



ChemPor 2023

**14th International Chemical and Biological
Engineering Conference**

Book of Abstracts

Instituto Politécnico de Bragança | September 12-15



ORDEM
DOS
ENGENHEIROS



This volume contains the extended abstracts presented at the 14th International Chemical and Biological Engineering Conference (CHEMPOR 2023), held in Bragança - Portugal, from the 12th to the 15th of September, 2023.

Instituto Politécnico de Bragança & Ordem dos Engenheiros

**14th International Chemical and Biological Engineering
Conference
(CHEMPOR-2023)**

Book of Abstracts

Edited by:

Ana Maria Alves Queiroz da Silva
António Manuel Coelho Lino Peres
António Manuel Esteves Ribeiro
Maria Filomena Filipe Barreiro
Maria Olga de Amorim e Sá Ferreira
Paulo Miguel Pereira de Brito
Simão Pedro de Almeida Pinho



Title

14th International Chemical and Biological Engineering Conference (CHEMPOR 2023): book of abstracts

Editors

Ana Maria Alves Queiroz da Silva

António Manuel Coelho Lino Peres

António Manuel Esteves Ribeiro

Maria Olga de Amorim e Sá Ferreira

Maria Filomena Filipe Barreiro

Paulo Miguel Pereira de Brito

Simão Pedro de Almeida Pinho

Publisher

Instituto Politécnico de Bragança

September 2023

ISBN 978-972-745-327-6

Sponsored by:

Diamond sponsors



Gold sponsors



Silver sponsors



Bronze sponsors



Organized with the support of:



Welcome Message

Dear Delegates,

Welcome to the 14th edition of the International Chemical and Biological Engineering Conference (ChemPor-2023) held at Bragança Polytechnic University (Instituto Politécnico de Bragança, IPB), Portugal, from 12 to 15 of September, 2023. This triennial conference, organized by a Portuguese Higher Education Institution and the Portuguese Engineers Association (Ordem dos Engenheiros), gathers experts from the chemical and biological engineering areas and related subjects to exchange knowledge and technological experiences within the academic, industrial, scientific, and technological communities. ChemPor-2023 addresses these research fields in different topics, from green chemistry to engineering education, always envisaging a sustainable development.

The etymology of the word “conference”, from the Medieval Latin, means literally “bring together”. This 14th edition comes with a two-year delay following the global sanitary crisis since only a full in-person meeting could fulfill this purpose. ChemPor-2023 encompasses a gathering in a vivid, enlightening, and convivial way, and this hiatus did not limit this spirit or its objectives. The conference aims to celebrate creativity, diversity, and friendship among participants, promoting ideas exchange and fruitful interactions. We have *circa* 300 delegates from 4 continents, and your active participation is highly acknowledged.

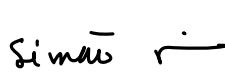

The general relevance of ChemPor-2023 is addressed in a variety of settings, including biorefinery, biotechnology, energy and environment, innovative materials, creation and design of novel reaction and separation processes, always foreseeing industrial applications for a sustainable shaping of the future. This edition includes an opening lecture by Jorge Calado in the immense but much less explored area of *ArtScience*, and an Honor Session dedicated to Alírio Rodrigues for his academic and scientific contributions, particularly regarding IPB. Besides, the conference includes 11 invited lectures from internationally recognized scientists and experts from the industry, 107 oral presentations distributed in 27 sessions, and 135 posters in two dedicated sessions. A session exclusively dedicated to companies and another for Ph.D. studies in industrial environments are to be highlighted.

The “Professor Almiro e Castro” award, established in 2014 by PARALAB – Equipamentos Industrial and Laboratory SA, to recognize the scientific merit of a Portuguese professor or researcher in the last three years in the fields of Chemical and Biological Engineering, and related areas, will be announced at the closing of the conference. In that ceremony, the two best posters and the best oral communication awards by young scientists will also be granted.

We want to reinforce our deepest appreciation to all the participants, but also to the members of the Honor, Scientific, and Local Organizing Committees for their invaluable contribution to the conference and acknowledge the institutional support of Instituto Politécnico de Bragança, Ordem dos Engenheiros, Centro de Investigação de Montanha, Sociedade Portuguesa de Química, and Câmara Municipal de Bragança. Expressing enormous gratitude is mandatory to all our Sponsors and associated scientific journals and publishers. Nothing could have been possible without all of you!

Finally, our best wishes for success for the next ChemPor organization.

Our warm regards,

 
Simão Pinho and Filomena Barreiro

Honor Committee

Orlando Afonso Rodrigues, Presidente do Instituto Politécnico de Bragança
 Hernâni Venâncio Dias, Presidente da Câmara Municipal de Bragança
 Fernando de Almeida Santos, Bastonário da Ordem dos Engenheiros
 Alírio Egídio Rodrigues, Faculdade de Engenharia da Universidade do Porto
 Clemente Pedro Nunes, Instituto Superior Técnico
 João Sobrinho Teixeira, Deputado à Assembleia da República e Presidente IPB 2006/2018
 João Carlos Moura Bordado, Instituto Superior Técnico
 José Luís Figueiredo, Faculdade de Engenharia da Universidade do Porto
 Manuel Teixeira Carrondo, Universidade Nova de Lisboa
 Rosa Maria Quinta-Ferreira, Universidade de Coimbra

Scientific Committee

Adélio Miguel Mendes – FEUP	José Nuno Canongia Lopes – IST
Ana Carreira Lopes – UBI	José Paulo Mota – FCT-UNL
Ana Margarida Azevedo – IST	Luísa Hora de Carvalho – IPV
António Gonçalves Silva – OE	Madalena Queiroz Dias – FEUP
António Luís Amaral – ISEC	Manuel Fernando Pereira – FEUP
Artur Manuel Silva – UA	Manuela Estima Gomes – 3Bs
Carlos Manuel Silva – UA	Marco Seabra dos Reis – UC
Eugénio Campos Ferreira – UM	Margarida Maria Quina – UC
Fernão Domingos Magalhães – ARCP	Maria Arminda Alves – FEUP
Francisco Manuel Gírio – BIOREF	Maria Ascensão Reis – FCT-UNL
Francisco Manuel Lemos – IST	Maria Filomena Barreiro – IPB
Henrique Aníbal Matos – IST	Maria Goreti Sales – UC
João Bernardo Campos – FEUP	Maria Teresa Duarte – IST
João Filipe Mano – UA	Miguel Abreu Teixeira – Colab4Food
João Araújo Pereira Coutinho – UA	Miguel Gama – UM
João Crespo – FCT-UNL	Nídia Sá Caetano – ISEP
Joaquim Luís Faria – LSRE-LCM/SPQ	Nuno Cerca – UM
Jorge Fernando Coelho – UC	Raquel Aires-Barros – IST
José António Teixeira - SPBT	Rui Manuel Oliveira – FCT-UNL
José Augusto Coelho – ISEL-IPL	Simão Pedro Pinho – IPB
José Manuel Martinho – IST	

Organizing Committee

Chairs:

Simão Pedro de Almeida Pinho – CIMO-SusTEC

Maria Filomena Filipe Barreiro – CIMO-SusTEC

Ana Isabel Pereira – CEDRI-SusTEC

Ana Maria Queiroz – CIMO-SusTEC

António Ribeiro – CIMO-SusTEC

António Manuel Peres – CIMO-SusTEC

Arantzazu Santamaria – CIMO-SusTEC

Helder Gomes – CIMO-SusTEC

Jacinta Costa – ESE

Joana Amaral – CIMO-SusTEC

Mónia Martins – CIMO-SusTEC

Olga Ferreira – CIMO-SusTEC

Paulo Brito – CIMO-SusTEC

Ramiro Martins – LSRE-LCM

Programme

Time		Tuesday 12	Wednesday 13			Thursday 14			Friday 15		
08:00	09:00		<i>Registration</i>								
09:00	09:15		Plenary lecture 1 Jarka Glassey - ADG			Plenary lecture 3 Raquel Aires-Barros - ADG			Plenary lecture 5 Rafael Luque - ADG		
09:15	09:30		S1-AAM	S1-ADG	S1-AP	S4-AAM	S4-ADG	S4-AP	S7-AAM	S7-ADG	S7-AP
09:30	09:45		O EE-01	O BS-01	O RS-01	O BT-04	O MS-13	O RS-09	O BS-07	O RS-12	O BT-10
09:45	10:00		O EE-02		O RS-02	O BT-05	O MS-02	O RS-10	O BS-02	O RS-13	O BT-11
Session-Room			O EE-03	O BS-03	O RS-03	O BT-06	O MS-03	O RS-11	O BS-09	O RS-14	O BT-12
10:00	10:15		Poster session 1			Poster session 2			<i>Coffee-break</i>		
10:15	10:30		<i>Coffee-break Topics - EE IA MS and RS</i>			<i>Coffee-break Topics - BS BT and IM</i>					
10:30	10:45		Keynote 1 - Juan F. Rodríguez - AAM			Keynote 3 - Maria José Ferreira - AAM			Keynote 5 - José Palomar - AAM		
10:45	11:00		Keynote 2 - Luís Madeira - ADG			Keynote 4 - Miguel Cerqueira - ADG			Keynote 6 - Mara Freire - ADG		
11:00	11:15		S2-AAM	S2-ADG	S2-AP	S5-AAM	S5-ADG	S5-AP	S8-AAM	S8-ADG	S8-AP
11:15	11:30		O IM-01	O EE-04	O BT-01	O BT-07	O BS-04	O IM-04	O RS-15		O BS-10
11:30	11:45		O IM-02	O EE-05	O BT-02	O BT-08	O BS-05	O IM-05	O RS-16	O IM-10	O BS-11
Session-Room			O IM-03	O EE-06	O BT-03	O BT-09	O BS-06	O IM-06	O RS-17	O IM-11	O BS-12
11:45	12:00		<i>Lunch</i>								
12:00	12:15		Plenary lecture 2 Joaquim Henrique Teles - ADG			Plenary lecture 4 Margarida Costa Gomes - ADG			S9-AAM	S9-ADG	S9-AP
12:15	12:30								O IA - 05	O RS-18	O BT-13
12:30	14:00								O IA - 06	O RS-19	O BT-14
Session-Room									O IA - 07	O RS-20	O BT-15
14:00	14:15									O RS-21	O BT-16
14:15	14:30		S3-AAM	S3-ADG	S3-AP	S6-AAM	S6-ADG	S6-AP			
14:30	14:45		Sysadvance	Paralab	O EE-07	O IA - 01	O MS-04	O EE-13	O EE-19	O MS-10	O IM-12
14:45	15:00		O RS-04	Bondalti	O EE-08	O IA - 02	O MS-05	O EE-14	O EE-20	O MS-11	O IM-13
15:00	15:15		O RS-05	Bruker	O EE-09	O IA - 03	O MS-06	O EE-15	O EE-21		O IM-14
15:15	15:30		O RS-06	Prio	O EE-10	O IA - 04	O MS-07	O EE-16	Awards ceremony - ADG		
15:30	15:45		O RS-07	Cires	O EE-11	O IM-07	O MS-08	O EE-17	CHEMPOR-2026		
15:45	16:00		O RS-08	Hovione	O EE-12	O IM-08	O MS-09	O EE-18	Closing session		
16:00	16:15	<i>Registration</i>	Poster session 1			Poster session 2					
16:15	16:30		<i>Coffee-break</i>			<i>Coffee-break</i>					
16:30	16:45		<i>Topics - EE IA MS and RS</i>			<i>Topics - BS BT and IM</i>					
16:45	17:00										
17:00	17:15										
17:15	17:30										
17:30	17:45										
17:45	18:00										
18:00	19:00										
19:00	19:30										
19:30	23:00		<i>Social program</i>								
			<i>Conference dinner</i>								

BS	Biorefinery and Sustainability
BT	Biotechnology
EE	Energy and Environment
IA	Industrial Applications
IM	Innovative Materials
MS	Modeling, Synthesis and Integration of Chemical Processes
RS	Reaction and Separation Processes

AAM	Auditório Alcínio Miguel
ADG	Auditório Dionísio Gonçalves
AP	Auditório Pequeno
TMB	Teatro Municipal de Bragança

Index

Welcome Message	i
Honor Committee	ii
Scientific Committee	ii
Organizing Committee	iii
Programme	iv
OPENING CEREMONY LECTURES	1
The Power of S.T.E.A.M	2
<i>J.C.G. Calado</i>	
Alírio E. Rodrigues, Chemical Engineering and Bragança	3
<i>L.S. Pais</i>	
Ups and Downs	4
<i>A.E. Rodrigues</i>	
PLENARY LECTURES	6
Chemical engineers for the future – are we asking too much?	7
<i>J. Glassey</i>	
Understanding the development of a large-scale chemical process - The HPPO technology	9
<i>J.H. Teles</i>	
Purification of biopharmaceuticals	11
<i>R.A.Barros</i>	
Gas separation and transformation using porous ionic liquids	12
<i>M.C. Gomes</i>	
Benign-by-design methodologies for a more sustainable future: from nanomaterials to biomass/waste valorization	14
<i>R. Luque</i>	
KEYNOTE PRESENTATIONS	15
Supercritical CO₂ synthesis and functionalization of biopolymers	16
<i>E. Gracia, T. Garcia, I. Gracia, J.F. Rodriguez</i>	
Integration of reaction and separation processes	18
<i>L.M. Madeira</i>	

Portuguese footwear cluster – Innovative green materials, processes and products	21
<i>M.J. Ferreira, V. Pinto, P. Costa</i>	
Bio-based materials for the development of innovative micro and nanostructures for the delivery of bioactive compounds	24
<i>M.A. Cerqueira</i>	
Towards industrial decarbonization: Challenges of carbon capture and utilization based on ionic liquids through process simulation analyses	26
<i>J. Palomar, P. Navarro, J. Lemus, C. Moya, R. Santiago, D. Hospital, E. Hernandez, A. Belinchon, R. El Bijou</i>	
Valorization of chicken feathers using aqueous solutions of ionic liquids	29
<i>C. Polesca, H. Passos, M.G. Freire</i>	
Oral Session BIOREFINERY AND SUSTAINABILITY	33
Biochar and bio-oil from spent coffee grounds valorization	34
<i>N. Caetano, T. Teixeira, W. Júnior</i>	
Understanding the behavior of chitin in Subcritical and Supercritical Water in a continuous reaction system.....	36
<i>S. Rodríguez Rojo, A. Casas González, E. Alonso</i>	
Method for the sustainability analysis of extraction processes: obtaining high value products from Soybean Oil Deodorization Distillate (SODD).....	38
<i>G.F. da Costa, L.N.S. Marçal, R.M. Cavalcante, A.F. Young</i>	
Applying two steps of DOE to microwave extraction from spent coffee.....	40
<i>J. Coelho, M. Robalo, R. Filipe, S. Boyadzhieva, R.P. Stateva</i>	
Multifunctional nanohybrids, zeotypes and modified macro and mesoporous silicas for the upgrading of the renewable platform chemical levulinic acid	42
<i>M.M. Antunes, K. Klan, A. Silva, A. Fernandes, M. Pillinger, F. Ribeiro, A.A. Valente</i>	
Efficient conversion of syngas to lipids through a two-stage bioconversion process	44
<i>R. Robles-Iglesias, M.C. Veiga, C. Kennes</i>	
From sulphite liquor production to valorization: challenges in vanillin crystallization.....	46
<i>C.A.E. Costa, F. Casimiro, A.E. Rodrigues</i>	
Microwave extraction of proteins from <i>Litopenaeus vannamei</i> molt shell using only water as a solvent.....	48
<i>M.M. de Souza-Ribeiro, H. Loya-Pérez, G.E. Alonso-Sánchez, S. Rodríguez-Rojo</i>	
Shrimp shells waste biorefinery: From the extraction to the production of designed biochar catalysts, biofuels, bioproducts and energy conversion.....	50
<i>I.S. Marques, R. Matos, M.M. Moreira, E. Surra, D.M. Fernandes, A.F. Peixoto</i>	

Modelling and optimisation of supercritical CO₂ extraction of fatty acids from rice bran	52
<i>J.P. Coelho, R.M. Filipe, M.P. Robalo, R.P. Stateva</i>	
Valorization of grain and cereal processing by-products as yeast substrates for carotenoids production.....	54
<i>T.R. Balbino, S. Sánchez-Muñoz, S.C. Inácio, G.C. Almeida, J.C. dos Santos, J.F.B. Pereira, S.S. da Silva</i>	
Oral Session BIOTECHNOLOGY.....	56
Biovalorization of agricultural by-products obtained through green extraction methodology	57
<i>I.M. Martins, A. Ribeiro, Y.A. Manrique, R. França, L. Rocha, R.C. Calhella, C.Caleja, E. Pereira, L. Barros, M.M. Dias</i>	
Development of K-carrageenan polymeric films incorporated with curcumin solid dispersion particles as a model packaging material for olive oil preservation	59
<i>S.C. Rezende, A. Santamaria-Echart, I. Marcet, M. Carpintero, M. Rendueles, M.M. Dias, M.F. Barreiro</i>	
Extraction of phenolic compounds from <i>Juglans regia</i> L. leaves using aqueous solutions of eutectic solvents.....	61
<i>I.W. Cordova, T. Oludemi, V. Vieira, T.C.S.P. Pires, S.P. Pinho, J.A.P. Coutinho, L. Barros, O. Ferreira</i>	
EPS and aggregates changes on activated sludge under atrazine exposure	63
<i>A. Melo, J.G. Costa, C. Quintelas, E.C. Ferreira, D.P. Mesquita</i>	
Development of an enzymatic biosensor based on boron-doped diamond surface	65
<i>B.L. Tavares, D.R. Fernandes, L.R. Freitas, V.C. Ebinuma-Santos, J.C.F. Nunes, M.C. Neves, A.V. Girão, M.A.C. Neto, A.P.M. Tavares</i>	
Enhanced extraction of RNA from recombinant lysates afforded by the use of biocompatible ionic liquids	67
<i>A.F. Pereira, A.Q. Pedro, L.S. Castro, M.J. Quental, A.P.M. Tavares, L.C. Branco, J.A.P. Coutinho, F. Sousa, M.G. Freire</i>	
Analysis and calculation of biofilm structural properties using 3D OCT images in BISCAP	69
<i>D. Narciso, A. Pereira, F.G. Martins</i>	
Valorization of agro-industrial wastes by hydrothermal carbonization: synthesis, nitrogen functionalization, and evaluation as carbocatalysts in water treatment.....	71
<i>S. Escudero-Curie, X.L. Rodríguez, A. Díez, M. Pazos, A. Sanromán</i>	
Development of an integrated process for the production and purification of laccase.....	73
<i>F.F. Magalhães, C. Alves, A.Q. Pedro, M.G. Freire, A.P. Tavares</i>	
Investigation of insulin nucleation kinetics under oscillatory flow mixing.....	75
<i>F. Castro, S. Araújo, J. Ferreira, A. Ferreira, J. Campos, J.A. Teixeira, F. Rocha</i>	

Valorization of agro-industrial by-products: the chemistry behind the biological properties of phenolic extracts and their potential for value-added products.....	77
<i>S. Ferreira, L. Santos</i>	
MLM-type structured lipids: synthesis and cytotoxic evaluate with murine fibroblast and human cervical adenocarcinoma cell lines	79
<i>R.H. Miotti Jr, S.R. do Amaral, F.L. Primo, J.F.B. Pereira, A.V. de Paula</i>	
Assessing the influence of long-chain fatty acids on aerobic granular sludge stability in a sequencing batch reactor	81
<i>S.A. Silva, M.S. Duarte, A.L. Amaral, E.C. Ferreira, M.M. Alves, D.P. Mesquita</i>	
Olive oil by-products as potential alternative substrates for xylooligosaccharides production.....	83
<i>A. Cordeiro, A. Fernandes, A.M. Peres, L. Rodrigues, C. Amorim</i>	
Microbial lipids production by <i>Yarrowia lipolytica</i> W29 from eucalyptus bark hydrolysate	85
<i>B. Dias, H. Fernandes, S. Marques, F. Gírio, M. Lopes, I. Belo</i>	
Batch cultures of <i>Y. lipolytica</i> CBS 2075 on hydrocarbons medium under different conditions of oxygenation	87
<i>S.M. Miranda, M. Lopes, I. Belo</i>	
Oral Session ENERGY AND ENVIRONMENT.....	89
Activated carbon 3D structures for carbon dioxide capture	90
<i>R.R. Dias, G. Al Khalil, I. Fonseca, J.P.B. Mota, I. Matos, R.P.P.L. Ribeiro</i>	
Hermetic encapsulation for long-lifetime printable perovskite solar cells and mini-modules.....	92
<i>M. Pereira, J. Martins, F. Santos, D. Ivanou, S. Emami, A. Mendes</i>	
Degradation of volatile organic compounds from gaseous streams by Fenton's oxidation over N-doped carbon-based materials	94
<i>E.F.S Sampaio, O.S.G.P. Soares, M.F.R. Pereira, C.S.D. Rodrigues, L.M. Madeira</i>	
Biochemical methane potential and biodegradability of brewery spent grain in different inoculum to substrate ratios	96
<i>P. Polastri, W.M. Moreira, A.L.G. Simões, D.T. Vareschini, M.L. Gimenes</i>	
Comparison of energy consumption and carbon footprint of perovskite solar cells with different architectures	98
<i>J. Príncipe, L. Andrade, T.M. Mata, A.A. Martins</i>	
Overcoming the upscaling challenges of Dye-sensitized solar cells with fluorine-doped tin oxide current collectors	100
<i>J. Capitão, D. Ivanou, A. Mendes</i>	
Highly stable noble metal-free bifunctional carbon black electrocatalysts for oxygen reduction and evolution reactions	102
<i>R.S. Ribeiro, M. Florent, M.F.R. Pereira, T.J. Bandoz</i>	

Low temperature hermetic encapsulation for long-term stable dye-sensitized solar cells	104
<i>J. Martins, S. Emami, D. Ivanou, A. Mendes</i>	
A novel approach for lead mitigation in perovskite solar cells glass encapsulated by laser sealing	106
<i>E. Loureiro, R. Madureira, S. Emami, D. Ivanou, A. Mendes</i>	
Magnetic properties of carbon nanotubes synthesized by chemical vapor deposition using polyolefins as carbon source	108
<i>A.S. Silva, L.F. Sanches, F.F. Roman, J.L. Diaz de Tuesta, A.I. Pereira, A.M.T. Silva, H.T. Gomes</i>	
When electroanalysis meets engineering: Validation of a methodology for the detection and monitoring of drugs' removal from water	110
<i>S. Caruncho-Pérez, N. Bernárdez, M. Pazos, M. A. Sanromán, E. González-Romero</i>	
Stable and Selective Cu-based catalysts supported on CNT-ZnO composites for the Reverse Water-Gas Shift Reaction	112
<i>A.R. Querido, L.P.L. Gonçalves, M.R. Pereira, O.S.G.P. Soares</i>	
Exhaustive characterization of petroleum sludges from different units of treatment and strategies for their valorization	114
<i>N. Corrochano, A. de Mora, J.L. Diaz de Tuesta, M.I. Pariente, Y. Segura, R. Molina, F. Martínez</i>	
Development of a method and analysis of levels of volatile methylsiloxanes in microplastics and sand from Azores beaches	116
<i>T. Ferreira, V. Homem, Y. Rodríguez, L. Herrera, C.K. Pham, N. Ratola</i>	
Treatment of a toluene-containing gas stream by application of an activated persulfate-based Advanced Oxidation Process	118
<i>A.S.P. Alves, C.S.D. Rodrigues, L.M. Madeira</i>	
Conversion of sewage sludge into catalyst for cytostatic removal	120
<i>D. Huber-Benito, M. Martin-Martinez, M. Larriba, V.I. Águeda, J. García</i>	
Numerical modelling and experimental measurement of wear in a cyclone separator	122
<i>P. Pacheco, M.A. Alves, J.B.L.M. Campos, J. Paiva</i>	
Biomass-based adsorbents for carbon capture	124
<i>A. Amorim, R.M. Filipe, C.K. Rojas-Mayorga, A. Bonilla-Petriciolet, H.A. Matos</i>	
Treatment of wastewater effluents using nanofiltration and low pressure UV treatment to produce high quality water that can be reused for irrigation for food production	126
<i>M.B. Cristóvão, A.P. Marques, A. Bento-Silva, M. Gossard, S. Tela, J. Sério, M.R. Bronze, P.B. de Oliveira, M. Nunes, M.T.B. Crespo, J.G. Crespo, V.J. Pereira</i>	
Efficient adsorption and regeneration of activated carbon used in the treatment of highly chlorinated organic emulsion using the Fenton Reaction	128
<i>A. Sánchez-Yepes, A. Santos, A. Romeros, D. Lorenzo</i>	

Synthesis of bimetallic ZnFe-MOF catalyst for the removal of emerging pollutants in wastewater by using radical-based treatment	130
<i>D. Terrón, E. Rosales, M. Pazos, M.A. Sanromán</i>	
Oral Session INDUSTRIAL APPLICATIONS	132
Green solvents for enhanced selective extraction of 1,3-butadiene: a comparative study	133
<i>J. Gomes, R. Silva, C. Nunes, D. Barbosa</i>	
Phosphorus recovery using calcined Layered Double Hydroxides from aqueous matrices	135
<i>I.D. Borges, C.M. Rocha, F. Maia, C.M. Silva, M.J. Quina</i>	
Static optimization and dynamic modelling of microalgae production in photobioreactors	137
<i>T.M. Taborda, J.C. Pires, S.M. Badenes, F. Lemos</i>	
Multi-class classification of melamine content in industrial formaldehyde-based resins using NIR spectroscopy and machine learning	139
<i>R. Magalhães, N.T. Paiva, F.D. Magalhães, F.G. Martins</i>	
Impact of visible light on natural textile dyes obtained from Yerba mate (<i>Ilex paraguariensis</i>)	141
<i>J. Santos, S. Oliveira, B. Freitas, R.A. Fernandes, S. Monteiro, P. Magalhães, F.D. Magalhães, J.M. Martins, L.H. Carvalho</i>	
Decentralized process monitoring: unlocking causal insights for enhanced fault detection and diagnosis	143
<i>R. Paredes, M.S. Reis</i>	
Multimodal data fusion in the chemical processing industry: a new methodology and case studies	145
<i>E. Strelet, I. Castillo, Y. Peng, R. Rendall, B. Braun, L. Chiang, M.S. Reis</i>	
The role of choline based ionic liquids in enhancing micellization of ionic surfactants in aqueous medium – comparative study	147
<i>A. Al-Farsi, I. Khan, J. Husband</i>	
Oral Session INNOVATIVE MATERIALS	149
Water capture from air: development of inks for 3D-printing using MOFs	150
<i>M. Barata, A. Pereira, A. Ferreira, A. Rodrigues, A.M. Ribeiro, M.J. Regufe</i>	
Modification of dextran with octenyl succinate. Evaluation of emulsifying and foaming properties	152
<i>F. Ridella, M. Carpintero, I. Marcet, M. Rendueles, M. Díaz</i>	
Facile process for the purification of (E)-resveratrol from grape stems using tailor-made sorbents	154
<i>A. Bzainia, R.C.S. Dias, M.R.P.F.N. Costa</i>	
Vitamin E-loaded hydroxyapatite Pickering emulsions as new product design for fortified food applications	156
<i>A. Ribeiro, R.F.S. Gonçalves, A.C. Pinheiro, Y.A. Manrique, M.F. Barreiro, J.C.B. Lopes, M.M. Dias</i>	

Recovery of chitin and chitosan from <i>Agaricus bisporus</i> mushrooms: optimisation of the extraction process and effect of different mushroom samples	158
<i>C.F. Almeida, I.L. Amorim, Y.A. Manrique, C.G. Silva, J.C.B. Lopes, F.G. Martins, M.M. Dias</i>	
Colloidal lignin particles as innovative oil-in-water Pickering stabilizers	160
<i>G. Colucci, L.G. Teixeira, S. C. Silva, A. Ribeiro, A. Santamaria-Echart, A. E. Rodrigues, M.F. Barreiro</i>	
Rheology of suspensions of charged cellulose nanofibrils	162
<i>L. Alves, J. Pedrosa, P.J.T. Ferreira, J.A.F. Gamelas, M.G. Rasteiro</i>	
Synthesis of nano-biocomposite hydrogel with graphene oxide for the separation of hemoprotein myoglobin: adsorption equilibrium and kinetics	163
<i>C.M.B. Araujo, M.A. Motta Sobrinho, M.G. Ghislandi, A.F.P. Ferreira, A.E. Rodrigues</i>	
Superabsorbent polymers: their uses and properties, and computation of their characteristic parameters	165
<i>M. Casquilho, A.M. Rodrigues, J.L. Miranda, J. Bordado</i>	
Hybrid adsorbents endowed with stereospecificity towards flavonoids present in olive oil and winemaking residues	167
<i>C.P. Gomes, R.C.S. Dias, M.R.P.F.N. Costa</i>	
Green affinity-driven biopurification materials: supercritical CO₂ technology versus mechanochemistry	169
<i>A.I. Furtado, R. Viveiros, V.D.B. Bonifácio, A. Melo, T. Casimiro</i>	
Agroindustry residues as powerful materials for environmental remediation and energy generation	171
<i>A.M. Díez, V. Laíño-Rodríguez, M. Bolaños-Vázquez, M.A. Sanromán, M. Pazos</i>	
Material development contribution to improve biorefinery sustainability	173
<i>T. Esteves, A.S. González, A. Gil, C.A.M. Afonso, F.C. Ferreira</i>	
Dyes removal using poly(ionic liquid)s	175
<i>G. Caetano, B. Soares, M.M. Correia, I.M. Marrucho</i>	
Oral Session MODELING, SYNTHESIS AND INTEGRATION OF CHEMICAL PROCESSES	177
Comparison of continuous chromatography for downstream processing of proteins using an analogy with single-column batch chromatography with recycle lag	178
<i>J.P.B. Mota, R.C.R. Ribeiro</i>	
Estimating the melting temperatures of type V deep eutectic solvents	180
<i>G. Teixeira, D. Abranches, O. Ferreira, J.A.P. Coutinho</i>	
Chemical recycling of poly(ethylene terephthalate) using low-cost ionic liquids	182
<i>H.L. Judah, M.Y. Suleman, A. Brandt-Talbot</i>	

Industrial process analytics: from case-based problem solving to a systematic discipline in chemical engineering.....	184
<i>M.S. Reis</i>	
An integrated approach of numerical topological optimization and 3D printed experimental validation.....	186
<i>J.M.R. Almeida, J.B.L.M. Campos, J.D.P. Araújo</i>	
A framework for predicting odor threshold values of perfumes by scientific machine learning and transfer learning.....	188
<i>L.M.C. Oliveira, V.V. Santana, A.E. Rodrigues, A.M. Ribeiro, I.B.R. Nogueira</i>	
Microdroplets flowing through microfluidic constrictions: experimental and numerical study.....	190
<i>A.T.S. Cerdeira, J.B.L.M. Campos, J.M. Miranda, J.D.P. Araújo</i>	
Understanding the behavior of an integrated process for microbial oil production from organic waste through modelling and simulation.....	192
<i>S. Abelleira, P.L. Cruz, D. Iribarren</i>	
A novel CFD approach to calculate the ozone mass transfer coefficient (<i>kL</i>) in a tube-in-tube membrane reactor: coupling numerical and analytical modeling.....	194
<i>M.P. Caixeta, P.H.M. de Oliveira, R.J. Santos, V.J.P. Vilar</i>	
Kinetic modeling of chemical reactions towards a faster chemical development in the pharmaceutical industry.....	196
<i>M.C. Pereira, N. Lousa</i>	
Analysis of the role of gasification within a waste management and valorization system using an artificial neural network as surrogate model.....	198
<i>N. Martínez-Ramón, J.L. Gálvez-Martos, E. Medina-Martos, I.R. Istrate, P.L. Cruz, J. Dufour</i>	
ReactorDesign App: An interactive software for self-directed explorative learning.....	200
<i>C.W. Lim, N. Yan</i>	
Structure and thermodynamics of empty clathrate hydrates bellow the freezing point of H₂O.....	202
<i>F.J.A.L. Cruz, J.P.B. Mota</i>	
Oral Session REACTION AND SEPARATION PROCESSES.....	204
Separation of n/iso-paraffins in a hierarchically structured 3D-printed porous carbon monolith.....	205
<i>A. Henrique, L.F.A.S. Zafanelli, E. Aly, H. Stedinger, J. Gläsel, A.E. Rodrigues, B.J.M. Etzold, J.A.C. Silva</i>	
Fenton and ion exchange processes for winery wastewaters treatment.....	207
<i>P.M. Reis, J.L. Alves, C.M. Matia, M.E. Quinta-Ferreira, L.M. Gando-Ferreira, R.M. Quinta-Ferreira</i>	
TiO₂-silver zeolites composites for ethylene removal and reduction of fruits and vegetable wastes.....	209
<i>R. Ferreira, A. Fernandes, J.P. Lourenço, J.M. Silva, I.M. João, S. Morales-Torres, L.M. Pastrana-Martínez, F.J. Maldonado-Hódar, M. F. Ribeiro</i>	

Methane upgrading on pelletized maxsorb by gas-phase simulated moving bed	211
<i>R.O.M. Dias, M.J. Regufe, A.A. Pereira, A.F.P. Ferreira, A.E. Rodrigues, A.M. Ribeiro</i>	
Silica-based supported ionic liquid-like phase materials for the flow-through downstream processing of L-asparaginase.....	213
<i>J.C.F. Nunes, M.R. Almeida, G.B. de Paiva, D.B. Pedrolli, V.C. Santos-Ebinuma, M.C. Neves, M.G. Freire, A.P.M. Tavares</i>	
Improving α-tocopherol extraction from <i>Moringa oleifera</i> L. leaves using SFE-CO₂	215
<i>J.C. Kessler, Y.A. Manrique, I.M. Martins, A.E. Rodrigues, M.F. Barreiro, M.M. Dias</i>	
Xylene isomerization in the liquid phase by MOR type zeolites.....	217
<i>B.A.C. Castro, A.F.P. Ferreira</i>	
A detailed study on the valorization of multilayer plastic waste based on the dissolution and precipitation technique	219
<i>A. Cavuquilha, C. Maganinho, M. Durão, A. Dias, G. Carreira, I. Portugal, C. Silva, A. Barros-Timmons</i>	
Complete separation of nadolol stereoisomers by fixed-bed and simulated moving bed chromatography.....	221
<i>R. Arafah, A. Ribeiro, A. Rodrigues, L. Pais</i>	
Influence of [emim][Tf₂N] in PES/SAPO-34 mixed matrix membranes for gas separation	223
<i>J.S. Cardoso, Z. Lin, P. Brito, L. Gando-Ferreira</i>	
Valorisation of sewage sludge producing an activated carbon as an adsorbent for the removal of cytostatic drugs from water	225
<i>E. Portillo, S. Flores, R. Carrizosa, S. Álvarez-Torrellas, J. Carbajo, V.I. Águeda, J. García</i>	
Pillared clays as cost-effective adsorbent for CO₂ capture in the cement Industry: experimental and simulation study	227
<i>A. Al Mohtar, T. Frade, M. Bordonhos, J. Tingelinas, C. Saragoça, M. Mateus, M.L. Pinto</i>	
Waste-derived carbon materials for adsorptive recovery of rare earth elements.....	229
<i>M. Nogueira, M. Bernardo, F. Pinto, I. Fonseca, N. Lapa, I. Matos</i>	
Biomethane production by PSA with sewage sludge-based adsorbents.....	231
<i>R. Calero-Berrocal, V.I. Águeda, J.A. Delgado</i>	
Evaluation of the cholinium chloride-based aqueous biphasic systems (ABS) hydrodynamics	233
<i>A.M.S. Jorge, J.A.P. Coutinho, J.F.B. Pereira</i>	
CO₂ capture and valorization to synthetic natural gas – process integration	235
<i>J. Martins, A. Rodrigues, L.M. Madeira</i>	
Green hydrogen recovery from natural gas grids by adsorption process	237
<i>L.F.A.S. Zafanelli, A. Henrique, E. Aly, A.E. Rodrigues, J.A.C. Silva</i>	

Solvent extraction in non-ideal eutectic solvents – application towards lanthanide separation	239
<i>U.G. Favero, N. Schaeffer, H. Passos, K.A.M.L. Cruz, D. Ananias, S. Dourdain, M.C. Hespanhol</i>	
Autothermal reforming of distillery wastewater for renewable hydrogen production	241
<i>P. Cerqueira, C. Rocha M.A. Soria, L.M. Madeira</i>	
A novel continuous flow multiphase installation for terpene-based extraction of acetic acid from wastewater streams	243
<i>D. Rodríguez-Llorente, J.C. de Mello, J. García, M. Larriba</i>	
Enhanced simulated moving bed reactor performance for the synthesis of solketal by implementing the ModiCon strategy.....	245
<i>I. Corrêa, R.P.V. Faria, A.E. Rodrigues</i>	
Oral Session COMPANY LECTURES.....	247
Optimization of supercritical fluid extraction and reaction systems for unique application requirements	248
<i>J. Carvalheira, S. Cardoso</i>	
RDI at Bondalti.....	249
<i>F. Franco</i>	
Monitoring of fermentation processes	250
<i>E. Monteiro, R. Rocha, H. Lutz</i>	
Six Sigma methodology applied in biodiesel production	251
<i>F. Pereira</i>	
PVC – a sustainable material.....	252
<i>A. Tomás</i>	
Sustainability at Hovione R&D process chemistry development	253
<i>N. Pereira</i>	
Advancing sustainability through gas adsorption and reaction technologies: SYSADVANCE's 20-year journey in gas purification	254
<i>P. Bárcia</i>	
Poster Session BIOREFINERY AND SUSTAINABILITY	257
Sustainable jet fuel production: assessment of reaction conditions in palmitic acid deoxygenation.....	258
<i>K.K. Ferreira, L. Ribeiro, M.F.R. Pereira</i>	
Studies on the hydrotropic enhancement of acetaminophen aqueous solubility.....	260
<i>J. Santos, A. Zambom, M.A.R. Martins, O. Ferreira, S.P. Pinho</i>	
Engineering of a recyclable crosslinked polyurethane with thermally reversible Diels-Alder adduct	262
<i>A.C. Restrepo, I. Larraza, N. Gabilondo, A. Saralegi, A. Eceiza</i>	

Innovative design of a more sustainable technology for microalgae protein recovery	264
<i>B. Pereira, C. Brazinha, J. G. Crespo, S. P. M. Ventura, C. T. Matos, L. Costa</i>	
Organosolv lignin extraction and characterization from three Costa Rican biomasses.....	266
<i>A. Valverde-Romero, J.M. Mata-Segreda; A. Hernández, C.A. Vega-Aguilar</i>	
Lignin-derived covalent adaptable networks (CANs): a sustainable approach to versatile material design.....	268
<i>F.A. Vicente, G. Tofani, D.B. Tiz, E. Jasiukaitytė-Grojdek, A.K.B. Likozar</i>	
Ionic liquids for essential oils processing: terpenes fractionation	270
<i>A. Zambom, S. Vilas-Boas, L.P. Silva, M.A.R. Martins, O. Ferreira, S.P. Pinho</i>	
Using COSMO-RS as a predictive tool to select potential deep eutectic solvents capable of dissolving lignin solubility and enhancing laccase activity.....	272
<i>P.V.A. Pontes, F.H.B. Sosa, J.A.P. Coutinho, A.M. da Costa Lopes, J. Andreus</i>	
Grape stalks of <i>Vitis vinifera</i> L.: a renewable source for bio-based adhesives	274
<i>R.A. Fernandes, N. Ferreira, S. Lopes, A.K. Barreto, J. Santos, J.M. Martins, L.H. Carvalho</i>	
Lycopene cream obtained by high-pressure homogenization of tomato waste	276
<i>H. Ribeiro, B. Schuur, J.F.B. Pereira</i>	
Development of polymeric adsorbent materials from the agar industry for removal of organic dyes in wastewaters.....	278
<i>M. Carpintero, I. Marcet, M. Rendueles, M. Díaz</i>	
Building a spent grain biorefinery using ionic liquids - with a focus on the extraction and valorisation of protein	280
<i>P. Kumar, P.Y.S Nakasu, A. Brandt-Talbot, J.P Hallett</i>	
Determination of Kraft lignin solubility in aprotic and protic ionic liquids aqueous solutions.....	282
<i>R.M. Dias, S.M. Vilas-Boas, M.C. Costa</i>	
Winery waste streams as potential natural pesticides	284
<i>J.P. Baixinho, F.B. Gaspar, P.J.A. Madeira, M.R. Bronze, N. Fernández</i>	
Recycling of poly(ethylene terephthalate) waste by efficient hydrolytic depolymerization with bio-based eutectic solvents.....	286
<i>V. de Paula, A.J.D. Silvestre, A.F. Sousa</i>	
Liquified biomass utilization in water co-electrolysis for Synthesis gas production	288
<i>D.M. Martins, T.M. Cabrita, J.C. Rodrigues, J.F. Puna, J.F. Gomes</i>	
Olive stone-based chemically modified carbon adsorbents for copper adsorption.....	290
<i>V. Rahimi, D. Gómez-Díaz, M.S. Freire, J. González-Álvarez</i>	
Effect of activation conditions of carbons derived from pine sawdust on wood dye removal	292
<i>C.H. Pimentel, M.S. Freire, D. Gómez-Díaz, J. González-Álvarez</i>	

Medium chain fatty acids production from syngas by a co-culture of <i>Clostridium acetivum</i> and <i>Clostridium kluyveri</i>.....	294
<i>C. Fernández-Blanco, M.C. Veiga, C. Kennes</i>	
Response surface methodology approach for keratin recovery using a bio-based ionic liquid	296
<i>C. Polesca, A. Al Ghatta, H. Passos, J.A.P. Coutinho, J.P. Hallett, M.G. Freire</i>	
Recovery of carotenoids from <i>Yarrowia lipolytica</i> using biosolvents.....	298
<i>C. Naveira-Pazos, M.C. Veiga, C. Kennes, J.F.B. Pereira</i>	
Obtaining liquid fuels by applying bifunctional catalysts in the Fischer-Tropsch process.....	300
<i>D. Costa, J. Joaquim, E. Falabella, C.M. Magalhães, B.F. Machado, M.F. Ribeiro</i>	
Impact of storage conditions on the chemical composition of wine industry by-products.....	302
<i>A.K. Barreto, R.A. Fernandes, J. Santos, P. Magalhães, J.M. Martins, I. Brás, L.H. Carvalho</i>	
Towards sustainable valorization of industrial waste - catalysts derived from sugar cane molasses for upgrading glycerol to fuel additives	304
<i>K.M. Eblagon, A. Malaika, K. Ptaczyńska, M. Kozłowski, J.L. Figueiredo</i>	
Production of 5-hydroxymethylfurfural from table sugar in water using bifunctional biochar catalysts	302
A. Malaika, K.M. Eblagon, M.A.C. Bravo, M. Kozłowski, J.L. Figueiredo	
Poster Session BIOTECHNOLOGY.....	308
Solubility of amino acids: the effect of chaotropic anions.....	309
<i>M. Aliyeva, P. Brandão, J.A.P. Coutinho, O. Ferreira, S.P. Pinho</i>	
Olive pomace extracts as antimicrobial agents for leather treatments	311
<i>K. Kebaili, H.H.S. Almeida, A.E.K. Benhlma, M.F. Barreiro, P.J.L. Crujeira</i>	
Development of acorn shell extract solid-in-oil-in-water (S/O/W) emulsion-based carriers envisaging cosmetic applications	313
<i>L.F. Fernandes, L.G. Teixeira, G. Colucci, M.P. Sousa, P.S. Babo, A. Santamaria-Echart, R.F. Canadas, M.F. Barreiro</i>	
Gellable aqueous biphasic systems as a novel strategy for mRNA nasal delivery	315
<i>B. Kopilovic, N. Laroui, J.A.P. Coutinho, C. Pichon, M.G. Freire</i>	
Exploiting winemaking residues as ingredients for cosmeceutical applications	316
<i>C.N. Duarte, A. dos Santos, T. Oludemi, C. Santos-Buelga, R.C.S. Dias, L. Barros, J.S. Amaral</i>	
Potassium evoked ROS signals in mitochondria.....	318
<i>J.L.R. Alves, M.S. Sousa, P.M. Reis, R.M. Quinta-Ferreira, M.E. Quinta-Ferreira, C. M. Matias</i>	
Near-infrared spectroscopy analysis of bread: study of shelf life and correlation with microbiological analysis	320
<i>D. Amendoeira, A. Teixeira, L.G. Dias, L. Estevinho</i>	

Analysis of bread using potentiometric electronic tongue: importance for quality control	322
<i>A. Teixeira, D. Amendoeira, L. Estevinho, L.G. Dias</i>	
Optimization of phenolic compounds extraction from mountain ash fruit pulp	324
<i>G. Vergara, N.L. Seixas, N.P. Mira, L. Estevinho, L.G. Dias</i>	
Extraction of phenolic compounds from <i>Sorbus aucuparia</i> tree leaves for use in food	325
<i>H.F. Rodrigues, N.L. Seixas, N.P. Mira, L.G. Dias, L.M. Estevinho</i>	
Laccase mediated grafting of pine sawdust for oil spill recovery	327
<i>N. Miguez, A. Sanromán, D. Moldes</i>	
Development of an integrated process for the recovery and purification of recombinant messenger RNA vaccines resorting to bio-based ionic liquids	329
<i>A.S.C. Marques, A.Q. Pedro, C. Gonçalves, A.P.M. Tavares, C. Pichon, M.G. Freire</i>	
Dextran-based hydrogel composites for tissue engineering	331
<i>P. Alves, A.F. Simões, M.F.P. Graça, I.J. Correia, P. Ferreira</i>	
Valorization of brewery spent grain to produce volatile fatty acids through acidogenic fermentation	333
<i>L. Ferreira, M.C. Veiga, C. Kennes</i>	
Predicting the shelf-life of extra virgin olive oil during storage at 22 and 50°C, using a kinetic modelling approach	335
<i>N. Ferreira, J.A. Pereira, N. Rodrigues, A.M. Peres</i>	
Metal-ion zeolites obtained by chemical and mechanochemical methods as Fenton-like catalysts for health applications	337
<i>J.T. Costa, V. Ivasiv, A.R. Bertão, N. Nunes, A.S. Mestre, A.P. Carvalho, A.M. Fonseca,</i> <i>F. Baltazar, J.N. Moreira, I.C. Neves, A. Martins</i>	
Computer-aided identification of trihalomethane degradation by haloalkane dehalogenase DhaA from <i>Rhodococcus</i> sp.	339
<i>M.M. Pereira, R.C. Martins</i>	
Ultrasound-assisted synthesis of inulin esters with antimicrobial and anti-inflammatory activities	341
<i>I. Hambarliyska, N. Petkova, Y. Tumbarski, D. Vassilev, M. Brazkova, A. Krastanov, I. Ivanov,</i> <i>P. Denev, I. Gotova, Z. Dimitrov</i>	
Urea as an alternative source of nitrogen for microalgae cultivation: effect on growth and biomass composition	342
<i>P.S. Corrêa, M.M.A. Freitas, N.S. Caetano</i>	
Microencapsulation of biocide benzisothiazolinone: a promising technique for the improvement of its aqueous solubility	344
<i>V.F.M. Silva, E.M.P.J. Garrido, F. Borges, J.M.P.J. Garrido</i>	

<i>In vitro</i> evaluation of avian immunoglobulin Y (IgY) antibodies to fight infectious illnesses caused by methicillin-resistance <i>Staphylococcus aureus</i> (MRSA)	346
<i>C. Almeida, M.C. Neves, M.G. Freire</i>	
Extraction study of bioactive compounds from ginger by ultrasound an analysis of antioxidant action	348
<i>S.S. Bernardoni, B.L. Schneider, D.A. Nardino, R.M. Suzuki, C.C. Sipoli</i>	
Validation of a prototype of a miniaturized near infrared spectrometer on complex organic samples.....	350
<i>L.L. Monteiro, P. Zoio, B.B. Carvalho, L.P. Fonseca, C.R.C. Calado</i>	
Interaction between <i>Chlorella vulgaris</i> and microplastic (PET) particles examined by optical and nuclear microscopy	352
<i>S.A. Vaz, T. Pinheiro, L.P. Monteiro, S.M. Badenes, R.C. Martins, H.M. Pinheiro</i>	
Polymer-based aqueous biphasic systems as a tool for the recovery of protein-based biopharmaceuticals.....	354
<i>L.S. Castro, A.Q. Pedro, M.G. Freire</i>	
Application of PNA-FISH based-methods for bacterial detection and localization in biofilms	356
<i>A. Barbosa, D. Goeres, N.F. Azevedo, L. Cerqueira</i>	
Development of efficient platforms for breast cancer biomarkers extraction resorting to ionic liquid-based aqueous biphasic systems	358
<i>M.S.M. Mendes, M.C. Souza, J.P. Conde, M.G. Freire, F.A. e Silva</i>	
Streamlining bacterial infection diagnosis: rapid Gram classification using FTIR spectroscopy.....	360
<i>R. Araújo, L. Ramalhete, T. Fonseca, C. von Rekowski, L. Bento, C. Calado</i>	
Enhancing plastic waste recycling: investigating the impact of additives on polymer degradation via laccase from <i>Trametes versicolor</i>	362
<i>M.I.S. Aguiar, A.F. Sousa, A.P.M. Tavares, A.M. Ferreira</i>	
Poster Session ENERGY AND ENVIRONMENT.....	364
Life cycle environmental impact assessment of a pajama shirt	365
<i>A.A. Martins, R. Lapa, B. Mota, S. Maia, J.C.G.E. da Silva, C. Soares, T.M. Mata</i>	
Life cycle assessment: a comparison of different tools using an academic case study	367
<i>R.N. Dias, N. Stamatopoulou, R.M. Filipe, H.A. Matos</i>	
Porous PDMS membranes as P25 supports for the photocatalytic degradation of parabens.....	369
<i>M.J. Silva, R. Alves, P. Alves, J. Gomes, P. Ferreira, R.C. Martins</i>	
Catalytic conversion of hemicellulose-derived pentoses into sugar/aliphatic acids	371
<i>V. Van-Dúnem, L.C. Duarte, L.M.D.R.S. Martins, F. Carvalheiro</i>	
Analysis of energy transition scenarios in industry, using RETScreen	373
<i>B. Moreira, C.G. Braz, M.C. Fernandes</i>	

Persulfate process activated by heterogeneous catalyst for synthetic olive mill wastewater treatment	375
<i>T. Vaz, M. Quina, R. Martins, J. Gomes</i>	
Self-supported 3D-printed plate-lattices with chitosan-based ink adsorbents for the removal of pollutants.....	377
<i>S. Fernández-Davila, M.A. Sanromán, E. Rosales</i>	
Renewable energy production in marine natural caves using Wells turbines.....	379
<i>T.F. Tavares, C.I.C. Pinheiro, R.M. Filipe</i>	
Biodiesel production from residual cooking oils and its purification through adsorption processes using activated carbon prepared from cork waste.....	381
<i>M.I.L. Garção, A.M. Queiroz, P. Brito, A.E. Ribeiro, M.C.S. Gomes</i>	
Recovery of phenolic compounds from olive mill wastewater using ion exchange process	383
<i>M.J. Fernandes, J. Gomes, R.C. Martins, E. Domingues</i>	
Novel photocatalysts for pharmaceuticals removal from wastewater: a literature survey and a perspective for healthy freshwater ecosystems	385
<i>F. Rodrigues, M.J. Feio, A.R. Calapez, N. Simões, A.M.P.T. Pereira, L.J.G. Silva, A. Freitas, L. Durães</i>	
Effect of steam on a fluidized-bed Calcium Lopping process using natural and waste resources	387
<i>A.C. Ferreira, P. Teixeira, C.I.C. Pinheiro</i>	
Removal of cytotoxic contaminants through advanced oxidation processes with a catalyst derived from sewage sludge	389
<i>D. Huber-Benito, M. Martin-Martinez, M. Larriba, V.I. Águeda, J. García</i>	
Sewage sludge as agricultural fertilizer - a screening of environmental risk assessment for PAHs, PCBs, synthetic musks and volatile methylsiloxanes	391
<i>F. Rocha, V. Homem</i>	
New copper-based solid heterogenous catalyst for peroxymonosulphate activation for disinfection of wastewater	393
<i>A. Giráldez, M.A. Sanromán, M. Pazos</i>	
Study of nanoplastics impact on seed germination of <i>Lactuca sativa</i>	395
<i>A.M. Barreiros, D.P. Varela, E.B. Moura, L.R. Araújo, M. Barrocas, H. F. Silva, J. Coelho, S. Piçarra, M. Matos, N. Silva, C. Oliveira</i>	
Evaluation of potential applications for poplar bark, a byproduct from food packaging	397
<i>S. Oliveira, S. Monteiro, J. Santos, R.A. Fernandes, B. Freitas, N. Ferreira, I. Ferreira, C. Vieira, F.D. Magalhães, J.M. Martins, L.H. de Carvalho</i>	
Study of biodiesel production from waste cooking oil by ethyl transesterification and its purification with the use of natural adsorbents	399
<i>G.L. Camilo, M.C.S. Gomes, A. Queiroz, A. Ribeiro, P. Brito</i>	

Energy rationalization plan of a road transport company: elaboration and monitoring	401
<i>P. Pereira, T. Santos, J. Puna</i>	
Comparison of environmental assessments of polyurethane foams	403
<i>R. Silva, A. Barros-Timmons, P. Quinteiro</i>	
Electrochemical recovery of phosphorus from aqueous solutions	405
<i>C. Afonso, A. Fernandes, L. Ciríaco, M.J. Pacheco, A. Lopes</i>	
Removal of estrogens from water using activated carbon adsorbent materials prepared from olive stones	407
<i>E.C. Milani, M.L. Menezes, J.L. de Tuesta, A.E. Ribeiro, P. Brito, A. Queiroz</i>	
Application of commercial activated carbon for removal of copper (II) ions from aqueous media.....	409
<i>R.S. Antônio, M. de Souza</i>	
Chlorine decay in water treatment and distribution	411
<i>P. Fernandes, M.T. Santos, T. Trindade</i>	
Optimization of electro-Fenton process parameters and subsequent reactor design for continuous flow treatment	413
<i>N. Bernárdez, B. Lomba, M. Pazos, E. Rosales, M.A. Sanromán</i>	
Comparison of test methods to assess formaldehyde emissions in coloured MDF	415
<i>M.L. Almeida, C. Coelho, J.M. Martins, R.M. Ramos, F.M. Magalhães, L.H. Carvalho</i>	
Catalytic hydrodechlorination of 4-chlorophenol in water	417
<i>C. Lopes, J. Restivo, C.A. Orge, M.F.R. Pereira, O.S.G.P. Soares</i>	
Influence of FeCu-MOF morphologies on peroxymonosulfate activation for rhodamine B degradation	419
<i>A. Fdez-Sanromán, B. Lomba-Fernández, M. Pazos, E. Rosales, M.A. Sanromán</i>	
Integrating Fenton's process with adsorption using <i>C. fluminea</i> shells: an iron recovery strategy	421
<i>E. Domingues, T. Vaz, P. Mazierski, J. Gomes, R.C. Martins</i>	
Water disinfection using UVC diodes that emit light at different wavelengths	423
<i>M.E. Martins, J. Sérgio, C. Santos, A.P. Marques, M.T. Crespo, V.J. Pereira</i>	
Catalysts screening for the CO₂ hydrogenation reaction in C₂₊ products	425
<i>M.B.S. Felgueiras, M.F.R. Pereira, O.S.G.P. Soares</i>	
Removal of heavy metals from aqueous solution using as adsorbent char derived from the pyrolysis of post-consumer plastic waste	427
<i>L. Pereira, M. Calero, R.R. Solís, A. Pérez, M.J. Muñoz, M.A. Martín-Lara</i>	
Development of low-cost adsorbent materials from char of pyrolysis of post-consumer mixed plastic waste and its application to effluent purification (CARBOPLASTIC project).....	429
<i>L. Pereira, R.R. Solís, M. Calero, G. Blázquez, M.A. Martín-Lara</i>	

A molecular simulation study of the structure and thermodynamics of empty clathrate hydrates below the freezing point of H₂O	431
<i>F.J.A.L. Cruz, J.P.B. Mota</i>	
Compost-derived catalyst for wet peroxide oxidation of leachate waters.....	433
<i>F.F. Roman, G.F. Batista, A.S. Silva, J.L. Diaz de Tuesta, R.V. Mambrini, H.T. Gomes</i>	
Water treatment station sludge with application in the production of ecological bricks	435
<i>R.M. Cabral, C. Akamatsu, N.C.M. Ross, R.J.E. Martins, M.T.A. Pietrobelli</i>	
Development and evaluation of an automatic monitoring and measurement system for electrodegradation processes	437
<i>M.R. Pereira, E. González-Romero, M. Pazos, E. Rosales, M.A. Sanromán</i>	
Poster Session INDUSTRIAL APPLICATIONS	439
Application of <i>Spirulina platensis</i> biomass and protein as an alternative emulsifier in the production of ice creams	440
<i>P. de Paula, S. Silva, P. Rodrigues, D. Drunkler, M. Barreiro, E. Ramalhosa</i>	
Effect of edible coatings on the chemical properties of chestnuts	442
<i>J. Correia, Y. Zbiss, F. Lema, L. Fernandes, I. Braga, A. Gonçalves, M. do C. Fidalgo, J. Moreira, E. Ramalhosa</i>	
Leather's surface and structural defects minimization with a sustainable approach	443
<i>M.J. Penayo, J.D. Rivaldi, S.E. Arantzazu, M.F. Barreiro</i>	
Innovation in cork: state of the art and future research possibilities	445
<i>R.N. da Silva</i>	
Application of different CuFe-MOFs for reduction of the environmental and sanitary impact of hospital effluents.....	447
<i>B. Lomba-Fernández, A. Fdez-Sanromán, M. Pazos, E. Rosales, M.A. Sanromán</i>	
Development of new PVC based products through emulsion process	449
<i>L. Lameiras, J. Marques, A.M.V. Barros-Timmons, F.D. Magalhães, A. Tomás</i>	
Evaluate the effectiveness and effects of ultraviolet light-emitting diodes for food production, preservation, and microbiological safety	451
<i>K. Luz, M.T. Crespo, V.J. Pereira, A.P. Marques</i>	
Poster Session INNOVATIVE MATERIALS	453
Development of chitosan/gum arabic films using Pickering emulsions envisaging hydrophobic compounds incorporation	454
<i>J.F.R. Vicente, T.L.B. Schreiner, C.C. Sipoli, A. Santamaria-Echart, M.F.F. Barreiro</i>	
Emulsion-based drug carriers for timolol maleate envisaging glaucoma treatment	456
<i>A.R. Teixeira, L.G. Teixeira, A. Santamaria-Echart, G.R. Silva, M.F. Barreiro</i>	

Structured foods based on Pickering emulsions as vitamin D3 vehicles	458
<i>L.S. Iwamura, L.C. Ghirro, E. Ramalhosa, B.D. Junior, A. Santamaria-Echart, M.F. Barreiro</i>	
Low-cost sanitizers derived from the biodiesel process: a study developed during the Covid-19 pandemic	460
<i>A.C.C.M. da Silva, B.K.F. Pussi, C.C.R.L. Santos, D.T.O.S. Romeiro, E.E.P. Céleri, F.H.C.N. Abreu, G.V.L. Júnior</i>	
Hydrogel formation from <i>Spirulina platensis</i> biomass: screening of process variables.....	462
<i>L.L. Aquino, S.C. Silva, E. Colla, E. Ramalhosa, A.Santamaria-Echart, M.F. Barreiro</i>	
Luminescent responsive lanthanide-doped silica films for biogenic amines recognition	464
<i>C.M.R. Almeida, J. Pina, J.M. S.C. Magalhães, M.F. Barroso, L. Durães</i>	
Development of a silica-based cryogel for the adsorption of perfluorooctanoic acid (PFOA) in water	466
<i>M.I. Roque, V. Rocha, E. Domingues, R.C. Martins, L. Durães</i>	
Ethosomes: an approach for bioactive plant extract preservation envisaging cosmetic applications.....	468
<i>P. Plasencia, A. Santamaria-Echart, S. Heleno, G. Colucci, P. Garcia, L. Barros, M.F. Barreiro</i>	
Formation and stabilisation of oil-in-water nanoemulsions using binary emulsifier mixtures of <i>Tribulus terrestris</i> extract and <i>Quillaja</i> bark saponin	470
<i>T.B. Schreiner, A. Santamaria-Echart, A.M. Peres, M.M. Dias, S.P. Pinho, M.F. Barreiro</i>	
Physicochemical characterization and functional properties of a pectic polysaccharide fraction isolated from celery tubers.....	472
<i>N. Petkova, D. Vassilev, M. Ognaynov, D. Yaneva, M. Krystijan, M. Todorova, I. Vasileva, I. Petrova, P. Denev</i>	
Design of functional polymers and sorption/desorption processes for the valorization of bioactive compounds in olive leaf	474
<i>A. Almeida, C. Martins, C.P. Gomes, R.C.S. Dias, M.R.P.F.N. Costa</i>	
Impregnating ionic liquids into a MOF: assessment of the cationic and anionic effects and their impact on sorbent properties.....	476
<i>T.J. Ferreira, A.T. Vera, B.A. de Moura, C. Cabral, L.M. Esteves, T.O. Carvalho, J. Pais, L.P.C. Silva, M. Tariq, P.M. Reis, J.M.S.S. Esperança, I.A.A.C. Esteves</i>	
Wet-spinning of lignin-nanocomposite fibres for stronger carbon fibres using low-cost ionic liquids	478
<i>Z. Kamora, A. Brandt-Talbot, M. Shaffer</i>	
Rationally developed injectable choline chloride-based hydrogel formulations for controlled and local therapeutic delivery applications	480
<i>T.A. Shmool, A.P. Constantinou, T.K. Georgiou, J.P. Hallett</i>	
Rice husks biochar as adsorbent for removal water pollutants: the use of porous 3D printed supports.....	482
<i>D.S.Gamarano, V.S. Guedes, F.C.C. Moura, M.L.B. Almeida, E. Ayres</i>	

Activated biochar from acai seeds (<i>Euterpe oleracea</i> Mart): the use of polyurethane foam as adsorbent device for water treatment	484
<i>M.L.B. Almeida, E.H.M. Nunes, B.R. Barrioni, L.A.F.P. Cohen, E. Ayres</i>	
Continuous oscillatory flow reactor: effect of liquid flow rate on gas-liquid mass transfer in a gas-liquid-solid system	486
<i>F. Almeida, F. Rocha, A. Ferreira</i>	
Development of bacterial cellulose composites for food packaging and textiles	488
<i>F.A.G.S. Silva, F. Dourado, M. Hummel, F. Poças, M. Gama</i>	
Poster Session MODELLING, SYNTHESIS AND INTEGRATION OF CHEMICAL PROCESSES.....	490
Modelling of reactive extrusion process by mixing two similar fluids in the extruder	491
<i>E. Delvar, M.S.C.A. Brito, A. Santamaria-Echart, M.F. Barreiro, C.G. Silva, R.J. Santos</i>	
Integration of a reaction-purification process to obtain pentyl acetate	493
<i>L. Domínguez, B. Lorenzo, J. Ortega, L. Fernández</i>	
Prediction of solubility and phase diagram of some pharmaceutical substances.....	495
<i>K. Bitchikn, N. Smakghi, A. H. Meniai</i>	
Heat integration of the Haber Bosch process for the production of green ammonia	497
<i>J. Leitão, C.G. Braz, H.A. Matos</i>	
Sorption assays of furanic compounds in transformers insulation oil and paper systems	499
<i>M.A.J. Teixeira, S.Y. Matharage, Z. Wang, M.M.Q. Simões, I. Portugal, C.M. Silva</i>	
Introducing the O-NETmix - a novel technology for continuous crystallisation	501
<i>A.F. Freitas, Y.A. Manrique, J.C.B. Lopes, R.J. Santos, A. Ferreira, M.M. Dias</i>	
Poster Session REACTION AND SEPARATION PROCESSES	503
Application of COSMO-RS to predict the phase equilibria of vanillin in aqueous mixtures	504
<i>I.W. Cordova, G. Teixeira, D.O. Abranches, S.P. Pinho, O. Ferreira, J.A.P. Coutinho</i>	
Solvent-free enzymatic esterification of pentyl propionate. Comparison of results using two types of reactors: BSTR and PBR.....	506
<i>B. Lorenzo, A. González, E. Martín, L. Domínguez, L. Fernández, J. Ortega</i>	
High-adsorption-performance carbon material for removal of fluoroquinolone from wastewater	508
<i>A.B.H. Abreu, S. Álvarez-Torrellas, V.I. Águeda, J.A. Delgado, J. Carbajo, J. García</i>	
Design of hierarchical Pt/zeolite catalysts for the hydrodeoxygenation of biomass-derived oxygenated molecules	510
<i>M. Matos, L.C. Silva, M. Araújo, N. Horta, B. Amaro, A.P. Carvalho, N. Nunes, J. Coelho, A. Martins</i>	

3D printed biomimetic flow fields for the electrochemical generation of free chlorine.....	512
<i>I. García-López, V.I. Águeda, A. Garrido-Escudero</i>	
Selective precipitation of gold from an aqua regia leachate of e-waste using a quaternary ammonium ionic liquid	514
<i>A.F.M. Nogueira, A.R.F. Carreira, S.J.R. Vargas, H. Passos, N. Schaeffer, J.A.P. Coutinho</i>	
Fractionation of citrus essential oil through extractive vacuum distillation using imidazolium-based ionic liquids as entrainers	516
<i>S.M. Vilas-Boas, F.R.M. Batista, R.M. Dias, J.A.P. Coutinho, O. Ferreira, M.C. da Costa, S.P. Pinho</i>	
DNA simultaneous extraction, purification, and preservation with ionic liquid-based aqueous biphasic systems.....	518
<i>A.I. Valente, T.B.V. Dinis, A.P.M. Tavares, F. Sousa, M.G. Freire</i>	
Polyamide chemical recycling processes: preliminary studies.....	520
<i>J. Araújo, N. Gama, A. Cavuquila, C.M. Silva, A. Barros-Timmons</i>	
Oxidative desulfurization of a simulated fuel using plastic waste-derived carbon nanotubes: a Pickering interfacial catalysis approach.....	522
<i>F.F. Roman, J.L. Diaz de Tuesta, A.M.T. Silva, J.L. Faria, H.T. Gomes</i>	
Hybrid hollow fiber membranes with encapsulated absorbents in sub-micron carbon capsules: A new technology for gas separation.....	524
<i>P.J. Carvalho, R.T. Pais, I. Souza, L.P. Silva</i>	
Experimental PSA reactor for methanol-enhanced production via CO₂ hydrogenation.....	525
<i>G. Pascual-Muñoz, M. Larriba, V.I. Águeda, J.A. Delgado</i>	
Symmetric and asymmetric PDMS membranes for CO₂/N₂ separation using the inorganic filler ZSM-5.....	527
<i>I. Rodrigues, L. Martínez-Izquierdo, C. Téllez, J. Coronas, A.E. Rodrigues, V.J.P. Vilar, A.F.P. Ferreira</i>	
Development of functionalized membranes for O₂/O₃ gas separation	529
<i>V.J.P. Vilar, I. Rodrigues, A.E. Rodrigues, A.F.P. Ferreira</i>	
Single- and multi-component fixed-bed adsorption of CO₂, CH₄, and N₂ on ion-exchanged binder-free NaY zeolites.....	531
<i>E. Aly, L.F.A.S. Zafanelli, A. Henrique, F.A. da Silva, A.E. Rodrigues, J.A.C. Silva</i>	
Sorption enhanced reaction process designed for CO₂ methanation from biogas using different Ni-based catalysts	533
<i>A. Cañada-Barcala, M. Larriba, V.I.A. Maté, J.A.D. Dobladez</i>	
Separation of volatile fatty acids with adsorption-based methods	535
<i>C. Gomes, A.M. Ribeiro, A. Rodrigues, A. Ferreira</i>	

The Power of S.T.E.A.M

J.C.G. Calado

Instituto Superior Técnico, Lisboa, Portugal.

jorge.calado@tecnico.ulisboa.pt

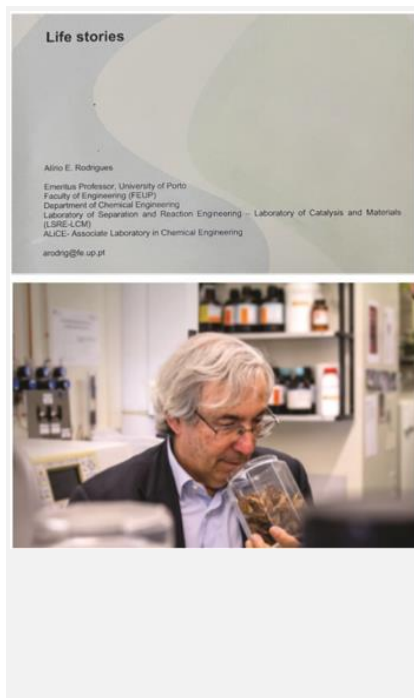


The Road to Innovation: A Walk through Scientific and Industrial Revolutions, the roles of Art and Mathematics and their Truth and Beauty.

Jorge Calado



Born and raised in Lisbon. Studied at Liceu de Pedro Nunes, graduated in Chemical Engineering from Instituto Superior Técnico (IST), and received a D.Phil. in physical-chemistry from the University of Oxford, UK. Professor of Physical-Chemistry and Chemical Thermodynamics at IST, he was also an Adjunct Professor of Chemical Engineering at Cornell University, USA. Awarded the 1st Ferreira da Silva Prize by the Portuguese Society of Chemistry (1982), was elected full-member of the Academy of Sciences of Lisbon in 1988, and received the University of Lisbon Prize (2016). Conceived and directed the first arts management courses in Portugal at the Instituto Nacional de Administração (1988-93) and founded IST Press in 1997. Interested in the relationships between science and the arts, collaborated with the *Times Literary Supplement* in the 1980s and has been a cultural critic for the *Expresso* since 1986. Over the last thirty years, Jorge Calado has curated more than 30 photography exhibitions in Portugal, France, Belgium, the UK, and the USA. He is the author of *Haja Luz! — A History of Chemistry Through Everything* (3rd edition, 2016), *Limites da Ciência* (2nd edition, 2021), and *Mocidade Portuguesa* (3rd edition, 2023), for which he was awarded the literary 2023 D. Diniz Prize.

Alírio E. Rodrigues, Chemical Engineering and Bragança*L.S. Pais**Instituto Politécnico de Bragança, Bragança, Portugal.**pais@ipb.pt*

Speaking about Alírio E. Rodrigues is to speak of Chemical Engineering. A life dedicated to teaching and research in Chemical Engineering, in Portugal and with many bridges around the world. After graduation at the University of Porto, he passed through Luanda and Évora before coming back to Porto and then founding the Laboratory of Separation and Reaction Engineering (LSRE), which later, together with the Laboratory of Catalysis and Materials (LCM), received the status of Associate Laboratory, the first and sole in Chemical Engineering, the LSRE-LCM. With many published books and granted patents, more than 800 publications, more than 90 supervised PhD students, he was visiting professor at several universities and the recipient of important awards, such as the “Prémio da Boa Esperança” (1993), the AIChE Adsorption and Ion Exchange Honorary Session (2014), and the MCTES Medal of Scientific Merit (2016). 80 years of life we had the pleasure of sharing and remembering through “Life Stories” that Professor Alírio Rodrigues recently offered us. This will be, therefore, a space of homage and conviviality with a unique personality. At the same time, and with ChemPor being held for the first time in Bragança, we also celebrate 25 years of Chemical Engineering at the Bragança Polytechnic University (Instituto Politécnico de Bragança, IPB). Since 1998, IPB has trained 368 bachelors and 186 masters in Chemical Engineering, plus 35 co-supervised PhD graduates in cooperation with Portuguese and international universities. These are not two separate celebrations, as Alírio Rodrigues and LSRE-LCM played a fundamental role in the offer of Chemical Engineering at IPB, training the teaching and research staff and developing research capacity through the LSRE-LCM Pole in Bragança.

Ups and Downs

A.E. Rodrigues

Faculdade de Engenharia da Universidade do Porto, Porto, Portugal.

arodrig@fe.up.pt



Alírio Rodrigues graduated in Chemical Engineering from the Faculty of Engineering of Porto University (FEUP) in 1968. After a training period in Angola at the brewery company CUCA and oil refinery FINA he joined the Department of Chemical Engineering of Luanda University as Teaching Assistant. In 1970 he started post-graduate studies at the Centre de Cinétique Physique et Chimique (CNRS) and ENSIC; in 1973 obtained his Ph.D. at Nancy University, France, in the area of Ion Exchange. Alírio Rodrigues went back to Luanda by the end of 1973, returned to Portugal (1975), joined for a short period, Évora University, and later (1976) the Department of Chemical Engineering of FEUP. He created a research group that became the Laboratory of Separation and Reaction Engineering (LSRE). He was the Director of LSRE until 2012. Under his leadership, LSRE created the pole at IPB and obtained the status of Associate Laboratory in partnership with LCM. He was visiting professor at UTC, France; Virginia, USA; Oviedo, Spain; and UFC, Brazil, universities. Since 2013 he is Emeritus Professor of Porto University. He supervised over 90 Ph.D. students and published over 800 papers in peer-reviewed journals.



Desenvolvemos protótipos e instalações experimentais "chave-na-mão"



EQUIPAMENTOS
CUSTOMIZADOS
E CHAVE-NA-MÃO



AUTOMAÇÃO DE
SISTEMAS
JÁ EXISTENTES



PROJETO
MECÂNICO

Equipamentos Customizados e Chave-na-mão

Trabalhamos a todas as escalas

Reatores

Bio-Reatores

Unidade SFE

Homogeneizador Laboratorial



Testing · Developing · Problem Solving
Industrial, Lab and Customized Solutions



bit.ly/3q6PYmH

+351 224 664 320

www.paralab.pt • info@paralab.pt

Porto • Lisboa • Santander • Barcelona • Madrid

Chemical engineers for the future – are we asking too much?

J. Glassey

Newcastle University, School of Engineering, Merz Court, Newcastle upon Tyne, UK.

jarka.glassey@ncl.ac.uk.

With rapidly spreading AI into all aspects of human life, the impact of climate change leading to radical changes in the sourcing and the use of raw materials for daily products and energy, chemical engineers entering their professional careers at this stage face unprecedented challenges. To be able to develop innovative solutions to some of the greatest challenges the society is facing, it is essential that education and training of engineers adapt to the changing context [1].

Given the significance of the role that chemical engineers play in the transition to a net zero circular economy as a requirement to mitigate the environmental impact of our activities, chemical engineering programmes need to incorporate considerations of sustainability more explicitly [2]. This is reflected in the more explicit requirements that the accrediting bodies are placing on the sustainability content in the curricular provision (see e.g. [3]).

At the same time, it is increasingly clear that the engineers will have to make decisions with far reaching ethical implications for which they will be held accountable more openly than ever before (consider for example the widely reported Volkswagen emissions scandal [4]). Thus including professional ethics in the curriculum is now also a clearly stated requirement of accrediting bodies [3].

However, at the same time, the engineers must remain highly competent technically and keep up with the latest technological development in their domain of expertise. This necessitates that they have solid foundations of the core chemical engineering concepts as well as practical skills in using the latest tools to implement these concepts. This includes the use of AI and machine learning algorithms for simulation and optimization of

process performance or fault detection [5]. Such tools are essential for engineers as we transition to Industry 4.0 (and beyond), yet it is still not clear how we can achieve all these requirements in the same timeframes that chemical engineering programmes used to be completed in decades ago.

The Bologna requirements of a 3-year bachelor studies with additional 2 years for masters are shortened in higher educational systems based on integrated 4-year master studies (e.g. in the UK). On completion of an IChemE master level accredited degree, the graduate is deemed to have fulfilled the educational requirement for registration as a Chartered Engineer, although achieving this recognition also requires the demonstration of further competence and commitment in their professional practice. The question of how prepared these graduates are for their professional practice and for the new challenges associated with the transition to a net zero circular economy continues to be hotly debated.

This contribution explores the possible means of ensuring that graduates are exposed to a sufficient level of additional areas of knowledge and skills to prepare them for their professional future whilst emphasizing the need for continuous professional development and the involvement of industry in the formation of chemical engineers.

An example of the acquisition of knowledge and skills in sustainability, ethics and digitalization will be used through various recent surveys of academics, students, and industry worldwide.

Finally, this plenary presentation will highlight further challenges and areas of development for the chemical engineering profession.

Acknowledgements

The contribution of Education Special Interest Group of IChemE, Working Party on Education of EFCE, colleagues and master students at Newcastle University as well as all respondents to various surveys is gratefully acknowledged. Ethical approval for various research projects discussed in this contribution was granted by Newcastle University, following its standard procedures for this type of research.

References

- [1] E.P. Byrne, *Educ. Chem. Eng.*, 43 (2023) 23-30.
- [2] A.A. Khalifa et al., *Sustainability*, 14 (2022) 11656.
- [3] L. Bolton et al., *Educ. Chem. Eng.*, 43 (2023) 31-36.
- [4] D. Jacobs et al., *CPA Journal*, Jul 2019, <https://www.cpajournal.com/2019/07/22/9187/>.
- [5] I.A. Udugama et al., *Educ. Chem. Eng.*, 44 (2023) 63-70.

Jarka Glassey



Prof Jarka Glassey completed her biochemical engineering studies at the Slovak Technical University in Bratislava and currently works at Newcastle University, UK. Her research approach is based on the use of machine learning, AI and hybrid modelling for bioprocess development, scale-up and process intensification. She is currently VP Executive of EFCE and VP Executive of ESBES and is actively involved in the EFCE working party on Education, WP on QbD as well as the Measurement, modelling, monitoring and control section of ESBES. She was elected a Fellow of Royal Academy of Engineering and is chairing the Board of Engineering Skills X, Engineering Skills for Safety. She is passionate about the education of future generations of chemical engineers and her research in this area includes active teaching methodologies (such virtual and augmented reality) in education and assessment of knowledge and professional skills.

Understanding the development of a large-scale chemical process - The HPPO technology

J.H. Teles

BASF Group Research, Ludwigshafen, Germany.

Henrique.Teles@BASF.com



In the second half of the 20th century chemical processes for basic chemicals and petrochemicals were developed and thoroughly optimized. For this reason, it has become seldom that completely new processes appear, which can compete with the established technologies. One such example is the HPPO technology, which stands for Hydrogen Peroxide based Propylene Oxide, for which the first plants were started in late 2007. The technology was developed in parallel by two competing consortia, BASF and Dow on the one side and Evonik and Krupp-Uhde on the other side. A comparison of the similarities and differences of the two process variants allows for a rare view into how such a large-scale process comes to be.

In the second half of the 20th century chemical processes for basic chemicals and petrochemicals were developed and thoroughly optimized. For this reason, it has become seldom that completely new processes appear, which can compete with the established technologies. For most basic chemicals and petrochemicals, meaning those produced at a worldwide scale of at least 1 million tons/year, only one process has survived and superseded all the others. On rare occasions several processes have thrive next to each other. The most notorious example is the case of propylene oxide (PO), a major building block for polyurethanes, whose world capacity is now around 12 million tons/year. The oldest technology for PO, dating back to the 1930's is based on the chlorohydrination of propylene with Cl₂ and water and subsequent dehydrochlorination with NaOH to form PO. Later, the 1970's brought about the era of the co-oxidation processes, where a hydrocarbon like isobutane or ethylbenzene is oxidized with O₂ to the corresponding hydroperoxide. The hydroperoxide is the used to epoxidize propylene, while the alcohol is transformed to a coupled product like MTBE and styrene respectively. In the early 2000's Sumitomo developed a variation of these processes using cumene. In this case the cumyl alcohol is hydrogenated back to cumene, so this was the first modern PO process without coupled products. The early 2000's was also the time when the HPPO process was being developed, enabled by the discovery of titanium silicalite (TS-1) as a catalyst by Enichem and the

evolution of hydrogen peroxide from a specialty to a commodity chemical, mostly by Solvay and Evonik. As of today, all these technologies are still in use, although HPPO has the highest growth rate.

The HPPO technology, which stands for Hydrogen Peroxide based Propylene Oxide, had the first plants coming online late 2007. Even more unusual was the fact that the technology was developed in parallel and almost simultaneously by two competing consortia, BASF and Dow on the one side and Evonik and Krupp-Uhde on the other side and the first plants started almost simultaneously. BASF/Dow built their first 300 kt/a plant in Antwerp, Belgium, while Evonik/Krupp-Uhde built their first 100 kt/a plant in Ulsan, South Korea as a license plant to SKC. In the meantime, several Chinese companies like Sinopec have also succeed to develop their own variations of the process.

One might imagine that two companies developing a process simultaneously and in parallel, using the same raw materials, the same solvent and essentially the same catalyst would come up with processes which are very similar. Curiously, this is absolutely not the case and the processes from BASF/Dow and Evonik/Krupp-Uhde are in fact very different. An analysis of the differences allows for a very rare and fascinating insight on how such a large-scale process is developed and how it comes to look the way it is.

Acknowledgements

The author would like to express his thanks to the hundreds of people who contributed to the process development both at BASF and Dow.

References

- [1] J. H. Teles et al., ChemSusChem, 2 (2009) 508-534.
- [2] J. H. Teles et al., Ullmann's Encyclopedia of Industrial Chemistry, (2015), a18_261.pub2.
- [3] J. H. Teles et al., Nature (London, United Kingdom), 586 (7831) (2020) 708-713.

J. Henrique Teles



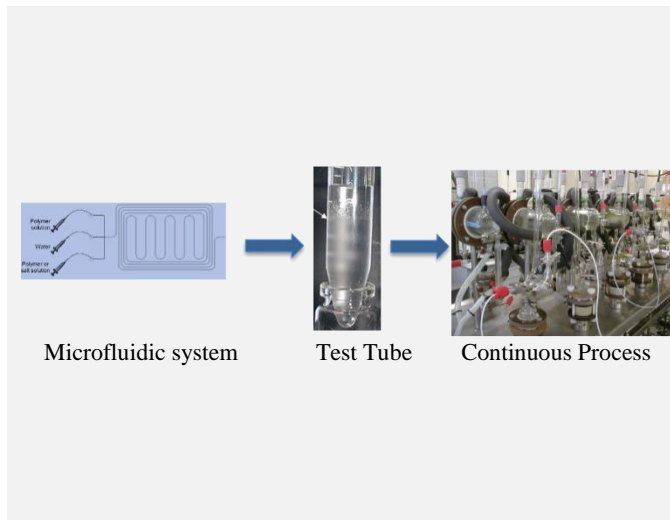
Born 1962 in Lisbon where he also did his high school studies at Liceu Camões. He then joined the IST, where he graduated in Chemical Engineering in 1985. There he started working with Prof. Silvia de Brito Costa and her group who gave him the chance to spend two months in Germany in 1984 with the group of Prof. Günther Maier. After concluding his graduation, he returned to the group of Prof. Maier at the Justus-Liebig University in Giessen, where he obtained his PhD degree in 1988. Soon after he joined the group of the late Prof. William von Eggers Doering at Harvard University for a post-doctoral stay. He returned to Germany as a Humboldt fellow before joining BASF's central research in 1991. Since 2021 he heads the research group responsible for oxidation technologies and phosgene chemistry. His group has developed several new large-scale processes like the HPPO process for propylene oxide, cyclododecanone and cyclopentanone using N₂O as the oxidant, and new processes for several carboxylic acids and phosgene derivatives, although outside industry he is better known for his seminal work on homogeneous gold catalysis and triazolium-NHC's. He has been a member of the advisory board of several high-profile journals and of Ullmann's Encyclopedia.

Purification of biopharmaceuticals

R.A. Barros

iBB—Institute for Bioengineering and Biosciences and Department of Bioengineering, Instituto Superior Técnico, Universidade de Lisboa, Lisboa, Portugal; Associate Laboratory i4HB—Institute for Health and Bioeconomy at Instituto Superior Técnico, Universidade de Lisboa, Lisboa, Portugal

rabarros@tecnico.ulisboa.pt



The biotechnology-based pharmaceuticals in the late-stage pipeline have seen a significant increase, with monoclonal antibodies alone accounting for a quarter of all biopharmaceuticals being tested in clinical trials. This has led to a greater demand for more efficient and cost-effective processes. Advancements in molecular biology, genetics, and media/feed development have played a crucial role in boosting production levels. However, the downstream processes, which pose a persistent bottleneck, need to be redesigned or improved to sustain this progress. Aqueous two-phase systems (ATPS) offer a promising alternative to the current platforms used for processing biopharmaceuticals. ATPS combines high biocompatibility and selectivity with easy scalability, reliability, and integration into a continuous process. Moreover, the potential of using microfluidic platforms to miniaturize ATPS is also explored, turning it into a high-throughput screening tool that can accelerate the design and optimization of bioprocesses.

Acknowledgements

iBB - Institute for Bioengineering and Biosciences acknowledges funding from FCT-Portuguese Foundation for Science and Technology (UID/05367/2020) and through pluriannual BASE and PROGRAMATICO financing (UID/04565/2020). This project has also received funding from the European Union's Horizon 2020 research and innovation program under the Marie Skłodowska-Curie grant agreement No 812909 CODOBIO, within the Marie Skłodowska-Curie European Training Networks framework.

Raquel Aires-Barros



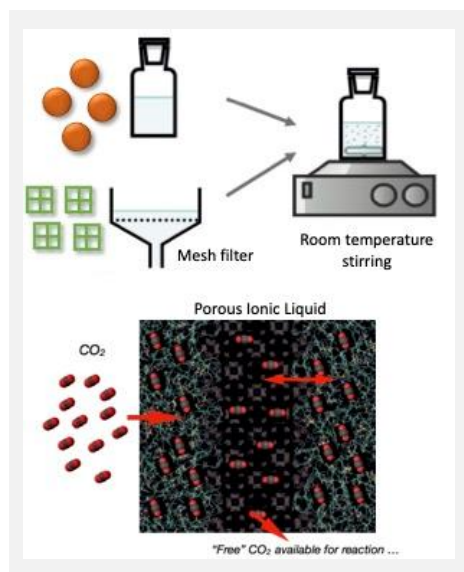
Full Professor at the Department of Bioengineering (DBE) at Instituto Superior Técnico (IST), Universidade de Lisboa, and Senior Researcher at Institute for Bioengineering and Biosciences (iBB). Coordinates the scientific-pedagogical area of Biomolecular and Bioprocessing Engineering of DBE at IST and is Vice-President of IST School Board. Current research interests include the development of new separation processes with high performance and efficiency for purification of biopharmaceuticals, with special emphasis on the purification of antibodies and the development of devices - "Lab-on-a-Chip" - for protein purification / separation of cells in the microscale. She is chair of the Session of Downstream Processing (DSP) of the European Society of Biochemical Engineering Sciences (ESBES), President of the Portuguese Society for Biotechnology and editor of Separation and Purification Technology Journal. Webpage: <http://ibb.ist.utl.pt>

Gas separation and transformation using porous ionic liquids

M.C. Gomes

CNRS Chemistry Laboratory, Ecole Normale Supérieure de Lyon, 46 allée d'Italie, 69634 Lyon, France.

Margarida.costa-gomes@ens-lyon.fr



Porous ionic liquids can be designed to improve the capacity and selectivity of gas absorption and prepared from *off-the-shelf* materials such as ionic liquids and metal organic frameworks. Porous ionic liquids also allow for the catalytic transformation of carbon dioxide under mild conditions thus providing a new, more sustainable platform for carbon capture and utilization.

Among the alternative sorbents potentially capable of outperforming current separation technologies, in particular gas separations, ionic liquids are promising candidates. Their most attractive feature is the possibility of tuning their physical and chemical properties through proper pairing of anions and cations, which can include reactive groups, enabling the selective absorption of different gases, even at low partial pressures [1].

We will describe ionic liquid-based absorbents which are liquids with permanent porosity [2], designed to selectively absorb different gases. The absorbents are stable suspensions of metal-organic frameworks (MOFs) in salts whose ion pairs are too voluminous to enter the solid pores [3]. The increase in gas absorption, when compared with the pure ionic liquids, is proportional to the amount of porous solid in suspension. The thermodynamic analysis of the absorption data, as well as molecular dynamics simulations, show that the driving force for gas absorption by the porous ionic liquids is energetic as well as structural and thus is controlled by gas-solid affinity or by the porous liquid free volume [4,5].

We have shown that porous ionic liquids prepared as stable suspensions of ZIF-8 in phosphonium acetate or levulinate salts can selectively absorb carbon dioxide with a capacity more than 100% higher than that of the pure MOF at 1 bar and 303 K [6]. Porous ionic liquids can also be designed to promote the reaction, at mild conditions of temperature and pressure, of the gases absorbed. Carbon dioxide can be catalytically coupled with epoxides to form cyclic carbonates in porous ionic liquids containing alkylphosphonium halides and ZIF-8. The high activity and selectivity observed at atmospheric pressure and room temperature indicate that porous ionic liquids are a promising and sustainable family of sorbents for both separating and transforming gases [7,8].

References

- [1] Bui et al., *Energy & Environmental Science*, 11(5) (2018) 1062–1176.
- [2] Giri et al., *Nature*, 527 (2015) 216–221.
- [3] Costa Gomes et al., *Angewandte Chemie International Edition*, 57 (2018) 11909–11912.
- [4] Avila et al., *Advanced Materials Interfaces*, 8 (2021) 2001982.
- [5] Avila et al., *Materials Advances*, 3 (2022) 8848–8863.
- [6] Avila et al., *Angewandte Chemie International Edition*, 60 (2021) 12876–12882.
- [7] Zhou et al., *Chemical Communications*, 57 (2021) 7922–7925.
- [8] Clark et al., *Journal of Chemistry Physics B*, 127 (2023) 3266–3277.

Margarida Costa Gomes



Margarida Costa Gomes obtained her Chemical Engineering diploma and her PhD in Experimental Thermodynamics in Lisbon, Portugal. She was a research associate at Imperial College in London and a post-doctoral fellow at the Blaise Pascal University in France before joining the CNRS in 1998 and becoming a CNRS Research Professor in 2010. She was awarded the CNRS Bronze Medal in 2003 and in 2004 she passed her Habilitation. Margarida was an invited researcher in 2008 at the Institute of Chemical and Biological Technology, Portugal and in 2014-15 she was a visiting scholar at the Massachusetts Institute of Technology, USA, where she maintained a position as research affiliate until 2020. Before moving to the Ecole Normale Supérieure de Lyon in 2018, she was responsible for the Thermodynamics and Molecular Interactions of Ionic Liquids research group at the Institute of Chemistry of Clermont-Ferrand.

Prof. Costa Gomes broad scientific interests are in the field of physical chemistry of solutions and concern the molecular and experimental thermodynamics of fluids, her research concerning chemistry, engineering and environmental aspects. She is driven by

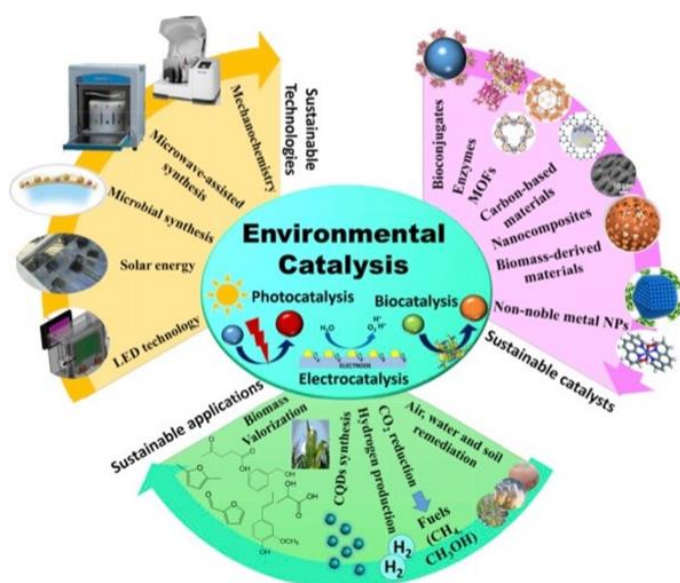
challenging questions at the intersection of these fields, especially where they have relevance to societal outcomes or to the advancement of science towards innovative applications. Her current research covers two major topics and several research actions funded by national research agencies, industrial partners and European projects. The first topic concerns the study of solvation in ionic liquid media aiming to engineer and design sustainable solvents. The molecular understanding of ionic fluids is necessary for new, lower energy and cleaner processes of separation and storage of gases or to transform and recycle polymers. The second topic is focused on materials and ionic liquids and is motivated by the development of new processes and devices: the discovery of porous liquids prepared easily from off-the-shelf materials and capable of absorbing large quantities of gases, requiring a better understanding of the interfaces between ionic liquids and different classes of materials leading to innovative devices and sensors. <https://perso.ens-lyon.fr/margarida.costa-gomes/>

Benign-by-design methodologies for a more sustainable future: from nanomaterials to biomass/waste valorization

R. Luque

King Saud University, Saudi Arabia.

rafael.luque@ksu.edu.sa



The design of benign and environmentally sound methodologies has been the driving force of scientists in recent years towards more sustainable methodologies.

Attractive and innovative protocols that nowadays are even part of industrial ventures including biomass-derived porous carbonaceous materials, designer nanomaterials for catalytic applications and catalytic strategies for biomass/waste conversion into useful materials, chemicals and fuels have been recently developed in our group in recent years. These topics have extensively covered the preparation and design of (nano)materials, biocatalysts and photocatalysts and their utilisation in heterogeneously (bio)(photo)(electro)catalysed processes, flow chemistry as well as in biomass/waste valorisation practices. An important research avenue from the group deals with the search for novel and alternative reaction media in Organic Synthesis including mechanochemistry, organocatalysis and photo-redox processes as well as greener catalytic processes in Organic Chemistry (flow chemistry) for the synthesis of APIs.

In this lecture, we aim to provide an overview of recent efforts from our group in leading the future of global scientists in benign-by-design methodologies for biomass valorization including and the “waste-to-pharma” concept.

Rafael Luque



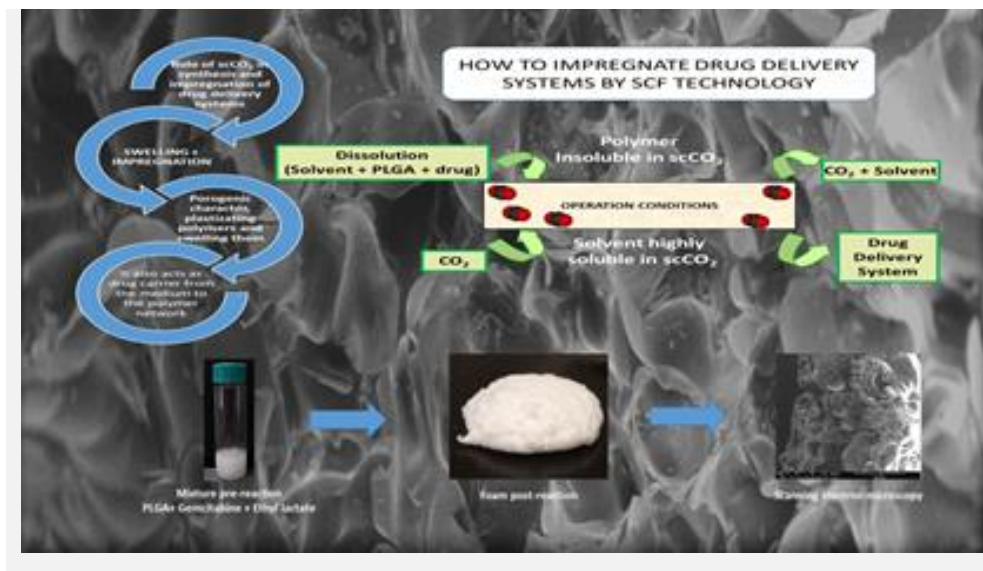
Rafael Luque (PhD in 2005, Universidad de Cordoba, Spain) has significant experience in biomass and waste valorization practices to materials, fuels and chemicals as well as nanoscale chemistry, green chemistry and catalysis (700+ publications, h-index 96, >45,000 citations, 7 patents, 10 edited books). He serves on the Advisory/Editorial Board of over 10 Q1 RSC, Wiley, ACS and Elsevier journals. He has been named 2018, 2019, 2020, 2021 and recently 2022 Highly Cited Researcher (Clarivate Analytics).

Supercritical CO₂ synthesis and functionalization of biopolymers

E. Gracia, T. Garcia, I. Gracia, J.F. Rodriguez*

Institute of Chemical and Environmental Technology, University of Castilla-La Mancha, Avenida de Camilo José Cela, 13071-Ciudad Real, Spain.

*juan.rromero@uclm.es



Most of the drug related allergies is suspected that could be in relation with a deficient removal of synthesis and manufacture residues. This issue is even more critical in polymers destined to controlled drug delivery because the objective is that have a prolonged stay in the body until being biodegraded and bioabsorbed by the body. Supercritical CO₂ (scCO₂) is finding application in the production of pharmaceutical related products due to their ability to solve difficult process, as particulation, foaming and formulation problems.

For those reasons, the use of scCO₂ as polymerization media looks very attractive because ideally makes easier the separation of unreacted monomers, allows a clean and complete removal of co-solvents or reaction additives, improves the mass transfer into a high swelled polymer bulk and permits the tuning of the final physical properties of the polymer obtained.

Nevertheless, not everything are advantages, the scCO₂ plays a key role into the polymerization process producing multiphase reaction processes of high complexity and also in the case of certain polymers as polylactic takes part in the polymerization process generating side reactions, mainly transesterifications and thermal non-radical random chain scission of difficult control.

For instance, for monomers as glycolide and lactide the polymerization rate is slower in bulk than in supercritical media due to the lower percent of crystallinity of the polymer obtained by supercritical polymerization. The production of cyclic chains and the presence of scCO₂ that favours a constant movement of chains readjusting continuously the molecular weight prevent the packing and reduce the crystallinity. So the crystallinity of the polymer is determined by the polymerization media. However, conversions achieved are not so different between the both methods. On the other hand, in supercritical media where part of the monomers can be soluble and only a small part of the polymer is solubilized, precipitation polymerization can be happening, and the molecular weight obtained is the maximum molecular weight of PLA soluble in scCO₂.

In such system, not only the reactivity of CO₂ plays a key role on the ring opening polymerizations on scCO₂. The matter of question to understand the behaviour of the system is whether in the operative conditions the monomers and/or the polymer are soluble in the scCO₂. The formation of particles or foams depends critically on the solubility and on the T_g of the polymer. For that reason, the knowledge of the complex equilibrium behaviour of monomers, oligomers and polymer into scCO₂ is fundamental and also is important to know the changes that the high pressure CO₂ exerts on the glass transition temperature, viscosity, surface tension, to understand and control the physical characteristics of the materials that can be obtained: particles, foams, bulks [1,3].

Using a polymer synthesized or not in scCO₂ a functionalization or impregnation with a drug has to be done to provide the biopolymer with therapeutic abilities. Porous biodegradable polymeric foams. The impregnation of drugs as additional step in the preparation of a polymeric substrate for the controlled delivery of drugs participates also of the same advantages and difficulties than the polymer synthesis in scCO₂. The plastization effect that scCO₂ exerts on the polymer favours greatly the homogeneous diffusion of the drug into the polymer matrix. The drug solubility in scCO₂ and the drug compatibility with the substrate are parameters that has be known to get a suitable impregnation of the drug into the polymer in scCO₂ [4-6].

Among different techniques for polymer functionalization where toxic organic solvents are used, click chemistry has emerged as one of the most promising reactions because it is classified as a very specific, efficient and versatile reaction which allow to obtain high products yields. When click functionalization is performed in scCO₂, the use of harmful solvents is completely avoided, getting similar reaction rates and yields than in conventional organic solvent. But the complete elimination of the catalyst remained being an unsolved issue. The use of copper wire bits as simple catalyst in a click chemistry reaction using supercritical CO₂ allows to remove the

whole amount of catalyst in the final product with a simple purification step using a green solvent as scCO₂ to synthesize the desired polymer-drugs adducts [7,8].

Acknowledgements

We gratefully acknowledge funding from the Ministerio de Economía y Competitividad through the projects Ref. CTQ2013-46380-P and CTQ2016-79811-P. The authors also acknowledge the support of the Ministerio de Economía y Competitividad for the fellowship of Mr. Gracia Cortes Ref. BES-2014-069313.

References

- [1] R. Mazarro et al., *Journal of Biomedical Materials Research Part B Applied Biomaterials*, 85(1) (2008) 196-203.
- [2] R. Mazarro et al., *Macromolecules Symposium*, 287(1) (2010) 111-118.
- [3] L.I. Cabezas et al., *Express Polymer Letters*, 7(11) (2013) 886-894.
- [4] L.I. Cabezas et al., *Journal of Supercritical Fluids*, 63 (2012) 155-160.
- [5] L.I. Cabezas et al., *Journal of Supercritical Fluids*, 80 (2013) 1-8.
- [6] C. Gutiérrez et al., *Journal of Supercritical Fluids*, 92 (2014) 288-298.
- [7] E. Gracia et al., *Journal of CO₂ Utilization*, 20 (2017) 20-26.
- [8] E. Gracia et al., *Catalysis Today*, 2018.
- [9] E. Gracia et al., *Journal Supercritical Fluids*, 141 (2018) 60-67.

Juan F. Rodriguez



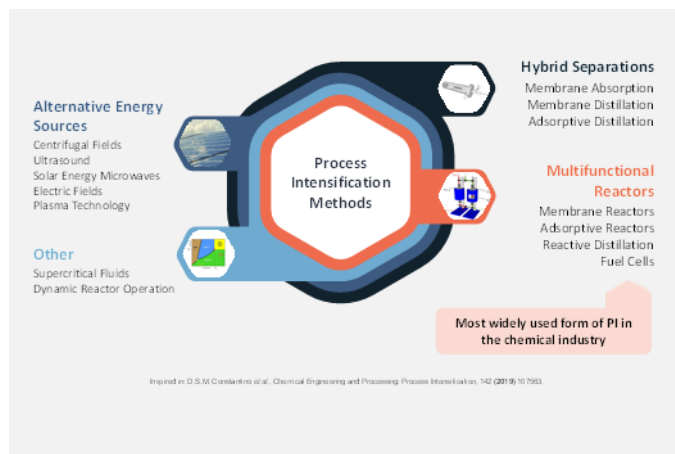
Full Professor and Head of Department of Chemical Engineering at the University of Castilla-La Mancha. Former Director for 14 years of the Institute of Chemical and Environmental Technology (ITQUIMA). Supervisor of 15 Doctoral Theses and author of 11 Patents, more than 240 papers published in national and international journals, 30 book chapters and more than 200 communications in national and international conferences. Main Responsible of more than 35 research projects funded by European (6), national and regional public organizations and more than one hundred research contracts with private companies. Active in the fields of biopolymer synthesis and processing in supercritical scCO₂, micro and nanoencapsulation and Polyurethane synthesis and recycling. Awarded with the Enterprise University Foundation Award in 2002, the Regional Merit Medal 2003 and the Best Research Centre of Castilla-La Mancha 2012.

Integration of reaction and separation processes

L.M. Madeira

LEPABE and ALiCE, Department of Chemical Engineering, Faculty of Engineering – University of Porto, Rua Dr. Roberto Frias, 4200-465 Porto, Portugal.

mmadeira@fe.up.pt



Process intensification is a topic of intensive research nowadays, particularly through the so-called multifunctional reactors, which are devices where reaction and another process operation is implemented, namely separation. Several examples of multifunctional reactors are presented, ranging from membrane reactors to membrane reactors integrated with adsorption; sorption-enhanced reactors are also addressed. The concept of each of the hybrid reactor typologies is explained, and some applications illustrated. Emphasis is given to the use of membrane reactors for hydrogen production/purification, to reactors integrated with carbon dioxide capture and its subsequent valorization into methane, and to membrane reactors integrated with carbon dioxide adsorption for hydrogen production/purification (namely by the water gas-shift and reforming processes).

Introduction

Process intensification (PI) is a term commonly used to describe the strategy of drastically reducing the physical size of an industrial unit, namely for obtaining chemical products, to achieve a certain production goal. The concept was developed by ICI (Imperial Chemical Industries) during the 1970s by Colin Ramshaw and his colleagues [1]. However, the definition and context of PI for chemical engineering has changed in recent decades [2]. PI has been applied across the chemical process industry to reduce plant investment and operating costs, increase profit and mitigate greenhouse gas emissions [3], without neglecting critical aspects such as safety, environmental impact, process flexibility and stability, as well as product quality [2]. Among the various forms of integration of operation units, the reactive separation process is considered the most widely applied form among the methods of intensification in the chemical industry [4]. PI therefore implies, among others, the use of multifunctional reactors, which are, in short, compact units where the reaction is combined with other unit operation(s), in particular with separation processes such as distillation, membranes or adsorption.

Many examples of multifunctional reactors could be provided and discussed, but only a few will be indicated. This is the case, for example, of the production/purification of hydrogen in membrane reactors (via the water-gas shift reaction – WGS), of reactors integrated with carbon dioxide adsorption, namely to capture CO₂ and proceed to its valorization by converting it into methane, or integrated membrane reactors with CO₂ adsorption for H₂ production via reforming processes.

Membrane reactors for hydrogen production

A relevant example of the possible application of membrane reactors (MRs) is the WGS reaction ($\text{CO} + \text{H}_2\text{O} \leftrightarrow \text{CO}_2 + \text{H}_2$; $\Delta H_{298K}^0 = -41.1 \text{ kJ/mol}$). The WGS is a key stage in the processing of fuels for the production of hydrogen, being an intermediate step used for the enrichment of H₂ and reduction of CO in the syngas with several industrial applications (including H₂-powered fuel cells, whose CO content must be minimized). The WGS is a moderately exothermic reversible reaction; consequently, its conversion is limited by equilibrium, particularly at high temperatures.

When using a H₂ perm-selective membrane, this product is extracted from the reaction medium, shifting forward the equilibrium of the WGS reaction. In Figure 1 are illustrated results obtained with a dense metallic permeation tube, obtained from a flat Pd-Ag commercial membrane [5]. Hydrogen permeation through the membrane can be improved by increasing the total feed pressure or by decreasing the pressure in the permeate side (e.g. using vacuum or, alternatively, a sweep gas). From a mechanical point of view, the difference between the (total) lumen and external pressure in such types of membranes cannot exceed ~2 bar. Thus, a strategy was designed to achieve higher pressures using a pressurized sweep gas [5]. The performance achieved with the MR, keeping the total pressure difference constant ($\Delta P = P_{\text{feed}} - P_{\text{permeate}}$) at 1 bar, is shown in Figure 1. Increasing the feed pressure from 2.0 to 4.0 bar improved the performance of the MR; under moderate conditions of temperature and pressure a CO conversion very close to 100% was reached (clearly above equilibrium – dashed line) with almost complete recovery of H₂.

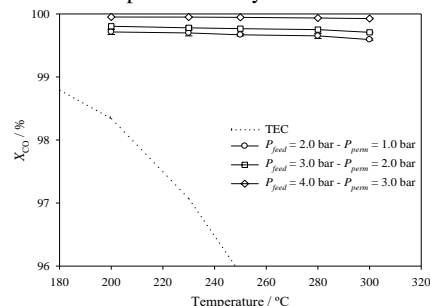


Figure 1. CO conversion as a function of the feed pressure for the WGS reaction at different temperatures in a Pd-Ag MR (N₂ flow rate used as sweep gas = 1000 mL_N min⁻¹, GHSV = 1200 L_N kg_{cat}⁻¹ h⁻¹, feed composition: 4.70% CO, 34.78% H₂O, 28.70% H₂, 10.16% CO₂ in N₂); TEC – thermodynamic equilibrium conversion. Source: [5].

Reactors integrated with carbon dioxide capture

In a perspective of processes that can be improved by adsorption, it is worth highlighting the proof of concept of another type of multifunctional reactor that benefits from the capture of CO₂ in a mixed bed of catalyst and adsorbent, in this case with the perspective of CO₂ valorization by conversion into methane [6]. Carbon dioxide may be available, for

example, from flue gas streams of various industrial processes. However, in such streams CO_2 is often too diluted for subsequent use. The work carried out aimed the demonstration of a cyclic adsorption and reaction unit, with continuous operation, capable of, simultaneously, removing CO_2 from flue gas streams (or from biogas [7]) and convert it into CH_4 . Such unit can be operated as schematically illustrated in Figure 2. In a first phase, one of the reactors (operating in adsorption mode) is fed with the flue gas, so that the CO_2 is retained in the selective adsorbent (e.g. hydrotalcite) contained in the mixed bed while the other species (N_2) leaves the column, until almost complete saturation of the bed. In the second stage – called reactive regeneration –, H_2 (obtained from a renewable source, for example via water electrolysis) is fed to the same column, which reacts with the CO_2 previously concentrated in the mixed bed (that contains both the CO_2 -selective sorbent and the methanation catalyst), producing methane by the Sabatier or methanation reaction ($\text{CO}_2 + 4\text{H}_2 \leftrightarrow \text{CH}_4 + 2\text{H}_2\text{O}$; $\Delta H_{298\text{K}}^\circ = -165 \text{ kJ/mol}$). Thus, to operate continuously, the process will require at least two columns operating in complementary steps: when a CO_2 -saturated bed is being regenerated (with green H_2) and is producing CH_4 , the other is in the CO_2 capture phase and vice-versa.

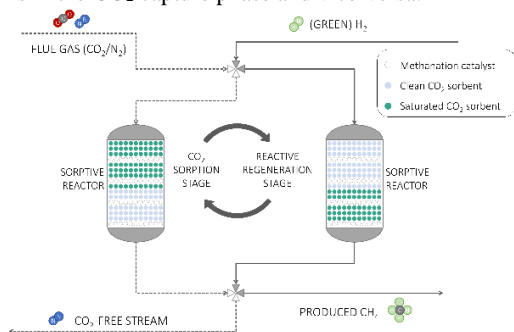


Figure 2. Scheme of the integrated process for capturing and converting CO_2 into CH_4 with two beds operating 180° out of phase.

The proof of concept of the integrated adsorption-reaction process has already been made, being possible to reach CH_4 purities above 80% (for biogas feed) and up to 70-80% (for flue gas). Furthermore, the tested materials showed absolute compatibility (a key factor for the success of the technology) and stability under operation for more than 150 h. Many operating conditions were varied, which will be useful for the subsequent modeling and optimization of the process, before the respective scale-up to reach a higher TRL level.

Acknowledgements

LMM acknowledges financial support by: (i) LA/P/0045/2020 (ALiCE), UIDB/00511/2020 and UIDP/00511/2020 (LEPABE), funded by national funds through FCT/MCTES (PIDDAC), and (ii) project HyGreen&LowEmissions, with reference NORTE-01-0145-FEDER-000077, supported by Norte Portugal Regional Operational Programme (NORTE 2020), under the PORTUGAL 2020 Partnership Agreement, through the European Regional Development Fund (ERDF).

References

- [1] D. Reay et al., *Process Intensification: Engineering for Efficiency, Sustainability and Flexibility*, Butterworth-Heinemann, Amsterdam, 2013.
- [2] A.E. Rodrigues et al., *Sorption Enhanced Reaction Processes*, World Scientific (Sustainable Chemistry Series vol. 1), London, 2017.
- [3] F.M. Dautzenberg, M. Mukherjee, *Chemical Engineering Science*, 56 (2001) 251-267.
- [4] K. Sundmacher, Z. Qi, 2010. *Chemical Engineering and Chemical Process Technology – Volume III: Chemical Reaction Engineering*, Encyclopedia of Life Support Systems, Eolss Publishers, Paris, 2010.
- [5] D. Mendes et al., *International Journal of Hydrogen Energy*, 35 (2010) 12596-12608.
- [6] L.M. Madeira et al., *PCT/IB2022/052657*.
- [7] J. Martins et al., *ACS Sustainable Chemistry & Engineering*, 10 (2022) 7833-7851.
- [8] J.M. Silva et al., *Journal of Power Sources*, 273 (2015) 423-430.
- [10] C. Rocha et al., *Chemical Engineering Journal*, 430 (2022) 132651.

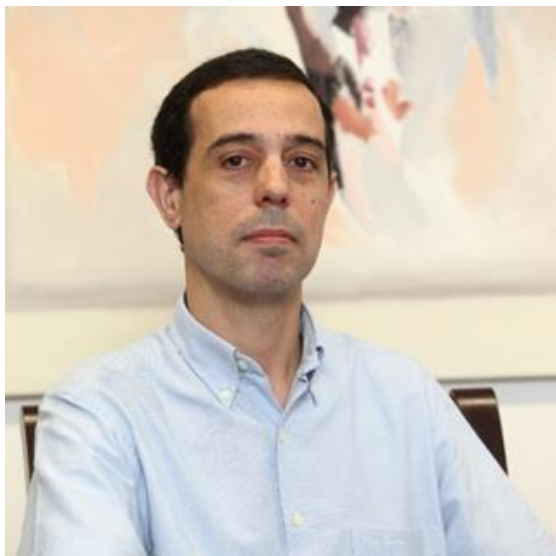
Membrane reactors integrated with CO_2 adsorption for H_2 production

The removal of any of the products in complex reaction systems, involving in particular reversible reactions, should improve the overall performance. However, such improvement is expected to be even more significant if more than one product is removed from the medium. For example, in the case of steam reforming of glycerol (a by-product of the biodiesel manufacturing process), the separation of H_2 (with a selective membrane) and/or CO_2 (with an appropriate adsorbent) was analyzed, from a thermodynamic point of view, by Silva *et al.* [8]. It was found that the yield of H_2 should improve either with the incorporation in the catalytic bed of an adsorbent for CO_2 capture (SER), or with the use of a perm-selective membrane towards H_2 (MR). However, compared to the conventional reactor, the best performance should be achieved in a reactor that integrates everything in the same device – the sorption-enhanced membrane reactor (SEMR); in this case, thermodynamic predictions pointed to over 200% improvement in the H_2 yield while also minimizing the occurrence of undesirable parallel reactions, namely methanation and coke formation [8].

Some of these trends have been corroborated by subsequent experimental studies, at the same time that high purity H_2 streams have been obtained [9]. Still, these multifunctional reactor concepts have also been successfully applied not only to glycerol but also to the WGS reaction and to effluents that represent a major concern in Mediterranean countries such as those resulting from the production of olive oil. Thus, not only is an environmental problem solved (because organic pollutant removals of more than 99.9% were achieved), but H_2 is also produced from renewable sources [10].

Conclusions

The multifunctionality resulting from the integration of reaction and separation operations in multifunctional reactors has significant advantages for improving the performance of many reactions, particularly those limited by equilibrium. However, the development of such reactors is a multi-step task, requiring efforts in several areas – more active and stable catalysts, highly permeable and selective membranes, adsorbents with fast capture and regeneration kinetics, together with advanced modeling, control and design strategies. Nevertheless, in recent years great progress has already been made; inherently, there are already some pilot-scale units and demonstration projects, pointing to the potential industrial scale-up in the short term.

Luís M. Madeira

Luís Miguel Madeira graduated in Chemical Engineering (1993) and received his PhD (1998) from the Technical University of Lisbon (IST) in Chemical Engineering - Heterogeneous Catalysis. He joined FEUP (Faculty of Engineering – University of Porto) in 1999 where is presently Full Professor in the Chemical Engineering Department. He is the Scientific Coordinator of the research unit LEPABE, and has been, from 2012 to 2023, Director of the undergraduate programmes in Chemical Engineering at FEUP (Bachelor, Master and Integrated Master). L.M. Madeira is member of the Working Parties on Chemical Reaction Engineering and Education, both from EFCE – European Federation of Chemical Engineering. His main research interests include multifunctional reactors, H₂ production and purification technologies, CO₂ capture and valorisation, and the use of Advanced Oxidation Processes for the treatment of gases and water/wastewater. L.M. Madeira authored/co-authored 215 articles in peer-reviewed international journals (h-index of 48; source: Scopus, August 2023), and co-authored over 220 communications in conferences. He has participated in ca. 40 research projects, either as a coordinator or as a member of the team. He was/is the coordinator/advisor/co-advisor of 16 postdoc level researchers, 30 PhD

students (23 theses already completed, 5 of them in companies) and >50 dissertations of master students

Portuguese footwear cluster – Innovative green materials, processes and products

M.J. Ferreira, V. Pinto, P. Costa*

CTCP, Rua de Fundões, Devesa Velha, São João da Madeira, Portugal.

**mjose.ferreira@ctcp.pt*



Our planet is facing challenges that are causing the footwear sector to accelerate its efforts to be sustainable by adopting green and digital solutions. There are, many potential areas of intervention and several variables remain, so significant research and innovation needs to be done. Firm steps are being accomplished within Portuguese projects GreenShoes4.0 and BioShoes4All. The global approach pursued in these projects will be shared, along with examples of the new and “next generation” of sustainable materials and processes, including biological and biobased materials, man-made bio-based materials, material-to-material recycling, and new concepts of functional, durable, or circular handbags or footwear. One important step towards sustainability in footwear is doing products life cycle assessment (LCA), to measure and reduce its environmental impact throughout its life cycle. Results and strategies to reduce the products carbon footprint will be introduced.

Green Shoes 4.0

Fashion businesses need to decarbonize and help minimize depletion of the planet’s resources and greenhouse gas (GHG) emissions. Realizing this transition is fundamental and will not happen spontaneously. It requires planning and collaborative efforts across the value chain involving both private and public sectors. While there are immediate opportunities for some businesses, namely some e-commerce platforms, others will benefit from research and innovation as is the case with biomaterials, traceability, and circular processes. Positive results were being achieved within GreenShoes4.0 a Portugal 2020 R&D collaborative project. It is promoted by a group of 15 companies covering the whole footwear value chain and includes leather, soles, software, production equipment, leather goods and footwear, representation and leadership, plus eight R&D bodies with complementary capabilities, coordinated by CTCP. The project developed new leathers, soling materials, software, production approaches, footwear concepts and business models (Figure 1).

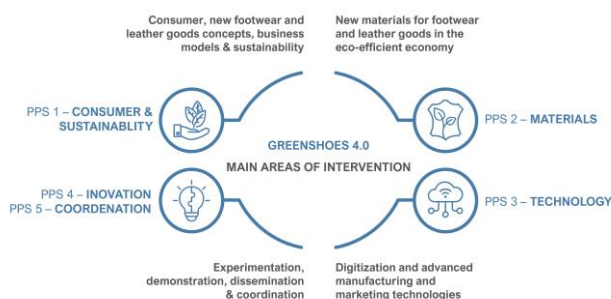


Figure 1. Main areas of R&D for the Green Shoes 4.0 project.

Functionalized circular leathers

Leather is a renewable biomaterial that presents excellent physical and comfort properties for use in footwear.⁷ It has high resistance to repeated flexion, tearing and abrasion, resistance to water penetration, good sweat absorption and desorption, and even resistance to heat/fire. However, may not be lightweight. From a sustainability point of view, it deserves to be highlighted

that leather is very durable, repairable and that its use contributes to recycling animal hides, an organic waste from the meat industry, even though leather production also results in waste. In this context, Green Shoes 4.0, partners IPB, CTIC, BOAVENTURA, FONTEVELHA and CTCP work included the modification of leather’s internal structure to reduce its density (weight), increase the area usable in final products and use of leather production waste. Leather functionalization was successfully promoted by hydrolyzed by-products obtained from solid leather residues from wet-white and wet-blue leather waste, with different molecular weights.

Recycled soling materials

Soles are very important footwear components contributing to its aesthetics, durability, comfort and also carbon footprint. GreenShoes4.0, partners ATLANTA, PROCALÇADO and CTCP studied new formulations and additives with the aim of obtaining high-quality materials. ATLANTA developed thermoplastics incorporating up to 90% recycled content. Test results confirm the materials and soles meet the specifications required by fashion and more demanding casual footwear. Additionally, the teams have worked on the development of materials incorporating soles and footwear production and post-consumer waste including rubber, fabrics, glues or leather. Soles developed by PROCALÇADO, and ATLANTA (Figure 2) were tested regarding density, hardness, resistance to abrasion and fatigue, tearing, traction and elongation at break. The results indicate present reduced carbon footprint and are ready to enter the market.



Figure 2. Illustration of soles from AtlantaSteps.

New product concepts and business models

Green Shoes 4.0 partners were actively deploying new products and concepts. One example is LeatherGoods by Belcinto (Figure 3). The new brand set itself the difficult objective of producing items only using surplus materials from previous collections and production, and using them fully, without generating new ‘leftovers’ in the process. This forced them to think the design through rigorously looking at a piece in every respect to fully satisfy functionality issues without failing to please consumers and keeping up to date without compromising on sustainability. The result is a deeply original line, producing prestigious leather goods made with exceptional world-class quality for markets around the world, while preserving the environment with eco-friendly providers.



Figure 3. LeatherGoods by Belcinto.

Several approaches may be followed in designing footwear for circularity. One approach is conceiving a product made mainly of one type of material that could, at the end of its useful life, be collected, cleaned and recycled into new shoes. An interesting example was developed by PROCALÇADO for its group brand Lemon Jelly (Figure 4). Through a recycling technology, the company can transform post-consumer Lemon shoes by grinding them down and incorporating them into the production of new Recycled Lemons. And because the factory runs entirely on renewable electrical energy, claims to generate new shoes with 90% less CO2 emissions.



Figure 4. Recycled Lemons by Procalçado/Lemon Jelly.

Digitization of the value chain

Green Shoes 4.0 has several new concepts in terms of digitization, with software company CEI by ZIPOR developing software and tools to digitally connect leather suppliers and their

Acknowledgements

The authors and consortiums acknowledge and thank the financial support of GreenShoes4.0 - Projeto de I&DT em mobilizador n. 046082, financiado pelo Compete 2020, Portugal 2020 e União Europeia Fundo Europeu de Desenvolvimento Regional; and BioShoes4All - Projeto n. 11 do PRR Medida C-12 Bioeconomia Sustentável, financiado pelo PRR Plano de Recuperação e Resiliência, República Portuguesa Ambiente e Ação Climática e União Europeia Next Generation EU.

clients to shorten the processes of leather digitalization, nesting and cutting. AMF, INESC TEC, ISEP, OFICINAWARE, and CTCF have been working on a consumer profile, trends and ‘forecast’ system, to boost sales. An innovative footwear injection planning system that increases overall productivity.

Future Steps: BioShoes4All

In footwear the materials, components and waste give the higher contribution to the total GHG emissions. The Portuguese footwear cluster aims to contribute to limit global warming to 1.5°C. To this end conceived a sustainability master plan and the integrated BioShoes4All project that includes 70 partners from industry, to retail and academia (Figure 5). BioShoes4All project is organized into five pillars – Biomaterials, Ecological Footwear, Circular Economy, Advanced Production Technologies, and Training & Promotion and intends to support the transition of the Footwear Cluster to a sustainable circular bioeconomy, reducing the dependency from the linear fossil-based economy, and maintaining a resilient and competitive national productive base and excellence positioning in the international market.



Figure 5. BioShoes4All Partnership.

The project objectives include the development and production of new biomaterials and components, based on the principles of circular bioeconomy and sustainable development, in all its dimensions, creating differentiated solutions, valued by customers and consumers, contributing to catalyze a new bioeconomy, efficient valuation of bioresources and decarbonization. There is also the need to “create new concepts of eco-products for footwear and leather goods, with lower carbon footprint, high durability, functionality and circularity, fundamental assets in the strategy of differentiation and creation of value in the long term, aimed at the consumer, who appreciates design and fashion, is informed, socially and environmentally demanding and responsible, and often digital”. Equally relevant will be the “design and application of new approaches and technologies aimed at minimizing and valuing production and post-consumption waste, in the context of a circular green economy, contributing to the extend the life cycle of materials and carbon neutrality. Within the scope of the BioShoes4All project, “the development and use of advanced technologies, within the framework of new technological and sustainability paradigms, are also a must, including tools for the traceability, automation and robotics, contributing to the increase of flexibility and competitiveness. The project will run until end of 2025. First results include promising leathers, man-made bio-based materials, material-to-material recycling.

Maria J. Ferreira

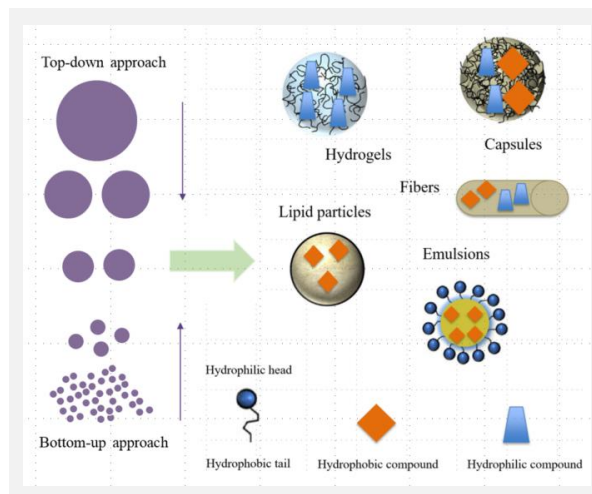
Maria José Pinto Ferreira is the Director of the Labs and Research and Sustainability Department at CTCP, the Portuguese Footwear Technological and Research Centre. Maria José holds a graduation in Chemistry, Master in Environmental Sciences, and a PhD in Environmental Engineering. She has experience in R&D projects preparation and coordination; physical and chemical testing of footwear and related materials (leather, plastics, rubber, composites, textiles, nanomaterials); and safety at work and environment management. Her research activity is carried out at CTCP in cooperation with industrial companies and R&D entities across Europe, being focused on new materials and processes, sustainability, products with lower environmental impact and recycling. She has coordinated for CTCP more than 60 projects. Maria José is a member of EU TAB for the EU Product Environment Footprint development and the delegate of Portugal in the Standardisation Committees enrolled in development of National, CEN and ISO Standards applicable to footwear and related materials.

Bio-based materials for the development of innovative micro and nanostructures for the delivery of bioactive compounds

M.A. Cerqueira

International Iberian Nanotechnology Laboratory, 4715-330 Braga, Portugal.

**miguel.cerqueira@inl.int*



Over the last few years there has been a clear evidence of the relationship between the rising of unhealthy diets and the incidence rate of chronic diseases, such as diabetes, obesity, and cardiovascular problems. As such, consumers are becoming more aware of the importance of their eating habits leading to a new demand for healthy and functional food products [1].

In addition to well-known micronutrients and vitamins, also bioactive compounds have been associated with several health benefits. However, the incorporation of those compounds in foods has some issues limiting its use, such as low solubility and bioavailability and low stability in the food matrix and under food processing.

These drawbacks can be minimized by exploring encapsulation technologies. Micro- and nanoencapsulation using new and innovative technologies have emerged in the last ten years and have been explored for the protection and control release of bioactive compounds in foods [2].

The top-down and bottom-up approaches using technologies such as electrohydrodynamic processing, nanoprecipitation, nanospray dryer and ultrasounds can be used to produce structures with different shapes and sizes. Among the food industry, the use of bio-based materials such as polysaccharides, proteins and lipids are the most interesting, thus maintaining their food-grade status. The developed structures can be used as carriers of bioactive compounds (lipophilic and hydrophilic) and used to deliver and control their release. They can also be used to stabilize these compounds during food processing, decreasing the possible changes in their bioactivity.

This work overviews some strategies for the encapsulation of bioactive compounds (e.g., vitamins, pro-vitamins, curcumin, caffeine, iron, resveratrol and quercetin) using well-known and innovative encapsulation technologies and food-grade materials (e.g., whey protein, corn zein, ethylcellulose, lactoferrin, hydroxypropyl methylcellulose, rhamnolipids). Microparticles, nanoparticles, nanofibers, nanohydrogels, lipid-based and multilayer nanosystems are presented being their main properties (size, polydispersity and zeta potential) disclosed and related to their behavior under different environments (pH and temperature) and during the *in vitro* gastrointestinal tract. Figure 1 shows some of the nanostructures developed and that will be presented.

Results showed that according to the compound of interest, the encapsulation technology should be optimized in combination with the materials used as carriers. In the case of the lipid-based nanosystems it was observed that the type of lipid could influence the size, stability and *in vitro* digestibility of the systems, which can then affect the bioaccessibility of vitamins. For the electrohydrodynamic processing besides the processing conditions also the viscosity of the solutions used can lead to the

formation of particles and fibers, which can be related with the entanglement of the biopolymer in the processed solutions.

It was possible to produce protein and polysaccharide-based nanoparticles using the nanoprecipitation method, model the nanosystem's digestibility, and increase the bioaccessibility of beta-carotene.

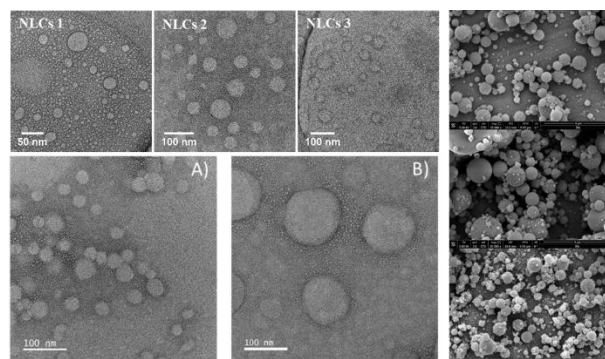


Figure 1. Images of micro and nanostructures obtained by ultrasounds using biosurfactants (top left) [3], electrospray using milk proteins (right) [4] and nanoprecipitation using a cellulose derivative and a plant protein (down right) [5].

Furthermore, some examples of how these encapsulated compounds can be incorporated into food products and influence their sensorial and physicochemical properties are presented.

References

- [1] Cerqueira et al. Nutrition, health and well-being in the world: The role of food structure design. In *Food Structure Engineering and Design for Improved Nutrition, Health and Well-being*, 2022, 3-15.
- [2] Guía-García et al., *Industrial Crops and Products*, 2022, 186, 115198.
- [3] Azevedo et al. *Food Chemistry*, 2021, 344, 128670.
- [4] Rodrigues et al., *Food Chemistry*, 2020, 314, 126157.
- [5] Afonso et al., *Molecules*, 2020, 25(19), 4497.

Miguel Cerqueira



Miguel Cerqueira holds a PhD degree in Biological Engineering from University of Minho. In 2011 he started as a Postdoctoral Researcher at University of Minho in collaboration with the University of Vigo aiming the development and characterization of bio-based nanostructures for food applications where he gained expertise on biodegradable films and coatings for food packaging, encapsulation of functional compounds using emergent encapsulation technologies, and the development and characterization of emulgels and oleogels for functional foods. In 2016 he joined the International Iberian Nanotechnology Laboratory, where he has been working on the development of bio-based micro and nanostructures for different applications. He has been involved in several projects as principal investigator and team member, and until now, raised approximately 6 M€ in funded projects and contracts with companies. He authored 145 Peer-reviewed scientific articles, published 27 book chapters, two patents and is editor of four books (achieving an h-index of 57). In 2014 he won the Young Scientist Award (sponsored by IUFOST). In 2018 he joined the list of "Highly Cited Researchers" presented by Clarivate Analytics (<http://orcid.org/0000-0001-6614-3942>).

Towards industrial decarbonization: Challenges of carbon capture and utilization based on ionic liquids through process simulation analyses

J. Palomar^{1*}, P. Navarro¹, J. Lemus¹, C. Moya², R. Santiago¹, D. Hospital¹, E. Hernandez¹, A. Belinchon¹, R. El Bijou¹

¹Universidad Autonoma de Madrid, Madrid 28049, Spain; ²Universidad Rey Juan Carlos, Madrid, Spain.

*pepe.palomar@uam.es



Industry is responsible for around a 30% of greenhouse gas emissions in Europe. Industrial decarbonization is a main strategy to reach the goal of net-zero emissions by 2050. Energy efficiency, industrial electrification, use of low carbon energy sources and raw materials and waste are key pathways to reduce industry's collective carbon footprint. Thus, CO₂-rich flue or process gases will continue being produced in several industrial processes in the near term. Therefore, Carbon Capture, Utilization, and Storage (CCUS) is a critical issue in the industrial decarbonization roadmap. Consequently, academy and industry are making significant efforts to develop new cost-effective CCU technology.

This work summarizes the main challenges of using multifunctional ionic liquids in the multi-component strategy of CO₂ capturing from diverse sources (biogas, post-combustion, etc.) and using the captured CO₂ to make value added products (carbonates, formic acid, urea, etc.). Process simulation is presented as useful tool in the multiscale development of new IL-based CCU technology.

Industry is responsible for around a 30 % of greenhouse gas emissions in Europe. Therefore, industrial decarbonization is a main strategy to reach the goal of net-zero emissions by 2050. Energy efficiency, industrial electrification, use of low carbon energy sources (biofuels, H₂) and raw materials and waste are key pathways to reduce industry's collective carbon footprint. However, current available technology in energy production, petroleum refining, chemical, cement, iron and steel manufacturing will continue need for using fossil fuels; therefore, CO₂-rich flue or process gases will continue be produced in the near term. Carbon Capture, Utilization, and Storage (CCUS) is a critical strategy in the industrial decarbonization roadmap. Consequently, academy and industry are making significant efforts to develop new cost-effective and sustainable CCU technology [1,2].

Ionic liquids (ILs) have been reported as promising CO₂ chemical absorbents [3, 4]. Taking advantage of their favorable properties (negligible volatility at mild operating conditions, structure tunability, chemical and thermal stability, etc.), new series of ILs (as example, aprotic heterocyclic anion based, AHA- ILs) have been designed with enhanced performance in carbon capture process for relevant systems as biogas, post-combustion and pre-combustion [5,6]. Further integrated molecular and process optimizations allowed obtained IL-based carbon capture processes with reduced chemical and energy consumptions [7-9], process costs [10-12], and environmental impacts [13]. Very recently, multiscale analyses, integrating molecular and process simulations, demonstrated that AHA-ILs can be adequately designed for direct carbon capture (DAC), obtaining competitive productivity, specific energy and process costs respect to conventional CO₂ absorbents and adsorbents [14]. On the other hand, ILs have been demonstrated excellent catalyst for CO₂ conversion to different added-value products (cyclic carbonates, dimethylcarbonate, urea, formic acid, etc.) [15,16]. Specifically, ILs have been widely used in the catalytic cycloaddition of CO₂ to epoxides for obtaining cyclic carbonates, added-value products for industry as solvent,

additive and reactant [17,18]. IL-based conversion systems as been demonstrated competitive in conversion and selectivity at mild conditions respect to conventional catalysts [19], allowing the effective catalyst recovery and product purification by distillation [20] or liquid-liquid extraction [21,22]. Further improvements in IL-based carbon conversion processes to produce cyclic carbonates have been reported to reach enhanced conversion and catalyst-product separation depending on IL and cyclic carbonate structure [23,24], minimizing energy demand [25] and environmental impacts [26]. Recently, bifunctional AHA-ILs have been successfully used for designing integrated CCU process, taking advantage of their excellent behavior as simultaneous CO₂ chemical absorbent and catalyst to promote process intensification and energy, emissions and cost savings [27].

This work summarizes the main challenges on using ILs in the multi-component strategy of capturing generated CO₂ from a point industrial source (biogas, post-combustion, blue H₂), or alternatively by direct air capture, and using the captured CO₂ to make value added products (carbonates, formic acid, urea, hydrocarbons) or storing it long-term to avoid release, with the aim of contributing to the current goal of industrial decarbonization. To this respect, the main contributions of process simulations in this research field are overviewed, including: i) the simultaneous product and process designs to select ILs with enhanced CCU process performance at industrial scale; ii) the multiscale experimental-computational research strategy for guiding process engineering developments; iii) the design of operation units and complete process, allowing techno-economic and environmental analysis; iv) The process optimization to promote the competitiveness of proposed IL-based CCU technologies respect current industrial ones; and iv) The development of digital prototype at TRL 4 to quickly advance in the development of IL-based CCU technology, for example, by pilot plant validation in relevant environment, enhancing the transferability to the industry.

References

- [1] M. Bui et al., *Energy & Environmental Science*, (2018).
- [2] C. Kim et al., *Journal of CO2 Utilization*, 65 (2022) 102239.
- [3] J. Haider et al., *Fuel* (2022) 314.
- [4] V.M. Shama et al., *Journal of CO2 Utilization*, (2021) 48.
- [5] D. Hospital-Benito et al., *Chemical Engineering Journal*, 11 (2020) 390.
- [6] B. Hong et al., *Industrial & Engineering Chemistry Research*, 55(30) (2016) 8432-8449.
- [7] C. Moya et al., *Chemical Engineering Journal*, (2022) 428.
- [8] D. Hospital-Benito et al., *Separation and Purification Technology*, 290 (2022) 7.
- [9] K. Seo et al., *ACS Sustainable Chemistry & Engineering*, 8(27) (2020) 10242-10258.
- [10] K. Seo et al., *ACS Sustainable Chemistry & Engineering*, 9(13) (2021) 4823-4839.
- [11] D. Hospital-Benito et al., *Chemical Engineering Journal*, 407 (2021) 9.
- [12] D. Hospital-Benito et al., *Chemical Engineering Journal Advances*, 10 (2022) 100291.
- [13] D. Hospital-Benito et al., *Sustainable Production and Consumption*, 38 (2023) 283-294.
- [14] D. Hospital-Benito et al., *Chemical Engineering Journal*, 468 (2023) 143630.
- [15] S.H. Lian et al., *Journal of Environmental Sciences*, 99 (2021) 281-295.
- [16] Y. Chen, T.C. Mu, *Green Chemistry*, 21(10) (2019) 2544-2574.
- [17] B.-H. Xu et al., *Green Chemistry*, 17(1) (2015) 108-122.
- [18] A. Rehman et al., *Journal of Environmental Chemical Engineering*, 9(2) (2021).
- [19] Y.F. Zhao et al., *Accounts of Chemical Research*, 54(16) (2021) 3172-3190.
- [20] K. Dong et al., *Chemical Reviews*, 117(10) (2017) 6636-6695.
- [21] E. Hernández et al., *Journal of CO2 Utilization*, 52 (2021) 101656.
- [22] R. Santiago et al., *Separation and Purification Technology*, 275 (2021) 119143.
- [23] A. Belinchón et al., *Journal of Cleaner Production*, 368 (2022) 133189.
- [24] E. Hernández et al., *Separation and Purification Technology*, 295 (2022) 121273.
- [25] E. Hernández et al., *Journal of CO2 Utilization*, 69 (2023) 102417.
- [26] E. Hernández et al., *Advanced Sustainable Systems*, 6(12) (2022) 2200384.
- [27] E. Hernandez, *Chemical Engineering Journal*, 446 (2022) 7.

José Palomar Herrero



José Palomar graduates in BSc on Chemistry in 1996 at Universidad Autónoma de Madrid Physical Chemistry. He holds his PhD in Science at Universidad Autónoma de Madrid in 2000, doing a postdoctoral stay at Florida State University (U.S.A). In 2001, he joined to Chemical Engineering Section/Department in UAM. The emergent group led by the tutor investigator, Prof. José Palomar, promotes, since 2007, new research lines focused on the development of knowledge and practical applications of ionic liquids (ILs), such as: i) CO₂ capture by IL-based systems; ii) Design of catalytic systems for the CO₂ conversion; iii) Development of advanced materials based on ILs with specific properties; iv) Treatment of gaseous contaminants by absorption with ILs; and v) Integration of molecular and process simulation computational tools for the conceptual design of industrial applications based on ILs. A multiscale research strategy -developed by a team of experts in molecular design, material science, environmental engineering and process simulation- is applied to the analysis of IL-based systems evolving gas-liquid, liquid-liquid and solid-liquid interfaces and their potential application to new sustainable processes. This methodology includes the selection of ILs with optimized properties by molecular simulation, experimental thermodynamic and kinetic tests to characterize the performance of selected ILs as separating agents or catalyst, the development of advanced materials based on LIs to improve the transport properties or recyclability of the system and, finally, process

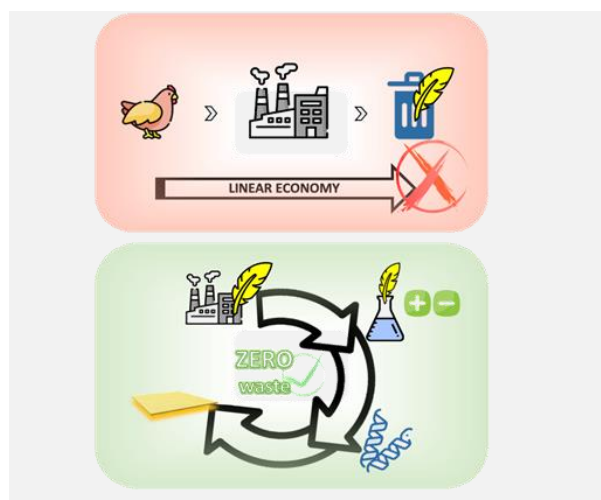
simulations to evaluate the performance of the new systems at industrial scale, their optimization attending to technical and economic criteria and viability analysis by comparing to available technologies. Prof. Palomar has participated in 20 competitive research projects and 5 contracts with companies, being the research leader in 19 of them, published 147 research articles in SCI journals (>5500 cites, h=47), 2 utility patents, and presented > 170 contributions to international and national meetings. The group maintains close collaborations with relevant research groups (International: Prof. Coutinho, Universidad de Aveiro; Prof. Brennecke, University of Texas; Prof. Fehrmann, Technical University of Denmark; Prof. Marrucho, Universidade Lisboa; Prof. Mischler, Ecole Polytechnique Fédérale de Lausanne; Prof. J. P. Hallet, Imperial College; Prof. Margarida Costa-Gomes, Ecole Normale Supérieure de Lyon; Prof. Canales, Pontificia Universidad Católica de Chile; among others. National: Prof. Rodríguez, UCM; Prof. Ortega, ULP; Prof. Díaz, UPM; Prof. Soto, USC. Prof. Tojo, UV. Prof. Martín, UG. among others); which have led to common projects, publications and stays. At this moment, the group participates in two research projects with important companies (Técnicas Reunidas, Aqualia) in the development of new CO₂ capture technology. In addition, cooperation with other companies such as Mahou, Vertech group, SENER, CEPSA, REPSOL, Cosmologic (Germany) and AspenTechnology (USA) has been established in the last years. An intense work in the formation of new researches is developed by the group, having directed 2 Juan de La Cierva contracts, 7 Doctoral Theses (another 4 currently in progress), more than 40 Master Thesis, 55 Bachelor Thesis and 19 scholar internships, as well as extensive teaching experience in Bachelor and Master subjects, in the organization of specialized training courses (3 UAM Summer Courses, 4 Continuous Training Courses, 1 International Course in India, etc.) and scientific events (Carbon 2018, "Iberoamerican Meeting of Ionic Liquids IMIL2015, "Twelfth meeting of the Spanish Carbon Group GEC2013" and several workshops).

Valorization of chicken feathers using aqueous solutions of ionic liquids

C. Polesca, H. Passos, *M.G. Freire**

CICECO - Aveiro Institute of Materials, Department of Chemistry, University of Aveiro, Aveiro, Portugal.

*maragfreire@ua.pt



Keratin, a fibrous protein with the potential for biomaterials production, represents around 90 wt % of chicken feathers. Aiming to achieve chicken feather waste valorization, we investigated the use of aqueous solutions of ionic liquids (ILs) to dissolve chicken feathers and produce keratin films. Different ILs were evaluated and the process operating conditions were optimized. Processes for the IL recovery and reuse were developed as well. A techno-economic analysis was performed, supporting the sustainable character of the developed process for keratin recovery. Hydrophilic and no cytotoxic keratin films were developed, with promising results for wound healing. The obtained results open the door for chicken feather waste valorization using an effective and sustainable process, as well as the use of keratin films in the biomedical field.

Introduction

Chicken is one of the most consumed meats in the world, resulting in an annual consumption of around 65 million tons worldwide. Consequently, a large amount of chicken feathers waste is generated, representing around 7 wt % of the total mass of chickens [1]–[3].

Chicken feather waste is generally disposed of through incineration or landfilling, resulting in serious environmental pollution. Therefore, it is critical to address this waste valorization using sustainable approaches [4], [5]. On this subject, it is essential to highlight that feathers are composed of 90 wt % of keratin, a fibrous protein, with potential application in cosmetics and in the biomedical field [1], [3].

Despite the potential applications of keratin, it is insoluble in water and has low solubility in traditional organic solvents due to the presence of inter- and intramolecular disulfide bonds in sulfur-containing amino acids [6], [7]. Traditional methods used (e.g. acid hydrolysis, alkaline hydrolysis and steam exposure) are still not efficient and present hazardous concerns, including negative impacts on the environment and on the keratin structure (e.g. amino acids degradation) [8], [9].

To overcome these concerns, researchers have investigated greener alternatives to recover keratin. Among the alternatives reported, the use of Ionic Liquids (ILs) has been highlighted. ILs are salts composed of large organic cations and organic or inorganic anions, which display lower melting temperatures than inorganic salts [6], [10], [11]. ILs have designer ability, and can be this designed to display high ability to dissolve biopolymers, including keratin. Based on this possibility, we focused on identifying an IL and develop a cost-effective process to dissolve chicken feathers and recover keratin. In addition, considering the challenges regarding the industrial application of ILs (their cost and requirement for recovery and reuse), we evaluated their recycling and performed a techno-economic assessment of the developed keratin recovery process. Finally, biological assays to prove the potential of the prepared keratin films in biomedical applications were carried out.

Methods

Chicken feathers were dissolved in an aqueous solution of IL (80 wt %) in a solid: liquid (chicken feathers: solvent) weight ratio of 1:20 w/w, at 100 °C, 650 rpm for 4 h [3], [12]. Different imidazolium and cholinium-based ILs were investigated, aiming to achieve the complete feathers dissolution. Then, keratin recovery conditions (solvent, time, and temperature) were optimized. The solution was centrifugated and keratin was washed with water to improve the IL removal and dried at 50 °C in an air oven for 48 h.

The recovery and reuse of IL were evaluated by removing the volatile compounds from the solution (IL + water + coagulant solvent), using a rotary evaporator. The purity of IL was determined using a Karl-Fischer titrator.

To address the cost-effectiveness of the developed process, a process simulation was carried out at Aspen Plus V11 for process modelling with the integrated Aspen Economics, following the principles described in the literature for biomass process [13].

Keratin films prepared from a keratin solution (15 wt %) with distilled water. The mixture was mixed at 60 °C for 30 min, cast on silicone molding, and dried at 50 °C for 24 h. Keratin films were characterized by physico-chemical and mechanical analysis. Aiming biomedical applications, the biocompatibility of keratin films, and their effect on the viability/metabolic activity of monocytes, macrophages, keratinocytes, and fibroblasts was assessed. Furthermore, *in vitro* wound healing assays were carried out.

Results

Most of the investigated ILs showed no ability to achieve the complete dissolution of chicken feathers under the reported conditions, with the exception of the following acetate-based ILs: 1-ethyl-3-methylimidazolium acetate ([C₂C₁im][C₁CO₂]), 1-butyl-3-methylimidazolium acetate ([C₄C₁im][C₁CO₂]), and cholinium acetate ([N_{111(20H)}][C₁CO₂]). This is due to the high hydrogen-bond basicity of the acetate anion, thus allowing strong hydrogen bonding with polymers, such as proteins [3].

The keratin recovery conditions were optimized for chicken feathers dissolved by $[C_4C_{1im}][C_1CO_2]$ and $[N_{111(2OH)}][C_1CO_2]$. Regarding the use of $[C_4C_{1im}][C_1CO_2]$, the best recovery conditions were with the addition of ethanol at 1:2 w/w (solution: coagulant ratio), at 5 °C for 1 h [3]. For $[N_{111(2OH)}][C_1CO_2]$, the optimized conditions were with the addition of ethanol solution (25 wt %), at 1:1.45 w/w, at 5 °C for 5 h [12]. These results highlight that the interactions established between the studied ILs and coagulants are different. The keratin recovery yields were 90 wt % and 93 wt % for $[C_4C_{1im}][C_1CO_2]$ and $[N_{111(2OH)}][C_1CO_2]$, respectively. It is essential to highlight that $[N_{111(2OH)}][C_1CO_2]$ presents greener properties – higher biocompatibility and low toxicity – than $[C_4C_{1im}][C_1CO_2]$, being reported for the first time, by us, for chicken feathers dissolution and keratin recovery [12].

Regarding the feasibility of the keratin recovery process and aiming to develop a sustainable process, $[C_4C_{1im}][C_1CO_2]$ and $[N_{111(2OH)}][C_1CO_2]$ were successfully recovered and reused for at least 3 cycles. Considering that $[N_{111(2OH)}][C_1CO_2]$ has the advantage of being a bio-based IL, the economic and environmental impact of $[N_{111(2OH)}][C_1CO_2]$ recovery was also evaluated. The developed keratin recovery process has a positive CO₂ emission, due to the unavailability of heat sources in pretreatment steps, in contrast with the common biomass-based process. Considering the annual productivity of 350 tons of keratin, its minimum selling price is 22 \$·kg⁻¹, making this process suitable for cosmetics and biomedical applications [12].

Acknowledgements

This work was developed within the scope of the project CICECO-Aveiro Institute of Materials, UIDB/50011/2020, UIDP/50011/2020 & LA/P/0006/2020, financed by national funds through the FCT/MCTES (PIDDAC). C. Polesca acknowledges FCT - Fundação para a Ciência e a Tecnologia for the Ph.D. grant with the reference UI/BD/151282/2021. H. Passos acknowledges FCT, I.P., for the researcher contract CEECIND/00831/2017, under the Scientific Employment Stimulus-Individual Call, 2017.

References

- [1] T. Tesfaye et al., *Sustainable Chemistry and Pharmacy*, 8 (2018) 38-49.
- [2] B. Mu et al., *Green Chemistry*, 22 (2020) 1726-1734.
- [3] C. Polesca et al., *Green Chemistry*, 25 (2023) 1424-1434.
- [4] S. Isarankura Na Ayutthaya et al., *Journal of Polymers and the Environment*, 23 (2015) 506-516.
- [5] M. Zhan et al., *Journal of Applied Polymer Science*, 133 (2016).
- [6] X. Liu et al., *ACS Sustainable Chemistry & Engineering*, 6 (2018) 17314-17322.
- [7] E.M. Nuutinen et al., *RSC Advances*, 11 (2021) 27512-27522.
- [8] C.R. Chilakamarry et al., *3 Biotech*, 11 (2021) 1-12.
- [9] A. Shavandi et al., *Biomaterials Science*, 5 (2017) 1699-1735.
- [10] A. Idris et al., *Green Chemistry*, 15 (2013) 525-534.
- [11] A. Idris et al., *Green Chemistry*, 16 (2014) 2857-2864.
- [12] C. Polesca et al., *Green Chemistry*, 2023.
- [13] A. Al-Ghatta et al., *ACS Sustainable Chemistry & Engineering*, 7 (2019) 16483-16492.

The keratin films obtained present a smooth and homogeneous topography, and a hydrophilic nature. Cytotoxicity tests have been successfully performed, without any significant impact on the cells, indicating that the keratin recovery process by ILs is efficient and may be safe for biomedical applications. Furthermore, the *in vitro* wound healing results showed that keratin film improves the proliferation of the cells, accelerating wound healing at 16 h (Figure 1) [3].

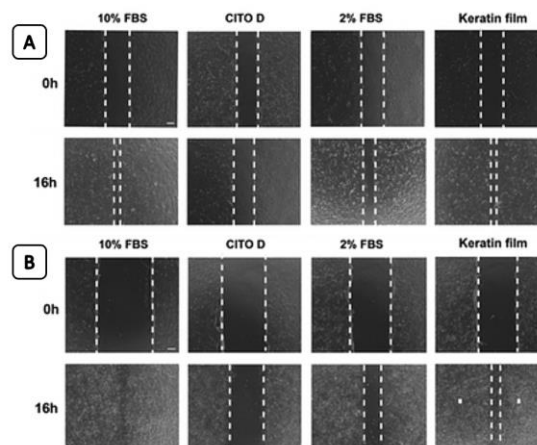


Figure 1. The wound healing ability of keratin film using (A) keratinocytes and (B) fibroblasts.

Mara G. Freire



Mara G. Freire graduated in Chemistry in 2003 by the University of Aveiro, Portugal, receiving the “Best Chemistry Student Award” from Dow Portugal. In 2007 she completed her PhD in Chemical Engineering by the University of Aveiro, with trainees at Federal University of Rio de Janeiro, Brazil, and Claude Bernard University, Lyon, France, followed by post-doctoral activities at ITQB2, New University of Lisbon, Portugal. In 2012, Freire was an invited professor at Tiradentes University, Sergipe, Brazil. In 2013, Freire was an Assistant Researcher and since 2014 she is a Coordinator Researcher at CICECO - Aveiro Institute of Materials, Chemistry Department, University of Aveiro, Portugal. Currently, Freire is the Coordinator of Group 5 - Biomedical and Biomimetic Materials - of CICECO, and Deputy Chair of the Scientific Council of the University of Aveiro. She is member of the European Academy of Sciences and of the Lisbon Academy of Sciences. In addition to being member of several journal editorial boards, Freire is one of the 17 Chairs of the Content Selection Advisory Board (CSAB) from Scopus. Freire published +300 papers in peer reviewed journals, +30 book chapters and two books, and has +16,000 citations and h-index of 71. She coordinated/participated in 25 R&D projects, among which two European Research Council (ERC) grants and 2 PathFinder projects from the European Innovation Council (EIC). She has filled +15 national/international patents, and is the co-founder of the RYAPURTECH spin-off. In addition to other awards and recognitions, Freire received the ECTP-NETZSCH Young Scientist Award in 2014, was recognized amongst the top 20 “Women in Science” in Portugal

in 2016, was recognized as one of the 14 rising stars in the Green Chemistry field by the Green Chemistry journal in 2017, was recognized as one of the 100 women in Chemistry by the Royal Society of Chemistry in 2018, was awarded with the “Vicente de Seabra Medal” in 2018, and received the 2021 Best Researcher Award from the University of Aveiro. Related to technology transfer and business ideas, she received the Born from Knowledge award by Agência Nacional de Inovação in the Health field in 2018, was finalist in the Everis Awards (2019) with the RYAPURTECH business case, and was awarded (2021) with the spin-off RYAPURTECH by the Macao Young Entrepreneur Incubation Centre (MYECI). Up to date, Freire has completed the supervision of 18 post-doctoral researchers, and 17 PhD, 60 MSc and 40 BSc students.

BONDALTI



A liderança é circular

Em matéria de química, a liderança faz-se de sustentabilidade. Somos a empresa #1 da Indústria química em Portugal, e renovámos o posicionamento Platina no ranking Mundial da Ecovadis. Uma conquista de hoje a pensar nas matérias do amanhã, incluindo o tratamento de águas e produção de energias verdes.

CHEMISTRY WATER ENERGY

TOMORROW MATTERS



BONDALTI.COM

Biochar and bio-oil from spent coffee grounds valorization

N. Caetano^{1,2,3}, T. Teixeira¹, W. Júnior¹*

¹School of Engineering (ISEP), Polytechnic of Porto (P. Porto), R. Dr. António Bernardino de Almeida 431, 4249-015 Porto, Portugal; ²LEPABE - Laboratory for Process Engineering, Environment, Biotechnology and Energy, Faculty of Engineering, University of Porto, Rua Dr. Roberto Frias, 4200-465 Porto, Portugal; ³ALiCE - Associate Laboratory in Chemical Engineering, Faculty of Engineering, University of Porto, Rua Dr. Roberto Frias, 4200-465 Porto, Portugal.

*nsc@isep.ipp.pt



Coffee is the world's most consumed beverage, and consequently spent coffee grounds (SCG) represent an important biowaste whose treatment and valorization must be considered not only for environment protection but also for resources conservation while promoting the circular economy. Therefore, the present work aimed at the valorization of spent coffee grounds through a thermochemical pyrolysis process yielding Biochar for use in soil, and bio-oil as a source of energy.

Pyrolysis was performed, in the range 400 to 600 °C, with an hold time of 5 to 15 min using SCG samples containing 9 to 44% moisture. A set of 23 experimental runs in a Central Composite Design allowed to model and maximize the yield of biochar/SCG or the yield of energy content of bio-oil/SCG. Finally, a maximum yield of 29% and 64%, was obtained respectively for biochar and bio-oil. In what concerns the energy content of bio-oil, a maximum 3894.45 kcal/kg dry SCG was obtained, showing the potential of this approach.

Introduction

Biomass and biowaste are used for energy production or as an energy carrier, such as biofuels, through various processes: pyrolysis, gasification, combustion or co-combustion [1]. Biomass can be used in pyrolysis, for the production of charcoal and activated carbon, with the aim of remediating soils or wastewater, and bio-oil, to be used as a fuel.

The coffee industry is considered the second most economically relevant industry in the world, after the oil industry, with coffee consumption estimated at more than 1.3 kg/year per capita. The estimated production for 2016/2017 was 9.34 million tons [2]. Spent coffee grounds (SCG), the biowaste that results after coffee extraction to prepare this beverage, have a moisture content of about 38%. Its uncontrolled disposal causes damage to the environment and the ecosystems, while valuable nutrients are lost and no energy is recovered. SCG is a type of biowaste with a relatively high moisture content. Its composition includes compounds toxic to the environment, as well as others such as tannins [3] that are of moderate or high value, being possible to explore its valorization within a biorefinery approach [4]. Valorization of SCG by thermal processes such as, for example, gasification, combustion or co-combustion is not recommended due to its usual high moisture content. However, it can be done through pyrolysis, allowing to obtain valuable energy products [5]. Pyrolysis is one of the few biofuel production technologies capable of processing a huge variety of biomass [6]. Chen et al. [7] performed a multi-objective optimization of SCG torrefaction, aiming at the production of carbon-neutral biochar. Akindolie & Choi [8] demonstrated the possibility of using biochar for the removal of phosphorus (P) from wastewater, therefore contributing to wastewater remediation and P recovery. Fu et al. [9] studied the co-circularity of SCG and polyethylene co-pyrolysis.

Following the agreement on the 17 Sustainable Development Goals (SDG) to create a global model of governance aimed at ending poverty, protecting the environment and promoting prosperity and well-being for all by 2030, it was proposed to evaluate the possibility of SCG valorization through the production of biochar and bio-oil via pyrolysis, therefore contributing to the SDG7, SDG12 and SDG15.

Materials and Methods

Spent coffee grounds collected from ISEP campus cafeteria were characterized for some important parameters, including particle size distribution (sieving followed by gravimetric analysis); moisture content (ISO 18134-3:2015); ash content (EN 14775:2009); lignin content (TAPPI T222om-11:2009); higher heating value (ASTM D586510); total organic carbon (Shimadzu, TOC-V CSN Analyzer and Shimadzu Solid Sample Module, SSM-5000[®]); total nitrogen (Kjeldahl method), cellulose content (NP ISO 6865:2009) and protein content. SCG were oven dried at 102 °C until constant weight, left to cool in a desiccator and stored until further use. Pyrolysis was performed using a vertical oven equipped with a control unit (Termolab) that allows controlling the heating rate, landing time and temperature (as shown in the Graphical Abstract). The oven was heated with 2000 W heating resistances, embedded in an insulating refractory carcass. The desired amount of SCG was inserted in a stainless steel mesh basket suspended in the center of a 1 m long refractory ceramic tube. The top and bottom of the tube were connected to the gas inlet and outlet, and nitrogen was fed to flush any traces of air/oxygen remaining in the tube. Then the desired temperature program was started, while the nitrogen flowrate was set to the required value. The gaseous product was bubbled into a 2 L flask with cool water (in an ice bath) where bio-oil condensed and the remaining cool gases were emitted to a vent. After the end of the temperature program, the oven was

left to cool up to 60 °C, after which the remaining solid (biochar) was left to cool to room temperature in a desiccator before further weighing and analysis. It was used the JMP Statistical Discovery v13 software to plan a set of 23 experimental runs in a Central Composite Design, and to model the effects of the parameters in the objective function. Therefore, for each specific goal (to maximize the ratio Biochar / dry SCG and to maximize the ratio energy content of the Bio-oil / dry SCG) a different expression was obtained.

Results and Discussion

SCG was characterized prior to any other procedure. Thus, moisture (37.43%); ash (1.81%); Kjeldahl nitrogen (12.33 g N / 100 g SCG); protein (12.33 g protein / 100 g SCG), higher heating value (5121.81 kcal / kg SCG); total organic carbon (88.97%); total lignin (32.81%); insoluble lignin (30.98%); soluble lignin (1.76%) were determined. Briefly, it was concluded that the values obtained for the SCG characterization do not significantly differ from those found in the literature [5,7] with only higher variation in the moisture content, what can be due to natural drying between production and time of analysis. In this work it was studied the influence of three parameters on the pyrolysis process: hold temperature (T) (400 to 600 °C), hold time (t) (5 to 15 min) and moisture content of the SCG (H) (9 to 44.4 %). As shown in Figure 1, the maximum yield obtained for the biochar and the bio-oil was 29% and 64%, respectively, corresponding to tests 9 (t=5 min, T=400 °C, H=44%) and 16 (t=5 min, T=400 °C, H=9 %) for biochar and to test 24 (t=10 min, T=500 °C, H=31%) for bio-oil, the heating speed for the test 9, 16 and 24 was 120, 120 and 30 °C/min respectively. It was concluded that the assay that promoted the maximization of the amount of energy in biochar was assay 16 (t=5 min, T=400 °C, H=9%), 1993.794 kcal/kg SCG (t=10 min, T=500 °C, H=31%), 3503.33 kcal/kg for the total amount of energy, the highest value was 11 (t=5 min, T=400 °C, H=9%), 5205.79 kcal/kg SCG. It was also realized a set of assays divided into two groups, A and B, that correspond to low heating rate and high heating rate tests (30 and 120 °C/min), respectively. These parameters were varied in order to obtain the maximum amount of biochar and the maximum amount of bio-oil energy per mass of SCG. For the set of tests, A, it was obtained a maximum biochar yield of 28% while the expected using the optimized model would be 34%. To maximize the amount of energy in bio-oil per mass of SCG, the result obtained experimentally was 3894.45 kcal/kg dry SCG and the expected was 3126.02 kcal/kg dry SCG. For the set of tests, B, it was obtained a maximum biochar yield of 29% while the expected using the optimized

model would be 30%. To maximize the amount of energy in bio-oil per mass of SCG, the result obtained experimentally was 956.89 kcal/kg dry SCG and the expected was 3576.94 kcal/kg dry SCG.

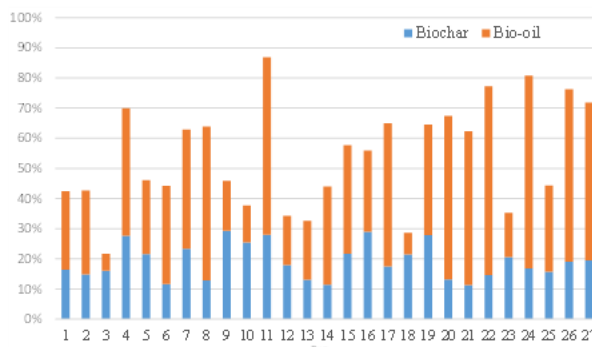


Figure 1. Yield of SCG pyrolysis products (biochar and bio-oil).

The difference between experimental and predicted values concerning the energy from bio-oil can be due to the difficulty in the recovery of the oil obtained from the pyrolysis process, particularly to the configuration of the oven, gas exhaust and liquid condensation system, as often it was observed the accumulation of oil in the output tubing, what negatively affected the results. It has been found that comparing with the values from the literature [10], the amount of energy of bio-oil when measured as a composite sample is closer (5481.64 kcal/kg) to the best assays analyzed alone (3894.45 and 956.89 kcal/kg). The amount of bio-oil required to replace the annual consumption (based on the year 2016) of diesel, gasoline and coal was also estimated as 1,218,460, 2,029,074; 4,885,295 t/year, respectively.

Conclusions

In this work it was demonstrated the technical feasibility of the thermochemical valorization of SCG through pyrolysis. The central composite design allowed to establish the best operating conditions to maximize the biochar yield or the bio-oil yield. The corresponding bio-oil energy yield was 3894.45 kcal/kg SCG. It was concluded that the maximum energy in biochar of 1993.79 kcal/kg SCG was achieved with a hold time of 5 min, at 400 °C, for SCG with a moisture content of 9%. In what concerns bio-oil, the maximum energy of 3503.33 kcal/kg SCG was achieved with a hold time of 10 min, at 500 °C, for SCG with a moisture content of 31%. For the total amount of energy, the highest value 5205.79 kcal/kg was achieved with a hold time of 5 min, at 400 °C, for SCG with a moisture content of 9%.

Acknowledgements

This work was financially supported by LA/P/0045/2020 (ALiCE), UIDB/00511/2020 and UIDP/00511/2020 (LEPABE), funded by national funds through FCT/MCTES (PIDDAC), UIDB/04730/2020 (CIETI), funded by national funds FCT/MCTES (PIDDAC).

References

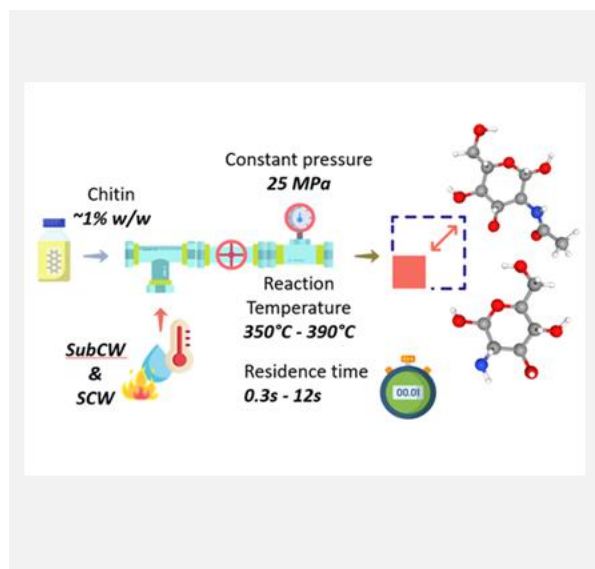
- [1] X. Yuan et al., *Renewable Energy*, 107 (2017) 489-496.
- [2] Y. Liu et al., *Fuel*, 199 (2017) 157-161.
- [3] M. Vilar et al., *Águas e Resíduos*, 11 (2022) 42-53.
- [4] T.M. Mata et al., *Bioresource Technology*, 247 (2018) 1077-1084.
- [5] N.S. Caetano et al., *Clean Technologies and Environmental Policy*, 16 (2014) 1423-1430.
- [6] P. Roy, G. Dias, *Renewable and Sustainable Energy Reviews*, 77 (2017) 59-69.
- [7] W.-H. Chen et al., *Bioresource Technology*, 370 (2023) 128584.
- [8] M. Akindolie, H. J. Choi, *Journal of Environmental Management*, 329 (2023) 117053.
- [9] J. Fu et al., *Fuel*, 337 (2023) 127061.
- [10] D. Meier, Chapter 14 in *Biorefineries. Advances in Biochemical Engineering/Biotechnology*, Wagemann, K., Tippkötter, N. Editors, vol 166. Springer, Berlin, Heidelberg, 2017, Cham. https://doi.org/10.1007/10_2016_68:Springer.

Understanding the behavior of chitin in Subcritical and Supercritical Water in a continuous reaction system

S. Rodríguez Rojo^{1,2*}, A. Casas González^{1,2}, E. Alonso^{1,2}

¹BioEcoUVA, Research Institute on Bioeconomy, PressTech Group, University of Valladolid, Spain; ²Dpt. of Chemical Engineering and Environmental Technology, School of Industrial Engineering, University of Valladolid, Spain.

*soraya.rodriguez@uva.es



Chitin ((1,4)- β -N-acetylglucosamine) is the second most widespread bio-polymer worldwide. Its high crystallinity and low solubility limit the exploitation of its antimicrobial, non-toxic and biodegradable properties, among others. So far, batch reactors and residence times longer than 1min with sub- and supercritical water have been tested to depolymerize chitin. In this work, we investigate the influence of temperature and residence time on chitin transformation in sub- and supercritical water (25MPa, 350 °C to 385 °C), using ultrafast continuous reactors (0.3s to 12s). Within the range studied, chitin gasification above 30% was detected when operating at high temperature ($T \geq 376$ °C) and a long residence time ($t \geq 5$ s). At these conditions, mean particle size of water-insoluble fraction was also reduced to ca. 280 nm. By-products such as glycolaldehyde, acetic acid and 5-HMF were identified in the water-soluble fraction, indicating the presence of side reactions.

Introduction

After cellulose, chitin is the second most widespread biopolymer worldwide. Its best-known applications, thanks to its antibacterial, toxicological and biocompatibility properties, are oriented to the medical and pharmaceutical industry, cosmetics, agriculture, and water treatment, among others. Being a biopolymer, chitin is formed by [β -1,4-poly(n-acetyl-D-glucosamine)] units, which can be treated to obtain oligomers and monomers, N-acetylglucosamine (depolymerization) and glucosamine (deacetylation). These monomers constitute nitrogen containing building blocks that open the way to seawaste biorefinery for obtaining molecules of interest, such as furan-based monomers or amines [1]. The physicochemical properties (density, viscosity, diffusivity, ionic product, and dielectric constant) of water vary drastically around the critical point (374 °C and 22 MPa); which gives it versatility to be used as a reaction and reagent medium altering its autoionization. In supercritical conditions (SCW) the concentration of $[H^+]$ and $[OH^-]$ ions is low ($\sim 10^{-9}$) favoring radical reactions, while the subcritical medium (SubCW) favors ionic reactions generating high ion concentrations ($\sim 10^{-5}$) [2]. Studies have shown that chitin, like cellulose, can be dissolved and hydrolyzed in sub- and supercritical water thanks to the change on its properties; however, due to its high crystallinity, this process occurs less easily [3]. Processes in the literature have used SubCW and SCW technology in batch-type systems as pre-treatments, managing to dissolve crab chitin in times of up to 1 minute [3]. However, degradation compounds (char) have been obtained or even the prevalence of side-reactions (5-HMF formation) competing with hydrolysis has been observed (depending on the reaction conditions) [4].

Objective

The present work aims to investigate the mechanisms of chitin transformation in SubCW and SCW media, using ultrafast

continuous reactors. Special attention is paid to the effect of residence time and reaction temperature on the solubilization and depolymerization processes.

Methodology

Experimental set-up. Commercial α -chitin from shrimp shells (coarse flake, Sigma Aldrich, 99% purity) was ground in a ball mill to a mean particle size ($d_{50,v}$) of 75 μ m. During the milling process, β -chitin is formed. The ground β -chitin was subjected to hydrolysis conditions under SubCW and SCW and short reactor residence times (0.3-12s). The reaction processes were carried out in the continuously operated pilot plant (Figure 1) used by Cantero et al. (2015) for cellulose hydrolysis [5]. An aqueous suspension of the ground chitin was introduced into the system at room temperature and mixed with hot pressurized water stream to reach the selected reaction temperature and a chitin concentration in the reactor of ca.1% w/w and 2% w/w. The reaction processes were carried out in a sudden expansion microreactor (SEMR) at constant pressure (25 MPa) and a temperature range between 350 °C and 390 °C, to achieve reaction times between 0.3s and 12s. The reaction mixture is then abruptly expanded in a decompression valve and cooled to room temperature to stop the reaction.

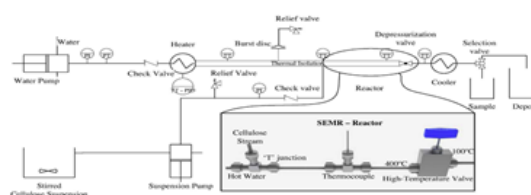


Figure 1. Experimental set-up (Cantero et al. 2015) [5].

Analytical methods. Raw material. Commercial chitin was characterized by elemental analysis, FT-IR, X-Ray diffraction and molecular weight by intrinsic viscosity analysis [6] to sketch

a picture of the starting structure for the reaction process. **Reaction products.** For characterization, the product was separated into water soluble and water insoluble fractions by centrifugation. The water-soluble fraction was characterized by HPLC chromatography, Total Organic Carbon (TOC), Total Nitrogen (TN) and pH. The water-insoluble fraction was characterized by elemental analysis (C, N, H), molecular weight [6], X-ray diffraction and particle size distribution by laser diffraction. Overall mass balance allowed to determine the chitin gasification fraction at the different operating conditions.

Results

The effect of reaction temperature and residence time on chitin depolymerization, and solid dissolution, is shown in Figure 2. When studying the influence of the residence time at constant temperature, an increase in the water-soluble fraction of the products was observed (19% in SCW conditions, and 8% in SubCW conditions). It was noticed that the SCW condition was more severe, observing a greater variation not only in the water-soluble fraction, but also a significant change in the gaseous fraction. The increase observed in the gas fraction is due mainly to the increase in reaction temperature rather than residence time in agreement with the behavior reported in the literature [4].

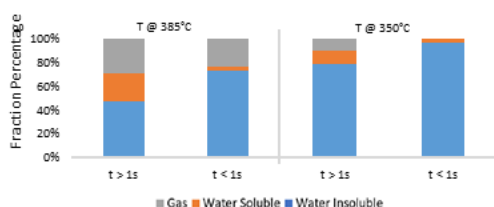


Figure 2. Influence of residence time and temperature on chitin processing.

The severity factor introduced by Overend and Chornet [7] for lignocellulosic biomass fractionation (Equation 1) has been used to consider the combined effect of temperature and time. The results in terms of severity factor are shown in Figure 3.

$$\text{Log}R_0 = \text{Log} \left(t \cdot \exp \left[\frac{T-100}{14.75} \right] \right) \quad (1)$$

The water-insoluble fraction decreases at the exit of the reactor when severity factor is increased, whereas the trend of the water-soluble and gas fractions is the opposite. Although similar trends are observed for the subcritical region and the supercritical region, different correlations are identified in each region. This behavior can be due to the drastic change of the water pK_w in the range 350 °C - 385°C, and this fact must be considered in the severity factor calculation. In addition, when increasing severity factor above 9, the mean particle size as $d_{50,v}$ of the water insoluble fraction was reduced from ca. 75 μm to approximately 0.28 μm . Besides the analyzed size reduction, a change of structure was detected by FT-IR techniques, identifying, among

Acknowledgements

This work was supported by Spanish Ministry of Science and Innovation (project PID2020-119481RA-I00), the Regional Government of Castilla y León and FEDER-EU, program CLU-2019-04.

References

- [1] X. Cai et al., Renewable and Sustainable Energy Reviews, 150 (2021) 111452.
- [2] M.J. Cocero et al., The Journal of Supercritical Fluids, 133 (2018) 550-565.
- [3] M. Osada et al., Carbohydrate Polymers, 134 (2015) 718-725.
- [4] T.M. Aida et al., Carbohydrate Polymers, 106 (2014) 172-178.
- [5] D. Cantero et al., The Journal of Supercritical Fluids, 96 (2015) 21-35.
- [6] G. Lamarque, et al. Biomacromolecules, 6 (2005) 1380-1388.
- [7] R. Overend, E. Chornet, Philosophical Transactions of the Royal Society A, 321 (1987) 523-536.
- [8] P.R. Sivashankari et al., Chitosan Based Biomaterials, 1 (2017) 117-133.

others, a possible transition from a β -structure to an α -structure. Results obtained by elemental analysis showed a deviation from the characteristic C/N ratio of chitin (6.85) [8] of almost +2 points. These results and a change in coloration in the water insoluble fraction (from light yellow chitin fed to dark brown products) could indicate the presence of degradation compounds (e.g., humic compounds) and reaffirm the presence of side reactions, as reported in the literature [4].

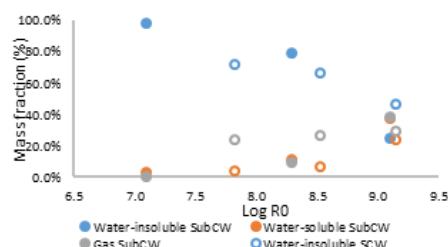


Figure 3. Water insoluble fraction, water soluble fraction, and gasification in terms of Severity Factor $\text{Log}R_0$.

Regarding the water-soluble fraction, it was observed that the composition profile was independent of the operating conditions, detecting the presence of glycolaldehyde, acetic acid, 5-HMF, and dihydroxyacetone (Figure 4) in all the evaluated conditions. Their concentration, in agreement with results in Figure 2, increased with increasing operating temperature and residence time.

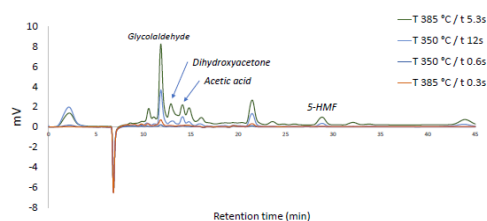


Figure 4. Liquid product composition profile.

Conclusions and on-going work

The results show that, within the studied range, chitin could not be fully depolymerized in sub and supercritical water and a solid product was get in all experimental conditions. Higher severity factors promoted gasification, particle size reduction of solid fraction and presence of by products as hint of side reactions competing with depolymerization. Also, the formation of humic acid is suggested due to the change in the visual appearance of the solid product (water-insoluble fraction). Experimental work is being oriented to develop a specific correlation of the severity factor in the range 350°C-400°C. Moreover, characterization of solid, liquid and gas products will be studied deeply. For instance, a flash and a gas capture system has been implemented to characterize the gas phase by GC-MS.

Method for the sustainability analysis of extraction processes: obtaining high value products from Soybean Oil Deodorization Distillate (SODD)

G.F. da Costa*, L.N.S. Marçal, R.M. Cavalcante, A.F. Young

Universidade Federal do Rio de Janeiro (UFRJ), Rio de Janeiro/RJ, Brazil; 2Universidade Federal Fluminense (UFF), Niterói/RJ, Brazil.

*gabriel.de.figueiredo@eq.ufrj.br

Solvent	QUANTITATIVE METRICS			QUALITATIVE METRICS				SM	CF	SI	SD				
	Efficiency	Price	Toxicity	Avg.	GDC#3	GDC#5	GDC#6					GDC#7	GDCI		
n-Propanol	1	1	1	1.00	9	9	1	1	5.00	5	5	15	23%	4.33	
Isopropanol	1	1	1	1.00	3	9	1	1	3.50	4	4	11	16%	6.19	
Acetone	1	1	1	1.00	9	9	1	1	5.00	5	5	15	23%	4.33	
Isobutanol	3	1	1	1.67	9	9	1	1	5.00	15	5	5	25	38%	2.60
Ethanol	1	3	1	1.67	3	1	1	1	1.50	2	5	2	8	12%	8.67
Ethyl Acetate	3	3	1	2.33	3	3	1	1	2.00	6	6	2	14	22%	4.64
n-Butanol	3	3	1	2.33	9	9	1	1	5.00	15	15	5	35	54%	1.86
Dimethyl carbonate	3	3	1	2.33	9	9	3	3	6.00	18	18	6	42	65%	1.55
Hexane	3	1	9	4.33	9	9	1	1	5.00	15	5	45	65	100%	1.00
Acetic Acid	1	1	9	3.67											
Pyridine	3	9	9	7.00											
1,4-Dioxane	1	9	1	3.67											
Isopropyl Acetate	3	9	1	4.33											
Tetrahydrofuran	3	9	1	4.33											
1,4-Diazabicyclooctane	9	9	1	6.33											
Propylamine	9	3	1	4.33											
Triethylamine	9	3	3	5.00											
Tripropylamine	9	1	9	6.33											

In a general sense, a solvent chosen for selective extraction must have (i) a high recovery efficiency; (ii) a competitive price; and (iii) relatively low toxicity to the human body and to the environment. Therefore, this work aims at developing a framework for assessing selective extraction processes, based on technical, economical and socioenvironmental parameters, that allows for the selection of the best solvents, as well as the application of the method on SODD processing. Ethanol was considered the most sustainable solvent for the selective extraction of SODD, with only 12% of the severity of the process using hexane (100% severity). Conversely, ethanol extraction is 8.67 times more sustainable than the one using hexane. Isopropanol is the second best solvent, (16% severity), while ethyl acetate would be the third option, (22% severity).

Introduction

Selective extraction methods can be employed to increase the value of plant residues, not only in the agricultural process but also in the energy and food sectors, considering vegetable fractions processing units of both segments. One of such residues is the Soybean Oil Deodorization Distillate (SODD), rich in tocopherols, squalene, and phytosterols, as well as other high value components [1]. In terms of extraction efficiency, in a general way, the size of the carbon chain and the presence or absence of functional groups in the solvent define the compounds that can be better extracted in each case; ketones, ethers and carboxylic acids have been shown to extract triglycerides, phospholipids and tocopherols from SODD with a higher efficiency, while alcohols and esters can present a higher overall efficiency with low selectivity [2].

When a selective extraction method employs liquid solvents, it is important to assess the toxicity of said solvent, regarding the possible uses for the extracts (e.g. pharmaceutical and food compounds can't contain residual solvents that are toxic), and also the impacts for the environment. The price is also an important factor to be observed, considering the economic feasibility of the extraction process. So, in a general sense, a solvent chosen for selective extraction must have (i) a high recovery efficiency; (ii) a competitive price; and (iii) relatively low toxicity to the human body and to the environment. Therefore, this work aims at developing a framework for assessing extraction processes, based on technical, economical and socioenvironmental parameters, that allows for the selection of the best solvents, exemplified on SODD processing.

Methodology

Through the work of Alcantara [2], a technical comparison was made regarding the extraction efficiency of 17 solvents compared to hexane, with a weighted average being made according to the mass fraction of each component of soybean oil to obtain a global efficiency metric. For the economic parameter (price), the values per liter of each solvent were obtained, with a

purity equal to or greater than 99%, through Sigma Aldrich database [3]. It was possible to check the parameters "Ecotoxicity, fresh water", "Human toxicity, carcinogenic" and "Human toxicity, non-carcinogenic", for each solvent. Using the OpenLCA software [4], and these parameters were normalized by the value for the worst solvent regarding each selected parameter. Then, the 3 parameters were summed for each solvent resulting in the Toxicity Index. Table 1 presents the results for each parameter.

Table 1. Technical, economical and socioenvironmental parameters for the 18 solvents.

Solvent	Efficiency	Price (R\$/L) 99% purity	Toxicity Index
n-Propanol	62.98%	500.00	0.0278
Isopropanol	63.07%	486.00	0.0230
Acetone	64.10%	250.00	0.0122
Isobutanol	55.49%	497.00	0.0827
Ethanol	67.35%	790.00	0.0302
Ethyl Acetate	55.54%	600.00	0.0555
n-Butanol	56.94%	574.00	0.0570
Dimethyl carbonate	46.37%	685.00	0.0215
Hexane	50.00%	453.00	0.6443
Acetic Acid	66.59%	238.00	0.4654
Pyridine	46.27%	900.00	2.5271
1,4-Dioxane	60.31%	927.00	0.1616
Isopropyl Acetate	50.81%	846.00	0.0861
Tetrahydrofuran	59.57%	851.00	0.0316
1,4-Diazabicyclooctane	5.08%	2076.72	0.2056
Propylamine	0.03%	767.00	0.1636
Triethylamine	0.68%	740.00	0.2785
Tripropylamine	0.83%	250.56	1.0000

Source: created by the authors based on [2], [3], [4].

These three quantitative parameters (efficiency, toxicity, price) were converted into degrees of conformity 1 (high conformity), 3 (medium conformity) and 9 (low conformity) corresponding to the desirable factors for the solvent regarding technical, economic and socioenvironmental aspects. Each solvent that

received a score of 9 in one phase was disqualified for the next analysis, in the aforementioned order.

For the efficiency, it was considered that values between 40% and 60% correspond to a medium conformity, indicating that the selective extraction is comparable to the process using hexane. Extraction efficiencies lower than 40% were considered to have a low conformity with the desirable standards, and efficiencies higher than 60% were considered as high conformity. In terms of price and toxicity, it was considered that values above 80% and below 120% of the average value for all 18 solvents had a medium conformity, while values lower than 80% of the average would represent a high conformity and values above 120% of the average present low conformity with the desirable traits.

The solvents that passed through the 3 quantitative evaluation phases were compared with hexane considering 4 of the 14 qualitative Green Degree Criteria (GDC) presented by Araújo *et al.* [5]. The production process for each of the solvents was assessed in terms of conformity to GDC#3 (using and generating compounds with low toxicity and minimizing dangerous substances), GDC#5 (preferably use renewable compounds), GDC#6 (minimize the formation of derivatives and the complexity of products) and GDC#7 (minimize the generation of byproducts by the use of selective catalysis), based on the analysis presented by Zhang *et al.* [6]. Then, the qualitative and quantitative metrics were used to generate a Severity Matrix

(SM) that was used to calculate the Criticality Factor (CF), the Severity Index (SI) and the Sustainability Degree (SD) for the selective extraction using each solvent.

Results and Discussion

From the total 17 alternative solvents, 4 were disqualified due to the efficiency criterion (less than 40% compared to hexane), 4 due to the price criterion (higher than 120% of the average price) and 1 due to the toxicity criterion (higher than 120% of the average toxicity). Results are shown in Table 2. Ethanol was considered the most sustainable solvent for the extraction of SODD, with only 12% of the severity of the process using hexane (100% severity). Conversely, ethanol extraction is 8.67 times more sustainable than the one using hexane. Isopropanol is the second best solvent, (16% severity), while ethyl acetate would be the third option, (22% severity).

Final Considerations

It can be observed that each one of the 7 criteria would result in a different solvent of choice, while the analysis by means of the SM and using CF, SI and SD metrics can provide a more integrated approach, revealing the best solvent regarding all these factors. A complete LCA assessment would be necessary in subsequent analysis steps, in order to confirm the conclusions obtained in the preliminary assessment.

Table 2. Quantitative and qualitative metrics, and results for the sustainability analysis of the solvents.

Solvent	QUANTITATIVE METRICS				QUALITATIVE METRICS				Severity Matrix (SM)	Criticality Factor (CF)	Severity Index (SI)	Sust. Degree (SD)			
	Efficiency	Price	Toxicity	Avg.	GDC #3	GDC #5	GDC #6	GDC #7					GDCI		
n-Propanol	1	1	1	1.00	9	9	1	1	5.00	5	5	15	23%	4.33	
Isopropanol	1	1	1	1.00	3	9	1	1	3.50	4	4	11	16%	6.19	
Acetone	1	1	1	1.00	9	9	1	1	5.00	5	5	15	23%	4.33	
Isobutanol	3	1	1	1.67	9	9	1	1	5.00	15	5	25	38%	2.60	
Ethanol	1	3	1	1.67	3	1	1	1	1.50	2	5	8	12%	8.67	
Ethyl Acetate	3	3	1	2.33	3	3	1	1	2.00	6	6	14	22%	4.64	
n-Butanol	3	3	1	2.33	9	9	1	1	5.00	15	15	35	54%	1.86	
Dimethyl carbonate	3	3	1	2.33	9	9	3	3	6.00	18	18	42	65%	1.55	
Hexane	3	1	9	4.33	9	9	1	1	5.00	15	5	45	65	100%	1.00
Acetic Acid	1	1	9	3.67											
Pyridine	3	9	9	7.00											
1,4-Dioxane	1	9	1	3.67											
Isopropyl Acetate	3	9	1	4.33											
Tetrahydrofuran	3	9	1	4.33											
1,4-Diazabicyclooctane	9	9	1	6.33											
Propylamine	9	3	1	4.33											
Triethylamine	9	3	3	5.00											
Tripropylamine	9	1	9	6.33											

Source: created by the authors following the methodology of [5].

Acknowledgements

This work was carried out with financial aid from the Human Resources Program of the National Agency of Petroleum, Natural Gas and Biofuels – PRH-ANP, supported with resources from the investment of oil companies qualified in the P, D&I Clause of ANP Resolution No. 50/2015; and also with scholarship support from the Institutional Scientific Initiation Scholarship Program (PIBIC) of the National Council for Scientific and Technological Development (CNPq).

References

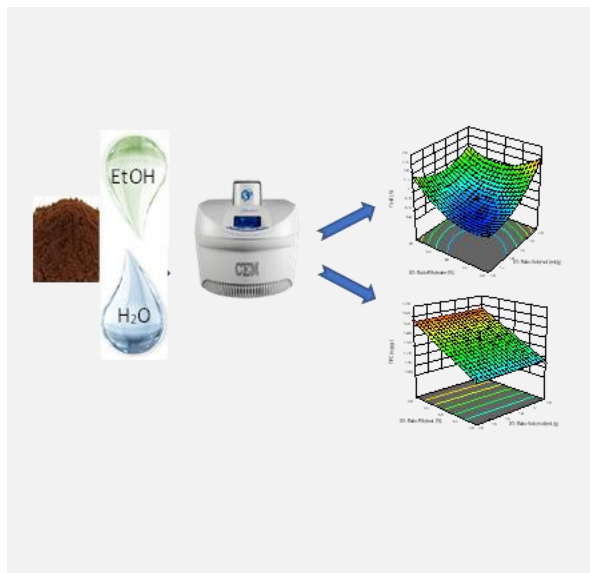
- [1] W. Lv *et al.*, ACS Omega, 6 (2021) 9141-9152.
- [2] A.C.R.V. Alcantara, Screening de solventes para extração seletiva de componentes do óleo de soja, Project carried out in School of Chemistry/UFRJ regarding the bachelor's degree in Chemical Engineering, July 2021.
- [3] Sigma Aldrich. Price consultation system, available at: <https://www.sigmaaldrich.com/> - Merck (2023).
- [4] OpenLCA. Open-Source Life Cycle Assessment software, available at: <https://www.openlca.org/> - Green Delta (2022).
- [5] O. Araújo *et al.*, Energy, 92 (2015) 556-568.
- [6] X. Zhang *et al.*, Industrial & Engineering Chemistry Research, 47 (2008) 1085-1094.

Applying two steps of DOE to microwave extraction from spent coffee

J. Coelho^{1,2*}, M. Robalo^{1,2}, R. Filipe^{1,3}, S. Boyadzhieva³, R.P. Stateva³

¹Instituto Superior de Engenharia de Lisboa, Instituto Politécnico de Lisboa, Rua Conselheiro Emídio Navarro 1, 1959-007 Lisboa, Portugal; ²Centro de Química Estrutural, Instituto Superior Técnico, Universidade de Lisboa, Av. Rovisco Pais 1, 1049-001 Lisboa, Portugal; ³PortugalCERENA, Centro de Recursos Naturais e Ambiente, Instituto Superior Técnico, Universidade de Lisboa, 1049-001, Lisboa, Portugal; ⁴Institute of Chemical Engineering, Bulgarian Academy of Sciences, Academic Georgi Bontchev str., 1113 Sofia, Bulgaria.

*jcoelho@deq.isel.ipl.pt



Two sequential design of experiments (DOE) were used to optimize the microwave-assisted extraction (MAE) with green solvents of bioactives from spent coffee grounds (SCGs). Initially, a 2^{4-1} two level Fractional Factorial Design was applied and ratios “solvent to solute” and “ethanol to water” were recognized as significant experimental factors. Consequently, Central Composite Design (CCD) was used to analyze the effects of the most significant factors on the responses yield, total polyphenols content (TPC), and antioxidant activity (AA) by the DPPH assay method, and quadratic surfaces to optimize those responses were generated. Values of 16.7 for the solvent/solute and 68.9% for ethanol/water optimized concurrently the yield (%) at 6.98 ± 0.27 , TPC (mg GAE/g) at 117.7 ± 6.1 , and AA ($\mu\text{mol TE/g}$) at 143.8 ± 8.6 , which were in excellent agreement with those predicted from the CCD model.

Introduction

Coffee is one of the most used plants in world. Its huge consumption produces large volumes of waste, which is almost as much as the quantity of coffee made worldwide. Storage of spent coffee grounds is a critical environmental problem and requires novel advanced approaches for its management and utilization. Within the concept of circular economy, a zero waste, one feed (SCGs) multiproduct Biorefinery targeted at a clean, safe production of high-value secondary metabolites and bioactives with enhanced properties and a wide spectrum of applications in the pharmaceutical, nutraceuticals, and cosmetic industries as well as in the development of functional foods, is the promising route for unlocking the full potential of SCGs [1,2].

The aim of this work was to combine two different design of experiments (DOE) methods in the optimization of the process conditions for the recovery of phenolic compounds from SCGs using the eco-friendly MAE technique. DOE methodology is a powerful research tool, which has proved to be more sensitive and robust than traditional methods, and which can be used efficiently at any stage of experimental development.

In this study, initially a Full Factorial Design (FFD), and subsequently a Central Composite Design (CCD) were applied to generate a mathematical model and consider the viable interrelationships among the independent parameters through minimizing the number of experiments and consequently saving time and resources. Extractions were performed with four independent parameters: *i*) solvent mixtures (ethanol/water); *ii*) microwave irradiation powers; *iii*) irradiation times and *iv*) solvent-to-SCGs ratios. Three response functions: yield, total polyphenols content and antioxidant activity by DPPH assay method were used to analyse the quality of the extracts. Finally,

the best conditions to recover extracts with high yield, total phenolic content and antioxidant activity were determined.

Experimental

The spent coffee grounds, a blended mixture of Arabica and Robusta species, obtained from an espresso machine of a Bulgarian coffee shop, was oven-dried to constant mass at 378 K and stored frozen in a refrigerator at 255 K. The moisture content (4.0 ± 0.3 %), was measured with a thermogravimetric balance (Kern MRS 120-3), and the average particle diameter, d_p , (0.273 ± 0.023) mm, calculated as described before [3]. The microwave-assisted extractions of the SCGs samples were carried out using a CEM Discover SP microwave reactor (2.45 GHz, 300 W) equipped with a non-contact infrared temperature sensor. Temperature was controlled by the variable microwave irradiations and the samples were cooled by nitrogen current and the end of extraction. The microwave radiation ranged from (60 to 120) W and was adjusted to stabilize the temperatures at 75 °C for different extraction times.

The DPPH assay of SCGs extracts was determined according to the method in a microplates system described by [4] with modifications. Total polyphenol content of the SCGs extracts was determined quantitatively using the Folin-Ciocalteu reagent in a microplates system with modifications [4].

Results and Discussion

In our work, in the first stage, four independent parameters (factors) were chosen and their influence on three important responses characterizing the quality of the extracts was studied. The main effects and the two-factors interactions were analysed [5]. That allowed us to understand which factors can be fixed in the second stage, where the Central Composite Design (CCD) was used to examine the effects of the variables in relation to

their responses and generate a quadratic surface to optimize the values with a minimum number of experiments.

For a 2^{4-1} two level FFD with four factors, 16 experimental runs are required. The maximum and minimum of the different factors and the respective coded values generated by the program Design-Expert 11 (DS-11) are shown in Table 1.

Based on the results of the FFD design applied at stage one, and with the aim to achieve extraction yield with a maximum of polyphenols and DPPH content, two independent parameters that have been indicated to have a low contribution to the microwave extraction, namely Power = 90 W and Time = 4.5 min, were fixed in the CCD.

The other two factors – Ratio Solv/sol (10-20 mL/g), and ratio of ethanol in water, Ratio Eth/water (50-70 % Ethanol) - were used to generate the CCD design.

Response surface analysis was designed centred on the model polynomial function defined in a three-dimensional model, establishing the effect on each observed response of the significant independent variables chosen. Contour response plots agreed with the visual identification of the optimal levels of each factor and a choice of the rightest values of the unique response factors.

In this work an FFD method followed by a CCD were effectively applied in the optimization of MAE of SCGs in terms of extraction yield, TPC and antioxidant content as DDPP assay.

The FFD design identified the independent variables Ratio (Solv/sol) and (Eth/water) as the most significant factors influencing the experimental extraction yield, TPC and DPPH content, while time and power of microwave irradiation, showed no significant influence. In the CCD design where the influence of the different factors (operating conditions) was tested, the Ratio (Eth/water) was indicated as the factor of principle significance in the extraction process. It was established that on the one hand the decrease of ethanol in the solvent mixture significantly decreased the extraction yield but, on the other - increased the TPC and antioxidant activity of the extracts obtained. The relation between a higher yield and lower TPC and antioxidant activity values exhibits an opposite trend.

Conclusions

Considering that the presence of bioactive compounds in SCGs is of great interest for the food, cosmetic and pharmaceutical industries, the results obtained in the present study can cover the way towards the design and scale-up of processes based on the application of MAE - an efficient, green and versatile technique - for the sustainable valorisation of the huge amounts of the easily obtainable waste generated from coffee processing.

Table 1. Range of parameters examined.

Factor	Name	Units	Minimum	Maximum	Coded Low	Coded High
F ₁	Power	Watt	60.00	120.00	-1 ↔ 60.00	+1 ↔ 120.00
F ₂	Ratio (Solv/sol)	mL/g	5.00	20.00	-1 ↔ 5.00	+1 ↔ 20.00
F ₃	Ratio(Eth/water)	% Ethanol	50.00	99.00	-1 ↔ 50.00	+1 ↔ 99.00
F ₄	Time	min	3.00	6.00	-1 ↔ 3.00	+1 ↔ 6.00

Acknowledgements

The authors acknowledge the European Union's Horizon 2020 research and innovation program under the Marie Skłodowska-Curie project IProPBio, grant N° 778168. J. P. Coelho and M. P. Robalo are thankful to Centro de Química Estrutural a Research Unit funded by Fundação para a Ciência e Tecnologia through projects UIDB/00100/2020 and UIDP/00100/2020. Institute of Molecular Sciences is an Associate Laboratory funded by FCT through project LA/P/0056/2020. R. M Filipe gratefully acknowledges the support of FCT through CERENA project UIDB/04028/2020.

References

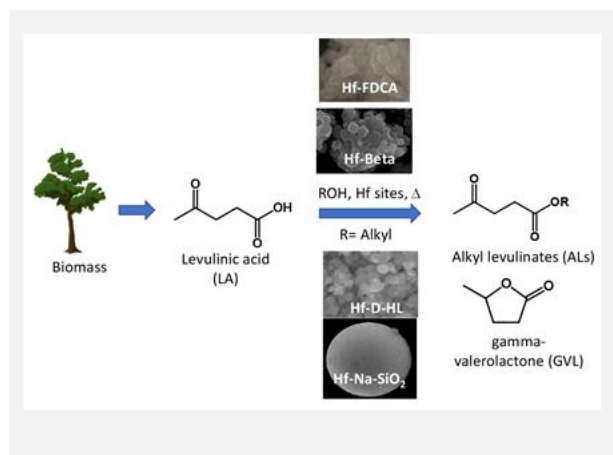
- [1] S. Georgieva et al., *Journal of Chemical Technology and Metallurgy*, 53 (2018) 640-646.
- [2] S.K. Karmee, *Waste Management*, 72 (2018) 240-254.
- [3] J.P. Coelho et al., *The Journal of Supercritical Fluids*, 161 (2020) 1-13.
- [4] G. Bobo-García et al., *Journal of the Science of Food and Agriculture*, 95 (2015) 204-209.
- [5] C.P. Santos et al., *Journal of Chemometrics*, 33 (2019) 1-18.

Multifunctional nano hybrids, zeotypes and modified macro and mesoporous silicas for the upgrading of the renewable platform chemical levulinic acid

M.M. Antunes^{1*}, K. Klan¹, A. Silva¹, A. Fernandes², M. Pillinger¹, F. Ribeiro¹, A.A. Valente¹

¹CICECO-Aveiro Institute of Materials, Department of Chemistry, University of Aveiro, Campus Universitário de Santiago, 3810-193 Aveiro, Portugal; ²Centro de Química Estrutural, Instituto Superior Técnico, University of Lisbon, Av. Rovisco Pais, 1049-001 Lisbon, Portugal.

*margarida.antunes@ua.pt



The present work deals with the conversion of the biomass-derived carbohydrate levulinic acid (LA) to gamma-valerolactone (GVL), via catalytic transfer hydrogenation (CTH) using heterogeneous Hf-containing catalysts. The catalysts were inorganic-organic nano hybrids Hf-FDCA synthesized from biobased 2,5-furandicarboxylic acid (FDCA) with a Hf precursor [1], hierarchical intracrystalline micro/mesoporous microcrystalline Hf-Beta [2], hierarchical Hf-D-HL derived from zeolite LTL [3], and Hf-containing macro- and mesoporous silica (under investigation). The catalysts were effective for the conversion of LA to GVL with yields of up to 99 % at 180 °C/24 h. Reaction kinetics and material characterization indicated that the catalytic reaction depends on a complex interplay of different factors including the textural and acid properties of the catalysts. Catalyst stability was studied by recovering, reusing, and characterising the used catalysts.

Introduction

Vegetable biomass (VB) is an established source of energy with potential to alleviate society's large dependency on fossil fuels, with several advantages such as the fact that VB is renewable, highly abundant on Earth and may contribute to reduce CO₂ emissions. The main components of VB include hemicelluloses and cellulose, which, in the presence of acid catalysts, undergo hydrolysis and dehydration reactions to give the furanic aldehydes furfural and 5-(hydroxymethyl)furfural, respectively. These furanic aldehydes can be converted to levulinic acid (LA) which is one of the most important carbohydrate biomass derived platform chemicals. LA has a growing applications profile, such as its use as an intermediate to produce gamma-valerolactone (GVL) and alkyl levulinates (ALS). GVL is a promising fuel additive and intermediate to liquid transportation fuels. LA conversion to GVL in alcohol medium may involve acid and reduction chemistry. High GVL yields were reported in the literature albeit using expensive noble metals and external supply of molecular hydrogen [4]. The use of organic hydrogen donors such as secondary alcohols (ROH) for catalytic transfer hydrogenation (CTH) is an attractive alternative to the external supply of H₂ because the former approach may avoid safety issues associated with high pressure H₂, H₂ transportation/storage and handling, and expensive infrastructures [5]. On the other hand, Lewis acid catalysts containing Hf may promote CTH reactions and substitute noble metal catalysts [6]. Our group used different types of non-noble metal heterogeneous catalysts for the LA-to-GVL conversion, namely hafnium-containing inorganic-organic nano hybrids (FDCA) prepared via a fast synthesis methodology (FT) [1], hierarchical microcrystalline Beta zeotype [2], hierarchical aluminosilicate derived from zeolite LTL [3] prepared via post-synthesis strategies and (for the first time) Hf-containing modified silica spheres with particles ranging from micron size (mSiO₂) to the nearly nano (LFS150) and nano (LFS50) size ranges, using 2-butanol (2BuOH) as reducing agent.

Objectives

To prepare new multifunctional heterogeneous catalysts with acid and reduction sites, able to convert LA to GVL via economic and safer strategies, without noble metals and avoiding external supply of high pressure H₂.

Methods

Synthesis

Hf-FDCA was prepared by a fast synthesis (FT) methodology (15 min) at 120 °C [1]. Hierarchical Hf-Beta and Hf-D-HL and macroporous silicates were prepared via top-down approaches starting from commercially available zeolites. The top-down strategies involved desilication, dealumination, impregnation of a hafnium precursor and calcination [2-3]. The mSiO₂ and LFS supports were subjected to post-synthesis modifications involving alkaline (NaOH or TPAOH) and acid treatments.

Characterisation of the catalysts

The acid and textural properties (herein reported) were measured by FT-IR spectroscopy of adsorbed pyridine and N₂ sorption isotherms at -196 °C, respectively.

Catalysis

LA conversion to GVL was carried out in stirred batch reactors in the reaction temperature range 150-200 °C, using 2BuOH as solvent. Reaction conditions: 25.6 g_{catalyst} L⁻¹; 0.45 M LA in 2BuOH.

Results

Table 1 gives the acid and textural properties of the prepared materials. Table 2 presents selected catalytic results for the conversion of LA to GVL, in the presence of the prepared materials.

Table 1. Acid properties (Lewis + Brønsted acid sites) and textural properties of the catalysts (S_{BET} = specific surface area; S_{E} = external surface area).

Catalyst	Total acid sites ($\mu\text{mol g}^{-1}$)	S_{BET} (S_{E}) ($\text{m}^2 \text{g}^{-1}$)
2.8Hf-FDCA	80	235 (144)
0.28Hf-Beta	110	564 (397)
1.12Hf-D-HL	67	96(74)
0.11Hf-Na-mSiO ₂	ui	89 (34)
0.11Hf-TPA-mSiO ₂	ui	116 (62)
0.11Hf-Na-LFS50	ui	218 (149)
0.11Hf-TPA-LFS50	ui	183 (162)

ui = under investigation.

Table 2. Best catalytic results for the studied catalysts in the conversion of levulinic acid (LA) to gamma-valerolactone (GVL) and 2-butyl levulinate (2BL).

Catalyst	T (°C)	Time (h)	LA conversion (%)	GVL yield (%)	2BL yield (%)
Blank	200	24	17	-	9
HfO ₂	200	24	24	-	8
2.8Hf-FDCA	180	24	100	87	10
0.28Hf-Beta	180	24	100	99	-
1.12Hf-D-HL	200	24	100	77	20
0.11Hf-Na-mSiO ₂	180	48	86	15	64
0.11Hf-TPA-mSiO ₂	180	48	90	23	62
0.11Hf-Na-LFS050	180	48	100	48	39
0.11Hf-TPA-LFS050	180	48	100	55	33

a) Reaction conditions: 0.45 M LA in 2BuOH, 25.6 $\text{g}_{\text{cat}} \text{L}^{-1}$ (materials possessing 0.11 - 2.8 $\text{mmol}_{\text{Hf}} \text{g}_{\text{cat}}^{-1}$).

Acknowledgements

This work was developed within the scope of the project CICECO-Aveiro Institute of Materials, UIDB/50011/2020, UIDP/50011/2020 & LA/P/0006/2020, financed by national funds through the FCT/MEC (PIDDAC). The positions held by MMA and AF were funded by national funds (OE), through FCT, IP, in the scope of the framework contract foreseen in the numbers 4, 5 and 6 of article 23 of the Decree-Law 57/2016 of 29 August, changed by Law 57/2017 of 19 July. The position held by AFS was funded by Project POCI-01-0145-FEDER-030075 (COMPETE 2020 Operational Thematic Program for Competitiveness and Internationalization) co-financed by national funds through the FCT/MCTES and the European Union through the European Regional Development Fund under the Portugal 2020 Partnership Agreement.

References

- [1] M.M. Antunes et al., *Catalysis Today*, 394-396 (2022) 268-281.
- [2] M.M. Antunes et al., *Journal of Catalysis*, 406 (2022) 56-71.
- [3] M.M. Antunes et al., *Frontiers in Chemistry*, 10 (2022) 1006981.
- [4] H.-T. Vu et al., *Chemical Engineering Journal*, 430 Part 2 (2022) 132763.
- [5] S. Dutta et al., *Chemical Engineering Journal*, 372 (2019) 992-1006.
- [6] W. Sun et al., *Frontiers in Chemistry*, 10 (2022) 863674.

Discussion and main conclusions

The prepared Hf-based materials possessed uniformly distributed hafnium (based on powder XRD and SEM-EDS, not shown). The prepared heterogeneous catalysts promoted the conversion of LA to GVL and 2BL, whereas commercial HfO₂ led to sluggish catalytic results. Hence adequate Hf sites are required to trigger the catalytic reaction of LA.

GVL yield seemed to increase with increasing specific surface area (S_{BET}) and increasing amount of total acid sites. A comparison of 0.28Hf-D-HL and 1.12 Hf-D-HL suggested that increasing the Hf loading favored GVL formation (51 and 77 % GVL yield, respectively, at 200 °C/24 h). The catalyst 0.28Hf-Beta led to the highest GVL yield (99 %), and 0.11Hf-Na-mSiO₂ led to the lowest (15 % GVL yield at the same temperature and greater reaction time, Table 2). However, the amount of Hf in 0.11Hf-Na-mSiO₂ was less than half of that in 0.28Hf-Beta. This might partly explain the lowest activity and selectivity towards GVL.

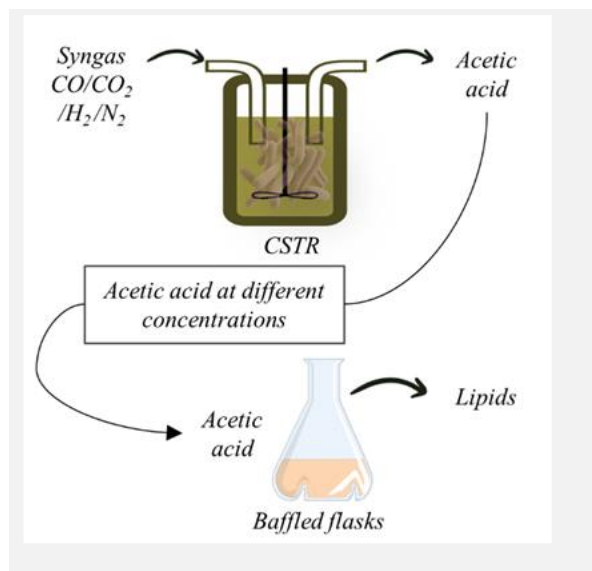
Importantly, the different types of heterogeneous catalysts were recoverable and stable in consecutive batch runs, enhancing the productivity.

Efficient conversion of syngas to lipids through a two-stage bioconversion process

R. Robles-Iglesias, M.C. Veiga, C. Kennes*

Chemical Engineering Laboratory, Faculty of Sciences and Center for Advanced Scientific Research – Centro de Investigaciones Científicas Avanzadas (CICA), BIOENGIN group, University of La Coruña, E-15008-La Coruña, Spain.

*kennes@udc.es



A two-stage process was set-up to effectively bioconvert syngas (CO, CO₂, H₂) into lipids. In the first stage, *Clostridium aceteticum* fermented C1-gases into acetic acid through the Wood-Ljungdahl metabolic pathway in a stirred tank bioreactor, reaching a maximum product concentration of 11.5 g/L and a production rate of 0.05 g/L·h. In the second stage, the yeast *Rhodosporidium toruloides* was inoculated in the acetogenic medium and it efficiently accumulated lipids from acetic acid produced in the first stage. The best results achieved were a lipid content of 39.5 % g/g dry cell weight, 3 g/L dry biomass, and biomass and lipid yields of 0.35 and 0.107, respectively. The lipid profile, in terms of decreasing abundance, was: C18:1 > C16:0 > C18:2 > C18:0 > Others. High concentrations of acetic acid were found to inhibit *R. toruloides* at acid levels reaching 18 g/L, being lethal at 22 g/L and above. This study provides a novel method for growing oleaginous yeasts for sustainable biofuel production from syngas or C1-pollutant gases.

Introduction

The need to minimize dependence on fossil fuels as well as issues related to greenhouse emissions have led to increased concern given the prospect of resource depletion and global warming problems. In order to solve those problems, gases such as carbon dioxide (CO₂) and carbon monoxide (CO), emitted from various sources, have been identified as suitable substrates to produce value-added chemicals.

Microorganisms capable of utilizing C1-gases, particularly acetogenic bacteria, have garnered considerable interest due to their ability to efficiently bioconvert CO₂ into organic acids, alcohols, and some other chemicals under anaerobic conditions. The Wood-Ljungdahl metabolic pathway is the most energy-efficient metabolic pathway in terms of CO₂ fixation, allowing acetogenic bacteria to use C1-gases and H₂ as sole energy and/or carbon sources [1]. However, due to bioenergetic restrictions during autotrophic metabolism and the lack of specific enzymes, acetogens are unable to synthesize energy-rich substances like lipids or biopolymers from C1-gases. Therefore, there is a need to engineer bacteria or combine different stages and/or microorganisms in order to expand the spectrum of products obtained. It is widely recognized that oleaginous yeasts exhibit a high degree of efficiency in the conversion of certain organic acids into lipids [2]. As such, the integration of these two processes, i.e., gas fermentation into fatty acids and subsequent acids conversion into lipids, may prove to be highly advantageous and offer numerous benefits.

This study tested the acetogenic bacterium *Clostridium aceteticum* for the bioconversion of C1-gases into acetic acid and the oleaginous yeast *Rhodosporidium toruloides* for the subsequent bioconversion of acetic acid into lipids. The research provides insight into the potential of combining different stages and/or microorganisms to expand the spectrum of products obtained from anaerobic C1-gas fermentation.

Materials and Methods

Clostridium aceteticum DSM 1496 was used for anaerobic fermentations. The medium employed is described on their commercial website. Two separate fermentations were carried out under identical experimental conditions. One experiment was conducted in 40 ml bottles using batch processing techniques, while the other experiment was performed in a 2 liter reactor with continuous gas feed. The experimental conditions for both experiments were a constant pH of 7.5, constant temperature of 30 °C, agitation at 150 rpm, and the flushed gas composition consisted of a syngas mixture of CO₂/CO/H₂/N₂ (10/30/20/40).

Rhodosporidium toruloides DSM 10134 was used for aerobic fermentations. Two experiments were conducted in 500 ml bottles, each containing 40 ml medium. In the first experiment, the culture medium was prepared by utilizing the acetic acid-rich medium obtained from the *C. aceteticum* batch experiments, in order to assess the acid toxicity to the yeast. In the second experiment, the medium obtained from the *C. aceteticum* bioreactor experiment was utilized to determine the lipid accumulation in *R. toruloides*. The initial pH in both experiments was adjusted to 6.0, 150 rpm agitation, and 30 °C.

Results and Discussion

The first assay investigated the growth and acetic acid production of *C. aceteticum* in bioreactor using syngas as a substrate. The strain efficiently grew on syngas and generated acetic acid, reaching 11.50 g/L after 387 hours. The growth rate was initially fast, but it subsequently slowed down and eventually ceased while acetic acid production kept going up. The strain continued producing acetic acid at high rates until its early decline phase, indicating that it remained highly metabolically active. During this assay, samples were extracted for the subsequent yeast experiments that focused on the production of microbial oils and lipids by using acetic acid generated from the syngas bioconversion experiment.

The second assay aimed at determining the potential toxicity of acetic acid on *R. toruloides* grown in the fermented medium of *C. acetivum*. First, an experiment in bottles was conducted with *C. acetivum*, reaching 1 g/L acetic acid in each bottle. Then, pure commercial acetic acid was added to reach concentrations between 5 and 35 g/L, and *R. toruloides* was cultivated in each flask with different acid concentrations. The results showed that inhibition started at approximately 18 g/L acetic acid, with a prolonged lag phase being observed. Concentrations exceeding 22 g/L significantly inhibited yeast growth. Complete substrate consumption was achieved in less than three days despite inhibition. The experiment allowed to conclude that the samples extracted from the *C. acetivum* bioreactor should not be diluted or have further acetic acid added in the third assay.

The third assay was set-up in order to check the potential of *R. toruloides* to accumulate lipids from acetic acid generated from syngas fermentation by the anaerobic bacterium *C. acetivum*. Figure 1 shows encouraging results in terms of growth of *R. toruloides* in the gas-fermented medium containing acetic acid, with no lag phase observed, although the consumption rate was slower than that observed in other of our related studies [3].

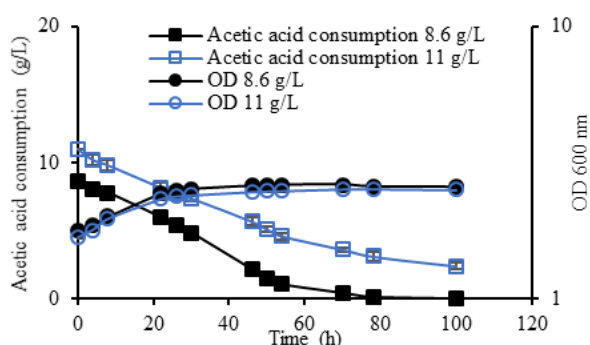


Figure 1. Growth (OD_{600nm}) and consumption of acetic acid by *R. toruloides* at various starting concentrations of acetic acid generated from *C. acetivum* anaerobic gas fermentation.

Table 1 shows a compilation of the results obtained at different initial acetic acid concentrations. According to the results, it was found that the initial acetic acid concentration affected the amount of lipid produced, with the highest total lipid content of 39.5 % (g/g DCW) achieved at an initial acetic acid concentration of 11 ± 0.5 g/L.

Table 1. Dry biomass of *R. toruloides*, maximum consumption rate of acetic acid, lipid content, lipid concentration, biomass yield, and lipid yield, at different initial acetic acid concentrations.

Initial acetic acid concentration (g/L)	Biomass (g/L)	Max. rate of acid consumption (g/L·h)	Lipid content % (g/gDCW)	Lipid concentration (g/L)	Biomass yield $Y_{(X/S)}$ (g/gC)	Lipid yield $Y_{(L/S)}$ (g/gC)
8.6 ± 0.5	2.56 ± 0.10	0.123	29.6	0.78	0.23 ± 0.02	0.088
11 ± 0.5	3.01 ± 0.04	0.113	39.5 ± 3.7	1.18 ± 0.12	0.35 ± 0.02	0.105 ± 0.015

Acknowledgements

This study was supported by the Spanish Ministry of Science and Innovation and European FEDER funding (PID2020-117805RB-I00). RRI thanks that Ministry for supporting his PhD contract financially (E-15-2019-0344365). The authors, who are members of the BIOENGIN group, are grateful to Xunta de Galicia for funding Competitive Reference Research Groups (ED431C 2021/55).

References

- [1] Á. Fernández-Naveira et al., Journal of Chemical Technology & Biotechnology, 92 (2017) 712-731.
- [2] R. Robles-Iglesias et al., Renewable and Sustainable Energy Reviews, 171 (2023) 113043.
- [3] R. Robles-Iglesias et al., Journal of CO₂ Utilization, 52 (2021) 101668.

The composition of lipids obtained from the yeast fermentation stage is crucial to assess possible applications, such as producing biodiesel or other fuels. Figure 2 illustrates the lipid profile obtained, showing a slightly dominant presence of oleic acid (C18:1) followed by palmitic acid (C16:0), with lower concentrations of stearic and linoleic acids. The experiment showed that, although palmitoleic acid (C16:1) was not detected, the high concentration of C18:1 in the lipid composition makes it highly suitable for biodiesel production. As a result, the study demonstrates that acetic acid produced by *C. acetivum* from C1-gas valorization can be efficiently converted into lipids with a fatty acid profile suitable for biodiesel production, indicating a high potential for biodiesel manufacture with this technique.

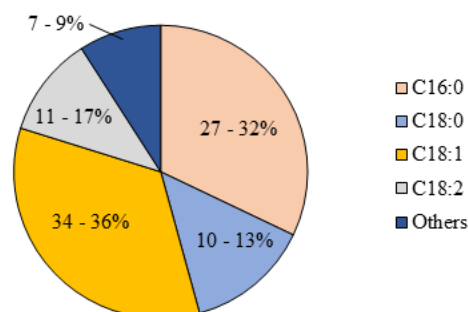


Figure 2. Average lipid composition obtained from different initial acetic acid concentrations.

Conclusions

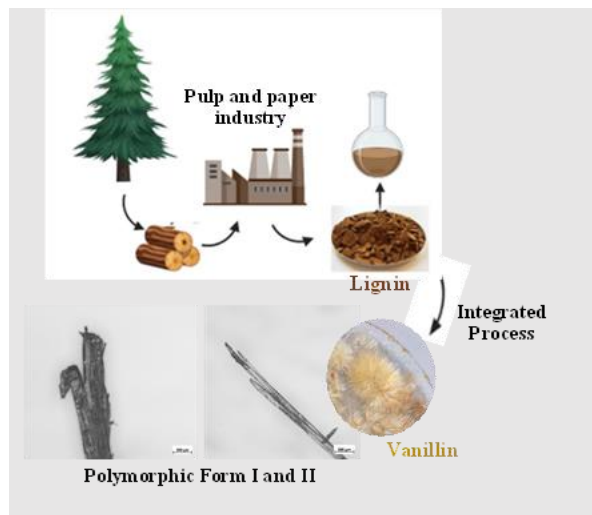
This research aimed to investigate the ability of the acetogenic bacterium *C. acetivum* to convert C1-gases, such as syngas, into acetic acid and evaluate the potential of using the fermented medium of *C. acetivum* for lipid production by the yeast *R. toruloides*. The results showed that syngas can be efficiently converted into acetic acid, and the resulting acetic acid can be used for lipid production by *R. toruloides*. However, the yeast started being inhibited at initial acetic acid concentrations around 18 g/L, and the acid was basically lethal at concentrations around 22 g/L and above. The study achieved encouraging results in terms of lipid content, with a maximum of 39.5 ± 3.7 % g/g dry cell weight, when the yeast was grown with 11 ± 0.5 g/L initial acetic acid concentration.

From sulphite liquor production to valorization: challenges in vanillin crystallization

C.A.E. Costa*, F. Casimiro, A.E. Rodrigues

LSRE-LCM - Laboratory of Separation and Reaction Engineering - Laboratory of Catalysis and Materials, Faculty of Engineering, University of Porto, Rua Dr. Roberto Frias, 4200-465 Porto, Portugal; ALiCE - Associate Laboratory in Chemical Engineering, Faculty of Engineering, University of Porto, Rua Dr. Roberto Frias, 4200-465 Porto, Portugal.

*carina.costa@fe.up.pt



An integrated process that is intended to produce added-value products, such as vanillin, by directing a stream of mother liquor from a pulp and paper mill has been developed over the years in LSRE/FEUP. In this process, vanillin obtained from lignin oxidative depolymerization is recovered using a combination of sequential steps of nano/ultrafiltration and adsorption/desorption experiments or ion-exchange processes. The final purification step of vanillin includes liquid-liquid extraction and crystallization.

In this work, different approaches for vanillin crystallization were performed, all of them using aqueous solutions rich in vanillin obtained from the integrated process applied to isolated lignin from softwood sulphite liquor. The main objective is to study the influence of the crystallization process on the yield, purity, and polymorphic forms of vanillin crystals.

Vanillin (4-hydroxy-3-methoxy-benzaldehyde) is a phenolic monomer with reactive methoxyl, hydroxyl, and aldehyde sites [1]. It has a strong aroma and is one of the most demanded ingredients in the flavor industry. In the global market, about 60 % of industrial vanillin is used as a food additive, while the remaining 40 % is used as cosmetic ingredients and pharmaceuticals [2]. The rising demand for vanillin for end-use industries is expected to substantially influence market growth in the next years. In 2016, the global demand for vanillin was about 18 600 tons and will grow by 6.2 % by 2025 [3]. Currently, the production of vanillin from wood accounts for about 15 % of its total production. Over the years, several methods have been employed to recover the vanillin in mother liquors, e.g., repeated recrystallization from methanol-water, distillation, and fractional precipitation of phenolate salts [4]. In LSRE/FEUP, an integrated process (Figure 1) to produce added-value products by directing a stream of mother liquor from biorefineries has been developed [5,6].

weight species. The permeate from nanofiltration proceeds to adsorption/desorption experiments and a fraction rich in vanillin is obtained. The final purification step, which includes liquid-liquid extraction and crystallization, represents a laborious task, and the final product could contain small amounts of impurities [14]. Crystallization is widely used as a method to isolate and purify products with specific physicochemical properties in pharmaceutical, food, fine chemicals, and bulk chemical industries.

This work studied the crystallization process applied to an aqueous solution rich in vanillin obtained from the integrated process applied to isolated lignin from softwood sulphite liquor [7]. Different approaches to cooling and evaporative vanillin crystallization were attempted. The crystallization yield and the vanillin crystals purity were determined (Table 1), and the thermal stability of different polymorphic forms obtained was analyzed. During the different crystallization processes, two distinct polymorphic forms of vanillin were observed: the stable Form I and the metastable Form II (Figure 2).

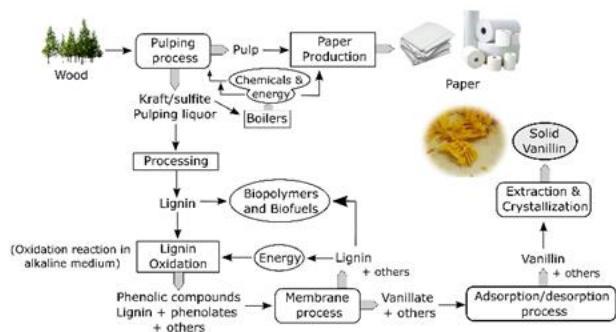


Figure 1. Scheme of the integrated process since the oxidation of lignin from pulping liquor until vanillin crystallization.

At the beginning of the process, lignin depolymerization is attained by oxidation in an alkaline medium using oxygen. The oxidized stream is submitted to ultra and nanofiltration to separate high molecular weight fractions from lower molecular

Table 1. Structural characteristics, purity, and yield of the vanillin polymorphic forms obtained from the different crystallization processes.

Crystallization process	Form	Color	Yield (%)	Purity (%)
Slow evaporation	I	Yellow	80	95
Cooling	I	Yellow	75	99
Swift cooling	II	White	52	98
Evaporation with heat	II	Yellow	55	95

From the slow evaporative and cooling process, vanillin crystallizes into stable polymorphic Form I with a yield of 80 and 75 %, respectively. For swift cooling and evaporation with heat, the crystallization process shows a lower yield, between 52 and 55 %, respectively, and gives origin to crystals with metastable Form II. It seems that, besides the influence of the crystallization process, the type of polymorphic form of vanillin formed also influences the process yield. The crystallization

processes that give origin to vanillin polymorphs of Form II, the metastable form, have lower yields.

The purity of the crystals that resulted from the evaporative crystallization is slightly lower than that from the cooling crystallization processes. From evaporation, the vanillin crystals present a purity of about 95 %, while for cooling processes the purity is slightly higher, with values around 99 %.

The melting points, observed in the DSC thermograms, of Form I and Form II of vanillin were found to be 82.6 °C and 81.0 °C, respectively. Proving that metastable Form II is less stable and highly energetic than stable Form I.

The polymorphic form of vanillin was found to be dependent on the crystallization method as well as the temperature variation during the process.

Acknowledgements

This work was financially supported by LA/P/0045/2020 (ALiCE), UIDB/50020/2020 and UIDP/50020/2020 (LSRE-LCM), funded by national funds through FCT/MCTES (PIDDAC).

References

- [1] C. Zhang et al., *Macromolecular Chemistry and Physics*, 216 (2015) 1816-1822.
- [2] P. Bajpai, *Biotechnology for Pulp and Paper Processing*, Springer, Singapore, (2018) 561-571.
- [3] G.A. Martão et al., *Trends in Food Science & Technology*, 109 (2021) 579-592.
- [4] O.Y. Abdelaziz et al., *ChemSusChem*, 15 (2022) e202201232.
- [5] A.E. Rodrigues et al., *An integrated approach for added-value products from lignocellulosic biorefineries*, Springer, 2018.
- [6] C.A.E. Costa et al., *Molecules*, 26 (2021) 4602-4623.
- [7] F.M. Casimiro et al., *International Journal of Biological Macromolecules*, 215 (2022) 272-279.

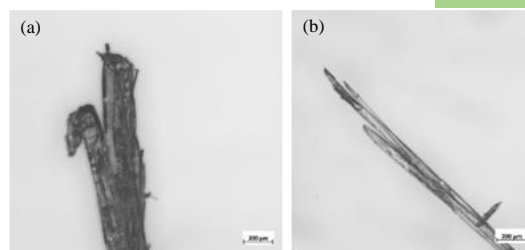


Figure 2. Microscope images of vanillin polymorph Form I (a) and Form II (b).

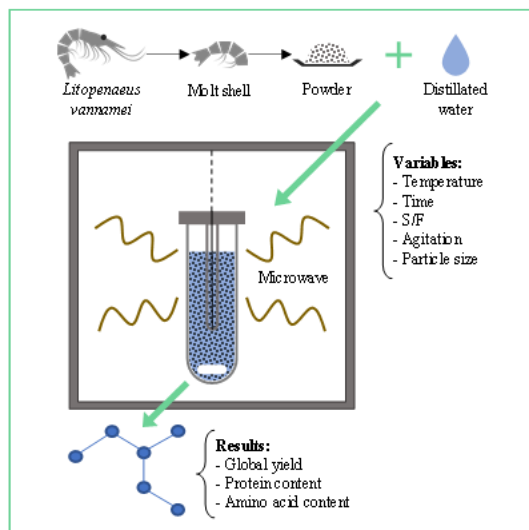
The evaporative and cooling crystallization processes studied in this work proved to be consistent and valuable considering the attaining of vanillin crystals. Moreover, each of the polymorphic forms of vanillin may have different industrial applications due to their different physicochemical properties.

Microwave extraction of proteins from *Litopenaeus vannamei* molt shell using only water as a solvent

*M.M. de-Souza-Ribeiro, H. Loya-Pérez, G.E. Alonso-Sánchez, S. Rodríguez-Rojo**

BioEcoUVa, Research Institute on Bioeconomy, PressTech Group, University of Valladolid, Valladolid, Spain; Dpt. of Chemical Engineering and Environmental Technology, Escuela de Ingenierías Industriales, Universidad de Valladolid, Valladolid, Spain.

*soraya.rodriguez@uva.es



This study aimed to apply microwave technique for the extraction of proteins from shrimp molt shell using water as the only solvent. The variables temperature, isothermal time, particle size, solid-liquid ratio (S/F) and stirring rate were studied to understand if they are significant variables. By varying the process parameters, it was possible to obtain an extraction yield of 16-31 g/100 g dry molt shell, extracted proteins of 3-7 g/100 g of dry molt shell, and extracted amino acids of 0.5-3 g/100 g dry molt shell. In addition, isothermal time was found to be the variable with the highest influence on the extracted protein content. The obtained results indicated the variables temperature, isothermal time, and S/F as significant variables for protein extraction, within the selected range.

Introduction

Crustacean production in 2022 represented 10% of world fisheries and aquaculture [1]. The consumption and production of shrimps generates as waste the cephalothorax and its exoskeleton (shell) [2]. The exoskeleton represents approximately 47% of the animal [2], and is a potential problem during the aquaculture process, since during the growth phases the molting process occurs with the exchange of the shell, releasing the old shell to the growth medium. These molt shells are not commonly valued, compared to the shell of the adult animal [3]. Currently the shrimp shell is used to obtain chitin [4]. However, the shell also contains other compounds of commercial interest, such as proteins (20-40%) [4]. During the conventional process, the proteins are separated from the shell using alkaline solutions (commonly sodium hydroxide solutions), which is not a sustainable process, and the protein obtained in this way cannot be reused [5]. To make the chitin extraction process more sustainable, some authors have studied the application of microwave technology, making the process more effective [6,7]. However, many of these processes use inorganic bases as extraction solvent.

Objective

In this context, this project aimed to study the use of microwave technology with only water as extraction solvent to obtain shrimp molt shell proteins.

Methods

For the extraction processes, the shrimp molt shell (supplied by the company Noray Seafood, Valladolid, Spain) was previously washed, dried in an oven at 105 °C for 24 h and grounded with a knife mill (SM 100, Retsch, Haan, Germany). The shell powder was initially characterized in terms of ash, protein, amino acids, fatty acids, and chitin content (Table 1).

A microwave oven with magnetic stirring and sensors of pressure and temperature (Monowave 300, Anton-Paar, Madrid, Spain) was used for all the experiments in closed system. Particle size distribution was evaluated by DLS (Mastersizer

2000, Malvern Panalytical, Malvern, UK). Stirring rate (N: 600 and 1000 rpm), temperature (T: 175 and 225 °C), isothermal time (t: 0, 10 and 20 min), solid-liquid ratio (S/F: 10 and 20 mL/g) and particle size (d_{90} : 483 and 125 μm) were studied as variables. The products were analyzed by the pH variation, extraction yield (X_0), proteins by BCA (bicinchoninic acid assay), and amino acids (AA) by ninhydrin method, all of them expressed as g per 100 g of dry molt shell. The process was carried out in duplicate. The results were statistically evaluated in the software statgraphics 19[®] 19.4.01 version (Statgraphics Technologies, Inc., VA, US) by one-way analysis of variance (ANOVA) with a statistical significance level of 5% by Tukey's test.

Table 1. Chemical composition of the shrimp molt shell

Compound	(g/100 g dry molt shell)
Ash	53.7 \pm 0.5
Protein	10.6 \pm 0.4
Amino acid	1.37 \pm 0.12
Fatty acid	3.8 \pm 0.9
Chitin	17.8 \pm 0.7

Results

Adding the raw material to the water (without applying any process) increased the pH of the water, making it alkaline (9.53 \pm 0.08), probably related to the release of minerals from the shell (CaCO_3). After the extraction processes the pH decreased to (8.8 \pm 0.2), which may be related to the release of proteins and other compounds (chitin and derivatives). This analysis indicates the possibility of using water instead of inorganic bases for this raw material, since the minerals contained in the shell can basify the medium.

For the effect of stirring rate the results indicate that increasing the rotation did not show any significant effect in terms of extracted proteins (6.1 \pm 0.3 g per 100 g of dry molt shell at 600 rpm and 6.2 \pm 0.2 g per 100 g of dry molt shell at 1000 rpm) and a lower stirring rate showed higher co-extraction (31 \pm 4 g per 100 g of dry molt shell at 600 rpm and 28.2 \pm 0.7 g per 100 g of dry molt shell at 1000 rpm) and dispersion of the data. Therefore,

a stirring rate of 1000 rpm was fixed to study the rest of variables. For the evaluation of the temperature effect, the results indicate that in terms of extracted protein, the temperature had no significant influence in this studied range (Table 2). Total proteins, considered as the sum of BCA analysis and AA increased from 7.4 ± 0.55 to 9.6 ± 0.4 g/100 g of dry molt shell. Increasing temperature promotes a significant increase in the content of free amino acids, which suggests a breakdown of the protein chain under such conditions (combination of temperature and time). In terms of global yield, results have shown that a higher co-extraction of other compounds may have occurred for a temperature of 225 °C.

Table 2. Effect of Temperature. (N = 1000 rpm, t = 10 min, S/F = 20 mL/g, $d_{90} = 483 \mu\text{m}$)

T (°C)	X_0	Extracted Proteins	AA
	(g/100 g of dry molt shell)		
175	22.8 ± 0.9^a	6.6 ± 0.5^a	0.80 ± 0.05^a
225	28.2 ± 0.7^b	6.2 ± 0.2^a	3.4 ± 0.2^b

^{a,b} Different lowercase letters in the same column indicate significant difference ($p < 0.05$).

Isothermal time was counted only after reaching the studied temperature, being the heating periods shorter than 90 s in all the experiments, where the equipment adapted the microwave power based on the set temperature to have rapid heating. As is shown in Table 3, the time of 10 and 20 minutes did not show significant differences for the X_0 . However, in terms of extracted protein and amino acid, the 10 min time performed better than the 20 min time, and it is possible to see a tendency for increased protein breakdown with a longer isothermal time. Based on these results it was possible to verify that the time of 20 min seems to be a long time in this temperature.

Table 3. Effect of isothermal time. (T = 175 °C, N = 1000 rpm, S/F = 20 mL/g, $d_{90} = 483 \mu\text{m}$)

t (min)	X_0	Extracted Proteins	AA
	(g/100 g of dry molt shell)		
0	16.8 ± 0.4^a	3.5 ± 0.2^a	0.54 ± 0.02^a
10	22.8 ± 0.9^b	6.6 ± 0.5^b	0.80 ± 0.05^b
20	23.9 ± 0.6^b	5.1 ± 0.5^c	1.06 ± 0.11^c

^{a,b,c} Different lowercase letters in the same column indicate significant difference ($p < 0.05$).

The effect of particle size has been studied modifying milling conditions to obtain two particle sizes: $d_{90} = 483$ and $125 \mu\text{m}$, and the results are included in Table 4. Based on the results (Table 4) it was verified that the reduction in the particle size has no effect on the improvement of the extracted protein content, under the studied conditions, however the decrease in particle

size has led to higher co-extraction of other compounds. Considering this co-extraction, the higher-energy demand of the milling pretreatment to achieve smaller particle size, and the difficulties derived to handle this smallest particle size in subsequent downstream steps, the particle size of $483 \mu\text{m}$ was selected for the next studies.

Table 4. Effect of particle size. (T = 175°C, N = 1000 rpm, t = 10 min S/F = 20 mL/g)

$d_{90} (\mu\text{m})$	X_0	Extracted Proteins	AA
	(g/100 g of dry molt shell)		
483	22.8 ± 0.9^a	6.6 ± 0.5^a	0.80 ± 0.05^a
125	28.4 ± 1.2^b	5.8 ± 0.3^b	0.92 ± 0.05^b

^{a,b} Different lowercase letters in the same column indicate significant difference ($p < 0.05$).

For the S/F analysis, the S/F was varied at 10, 20 and 40 mL/g, and results are shown in Table 5. The results indicate that increasing the S/F from 20 to 40 led to a higher co-extraction.

Table 5. Effect of S/F. (T = 175°C, N = 1000 rpm, t = 0, $d_{90} = 483 \mu\text{m}$)

S/F (mL/g)	X_0	Extracted Proteins	AA
	(g/100 g of dry molt shell)		
10	16.4 ± 0.5^a	2.5 ± 0.2^a	0.58 ± 0.06^a
20	16.8 ± 0.4^a	3.5 ± 0.2^b	0.54 ± 0.02^a
40	18.65 ± 0.04^b	4.2 ± 0.4^c	0.58 ± 0.03^a

^{a,b} Different lowercase letters in the same column indicate significant difference ($p < 0.05$).

The results obtained in these experiments demonstrated that temperature, isothermal time, and S/F are variables that need to be studied in an experiment design to optimize operational condition for microwave assisted extraction of proteins using only water.

Conclusions

This study showed that the use of microwave technology with water as the only solvent is an effective method to extract proteins from shrimp molt shells with the possibility of using these proteins in industrial sectors, which is a differential of this technique compared to the conventional alkaline extraction method. Besides that, this technique presents shorter process times and does not generate harmful waste compared to the conventional process. Following these results, an experimental design is being carried out and experimental results will be shown during the congress. In addition, a study will also be conducted to identify the co-extracted compounds, and the molecular weight of the extracted proteins.

Acknowledgements

This work/project (project PID2020-119481RA-I00) was supported by the Regional Government of Castilla y León and the EU-FEDER program (CLU-2019-04). M.M. de-Souza-Ribeiro thanks the Department of Education of the Regional Government of Castilla y León and the European Social Fund Plus (ESF+) for his doctoral grant.

References

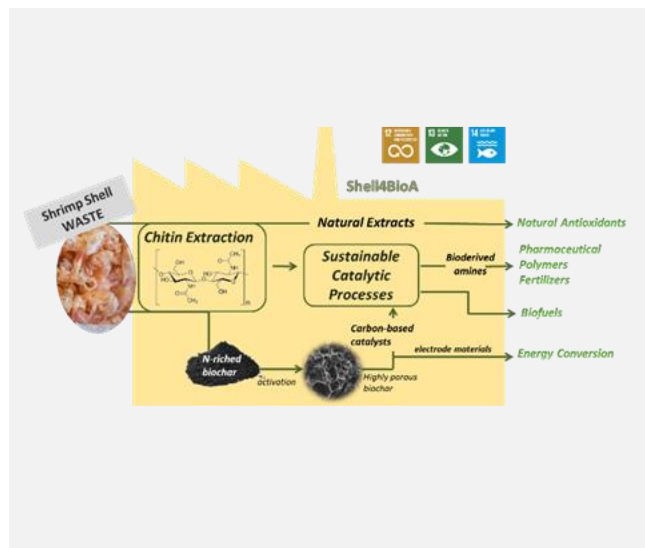
- [1] FAO, World Food and Agriculture – Statistical Yearbook 2022, FAO, Rome, 2022.
- [2] N. Mezzomo et al., Journal of Supercritical Fluids, 74 (2013) 22-33.
- [3] P.T.D. Phuong et al., Waste Biomass Valorization, 13 (2022) 823-830.
- [4] X. Hu et al., ACS Omega, 5 (2020) 19227-19235.
- [5] H. El Knidri et al., International Journal of Biological Macromolecules, 120 (2018) 1181-1189.
- [6] H. EL Knidri et al., International Journal of Biological Macromolecules, 139 (2019) 1092-1102.
- [7] H. El Knidri et al., Process Safety and Environmental Protection, 104 (2016) 395-405.

Shrimp shells waste biorefinery: From the extraction to the production of designed biochar catalysts, biofuels, bioproducts and energy conversion

I.S. Marques¹, R. Matos¹, M.M. Moreira², E. Surra², D.M. Fernandes¹, A.F. Peixoto^{1*}

¹LAQV/REQUIMTE, Departamento de Química e Bioquímica, Faculdade de Ciências, Universidade do Porto, Rua do Campo Alegre s/n, 4169-007 Porto, Portugal; ²LAQV/REQUIMTE, Instituto Superior de Engenharia do Porto, Instituto Politécnico do Porto, Rua Dr. António Bernardino de Almeida, 431, 4249-015 Porto, Portugal.

*andrea.peixoto@fc.up.pt



Circular bioeconomy is emerging motivated by a variety of sustainability concerns. Biomass valorisation to value-added chemicals is rapidly emerging as the basis for future Chemical Industry. In this context, biorefinery concept is used to define facilities in which biomass is converted through sustainable (catalytic) technologies to a wide range of bioproducts. Shrimp shell waste (SSW) is an abundant natural source of N-containing products and materials and should deserve adequate attention within next generation of biorefineries schemes. Here in, we present and discuss the results obtained in the scope of the Shell4BioA project regarding the extraction of bioactive compounds and chitin using advanced extraction technologies, the production of N-derived biochar materials (catalysts/electrocatalysts) obtained from SSW to be used in catalytic reactions for production of biofuels and N-derived bioproducts and, energy conversion (Oxygen oxygen reduction reaction, ORR) contributing thus to a future innovative and disruptive chemical industry aligned with green chemical principals and sustainable development.

Introduction

Despite the abundance of carbon in nature, a significant portion of the existing biomass carbon materials in livestock, agriculture, and marine fishery industry are currently being wasted. Most of shrimp shell waste (SSW) is disposed into landfills or back into the ocean being associated with several environmental issues. Because of the reactive amino-group, chitin-derivatives can serve as novel platform molecules for the synthesis of a plethora of industrially valuable chemicals and materials [1,2]. Following the concept of biorefinery and circular bioeconomy, the Shell4BioA project arise to meet these challenges targeting the extraction of bioactive compounds, chitin or chitosan from SSW using advanced extraction methodologies [3,4]; production of designed biochar materials from SSW for the production of biofuels[5], biobased products and for energy conversion using electrochemical processes, including the oxygen reduction reaction (ORR)[6]. Finally the environmental impacts of the extraction and production of SSW-biochar catalysts will be analysed in a Life Cycle Analysis (LCA) perspective.

Methods

Shrimp shells obtained from Portuguese fishery industry (Mar Cabo company) were frozen, dried, grounded (particle size < 0.5 mm) and stored in sealed bags at room temperature until use. Extractions of SSW were performed following the methodologies previously developed by our group for the extraction of natural antioxidants from vineyard pruning waste [3,4]. Obtained extracts were further characterized with different colorimetric methods, namely total phenolic (TPC) and carotenoid content (TCC), ABTS radical scavenging activity and Ferric Reducing Antioxidant power; The remaining solid was treated with organic acids (including citric acid) and hydrochloric acid to obtain the purified chitin.

Biochar-based catalysts (sulfonic acid-catalysts and metal supported catalysts) were prepared according to modified procedures from literature [5,6]. Metals or metal oxides were supported on the N-doped SSW-biochar using co-precipitation, wet impregnation and ball milling mechanic impregnation [6]. The prepared materials were characterized by SEM, Raman, XPS and XRD and sulfonic acid-catalysts by potentiometric titration All catalysts have been used in catalytic reactions for the production of biobased products: ethyl levulinate, furfuryl alcohol, methylfuran and bio-based amines [5,6]. Some of the prepared materials, namely the N-doped and metal/metal oxide supported biochars, were also applied as electrocatalysts in ORR in KOH 0.1 mol dm⁻³ electrolyte.

The environmental benefits generated by the production of biochar-based catalysts are assessed according to ISO 14040 and ISO 14044 standard in SimaPro 9.5 software package equipped by Ecoinvent 3.9.1 database. The results obtained are compared to the environmental impacts associated to equivalent commercial catalysts.

Results

From the tested techniques to recover antioxidant compounds from SSW, namely ultrasound assisted extraction, subcritical water extraction and conventional extraction, SWE at 200°C presented the best results, with a TPC and TCC of 5.36 ± 0.07 mg GAE/g dw and 59.8 ± 1.0 µg carotenoids/g dw. The reported values were at least 5-fold higher than the values reported for the CE (1.2±0.3 mg GAE/g dw and 9.0±0.1 µg carotenoids/g dw, respectively). Work is under progress to try to incorporate the best extract in chitosan-based biofilms.

Regarding the valorization of SSW through biochar catalysts production, characterization results revealed the correct preparation of the original, N-doped biochars and catalysts. XPS analysis, in particular, showed that SSW already contained small amounts of N and S, which significantly increased during the

doping procedures. All the prepared N-doped biochars and metal supported biochars were catalytic active towards ORR. Indeed, the resulting hybrid materials showed excellent electrocatalytic performance in alkaline medium, displaying faster kinetics and lower overpotentials compared with the original biochar and even outcompeted state-of-the-art Pt-based catalysts in terms of selectivity towards the 4-electron reduction and Tafel slopes. In particular, a hybrid catalyst consisting of SSW-derived biochar and Co_3O_4 nanoparticles achieved E_{onset} of 0.85 V vs. RHE, j_L of -3.45 mA cm^{-2} , n_{O_2} of 3.50 and a Tafel slope of only 35 mV dec^{-1} . Ru dispersed on SSW-derived biochar also showed a very promising electrocatalytic performance, obtaining E_{onset} of 0.84 V vs. RHE, j_L of -3.65 mA cm^{-2} , n_{O_2} of 3.32 and a Tafel slope of 81 mV dec^{-1} .

Ethyl levulinate (EL) was obtained from 5-HMF with (EL yield = 90%) at 130°C , after 6h reaction, over the sulfonic acid functionalized biochar prepared from sulfanilic acid with an acidity of $2.0 \text{ mmol H}^+/\text{g}$, determined by potentiometric titration. The inventory data collection and preparation of an LCA modeling is ongoing, based on the flowsheet of the novel process developed. The research strategies adopted as well as the

laboratorial approach are going to be supported by sustainability criteria and driven towards the most environmentally advantageous solution during every step of the laboratorial experiments [7].

Conclusions

Seafood waste should be considered wealth and its valorisation should be aligned with circular economy. The use of SSW as raw-material for different value-chains was demonstrated by the different approaches and applications here presented. The use of SSW as bioactive compounds and chitin derivatives sources was evaluated and the results demonstrated that the extraction technologies and type of solvents affect the target final products. In this research a class of new promising (electro)catalysts were developed based on SSW for bifunctional applications biomass valorisation and energy conversion as an important contribution to the future of biorefineries implementation. The LCA perspective suggests that the production process of the novel biochar-based catalysts is an environmentally promising alternative to the production processes of equivalent commercial materials obtained from non-renewable precursors.

Acknowledgements

This work was funded by Portuguese funds through Fundação para a Ciência e a Tecnologia (FCT/MCTES) in the framework of the project EXPL/BII-BIO/0436/2021. Thanks are also due to the projects UIDB/50006/2020, UIDP/50006/2020 and LA/P/0008/2020. I.S.M. thanks FCT for her working contract in the framework of Project EXPL/BII-BIO/0436/2021. A.F.P., D.M.F. and M.M.M. thank FCT for funding through the Individual Call to Scientific Employment Stimulus (Refs. 2020.01614.CEECIND/CP1596/CT0007, 2021.00771.CEECIND/CP1662/CT0007 and CEECIND/02702/2017, respectively). R.M. thanks FCT for the PhD fellowship 2020.05342.BD. We also thank the company Mar Cabo for providing shrimp shells.

References

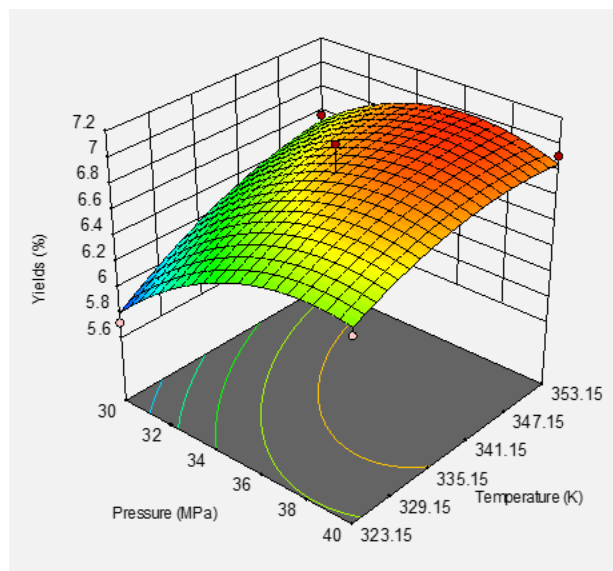
- [1] M.J. Hülsey, Green Energy & Environment, 3 (2018) 318-327.
- [2] N. Yan et al., Nature, 524 (2015) 155-157.
- [3] O. Dorosh et al., Foods, 9 (2020) 872.
- [4] O. Dorosh et al., Molecules, 25 (2020) 1739.
- [5] A.F. Peixoto et al., Fuel, 303 (2021) 121227.
- [6] I.S. Marques et al., Catalysis Today, 418 (2023) 114080.
- [7] O. Dorosh et al., ACS Sustainable Chemistry & Engineering, 11 (2023) 8084-8095.

Modelling and optimisation of supercritical CO₂ extraction of fatty acids from rice bran

J.P. Coelho^{1,2}, R.M. Filipe^{1,3*}, M.P. Robalo^{1,2}, R.P. Stateva⁴

¹Instituto Superior de Engenharia de Lisboa, Instituto Politécnico de Lisboa, Rua Conselheiro Emídio Navarro 1, 1959-007 Lisboa, Portugal; ²Centro de Química Estrutural, Instituto Superior Técnico, Universidade de Lisboa, Av. Rovisco Pais 1, 1049 001 Lisboa, Portugal; ³Centro de Recursos Naturais e Ambiente (CERENA), Instituto Superior Técnico, Universidade de Lisboa, 1049-001, Lisbon, Portugal; ⁴Institute of Chemical Engineering, Bulgarian Academy of Sciences, Academic Georgi Bontchev str., 1113 Sofia, Bulgaria.

*rfilipe@isel.ipl.pt



This study presents an optimisation strategy for the recovery of oil from *Japonica* Luna rice bran using supercritical carbon dioxide (scCO₂), based on design of experiments. Initially, a 2⁴⁻¹ two level fractional factorial design was used, and pressure, temperature, and scCO₂ flow rate were identified as the significant variables. Yield, total flavonoids content, and total polyphenols content were the response functions used to analyse the quality of the extracts recovered. A central composite design was then used to study the effects of the significant variables on the responses and create quadratic surfaces that optimize the latter. Finally, two mass transfer models were applied to determine the mass transfer coefficients and assess the cumulative extraction curves. The results obtained applying two different solution techniques for the models were analysed and a good fitting between the experimental and simulated were obtained.

Introduction

Rice is the world's leading cereal crop in 2021/22, and the by-product rice bran contains 8-20 % by weight of bio-oil with an excellent calorific value for energy applications. It is also a rich source of vitamins, antioxidants, and minerals [1,2]. Therefore, the integral use of these grains can add value to their production. For example, the processing of white rice (*Oryza sativa* L.), the main variety used in the rice milling industry, generates large quantities of solid waste from the removal of the outer layers of the grain, consisting mainly of two by-products: rice bran (8-10 %) and rice husk (about 20 %) [1,3]. The huge quantities of waste generated by this industry pose a significant challenge to its economic and sustainable management. Hence, instead of disposing of these quantities, processes that can be used to recover high value-added products should be explored, as their successful implementation will not only ensure the valorisation of bio-waste but will also contribute to a sustainable industrial production.

Rice bran oil (RBO) is often extracted using *n*-hexane. However, the oil obtained contains several impurities, such as phosphorus and wax, requiring further refining. It is therefore important to use processes that apply green, sustainable, and environmentally friendly technologies, such as pressurised fluids, that perform better and render better quality RBOs extracts with lower levels of impurities.

The influence of the predominant extraction processes, namely cold press, solvent, and scCO₂ extraction on the quality and composition of RBO obtained from different rice varieties was analysed by several authors [4,5].

A number of studies examined and reported the effect of scCO₂ extraction parameters (pressure, temperature, scCO₂ flow rate, and co-solvents) on the quality of the RBO and its composition, in terms of antioxidant activity, fatty acid profile, bioactive and

phytochemical constituents such as phytosterols, tocopherols and γ -oryzanol [1,3,6].

In this work, the optimisation of the operating conditions for the RBO extraction by scCO₂ from rice variety *Japonica* Luna was carried out using Design of Experiments (DoE), followed by the application of two mass transfer models to simulate the extraction conditions.

Methods

An important advantage of the DoE method is that it maximizes the extent of suitable information gained with the minimum number of experiments [7] allowing the optimisation of the process operational parameters.

The initial application of Fractional Factorial Design (FFD) and subsequently a Central Composite Design (CCD) allowed to determine the optimal values of the operating conditions of the scCO₂ extraction process. The response parameters delineated were yield of the oil recovered, total phenolic and flavonoids contents of the RBOs. The fatty acid profile of the oils was characterized by GC-FID.

The extraction kinetics results from the assays were modelled by applying two mass transfer models to simulate the experimental cumulative extraction yield curves obtained. Two different solution techniques were used to solve the models. The first one solved the analytically integrated model equations using Microsoft Excel, and the mass transfer parameters were found using Microsoft Excel Solver. The second one used gPROMS ModelBuilder [8], where the ordinary differential equations were numerically integrated, and a parameter estimation tool used to estimate the mass transfer parameters.

Results

It was found that the acids in largest quantities in the RBO are C16:0 (15-16 %), C18:1 (41 %), and C18:2 (38-39 %).

The markers in Figure 1 show the extraction yield points obtained experimentally for different operating conditions, namely pressure, temperature, and CO₂ flow rate. A positive but uneven effect on the extraction rate is observed as each of the three parameters studied is increased.

The extraction yield curves obtained with the two models are also shown in Figure 1, together with the experimental results. The mass transfer coefficients were evaluated, and it was shown that their values are in a good agreement with those found in the literature for similar matrices.

Conclusions

The operating conditions for the RBO extraction with scCO₂ from rice variety *Japonica* Luna were optimised using DoE. The experimental extraction yield results were then used to apply two mass transfer models and simulate the extraction yield curves under different conditions. The effect of the operating conditions was analysed, and the obtained mass transfer

coefficients were found to agree well with those previously reported for similar matrices.

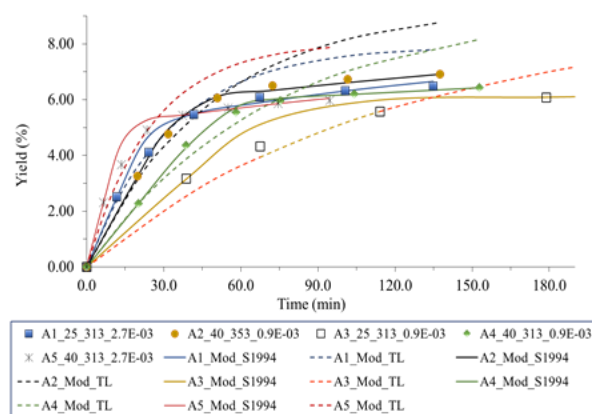


Figure 1. Extraction yield curves representing the influence of pressure (MPa), temperature (K) and CO₂ flow rates (kg/min), on RBO yield, as a function of time. The symbols are the experimental data, and the line the predictions by the models, for cases A1 to A5.

Acknowledgements

The authors acknowledge the funding received from the European Union's Horizon 2020 research and innovation programme under the Marie Skłodowska-Curie grant agreement No 778168. J. P. Coelho and M. P. Robalo are thankful to Centro de Química Estrutural a Research Unit funded by Fundação para a Ciência e Tecnologia (FCT) through projects UIDB/00100/2020 and UIDP/00100/2020. Institute of Molecular Sciences is an Associate Laboratory funded by FCT through project LA/P/0056/2020. R. M Filipe gratefully acknowledges the support of FCT through CERENA project UIDB/04028/2020.

References

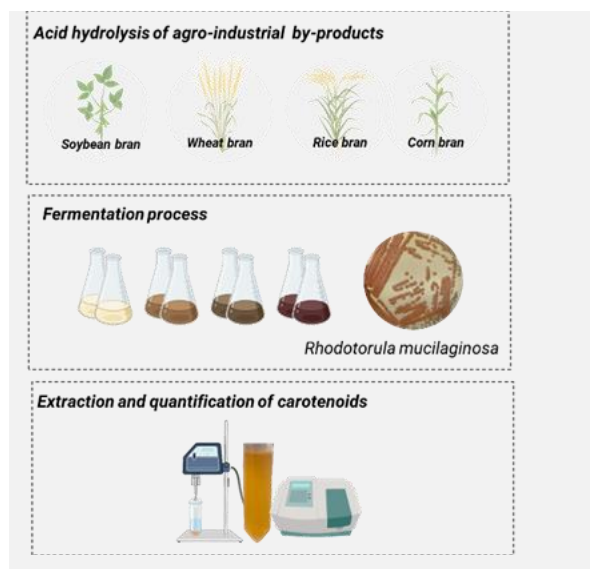
- [1] I. Okajima et al., *Energies*, 15 (2022) 2594.
- [2] N. El Boulifi et al., *Renewable Energy*, 53 (2013) 141-147.
- [3] T. Pinto et al., *Separations*, 8 (2021) 115.
- [4] S. Mingyai et al., *Journal of Oleo Science*, 66 (2017) 565-572.
- [5] S. Mingyai et al., *Journal of Oleo Science*, 67 (2018) 135-142.
- [6] J.P. Coelho et al., *ChemEngineering*, 6 (2022) 1-16.
- [7] C.P. Santos et al., *Journal of Chemometrics*, 33 (2019) 1-18.
- [8] Process Systems Enterprise, www.psenterprise.com/products/gproms 1997-2020.

Valorization of grain and cereal processing by-products as yeast substrates for carotenoids production

T.R. Balbino^{1*}, S. Sánchez-Muñoz¹, S.C. Inácio¹, G.C. Almeida¹, J.C. dos Santos¹, J.F.B. Pereira², S.S. da Silva¹

¹University of São Paulo, Engineering School of Lorena, Department of Biotechnology, Estrada Municipal do Campinho, n100, 12602-810, Lorena, SP, Brazil; ²University of Coimbra, CIEPQPF, Department of Chemical Engineering, Rua Sílvio Lima, Pólo II, 3030-790 Coimbra, Portugal.

*tbalbino@usp.br



Carotenoids are high-value-added products that can be used as active ingredients in various industries, such as food, pharmaceutical and cosmetic. These natural pigmented compounds have special properties (e.g., antioxidants and antimicrobials), which are highly valued in the market. Despite the great demand and variety of applications for carotenoids, the high cost of biotechnological production is still the main obstacle that makes microbial carotenoids less competitive in the market when compared to synthetic pigments. To improve the economic viability of bioprocesses, in this work, it was used low-cost raw materials, namely, agro-industrial by-products generated from the cultivation and processing of grains and cereals, to produce microbial carotenoids. Hydrolysates of soybean, wheat, corn, and rice bran were evaluated as cultivation media for producing carotenoids by the yeast *Rhodotorula mucilaginosa*. The main promising nutritional low-cost feedstock was rice bran.

Introduction

Different by-products are generated in the industrial processing of grains and cereals, which are rich sources of proteins and carbohydrates. These by-products are often burned in industries or improperly discarded in the environment, practices that generate environmental problems [1,2]. Considering the rich composition of these by-products, the use of bran as a source of carbon, nitrogen, and nutrients in bioprocesses becomes an interesting alternative to improve the economic feasibility and the sustainable factor of the overall process of obtaining bioproducts with high added market value. Among the highly valued microbial compounds, a special interest is given to carotenoids. These natural pigments are a sustainable alternative to synthetic compounds with great commercial interest for food and non-food applications, such as by the cosmetic and textile industries. Carotenoids are high-value-added products that can be used as active ingredients, mainly due to special properties such as antioxidant and antimicrobial activities, highly valued in the market [3]. The objective of this study was to evaluate the potential of the use of agro-industrial by-products (brans) to obtain carotenoids using *R. mucilaginosa* yeasts.

Methods

Initially, acidic hydrolysis of brans was carried out in an autoclave, by adding 2% of sulfuric acid to 15% (w/v) total solids loading and by reacting at 121 °C for 60 min. This approach was used to produce soybean bran hydrolysate (SBH), wheat bran hydrolysate (WBH), rice bran hydrolysate (RBH), and corn bran hydrolysate (CBH).

For the yeast production of carotenoids assays, the initial concentration of carbohydrates (sum of glucose, xylose, and arabinose) of all hydrolysates was standardized for about 11 g/L and the initial pH of each one adjusted to 5.5 by adding sodium hydroxide micro pearls. Then, Erlenmeyer-type flasks (250 mL)

containing 60 mL of SBH, WBH, RBH, or CBH were inoculated with previously activated cells of *Rhodotorula mucilaginosa* and incubated at 30 °C and 300 rpm for 72 h.

Samples were collected during the growth to determine: cellular biomass concentration; total carotenoids content; maximum specific growth rate (μ_{max} , h⁻¹); carotenoids yield in relation to substrate consumption ($Y_{P/S}$, g_P/g_S); and biomass growth in relation to the substrate consumption ($Y_{X/S}$, g_X/g_S).

Since carotenoids are produced intracellularly, these were properly subjected to a cell-disruption process. Therefore, the harvested cell pellets were dried at 60 °C for 24 h. Afterwards 0.1 g of dry cells were resuspended in 10 ml of methanol: acetone solution (7:3, v/v) and homogenized by ultrasonication with cycles of 20 s ON/5 s OFF for a total of 10 min to achieve a complete cell disruption and the release of intracellular carotenoids. The cells debris were separated by centrifugation, the colored supernatants (carotenoid-rich extracts) were collected and the total carotenoids concentration quantified as β -carotene equivalent using calibration curves of a β -carotene standard solution in a Thermo Scientific® UV-Vis spectrophotometer (model Genesis 10S, China).

Results and Discussion

After the preparation of the hydrolysates, the yeast was inoculated in the SBH, WBH, RBH, and CBH and cultivated for the carotenoids production. It was observed that the yeast grew and produced carotenoids using all bran hydrolysates as the sole source of carbon, nitrogen, and nutrients, with no steps required for culture medium detoxification or supplementation.

Concerning the production of yeast cell biomass, similar patterns were observed when using SBH, WBH, and RBH, with final cell concentrations ranging from 20 to 30 g/L and specific velocities maximum growth (μ_{max}) around 0.25 to 0.27 (h⁻¹). The highest cell biomass concentration (29.74 g/L) was

achieved with the yeast cultivation in SBH media. Contrarily, when using WBH, the yeast *R. mucilaginosa* showed lower final production of cell biomass and μ_{max} (9.75 ± 0.52 g/L and 0.16 ± 0.01 h⁻¹, respectively) (cf. Figure 1).

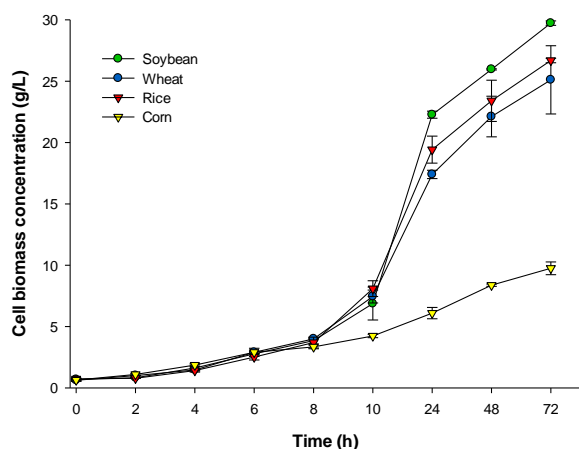


Figure 1. Cell biomass concentration (g/L) during cultivation of *R. mucilaginosa* using Soybean Bran Hydrolysate; Wheat Bran Hydrolysate; Rice Bran Hydrolysate, and Corn Bran Hydrolysate at 30 °C and 300 rpm for 72 h.

As shown in Figure 2, RBH and CBH were the growth media that enhanced the production of carotenoids after 72 h of *R. mucilaginosa* cultivation (105.55 and 105.21 $\mu\text{g/g}$, respectively), whereas cultivation in SBH and WBH resulted in a carotenoids production of circa 1.4-times lower than that of RBH and CBH. Evaluating fermentations in SBH and WBH, it was observed that the yeast *R. mucilaginosa* preferred the primary metabolism, directing the greater expenditure of energy to cell growth, with $Y_{X/S}$ greater than $Y_{P/S}$, consistent with the low values of specific concentration of total carotenoids observed. However, due to the higher biomass production, the concentration of total carotenoids per volume of culture medium were higher when using the SBH. On the other hand, when used CBH as growth

medium, a small production of cellular biomass was observed, resulting in low $Y_{X/S}$. The high specific concentration of total carotenoids was achieved in CBH, similar to that obtained in RBH and higher than SBH and WBH. When using RBH, the yeast showed similar $Y_{P/S}$ and $Y_{X/S}$, with similar metabolic activities for primary and secondary metabolisms. The highest concentration of total carotenoids per volume of growth medium was obtained when using RBH, showing the high potential of using rice bran as a substrate for the biopigments production.

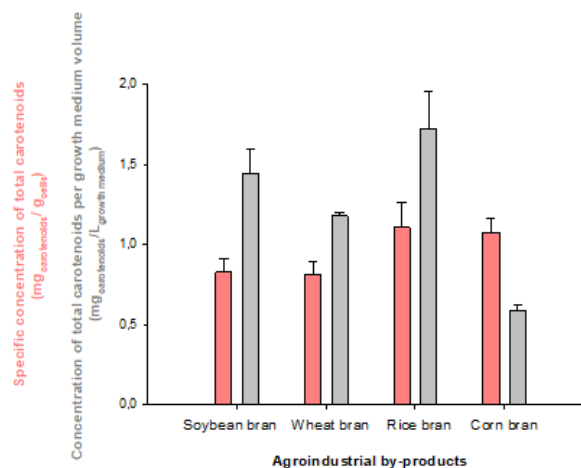


Figure 2. Specific concentration of total carotenoids and concentration of total carotenoids per growth medium volume observed after 72 h of cultivation of *R. mucilaginosa* using Soybean Bran Hydrolysate; Wheat Bran Hydrolysate; Rice Bran Hydrolysate, and Corn Bran Hydrolysate.

Conclusions

Despite the divergences in the metabolism of the yeast *R. mucilaginosa*, this work demonstrated that is possible of using four different types of bran for microbial growth and production of carotenoids, with a high potential of RBH. This works shows the potential of this yeast species for developing biorefineries for producing valuable biomolecules using low-cost by agro-industrial by-products as nutritional feedstocks.

Acknowledgements

This work was financed by the Fundação de Amparo à Pesquisa do Estado de São Paulo (FAPESP – 2016/10636-8); Conselho Nacional de Desenvolvimento Científico e Tecnológico (CNPq – 303943/2017-3); Coordenação de Aperfeiçoamento de Pessoal de Nível Superior - Brasil (CAPES - Finance Code 001). This work is part of the project “INCT Yeasts: Biodiversity, preservation and biotechnological innovation”, funded by CNPq, Brasília, Brazil, grant #406564/2022-1. CIEPQPF is supported by the Fundação para a Ciência e Tecnologia (FCT) through the projects UIDB/EQU/00102/2020 and UIDP/EQU/00102/2020.

References

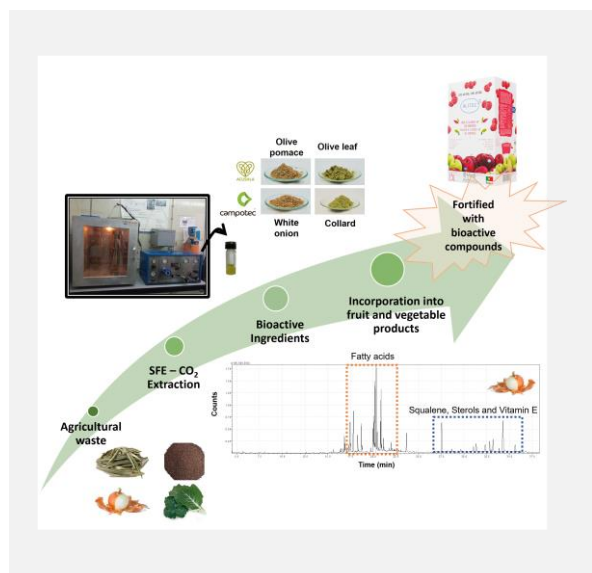
- [1] E.R. Abaide et al., Biomass Bioenergy, 120 (2019) 240-256.
- [2] M. Peanparkdee, S. Iwamoto, Trends in Food Science and Technology, 86 (2019) 109-117.
- [3] L.C. Foong et al., World Journal of Microbiology and Biotechnology, 37 (2021) 1-11.

Biovalorization of agricultural by-products obtained through green extraction methodology

I.M. Martins^{1,2*}, *A. Ribeiro*^{1,2}, *Y.A. Manrique*^{1,2}, *R. França*^{1,2}, *L. Rocha*^{1,2}, *R.C. Calhelha*³, *C. Caleja*³, *E. Pereira*³, *L. Barros*³, *M.M. Dias*^{1,2}

¹LSRE-LCM - Laboratory of Separation and Reaction Engineering – Laboratory of Catalysis and Materials, Faculty of Engineering, University of Porto, Rua Dr. Roberto Frias, 4200-465 Porto, Portugal; ²ALiCE - Associate Laboratory in Chemical Engineering, Faculty of Engineering, University of Porto, Rua Dr Roberto Frias, 4200-465 Porto, Portugal; ³Centro de Investigação da Montanha (CIMO), Instituto Politécnico de Bragança, Campus de Santa Apolónia, 5300-253 Bragança, Portugal.

*isa@fe.up.pt



The world population is increasing, and consequently, it will be necessary to increase food production to meet its needs. This results in the intensification of food waste, which causes a loss of resources and has a considerable environmental impact due to the numerous processes involved in the food life cycle. Therefore, finding methodologies capable of adding commercial value to these residues is crucial.

The present work aims to evaluate the bioactivity of extracts using agricultural residues of olive pomace, olive leaf, white onion and collard greens. These agricultural by-products are rich in bioactive compounds with functional properties. To increase the selectivity and preserve the substances of interest, supercritical fluid extraction using carbon dioxide as solvent (SFE-CO₂), a sustainable and green technology, was used.

In the future, it is expected to incorporate these bio-compounds into food matrices.

Introduction

The world's population, determined by the United Nations, is currently around 8 billion people, with an expected growth of another 2 billion by the end of 2100 [1], and it will be necessary to increase approximately 80% of world food production to meet the population's needs [2].

The result of this increase in production is the intensification of food waste and loss, which negatively affects the environment [3,4]. Worldwide, the rate of wasted food reaches 17%. Roots, fruits, vegetables and oilseeds are about 40 – 50% of this total [3]. Therefore, many studies have been conducted to find methodologies capable of adding commercial value to waste products [5]. Residues and by-products have several bioactive ingredients, such as phenolic compounds, carotenoids and vitamins [4,6].

Objectives

The present work aims to evaluate the bioactivity of extracts using agricultural by-products of olive pomace, olive leaf, white onion and collard and optimise the extraction conditions using SFE-CO₂ (supercritical fluid extraction using carbon dioxide) - a sustainable and green technology [7,8,9]. These products are rich in bioactive compounds with functional properties. Therefore, the evaluation of extracts obtained using this methodology, as well as research around the parameters that provide better yields for extraction, are of interest in the nutraceutical and food industries [10, 11].

Methods

The chemical composition of the obtained extracts was evaluated by liquid chromatography (HPLC) and gas chromatography-mass spectrometry (GC-MS), and their toxicity

was evaluated through a non-tumour cell line. Extractions were carried out using a 1L extractor with a pressure range of 80, 90 and 100 bar, a temperature of 50 °C and two hours of extraction time.

Results and Conclusions

In general, higher pressures have allowed higher extraction yields (Figures 1 and 2). The higher pressure favoured the extraction of the active compounds since a higher amount of extract was obtained.

Concerning the chemical composition (Figure 3), GC-MS analysis revealed the presence of palmitic acid, linolenic acid (compound only present in white onion), linoleic acid, stearic acid, oleic acid, squalene and vitamin E.

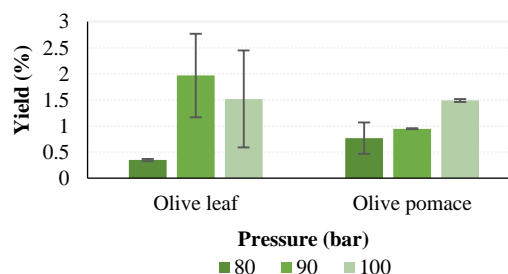


Figure 1. SFE-CO₂ extraction yields for olive leaf and olive pomace at pressures of 80, 90, and 100 bar.

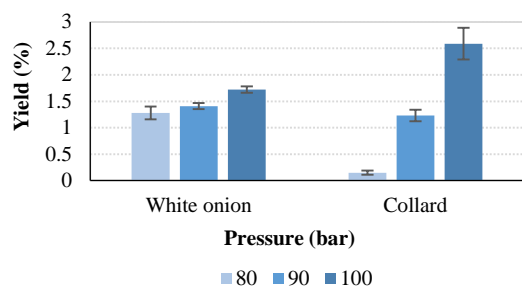


Figure 2. SFE-CO₂ extraction yields for white onion and collard at pressures of 80,90, and 100 bar.

Antioxidant (EC₅₀, TBARS), anti-inflammatory (IC₅₀, RAW 264.7 rat macrophages) and cytotoxicity (GI₅₀, non-tumoral pig liver and renal cells) activities were determined with specific methodologies, and the results are shown in Table 1.

Table 1. Bioactivity analysis of olive leaf, olive pomace, white onion and collard extracts (mean ± SD).

	Olive leaf	Olive pomace	White onion	Collard
GI ₅₀ /μg·mL ⁻¹	>400	197±11	>400	>400
IC ₅₀ /μg·mL ⁻¹	>400	390±13	nd	nd
EC ₅₀ /mg·mL ⁻¹	nd	nd	33.37±1.38	10.70±0.22

nd-not determined.

The SFE-CO₂ extracts of olive leaf, olive pomace, white onion and collard presented interesting bioactivities (antioxidant and anti-inflammatory) and did not show cytotoxicity, with the exception of the olive pomace.

As future work, it will be expected that all the extracts could be incorporated (in free or stabilised forms) into food matrices to increase the bioactive compound content and thus produce fortified fruits and vegetable products with natural functional properties.

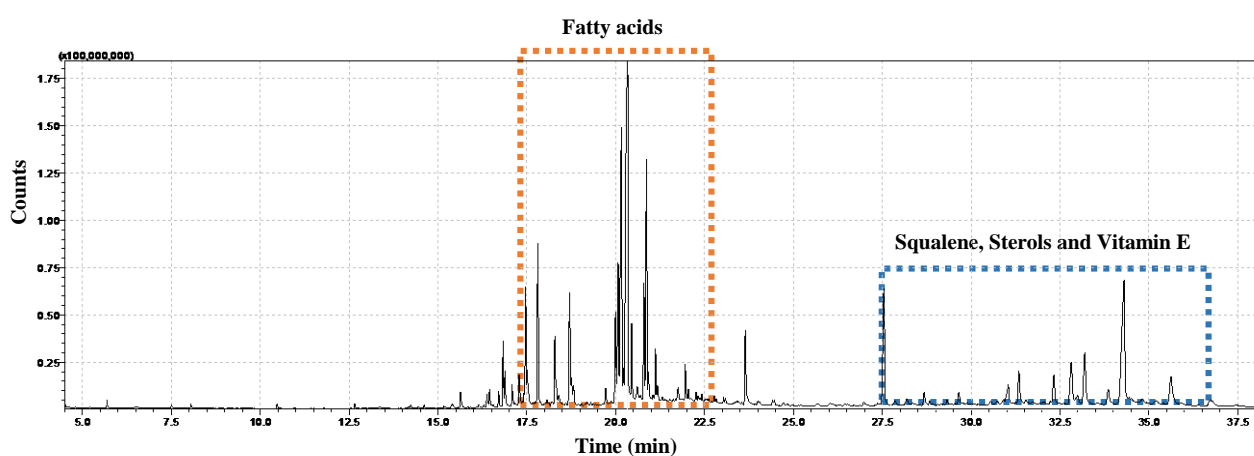


Figure 3. GC-MS profile of the SFE-CO₂ onion extract (80 bar, 50 °C, 2 h).

Acknowledgements

This work was financially supported by LA/P/0045/2020 (ALiCE), UIDB/50020/2020 and UIDP/50020/2020 (LSRE-LCM), funded by national funds through FCT/MCTES (PIDDAC). This work is also a result of project “BIOMA - Soluções Integradas de Bioeconomia para Mobilização da Cadeia Alimentar”, with reference POCI-01-0247-FEDER-046112, co-funded by the European Regional Development Fund (ERDF), through the Operational Programme for Competitiveness and Internationalization (COMPETE 2020) and the Lisbon Regional Operational Programme (LISBOA 2020), under the PORTUGAL 2020 Partnership Agreement. The authors are thankful for the samples provided by Acushla (<https://www.acushla.pt/>) and Campotec (<https://campotec.pt/>).

References

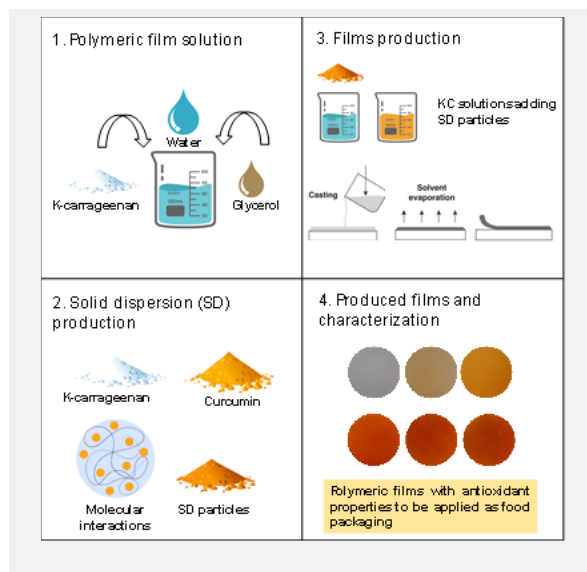
- [1] United Nations. Department of Economic and Social Affairs - Population Division. “World Population Prospects 2022”. Web. 20 February 2023. <https://population.un.org/wpp/>.
- [2] Population Matters. “Larger Population, Larger People: Humanity Will Require 80% More Food By 2100”. Web. 20 February 2023. <https://populationmatters.org/news/2019/12/larger-population-larger-people-humanity-will-require-80-more-food-by-2100/>.
- [3] P. Morone et al., *Journal of Cleaner Production*, 221 (2019) 10.
- [4] H.V. Annegowda et al., *Valuable bioactives from vegetable wastes. Valorization of Agri-Food Wastes and By-Products: Recent Trends, Innovations and Sustainability Challenges*, (2021) 83.
- [5] P. Schreinemachers et al., *Global Food Security*, 16 (2018) 36.
- [6] V. Marcillo-Parra et al., *Trends in Food Science & Technology*, 116 (2021) 11.
- [7] J.C. Kessler et al., *Food Chemistry*, 384 (2022) 132514.
- [8] J.C. Kessler et al., *Molecules*, 27(3) (2022) 694.
- [9] J.C. Kessler et al., *Food Chemistry*, 41 (2023) 135845.
- [10] J. Azmir et al., *Journal of Food Engineering*, 117 (2013) 426.
- [11] T. Arumugham et al., *Chemosphere*, 271 (2021) 129525.

Development of K-carrageenan polymeric films incorporated with curcumin solid dispersion particles as a model packaging material for olive oil preservation

S.C. Rezende^{1,2,3,4}, A. Santamaria-Echart^{1,2}, I. Marcet⁵, M. Carpintero⁵, M. Rendueles⁵, M.M. Dias^{3,4}, M.F. Barreiro^{1,2*}

¹Centro de Investigação de Montanha (CIMO), Instituto Politécnico de Bragança, Campus de Santa Apolónia, 5300-253 Bragança, Portugal; ²Laboratório Associado para a Sustentabilidade e Tecnologia em Regiões de Montanha (SusTEC), Instituto Politécnico de Bragança, Campus de Santa Apolónia, 5300-253 Bragança, Portugal; ³Laboratory of Separation and Reaction Engineering – Laboratory of Catalysis and Materials (LSRE-LCM), Department of Chemical Engineering, Faculty of Engineering University of Porto, Rua Dr. Roberto Frias, 4200-465 Porto, Portugal; ⁴Associate Laboratory in Chemical Engineering (ALiCE), Faculdade de Engenharia, Universidade do Porto, R. Dr. Roberto Frias, 4200-465, Porto, Portugal; ⁵Department of Chemical and Environmental Engineering, University of Oviedo, C/Julián Clavería 8, 33006 Oviedo, Spain.

*barreiro@ipb.pt



This work addresses the development of k-carrageenan polymeric films added with curcumin-based solid dispersion particles to be used as a model food packaging material for olive oil preservation. The aim was to create a sustainable packaging alternative to replace conventional petroleum-based films. The solid dispersion technique was used to encapsulate curcumin and increase water compatibility, facilitating the posterior incorporation in hydrophilic polymeric films. The characterization results indicated that using 10% particles was the most effective concentration to improve the mechanical and barrier properties of the films. This study demonstrated the potential of adding hydrophobic bioactive compounds (curcumin) to hydrophilic matrices. The materials are expected to find applications as packaging materials aiming to extend food products' shelf life.

Introduction

Polymeric food packaging films are thin, flexible sheets or coatings made from various polymers, used to package, and preserve food products. These films are typically made from petroleum-based polymers. They are designed to provide a barrier against oxygen, moisture, and other contaminants that can compromise the quality and safety of food [1, 2].

Considering the high demand for packaging materials to preserve foods and the growing environmental concern about their biodegradability, the use of natural-based products is one of the main alternatives to explore (together with recycling) [3]. The potential of natural polymers has been extensively investigated to offer simple and sustainable discarding products. However, they can present limitations when compared with their synthetic counterparts (e.g., weaker mechanical and barrier properties and poor resistance to water) [1], needing to be reinforced, (i.e., with particles).

The addition of active compounds is another trending topic related to bio-based films. Bioactive substances are usually proposed to improve the shelf life of products, as is the case of high-content lipid products, by slowing down the oxidation rate. Nevertheless, most natural polymers are hydrophilic, and many of bioactive compounds with properties of interest, i.e., antimicrobial, are hydrophobic, making it difficult to disperse a significant quantity in the polymeric matrix [4].

Solid dispersion (SD) is an encapsulation technique, where an active compound is molecularly dispersed into a polymer, promoting hydrogen bonding between both components, resulting in particles formation. This method allows the change in the crystallinity pattern of the active compound, improving its water solubility [5, 6].

Objectives

This work comprehends the development of k-carrageenan polymeric films added with curcumin-based solid dispersions particles to confer functionality and reinforcement. The obtained films were tested as a model food packaging material for olive oil preservation as proof of concept.

Methods

For the SD production, the kappa-carrageenan (0.4g) and the surfactant Tween 80 (15% w/w, polymer-basis) were dissolved in 100 mL of distilled water, whereas curcumin (15% w/w, polymer-basis) was dissolved in 50 mL of ethanol. The aqueous solution was poured into the ethanolic one. The mixture was sonicated at 70% amplitude for 10 min (30 s on and 10 s off). After sonication, the mixture was submitted to a solvent evaporation step to remove the ethanol using a vacuum rotary evaporator at 40 °C and 175 mbar. The sample was frozen at -20 °C and dried in a freeze-dryer at -106 °C. The polymeric films were prepared based on the film casting method. Kappa-carrageenan at 2.5% (w/w) was dissolved in distilled water, under constant heating at 90 °C and stirring. Glycerol was added to the solution as a plasticizer (30% (w/w), polymer-basis). Films containing different SD percentages were prepared: 0, 1, 5, 10, 15, and 20% (w/w, polymer-basis). The samples were coded as KCX, where "X" corresponds to the solid dispersion added amount. A total of 25 mL of solution was poured into a Petri dish (9 cm diameter) and left to dry at 35 °C in a drying oven for 12 hours. The characterization included the thickness, transparency, color, water solubility (WS) [7], water vapor permeability (WVP) (ASTM E96-95), and mechanical

properties. The promising formulations concerning mechanical properties were analyzed for antioxidant activity, and olive oil oxidation expressed as peroxide values following the methodologies described elsewhere [8, 9].

Results

The film thickness values, 85.00 ± 4.47 and 100.00 ± 7.07 μm , indicated they were dimensionally homogeneous. Regarding the color, all the samples presented yellowish tone, except the KC0 (without SD particles). The L^* (lightness) decreased from KC1 to KC20, while the parameter a^* , referent to the red influence, increased. In the coordinate b^* (yellow), the value increased from KC1 to KC10, showing then a decreasing tendency. The transparency decreased from KC0 (71.28%) to KC20 (5.02%).

The WS values were similar for all the samples (from 82.33 to 84.86%), except for the KC10 sample, which showed a lower value of 77.18%. The WVP and mechanical properties values are described in Table 1. The WVP values were similar among the samples, except for formulation KC20. This higher value was expected, once this sample contained more particles, contributing to an increase in the barrier.

Considering the films with SD particles, the mechanical properties improved up to 10 % of particles; thereafter, the values decreased. According to the literature [10], the curcumin concentration and the physical and chemical interactions between the polymer and curcumin, commonly hydrophobic forces, and hydrogen bonds can affect the mechanical properties. The sample KC10 presented significant improvements regarding tensile modulus and stress at break compared to all samples. Moreover, KC10 was the film showing the higher yield strength among the samples added with SD.

It was noticeable that the concentration of 10% of SD favored the final properties of the films. Therefore, the films with 10% (KC10), a concentration below 5% (KC5), and the film without SD (KC0), were selected to perform the antioxidant activity analysis and the proof of concept as food packaging for olive oil.

The antioxidant activity was analyzed by the FRAP and ABTS+ assays. The antioxidant activity was superior in the KC10 film compared to the KC5, a behavior justified by the higher concentration of curcumin. No activity was found for the sample KC0.

The films KC0, KC5, and KC10 were used to pack olive oil, and their oxidation state was evaluated under accelerated oxidative stability conditions (60 °C, 6 days). The peroxide value (PV) (Commission Regulation (EEC) No 2568/91 of 11 July 1991) was determined at times 0, 3, and 6 days. The control (no film) and the sample with the base film, KC0, presented values reaching 20 mEq. O_2/kg oil (maximum allowed by legislation), while the samples with SD revealed better oil protection from environmental conditions (light and temperature).

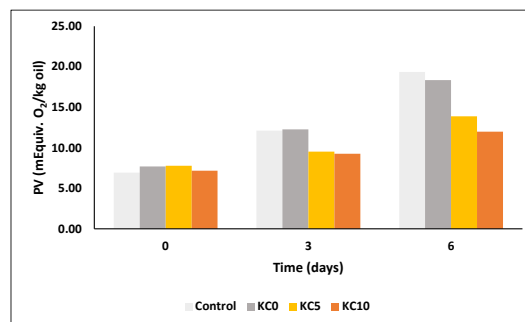


Figure 1. Peroxide values of the produced films for 6 days.

Conclusions

Adding curcumin SD in the k-carrageenan polymeric films improved their final properties, especially with 10% concentration. The formulations KC5 and KC10 demonstrated effectiveness in protecting the olive oil against lipid oxidation. Films with a natural polymer combining the curcumin in an encapsulated form could provide a good alternative for food packaging materials with potential application in high-content lipid product preservation.

Table 1. Water vapor permeability and mechanical properties of all the produced films.

Sample	WVP ($\text{g} \times \text{mm}/\text{m}^2 \times \text{h} \times \text{kPa}$)	Tensile modulus (MPa)	Yield strength (MPa)	Stress at break (MPa)	Strain at break (%)
KC0	1.07 ± 0.03	214.62 ± 11.44	2.57 ± 0.25	3.37 ± 0.86	2.26 ± 0.88
KC1	1.02 ± 0.07	186.34 ± 10.65	1.91 ± 0.25	2.10 ± 0.22	1.36 ± 0.19
KC5	1.05 ± 0.07	207.41 ± 24.03	2.25 ± 0.42	2.50 ± 0.43	1.48 ± 0.08
KC10	1.06 ± 0.13	241.47 ± 28.13	2.40 ± 0.76	3.50 ± 0.98	2.36 ± 1.19
KC15	1.03 ± 0.03	187.36 ± 15.52	2.10 ± 0.36	2.20 ± 0.37	1.31 ± 0.23
KC20	1.15 ± 0.12	185.26 ± 7.03	1.80 ± 0.23	1.91 ± 0.21	1.18 ± 0.10

Acknowledgments

The authors are grateful to the Foundation for Science and Technology (FCT, Portugal) and FEDER under Programme PT2020 for financial support to CIMO (UIDB/00690/2020 and UIDP/00690/2020), SusTEC (LA/P/0007/2021), ALiCE (LA/P/0045/2020), and LSRE-LCM (UIDB/50020/2020 and UIDP/50020/2020). FCT for the research grant SFRH/BD/147326/2019 of Stephany C. de Rezende and the scientific employment program-contract of Arantzazu Santamaria-Echart. Red CYTED ENVABIO100 121RT0108.

References

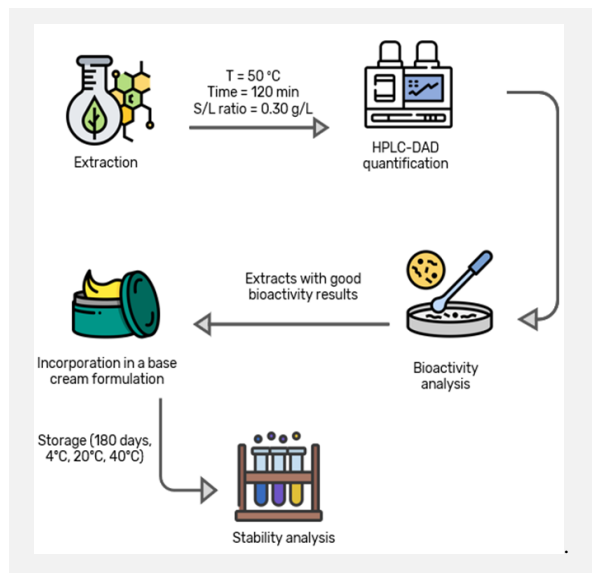
- [1] A.G. Azevedo et al., *Polymers* 14 (2022) 1-32.
- [2] V. Gupta et al., *Materials*, 15 (2022) 5899.
- [3] F. Versino et al., *Foods*, 12 (2023) 1057.
- [4] R.Q. Assis et al., *Packaging Technology Science*, 31 (2018) 157-166.
- [5] Y. Lan et al., *Food Chemistry*, 278 (2019) 665-673.
- [6] Y. Umemoto et al., *Journal of Drug Delivery Science and Technology*, 55 (2020) 101401.
- [7] P. Velázquez et al., *Food Hydrocolloids*, 124 (2022) 107250.
- [8] S.S. de Campos et al., *Food Packaging and Shelf Life*, 22 (2019) 100424.
- [9] M. Carpintero et al., *Membranes*, 12 (2022) 12010046.
- [10] J.G. Oliveira Filho et al., *Food Science and Technology*, 118 (2021) 840-849.

Extraction of phenolic compounds from *Juglans regia* L. leaves using aqueous solutions of eutectic solvents

I.W. Cordova^{1,2,3}, T. Oludemi^{1,2}, V. Vieira^{1,3}, T.C.S.P. Pires^{1,2}, S.P. Pinho^{1,2}, J.A.P. Coutinho³, L. Barros^{1,2}, O. Ferreira^{1,2*}

¹Centro de Investigação de Montanha (CIMO), Instituto Politécnico de Bragança, Campus de Santa Apolónia, Bragança, Portugal; ²Laboratório para a Sustentabilidade e Tecnologia em Regiões de Montanha (SusTEC), Instituto Politécnico de Bragança, Campus de Santa Apolónia, Bragança, Portugal; ³CICECO, Aveiro Institute of Materials, Complexo de Laboratórios Tecnológicos, Aveiro University, Campus Universitário de Santiago, Aveiro, Portugal.

*oferreira@ipb.pt



Juglans regia L. leaves are a source of extracts rich in phenolic compounds with well-studied antimicrobial, antioxidant, and anti-inflammatory properties, when conventionally obtained with volatile organic solvents. In this work, a new extraction process using aqueous solutions of eutectic solvents composed of urea, 1,3-propanediol and/or betaine was developed. These compounds were selected considering the potential application of the extracts (in the solvents) as functional additives in the cosmetic industry. The solvents with the best extraction yield in phenolic compounds were chosen for additional bioactivity (antimicrobial, antioxidant and anti-tyrosinase properties) and photostability studies. Finally, the extracts dissolved in the low volatile eutectic solvents with the best combined results in terms of extraction and bioactivity were incorporated in a commercial base cream. Those formulations were evaluated at three temperatures over 180 days, showing excellent pH and colour stability. Moreover, the incorporated creams maintained high antioxidant activity and total phenolic content.

Introduction

Phenolic compounds can be found in plants and fungi, being responsible for their colour, flavour, and protection against UV radiation and pathogens [1–3]. The extracts of the leaves of *Juglans regia* L. (walnut tree) have remarkable biological properties such as antimicrobial, antioxidant, and anti-inflammatory activities due to the presence of such phenolic compounds, presenting potential application in the food, pharmaceutical or cosmetics areas [4,5]. These compounds are usually extracted using conventional volatile organic solvents [3,4,6].

Objectives

The main aim of this work is to design a more sustainable extraction process using aqueous solutions of eutectic solvents (ES) to be directly incorporated in cream formulations. Aqueous solutions of ES betaine + urea and betaine + 1,3-propanediol (1,3-PPD) were selected considering their potential application as ingredients in cosmetics, eliminating the separation step of the extract from the solvent. Finally, to support the development of new applications, besides determining the extraction yield of the main phenolic compounds, the photostability and the bioactivity in several dimensions of the extracts were evaluated.

Methods

A solvent screening was carried out considering the aqueous solutions (25, 50 and 75%, water content) of the individual components and of the ES (in the proportions 1:1, 1:2, 2:1) at fixed extraction conditions [4], using a heat-assisted extraction technique. The quantification of the phenolic compounds was performed by HPLC-DAD. The antioxidant activity was evaluated by the ferric reducing power, DPPH radical scavenging and thiobarbituric acid reactive substances assays.

The antibacterial activity was assessed by the microdilution method in microtiter plates. The incorporation of the extracts in a commercial base cream and the stability assays were followed a methodology previously described [7]. The photostability of the incorporated extracts, as well as their total phenol content and antioxidant activity were determined using methodologies previously described [7].

Results and conclusions

High extraction yields of both phenolic acids (in the range of 2–3 mg/g of dry plant) and flavonoids (6–11 mg/g of dry plant) were achieved with a wide set of aqueous solutions of ES. On the other hand, when using pure water as solvent, the maximum extraction yield was obtained for the phenolic acids (3 mg/g of dry plant), but for the flavonoids only 2 mg/g of dry plant were obtained.

Considering the maximum extraction yield, four solvents were selected for additional photostability and bioactivity studies (antimicrobial, anti-tyrosinase, and antioxidant). Regarding photostability, all extracts were stable under UVA and UVB radiation in the pH range typical in human skin [8]. All extracts presented antimicrobial activity against selected Gram-negative bacteria, Gram-positive bacteria and yeast (*Candida albicans*). Only the aqueous extract presented tyrosinase inhibition at the maximum concentration tested, showing that the extracts obtained with different solvents can be used to explore a variety of biological properties of the leaves of *J. regia*. Finally, for the antioxidant assays, the best results were found for the extracts in the aqueous solutions of 1,3-PPD or betaine. No antioxidant activity was observed in the pure solvents. These solutions were selected for incorporation in a commercial base cream. The stability of these formulations was evaluated, using the pure base cream as control and the formulation incorporated with the pure

water extract as reference. The creams were stored in a light-protective and airtight container at different temperature conditions (4, 20 and 40 °C). The colour, pH, antioxidant activity and total phenolic content of the formulations were evaluated at the initial time and after 180 days. The formulations containing the aqueous solutions of eutectic solvents showed excellent pH and colour stability during the evaluated time, at all tested temperatures. Regarding the antioxidant activity, a decrease was observed after 180 days, though it remained at higher values than the pure water extract, as can be seen in Figure 1.

In conclusion, this study showed that aqueous solutions of eutectic solvents can be used as efficient solvents for the extraction of phenolic compounds from the leaves of *J. regia* L. Preliminary studies were carried out to directly incorporate these solutions in a commercial base cream and the promising results suggest that future work should be focused on evaluating its performance in terms of skin permeation, together with more detailed toxicological and stability studies.

Acknowledgements

This work was developed within the scope of the project AllNat – “Using natural deep eutectic solvents for the extraction of bioactive compounds from plant material” (reference POCI-01-0145-FEDER-030463, PTDC/EQU-EPQ/30463/2017), funded by FEDER funds through COMPETE2020 – Programa Operacional Competitividade e Internacionalização (POCI), Portugal 2020 and by national funds through Foundation for Science and Technology (FCT/MCTES) and project GreenHealth – “Digital strategies in biological assets to improve well-being and promote green health” (reference Norte-01-0145-FEDER-000042), funded by the FEDER funds through the Regional Operational Program North 2020. The authors are grateful to FCT (Portugal) for financial support through national funds FCT/MCTES (PIDDAC) to CIMO (UIDB/00690/2020 and UIDP/00690/2020) and SusTEC (LA/P/0007/2020) and CICECO-Aveiro Institute of Materials, UIDB/50011/2020 & UIDP/50011/2020. I. W. Cordova is grateful to FCT for her contract 2022.12407.BD. To the MICINN for the Juan de la Cierva Formación contracts of Tânia C.S.P. Pires (FJC20120-045405-I) and T. Oludemi (FJC2019-042549-I).

References

- [1] O. Taofiq et al., *Molecules*, 22 (2017) 1-24.
- [2] D. Cao et al., *ACS Sustainable Chemistry & Engineering*, 8 (2020) 19169-19177.
- [3] M. Ruesgas-Ramón et al., *Journal of Agricultural and Food Chemistry*, 65 (2017) 3591-3601.
- [4] V. Vieira et al., *Molecules*, 25 (2020) 2497-2510.
- [5] V. Vieira et al., *Industrial Crops and Products*, 134 (2019) 347-355.
- [6] F. Chemat et al., *Molecules*, 24 (2019) 1-27.
- [7] N. Besrouer et al., *Antioxidants*, 11 (2022) 677.
- [8] E. Proksch, *Journal of Dermatology* 45 (2018) 1044-1052.

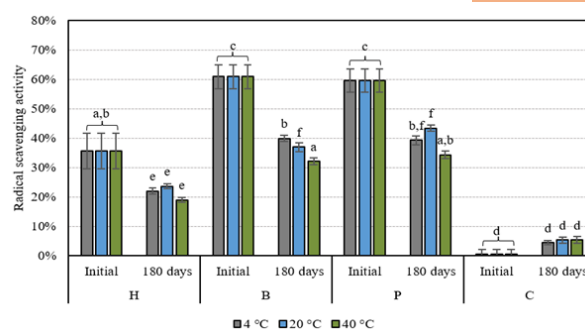


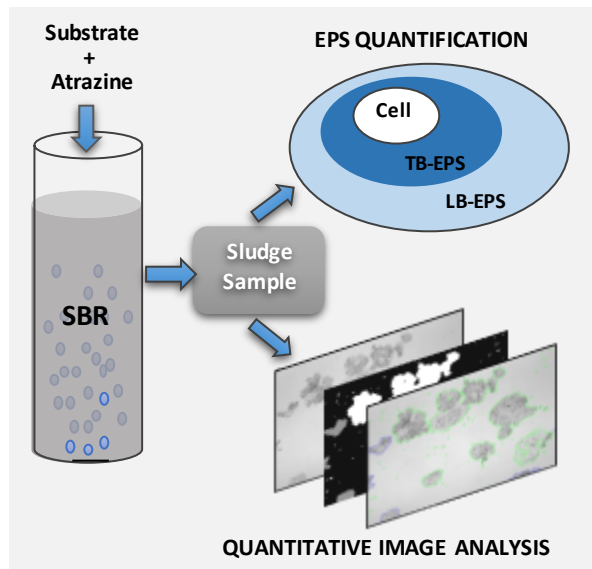
Figure 1. Radical scavenging activity by the DPPH method in formulations containing: aqueous extract (H), aqueous solution of betaine extract (B), aqueous solution of 1,3-propanediol extract (P) and control base cream (C). Each value is the mean of at least three replicated determinations \pm standard deviation. Means with different letters are significantly different ($p < 0.01$).

EPS and aggregates changes on activated sludge under atrazine exposure

A. Melo, J.G. Costa, C. Quintelas, E.C. Ferreira, D.P. Mesquita*

CEB – Centre of Biological Engineering, University of Minho, Braga, Portugal; LABELS –Associate Laboratory, Braga/Guimarães, Portugal.

*daniela@deb.uminho.pt



Extracellular polymeric substances (EPS) play a vital role in biological wastewater treatment systems, affecting their performance in aggregates settling, structure and arrangement, and interacting with micropollutants present in wastewater. In this study, the effects of herbicide atrazine (ATZ) on the EPS yield and composition and aggregates structure were investigated on activated sludge (AS) in a sequencing batch reactor (SBR). The results demonstrated that TB-EPS and LB-EPS increased under ATZ exposure, indicating that microorganisms release EPS as a self-mechanism of defense against environmental changes. Above 5.5 mg L^{-1} of ATZ aggregates become larger. Principal component analysis (PCA) was useful in highlighting biomass changes during the experimental phases, and Pearson correlation revealed that TB-EPS content correlate well with large aggregates (0.996).

Introduction

Among pesticides, atrazine (ATZ) is commonly used in agricultural activity worldwide. As a consequence, ATZ can be found in wastewater treatment (WWT) systems and natural aquatic environments. In biological WWT, microorganisms live and grow held together by a slime matrix comprised of extracellular polymeric substances (EPS), forming a three-dimensional microbial structure of aggregates and by chemical binding forces. The EPS are typically composed of organic substances such as polysaccharides (PS), proteins (PN), humic acid substances (HAS), nucleic acids, and lipids. In biological WWT, EPS is important because they play an essential role in aggregates flocculation, settling, and dewatering [1]. Moreover, in the presence of toxic substances, such as pesticides, EPS forms a protective layer for the aggregated biomass against environmental disturbances that might play an important role in the transport and transformation of micropollutants [2]. Also, the increase of EPS concentration under toxic conditions have been reported [2]. Besides that, the content of EPS and its components (PS, PN, HAS), and variation in the PN/PS ratio have been associated with the stability and size of aggregates in WWT. Quantitative Image Analysis (QIA) has proven to be a suitable tool for monitoring biological WWT systems, and for the assessment of aggregates in AS as well [3]. Furthermore, multivariate statistics, such as principal component analysis (PCA), have become important in organizing and extracting relevant information from such comprehensive datasets [4]. In this context, this work presents the effect on EPS production and on aggregates structure of different concentrations of atrazine (ATR).

Methods

A sequencing batch reactor (SBR) consisting of a 2 L working volume was operated at room temperature. SBR was fed with synthetic medium containing ATZ at 2.0 (phase II for 32 days), 5.5 (phase III for 32 days), and 12.0 mg L^{-1} (phase IV for 33

days), and without ATZ (phase I for 34 days). EPS was determined as loosely bound (LB-EPS), tightly bound (TB-EPS), and total EPS according to [5]. Aggregates were evaluated by QIA where an Olympus BX51 microscope (Olympus, Shinjuku, Japan) at $40\times$ coupled to an Olympus DP72 camera (Olympus, Tokyo, Japan) was used. Images were then processed, and aggregates size was classified considering their equivalent diameter (Deq) as: small ($\text{Deq} < 25 \mu\text{m}$), intermediate ($25 < \text{Deq} < 250 \mu\text{m}$), and large ($\text{Deq} > 250 \mu\text{m}$). The aggregate area percentage (%Area) was also determined for the small (%Area_{small}), intermediate (%Area_{intermediate}), and large aggregates (%Area_{large}). PCA was performed using EPS and QIA aggregates data. More detail about the techniques employed can be found elsewhere [5]. QIA procedures and PCA were conducted using Matlab™ 8.5 (The MathWorks Inc, USA). Pearson correlation was used to relate EPS production and QIA data.

Results

Different concentrations of ATZ had some impact on biomass activity by increasing LB-EPS from 18 to 45, TB-EPS from 34 to 66, and from 53 to $111 \text{ mg EPS g MLVSS}^{-1}$ (Table 1). When the aggregates were exposed to the highest ATZ concentrations (5.5 and 12 mg L^{-1}) the aggregates became larger (Figure 1a). Principal components analysis (PCA) was performed and is present in Figure 1b. The explained variance was 41, 15 and 12% for PC1, PC2, and PC3, respectively, performing 68% of the total explained variance. Two well-defined clusters were found corresponding to phase I and phase II. Considering PC1 axis, phase I was placed in the right side and phase II was placed from the middle to the left side. In contrast, for phases III and IV, samples were combined in two close clusters located in the bottom and upper of the left side, demonstrating that ATZ above 5.5 mg L^{-1} did not cause significant changes on biomass

properties. These results showed the usefulness of this technique identifying changes in AS properties, showing the transition from predominantly small and intermediate aggregates to large aggregates as well as the increase in EPS content under ATZ exposure. From Pearson correlation (Table 2), it was verified the strong relationship between EPS content (mainly TB-EPS) and the %Area_{large}. Therefore, the present results showed a close relationship between large aggregates and high EPS content. Additionally, the increase of EPS content can be also considered a self-defense mechanism from microorganisms when exposed to toxic compounds.

Table 1. Average values followed by the standard deviation of EPS (mg EPS g MLVSS⁻¹).

EPS	Phase	Mean	Standard Deviation
LB-EPS	I	17.71	0.98
	II	49.26	1.10
	III	37.12	1.20
	IV	44.74	1.23
TB-EPS	I	34.12	1.71
	II	46.51	1.13
	III	57.27	1.73
	IV	66.40	1.14
Total EPS	I	51.82	1.97
	II	95.77	1.57
	III	94.39	2.10
	IV	111.14	1.68

Conclusions

Changes of aggregates size and EPS content were studied to assess the impact of ATZ on AS system. The effect was more evident above 5.5 mg L⁻¹. TB-EPS had values greater than LB-EPS during all experimental phases, indicating their interaction with ATZ as a response mechanism of the biomass. PCA accomplished with QIA and EPS data provided insights into the EPS role in the biomass structure changes along operation and allowed to distinguish the experimental phases as well. Pearson correlation revealed that total EPS and TB-EPS were strongly correlated to %Area of aggregates, rather than LB-EPS forms.

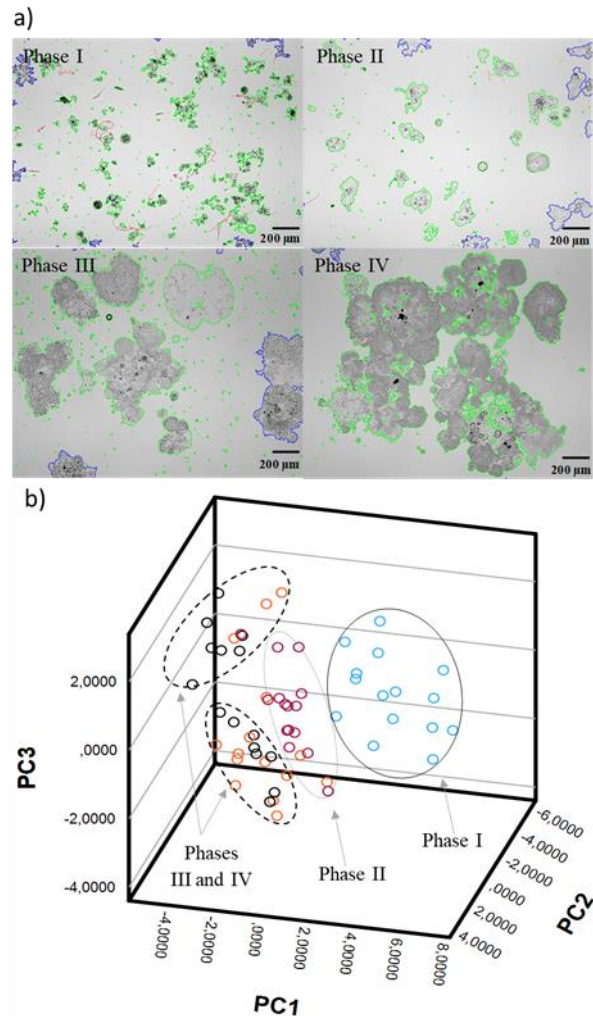


Figure 1. (a) Microscopic view of AS during reactor operation. The image corresponds to the beginning of each phase. (b) PCA scores plot of the SBR operational parameters, EPS and QIA dataset.

Table 2. Pearson correlation coefficients computed between EPS components and %Area of aggregates.

	LB-EPS	TB-EPS	Total EPS	%Area _{small}	%Area _{intermediate}	%Area _{large}
LB-EPS	1.000					
TB-EPS	0.658	1.000				
Total EPS	0.913	0.908	1.000			
%Area _{small}	0.239	-0.494	-0.135	1.000		
%Area _{intermediate}	-0.672	-0.992	-0.912	0.418	1.000	
%Area _{large}	0.630	0.996	0.891	-0.481	-0.998	1.000

Acknowledgements

The authors thank the Portuguese Foundation for Science and Technology (FCT) under the scope of the strategic funding of UIDB/04469/2020 unit, and by LABBELS – Associate Laboratory in Biotechnology, Bioengineering and Microelectromechanical Systems, LA/P/0029/2020. The authors also acknowledge the financial support to A. Melo through the grant 240-20170220 provided by Instituto Federal de Educação, Ciência e Tecnologia de Pernambuco (IFPE). D.P. Mesquita and C. Quintelas acknowledge FCT funding under DL57/2016 Transitory Norm Programme.

References

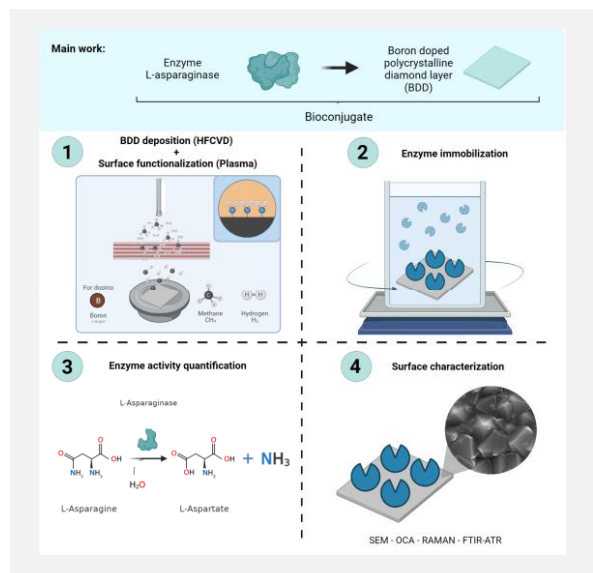
- [1] G.-P. Sheng et al., *Biotechnology Advances*, 28 (2010) 882-894.
- [2] A. Melo et al., *Frontiers in Chemical Engineering*, 4 (2022) 778469.
- [3] A.L. Amaral, E.C. Ferreira, *Analytica Chimica Acta*, 544 (2005) 246-253.
- [4] C.S. Leal et al., *Journal of Environmental Management*, 289 (2021) 112474.
- [5] A. Melo et al., *Journal of Environmental Chemical Engineering*, 10 (2022) 108415.

Development of an enzymatic biosensor based on boron-doped diamond surface

B.L. Tavares^{1*}, D.R. Fernandes¹, L.R. Freitas¹, V.C. Ebinuma-Santos², J.C.F. Nunes¹, M.C. Neves¹, A.V. Girão³, M.A.C. Neto³, A.P.M. Tavares¹

¹Chemistry Department, CICECO—Aveiro Institute of Materials, University of Aveiro, 3810-193 Aveiro, Portugal; ²Department of Engineering of Bioprocesses and Biotechnology, School of Pharmaceutical Sciences, São Paulo State University (UNESP), Brazil; ³Department of Materials and Ceramics Engineering, CICECO—Aveiro Institute of Materials, University of Aveiro, 3810-193 Aveiro, Portugal.

*bernardo.tavares@ua.pt



L-asparaginase (ASNase) is a biopharmaceutical enzyme that acts in the hydrolysis of L-asparagine, an amino acid that favors tumoral growth in patients with acute lymphoblastic leukemia. Monitoring L-asparagine depletion is vital, but current methods are expensive and complex. Alternative strategies that are more efficient and cost-effective are being researched. In this regard, ASNase-based biosensors have been developed for the quantification of L-asparagine. Due to its unique properties, diamond has been used as an ideal platform for the development of a new generation of biosensors. This study aimed to immobilize ASNase on plasma-functionalized polycrystalline chemical vapor deposition diamond. The diamond films were used for physical adsorption of ASNase, which was confirmed via activity tests. Surface characterization provided further understanding of the immobilization conditions. The results support the development of the proposed diamond-based biosensor.

Introduction

L-Asparaginase (ASNase) is a versatile enzyme with both medical and industrial applications. ASNase catalyzes the hydrolysis of L-asparagine (asn) into L-aspartate (asp) and ammonium, a reaction that can be used for relevant purposes [1]. In industrial applications, ASNase has been used as a food processing aid to reduce acrylamide formation (relevant due to its various adverse effects, such as neurotoxicity, and carcinogenicity) caused by the Maillard Reaction, in starch-rich foods cooked at $>120^\circ\text{C}$, including potato chips, and bakery products [2].

As a biopharmaceutical, ASNase is an important therapeutic protein used in the treatment of cancer, particularly acute lymphoblastic leukemia (ALL) [3]. However, the use of non-human-origin enzymes can lead to the production of anti-drug antibodies and therapeutic inefficiency, as well as side effects such as edema, skin rashes, hepatic dysfunction, fever, and even anaphylactic shock. Monitoring the activity of ASNase is crucial to ensure treatment efficiency and detect early isozyme incompatibility. The most common monitoring strategy involves the quantification of released ammonia through spectrophotometric methods, but these are limited by their toxicity and susceptibility to temperature and light exposure variations [4]. Thus, there is a need for rapid and resilient techniques that can detect reactions at low substrate concentrations to improve the quality of enzymatic activity measurement while avoiding the use of hazardous substances.

Recently, diamond surfaces have been used as platforms for the development of modern screening techniques, such as sensors capable of detecting biomolecular interactions, and biological signals, which is called biosensing. Biosensors are a particular type of sensor since they can detect different types of biological signals, depending on the adopted strategy and material. There are two main biosensor classification methods, based on the used

bioreceptor (enzyme, antibody, aptamer, cell, other biomolecules) and the transducer type (electrochemical, optical, thermal, gravimetric, acoustic) [5].

Diamond is a highly stable allotrope form of carbon with a face-centered cubic structure with each carbon covalently bonded to the nearest carbon in a regular tetrahedron. The structural arrangement composed of sp^3 carbons exhibit extraordinary chemical and physical properties, as it has a broad wavelength transparency, a high thermal conductivity ($2,600 \text{ W}\cdot\text{m}^{-1}\cdot\text{K}^{-1}$), and while being the hardest known material, it also shows great resistance to chemical corrosion, and it is biocompatible [6]. The incorporation of boron atoms into the diamond lattice leads to a p-type semiconducting behavior with acceptor energy levels in the band gap, 0.39 eV above the valence. Furthermore, by doping the diamond with boron, it is possible to obtain a negative temperature coefficient (NTC) thermistor behavior, which is characterized by a resistance decrease as the temperature at which is exposed to, rises [7].

This study aims at the immobilization of ASNase on the surface of O_2 and NH_3 plasma functionalized polycrystalline chemical vapor deposition (CVD) diamond surfaces, made from the hot-filament chemical vapor deposition (HFCVD) technique, on monocrystalline silicon substrates. We want to evaluate the enzyme compatibility with the diamond surface which will be crucial to the future development of a biosensor for the treatment monitorization of ALL.

Methods

Boron-doped diamond thin films were deposited using the HFCVD technique, throughout 3 h of deposition on $0.5 \times 0.5 \text{ cm}$ silicon wafers at $700\text{--}800^\circ\text{C}$, with a cooling step of 30 min with hydrogen, to give hydrogenated diamond surfaces. The quality of the films was accessed by Raman spectroscopy.

In order to study the enzyme attachment to the material, plasma functionalization with NH_3 and O_2 gases was performed in a plasma etching equipment, for 15 min. To analyze the functionalization effects of both gases, Optical Contact Angle measurements were performed for 10s per assay, through the sessile drop method for non-functionalized and functionalized samples. Scanning electron microscopy and profilometry were used to characterize the surface morphology and crystal size.

The obtained diamond samples were immersed in a 1.00 mL solution containing the respective enzyme [ASNase] = 0.06 mg/mL at 37°C for 1 hour with agitation. The supernatant was then collected for quantification, and the material was scanned by ATR-FTIR to detect the amino groups of the enzyme in the diamond surface.

Enzymatic activity was determined through a reaction with [L-asparagine] = 198 μM at pH 8, considering the following volumes: 500 μL of Tris/HCl buffer, 450 μL of distilled water, and 50 μL of asparagine solution for 30 min at 37°C, followed by a reaction through the Nessler method, for an additional 30 min and absorbance measurement ($\lambda = 420 \text{ nm}$).

Results

Scanning electron microscopy imaging shows a crystallite size of similar dimensions, around $\sim 1.8 \mu\text{m}$ for all diamond samples. The enzyme is immobilized on the surface of polycrystalline diamond. The amount of adsorbed enzyme is similar in all materials presented (10-20%), slightly higher, particularly when functionalized with NH_3 and O_2 plasma (20-30%). The enzymatic activity also decreases by about 30-40% in the second reaction and 5-10% in the third reaction when functionalized with NH_3 , and about 80% in the second reaction and 5-10% in the third reaction when functionalized with O_2 .

Functionalizing the diamond films with O_2 and NH_3 plasma resulted in a 10% increase in the immobilization yield while

maintaining the activity of the immobilized ASNase, with the activity persisting for more cycles in films immobilized with NH_3 .

In the ATR-FTIR spectra, bands of N-H, O-H, and C-H vibrations (of amino acids) are found at 3240 cm^{-1} , 3100 cm^{-1} , and 2934 cm^{-1} , respectively. These bands are not detected in the non-immobilized diamond. Bands at 1638 cm^{-1} and 1530 cm^{-1} correspond to N-H stretching of amine groups I and bending N-H of amine groups II of Asparaginase, respectively. The band at 1390 cm^{-1} corresponds to the asymmetric stretching vibrations of the carboxyl groups of amino acids, and finally, bands between 1200-800 cm^{-1} correspond to C-C, C-O, C-N, N-H, and C-H bonds in the structure of amino acids, with emphasis on the first two, which, despite being slightly shifted, indicate the presence of the immobilized enzyme in the material.

Conclusions

This study investigated the immobilization of L-asparaginase on polycrystalline CVD diamond by adsorption, with the scope to develop a biosensor for the monitoring of cancer treatment. The HFCVD technique was used to deposit boron-doped diamond thin films on silicon wafers, and then the films were functionalized with NH_3 and O_2 plasma to enhance the attachment of the enzyme. The study found that the enzyme was successfully immobilized on the diamond surface, with similar amounts of adsorbed enzyme across all materials presented, and slightly higher when functionalized with NH_3 and O_2 plasma. The enzymatic activity of ASNase was also found to decrease slightly after the functionalization process, but still remained within acceptable levels. Overall, the results suggest that diamond-based biosensors could be a promising approach for the development of more efficient and reliable methods for monitoring ASNase activity in cancer treatment.

Acknowledgements

This work was developed within the scope of the project CICECO-Aveiro Institute of Materials, UIDB/50011/2020, UIDP/50011/2020 & LA/P/0006/2020, financed by national funds through the FCT/MEC (PIDDAC). Miguel A.C. Neto thanks the FCT for the research contract funded by national funds (OE), through FCT, in the scope of the framework contract foreseen in the numbers 4, 5, and 6 of article 23, of the Decree-Law 57/2016, of August 29, changed by Law 57/2017, of July 19. Ana P.M. Tavares and Márcia C. Neves acknowledge FCT for the research contract CEECIND/2020/01867 and CEECIND/00383/2017, respectively. Valéria C. Santos-Ebinuma acknowledges FAPESP for financial support. João C.F. Nunes acknowledges SPQ and FCT for the PhD fellowship (SFRH/BD/150671/2020).

References

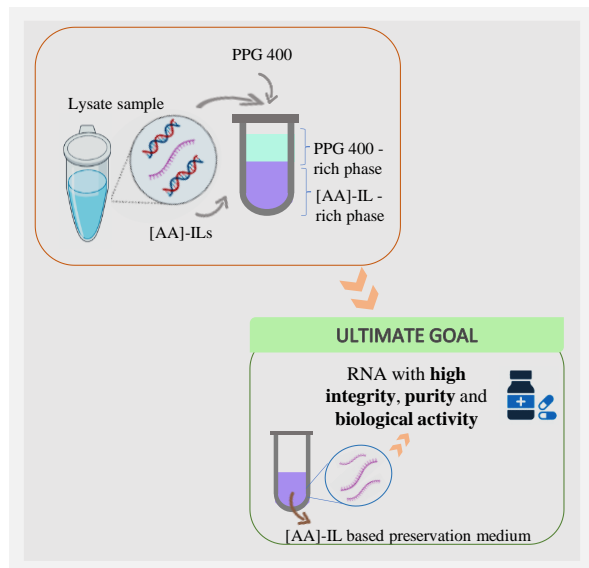
- [1] J.C.F. Nunes et al., *Molecules*, 25 (2020) 5827.
- [2] R. Jia et al., *Microorganisms*, 9 (2021) 1659.
- [3] T. Terwilliger, M. Abdul-Hay, *Blood Cancer Journal*, 7 (2017) e577.
- [4] D.K. Ceconello et al., *Scientific Reports*, 10 (2020) 21481.
- [5] H.H. Nguyen et al., *Materials*, 12 (2019) 1-34.
- [6] S.J. Cobb et al., *Annual Review of Analytical Chemistry*, 11 (2018) 463-484.
- [7] R. Kalish, *Carbon*, 37 (1999) 781-785.

Enhanced extraction of RNA from recombinant lysates afforded by the use of biocompatible ionic liquids

A.F. Pereira^{1*}, A.Q. Pedro¹, L.S. Castro¹, M.J. Quental¹, A.P.M. Tavares¹, L.C. Branco², J.A.P. Coutinho¹, F. Sousa³, M.G. Freire¹

¹CICECO – Instituto de Materiais de Aveiro, Departamento de Química, Universidade de Aveiro, Campus Universitário de Santiago 3810-193, Aveiro, Portugal; ²LAQV-REQUIMTE, Departamento de Química, Faculdade de Ciências e Tecnologia, Universidade Nova de Lisboa, 2829-516 Caparica, Lisboa, Portugal; ³CICS-UBI – Centro de Investigação em Ciências da Saúde, Universidade da Beira Interior, Convento de Sto. António 6201-001, Covilhã, Portugal.

*anafilipa98@ua.pt



RNA-based biopharmaceuticals are being envisioned as a powerful tool for the development of innovative medicines for prevalent diseases, but its widespread application is still challenging due to issues regarding RNA stability and purification. In this context, ionic-liquid-based aqueous biphasic systems (IL-based ABS) are herein investigated as more sustainable and efficient techniques for RNA purification. Amino-acid-based ILs (AA-ILs) were successfully synthesized and characterized. It was verified that all AA-ILs in study were able to form ABS with polypropylene glycol with a molecular weight of 400 g.mol⁻¹ (PPG 400). Overall, the obtained results show that depending on the chemical structure of AA-IL, RNA was successfully extracted with high yield either to the IL-rich phase or precipitated, thus confirming the versatility and improved selectivity of these systems. RNA integrity and stability are preserved throughout the extraction process.

Introduction

RNA has emerged as a promising biopharmaceutical, paving the way for the development of innovative medicines with broad therapeutic and prophylactic efficiencies. Nevertheless, for its use as biotherapeutics, the biopolymer integrity, purity and biological activity are essential requirements. RNA has a highly labile nature and intrinsic low stability, which coupled with the laborious and costly methods of extraction and purification of this biopolymer constitute the main challenge toward its widespread application [1].

To surpass the described bottlenecks, more competitive, effective and sustainable strategies for purifying RNA are of paramount relevance, where AA-ILs may play a prominent role on this field. By virtue of the high affinity between amino-acids and RNA as well as the favorable nucleic acids-stabilization properties exhibited by AA-ILs, a set of ILs is herein studied both as preservation media and components of aqueous biphasic systems (ABS) [2].

Objectives

This work aims to develop alternative cost-effective and sustainable purification-preservation platforms for RNA, taking advantage of the “designer solvent” character of ILs, with the ultimate goal of purifying RNA from a complex recombinant lysate.

Methods

AA-ILs comprising cholinium, L-arginine, L-lysine and L-histidine as cations combined with chloride, DL-aspartate, L-tyrosine or L-phenylalanine were synthesized, characterized, and their ability to form ABS with distinct salts and polymers investigated. All systems were further investigated as potential

extraction and preservation platforms for RNA. The respective ternary phase diagrams, comprising the binodal curve, were determined by the cloud point titration method at 25 °C, as previously reported [3]. Moreover, a common mixture point was selected (although with two exceptions) for the extraction procedures. Each ABS was prepared, followed by the separation of two phases and recovery of RNA (by alcohol precipitation or ultrafiltration). The partitioning of RNA was evaluated by agarose gel electrophoresis, as well as the integrity of RNA.

Results

Initially, the integrity of RNA was evaluated in aqueous solutions of AA-ILs through electrophoretic analysis. A low molecular weight band corresponding to bacterial RNA was observed for all the investigated AA-ILs, thus confirming the potential of these ILs to act as preservation media of RNA up to its usage. Moreover, all the AA-ILs in study formed ABS with PPG 400, envisaging the creation of integrated extraction-preservation platforms for RNA. Extraction studies were performed with a common mixture point (20 wt % of AA-IL + 30 wt % of PPG 400), although with two exceptions. It was demonstrated that RNA was majorly extracted to the IL-rich phase or precipitated (in the ABS composed of the dicationic AA-ILs). The structural integrity of RNA was generally maintained during the extraction process, thus confirming that AA-IL-based ABS can be considered as promising extraction-preservation platforms for RNA. Ongoing work is focusing on the application of the most promising IL-based ABS for the separation of RNA from complex recombinant lysates.

Conclusions

It was verified a preferential migration of RNA to the IL-rich phase or precipitated, without compromising its integrity, thus demonstrating the ability of these ABS to act as potential integrated extraction-preservation platforms for RNA. Overall,

the approach herein developed represents a promising strategy to surpass the critical demand of RNA with high integrity, purity and biological activity, envisaging its potential use as biotherapeutics.

Acknowledgements

This work was developed within the scope of the projects: CICECO-Aveiro Institute of Materials, UIDB/50011/2020, UIDP/50011/2020 & LA/P/0006/2020, financed by national funds through the FCT/MCTES (PIDDAC); EIC-Pathfinder YSCRIPT project with reference 101047214, supported by the budgets of the Horizon Europe Program; and mVACCIL (EXPL/BII-BTI/0731/2021), financially supported by national funds (OE), through FCT/MCTES. Ana Pereira, Leonor Castro, Augusto Pedro and Ana Tavares acknowledge FCT, respectively, for the PhD grants 2022/13247/BD and 2020/05090/BD and the research contracts CEECIND/2020/02599 and CEECIND/2020/01867 under the Scientific Stimulus – Individual Call.

References

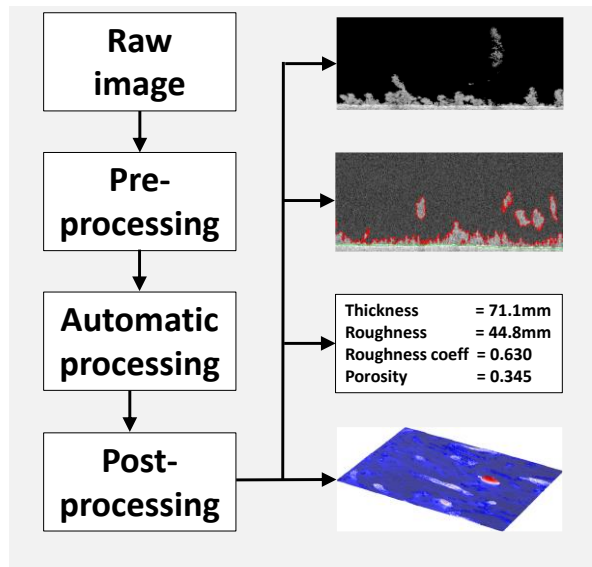
- [1] A.Q. Pedro et al, ACS Sustainable Chemical Engineering, 6 (2018) 16645-16656.
- [2] M.V. Quental et al., ACS Sustainable Chemical Engineering, 7 (2019) 9439-9448.
- [3] F.A.E. Silva et al., ACS Sustainable Chemical Engineering, 5 (2017) 6409-6419.

Analysis and calculation of biofilm structural properties using 3D OCT images in BISCAP

D. Narciso*, A. Pereira, F.G. Martins

LEPABE - Laboratory for Process Engineering, Environment, Biotechnology and Energy, Faculty of Engineering, University of Porto, Rua Dr. Roberto Frias, 4200-465 Porto, Portugal; ALiCE - Associate Laboratory in Chemical Engineering, Faculty of Engineering, University of Porto, Rua Dr. Roberto Frias, 4200-465 Porto, Portugal.

*dnarciso@fe.up.pt



A fully automatic image processing strategy was proposed in Narciso et al. 2022 to obtain the structural parameters of 2D biofilm images obtained via Optical Coherence Tomography (OCT). This is achieved via a novel software tool BISCAP (Biofilm Imaging and Structure Classification Automatic Processor), managing all image processing tasks. This work shows preliminary results concerning the extension of this strategy from the 2D to the more complex and general 3D case. The critical image processing principles and how to adapt them to the 3D case are discussed briefly. The new features of BISCAP in the context of 3D OCT image processing are highlighted via an example, further solidifying it as an advanced tool for biofilm image analysis.

Introduction

Biofilms are colonies of microorganisms bound together via symbiotic relationships attached to a substratum surface. Their study has received considerable attention owing to their strong relevance in biological and industrial applications [1].

Biofilm thicknesses are in the order of μm , which requires the use of microscopy techniques, such as Confocal Laser Scanning Microscopy, in all R&D activities. More recently, Optical Coherence Tomography (OCT) has proved valuable in biofilm research, given its many advantages over other microscopy techniques [2].

To the authors' best knowledge, the only systematic and fully automatic approach enabling the processing of biofilm OCT images is presented in [3]. It builds on key concepts in earlier work and introduces new algorithms covering all aspects of 2D OCT biofilm image processing. Biofilm Imaging and Structure Classification Automatic Processor (BISCAP) was delivered as a Graphical User Interface from which biofilm structural properties and image outputs are calculated.

Building on [3], the authors have been working on expanding the approach to the 3D case. This work is ongoing, and some results towards this extension are presented here.

Methods

A set of algorithms was developed in Python [4] to enable the automatic processing of raw 3D OCT images. Four classification steps are required as follows:

- Bottom interface
- Biomass
- Biofilm
- Top interface

All image processing principles and algorithms for the 2D case are presented in detail in [3]. All principles also apply to 3D

image processing, subject to an adaptation to the more complex geometry of these images.

Calculation of the bottom interface requires minimal adaptation from 2D. Since 3D images comprise a collection of 2D image slices along the new depth axis, using the bottom interface detection strategy developed earlier on all slices suffices. A final smoothing step along the horizontal axis removes any spurious estimates from the first round.

Calculating all biomass voxels is a trivial extension from the 2D case, where it suffices to enlarge the classification along the depth axis.

Calculating the biofilm structure and its top interface requires the most significant adaptations. Both are based on a connected-volume strategy [5], testing continuity on neighbor voxels. In 2D, the maximum number of neighbor pixels is 8, whereas in 3D, this number rises to 26. This requires, in turn, a careful adaptation to compute neighbor voxels in all domains of 3D images.

These continuity-based calculations are, in fact, the most computationally challenging image processing steps, and to speed them up, two additional developments are introduced: (i) a more efficient strategy to keep track of voxels to process and (ii) a parallel processing architecture was developed, where classification tasks are distributed over several independent processes, each dealing with a portion of the full image.

Once all classification tasks are completed, this information may be used to calculate the structural properties of biofilms and create a set of output images for detailed biofilm analysis. All steps were programmed in BISCAP. It includes multiple screens for all processing tasks: Pre-Processing, Automatic Processing, and Post-Processing. All tasks and options are configured via intuitive buttons, where no programming knowledge is strictly necessary.

Results

For brevity, details on biofilm preparation and image acquisition are omitted. These are described in detail in [3]. Some preliminary results are illustrated for such a biofilm culture. A 3D OCT image of 519*317*730 voxels (depth, vertical and horizontal axes) is used for this purpose. Total processing time in BISCAP was ~9 min on a standard laptop machine.

Multiple outputs are calculated automatically during automatic processing, some presented here for illustration purposes. The biofilm structure is shown in Figure 1.

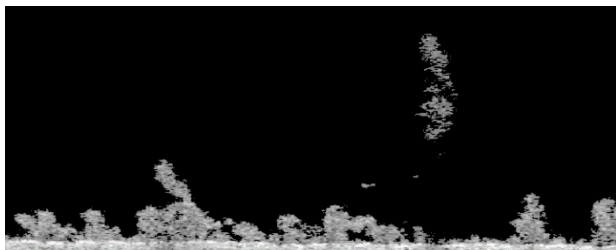


Figure 1. 2D view of biofilm structure.

It shows a 2D slice at a constant depth position. All voxels in the biofilm region retain their original grayscale intensities, whereas all others are displayed in black to emphasize the biofilm structure. Figure 2 shows the bottom and top interface voxels, highlighting biofilm contours (green and red, respectively).

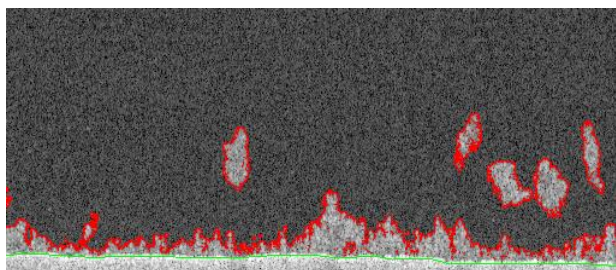


Figure 2. 2D view of biofilm contours.

Any 2D slice along any axis may be selected for inspection in BISCAP. Users may also inspect the outcomes of biomass and biofilm classification as a set of white/black voxels.

Acknowledgements

This work is financially supported by: LA/P/0045/2020 (ALiCE), UIDB/00511/2020 and UIDP/00511/2020 (LEPABE), funded by national funds through FCT/MCTES (PIDDAC).

References

- [1] Z.B. Lewandowski, H. Beyenal, Fundamentals of Biofilm Research, 2nd ed, CRC Press, Boca Raton, FL, 2013.
- [2] J. Hou et al., Scientific Reports, 9.9794 (2019) 1-12.
- [3] D. Narciso et al., Bioinformatics, 38(6), (2022) 1708-1715.
- [4] G. Van Rossum, F. L. Drake, Python 3 Reference Manual, CreateSpace, Scotts Valley, CA, 2009.
- [5] A. Heydorn et al., Microbiology, 146 (2000) 2395-2407.

A 3D representation of the entire collection of top interface voxels is shown in Figure 3. Voxels at high/low positions in the vertical axis are shown as predominantly red/blue, respectively, and offer complementary insight into biofilm structure.

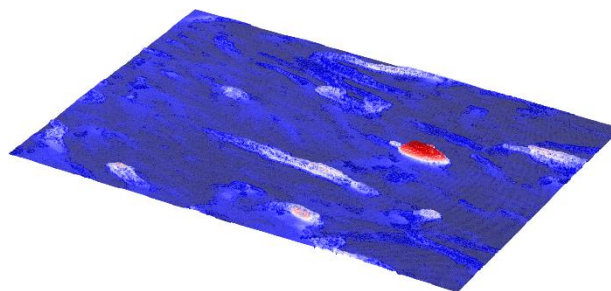


Figure 3. 3D representation of the top interface.

By default, structural parameters are calculated for the full image. This includes the average biofilm thickness, rugosity, rugosity coefficient, and porosity.

Table 1. Biofilm structural parameters.

Thickness (μm)	Roughness (μm)	Roughness coeff (-)	Porosity (-)
71.1	44.8	0.630	0.345

Users may also define regions of interest in the horizontal and depth axes to obtain the corresponding structural parameters.

Conclusions

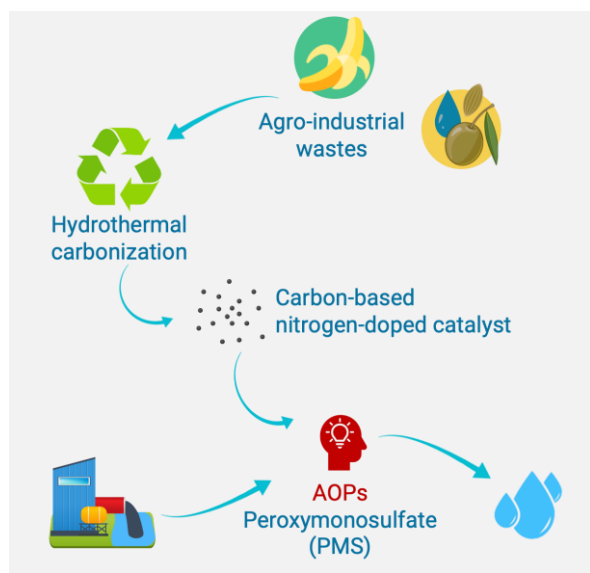
This work reports preliminary results from the planned extension of BISCAP to deal not only with 2D but also with the more general and complex 3D case. All image principles have been successfully adapted to the 3D case, and additional improvements have been included for increased performance. BISCAP now offers a rich insight into 3D biofilm structures, where many image outputs are available for analysis. Development work is ongoing and will be reported in full soon. The most current version of BISCAP is available at: <https://github.com/diogonarciso/BISCAP>.

Valorization of agro-industrial wastes by hydrothermal carbonization: synthesis, nitrogen functionalization, and evaluation as carbocatalysts in water treatment

S. Escudero-Curie*, X.L. Rodríguez, A. Díez, M. Pazos, A. Sanromán

CINTECX. Universidade de Vigo, Department of Chemical Engineering. Campus As Lagoas-Marcosende, 36310 Vigo, Spain.

*sescudero@uvigo.gal



The transition to a circular economy model is essential to reduce the rate of resource consumption and waste generation. The valorization of waste is a key strategy to extend the life cycle of products and transform waste into energy or raw materials. Agro-industrial wastes can be valorized through a hydrothermal carbonization (HTC) process, resulting in the production of hydrochar (HC). HC can be used as a carbocatalyst in advanced oxidation processes (AOPs), such as systems based on the activation of peroxymonosulfate (PMS), for water treatment. Although carbocatalysts are not as efficient as traditional metallic catalysts, they can be functionalized with nitrogen to enhance their performance. In this study, valorization of two residues, namely alperujo (A) and banana peel (B), was performed by producing and functionalizing four types of N-HCs for the removal of the dye Reactive Black 5 (RB5). Results showed that N-HCs derived from A were more effective in removing RB5 than those derived from B, with N-HCA functionalized with the crosslinker EDC achieving an 80% removal of RB5. The main mechanism of action was attributed to the active complexes on the surface of the material.

Introduction

The current rate of resource consumption and waste generation is not sustainable for the planet. One way to tackle this problem is by transitioning to a circular economy model, which involves reusing, recycling, and adding value to existing materials and products, thereby optimizing the utilization of raw materials, and increasing the efficiency of industrial processes. The valorization of waste is a key strategy that aims to extend the life cycle of products and transform waste into energy or raw materials, avoiding landfills.

Despite this, the only residual product of human activity is not just materials or products that can be reused. The issue of pollution arises in various ways, but one of the most concerning is the presence of contaminants in masses and streams of water, which is evident worldwide. Particularly, organic compounds interact more with living beings and are more difficult to eliminate from ecosystems. These bio-recalcitrant substances disrupt the natural cycle of ecosystems and enter aquatic systems through human-generated waste. Thus, effective regulations and processes for degrading organic contaminants in water are needed.

Conventional water decontamination processes are sometimes ineffective in achieving an adequate degree of purity. Therefore, the development of new processes that can more effectively eliminate or reduce contamination levels has been necessary. Among these new decontamination methods, one of the most prominent is the so-called AOPs. In addition, it has been demonstrated that when combined with other processes such as adsorption or biological processes, they reach their potential in terms of economic efficiency due to savings in chemicals and/or energy [1]. AOPs based on sulfate, such as the use of PMS, require catalysts, with metallic catalysts being the most used (Fenton-like processes). These catalysts produce secondary contamination through leaching or sludge generation, which leads to additional costs and operational problems. To avoid these drawbacks, studies are being conducted on carbon-based catalysts, known as carbocatalysts, as a greener alternative to

traditional methods. Agro-industrial waste can be valorized by HTC to obtain HC. This HC might be an excellent starting material for generating carbocatalysts. This way, two environmental problems could be solved at the same time, promoting a circular economy and using these wastes to fight against water pollution. Nevertheless, the catalytic activity of pristine HCs is generally lower than that of metallic catalysts, but HCs can be easily modified to adjust their electronic and physicochemical properties to make them more suitable for catalysis. Incorporating certain elements into the C atom matrix can break the original surface charge balance and induce polarization of the bonds at the point of inclusion, resulting in a more favorable material for chemical catalysis [2]. Doping with heteroatoms is a way to modify the surface properties of HCs to favor the electron transfer mechanisms that trigger different pathways of persulfate activation such as PMS. Among heteroatoms, nitrogen (N) is the most common and readily available for functionalization.

Objectives

The specific objectives of this study are to:

- Valorize two abundant agro-industrial wastes using HTC to produce HC as carbocatalysts.
- Functionalize the HC with nitrogen (N-HC) to enhance their catalytic capacity.
- Evaluate the catalytic capacity of the N-HC in a N-HC/PMS system for the removal of a model organic contaminant, Reactive Black 5 (RB5).
- Elucidate the mechanism of action of the N-HC in N-HC/PMS systems.

Materials and methods

Alperujo (A), main olive oil production waste, and banana peel (B) were used as HC precursors and were kindly provided by local companies (Aceites Abril S.L. and FreshCut S.L. respectively). RB5, Polyethyleneimine (PEI) and glutaraldehyde

(GTA) were purchased at Merck and 1-ethyl-3-(3-dimethylaminopropyl)carbodiimide (EDC) at TCI Europe N.V. HCs were synthesized for 2.5 h at 220 °C in a cylindrical stained steel hydrothermal reactor. A and B were introduced in a Teflon inner chamber of the reactor in a 1:3 solid:liquid ratio. After the necessary cooling time, the reactors were opened, and the corresponding HCs were washed and filtered. After that HCA and HCB were obtained and stored for further use.

The N-HC functionalization was carried out with PEI and two different methodologies using two different crosslinkers, GTA and EDC, as a post-treatment applied to the obtained HCs. Firstly, to obtain N-HC-GTA, 2 g of pristine HCA or HCB were added to 10 mL of a 10% w/v PEI/methanol solution and stirred at 180 rpm for 24 h at 30°C. The mixture was filtered and washed with methanol and dried. After that, the solid with PEI was added to 150 mL of a 2% GTA aqueous solution for 25 min at 30°C and 180 rpm. Then it was washed and dried. Secondly, to obtain N-HC-EDC, 1g of HCA or HCB was added to 100 mL of distilled water that contained 15.33 mL of a 50% w/w PEI/methanol solution and 1.1 g of EDC. The mixture was stirred at room temperature for 6 h. The resulting mixture was washed, filtered, and dried.

The catalytic activity was assessed in cylindrical, amber-colored reactor tubes. A catalyst load of 0.1 g/L and 2 mM PMS were added to 50 mL of RB5 and subjected to agitation using a rotary shaker for 2 h. Additionally, an adsorption control for each HC tested was performed in parallel, as well as a control of the PMS activity alone.

The quenching experiments were performed under the same conditions as the catalytic evaluation assays, with the addition of one of the quenchers NaN_3 (singlet oxygen inhibitor), KI (surface-active complexes inhibitor), or methanol (free radicals inhibitor).

Results

The results obtained from the catalytic capacity evaluation experiments can be observed in Figure 1. As shown, it can be observed that the performance of the materials derived from B is much lower than that of those derived from A. The adsorption exhibited by both A and B materials was very low, but it increased significantly for all N-HCs. Increased adsorption can facilitate greater interaction between active complexes on the surface and pollutants [3], which is consistent with their higher catalytic capacity. Both N-HCs showed that EDC was the crosslinker that provided the highest yield in removing RB5, indicating that this compound is much more efficient in introducing nitrogen into the HC structure so that it acts better in the N-HC/PMS system.

To elucidate the activation mechanism of PMS, it is necessary to identify the dominant oxidizing species in the N-HC/PMS

Acknowledgements

This research has been financially supported by MCIN / AEI /10.13039/501100011033 (Project PID2020-113667GB-I00 and PDC2021-121394-I00) and Project CINTECX-CHALLENGE 2023.

References

- [1] S. Monge et al. [Online] (2016). Available: http://www.cyted.org/sites/default/files/manual_sobre_oxidaciones_avanzadas_0.pdf
- [2] L. Dai et al., *Small*, 8 (2012) 1130-1166.
- [3] S. Navalón et al., *Chemical Reviews*, 114 (2014) 6179-6212.
- [4] H. Wang et al., *Water Research*, 160 (2019) 405-414.

system. As the material that exhibited the best performance in RB5 removal was N-HCA-EDC, achieving approximately 80%, experiments with various scavengers were carried out using this material. It was observed that almost all of the decolorizing capacity of the N-HC/PMS system was due to the action of the active complexes, with singlet oxygen in second place. This test confirms that the non-radical pathway is the main mechanism of PMS activation by N-HCA-EDC.

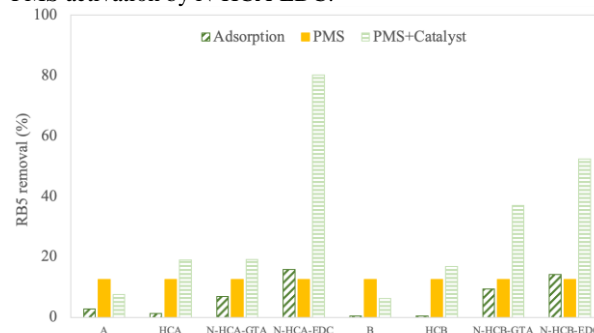


Figure 1. Comparison of the catalytic activity in the removal of RB5 of precursors, A and B, HCA and HCB, and all N-HCs tested.

Considering the kinetics, when the action of the surface-active complexes is blocked, decolorization reaches its maximum at 15 min and then the reaction stops completely at only 20% of RB5 removal. On the other hand, when free radicals are inhibited, the reaction continues fully. This is because free radicals and singlet oxygen are reactive oxygen species that are consumed by participating in the degradation reaction, while active complexes act by the mechanism of surface electron conduction and are able to degrade pollutants without becoming depleted immediately [4].

Conclusions

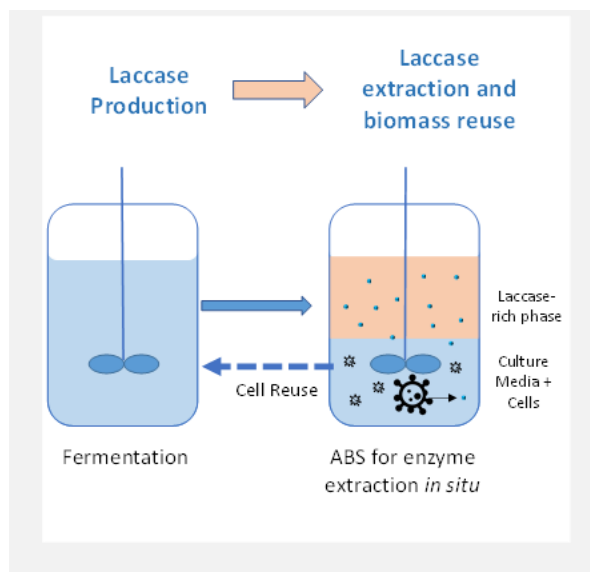
The use of functionalized HCs, N-HCs, for catalytic processes in waste treatments might contribute to the valorization of agro-industrial wastes and the implementation of circular economy principles. Functionalization of carbon materials is a promising approach to improving their catalytic activity. By modifying the electronic and physicochemical properties of the carbon matrix, it is possible to make it more suitable for catalytic processes, such as the activation of PMS in N-HC/PMS systems. As has been shown, nitrogen doping can significantly improve the catalytic performance of N-HCs, particularly using EDC as crosslinker. This strategy presents a low-cost, sustainable, and environmentally friendly alternative to traditional metal-based catalysts, which often require the use of non-renewable resources and generate high amounts of waste.

Development of an integrated process for the production and purification of laccase

F.F. Magalhães*, C. Alves, A.Q. Pedro, M.G. Freire, A.P. Tavares

CICECO - Aveiro Institute of Materials, Department of Chemistry, University of Aveiro, Aveiro, Portugal

*flaviamagalhaes@ua.pt



Extractive fermentation is an integrated process that uses aqueous biphasic systems to combine the production and primary purification procedures into a single step. With this concept, the main goal of this work was to design a bioprocess that integrates laccase production and purification using a genetically engineered yeast (*Pichia pastoris*), creating a competitive and sustainable process.

Successful expression in *P. pastoris* resulted in the production of extracellular recombinant laccase. Microbial growth and laccase production in fermentation was evaluated in media with ABS constituents to integrate the purification step. The laccase produced was recovered, concentrated by precipitation, and characterised.

This work demonstrates that ABS is a promising alternative for integrative protein production platforms, with the potential to minimise production steps and, consequently, process costs.

Introduction

Laccases (EC 1.10.3.2) are multicopper enzymes that use molecular oxygen to catalyse the oxidation of several substrates, such as phenolic compounds and aromatic amines [1]. Laccases are used in a wide range of industrial and biotechnological processes, including wastewater treatment, paper and pulp industry, clarification of wine, synthesis of organic compounds, and polymerisation reactions. However, enzymes' production and purification costs are high due to low productivity and the multi-step purification process [2].

Aqueous biphasic systems (ABS) are liquid-liquid extraction systems composed mainly of water, which creates a biocompatible environment ideal for applications within the biotechnology field [3]. These advantages have led to extensive research on ABS in the downstream processing of value-added biomolecules, such as enzymes. For the purpose of creating competitive and more environmentally friendly downstream processes than those currently in use, the development of integrated bioprocesses is necessary, such as extractive fermentation [3]. In this process, the microorganism is restrained in one of the ABS phases, while the target compound produced is partitioned to the other phase, combining the production and primary purification steps process in a single step.

This work aims to develop a bioprocess to integrate the production and purification of laccase while creating a sustainable and low-cost process. For this, fermentation processes were evaluated using a genetically modified yeast (*Pichia pastoris*) to produce laccase in media with ABS constituents to integrate the purification step.

Methods

Recombinant laccase from *Trametes versicolor* expressed in *P. pastoris* was produced. *P. pastoris* was cultivated in BMGY medium for 24 h at 30° C and 200 rpm, and further used to inoculate the fermentation assays with an initial OD₆₀₀ (Optical Density) of 1. Fermentation occurred in BMMY with copper supplementation for 13 days at 30°C and 200 rpm, with daily

methanol supplementation. Laccase production was monitored by the quantification of enzymatic activity by UV-Vis spectrophotometer at 420 nm measuring 2,2'-azino-bis(3-ethylbenzothiazoline-6-sulfonic acid) (ABTS) kinetic oxidative reaction.

To study extractive fermentation, the fermentation medium was supplemented with multiple ABS constituents (salts, polymers, and ionic liquids) with concentrations between 10-20 wt% and microbial growth was monitored by OD₆₀₀ measurement. Using the best ABS compounds for microbial growth, laccase production was studied in the BMMY fermentation medium supplemented with the compounds.

The protein was characterised by SDS-PAGE and biological activity, and optimal pH and temperature for enzyme activity were found.

Results

The expression in *P. pastoris* was successful, and the extracellular recombinant laccase was produced (Figure 1). Laccase was detected after six days of fermentation, achieving the highest enzymatic activity on day 13.

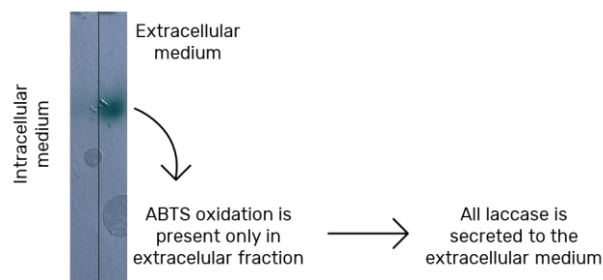


Figure 1. Semi-native SDS-PAGE gel with ABTS revelation

Several ABS constituents were tested to evaluate the microbial growth. Using 10 wt% propylene glycol with a molecular weight of 400 g mol⁻¹ (PPG 400), cholinium chloride and ammonium sulfate inhibit yeast growth. The best growth results were

achieved using 10 wt% polyethylene glycol with a molecular weight of 2000 g mol⁻¹ (PEG 2000) and 10 wt% phosphate buffer pH 6.

Fermentation for laccase production in ABS was performed in the best ABS constituents for microbial growth, and phase separation was achieved, allowing microbial recovery for future reuse and laccase extraction. Further purification steps applied were protein precipitation with ammonium sulfate, methanol, and acetone.

Acknowledgements

This work was developed within the scope of the project CICECO-Aveiro Institute of Materials, UIDB/50011/2020, UIDP/50011/2020 & LA/P/0006/2020, financed by national funds through the FCT/MCTES (PIDDAC). Ana P. M. Tavares and Augusto Pedro acknowledge FCT for the research contract CEECIND/01867/2020 and CEEC-IND/02599/2020, respectively. Flávia Magalhães acknowledges the SPQ/FCT PhD grant SFRH/BD/150669/2020.

References

- [1] J.R. Jeon et al., *Microbial Biotechnology*, 5 (2012) 318-332.
- [2] D. Raina et al., *Chemosphere*, 294 (2022) 133712.
- [3] F.F. Magalhães et al., *Current Opinion in Green and Sustainable Chemistry*, 27 (2021) 100417.

The laccase produced presents a high thermal stability, keeping its activity stable between 20 and 40 °C (tested range).

Conclusions

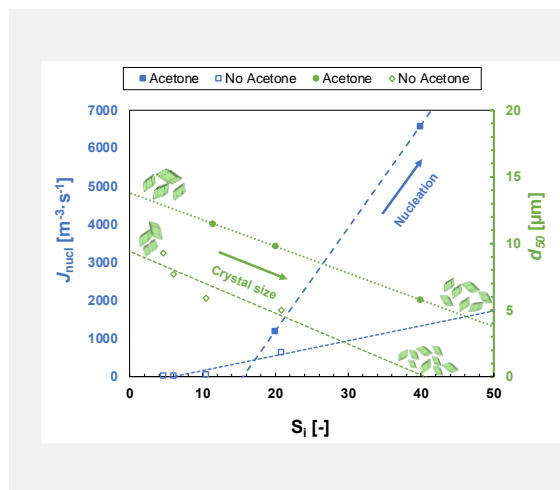
This work shows ABS as a promising option for integrative platforms for protein production, with the possible ability to reduce production steps, thus reducing process costs.

Investigation of insulin nucleation kinetics under oscillatory flow mixing

F. Castro^{1*}, S. Araújo¹, J. Ferreira¹, A. Ferreira¹, J. Campos¹, J.A. Teixeira², F. Rocha¹

¹Faculty of Engineering of the University of Porto, s/n, R. Dr. Roberto Frias 4200-465, Porto, Portugal; ²Centre of Biological Engineering of the University of Minho, Campus de Gualtar 4710-057, Braga, Portugal.

*filipaj@fe.up.pt



Crystallization can represent a cost-effective and scalable alternative for protein separation and purification. However, it is still not widely implemented in biopharmaceutical industry due to limited understanding of the underlying phenomena.

Herein, insulin crystallization was investigated in an oscillatory flow reactor in the presence and absence of acetone. The results show the impact of both supersaturation (i.e., insulin concentration) and acetone on nucleation kinetics and crystal size distribution (CSD). As supersaturation increases, the nucleation rate increases and mean crystal size decreases. In its turn, acetone allows faster nucleation, a narrower CSD and larger mean crystal size. The kinetic parameter A derived from the classical nucleation theory (CNT) also indicate the acceleration of the kinetics of molecular attachment in the presence of acetone.

These findings contribute to the better understanding of insulin crystallization mechanism under oscillatory flow mixing.

Introduction

Protein therapeutics have become an important segment of biopharma due to their increasing use to treat diseases [1]. While chromatography has been the main bioseparation method, the future of the industry relies on its ability to develop more cost-effective and scalable separation techniques. In this context, protein crystallization requires no costly equipment and consumables, handles high process volumes and protein titers, and yields highly pure products in a single-step [2]. Despite its huge potential, barriers to the industrial adoption of crystallization as a bioseparation method remain. This is namely due to the complexity of the occurring phenomena and the unavailability of generalized crystallization strategies in the case of proteins [3].

Objectives

The present work aims to develop a unique platform for protein crystallization based on oscillatory flow technology [4]. The target system is insulin, the first crystalline protein to be approved for therapeutic uses [5]. However, limited research has been conducted on agitated/sheared crystallization of insulin, in particular exploring crystallization kinetics. Therefore, insulin batch crystallization assays were carried out in a meso scale oscillatory flow reactor provided with smooth periodic constrictions (OFR-SPC) coupled to a spectrometer for *in-situ* measurements of solution turbidity. Herein, the influence of supersaturation (i.e., insulin concentration) and presence of acetone on nucleation kinetics and crystal size distribution (CSD) were assessed.

Methods

The experimental set-up is shown in Figure 1. The mixing intensity is controlled by the oscillation frequency (f) and amplitude (x_0), fixed at 1.83 Hz and 5.3 mm, respectively. Isothermal batch insulin crystallization trials were carried out at 20 °C and pH 5.7 during 150 min. Experiments started by

injecting simultaneously equal volumes of insulin (0.3 to 5.0 mg.mL⁻¹ in 20 mM HCl) and precipitant (7.50 mM ZnCl₂, 75.0 mM trisodium citrate and 0% or 30% (v/v) acetone in 20 mM HCl) solutions in the meso OFR-SPC.

The solution turbidity was monitored over time through UV-Vis spectrophotometry ($\lambda = 400$ nm) to estimate the induction time (t_{ind}) and then determine the nucleation rate (J_{nucl}) following the classical nucleation theory (CNT). Insulin solubility was measured, and crystal yield was estimated. For this, insulin concentration in solution was measured by UV-Vis spectrophotometry, at 280 nm and at 562 nm through BCA protein assay, in the absence and presence of acetone, respectively. The collected suspensions were observed under an optical microscope coupled to a camera to measure CSD. A minimum of 500 crystals were measured (Feret diameter) using Image J software to ensure a representative population of crystals with a 90% confidence interval.

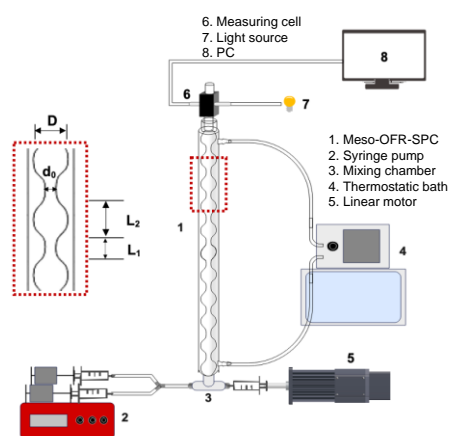


Figure 1. Schematic representation of the experimental set-up and characteristic dimensions of the meso-OFR-SPC [4]: $D = 3$ mm, $d_0 = 1.6$ mm, $L_1 = 6$ mm, and $L_2 = 13$ mm.

Results

An overview of the main results from the insulin crystallization assays carried out in the meso-OFR-SPC is given in Figure 2 and Table 1. It is possible to verify a faster insulin nucleation event with the increase of the initial supersaturation ratio (S_i) (i.e., increase of protein concentration) both in the presence and absence of acetone, though dependence of insulin nucleation kinetics on S_i is more pronounced at higher S_i . According to the CNT, there is a strong correlation between (primary) homogeneous nucleation rate and supersaturation. As shown in Figure 2, results suggest a (primary) homogeneous nucleation mechanism at higher S_i and a (primary) heterogeneous nucleation mechanism at lower S_i .

The results also evidence the key role of acetone on the insulin nucleation kinetics. At similar S_i , nucleation rate J_{nuc} is ~ 2 times higher for insulin crystallization assays performed with acetone (Table 1). The kinetic (A) and thermodynamic (B) parameters following the CNT were derived for homogeneous nucleation (Table 1). It was verified that A increases ~ 2.5 times in the presence of acetone, indicating an acceleration of the kinetics of molecular attachment.

CSD results (Table 1) show a smaller mean crystal size (d_{50}) as S_i increases and higher mean crystal size (d_{50}) in the presence of acetone when compared to the assays without acetone. Further, narrower CSD is verified in the presence of acetone. This corroborates the nucleation kinetics results (Figure 2 and Table 1), since high J_{nuc} were verified at higher S_i leading to the formation of numerous small crystals, while at lower S_i nucleation is slower leading thus to the formation of fewer but larger crystals. Insulin crystallized under a rhombohedral shape for all the studied experimental conditions.

Regarding crystal yield, values higher than 60% were obtained. Table 1 also shows the critical impact of S_i on crystal yield, where higher S_i led to higher crystal yields.

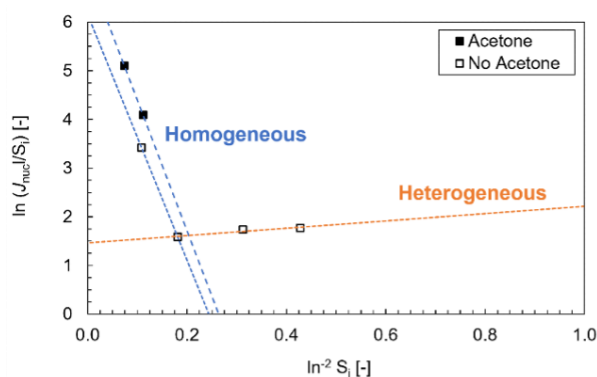


Figure 2. Overview of insulin nucleation kinetics in the meso OFR-SPC.

Conclusions

The present study describes the investigation of insulin nucleation kinetics in a meso OFR-SPC. The significant impact of the initial supersaturation ratio (i.e., insulin concentration) on insulin nucleation kinetics was confirmed. At higher supersaturations, faster nucleation kinetics were verified and consequently a higher number of smaller crystals was formed, whereas at lower supersaturations, slower nucleation kinetics were obtained leading to the formation of fewer but larger crystals. Further, it was verified that acetone accelerates the insulin nucleation kinetics and led to the formation of a more uniform insulin crystals population. In conclusion, this works gives insights into insulin crystallization mechanism under oscillatory flow mixing, which can boost the exploitation of oscillatory flow reactors for technical scale protein crystallization.

Table 1. Summary of the insulin crystallization assays performed in the meso-OFR-SPC at 20 °C and pH 5.7.

	S_i^* [-]	Nucleation kinetics		Parameters of homogeneous nucleation		CSD		Yield [%]
		t_{ind} [s]	J_{nuc} [$m^{-3}.s^{-1}$]	A [$m^{-3}.s^{-1}$]	B [-]	d_{50} [μm]	Span [-]	
Acetone	39.9	19	6579	1.2×10^{-9}	26.8	5.8	0.7	
15% (v/v)	20.0	104	1202			9.8	0.6	
	11.4					11.5	0.7	
No acetone	20.8	196	638	4.7×10^{-10}	25.2	5.0	2.0	99.6
	10.5	2446	51			5.9	2.1	87.1
	6.0	3677	34			7.7	1.8	83.0
	4.6	4624	27			9.3	1.0	61.6

* S_i is defined as the ratio between insulin initial concentration and insulin solubility in the studied conditions.

Acknowledgements

J. F. acknowledges funding from CEFT under FCT/MCTES (PIDDAC) through a postdoctoral scholarship. This work was financially supported by: HealthyWaters (NORTE-01-0145-FEDER-000069), supported by Norte Portugal Regional Operational Programme (NORTE 2020), under the PORTUGAL 2020 Partnership Agreement, through the European Regional Development Fund (ERDF); and LA/P/0045/2020 (ALiCE), UIDB/00532/2020 and UIDP/00532/2020 (CEFT), UIDB/00511/2020 and UIDP/00511/2020 (LEPABE), funded by national funds through FCT/MCTES (PIDDAC).

References

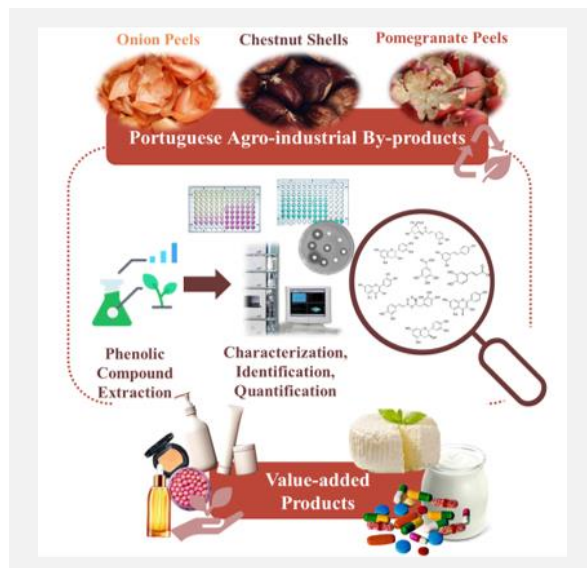
- [1] D. Agyei et al., Protein & Peptide Letters, 24 (2017) 94-101.
- [2] R. dos Santos et al., Biotechnology Advances, 35 (2017) 41-50.
- [3] C.N. Nanev, Progress in Crystal Growth and Characterization of Materials, 66 (2020) 100484.
- [4] A. Ferreira et al., PCT/IB2014/065273;WO/2015/056156; EP3057694 (B1), 2019.
- [5] S.K. Basu et al., Expert Opinion on Biological Therapy, 4 (2004) 301-317.

Valorization of agro-industrial by-products: the chemistry behind the biological properties of phenolic extracts and their potential for value-added products

*S. Ferreira**, *L. Santos*

LEPABE - Laboratory for Process Engineering, Environment, Biotechnology and Energy, Faculty of Engineering, University of Porto, Rua Dr. Roberto Frias, 4200-465 Porto, Portugal; ALiCE - Associate Laboratory in Chemical Engineering, Faculty of Engineering, University of Porto, Rua Dr. Roberto Frias, 4200-465 Porto, Portugal.

**up201604659@fe.up.pt*



Population expansion has increased the demand for food processing, leading to the production of agricultural by-products such as chestnut shells, onion peels, and pomegranate peels. These by-products are rich in bioactive substances, such as phenolic compounds, which can be extracted and incorporated into different products from the food, pharmaceutical and cosmetic industries. Knowledge of the phenolic compounds composition in these extracts is essential to appreciate their health benefits. High-performance liquid chromatography (HPLC) is essential to identify and quantify phenolic compounds. In this study, an HPLC screening method was developed and validated for nine phenolic compounds (caffeic acid, catechin, chlorogenic acid, epicatechin, and gallic acid). Three different phenolic extracts were analyzed by the HPLC method and characterized regarding their biological properties, to understand how the chemical composition can influence the biological activity of these extracts.

Introduction

The growing human population have been accompanied by an increase in agricultural waste and by-products generated. This heightened concern about this issue prompted the scientific community to research and create solutions to valorize these byproducts and lessen their harmful consequences. Indeed, to create a more sustainable world, one of the United Nations' 2030 goals is to minimize food waste generation [1]. By-products are rich in bioactive compounds, including antioxidants, fibers, and vitamins, among other substances [2]. Phenolic compounds (PC) are some of the main substances found in agro-industrial by-products, such as peels, seeds, and shells. These compounds are secondary metabolites from plants and act as protective agents towards external aggression [1]. Literature studies reveal that PC have a vast set of biological activities, antimicrobial, antiviral, anti-allergic, and anti-cancer; however, their antioxidant capacity stands out the most. These molecules can act as natural antioxidants due to their ability to reduce oxidative stress [3]. Due to their biological properties, PC have been gaining attention since they can be beneficial for human health. Therefore, these compounds have been incorporated into different matrices, in different industries, such as food, pharmaceutical and cosmetics [4]. Even though the evaluation of the physicochemical and biological activities of PC can be found in the literature, the correlation between these activities and the composition of the extracts is not always studied. The identification and quantification of the molecules present in phenolic extracts added to a product can explain their bioactive capabilities; therefore, the development of analytical screening methods is necessary.

Objectives

The main purpose of the present work was the development of a screening method using an HPLC-DAD technique to identify and measure the primary phenolic compounds contained in extracts from Portuguese agro-industrial (chestnut shells – CS -, onion peels – OP - and pomegranate peels - PP). Furthermore, it also aimed to associate the biological characteristics of the extracts with their composition.

Methods

The extracts were obtained through solid-liquid extraction, with a Soxhlet apparatus, using ethanol as extraction solvent. The solvent was evaporated with a rotary evaporator, followed by evaporation with nitrogen. Afterwards, the extracts were characterized regarding their total phenolic content through the reaction with the Folin-Ciocalteu reagent. Additionally, their antioxidant properties were assessed via the assay with the radical DPPH and ABTS. The antibacterial capacity of the different extracts was also evaluated using a disc diffusion assay. Their effect was evaluated against two Gram-positive bacteria *Staphylococcus aureus* e *Staphylococcus epidermidis* and against one Gram-negative bacteria *Escherichia coli*. The sun protection value (SPF) was also evaluated. These assays were all performed using literature protocols [5], [6]. The chemical composition of the extracts was evaluated using High-Performance Liquid Chromatography with a diode array detector (HPLC-DAD). The preparation of the samples and the composition of the mobile phase is described in Figure 1.

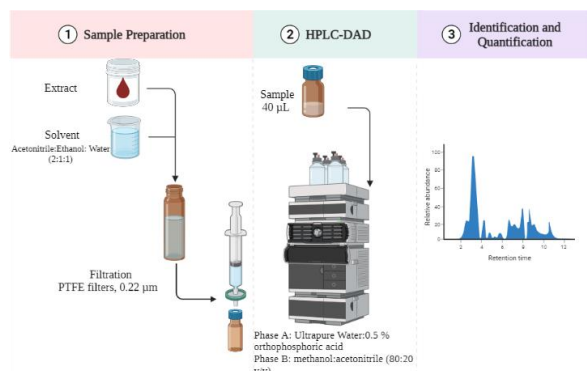


Figure 1. Protocol for the sample preparations and composition of the mobile phase for the analysis with HPLC-DAD.

Results

For the validation of the HPLC method, the validation parameters were selected accordingly to the recommendation of the Q2(R2) guidance of the International Council for Harmonization. The selected parameters were linearity, sensitivity, precision, robustness and accuracy. The developed HPLC-DAD technique demonstrated adequate accuracy (recovery levels between 70% and 120%), suitable linearity, sensitivity, precision, and durability (RSD values inferior to 10%). After the validation, the screening method was applied to identify the main PC in the composition of the chestnut shell, onion peel and pomegranate peel extracts. The results are displayed in Table 1.

Table 1. Phenolic compounds identified in the different extracts.

Compound (mg _{compound} /g _{extract})	Chestnut Shell	Onion Peel	Pomegranate Peel
Caffeic acid	-	-	0.15 ± 0.01
Catechin	2.59 ± 0.15	0.28 ± 0.01	1.32 ± 0.06
Chlorogenic acid	-	-	0.40 ± 0.05
Epicatechin	-	-	2.21 ± 0.27
Gallic Acid	0.97 ± 0.10	-	0.19 ± 0.05
Kaempferol	-	0.87 ± 0.01	-
Quercetin	-	21.90 ± 0.19	-
Resveratrol	0.07 ± 0.02	4.68 ± 0.49	0.48 ± 0.18
Rosmarinic acid	0.11 ± 0.00	1.22 ± 0.33	-

From Table 1, it is possible to verify that all of the extracts evaluated display a different chemical composition; as consequence, their biological properties will also be dissimilar.

Acknowledgements

This work was financially supported by: LA/P/0045/2020 (ALiCE), UIDB/00511/2020 and UIDP/00511/2020 (LEPABE), funded by national funds through FCT/MCTES (PIDDAC). Sara M. Ferreira would like to thank the Portuguese Foundation for Science and Technology (FCT) for her PhD grant (2022.10910.BD).

References

- [1] A.D. Rodriguez-Lopez et al., Chapter 5 in Sustainability of the Food System, N. Betoret and E. Betoret, Eds. Academic Press, 2020, 71-99.
- [2] E. Capanoglu et al., Journal of Agricultural and Food Chemistry, 70 (2022) 6787-6804.
- [3] S.M. Ferreira et al., Molecules, 27 (2022) 969.
- [4] C. Jimenez-Lopez et al., Food & Function, 11 (2020) 4853-4877.
- [5] S.M. Ferreira et al., Food Bioscience, 51 (2023) 102293.
- [6] S.M. Ferreira et al., Molecules, 28 (2023) 2037.

Considering CS extract, it is noticeable that the main PC are gallic acid and catechin. Both these compounds are associated with high scavenging ability, having the capacity to work as antioxidants. Indeed, this result is following the extracts characterization since this extract displayed better antioxidant properties than the OP and PP extracts. From the assay with DPPH, this extract exhibited a IC_{50} value of 4.9 mg/mL; for the ABTS assay, the value of Trolox equivalents was 620 mg_{TE}/g. Hence, CS extract is an interesting option to be incorporated in food, cosmetic and pharmaceutical formulations as an antioxidant agent.

In the OP extract the main phenolic was quercetin. This molecule is capable of absorbing UV radiation efficiently, due to its chemical structure. Undeniably, quercetin is known to exhibit exceptional characteristics to act as a UV agent. From the SPF values obtained, the extract that exhibited higher value was the OP extract, proving its potential to serve as a UV filter, since it can absorb radiation in the UV region and function as UV filters. Therefore, the obtained results display that OP extract is more suitable for cosmetic applications than for food. Regarding the PP extract, the main PC found were catechin and epicatechin. These compounds exhibit high antibacterial action towards both Gram-positive and Gram-negative bacteria, as a result of their ability to disrupt the bacterial membrane. Indeed, this extract was the one that revealed a higher capacity to inhibit the studied microorganisms, proving to have a better antibacterial capacity. Thus, as a result of its chemical composition, PP extract is a suitable option to be used as an antibacterial agent in multiple industries.

Conclusions

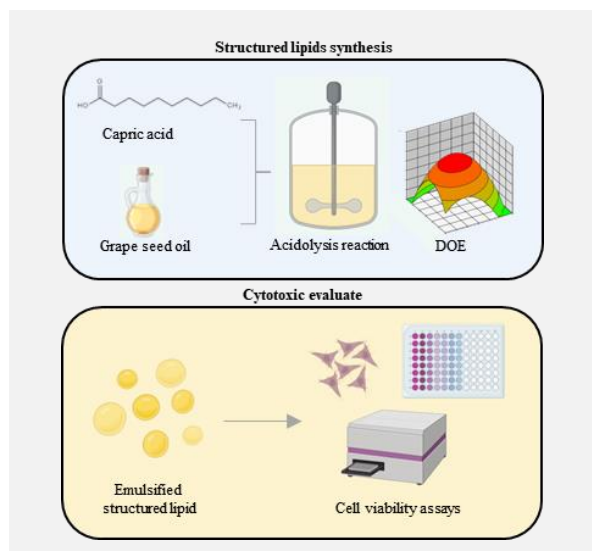
The present study aimed to develop an HPLC screening method to identify the main phenolic compounds present in phenolic extracts of different agro-industrial by-products. Furthermore, it aimed to demonstrate the relevance and influence of the chemical composition of phenolic extracts on their biological activities. Thus, it was demonstrated that, although there are some similarities in the composition of the extracts, the difference between the amounts of CP and the majority of compounds considerably influences the biological activity of the extracts and, consequently, their final application.

MLM-type structured lipids: synthesis and cytotoxic evaluate with murine fibroblast and human cervical adenocarcinoma cell lines

R.H. Miotti Jr^{1,2*}, S.R. do Amaral¹, F.L. Primo¹, J.F.B. Pereira^{1,2}, A.V. de Paula¹

¹São Paulo State University (UNESP), Department of Engineering of Bioprocesses and Biotechnology, School of Pharmaceutical Sciences Institution, Highway Araraquara-Jaú, Km 1, Araraquara, Brazil; ²University of Coimbra, CIEPQPF, Department of Chemical Engineering, Faculty of Sciences and Technology, Street Silvio Lima, Polo II, Coimbra, Portugal.

*rodney.miotti@unesp.br



The present work aimed to produce and evaluate the cytotoxic capacity of MLM-type structured lipids (MLM-SL). At first, synthesis of structured lipids by *Rhizopus oryzae* lipase immobilized on styrene-divinylbenzene, which were capable of incorporating 61.05 ± 0.51 mol% of capric acid in the sn-1 and sn-3 position of the triacylglycerol structure of grape seed oil. From this high incorporation degree, cell viability assays were performed with murine fibroblast cell lines and human cervical adenocarcinoma cell lines. Concerning the cytotoxicity assays, the less concentrated MLM-SL emulsions were unable to deactivate cells in both strains. On the other hand, increasing the concentration of MLM-SL to 1.75 and 2% v/v, the emulsions were able to induce cell death in 56% and 64% of adenocarcinoma cells, respectively. Human cervical adenocarcinoma cells showed greater sensitivity to the induction of cell death when using emulsions with MLM-SL > 1.75% v/v compared to emulsions with lower content indicating a potential for combating carcinogenic cells.

Introduction

In the search for new technologies for the production of healthier foods, the use of modified oils and fats has become a relevant strategy in new food formulations. In addition to having basic nutraceutical properties, they also contribute to the physiological processes used in the prevention and treatment of diseases [1]. Among the modifications of oils and fats, a specific group of structured lipids (SL) can be mentioned, this being the MLM type. MLM-type structured lipids are those with long-chain fatty acids at the sn-2 position of triacylglycerol and medium-chain fatty acids at sn-1 and sn-3 of triacylglycerol [2]. They can be synthesized by the enzymatic route and catalyzed by lipases (triacylglycerol acyl hydrolases, EC 3.1.1.3), thus enabling the formation of specific structured compounds particularly unable to be obtained using chemical catalysts [1-2]. There is great interest in the production of this triglyceride because its low caloric index, in addition to have unsaturated fatty acids in its central region. Thus, the choice of grape seed oil as a starting material for the synthesis of MLM-type structured lipid is due to high amount of unsaturated fatty acids, which are predominantly in the inner position of triacylglycerol, such as linoleic acid (58-78%). Therefore, this oil allows to obtain a higher amount in the sn-2 position when compared to corn oil (34-65.5%) and soybean oil (48-59%) [1], which advocates the synthesis of fatty acids polyunsaturated fatty acids (PUFAs) [2-3]. PUFAs exhibit anticarcinogenic and anti-inflammatory potential [5-6], acting in the process of apoptosis and death of cancer cells. This work aimed the production MLM-SL having high degree of capric acid incorporation, given that an acidolysis reaction is catalyzed by lipase immobilized from *Rhizopus oryzae*. Furthermore, the MLM-SL was applied in cell viability assays whit murine embryonic fibroblast (NIH- 3T3 - ATCC® CRL-1658™) and cervical cancer cells (HeLa, ATCC® CCL-2, aiming the development of nanoemulsion as a new therapeutic approach.

Materials and Methods

Production of SL

Commercial lipase from *Rhizopus oryzae* (Prozyn - São Paulo) were immobilized on styrene-divinylbenzene. The reactions were carried out in a jacketed glass reactor (diameter 3 cm; height 6 cm) equipped with a heating jacket connected to a water bath. The reaction mixture contained grape seed oil and capric acid with different molar ratios were optimized following a CCRD (Table 1). The incorporation degree (ID) of capric acid in the structure of triacylglycerols was determined by gas chromatography [1]. The modified grape seed oil was concentrated in the nano emulsions carried out following [7].

Table 1. Matrix of factorial design used to acidolysis reaction.

Run	Coded variables		ID
	MR	T (°C)	(mol%)
1	-1	-1	21.97 ± 2.82
2	1	-1	45.96 ± 1.63
3	-1	1	14.67 ± 2.25
4	1	1	15.45 ± 2.26
5	-1.41	0	8.18 ± 2.09
6	1.41	0	29.15 ± 3.27
7	0	-1.41	36.93 ± 1.98
8	0	1.41	17.18 ± 4.86
9	0	0	56.33 ± 3.51
10	0	0	53.50 ± 2.87
11	0	0	54.00 ± 1.00

Cell Culture and In Vitro Cell Viability

Murine embryonic fibroblast (NIH- 3T3 - ATCC® CRL-1658™) and cervical cancer cells (HeLa, ATCC® CCL-2) were cultured following [8]. *In Vitro* cell viability was carried out with resazurin, NIH/3T3 and HeLa cells were seeded into a 96-wells plate (5x10³ cells/well) and incubated for 24h following [8].

Results

The immobilized enzyme showed high catalytic capacity reaching values of 1872 ± 37 U/g. When applied in the acidolysis reactions of capric acid with grape seed oil, the degree of incorporation varied from 8.18 ± 2.09 to 56.33 ± 3.51 mol%. These trials correspond to the lowest level of molar ratio and to the moderate level of design, respectively. At the optimal point of the factorial design, the degree of incorporation reached a value of 61.05 ± 0.51 mol%, and this final product was used in the following cytotoxicity assays.

Cell viability assays were used as a preliminary test for assessing the toxicity of the structured lipid. As shown in Figure 1, low concentrations of the nanoemulsions (1.125 and 1.5% v/v) did not cause cytotoxicity. However, with the increase of structured lipid concentrations, i.e., 1.75 and 2% v/v, the cell viability decreased to 15 and 9%, respectively. From these results, following *in vitro* cytotoxicity assays using HeLa human cervical adenocarcinoma cell lines (ATCC® CCL-2) were performed.

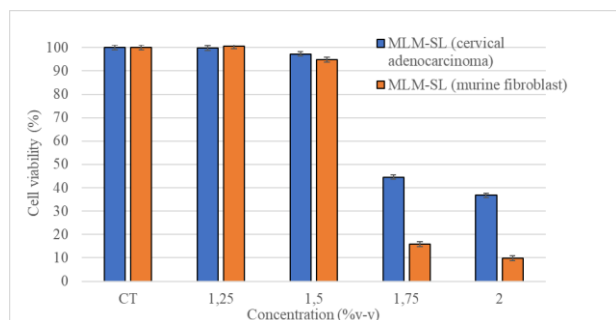


Figure 1. *In vitro* cytotoxicity test in fibroblast cells and human cervical adenocarcinoma cell lines.

Acknowledgements

CAPES (Finance Code 001), FAPESP (Process 2017/11482-7 and 2020/09592-1) and CNPq (Process 304399/2022-1 and Universal Grants (S.R.A and F.L.P. – Process 404416/2021-7)). CIEQPFF is supported by the Fundação para a Ciência e Tecnologia (FCT) through the projects UIDB/EQU/00102/2020 and UIDP/EQU/00102/2020.

References

- [1] N. Bassan et al., *LWT – Food Science and Technology*, 99 (2019) 600-606.
- [2] S. Rehman et al., *International Journal of Biological Macromolecules*, 97 (2017) 279-286.
- [3] S. Huerta-Yépez et al., *Boletín Médico del Hospital Infantil de México*, 73 (2016) 446-456.
- [4] R. Morales-Medina et al., *Food Chemistry*, 228 (2017) 634-642.
- [5] A.M. Eltweri et al., *Clinical Nutrition*, 36 (2017) 65-78.
- [6] N.R. Fuentes et al., *Molecular Aspects of Medicine*, 64 (2018) 79-91.
- [7] M.P. Siqueira-Moura et al., *Die Pharmazie*, 65 (2010) 9-14.
- [8] S.R. do Amaral et al., *Lasers in Medical Science*, 37 (2022) 3443-3450.
- [9] E.G. Lanna et al., *Biomedicine & Pharmacotherapy*, 134 (2021) 111114.
- [10] J. Roy et al., *Journal of Experimental & Clinical Cancer Research*, 34 (2015) 1-12.

The results of the viability assay with HeLa cells are presented in Figure 1. It can be observed that at low concentrations of the active lipid, there was no decrease in cell viability, indicating high biocompatibility. However, as the concentration increased to 1.75 and 2% v/v, the nanomaterial was capable of inducing cell death of 56 and 64% of adenocarcinoma cells, respectively. Lanna et al. [9] evaluated the action of the triglyceride of docosahexaenoic acid in breast cancer cells, as a lipid-core in nanoemulsion systems (nanoemulsions, nanocapsules, and nanostructured lipid carriers). They observed that all three nanocarriers decreased viability in a dose-dependent manner, while increasing treatment selectivity. Roy et al [10] develop a new polymeric nanocapsule containing polyunsaturated fatty acids. The authors observed that the nanomaterial can better internalize the active when tested in breast cancer cells, controlling the release of fatty acids into the cells. Based on the results obtained, it is possible to propose the developed nanoemulsion as a new therapeutic approach.

Conclusions

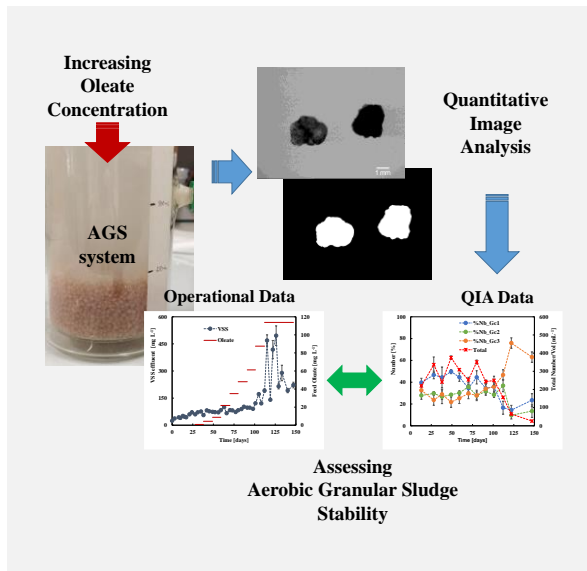
The immobilized lipase from *Rhizopus oryzae* demonstrated the ability to incorporate capric acid into the triacylglycerol structure of grape seed oil, reaching a level of 92% of the maximum theoretical capacity. Additionally, the final product was found to induce cell death when emulsified at concentrations exceeding 1.5% v/v.

Assessing the influence of long-chain fatty acids on aerobic granular sludge stability in a sequencing batch reactor

S.A. Silva^{1,2}, M.S. Duarte^{1,2}, A.L. Amaral^{1,2,3,4}, E.C. Ferreira^{1,2}, M.M. Alves^{1,2}, D.P. Mesquita^{1,2*}

¹CEB - Centre of Biological Engineering, Universidade do Minho, Campus de Gualtar, 4710-057 Braga, Portugal; ²LABELS - Associate Laboratory, Braga/Guimarães, Portugal; ³Polytechnic Institute of Coimbra, Coimbra Institute of Engineering, Rua Pedro Nunes, Quinta da Nora, 3030-199 Coimbra, Portugal; ⁴Polytechnic Institute of Coimbra, Applied Research Institute, Rua da Misericórdia, Lagar dos Cortiços - S. Martinho do Bispo, 3045-093 Coimbra, Portugal.

*daniela@deb.uminho.pt



The presence of long-chain fatty acids (LCFA) in biological wastewater treatment systems can cause various operational issues. This study evaluated the effect of LCFA, at typical concentrations found in domestic wastewater, on the performance and stability of aerobic granular sludge (AGS) in a sequencing batch reactor. At an oleate concentration of $61 \pm 2 \text{ mg L}^{-1}$, oleate started to accumulate in the reactor, resulting in an increase of volatile suspended solids concentration in the effluent. This caused small granules to be washed out due to their larger specific surface area for oleate adsorption. Selecting large granules could minimize oleate adsorption, preventing sludge washout and maintaining the reactor stability. Overall, the study demonstrates the feasibility of using AGS systems for treatment of oleate-containing wastewater for concentrations below $61 \pm 2 \text{ mg L}^{-1}$ and highlights the importance of limiting oleate adsorption for the stability of AGS systems.

Introduction

AGS technology is a promising alternative to conventional activated sludge systems for wastewater treatment due to its higher energy efficiency and cost-effectiveness [1]. However, AGS instability limits its widespread use. LCFA result from lipids hydrolysis, one of the most significant components of organic matter present in wastewaters, which may cause microbial inhibition and sludge settling problems in biological treatment systems [2,3]. However, the impact of LCFA on AGS systems is not yet fully understood, particularly at typical concentrations found in domestic wastewater. Quantitative image analysis (QIA) has emerged as a valuable tool for monitoring the morphology of sludge aggregates in both aerobic and anaerobic treatment processes, providing insight into the granulation process and stability of AGS systems [4]. By analyzing the morphology, size and content of granules, QIA can anticipate potential problems and assess process stability. This study aimed to investigate the impact on the stability of AGS systems of different concentrations of LCFA commonly found in domestic wastewater. The potential effects of LCFA on the morphology, size and content of granules using QIA was also evaluated.

Methods

A sequencing batch reactor (SBR) with a working volume of 1 L and dimensions of 18.5 cm height and 9 cm diameter ($H/D = 2$) was operated at room temperature with cycles of 6 h. The reactor was inoculated with AGS produced from activated sludge and fed with sodium acetate as carbon source. After 28 days, sodium oleate was added to the feed at concentrations ranging from $1 \pm 0.03 \text{ mg L}^{-1}$ to $114 \pm 4 \text{ mg L}^{-1}$. Oleate was used as the model LCFA due to its prevalence in raw products, sewage grease deposits, and wastewater treatment plants. The

volatile suspended solids in the effluent (VSS_{effluent}) and the sludge volume index at 5 min (SVI_5) and 30 min (SVI_{30}) were determined according to standard methods [5]. Oleate concentration was determined by gas chromatography according to [6]. The morphological changes of AGS, due to the increase in oleate concentration, were evaluated by QIA. Granules images were captured using an Olympus SZ-40 stereomicroscope (Olympus, Shinjuku, Japan) at a $15\times$ magnification. After images pre-treatment, segmentation, and debris removal, binary images of the granules were created, and further used to determine the granules' size, content and morphology [7]. The granules were characterized into three size classes based on their equivalent diameter (Deq): small - Gc1 ($0.2 \text{ mm} \leq Deq \leq 0.6 \text{ mm}$), intermediary - Gc2 ($0.6 \text{ mm} < Deq < 1 \text{ mm}$), and large - Gc3 ($Deq \geq 1 \text{ mm}$). Image analysis was conducted using Matlab™ 8.5 (The MathWorks Inc, USA).

Results

Oleate accumulation in the reactor (solid and liquid fractions) was detected when a concentration of $61 \pm 2 \text{ mg L}^{-1}$ was added to the feed. However, increasing the oleate concentration in the feed up to $114 \pm 4 \text{ mg L}^{-1}$ did not result in further accumulation inside the reactor (Figure 1A). At the highest oleate concentration, VSS_{effluent} increased drastically to $496 \pm 55 \text{ mg L}^{-1}$ (Figure 1B). The observed phenomenon is likely due to the adsorption of oleate onto granules, leading to sludge flotation and subsequent washout from the system. Before the addition of oleate, the sum of the fraction of small ($\%Nb_Gc1$) and intermediary ($\%Nb_Gc2$) granules (i.e., $Deq < 1 \text{ mm}$) represented 70% of the AGS, while the large granules ($\%Nb_Gc3$) accounted for the remaining 30% (Figure 1C). The granules distribution changed when AGS was exposed to the highest concentration of oleate, accompanied by a decrease in

the total number of granules (Figure 1C). On day 122, the prevalence of granules with $Deq < 1$ mm (Gc1 and Gc2) decreased to 25% and granules with $Deq \geq 1$ mm (Gc3) became predominant in the system. Thus, the sludge was selectively washed out, primarily consisting of smaller granules (i.e., $Deq < 1$ mm), while larger granules (i.e., $Deq \geq 1$ mm) were able to persist in the system (Figure 1C).

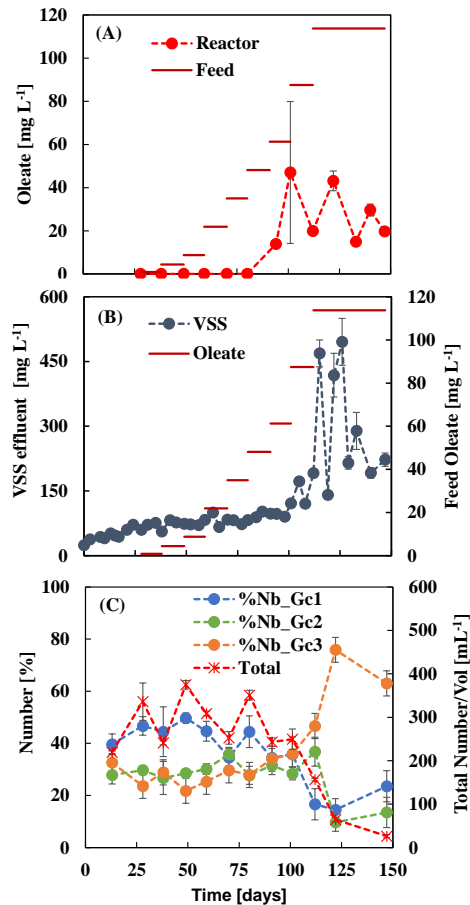


Figure 1. Operation and AGS profiles during the SBR operation. (A) Oleate concentration in the reactor and in the feed. (B) VSS concentration in the effluent. (C) Number distribution of small (%Nb_Gc1), intermediary (%Nb_Gc2) and large (%Nb_Gc3) granules.

Although the sludge exhibited good settling properties throughout the experiment, the settling velocity of the granules decreased when large granules were predominant (Figure 2A). In fact, the Deq of the overall granules size

increased considerably from 0.8 ± 0.03 mm (at day 80) to 2.0 ± 0.2 mm (at day 147), confirming that mostly large granules were able to endure in the system (Figure 2B). A significant decrease in the convexity of the overall granules underlined the appearance of protruding filaments on the granules outer layer, concomitant to the decrease of the sludge settling properties (Figure 2AB).

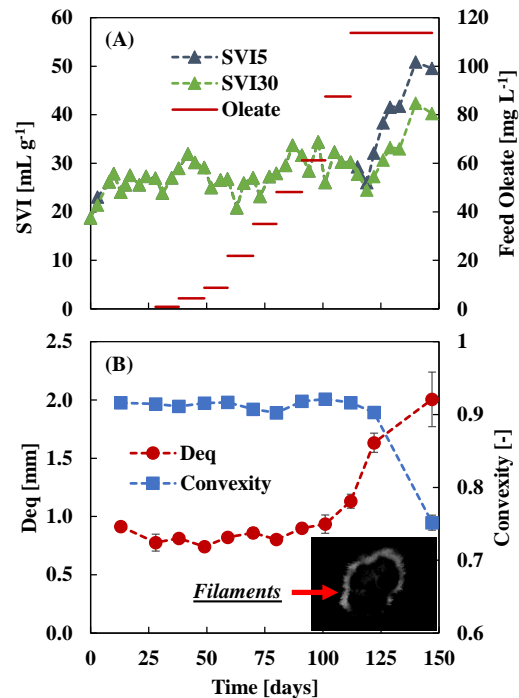


Figure 2. AGS profile during SBR operation. (A) Sludge volume index. (B) Equivalent diameter (Deq) and convexity of the overall granules.

Conclusions

This study suggests that oleate can have significant effects on the operation of an SBR system with AGS. The adsorption of oleate onto granules led to sludge flotation and washout from the system. Granules with $Deq < 1$ mm were selectively removed from the system due to their larger specific surface area, while larger granules remained. Limiting oleate adsorption appears to be a key factor in maintaining AGS stability in the presence of oleate-containing wastewaters. In this sense, the impact of oleate adsorption onto AGS could be minimized through the selective use of large granules, thus preventing extreme sludge washout.

Acknowledgements

The authors thank the Portuguese Foundation for Science and Technology (FCT) under the scope of the strategic funding of UIDB/04469/2020 unit, and by LABBELS – Associate Laboratory in Biotechnology, Bioengineering and Microelectromechanical Systems, LA/P/0029/2020. The authors also acknowledge the financial support to Sérgio A. Silva through the grant SFRH/BD/122623/2016 and COVID/BD/151748/2021 provided by FCT. Daniela P. Mesquita acknowledges FCT funding under DL57/2016 Transitory Norm Programme.

References

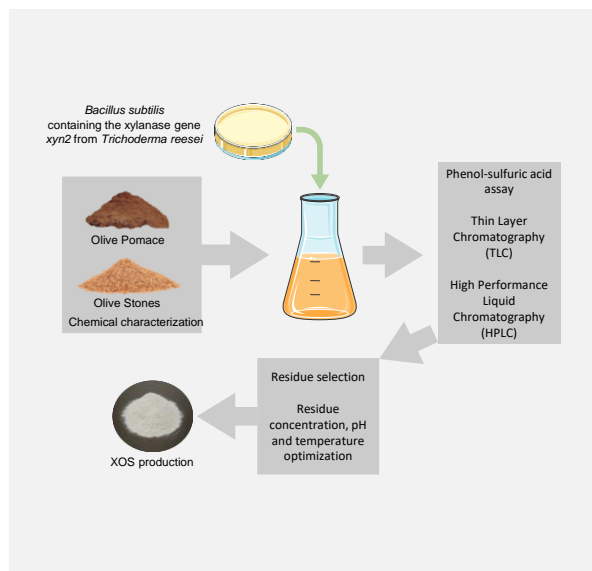
- [1] S. Bengtsson et al., *Environmental Technology*, 40 (2019) 2769-2778.
- [2] J.L. Chen et al., *Biotechnology Advances*, 32 (2014) 1523-1534.
- [3] S. Singh et al., *Science of the Total Environment*, 691 (2019) 960-968.
- [4] S.A. Silva et al., *Chemosphere*, 286 (2022) 131637.
- [5] APHA et al., *Standard Methods for the Examination of Water & Wastewater*, 21st Ed., APHA Press, Washington DC, 2005.
- [6] L. Neves et al., *Bioresource Technology*, 100 (2009) 91-96.
- [7] A.L. Amaral, PhD Thesis, University of Minho, Braga, 2003.

Olive oil by-products as potential alternative substrates for xylooligosaccharides production

A. Cordeiro^{1,2,3,4*}, A. Fernandes^{3,4}, A.M. Peres^{1,2}, L. Rodrigues^{3,4}, C. Amorim^{3,4}

¹Centro de Investigação de Montanha (CIMO), Instituto Politécnico de Bragança, Campus de Santa Apolónia, 5300-253 Bragança; ²Laboratório Associado para a Sustentabilidade e Tecnologia em Região de Montanha (SusTEC), Instituto Politécnico de Bragança, Campus de Santa Apolónia, 5300-253 Bragança, Portugal; ³CEB – Centre of Biological Engineering, Universidade do Minho, Campus de Gualtar, 4710-057, Braga, Portugal; ⁴LABELLS – Associate Laboratory, Guimarães, Braga, Portugal.

*anacordeiro.ac03@gmail.com



Olive pomace (OP) and olive stones (OS) are industrial by-products from the olive oil production. These residues have a high percentage of cellulose, hemicellulose, and lignin, which makes them a good source of fermentable sugars and xylan, as well as a potential alternative substrate for xylooligosaccharides (XOS) production. In this work, OP and OS were chemically characterized and used for the first time as a xylan source to produce XOS through direct fermentation by *Bacillus subtilis* 3610 containing the xylanase gene *xyn2* from *Trichoderma reesei*. OS presented the highest potential for XOS production. The fermentation process was further optimized for this residue in terms of residue concentration (5, 10, 20, 40 and 60 g L⁻¹), pH (5.0, 6.0, 7.0 and 8.0), and temperature (30, 37, 45 and 50°C). The highest total sugars yield (27 ± 2 mg g⁻¹) was achieved after 12 h, using 20 g L⁻¹ of OS at pH 7.0 and 45°C.

Introduction

Mediterranean countries, including Portugal, are the main producers of olive oil. According to the International Olive Oil Council, these countries produce 93.3% of the total olive oil in the world (www.internationaloliveoil.org). The olive oil extraction is done by mechanical processes, which originate large amounts of different residues that the producers have difficulties to discard, *e.g.*, olive pomace (OP). Depending on the extraction methods, OP can have different percentages of moisture, being rich in polyphenols, tocopherols, proteins, and squalene [1]. The olive stones (OS) are another residue obtained from the olive oil industry, which can be separated from the olive pulp by centrifugation and used as fuel for heating dryers [2].

Both residues have a significant percentage of hemicellulose, particularly xylan, which makes them a potential alternative substrate to produce prebiotic xylooligosaccharides (XOS), by direct fermentation [3].

XOS have been reported to have prebiotic effects, and beneficial health effects such as anti-cancer, anti-inflammatory, and anti-diabetic properties. Additionally, these compounds can also improve the organoleptic properties of foods, being interesting its incorporation into functional foods [4].

XOS are short chain oligosaccharides composed of 2 to 10 xylose units and are conventionally produced through enzymatic hydrolysis or autohydrolysis methodologies, or a combination thereof. However, an emerging production approach based on direct fermentation has the potential to compete with the established processes by reducing the operational costs [5].

In this work, we evaluated the potential of OP and OS for XOS production by direct fermentation, using *Bacillus subtilis* 3610 containing the xylanase gene *xyn2* from *Trichoderma reesei* previously reported as a successful microbial XOS produced with other residues [6].

Materials and Methods

Chemical characterization of olive pomace and stones

The OP and OS were provided by Cooperativa Agrícola de Macedo de Cavaleiros (Portugal). The lignin, cellulose and hemicellulose were quantified according to the protocols of the National Renewable Energy Laboratory (NREL) (www.nrel.gov/docs/gen/fy13/42618.pdf).

Microorganism and culture conditions

Engineered *Bacillus subtilis* 3610, containing the xylanase gene *xyn2* from *Trichoderma reesei* [7], was grown on LB agar, overnight, at 37°C. The pre-inoculum was prepared by picking one colony into 4 mL of LB medium and cultivated at 40°C and 250 rpm during approximately 2 h until reaching an OD_{600nm} ~ 1.0. This culture was then diluted to an OD_{600nm} ~ 0.020 with the fermentation medium, being grown at 150 rpm [7]. The fermentation medium consisted in a mixture of grinded residue in 2% (v/v) of basal Vogel medium, autoclaved at 121°C for 15 min. Different residue concentrations (5, 10, 20, 40 and 60 g L⁻¹), pH values (5.0, 6.0, 7.0 and 8.0) and temperatures (30, 37, 45 and 50°C) were tested to optimize the process. Samples were collected over time and evaluated using different analytical methods [8].

Analytical methods

Phenol - sulphuric acid assay was used to analyse the total sugar content [9]. Thin Layer Chromatography (TLC) was performed using TLC plates (Macherey-Nagel, Duren, Germany) and butanol, acetic acid, and water (2:1:1 v/v/v) as mobile phase. The bands were detected by spraying with a staining solution containing 1% (w/v) diphenylamine and 1% (v/v) aniline in acetone, followed by heating at 120°C during 10 min [8]. For monosaccharides quantification, a High Performance Liquid Chromatography (HPLC) (Agilent Technologies, USA) fitted an Aminex HPX 87H column (300 mm × 7.8; Biorad, USA) was used. A 5mM H₂SO₄ solution was used as the mobile phase at a

flow rate of 0.7 mL min^{-1} and 60°C . For the oligosaccharides' quantification, a HPLC (JASCO, Japan) fitted with a Shodex HILICpak VG-50 4E column ($4.6 \text{ mm} \times 250 \text{ mm}$; Shodex, Tokyo, Japan), was used. A 75:20:5 (v/v) acetonitrile/methanol/water mixture was used at a flow rate of 0.9 mL min^{-1} , at 40°C .

Results

The chemical composition of OP and OS, particularly their content in xylan, provides an important indication of their potential as alternative substrate for XOS production by direct fermentation.

OP presented $31.4 \pm 0.7\%$ of lignin ($7.0 \pm 0.5\%$ of soluble lignin and $27.6 \pm 0.6\%$ of Klason lignin), $18.5 \pm 0.5\%$ of cellulose and $25.5 \pm 0.5\%$ of hemicellulose, of which $12.9 \pm 0.4\%$ correspond to the xylan, $0.68 \pm 0.03\%$ of arabinan and $8.3 \pm 0.3\%$ of acetic groups. While OS was composed by $27.6 \pm 0.9\%$ of lignin ($3.8 \pm 0.2\%$ of soluble lignin and $23.1 \pm 0.9\%$ of Klason lignin), $21.1 \pm 0.8\%$ of cellulose and $26.8 \pm 0.9\%$ of hemicellulose, of which $14.8 \pm 0.4\%$ correspond to the xylan and $10.1 \pm 0.6\%$ of acetic groups. The values were expressed in % of dry weight and are in accordance with the literature [1],[2]. When compared with brewers' spent grain composition, previously reported as XOS fermentative substrate [6], OP and OS have comparable xylan contents, thus presenting potential for XOS production.

OP and OS potential for XOS production was then compared between each other by performing a fermentation with 20 g L^{-1} of residue, at pH 7.0, 45°C and 150 rpm. OS was the residue with the highest potential, presenting an increase of the total sugars yield from 0 h ($15 \pm 1 \text{ mg g}^{-1}$) until 12 h ($27 \pm 2 \text{ mg g}^{-1}$) and low amounts of undesired free sugars ($0.02 \pm 0.01 \text{ g L}^{-1}$), thus being selected for further optimization studies. The TLC and HPLC results suggested that XOS with a degree of

polymerization superior to 6 were produced with OS (Figure 1). After optimization, the highest total sugars yield ($27 \pm 2 \text{ mg g}^{-1}$) was achieved at 12 h with low amounts of free xylose ($0.02 \pm 0.01 \text{ g L}^{-1}$), using 20 g L^{-1} of OS at pH 7.0 and 45°C .

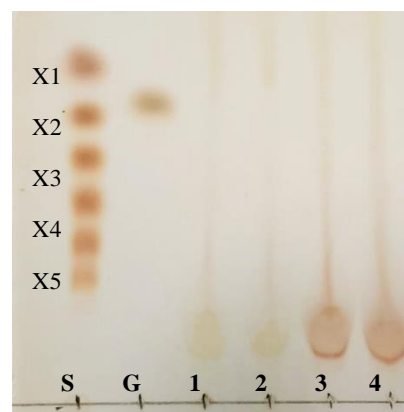


Figure 1. TLC of the supernatants obtained from the direct fermentation of OS under optimal conditions at 0 h (1 and 2) and 12 h (3 and 4) (optimal time). A mixture (S) containing 2 g L^{-1} of xylose (X1) and XOS with a degree of polymerization between 2 and 6 (X2-X6) and a solution of 1 g L^{-1} of glucose (G) were used as standard.

Conclusions

OS presented the highest potential for XOS production by direct fermentation. The optimization of the fermentation process allows to increase 1.8-fold the yield in total sugars, achieving its maximum value at 12 h ($27 \pm 2 \text{ mg g}^{-1}$). Direct fermentation of OS revealed to be a promising and competitive strategy to produce XOS likely to significantly reduce their production cost.

Acknowledgements

CA and AC acknowledges her junior researcher contract (CEECIND/00293/2020) and her PhD scholarship (UI/BD/153689/2022), respectively, from the Portuguese Foundation of Science and Technology (FCT). This study was supported by FCT under the scope of the strategic funding of CIMO (UIDB/00690/2020 and UIDP/00690/2020), CEB (UIDB/04469/2020) and Associate Laboratory SusTEC (LA/P/0007/2020).

References

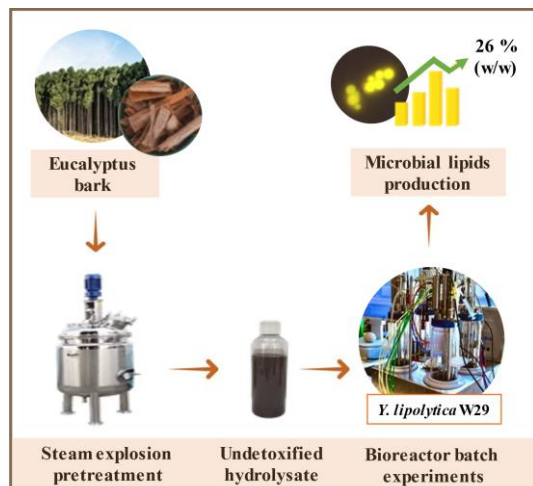
- [1] T.B. Ribeiro et al., *Applied Sciences*, 10 (2020) 6785.
- [2] I. Miranda et al., *Bioresource Technology*, 292 (2019) 121936.
- [3] S. Dermeche et al., *Process Biochemistry*, 48 (2013) 1532-1552.
- [4] C. Amorim et al., *Biotechnology Advances*, 37 (2019) 107397.
- [5] A. Palaniappan et al., *Food Biotechnology*, 31 (2017) 264-280.
- [6] C. Amorim et al., *Food Chemistry*, 270 (2019), 86-94.
- [7] C. Amorim et al., *Carbohydrate Polymers*, 199 (2018) 546-554.
- [8] C. Amorim et al., *Carbohydrate Polymers*, 205 (2019) 176-183.
- [9] L. Freitas et al., *Catalysts*, 12 (2022) 788.

Microbial lipids production by *Yarrowia lipolytica* W29 from eucalyptus bark hydrolysate

B. Dias^{1,2}, H. Fernandes^{1,2}, S. Marques³, F. Gírio³, M. Lopes^{1,2}, I. Belo^{1,2*}

¹Centre of Biological Engineering, University of Minho, Campus de Gualtar, Braga, Portugal; ²LABBELS – Associate Laboratory, Braga/Guimarães, Portugal; ³Unit of Bioenergy and Biorefineries, LNEG, Estrada do Paço do Lumiar, 22, 1649-038 Lisboa.

*ibelo@deb.uminho.pt



Eucalyptus bark hydrolysate (EBH) is an abundant and renewable source of fermentable sugars for microbial lipids production. However, microorganisms need to be tolerant to antimicrobial compounds present in these type-hydrolysates and formed during lignocellulosic biomass processing. The ability of *Y. lipolytica* W29 to grow and produce lipids in undetoxified and undiluted EBH was evaluated in stirred tank bioreactor. The effect of medium composition and volumetric oxygen transfer coefficient on biomass and lipids production was also studied. A final biomass concentration of 21.8 g·L⁻¹ and 26 % (w/w) of lipids (5.6 g·L⁻¹) were obtained at optimum conditions (2 g·L⁻¹ corn steep liquor supplementation and volumetric oxygen transfer coefficient of 66 h⁻¹). *Yarrowia lipolytica* W29 demonstrated robust characteristics to be used as a platform for lipids production into a lignocellulose-based biorefinery bioprocess.

Introduction

The increase in the world population drove researchers to search for alternative lipidic sources to vegetable oils used in biofuels, food, feeds, and pharmaceutical industries [1]. Agricultural waste and lignocellulosic biomass can guarantee a cost-effective and sustainable production pattern to meet the lipids market demand [2]. Eucalyptus bark is an example of abundant and renewable lignocellulosic biomass that can be used for microbial cultures after appropriate pretreatments [3]. In pretreatments, the cleavage of main biomass constituents' chemical bonds (lignin, cellulose, and hemicellulose) results in the release of monomeric assimilable sugars and some compounds (e.g., organic acids, furans, phenolic compounds) with antimicrobial activity [3]. The microbial lipids production from eucalyptus bark hydrolysate (EBH) is highly dependent on the microorganism's suitability to consume hexoses and pentoses and its tolerance to EBH-derived compounds (EBH-C) [4]. This work evaluated the potential of using EBH as a low-cost substrate for microbial lipids production by *Y. lipolytica* W29, studying the effects of medium composition and volumetric oxygen transfer coefficient (k_{La}).

Methods

Eucalyptus bark hydrolysate preparation

EBH was obtained by steam explosion pre-treatment of eucalyptus bark, followed by enzymatic treatment with Cellic® CTec3 and was composed of 56 g·L⁻¹ glucose, 9 g·L⁻¹ xylose, 6 g·L⁻¹ acetic acid, 0.6 g·L⁻¹ formic acid, 0.2 g·L⁻¹ 5-HMF, 0.7 g·L⁻¹ total phenolic compounds, 0.4 g·L⁻¹ total nitrogen and 0.01 g·L⁻¹ total phosphorus.

Bioreactor experiments

Yarrowia lipolytica W29 batch cultures were carried out in 2-L DASGIP Parallel Bioreactor System (Eppendorf, Hamburg, Germany) filled with 400 mL of undiluted EBH. To study the effect of EBH supplementation, corn steep liquor (CSL) (0.5 g·L⁻¹ and 2 g·L⁻¹) and KH₂PO₄ (0.3 g·L⁻¹) was added to EBH with a C/N ratio of 75 by the addition of (NH₄)₂SO₄. The

experiments were conducted at constant agitation of 600 rpm and an aeration rate of 2 vvm. The effect of k_{La} was studied in a medium composed of undiluted EBH, 2 g·L⁻¹ CSL and 1.8 g·L⁻¹ (NH₄)₂SO₄, by varying the agitation and aeration rates, obtaining values of k_{La} equal to 44 h⁻¹ (600 rpm, 2 vvm), 54 h⁻¹ (800 rpm, 2 vvm) and 66 h⁻¹ (800 rpm, 3 vvm). All bioreactor experiments were conducted at 27 °C and a constant pH of 5.5.

Analytical methods

Biomass concentration was determined by cell counting using a Neubauer counting chamber and converted to cell dry weight (g·L⁻¹) through a conversion factor. Glucose, xylose and EBH-C (acetic acid, formic acid and 5-HMF) were quantified by HPLC using an Aminex HPX-87H column at 60 °C, coupled with RI and UV detectors. Sulfuric acid 5 mM was used in the mobile phase at a flow rate of 0.7 mL·min⁻¹. Microbial lipids were quantified using the phospho-vanillin colorimetric procedure according to Lopes et al. [5]. The fatty acid composition of microbial lipids was determined by analysis of fatty acid methyl esters, according to the protocol described by Lopes et al. [5].

Results

Yarrowia lipolytica W29 grew in undiluted EBH without the removal of EBH-C and no latent phase was observed (Figure 1). Increasing CSL concentration from 0.5 g·L⁻¹ to 2 g·L⁻¹ led to approximately 1.5-fold improvement of biomass concentration at the end of the exponential growth phase (Figure 1) and specific growth rate (from 0.06 h⁻¹ to 0.09 h⁻¹). Furthermore, the addition of 2 g·L⁻¹ of CSL to the EBH medium also led to faster consumption of glucose and xylose (Figure 1). CSL is a by-product of the corn steeping process, which can promote yeast growth by providing "unidentified growth factors" [6]. Although the specific growth rate and sugars and acetic acid consumption were higher in the medium containing 0.3 g·L⁻¹ KH₂PO₄ compared to cultures without phosphorus supplementation, the final biomass (Figure 1) and biomass yield were statistically equal. It is important to highlight that both sugars (glucose and

xylose) and EBH-C (acetic acid, formic acid, and 5-HMF) were completely and simultaneously consumed, proving that *Y. lipolytica* W29 was able to assimilate all compounds of EBH without needing detoxifying methods, which agrees with previous *Y. lipolytica* studies in sugarcane bagasse hydrolysate [2]. Medium supplementation also influenced microbial lipids production. Although maximum lipids contents obtained were statistically equal regardless of CSL concentration (Table 1), lipids concentration at 48 h was 2.7-fold higher in 2 g·L⁻¹ CSL compared to 0.5 g·L⁻¹ CSL. Lipids accumulation was lower in KH₂PO₄-supplemented hydrolysate in comparison with non-phosphorus-supplemented medium (Table 1).

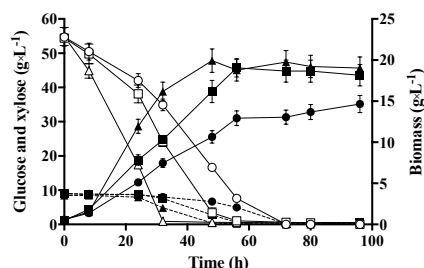


Figure 1. Time course of biomass (closed symbols), glucose (open symbols), and xylose (dashed line) concentration obtained in *Y. lipolytica* W29 batch cultures carried out with undiluted eucalyptus bark hydrolysate supplemented with 0.5 g·L⁻¹ CSL (●, ○); 2 g·L⁻¹ CSL (■, □); 2 g·L⁻¹ CSL and 0.3 g·L⁻¹ KH₂PO₄ (▲, △). The error bars represent the standard deviation of two independent replicates.

Table 1. Values of maximum lipids content and lipids concentration at 48 h obtained in experiments carried out with undiluted eucalyptus bark hydrolysate supplemented with CSL and KH₂PO₄. Data are present as average ± standard deviation of two independent replicates. Statistical analysis was performed by columns and values with the same letter are not significantly different ($p \geq 0.05$).

Medium (g·L ⁻¹)	Maximum lipids content (%)	Lipids conc. (g·L ⁻¹)
0.5 CSL	16.2 ± 2.0 ^a	1.0 ± 0.1 ^a
2 CSL	13.6 ± 2.2 ^a	2.6 ± 0.5 ^b
2 CSL + 0.3 KH ₂ PO ₄	8.5 ± 1.4 ^b	1.2 ± 0.2 ^a

The effect of k_{LA} on biomass and lipids production by *Y. lipolytica* was also studied. Although the increase of k_{LA} did not affect the specific growth rate, with values varying between 0.095 h⁻¹ and 0.103 h⁻¹, biomass yield, with values between 0.27 g·g⁻¹ and 0.32 g·g⁻¹, final biomass and glucose and xylose

consumption (Figure 2), the stationary growth phase was reached early at k_{LA} of 66 h⁻¹ condition than in lower k_{LA} conditions. Lipids content was positively affected by k_{LA} increase (Table 2). Furthermore, a 1.4- and 1.6-fold improvement in microbial lipids concentration were attained increasing k_{LA} from 44 h⁻¹ to 54 h⁻¹ and to 66 h⁻¹, respectively. The main fatty acids of the lipids were oleic (48 % - 64 %), palmitoleic (20 % - 21 %), palmitic (10 % - 14 %) and stearic acids (6 % - 17 %), making these lipids suitable feedstock for biofuel industry.

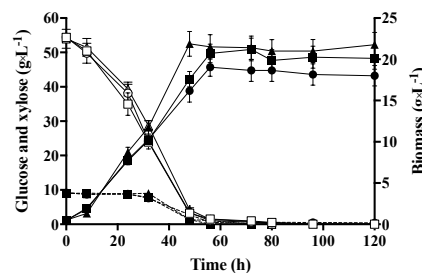


Figure 2. Time course of biomass (closed symbols), glucose (open symbols), and xylose (dashed line) concentration obtained in *Y. lipolytica* W29 batch cultures carried out at different k_{LA} conditions: 44 h⁻¹ (●, ○, black line); 54 h⁻¹ (■, □, dark grey line); and 66 h⁻¹ (▲, △, light grey line). The error bars represent the standard deviation of two independent replicates.

Table 2. Values of lipids content and concentration at 48 h obtained in *Y. lipolytica* W29 experiments carried out at different k_{LA} conditions. Data are present as average ± standard deviation of two independent replicates. Statistical analysis was performed by columns and values with the same letter are not significantly different ($p \geq 0.05$).

k_{LA} (h ⁻¹)	Lipids content (%)	Lipids conc. (g·L ⁻¹)
44	16.2 ± 2.0 ^a	2.6 ± 0.5 ^a
54	20.7 ± 3.8 ^{ab}	3.6 ± 0.5 ^a
66	25.6 ± 4.4 ^b	5.6 ± 0.9 ^b

Conclusions

This work demonstrates the possibility of using undetoxified EBH for *Y. lipolytica* W29 growth and microbial lipids accumulation, being media composition and k_{LA} important factors in bioprocess optimization. The reuse and valorization of lignocellulosic biomass through *Y. lipolytica* W29 lipids production fulfill the assumptions of the biorefinery and circular bioeconomy.

Acknowledgements

This study was supported by the Move2LowC project (POCI-01-0247-FEDER-046117), cofinanced by Programa Operacional Competitividade e Internacionalização, Programa Operacional Regional de Lisboa, Portugal 2020 and the European Union, through the European Regional Development Fund. It was also supported by the Portuguese Foundation for Science and Technology (FCT) under the scope of the strategic funding of UIDB/04469/2020 unit and the Doctoral grant (2021.05799.BD) and by LABBELS – Associate Laboratory in Biotechnology, Bioengineering and Microelectromechanical Systems, LA/P/0029/2020.

References

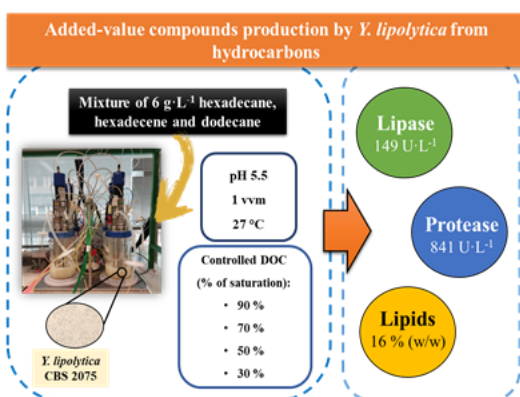
- [1] B. Vasconcelos et al., *Applied Microbiology and Biotechnology*, 103 (2019) 3651-3667.
- [2] Y.A. Tsigie et al., *Bioresource Technology*, 102 (2011) 9216-9222.
- [3] B.R. Prasad et al., *International Journal of Environmental Science and Technology* (2022).
- [4] V.S. Nogué et al., *Green Chemistry*, 20 (2018) 4349-4365.
- [5] M. Lopes et al., *European Journal of Lipid Science and Technology*, 121 (2019) 1-9.
- [6] D.D. Loy, E.L. Lundry, Chapter 23 in *Corn: Chemistry and Technology*, 3rd Ed., Elsevier Inc., Amsterdam, 2019, 633-659.

Batch cultures of *Y. lipolytica* CBS 2075 on hydrocarbons medium under different conditions of oxygenation

S.M. Miranda, M. Lopes, I. Belo*

Centre of Biological Engineering, University of Minho, Campus de Gualtar, Braga, Portugal; LABELS – Associate Laboratory, University of Minho, Braga/Guimarães, Portugal.

*ibelo@deb.uminho.pt



Hydrocarbons are hydrophobic pollutants that can be used as a carbon source in microbial-based processes. *Yarrowia lipolytica* is a nonconventional yeast known for its ability to assimilate hydrophobic substrates to growth and simultaneously produce added-value compounds. The effect of dissolved oxygen concentration on the assimilation of a hydrocarbons mixture, biomass and metabolites production by *Y. lipolytica* CBS 2075 was studied for the first time. The yeast grew in a mixture of hexadecane, hexadecene, and dodecane, producing enzymes (lipase and protease) and intracellular lipids. Though the amount of dissolved oxygen concentration did not affect *Y. lipolytica* CBS 2075 cellular growth, the hydrocarbons consumption rate was slightly dependent on the dissolved oxygen concentration. Low amounts of dissolved oxygen concentration had a clear negative effect on lipase production but no differences were found among all dissolved oxygen conditions for lipids and protease production.

Introduction

Environmental pollution with petroleum hydrocarbons has emerged as a serious ecological and human health concern due to the improper disposal of petroleum-derived effluents. Different techniques have been applied to treat oily wastewaters, but, physicochemical remediation methods are costly and generate other pollutant compounds [1,2]. Therefore, microbial-based processes are environment-friendly technologies and feasible alternatives for the sustainable management of hydrocarbon-polluted effluents [3,4]. Hydrocarbons are hydrophobic pollutants compounds that can be used as a carbon source for microbial growth, but most of the studies are focused on the biodegradation of aliphatic and aromatic hydrocarbons by bacteria species [5]. *Yarrowia lipolytica*, often isolated from oil-contaminated environments, has the ability to assimilate hydrophobic substrates with the simultaneous production of added-value compounds. Although the potential of *Y. lipolytica* to degrade aliphatic hydrocarbons has already been explored, the biotransformation of these compounds into valuable metabolites is much less researched [6]. Since *Y. lipolytica* is a strictly aerobic yeast, the amount of dissolved oxygen in the culture medium is a crucial parameter for bioprocess and may affect intracellular lipids accumulation and the production of enzymes [7]. This work aimed to study the effect of dissolved oxygen concentration (DOC) on the assimilation of a hydrocarbons mixture of hexadecane, hexadecene, and dodecane by *Y. lipolytica* CBS 2075 in bioreactor batch cultures. Furthermore, its impact on yeast growth and the production of added-value compounds (lipids and enzymes) was also evaluated.

Methods

Yeast strain

Yarrowia lipolytica CBS 2075 pre-grow overnight in a YPD medium to prepare cryo-stocks in sterile microtubes (800 μ L of yeast culture and 200 μ L of glycerol 99.5 %), which were preserved at -80 °C. Each pre-inoculum was inoculated with one microtube and incubated in an orbital incubator at 27 °C and 200 rpm.

Bioreactor batch cultures

Several experiments were carried out in a 2-L DASGIP Parallel Bioreactor System at 27 °C and pH 5.5 with 1200 mL of culture medium composed of 6 g·L⁻¹ hydrocarbons mixture (2 g·L⁻¹ dodecane, 2 g·L⁻¹ hexadecane and 2 g·L⁻¹ hexadecene), 0.5 g·L⁻¹ ammonium sulfate and 3.4 g·L⁻¹ corn steep liquor. To evaluate the effect of DOC, four conditions of controlled DOC, from 30 % to 90 % (± 10 %) were studied by automatic variation of stirring rates between 200 rpm and 700 rpm. All experiments were conducted at a specific airflow rate of 1 vvm.

Analytical methods

Biomass concentration was quantified by optical density and converted to cell dry weight by a calibration curve. Lipase and protease activities were quantified in accordance with the methods described by Lopes et al. [8]. Microbial lipids were quantified by the phospho-vanillin colorimetric method, after extraction with methanol and chloroform (1:1, v/v) from lyophilized cells as described by Pereira et al. [9]. Hydrocarbons were extracted from the culture medium samples by liquid-liquid extraction, using hexane as solvent (1:6, v/v) and undecane as the internal standard.

Results

Y. lipolytica CBS 2075 grew in a 6 g·L⁻¹ hydrocarbons mixture without inhibition, and, regardless of DOC in the culture medium, no differences were found in the yeast growth profile, final biomass concentration (Figure 1) and specific growth rates (values ranged between 0.068 h⁻¹ to 0.072 h⁻¹). By contrast, the assimilation of hydrocarbons by *Y. lipolytica* CBS 2075 was dependent on the concentration of dissolved oxygen in the culture medium. All hydrocarbons were completely assimilated after 24 h of cultivation, but in the lowest DOC value, total assimilation of hydrocarbons was reached only at 48 h (Figure 1). Although hydrocarbons were assimilated faster in the cultures with 90 %, 70 % and 50 % of DOC when compared to experiments conducted at 30 %, no improvement was attained in biomass yield ($Y_{x/s}$) (values ranged from 1.0 g·g⁻¹ and 1.3 g·g⁻¹) since hydrocarbons were totally consumed.

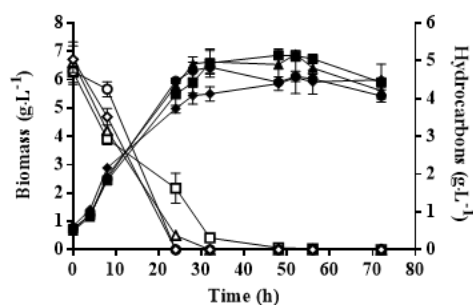


Figure 1. Time course of biomass (closed symbols) and total hydrocarbons (open symbols) concentration obtained in batch cultures of *Y. lipolytica* CBS 2075 carried out in bioreactor at different DOC: 90 % (◆, ◇), 70 % (●, ○), 50 % (▲, △) and 30 % (■, □). The error bars represent the standard deviation of two independent replicates.

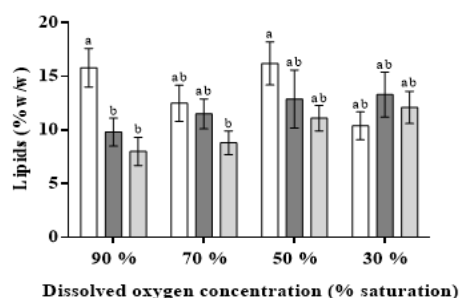


Figure 2. Lipids content of *Y. lipolytica* CBS 2075 at 24 h (white bars), 48 h (dark grey bars) and 72 h (light grey bars) in different DOC (% saturation): 90 %, 70 %, 50 % and 30 %. The error bars represent the standard deviation of two independent replicates.

The effect of DOC on added-value compounds production by *Y. lipolytica* CBS 2075 was also studied. As observed for biomass concentration, lipids content (% w/w) and lipids concentration (values ranged between 0.8 g·L⁻¹ and 0.9 g·L⁻¹) were not affected by DOC conditions, and a similar pattern for lipids accumulation was observed in all DOC conditions (Figure 2). At DOC conditions of 90 %, 70 % and 50 %, a higher amount of lipids was accumulated at 24 h by yeast cells, then a decrease in lipidic content at 48 h and 72 h of cultivation occurred owing to intracellular lipids mobilization by cells, which coincide with the total depletion of hydrocarbons from the medium (Figure 1). By contrast, at DOC of 30 %, no decrease in lipids content was observed from 24 h to 48 h, considering that the total depletion of hydrocarbons from the medium was only reached at 48 h of cultivation time (Figure 1). In addition to lipids accumulation,

Acknowledgements

This study was supported by the Portuguese Foundation for Science and Technology (FCT) under the scope of the strategic funding of UIDB/04469/2020 unit and doctoral grant (SFRH/BD/144188/2019), and by LABBELS – Associate Laboratory in Biotechnology, Bioengineering and Microelectromechanical Systems, LA/P/0029/2020.

References

- [1] S. Varjani et al., Sustainable Industrial and Environmental Bioprocesses, 27 (2020) 27172-27180.
- [2] K. Abuhasel et al., Water, 13 (2021) 980.
- [3] E.O. Atakpa et al., Chemosphere, 290 (2022) 133337.
- [4] O. Matatkova et al., International Journal of Analytical Chemistry, 2017 (2017) 8195329.
- [5] F. Abbaasian, R. Lockington, M. Mallavarapu, R. Naidu, Applied Biochemistry and Biotechnology, 176 (2015) 670-699.
- [6] M. Lopes et al., Critical Reviews in Biotechnology, 42 (2022) 163-183.
- [7] M. Lopes, A.S. Gomes, C.M. Silva, I. Belo, Journal of Biotechnology, 265 (2018) 76-85.
- [8] M. Lopes et al., European Journal of Lipid Science and Technology, 121 (2019) 1800188.
- [9] A.S. Pereira et al., Biotechnological Products and Process Engineering, 106 (2022) 2869-2881.

the synthesis of extracellular lipase and protease was also observed (Table 1). Lipase activity was enhanced by the increase of DOC, and an 8-fold improvement in lipase activity was attained by increasing DOC in the culture medium from 30 % to 90 %. By contrast, no statistical differences were observed for proteolytic activity at different DOC conditions (Table 1).

Table 1. Values of maximum lipase (Lip_{max}) and protease ($Prot_{max}$) activities obtained in *Y. lipolytica* CBS 2075 batch cultures carried out in STR bioreactor. Data are average \pm standard deviation for two independent replicates. Statistical analysis was performed by columns and values with the same letter are not significantly different ($p \geq 0.05$).

Dissolved oxygen concentration (% saturation)	Lip_{max} (U·L ⁻¹)	$Prot_{max}$ (U·L ⁻¹)
90	149 \pm 2 ^a	841 \pm 42 ^a
70	87 \pm 0.3 ^b	585 \pm 71 ^a
50	22 \pm 3 ^c	628 \pm 77 ^a
30	19 \pm 0.2 ^c	648 \pm 70 ^a

Conclusions

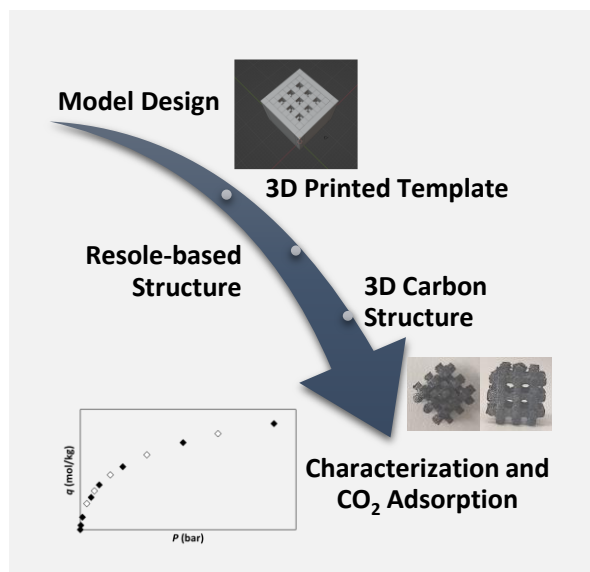
This work demonstrates the ability of *Y. lipolytica* CBS 2075 to grow in a mixture of hydrocarbons (dodecane, hexadecane, hexadecene) without lag phase or inhibition of biomass proliferation. Regardless of DOC in the culture medium, *Y. lipolytica* CBS 2075 growth profiles were similar and no differences were found in specific growth rate, biomass concentration, and biomass yield. By contrast, faster assimilation of hydrocarbons was achieved at DOC conditions of 90 %, 70 % and 50 % when compared to the lowest DOC conditions. Simultaneous with biomass production, the synthesis of intracellular lipids and extracellular enzymes was observed. Whereas lipase activity was positively affected by increasing DOC from 30 % to 90 %, no differences were found for protease activity at different DOC conditions. Although *Y. lipolytica* is known for being a strictly aerobic yeast, in the present study, the decrease of dissolved oxygen in the culture medium was not a limiting factor, thus representing a cost-saving in operating costs (power consumption) owing to the lower stirring rates needed to achieve these dissolved oxygen concentrations. The biotechnological approach presented here opens a new perspective on the application of *Y. lipolytica*-based cultures for the valorization of hydrocarbons, which intend to be helpful in the further development of sustainable strategies from the economic and environmental point of view, fulfilling the guidelines proposed in the circular economy concept.

Activated carbon 3D structures for carbon dioxide capture

R.R. Dias, G. Al Khalil, I. Fonseca, J.P.B. Mota, I. Matos, R.P.P.L. Ribeiro*

LAQV-REQUIMTE, NOVA School of Science and Technology, NOVA University of Lisbon, Caparica, Portugal.

*rpp.ribeiro@fct.unl.pt



Recently, 3D printing techniques became interesting options in several industries such as the automotive, space, footwear, clothing, jewelry, etc. In the field of chemical engineering, 3D printing is also increasingly becoming a valuable option, with a huge potential of application. Reactors and mixers have been printed as well as structured catalysts and adsorbents. Several structures have been 3D printed using different adsorbents such as zeolites, activated carbons, metal-organic frameworks, and others.

In this work, we present a straightforward approach for the preparation of three-dimensional activated carbon structures. The procedure is based in the 3D printing of a PVA structure that is filled with a phenol-formaldehyde resole resin. The PVA template is then removed, and the resin is used as precursor for carbon preparation.

The 3D carbon structures are characterized and evaluated for the adsorption of CO₂, showing good potential of utilization on CO₂ removal processes.

Introduction

3D printing has recently become a widely available tool that enables anyone to create objects from scratch. This disruptive approach has potential to influence procedures in virtually every field of work. 3D printing is already being used in the automotive, space, footwear, clothing, and jewelry industries. Naturally, the introduction of 3D printing in the chemical engineering field is also occurring at a fast pace. Novel reactors, mixers, structured catalysts and adsorbents have been 3D printed. [1] Regarding the printing of adsorbent structures, it can have a huge impact on adsorption processes. Many adsorbents are synthesized as powders that are unfeasible for utilization in processes, due to the huge pressure drop generated, and must be shaped into bigger particles. Traditionally, pellets or beads are used although the use of structured adsorbents such as honeycomb monoliths presents several advantages [2]. These monoliths are typically obtained by extrusion which limits the obtainable structures to monoliths with parallel (non-interconnected) channels. On the other hand, with 3D printing novel and more complex shapes can be obtained, adding more degrees of freedom in the design of structured adsorbents. Furthermore, the use of computer aided design tools allows changing the structures with ease, permitting the rapid prototyping of different shapes.

Among the several 3D printing techniques available, most of the adsorbent structures printed were based on the direct ink writing (DIW) technique. [3, 4] Some studies have also focused on the development of novel formulations for use in stereolithography 3D printers [5]. In this work, we have developed a straightforward templating methodology for the preparation of carbon-based adsorbent structures for carbon dioxide (CO₂) capture.

Methods

The 3D structures are designed in Blender™ software, generating STL files that can be 3D-printed. The structures are printed in an CreatBot F160 printer using a commercial

polyvinyl alcohol (PVA) filament. Subsequently, the three-dimensional piece is filled with a previously prepared phenol-formaldehyde resole resin and left curing at 353 K for approximately one week. Then, the template is removed in water and the self-sustained resole structure is pyrolyzed. Various activation conditions with CO₂ were tested to evaluate its influence in the porosity of the obtained activated carbons.

The obtained materials are thoroughly characterized through nitrogen (N₂) adsorption at 77 K, SEM, Hg porosimetry. The CO₂ and N₂ adsorption equilibrium are also determined to evaluate the potential of the materials for CO₂ capture applications.

Results

The structured activated carbons present microporosity suitable for gas adsorption. The adsorption equilibrium isotherms of CO₂ at 303 K on a pristine carbon sample and a sample activated with CO₂ are shown in Figure 1 for comparison. The data obtained demonstrates that upon activation with CO₂ the amount adsorbed is significantly increased.

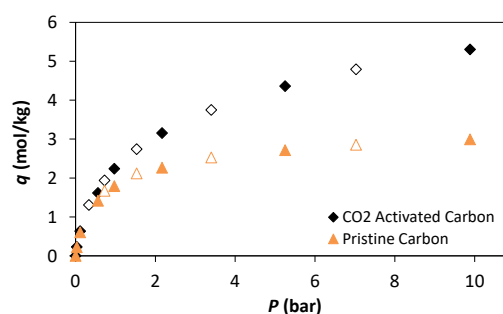


Figure 1. Adsorption equilibrium isotherms of CO₂, at 303 K, on the pristine carbon sample and a carbon sample activated with CO₂.

Conclusions

The results obtained show that the approach proposed presents a straightforward and efficient option for the preparation of 3D adsorbent structures with good potential for CO₂ capture. It is

once more showed that 3D printing will surely be an important tool in the chemical engineering sector in the near future. concept.

Acknowledgements

This work was financed by national funds from FCT/MCTES (Portugal) through Associate Laboratory for Green Chemistry–LAQV [UIDB/50006/2020 | UIDP/50006/2020], the Norma Transitória DL 57/2016 Program Contract (Rui Ribeiro), and the Individual Call to Scientific Employment Stimulus contract CEECIND 004431/2022 (Inês Matos).

References

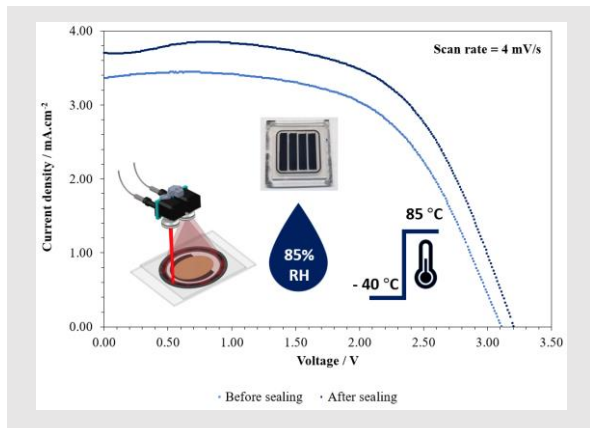
- [1] C. Parra-Cabrera et al., *Chemical Society Reviews*, 47 (2018) 209-230.
- [2] Y. Y. Li et al., *Chemical Engineering Research & Design*, 76 (1998) 931-941.
- [3] S. Couck et al., *Chemical Engineering Journal*, 308 (2017) 719-726.
- [4] H. Thakkar et al., *ACS Applied Materials & Interfaces*, 8 (2016) 27753-27761.
- [5] L.F.A.S. Zafaneli et al., *Microporous and Mesoporous Materials*, 335 (2022) 111818.

Hermetic encapsulation for long-lifetime printable perovskite solar cells and mini-modules

M. Pereira, J. Martins, F. Santos, D. Ivanou, S. Emami, A. Mendes*

LEPABE - Laboratory for Process Engineering, Environment, Biotechnology and Energy, Faculdade de Engenharia, Universidade do Porto, rua Dr. Roberto Frias, 4200-465 Porto, Portugal; ALiCE - Associate Laboratory in Chemical Engineering, Faculty of Engineering, University of Porto, Rua Dr. Roberto Frias, 4200-465 Porto, Portugal.

*mendes@fe.up.pt



Perovskite solar cells (PSCs) are rapidly gathering attention in the photovoltaic (PV) community. While this technology offers exciting potential, its long-term stability and scalability is the major challenge that needs to be addressed before they can be commercialized. PSCs are sensitive to humidity and temperature; therefore, hermetic encapsulation is essential to protect them from external environmental factors and to prevent lead-containing materials from leaking out. Therefore, to continue the path to industrialization, PSCs should be fabricated with thermally stable layers through scalable deposition methods and protected by a long-term stable hermetic encapsulation. In this work, we present for the first-time laser-sealed printable perovskite solar cells and mini-modules, encapsulated at low process temperature. This innovative technology allows to glass encapsulate the cells without them losing any energy performance during the process.

Introduction

A hermetic encapsulation is required to protect perovskite solar cells (PSCs) from the most common sources of degradation – humidity and oxygen [1]. According to IEC61646 PV standard test, commercial photovoltaic devices must be stable at the temperature range of $-40\text{ }^{\circ}\text{C}$ to $85\text{ }^{\circ}\text{C}$ and relative humidity of 85 % [2]. Therefore, to achieve the mentioned requirements, the PSCs should be fabricated with thermally stable layers deposited through scalable deposition methods and protected by a long-term stable hermetic encapsulation.

Laser-assisted glass frit encapsulation has been successfully used to achieve long-term stability for PSCs with n-i-p and HTM-free structures [3,4]. The laser-sealing can be achieved with a single laser beam or dual laser beams. The advanced novel dual laser beam glass frit sealing was previously developed and optimized to hermetically encapsulate n-i-p PSCs at $65 \pm 5\text{ }^{\circ}\text{C}$ for a short processing time of $< 60\text{ s}$ [3]. In contrast, printable HTM-free perovskite solar cells have been only reported to be sealed with a single laser beam at $100\text{ }^{\circ}\text{C}$ for a long processing time of 35 min [4]. In the present work, the application of dual laser beam sealing to encapsulate HTM-free PSCs and mini-modules fabricated with $(5\text{-AVA})_{0.05}(\text{MA})_{0.95}\text{PbI}_3$ perovskite absorber is studied. During the laser-sealing process, the cells were subjected to $65\text{ }^{\circ}\text{C}$ and the mini-modules to $80\text{ }^{\circ}\text{C}$ for a short time of $< 90\text{ s}$.

Results and discussion

The previously reported single beam sealing of HTM-free PSCs at $100\text{ }^{\circ}\text{C}$, caused a slight decrease in the performance of the devices, due to the long thermal exposure during the encapsulation process [4]. In the present work, the average power conversion efficiency (PCE) of the small-area PSCs increased from $(6.13 \pm 0.63)\%$ to $(6.20 \pm 0.40)\%$ after the encapsulation process at $65\text{ }^{\circ}\text{C}$ with dual laser beam method. While using the same procedure for the mini-modules, the average PCE increased from $(6.08 \pm 0.32)\%$ to $(6.60 \pm 0.49)\%$ after being laser-sealed at $80\text{ }^{\circ}\text{C}$. The photovoltaic parameters of the champion small-area and mini-module PSC before and after the sealing process are presented on table 1 and the photocurrent vs voltage (J - V) curves are shown in Figure 1 and in the

graphical abstract, respectively. A picture of a laser-sealed small-area and a mini-module PSC devices are presented in Figures 2 and 3, respectively.

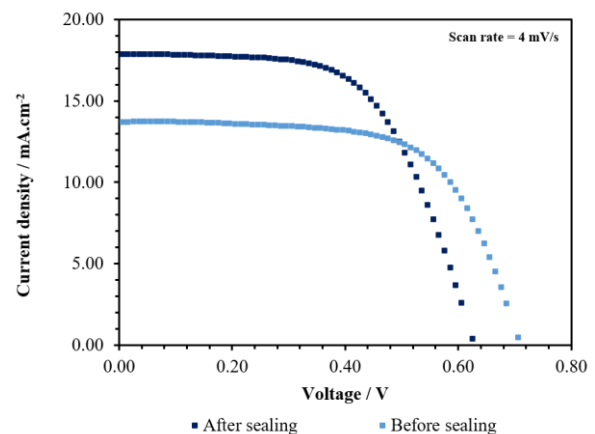


Figure 1. J - V curve for the champion PSC before and after sealing.

Table 1. Photovoltaic parameters of the champion PSC and mini-module.

Champion devices	PSC		Mini-module	
	Before	After	Before	After
$J_{sc} / \text{mA.cm}^{-2}$	13.72	17.91	3.36	3.69
V_{oc} / V	0.71	0.63	3.11	3.21
FF	0.65	0.60	0.59	0.61
PCE / %	6.29	6.75	6.20	7.25



Figure 2. Picture of a laser-sealed small PSC.



Figure 3. Picture of a laser-sealed mini-module.

The average performance improvement of encapsulated cells is related to the increase in short circuit current (J_{sc}) from (13.84

± 1.01) to (15.48 ± 1.46) mA cm^{-2} for small-area cells and from (3.22 ± 0.14) to (3.50 ± 0.13) mA cm^{-2} for the mini-modules. Concerning the open circuit potential (V_{oc}) and the fill factor (FF), the glass encapsulation process decreased the V_{oc} from (0.72 ± 0.03) V to (0.66 ± 0.06) V and increased the FF from 0.61 ± 0.02 to 0.62 ± 0.09 for small-area PSCs; in the case of the mini-modules the V_{oc} decreased slightly from (3.25 ± 0.10) V to (3.21 ± 0.00) V and the FF was mostly constant at 0.56 ± 0.02 . The variations in V_{oc} and J_{sc} were assigned to the recrystallization of the perovskite absorber at the TiO_2 and at the carbon layer, respectively. Recrystallization at the carbon layer improves the charge transfer, therefore increasing the current. However, at the TiO_2 scaffold the recrystallization leads to the reduction of the V_{oc} which was assigned to surface recombination due to the increase of defects at the grain boundary interfaces [5].

Conclusions

In conclusion, this work indicates that dual laser sealing has a low impact on the performance on both lab-scale devices and mini-modules. This is a very important step towards the commercialization of this PV technology since one of the main concerns for the industrialization of PSCs is the scalability and stability. With this study it was possible to ensure that laser-assisted glass frit encapsulation is suitable for large area PSCs. Further intrinsic stability studies towards UV light and electrical bias will be followed in future to demonstrate the robustness of the glass frit sealing.

Acknowledgements

Marta Pereira and Jorge Martins are grateful to the Portuguese Foundation for Science and Technology (FCT) for their PhD grants (references: 2021.06451.BD and SFRH/BD/147201/2019). The authors acknowledge the financial support of the project Baterias 2030, with the reference POCI-01-0247-FEDER-046109, co-funded by Operational Programme for Competitiveness and Internationalization (COMPETE 2020), under the Portugal 2020 Partnership Agreement, through the European Regional Development Fund (ERDF)”. LA/P/0045/2020 (ALiCE), UIDB/00511/2020 and UIDP/00511/2020 (LEPABE), funded by national funds through FCT/MCTES (PIDDAC). 2022.05826.PTDC, funded by FEDER funds through COMPETE2020 – Programa Operacional Competitividade e Internacionalização (POCI) and by national funds (PIDDAC) through FCT/MCTES. This work has received funding from the European Union’s Horizon 2020 programme, through a FET Proactive research and innovation action under grant agreement No. 101084124.

References

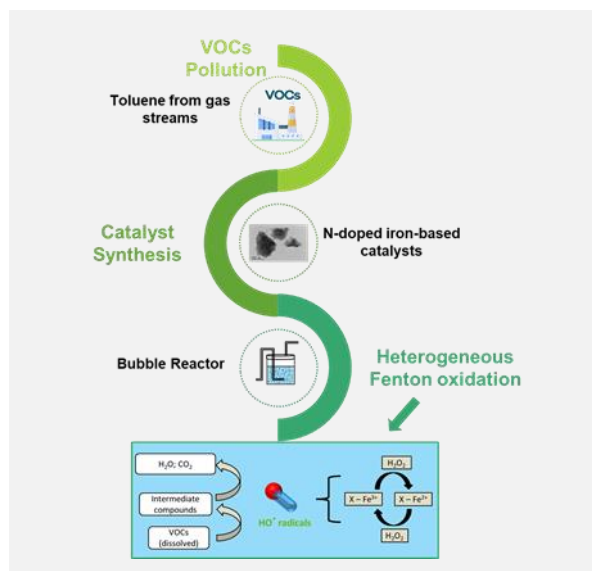
- [1] D. Wang et al., *Solar Energy Materials and Solar Cells*, 147 (2016) 255-75.
- [2] IEC61646, International Electrotechnical Commission, 2008.
- [3] S. Emami et al., *Journal of Materials Chemistry A*, 8 (2020) 2654-2662.
- [4] J. Martins et al., *Journal of Materials Chemistry A*, 8 (2020) 20037-20046.
- [5] K. Liao et al., *Nano-Micro Letters*, 12 (2020) 156.

Degradation of volatile organic compounds from gaseous streams by Fenton's oxidation over N-doped carbon-based materials

E.F.S. Sampaio^{1,2,3*}, O.S.G.P. Soares^{2,3}, M.F.R. Pereira^{2,3}, C.S.D. Rodrigues^{1,2}, L.M. Madeira^{1,2}

¹Laboratory for Process Engineering, Environment, Biotechnology and Energy (LEPABE), Faculty of Engineering, University of Porto, Rua Dr. Roberto Frias, 4200-465 Porto, Portugal; ²Associated Laboratory in Chemical Engineering (ALiCE), Faculty of Engineering, University of Porto, Rua Dr. Roberto Frias, 4200-465 Porto, Portugal; ³Laboratory of Separation and Reaction Engineering – Laboratory of Catalysis and Materials (LSRE-LCM), Faculty of Engineering, University of Porto, Rua Dr. Roberto Frias, 4200-465 Porto, Portugal.

*sampaioemanuel16@gmail.com



Volatile organic compounds (VOCs) released into the atmosphere by industries cause risks to public health and the environment, making removing or minimizing their concentration in polluted gas streams essential. A novel treatment technology for VOCs abatement from gaseous streams was developed using a semi-batch bubble reactor, with the goal of assessing the toluene (selected as model compound) degradation from gaseous streams via heterogeneous Fenton oxidation over N-doped carbon-based materials.

Activated carbon (AC), carbon nanotubes (CNTs) and carbon xerogel (XG) doped with N-groups and impregnated with 2 wt.% of iron were prepared and used as catalysts. The materials were characterized by several techniques (including N₂ adsorption at – 196 °C and elemental analysis - EA).

The effect of the textural and chemical properties of the different carbon materials with different nitrogen functionalities in the adsorption and heterogeneous Fenton oxidation of toluene was assessed.

Introduction

The emission of volatile organic compounds (VOCs) from several industries into the atmosphere causes adverse effects on the environment and public health and, therefore, it is crucial to remove them from gas polluted streams or, at least, reduce their concentrations.

Advanced oxidation processes (AOPs) are interesting for VOCs abatement when compared with other treating technologies available. AOPs are based on the generation of hydroxyl radicals (HO[•]), non-selective species with high oxidation potential (2.8 eV), which are responsible for the oxidation of VOCs into intermediate compounds or, in some cases, into carbon dioxide (CO₂) and water (H₂O) [1]. Heterogeneous Fenton's reaction is one of the most studied AOPs and it is a promising treatment process that can be applied for VOCs degradation, wherein the hydroxyl radicals are generated by the catalytic decomposition of hydrogen peroxide (H₂O₂) in the presence of ferrous ions (Fe²⁺) supported on a solid matrix [2,3].

Degradation of VOCs present in gaseous effluents by AOPs involves firstly the transfer of the pollutants from the gas to the liquid phase; for that, it is necessary the gas bubbling into the liquid; then, the dissolved VOCs are oxidized by the radicals generated in the liquid phase. Moreover, the degradation of the dissolved VOCs increases the driving force and consequently more VOCs are transferred from the gas to the liquid phase [1,4]. For this purpose, a bubble reactor (BR) was used in this work. This reactor configuration presents as advantages easy operation and maintenance, good control, absence of mechanical stirring devices and effective mass and heat transfer. Furthermore, it leads to reduced operating and maintenance costs. However, some VOCs are hydrophobic compounds and present low water solubilities; thus, applying carbon materials as heterogeneous catalysts seems promising as they significantly increase the gas-

liquid transfer of VOCs by adsorption on their surface. This way, one also takes advantage of the heterogeneous Fenton oxidation in the gas-liquid-solid system [4].

Carbon materials are extensively used as catalysts/adsorbents because they are very flexible materials, since their textural and chemical properties can be easily modified by physical or chemical treatment. Among the carbon materials, activated carbons (ACs) are particularly attractive as iron support due to their developed porosity and high surface area and tunable surface chemistry. Recently, carbon nanotubes (CNTs) and carbon xerogels (XGs) have emerged as iron supports due to their attractive properties when compared with other carbon materials, such as low limitations to mass transfer, and high electronic properties for CNTs, and high purity, and mesoporous structure with good pore distribution for XGs [5].

On the other hand, the presence of N-groups on the surface of carbon-based materials improved their catalytic performance for AOPs applications [3,5].

The main objective of this work is to evaluate the effect of the N-doped carbon materials nature with different textural properties in the efficiency of gaseous toluene removal by adsorption and heterogeneous Fenton oxidation in a bubble reactor.

Methods

A commercial Norit GAC 1240 AF activated carbon was ground and sieved to obtain a particle diameter of 0.1-0.3 mm. Then, the AC sample was doped using melamine as a nitrogen precursor. For that, 0.6 g of the AC sample and 0.4 g of melamine were dipped into 0.050 dm³ of a 1 mol dm⁻³ aqueous solution of ethanol (96% v/v), and stirred at room temperature for 24 h, as described elsewhere [3,5]. The resulting sample was called as

ACM. For obtaining the N-doped CNTs, 0.6 g of commercial Nanocyl NC 7000 multiwalled carbon nanotubes, and 0.39 g of melamine as N-source, were ball-milled in a closed pot at a vibration frequency of 15 vibrations s^{-1} for 4 h using a MM200 ball-milling as described in a previous work [6]. The resulted sample was called as CNTM.

Carbon xerogels doped with nitrogen were prepared with 15 g of resorcinol and 3 g of melamine in 18 mL of distilled water. The solution was heated to 90 °C under stirring until the melamine was completely dissolved. Then, it was cooled to room temperature and 20 mL of formaldehyde were added. The pH was adjusted to 6.9. After this step, the procedure adopted is the same as described elsewhere [5]. The sample was called as XGM. The iron-based catalysts were prepared using the incipient wetness impregnation method, using iron (III) nitrate nonahydrate as a precursor solution to obtain an iron content of 2 wt.%. Thereafter, samples were dried at 100 °C overnight, heat treated under N_2 flow for 1 h, and finally reduced under H_2 flow for 3 h at 400 °C [3, 5]. The samples were called as ACM-Fe, CNTM-Fe and XGM-Fe. The textural characterization of the samples was assessed by N_2 adsorption isotherms, determined at -196 °C with a Quantachrome NOVA 4200e apparatus. The samples (~0.1 g) were outgassed at 150 °C for 3 h under vacuum. The surface area (S_{BET}) was determined using the Brunauer–Emmett–Teller (BET) equation. The mesopore surface area (S_{meso}) and the micropore volume (V_{micro}) were calculated using the t -method. The total specific pore volume (V_p) was determined from the amount of N_2 adsorbed at $P/P_0 = 0.95$ [3]. The N-content of the carbon materials was obtained by elemental analysis using a Vario micro cube analyzer (Elementar GmbH) [3]. The experimental procedure adopted for the adsorption and catalytic runs aiming toluene removal from a gas stream is described in detail elsewhere [1], but in this work a semi-batch bubble reactor (BR) was used – Figure 1. The toluene-containing gas stream was simulated by stripping. In a gas scrubber bottle at 5 °C, an air stream ($Q_{air} = 100 \text{ cm}^3/\text{min}$) was injected into a 300 mL of toluene pure liquid. The concentrated toluene-containing stream was diluted in another gas scrubber bottle through a clean air stream

($Q_{air} = 100 \text{ cm}^3/\text{min}$). Finally, the diluted toluene gaseous stream was fed to the BR.

The catalytic experiments were performed in a semi-batch BR equipped with an internal cylindrical air diffuser to form the gas bubbles. In each experiment, 0.3 L of water with an adjusted pH of ~3.0 was added into the BR. Then, the carbon material was added (adsorption experiment) and, in heterogeneous Fenton experiments, the desired amount of H_2O_2 was also added to the reactor immediately before bubbling the diluted gas stream.

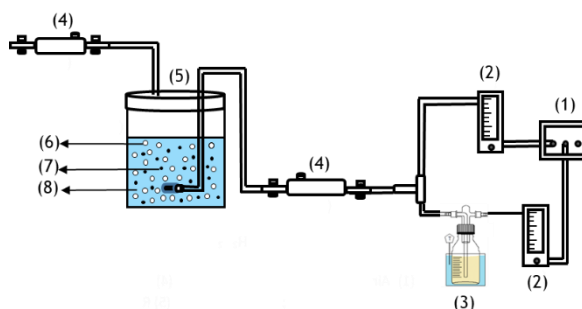


Figure 1. Scheme of the experimental setup; (1) – air pumps; (2) – flowmeters; (3) – toluene saturated solution; (4) – gas sampling points; (5) – bubble reactor; (6) – gas bubbles; (7) – catalyst particles; (8) – water + H_2O_2 .

Results

Table 1 summarises the textural properties of the different iron-impregnated carbon materials prepared. As can be seen, ACM-Fe presents the largest BET specific surface area ($823 \text{ m}^2 \text{ g}^{-1}$), while the CNTM-Fe sample presents the lowest surface area ($182 \text{ m}^2 \text{ g}^{-1}$). Moreover, ACM-Fe is a microporous material, while CNT-M-Fe presents a mesoporous nature. The XGM-Fe sample shows intermediate properties with a BET specific surface area of $495 \text{ m}^2 \text{ g}^{-1}$ and a mesoporous area (S_{meso}) of $95 \text{ m}^2 \text{ g}^{-1}$. Moreover, all samples show a similar N-content, approximately 7 wt.%, measured by elemental analysis. The N-doped carbon-based materials with different textural properties are being tested in a bubble reactor and the process efficiency will be evaluated in terms of toluene transferred, dissolved organic carbon and H_2O_2 consumption.

Table 1. Textural properties of the N-doped carbon-based catalysts.

Catalysts	S_{BET} ($\pm 10 \text{ m}^2 \text{ g}^{-1}$)	S_{meso} ($\pm 10 \text{ m}^2 \text{ g}^{-1}$)	V_{micro} ($\pm 0.01 \text{ cm}^3 \text{ g}^{-1}$)	V_p ($\pm 0.01 \text{ cm}^3 \text{ g}^{-1}$)
ACM-Fe	823	84	0.323	0.435
XGM-Fe	495	95	0.166	0.306
CNTM-Fe	182	182	0	0.461

Acknowledgements

This work was financially supported by: UIDB/00511/2020 and UIDP/00511/2020 (LEPABE), UIDB/50020/2020 and UIDP/50020/2020 (LSRE-LCM) and LA/P/0045/2020 (ALICE) funded by national funds through FCT/MCTES (PIDDAC); Project PTDC/EAM-AMB/29642/2017 - POCI-01-0145-FEDER-029642 - funded by FEDER funds through COMPETE2020 - Programa Operacional Competitividade e Internacionalização (POCI) and by national funds (PIDDAC) through FCT/MCTES. EFSS thanks the Portuguese Foundation for Science and Technology (FCT) for his PhD grant (2020.04593.BD), financed by national funds of the Ministry of Science, Technology and Higher Education and the European Social Fund (ESF) through the Human Capital Operational Programme (POCH). OSGPS acknowledges FCT funding under the Scientific Employment Stimulus - Institutional Call (CEECINST/00049/2018). CSDR acknowledges FCT for the financial support of her work contract through the Scientific Employment Support Program (Norma Transitória DL 57/2017).

References

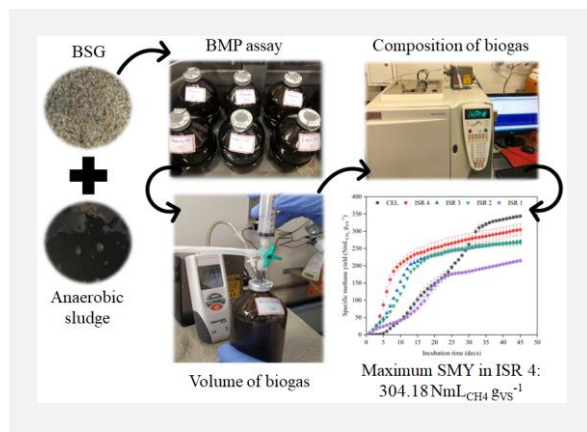
- [1] C.S.D. Rodrigues et al., Journal of Environmental Management, 322 (2022) 116084.
- [2] C. Walling, Accounts of Chemical Research, 8 (1975) 125-131
- [3] C.S.D. Rodrigues et al., Applied Catalysis B: Environmental, 219 (2017) 109-122.
- [4] R. Xie et al., Chemosphere, 227 (2019) 401-408.
- [5] O.S.G.P. Soares et al., Catalysts, 9 (2019) 258.
- [6] O.S.G.P. Soares et al., Carbon, 91, 249 (2015) 114-121.

Biochemical methane potential and biodegradability of brewery spent grain in different inoculum to substrate ratios

P. Polastri*, W.M. Moreira, A.L.G. Simões, D.T. Vareschini, M.L. Gimenes

State University of Maringá, 5790 Columbus Avenue, Maringá, PR 87020-900, Brazil.

*paulapolastri1983@gmail.com



This study aims to evaluate the influence of different inoculum to substrate ratios (ISR) on the methane production using brewery spent grain (BSG) as substrate. The biochemical methane potential (BMP) assay was conducted to evaluate the effect on methane yield of different ISR (4, 3, 2 and 1) based on volatile solids. In addition, the performance of the inoculum using microcrystalline cellulose as a standard substrate, the theoretical methane potential and the biodegradability of the substrates were evaluated. The BMP assay pointed that the best methane production was in ISR 4, with a specific methane yield of 304.18 NmL_{CH₄} g_{VS}⁻¹. On the other hand, ISR 1 showed the lowest production, showing a profile of the accumulated production curve of biogas and methane with possible inhibition and difficult biodegradability. Therefore, the inoculum used in the BMP assay met the mandatory quality criteria and the increase in BSG methane yield was directly proportional to the increase in ISR.

Introduction

Nowadays, Brazil is the third largest beer producer in the world, behind only China and the United States [1]. In addition, to produce 100 liters of beer, approximately 20 kg of brewery spent grain (BSG) are generated, representing 85% of the total solid waste produced [2].

The main current application of BSG is as a feed for cattle. However, several studies have been proposing the use of BSG in energy production [2], such as a substrate in anaerobic digestion (AD) processes for production biogas [3–5]. Thus, the determination of the biochemical methane potential (BMP) of organic substrates is a key component of AD research, and the BMP assay is widely used to determine the biodegradability and methane yield of different substrates [6].

In BMP assays, the inoculum to substrate ratio (ISR) is an important parameter, as it affects the efficiency of AD [7]. It is recommended that the volatile solids (VS) portion of the inoculum be greater than that of the substrate to minimize acidification or inhibition problems, and the use of an ISR ≥ 2 is considered a standard [8,9]. Previous studies have shown that increasing ISR positively affects the methane yield [10,11].

Therefore, this study aims to determine the biochemical methane potential (BMP) using the brewery spent grain (BSG) as a substrate. The BMP was evaluated in different inoculum to substrate ratios (ISR) and the inoculum activity was validated using a standard substrate to compare the results.

Materials and methods

The BSG was obtained by a local brewery (Maringá, Paraná, Brazil), after producing Pilsen-type beer. Microcrystalline cellulose (CEL) was used as the standard substrate. The inoculum is the mixture of anaerobic sludge from a municipal wastewater treatment plant (MWTP) and the treatment of wastewater from swine farming. The physical-chemical characterization of the inoculum and substrates followed the methodologies described in [12]. The elemental composition of BSG was determined using a CHNS elemental analyzer (Thermo Scientific, FlashSmart).

After the characterization of the inoculum and substrates, the BMP assay was performed according to the recommendations

described in [8,9] and conducted in a 250 mL glass bottle reactor, with a headspace volume of 75 mL. Blank controls were performed to obtain BMP from the inoculum activity, and positive control reactors were used to evaluate the quality of the inoculum using CEL. The ISR was calculated on VS basis, and ISR 4, 3, 2, and 1 were investigated, except from CEL, where the ISR was fixed at 2. All bioreactors were maintained at mesophilic temperatures (37 ± 1 °C) in a thermostatic bath for 45 days and manually agitated once a day.

The biogas composition was measured on a gas chromatograph (Trace GC Ultra, Thermo Scientific), equipped with a thermal conductivity detector (TCD). Results were expressed in normal milliliter (NmL) at 273.15 K and 1013.25 mbar. The theoretical biochemical methane potential (TBMP) was calculated using Buswell equation [13] and TBMP values were used to evaluate the biodegradability of the substrates, through the relationship between the measured BMP and the TBMP [14]. The biogas production and specific methane yield (SMY) were analyzed using analysis of variance (ANOVA) followed by the Tukey test ($p < 0.05$).

Results and discussion

The characteristics of substrates and the inoculum are shown in Table 1. Table 1 shows that the BSG VS/TS ratio (0.96) indicates a high potential for organic transformation, since substrates that present VS/TS greater than 0.70 can be considered easily biodegradable [15]. Moreover, the C/N ratio obtained for BSG (12.52) is below the value considered optimal for anaerobic digestion (20–30) [16]. Therefore, considering the optimal C/N ratio, the substrates can be successfully digested. However, for low C/N ratios, as obtained for BSG, the use of higher ISR in BMP tests [5] and anaerobic co-digestion is indicated to improve the C/N ratios [17]. In [3] C/N ratio was 12.4, the closest value found compared to the result obtained in this study.

The accumulated production of biogas and methane, methane concentration, and the biodegradability of the substrates are shown in Table 2. The curves profile of the accumulated production of methane for each ISR is shown in Figure 1.

The ISR 4 presented the best performance in the BMP, showing that this concentration range is the most suitable for producing biogas and methane from BSG. However, an ISR 1 resulted in the lowest SMY, this result may be related to the overload of the bioreactors at this concentration. For this reason, the amount of hydrolysable substrate available to microorganisms may have caused the accumulation of volatile fatty acids and, consequently, possible inhibitions of the AD.

Table 1. Composition of inoculum and substrates.

Parameter	Inoculum ^(a)	Brewery spent grain	Microcrystalline cellulose ^(b)
TS (%)	3.57 (± 0.07)	22.27 (± 0.08)	94.40 (± 0.09)
VS (%)	2.38 (± 0.09)	21.49 (± 0.03)	94.34 (± 0.11)
VS/TS (-)	0.66	0.96	0.99
C (% TS)	ND	45.71 (± 1.07)	ND
H (% TS)	ND	6.07 (± 0.12)	ND
N (% TS)	ND	3.65 (± 0.21)	ND
S (% TS)	ND	0.15 (± 0.00)	ND
O ^(c) (% TS)	ND	43.64	ND
C/N ratio (-)	ND	12.52	ND
Chemical formula	ND	C ₁₅ H ₂₃ O ₁₀ N	C ₆ H ₁₀ O ₅ ^(d)
TBMP (NmL _{CH₄} g _{SV} ⁻¹)	ND	446	414 ^(d)

ND: not determined; TS: total solids; VS: volatile solids; C/N ratio: carbon to nitrogen ratio; TBMP: theoretical biochemical methane potential based on elemental composition; (a) anaerobic sludge mixture; (b) standard substrate; (c) calculated by difference; (d) from literature. Average values are reported and values in parenthesis represent standard deviation (n = 3).

In comparison, [5] applied an ISR 3 and reported a SMY for two different BSG samples between 306.40-356.20 NmL_{CH₄} g_{VS}⁻¹. In [3], reported a degree of conversion or biodegradability of 81.10% for BSG, while in this study the highest value obtained was 68.20% for ISR 4.

The biological activity of the inoculum was evaluated by the BMP in the positive control bioreactors. The biogas production

of 598.61 NmL g_{VS}⁻¹, corresponding to 80.35% of the theoretical potential value of CEL. In [9], considering cellulose with 100% conversion, the average biogas production is 745 NmL g_{VS}⁻¹. In addition, [6] reported that the BMP results can be validated only if the BMP of CEL is between 340 and 395 NmL_{CH₄} g_{VS}⁻¹. Thus, the BMP test performed was valid, since 343.67 NmL_{CH₄} g_{VS}⁻¹ was obtained for the average of the positive control bioreactors.

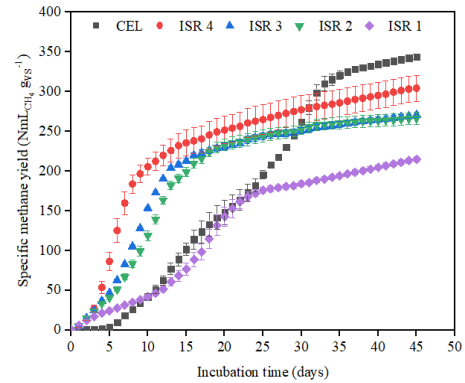


Figure 1. Curves of cumulative methane production of the BMP test in 45 days of BSG in ISR 4, 3, 2 and 1, and CEL as positive control in ISR 2. Average values are reported and standard deviations represent vertical bars (n = 4).

Conclusions

All in all, the SMY of BSG on the ISR 4 showed better performance in the BMP assay. Therefore, the increase in SMY was directly proportional to the increase in ISR, and the anaerobic sludge used showed good performance, meeting the quality criteria necessary for application as inoculum in BMP assay.

Table 2. Biogas and methane production, methane content and biodegradability for different inoculum to substrate ratios in 45 days.

Bioreactor	ISR	Cumulative biogas production (NmL g _{VS} ⁻¹)	Cumulative methane production (NmL _{CH₄} g _{VS} ⁻¹)	Methane content (% of CH ₄)	Biodegradability (%) ^(*)
CEL	2	598.61 (± 10.64)	343.67 (± 3.33)	53.35 (± 0.57)	83.01
BSG 4	4	524.78 (± 30.43) ^a	304.18 (± 16.39) ^a	55.61 (± 0.79)	68.20
BSG 3	3	486.55 (± 12.56) ^{ab}	270.62 (± 3.53) ^b	54.83 (± 0.48)	60.67
BSG 2	2	468.34 (± 10.19) ^b	267.17 (± 8.90) ^b	55.74 (± 0.28)	59.69
BSG 1	1	390.55 (± 13.67) ^c	214.79 (± 3.61) ^c	53.76 (± 1.06)	48.16

Different letters indicate that the difference of the means is significant at the 0.05 level; BSG: brewery spent grain; CEL: positive control; ISR: inoculum to substrate ratio; VS: volatile solids; (*) Biodegradability = (BMP/TBMP) x 100. Average values are reported and values in parenthesis represent standard deviation (n = 4).

References

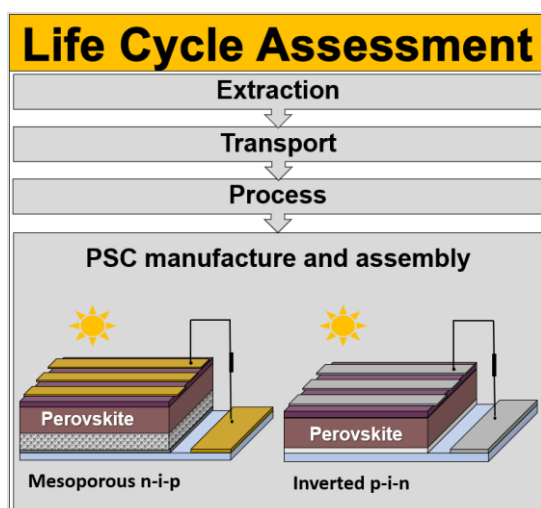
- [1] BarthHaas, BarthHaas Report 2021/2022, BarthHaas GmbH & Co. KG, Nuremberg, 2022, 3-40.
- [2] S.I. Mussatto, Journal of the Science of Food and Agriculture, 94 (2014) 1264-1275.
- [3] R. Vitanza et al., Chemical and Biochemical Engineering Quarterly, 30 (2016) 351-357.
- [4] C. Bougrier et al., Journal of Environmental Management, 223 (2018) 101-107.
- [5] M. Mainardis et al., Journal of Environmental Chemical Engineering, 7 (2019) 1-9.
- [6] S. D. Hafner et al., Water, 12 (2020) 1752.
- [7] S. Dechruga et al., Bioresource Technology, 146 (2013) 101-108.
- [8] C. Holliger et al., Water Science and Technology, 74 (2016) 2515-2522.
- [9] Verein Deutscher Ingenieure, VDI 4630 Fermentation of organic materials, VDI, Düsseldorf, 2016, 1-132.
- [10] H. Caillet et al., Procedia Manufacturing, 35 (2019) 259-264.
- [11] H.C. Yoruklu et al., Journal of Material Cycles and Waste Management, 20 (2018) 800-809.
- [12] American Public Health Association, Standard methods for the examination of water and wastewater, 20 Ed., APHA, Washington, 1998, 1-2671.
- [13] G.E. Symons, A.M. Buswell. Journal of the American Chemical Society, 55 (1933) 2028-2036.
- [14] A. H. Vazifekhoran, J. M. Triolo. Journal of Cleaner Production, 220 (2019) 1222-1230.
- [15] P. Pavan et al., Water Science and Technology, 41 (2000) 75-81.
- [16] G. F. Parkin, W. F. Owen. Journal of Environmental Engineering, 112 (1986) 867-920.
- [17] J. Mata-Alvarez et al., Renewable and Sustainable Energy Reviews, 36 (2014) 412-427.

Comparison of energy consumption and carbon footprint of perovskite solar cells with different architectures

J. Príncipe^{1,2}, L. Andrade^{1,2}, T.M. Mata³, A.A. Martins^{1,2*}

¹LEPABE - Laboratory for Process Engineering, Environment, Biotechnology and Energy, Faculty of Engineering, University of Porto, R. Dr. Roberto Frias, 4200-465 Porto, Portugal; ²ALiCE - Associate Laboratory in Chemical Engineering, Faculty of Engineering, University of Porto, R. Dr. Roberto Frias, 4200-465 Porto, Portugal; ³LAETA-INEGI, Associated Laboratory for Energy and Aeronautics - Institute of Science and Innovation in Mechanical and Industrial Engineering, R. Dr. Roberto Frias 400, 4200-465 Porto, Portugal.

*aamartins@fe.up.pt



Perovskite Solar Cells (PSCs) are an emerging photovoltaic technology that currently is seen as an alternative to silicon-based technologies. A proper technology development requires the evaluation and optimization of their environmental performance. This work compares the energy consumption and the carbon footprint (CF) of producing PSCs with mesoporous n-i-p and inverted p-i-n architectures. An inverted PSC with 2.4 cm x 1.2 cm of area was considered. A cradle-to-gate study is done, and the life cycle inventory was built using primary data from the PSC production complemented with literature information and the EcoInvent V3.5 database. The ILCD methodology was considered to evaluate the CF in SimaProTM V8.5.2.0. Results show that the mesoporous n-i-p PSC has significantly higher energy consumption (123.33 MJ) and CF (32.88 kg CO₂ eq) when compared with the inverted p-i-n PSC (20.88 MJ and 0.50 kg CO₂ eq). Suggestions of improvement are proposed and evaluated to reduce those values.

Introduction

Presently, fossil fuels provide about 80 % of the world's energy needs [1]. Beyond being finite and unevenly distributed globally, energy use has resulted in significant environmental, economic and social impacts, of which greenhouse gas (GHG) emissions are a major culprit. More concretely, the combustion of fossil fuels for power generation accounts for more than 40 % of all energy-related carbon dioxide (CO₂) emissions [2]. Production of energy through renewable sources is the main alternative to fossil fuels. Among them, solar energy has shown great potential to contribute positively to changing the energy paradigm. PSCs are an attractive emerging photovoltaic technology not only because of their high power conversion efficiency (PCE) but also, due to their easy manufacturing and scalability potential [3, 4]. This type of technology already achieved PCEs of 25.7 % and has great potential to compete with the currently used photovoltaic panels [5]. Different device architectures have been reported, but mesoporous n-i-p and inverted p-i-n structures are the most used. In the mesoporous structure, the perovskite layer is deposited on top of an electron transport layer (ETL) and then a hole transport layer (HTL) is coated on top of the perovskite layer, while in the inverted structure, the order of the charge extracting layers is inverted [6], as seen in Figure 1.

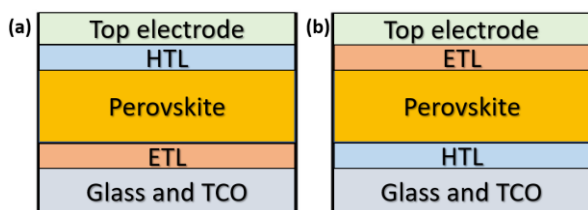


Figure 1. Most common PSCs architectures: a) mesoporous n-i-p and b) inverted p-i-n (adapted from [3]).

Despite the advantages that this technology presents, PSCs still have some limitations, mainly in terms of stability and possible environmental impacts. Thus, this represents an opportunity to improve the PSC technical performance, while ensuring that the environmental impacts of their production are reduced.

Objective and methodology

Notwithstanding the importance of having high PCE values, from an environmental impacts perspective the production of PSC is also relevant, as it may be energy intensive and/or use rare materials. Hence, in this work the energy consumption and carbon footprint of producing an inverted p-i-n PSC is assessed and compared with the results obtained for a PSC with mesoporous n-i-p architecture by Carneiro et al. [7]. The CF was evaluated using the Life Cycle Assessment (LCA) methodology, as defined in the ISO standards [8, 9]. An attributive "cradle-to-gate" study is done for a PSC structure with 1.2 cm x 2.4 cm of area, the same dimensions considered by Carneiro et al. [7]. Thus, only activities that occur from raw materials extraction to transportation, processing, manufacturing and assembly of the PSCs were considered, excluding the utilization and end-of-life stages. Even though commercial PSCs have much larger dimensions than those of laboratory scale manufactured in this work, the development of an LCA study will allow the identification of the environmental hotspots during production of a PSC, allowing R&D efforts to be concentrated on them in order to reduce the environmental impacts.

The Life Cycle Inventory (LCI) includes primary data from the PSCs production at the laboratory scale, complemented with secondary data from the literature and the EcoInvent database V3.5 available in the SimaProTM V8.5.2.0 software. For the background data, Portuguese and European conditions were considered whenever possible. The CF was evaluated using the

International Reference Life Cycle Data System (ILCD) 2011 Midpoint+ V.1.10 [10] methodology to ensure a proper comparison with the Carneiro et al. [7] results.

Results

As shown in Figure 1, the PSCs consist of various layers that are deposited consecutively, from bottom to top. Hence, a good way of comparing both PSC architectures involves not only comparing the values for the whole life-cycle, but also compare the values for each layer. In this way, it will be possible to better compare the two architectures and identify which are the layers where the improvement work should focus. For the energy consumption, the mesoporous n-i-p architecture consumes 123.33 MJ per PSC compared with 20.88 MJ for the inverted p-i-n. Figure 2 presents the energy consumption values for each layer. The results show that, with the exception of the fourth layer (HTL/ETL) deposition, the mesoporous n-i-p architecture always consumes more energy than the inverted p-i-n.

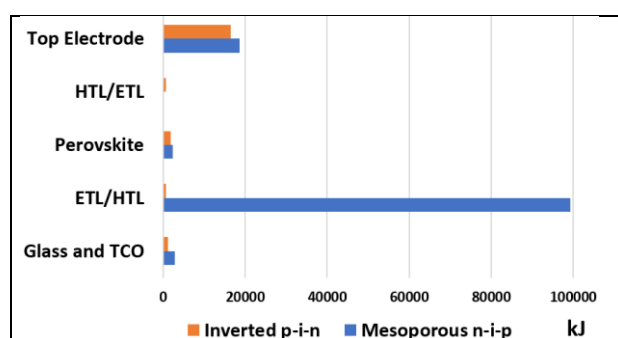


Figure 2. Energy consumption involved in the production of the PSC layers for the two architectures considered: mesoporous n-i-p and inverted p-i-n.

The difference is particularly relevant for the second layer that represents the controlling factor in the mesoporous n-i-p architecture, where the creation of the ETL layer involves an oven with a significant consumption of energy. Even though the CF is related to the energy consumption, as energy generation

Acknowledgements

Joana Príncipe was supported by the doctoral grant RT/BD/152838/2021 financed by the Portuguese Foundation for Science and Technology (FCT), through the state budget, under MIT Portugal Program. This work was also financially supported by LA/P/0045/2020 (ALiCE), UIDB/00511/2020 and UIDP/00511/2020 (LEPABE), funded by national funds through FCT/MCTES (PIDDAC) and project InPSC - PTDC/EQU-EQU/4193/2021 funded by national funds through the FCT/MCTES (PIDDAC). Teresa Mata gratefully acknowledges the funding of Project NORTE-06-3559-FSE-000107, cofinanced by Programa Operacional Regional do Norte (NORTE2020), through Fundo Social Europeu (FSE). António Martins gratefully acknowledges the Portuguese national funding agency for science, research and technology (FCT) for funding through program DL 57/2016 – Norma transitória.

References

- [1] Environmental and Energy Study Institute, Fossil Fuels, <https://www.eesi.org/topics/fossil-fuels/description>, (accessed on 23-03-2023).
- [2] World Nuclear Association, Carbon Dioxide Emissions from Electricity, <https://www.world-nuclear.org/information-library/energy-and-the-environment/carbon-dioxide-emissions-from-electricity.aspx>, (accessed on 23-03-2023).
- [3] J. Príncipe et al., *Energy Technol-Ger*, 10 (2022).
- [4] Q. Wang et al., *Renewable Sustainable Energy Reviews*, 56 (2016) 347-361.
- [5] National Renewable Energy Laboratory, Best Research-Cell Efficiency Chart, <https://www.nrel.gov/pv/cell-efficiency.html>, (accessed on 23-03-2023).
- [6] A.A. Said et al., *Small*, 15 (2019) 1900854.
- [7] A.L. Carneiro et al., *Energy Reports*, 8 (2022) 475-481.
- [8] International Organization for Standardization, ISO 14040: Environmental Management - Life Cycle Assessment - Principles and Framework, 2006.
- [9] International Organization for Standardization, ISO 14044: Life Cycle Assessment - Requirements and Guidelines, 2006.
- [10] European Commission -Joint Research Centre - Institute for Environment and Sustainability, International Reference Life Cycle Data System (ILCD) Handbook - General guide for Life Cycle Assessment - Provisions and action steps, First ed., Publications Office of the European Union, Luxembourg, 2011.

involves the combustion of fossil fuels with the corresponding GHG, the emissions due to processing of raw materials are also accounted for a life cycle perspective. Values of CF of 32.88 kg CO₂ eq and 0.50 kg CO₂ eq per cell were obtained for the mesoporous n-i-p and inverted p-i-n architecture, respectively. The difference in the CF of both PSC architectures is about 66 times greater than the difference observed for energy consumption, which is 6 times greater. This is due to the materials used in both cases, in particular the utilization of gold as top electrode in mesoporous n-i-p PSC, that change the relative importance of the various layers on the CF when compared to the situation observed in the energy consumption. This is shown in Figure 3, where it can be seen that the CF dominant layers changed when compared with Figure 2.

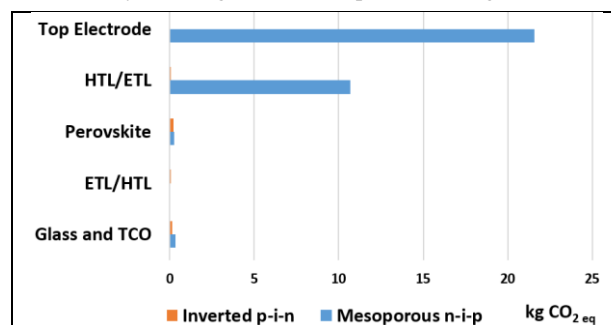


Figure 3. Values of the CF involved in producing the various layers of PSCs for both architectures.

Conclusions

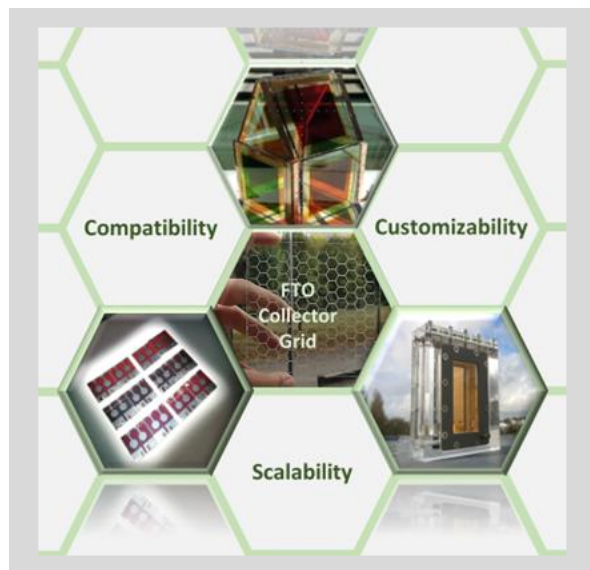
In this work the energy consumption and CF of producing PSCs with two different architectures were evaluated and compared on a life cycle perspective. The results show that the mesoporous n-i-p architecture has higher energy consumption and CF than the inverted p-i-n architecture, supporting the conclusion that further R&D work should focus on the later. Based on the results obtained some suggestions for improvements were proposed and evaluated, and the results will be presented in the oral communication to be made at the congress.

Overcoming the upscaling challenges of Dye-sensitized solar cells with fluorine-doped tin oxide current collectors

*J. Capitão**, *D. Ivanou*, *A. Mendes*

LEPABE – Laboratory for Process Engineering, Environment, Biotechnology and Energy, University of Porto, Rua Dr. Roberto Frias, 4200-465, Porto, Portugal; ALiCE – Associate Laboratory in Chemical Engineering, University of Porto, Rua Dr. Roberto Frias, 4200-465, Porto, Portugal.

**up200606001@edu.fe.up.pt*



The potential of Dye-Sensitized Solar Cells (DSSCs) for photovoltaic integration into buildings and low-power electronics is significant due to their low cost, adaptability, and semi-transparency. However, one of the main challenges of upscaling DSSCs is the poor performance due to electron transport resistance. To overcome this, highly conductive collectors with chemical and thermal stability can be added to the DSSC electrode. This work presents a study on the use of fluorine-doped tin oxide (FTO) as a conductive material for current collectors. By using a heat-resistant ink solution to mask the electrode for the spray pyrolysis technique, a mesh-like FTO current collector was created that significantly improved the performance of large-area DSSCs. The practical results show an increase in photoconversion efficiency from 0.77% to 2.44%. The proposed method of using FTO current collectors offers a simple and promising solution for improving the performance of large-area DSSCs.

Introduction

The market for photovoltaic (PV) integration into buildings and consumer items, such as low-power electronics, is becoming essential for solving the constantly growing demand for local energy supply. DSSCs are one of the most promising 3rd generation PV for this application as they are inexpensive to produce and can be built with low-cost materials; they excel under diffuse natural and artificial light because they can absorb more light spectrum; they are simple to process and adaptable for use in indoor electronics; and they are also semi-transparent with pleasing colors adapted for living and working interiors, making them ideal for solar windows [1]. One of the main challenges of introducing DSSCs into the PV integration market is poor performance when upscaled to large areas. The current (J) extracted from DSSCs, in the presence of series (R_S) and shunt resistance (R_{Sh}) can be described by the general diode equation [2]:

$$J = J_L - J_0 \times e^{\left[\frac{F \times (V + J \times R_S)}{n \times k \times T} \right]} - \frac{V + J \times R_S}{R_{Sh}} \quad (1)$$

Where J_L is the photogenerated current, J_0 is the reverse saturated current, F is the Faraday constant, n is the diode ideality factor, R is the universal gas constant, T is the absolute temperature, and V the voltage. The R_S is associated with the electron transport resistance factors, and the most impactful is the conductive electrode. FTO-coated glass is commonly used due to its good chemical and thermal stability, good conductivity, and high solar transmittance [3]. By correlating the R_S with the FTO sheet resistance (R_{Sheet}), the voltage drop can be expressed for a device of length, L , and width, w :

$$V = V_0 - J \times R_S = V_0 - J \times \frac{R_{Sheet} \times w}{L} \quad (2)$$

Where V_0 is the cells' voltage considering null resistance. The photovoltaic performance of large devices can be evaluated by

solving equations (1) and (2). As seen in Figure 1, the FTO conductivity is insufficient to maintain efficiency as the area increases.

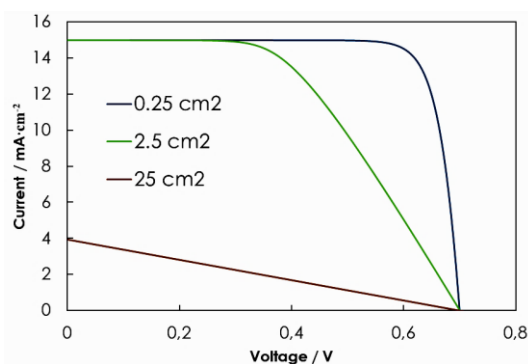


Figure 1. J - V curve response for different DSSCs areas.

Methods

The current extraction from DSSCs can be maximized by adding a grid of highly conductive current collectors, dividing the large area device into smaller, parallel operating units [4]. Due to their superior conductivity, metals are the preferred choice; however, the chemical interaction with DSSCs organic components jeopardizes the long-term functionality of the metal collector by promoting recombination reactions. Furthermore, the ongoing research for better dyes and electrolytes makes it impossible to predict whether the metal will still be a viable assembly option [5]. Therefore, the ideal conductive material must possess chemical and thermal stability towards DSSCs, regardless of any future modification to the solar cell. Since FTO already meets these requirements, it seems logical to conceptualize FTO current collectors. The most common method of deposition is spray pyrolysis because it allows the optimization of the FTO solution and deposition temperature (between 400 to 500 °C) to

achieve a relatively high conductivity while maintaining transparency [3]. However, masking the substrate for the required high-temperature deposition has not been scientifically pursued and achieved in this work by spraying a heat-resistant ink solution, providing a simple and quick curing process, and the flexibility with laser ablation, to develop various collectors designs (Figure 2) that can be studied regarding the mesh geometry and dimensions with Multiphysics simulation for the optimization of current extraction [6].

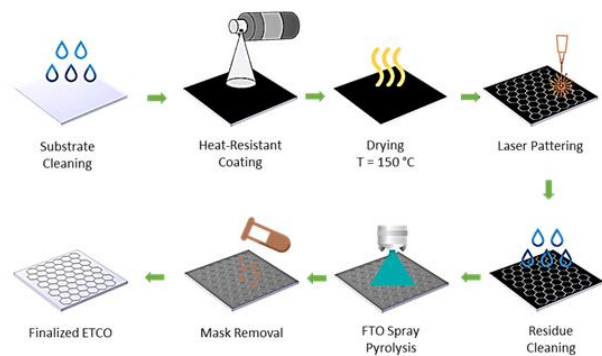


Figure 2. Illustration of FTO collector development process.

Results

Four types of conductive electrodes were simulated and produced for experimental validation of large-area DSCs, seen in Figure 3: plain commercial FTO ($7 \Omega \cdot \text{cm}^{-1}$) as a reference, a highly conductive FTO perimeter, and two samples containing a mesh: square and honeycomb; that retains 15% of light transmittance. The simulation shows that the reference has a substantial potential drop that can be decreased by adding a conductive perimeter, leaving only one critical area with high-level resistance. Inserting collector lines in this area can improve conductivity even further. This impact is amplified when the design is improved to the honeycomb mesh.

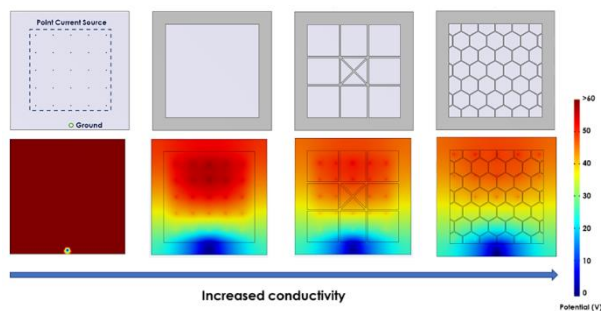


Figure 3. Simulation results for 25cm² collector designs.

Acknowledgements

LEPABE for the PhD grant reference UI/BD/150993/2021. The research leading to these results also received funding from: i) project 2SMART - engineered Smart materials for Smart citizens, with reference NORTE-01-0145-FEDER-000054, supported by Norte Portugal Regional Operational Programme (NORTE 2020), under the PORTUGAL 2020 Partnership Agreement, through the European Regional Development Fund (ERDF); ii) project HopeH2, with reference POCI-01-0145-FEDER-030760; iii) ALICE - Laboratório Associado para a Inovação em Engenharia Química, under reference LA/P/0045/2020; and iv) Base - UIDB/00511/2020 and Programmatic - UIDP/00511/2020 Funding of the Laboratory for Process Engineering, Environment, Biotechnology and Energy – LEPABE - funded by national funds through the FCT/MCTES (PIDDAC).

References

- [1] E. Mirabi et al., *Clean Energy*, 5 (2021) 505-526.
- [2] L. Han et al., *Comptes Rendus Chimie*, 9 (2006) 645-651.
- [3] J. Kim et al., *Journal of Materials Chemistry C*, 8 (2020) 14531-14539.
- [4] H. Serreze et al., *Conference Record of the 13th IEEE Photovoltaic Specialists Conference*, Washington, D.C, USA, 1978, 609-614.
- [5] G. Reynolds et al., *Electrochemical Society Transactions*, 33 (2011) 129-138.
- [6] D.K. Gupta et al., *Structural and Multidisciplinary Optimization*, 51 (2015) 941-955.

The photovoltaic metrics: Open circuit potential (V_{OC}); short circuit current (J_{SC}), Fill Factor (FF); and Power Conversion Efficiency (η_{PCE}) presented in (Table 1) were extracted from the current-voltage characterization of the DSSCs (Figure 4) and validated the simulation results. In comparison, the perimeter design results in an 83% increase in maximum current extraction, while the honeycomb design increases an additional 38%. Furthermore, the power output, directly related to the FF , benefits significantly from adding the mesh collector, enhancing this factor by 44%. Overall, the practical results corroborate the simulation and show an increase in PCE from 0.77% to 2.44%.

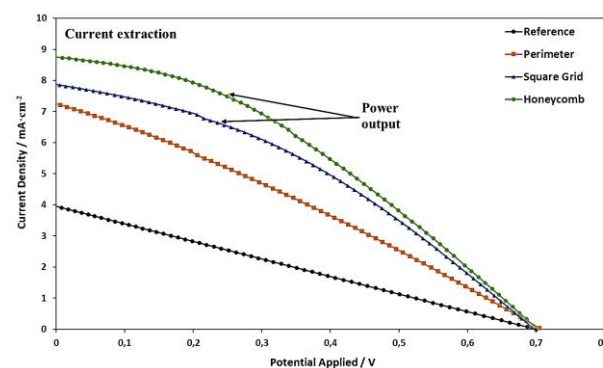


Figure 4. J - V characterization of 25cm² simulated DSSCs.

Table 1. Photovoltaic parameters extracted from J - V characterization.

	Reference	Perimeter	Square Grid	Honeycomb
V_{OC} (V)	0.70	0.71	0.70	0.70
J_{SC} (mA·cm ⁻²)	3.95	7.25	7.87	8.75
FF	0.25	0.29	0.36	0.37
η_{PCE} (%)	0.77	1.63	2.21	2.44

Conclusions

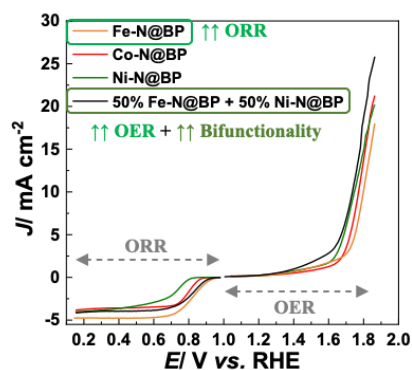
Although DSSCs demonstrate potential for the PV integration market, scalability remains a challenge that must be addressed. Adding current collectors displays a prominent solution, yet the conductive material requires chemical and thermal compatibility for long-term photovoltaic operation. A method was achieved to develop customizable FTO current collectors deposited by high-temperature spray pyrolysis. Different designs were assessed with Multiphysics simulation and then produced for large-area DSSCs. The results demonstrate a PCE improvement from 0.77% of the reference (no collectors) to 2.44% using the honeycomb mesh. congress.

Highly stable noble metal-free bifunctional carbon black electrocatalysts for oxygen reduction and evolution reactions

R.S. Ribeiro^{1,2,3*}, M. Florent¹, M.F.R. Pereira^{2,3}, T.J. Bandosz¹

¹Department of Chemistry and Biochemistry, The City College of the City University of New York, 160 Convent Avenue, New York, NY 10031, USA; ²LSRE-LCM - Laboratory of Separation and Reaction Engineering – Laboratory of Catalysis and Materials, Faculty of Engineering, University of Porto, Rua Dr. Roberto Frias, 4200-465 Porto, Portugal; ³AlICE - Associate Laboratory in Chemical Engineering, Faculty of Engineering, University of Porto, Rua Dr. Roberto Frias, 4200-465 Porto, Portugal.

*rsribeiro@fe.up.pt



This communication features our contribution to advance the design of carbon-based electrocatalysts, focusing on the main parameters to consider when aiming precise surface tuning with highly stable transition metals as active sites. The quality and dispersion of Fe species are the main parameters governing the electrocatalytic activity. For this, a simultaneous incorporation of nitrogen (to anchor individual metal centers and modulate the charge density nearby the active sites) and glucose (as chelating agent to enhance metal dispersion) was found crucial. The optimized Fe-containing carbon black electrocatalyst revealed a superior performance in ORR (*e.g.*, higher onset potential and current density) compared to a benchmark electrocatalyst containing 20 wt.% of platinum. The best bifunctionality features for oxygen reduction (ORR) and evolution (OER) reactions were obtained when employing a physical mixture of Fe- and Ni-containing carbon blacks as a catalyst.

Introduction

In May 2021, the International Energy Agency established the Net Zero Emissions by 2050 Scenario, as landmark, detailing the sustainable energy-related goals needed to ensure the feasibility of the roadmap to a 1.5 °C stabilization in rising global temperatures [1]. Renewable electricity generation is expected to play a central role in this endeavor, accounting for 50% of the final energy consumption by 2050 [1]. However, renewable energy sources are intermittent, *i.e.*, their output is dependent upon the weather. Moreover, the storage devices currently available (*e.g.*, batteries) lack the capacity needed to store the oversupply of renewable energy until peak demands occur [2]. Therefore, new solutions are needed to balance the renewable electricity supply and demand. The use of hydrogen as an energy vector can be that solution. Excess electrical energy can be converted into storable chemical energy in an electrolyzer, yielding hydrogen and oxygen [3], through the so-called hydrogen (HER) and oxygen (OER) evolution reactions [4]. The net zero-carbon fuel and oxidant can then be converted back to electrical energy in a fuel cell, through the so-called hydrogen oxidation (HOR) and oxygen reduction (ORR) reactions [3, 4]. Under a more innovative approach, unitized regenerative fuel cells (*i.e.*, compact systems with a single electrochemical cell operating alternatively in electrolyzer and fuel cell mode) can be used to decrease capital costs and render an operation easier [4]. However, it poses the need for bifunctional electrocatalysts, *i.e.*, one suitable for ORR and OER, and another for HOR and HER. ORR is the bottleneck of a hydrogen-based energy cycle. Therefore, oxygen reactions have been the focus of our study. ORR and OER electrocatalysts have been traditionally based on noble metals-containing nanoparticles supported on carbon black – mostly platinum (Pt) and its alloys [5-8]. Thus, the widespread use of hydrogen as the energy vector has been hindered both by the scarcity (and unsustainability) of these precious metals, as well as by the major impact of their high price on the overall costs [5, 9]. Bearing this in mind, highly active and stable noble metal-free carbon black electrocatalysts were developed in this study as an alternative to traditional noble

metals-containing materials. A molecular engineering approach was taken for that purpose, through which highly porous carbon black with promising features for ORR [10] was meticulously tailored with Fe, Ni, and Co species as active sites.

Experimental

Materials

Commercial carbon black – Black Pearls 2000 (BP), was purchased from Cabot Corporation (Boston, MA, USA). Iron species were introduced on the surface of BP using iron (III) nitrate, iron (II) chloride, or iron (II) acetate as precursor. Nickel (II) and cobalt (II) acetates were used as a source of nickel and cobalt, respectively. Melamine was used as a source of nitrogen and glucose was added as a chelating agent. Various ratios of the precursors were considered. The samples containing iron, nickel, cobalt, nitrogen, and/or glucose were subjected to a final thermal treatment under an inert atmosphere at 800 °C.

Characterization

Samples were characterized by N₂ physisorption; thermogravimetric analysis (TGA) coupled with a MS detector; X-ray Diffraction (XRD); X-ray photoelectron spectroscopy (XPS); and high-resolution transmission electron microscopy (HR-TEM).

Electrochemical measurements

A standard three-electrode configuration was used for the electrochemical measurements, with a Ag/AgCl reference electrode; a carbon rod counter electrode; and, as a working electrode, a rotating ring-disc electrode with a glassy carbon disc and a gold ring (ORR), or a glassy carbon rotating disc electrode (OER). Incorporation of carbon materials was performed by surface modification of the working electrodes by the drop-casting method. Cyclic voltammetry (CV), linear sweep voltammetry (LSV), and chronoamperometry measurements were carried out in basic media (0.1 mol L⁻¹ KOH) pre-saturated with nitrogen or oxygen by bubbling corresponding gas through the electrolyte solution for at least 30 min. Common indicators used to characterize the performance of electrocatalysts in ORR were determined from experiments performed with a rotation speed of 1600 rpm: onset potential (E_{onset} ; defined as the

maximum of the second derivative of the current density-potential curve); half-wave potential ($E_{1/2}$; defined as the maximum of the first derivative of the current density-potential curve); limiting current density (J_L ; defined as the current density at 0.2 V vs. RHE); hydrogen peroxide (H_2O_2) formation; and average number of electrons transferred during the ORR (n_E). The potential needed to achieve a current density of 10 mA cm^{-2} (E_{10}) was used to characterize the performance of the electrocatalysts in OER; whereas the potential gap between E_{10} and $E_{1/2}$ (ΔE) was used to evaluate bifunctionality.

Results and discussion

The synthesis methodology (Figure 1) was optimized upon introduction of Fe functionalities to the surface of BP and by a subsequent evaluation of the ORR activity. The effect of Fe precursor was studied first (results not shown), followed by the role of each synthesis precursor. The results confirmed the importance of adding nitrogen during the synthesis to anchor individual metal centers and to modulate a charge density nearby the active sites ($Fe_5-N@BP$ vs. $Fe_5@BP$; Table 1); whereas adding glucose as a chelating agent impacts the dispersion of active sites on the carbon surface and the subsequent performance ($Fe_5-N@BP$ vs. $Fe_5, No\ glucose-N @BP$; Table 1).

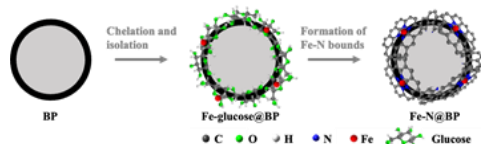


Figure 1. Strategy employed for the design of Fe-N active sites on BP.

Proper selection of the Fe load was also found important. Briefly, the performance in ORR obtained with $Fe-N@BP$ (Table 2) was better than that of $Fe_5-N@BP$ (Table 1), despite a 5-fold larger metal load on the latter.

Table 1. Summary of ORR results obtained with carbon black electrocatalysts prepared under various synthesis conditions.

Material	E_{onset}/V	$E_{1/2}/V$	$J_L/mA\ cm^{-2}$
BP	0.772	0.727	3.480
$Fe_5-N@BP$	0.917	0.852	4.361
$Fe_5@BP$	0.767	0.717	4.066
$Fe_5, No\ glucose-N @BP$	0.822	0.742	4.740

These ORR results, together with the advanced characterization results obtained by XRD, XPS, and HR-TEM (not shown), highlight the quality and dispersion of Fe species as crucial parameters governing the electrocatalytic activity. A catalyst benchmark study revealed that $Fe-N@BP$ enables a higher E_{onset} than that on Pt/C and similar $E_{1/2}$ (Figure 2 and Table 2). Moreover, the current density (J) yielded by the former after 24 h was still higher than that yielded by the latter at the beginning of the chronoamperometry experiment (Figure 2). The optimized synthesis methodology was employed for the introduction of Co and Ni. The best performance in OER and bifunctionality for oxygen reactions were obtained when employing a physical mixture of the Fe- and Ni-containing carbon blacks as a catalyst (Table 2 and Graphical abstract).

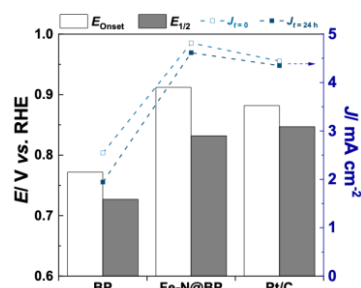


Figure 2. E_{onset} and $E_{1/2}$ (left axis); and current density (J) obtained after 0 ($J_{t=0}$) and 24 h ($J_{t=24h}$) at 0.4 V vs. RHE (right axis).

Conclusions

The methodology herein developed opens a window of opportunity for the development of electrocatalysts with enhanced bifunctionality features for ORR and OE.

Table 2. Summary of ORR and OER results obtained with Fe-, Co-, and Ni-containing carbon black electrocatalysts prepared under the optimized synthesis conditions.

Material	ORR					OER		Bifunctionality
	E_{onset}/V	$E_{1/2}/V$	$J_L/mA\ cm^{-2}$	$H_2O_2/\%$	n_E	E_{10}/V	$\Delta E/V$	
$Fe-N@BP$	0.912	0.832	4.757	1.8	3.97	1.798	0.966	
$Co-N@BP$	0.857	0.802	3.833	18.3	3.63	1.771	0.969	
$Ni-N@BP$	0.787	0.747	4.037	10.6	3.79	1.747	1.000	
50% $Fe-N@BP$ + 50% $Ni-N@BP$	0.892	0.837	4.152	8.3	3.84	1.736	0.899	
Pt/C	0.882	0.847	4.657	2.2	3.96	Not achieved	-	

Acknowledgements

This work was financially supported by project BiCat4Energy (PTDC/EQU-EQU/1707/2020), funded by national funds (PIDDAC) through FCT/MCTES; LA/P/0045/2020 (ALiCE), UIDB/50020/2020 and UIDP/50020/2020 (LSRE-LCM) funded by national funds through FCT/MCTES (PIDDAC). R.S.R. acknowledges the Fulbright Grant for Professors and Researchers with PhD awarded by Fulbright Commission Portugal.

References

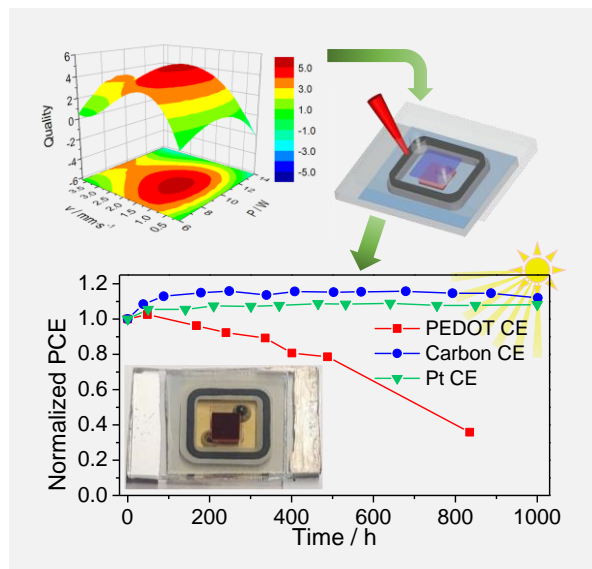
- [1] International Energy Agency, World Energy Outlook 2021, Paris, 2021.
- [2] A.S. Brouwer et al., Renewable and Sustainable Energy Reviews, 33 (2014) 443-466.
- [3] I. Staffell et al., Energy & Environmental Science Journal, 12 (2019) 463-491.
- [4] Y. Wang et al., Renewable and Sustainable Energy Reviews, 65 (2016) 961-977.
- [5] M.K. Debe, Nature, 486 (2012) 43-51.
- [6] K.C. Tsao et al., Oxygen reduction catalysts on nanoparticle electrodes, in: Encyclopedia of Interfacial Chemistry, K. Wandelt (Ed.), Elsevier, Oxford, 2018, 796-811.
- [7] C. Fu et al., Computational Materials Science, 170 (2019) 109202.
- [8] M. Tahir et al., Nano Energy, 37 (2017) 136-157.
- [9] R. Ma et al., npj Computational Materials, 5 (2019) 78.
- [10] M. Florent et al., Nanomaterials, 12 (2022) 4432.

Low temperature hermetic encapsulation for long-term stable dye-sensitized solar cells

J. Martins, S. Emami, D. Ivanou, A. Mendes*

LEPABE - Laboratory for Process, Environment, Biotechnology and Energy, Department of Chemical Engineering, Faculty of Engineering of University of Porto, Rua Dr. Roberto Frias s/n 4200-465 Porto, Portugal; ALiCE - Associate Laboratory in Chemical Engineering, Faculty of Engineering, University of Porto, Rua Dr. Roberto Frias, 4200-465 Porto, Portugal.

*mendes@fe.up.pt



A hermetic encapsulation is essential for producing long-term stable dye-sensitized solar cells (DSSCs). A new laser-assisted glass frit sealing method was developed to encapsulate DSSCs at a low temperature of 110 °C. This technique allowed, for the first time, the use of heat sensitive materials in the preparation of DSSCs before sealing process. The achieved encapsulation was characterized according to MIL-STD-883 and IEC61646 standards, concerning hermeticity and robustness. Glass frit sealed devices showed high stability with no performance loss after 1000 h under accelerated light ageing conditions, according to standard ISOS-L-2. The new low-temperature sealing method allows to simplify the fabrication process of DSSCs and produces long-lasting devices.

Introduction

Dye sensitized solar cells (DSSCs) are an emerging photovoltaic (PV) technology that combines moderate energy efficiencies with low-cost fabrication processes [1]. The attractive aesthetic and high performance under diffuse and low light conditions make DSSCs appealing for buildings and agriculture-integrated PV and has energy source for low-power devices such as Internet of Things (IoT) [2]. DSSCs are composed of a photoelectrode (PE) and a counter-electrode (CE) substrate connected by an electrolyte. DSSCs based on a liquid electrolyte use normally acetonitrile (ACN) solvent. However, the low boiling point of ACN causes loss of electrolyte by evaporation and low stability of the devices [3]. The electrolyte leakage can be prevented with a hermetic and robust encapsulation. Traditional polymer-based sealant materials do not provide a hermetic and long-lasting encapsulation [4]. Alternatively, glass frits are sealant materials that can provide airtight and stable encapsulation. These materials have high melting temperatures of > 380 °C and the components in the cell before the encapsulation process is limited to only heat-resistance materials. Using a laser beam as heating source it is possible to locally heat the glass frit to its melting point, bonding the substrates while keeping the cells at low process temperatures of < 120 °C [5]. In this work, a new glass frit encapsulation method was developed to encapsulate DSSCs at the low processing temperature of 110 °C. This new technique allowed for the first time the use of temperature sensitive components before the encapsulation process and the sealed devices show outstanding stability.

Methods

The sealant configuration is composed of two glass frits denoted as frit A and B, sequentially deposited by screen printing on the PE substrate and glazed at 500 °C and 400 °C. The sealing process is accomplished in an in-house made machine composed of i) a furnace, ii) a continuous wave (CW) laser source with the wavelength of 1070 nm, iii) an optic set of 2D scan head/f-theta lens, and iv) a four-axis Selective Compliance Assembly Robot

Arm (SCARA). The encapsulation process is performed by placing together the PE (bottom) and CE (top) substrate, in the furnace at the process temperature of 110 °C for 1 h. Then, the laser beam path is aligned with the glass frit sealing perimeter using the SCARA arm/optic set before the firing the laser beam through the CE substrate into the glass frit B, melting and joining frit B to the CE substrate. The hermeticity of the encapsulation was tested according to the helium leak test of MIL-STD-883 standard; method 1014.13, A2 using Adixen ASM 142 mass spectrometer. The robustness of empty sealed cells was tested following the humidity-freeze cycle test (-40 °C to 85 °C with 85 % RH) and damp heat test (70 °C with 85 % of RH for 500 h). Three different DSSCs configurations were encapsulated using the method above denoted as i) S_YCoP, ii) S_NiPt and iii) M_YCoC. A TiO₂ blocking layer by spray pyrolysis was deposited in all PE substrates. The PE of S_YCoP is composed of sequentially deposited transparent and reflector TiO₂ layer, followed by frits A and B. After sintering, the PE was sensitized using Y123 dye. The CE is constituted by a PEDOT:PSS layer. In the PE of S_NiPt was sequentially deposited two transparent and one opaque TiO₂ layer, frit A and B. The substrate was then sensitized with N719 dye. In the CE was deposited a Pt layer. In the PE of M_YCoC was deposited a transparent and reflector TiO₂ layer, frit A, a carbon layer and frit B, followed by sensitization with Y123 dye. No component is deposited in the CE of M_YCoC. The PE and CE are sandwiched together and bonded using the laser sealing method. After sealing, the electrolyte is injected into the cells. Cobalt electrolyte based in ACN solvent for S_YCoP and M_YCoC devices configurations and iodide electrolyte based on 3-methoxypropionitrile (MPN) solvent for S_NiPt cells. The stability of the sealed devices was assessed under accelerated light ageing test at the light intensity of 900 W·m⁻² in a test chamber at 50 ± 5 °C and under passive load at ca. 0.55 V according to the modified ISOS-L-2 protocol.

Results

The laser parameters, power, velocity and spot size, were optimized using response surface methodology (RSM). The

response of the model was the qualitative sealing quality on a scale of -5 to +5, where a negative response is associated with defects and +5 is the highest quality possible. Based on the quality response of the model as shown in the Graphical Abstract, the optimal laser parameters were laser power of 9.3 W, sealing velocity of 1.25 mm·s⁻¹, and beam spot size of 1.3 mm. Using these conditions, a reproducibility of ca. 80 % was achieved. No pin-holes were presented in the bonding interface and the thickness of the sealing line was ca. 38 μm.

Empty-sealed packages displayed helium leak rates below the reject limit of 1×10^{-7} atm·cm³·s⁻¹ before and after being submitted to the accelerated ageing tests of the IEC61646 standard; 10 humidity-freeze cycles and 500 h of damp heating. The optimized sealing conditions allows to achieve a hermetic and robust encapsulation that offers long-lasting protection.

The laser sealing process is performed at 110 °C and the cells are stabilized at this temperature for 1 h. This prolonged dwell time might affect the temperature sensitive components used in the devices; the dye load on the PE substrate and the polymer CE of PEDOT:PSS. To evaluate this effect, four groups of devices were prepared: i) without being submitted to 110 °C (N); ii) only the PE with dye loaded was submitted to 110 °C (PE); iii) only the CE with PEDOT:PSS was submitted to 110 °C (CE) and (iv) both, PE and CE substrates, were submitted to 110 °C (PE&CE). **Figure 1** show the characteristic photocurrent density vs. potential (*J-V*) curves of the devices. The performance of all devices are similar and therefore can be concluded the exposure to the laser process temperature and dwell time does not affect the loaded temperature sensitive components in DSSCs.

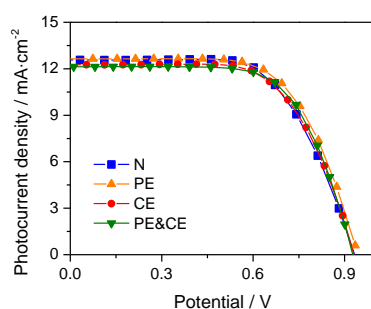


Figure 1. *J-V* curves of N, PE, CE, and PE&CE devices.

The DSSCs were encapsulated with the developed sealing method and their stability was evaluated under 1000 h of light ageing at 900 W·m⁻² of light intensity and at 50 ± 5 °C. S₂NIPt devices composed of electrolyte with MPN solvent, N719 dye

Acknowledgements

Jorge Martins is grateful to the Portuguese Foundation for Science and Technology (FCT) for his PhD grant (reference: SFRH/BD/147201/2019). This work was financially supported by: (i) LA/P/0045/2020 (ALiCE), UIDB/00511/2020 and UIDP/00511/2020 (LEPABE), funded by national funds through FCT/MCTES (PIDDAC); (ii) project 2SMART (NORTE-01-0145-FEDER-000054), supported by Norte Portugal Regional Operational Programme (NORTE 2020), under the PORTUGAL 2020 Partnership Agreement, through the European Regional Development Fund (ERDF); (iii) project BATERIAS 2030 with the reference POCI-01-0247-FEDER-046109 co-funded by Operational Programme for Competitiveness and Internationalisation (COMPETE 2020), under the Portugal 2020 Partnership Agreement, through the European Regional Development Fund (ERDF); (iv) project PorphSol (POCI-01-0145-FEDER-030357), funded by FEDER funds through COMPETE2020 – Programa Operacional Competitividade e Internacionalização (POCI) and by national funds (PIDDAC) through FCT/MCTES; national funds through FCT – Fundação para a Ciência e a Tecnologia, I.P., within the scope of project “TanPT - 2022. 05826.PTDC”.

References

- [1] M. Kokkonen et al., *Journal of Materials Chemistry A*, 9 (2021) 10527-10545.
- [2] H. Michaels et al., *Chemical Science*, 11 (2020) 2895-2906.
- [3] J. Gao et al., *Chemical Communications*, 50 (2014) 6249-6251.
- [4] A. Fakhruddin et al., *Energy & Environmental Science*, 7 (2014) 3952-3981.
- [5] S. Emami et al., *Journal of Materials Chemistry A*, 8 (2020) 2654-2662.
- [6] J. Maçaira et al., *Solar Energy Materials and Solar Cells*, 157 (2014) 134-138.
- [7] R. Jiang et al., *Journal of Materials Chemistry A*, 2 (2014) 4751-4757.
- [8] A. Kamppinen et al., *Electrochimica Acta*, 335 (2020) 135652.

and Pt as CE were shown to be stable and did not show any electrolyte leakage as illustrated in the Graphical Abstract. The devices had an increase in performance after the 1000 h of 10 % due to an increase in photocurrent. Good stability was previously reported for this configuration of cells [6].

S₂YCoP and M₂YCoC configurations constituted of a cobalt-mediated electrolyte in ACN solvent, Y123 dye, and CE of PEDOT:PSS and carbon, respectively, have more challenging stability issues [7] and therefore proper encapsulation is imperative. Polymer-sealed S₂YCoP cells show a large drop in performance after 50 h of ageing due to electrolyte/solvent leakage. Glass frit sealed devices show no electrolyte leakage. However, S₂YCoP cells displayed a continuous performance degradation as shown in the Graphical Abstract due to a sharp drop in fill factor and photocurrent. Kamppinen et al. observed similar performance deterioration behavior in light ageing test of cobalt+ACN electrolyte with PEDOT CE. These authors attributed the observed deterioration of power conversion efficiency (PCE) to a decrease of charge carriers and fast degradation of the electrolyte [8]. Glass-sealed M₂YCoC cells with carbon CE showed high stability during 1000 h of light ageing with ca. 13 % increase in efficiency, as shown in the Graphical Abstract, mostly due to an increase in photocurrent. This is the highest recorded stability for DSSCs with ACN-based electrolyte.

Conclusions

A new glass frit encapsulation process was developed to seal DSSC at the low process temperature of 110 °C, for the first time. The obtained encapsulated cells were characterized as hermetic and long-term stable according to the fine leak test of the MIL-STD-883 standard and the humidity-freeze cycle and damp heating tests of the IEC 61646 protocol.

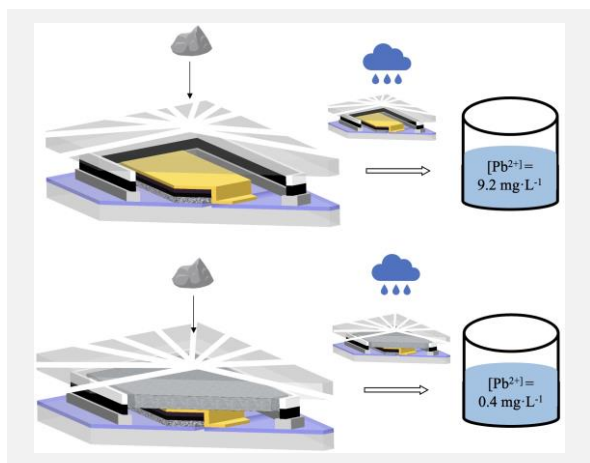
Glass-sealed DSSCs with MPN-based electrolyte show high stability after 1000 h of continuous illumination under simulated sunlight. Glass-sealed devices with cobalt-based electrolyte in ACN solvent and carbon counter-electrode show outstanding stability, displaying 13 % of PCE improvement after 1000 h of light ageing. However, glass-sealed devices with cobalt-based electrolyte in ACN solvent and PEDOT:PSS counter-electrode showed a continuous reduction of performance during the light ageing test due to electrolyte deterioration. Polymer-sealed devices had electrolyte leakage while no leakage was observed in glass-sealed cells. The developed sealing process prevents electrolyte leakage and eliminates extrinsic degradation factors producing stable DSSCs.

A novel approach for lead mitigation in perovskite solar cells glass encapsulated by laser sealing

E. Loureiro^{1,2}, R. Madureira^{1,2,3}, S. Emami^{1,2}, D. Ivanou^{1,2}, A. Mendes^{1,2*}

¹LEPABE - Laboratory for Process Engineering, Environment, Biotechnology and Energy, Faculty of Engineering, University of Porto, Rua Dr. Roberto Frias, 4200-465 Porto, Portugal; ²ALiCE - Associate Laboratory in Chemical Engineering, Faculty of Engineering, University of Porto, Rua Dr. Roberto Frias, 4200-465 Porto, Portugal; ³INEGI - Institute of Science and Innovation in Mechanical and Industrial Engineering, Faculty of Engineering, University of Porto, Rua Dr. Roberto Frias, 4200-465 Porto, Portugal.

*mendes@fe.up.pt

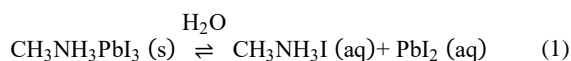


The use of lead-based perovskite solar cells (PSCs) rises public concerns due to the great water solubility of this light absorber. Simultaneously, the stability of these solar devices also represents an essential factor for their commercialization. The use of fully encapsulated cells fully addresses lead leakage in the case normal operation. However, in the case of an accident, when the cell breaks, other strategies must be put in place. The laser-assisted glass frit sealing process allows full hermeticity and long-term stable devices [1]. For addressing accident cell breakage events, this work discloses a chemisorption layer able to capture > 93 % of the water-soluble lead present in PSCs.

Introduction

Exposure to lead-contaminated environments is harmful to humans, animals, and plants; therefore, it is necessary to minimize its presence in the environment. Various studies show that exposure to shallow levels of lead (Pb) causes severe damage to human health [2]. In 2020, the European Parliament and the Council recast the directive on the quality of water intended for human consumption and set the maximum concentration limit for Pb present in drinking water equal to 5 µg L⁻¹ [3]. In the outdoor operation of perovskite solar cells PSCs, the devices are exposed to uncontrolled conditions related to environmental phenomena that may damage or break the device. If a broken perovskite solar cell enters in contact with water, the lead-perovskite layer onsets dissolution and ultimately water-soluble lead may be released in the environment.

Humidity directly influences the stability of the perovskite absorber. Niu *et al.* suggested a degradation mechanism according as described by equation (1) [4]:



Low-toxic/Pb-free metal halide perovskites have been proposed for applications in PSCs through the partial or total replacement of Pb by other metals, including tin (Sn), germanium (Ge), bismuth (Bi), or antimony (Sb) [5]. However, using these ions as Pb substitutes in the chemical structure of perovskite the performance of the PSCs becomes considerably decreased. Therefore, various strategies mitigating the lead release in the environment have been proposed.

Developing and improving Pb mitigation methods will make Pb-based PSCs environmentally safer and will be a crucial step towards the general acceptance of the PSC technology in the photovoltaic market. Simultaneously, the stability of the devices is also a critical factor in the commercialization of PSCs.

Although several strategies already exist to capture Pb in case of damage or breakage of PSCs, none of them address the device stability and the lead release mitigation in the case of leakage. Our recent developments in laser-assisted glass encapsulation of the PSCs [1, 6], contribute largely to increase the stability of the device and prevents the release of lead to the environment in the case of normal operation of the cells. However, there is still concern about the possibility of the breakage of these solar devices. Thus, it is essential to study a lead mitigation layer that can be integrated inside the cavity of the encapsulated PSCs. There are two possible strategies for applying a Pb mitigation layer inside a hermetic laser-sealed PSC: applying this layer directly above the solar cell active layers or on the inner side of the cover glass – Figure 1.

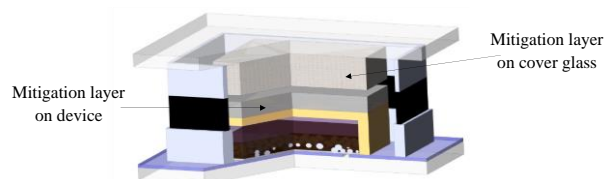
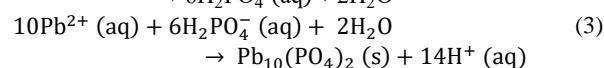
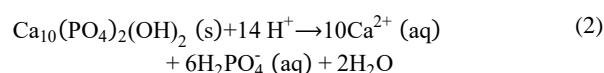


Figure 1. Schematic presentation of hermetically sealed PSC device incorporating two Pb mitigation layers strategies.

Methods and Results

In the present work, the Pb mitigation layer was applied the inner side of cover glass. The lead capture was investigated using a mesoporous paste of hydroxyapatite (HAp). The water soluble Pb is easily and efficiently chemisorbed at this layer. The Pb adsorption occurs according to following dissolution-precipitation mechanism – equations (2) and (3):



In this mechanism, Ca^{2+} ions are replaced by Pb^{2+} ions, transforming HAp into hydroxypyromorphite (Pb-HAp) [7]. Analyses of scanning electron microscopy (SEM), energy-dispersive x-ray spectroscopy (EDS), and x-ray photoelectron spectroscopy (XPS), validated the Pb capture by the HAp layer. The preliminary results revealed a $[\text{Pb}^{2+}] = (9.19 \pm 0.42) \text{ mg L}^{-1}$ and $[\text{Pb}^{2+}] = (0.68 \pm 0.21) \text{ mg L}^{-1}$, in the control and HAp devices, respectively. The presence of the HAp layer on cover glass did not influence the performance of the laser sealed device.

Acknowledgements

Eliana Loureiro and Rúben Madureira are grateful for the funding support from Foundation for Science and Technology (FCT) for their PhD grants (references: UI/BD/150991/2021 and SFRH/BD/137782/2018). This work was financially supported by LA/P/0045/2020 (ALiCE), UIDB/00511/2020 and UIDP/00511/2020 (LEPABE), funded by national funds through FCT/MCTES (PIDDAC); project 2SMART (NORTE-01-0145-FEDER-000054), supported by Norte Portugal Regional Operational Programme (NORTE 2020), under the PORTUGAL 2020 Partnership Agreement, through the European Regional Development Fund (ERDF), project Baterias 2030 (POCI-01-0247-FEDER-046109), supported by Operational Programme for Competitiveness and Internationalization (COMPETE 2020), under the Portugal 2020 Partnership Agreement, through the European Regional Development Fund (ERDF); project TanPT (2022.05826.PTDC), funded by FEDER funds through COMPETE2020 – Programa Operacional Competitividade e Internacionalização (POCI) and by national funds (PIDDAC) through FCT/MCTES. This work has received funding from the European Union's Horizon 2020 programme, through a FET Proactive research and innovation action under grant agreement No. 101084124.

References

- [1] S. Emami et al., *Journal of Materials Chemistry A*, 8 (2020) 2654-2662.
- [2] R.M. Pearson, *Medical Toxicology: Diagnosis and Treatment of Human Poisoning*, M.J. Ellenhorn and D.G. Barceloux. Elsevier, Amsterdam, 1987, 1512.
- [3] Directive (EU) 2020/2184 of the European Parliament and of the Council of 16 December 2020 on the quality of water intended for human consumption (recast), E.P.a.t.C.o.t.E. Union, Editor. 2020: Official Journal of the European Union. 62.
- [4] G. Niu et al., *Journal of Materials Chemistry A*, 2 (2014) 705-710.
- [5] A. Babayigit et al., *Scientific Reports*, 6 (2016) 18721.
- [6] J. Martins et al., *Journal of Materials Chemistry A*, 8 (2020) 20037-20046.
- [7] S. Sugiyama et al., *Journal of Colloid and Interface Science*, 332 (2009) 439-443.

Conclusions

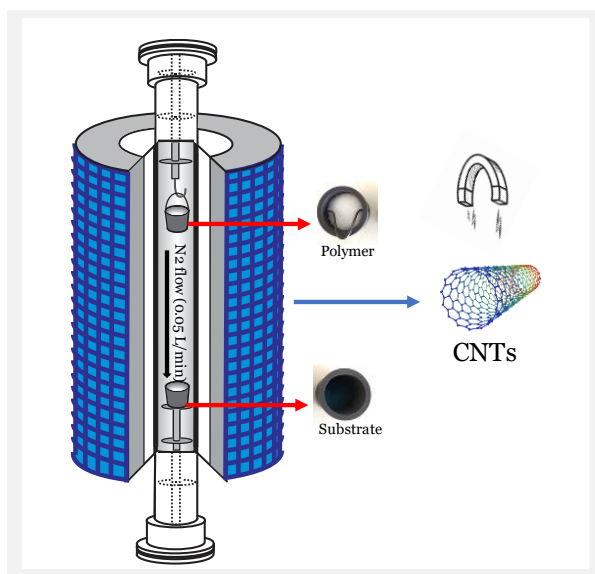
The effect of the HAp layer in capturing the Pb^{2+} released from a damaged PSCs were studied according to test procedures provided in Specification Test Standard for Impact Resistance Testing of Rigid Roofing Materials by Impacting with Freezer Ice Balls and BS EN 60529:1992+A2:2013 Degrees of protection provided by enclosures (IP Code).

Magnetic properties of carbon nanotubes synthesized by chemical vapor deposition using polyolefins as carbon source

A.S. Silva^{1,2,3,4,5*}, L.F. Sanches^{1,3}, F.F. Roman^{1,3,4,5}, J.L. Diaz de Tuesta^{1,3,6}, A.I. Pereira^{2,3}, A.M.T. Silva^{4,5}, H.T. Gomes^{1,3}

¹Centro de Investigação de Montanha (CIMO), Instituto Politécnico de Bragança (IPB), Bragança, Portugal; ²Centro de Investigação em Digitalização e Robótica Inteligente (CeDRI), IPB, Bragança, Portugal; ³Laboratório Associado para a Sustentabilidade e Tecnologia em Regiões de Montanha (SusTEC), IPB, Bragança, Portugal; ⁴Laboratory of Separation and Reaction Engineering – Laboratory of Catalysis and Materials (LSRE-LCM), Faculty of Engineering of the University of Porto (FEUP), Porto, Portugal; ⁵ALiCE - Associate Laboratory in Chemical Engineering, FEUP, Porto, Portugal; ⁶Department of Chemical and Environmental Technology, ESCET, Rey Juan Carlos University, Móstoles, Spain.

*adriano.santossilva@ipb.pt



Plastic recycling technologies are needed to ensure the sustainability of plastic use. In this respect, chemical recycling through plastic pyrolysis has promising results. In this regard, polyolefins as carbon source were valorized into carbon nanotubes (CNTs) using chemical vapor deposition (CVD), over a synthesized iron metal substrate. The recovered CNTs showed magnetic properties that are useful for liquid phase reactions, since they are easily recovered with the help of magnetic fields. The magnetic properties of nanomaterials were characterized by X-ray diffraction (XRD) to determine the origin of the magnetic properties. The results obtained from this analysis showed the existence of graphite and cementite phases, the latter being responsible for the magnetic properties.

Introduction

Urbanization has been increasing in the last few years, with uncontrolled city growth in most cases. The lack of planning in cities to deal with basic services has severe environmental consequences. As an example, the municipal solid waste management system is often neglected in urban areas, leading to sanitary issues. In this scenario, plastic solid wastes (PSWs) are recognized as major waste streams that can be a source of serious environmental problems. Plastics have become one of the most important modern resources due to their good properties, such as light weight, strength, fabrication capabilities, and low-cost nature. For instance, the plastic industry maintained high-level employment in Europe during the COVID-19 crisis, with over 1.5 million people working in about 50000 companies. Despite the importance of plastics to human life, alternatives to post-consumer plastic are in high demand to increase the sustainability of plastic usage.

Recycling is recognized as one of the most efficient methods to tackle plastic pollution. The traditional method of plastic recycling is mechanical, which includes collection, sorting, washing, and grinding of the material [1]. The steps mentioned may occur in a different order or not at all, depending on the source of the waste. The broadest amount of plastic waste comes from post-consumer mixed plastics packaging, requiring collection from the consumers, sorting to select the PET bottles, washing to remove food and paper residues, and grinding. Another alternative for the final disposition of PSWs is related to the construction industry to substitute virgin construction materials in mortars and concrete [2]. The amount of plastic available as waste can also be used as feedstock to produce valuable chemicals or for energy recovery [3]. However, the

energy recovery route is mainly performed via incineration, which has strong regulation laws established by the EU Hazardous Waste Incineration Directive. Several aspects of plastic waste characteristics can be challenging for mechanical recycling, such as using paints and coatings on plastics and limitations in the recycled plastics market. For the energy recovery route, toxic and obnoxious dioxins are released during incineration and should be carefully monitored to avoid environmental problems, increasing operational costs.

Due to the drawbacks associated with mechanical recycling and energy recovery, another approach that has received increasing interest is the chemical recycling route. In this regard, studies are reporting the synthesis of carbon nanotubes using plastics as carbon source, as well as studies dealing with valorization of the liquid fraction arising from plastic pyrolysis. In most cases, the synthesis of carbon nanomaterials is performed by chemical vapor deposition, requiring the utilization of a proper metal substrate. In this methodology, the obtention of magnetic CNTs was already reported, but the mechanism behind the synthesis still needs to be explored.

In this regard, CNTs were prepared in this work by CVD using polyolefins as carbon source and iron supported on alumina as a metal substrate. The nanomaterials recovered from the synthesis procedure exhibited magnetic properties useful for liquid-phase reactions due to easy recovery with a magnetic field. The magnetic properties of the nanomaterials will be discussed here in more detail.

Methodology

The CNTs were prepared by CVD using iron oxide nanoparticles supported on alumina (IO/Al₂O₃) as a metal

substrate. The metal substrate was prepared by adapting a sol-gel procedure. In brief, an Fe^{2+} solution in ethanol and an Fe^{3+} solution in ethylene glycol were mixed and stirred for 2 h with 6.6 g of alumina to homogenize the solution. The mixture was further heated to 120 °C, remaining at this temperature for 4 h until the formation of the gel. At last, the temperature was raised to 189 °C (boiling point of ethylene glycol) to remove the solvents. The final solid was calcined at 300 °C for 6 h and at 600 °C for 12 h.

For the CVD process, a one-chamber reactor was used. The reactor is equipped with 3 heating zones controlled independently and with 2 crucibles. The upper crucible was loaded with 5 g of polymer (LDPE, HDPE, or PP), and the lower crucible was loaded with 1 g of IO/ Al_2O_3 . During the synthesis, the temperature was set to 850 °C for the lower crucible for 1 h with an N_2 flow of 50 mL min^{-1} . The nanomaterial recovered from the lower crucible was washed with H_2SO_4 solution (50% v/v) at 140 °C for 3 h, to remove the metal phase. The final materials were named according to the plastic precursor considered for their synthesis as CNT@LDPE, CNT@HDPE, and CNT@PP. A blank run was performed without polymer to evaluate changes in the metal phase due to the heat treatment.

A strong neodymium magnet was used to evaluate the magnetic response from the samples. X-ray diffraction (XRD) analyses were made with a PANalytical X'Pert Pro diffractometer equipped with an X'Celerator detector and secondary monochromator in $\theta/2\theta$ Bragg-Brentano geometry. The measurements were carried out using 40 kV and 30 mA, a $\text{CuK}\alpha$ radiation ($\lambda_{a1} = 1.54060 \text{ \AA}$ and $\lambda_{a2} = 1.54443 \text{ \AA}$), $0.017^\circ/\text{step}$, 100 s/step, in a 10–80° 2θ angular range. TEM images were recorded in JEOL 2100 high-resolution transmission electron microscope (HR-TEM).

Results

The TEM images obtained for the washed nanomaterials and the interaction of samples with a strong magnet are shown in Figure 1. The results obtained in this analysis demonstrates that the synthesis procedure can be used to produce CNTs successfully. In addition, it's possible to observe the presence of iron grains encapsulated in the CNTs, that remain in the nanomaterials even after acid washing. The presence of the metal phase is enough to confer magnetic properties to the materials, as shown in Figure 1.

The XRD results of the metal substrate revealed a composition of 78% alumina, 19% hematite and 3% magnetite (diffractogram not shown here).

Acknowledgements

Adriano S. Silva thanks his doctoral Grant with reference SFRH/BD/151346/2021 financed by the Portuguese Foundation for Science and Technology (FCT), with funds from NORTE2020, under MIT Portugal Program. This work was financially supported by UIDB/05757/2020 (CeDRI), UIDB/00690/2020 (CIMO), LA/P/0045/2020 (ALiCE), UIDB/50020/2020, UI-DP/50020/2020 (LSRE-LCM) and by national funds through FCT/MCTES (PIDDAC). Fernanda F. Roman acknowledges the national funding by FCT through the individual research grant SFRH/BD/143224/2019. Jose L. Diaz De Tuesta acknowledges the financial support through the program of Atracción al Talento of Comunidad de Madrid (Spain) for the individual research grant 2022-T1/AMB-23946.

References

- [1] K. Ragaert et al., *Waste Management*, 69 (2017) 24–58.
- [2] L. Lizárraga-Mendiola et al., *Sustainability*, 14 (2022) 24.
- [3] S.M. Al-Salem et al., *Progress in Energy and Combustion Science*, 36 (2010) 103–129.
- [4] A.A.S. Oliveira et al., *Applied Catalysis B: Environmental*, 144 (2010) 144–151.

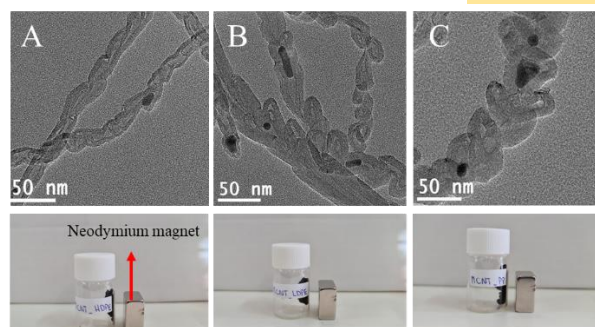


Figure 1. TEM images and interaction with a strong magnet of (A) CNT@LDPE, (B) CNT@HDPE, and (C) CNT@PP

The blank test performed in the absence of polymer revealed that the thermal treatment is not responsible for ascribing magnetic properties to the final CNTs since the sample did not present the response to the presence of an external magnetic field. The results obtained for XRD analysis before and after acid washing of the CNT@LDPE sample are shown in Figure 2.

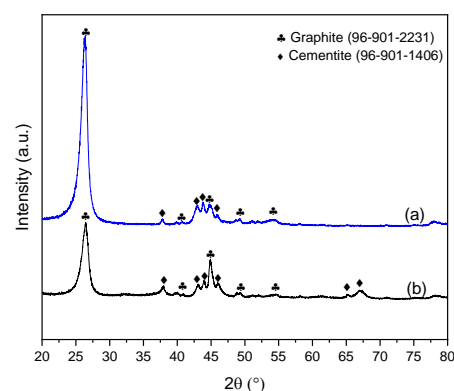


Figure 2. XRD results of LDPE sample (a) after and (b) before acid washing.

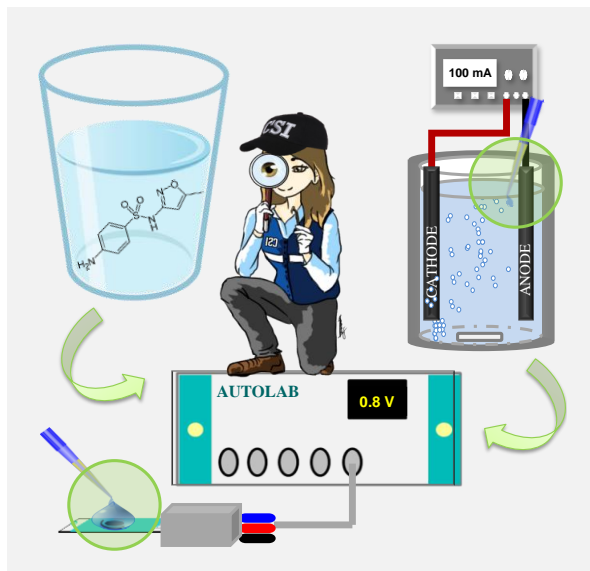
The results were processed using the X'Pert HighScore Plus software to identify the phases present in the nanomaterials using the Crystallography Open Database reference cards. The qualitative analysis showed the presence of graphite phase and of cementite, the last being responsible for the magnetic characteristics. The semi-quantitative analysis resulted in 32% cementite composition before washing and 19% after washing, which was expected due to metal-phase removal with the procedure. The phase change observed here from iron oxides to cementite was already reported in other studies and is related to hydrogen reduction faced by the metal substrate during the CVD process [4].

When electroanalysis meets engineering: Validation of a methodology for the detection and monitoring of drugs' removal from water

S. Caruncho-Pérez^{1,2}, N. Bernárdez², M. Pazos², M. A. Sanromán², E. González-Romero^{1*}

¹Department of Analytical and Food Chemistry, University of Vigo, Campus Lagoas-Marcosende, 36310 Vigo, Spain; ²CINTECX – Universidade de Vigo, Campus Lagoas-Marcosende, Vigo University, 36310 Vigo, Spain.

*sara.caruncho@uvigo.es



Sulfamethoxazole is an antibiotic which is commonly used nowadays. Unfortunately, this type of organic substances is so stable that they can easily get accumulated in the aquatic ecosystem at ultra-trace levels. Due to this, it is important to develop a reliable methodology that allows the detection of this drug in water samples. Voltammetric techniques are not only highly sensitive and selective, but also fast and eco-friendly since the generated amount of waste is minimal. Cyclic voltammetry is used to characterize the electrochemical process, while differential pulse voltammetry is selected for the analysis after optimizing the corresponding instrumental parameters. Moreover, the effect of pH, waters' composition and interactions with trimethoprim are studied to ensure the robustness of the proposed methodology. Validation studies both inter and intra-laboratory are also performed. Once the electroanalytical method is ready, it is applied for the monitoring of sulfamethoxazole's removal from water samples. In this work, this is mainly achieved by anodic oxidation while the voltammetric measurements are performed *in situ*. This way, the effectiveness of the degradation process as well as its kinetics can be determined successfully.

Introduction

Currently, the potential risks derived from the excessive consumption of drugs and their poor waste management has led to their inclusion in the list of emerging pollutants. In spite of the fact that no direct impact on the environment has been observed yet, the concern of the scientific community about their presence in waters around the world has driven the search for methodologies that allow thoroughly controlling this type of compounds. Moreover, most of the drugs have such a high chemical stability that many water treatment plants are not capable of removing them successfully. Some sulfonamides are an example of this due to the presence of aromatic rings in their chemical structure. Among this class of drugs, sulfamethoxazole stands out for having been included by the European Union in the watch list of substances in the field of water policy [1].

Objectives

Due to the mentioned above, sulfamethoxazole is the drug selected as a model to develop a sensitive and selective methodology that allows not only detecting but also quantifying the amount of the sulfonamide in water samples to be able to monitor its elimination afterwards. For this purpose, voltammetric techniques together with the screen-printed electrodes are selected due to the possibility of performing fast measurements with only about 50 μL of solution. After optimizing the electroanalytical method, its application to the monitoring of the sulfamethoxazole's removal based on advanced oxidation processes is described.

Methods

Firstly, the characterization of the electrochemical process that takes place must be performed by cyclic voltammetry. With this technique, the reversibility of the process can be studied as

well as the nature of matter transport. The oxidation reaction of sulfamethoxazole is depicted in Figure 1.

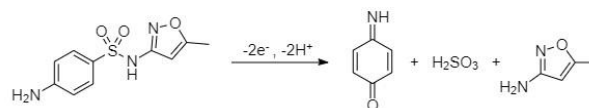


Figure 1. Oxidation reaction of sulfamethoxazole [2].

Once the electrochemical process is properly studied, a more sensitive technique must be selected for the analysis. In this sense, differential pulse voltammetry is chosen [3]. After optimizing the instrumental parameters, waters of different compositions are also studied to evaluate whether there is a significant matrix effect or not. Furthermore, the effects of trimethoprim on sulfamethoxazole must be evaluated as well since both drugs are usually found together in the pharmaceutical formulations due to their synergistic effects.

On the other hand, it must be taken into account that electronic transference in organic molecules also involves a proton exchange, so it is necessary to study how pH affects the morphology of the peak of sulfamethoxazole. Moreover, a quantitative variable which is independent of pH is needed to achieve a robust methodology since at pH values close to the pK_a the oxidation peak is due to the presence of both protonated and deprotonated forms [4]. Thus, the peak area is preferable for the validation instead of the peak current.

As far as the drug's elimination is concerned, different methodologies are studied for this purpose, from a simple adsorption to more complex degradation processes such as anodic oxidation [5]. In all cases, the monitoring of the sulfamethoxazole's removal can be successfully performed *in situ* via electroanalysis, being able not only to ensure the effectiveness of the elimination process but also to determine its kinetics.

Results

By cyclic voltammetry it can be concluded that sulfamethoxazole's oxidation is an irreversible process whose matter transport is governed by the diffusion of the analyte from the bulk solution towards the interface with the working electrode. The cyclic voltammogram is shown in Figure 2 together with a differential pulse voltammogram at pH values of 3 and 6, where the higher sensitivity at pH 3 can be appreciated. After confirming that pH does affect the morphology of the oxidation peak in terms of potential and intensity, a more comprehensive pH study must be performed.

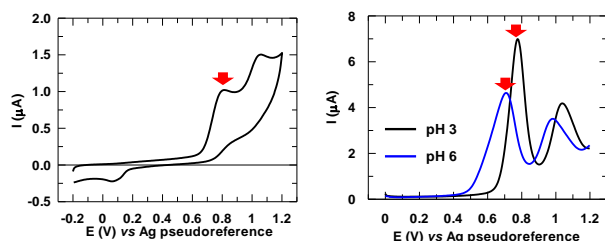


Figure 2. Voltammograms obtained of sulfamethoxazole 150 μM in Na_2SO_4 10 mM by cyclic voltammetry at pH 3 (right picture) and differential pulse voltammetry at pH 3 and 6 (left picture).

Thus, Britton-Robinson buffer is selected to study the influence of pH while keeping a constant ionic strength. This way the pK_a can be experimentally determined by differential pulse voltammetry, and it is found to be 6.73. From this point, the drug is studied at pH values of 3 and 6, the most sensitive and the closest to the pK_a , respectively. In addition, matrix effect is also evaluated with water of different natures, specifically distilled water, tap water and a synthetic hospital wastewater. Furthermore, validation studies with different measuring instruments and operators are carried out. In all cases the RSD does not exceed the 5%, and the limits of detection and quantification achieved from the peak area measurements in distilled water are collected in Table 1.

Table 1. Limits of detection (LOD) and quantification (LOQ) in distilled water by differential pulse voltammetry.

pH	LOD ($\mu\text{mol L}^{-1}$)	LOQ ($\mu\text{mol L}^{-1}$)
3	4.2	13.9
6	7.2	23.8

Trimethoprim's effects on sulfamethoxazole are also studied since in real samples it is expected to find the two drugs together due to their combined prescription. Since the oxidation peak of trimethoprim does not interfere with the main peak of sulfamethoxazole and no enhancement or decrease on its signal is observed, it can be ensured that the former does not constitute an interference when it comes to sulfamethoxazole's analysis, thus confirming the selectivity of the voltammetric techniques.

Acknowledgements

This research has been financially supported by Project PID2020-113667GB-I00 funded by the Spanish Ministry of Sciences and Innovation MCIN/AEI/10.13039/501100011033 and European Union Next Generation EU/ PRTR (PDC2021-121394-I00 and PCI2022-132941).

References

- [1] European Union. Decision (EU) 2020/1161 of 4 August 2020. Official Journal of the European Union, L 257, 6 August 2020, 32-35.
- [2] Vinícius et al., *Analytica Chimica Acta*, 1173 (2021) 338569.
- [3] Melo et al., *Microchemical Journal*, 170 (2021) 106701.
- [4] Mangalgi et al., *Science of the Total Environment*, 835 (2022) 155508.
- [5] Poza-Nogueiras et al., *Journal of Environmental Chemical Engineering*, 10 (2022) 107506.

As far as the sulfamethoxazole's removal is concerned, and bearing in mind that pH is modified with the course of the degradation process, kinetics must be studied under pH values of 3 and 6 to verify there are no significant differences between these conditions. Experimental parameters such as the applied current and the aeration are also evaluated. Thus, the degradation process via adsorption with active carbon combined with anodic oxidation in a continuous flow system, applied current 100 mA and aeration 1 L/min, shows the peak decreases around 92% in the first hour, following pseudo-first order kinetics with an observed kinetic constant of $(0.17 \pm 0.02) \text{ min}^{-1}$ and $(0.14 \pm 0.04) \text{ min}^{-1}$ for pH values of 3 and 6, respectively. The corresponding voltammograms are shown in Figure 3.

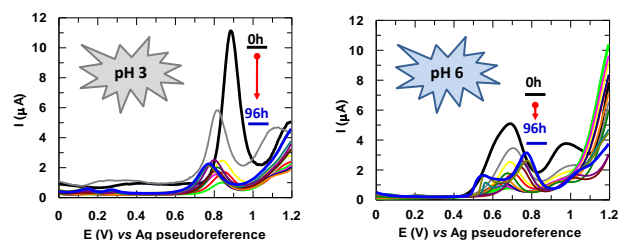


Figure 3. Voltammograms obtained for the anodic oxidation of sulfamethoxazole 200 μM in Na_2SO_4 10 mM during 96 h at pH values of 3 (right picture) and 6 (left picture).

Lastly, the electrochemical methodology needs to be validated with other techniques to corroborate that it is actually valid for the proposed goal. For this purpose, the degradation process was monitored with differential pulse voltammetry and HPLC-UV, and comparing the peak areas it can be concluded that differences between both methods are almost negligible ($\approx 4\%$) but, while the measurements with the former only takes a few minutes, with the latter it is necessary to respect the chromatographic elution time (20 min.), as well as to include a previous sample treatment step to ensure the proper operation of the chromatographic system.

Conclusions

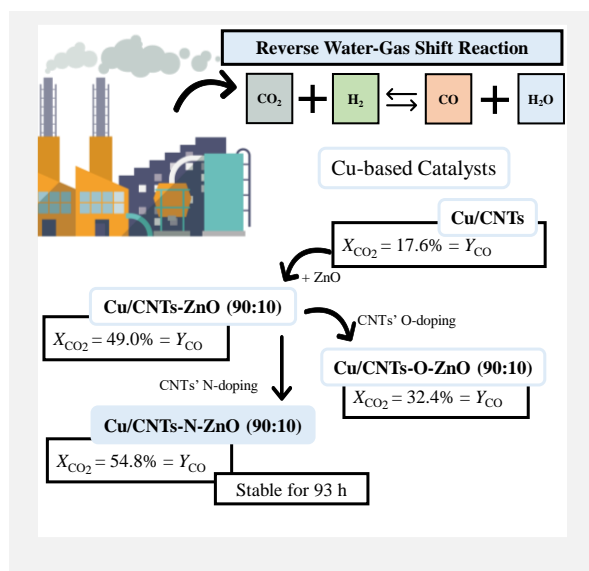
In conclusion, electroanalysis working in tandem with elimination processes does constitute a reliable and effective methodology to promote both the analysis and the removal of stable organic compounds such as sulfamethoxazole. Voltammetric techniques offer high sensitivity, reproducibility and robustness in short time periods while minimizing the amount of waste generated, and it provides a simple way to monitor the degradation process *in situ*. The latter also shows high removal efficiency regardless of the pH of the medium. Overall, it constitutes promising methodology that could be implemented in water treatment plants in a near future, but for this to happen further scaling studies must be performed with continuous flow systems in order to ensure its successful operation.

Stable and Selective Cu-based catalysts supported on CNT-ZnO composites for the Reverse Water-Gas Shift Reaction

A.R. Querido*, L.P.L. Gonçalves, M.R. Pereira, O.S.G.P. Soares

LSRE-LCM – Laboratory of Separation and Reaction Engineering – Laboratory of Catalysis and Materials, Faculty of Engineering, University of Porto, Rua Dr. Roberto Frias, 4200-465 Porto, Portugal; ALiCE – Associate Laboratory in Chemical Engineering, Faculty of Engineering, University of Porto, University of Porto, Rua Dr. Roberto Frias, 4200-465 Porto, Portugal.

*anarnquerido@fe.up.pt

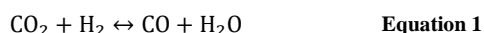


Fossil fuel combustion releases carbon dioxide (CO_2), a greenhouse gas contributing to global warming. It is urgent to develop processes capable of decreasing CO_2 emissions. The Reverse Water-Gas Shift reaction (RWGS) converts CO_2 to CO , which mixed with H_2 forms syngas, the feedstock for chemicals and synthetic fuels production. In this work, Cu-based catalysts supported on pristine CNT and composites of pristine and functionalized CNT:ZnO were developed for the RWGS reaction. The RWGS catalytic experiments were conducted between 100-600 °C and at 1 bar (GHSV= 60 000 $\text{cm}^3 \text{g}^{-1} \text{h}^{-1}$). The catalysts supported on pristine CNT achieved a CO_2 conversion of 17.6%, whereas the catalyst supported on a CNT:ZnO composite obtained a CO_2 conversion of 49.0%. O-doping of the CNT's surface resulted in a decrease of CO_2 conversion to 32.4%; notably, N-doping CNT's surface enhanced CO_2 conversion up to 54.8%, with the catalyst being stable for 93 h. All catalysts developed were 100% selective to CO.

Introduction

Carbon dioxide (CO_2) is one of the main products of fossil fuels combustion, the world's primary energy resource and, as a greenhouse gas, its emissions contribute massively to climate change. Therefore, it is essential to develop processes capable of converting CO_2 into valuable products [1].

The Reverse Water-Gas Shift (RWGS) reaction (Equation 1) has attracted attention from researchers, since it allows the conversion of CO_2 to CO . As CO offers higher reactivity than CO_2 , processes such as methanol synthesis by the CAMERE process or Fischer-Tropsch synthesis, use syngas (mixture of CO and H_2) as their feedstock [2,3].



Most catalysts already developed for this reaction comprise an active phase of metal nanoparticles (NPs) and a metal oxide support. The most used metal NPs for this reaction consist of Cu, which provides great CO_2 conversion and CO selectivity and is also less expensive than most metals. Nevertheless, Cu-based catalysts often deactivate due to sintering or reoxidation as these catalysts are not capable of sustaining the high temperatures needed to achieve a good catalytic performance (RWGS reaction is endothermic, $\Delta H_{25\text{ }^\circ\text{C}} = +41.1 \text{ kJ/mol}$) [3-5].

Metal oxides are used as supporting materials due to their ability to improve the active phase dispersion and CO_2 activation [3]. Carbon materials, such as carbon nanotubes (CNT) have emerged as possible supporting materials as they present great stability at high temperatures and a higher surface area, facilitate the active phase reduction and, it is possible to modify their surfaces by replacing carbon atoms by heteroatoms (e.g. N) or adding functional groups (e.g. O-groups) [6,7].

Objectives

The main objectives of this work consisted in developing Cu-based catalysts supported on CNT materials: pristine, CNT:ZnO composite and functionalized CNT:ZnO composite. The catalysts were tested and characterized thoroughly.

Methods

To synthesize the composites, pristine CNT (90% wt) and ZnO (10% wt) were co-ball-milled at a frequency of 20 vibrations/s for 30 min.

To obtain N-doped CNT (CNT-N), commercial CNT and melamine were co-ball-milled for 4 h at a frequency of 15 vibrations/s. Then, the mixture obtained was annealed at 600 °C for 1 h, under a N_2 flow. To obtain O-doped CNT (CNT-O), commercial CNT were placed in a round bottom flask with a solution of HNO_3 . The mixture was heated until its boiling point and refluxed for 180 min. Afterwards, the mixture was washed with distilled water until it reached neutral pH, and the resultant product was dried overnight at 100 °C.

The catalysts were prepared by incipient wetness impregnation: the support was placed under ultrasonic vibration, and a solution of copper nitrate was added to achieve 15% wt of Cu. The catalysts were impregnated under ultrasonic vibration for 90 min and then dried overnight. The catalysts were calcinated for 1 h at the reduction temperature, under a N_2 flowrate. Afterwards, the catalysts were reduced for 3 h under a H_2 flowrate.

The catalytic experiments were carried out in a Microactivity XS15 reactor (PID Eng & Tech). The gaseous products were analyzed by a GC 1000 gas chromatograph (DANI) equipped with a thermal conductivity detector (TCD) and a GS-CarbonPLOT capillary column. He was used as carrier gas, while N_2 was used as internal standard. In the catalytic experiments, 100 mg of the catalyst was mixed with SiC and placed into a fixed bed quartz reactor. The reactor was fed with

10 cm³ min⁻¹ of CO₂, 40 cm³ min⁻¹ of H₂, and 50 cm³ min⁻¹ of He, at 1 bar ($GHSV = 60\,000\text{ cm}^3\text{ g}^{-1}\text{ h}^{-1}$). The experiments were conducted between 100 °C to 600 °C at 5 °C min⁻¹ to assess the performance of each catalyst at different temperatures and at 1 bar. Lastly, the stability of the best performing catalyst was then evaluated for 93 h.

The catalysts and their supports were characterized by N₂ physisorption at -196 °C, elemental analysis (EA), temperature programmed desorption (TPD), hydrogen temperature programmed reduction (H₂-TPR), powder X-ray diffraction analysis (XRD), X-ray photoelectron spectroscopy (XPS), and transmission electron microscopy (TEM).

Results

The catalytic results, CO₂ conversion (X_{CO_2}) and CO selectivity (S_{CO}), are presented in Table 1. All the developed catalysts achieved their best catalytic performance at the highest temperature tested, 600 °C, because the RWGS is an endothermic reaction.

As the catalyst supported on pristine CNT, Cu/CNT, did not achieve a better catalytic performance than the reference catalysts, a new catalyst combining both CNT and ZnO, Cu/CNT-ZnO (90:10), was prepared. This catalyst topped the catalytic performance of the Cu/CNT and Cu/ZnO catalysts, achieving a $X_{\text{CO}_2} = 49.0\%$, indicating the benefits of combining the properties of CNT and ZnO. Furthermore, catalysts supported on functionalized CNT:ZnO composites were synthesized: Cu/CNT-O-ZnO (90:10) and Cu/CNT-N-ZnO (90:10). An even better catalytic performance was attained with the catalyst supported on CNT-N-ZnO (90:10), obtaining a CO₂ conversion 6% higher, when compared to Cu/CNT-ZnO (90:10) ($X_{\text{CO}_2} = 54.8\%$). The N-groups present in the CNTs' surface might enhance CO₂ adsorption and, therefore, improve the overall performance of the catalyst [8]. The catalyst supported

on CNT-O-ZnO (90:10) achieved a $X_{\text{CO}_2} = 32.4\%$. This lower conversion result could be due to the number of acidic groups present on CNT's surface, as CO₂'s adsorption is facilitated by basic groups [7]. Notably, all catalysts are 100% selective to CO and, Cu/CNT-N-ZnO (90:10), as the best catalyst developed, was submitted to a stability test for 93 h, presenting excellent stability and maintaining its CO selectivity equal to 100%.

Table 1. CO₂ conversion and CO selectivity for the developed catalysts at 600 °C.

Catalyst	X_{CO_2} (%)	S_{CO} (%)
Cu/ZnO	34.9	100
Cu/CNT	17.9	100
Cu/CNT-ZnO (90:10)	49.0	100
Cu/CNT-O-ZnO (90:10)	32.4	100
Cu/CNT-N-ZnO (90:10)	54.8	100

Conclusions

The main objective of this work was to evaluate the catalytic performance of Cu-based catalysts supported on CNT:ZnO composites for the RWGS reaction. Compositing CNT and ZnO proved to be beneficial for the catalytic results, with an increase in CO₂ conversion being observed. N-doping of the surface of the CNT further enhanced the catalytic performance of the catalyst, with a maximum CO₂ conversion of 54.8%. This functionalization treatment likely increases CNT's ability to adsorb CO₂, promoting a better catalytic performance for the catalyst as well. All catalysts provide a complete CO selectivity and the top performing catalyst showed excellent stability for 93 h. For this reason, it is possible to conclude that the catalytic performance of the RWGS reaction may benefit from combining the properties of CNT materials and metal oxide on composites, turning this approach an interesting toolbox for developing highly efficient catalysts for this reaction.

Acknowledgements

This research was financially supported by national funds through the FCT/MCTES (PIDDAC), under the CM4Methane project PTDC/BTA-BTA/2249/2021, the Move2LowC project (n. 46117), cofinanced by Programa Operacional Competitividade e Internacionalização (POCI); Programa Operacional Regional de Lisboa, Portugal 2020 and the European Union, through the European Regional Development Fund (ERDF), and by Project HyGreen&LowEmissions, reference NORTE-01-0145-FEDER-000077, Co-financed by the European Regional Development Fund (FEDER), through the North Portugal Regional Operational Programme (NORTE2020); LA/P/0045/2020 (ALiCE), UIDB/50020/2020 and UIDP/50020/2020 (LSRE-LCM), funded by national funds through FCT/MCTES (PIDDAC). O.S.G.P.S. acknowledges FCT funding under the Scientific Employment Stimulus - Institutional Call CEECINST/00049/2018.

References

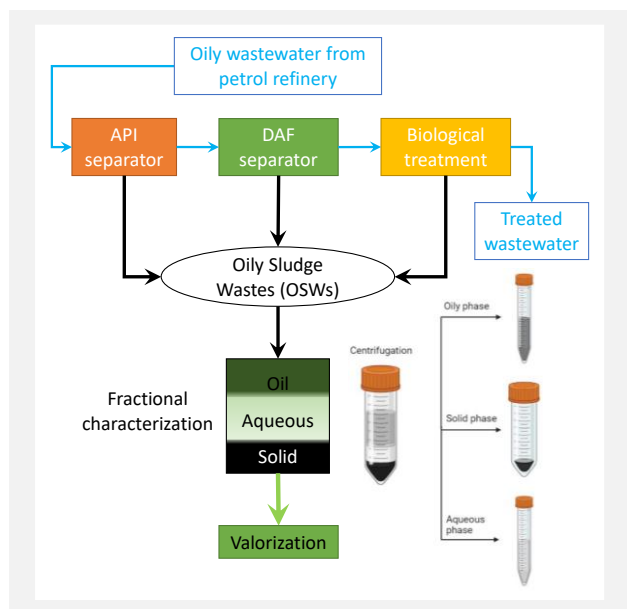
- [1] I.U. Din et al., Journal of CO₂ Utilization, 34 (2019) 20-33.
- [2] A.M. Bahmanpour et al., Applied Catalysis B: Environmental, 295 (2021) 120319-120330.
- [3] X. Chen et al., Frontiers in Chemistry, 8 (2020) 1-21.
- [4] C.Y. Chou et al., Catalysts, 9 (2019) 773-784.
- [5] H.X. Liu et al., Nature Communications, 13 (2022) 1-11.
- [6] P. Serp et al., Nanostructured Carbon Materials for Catalysis, 1st edition, The Royal Society of Chemistry, Cambridge, 2015, 164-170.
- [7] P. Serp et al., Carbon Materials for Catalysis, 1st edition, John Wiley & Sons, Hoboken New Jersey, 2009, 45-56.
- [8] M.S. Shafeeyan et al., Journal of Analytical and Applied Pyrolysis, 89 (2010) 143-151.

Exhaustive characterization of petroleum sludges from different units of treatment and strategies for their valorization

N. Corrochano, A. de Mora, J.L. Diaz de Tuesta*, M.I. Pariente, Y. Segura, R. Molina, F. Martínez

Department of Chemical and Environmental Technology, ESCET, Rey Juan Carlos University, C/Tulipan s/n, 28933, Móstoles, Spain.

*jose Luis.diaz@urjc.es



Oily sludge wastes (OSWs) are generated in refinery treatment plants during the petroleum refining processes. The hazardousness associated with the disposal of these OSWs, makes necessary the development of innovative technologies to handle them adequately to further reach the desirable circular economy and environmental sustainability concepts. This work provides a deep characterization of these waste streams and proposes a way to valorize them through their transformation into more added-high value products, for example carbon-based materials. In this work, three OSWs coming from different units, namely API, DAF and BIO OSW, coming from API Oil-Water separator, and DAF (Dissolved Air Flotation) units, as well as the biological treatment process, respectively, were characterized. The characterization of the OSW samples in terms of TCOD, TS, VTS, TKN, and TPH, coupled with the fractional characterization of aqueous, oily and solid phases, were performed. The OSW coming from the API unit contains the highest content of the solid phase, whereas the OSW from the DAF unit has the highest quantity in the oil phase. Both oily and solid phases could be valorized through thermochemical processes into more biodegradable substrates or carbon-based materials of high-added value.

Introduction

The petroleum industry generates large quantities of oily sludge wastes (OSWs) during different steps of oil treatment, such as mining, transportation, storage, and refine treatments [1]. The OSW generated depends on the crude properties, oil storage system, and processing scheme, but it is assumed that one ton of OSW is generated for every 500 tons of crude oil [2]. The OSW typically is a recalcitrant residue characterized by being a stable water-oil emulsion of water, solids, petroleum hydrocarbons and metals [3]. As being recognized as hazardous waste, improper disposal or insufficient treatment of OSW can seriously threaten the environment and human health [4]. The chemical composition of the OSW varies in a wide range and accordingly, its physical properties, such as density, viscosity, and HHV, can vary significantly [1]. Moreover, the properties obtained from one OSW source cannot be extended to those from the same source collected on a different day or different location [2]. Thus, deep sludge characterization is required as a preliminary step before proposing a treatment and/or valorization approach. Strategies typically found in the literature for the treatment of OSW are the recovery of the valuable oily phase solvent extraction [4] or centrifugation [2] and then take that fraction back to the refining scheme. The remaining fraction is disposed of without further valorization. Novel approaches to introduce more commercially achievable options and/or products to reduce socio-economic and environmental problems must be studied. This work deals with the fractional characterization of the different phases (oily, aqueous, and solid phases) involved in up to three OSWs coming from an API and DAF separators and biological treatment. The characterization of the OSWs (and the different phases) is discussed regarding physical and chemical composition.

Methodology

The OSWs were collected from an API and DAF separators and from a biological treatment (API, DAF and BIO samples, respectively) placed in a petroleum refinery wastewater treatment plant located in Spain. All samples are mainly composed of three different fractions: oily (Oil. P.), aqueous phases (Aq. P.) and solid (Solid P.) phases. These fractions were separated by centrifugation at 30,000 rpm for 15 min, following the method described elsewhere [1]. Total Chemical Oxygen Demand (TCOD), Total Solids (TS), Volatile Total Solids (VTS), and Total Kjeldahl Nitrogen (TKN) were measured following APHA-AWWA Standard Methods 5220.D, 2540.B, 2540.E, and 4500-Norg C, respectively. For Total Petroleum Hydrocarbon (TPH) determination, OSWs were dissolved into cyclohexane and added into a glass column previously packed with silica gel and anhydrous sodium sulphate to remove solid particles. Then, TPHs were eluted with cyclohexane and dichloromethane (1:1 vol:vol), the elution volume was collected, and the solvents were allowed to volatilize in a rotary evaporator [1].

Results

API and DAF OSWs show a dark colour and are similar in aspect and texture to that of crude oil, whereas BIO OSW is similar to water but brown. Table 1 shows all the macroscopic parameters measured for the bulk OSWs. Density, pH, and TPH are similar to those found in the literature (0.9-1.3 Kg L⁻¹, 6-8, and 5-86%, respectively), whereas TS and VTS are values slightly lower than those reported for others OSWs (100-200 g L⁻¹ and 120-850 g L⁻¹, respectively) [1]. As observed, the properties among the collected OSWs are different depending on their origin. OSW coming from the API separator presents the highest values of density, pH, TS, VTS, TCOD and weight

percentage of the solid phase, whereas OSW obtained from DAF show the highest values in TKN, TPH and weight percentage of oily phase. Table 2 summarizes the fractional characterization of aqueous, oily, and solid phases for all the OSWs.

Table 2. Fractional characterization of the different OSWs.

OSW	Aqueous phase				
	TOC (g L ⁻¹)	TCOD (g L ⁻¹)	TN (g L ⁻¹)	pH	κ* (μS/cm)
API	0.36	1.8	397	8.8	4.91
DAF	0.82	3.0	-	7.6	3.94
BIO	0.26	0.7	75.4	7.0	2.30
OSW	Oily phase				
	N (wt.%)	C (wt.%)	H (wt.%)	S (wt.%)	
API	0.9	84.0	12.0	<0.1	
DAF	1.5	83.1	12.1	<0.1	
BIO	-	-	-	-	
OSW	Solid phase				
	N (wt.%)	C (wt.%)	H (wt.%)	S (wt.%)	Ashes (wt.%)
API	0.8	41.6	3.4	5.6	32
DAF	1.5	44.0	3.5	5.4	43
BIO	5.0	50.3	6.4	0.5	15

* Conductivity.

Notably, the main inorganic content was detected in solid phases for all OSWs, whereas carbon content is mainly present in the oily phase of the OSWs. Related to the aqueous phase, it can be observed that the BIO OSW sample presents the lowest contents in TOC, TCOD, TN and in values of pH and conductivity, as expected, since the biological treatment is the last treatment present in the wastewater treatment line. The oily phase shows similar C, N and H contents in both API and DAF OSW samples. However, the solid phase displays more significant differences among the OSW samples, with higher content of carbon for the BIO sample, and ashes for the sample taken from the DAF separator. The management strategy of these OSWs is normally focused on recovering and reclaiming valuable fuel and disposing of unrecoverable residues. Still, disposal is becoming less accepted and more expensive due to stringent environmental regulations. Hu et al., 2020 recently studied a comparative life cycle assessment of traditional treatments (incineration, landfilling, solvent extraction and pyrolysis) for hazardous refinery OSWs, concluding that traditional oily sludge treatment approaches are generally associated with relatively high global warming potential, ecotoxicity, and adverse human health

Table 1. Sludge macroscopic characterization.

OSW	Density (Kg L ⁻¹)	pH	TS (g L ⁻¹)	VTS (g L ⁻¹)	TCOD (g L ⁻¹)	TKN (g L ⁻¹)	TPH (%)	Aq. P. (wt.%)	Oil. P. (wt.%)	Solid P. (wt.%)
API	1.56	7.9	76.0	51.3	16.5	0.54	9.1	56.2	35.6	8.2
DAF	0.93	7.1	38.5	23.6	16.4	2.26	34.9	7.7	88.3	4.1
BIO	0.94	6.8	16.0	13.4	4.0	1.28	-	98.4	-	1.6

Acknowledgements

The financial support of the Ministry of Research and Innovation of Spain through the project [PID2021-122883OB-I00] and of the Regional Government of Madrid through the project REMTAVARES-CM [S2018/EMT-4341] is gratefully acknowledged. Jose L. Diaz De Tuesta acknowledges the financial support through the program of *Atracción al Talento de Comunidad de Madrid* (Spain) for the individual research grant 2022-T1/AMB-23946. Noelia Corrochano and Alberto de Mora also acknowledges the financial support through the INVESTIGO [LG1-006257-128] and [PEJ-2020-AI/AMB-19011] programs.

References

- [1] S. Jerez et al., *Journal of Environmental Management*, 285 (2021) 112124.
- [2] G. Hu et al., *Journal of Hazardous Materials*, 261 (2013) 470-490.
- [3] E.A. Mazlova et al., *Chemistry and Technology of Fuels and Oils*, 35 (1999) 49-53.
- [4] M. Zhao et al., *Journal of Hazardous Materials*, 389 (2020) 121826.
- [5] G. Hu et al., *Journal of Cleaner Production*, 251 (2020) 119594.

effects [5]. Thus, new technologies must be proposed to handle these OSWs, decreasing adverse environmental and societal impacts. The fractional characterization of the OSWs presented above offers insights into innovative and alternative approaches for its valorization. A novel approach can deal with the valorisation of solids and oily fractions through their transformation into a carbon-based material, such as activated carbon, or hydrochars, among others, which can be used as an adsorbent, electrodes or catalyst. After that, wet air oxidation process can be used to accumulate a high concentration of dissolved organic compounds in the aqueous phase and, additionally, break down biologically refractory compounds into simpler ones, increasing the biodegradability of the sludge [1].

Conclusions

This work reports the use of different and complementary analytical techniques for the fractional characterization of OSWs coming from different units, such as API and DAF separators, as well as a biological treatment (BIO OSW). API, DAF and BIO OSW samples before fractional separation show values of density, pH, TS, VTS and TCOD in the range of 0.93-1.56 Kg L⁻¹, 6.8-7.9, 16.0-76.0 g L⁻¹, 13.4-51.3 g L⁻¹ and 4.0-16.5 g L⁻¹, respectively, finding the highest values for API OSW. OSW coming from API show the highest quantity of solid phase (8.2 wt.%), whereas DAF OSW present the largest content in oily fraction (88.3 wt.%) and then the highest value of TPH (34.9%). Hydrocarbons form the oily phase, and it has a carbon content of 84.0 and 83.1 wt.% for the oily phases found in API and DAF, respectively. The solid phase is a complex mixture of inorganic matter (15-43 wt.% of ashes) and amorphous carbonaceous species (41.6-50.3 wt.% of carbon content). The aqueous phase is lowly concentrated in organic matter and nutrients and has some dissolved metals (results are not shown). According to the characterization results, several potential strategies can be proposed for the integral valorization of oily sludge to produce valuable by-products through thermochemical processes based on wet air oxidation process or hydrothermal carbonization to produce more biodegradable substrates that enhance the biochemical methane potential of OSW in anaerobic digestion systems or solid hydrochar materials with remarkable power heat as fuel or high-added carbon materials as electrodes for advanced electroFenton processes or conductive materials for enhancement of the performance of constructed wetlands.

Development of a method and analysis of levels of volatile methylsiloxanes in microplastics and sand from Azores beaches

T. Ferreira^{1,2*}, V. Homem^{1,2}, Y. Rodríguez³, L. Herrera³, C.K. Pham³, N. Ratola^{1,2}

¹LEPABE – Laboratory for Process Engineering, Biotechnology and Energy, Faculty of Engineering, University of Porto, Rua Dr. Roberto Frias, 4200-465 Porto, Portugal; ²ALiCE – Associate Laboratory in Chemical Engineering, Faculty of Engineering, University of Porto, Rua Dr. Roberto Frias, 4200-465 Porto, Portugal; ³Instituto de Investigação em Ciências do Mar – OKEANOS, Universidade dos Açores, 9900-138 Horta, Portugal.

*tferreira@fe.up.pt



A large portion of microplastics (MPs) found in the environment eventually end up in coastal areas. These plastic fragments can act as carriers of organic pollutants, with volatile methylsiloxanes (VMSs) potentially being one of them, considering their mass-production and distinct physicochemical properties. This work presents a novel approach for the extraction, analysis and quantification of cyclic (D3-D6) and linear (L3-L5) VMSs in complex samples of MPs, with a method tested on four of the most common types of plastic: polypropylene, polystyrene, and high- and low-density polyethylene. The method – two sequential ultrasound-assisted extractions with acetone and analysis by GC-MS – was validated and applied to MP samples collected from Azores beaches. The samples demonstrated the detection of VMSs, and the respective concentrations will be used to estimate the magnitude of the human exposure to these chemicals that occurs on beaches during summertime. Sand samples were also collected in some of the same beaches, and the results of VMSs are compared to try to understand the sources of their presence in the MPs.

Introduction

An increase in plastic consumption over recent years has inevitably intensified the disposal of plastic waste and, consequently, the prevalence of microplastics (MPs) in remote coastal areas. Various additives (*e.g.*, plasticizers, fillers and reinforcements) are typically added to plastic polymers to enhance specific properties [1], and although the composition of a MP generally bears a close resemblance to the plastic it originates from, their strong hydrophobicity and large surface area are responsible for the adsorption of organic pollutants present in the environment [2], as shown by the presence of chemicals unknown to be plastic additives – polycyclic aromatic hydrocarbons (PAHs), polychlorinated biphenyls (PCBs) and dichlorodiphenyltrichloroethane (DDT) – in beach MPs [3]. As of late, volatile methylsiloxanes (VMSs) have received the status of emerging pollutants [4] due to the substantial use of siloxanes in several consumer and industrial products coupled with their distinctive physicochemical properties (*e.g.*, high hydrophobicity, durability and, volatility) which leads to their persistence in the environment [5]. Thus, when considering the adsorption capacity of MPs, there are reasons to believe that VMSs may be also present on the surface of MPs.

Objectives

Given that the targeting of VMSs in MPs is a pioneering approach, the present work aimed, first and foremost, to implement a reliable and robust scientific method for the extraction, analysis and quantification of VMSs in environmental samples of MPs. Upon its validation, the method is applied to beach MP samples from the Azores, and the results used in a risk assessment study dedicated to VMS exposure in these locations and compared with levels of VMS in the sand to understand possible sources.

Methods

The process of developing and optimizing the analytical method for VMSs in MPs consisted of a series of tests (recovery assays) with the following commercial MPs: polypropylene (PP), polystyrene (PS), high-density polyethylene (HDPE) and low-density polyethylene (LDPE) – as they are some of the most commonly used plastics [6] and thus will likely comprise the large majority of MPs found in the environment. The extraction protocol which served as a starting point for this process was previously developed by the LEPABE research group for VMSs in recycled rubber granulate [7] – consisting of an ultrasound-assisted extraction (UAE) with 1:1 (v/v) of hexane:dichloromethane (Hex:DCM) as a solvent, followed by a QuEChERS clean-up step. First, it had to be assured that the solvent used in the extractions was compatible with all four types of plastic. As such, the following solvents were tested with each plastic individually: 1:1 (v/v) Hex:DCM, Hex, acetone (Ace) and ethyl acetate (EtAc). After selecting the extraction solvent, the remaining assays were carried out with a mix of the four plastics in equal parts (*i.e.*, 25% (w/w) of each). The next steps in the method optimization consisted of modifying some details in the protocol (*e.g.*, sample mass, solvent volume, number of extractions, vortex/ultrasound duration, necessity of having a QuEChERS clean-up) in order to maximize the obtained recoveries. The final method was validated according to the following parameters: linearity, limits of detection and quantification (instrumental and method), accuracy and precision. The methodology used for the analysis of sand (based on QuEChERS) was previously validated by LEPABE [8].

Results

Method validation

The optimized protocol for VMS extraction and analysis in environmental samples of MPs is presented in Figure 1.

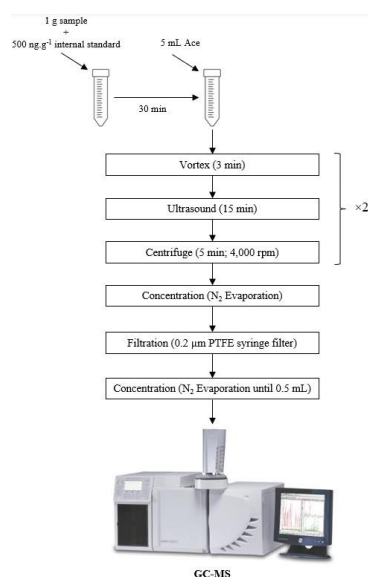


Figure 1. Schematic representation of the method used for the analysis of volatile methyl siloxanes in microplastics.

The method detection limits (MDL) ranged from 0.0003 to 0.23 $\text{ng}\cdot\text{g}^{-1}$ and the method quantification limits (MQL) from 0.0007 to 0.77 $\text{ng}\cdot\text{g}^{-1}$ (values referring to D5 and L5, respectively). The accuracy and precision were evaluated by recovery assays performed with two VMS spike levels: 100 and

500 $\text{ng}\cdot\text{g}^{-1}$. The mean accuracy/recovery of the method (accounting for the seven target VMSs) was 84% at 100 $\text{ng}\cdot\text{g}^{-1}$ and 94% at 500 $\text{ng}\cdot\text{g}^{-1}$. In terms of precision, on the other hand, the repeatability RSD was 9% at 100 $\text{ng}\cdot\text{g}^{-1}$ and 6% at 500 $\text{ng}\cdot\text{g}^{-1}$; the one for intermediate precision was 6% at 100 $\text{ng}\cdot\text{g}^{-1}$ and 2% at 500 $\text{ng}\cdot\text{g}^{-1}$.

Levels of VMSs in microplastics and sand

For the quantification of the beach MP samples (67 from 5 islands in total), these were first pre-treated with liquid nitrogen to facilitate its mechanical grinding (this way, it is possible to obtain a representative sample from every beach and minimize heterogeneity between replicates). The total VMS concentrations reached 122 $\text{ng}\cdot\text{g}^{-1}$, with a clear predominance of the cyclic compounds and no apparent geographical trend. In 16 samples it was possible to compare the VMS levels with those in the sand (4 to 15 $\text{ng}\cdot\text{g}^{-1}$), but there was no statistically significant correlation, which means the sources of VMS in both matrices are likely different. MPs may have some impact from the manufacturing processes and sand is more dependent on the atmospheric deposition or the presence of sunbathers using sunscreens and related personal care products.

Conclusions

The present work provides a novel scientific method applicable to environmental samples of microplastics for the extraction, analysis and quantification of VMSs in MPs. MPs may function as vectors of VMS contamination in the environment but results in sand tend to indicate different sources. Future work will focus on assessing the risk associated with human exposure to these contaminants, comparing to reference values provided by the European Chemicals Agency.

Acknowledgements

This work was financially supported by: (i) Projects LA/P/0045/2020 (ALiCE) and UIDB/00511/2020 and UIDP/00511/2020 (LEPABE), funded by national funds through FCT/MCTES (PIDDAC); (ii) Project “HealthyWaters – Identification, Elimination, Social Awareness and Education of Water Chemical and Biological Micropollutants with Health and Environmental Implications” (NORTE-01-0145-FEDER-000069), co-financed by Programa Operacional Regional do Norte (NORTE 2020), through Portugal 2020 and FEDER; (iii) VH thanks national funds through FCT, under the Scientific Employment Stimulus-Individual Call - CEECIND/00676/2017. YR, LH, and CKP also acknowledge funds and support from the FCT through the strategic project (UIDB/05634/2020 and UIDP/05634/2020) granted to OKEANOS and through the FCT Regional Government of the Azores under the project M1.1.A/REEQ.CIENTÍFICO UI&D/2021/010. YR is supported by a PhD Fellowship (reference: M3.1.a/F/022/2020) funded by the Regional Fund of Science and Technology, from the Regional Government of the Azores. CKP was co-financed by the Operational Program AZORES 2020, through the Fund 01-0145-FEDER-000140 “MarAZ Researchers: Consolidate a body of researchers in Marine Sciences in the Azores” of the European Union. The authors wish to thank the volunteers that helped in the collection of the samples.

References

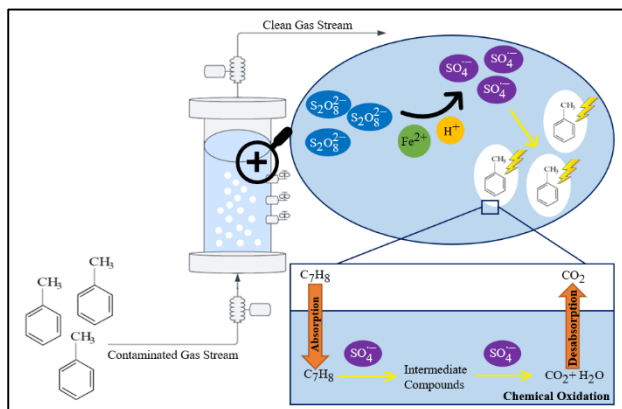
- [1] J.N. Hahladakis, et al., *Journal of Hazardous Materials*, 344 (2018) 179-199.
- [2] L. Fu et al., *Ecotoxicology and Environmental Safety*, 217 (2021) 112207.
- [3] J.P.G.L. Frias et al., *Marine Pollution Bulletin*, 60 (2010) 1988-1992.
- [4] K. Kumari et al., *Environmental Science and Pollution Research*, in press.
- [5] K. Gaj, Properties, Potential Toxicity, and Transformations of VMSs in the Environment. In: V. Homem & N. Ratola (Eds.), *Volatile Methylsiloxanes in the Environment* (pp. 1-31). Springer International Publishing.
- [6] Organisation for Economic Co-operation and Development (OECD) (2022). *Global Plastics Outlook: Economic Drivers, Environmental Impacts and Policy Options*, OECD Publishing, Paris. 201 p.
- [7] N. Ratola, T. Ferreira, A. Alves, V. Homem, In: *Book of Abstracts of SETAC Europe 2023*, 688-689 (ISSN 2309-8031).
- [8] D. Capela et al., *Marine Pollution Bulletin*, 140 (2019) 9-16.

Treatment of a toluene-containing gas stream by application of an activated persulfate-based Advanced Oxidation Process

A.S.P. Alves, C.S.D. Rodrigues, L.M. Madeira*

LEPABE – Laboratory for Process Engineering, Environment, Biotechnology and Energy, Chemical Engineering Department, Faculty of Engineering – University of Porto, R. Dr. Roberto Frias, 4200-465 Porto, Portugal; ALiCE – Associate Laboratory in Chemical Engineering, Chemical Engineering Department, Faculty of Engineering – University of Porto, R. Dr. Roberto Frias, 4200-465 Porto, Portugal.

*mmadeira@fe.up.pt



This work focused on the degradation of a gaseous toluene stream by the application of a persulfate-based advanced oxidation process, using for that a bubble column reactor. A parametric study was performed, being analyzed the influence of some operating variables in the process performance, namely: the catalyst (0-0.27 gFe²⁺/L) and oxidizing agent (0.80-2.40 gS₂O₈²⁻/L) dosage and the initial pH (2.0-6.8). The best treatment performance was achieved for the assay performed with [Fe²⁺]=0.20 g/L, [S₂O₈²⁻]=1.70 g/L and initial pH=3.0, being the treatment process extended for 6 h. Under these conditions, the toluene transferred from the gaseous stream to the liquid phase, wherein it was then degraded by the sulfate radicals, assumed a value of 0.073 mol/L, which represents an improvement of 12 times when compared with the toluene solubility in water.

Introduction

Volatile Organic Compounds (VOCs), among which is toluene, are the most common pollutants found in gaseous effluents derived from chemical and petrochemical industries. In general, VOCs are volatile and photo-chemically reactive species, which exhibit physical and chemical properties that allow them a great capacity for dispersion. Due to their toxic properties, VOCs are responsible for numerous environmental and health problems. Currently, several methods are available for treating gaseous effluents that are contaminated with this type of chemical compounds; however, all present some disadvantages, making them not the most appropriate technology to use: either because only transfer the pollutants from one phase to another (as in absorption or adsorption) [1,2], or because VOCs are very toxic substances capable of inhibiting the microorganisms' action (for biological degradation) [3]; or even because of the demanding operating conditions required by the process (e.g. thermal destruction/catalytic incineration) [4].

So, the scientific community has been addressing this issue by employing advanced oxidation processes (AOPs), which have shown to be promising in terms of treating priority pollutants, as they allow the real elimination of toxic and non-biodegradable compounds in an efficient, fast and not expensive way, making use of environmentally friendly reagents and mild conditions of temperature and pressure. This type of processes focuses on the *in situ* generation of active species – free radicals - which, due to their high oxidation power, react with the organic pollutants, degrading them. In this work, an activated persulfate-based AOP is implemented, being the degradation of the target pollutant carried out by the sulfate radicals, SO₄^{•-}.

Persulfate (PS) has been playing an important role as an oxidizing agent in wastewater remediation processes; however, as it is a very stable compound, its ion reacts very slowly with the organic pollutants, being its activation before the degradation reactions essential. This activation will lead to the formation of free sulfate radicals, which are stronger from the oxidative point of view (2.01 eV for PS vs. 2.60 eV for sulfate

radicals), making the degradative process more efficient. This activation can be performed by the application of several methods (heat, radiation, ultrasounds, presence of transition metal ions/catalyst and pH change), having been selected for this work the last two.

In this work is aimed to treat a contaminated gas stream through a liquid phase oxidation, being for that necessary to use a bubble column reactor (BCR). The contaminated gas stream is continuously dispersed within the liquid phase present inside the BCR, which will provide the contact needed between the target pollutant present in the gas stream and the oxidizing agent present in the liquid phase. In fact, this contact is the key for the success of this technology, since it is through the bubbling that the gaseous pollutant is transferred to the liquid phase, by absorption, and then, once dissolved in the liquid effluent, degraded/oxidized [5]. This oxidation will lower the concentration of the target VOC within the liquid phase, increasing the driving force for the transfer of more pollutant from the gas stream [5] (please refer to the graphical abstract presented above).

In the literature it was possible to find some studies that applied Fenton [5,6], photo-Fenton [7] or catalytic ozonation [8] to decontaminate toluene-containing gaseous streams, however, up to the authors' knowledge, this is the first time that an activated persulfate-based AOP has been applied.

Methods

In this work, a toluene gas stream was treated by application of an activated persulfate-based AOP, using for that a BCR. A detailed parametric study was performed - the effect of the iron dose was evaluated in the range of 0 to 0.27 g/L and the effect of the initial persulfate concentration was assessed between 0.80 and 2.40 g/L; the initial pH was varied between 2.0 and 6.8 (pH of the distilled water used) -, and the operating conditions that allow maximizing the toluene removal and the organics mineralization were found.

Both the experimental facility and methodology used have been described in detail elsewhere [5,6]. In order to proceed with the study, several samples were collected throughout the reaction time. In the case of the gas effluent, the samples were taken from the inlet and outlet streams of the BCR to quantify toluene; in the case of the liquid phase, the samples were taken to analyze the dissolved organic carbon (DOC), concentration of persulfate remaining in the solution, and pH.

Results and Discussion

Along the parametric study two different types of experiments were realized, the absorption runs (without the addition of PS and iron) and the (normal) experimental runs. The realization of the first type of experiments had as the main objective to understand what happened to the toluene if no treatment was conducted, being used as a reference or control. The amount of toluene transferred obtained here was 0.006 mol/L, which is very similar to the reported solubility of toluene in water (0.516 g/L at 25 °C [9]), being the difference between them of 5%. Additionally, the experimental Henry's constant was also determined (6.257 atm/(mol/L)) and compared with the value presented in the literature (6.397 atm/(mol/L) [10]), being the difference between them of about 2%.

After being analyzed the influence that some parameters have on the degradation of toluene, it was possible to conclude that the performance of the treatment system was affected both by the iron and persulfate doses and the initial pH, being reached as the best operating conditions, i.e., the ones that lead to a higher amount of toluene transferred, an iron concentration of 0.20 g/L, an initial persulfate concentration of 1.70 g/L and an initial pH value of 3.0. Under such conditions, it was obtained a value of 0.073 mol/L of toluene transferred, which represents an improvement of 12 times when compared to the value obtained during the absorption run.

Although there are already published in the literature some studies where other AOPs were applied with the aim of carrying out the treatment of a toluene gas stream, most of them do not report the amount of toluene transferred, except for some works that focused on Fenton's reaction application [5,6] – see Figure 1. Thus, although the AOP applied here and Fenton's reaction work in a similar way, they have as main difference the type of radical specie used: while the activated PS-based AOP counts on with the presence of sulfate radicals, Fenton's reaction is based on hydroxyl radicals. So, comparing the value obtained in this work with the (best) one obtained when Fenton's process is

applied [5], one can conclude that the overall amount of toluene transferred almost dropped by half, going from 0.073 to 0.041 mol/L. This puts into evidence the advantage of using sulfate radicals to conduct degradation treatments, particularly of toluene-containing gas streams. Although both species have a similar redox potential (2.60 eV for $\text{SO}_4^{\cdot-}$ and 2.80 eV for HO^{\cdot}) [11], sulfate radicals have been shown to be more stable and have much longer half-life time ($3\text{-}4 \times 10^{-5}$ s for $\text{SO}_4^{\cdot-}$ and 2×10^{-8} s for HO^{\cdot}) [11], which contributes to a more efficient treatment.

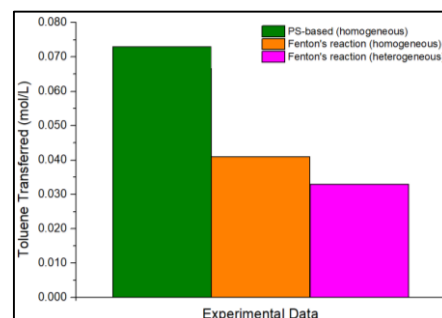


Figure 1. Amount of toluene transferred for different treatment processes: persulfate-based AOP (homogeneous) and Fenton's reaction (homogeneous and heterogeneous). The dose of catalyst used on the heterogeneous test was 2.30 g/L [6].

Conclusions

This work focused on the decontamination of a gaseous effluent rich in toluene, through the application of an activated persulfate-based AOP, where a bubble column reactor was used. A detailed parametric study was performed, and the influence that some operating conditions have on the degradative process was analyzed. Under the best operating conditions found ($[\text{Fe}^{2+}] = 0.20$ g/L, $[\text{S}_2\text{O}_8^{2-}] = 1.70$ g/L and an initial pH of 3.0) an amount of toluene transferred of 0.073 mol/L was obtained, which represents, first, an improvement of 12 times when compared to the solubility of toluene in water; and secondly, such value is, at least, the double of that achieved by other authors, who applied the Fenton's reaction.

Acknowledgements

This work was financially supported by: UIDB/00511/2020 and UIDP/00511/2020 (LEPABE) and LA/P/0045/2020 (ALiCE) funded by national funds through FCT/MCTES (PIDDAC). Ana S. P. Alves is grateful to the Portuguese Foundation for Science and Technology (FCT) for her PhD grant (2021.08505.BD), financed by national funds of the Ministry of Science, Technology and Higher Education, and the European Social Fund (ESF) through the Human Capital Operating Program (POCH). Carmen S. D. Rodrigues thanks the FCT for the financial support of her work contract through the Scientific Employment Support Program (Norma Transitória DL 57/2017).

References

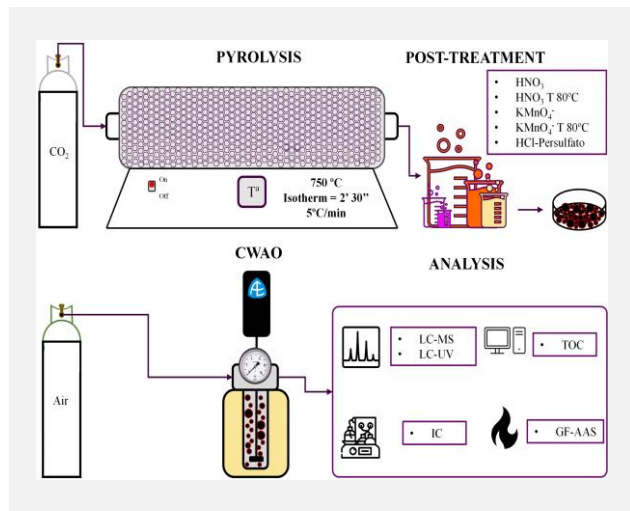
- [1] H.J. Kim et al., *Chemical Engineering Journal*, 230 (2013) 244-250.
- [2] B. Ambrozek et al., *Energy Conversion and Management*, 85 (2014) 646-654.
- [3] J.M.M. de Mello et al., *Journal of Petroleum Science and Engineering*, 70 (2010) 131-139.
- [4] M.A. Campesi et al., *Journal of Environmental Management*, 154 (2015) 216-224.
- [5] V.N. Lima et al., *Journal of Environmental Chemical Engineering*, 8 (2020) 103796-103809.
- [6] C.S.D. Rodrigues et al., *Journal of Environmental Management*, 322 (2022) 116084-116093.
- [7] W. Guo et al., *Chemosphere*, 275 (2021) 129998-130007.
- [8] A. Cabrol et al., *Chemical Engineering Research and Design*, 168 (2021) 453-464.
- [9] D.-H. Lee et al., *Environment International*, 27 (2002) 681-688.
- [10] D.W. Green et al., *Perry's Chemical Engineers' Handbook*, 8th edition, The McGraw-Hill Companies, 2008.
- [11] J. Li et al., *Journal of the Taiwan Institute of Chemical Engineers*, 80 (2017) 686-694.

Conversion of sewage sludge into catalyst for cytostatic removal

*D. Huber-Benito**, *M. Martin-Martinez*, *M. Larriba*, *V.I. Águeda*, *J. García*

Catalysis and Separation Processes Group (CyPS), Chemical Engineering and Materials Department, Faculty of Chemistry, Complutense University of Madrid, Avda. Complutense s/n, 28040 Madrid, Spain.

**dihuber@ucm.es*



In the present work, sewage sludge-derived catalysts are synthesised by pyrolysis in CO₂ atmosphere followed by a post-treatment with different agents. The activity of these materials is evaluated in prednisone removal through CWAO, testing different conditions to assess their behaviour. The most relevant parameters studied have been the removal of prednisone, the intermediates and the organic acids remaining in the treated water. After analysing the results obtained by different analytical techniques, the best catalyst found is the one treated with HNO₃ at ambient temperature. This develops the porosity without introducing a considerable quantity of functional groups that disfavoured the process.

Introduction

Sewage sludge is a byproduct of water treatment which receives significant attention. Over 9.8 million tons are produced annually in the European wastewater treatment plants (WWTP) [1], and generation is predicted to increase by up to 2% by volume annually. Due to environmental concerns, sewage sludge disposals, such as incineration, fertiliser or compost, are limited in many countries, and new techniques are needed for this residue [2]. Thanks to the high portions of carbon, iron, silicon and other metals, sewage sludge can be used as an efficient heterogeneous carbonaceous catalyst.

On the other hand, active pharmaceutical compounds are one of the most critical emerging pollutants nowadays. The growing use of anticancer treatments has led to the presence of cytostatic drugs in the environment, which entails high risk due to their mutagenic and teratogenic properties. These compounds have been detected in wastewaters at low concentrations ranging from mg·L⁻¹ in hospital wastewaters to ng·L⁻¹ in urban wastewaters [3]. Due to WWTP cannot remove these compounds, an advanced process must be considered, such as adsorption, catalysis, electro-oxidation, etc. Prednisone is highly used because of its anti-inflammatory effect [4]. In addition, it is considered an anticancer drug with a higher PEC than other anticancer drugs in Spain [5]. This molecule is taken as a model in exchange for determining the behaviour of each catalyst synthesised.

Among the heterogeneous catalysis technologies, catalytic wet air oxidation (CWAO) is proposed, which consists of treating the wastewater at high-pressure air and high temperature using the appropriate catalysts. Recently, a series of noble metal catalysts have been used in CWAO, exhibiting high activities, but they are quite expensive. The use of sewage sludge as a catalyst has been reported in the CWAO of phenolic compounds, in the catalytic ozonation of oxalic acid and as supports for heterogeneous Fenton-like catalysts [6]. The synthesis of catalysts using sewage sludge is a low-cost way of using this residue. Furthermore, the control of physical-chemical surface

properties through different treatments and operation conditions can be achieved.

Methods

For the catalyst synthesis dried sludge was pyrolyzed in a horizontal quartz reactor for 2h 30 mins at 750 °C in CO₂ atmosphere and a heating rate of 5 °C/min. CWAO experiments were performed using prednisone solutions with an initial concentration of 20 ppm, in a Hastelloy autoclave reactor equipped with a heating jacket and a mechanically controlled paddle stirrer. Liquid samples were collected periodically for 2 h and immediately filtered through 0.45 μm PTFE filters for further analysis.

Results

The physical-chemical surface of the catalysts is characterised through BET and FTIR analysis. Table 1 and Figure 1 show the results of these techniques. The BET results reveal an enhancement of the S_{bet} after the acid treatment. The FTIR spectrum exhibits a prominent peak at 1050 cm⁻¹, band related to the silicon content of the materials. The band of 1500 cm⁻¹ can be attributed to carbonyl (C=O) groups. Finally, the broad band at 3500 cm⁻¹ is the characteristic of -OH and -NH surface functional groups.

Table 1. Porous structure of the SBCs.

Carbon	S _{bet} (m ² /g)	V _t (cm ³ /g)	V _{micro} (cm ³ /g)	V _{meso} (cm ³ /g)	V _{micro} /V _t (cm ³ /g)
CO ₂ 750	131	0.144	0.030	0.114	0.207
CO ₂ HNO ₃	372	0.432	0.088	0.345	0.203
CO ₂ HNO ₃ T	387	0.455	0.089	0.367	0.194
CCO ₂ KMNO ₄	133	0.124	0.032	0.092	0.258
CCO ₂ KMNO ₄ T	147	0.126	0.034	0.092	0.267
CCO ₂ HClPer	300	0.401	0.062	0.339	0.154

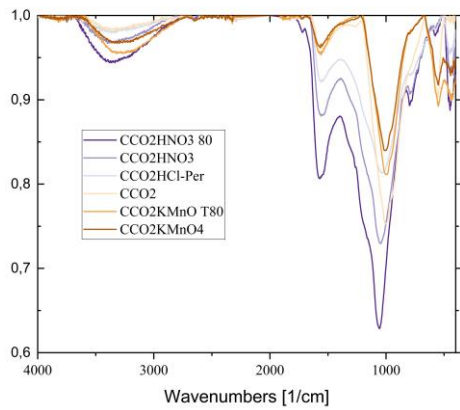


Figure 1. FTIR spectra of SBCs with different treatments.

The application of these materials in CWAO at 100 °C and 15 bar is shown in Figure 2, where an enhancement of prednisone degradation after acid treatment is exhibited, effect derived from the development of the specific surface. Different operation conditions of CWAO are tested to favour either the adsorption or the catalytic process. Figure 3 summarises the results for CO_2HNO_3 , $\text{CO}_2\text{HNO}_3\text{T}$ and $\text{CO}_2\text{HCl-Per}$ in adsorption experiments or the different catalytic conditions specified in the figure. CCO_2HNO_3 achieves the highest TOC reduction; this material gives an IC value of 7.7 mg/L. Analysing all the results, hydroxyl groups disfavour prednisone adsorption, while carbonyl groups support the catalytic process. Once this material is selected, further analysis will be done to evaluate the intermediates and the organic acids that remain after the treatment.

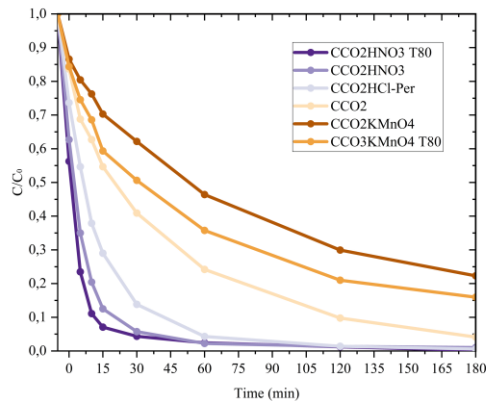


Figure 2. CWAO experiments at 100 °C, P=15 bar, $D_{\text{cat}}=0$, g/L and $[\text{Pred}]_0=20$ ppm.

Acknowledgements

This work has been supported by the MICINN through the CATAD3.0 project PID2020-116478RB-I00. In addition, the authors acknowledge funding from the Comunidad de Madrid (Spain), through the REMTAVARES Network (S2018/EMT-4341).

References

- [1] M.M. Mian et al., *Science of the Total Environment*, 666 (2019) 525-539.
- [2] T.J. Bandoz et al., *Applied Catalysis B Environmental*, 67 (2006) 77-85.
- [3] P. Hamon et al., *Journal of Water Process Engineering*, 21 (2018) 9-26.
- [4] K. Yin et al., *Chemosphere*, 212 (2018) 56-66.
- [5] H. Franquet-Griell et al., *Environmental Pollution*, 229 (2017) 505-515.
- [6] Y. Tua et al., *Journal of Hazardous Materials*, 276 (2014) 88-96.

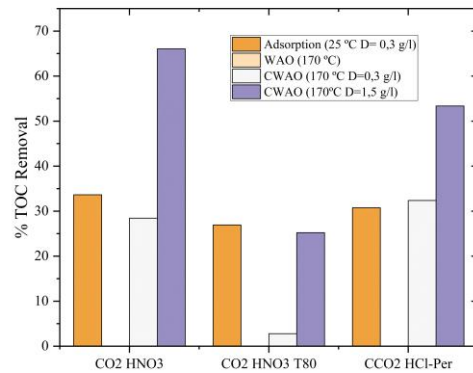


Figure 3. TOC reduction after 3 h of CWAO process at different conditions.

Conclusions

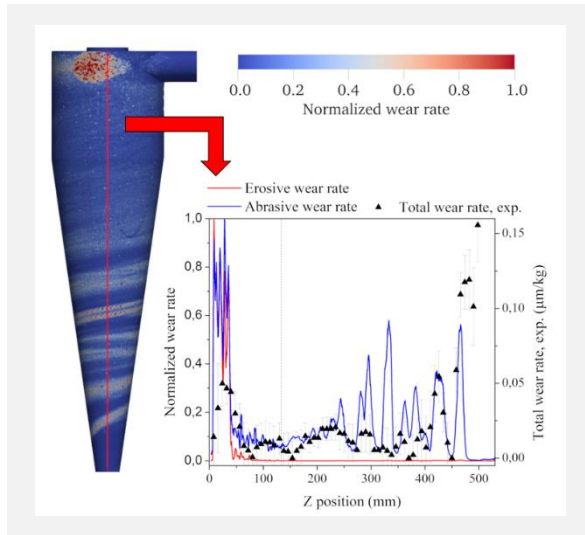
Sewage sludge is a residue that can be valorised with pyrolysis in CO_2 atmosphere followed by an acid treatment. Thanks to controlling the operating conditions of the synthesis, the surface functional groups of the obtained carbonaceous material can be modified. The best material for the CWAO process is CCO_2HNO_3 due to the development of the porosity and the increase of carbonyl surface groups. Hydroxyl functional groups hinder the adsorption process, disfavoring the catalytic process as well. 3 hours at a temperature of 170 °C using a catalyst dosage of 1.5 g/L are enough for the complete removal of prednisone, and a 66% of TOC reduction, obtaining an IC value of 7.7 mg/L. Longer times increase the IC value, achieving 14 mg/L after 6 hours.

Numerical modelling and experimental measurement of wear in a cyclone separator

P. Pacheco^{1,2*}, M.A. Alves^{1,2}, J.B.L.M. Campos^{1,2}, J. Paiva^{1,2,3}

¹Centro de Estudos de Fenómenos de Transporte (CEFT), Departamento de Engenharia Química, Faculdade de Engenharia da Universidade do Porto, Rua Dr. Roberto Frias, 4200-465 Porto, Portugal; ²Associate Laboratory in Chemical Engineering (ALiCE), Departamento de Engenharia Química, Faculdade de Engenharia, Universidade do Porto, Rua Dr. Roberto Frias, 4200-465 Porto, Portugal; ³Advanced Cyclone Systems, SA, Rua de Vilar, 235, 3^oE, 4050-626 Porto, Portugal.

*up201304015@edu.fe.up.pt



Gas-solid cyclones are often subject to rapid wear. This may lead to reduced efficiency and cause equipment shutdown or even failure. There is significant interest in modelling cyclone wear to decrease uncertainty and decreased maintenance frequency and costs. Numerical modelling efforts so far have centered on erosion as the main mode of wear in cyclones. In this work, we propose that three-body abrasion by particle sliding and rolling is determinant for observed wear magnitude and distribution throughout the cyclone interior. To test this hypothesis, we have developed a multiphase numerical model of a gas-solid cyclone, with sub-models for erosive and abrasive modes of wear. Model predictions are compared against experimental data obtained in a laboratory scale installation. While the erosive model only predicts wear at the inlet target zone, the abrasive model also predicts wear tracks left by particle strands, agreeing with experimental mapping of wear rates and supporting the formulated hypothesis.

Introduction

Cyclone separators are cost-effective solutions for gas-solid separation due to simple fabrication and lack of moving parts, allowing for continuous operation even at high temperatures, and having reduced maintenance needs compared to alternatives such as filter separation. However, the inner walls of cyclones are susceptible to rapid wear in some operating environments [1], which is a concern as it may cause reduced efficiency and is the main cause of unexpected downtime due to equipment failure. Engineers intervene at the design stage to mitigate wear, through material selection, surface finishing and coating application to increase equipment service life, and at the operation stage by implementing maintenance practices for monitoring and managing wear.

Accurate modeling of wear in cyclones has the potential to reduce uncertainty at both the design and operation stages, lowering maintenance costs. Researchers modelling wear in gas-solid cyclones have focused disproportionately on erosive wear by solid particle impact, whereas the occurrence of wear through other modes has been mostly neglected. Moreover, there is scarce experimental data regarding cyclone wear rates.

The authors propose that three-body abrasion by particle sliding and rolling is determinant in wear processes throughout the cyclone interior. To test this hypothesis, we have developed a multiphase numerical model of a gas-solid cyclone with sub-models for the erosive and abrasive wear modes. Additionally, we test predictions by both models against experimental data obtained at a laboratory-scale installation.

Methods

Wear in cyclones is highly localized, with a strong dependence on the dynamics of the solid phase, and, by extension, the fluid dynamics of the gas phase. In this work, we used the numerical code CFDEM@coupling-PFM [2] to simulate wear in a gas cyclone loaded with spherical steel grit. This numerical code is

well suited for multiphase simulations, coupling computational fluid dynamics (CFD) to the discrete element method (DEM). The fluid phase is modelled through implicit Large Eddy Simulation (LES), using the finite volume method to solve the Navier-Stokes equations for incompressible flow. Turbulence closure is achieved by using the Wall Adapting Local Eddy-Viscosity method to model the sub-grid scale tensor [3]. The Navier-Stokes equations are modified to account for the presence of a solid phase, including particle-fluid coupling as a source term. This term is composed by several force sub-models, accounting for the pressure gradient force, the viscous force and drag through the Koch-Hill model [4]. The DEM is used to model the solid phase. Newton's laws of motion are solved for the translational and rotational motion of each particle in the ensemble. The Hertzian contact model is used to calculate particle-particle and particle-wall interaction forces. Erosive wear is modelled using the Finnie model [5], while abrasive wear is modelled using the Archard model [6]. Constants for both wear models are dependent on the specific mechanical system under consideration, and cannot be estimated reliably *a priori*. For this reason, numerical wear rates were normalized by the maximum value at the surface of the cyclone for qualitative analysis.

Wear rates are measured experimentally in a laboratory-scale cyclone made of structural steel (S235). The cyclone is operated at an inlet gas velocity of 28 m/s. Spherical steel grit is injected at a mass flowrate of 40 kg/h, with a particle size distribution ranging from 200–400 μm , and a solid density of 7000 kg/m^3 . The operating conditions and material properties used for the CFD-DEM simulations match those used in the experimental work as closely as possible, excepting particle mass flowrate. This variable was increased to 40 kg/h to accelerate wear in the experimental installation, compared to 7 kg/h in the CFD-DEM simulation. The wall thickness of the cyclone is periodically monitored at 62 measurement points along its height, each time an additional 100 kg of steel grit is injected. Wall thickness is

measured non-destructively by an ultrasonic thickness gauge (Elcometer PTG8 with 20 MHz monocrystalline transducer and acrylic delay line).

Results

The results of numerical simulations are summarized in Figure 1. Figure 1a shows an instantaneous snapshot of particle positions and velocities in the cyclone body. Figure 1b presents the surface maps of normalized wear rates predicted by the erosion and abrasion models.

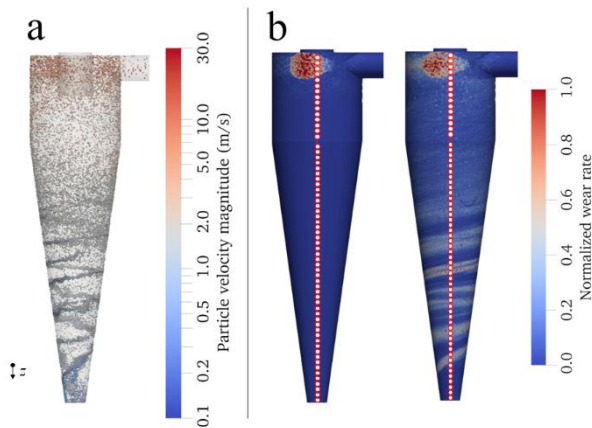


Figure 1. XZ plane view of particle snapshot colored by velocity magnitude (a), and normalized wear rate by erosive (b, left) and abrasive modes (b, right), indicate wall thickness measurement points.

Two distinct particle flow regimes can be observed in the cylinder and cone sections of the cyclone, with a transition zone in-between. In the cylinder section, incoming particles strike the inlet target zone (directly opposite the inlet) at high velocities, dissipating a large fraction of their kinetic energy in this initial collision. The effect of these high kinetic energy impacts is observable in Figure 1b, with both erosive and abrasive wear maps showing maximum wear in the inlet target zone.

Particles follow a ballistic trajectory until they are confined to the wall, driven by the dissipation of kinetic energy in successive collisions and the centrifugal force imparted by the fluid phase. From that point onwards, each particle travels along the wall in a tight spiral, suffering tangential deceleration due to sliding and rolling friction. This process causes particles to pile up, particularly in the transition from the cylindrical to the conical section, forming increasingly denser spiral strands as particles travel towards the collection bin. As the individual particles in the helical strands travel at low velocities, with low kinetic

Acknowledgements

This work was financially supported by: Base Funding - UIDB/00532/2020 and Programmatic Funding - UIDP/00532/2020 of CEFT - funded by national funds through the FCT/MCTES (PIDDAC); PhD grant of Pedro Teixeira Pacheco was funded by Advanced Cyclone Systems, S.A; and ALiCE through project LA/P/0045/2020.

References

- [1] A.C. Hoffmann, L.E. Stein, *Gas Cyclones and Swirl Tubes*, 2nd ed., Springer, New York, 2007, 257-268.
- [2] S. Pietsch et al., *Proc. of Fluidization XV - ECI Symposium Series*, Quebec, Canada, 2016.
- [3] R. Hreiz et al., *Chemical Engineering Research and Design*, 89 (2011) 2521-2539.
- [4] Z.Y. Zhou et al., *Journal of Fluid Mechanics*, 661 (2010) 482-510.
- [5] I. Finnie, *Wear*, 3 (1960) 87-103.
- [6] J.F. Archard, W. Hirst, *Proc. of Royal Society A*, London, United Kingdom, 1956, 397-410.

energy and near tangent angles, the normalized wear rate predicted by the Finnie mode is near zero in the cone region of the cyclone. By contrast, the normalized abrasive wear map shows pronounced wear tracks along the spirals, with wear rates up to 60% of the maximum in the inlet target zone.

In Figure 2, the predictions of the erosive and abrasive wear models are compared to experimental measurements. Plots for normalized wear rates by both models are extracted from a line extending through the full height of the cyclone, coinciding with the thickness measurement positions, as shown in Figure 1b.

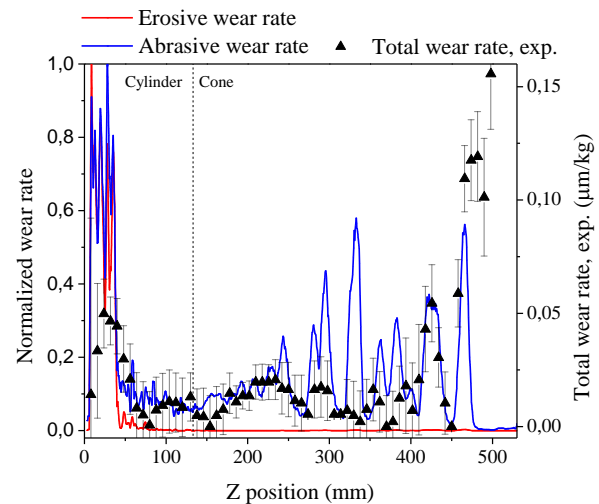


Figure 2. Wear rates along the height of cyclone. Normalized numerical wear rates are shown on left y-axis, while experimental wear rates are shown on the right y-axis.

There is considerable wear in the inlet target zone according to experimental measurements, corresponding to the region from $Z = 0$ to $Z = 40$ mm. Further down the cyclone, experimental measurements show peaks and valleys of wear, consistent with the hypothesis of three-body abrasion in the particle strands. The maximum wear rate is observed in the bottom of the cone, with severe wear in the region $Z > 450$ mm.

Conclusions

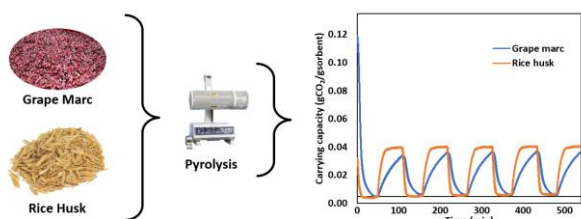
The predictive power of the Archard abrasion model was found to outperform that of the Finnie erosion model, in terms of the qualitative wear pattern. This supports the hypothesis that three-body abrasion is a relevant mode of wear in gas-solid cyclones. Neither model was able to predict the critical region of wear near the bottom of the cone section of the cyclone.

Biomass-based adsorbents for carbon capture

A. Amorim^{1,2*}, R.M. Filipe^{2,3}, C.K. Rojas-Mayorga⁴, A. Bonilla-Petriciolet⁴, H.A. Matos²

¹c5Lab – Sustainable Construction Materials, 2795-242, Linda-a-Velha, Portugal; ²CERENA, Instituto Superior Técnico, Universidade de Lisboa, 1049-001, Lisbon, Portugal; ³Instituto Superior de Engenharia de Lisboa, Instituto Politécnico de Lisboa, 1959-007, Lisbon, Portugal; ⁴Instituto Tecnológico de Aguascalientes, Aguascalientes 20256, Mexico.

*aamorim@c5lab.pt



Two different precursors, grape marc and rice husk, were pyrolyzed to obtain adsorbents for CO₂ capture. The adsorbents were submitted to consecutive cycles of desorption, at 120 °C under N₂ atmosphere, and adsorption, at 30 °C under CO₂ atmosphere. The results show faster adsorption kinetics using the rice husk-based adsorbent, for which a 0.04 g CO₂/g adsorbent carrying capacity was obtained. It is also possible to verify the maintenance of the carbon capture efficiency over multiple cycles. This means that, for a future industrial application, the fresh adsorbent requirement is low.

Introduction

To achieve the sustainable goals defined by the Paris agreement, EU countries must become carbon neutral by 2050. One of the main strategies to meet this goal is CO₂ capture and sequestration/reutilization. Adsorption is a cost-effective and efficient carbon-capturing technology. Popular adsorbents include carbon materials, zeolites and metal-organic frameworks (MOFs). Unlike zeolites and MOFs, carbon materials are not sensitive to the presence of moisture. Recent studies are focused on the study of carbon biomass-based adsorbents, since biomass is an abundant, renewable and cheap source [1]. These adsorbents are reported to present carrying capacities up to 0.47 g CO₂/g adsorbent at atmospheric pressure, which is similar to the values reported for calcium-based adsorbents before deactivation [2]. In this work, two waste materials easily available in Portugal, rice husk and grape marc, were chosen as precursors for CO₂ adsorbents. The objective of this work was the evaluation and comparison of the multicyclic CO₂ capture of these low-cost adsorbents.

Methods

The adsorbent precursors were crushed and sieved before being submitted to pyrolysis at 600 °C in an N₂ atmosphere for 2 hours with a heating ramp of 10 °C/min. After pyrolysis, the materials were sieved to obtain particle sizes in the range of 420-500 μm. The ability to maintain the performance during multiple adsorption and desorption cycles was evaluated using thermogravimetric analysis. The adsorption and desorption conditions are presented in Table 1. Flowrates of 200 mL/min were used to provide the specified atmosphere for each cycle step. Five cycles were performed for each material, starting with desorption and ending with an adsorption step.

Table 1. The adsorption and desorption conditions used in the thermogravimetric analyzer for each cycle and material.

Process	Atmosphere	Temperature (°C)	Duration (min)
Desorption	N ₂	120	30
Cooling ramp	N ₂	120-30	9
Adsorption	CO ₂	30	60
Heating ramp	N ₂	30-120	9

Results

The yield of the pyrolysis for both materials is presented in Table 2. The process yields obtained are similar to the biochar yields found in the literature for slow pyrolysis (~35 %) [3].

Table 2. Mass yield of pyrolysis for grape marc and rice husk.

Adsorbent precursor	Biochar yield (%)
Grape marc	33.5
Rice husk	37.2

The results obtained in the thermogravimetric analysis for both materials are shown in Figure 1.

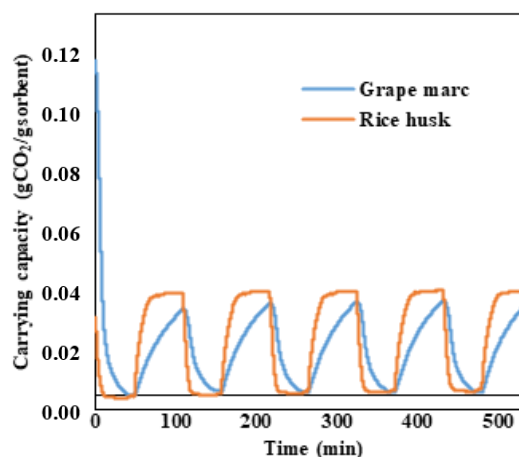


Figure 1. The multicyclic activity of grape marc and rice husk-based adsorbents for carbon capture. The desorption was performed at 120 °C in an inert atmosphere and the adsorption at 30 °C under CO₂ flow.

The carrying capacity of both adsorbents after 1 hour of adsorption is between 0.03 and 0.04 g CO₂/g adsorbent and no deactivation was observed through the five cycles performed. This value is lower than the carrying capacity of rice husk and grape marc-based adsorbents found in the literature, which highlights the importance of a further activation step after pyrolysis [4,5]. The grape marc-based adsorbent adsorption kinetics is significantly slower than the rice husk-based adsorbent kinetics. For grape marc biochar, 1 hour is not enough to achieve equilibrium. Given more adsorption time, the carrying capacity of this adsorbent could increase. On the other hand, the adsorption, and desorption kinetics of the rice husk

biochar are fast and thus it does not need 1 hour of adsorption to achieve the maximum conversion (~20 minutes needed) nor 30 minutes of desorption to release all the CO₂ (~10 minutes needed). Rice husk biochar is thus best suited for industrial application since it can achieve the same carrying capacity in a short time. The maintenance of the activity over consecutive cycles is also an advantage, as it means the material can operate continually without deactivation. Thus, the adsorbent synthesis, which is an energy-consuming step, is minimized. Nevertheless, an economic analysis is required to validate this technology as a competing one for industrial implementation.

Acknowledgements

This work is funded by European Union's Horizon 2020 under the scope of the IProPBio project. The authors also gratefully acknowledge the support of the CERENA (strategic project FCT-UIDB/04028/2020) and c⁵Lab – Sustainable Construction Materials Association.

References

- [1] C. Quan et al., *Journal of CO2 Utilization*, 68 (2023) 102373.
- [2] Y.Q. Geng et al., *Journal of Fuel Chemistry and Technology*, 49 (2021) 998-1013.
- [3] G. Singh et al., *Carbon*, 148 (2019) 164-186.
- [4] I.S. Ismail et al., *Carbon*, 160 (2020) 113-124.
- [5] P. Murge et al., *Energy and Fuels*, 32 (2018) 10786-10795.

Conclusions

Carbon capture adsorbents were synthesized using grape marc and rice husk as precursors. Pyrolyzed grape marc and rice husk show a carrying capacity between 0.03 and 0.04 g CO₂/g adsorbent. The multicyclic activity is maintained for at least 5 cycles, using moderate temperatures for absorption and desorption. Further investigation is needed to evaluate the selectivity of these materials and to compare the process costs of this process, when compared to benchmark technologies, such as MEA absorption or calcium-looping.

Treatment of wastewater effluents using nanofiltration and low pressure UV treatment to produce high quality water that can be reused for irrigation for food production

M.B. Cristóvão^{1,2}, A.P. Marques¹, A. Bento-Silva³, M. Gossard¹, S. Tela^{1,2}, J. Sério^{1,4}, M.R. Bronze^{1,3,4}, P.B. de Oliveira⁵, M. Nunes^{1,4}, M.T.B. Crespo^{1,4}, J.G. Crespo², V.J. Pereira^{1,4*}

¹iBET, Instituto de Biologia Experimental e Tecnológica, Portugal; ²LAQV-REQUIMTE, Department of Chemistry, NOVA School of Science and Technology, Universidade NOVA de Lisboa, Portugal; ³Faculdade de Farmácia Universidade de Lisboa, Portugal; ⁴Instituto de Tecnologia Química e Biológica António Xavier, Universidade Nova de Lisboa, Portugal; ⁵Instituto Nacional de Investigação Agrária e Veterinária, Portugal.

*vanessap@ibet.pt



Agriculture irrigation accounts for approximately 70% of all water withdrawals. Climate change and the increase in human population will lead to a higher food and water demand. Hence, it is crucial to explore new water sources for agriculture irrigation, such as the reuse of wastewater effluents. Prior to irrigation with wastewater effluents, it is important to evaluate the potential uptake of contaminants by food crops. In this study, different water sources (wastewater effluents, wastewater effluent after nanofiltration treatment and tap water) were used for the irrigation of raspberries. Several antibiotics (ciprofloxacin, levofloxacin, ampicillin, ertapenem and meropenem) as well as total coliforms and *Escherichia coli* resistant to different antibiotics (ciprofloxacin, levofloxacin, meropenem, streptomycin and ampicillin) were quantified in the different irrigation waters over a 5-month irrigation period.

Methods

Figure 1 summarizes the experimental procedure.

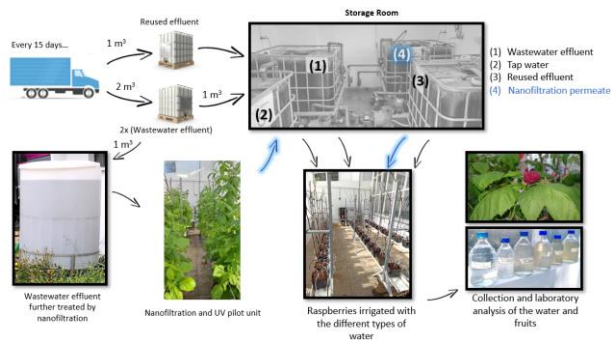


Figure 1. Experimental procedure.

Results

Of all the target antibiotics, only ciprofloxacin, levofloxacin, and meropenem were detected at different concentrations in the different irrigation waters. The discharged wastewater effluent had higher levels of ciprofloxacin and levofloxacin, ranging from 174 to 1335 ng/L.

The best nanofiltration operating conditions were defined [1,2]. The combination of UV photolysis with membrane filtration was tested to further treat the permeate and retentate samples from the nanofiltration unit. When ciprofloxacin was present in the permeate samples, after exposure to UV photolysis using a low pressure mercury lamp the antibiotic was not detected. In the highly concentrated retentate samples, 57% of ciprofloxacin and 31% of levofloxacin were degraded by UV photolysis using an extremely low UV fluence. If a higher exposure time was used,

the higher degradation levels would be achieved. These low UV fluences were able to inactivate successfully the antibiotic resistant bacteria in the highly concentrated retentate samples (with percent inactivation's higher than 4-log).

Analytical methods were validated for the detection of the target contaminants in the solid matrices and the potential uptake of the target contaminants by the fruits evaluated. The target antibiotics were not detected in the raspberries nor the leaves at levels above 10 µg.kg⁻¹.

Conclusions

Four different waters were used to irrigate raspberries and characterized in terms of the concentration of the target antibiotics and antibiotic resistant bacteria.

One of the irrigation waters was produced by nanofiltration of the wastewater effluent using the best operating conditions that minimize fouling and maximize water production and rejection of the target contaminants.

Rejections higher than 94% were obtained for the target antibiotics and resistant bacteria. Nanofiltration can be used to ensure a high removal of the target antibiotics and antibiotic resistant bacteria from wastewater effluents as well as to produce water suitable for irrigation.

Low pressure UV photolysis was extremely effective to treat the target bacteria in the concentrated retentate.

The target antibiotics were not detected in the fruits nor the leaves at levels above 10 µg.kg⁻¹.

The combination of nanofiltration and UV photolysis produced extremely high quality water for irrigation in terms of the antibiotics and antibiotic resistant bacteria monitored in this study.

Acknowledgements

This research was funded by Fundação para a Ciência e a Tecnologia through the project PTDC/CTA-AMB/29586/2017. We also acknowledge the financial support from Fundação para a Ciência e Tecnologia and Portugal 2020 to the Portuguese Mass Spectrometry Network (LISBOA-01-0145-FEDER-402-022125), iNOVA4Health (UIDB/04462/2020 and UIDP/04462/2020), the Associate Laboratory LS4FUTURE (LA/P/0087/2020), and the Associate Laboratory for Green Chemistry – LAQV (UIDB/50006/2020 and UIDP/50006/2020). Funding from INTERFACE Programme, through the Innovation, Technology and Circular Economy Fund (FITEC), is gratefully acknowledged.

References

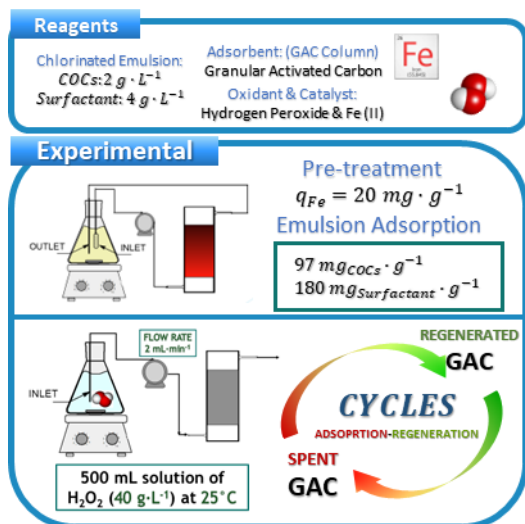
- [1] M.B. Cristóvão et al., *Membranes*, 11 (2021) 9.
- [2] M.B. Cristóvão et al., *Separation and Purification Technology*, 288 (2022) 120565.

Efficient adsorption and regeneration of activated carbon used in the treatment of highly chlorinated organic emulsion using the Fenton Reaction

A. Sánchez-Yepes*, A. Santos, A. Romero, D. Lorenzo

Chemical Engineering and Materials Department, Complutense University of Madrid, Spain.

*andsan28@ucm.es



The uncontrolled disposal of persistent compounds has generated an important environmental issue, generating dense nonaqueous liquid phase (DNAPL) of hydrophobic nature. One of the most promising remediation technologies is the extraction using a surfactant. However, the contamination is transferred from the subsurface to the extracted emulsion containing surfactant and organic pollutants. In this work, an emulsion composed of highly chlorinated organic phase and E-Mulse 3® was treated adsorbing those in granular activated carbon previously saturated with Fe. After that, the subsequent recovery and reuse of the adsorbent was performed. It was found after adsorption-regeneration cycles that the adsorbent capacity of the carbon was recovered, obtaining a selective COCs adsorption efficiently achieved with surfactant and adsorbent recovery, which improved the circular economy without generating secondary waste.

Introduction

Bad practices in disposing of obsolete and toxic pesticide production waste have caused significant environmental risks in many parts of Europe. An example is the dumping in unlined landfills of residues from the lindane (γ -hexachlorocyclohexane, γ -HCH) manufacturing process [1]. The liquid residuum was a dense nonaqueous liquid phase (DNAPL) of hydrophobic nature comprising more than 28 chlorinated organic compounds (COCs) [2]. This DNAPL percolated through the subsurface and accumulated in the nonpermeable layers, polluting the soil and groundwater.

Injection of biodegradable surfactant aqueous emulsions into the subsurface with further extraction of polluted fluids [3, 4] can be applied to remove the residual DNAPL. However, the contamination is transferred from the subsurface to the extracted emulsion containing surfactant and organic pollutants. This highly contaminated emulsion must be treated on-site to remove the extracted DNAPL and, if possible, recover the surfactant. This work studied the management of polluted emulsions by selective adsorption of pollutants in granular activated carbon (GAC) and regeneration of the spent GAC. The adsorbent was regenerated under mild conditions, with hydrogen peroxide as the oxidant and immobilised iron in GAC as a catalyst (heterogeneous Fenton reaction). A commercial GAC was used in a real wastewater treatment plant was used. The surfactant selected was a non-ionic biodegradable surfactant produced by EthicalChem (E-Mulse 3®) (E3).

Experimental

Treatment of E3-containing and real DNAPL obtained from the Bailin landfill (Sabiñánigo, Spain) was performed at a laboratory scale. In the first approach, the adsorption isotherms of surfactant and COCs were obtained in batch runs. Subsequently, the adsorption-regeneration cycles of the adsorbent were studied in column experiments (glass, diameter 28 mm and height 50 mm) filled with 20 g of commercial GAC previously spiked with Fe ($20 \text{ mg}_{\text{Fe}}/\text{g}_{\text{GAC}}$).

The unproductive consumption of H_2O_2 was studied (R1). A 500 mL solution of H_2O_2 (40 g/L) was fed through the column at a flow rate of $2 \text{ mL} / \text{min}$. The reaction between GAC and the oxidant was monitored, quantifying the flow rate of O_2 generated and the remaining concentration of oxidant obtained in the column outlet stream.

Absorption-regeneration experiments were performed (R2) using the same experimental setup. 1100 mL of the emulsion composed of $2 \text{ g}_{\text{COCs}}/\text{L}$ and 4 g/L of surfactant were recirculated through the GAC. The saturation concentrations were $97 \text{ mg}_{\text{COCs}}/\text{g}_{\text{GAC}}$ and $180 \text{ mg}_{\text{E3}}/\text{g}_{\text{GAC}}$ of COC and E3, respectively.

Results and Discussions

The regeneration of the spent GAC was carried out by feeding 500 mL of a solution of H_2O_2 (40 g/L) at $2 \text{ mL}/\text{min}$. A sample of the output stream was taken and analysed at different reaction times. The pH, iron leachates and by-products were quantified. Furthermore, the volumetric flow of the gases generated during the reaction was also monitored. After regeneration, the column was raised with 150 mL milli-Q water at $2 \text{ mL}/\text{min}$.

The gas flows generated during the reaction of GAC and the oxidant (R1 in Figure 1) and the regeneration of saturated GAC (R2 in Figure 1) are compared in Figure 1. In R1, the gas flow rate generated reaches the steady state after 60 min obtaining a gas flow rate of $25 \text{ mL}/\text{min}$. Meanwhile, $9 \text{ mL}/\text{min}$ of gas was obtained during the saturated GAC regeneration, as shown in Figure 1.

This experimental evidence is explained by assuming that the COCs and E3 hide the surface of the GAC, and the unproductive reaction is considerably reduced. The latter agrees with the H_2O_2 consumption measured between the input and output streams after the steady state conditions. In R1, the H_2O_2 was consumed entirely, but in R2, the consumption was 25%.

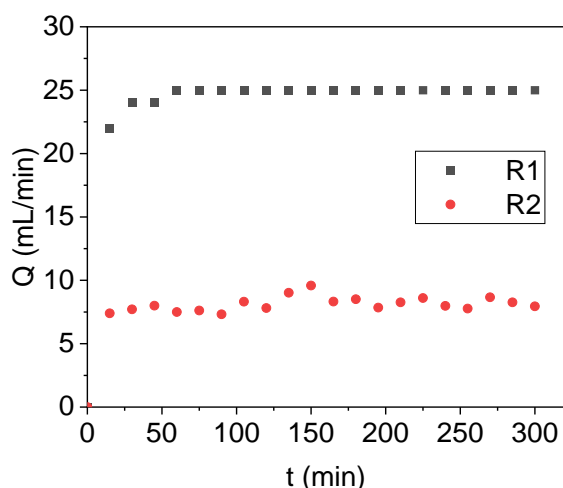


Figure 1. Gas flow rate at the outlet of the column.

The aqueous phase was measured. In the steady state, relevant concentrations of short-chain acids were obtained, and these acids were identified as acetic and formic. After 120 min of the

Acknowledgements

This research was supported by the project PID2019-105934RB-I00 funded by MCINN/AEI/10.13039/501100011033 and the project S2018/EMT-4317 (CARESOIL CM) co-funded by the European Social Fund and the European Regional Development Fund. Andrés Sánchez-Yepes thanks the Ministry of Science and Innovation for supporting pre-doctoral contracts with FPI grant PRE2020-093195.

References

- [1] J. Vijgen et al., *Environmental Pollution*, 248 (2019) 696-705.
- [2] A. Santos et al., *Environmental Pollution*, 242 (2018) 1616-1624.
- [3] M.D. Lin, D.C. McKinney, Optimal remediation of DNAPL contaminated aquifers using surfactant enhanced pump-and-treat systems, *Proceedings of the International Symposium on Groundwater Management*, 41-45.
- [4] L. Huo et al., *Chemosphere*, 252 (2020) 126620.

oxidant feed stream, an acid concentration of approximately 750 ppm was obtained, and the presence of chlorines was detected, confirming the reduction of the adsorbed compounds. These acids produced a drop in the pH of the aqueous phase below 3. Finally, negligible iron leaches were found in R1 and R2 (less than 3 %).

After regeneration, the column was re-saturated with a new emulsion stream. The adsorption process was performed under the same conditions as previously described. Once the column has been saturated, the recovery capacity of the adsorbent was obtained.

Conclusions

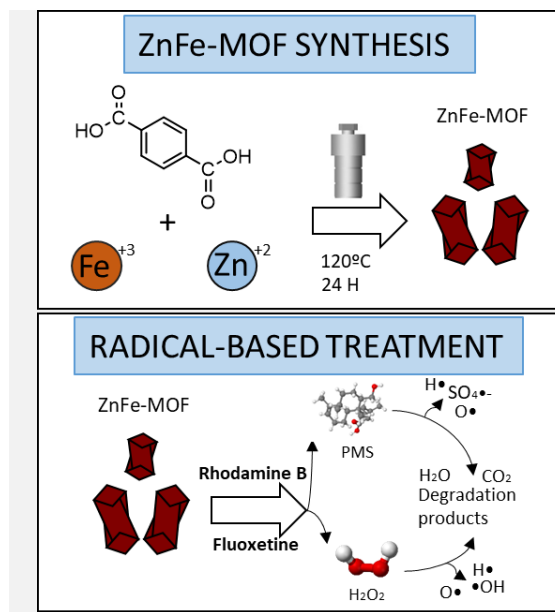
Recovery of the adsorbent capacity was studied by successive adsorption cycles after GAG regeneration. After each regeneration cycle, it was found that the surfactant adsorption decreased, but the COCs adsorption kept almost constant. In this way, selective COCs adsorption and adsorbent recovery and reuse were efficiently achieved, which improved the circular economy without generating secondary waste.

Synthesis of bimetallic ZnFe-MOF catalyst for the removal of emerging pollutants in wastewater by using radical-based treatment

D. Terrón*, E. Rosales, M. Pazos, M.A. Sanromán

Department of Chemical Engineering, University of Vigo, Isaac Newton Building, Campus as Lagoas Marcosende 36310, Vigo, Spain.

*daniel.terron@uvigo.gal



The presence of emerging pollutants, such as drugs or dyes, is increasing in wastewater. Given the difficulty and cost of removing them from the water, several treatments have been developed. Among them, methods based on Advanced Oxidation Processes (AOPs), have aroused great interest in the scientific community. In this framework, new materials such as Metal-Organic Frameworks (MOFs) capable to adsorb the pollutant and catalyze the AOPs are necessary. In this study, a novel bimetallic material denoted ZnFe-MOF was synthesized from a one-step solvothermal method. After the characterization of the ZnFe-MOF, it was verified its good properties as dual material: adsorbent and catalyst. For this reason, it was tested in the removal of a model dye Rhodamine B. The results have been very promising, being capable of the removal of more than 99% of the pollutant. However, it was detected better results when hydroxyl radicals were generated in comparison with sulphate radicals, achieving total degradation in 90 min for the hydroxyl radical process and 100% in 120 min for peroxymonosulfate activated system. Finally, their efficacy was also tested by degrading drugs such as Fluoxetine, reaching, in the first instance, more than 80% in 900 min.

Introduction

In the last years, there has been a growing interest in emerging pollutants, such as certain dyes or drugs like Rhodamine B or Fluoxetine, which are the subject of this research. In addition, the increase in population year after year leads to an increased presence and therefore toxicity of these chemicals in wastewater. However, the current conventional procedure in a wastewater treatment plant is ineffective against these emerging pollutants, as it uses a costly or unsuccessful amount of time, resources and energy. Thus, it is leading to the development of new treatments, such as Advanced Oxidation Processes (AOPs) alone or combined with other processes, such as adsorption, capable of degrading or removing these pollutants from the polluted water [1]. Among different adsorbents in recent times, new composites have been developed, namely MOFs, which are materials with a very porous surface, with a specific dimensional structure given by the bonding of a linker with one or more metals inside. These composites have the ability to adsorb a large amount of contaminants into their pores as well as act as powerful and reusable catalysts [2]. Recent studies mention the use of MOFs in AOPs for pollutant removal favorably and with a promising future, achieving 100% reductions for the presence of many of these pollutants, as well as reducing the need for the use of ozone or hydrogen peroxide mostly. Bimetallic MOF of iron and zinc can be really interesting, since iron is a catalyst commonly used in Fenton processes for pollutant degradation [3], and zinc is an inhibitor of microbial growth at low concentrations [4]. Mixing both, results in a material with the potential to adsorb and catalyze AOPs. In addition, the reaction between the two metals is expected to result in enhanced catalytic performance and a better recovery or reuse of the material than just one [5].

Objectives

The aim is to synthesize in a simple way, bimetallic and stable MOFs, capable of adsorbing and catalyzing the degradation of emerging pollutants through their application in AOPs such as radical-based processes.

Methods

Bimetallic ZnFe-MOF one step solvothermal synthesis:

Terephthalic acid (H₂BDC), iron(III) chloride hexahydrate and zinc nitrate hexahydrate were added into a beaker, dissolved in 200 mL of dimethylsulfamide (DMF) and stirred for 30 min. Then, the solution was transferred into a stainless-steel autoclave and put into a 120°C oven overnight. After this, the autoclave was cooled to room temperature for several hours until it is openable and transferred into a beaker. After that samples were centrifugally collected and washed in different falcon tubes, eliminating the supernatant, and suspending the pellet in 25 mL of ethanol and DMF. Repeat this step 3 times and put the final supernatant into a vacuum oven at 60°C, for at least 12 h [6]. The obtained solid is a dusty stone-like shape, orange-red coloured MIL-MOF [7], which has to be crushed in a mortar to obtain the final MOF dust.

Material characterization: To understand the effect of the crystalline structure and the functional groups on the AOPs, the ZnFe-MOF dust was structurally evaluated by XRD (XPert Pro 3) and FTIR (Nicolet 6700) analysis (CACTI University of Vigo).

Degradation and reuse tests: Simulated polluted water with 100 ppm of Rhodamine B or 10 ppm of fluoxetine were used. Both pollutants were degraded by two methods: i) generation of sulfate radicals in which (peroxymonosulfate (PMS) at a concentration of 0.6 mM was activated by the MOF; and ii) generation of hydroxyl radicals in which the solution was mixtures with H₂O₂ (32 mM) and MOF. In all cases, the effect

of ZnFe-MOF dosage was evaluated in a range of 0.5-3.2mM. The mixtures were homogenized by magnetic agitation. Samples were taken at 5, 15, 30, 45, 60 and 90 min. for Rhodamine B tests, and 5, 15, 30, 60, 260, 390 and 900 min. for Fluoxetine. The samples of Rhodamine B were centrifuged and measured without interference in the spectrophotometer (554 nm). For fluoxetine assays, the sample was filtered with a syringe and measured in HPLC following the referenced method [1]. For the reuses, a sample from a previous test was centrifuged and the ZnFe-MOF pellet was resuspended in a new simulated polluted water with 100ppm of Rhodamine B.

Results

Materials characterization: The obtained ZnFe-MOF from the synthesis was analyzed by FTIR (Figure 1). From the spectrum is highlighted the strong bands attributed to the C=O, -COO, C-O and C-H bending vibrations of the benzene ring (1503-1656, 1391, 1017 and 749 cm^{-1}). In addition, confirms the correct coordination of the Zn (528 cm^{-1}) and Fe (560 cm^{-1}) metal ions with the H₂BDC to form MIL-MOF crystals [6].

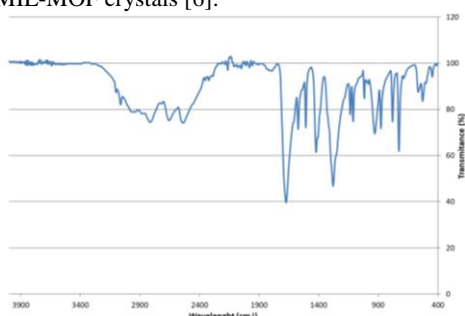


Figure 1. FTIR spectrum of ZnFe-MOF.

The key diffraction peaks for ZnFe-MOF at 2-theta, for XRD pattern, are found at 5.47, 8.51, 9.08 and 10.38 which is a similar range to previous synthesized ZnFe-MOFs with this structure [5]. It also confirms a high crystallization using the equation, that outputs a value of 90%.

Degradation by sulfate radicals: Figure 2 shows the results of the degradation process by PMS activation method. The addition of ZnFe-MOF as catalyst improves the process, reducing 84% of the contaminant present in water in 60 min., compared to 58% or 61% in the same timeframe for PMS or MOF adsorption experiments, respectively.

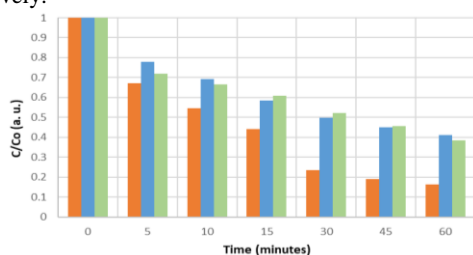


Figure 2. Degradation of Rhodamine B by PMS/ZnFe-MOF (orange bar) control-PMS (blue bar) and adsorption (green).

Acknowledgements

This research has been financially supported by MCIN / AEI / 10.13039/501100011033 Project PID2020-113667GB-I00 and Xunta de Galicia, and the European Regional Development Fund (ED431C 2021-43).

References

- [1] S. Escudero et al., Chemosphere, 268 (2021) 129318.
- [2] X. Liu et al., Green Energy & Environment, (2022) 2468-0257.
- [3] Virender K. Sharma et al., Journal of Hazardous Materials, 372 (2019) 5-7.
- [4] F. Akbarzadeh et al., Heliyon, 6 (2020) e03231.
- [5] D. Wu et al., Chemosphere, 327 (2023) 0045-6535.
- [6] Y. Shi et al., Optical Materials, 131 (2022) 0925-3467.
- [7] S. Cohen et al., Optical Materials, 131 (2022) 0910-1039.

The fluoxetine test outputs under sulfate radicals action are presented in the following Table 1. It is observed that ZnFe-MOF retains its capacity of a good catalyzer for PMS (0.45mM), being capable of the total removal of this drug in 900 min.

Table 1. Fluoxetine degradation by PMS/ZnFe-MOF, PMS and adsorption.

Time (min)	PMS/ZnFe-MOF Degradation (%)	Control-PMS Degradation (%)	Adsorption Removal (%)
5	10.93	9.55	3.02
15	27.73	13.38	18.13
30	23.77	17.83	16.93
60	35.69	19.31	22.90
260	71.37	20.13	20.42
390	92.91	21.55	22.05
900	99.68	22.34	22.26

Degradation by hydroxyl radicals: Table 2 shows that ZnFe-MOF is a perfect catalyzer, achieving the total degradation after 90 min, while adsorption and H₂O₂ controls cannot degrade furthermore than 1% and 63% respectively for the same time.

Table 2. Heterogenous Fenton (H₂O₂/ZnFe-MOF) for degradation of 100 ppm Rhodamine B.

Time (min)	H ₂ O ₂ /ZnFe-MOF Degradation (%)	Control-H ₂ O ₂ Degradation (%)	Adsorption Removal (%)
5	31.98	0.04	10.70
15	45.98	0.11	21.70
30	63.55	0.17	36.77
45	67.20	0.25	49.27
60	75.41	0.32	60.26
90	99.36	0.38	62.83

In addition, the properties as catalyst remain after 3 uses in the Fenton process, reaching 100% degradation and starting to drop in the 4th test. The reuses keep the trends determined previously, slowing the adsorption rate and affecting its catalytic ability with each reuse.



Figure 3. Samples from different tests, from left to right: Rhodamine B solution, Rhodamine B + H₂O₂, Rhodamine B adsorption and Fenton after 3 cycles.

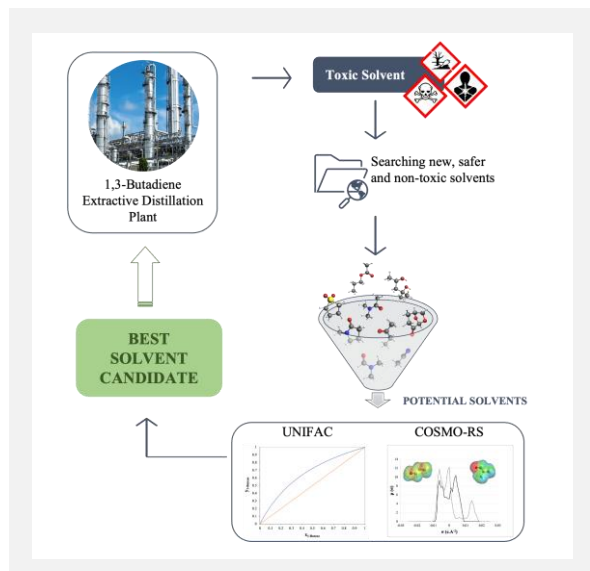
Conclusions

A novel ZnFe-MOF material synthesized quickly and easily is able to act multifunctionally in different AOPs, being both adsorbent and catalyst. In addition, it has an acceptable reusability, being understood as a cycle of 3 uses in its useful life. Therefore, a new material with promising results to remove pollutants under AOPs in a fast and cheap way is being developed. Future studies will be carried out to study its anti-pathogenic capacity.

Green solvents for enhanced selective extraction of 1,3-butadiene: a comparative study

J. Gomes¹*, R. Silva², C. Nunes³, D. Barbosa¹

¹LEPABE, Faculdade de Engenharia da Universidade do Porto, Rua Dr. Roberto Frias, 4200-465 Porto, Portugal; ²Repsol Polímeros, S.A., Complexo Petroquímico, Aptd. 41 Monte Feio, Sines, Portugal; ³CERENA, Instituto Superior Técnico, Av. Rovisco Pais 1, 1049-001 Lisboa, Portugal;
*e-mail: joaopedrosgomes@gmail.com



The use of solvents in the petrochemical industry for separation processes may pose a potential threat to the environment and workers' health. REACH regulations have prompted the search for non-toxic and safer solvents. In the extraction of 1,3-butadiene from crude C₄ streams, the choice of solvent is critical to achieving the desired purity. However, finding high-performance solvents for extractive distillation using heuristic guidelines or experimental techniques is challenging as they are typically inefficient, time-consuming, and costly. The UNIFAC model and COSMO-RS method were used to screen potential solvents and reduce the experimental workload to address this issue. This study analyzed 70 solvents for their physical and thermodynamic properties, toxicity, flammability, environmental impact, selectivity, capacity, and boiling point. The study identified four solvent alternatives that are safer, greener, and non-toxic substitutes for the solvents currently used in 1,3-butadiene production.

Introduction

The use of solvents in the petrochemical industry for separation processes may typically pose a potential risk to the environment and workers' health. Therefore, the use of safer and non-toxic solvents is an emerging strategy within the European Union to comply with the Registration, Evaluation, Authorisation and Restriction of Chemicals (REACH) legislation. Most of the 1,3-butadiene, an important commodity for the chemical and petrochemical industry, is obtained through a series of extractive and conventional distillation columns from a crude C₄ stream, which is generated by the naphtha or natural gas cracking process for olefin production [1,2]. Extractive distillation is required due to its ability to separate components with similar boiling points or azeotropes by adding a solvent that conveniently changes the relative volatility of the components to be separated. The selection of this solvent is critical to achieve the desired level of purity for 1,3-butadiene. The most common used solvents for this process are N,N-dimethylformamide (DMF), N-methyl-2-pyrrolidone (NMP) and acetonitrile (ACN). Although all these solvents are highly efficient and selective, they may be harmful and toxic to humans, potentially causing skin problems, liver damage and cancer [3]. This work seeks to comply with the proposed REACH regulations by replacing the DMF solvent presently used in an existing 1,3-butadiene plant with an appropriate and safer one.

Methods

A comprehensive database of 70 solvents was the starting point for the evaluation process. The solvents under investigation were assessed using a set of green solvent selection criteria, including the degree of toxicity in terms of both environmental and human health impacts, as well as compliance with restrictions established by the REACH legislation. Additionally, the physical and thermochemical properties of each solvent were considered during the evaluation process. The UNIFAC model was used to predict the activity coefficients of the systems considered. This allowed the determination of solvent selectivity and capacity at infinite dilution and typical operating conditions

(60 °C and 4 bar). Subsequently, the COSMO-RS method was used to provide molecular surface charge density (σ), perform virtual experiments with new possible solvents and evaluate their activity coefficients and solubilities at typical operating conditions and infinite dilution. In addition, σ -profiles were generated to analyse the polarity of each molecule and understand its affinity to 1,3-butadiene as well as its behaviour in the liquid solvent matrix.

Results

As can be seen in Figure 1, the vapor-liquid equilibrium of components 1-butene and 1,3-butadiene shows how difficult their separation is due to their close boiling points (−6.3 °C and −4.4 °C, respectively) and relative volatility close to one.

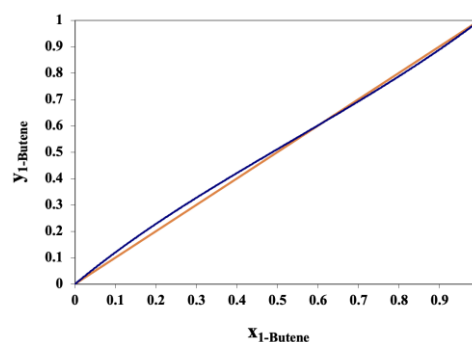


Figure 1. Vapor-liquid equilibrium for system 1-butene/1,3-butadiene at 4 bar, predicted by the UNIFAC method.

Adding a conveniently chosen solvent will enhance the relative volatility of the 1-butene/1,3-butadiene system allowing an easier separation. In Figure 2 it is possible to observe this effect as the equilibrium curve moves away from the line $y=x$. To observe the differences among solvents, ethylene carbonate, anisole, methyl oleate and cyrene™ were selected as representative of green solvents and compared with typical used

solvents. It is important to clarify that it was considered a solvent molar fraction of 0.6 for the system solvent/1-butene/1,3-butadiene and the y and x values of the solutes are expressed in a solvent free basis.

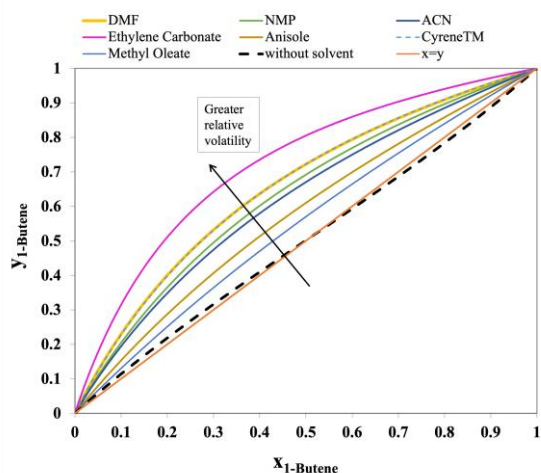


Figure 2. Solvent effect on the separation of 1-butene/1,3-butadiene.

In order to interpret the difference in the separation performance between a well-known solvent such as DMF and a potential greener solvent as cyreneTM, the σ -profiles and σ -potential were reviewed.

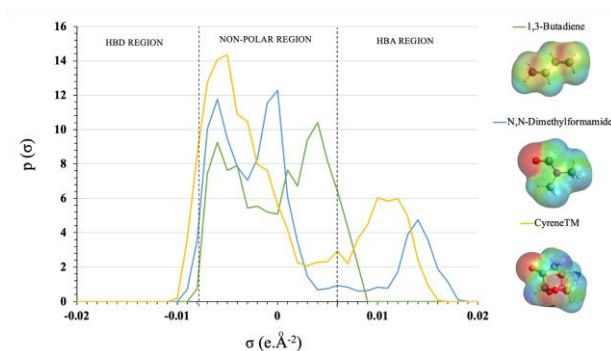


Figure 3. σ -profiles of 1,3-butadiene, DMF and CyreneTM and their respective charge density molecular surface.

From Figure 3, σ -profile analysis allows to understand the hydrogen bonding donor (HBD) ability ($\sigma < -0.008 \text{ e}\cdot\text{\AA}^{-2}$) and hydrogen bonding acceptor (HBA) ability ($\sigma > 0.008 \text{ e}\cdot\text{\AA}^{-2}$) of a molecule. The peaks in the HBA region reveal that cyreneTM has stronger hydrogen bond interaction with 1,3-butadiene than DMF. As it can be seen from the charge density surface area of the molecules (red surface) this results in higher selectivity for this solvent, and therefore, an easier separation.

Acknowledgements

This research was funded by: (a) Fundação para a Ciência e a Tecnologia (FCT) through the Ph.D. Grant PRT/BD/153600/2022. (b). Base Funding—UIDB/00511/2020 of the Laboratory for Process Engineering, Environment, Biotechnology and Energy—LEPABE—Funded by national funds through the FCT/MCTES (PIDDAC); (c) Project 2SMART – engineered Smart materials for Smart citizens, with reference NORTE-01-0145-FEDER-000054, supported by Norte Portugal Regional Operational Programme (NORTE 2020), under the PORTUGAL 2020 Partnership Agreement, through the European Regional Development Fund (ERDF).

References

- [1] K. Weissermel et al., Chapter 3 in Industrial Organic Chemistry, L. Charlet, 3rd edition, VCH Verlagsgesellschaft mbH and VCH Publishers, Weinheim, (1997) 105-123.
- [2] J. Schulze, Chapter 3 in C₄-Hydrocarbons and derivatives, Springer, Berlin, 35-104.
- [3] F. Kerton, Journal of the American Chemical Society, 33 (2009) 1-226.

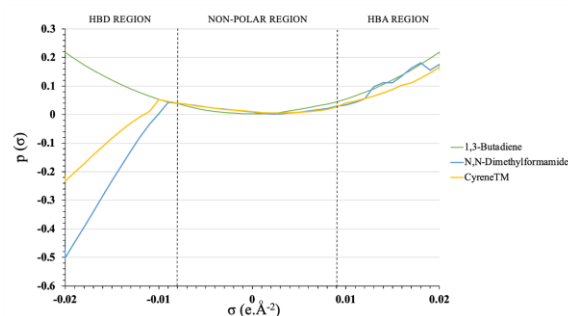


Figure 4. σ -potential of 1,3-butadiene, DMF and CyreneTM.

As illustrated in Figure 4, the σ -potential indicates the affinity of a component in the mixture towards another. In the three regions of σ -potential, a higher negative value for a component indicates a stronger affinity, while a higher positive value indicates a stronger repulsive interaction. For 1,3-butadiene, its σ -potential presents a low positive value in the non-polar region, suggesting that 1,3-butadiene has a stronger affinity and attractive interaction towards non-polar molecules. Despite cyreneTM and DMF have similar thermodynamic properties, cyreneTM is slightly better than DMF as it has a lower positive value in the non-polar region. These results are being validated, and ongoing studies include the evaluation of the optimal green solvent for this process.

Conclusions

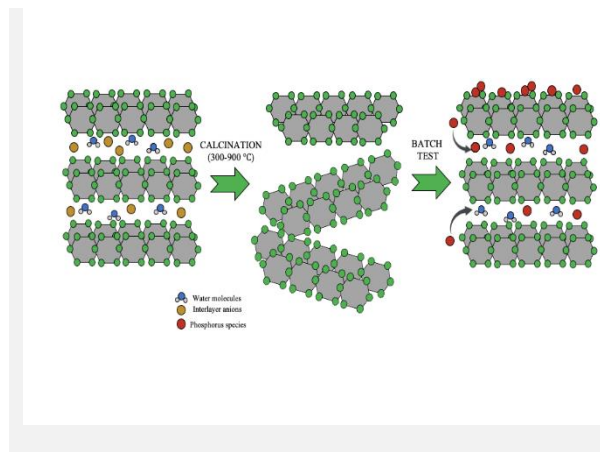
Several green solvents with very high potential to replace the potentially toxic solvents currently used in the 1,3-butadiene extractive distillation plant have been identified as potential candidates. Systematic evaluation and comparison of individual solvents is crucial. The effect on the industrial process will also be analyzed using ASPEN PLUS software to simulate the actual plant. These screening methods offer a more cost-effective, time-efficient, and sustainable alternative to the traditional trial-and-error experimental approach. Furthermore, theoretical modeling can expand the range of experimental data and enable predictions for unexplored solvent mixtures. This research has the potential to identify the use of safe, non-toxic, and sustainable solvents for the 1,3-butadiene extraction process, resulting in an enhanced and sustainable process. Ethylene carbonate has an equilibrium curve shifted further away from the other solvents, showing an improved separation between 1-butene and 1,3-butadiene, indicating that it is a promising solvent for this separation. Nevertheless, cyreneTM seems also to be a good alternative for the 1,3-butadiene process, because of its characteristics that are similar to solvents already used in the industry, such as DMF.

Phosphorus recovery using calcined layered double hydroxides from aqueous matrices

I.D. Borges^{1,2,3}, C.M. Rocha², F. Maia², C.M. Silva³, M.J. Quina¹*

¹University of Coimbra, CIEPQPF, Department of Chemical Engineering, Rua Sílvio Lima, Pólo II-Pinhal de Marrocos, 3030-790 Coimbra; ²Smallmatek-Small Materials and Technologies, Lda, 3810-075 Aveiro, Portugal; ³CICECO-Aveiro Institute of Materials, Department of Chemistry, University of Aveiro, 3810-193 Aveiro, Portugal.

*ines.borges@smallmatek.pt



This study aims to evaluate calcined layered double hydroxides (LDH) for phosphate removal in batch conditions. For that, the influence of pH, LDH dosage, temperature, competitive anions, initial phosphate concentration, and contact time on sorption were studied. The materials were characterized by X-ray diffraction (XRD) and Fourier transform infrared (FTIR) before and after sorption. The results showed that phosphate ion uptake decreases in the presence of other anions, such as nitrate. The temperature has no significant impact on phosphate removal and a neutral pH is the most favorable for this process. Based on XRD and FTIR results, it was confirmed that phosphate was sorbed by Mg-Al LDH and the material was capable to reacquire the original LDH structure before the calcination process. Instead, calcined Zn-Al sorbed phosphate at external surface. The maximum sorption loadings observed were 31 mg g⁻¹ and 107 mg g⁻¹ for Mg-Al and Zn-Al LDH, respectively.

Introduction

In the last 2-3 decades, the world population has grown by more than 2 billion and could reach about 8.4 billion in 2030. With population growth, better living conditions, and rising energy consumption, the limited natural resources are increasingly under pressure. Phosphorus (P), mainly in the form of phosphate (PO_4^{3-}), is a crucial component for plant growth and is regularly used as a fertilizer for growing crops. However, the natural reserves of P can be exhausted in the next 50-100 years. Only about 16 % of the P in fertilizers reaches human food, with very high losses through soil erosion or agrowaste [1]. In addition, the consumption of P in food in developed countries exceeds nutritional needs, which results in losses in wastewater treatment plants. Thus, the recovery of P from wastewater and inland waters such as lakes or rivers must be considered, not only due to its market value but also to mitigate pollution problems, usually referred to as eutrophication. Thus, in the future, it is essential to find alternative and sustainable sources of P through efficient management at the environmental and economic levels [2-4]. Layered double hydroxides (LDH) are a kind of nanoclays that have gained interest in the last years in environmental applications. LDH belongs to a family of inorganic crystalline materials known to have positively charged layers with the difference balanced by interlayered anions. The most important group of LDH may be represented by the formula $[M^{2+}_{1-x}M^{3+}_x(OH)_2]A^{n-}_{\frac{x}{n}} \cdot mH_2O$, where M^{2+} and M^{3+} are divalent and trivalent cations, respectively; x is equal to the ratio $M^{3+}/(M^{2+}+M^{3+})$ and A is an anion of divalent n (if $n = 0$ indicates that neutral layers are attracted by weak van der Waals forces and the value of x lies in the range of 0.2-0.33). The divalent and trivalent metal cations in the layers of LDH are mainly from the third and fourth periods of the periodic table and several different types of LDH could be produced with various elemental compositions. Calcination is a post-synthesis treatment usually applied to LDH to improve its sorption capacity, because it enhances the specific surface area and remove the interlayer anions and water molecules, leading to a higher number of binding sites to intercalate the molecules of interest. This work aims to evaluate the performance of calcined

LDH as sorbents for recovering phosphates from liquid synthetic matrices and optimizing operating conditions.

Methods

The LDH (Zn-Al and Mg-Al) were obtained by the coprecipitation method and then calcined at 650 °C for 4 h and milled to obtain a fine powder. These materials were characterized with respect to diverse properties, such as specific surface area, pore structure, and particle size distribution. Their structural and chemical properties were evaluated by XRD and FTIR, respectively. The sorption kinetics of phosphate on Zn-Al and Mg-Al materials was measured by batch tests for an initial phosphorus concentration of 100 mg L⁻¹ using a dosage of 10 g L⁻¹.

Results

Sorption kinetics

Investigating the phosphate sorption behavior as function of time is crucial for the successful application of LDH for removing phosphate from wastewater. The kinetic results for the particular case of calcined Mg-Al are present in Figure 1. The fitted parameters of the calcined LDH for the pseudo-first order, pseudo-second order, and Elovich models are summarized in Table 1. Based on fitting results, the model that better describes the kinetics of phosphate sorption in both materials is the pseudo-second order model. Nonetheless, the Elovich model also presents a good fitting of experimental results.

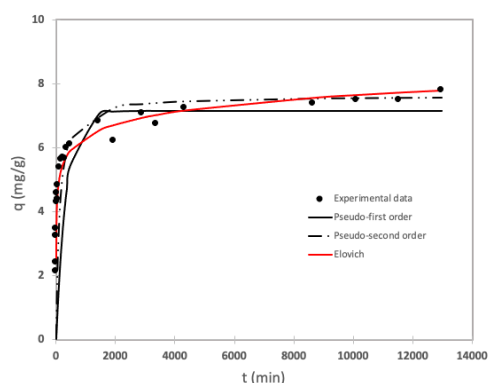


Figure 1. Kinetics studies of calcined Mg-Al LDH and fittings with pseudo-first order, pseudo-second order, and Elovich models.

Table 1. Isotherms parameters obtained for phosphate/(Zn-Al LDH) and phosphate/(Mg-Al LDH) systems.

	Mg-Al	Zn-Al
Pseudo-first order	$q_e = 7.14 \text{ mg P g}^{-1}$ $k_1 = 0.00300 \text{ h}^{-1}$ $R^2 = 0.811$	$q_e = 9.57 \text{ mg P g}^{-1}$ $k_1 = 4.00 \times 10^{-3} \text{ h}^{-1}$ $R^2 = 0.873$
Pseudo-second order	$q_e = 7.61 \text{ mg P g}^{-1}$ $k_2 = 1.26 \times 10^{-3} \text{ g mg P}^{-1} \text{ h}^{-1}$ $R^2 = 0.999$	$q_e = 9.75 \text{ mg P g}^{-1}$ $k_2 = 4.30 \times 10^{-4} \text{ g mg P}^{-1} \text{ h}^{-1}$ $R^2 = 0.995$
Elovich	$\alpha = 37.9 \text{ mg P g}^{-1} \text{ h}^{-1}$ $\beta = 1.76 \text{ g mg P}^{-1}$ $R^2 = 0.976$	$\alpha = 2.89 \text{ mg P g}^{-1} \text{ h}^{-1}$ $\beta = 1.74 \text{ g mg P}^{-1}$ $R^2 = 0.947$

Based on the Mg-Al kinetics study, the sorption process comprised two different stages. A faster sorption and approximately linear period of 2 h, which reached about 50 % of maximum uptake. After that, a slower sorption stage between 2 h and 24 h, during which the P removal increases slightly and equilibrium is reached.

Sorption isotherms

The sorption isotherms of phosphate on calcined materials were studied within an initial phosphate concentration of 100 mg L^{-1} under different LDH dosages at room temperature. As expected, the solid concentration gradually decreases with increasing dosage. The maximum sorption loadings were 31 mg g^{-1} and 107 mg g^{-1} for Mg-Al and Zn-Al LDH, respectively.

Conclusions

In this work, the kinetics and sorption capacity of calcined LDH (Mg-Al and Zn-Al) were evaluated regarding phosphorus recovery from synthetic water matrices. The LDH showed good potential for this application, while the kinetics was relatively slow. Further studies are still needed to define which mechanisms are involved in the phosphorus sorption process.

Acknowledgements

This work was partially supported by project “NATURAL- Nano-argilas para remoção/captura de fosfatos (P) e sua reutilização como fertilizante”, with the reference CENTER-01-0247-FEDER-047080, supported by Centro Portugal Regional Operational Programme (CENTRO 2020), under the Portugal 2020 (P 2020) Partnership Agreement, through the European Regional Development Fund (ERDF). Inês D. Borges acknowledges the financial support provided by the Portuguese Fundação para a Ciência e a Tecnologia (FCT) grant PD/BD/153599/2022.

References

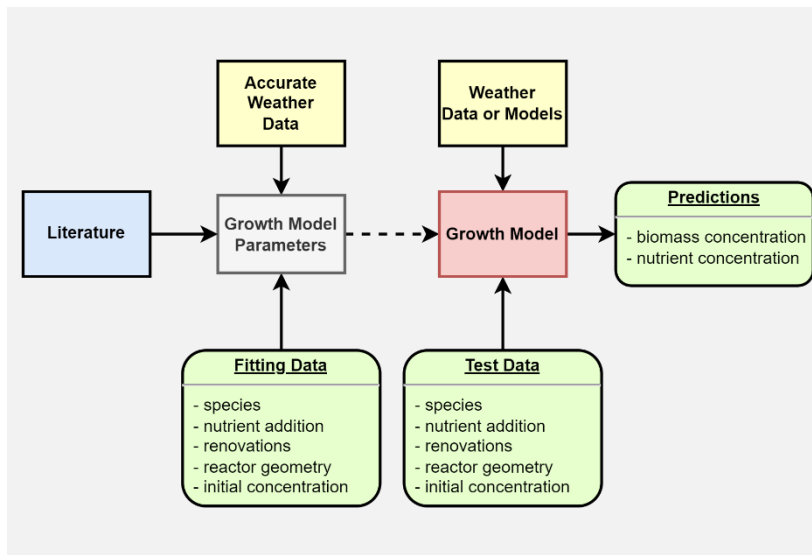
- [1] S. Daneshgar et al., Resources, 7 (2018) 37.
- [2] B. Cieřlik, P. Konieczka., Journal of Cleaner Production, 142 (2017) 1728-1740.
- [3] European Sustainable Phosphorus Platform. (n.d.). About the European Sustainable Phosphorus Platform (ESPP). Retrieved September 12, 2022, from <https://phosphorusplatform.eu/platform/about-espp>
- [4] A.F. Santos et al., Chemosphere, 284 (2021) 131258.

Static optimization and dynamic modelling of microalgae production in photobioreactors

T.M. Taborda^{1,2,3*}, J.C. Pires^{3,4}, S.M. Badenes², F. Lemos¹

¹Cerena, Instituto Superior Técnico, Av. Rovisco Pais 1, 1049-001 Lisboa, Portugal; ²A4F – Algae for Future, Campus do Lumiar, Estrada do Paço do Lumiar, Edif. E, R/C, 1649-038 Lisboa, Portugal; ³LEPABE - Laboratory for Process Engineering, Environment, Biotechnology and Energy, Faculty of Engineering, University of Porto, Rua Dr. Roberto Frias, 4200-465 Porto, Portugal; ⁴ALiCE - Associate Laboratory in Chemical Engineering, Faculty of Engineering, University of Porto, Rua Dr. Roberto Frias, 4200-465 Porto, Portugal.

*tiago.taborda@tecnico.ulisboa.pt



This work proposes a methodology for constructing models to predict the growth of microalgae in closed photobioreactors. Two models were constructed: one considering the effects of nutrients and another not considering the effect of nutrients (nitrate). The models were based on a Monod-like equation for the effect of irradiation, with the Lambert-Beer law being used to consider the effect of light inhibition inside the dense cultures. The effect of nitrate was based on the nitrogen quota model by Flynn. The models were trained on six *Nannochloropsis sp.* cultivations in three different types of reactors and compared with six other cultivations done in the same reactors. The results are promising, with R^2 above 80% for both models tested.

Introduction

Modeling of photobioreactors is of vital importance towards the production of photosynthetic microalgae biomass at an industrial scale. With such a model, it will be possible to better estimate the productivity of a given culture in different weather conditions and locations, as well as better monitor the culture. This project proposes a framework for the use of previously obtained process data to develop flexible and robust models for closed outdoor photobioreactors. The objective of this work is to create a model based on the analysis of data obtained from previous cultivations that is aimed at predicting the outcome of future cultivations (namely biomass concentration and nutrient consumption) of the same microalgae species under varying conditions, including light and nutrient concentration, and for different reactor configurations. This model can also be continuously improved based on constantly acquired data.

Methods

The microalgae species analyzed was a strain of *Nannochloropsis sp.*; cultures were carried-out in horizontal unilayer photobioreactors (UHT) and multilayer horizontal photobioreactors (MHT). Twelve assays were considered: seven in UHT reactors (assays labelled U1 and U2) and five in MHT reactors (assays labeled M1). The data used as input for the construction of the model were the biomass concentration (measured indirectly as optical density), solar irradiation, volume of the culture, nitrate concentration in the medium, temperature of the reactor, and the amount of nutrient medium added throughout the cultivation. Renovations of the medium were done periodically, where a part of the culture volume is removed and replaced by fresh medium; the volume and frequency of these medium renovations were also used as input for the model.

Two models were considered: one without the effect of nutrients (Model 1) and one with the effect of nutrients (Model 2). The effect of nutrients in Model 2 was based on the nitrogen quota

model by Flynn [2]. The models were developed using a semi-empirical approach, based on first principles equation but fitting the relevant parameters to describe the available data.

For the effect of irradiation on the culture in both Model 1 and Model 2, a Monod-like equation was chosen [1]. The effect of biomass concentration on irradiation was considered using the Lambert-Beer equation. The growth equation used for Model 1 is shown in Equation 1.

$$\mu = \mu_{\max} \frac{I \cdot \exp(-\alpha X)}{K_I + I \cdot \exp(-\alpha X)} \quad (1)$$

where X is the concentration of biomass (g L^{-1}), I is the irradiation (in $\text{MJ m}^{-2} \text{h}^{-1}$), and α is the Lambert-Beer constant (L g^{-1}). The parameters to be fitted are μ_{\max} , K_I and α .

Model 2 uses the nitrogen quota of the culture in a logistic equation where the higher the rate of carbon to nitrogen in the system, the faster the growth rate. The equation used for Model 2 is shown in Equation 2.

$$\mu = \mu_{\max} \frac{I \cdot \exp(-\alpha X)}{K_I + I \cdot \exp(-\alpha X)} \frac{1}{1 + \exp(-\beta N/C - \gamma)} \quad (2)$$

where N_{alg}/C_{alg} is nitrogen quota (the ratio of nitrogen to carbon in the cell), β (gC gN^{-1}) and γ (dimensionless) are parameters for the logistic equation for the nutrient influence.

Unlike in Model 1, the growth equation in Model 2 is used to calculate the amount of carbon in the system (C_{alg} , g L^{-1}). The mass concentration of nitrogen in the system is defined as N_{alg} (g L^{-1}). The value of N_{alg} at time t is determined from Equation 3 (using Euler's method).

$$N_{alg,t} = N_{alg,t-1} + h \frac{N_{\text{cons}} \cdot MM(N)}{N_{alg}/C_{alg}} - \delta_{ij} \frac{V_{\text{recirc}} N_{alg}}{V} \quad (3)$$

where N_{cons} is the consumption of nitrogen in the medium per nitrogen quota, per volume of medium and per hour ($\text{mol}_N \text{gN gC}^{-1} \text{h}^{-1} \text{L}^{-1}$), $MM(N)$ is the atomic mass of nitrogen (14 g mol^{-1}), V

is the total volume of the system (L), V_{recirc} is the volume recirculated in time period j , δ is the Kronecker delta, i is a discrete variable with all the periods considered in the integration, j is a discrete variable with all the periods where a renovation occurred and h is the step for Euler's method.

The value of the concentration of nutrients in the medium, S (mol L^{-1}), at time t , is calculated by Equation 4 using Euler's method.

$$S_t = S_{t-1} + h \frac{-N_{cons}}{N_{alg}/C_{alg}} - \frac{\delta_{ij} V_{recirc} S + \delta_{i,k} Q}{V} \quad (4)$$

where Q (mol) is the addition of nutrients in time period k and k is a discrete variable with all the periods where nutrient addition occurred.

The dry cell weight is estimated using the empirical chemical formula for *Nannochloropsis salina* ($\text{CN}_{0.125}\text{O}_{0.275}\text{H}_{1.82}\text{P}_{0.014}\text{S}_{0.002}$ [3]). It's assumed that the amount of elements other than carbon and nitrogen remain constant in relation to the amount of carbon. The amount of nitrogen varies independently of the others. The models were trained on six of the twelve assays (named fitting assays) using the Solver add-on in MS Excel; the model was then used with those same parameters on the other six (named test assays). There is a total of 232 data points in the fitting assays and 243 data points in the test assays.

Results and Discussion

The values obtained for the parameters from the fitting of the models to the data are:

- Model 1: $\mu_{max}=0.074 \text{ h}^{-1}$; $K_I=1.26 \text{ MJ m}^{-2} \text{ h}^{-1}$; $\alpha=1.717 \text{ m}^3 \text{ kg}^{-1}$.
- Model 2: $\mu_{max}=0.085 \text{ h}^{-1}$; $K_I=1.83 \text{ MJ m}^{-2} \text{ h}^{-1}$; $\alpha=1.287 \text{ m}^3 \text{ kg}^{-1}$; $N_{cons}=0.0066 \text{ mol}_N \text{ g}_N \text{ gC}^{-1} \text{ h}^{-1} \text{ L}^{-1}$; $\beta=26.278 \text{ gC gN}^{-1}$; $\gamma=-2.651$.

The fitting of both models for one of the fitting assays (labelled M1-3) is shown in the Figure 1.

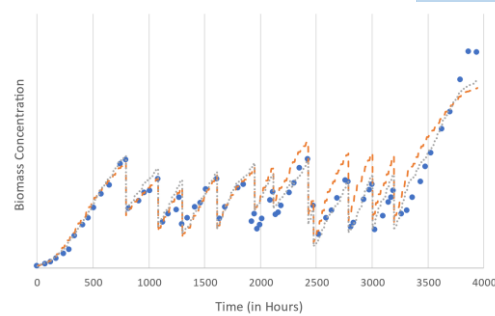


Figure 1. Measured (symbols), fitted by Model 1 (dashed line) and fitted by Model 2 (dotted line) dry cell weight for the *Nannochloropsis sp.* assay labelled M1-3. The sudden drops in measured dry cell weight correspond to renovations of the culture, where a significant portion is removed and replaced with fresh medium.

Table 1 contains the R^2 for all the assays tested for both models. Model 1 had a global coefficient of determination (R^2) of 83.0% while Model 2 had a global R^2 of 89.0% on the same data. These values are high and show both models fit the data well. However, the results of the test assays are not as good, with several assays even having negative R^2 (which means the model is worse at predicting the data points than the average value of the data of that assay). The M1-1 assay in particular has a low R^2 for both models, which implies there is a problem with the assay itself. Although Model 2 has another assay with a negative R^2 (U1-4), it is also able to predict the U1-1 assay much better than Model 1. To compare both models, the AIC (Akaike information criterion) was calculated [4]. Model 1 had an ΔAIC of -678, while Model 2 had an ΔAIC of -779. Therefore, Model 2 is a better model at fitting the data than Model 1.

Conclusions and Future Work

From analysis of the values of R^2 for the fitting assays, it can be concluded that Model 2 has overall a better fitting. The lower AIC for Model 2 implies it is a better model than Model 1. However, Model 1 might be a better option if the nutrient consumption is not necessary to explain the behavior of the culture. The results from the test assays are inconclusive.

Future work involves correlating these models with other cultivations of the same species to determine their validity, analyzing cultivations of different species, and applying these models to real life cultivations in similar photobioreactor configurations.

Table 1. Table with the obtained Coefficients of Determination for each of the assays.

Models \ Assays	Fitting Assays						Test Assays					
	M1-2	M1-3	U1-2	U1-3	U2-1	U2-3	M1-1	M1-4	M1-5	U1-1	U1-4	U2-2
Model 1	97.0%	78.1%	93.0%	93.5%	76.9%	84.6%	-211.7%	77.6%	84.8%	31.3%	85.8%	86.4%
Model 2	92.0%	86.8%	93.8%	97.8%	84.0%	92.7%	40.7%	75.4%	72.1%	68.2%	-3.0%	88.1%

Acknowledgements

This project was financially supported by FCT (Fundação para a Ciência e Tecnologia) with the PhD grant SFRH/BD/151226/2021. The author wishes to thank CERENA, Lepabe and A4F – Algae for Future for their support in this project.

References

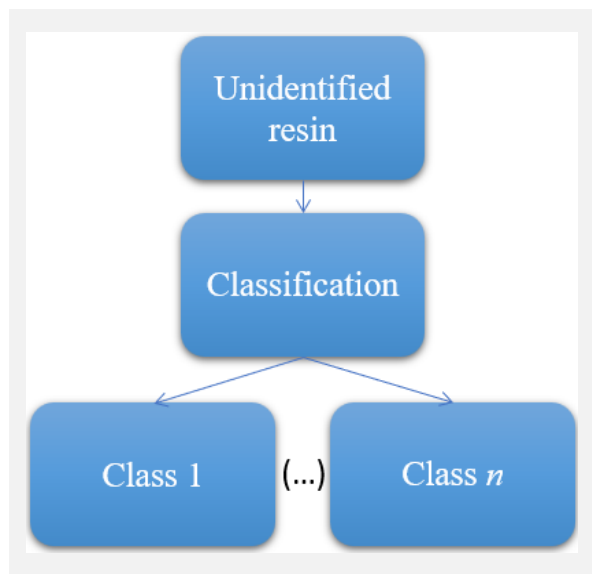
- [1] P. Darvehei et al., Renewable and Sustainable Energy Reviews, 97 (2018) 233-258.
- [2] K. Flynn, "Enhancing Microalgal Production - constructing decision support tools using system dynamics modelling", Zenodo, 2021.
- [3] M.C. Picardo et al., Clean Technologies and Environmental Policy, 15 (2013) 275-291.
- [4] K.P. Burnham & D.R. Anderson, "Model Selection and Inference.", Springer, New York, 1998, 75-117.

Multi-class classification of melamine content in industrial formaldehyde-based resins using NIR spectroscopy and machine learning

R. Magalhães^{1,2,3}, N.T. Paiva⁴, F.D. Magalhães^{1,2}, F.G. Martins^{1,2*}

¹LEPABE - Laboratory for Process Engineering, Environment, Biotechnology and Energy, Faculty of Engineering, University of Porto, Rua Dr. Roberto Frias, 4200-465 Porto, Portugal; ²ALiCE - Associate Laboratory in Chemical Engineering, Faculty of Engineering, University of Porto, Rua Dr. Roberto Frias, 4200-465 Porto, Portugal; ³EuroResinas - Indústrias Químicas, 7520-195 Sines, Portugal; ⁴Sonae Arauco Portugal S.A., 4470-177 Porto, Portugal.

*fgm@fe.up.pt



This study implements Near-Infrared (NIR) spectroscopy and Python's Scikit-learn library to classify formaldehyde-based resins with varying melamine content. NIR spectroscopy is a non-destructive analytical technique that determines the chemical composition of a sample by measuring light absorption in the NIR region. Scikit-learn is a popular Python machine learning library for classification, regression, and clustering.

The models were developed using a dataset of 2119 spectra from industrial samples of formaldehyde-based resins with varying melamine contents in the range 0 to 18 % (m/m).

The study observed that resins with 0 % melamine were easier to distinguish from those with melamine. In models that did not achieve 100 % accuracy, misclassifications were observed in only a few cases, typically for samples containing more than 5 % melamine. The best models achieved 100 % accuracy in both calibration and test samples. The developed models are particularly useful for process control and optimization in the wood-based panel industry.

Introduction

Formaldehyde-based resins, such as urea-formaldehyde (UF), melamine-formaldehyde (MF), and melamine-urea-formaldehyde (MUF), are primarily used in the wood-based panel (WBP) industry [1]. MUF resins are an intermediate polymer that combines the performance and cost benefits of UF and MF resins. Melamine, with its more stable molecular structure, outperforms urea in terms of water resistance and formaldehyde emissions. Because the resin is the most expensive component of wood-based products, lowering the melamine content (the costliest component in the resin), is critical for optimizing MUF resin economic competitiveness [2]. Standard industrial methods for evaluating the quality of amino resins include analyzing properties such as pH, viscosity, density, solid content, and melamine content, which are indicators of the resin's performance. Methods supported in NIR (near infrared) spectra can be developed as an alternative to standard testing methods. NIR spectroscopy requires little sample preparation and is primarily an indirect analytical technique, requiring calibration with samples of known composition determined by using standard methods. In the field related to formaldehyde-based resins, few studies on classification and melamine determination have been published. Previous research using NIR spectroscopy and chemometric methods to classify resins and predict melamine content yielded promising results [3-5]. In this study, new NIR-based methods are proposed for correctly classifying an unidentified resin from industrial samples containing up to 18 % (m/m) melamine.

Materials and Methods

NIR spectra of industrial samples of formaldehyde-based resins were provided by EuroResinas.

Scikit-learn, a Python library, was used to develop the proposed chemometric models. The Jupyter notebook environment was used to process the data.

The samples were divided into calibration and test sets, and various models were fitted to them, such as logistic regression (LR), k-nearest neighbors (KNN) and support vector machines (SVM).

The models were tuned by adjusting the most relevant hyperparameters. These are parameters that are optimized during the model's development for avoiding underfitting or overfitting phenomena and thus to select the best model during the calibration step.

Choosing the right hyperparameters for a given machine learning task typically involves a systematic search in a range of values for the set of hyperparameters, to achieve the best performance index during the calibration step.

Finally, predictions were made on the test set using the best-performing model as a final check. The obtained results demonstrate the utility of scikit-learn library and Python in the development of chemometric models for the classification of formaldehyde-based resins containing up to 18 % (m/m) melamine. The models developed in this study can be used to predict the melamine range of new samples and can be used in process control and optimization.

Results and discussion

Industrial samples of resins with melamine contents up to 18 % (m/m) were studied. A dataset containing 2119 spectra was splitted in a calibration set – used to develop the models – and a test set containing ≈ 33 % of the samples – used for the final performance check of the models.

Following are three cases in which samples were separated based on their melamine content.

As shown in Table 1, the samples in Case #1 were divided into those with and without melamine.

Table 1. Resin classes in Case #1.

Class	Melamine Range	Full Dataset	Spectra on Test set
A	0 %	548	187
B]0-18 %]	1571	513

Three models were fitted to them: logistic regression (LR), k-nearest neighbors (KNN) and support vector machines (SVM). GridSearchCV was used for model tuning. GridSearchCV is a hyperparameter tuning function that searches the best hyperparameters through a cross-validation procedure (5-fold). For example, for a support vector machine (SVM) model, a grid of values for the regularization parameter C was created. The GridSearchCV algorithm then evaluates the SVM model for C with the best performance in terms of accuracy, defined as the ratio of correctly identified samples to the total number of samples in the dataset.

In Case #1, all the models achieved 100 % correct classification on the calibration and test sets.

The samples in Case #2 were divided into three classes based on their melamine content, as shown in Table 2.

Table 2. Resin classes in Case #2.

Class	Melamine Range	Full Dataset	Spectra on Test set
A	0 %	548	187
B]0-5 %]	1343	436
C]5-18 %]	228	77

The best KNN and SVM models in this case achieved 100 % correct classification on the calibration and test sets. In the case of Logistic Regression, the best model achieved 99.9 % accuracy since misclassified one sample on test set.

Table 3 shows how the samples in Case #3 were classified into four classes based on their melamine content.

Table 3. Resin classes in Case #3.

Class	Melamine Range	Full Dataset	Spectra on Test set
A	0 %	548	187
B]0-5 %]	1343	436
C]5-10 %]	95	30
D]10-18 %]	133	47

In this case, the best LR model misclassified 11 samples (98.4 % accuracy) on test set, the best KNN model misclassified 4 samples (99.4 % accuracy) on test set and the best SVM model achieved 100 % correct classification for a regularization parameter of $C = 9.0$

of Logistic Regression, the best model achieved 99.9 % accuracy since misclassified one sample on test set.

Acknowledgements

This work was financially supported by LA/P/0045/2020 (ALiCE), UIDB/00511/2020 and UIDP/00511/2020 (LEPABE), funded by national funds through FCT/MCTES (PIDDAC). Roberto Magalhães thanks the individual research grant SFRH/BD/151225/2021, funded by the Portuguese Foundation for Science and Technology (FCT). The authors kindly acknowledge EuroResinas - Indústrias Químicas and Sonae Arauco Portugal S.A. for support with data, equipment, and materials.

References

- [1] C. Gonçalves et al., *Holzforschung*, 72 (2018) 653-671.
- [2] J. Zhang et al. *Bioresources*, 8 (2013) 5500-5514.
- [3] M. Gonçalves et al., *Journal of near Infrared Spectroscopy*, 27 (2019) 345-353.
- [4] M. Gonçalves et al., *International Journal of Adhesion and Adhesives*, 93 (2019) 102327.
- [5] A. Henriques et al., *Wood Science and Technology*, 47 (2013) 939-948.
- [6] European Standard EN 312:2011 - Particleboards – Specifications.

Table 3 shows how the samples in Case #3 were classified into four classes based on their melamine content.

Gonçalves et al. (2019) [3] reported 96.1 % accuracy using KNN classification of several classes of resins in the range 8-19 %.

Figure 1 depicts the optimal value of $C=9.0$ for the SVM model proposed in this study for the Case #3. The standard deviation of the cross-validation score at each value of C was considered and it is shown in the shadowed area. If the standard deviation is high, it indicates that the model's performance is sensitive to the training and validation splits used in the cross-validation procedure. For C values equal or greater than 9.0, 100 % accuracy is obtained in this dataset.

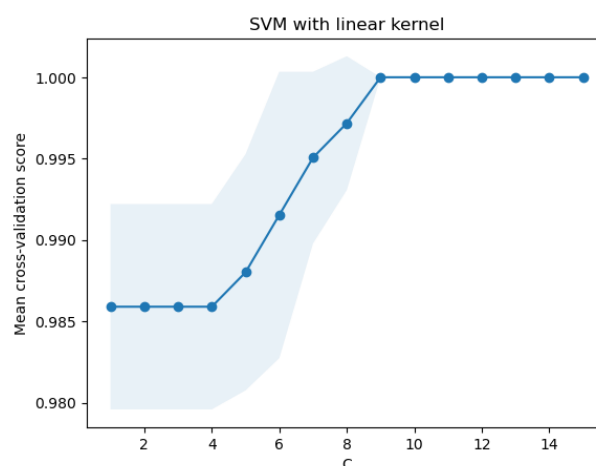


Figure 1. Effect of regularization parameter C on SVM model.

These three cases were identified as the most practical categorization for industrial applications in WBP production. EN312 standard [6] defines several usage classes for panels. For Case #3, class B resins are primarily used for P2 panels that will be used in dry conditions. Class C resins are typically required for P3 panels that will be exposed to wet conditions. Finally, class D resins are required for P5 panels, which are used in wet conditions and as load-bearing or stiffening building elements.

Conclusions

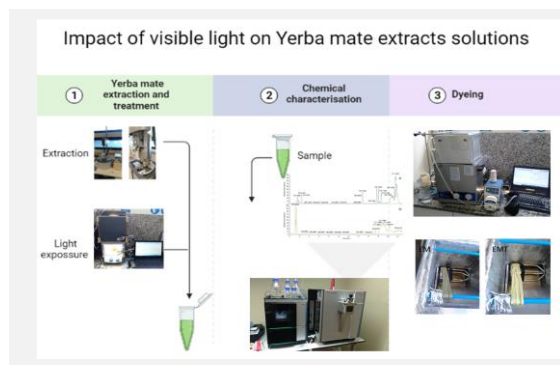
NIR spectroscopy and chemometric techniques were used to develop classification models able to categorize resins containing melamine in concentrations ranging from 0 % to 18 % into two to four distinct classes. The most effective models, which were based on support vector machines (SVM), achieved 100% correct classification in a test set of unknown resins. These models outperformed previously reported literature results.

Impact of visible light on natural textile dyes obtained from Yerba mate (*Ilex paraguariensis*)

J. Santos^{1,2,3*}, S. Oliveira¹, B. Freitas¹, R.A. Fernandes^{1,2,3}, S. Monteiro^{1,2,3}, P. Magalhães⁴, F.D. Magalhães^{2,3}, J.M. Martins^{2,3,5}, L.H. Carvalho^{2,3,5}

¹ARCP-Associação Rede de Competência em Polímeros, 4200-355 Porto, Portugal; ²LEPABE - Faculty of Engineering, University of Porto, Rua Dr. Roberto Frias, s/n 4200-465 Porto, Portugal; ³ALiCE - Associate Laboratory in Chemical Engineering, Faculty of Engineering, University of Porto, Rua Dr. Roberto Frias, 4200-465 Porto, Portugal; ⁴Tintex Textiles SA, Zona Industrial, Polo I, Campos, 4924-909 Vila Nova de Cerveira, Portugal; ⁵DEMad-Department of Wood Engineering, Instituto Politécnico de Viseu, Campus Politécnico de Repeses, 3504-510 Viseu, Portugal.

*jorge.ucha@arcp.pt



The use of natural dyes obtained from biological sources is a good alternative to reduce the environmental impact of the textile industry. This approach is even more interesting when the natural dyes are obtainable from by-products of industrial processes. However, colour fastness to light is a major challenge in the industrial application of most natural dyes. This work aims to study the chemical changes produced by a white light lamp on yerba mate (*Ilex paraguariensis*) extracts. The impact of light on the phenolic content and on the antioxidant activity was evaluated. In addition, the chemical changes were evaluated by FTIR-ATR and HPLC-MS. The changes in the colour properties of the extract solution were monitored by UV-Vis spectroscopy.

Introduction

Yerba mate (*Ilex paraguariensis*) has been commonly used to prepare tea-like beverages in Argentina, Paraguay, Uruguay, and southern Brazil. Its extracts are composed mainly of polyphenolic compounds (chlorogenic acid) and xanthines (caffeine and theobromine) [1]. Due to its properties, the leaves and branches of yerba mate are also used industrially in producing energy drinks, beers, soft drinks, and liqueurs. In addition, they also have interesting applications in other industries, like the production of functional foods, or natural antioxidant additives, or in the cosmetic or pharmaceutical industries [2]. During the industrial production process of yerba mate-based products, large quantities of by-products are generated [1], which creates an opportunity for investigating their valorisation routes. One example is to use these by-products as raw materials to obtain extracts that could be used as dyes in the textile industry [3,4]. However, one of the properties that will influence the industrial applicability of a natural dye is colour fastness to light of the resulting textile products. This work aims to study the chemical changes produced by a white light lamp on a yerba mate (*Ilex paraguariensis*) extract solution. The impact of light on the phenolic content and the antioxidant activity was evaluated. In addition, the chemical changes were evaluated by FTIR-ATR and HPLC-MS. The changes in the colour properties of the extract solution were monitored by UV-Vis spectroscopy.

Methods. *Extraction.* The extraction experiments were performed in a 4 l Pyrex glass reactor with mechanical stirring and temperature control. Solid/liquid ratio was fixed at 1/10 (w/w) for all the extraction experiments. Aqueous solutions of sodium hydroxide were used as extraction agent and the selected temperature was 60 °C. The extract was dried in a laboratory scale Spray dryer SD-60 (Labplant, UK).

Total phenolic content. Total phenolic content was determined by the Folin-Ciocalteu method. The phenolic content was calculated as a gallic acid equivalent from the calibration curve of gallic acid standard solutions (2–40 µg/ml). Results were

expressed as mass of gallic acid equivalent (g) (GAE)/100 g of extract (on dry basis).

Antioxidant activity. The antioxidant activity of the extracts was determined by the FRAP (ferric reducing/antioxidant power) assay. The relative antioxidant activity of the Yerba mate extracts was calculated from the calibration curve of L-ascorbic acid (0.1–0.2–0.3–0.4–0.5–0.6 mmol/l), and the results were expressed as nmol of ascorbic acid equivalent (AAE) per mg of EM extract (on dry basis).

Fourier Transform Infrared Spectroscopy (FTIR) assay. FTIR spectra were recorded on a VERTEX 70 FTIR spectrometer (BRUKER, Billerica, MA, USA) equipped with a high sensitivity DLATGS detector at room temperature. Samples were measured in ATR mode, with an A225/Q PLATINUM ATR Diamond crystal with a single reflection accessory. The spectra were recorded from 4000 to 400 cm⁻¹ with a resolution of 4 cm⁻¹.

LC-ESI-LTQ-Orbitrap-MS analyses. Liquid chromatography (LC) analysis was conducted using a Vanquish HPLC (Thermo Scientific). Chromatographic separation was performed in an Atlantis T3 column 2.1 × 100 mm, 3µm (Waters, Milford, MA, USA). The LC equipment was coupled to an Orbitrap Exploris 120.

Dyeing Process. The dyeing of the cotton samples was carried out using a water solution of the extracts of Yerba mate treated (with light) and untreated as dyes, with a liquor ratio of 1/15 (mass of dry textile product/mass of dyeing solution). Samples were dyed in laboratory dyeing equipment. Cotton knit samples of 5±0.5 g were mixed with the dyeing liquor (2% g dry extract/g textile sample). Once the dyeing stage was finished, the dyed textile samples were washed first with cold water, then, with water at 40±5 °C and Cottoblanco STM (CHT, Tübingen, Germany) as a soap agent, and, finally, with cold water.

Monitoring of Light impact by UV-VIS Spectroscopy. The impact of the light (LED A67;2000 Lm (6400 K), Aigostar) in the EM extracts solutions was characterized using a FLEX-STD-UV-Vis (IS) 25 µm spectrometer (Sarspec, Vila Nova de

Gaia, Portugal) with light source LS-DW (Deuterium Tungsten), an a transmission probe with 400 μm core diameter fibres and 200 cm stainless steel (Sarspec, Vila Nova de Gaia, Portugal).

Results and Discussion

The impact of light exposure on the Yerba mate extracts solutions properties was evaluated (Table 1).

Table 1. Impact of light on Yerba mate extract properties.

Samples	Total phenols content (g GAE/100 g extract)	Antioxidant activity (nmol AAE/mg EM dry extract)
EM	47.04 \pm 4.68	1095.6 \pm 60.9
EMT	28.98 \pm 2.27	101.1 \pm 5.9

Regarding the values obtained, a high impact of light on the antioxidant activity of the extract solutions was demonstrated. Furthermore, the phenolic content also decreased, showing that some phenolic compounds were degraded in the process. The impact of light exposure on the Yerba mate extract solution was monitored by UV-Vis spectroscopy and the obtained spectra are shown in Figure 1.

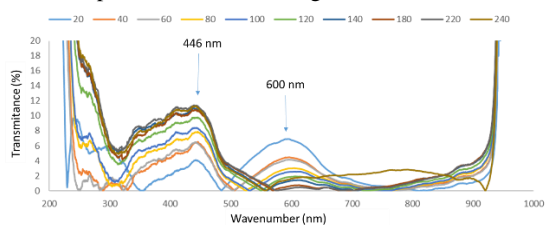


Figure 1. Monitoring by UV-Vis of light impact on yerba mate extract solution at (20-240 min).

The changes observed in the UV-VIS spectra allowed us to follow the degradation process of the Yerba Mate extracts by light. FTIR-ATR spectroscopy was used to study the chemical changes (Figure 2).

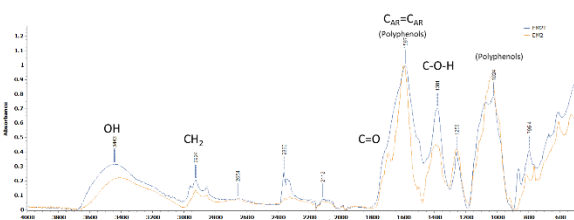


Figure 2. FTIR spectra of dry extracts of Yerba mate (400-4000 cm^{-1}) before (EM) and after (EMT) exposure to light.

By the FTIR-ATR analysis, changes in the characteristic bands of the presence of phenolic compounds were detected due to light treatment. To complete the study HPLC-MS of Yerba Mate extracts before (EM) and after the light treatment (EMT) was done (Figure 3).

Acknowledgements

The authors gratefully acknowledge the funding by: LA/P/0045/2020 (ALICE) and UIDB/00511/2020—UIDP/00511/2020 (LEPABE) funded by national funds through FCT/MCTES (PIDDAC); This work was supported by the Integrated Project Be@t – Textile Bioeconomy, to strengthen the National Bioeconomy, financed by the Environmental Fund through Component 12 – Promotion of Sustainable Bioeconomy (Investment TC-C12-i01 – Sustainable Bioeconomy No. 02/C12-i01/202), of European funds allocated to Portugal by the Recovery and Resilience Plan (RRP), within the scope of the European Union (EU) Recovery and Resilience Mechanism, framed in the Next Generation EU, for the period 2021 – 2026.

References

- [1] B. Gullón et al., *Industrial Crops and Products*, 113 (2018) 398-405.
- [2] C.P. Croge et al., *Scientia Agricola*, 78 (2021) e20190259.
- [3] F. Giacomini et al., *Textile Research Journal*, 87 (2017) 829-837.
- [4] H. Ja et al., *Journal of the Korean Society of Clothing and Textiles*, 36 (2012) 412-421.

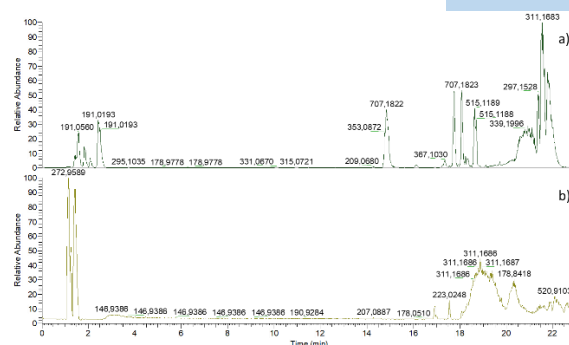


Figure 3. Base peak chromatogram of Yerba Mate extracts: a) before (EM) and b) after the light treatment (EMT).

The HPLC-MS assay confirms the observed changes in the chemical composition of the extracts due to exposure to light. The chlorogenic acids present in the Yerba mate extract are highly sensitive to light exposure.

Finally, both extracts were used to dye cotton textile samples and the impact of light exposure on the colour of the dyed cotton fabric was evaluated (Figure 4).



Figure 4. Cotton textile samples dyed with Yerba Mate extract before (EM) and b) after the light treatment (EMT).

The colour of the cotton samples dyed with the two extracts of Yerba mate EM and EMT and their colour fastness to light were evaluated.

Table 2. Colour coordinates (CIELab) of Cotton samples dyed with EM and EMT and colour fastness to light assessed by colour change.

Samples	L*	a*	b*	$\Delta\text{E}_{\text{cmc}}^{\text{1}}$
EM	67.59 \pm 1.3	-3.38 \pm 0.2	14.14 \pm 1.0	4.39 \pm 0.2
EMT	74.88 \pm 0.9	4.08 \pm 0.6.	18.02 \pm 0.8.	3.17 \pm 0.1

*1 $\Delta\text{E}_{\text{cmc}}$: Colour changes in the dyed cotton samples colour due to 1-week light exposure.

Conclusions

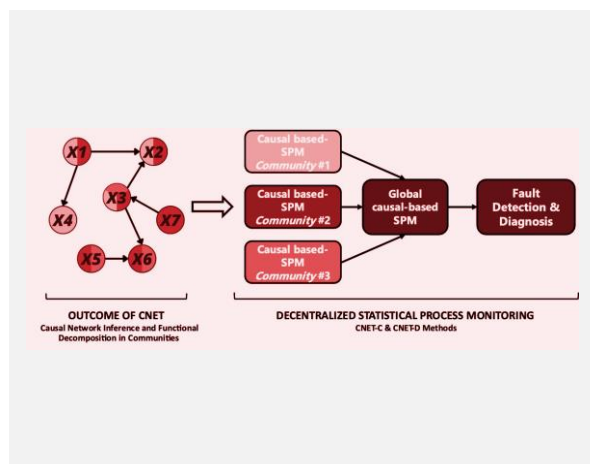
The light treatment carried out on the Yerba mate extract had a high impact on the colour of dyed cotton textile samples and on their colour fastness to light. It was confirmed that the chemical changes observed in the extracts (mainly in the polyphenolic components) affected their properties as a textile dye.

Decentralized process monitoring: unlocking causal insights for enhanced fault detection and diagnosis

R. Paredes, M.S. Reis*

University of Coimbra, CIEPQPF, Department of Chemical Engineering, Rua Silvio Lima, Pólo II – Pinhal de Marrocos, 3030-790 Coimbra, Portugal.

*marco@eq.uc.pt



As data collection systems continue to expand, Multivariate Statistical Process Monitoring (SPM) methods must evolve to maintain their ability to detect localized faults. We introduce a novel method for decentralized SPM by breaking down its causal network into functional modules. Our approach involves inferring the causal network from normal operating data, identifying strongly connected variables as communities, and extending them with the relevant Markov blankets to account both for micro- and macro-causality. We propose two alternative hierarchical monitoring schemes for distributed monitoring: Causal Network-Centralized (CNET-C) and Causal Network-Distributed (CNET-D). Our results show that CNET is more effective at detecting faults than conventional non-causal methods and centralized causal methods. Moreover, it leads to more conclusive and unambiguous fault diagnosis.

Introduction

Causal networks contain valuable information about the causal connections between process variables. However, current Statistical Process Monitoring (SPM) methodologies, including those based on Principal Component Analysis (PCA), Partial Least Squares (PLS), and Independent Component Analysis (ICA), do not take causality into account. This reduces the fault detection sensitivity and the diagnosis capability due to the “smearing-out”. Causal SPM methodologies, like Sensitivity Enhancing Transformation (SET) [1], uses causality to identify the propagation path, increasing fault diagnosis capabilities. However, these methods lose sensitivity as process dimensionality increases. Decentralized monitoring groups process variables into modules for local monitoring. To combine the benefits of both causal and decentralized monitoring, we propose two hierarchical monitoring schemes based on community detection of closely related variables. Community detection algorithms evaluate network topology and association density to identify communities. By monitoring at the community level, the proposed methodologies become more sensitive to localized faults, while retaining the benefits of causal-based methods for enhancing fault diagnosis.

Causal Network SPM: CNET

Two Causal Network SPM schemes are presented: Causal Network-Centralized (CNET-C) and Causal Network-Distributed (CNET-D). Both methods start by inferring the causal graph using partial correlations and determining causality directions through cross-correlation or Granger causality analysis. Variables are then subdivided into communities based on topology and edge density, with each community expanded to include the Markov-blanket of each causal parent (Figure 1). Then the SET-SPM methodology [1] is implemented for each community. It essentially consists of first computing a whitening filter by regressing variables onto their causal parents. This filtering operation produces causally decorrelated variables, which are monitored by a Hotelling's T^2 statistic. In CNET-D, the T^2 statistics are aggregated through an “OR” gate, and a

global alarm is triggered if at least one community detects an abnormality. In CNET-C, all T^2 statistics are concatenated to build a single monitoring statistic, triggering a global alarm if it exceeds its control limit.

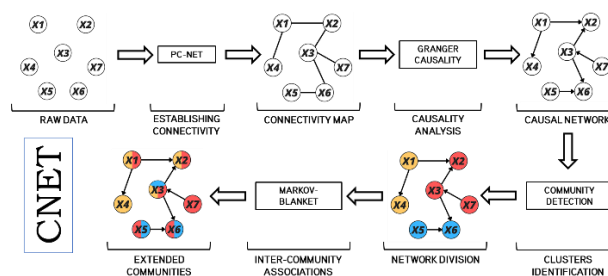


Figure 1. Representation of the main steps of CNET.

Fault diagnosis occurs in two levels: identifying *communities* with abnormalities in the first level and identifying *variables* within those communities that may be the origin of such behavior, in the second level. The CNET-D methodology carries out fault detection directly at the community level by observing which communities triggered an alarm in the logical “OR” gate. On the other hand, the first diagnosis level in CNET-C methodology assesses the contributions of each community to the statistic. After identifying the abnormal communities, in the second diagnosis level one evaluates the contribution of each variable to the T^2 statistics of the abnormal communities. The contribution of each variable is compared against a control limit to determine if it is a candidate for the fault's root cause.

Results

To establish the performance of the causal network inference and the proposed distributed monitoring methodologies in a rigorous way, we performed a Monte Carlo simulation study (100 replicates). In this way, the relevant quantities under analysis (network structure, type of fault, fault time, fault magnitude, root-cause, level of noise, etc.) are known and controlled, enabling the precise computation of performance metrics based on the ground truth. This approach is preferable

when proposing a new methodology, where the priority is to characterize the statistical properties of the method in well-defined testing scenarios. We tested the proposed approach in several scenarios with an artificial network system composed of 16 nodes to generate normal operating conditions (NOC) and faulty data [2]; see Figure 2. Both static and dynamic linear models were contemplated. Furthermore, the causal network was divided into 3 communities using an algorithm based on network density and topology. All monitoring methodologies were trained on a NOC dataset with 5000 observations and were set for an overall false alarm rate of $\alpha=0.01$. For each monitoring scheme, the significance level of its control limits was adjusted with the Šidák correction.

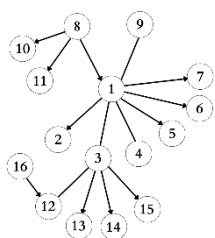


Figure 2. Graphical representation of the causal structure for the artificial network system.

Figure 3 shows one of the fault detection sensitivity studies (True Positive Rate, TPR, *versus* Fault Magnitude) of the proposed methodologies against two benchmark methodologies (SET-Hotelling- T^2 and PCA) for a process fault in variable 1. This figure clearly shows that CNET-C and CNET-D have consistently significantly higher TPR than the benchmarks. This improvement is a result of the functional decomposition into communities as it increases the sensitivity to localized faults.

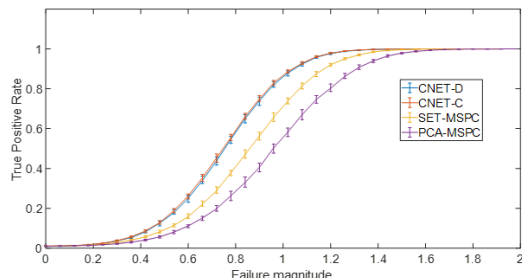


Figure 3. Median of the true positive rate and interquartile range for a simulated process fault in variable X_1 .

To demonstrate the fault diagnosis capabilities of the proposed methodologies, a process fault in variable 1 with a failure magnitude of 1 standard deviation was simulated. Fault diagnosis was performed with contribution plots for PCA [3] and the contributions to the SET-Hotelling- T^2 [1]. In Figure 4, the root cause diagnosis for the PCA-MSPC benchmark is graphically represented. Figure 5 shows the two diagnostic levels of the proposed CNET-C methodology. For this case, only SET-Hotelling- T^2 and CNET-C (as well as CNET-D) provide an unambiguous diagnosis, correctly identifying variable 1 in all replicates.

Acknowledgements

Rodrigo Paredes is supported by the doctoral Grant (PRT/BD/154267/2022) financed by the Portuguese Foundation for Science and Technology (FCT), and with funds from POR Centro - Portugal 2020, under MIT Portugal Program. The authors also acknowledge the support of Portuguese FCT, through the project with reference UIDB/00102/2020.

References

- [1] T.J. Rato, M.S. Reis, *Chemical Engineering Science*, 163 (2017) 223-233.
- [2] T.J. Rato, M.S. Reis, *Computers & Chemical Engineering*, 71 (2014) 307-322.
- [3] S.J. Qin et al., *Journal of Chemometrics*, 15 (2001) 715-742.

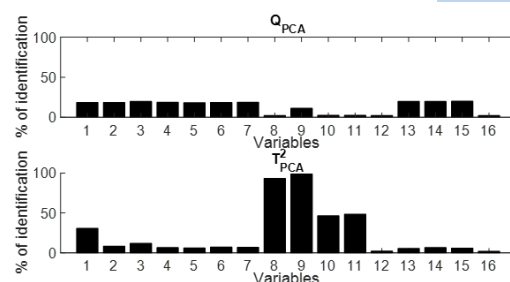


Figure 4. Percentage of times that each variable is significant in the PCA-based methodology. Process fault in variable 1 with a magnitude of 1 standard deviation.

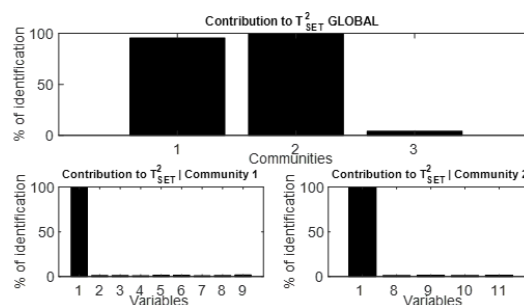


Figure 5. Percentage of times a community is significant: for the CNET-C methodology monitoring statistic (first diagnostic level; on top), and for each community's T^2 monitoring statistic (second diagnostic level; on bottom). Process fault in variable 1 with a magnitude of 1 standard deviation.

Conclusions

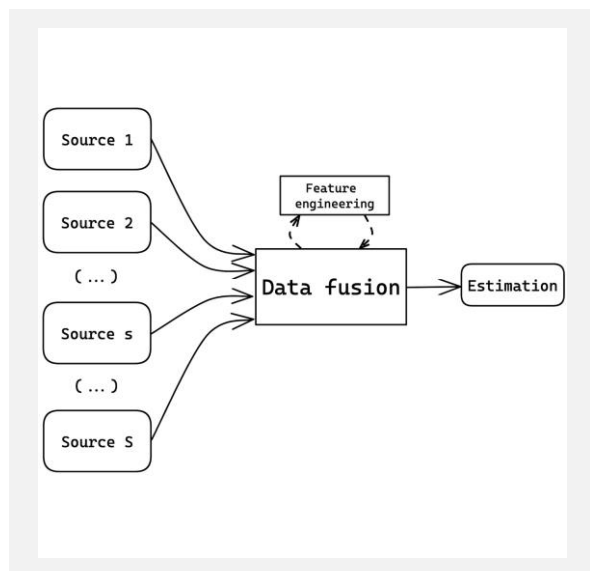
Causal networks contain information about systems that is typically not used by standard SPM methodologies. These networks can be inferred based on observational data, using methods such as Granger causality. In this work, we present a methodology that extends the benefits of causal-based monitoring methods to the distributed SPM arena. Our methodology consists of performing inference of the causal network and the identification of extended communities through CNET, after which two hierarchical distributed monitoring methodologies can be used, CNET-C and CNET-D. The main difference between these methodologies lies in how monitoring information generated at the sub-block level can be aggregated to provide a decision about the process status. The proposed causal network functional decomposition into several communities reduces the dimensionality of the monitoring system from the overall system to meaningful sub-blocks, which increases the sensitivity to localized faults. In addition, the extension to the Markov-blankets of the causal parents from each community accommodates the inter-community associations in the models. The proposed methods were tested, and their fault detection and diagnosis performance were analyzed against two benchmark methodologies, PCA-MSPC and SET-MSPC. For all types of faults (process perturbations, sensor faults, correlation changes), causal-based methods presented better detection sensitivity. The fault diagnosis was also less unambiguous and clearly more informative when compared to correlation-based methods.

Multimodal data fusion in the chemical processing industry: a new methodology and case studies

E. Strelet¹, I. Castillo², Y. Peng², R. Rendall², B. Braun², L. Chiang², M.S. Reis^{1*}

¹Univ Coimbra, CIEPQPF, Department of Chemical Engineering, Rua Sílvia Lima, Pólo II – Pinhal de Marrocos, 3030-790, Portugal; ²The Dow Chemical Company, Lake Jackson, USA.

*marco@eq.uc.pt



With the rise of Industry 4.0 and the technological boom, industrial plants have access to a wide range of sensor technology. However, this also means that there is an abundance of data from different sources, which can make data processing and integration quite complex. To effectively estimate the state of a given process, data fusion can be used to combine information from various sources and achieve a more accurate and robust estimate. We propose a new data fusion methodology, Regularized Bayesian fusion (RegBF), that handles multiple heterogeneous sources to estimate a parameter of interest. The proposed method also takes into account the quality of each source. The performance of RegBF was assessed in two case studies, one simulated and another real. The results confirm that the method can effectively estimate the parameter of interest and maintain good performance even when there is a lack of more accurate sources.

Introduction

The technological boom of the last decades provided conditions for sensors diversification and their growing number. A wide spectrum of sensor technology is currently available in industrial settings, providing data with different structures and formats. Examples include classical sensors (pressure, temperature, flow, pH, conductivity, etc.); process analytical technology (PAT) (such as Raman spectroscopy, near-infrared spectra (NIR), nuclear magnetic resonance (NMR), chromatography); surface profilometry; grey-level images; color and hyperspectral images; hyphenated instruments; among others. These examples include scalar sensors, as well as first-, second-, and high-order tensorial data structures, creating in this way complex Big Data environments.

By variety of sources it is meant heterogeneity in data characteristics. As was defined by Goh [1], data heterogeneity is "different ways in which data is organized or interpreted in disparate system". This characteristic is intrinsic to all kinds of systems due to various reasons as different scales, accuracies, granularity, data structure, acquisition rate, modality, etc. [2]. Data collected also present additional complexity features, such as noise, outliers, sensor drift, and degradation - that increase its uncertainty - as well as missing values, etc.

Data fusion methods synergistically combine data from various sources into more accurate and complete estimation [3]. However, the poor quality of its data sources can jeopardize its performance. Despite the appealing advantages of the data fusion methods, they have an Achilles' heel. All data-driven methods follow the garbage in garbage out (GIGO) principle. The success of the fusion platform depends on the careful design of its components, namely the handling of its data sources.

Important to the development of data-centric activities is the quality of the data and the information generated by integrating data and analytical methods for the achievement of a given

goal, *InfoQ* [4]. This principle has been a guide for the works discussed here.

The main goal of the present work is to develop a data fusion framework that can handle properly the heterogeneous data sources, to estimate a given state parameter.

Regularized Bayesian Fusion

Several steps were carefully designed to achieve the proposed goal and ensure the *InfoQ* throughout the data analysis and processing tasks. In order to make possible the fusion of heterogeneous data, feature engineering was first applied to deal with structural heterogeneity of the considered data sources. Next, to work out the dimensional heterogeneity, several soft sensors predicting desired parameter level were developed. Next, data was combined via the developed fusion algorithm, called Regularized Bayesian Fusion (RegBF); see Figure 1.

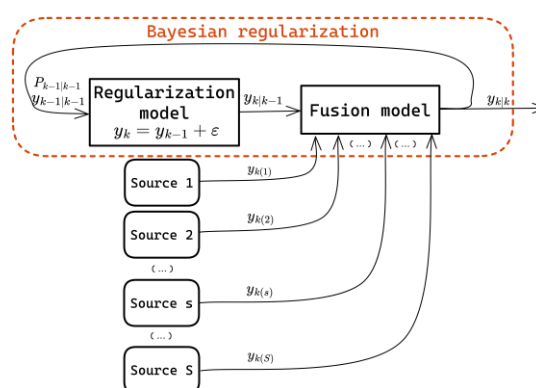


Figure 1. Scheme of RegBF – Regularized Bayesian fusion.

RegBF is a fusion method that combines estimations from different sources into one more accurate estimate, Figure 1. To this, similarly to Bayesian fusion (BF), RegBF use the estimates and the corresponding uncertainties of the given sources, but with crucial a difference: regularization occurs at the same time as fusion. Regularization case means that the fused estimate, y , at time step k , y_k , is regularized by the previous estimation at time step $k - 1$, y_{k-1} . In this case regularization works as smoother and not as the generalization ability of a model, as defined in Deep Learning (DL) field.

Benchmark methods

Besides the proposed method, in this work several benchmark methods were used as well as machine learning methods applied to single sources (Random Forest (RF) [5]), as well as data fusion algorithms as BF [6] and Data-driven Aggregation (DAG) [7] method for parameter estimation.

Case studies

All considered methods were applied to two case studies, one simulated (Kamyr digester) and another real (WWTP). In the Kamyr digester case study, several sources were simulated. Those sources give Kappa measurements at any desirable rates and accuracy (not shown). Kappa is the remaining lignin content of the outflow of Kamyr digester. Using this case study, the methods advantages and drawbacks were further explored.

In the real case study, data from a waste water treatment plant (WWTP) at a Dow Chemical Co. site was considered. One of the main goals of the WWTP is to treat wastewater so that a toxin level does not damage the environment and does not exceed the environmental protection agency (EPA) compliance level for disposal. WWTP operation presents several challenges due to its non-linear and non-stationary nature of biological process. Additionally, the heterogeneity of the collected data is not easy to workout. Even though such data is difficult to handle, it provides the only viable source of information to support WWTP management and optimization. In this case study, the methods were tested on real data. Due to confidentiality reasons, the data were normalized.

Acknowledgements

The authors acknowledge support from the Fundação para a Ciência e Tecnologia (FCT, Portugal), project reference UIDB/00102/2020.

References

- [1] C.H. Goh, "Representing and reasoning about semantic conflicts in heterogeneous information systems," Thesis, Massachusetts Institute of Technology, 1997. Accessed: Oct. 23, 2019. [Online]. Available: <https://dspace.mit.edu/handle/1721.1/10713>
- [2] V. Sheokand, V. Singh, "Modeling Data Heterogeneity Using Big DataSpace Architecture," in *Advanced Computing and Communication Technologies*, vol. 452, R. K. Choudhary, J. K. Mandal, N. Auluck, and H. A. Nagarajaram, Eds. Singapore: Springer Singapore, 2016, 259-268.
- [3] A. Diez-Olivan et al., *Information Fusion*, 50 (2019) 92-111.
- [4] M.S. Reis, R. Kenett, *AIChE Journal*, 64 (2018) 3868-3881.
- [5] L. Breiman, *Machine Learning*, 45 (2001) 5-32.
- [6] O. Punska, "Bayesian Approaches to Multi-Sensor Data Fusion," University of Cambridge, 1999. Accessed: Feb. 14, 2023. [Online]. Available: <https://www.semanticscholar.org/paper/Bayesian-Approaches-to-Multi-Sensor-Data-Fusion-Punska-Doucet/1cc028b780751e53fb4c0177ae3202a068b63212>
- [7] M.P. Campos et al., *Talanta*, 171 (2017) 132-142.

Main results and conclusions

The proposed fusion method, RegBF, in combination with properly trained soft sensors, was able to effectively integrate heterogeneous data sources and accurately estimate a parameter. The simulated case study demonstrated the advantages of using regularized fusion. By utilizing regularization, the RegBF method maintained good performance even in situations where accurate sources were lacking. In a real case scenario, while the DAG, BF, and RegBF methods had similar median performance, the RegBF was the only fusion method that successfully achieved the goal of timely and accurate estimation (Figure 2).

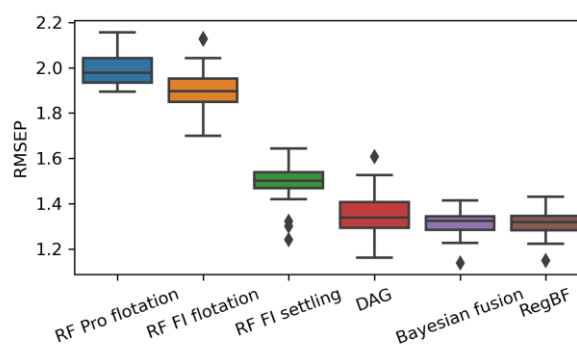


Figure 2. Performance under testing conditions of single- and multi-source prediction methods (WWTP).

However, it is important to note that, as for any fusion algorithm, the performance of RegBF strongly relies on the quality of the information sources. Therefore, a quality monitoring framework for the sources must be employed in conjunction with the RegBF to ensure a robust estimation performance and *InfoQ*. Using toxin level distribution analysis and PCA was possible to verify the shift between the training and test domain that could potentially jeopardize the soft sensors' performance. Nevertheless, further efforts will be employed to develop an *InfoQ* assessment approach.

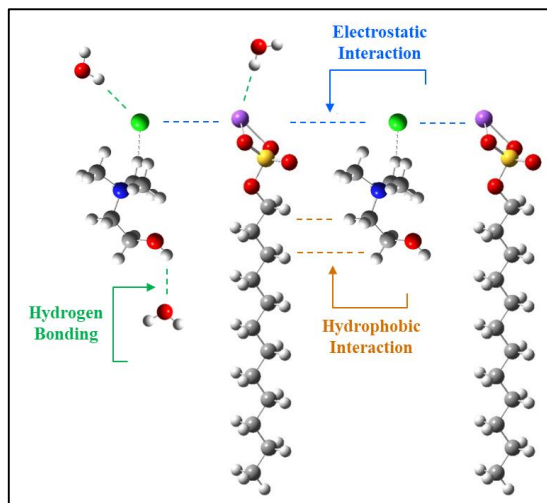
Overall, the findings presented in this paper confirm the potential of RegBF for data fusion applications and the importance of taking data quality into account.

The role of choline based ionic liquids in enhancing micellization of ionic surfactants in aqueous medium – comparative study

A. Al-Farsi*, I. Khan, J. Husband

Department of Chemistry, College of Science, Sultan Qaboos University, Muscat, Oman, Jordania

*s12273@student.squ.edu.om



Understanding the effect of ionic liquids (ILs) as additives on the properties of aqueous surfactant solutions is intensely significant because of the plentiful applications of surfactant-based frameworks in the industry. In this work the effect of six choline based ionic liquids ([Ch][DiHCit], [Ch][Ac], [Ch][Cl], [Ch][Bit], [Ch][DBP] and [Ch][BEHP]) on the aggregation behavior of DTAB and SDS surfactants. Moreover, the thermodynamic parameters of micellization such as standard free energy (ΔG_m°), standard enthalpy (ΔH_m°), and standard entropy of the micellization (ΔS_m°) have been determined.

The interaction between ILs and surfactants is of electrostatic, hydrophobic and van der Waals interaction types which lead to the formation of micelles and enhance spontaneity of micellization process. The main IL-surfactant interaction is the electrostatic interaction between the surfactant's head group with oppositely charged counterion and vice versa at the micelle's polar shell. Moreover, SAILs can interact with surfactants via hydrophobic bonding as well as van der Waals interactions at the hydrophobic tail of both. All mentioned interactions are willing to create a co-surfactant effect which declines the CMC. However, it was approved that the hydrogen bonding is not the main reason for the reduction of CMC value in the polar shell [1-2]. ILs usually used to amend physicochemical properties of surfactants in order to improve the interaction between the hydrophobic sites of the surfactant molecules with water molecules. Their composition of ionic heads groups increases the polarity of the solvent and consequently the tendency of the hydrophobic tails of surfactants molecules to reduce their exposure to the polar environment by forming aggregates [3]. These interactions depend mainly on the structures of ILs ions and the surfactant's head and tail interactions [4]. The aggregation behavior of the anionic surfactant Sodium Dodecyl Sulfate (SDS) and the cationic surfactant Dodecyltrimethylammonium Bromide (DTAB) has been investigated in the absence and presence of (0.1) wt.% ionic liquids (ILs) in aqueous solutions. Room temperature ionic liquids (RTILs) including choline dihydrogen citrate [Ch][DiHCit], choline acetate [Ch][Ac], choline chloride, and choline bitartrate [Ch][Bit] have been used. In addition, two surface active ionic liquids (SAILs); choline dibutyl phosphate [Ch][DBP] and choline bis(2-ethylhexyl) phosphate [Ch][BEHP]. The Critical Micelle Concentration (CMC) values have been evaluated at different temperatures between 283.15 and 313.15 K by employing electrical conductivity techniques.

In the absence of ILs, the CMC values of DTAB and SDS at 298.15 K were found to be around 14.95, and 7.95 mM respectively which are consistent with the literature values. The results indicate that the addition of all employed ILs to both kinds of surfactants lead to a dramatic decrease in the CMC. In terms of RTILs, the cationic surfactants DTAB was highly influenced by [Ch][DHCit] were the average reduction on CMC to 14.31 mM. While the [Ch][Ac] was the highest influencer on SDS and the average reduction was equals to 4.31 mM. The effect of SAILs was recorded more on cationic surfactants as presented in Table 1.

Table 1. Critical micelle concentration (CMC) of DTAB, SDS surfactant in aqueous solution and in presence of 0.1 wt% Choline-based ILs systems at 298.15 K by electrical conductivity (κ).

Solvent system	DTAB	SDS
Water	14.97 (15.30) [5] (14.50) [6]	8.10 (8.10) [7] -
[Ch][DHCit]	14.02	5.30
[Ch][Ac]	14.68	4.32
[Ch][Cl]	14.35	4.46
[Ch][Bit]	14.17	5.09
[Ch][DBP]	11.86	5.16
[Ch][BEHP]	-	4.56

The obtained CMC values have been employed to determine the thermodynamic parameters of micellization such as standard free energy (ΔG_m°), standard enthalpy (ΔH_m°), and standard entropy of the micellization (ΔS_m°). The results found in this study are consistent with the results presented by Inoue et al. [8]. For all cases in the studied system on increasing the temperature from 283.15 to 313.15 K; the value of ΔH_m° decreases linearly and changed its sign from positive to negative at a point around room temperature between 288.15 K and 308.15 K. This indicates that the micellization process starts to be endothermic (positive) at very low temperature. After T_{min} it turned to be exothermic (negative) as the medium become warmer and the

London-dispersion force become dominant between monomers. This large negativity in ΔH_m° is because with increasing temperature the hydrogen bonding among water molecules weakened, and the energy required to dehydrate the surrounding of the hydrophobic tail reduced.⁹ Furthermore, the increase in temperature leads to an increase in the molecular motion, which makes the self-aggregation to be poor at high temperature and this interprets the contentious reduction in ΔS_m° values [9]. However, the entropy term $-T\Delta S_m^\circ$ increased with temperature

and it cross ΔH_m° at a certain temperature. It was found also that the values of standard Gibbs energy of micellization (ΔG_m°) negative for all systems indicating a spontaneous process of the aggregation [10]. The negativity of ΔG_m° value does not depend on the temperature or the type of additive including ILs [11]. The results show that ΔG_m° values are negative in all cases and lay in the range of -32.36 to -36.57 KJ/mol for DTAB and from -30.61 to -36.22 KJ/mol for SDS.

Acknowledgements

Authors would like to thank Sultan Qaboos University (SQU), Ministry of Education (MOE), and the Department of Chemistry for providing the research facilities.

References

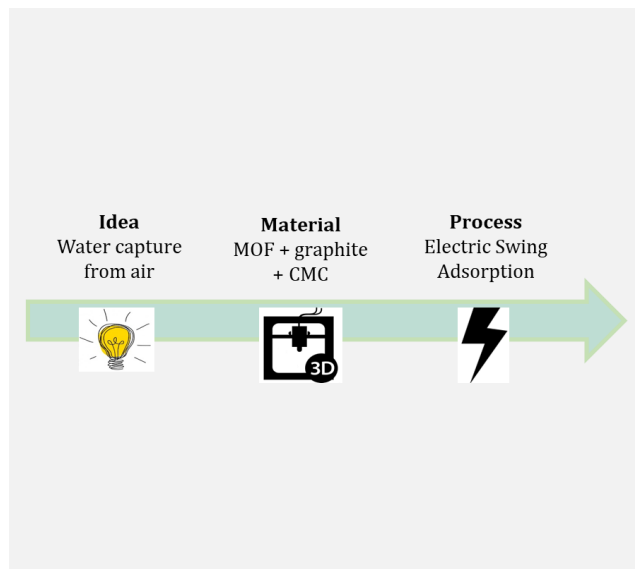
- [1] M.K. Banjare et al., Journal of Molecular Liquids, 241 (2017) 622-632.
- [2] E.A. Turner et al., The Journal of Physical Chemistry A, 107 (2003) 2277-2288.
- [3] T.S. Banipal et al., Journal of Molecular Liquids, 218 (2016) 112-119.
- [4] S. Javadian et al., Industrial & Engineering Chemistry Research, 52 (2013) 4517-4526.
- [5] K.D. Danov et al., Advances in colloid and interface science, 206 (2014) 17-45.
- [6] S.K. Shah et al., Journal of Molecular Liquids, 222 (2016) 906-914.
- [7] M.K. Mandal et al., Journal of Oleo Science, 70 (2021) 185-194.
- [8] T. Inoue et al., Journal of colloid and interface science, 314 (2007) 236-241.
- [9] H. Kumar et al., Journal of Physics: Conference Series, IOP Publishing, (2020) 012099.
- [10] J. Wang et al., The Journal of Physical Chemistry B, 111 (2007) 6181-6188.
- [11] S. Chauhan et al., The Journal of Chemical Thermodynamics, 78 (2014) 175-181.

Water capture from air: development of inks for 3D-printing using MOFs

M. Barata, A. Pereira, A. Ferreira, A. Rodrigues, A.M. Ribeiro, M.J. Regufe*

LSRE-LCM - Laboratory of Separation and Reaction Engineering – Laboratory of Catalysis and Materials, Faculty of Engineering, University of Porto, Rua Dr. Roberto Frias, 4200-465 Porto, Portugal; ALiCE - Associate Laboratory in Chemical Engineering, Faculty of Engineering, University of Porto, Rua Dr. Roberto Frias, 4200-465 Porto, Portugal

*mjregufe@fe.up.pt



This work intends to study new adsorbent materials to be used to directly capture water from the air by adsorption with high water adsorption capacity and excellent electrical properties. In this work, four adsorbent structures were prepared to study their availability to be used in Electric Swing Adsorption process. The inks were prepared using four types of MOFs, graphite as conductive material and carboxymethylcellulose as binder: Al-Fumarate + Graphite + CMC; CAU-10 + Graphite + CMC; MIL-100(Fe) + Graphite + CMC; MIL-160(Al) + Graphite + CMC. Rheological properties of the inks were examined, demonstrating pseudoplastic properties. The powders MOFs and the inks were characterized by N₂ physisorption at 77 K and CO₂ adsorption at 273 K, demonstrating a loss in the surface area and the volume of pores in the case of inks, when compared with the raw MOFs materials. Al-Fumarate + Graphite + CMC demonstrated high viability to H₂O adsorption and good electrical conductivity.

Introduction

The Intergovernmental Panel on Climate Change (IPCC) has reported that Europe has experienced temperature increases and decreases in precipitation due to climate change. Portugal, in particular, mean and extreme temperatures have increased in the past decades and are projected to continue to do so. Annual precipitation has decreased, and climate models project that this decrease will continue: under a scenario where global warming reaches about 3°C by 2100, precipitation will decrease by about 30% in the southern part and 15% in the northern part of the country [1]. The direct capture of water by adsorption is a technology that can be explored to reduce this problem. Low amount of electric energy, simple structures, and low cost are some advantages of an adsorption method [2]. Adsorption-based processes, namely Electric Swing Adsorption (ESA), are a promising alternatives for H₂O harvesting. The regeneration occurs when the adsorbent is heated by the Joule effect, promoting faster heating that increases the process productivity and decreases the unit size. Furthermore, ESA can be used when no heat sources are available, demonstrating low dependency on ambient relative humidity and temperature [3]. Several Metal-organic frameworks (MOFs) have been reported as excellent candidates for H₂O adsorption. Although these adsorbents are non-conductive, these materials must be combined with conductive materials to obtain suitable adsorbents for ESA. This way, four mixtures containing one type of MOF, graphite, and CMC were tested. The inks were prepared using four types of MOFs: aluminium fumarate, CAU-10, and MIL-160(Al), and MIL-100(Fe).

Material and Methods

Adsorbents. MIL-100(Fe), MIL 160(Al), CAU-10, and Al-Fumarate, provided by KRICT, were used as adsorbents in the preparation of the ink. These materials were mixed with graphite to obtain the electrical conductivity required for the

ESA process. Also carboxymethylcellulose (CMC) was added as a binder to give mechanical strength to the 3D-printed structures and to provide the ink pseudoplastic behaviour.

Ink Preparation. The inks were prepared by mixing each MOF, MIL-100(Fe), MIL 160(Al), CAU-10 and Al-Fumarate, with graphite, commercial CMC, and water. The quantities used were 45% wt. of MOF, 45% wt. of graphite, and 10% wt. of CMC.

To do the mixtures, the mixing chamber of Caleva Multi Lab Extruder was used. First, the dry components were mixed without any solvent. Afterward, distilled water was added dropwise until a homogeneous printable paste was obtained.

Rheology. To evaluate the ink behaviour, rheological analyses of the inks were performed using a rheometer Anton Paar GmbH MCR 92, Austria. Rotation and oscillatory tests were made. On the first ones, the viscosity as a function of the shear rate was assessed. Through oscillatory tests, the storage (G') and loss (G'') moduli were evaluated as a function of the deformation of the ink. The tests were performed at 298 K using a distance between the parallel plates of 0.5 mm.

3D-printing. To develop structured adsorbents, an extruder module (Structur3D Printing, Canada) coupled with the Ultimaker 2+ 3D-printer was used. Afterward achieving the homogeneity, the ink was inserted in a syringe which was positioned in the extruder module. Firstly, the prepared inks were tested in a syringe, pressing by hand, to print small lines. These lines were dried during 24 hours at room temperature. The four inks were observed and the best one was printed using the 3D-printer and Discovery module.

Textural characterization. The prepared inks and the powders MOFs were characterized by N₂ adsorption at 77 K and CO₂ adsorption isotherm at 273 K. The analyses were performed with a Micromeritics ASAP 2420 Accelerated Surface Area and Porosimetry System (USA). The samples were degassed and activated at 423 K under vacuum. This

characterization allowed to estimate the specific surface area and volume of pores.

Results and Discussion

Rheology. Rotational tests were operated, and the variation of the viscosity with the increase of the shear rate was measured. The viscosity of the paste decreased when shear rate increased, which is typical of a pseudoplastic material. Amplitude sweep analysis was also performed, and the storage and loss moduli were plotted as a function of the deformation imposed on the ink. Initially, for low deformation values, the storage modulus presented higher values than the loss modulus, but at a certain deformation, that behaviour changes, and the loss modulus surpasses the storage modulus. Rotational and amplitude sweep results for the Al-fumarate + Graphite + CMC ink is presented in Figure 1.

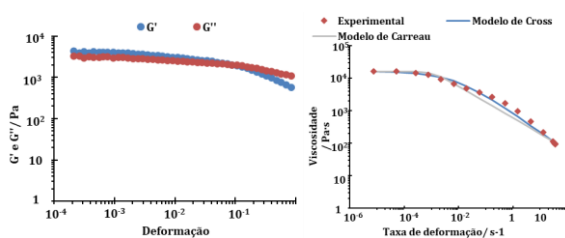


Figure 1. Viscosity vs shear rate; G' and G'' vs deformation.

Syringe printings by hand. Four inks were prepared:

- 1) MIL-100(Fe) + Graphite + CMC

The length of lines was decreased during the drying, due to solvent evaporation. The dried lines maintained the shape and presented some resistance when applying pressure.

- 2) MIL-160(Al) + Graphite + CMC

The length of the lines was reduced during the drying step. However, during the extrusion, it was observed a slightly flattening, maybe due to the high quantity of water in the ink. Small resistance was observed in the dried lines.

- 3) Al-fumarate + Graphite + CMC

The extruded lines maintained their shape after drying step. Some mechanical resistance is observed.

- 4) CAU-10 + Graphite + CMC

The extruded lines maintained their shape after the drying step. Some mechanical resistance is observed.

Electrical resistance measurements. After drying step, all inks were maintained at room temperature. Electrical resistances were measured using a multimeter to evaluate the potential of each material to be heated by Joule effect, when an electric current is applied. Al-Fumarate + Graphite + CMC material presented low resistance, followed by CAU-10 + Graphite + CMC, MIL-100(Fe) + Graphite + CMC and MIL-160(Al) + Graphite + CMC, as it is possible to observe in Table 1.

Acknowledgements

This work is financially supported by national funds through the FCT/MCTES (PIDDAC), under the project 2022.01973.PTDC. This work was financially supported by LA/P/0045/2020 (ALiCe), UIDB/50020/2020 and UIDP/50020/2020 (LSRE-LCM), funded by national funds through FCT/MCTES (PIDDAC). The authors also acknowledge the financially supported by national funds through the FCT/MCTES (PIDDAC), under the “Emprego Científico na Modalidade de Apoio Institucional: Concurso de 2018” and the Ph.D. scholarship 2022.10612.BD.

References

- [1] C.-F. Schleussner et al., Climate Analytics - Climate Impacts in Portugal, 2020.
- [2] C.A. Grande et al., Energy Procedia, 1 (2009) 1219-1225.
- [3] P.D. Sullivan et al., Environmental Science & Technology, 38 (2004) 4865-4877.

Table 1. Electrical resistances of the dried inks.

Adsorbent	Resistance (Ohm)
MIL-100(Fe) + Graphite + CMC	$(30 - 50) \times 10^4$
MIL-160(Al) + Graphite + CMC	$(80 - 120) \times 10^4$
Al-Fumarate + Graphite + CMC	$(0.18 - 0.24) \times 10^3$
CAU-10 + Graphite + CMC	$(0.50 - 0.72) \times 10^3$

Textural characterization. The results from N_2 adsorption at 77 K and CO_2 isotherm at 273 K allowed to estimate the values of specific surface area and pore volumes for each dried ink (Table 2).

Table 2. Surface areas and volume of pores.

Adsorbent	Surface Area (m^2/g)	Volume of Pores (diameter < 8 Å) (cm^3/g)
MIL-100(Fe) + Graphite + CMC	825	0.05
MIL-100(Fe) powder	2437	0.16
MIL-160(Al) + Graphite + CMC	477	0.08
MIL-160(Al) powder	1285	0.22
Al-Fumarate + Graphite + CMC	515	0.08
Al-Fumarate powder	1204	0.17
CAU-10 + Graphite + CMC	227	0.07
CAU-10 powder	743	0.15
Graphite	14	0.003

Based on the results, it is possible to observe a decrease in the surface area and volume of pores for all inks when compared with the original MOFs, due to the shaping and the addition of graphite, which has very low surface area. Taking into account the results of the printed lines by hand, the textural characterization and the electrical resistance measurements, Al-Fumarate + Graphite + CMC ink was selected to be printed. **3D-printing test.** Al-Fumarate + Graphite + CMC material was chosen to be printed (Figure 2). Monolith with cross-section dimensions of 3 cm x 3 cm was printed. No reduction or deformation of the structure was seen during the drying.

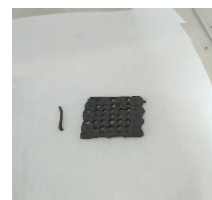


Figure 2. 3D-printed Al-Fumarate + Graphite + CMC monolith.

Conclusions

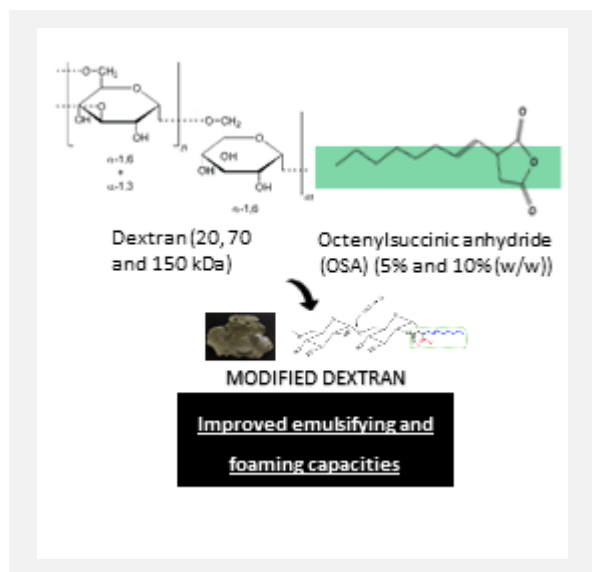
The ink containing Al-fumarate + Graphite + CMC demonstrated better conditions to be tested, due to the pseudoplastic behaviour, the low electrical resistance, and the surface area and volume of pores measured, when compared with the others. The 3D-printed material presented good resistance to be used in the adsorption tests for water capture.

Modification of dextran with octenyl succinate. Evaluation of emulsifying and foaming properties

F. Ridella, M. Carpintero, I. Marcet, M. Rendueles*, M. Díaz

Department of Chemical Engineering and Environmental Technology, University of Oviedo, Oviedo, Spain.

*mrenduel@uniovi.es



Dextran is an exopolysaccharide commonly employed in the pharmaceutical and food industries. However, due to its strong hydrophilic nature, it lacks surface-active properties, which can limit its range of applications. In recent times, many polysaccharides have been chemically modified using Octenyl Succinic Anhydride (OSA) to partially reverse their hydrophilic behaviour. In this study, for the first time, dextran molecules of several molecular weights (20, 70, and 150 kDa) were modified with two concentrations of OSA (5% and 10% (w/w)), and the resultant modified dextran's foaming and emulsifying properties were assessed. The findings suggest that the chemical modification of dextran by OSA was dependent on the amount of OSA used, leading to an increase in the amphipathic character of the modified dextran as the concentration of OSA increased. Furthermore, the emulsifying and foaming properties of the modified dextran were affected by the molecular weight of the polysaccharide.

Introduction

Dextran is a complex glucan synthesized by microorganisms, consisting of a main backbone of D-glucose units linked by α -(1 \rightarrow 6) bonds with possible branching by α -(1 \rightarrow 2), α -(1 \rightarrow 3), or α -(1 \rightarrow 4) bonds. This natural polysaccharide has been used as an encapsulating, thickener, binder, and lubricant agent in the pharmaceutical, cosmetic, and food industries.

Dextran is considered a highly water-soluble molecule due to its marked polar character and the presence of hydroxyl groups (-OH) that participate in the formation of hydrogen bonds with water molecules. Despite the multiple industrial applications of dextran mentioned above, this same polar and highly hydrophilic character ultimately limits its use, as it lacks emulsifying and foaming properties. One of the most applicable compounds for the chemical modification of the surface properties of hydrocolloids is octenyl succinic anhydride (OSA). OSA is an alkenyl succinic anhydride approved by the Food and Drug Administration (FDA) for use in food products [1].

It is for this reason, and due to the importance of the surface and emulsifying properties of polysaccharides for their use in the formulation of food, cosmetic, and pharmaceutical products, that this study was conducted on the modification of dextran synthesized by *Leuconostoc mesenteroides* with OSA.

Materials and Methods

Dextran of 20 kDa, 70 kDa, and 150 kDa were modified with 5% and 10% (w/w) of OSA relative to the amount of polymer. The emulsifying and foaming properties of the modified dextran were analysed.

For the comparative study of foaming capacity and stability of modified and unmodified dextran, the methodology described by Bayar et al. [2] with slight modifications was followed. For this purpose, dextran was dissolved in 15 mL of distilled water at a concentration of 0.5% (w/w) using a homogenizer (SilentCrusher M, Heidolph) at 12,000 rpm for 3 minutes in 50 mL centrifuge tubes and the height of the foam produced was measured.

For the preparation of the emulsions, the technique described by Asgari et al. [3] was followed with slight variations. In 50 mL centrifuge tubes, 20 mL of a solution of modified or unmodified dextran at 0.5% (w/w) were placed. These solutions were mixed with an equal amount of sunflower oil, preparing an emulsion using a homogenizer (SilentCrusher M, Heidolph) at 12,000 rpm for 3 minutes for each sample. The stability of these emulsions under the storage time (10 days) was carried out by using a Turbiscan Lab Expert device.

Results

According to the results obtained, the unmodified dextran samples not showed foaming capacity, while the samples modified with OSA produced stable foams over the storage time tested. Additionally, it could be observed that, except for the 20 kDa dextran samples, the foaming capacity of the rest of the samples increased with the dextran molecular weight and with the concentration of OSA used, which could be associated with a higher degree of esterification of the polysaccharide and therefore with an increase in its amphiphilic character.

Regarding the emulsifying properties, the results obtained showed that the modified dextran emulsifying capacity increased proportionally with the concentration of OSA used in the reaction (Table 1), which also suggest that the larger the amount of OSA in the reaction medium, the higher the amphiphilic character of the dextran obtained. These emulsions proved to be very stable after 10 days of storage, showing a Turbiscan Stability Index (TSI) below 15 in the case of using 10% (w/w) OSA concentration. In addition, dextran molecules modified with 10% OSA resulted in emulsions with a droplet size of less than 50 μ m (Figure 1), showing a high resistance to coalescence after 10 days of storage.

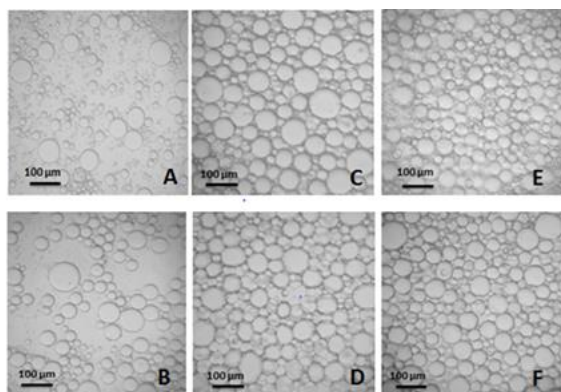


Figure 1. Images of emulsion droplets carried out using the microscope Olympus CX31 (Olympus) at 20X of magnification. (A, B) 20 kDa 10% emulsion at t=0 days and t=10 days, respectively. (C, D) 70 kDa 10%

emulsion at t=0 days and t=10 days, respectively. (E, F) 150 kDa 10% emulsion at t=0 days and t=10 days, respectively.

Conclusions

All these results suggest that the dextran has been chemically modified joining OSA following a dose dependant behaviour, so the higher the amount of OSA introduced, the higher the amphipathic character of the dextran obtained. Moreover, the size of the polysaccharide also influenced on the emulsifier and foaming properties of the modified dextran, showing the worst surface-active properties the 20 kDa dextran, which was the smallest one tested.

All in all, the modification of dextran with OSA confers on this polysaccharide emulsifying and foaming properties important enough to expand its range of applications in the industries in which it is commonly used. column.

Table 1: Emulsion volume and emulsifying capacity of the dextran modified with OSA and unmodified measured immediately and 7 days after the preparation of the emulsions. The total volume was 10 mL

Samples	Emulsion volume (mL)		Emulsifying capacity (%)	
	t=0 days	t=7 days	t=0 days	t=7 days
20 kDa	3.1	0	31	0
70 kDa	4.3	0	43	0
150 kDa	4.5	0	45	0
20 kDa 5% OSA	4.4	4	44	40
70 kDa 5% OSA	5.3	3.3	53	33
150 kDa 5% OSA	5.4	5	54	50
20 kDa 10% OSA	5	4.2	50	42
70 kDa 10% OSA	6.8	6	68	60
150 kDa 10% OSA	6.75	6.1	67.5	61

References

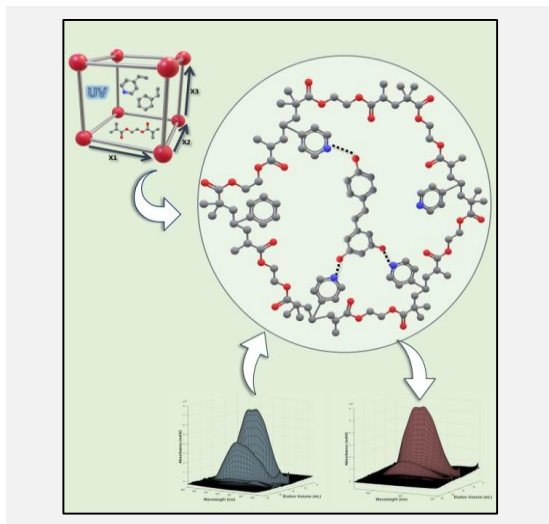
- [1] L. Altuna et al., *Food Hydrocolloids*, 80 (2018) 97-110.
- [2] N. Bayaret al., *Food Chemistry*, 235 (2017) 275-282.
- [3] K. Asgari et al., *International Journal of Biological Macromolecules*, 152 (2020) 1274-1282

Facile process for the purification of (E)-resveratrol from grape stems using tailor-made sorbents

A. Bzainia^{1,2*}, R.C.S. Dias^{1,2}, M.R.P.F.N. Costa¹

¹LSRE-LCM-Laboratory of Separation and Reaction Engineering—Laboratory of Catalysis and Materials Faculty of Engineering-University of Porto, Porto 4200-465, Portugal; ²Polytechnic Institute of Bragança-Mountain Research Center (CIMO), Bragança 5300-253, Portugal.

*amir.bzainia@ipb.pt



Stereoselective sorbents were synthesized using molecular imprinted technology to target the phenolic compound (E)-resveratrol present in grape stems. Photoinitiation permitted the preservation of the intermolecular interactions between (E)-resveratrol and the functional monomers which resulted in highly selective sorbents. Sorption tests were carried out to assess the performance of the materials allowing to describe the impact of the synthesis parameters on the final material's characteristics. Furthermore, the synthesized sorbents were used to purify (E)-resveratrol from grape stems extract in a simple continuous process of sorption-desorption. The purity of (E)-resveratrol was increased from 29% in the extract to 87% in the desorbed hydroalcoholic fractions.

Introduction

Winemaking residues contain a diverse array of phenolic compounds ranging from flavonoids, phenolic acids, stilbenes and even macro compounds such as tannins [1,2]. Among this plethora of polyphenols, (E)-resveratrol is of particular interest due to its inherent antioxidant and anti-inflammatory activities. As a matter of fact, (E)-resveratrol has been reported to limit heart-related diseases [3], confer neuroprotection against Alzheimer's disease [4] and improve energy utilization when performing short-duration high-intensity exercises [5]. The present work focused on the development of a sorption-desorption process to purify (E)-resveratrol found in winemaking residues, specifically from the crude extract of grape stems. The core element of this process is a photo-molecularly imprinted sorbent (MIS) synthesized by means of the molecular imprinting technique (MIT). In brief, a MIS is a polymer endowed with stereospecificity for a compound (or a fragment of that compound), referred to as template. The technology of MISs is inspired from the antibody-antigen interaction during which a pathogenic foreign body is inserted into the antigenic binding site of the antibody. The synthesized materials used herein, were based on the functional monomer 4-vinylpyridine (4VP) and were polymerized through UV irradiation at ambient room temperature using (E)-resveratrol as the imprinting molecule. Eventually, a MIS with high affinity towards (E)-resveratrol was chosen to treat grape stems extract, therefore leading to pure hydroalcoholic fractions of (E)-resveratrol.

Methodology

The synthesis of sorbents was based on a statistical design of experiments allowing the generation of eight MISs and their corresponding non-imprinting sorbents (NISs) (total of sixteen materials). The statistical design of experiments considered three factors with large impact on the material's performance. These factors are the amount of crosslinker, the total monomer's

concentration, and the ratio of (E)-resveratrol to the functional monomer of 4-vinylpyridine in the initial polymerization mixture.

Following their synthesis, the binding capacities and the selectivity of the sorbents were assessed through sorption experiments in pure acetonitrile and hydroalcoholic media. Consequently, a multivariate linear regression analysis led to a description of the uptake of (E)-resveratrol by the materials in these two media. These experiments allowed the selection of a MIS to purify (E)-resveratrol from grape stems extract in a two-step process and relying on sorption-desorption principles.

Results

The sorption experiments using (E)-resveratrol standard permitted to decipher the impact of the polymerization conditions on the selectivity (IF = imprinting factor) and the binding capacity (Q) of the sorbents as shown by the contour plots in Figure 1. Both crosslinker content and the ratio of (E)-resveratrol to 4VP were found to be impactful parameters in the design of such materials [6].

Among the different synthesized materials, one specific MIS was chosen (referred to as MIP7 in our previous work [6]) due to its dual imprinting factor and binding capacity for (E)-resveratrol. This MIS played the role of the core element of the purification process where it was possible to isolate the bioactive compound of (E)-resveratrol in hydroalcoholic medium throughout two steps of purification as shown in Figure 2.

This latter shows the 3D chromatograms where the clear enrichment of (E)-resveratrol can be observed along the process. In fact, the purify was increased from 28% in the initial extract (Figure 2.1) to 78% in the 1st purified solution (Figure 2.2). Furthermore, the purify of (E)-resveratrol was increased to 87% in the 2nd purified solution of (E)-resveratrol (Figure 2.3).

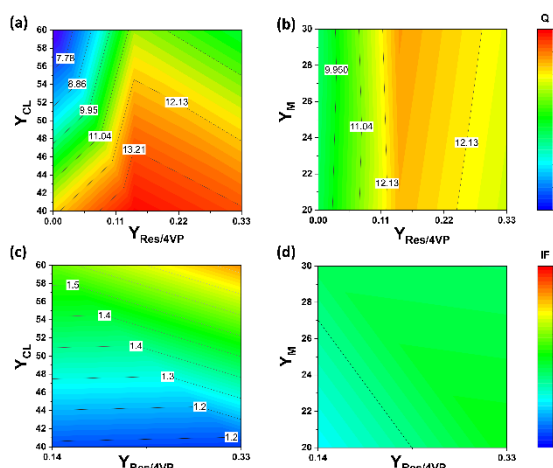


Figure 1. (a); (b): Contour plots of the combined effects of the crosslinker content (Y_{CL}), total monomer concentration (Y_M) and resveratrol content ($Y_{Res/4VP}$) on Q . (c); (d): Contour plots of the combined effects of the crosslinker content (Y_{CL}), total monomer concentration (Y_M) and resveratrol content ($Y_{Res/4VP}$) on IF .

Conclusions

The present work demonstrates the proof of concept of molecularly imprinted sorbents as materials for the practical purification of (E)-resveratrol from grape stems. These sorbents were developed at room temperature through photopolymerization with (E)-resveratrol as template. The molecular imprinting technique yielded materials with specific binding sites for (E)-resveratrol and a morphology adequate for its implementation in a continuous sorption-desorption process. This latter permitted to isolate (E)-resveratrol from grape stems extract leading to a purity of 87%. In addition, other stilbenes present in grape stems (e.g. viniferin) were also identified and enriched with the proposed approach. It is noteworthy that the purified fractions of (E)-resveratrol were obtained in

hydroalcoholic media which has important implications in real-life applications.

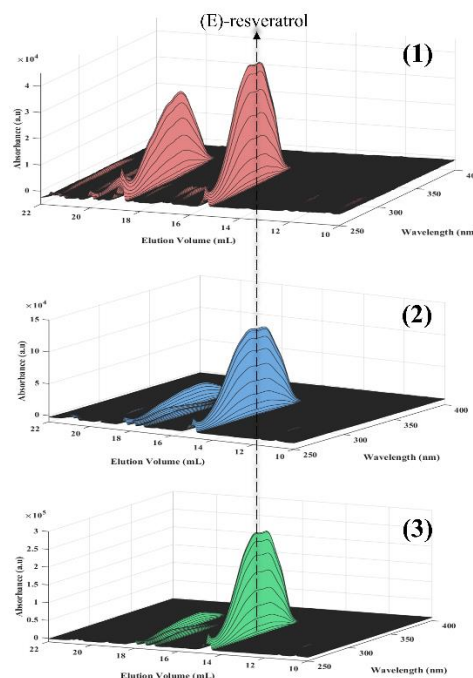


Figure 2. 3D chromatogram of (1) ACN extract; (2) the 1st purified solution obtained in water-ethanol (6:4, v/v) and (3) the 2nd purified solution obtained also in water-ethanol (6:4, v/v). The peak of (E)-resveratrol is around $V_R = 15.1$ ml whereas its derivative (E)- ϵ -viniferin is around $V_R = 18.5$ ml.

Acknowledgements

The authors are thankful for the financial aid provided by “BacchusTech-Integrated Approach for the Valorization of Winemaking Residues” (POCI-01-0247-FEDER-069583), supported by the Competitiveness and Internationalization Operational Program (COMPETE 2020), under the PORTUGAL 2020 Partnership Agreement, through the European Regional Development Fund (ERDF). A. Bzainia is grateful to the national funding by the Foundation for Science and Technology (FCT, Portugal) through the PhD grant of UI/BD/153688/2022. R.D. is grateful to the Foundation for Science and Technology (FCT, Portugal) for financial support through national funds FCT/MCTES (PIDDAC) to CIMO (UIDB/00690/2020 and UIDP/00690/2020) and SusTEC (LA/P/0007/2020). M.R.C. acknowledges the support by LA/P/0045/2020 (ALiCE), UIDB/50020/2020, and UIDP/50020/2020 (LSRE-LCM), funded by national funds through FCT/MCTES (PIDDAC).

References

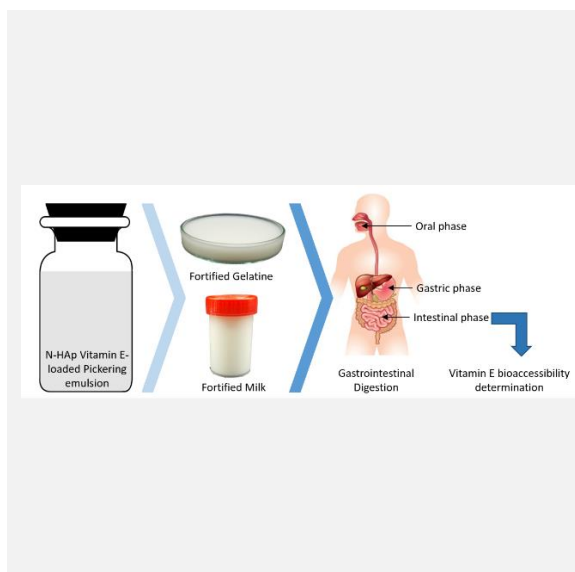
- [1] P. Tapia-Quirós et al., *Science of The Total Environment*, 835 (2022) 155552.
- [2] S. Acquadro et al., *Molecules*, 25 (2023) 464.
- [3] H. Chopra et al., *Journal of Nanomaterials*, (2022)1-17.
- [4] F. Islam et al., *Molecular Neurobiology*, 59 (2022) 4384-4404.
- [5] L.Y. Su et al., *Nutrients*, 15 (2023) 249.
- [6] A. Bzainia et al., *Macromolecular Reaction Engineering*, 2200076 (2023).

Vitamin E-loaded hydroxyapatite Pickering emulsions as new product design for fortified food applications

A. Ribeiro^{1,2,3*}, R.F.S. Gonçalves⁴, A.C. Pinheiro⁴, Y.A. Manrique^{1,2}, M.F. Barreiro^{3,5}, J.C.B. Lopes^{1,2,6}, M.M. Dias^{1,2}

¹LSRE-LCM - Laboratory of Separation and Reaction Engineering – Laboratory of Catalysis and Materials, Faculdade de Engenharia, Universidade do Porto, Rua Dr. Roberto Frias, 4200-465 Porto, Portugal; ²ALiCE - Associate Laboratory in Chemical Engineering, Faculdade de Engenharia, Universidade do Porto, Rua Dr. Roberto Frias, 4200-465 Porto, Portugal; ³Centro de Investigação de Montanha (CIMO), Instituto Politécnico de Bragança, Campus de Santa Apolónia, 5300-253 Bragança, Portugal; ⁴Centre of Biological Engineering (CEB), University of Minho, 4710-057 Braga, Portugal; ⁵LA SusTEC - Laboratório Associado para a Sustentabilidade e Tecnologia em Regiões de Montanha, Instituto Politécnico de Bragança, Campus de Santa Apolónia, 5300-253 Bragança, Portugal; ⁶CoLAB Net4CO2 – Network for a Sustainable CO2 Economy, Rua Dr. Júlio de Matos 828-882, 4200-355 Porto, Portugal.

*asribeiro@fe.up.pt



Lipophilic vitamin E is a vital component of human health; however, it degrades quickly and loses bioactivity due to oxidative instability. In this study, vitamin E-loaded Pickering emulsions stabilised by nano-hydroxyapatite (n-HAp) were produced using a static mixer (NETmix), a technique enabling continuous production and droplet size tailoring. Thus, oil-in-water (O/W) emulsions containing vitamin E at a content of 1mg/mL were produced with different droplet sizes using an O/W ratio of 20/80 (v/v). Their stability during *in vitro* gastrointestinal digestion and vitamin E bioaccessibility was studied. It was observed that n-HAp particles break in the stomach and subsequently aggregate as random calcium phosphates in the small intestine, leading to low vitamin E bioaccessibility due to oil entrapment. The emulsion showing the highest vitamin E bioaccessibility ($3.29\pm 0.57\%$, sample with the larger average droplet size) was used to produce fortified gelatine and milk, resulting in an increased bioaccessibility ($10.87\pm 1.04\%$ and $18.07\pm 2.90\%$, respectively), associated to the presence of macronutrients. Overall, n-HAp Pickering emulsions offer advantages for vitamin E encapsulation directed to fortified foods development, a process that can be extended to other lipophilic vitamins.

Introduction

Emulsions are widely used in various fields (food, pharmaceuticals, and agrochemical), playing an important role in traditional and novel emulsion-based products [1]. Emulsions are bi-phasic systems where a third component is needed to stabilise the two immiscible phases. In Pickering emulsions, the third component, acting as the stabiliser, corresponds to solid particles. These emulsions provide high physical and chemical stability due to their irreversible solid particles' adsorption at the oil-water interface [2]. Thus, Pickering emulsion stabilisation arose as an alternative to traditional emulsifiers, contributing to the development of clean-label products [3] and promising encapsulation systems for bioactive compounds such as vitamins [4], receiving high interest, both from academic and industrial perspectives.

Vitamin E is essential in human health, avoiding cellular ageing and reducing diseases such as dementia, cancer, and cardiovascular disorders [5]. However, vitamin E has a high lipophilic character needing to be encapsulated to increase the stability and compatibility with hydrophilic food matrices. Hydroxyapatite (HAp) has been described as a suitable Pickering stabiliser, stabilising O/W emulsions due to its hydrophilicity [6]. Thus, HAp is appropriate for developing Pickering emulsions systems to protect and deliver lipophilic compounds and further develop functional foods.

Pickering emulsions are usually produced through batch processes, which makes it difficult for large-scale production (industrial implementation). Aiming at achieving a more feasible industrial process, in this work, the NETmix technology

was tested to produce vitamin E-loaded Pickering emulsions in continuous mode with high reproducibility. NETmix is a structured mixer and reactor consisting of a network of static mixing chambers interconnected by transport channels (Figure 1A).

Following reported results pointing out Pickering emulsions as promising systems to improve vitamins bioaccessibility, n-HAp Pickering emulsions were firstly tested as vitamin E carriers, then used to produce fortified milk and gelatine, and their behaviour in the gastrointestinal tract (GIT), and vitamin bioaccessibility evaluated.

Materials and methods

To produce the vitamin E-loaded Pickering emulsions, sunflower oil and vitamin E were used as the oil phase, and water containing dispersed n-HAp particles as the aqueous phase. Firstly, the two phases were fed into NETmix in the pre-mixed mode (Figure 1A), with the total flow rate adjusted according to the desired Reynolds number. Next, to reduce the droplet size, 17 cycles were performed.

Results

Figure 1B shows the optical microscope image of the obtained vitamin E-loaded Pickering emulsion, where it is possible to observe an emulsion with a spherical shape and reduced-size droplets. The Cryo-SEM image shows a Pickering droplet evidencing the n-HAp layer around the oil core, and EDS analysis (data not shown) confirmed the presence of this material at the oil surface. The results are promising and show

the feasibility of using the NETmix technology to produce vitamin E-loaded Pickering emulsions. This fact is an advantage from an energy point of view (NETmix is a low-energy device) and allows continuous production that supports a high-volume scale compatible with industrial production, facilitating the development of end-user applications, namely food applications loaded with lipophilic vitamins.

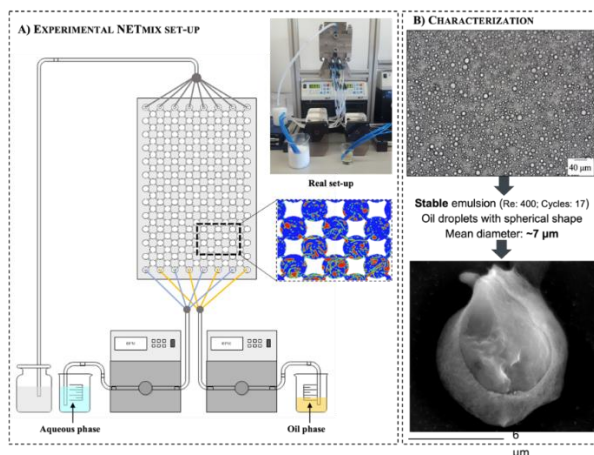


Figure 1. A – Experimental NETmix set-up and B – Optical and cryo-SEM Pickering emulsion characterisation.

The vitamin E-loaded Pickering emulsions were digested in vitro through a simulated GIT: mouth, gastric, and small intestine. Regarding digestion, the tested vitamin E-loaded Pickering emulsions presented similar behaviour along GIT, with n-HAp particles being dissolved in gastric conditions with subsequent formation of aggregates under the intestinal

Acknowledgements

This work was financially supported by LA/P/0045/2020 (ALiCE), UIDB/50020/2020, UIDP/50020/2020 (LSRE-LCM), LA/P/0007/2021 (LA SusTEC), UIDB/00690/2020 and UIDP/00690/2020 (CIMO), and funded by national funds through FCT/MCTES (PIDDAC).

References

- [1] C. Berton-Carabin, K. Schroen, *Annual Review of Food Science and Technology*, 6 (2015) 263-297.
- [2] D. Ortiz et al., *Engineering*, 6 (2020) 468-482.
- [3] M. Zembyla et al., *Journal of Colloid and Interface Science*, 548 (2019) 88-99.
- [4] A. Ribeiro et al., *LWT*, 154 (2022) 112706-112714.
- [5] E. Niki, N. Noguchi, *Free Radical Research*, 55 (2021) 352-363.
- [6] M. Zhang et al., *Materials Science and Engineering C*, 70 (2017) 396-404.

environment. When the vitamin E-loaded PE NET-high was incorporated in food matrices (gelatine and milk, Figure 2 B), vitamin E bioaccessibility increased significantly ($10.87 \pm 1.04\%$ for gelatine and $18.07 \pm 2.90\%$ for milk), putting in evidence the positive effect of the food matrix in the bioaccessibility (Figure 2 A).

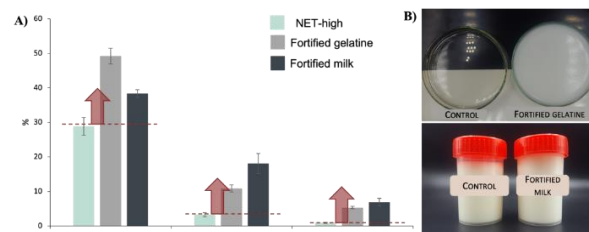


Figure 2. A – Stability, bioaccessibility, and effective bioavailability of vitamin E loaded Pickering emulsions after in vitro digestion; and B – Photographic register of control samples and fortified foods.

Conclusions

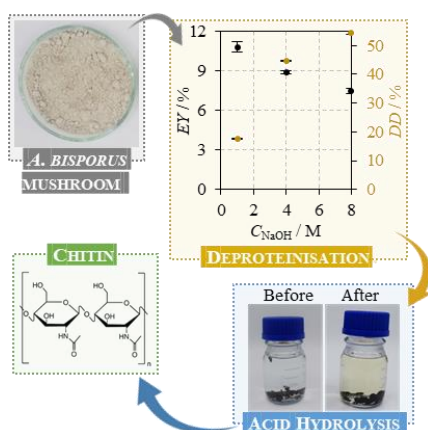
Overall, n-HAp Pickering emulsions offer advantages for vitamin E encapsulation directed to fortified foods development, a process that can be extended to other lipophilic vitamins and other Pickering stabilisers. The obtained results also pointed out the interest in proceeding with further studies to understand the effect of the food matrix composition on the achieved bioaccessibility. Moreover, it also highlights the importance of combining the study of PEs with their final applications to evaluate more accurately the real potential of these innovative solutions. More information on the developed work can be consulted in Ribeiro et al. [4].

Recovery of chitin and chitosan from *Agaricus bisporus* mushrooms: optimisation of the extraction process and effect of different mushroom samples

C.F. Almeida^{1,2,3*}, I.L. Amorim^{1,3}, Y.A. Manrique^{1,3}, C.G. Silva^{1,3}, J.C.B. Lopes^{1,3}, F.G. Martins^{2,3}, M.M. Dias^{1,3}

¹LSRE-LCM – Laboratory of Separation and Reaction Engineering – Laboratory of Catalysis and Materials, Faculty of Engineering, University of Porto, Rua Dr. Roberto Frias, 4200-465 Porto, Portugal; ²LEPABE – Laboratory of Process Engineering, Environment, Biotechnology and Energy, Faculty of Engineering, University of Porto, Rua Dr. Roberto Frias, 4200-465 Porto, Portugal; ³ALiCE – Associate Laboratory in Chemical Engineering, Faculty of Engineering, University of Porto, Rua Dr. Roberto Frias, 4200-465 Porto, Portugal.

*ccalmeida@fe.up.pt



Chitin and chitosan are high-added value compounds currently extracted primarily from crustaceans. In this work, chitin was extracted from *Agaricus bisporus*, a common type of mushroom, and the effect of the deproteinisation conditions on the chitin's extraction yield and degree of deacetylation was studied. The extraction time did not significantly affect chitin's extraction yield; however, the degree of deacetylation increased with extraction time up to 60 minutes. The more impactful parameter was the sodium hydroxide concentration, whose increase produced higher deacetylated chitin and lower extraction yields. Different samples, including fresh and production residue mushrooms, and before and after extraction with supercritical carbon dioxide, were tested. No significant differences were observed regarding extraction yield and degree of deacetylation. Thus, this work evidences the viability of using *Agaricus bisporus* mushrooms' bio-residues for the sustainable recovery of chitin.

Introduction

Chitin, second to cellulose, is the most abundant biopolymer in nature. Many living organisms synthesise it, including crustaceans (e.g., shrimps, crabs, lobsters and squids), insects, algae, yeasts and fungi [1,2]. Currently, chitin is primarily extracted and isolated from shellfish industry wastes by a process requiring harsh chemical reagents and high temperatures [3,4]. Chitosan is then obtained by chitin's deacetylation [5]. However, using seafood by-products for chitin recovery has several shortcomings, namely seasonal supply restrictions and geographical limitations, extraction of potential allergens (tropomyosin, myosin light chain and arginine kinase), and difficulty in maintaining consistent product composition and physicochemical properties [4,5]. These inconveniences potentiated the interest in chitin extraction from other sources. Fungal chitin is an attractive alternative with numerous advantages: use of a non-animal source; chitin free of potential allergens; milder extraction conditions due to the low levels of minerals, which consequently leads to less chitin degradation and lower costs; fewer steps required in the extraction process; and better control of the physicochemical properties of chitin, known to differ in crustaceans depending on the species and harvesting period [4,6-7]. *Agaricus bisporus*, rich in chitinous biopolymers, easy to grow and with a fast-growing cycle, is the most consumed mushroom species representing over 38% of the world's production [6,8]. On top of that, mushroom harvesting and production generate waste up to 30% of the production volume, mainly consisting of discarded bases or stripes commonly used in low-economic-value animal feed and compost [9]. Thus, using *Agaricus bisporus* mushrooms, particularly its production bio-residues, is an appealing approach for chitin recovery. This work aims the recovery of fungal chitin from *A. bisporus* mushrooms. The effect of the deproteinisation conditions and use of different mushroom samples on the

extraction yield (EY) and degree of deacetylation (DD) were evaluated.

Methods

Chitin's extraction from *Agaricus bisporus* was adapted from Hassainia et al. (2018) and is divided into two main steps. The first step, deproteinisation, consists of an alkaline treatment where the mushroom powder was treated with sodium hydroxide (NaOH) at a mass-to-volume ratio of 1:30 (w/v) and temperature of 85 °C. The resulting alkali-insoluble matter (AIM) was submitted to several washing steps until neutral pH. In the second step, acid hydrolysis, a 2% v/v acetic acid (100 ml) was added to the AIM and placed inside an autoclave at 100 °C for 5 hours. Extracted chitin was then washed until neutral pH.

Results

The effect of deproteinisation conditions (number of successive extractions, n , NaOH concentration, C_{NaOH} , and reaction time, t) and of using different samples on EY and DD was studied. Extraction yields were determined as the ratio between the mass of AIM or chitin and the dried mushroom mass. Chitin's deacetylation degree was estimated from the FTIR spectra using the methodology proposed by Baxter et al. (1992), which relates the infrared absorbances of the C=O amide bond and the hydroxyl group (O-H). Results are shown in Table 1. Experiments E01 through E09 were performed on fresh mushroom samples. The effect of reaction time, t , is shown in experiments E01-E04. A slight decrease in the extraction yield is observed for higher deproteinisation times. The deacetylation degree increases with extraction time up to 60 minutes, remaining nearly constant at 17% for higher times. Experiments E04-E07 show that increasing the number of successive extractions, n , with increasing NaOH concentrations, C_{NaOH} , decreases the extraction yields for both AIM and chitin, while

chitin's DD increases. The decrease in extraction yield is likely a cumulative effect of the following factors: an increase in the compounds' removal efficiency due to the successive deproteinisation steps and the consequent addition of new NaOH solutions; and more significant mass losses deriving from a higher number of washing steps, including centrifugation and vacuum-filtration. However, the increase in chitin's DD for increased n directly results from the higher sodium hydroxide concentrations used rather than the number of deproteinisation steps. This observation is evident upon comparing chitin's DD from experiment E07 ($n = 4$; $C_{\text{NaOH}} = 1, 2, 3$ and 4 M) with experiment E08 ($n = 1$, $C_{\text{NaOH}} = 4$ M), where a slightly higher value is observed. Lastly, experiments E04, E08 and E9 show that increasingly concentrated NaOH solutions decrease chitin's extraction yield and increase chitin's DD, which can also be observed in the Graphical Abstract (black points refer to chitin's EY and the yellow to the DD). The decrease in extraction yields is associated with chitin's deacetylation and conversion to chitosan, as well as with a potential increase in deproteinisation efficiency by using concentrated solutions. Experiments E10 and E11 also evaluate the effect of NaOH concentration during the deproteinisation of fresh *Agaricus bisporus* mushrooms after extraction with supercritical carbon dioxide (scCO_2), showing decreasing EYs and increasing chitin's DD for higher sodium hydroxide concentrations. Experiments E12 and E13 were

performed in production residue samples again with similar results compared to fresh mushroom samples (E04 and E10). A slight decrease in the difference between the AIM and chitin EYs is observed for samples of experiments E10 and E13, which were previously extracted with scCO_2 , compared to unaltered mushroom samples of experiments E04 and E12. This likely occurs due to the compounds' extraction with the scCO_2 , which would otherwise be soluble in the acetic acid solution. No significant variations are observed regarding the DD.

Conclusions

In this work, chitin recovery from *Agaricus bisporus* was optimised regarding the deproteinisation conditions, including time, sodium hydroxide concentration and number of successive extractions. The sodium hydroxide concentration was the most influential parameter on extraction yield and chitin's deacetylation degree. Higher concentrations resulted in lower extraction yields and higher DD. Moreover, different *A. bisporus* samples (fresh mushrooms and production residues, before and after supercritical carbon dioxide extraction) were also tested. No significant differences were observed regarding chitin's EY (maximum variation of 3.0%) and DD (maximum variation of 1.4%), thus evidencing the viability of using *Agaricus bisporus* bio-residues for the sustainable recovery of chitin.

Table 1. Chitin extraction from *Agaricus bisporus* mushrooms: summary of experiments and main results (EY and chitin's DD).

ID	Raw material	Deproteinisation			EY _{AIM} / %	EY _{chitin} / %	DD / %
		n	$C_{\text{NaOH}} / \text{M}$	t / min			
E01		1	1	30	14.7 ± 0.1	11.7 ± 0.3	8.3 ± 0.3
E02		1	1	60	14.1 ± 0.8	11.4 ± 0.5	17.2 ± 0.2
E03		1	1	90	13.1 ± 0.3	11.5 ± 0.4	17.4 ± 0.4
E04		1	1	120	13.4 ± 0.3	10.8 ± 0.4	17.7 ± 0.3
E05	Fresh mushrooms	2	1 and 2*	120	11.1 ± 0.1	9.1 ± 0.3	23.1 ± 0.7
E06		3	1, 2 and 3*	120	10.0 ± 0.5	8.0 ± 0.2	34.1 ± 0.5
E07		4	1, 2, 3 and 4*	120	7.5 ± 0.1	5.3 ± 0.1	39.9 ± 0.5
E08		1	4	120	9.7 ± 0.3	8.9 ± 0.1	44.7 ± 0.2
E09		1	8	120	10.3 ± 0.0	7.5 ± 0.2	54.3 ± 0.5
E10	Fresh mushrooms after scCO_2 extraction	1	1	120	11.6 ± 0.2	11.1 ± 0.2	16.9 ± 0.4
E11		1	8	120	8.7 ± 0.3	7.1 ± 0.0	54.1 ± 0.2
E12	Production residue	1	1	120	14.1 ± 0.3	12.9 ± 0.2	17.6 ± 0.2
E13	Production residue after scCO_2 extraction	1	1	120	14.4 ± 0.1	13.8 ± 0.1	18.3 ± 0.1

*successive 120-minute extractions for increasing NaOH concentrations.

Acknowledgements

This work was financially supported by: LA/P/0045/2020 (ALiCe), UIDB/50020/2020 and UIDP/50020/2020 (LSRE-LCM), and UIDB/00511/2020 and UIDP/50020/2020 (LEPABE), funded by national funds through FCT/MCTES (PIDDAC). Ivan Amorim acknowledges his scholarship from FCT's "Verão com Ciência 2022" – Summer@LSRE-LCM_2022 and Cláudia Almeida her PhD scholarship from FCT (2020.04470.BD). The authors express gratitude to the following entities for the services provided: Centro de Materiais da Universidade do Porto (CEMUP) for the SEM images; and the Universidade de Trás-os-Montes e Alto Douro (UTAD) for the XRD analysis.

References

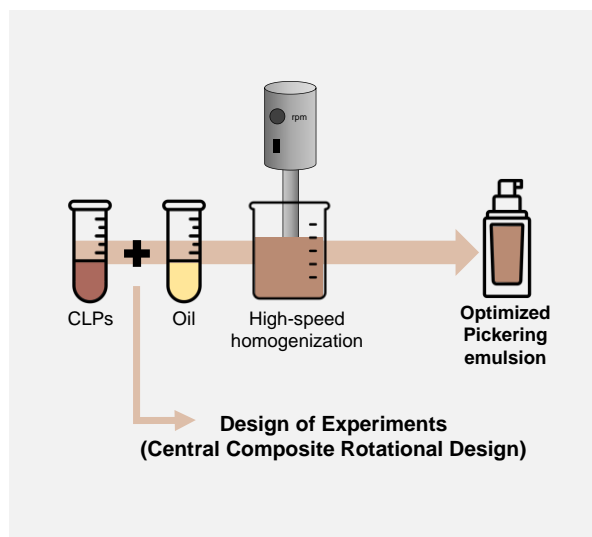
- [1] R.S. Dassanayake et al., Chapter 1 in *Advanced Sorption Process Applications*, Serpil Edebali, IntechOpen, Rijeka, 2018.
- [2] K.J. Kasongo et al., *SN Applied Sciences*, 2 (2020) 406.
- [3] T. Wu et al., *Journal of Agricultural and Food Chemistry*, 52 (2004) 7905-7910.
- [4] A. Papadaki et al., *Foods*, 8 (2019) 239.
- [5] A. Hassainia et al., *Journal of Renewable Materials*, 8 (2020) 101-111.
- [6] A. Hassainia et al., *International Journal of Biological Macromolecules*, 117 (2018) 1334-1342.
- [7] Y. Bouregghda et al., *Waste and Biomass Valorization*, 12 (2021) 6139-6153.
- [8] F. Naisiri et al., *Journal of Food Biosciences and Technology*, 3 (2013) 41-48.
- [9] P.A. Diamantopoulou, A.N. Philippoussis, Chapter 22 in *Handbook of Vegetable Preservation and Processing*, Y. H. Hui and E. Özgül Evranuz Editors, 2nd Ed., CRC Press, 2015, 495-526.
- [10] A. Baxter et al., *International Journal of Biological Macromolecules*, 8 (1992) 166-169.

Colloidal lignin particles as innovative oil-in-water Pickering stabilizers

G. Colucci^{1,2,3,4}, L.G. Teixeira^{1,2,3,4}, S. C. Silva^{1,2,3,4}, A. Ribeiro^{3,4}, A. Santamaria-Echart^{1,2}, A. E. Rodrigues^{3,4}, M.F. Barreiro^{1,2*}

¹Centro de Investigação de Montanha (CIMO), Instituto Politécnico de Bragança, Campus de Santa Apolónia, 5300–253, Bragança, Portugal; ²Laboratório Associado para a Sustentabilidade e Tecnologia em Regiões de Montanha (SusTEC), Instituto Politécnico de Bragança, Campus de Santa Apolónia, 5300–253, Bragança, Portugal; ³Laboratory of Separation and Reaction Engineering (LSRE-LCM), Faculdade de Engenharia, Universidade do Porto, R. Dr. Roberto Frias, S/N, 4200–465, Porto, Portugal; ⁴Associate Laboratory in Chemical Engineering (ALiCE), Faculdade de Engenharia, Universidade do Porto, R. Dr. Roberto Frias, S/N, 4200–465, Porto, Portugal.

*barreiro@ipb.pt



The valorization of lignin, an abundant phenolic biopolymer with remarkable properties, plays a key role in the transition to a sustainable and bio-based economy. This work addresses the emerging use of colloidal lignin particles (CLPs) as stabilizers of multifunctional Pickering emulsions, an innovative approach to replace the conventional synthetic emulsifiers used in commercial emulsions. The composition of the Pickering emulsions stabilized with CLPs was optimized using a Central Composite Rotational Design (CCRD) to obtain stable formulations. For this, the CLPs concentration and oil volume fraction were studied and revealed to be significant factors in emulsion stability. From the CCRD, an optimized formulation was defined and revealed high stability over 30 days of storage. This formulation can be further explored as a delivery system, finding applications in sectors such as cosmetics and healthcare.

Introduction

Lignin, the most abundant phenolic biopolymer on earth, has been extensively studied as a potential material to replace fossil-based chemicals and products, due to its carbon-rich chemical structure [1]. Lignin is largely available as technical lignins, by-products of the paper/pulp and bioethanol industries. Although most of the technical lignins are still burned for energy recovery of the industrial process, the lignin valorization into high-value products is considered a key factor towards a sustainable and bio-based economy [2,3]. Among the several applications of lignin, colloidal lignin particles (CLPs) are interesting systems reported to show improved features when compared to pristine lignin, such as water dispersibility, lighter brown color, and improved functional properties [4]. Recently, CLPs have been explored as stabilizers of Pickering emulsion figures, where solid particles stabilize the emulsions instead of environmentally harmful synthetic surfactants [4,5]. In this context, this study covers the development of lignin-based Pickering emulsions, where the emulsion composition was optimized to obtain stable emulsions. The optimized formulation was further characterized to investigate its stability over time.

Methods

CLPs were produced according to a previous work of the group [6] using the antisolvent precipitation method, with an initial lignin concentration of 50 g/L. To produce oil-in-water Pickering emulsions with CLPs, a cosmetic-grade oil was added to the CLPs dispersion and stirred in a rotor-stator homogenizer at 13500 rpm for 5 minutes. 11 formulations (Table 1) were prepared using a two-factor Central Composite Rotational Design (CCRD). The factors were the CLPs concentration (X_1 , from 10 to 50 g/L) and the oil volume fraction (X_2 , from 0.3 to 0.7). The evaluated response was the creaming index (CI), which indicates the emulsion stability against phase separation, calculated according to Equation 1.

$$CI (\%) = H_S \times 100 / H_T \quad (1)$$

where H_S is the height of the serum layer and H_T is the total sample height.

Table 1. Coded and real values (in parentheses) of the studied factors from the Central Composite Rotational Design and the obtained response for each run.

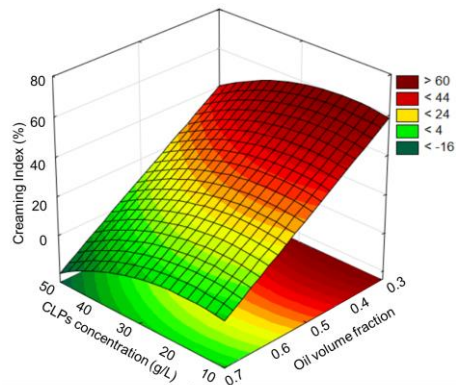
Run	Factors		Response
	X_1 CLPs concentration (g/L)	X_2 Oil volume fraction	Y Creaming Index (%)
1	-1 (16)	-1 (0.36)	52
2	+1 (44)	-1 (0.36)	39
3	-1 (16)	+1 (0.64)	2
4	+1 (44)	+1 (0.64)	0
5	-1.41 (10)	0 (0.50)	34
6	+1.41 (50)	0 (0.50)	6
7	0 (30)	-1.41 (0.30)	58
8	0 (30)	+1.41 (0.70)	0
9	0 (30)	0 (0.50)	29
10	0 (30)	0 (0.50)	29
11	0 (30)	0 (0.50)	26

The optimized emulsion was further characterized after 1 and 30 days of storage by optical microscopy using a Nikon Eclipse 50i (Nikon Corporation, Japan) equipped with Nikon Digital, and the droplet size distribution was obtained through laser diffraction using a Mastersizer 3000 equipped with a Hydro MV dispersion unit (Malvern Instruments Ltd., United Kingdom).

Results

An experimental design (CCRD) was conducted to study the effect and significance of the particle concentration and oil volume fraction in the emulsion stability, to optimize the emulsion composition. From the CCRD, both factors presented negative and significant (p-value ≤ 0.05) effects on the creaming

index, suggesting that the increase in the CLPs concentration and oil volume fraction decreases the creaming index of emulsions. Figure 1 shows the obtained response surface from the regression coefficients after reparametrization ($R^2 = 0.97022$ and validated by the ANOVA F-test). The graph reveals that the optimized formulation with the lowest creaming index is obtained using the highest CLPs concentration and oil volume fraction values, in this case, 50 g/L and 0.7, respectively.



$$Y = 28.30 - 6.55X_1 - 4.46X_1^2 - 21.34X_2 - 0.05X_2^2$$

Figure 1. Response surface obtained for the creaming index (Y) response from the Central Composite Rotational Design of Pickering emulsion composition (X_1 : Colloidal lignin particles concentration and X_2 : Oil volume fraction).

Therefore, the optimized formulation was prepared, and its droplet size and optical microscopy were evaluated after 1 and 30 days of storage (Figure 2). The emulsion exhibited round droplets with a volume-mean droplet size of about 4 μm . Furthermore, after 30 days of storage, the emulsion morphology and size did not significantly change, indicating the high stability of the formulation.

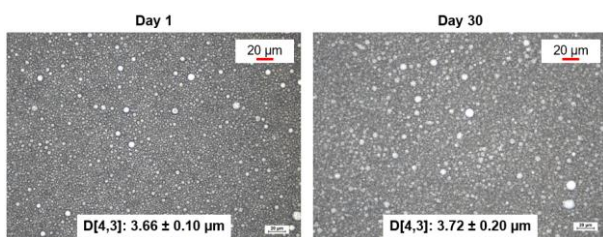


Figure 2. Optical microscopy images and volume-mean droplet size (D[4,3]) of optimized Pickering emulsion after 1 and 30 days of storage.

Acknowledgments

The authors are grateful to the Foundation for Science and Technology (FCT, Portugal) for financial support through national funds FCT/MCTES (PIDDAC) to CIMO (UIDB/00690/2020 and UIDP/00690/2020), SusTEC (LA/P/0007/2021), LSRE-LCM (UIDB/50020/2020 and UIDP/00690/2020), and ALICE (LA/P/0045/2020). National funding by FCT, P.I., through the institutional scientific employment program contract of A. Santamaria-Echart. FCT for the Ph.D. research grants of G. Colucci (2021.05215. BD), S.C. Silva (SFRH/BD/148281/2019), and L. G. Teixeira (2020.08803. BD). Ingevity™ for the kind supply of Indulin AT lignin. COST Action LignoCOST (CA17128), supported by COST (European Cooperation in Science and Technology), in promoting interaction, exchange of knowledge, and collaborations in the field of lignin valorization.

References

- [1] A. Boarino et al., *Biomacromolecules*, 24 (2023) 1065-1077.
- [2] W.D.H. Schneider et al., *Biotechnology Advances*, 47 (2021) 107685.
- [3] M. Österberg et al., *Green Chemistry*, 22 (2020) 2712-2733.
- [4] O. Gordobil et al., *International Journal of Biological Macromolecules*, 233 (2023).
- [5] J. Tomasich et al., *Sustainability*, 15 (2023).
- [6] G. Colucci et al., *Colloids and Surfaces A: Physicochemical and Engineering Aspects*, 666 (2023) 131287.

The CI of the formulation was measured after 1, 7, 15, and 30 days (Figure 3). As suggested by the CCRD, no phase separation was detected after 1 day of storage. However, after 15 and 30 days, CI values of $3.7 \pm 0.1\%$ and $6.3 \pm 1.0\%$ were detected, respectively. Even so, the formulation was considered stable since CI values lower than 10% were obtained. Finally, the emulsion type was confirmed by the drop test. Figure 4 reveals that the optimized Pickering emulsion is an oil-in-water type since it was easily dispersed in water and not miscible in the oil.

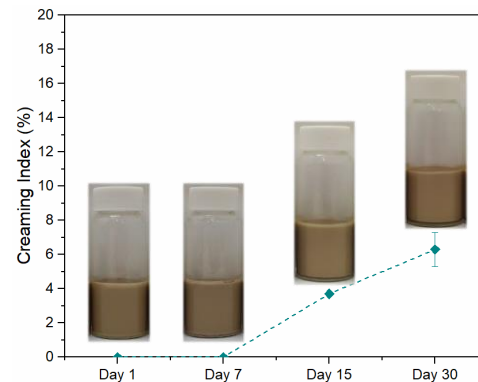


Figure 3. Creaming Index (%) and visual aspect of the optimized Pickering emulsion after 1, 7, 15, and 30 days of storage.

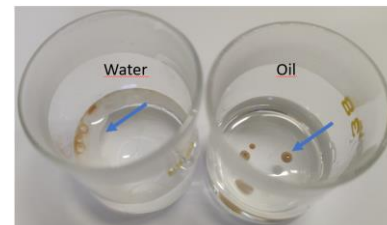


Figure 4. Drop test to determine emulsion type.

Conclusions

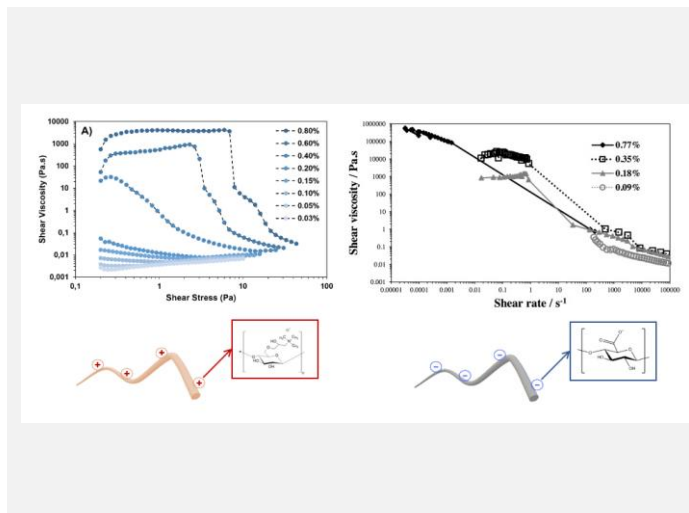
In this work, Pickering emulsions stabilized by CLPs are proposed as a sustainable alternative over conventional synthetic emulsifiers. A design of experiments, namely a Central Composite Rotational Design (CCRD), was performed to optimize the emulsion composition. Two parameters were evaluated, the CLPs concentration and the oil volume fraction, with both variables revealing negative and significant effects on the emulsion stability. From the CCRD, an optimized formulation was prepared, revealing high stability over 30 days of storage. Overall, CLPs have proven to be effective emulsifiers with a high potential to be applied in the cosmetic and healthcare sectors.

Rheology of suspensions of charged cellulose nanofibrils

L. Alves*, J. Pedrosa, P.J.T. Ferreira, J.A.F. Gamelas, M.G. Rasteiro

Univ Coimbra, CIEPQPF, FCTUC, Department of Chemical Engineering, Rua Sílvia Lima, Pólo II – Pinhal de Marrocos, 3030-790 Coimbra, Portugal.

*luisalves@ci.uc.pt



Cellulose nanofibrils (CNF) are materials with high aspect ratio. Typically, TEMPO-oxidised, or cationic CNF consist of long fibrils (up to 2 μm) with very low thickness (less than 10 nm). Derived from their high crystallinity and high aspect ratio, CNF form strong hydrogels with high elasticity at a relatively low concentration. Thus, CNF suspensions appear as an interesting rheology modifier to be applied in cosmetics, paints, food, as mineral suspending agent, among other applications.

Introduction

Cellulose nanofibrils (CNF) are materials with high aspect ratio. Typically, TEMPO-oxidised, or cationic CNF consist of long fibrils (up to 2 μm) with very low thickness (less than 10 nm). Derived from their high crystallinity and high aspect ratio, CNF form strong hydrogels with high elasticity at a relatively low concentration. Thus, CNF suspensions appear as an interesting rheology modifier to be applied in cosmetics, paints, food, as mineral suspending agent, among other applications.

Methods

The CNF used in the present work were produced from an industrial never dried bleached Eucalyptus globulus kraft pulp. The TEMPO CNF were produced by oxidising the cellulose fibres with NaClO, in the presence of catalytic amounts of TEMPO and NaBr, and mechanically treated in a high-pressure homogenizer [1]. On the other hand, cationic CNF were produced by quaternization of the cellulose fibres, with the same characteristics, through a direct reaction with 2,3-epoxypropyltrimethylammonium chloride (EPTAC) in an alkaline medium or a dual step reaction (sodium periodate oxidation + cationization with Girard's reagent T) followed by mechanical treatment in a high-pressure homogenizer [2].

Results

The obtained CNFs suspensions were submitted to rheological tests, with flow curves being obtained for distinct concentrations (ranging from 0.09 to 0.77wt% for TEMPO CNF, and from 0.03

to 0.80 wt% for cationic CNF) in controlled stress mode. It was concluded that the pre-treatment done to cellulose fibres plays a key role on the rheological behaviour of the CNFs suspensions. The fibres treated with EPTAC and TEMPO-oxidised resulted in suspensions with higher viscosity compared to those obtained from fibres treated with Girard's reagent T.

This higher viscosity results from the strong 3D fibril network, which is related to a good fibrillation of the material and to the long and thin fibrils that can overlap. The c^* concentration was found to vary from ca. 0.13 to ca. 0.4wt% depending on the type and intensity of the pre-treatment applied. The results confirm the higher tendency for the fibres treated with EPTAC and TEMPO to form a 3D network, resulting in lowest c^* .

For the TEMPO-oxidised CNF suspensions it was also found that aggregation is improved at acidic pH conditions due to lower charge repulsion among fibrils, leading to an increase of the suspension viscosity, as well as to higher apparent yield stresses. Moreover, distinct rheological behaviours were found as different acids were applied, being observed that phosphate ions resulted in an extended aggregation and formation of very strong gels, at pH 2.3, and on the other hand, the presence of acetate ions resulted in lower aggregation and weaker gels, for the same pH value.

Conclusions

The fibrillation degree and the length and width of CNF play key roles on the rheology of cellulose nanofibril suspensions.

Acknowledgements

The authors want to acknowledge the Strategic Research Centre Project UIDB/00102/2020, funded by the Fundação para a Ciência e Tecnologia (FCT).

References

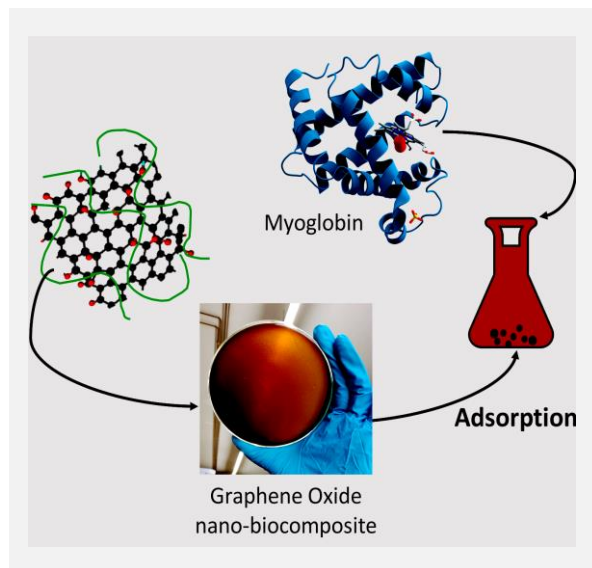
- [1] L. Alves et al., Carbohydrate Polymers 237 (2020) 116109.
- [2] J.F.S. Pedrosa et al., International Journal of Biological Macromolecules 201 (2022) 468.

Synthesis of nano-biocomposite hydrogel with graphene oxide for the separation of hemoprotein myoglobin: adsorption equilibrium and kinetics

C.M.B. Araujo^{1*}, M.A. Motta Sobrinho², M.G. Ghislandi³, A.F.P. Ferreira¹, A.E. Rodrigues¹

¹Faculty of Engineering, University of Porto, s/n, R. Dr. Roberto Frias, 4200-465, Porto, Portugal; ²Federal University of Pernambuco, Av. Prof. Moraes Rego, 1235, 50670-901, Recife-PE, Brazil; ³Federal Rural University of Pernambuco, R. Cento e Sessenta e Três, 300, Cabo de Santo Agostinho – PE, Brazil.

*carolinemariaba@gmail.com



Proteins and amino acids are essential to humans and in all living beings. In addition to their biological importance, these compounds are present in the pharmaceutical, food and cosmetic industries. To be used in industry, proteins need to be separated. This work aims to synthesize and apply nano-biocomposite hydrogels based on graphene oxide (GO) and agar for protein separation and purification. The hydrogel was tested as an effective method for the adsorption of the hemoprotein myoglobin in batch, exhibiting a notorious potential for protein adsorption, showing maximum adsorptive capacity predicted by the Langmuir model over 1500 mg.g⁻¹ at pH = 5 and 25 °C. As GO interacts with the polymeric matrix agar, resulting in a 3D material, in the following steps, it is expected that the material developed will be able to adsorb myoglobin in a fixed-bed system in successive adsorption-desorption cycles.

Introduction

Polysaccharide hydrogels are materials consisting of interconnected networks filled with water. They have non-toxicity, biodegradable and recyclable properties, exhibiting low cost, simple manufacturing, and high adsorption capacity [1]. Incorporating graphene oxide (GO) into the structure of these materials gives them properties and functions, such as increased mechanical strength and adsorptive capacity [2].

Graphene-based materials have, among their innumerable characteristics: high theoretical specific surface area, great regeneration capacity, versatility, and unique chemical and mechanical properties, being considered promising materials for adsorption [3]. The abundance of oxygen groups on GO surface has been explored in studies related to the production of composites and biocomposites, including hydrogels [4].

On the other hand, proteins and amino acids are essential to humans and in all living beings. In addition to their biological importance, these compounds are part of everyday life, being present in the pharmaceutical, food, and cosmetic industries. To be used in industry, proteins must be separated and/or purified [5]. The functional groups on the surface of the GO allow these molecules to be efficiently adsorbed on its surface [6].

Objectives

This work aims to synthesize nano-biocomposite hydrogels based on GO and agar for protein separation and purification. The hydrogel was tested as an effective method for adsorbing the hemoprotein myoglobin in batch experiments.

Methods

GO was synthesized by the modified Hummers method. Hydrogel production was carried out following the methodology presented by Araujo et al. [7], placing powdered agar (0.30 g) diluted in 20 mL deionized water under constant stirring at 85 °C

for 20 min. Then, with the system under stirring, a volume of the OG suspension (10 g.L⁻¹) was added. The hydrogel was cooled and jellified at room temperature (picture in the graphical abstract). Afterwards, the sample was manually crushed into pieces (3 mm average particle size), sealed, and stored at 4 °C. Batch adsorption experiments were performed evaluating the effect of initial pH, NaCl concentration, kinetics, and adsorption equilibrium isotherms for myoglobin (Sigma-Aldrich, USA). Assays were performed in a shaker at 25 °C, 250 rpm for 24 h. The initial volume of the protein solution was 25 mL, and the adsorbent dry mass was 0.004 g. Initial and final protein concentrations were quantified using a UV-Visible spectrophotometer (Jasco 7800), considering the maximum wavelength of 405 nm [5]. The experimental data obtained for the equilibrium isotherms were modeled according to the Langmuir, Freundlich and Sips equations [7].

Protein was dissolved in different buffer solutions (20 mM) - citrate buffer was used for pH = 5 and 6 (citric acid, 192.12 g.mol⁻¹ with tri-sodium citrate di-hydrate, 294.10 g.mol⁻¹); phosphate buffer was used for pH = 7 (sodium di-hydrogen phosphate di-hydrate, 156.01 g.mol⁻¹ with di-sodium hydrogen phosphate, 141.96 g.mol⁻¹); and a Tris-HCl buffer for pH = 8 (157.64 g.mol⁻¹). The final solution pH was adjusted with NaOH or HCl (1 M) when needed [8].

Results

Scan electron microscopy (SEM) was carried out in the TESCAN VEGA3 (Tescan Analytics) scanning electron microscope, and micrographs of the composite produced are depicted in Figure 1. It reveals evidence of GO interaction with the polymeric matrix agar, resulting in a 3D material with many tiny layers, ascribed to the disarranged GO sheets, channels, and a visually disordered morphology.

By varying the initial pH (Figure 2a), it is notorious that adsorption capacity values were approximately the same when pH = 5 and 6. For higher pH values, the adsorption capacity decreased considerably. That could be attributed to the electrostatic interactions between the charges on the adsorbate and adsorbent surface. The isoelectric point of myoglobin is ~ 7.0 , which means that the protein is positively charged when $\text{pH} < 7.0$. Conversely, the composite is negatively charged in a pH range from 2.0 to 10.0 [9]. Evaluating the effect of NaCl concentration in the medium (Figure 2b), it is observed that, in general, the increase in NaCl concentration does not seem to affect the adsorptive capacity for myoglobin. For pH = 5, only a small reduction in the adsorption capacity value is observed when it increases from 0.15 to 0.20 M NaCl.

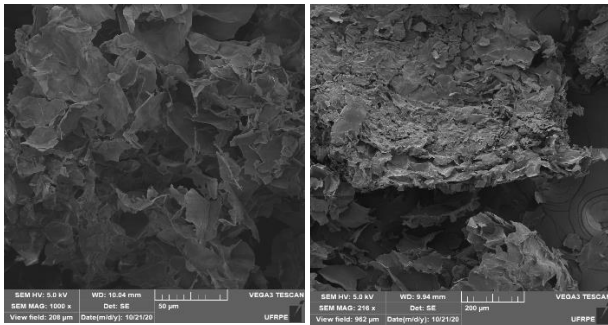


Figure 1. SEM micrographs of the freeze-dried hydrogel with 1000x (left) and 216x (right) of magnification.

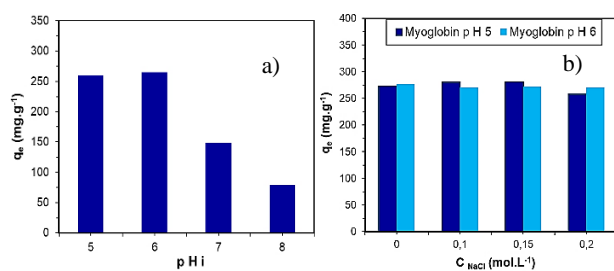


Figure 2. Effect of initial pH (a) and NaCl concentration (b) on the adsorption of myoglobin by the hydrogel ($T = 25\text{ }^{\circ}\text{C}$).

Adsorption kinetic curves obtained experimentally are depicted in Figure 3 for two different initial concentrations and pH values. Overall, when $C_0 = 100\text{ mg.L}^{-1}$, the adsorption capacities were higher for pH = 5 than 6. It was observed that 24 h was sufficient to guarantee the equilibrium was reached.

Acknowledgements

To the Conselho Nacional de Desenvolvimento Científico e Tecnológico (CNPq, Brazil), and Fundação para a Ciência e a Tecnologia (FCT, Portugal). This work was funded by national funds through FCT/MCTES (PIDDAC), under the base funding - UIDB/50020/2020 from the LSRE-LCM Associate Laboratory; and by the CNPq (grant number: 200138/2022-7).

References

- [1] O. Duman et al., *International Journal of Biological Macromolecules*, 160 (2020) 823-835.
- [2] A. Khalil et al., *International Journal of Biological Macromolecules*, 164 (2020) 2922-2930.
- [3] T.J. M. Fraga et al., *Adsorption*, 26 (2020) 283-301.
- [4] L. Chen et al., *Carbohydrate Polymers*, 155 (2017) 345-353.
- [5] A.G. Rios et al., *Journal of Chromatography A*, 1628 (2020) 461431.
- [6] D. Huang et al., *Environmental Chemistry Letters*, 18 (2020) 251-255.
- [7] C.M.B. de Araujo et al., *Colloids and Surfaces A: Physicochemical and Engineering Aspects*, 639 (2022) 128357.
- [8] P.F. Gomes et al., *Adsorption*, 23 (2017) 491-505.
- [9] C.M. Bezerra de Araujo et al., *Environmental Research*, 216 (2023) 114425.

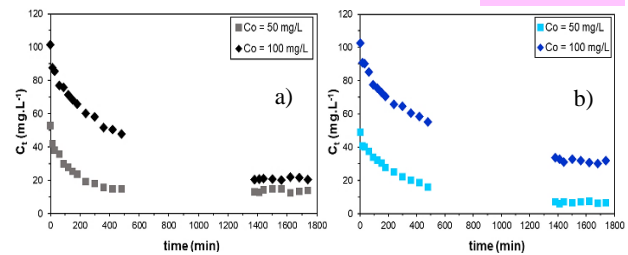


Figure 3. Adsorption kinetics for myoglobin at $T = 25\text{ }^{\circ}\text{C}$ with pH= 5 (a) and pH= 6 (b).

Regarding the adsorption equilibrium isotherms (see Figure 4), overall, the Sips model satisfactorily fit the equilibrium data, although the Langmuir model also exhibited good results (Table 1). In this case, the compatibility of Sips isotherm indicates the combined features of Freundlich and Langmuir equations [7].

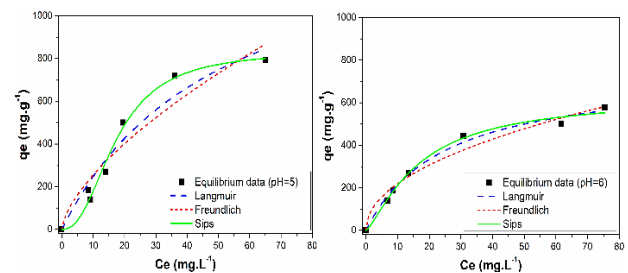


Figure 4. Adsorption equilibrium isotherms for myoglobin ($T = 25\text{ }^{\circ}\text{C}$).

Table 1. Adsorption isotherms parameters.

Model	Parameter	Value (pH=5)	Value (pH=6)
Langmuir	q_m (mg.g^{-1})	1503.613	746.914
	K_L (L.mg^{-1})	0.0197	0.0404
	Adj. R^2	0.932	0.988
Freundlich	n	1.528	2.073
	K_F ($\text{mg}^{1-(1/n)}, (\text{g}^{-1}).\text{L}^{1/n}$)	56.487	72.305
	Adj. R^2	0.894	0.967
Sips	q_m (mg.g^{-1})	836.182	628.465
	m	2.355	1.319
	K_S (L.mg^{-1}) ^m	0.00121	0.0243
	Adj. R^2	0.984	0.989

Conclusions

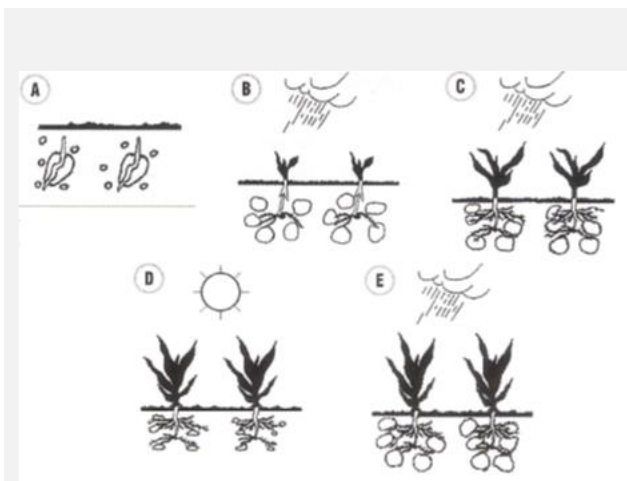
The hydrogel has a notorious potential for myoglobin adsorption, showing maximum adsorptive capacity predicted by the Langmuir model over 1500 mg.g^{-1} at pH = 5. In the following steps, tests will be carried out to evaluate the protein adsorption and desorption using the hydrogel in a fixed-bed column.

Superabsorbent polymers: their uses and properties, and computation of their characteristic parameters

M. Casquilho¹*, A.M. Rodrigues², J.L. Miranda³, J. Bordado¹

¹Instituto Superior Técnico (IST), University of Lisbon; Ave. Rovisco Pais, IST; Lisbon, Portugal; ²Instituto Nacional de Investigação Agrária e Veterinária (INIAV), Ave. República, Oeiras, Portugal; ³Instituto Politécnico de Portalegre; Campus Tecnológico, Portalegre, Portugal.

*mcasquilho@tecnico.ulisboa.pt



The development of macromolecular compounds able to absorb large quantities of water or aqueous solutions has been an important research area in the chemistry of polymers in the recent decades. An amount of, say, 1 g of one of these polymers, can absorb hundreds of times that mass of water, even 1000 g. This property has been used to make hygiene products, medical devices, and, in agriculture and forestry, to add it to the soil to improve its humidity, namely to fight desertification.

In this document, we briefly address: the uses of the superabsorbent polymers; their properties; and how to compute their characteristic parameters. These parameters allow us to understand the polymers' behavior, and help in selecting them for the particular applications envisaged.

For computing the characteristic parameters of superabsorbent polymers, we supply a webpage for direct use, permitting to obtain the usual 3 parameters from experimental data, based on the accepted theory of absorption-relaxation.

Introduction

Superabsorbent polymers are hydrophilic materials able to absorb large quantities of water or aqueous solutions, these substances being mentioned because they are the typical ones of practical interest.

The first remarkable results on superabsorbents were obtained around 1980 in the Northern Laboratory, US Department of Agriculture 0 and their study has continued. (e.g., 0).

Uses and properties

Several applications of superabsorbent polymers have shown particular interest. A significant part of the current market relates to hygiene and several others, such as agriculture and medicine.

Agriculture

Water being essential to life on Earth, one of the largest challenges in agriculture is its scarcity in several continents, which makes difficult the development and survival of plants, with as a consequence the decrease of production. Another, more recent, rising problem is the contamination of soils and underground waters from the leaching by fertilizers, phytopharmaceuticals and their biodegradability products (metabolites).

Superabsorbents can be useful by enhancing the retention capacity of water and nutrients in soils, thus leading to a better management of available hydric resources. Besides losses from surface evaporation, losses by infiltration to deeper layers may be relevant, the more damaging the lighter or sandier the soil texture. Both cases make it more difficult for the plants to reach the necessary water.

Regarding soil contamination, superabsorbents mixed with earth absorb part of the existing fertilizer, which is retained in particles of gelatinous consistency. Around these, roots can grow and extract, progressively, the fertilizing spots retained in the

superficial zone of the soil, precisely where they are more efficient. This can be decisive (i) in plant nurseries and upon transplantation, (ii) in forest species, (iii) in agricultural species and (iv) in gardening 0. The Graphical Abstract (initial figure) represents schematically the phases of the superabsorbent action:

- A — The particles of superabsorbent are dispersed in the soil at the depth where the seed will be laid.
- B — The superabsorbent retains part of the water from rain or irrigation
- C — The superabsorbent supplies gradually retained water to the plant, and rehydrates itself with rain or irrigation.
- D — After the available water runs out, the particles “shrink” and leave cavities that aerate the soil.
- E — The process is reversible and, upon new water supply, the particles retain again part of the infiltrated water.

Medicine

As regards polymers, in general, and superabsorbents, in particular, the research directed to materials (somehow inappropriately called “biomaterials”) compatible with uses in medicine is active.

It is frequent to apply superabsorbents as support for medication to be diffused progressively, which is managed through the aggregate of polymer molecules. Among commercial applications are the liberation of prostaglandin E2 to induce labour (childbirth), supply adequate levels of morphine in post-surgical analgesia; and supply insulin to diabetics.

Computing the characteristic parameters of superabsorbents

The main contribution of the present document is to provide a simple webpage where a user or researcher can introduce experimental data of absorbency vs. time in order to determine

the classical parameters that characterize the superabsorbent. The progressive increase in volume of a given quantity of superabsorbent is called “swelling” (Pt, “inchamento”). According to the accepted theory explaining swelling, two phenomena are considered: diffusion and relaxation. “Diffusion” is the contribution due to the well-known Fickian diffusion, and “relaxation” is the geometric increase in volume due to the interspersation of molecules of water in the polymer network.

The above leads to 3 parameters: ϕ , weight (fraction) of diffusion (with, of course, $1 - \phi$ the weight of relaxation); k_F , diffusion parameter; and k_R , relaxation parameter. Thus, the swelling ratio is

$$r(t) = \phi \left[1 - \frac{6}{\pi^2} \sum_{n=1}^{\infty} \frac{1}{n^2} \exp(-n^2 k_F t) \right] + (1 - \phi) [1 - \exp(-k_R t)]$$

with r going from 0 (initially, no swelling) to 1 (finally, total swelling) as t , time, goes from 0 to ∞ , which is simply the moment when no more swelling will be observed (“equilibrium swelling”). The problem is, thus, a regression to find the three parameters mentioned. From the data in Table 1, inserted in the webpage constructed for the problem, the parameters (the k 's in the units used) are

$$\phi = 0.6363 \quad k_F = 5.361e-03 \quad k_R = 5.345e-03$$

meaning, namely, that, for the superabsorbent used, the Fickian diffusion has a weight of ~64 % (so, relaxation, 36 %).

As mentioned, the parameters can be simply obtained by dropping (possibly by copy-paste) the data, such as those in Table 1, in the adequate space in the webpage,

Ref. 0

and clicking ‘Execute’.

Acknowledgements

MC (Department of Chemical Engineering [DEQ], Instituto Superior Técnico [IST], University of Lisbon [ULisboa]) does research at CERENA, “Centro de Recursos Naturais e Ambiente” (Centre for Natural Resources and the Environment); AMR does research at INIAV, GeoBiotec (FCT-UNL) and IDMEC (IST); JLM (Department of Technologies, Escola Superior de Tecnologia e Gestão [School of Technology and Management], Polytechnic Institute of Portalegre) does research at CERENA; and JB (DEQ, IST, ULisboa) does research at CERENA. CERENA’s support is through Project UID/04028/2020, from FCT, “Fundação para a Ciência e a Tecnologia” (Portuguese “National Science Foundation”). The computing is based on the IST computing system, maintained by CIIST, “Centro de Informática do IST” (Informatics Centre of IST).

References

- [1] M. Yamaguchi et al., Carbohydrate Polymers, 7 (1987) 71-82.
- [2] F. Rosa, M. Casquilho, Fuel Processing Technology, 103 (2012) 174-177.
- [3] F. Masuda, Chemical Economy & Engineering Review, 15 (1983) 19-22.
- [4] M. Casquilho, “Superabsorbent polymers: parameters” (2022), http://web.tecnico.ulisboa.pt/~mcasquilho/compute/CISTI_2022/P-SuperAPolymer.php, accessed 10-Apr-2023.

Table 1. Increment in weight of superabsorbent

Data
time;increment
0;0
1;61
2;87
4;114
6;126
8;135
10;144

With the data from Table 1, the result is depicted in Figure 1, showing, in good agreement, the experimental and computed curves of the fraction swelling versus time for a given superabsorbent.

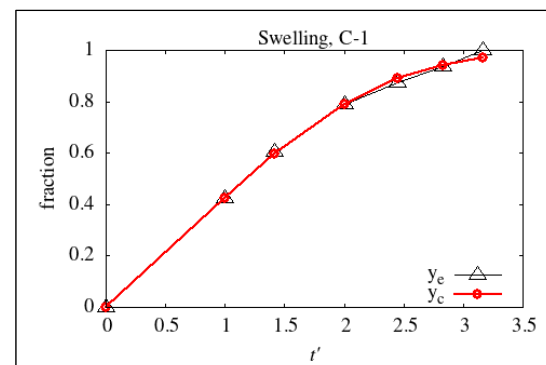


Figure 1. Experimental, y_e , and computed curves, y_c , of swelling for a given superabsorbent.

Conclusions

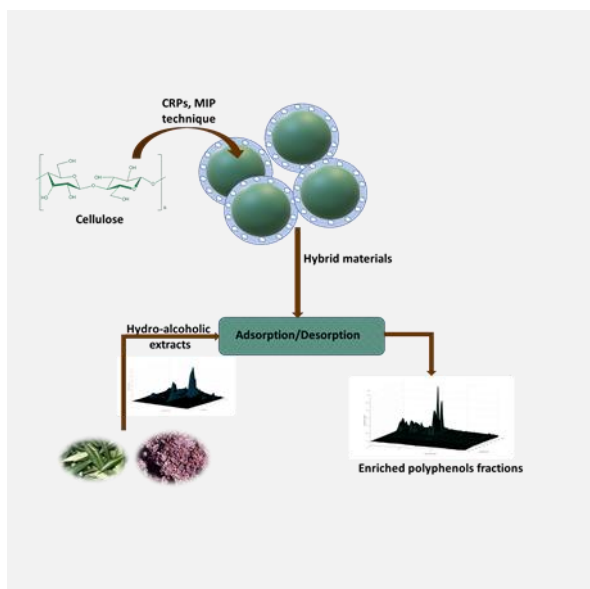
The typical property of superabsorbent polymers, i.e., being able to absorb water and “swell” without dissolving, finds application in hygiene, medicine and, significantly, in agriculture and forestry. The trend is that the applications of these polymers continue to grow, as they not only solve several technical problems, but also contribute to protect the environment and improve water management. The mathematical procedure shown permits to characterize the essential parameters of a superabsorbent, in order to predict its behavior, just using computation freely available on a webpage.

Hybrid adsorbents endowed with stereospecificity towards flavonoids present in olive oil and winemaking residues

C.P. Gomes¹*, R.C.S. Dias¹, M.R.P.F.N. Costa²

¹Mountain Research Center (CIMO), Polytechnic Institute of Bragança-, Bragança 5300-253, Portugal; ²LSRE-LCM-Laboratory of Separation and Reaction Engineering—Laboratory of Catalysis and Materials Faculty of Engineering-University of Porto, Porto 4200-465, Portugal.

*cpgomes@ipb.pt



This research is devoted to the design and synthesis of molecularly imprinted cellulose-synthetic hybrid particles via surface atom transfer radical polymerization (SI-ATRP). The two-step process involves the immobilization of α -bromoisobutyryl bromide in the pristine microcrystalline cellulose, to generate ATRP macro-initiator particles, and then the creation of a crosslinked-imprinted shell in the particles surface considering ATRP of co-monomers 4-vinylpyridine (4VP) and ethylene glycol dimethacrylate (EGDMA) with quercetin as imprinting template molecule. Different combinations recipes were tested, and a system with ethanol as solvent and 4VP/EGDMA as co-monomers was demonstrating a good performance suitable to be used as adsorbent to polyphenols. Adsorption/desorption processes with standard molecules were considered to prove the modification of pristine cellulose and also the effect of molecular imprinting (imprinting factor ~ 2.6). Considering these particles as adsorbents for the enrichment of flavonoids in olive leaves and grape pomace extracts we estimate enrichment factors up to 4. These results point up for the usefulness of natural-synthetic materials with processes to get high-added value compounds in the framework of circular bio-economy.

Introduction

The valorization of agricultural residues and sub-products is becoming a major occupation of several industries namely the enrichment and isolation of molecules with high added-value. It is estimated that about 1300 million tons of agriculture residues is annually produced [1]. Considering our geographical location, Trás-os-Montes e Alto Douro (region with high wine and olive oil production) there is an enormous interest in the valorization of the residues resulting from this production. In case of olive and olive oil production, around 4.5 million of olive leaves are annually generated and are usually discharged in fields, burned or used to feed animals. The same with the winemaking industries, that are responsible for generating a large number of residues and sub-products, such as grape pomace (grape skins, seed and stems), wine lees and other undervalued residues (diatomaceous earth used to filtrate the wine) which are disposed of and not valorized. However, these residues are extremely rich in bioresources, in case of olive leaves it has been estimated that around 1 million tons of bioactive compounds, 1 million tons of cellulose and 1.5 million tons of lignin are currently underexploited [2]. In particular, the extraction and isolation of bioactive compounds with high added value present in olive leaves and winemaking residues are particularly interesting due to their high market potential in different sectors as food, feed, chemical, cosmetic and pharmaceutical [2]. Therefore, it is of great interest to find an effective methodology to valorize bioactive compounds and to facilitate their use in the aforementioned sectors.

Adsorption/desorption processes are commonly used in industry and in analytical procedures to purify, fractionate and concentrate target molecules. For these applications, different kinds of adsorbents from natural (e.g., activated carbons, minerals, lignocellulosic/polysaccharides) to synthetic

polymeric resins (e.g. Amberlite®, Supellite™ or Reillex™) have been considered. Characteristics like durability, stability, ease of regeneration and the possibility to create tailored active materials are important benefits associated to synthetic polymer resins. Pharmaceuticals, biotechnological, environmental and chemical production are some application fields with a high use of polymer resins for the separation and purification of desired compounds. Improvement of the selectivity and binding capacity of the materials for target compounds can be achieved through synthetic routes allowing their functionalization. In this context, the introduction of stereospecificity in the materials considering molecular imprinting techniques is a way of functionalization. Our research group has demonstrated the use of synthetic polymers with the molecular recognition for the valorization of polyphenols present in some agriculture residues (some example olive leaves [3], winemaking residual diatomaceous earth [4] onion shell [5])

The development of hybrid materials, combining natural and synthetic polymers, is also possible using appropriate synthesis routes, namely controlled radical polymerization (CRP), allowing to address the eco-sustainability requirements with the inclusion of the natural materials.

In this work, we address the development of tailored hybrid adsorbents and their application in sorption/desorption processes for the enrichment of flavonoids present in olive leaf extracts and winemaking residues extracts (namely in grape pomace and diatomaceous earth) as shown in graphical abstract. Surface molecularly imprinted cellulose-synthetic hybrid particles, prepared via atom transfer radical polymerization (ATRP) were developed to assess the combination in the same material of high retention capability (selection of appropriated synthetic functional monomers), selectivity towards target compounds (molecular imprinting), enhancement of binding site

accessibility and high mass transfer (particles with active surface). All these characteristics were combined in core-shell particles with cellulose core, highlighting the possibility for generation of advanced natural-synthetic materials with application in the development of sustainable processes in the framework of circular bioeconomy.

Methodology

The synthesis approach here considered for surface molecular imprinting (as shown in our recent paper [6]): (i) the immobilization of α -bromoisobutyryl bromide (BIBB) in pristine microcrystalline cellulose (MCC) to generate ATRP macro-initiator particles (MCC-Br) and, (ii) the grafting of a crosslinked-imprinted shell in the surface of these particles through ATRP with 4-vinylpyridine (4VP) as functional monomer, ethylene glycol dimethacrylate (EGDMA) as crosslinker and quercetin as the flavonoid template. Selected imprinted particles are assessed in adsorption and desorption processes using standard polyphenol compounds and then progressing to residues' extracts originating from olive leaves and winemaking. The adsorbed and desorbed fractions were analyzed in HPLC.

Discussion

In Figure 1 are presented examples of the analysis of some elution fractions collected during the desorption of the selected material, pre-loaded with an olive leaves extract dissolved in ethanol/water (50/50) at 5mg/ml. These results highlight the performance of the developed MCC_MIP particles in compounds separation due to the different binding strengths. Key compounds such as oleuropein, verbascoside, oleurosides, luteolin-7-O-glucoside, apigenin-7-O-glucoside, luteolin-4-O-glucoside, and quercetin are considered to illustrate these aspects. The fraction recovered in water is enriched with oleuropein, verbascoside and oleurosides comparatively to the initial extract. When the elution strength of the solvent increase substantially (alcohol content and pH), as in case of Methanol/Acetic Acid (90/10) the compounds with a strong binding to the MMC_MIP can be recovered. This is observed for example with luteolin-4-O-glucoside, and quercetin (the template used to synthesize the materials) due to the strong

interaction with the material, thus their removal was only possible with MeOH/Acetic Acid (90/10). In terms of quantities analysis, we estimated the enrichment factor to be around 4 for the flavonoid's family and in particular 3.5 for the imprinting template quercetin, comparatively to the initial extract [6]. Similar results were also obtained considering grape pomace and diatomaceous earth extracts. Furthermore, the synthesized particles are able to retain polyphenols in low-water content solvents which is advantageous compared to the commercial resins that require high water content in order to function properly.

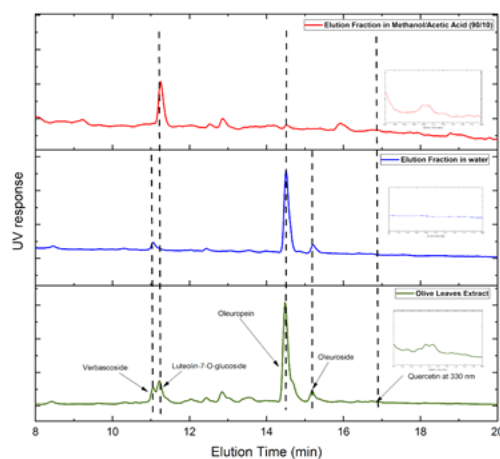


Figure 1. HPLC-DAD chromatograms for two elution fractions collected during the desorption of selected MIP material, pre-loaded with the olive leaf extract in ethanol/water 50/50 at 5 mg/mL. Measurement at 280 nm are presented to highlight the fractionation of flavonoid and non-flavonoid compounds. The inset demonstrates the peak of quercetin obtained at 330 nm, since it is not possible to see the peak at 280 nm (it is present in initial extract in very small concentration).

Conclusions

With these very interesting results, we highlight the production of flavonoid-enriched fractions from the complex olive leaf extract through sorption/desorption processes with developed imprinted particles.

Acknowledgements

We acknowledge the support through the OLEAF4VALUE project. This project has received funding from the Bio-Based Industries Joint Undertaking under the European Union's Horizon 2020 research and innovation programme under grant agreement n° 101023256. We also acknowledge the funded of "BacchusTech-Integrated Approach for the Valorization of Winemaking Residues" (POCI-01-0247-FEDER-069583), supported by the Competitiveness and Internationalization Operational Program (COMPETE 2020), under the PORTUGAL 2020 Partnership Agreement, through the European Regional Development Fund (ERDF). Catarina Gomes acknowledges to FCT for the PhD scholarship 2020.06057.BD. We also thank to NATAC for providing the olive leaf extracts and the aid with the identification by LC-MS of compounds there contained. Rolando Dias is grateful to the Foundation for Science and Technology (FCT, Portugal) for financial support through national funds FCT/MCTES (PIDDAC) to CIMO (UIDB/00690/2020 and UIDP/00690/2020) and SusTEC (LA/P/0007/2020). Mário Rui Costa acknowledges the support by LA/P/0045/2020 (ALiCE), UIDB/50020/2020 and UIDP/50020/2020 (LSRE-LCM), funded by national funds through FCT/MCTES (PIDDAC).

References

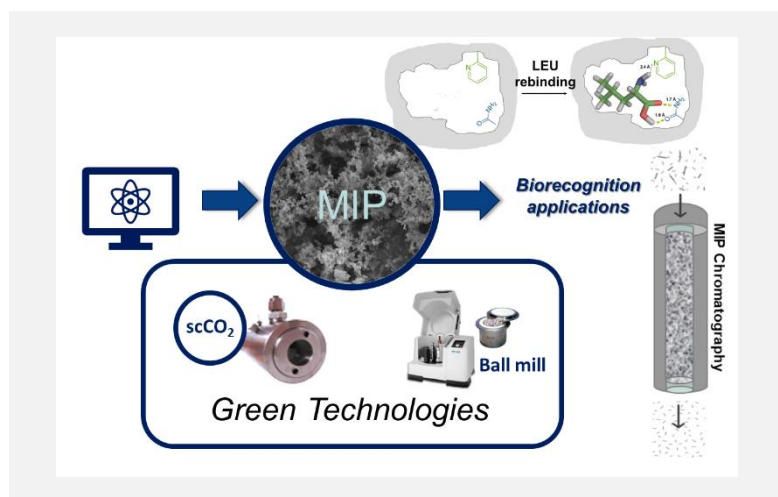
- [1] M.A. Amran et al., *Sustainability*, 13 (2021) 11432.
- [2] "OLEAF4VALUE, Olive leaf multi-product cascade based biorefinery." <https://oleaf4value.eu> (accessed Mar. 22, 2023).
- [3] C.P. Gomes et al., *Reactive and Functional Polymers*, 164 (2021) 104930.
- [4] A. Bzainia et al., *Molecules*, 27 (2022), 6406.
- [5] C.P. Gomes et al., *Chromatographia*, 83 (2020) 1539-1551.
- [6] C.P. Gomes et al., *Macromolecular Reaction Engineering*, 17 (2023) 2300011.

Green affinity-driven biopurification materials: supercritical CO₂ technology versus mechanochemistry

A.I. Furtado^{1,2*}, R. Viveiros¹, V.D.B. Bonifácio², A. Melo³, T. Casimiro¹

¹LAQV-REQUIMTE, Chemistry Department, NOVA School of Science & Technology, NOVA University of Lisbon, 2829-516 Caparica, Portugal; ²iBB-Institute for Bioengineering and Biosciences and i4HB-Institute for Health and Bioeconomy, Instituto Superior Técnico, University of Lisbon, Av. Rovisco Pais, 1049-001 Lisbon, Portugal; ³LAQV-REQUIMTE, Departamento de Química e Bioquímica, Faculdade de Ciências, Universidade do Porto, Rua do Campo Alegre, 4169-007 Porto, Portugal.

*ai.furtado@campus.fct.unl.pt



The production of biological products is increasing, with a consequent intensification of separation and purification processes. According to recent market research, the global market for bioseparation/purification systems is valued in EUR 13 billion in 2022 and have a compound annual growth rate (CAGR) of 13 % (2022-2026) [1]. However, current separation and purification processes in bioprocesses are expensive and, in some cases, inefficient and/or with low-specific solutions [2]. To address this demand, herein, the sustainable development of innovative affinity polymeric materials towards biomolecule(s) is proposed, specially designed to overcome the current limitations in biopharmaceutical industry field, using green technologies such as supercritical CO₂ (scCO₂) and mechanochemistry (ball milling).

Introduction

Molecular Imprinting Technique (MIT) is a synthetic way to create specific affinity sites within crosslinked polymers, complementary in terms of size, conformation and functionality with the target molecule, known as Molecularly Imprinted Polymers (MIPs). Conventional MIP synthesis for biomolecules typically uses organic solvents with a small fraction of water to increase their solubility [3]. The water molecules interfere with the interactions between the template and the functional monomer, and negatively affect the stabilization of the template-monomer complex. Moreover, in the conventional strategies, MIPs are obtained as hard blocks that need to be further crushed, which can destroy the affinity cavities created during the molecular imprinting process [4]. Therefore, the combination of MIT with green technologies (scCO₂ and mechanochemistry) overcomes the conventional MIP drawbacks and brings new features to the materials compared to conventional ones. CO₂ is abundant, non-toxic, non-flammable, has a very accessible critical point and its properties are easily tuned. By simply adjusting pressure and temperature, it is possible to tune its solvent power which make it very attractive as an alternative solvent for polymerization reactions [5]. On the other hand, mechanochemistry is an expanding technology that is easily scalable, that besides the requirement of a low-cost equipment, operates under solventless conditions, and has shown to be a fast, simple and efficient route for polymerization reactions, avoiding solubility issues [6]. Herein, it is described the rational design and green synthesis of MIPs with molecular recognition ability for L-leucine (LEU) (LEU-MIPs) [3].

Methods

The LEU-MIPs were developed as sustainable affinity polymers from a bottom-up perspective. Firstly, rational design using quantum mechanics calculations through Gaussian 09 software and molecular modeling through Autodock Vina 1.2.0 software

were performed to select the most appropriate functional monomers. Nine functional monomers, commonly used in molecular imprinting polymerization reactions, such as: 2-vinylpyridine (2VP), 4-vinylpyridine (4VP), acrylic acid (AA), acrylamide (AM), 2-acrylamido-2-methylpropane sulfonic acid (AMPS), itaconic acid (ITA), N-vinylpyrrolidone (NVP), styrene (STY) and 1-vinylimidazole (VIIM), were investigated as potential monomers for LEU-MIP synthesis. Then, LEU-MIPs were synthesized by both green technologies. The scCO₂-assisted LEU-MIP polymerization, was carried out in a 33 mL stainless steel high-pressure cell, using a Template:Monomer:Crosslinker (T:M:C) molar ratio of 1:50:100, using 2VP and AM as functional monomers, ethylene glycol dimethacrylate (EGDMA) as crosslinker, and 2 wt.% V-65 (total weight % of monomer and crosslinker) as the thermal initiator. LEU (3 mg) was previously dissolved in 0.5 mL of ethyl acetate (EtOAc) and kept under stirring for 4 h. All reagents were placed in the high-pressure cell, with a magnetic stirring bar, and immersed in a thermostatted water bath at 45 °C. CO₂ was loaded up to 200 bar using a Knauer – 1900 liquid pump. After 24 h of reaction, a homogeneous crosslinked polymer was obtained. At the end of the reaction, the polymer was slowly washed with fresh CO₂ for 1 h to remove unreacted starting materials. For the LEU-MIPs mechanochemistry, the mechanochemical polymerization reaction was performed in a PM100 planetary ball mill (Retsch) using a zirconium oxide reactor containing 200 zirconium oxide balls of 5 mm diameter. The reaction occurred for 6 h, at 500 rpm, with rotation inversion cycles of 30 min. The T:M:C molar ratio (1:50:100) was the same used in the scCO₂-assisted polymerization reactions. Sodium persulfate, 10 wt.% (total weight % of monomer and crosslinker) was used as the initiator, and NaCl (twice the total weight of reactants) was added as a porogenic agent. At the end of the reaction, the polymer was washed with water and methanol to remove unreacted starting materials, filtered and

dried under vacuum system. In both technologies, the NIP was synthesized following the same procedure, but without template (LEU) addition. The MIPs obtained by both technologies were submitted to a template-desorption process in scCO₂ to remove the LEU using the well-established conditions of 40 °C and 200 bar and 1% (v/v) of EtOAc co-solvent in continuous mode during 3 h. Then, the performance of the produced materials was assessed by static binding tests for two different LEU aqueous solutions (0.5 and 1.5 mg/mL) at room temperature using an orbital shaker equipment (100 rpm) for 24 h.

Results

The computational studies (Table 1) suggest that AM was the most suitable monomer to achieve a more stable LEU-monomer complex, corresponding to the lowest binding energy. On the other hand, 2VP was found to be the monomer less favored to form stable LEU-monomer complexes. Both green technologies were effectively applied in the synthesis of LEU-MIPs using both functional monomers (AM and 2VP). The LEU-MIPs were obtained in both technologies, as dry, free-flowing and ready-to-use powders.

Table 1. Binding energies ($\langle \Delta_{bind} H^{\circ} \rangle$) of LEU-monomer complexes, for each lowest energy conformation complex, divided by cluster (1 – more suitable complex to 3 – less suitable complex).

Cluster	LEU-monomer complex	$\langle \Delta_{bind} H^{\circ} \rangle$ (kJ/mol)
1	LEU-AM	-57.86
	LEU-AMPS	-45.63
2	LEU-NVP	-42.69
	LEU-ITA	-41.26
	LEU-AA	-33.26
3	LEU-4VP	-26.03
	LEU-STY	-23.27
	LEU-VIIM	-22.61
	LEU-2VP	-21.25

According to the binding performance (Figure 1 and Table 2), LEU-MIPs prepared by ball milling showed a binding performance in line with the computational studies (Table 1), since higher binding capacity was obtained for the LEU-MIP that used AM as functional monomer. On the other hand, LEU-MIP prepared in scCO₂ did not follow the computational prediction, obtaining a higher binding performance for the LEU-MIP that used 2VP as functional monomer. According to the

Acknowledgements

The authors would like to thank financial support from Fundação para a Ciência e a Tecnologia, Ministério da Ciência, Tecnologia e Ensino Superior (FCT/MCTES), Portugal, through projects PTDC/EQU-EQU/32473/2017, PTDC/MEC-ONC/29327/2017 and PTDC/QUI-QIN/30649/2017 (REALM). A.I.F. acknowledges her PhD grant (SFRH/BD/150696/2020) in the aim of the International Year of the Periodic Table - a Protocol established between the Portuguese Chemical Society (SPQ) and the FCT/MCTES. R.V. would like to acknowledge to Individual Scientific Employment Stimulus (CEEC-IND), reference 2020.00377.CEECIND from the FCT/MCTES, Portugal. The Associate Laboratory Research Unit for Green Chemistry – Clean Technologies and Processes – LAQV-REQUIMTE is financed by national funds from FCT/MCTES (UIDB/50006/2020, UIDP/50006/2020, and UID/QUI/50006/2020) and co-financed by the ERDF under the PT2020 Partnership Agreement (POCI-01-0145-FEDER – 007265).

References

- [1] Biopharmaceutical biopurification systems market to value \$20bn. <https://www.europeanpharmaceuticalreview.com/news/172719/biopharmaceutical-biopurification-systems-market-to-value-20bn/> (accessed March 3, 2023).
- [2] O. Khanal, A.M. Lenhoff, mAbs, 13 (2021) 1-13.
- [3] A.I. Furtado et al., ACS Omega, 8 (2023) 9179-9186.
- [4] R. Viveiros et al., Polymers, 10 (2018) 1-27.
- [5] A.I. Furtado et al., Methods in Molecular Biology, 2359 (2021) 19-42.
- [6] K.J. Ardila-Fierro, J.G. Hernández, ChemSusChem, 14 (2021) 2145-2162.

binding results, a significant imprinting factor (IF , Q_{MIP}/Q_{NIP}) of 12 was obtained for the LEU-MIP synthesized in scCO₂ using 2VP as functional monomer, while the LEU-MIP using AM as functional monomer synthesized by ball milling, showed an IF of 1.4, both systems at 0.5 mg LEU/mL.

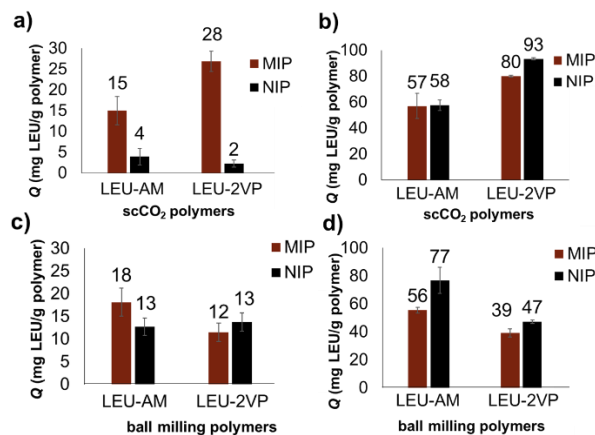


Figure 1. Binding capacities (Q) of LEU-MIPs obtained using scCO₂ at a) 0.5 mg LEU/mL and b) 1.5 mg LEU/mL, and for LEU-MIPs obtained by ball milling at c) 0.5 mg LEU/mL and d) 1.5 mg LEU/mL.

Table 2. Imprinting factors (IF s) for LEU-MIPs.

Polymer		0.5 mg LEU/mL	1.5 mg LEU/mL
Technology	Complex		
ScCO ₂	LEU-AM	3.9	1.0
ScCO ₂	LEU-2VP	12.1	0.9
Ball milling	LEU-AM	1.4	0.7
Ball milling	LEU-2VP	0.8	0.8

As expected, at the highest concentration (1.5 mg LEU/mL), the binding capacity was considerably increased, but low imprinting factors were obtained.

Conclusion

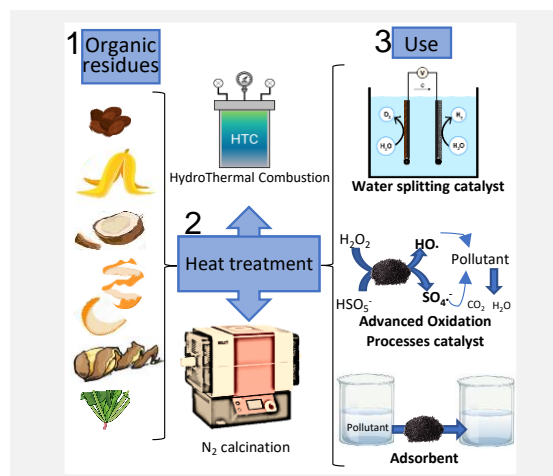
LEU-MIPs were successfully synthesized using both green strategies (scCO₂-assisted polymerization and mechanosynthesis), and showed to have high potential in obtaining innovative, ready-to-use, stable, low-cost affinity polymers with biorecognition ability for LEU. These LEU-MIPs are envisaged to act as advanced cost-effective materials for demanding biopurification downstream processes in which affinity, efficiency, and cost are critical issues.

Agroindustry residues as powerful materials for environmental remediation and energy generation

A.M. Díez*, V. Laíño-Rodríguez, M. Bolaños-Vázquez, M.A. Sanromán, M. Pazos

BIOSUV Research Group, CINTECX, University of Vigo, As Lagoas Marcosende s/n, Vigo, Spain.

*adiez@uvigo.gal



The growing world population is causing an increase in water pollution with organic residues, and energy demand. As a solution for water pollution, adsorption process is regarded as quick and easy-to-apply process. Another option for contaminants abatement is the application of Advanced Oxidation Processes (AOPs) which are based on the generation of radical species which attack quickly and non-selectively the organic matter, degrading it. On the other hand, to cope with the energy demand, water splitting reactions are proposed as an environmentally friendly process for H₂ and H₂O₂ generation. Those three processes (adsorption, AOPs and water splitting) can be applied to lower their cost and reduce environmental problems by the utilization of organic residues from several industry sectors. Thus, agroindustry residues can be thermally treated (hydrothermal treatment or N₂ calcination) in order to have carbonaceous materials which may be used either as adsorbents or AOPs and water splitting catalysts. The results hereby presented demonstrate it is possible to apply a circular economy approach to several agroindustry residues.

Introduction

The exponential population growth has been related to an increase in contaminants in water. This is related to inefficient wastewater treatments. The typical wastewater treatment plant is based on the application of a biological degradation process which can be slow and unsuitable for the treatment of toxic pollutants. Both adsorption processes and AOPs are proposed as a quick remediation alternative and as an option for the elimination of toxic pollutants such as pharmaceuticals or pesticides [1].

Adsorption processes could be applied at a real scale by using low-cost and high-performance adsorbents. Carbon-based materials have been widely proposed, considering their porous structure. Regarding AOPs, they require catalysts for radicals generation. On this sense, several oxidants can be activated with carbonaceous materials such as peroxymonosulphate (PMS) or peroxydisulfate (PDS) [2], for the generation of SO₄^{•-}. Moreover, the slight addition of some metals (specifically Fe) can favour the activation of hydrogen peroxide (H₂O₂) on the so-called Fenton process for the generation of HO· [3]. The immobilization of metals on carbonaceous materials is an interesting way of using environmentally friendly heterogeneous AOPs catalysts.

Both elimination processes can be used for the treatment of wastewaters polluted with pharmaceutical compounds, considering their stability to traditional treatments [1]. Specifically, this study is focused on the elimination of the antidepressant fluoxetine, which usage has been increased during the last years [4].

On the other hand, energy expenditure has increased meanwhile fossil fuels are being extinguished. Thus, water splitting reactions are being used as H₂ and H₂O₂ source. On this electrochemical process, a catalyst should be added in order to reduce the overpotential required for the electrochemical reaction to happen. However, the typically used catalysts are based on the utilization of rare metals, increasing both the price and the toxicity of the process. Some authors have tried to use carbon-based materials as catalysts although this research is on early stage [5].

Objectives

The main aim of this study is to synthesize different carbon-based materials from agroindustry residues. Those materials will be screened as adsorbents and catalysts for AOPs as well as for water splitting reactions. Moreover, some modifications would be carried out in order to enhance the attained results.

Methods

Carbon-based materials synthesis

The agroindustry residues (spent coffee, spinach stem, rice bran and potato, corn, banana and chestnut peels) were washed, dried and grounded prior to synthesis.

In the case of hydrothermal synthesis (HTC) a 50 mL autoclave was used, where 40 mL of water and 8 g of the agroindustry residue were added. Then the synthesis took place for 2 h at 220°C, attaining the so labelled hydrochars.

For N₂-calcination synthesis, a tubular furnace (Aero-360) was used and N₂ was fixed at 2 L/min. Initially, 400 or 800°C were essayed, although the best performing materials were further optimized. In all cases, the residues were heat-treated for 2 h, having reached the fixed temperature at a rate of 10°C/min, attaining the so-called biochars.

Water splitting reactions

Hydrogen Evolution Reaction (HER), Oxygen Evolution Reaction (OER) and Oxygen Reduction Reaction (ORR) were evaluated. In all cases, Hg₂Cl₂ was used as the reference electrode. HER and ORR were carried out under acid conditions (0.5 M H₂SO₄) and using carbon paper as the working electrode where the biochars were placed (0.25 mg/cm²) and carbon stick as the counter electrode. In the case of alkaline OER (1 M NaOH), Ni-foam was used as the working electrode and Pt wire as the counter electrode.

Adsorption and AOPs tests

The removal of 30 ppm of fluoxetine was evaluated. For that, 10 mg of the as-prepared carbon-based materials were mixed with 50 mL of the fluoxetine solution in a glass tube which was placed in a rotary shaker. Adsorption tests were left for 24 h at 80 rpm. For AOPs, 2 mM of either PMS, PDS or H₂O₂ was added to the reactor tubes and a sample was taken after 1 h of reaction. In order to improve the AOPs performance, the

hydrochars were doped with Fe so they were left for 5 h under stirring in a FeCl_3 solution (50 mM) and then dried overnight at 100°C , attaining Fe-hydrochars.

Results

Materials characterization

The biochars (after N_2 calcination) and hydrochars (after HTC synthesis) were attained from spent coffee, spinach stem, rice bran and potato, corn, banana and chestnut peels. Moreover, Fe-biochars were gotten after Fe impregnation. All of them were evaluated in terms of porosity (N_2 isotherms), ratio C/N (macro analysis), pH (measurement of the Point of Zero Charge:PZC) and structure (SEM and EDS analysis). This demonstrated the synthesis procedure and the raw agroindustry residue has an important effect on the final properties of the synthesized carbon-based materials.

Materials screening for HER, OER and ORR

Figure 1 shows the results of the best performant carbon-based materials for water splitting reactions. The synthesized materials did not show activity as acid HER catalysts. However, some of the natural materials provided promising results as acid ORR and alkaline OER catalysts. Specifically, all the hydrochars showed activity on ORR and some of the biochars and hydrochars demonstrated to favour OER. The differences in the performance are related to the porosity, the PZC and the ratio C/N.

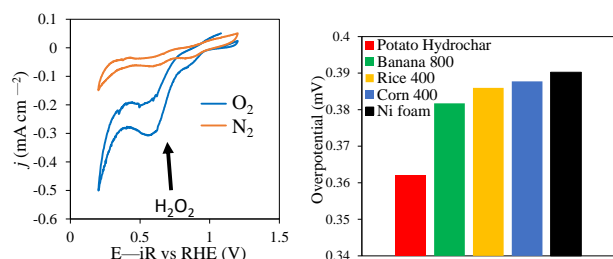


Figure 1. Acid ORR generation of chestnut HTC (left graph) and alkaline OER performance of biochars at different temperatures and potato hydrochar (right graph).

Materials screening for fluoxetine removal

The evaluation of the adsorption capacity of the synthesized materials led to interesting results. To begin with, most of them

present an acceptable uptake, surpassing 20 mg/g, which defeats previously reported data [6]. Moreover, the heat-treatment process selection has been demonstrated to have a great impact on the adsorption performance. For instance, rice bran provided an uptake of 65.5 mg/g when being HTC-synthesized (hydrochar) whereas 21.2 mg/g was attained when using N_2 -carbonization (biochar). Additionally, it can be seen how the temperature effect on N_2 -carbonization varies depending on the treated agroindustry residue. Being more significant in the case of banana peel (Table 1) and almost negligible in the case of rice bran or chestnut peels. This fact can be explained by the different properties of the raw and heat-treated materials, mainly in terms of porosity and C/N ratio.

In order to avoid spent adsorbent disposal, regeneration assays were performed. Fenton-like and PMS oxidation did not cause any fluoxetine degradation. On the case of PDS, the best regeneration degree was 40% for the spinach biochar.

Considering hydrochars were more economic to synthesize (220°C), provided higher adsorption uptakes and were more difficult to regenerate, Fe impregnation was done. Thus, Fe-hydrochars were tested and not only this modification improved the attained uptakes by more than 100%, but also the regeneration by Fenton-like processes was highly efficient (Table 1).

Conclusions

Several porous carbonaceous materials were synthesized using agroindustry residues as starting point. Thus, biochars and hydrochars were attained which demonstrated to have widely different properties depending on the synthesis process or the temperature. The vast majority of the attained materials demonstrated a high adsorption degree of fluoxetine. AOPs regeneration process was difficult unless the addition of Fe take place. Parallely, the synthesized materials showed catalytic behaviour on alkaline OER and acid ORR, reducing the overpotential required for water splitting reactions.

These results demonstrate that not only it is possible to apply circular economy to agroindustry residues but also that metal-free compounds can act as efficient catalysts for adsorption and water splitting reactions. Moreover, slight Fe additions make also these agroindustry residues to act as Fenton-like catalysts.

Table 1. Best results for the elimination of fluoxetine after 24 h adsorption and after 1 h Fenton-like regeneration.

Synthesis (T^a) biochar	Uptake (mg/g)	Fe-hydrochar	Uptake (mg/g)	Fenton-like degradation (%)
banana				
220	146.48	Rice	135.14	50.92
400	69.67	Coffee	151.69	83.50
600	56.86	Potato	151.81	66.76
800	57.68	Banana	151.99	33.40

Acknowledgements

The researcher Aida M. Díez is grateful to Xunta de Galicia for the financial support obtained (ED481B 2019/091) and to the project CINTECX-CHALLENGE 2023. This research has been financially supported by Project PID2020-113667GBI00 funded by MCIN/AEI/10.13039/501100011033.

References

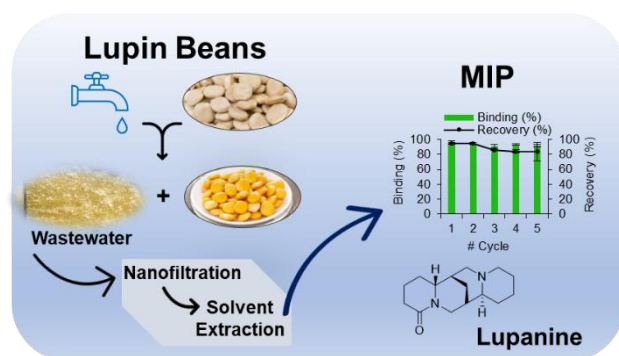
- [1] S. Escudero et al. Chemosphere, 268 (2021) 129318-129326.
- [2] S. Gao et al., Applied Surface Science, 599 (2022) 153917-153929.
- [3] Z. Zhang et al., Journal of Water Process Engineering, 51 (2023) 103391-103400.
- [4] J.L.B. Simões et al. Cellular and Molecular Neurobiology, 43 (2022) 621-637.
- [5] Y. Du et al., International Journal of Hydrogen Energy, 48 (2023) 894-908.
- [6] A. Puga et al., Journal of Environmental Chemical Engineering, 10 (2022) 106977-106919.

Material development contribution to improve biorefinery sustainability

T. Esteves^{1*}, A.S. González², A. Gil², C.A.M. Afonso³, F.C. Ferreira¹

¹iBB-Institute for Bioengineering and Biosciences and Department of Bioengineering, Instituto Superior Técnico, Universidade de Lisboa, 1049-001 Lisboa, Portugal; Associate Laboratory i4HB-Institute for Health and Bioeconomy at Instituto Superior Técnico, Universidade de Lisboa, 1049-001 Lisboa, Portugal; ²Centro de Química e Bioquímica and BioISI-Biosystems and Integrative Sciences Institute, DQB, Faculdade de Ciências, Universidade de Lisboa, 1749-016 Lisboa, Portugal; ³Research Institute for Medicine (iMED, ULisboa); Faculty of Pharmacy, Universidade de Lisboa, 1649-003 Lisboa, Portugal.

*teresa.esteves@tecnico.ulisboa.pt



Lupanine is an alkaloid explored in the pharma industry as a precursor for the synthesis of sparteine, which is used as a chiral selector. This alkaloid is found in lupin beans processing wastewaters originated from the debittering process to make these beans edible. Molecular modeling was pursued to design a molecularly imprinted polymer (MIP) with itaconic acid, a biobased building block, as a functional monomer with high affinity for lupanine, and ethylene glycol dimethacrylate as a cross-linker, by bulk polymerization. Lupanine was concentrated from lupin bean wastewater by nanofiltration, extracted with ethyl acetate, and its purity was improved from 78 to 88%, using the MIP, that was able to selectively recognize lupanine, with an overall 82% recovery of the alkaloid. These results show the potential of the contribution of innovative material development to render an industrial process more sustainable.

Introduction

Lupin beans are highly nutritious seeds, low in fats and sugars, with a high fiber content, being used as snack or protein source in food products (pastry products, bread, mayonnaise, and hamburgers) [1]. The seeds have a bitter taste due to the presence of a toxic alkaloid (lupanine) and, to become edible, the alkaloid must be removed using several m³ of fresh water [2] in a process called debittering that comprises several stages: hydration, cooking, and thorough washing of the seeds. At the end, edible seeds are obtained together with high volumes of wastewater with high lupanine content. Lupanine toxic effects are documented [3], and regulated values are followed for incorporation in food products [4]. However, it is a versatile building block with application in the pharmaceutical industry, being assessed for the treatment of type 2 diabetes and as the precursor of sparteine, which is a recognized chiral selector [5]. Its complex chemical structure makes its synthesis quite challenging, therefore its recovery from the wastewaters of lupin bean processing is important, making this an added-value compound of great interest. We explored nanofiltration (NF) coupled to solvent extraction (SE) to recover lupanine [6]. However, further selective separation is still required because of the coexistence of compounds with similar functional groups, for example, from the alkaloid family, such as lupanine and sparteine. We therefore designed an adsorber with high affinity for lupanine, compatible with its recovery from the ethyl acetate (EtOAc) fraction, ultimately improving its purity.

Since there is an urge for sustainable polymer production, using building blocks derived from green sources, itaconic acid (IA) was assessed as functional monomer to obtain a molecularly imprinted polymer (MIP). IA is obtained by biofermentation of lignocellulosic biomass [7] and presents two carboxylic acid groups and one vinyl group, that makes it a versatile bio-based platform for the synthesis of the envisaged polymeric material for lupanine isolation [8].

The strategy disclosed presents versatility to be further explored in other food processing industries, originating alkaloid-rich

waste streams, comprising added-value compound recovery at the same time as lowering fresh water consumption, with recycling of water used in the industrial processes, tackling environmental water scarcity burden.

Material Development

MIPs were prepared by bulk polymerization, using lupanine as the template, ethylene glycol dimethacrylate (EGDMA) as cross-linker, and AIBN as the initiator. Several functional monomers were assessed, with molecular modeling studies supporting the choice of IA as the functional monomer (Figure 1). Complete characterization of this MIP was performed including, isotherm binding, kinetic, and reutilization studies. The recovery of lupanine was assessed using industrial wastewaters.

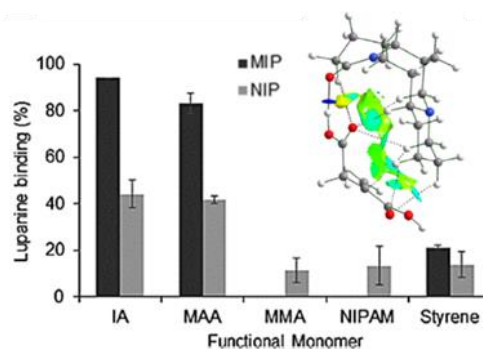


Figure 1. Top: Binding of lupanine in MIP and NIP polymers, obtained with several functional monomers, in EtOAc. Lupanine solutions of 1 g/L were loaded on 50 mg/mL of scavengers ($n = 2$). Inset: complex formed between lupanine and IA (blue: attractive forces, green: weak interactions). MAA – methacrylic acid, MMA – methyl methacrylate, NIPAM – N-isopropylacrylamide.

A higher performance for lupanine recognition (>95%) than the respective NIP (<40%), in several organic solvents (EtOAc, MTBE, EtOH, and DCM), was obtained (Figure 1), despite a

smaller surface area of MIP (37.53 m²/g) compared to NIP (271.23 m²/g). The MIP showed an adsorption process following the Freundlich model, reaching equilibrium within 1 h by a pseudo-second-order kinetic model. This adsorber allowed a good recovery yield of lupanine (82–87%) both for pure samples and the ones from industrial wastewaters. It also maintained its performance for at least 5 consecutive cycles of binding/recovery as shown in the Graphical Abstract.

Process Design

Unit operations were assessed separately and optimized for lupin beans wastewater treatment and recycling, and lupanine recovery. From the nanofiltration (NF) the NF270 membrane showed the highest lupanine (99.5%) and remaining organic matter (94%) rejections. Therefore, further isolation of lupanine from this stream was evaluated by solvent extraction (SE), with EtOAc as the best performing solvent, allowing a recovery of 98% of lupanine, with 78% purity, achieved after 3 successive extractions.

By coupling the MIP adsorption stage to NF and SE (NF+SE+MIP), it was possible to recover lupanine with 88% purity (Figure 2). These results show the potential applicability of a high-affinity material to isolate an added-value compound from waste generated from the food industry, rendering the process more sustainable.

Acknowledgements

The authors acknowledge Tremoceira M. Ferreira Bastos Lda., Portugal, for providing the industrial wastewater samples and dedicated funding from Water-Works2014 ERA-NET Cofunded Call, through the collaborative project ID 278-Biorg4WasteWaterVal+, Fundação para a Ciência e Tecnologia (FCT) through the projects WaterJPI/0002/2014, PTDC/QUI-QFI/29236/2017, and PTDC/QEQ-PRS/4157/2014 (SelectHost), and the iBB-Institute for Bioengineering and Biosciences (UIDB/04565/2020), from Programa Operacional Regional de Lisboa 2020 (Lisboa-01-0145-FEDER-007317).

References

- [1] F.E. Carvajal-Larenas et al., *Critical Reviews in Food Science and Nutrition*, 56 (2016) 1454-1487.
- [2] P.J. Bebeli et al., *Agronomy*, 10 (2020) 1038.
- [3] A. Al-Abdoun et al., *Journal of Research in Health Sciences*, 5 (2020) 22-26.
- [4] D. Resta et al., *Molecular Nutrition & Food Research*, 52 (2008) 490-495.
- [5] O. Chuzel et al., *Sparteine as a Chiral Ligand for Asymmetric Catalysis in Chiral Diazaligands for Asymmetric Synthesis*. Topics in Organometallic Chemistry, M. Lemaire and P. Mangeney Editors, Springer, Berlin, 2005, 15, 59-92.
- [6] T. Esteves et al., *Journal of Cleaner Production*, 277 (2020) 123349.
- [7] B.E. Teleky et al., *Polymers*, 11 (2019) 1035.
- [8] T. Esteves et al., *ACS Applied Materials & Interfaces*, 14 (2022) 18910-18921.

The treated water obtained in the NF permeate, representing 80% of the debittering step wastewater, can be further re-used within the industrial process addressing a major environmental issue concerning savings in the use of high amounts of fresh water in the lupin beans debittering process.

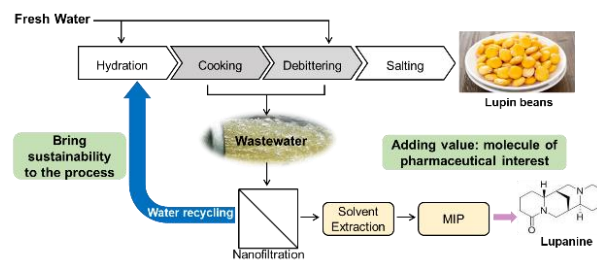


Figure 2. Proposed strategy for lupanine isolation from lupin beans wastewaters with water recycling.

Conclusions

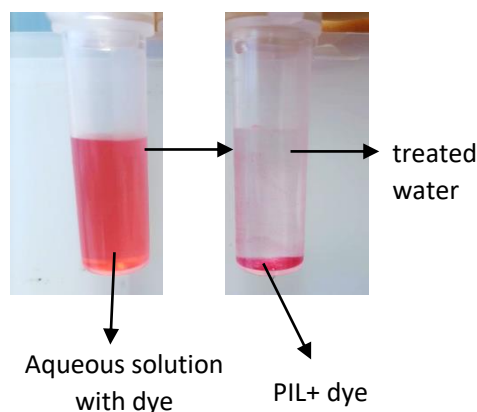
The new bio-based polymer here described allowed the isolation of an alkaloid from a very complex matrix, wastewater, by simple solvent extraction followed by a simple polishing step with a MIP. This strategy presents the versatility to be further explored in other food processing industries, originating alkaloid-rich waste streams, allowing the recovery of added-value products and recycling of 80% of water used in the industrial process contributing to its sustainability.

Dyes removal using poly(ionic liquids)

G. Caetano¹, B. Soares¹, M.M. Correia², I.M. Marrucho^{1*}

¹Centro de Química Estrutural, Departamento de Engenharia Química, Instituto Superior Técnico, Universidade de Lisboa, Avenida Rovisco Pais, 1049-00 Lisboa, Portugal; ²REQUIMTE/LAQV, Instituto Superior de Engenharia do Porto, Instituto Politécnico do Porto, Rua Dr. António Bernardino de Almeida, 431, 4249-015 Porto, Portugal.

*isabel.marrucho@tecnico.ulisboa.pt



Contamination of water by micropollutants, such as dyes from the textile industry, represents a serious environmental and public health challenge. In this way, it becomes necessary to develop new materials that can be readjusted and processed, in order to present high surface areas. In this context, poly(ionic liquid)s (PILs), that combine the attractive features of ionic liquids (ILs) with the mechanical properties of polymers, have been playing prominent roles in the design of highly performant smart materials. This study focuses on the extraction of dyes in aqueous solution, using the polymer poly(diallyldimethylammonium) bis(trifluoromethylsulfonyl)imide (Poly[Pyrr11][NTf2]), proceeding to increase the surface area through the grinding of the PIL itself, and the introduction of porosity under supercritical CO₂ admissions.

Introduction

Dyes are believed to have been used over 180,000 years ago, mostly extracted from plants, but nowadays more than 1 million tons are industrially produced each year and used primarily by textile industries [1]. In these industries, for the textile dyeing process, the dye is hydrolysed. As a result, about 10 to 15% of the dye used remains unused and discharged into the environment [2]. This causes problems to the aquatic life and therefore industrial wastewater treatment needs to be performed before releasing. Poly(ionic liquid)s (PILs) have already been explored as adsorbents for the extraction of acid, basic and azo dyes such as bromo phenyl blue, methyl blue, orange II, sunset yellow or amarant, mainly through the use of imidazolium based PILs [3-4]. The final objective is to use oxidation methods to oxidize the dye, while keeping the integrity of the PIL.

Objectives

This work aims to further evaluate the real potential of PILs, namely poly(diallyldimethylammonium bis(trifluoromethylsulfonyl)imide) (Poly[pyrr11][NTf2]), as sorbent materials for removing direct red 80 dye from aqueous solutions. Furthermore, the optimization of extraction parameters such as time, initial dye concentration, ratio of PIL to aqueous solution, PIL particle size and PIL porosity were evaluated.

Methods

For that purpose, Poly[pyrr11][NTf2] was synthesized by anion exchange, which basically consists of adding an aqueous solution of LiNTf2 in molar excess to an aqueous solution of poly(diallyldimethylammonium chloride) (Poly[Pyrr11]Cl), under vigorous stirring. At the end, the white precipitate is consecutively washed with water to extract LiNTf2 and LiCl and dried in an oven ($T = 40^{\circ}\text{C}$ and $p = 1\text{ Pa}$) until constant weight. The introduction of porosity in the Poly[pyrr11][NTf2] was carried out the use of supercritical CO₂.

For the study of dye removal from the aqueous solution, dye samples were prepared and Poly[pyrr11][NTf2] was added and stirred in a Thermomixer. The effect of experimental parameters such as the initial dye concentration, extraction time, ratio of Poly[pyrr11][NTf2] to liquid, PIL particle size and porosity in the dye extraction efficiency were studied using the STATISTICA Software. Analysis of dye removal efficiency was performed with a UV-vis spectrophotometer (Shimadzu UV Spectrophotometer).

Results and Conclusion

Using the STATISTICA software, a mathematical equation capable of predicting dye extraction efficiencies as a function of initial dye concentration, extraction time and aqueous solution and aqueous dye solution to PIL ratio (LSR) was obtained for two different PIL particle sizes: $< 71\mu\text{m}$ and between 0.45 and 1.00mm, before being submitted to CO₂, as shown in Equations 1 and 2, respectively.

$$\%Efficiency = 9.63 \times 10^{-1} + 5.64 \times 10^{-2}X_1 - 1.64 \times 10^{-3}X_1^2 - 2.63 \times 10^{-3}X_2 - 7.21 \times 10^{-3}X_3 \quad (1)$$

$$\%Efficiency = 1.02 + 1.08 \times 10^{-2}X_1 - 6.50 \times 10^{-4}X_1^2 - 1.36 \times 10^{-3}X_2 - 4.32 \times 10^{-6}X_3^2 + 9.11 \times 10^{-5}X_1 X_2 - 2.01 \times 10^{-6}X_1 X_3 \quad (2)$$

The optimal extraction point was obtained for both studies, predicting an efficiency of $101.1\% \pm 6.8\%$ for Poly[pyrr11][NTf2] of $< 0.71\mu\text{m}$, for a time of 15.2 minutes, initial dye concentration of 47.2 mg/L and a LSR of 63.3. For the PIL of 0.45-1.00mm, an efficiency of $96.2\% \pm 11.6\%$ is predicted, for a time of 23.7 minutes, initial dye concentration of 51.4mg/L and a LSR of 38.6. For each of the optimized parameters, the remaining variables were studied for PIL $< 0.71\mu\text{m}$ and 0.45-1.00mm, as shown in Figures 1 and 2, respectively. In conclusion, Poly[pyrr11][NTf2] allows to adsorb the direct red 80 dye with very high efficiencies and that the use of a smaller particle size has a high influence in the kinetics and in the adsorption capacity.

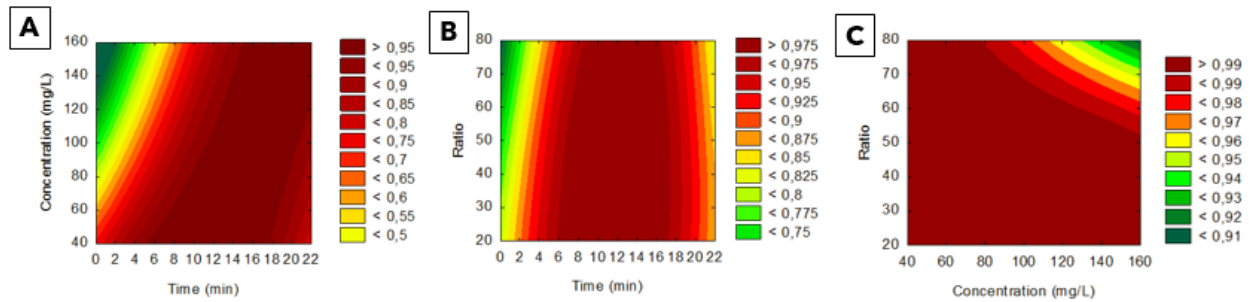


Figure 1. Contour plots/surface plots for the dye extraction efficiency obtained A) relating the time to the initial concentration of dye, keeping the ratio at 63.3 B) relating ratio to the time, keeping the initial concentration of 47.2 mg/L C) relating ratio to the initial concentration, maintaining a time of 15.2 minutes.

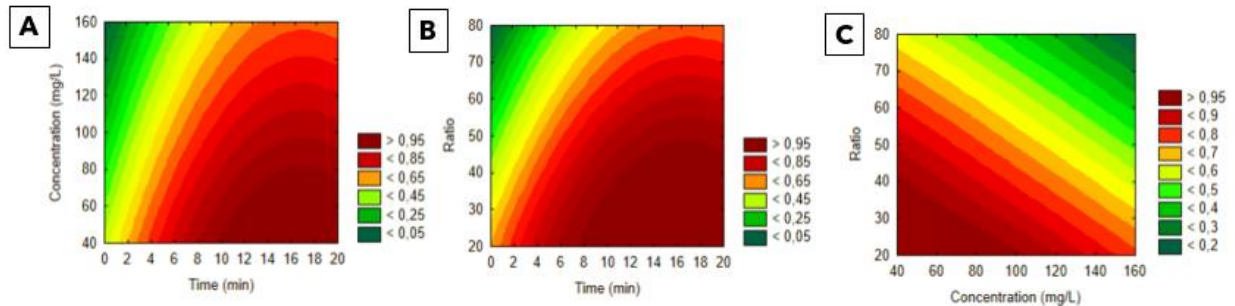


Figure 2. Contour plots/surface plots for the dye extraction efficiency obtained A) relating the time to the initial concentration of dye, keeping the ratio at 38.6 B) relating ratio to the time, keeping the initial concentration of 51.4 mg/L C) relating ratio to the initial concentration, maintaining a time of 23.7 minutes.

Acknowledgements

Gabriela Caetano gratefully acknowledges the financial support of FCT/MCTES (Portugal) for PhD fellowship 2022.11532.BD. This work was financed by CQE project (UIDB/00100/2020 and UIDP/00100/2020). This work was financed by CQE project (UID/QUI/00100/2013) and PTDC/EAMAMB/2023/2021.

References

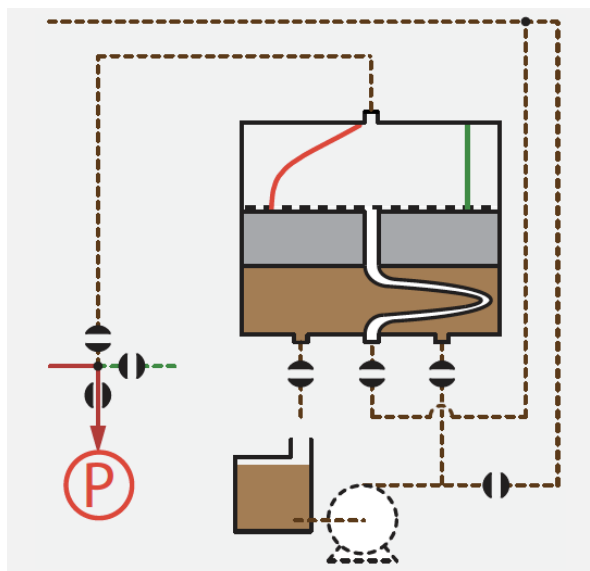
- [1] B. Okutucu et al., *Preparative Biochemistry & Biotechnology*, 40 (2010) 366-376.
- [2] V.K. Gupta, Suhas, *Journal of Environmental Management*, 90 (2009) 2313-2342.
- [3] H. Mi et al., *Polymers (Basel)*, 5 (2013) 1203-1214.
- [4] A.M. Ferreira et al., *Separation and Purification Technology*, 128 (2014) 58-66.

Comparison of continuous chromatography for downstream processing of proteins using an analogy with single-column batch chromatography with recycle lag

J.P.B. Mota, R.C.R. Ribeiro*

LAQV-REQUIMTE, Chemistry Department, NOVA School of Science and Technology, NOVA University Lisbon, 2829-516 Caparica, Portugal.

**pmota@gmail.com*



Two of the main types of continuous chromatographic processes for downstream protein processing are the three- or four-column periodic counter-current chromatography (3C-PCC and 4C-PCC) and the two-column Capture SMB.

Here we derive a corresponding single-column batch analog for each of these multicolumn processes and demonstrate their similarities. Using a benchmark case of monoclonal antibody (mAb) capture on protein A at various mAb and feed doses, the chromatographic processes are designed for optimal performance using state-of-the-art mathematical programming tools and their performances are compared.

Continuous chromatography is becoming increasingly attractive for process intensification due to its high efficiency and cost-effectiveness [1]. Two of the main types of continuous chromatographic processes for downstream protein processing are three- or four-column periodic counter-current chromatography (3C-PCC and 4C-PCC) [2,3] and two-column Capture SMB [4].

These methods involve cyclically switching columns between loading and non-loading zones, enabling continuous loading. When a loading column reaches its predetermined

breakthrough point, it is disconnected and the load is redirected to the next column. Meanwhile, the disconnected column can be washed, eluted, and regenerated.

Compared to traditional batch chromatography, continuous chromatography maximizes the use of chromatography resin capacity, allowing for higher sample loads without compromising safety. Additionally, the second column in the loading zone captures any product breakthrough, reducing the loss of valuable product

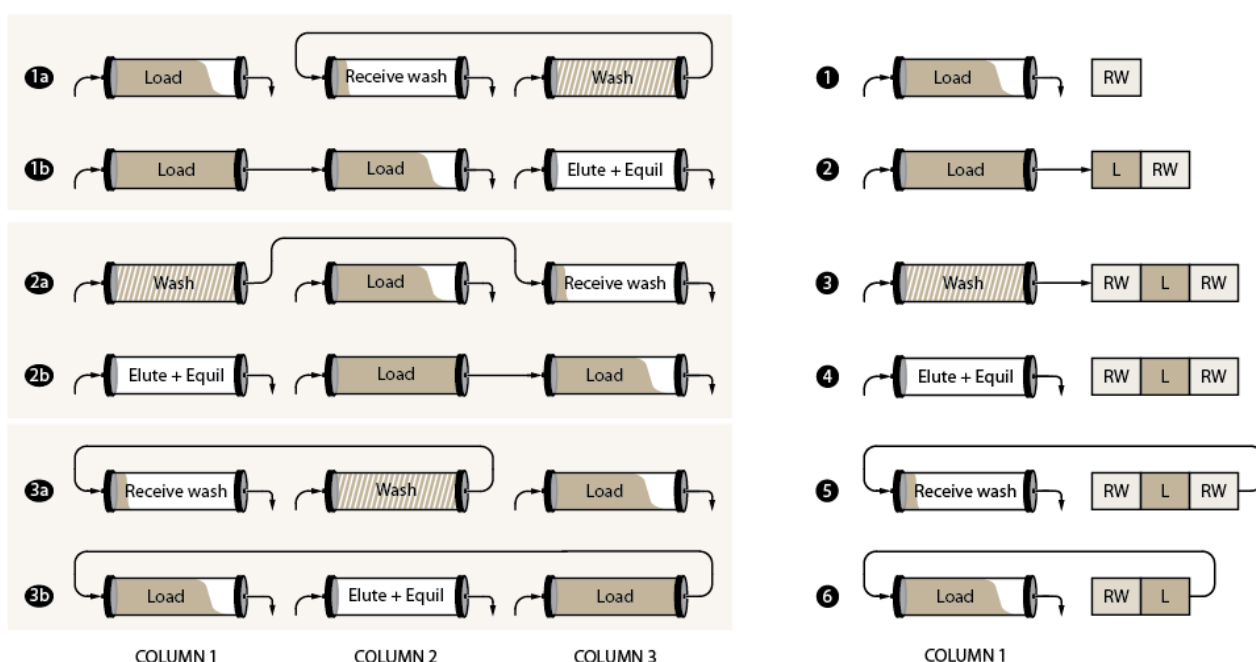
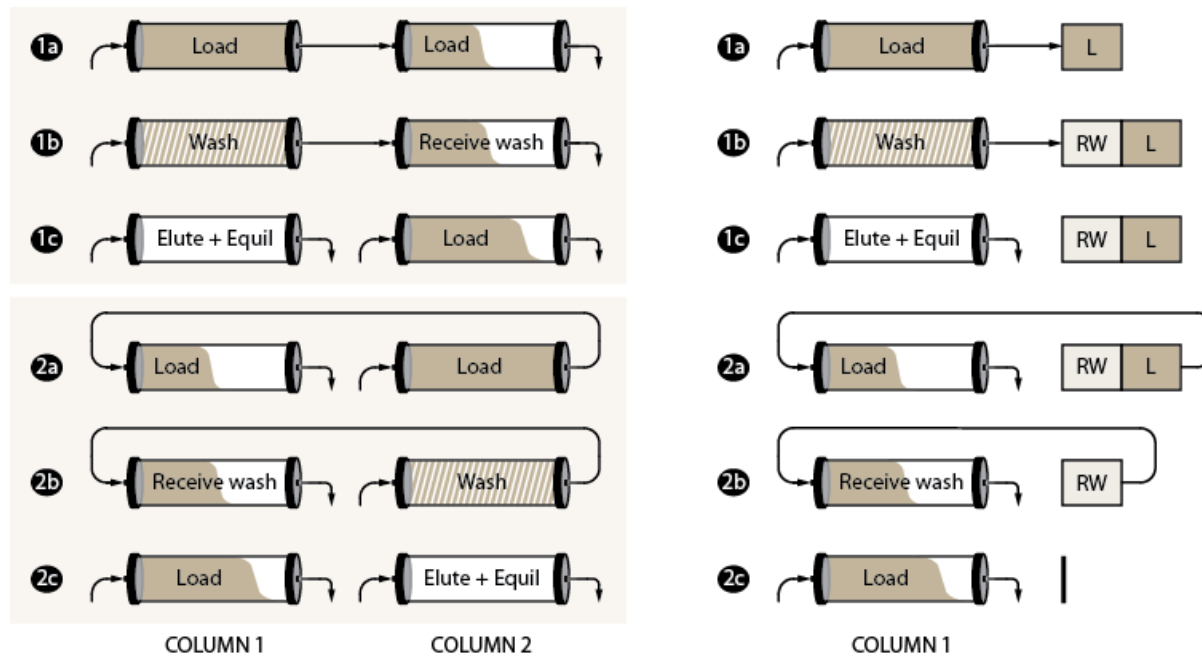


Figure 1. Schematic of the 3C-PCC cycle (left) and its one-column analog (right).

We derive a corresponding single-column batch analog [5,6] for each of these multicolumn processes and demonstrate their similarities.

Using a benchmark case of monoclonal antibody (mAb) capture on protein A at various mAb and feed doses, the compared.

chromatographic processes are designed for optimal performance using state-of-the-art mathematical programming tools [7] and their performances are compared.



References

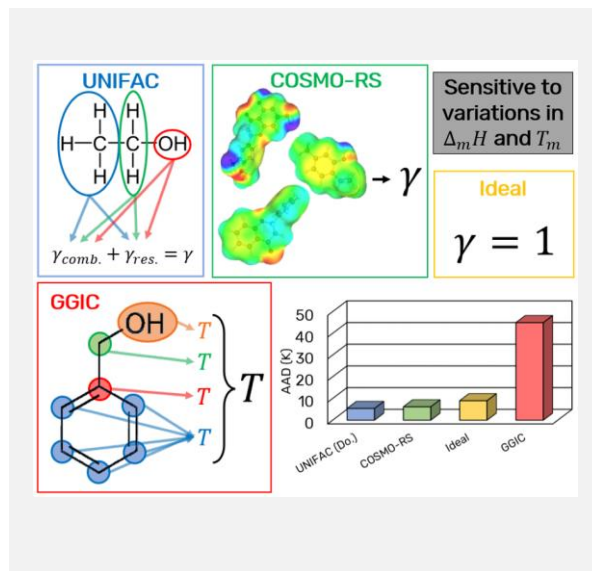
- [1] F. Steinebach et al., *Biotechnology Journal*, 11 (2011) 1126-1141.
- [2] V. Warikoo et al., *Biotechnology Bioengineering*, 109 (2012) 3018-3029.
- [3] R. Godawat et al., *Biotechnology Journal*, 7 (2012) 1496-1508.
- [4] M. Angarita et al., *Journal of Chromatography A*, 1389 (2015) 85-95.
- [5] A.S. Chibério et al., *Journal of Chromatography A*, 1623 (2020) 461199.
- [6] A.S. Chibério et al., *Journal of Chromatography A*, 1623 (2020) 461211.
- [7] T.P.D. Santos et al., *Digital Chemical Engineering*, 6 (2023) 100081.

Estimating the melting temperatures of type V deep eutectic solvents

G. Teixeira^{1*}, D. Abranches¹, O. Ferreira^{2,3}, J.A.P. Coutinho¹

¹CICECO, Aveiro Institute of Materials, Complexo de Laboratórios Tecnológicos, University of Aveiro, Campus Universitário de Santiago, Aveiro, Portugal; ²Centro de Investigação de Montanha (CIMO), Instituto Politécnico de Bragança, Campus de Santa Apolónia, 5300-253 Bragança, Portugal; ³Laboratório para a Sustentabilidade e Tecnologia em Regiões de Montanha, Instituto Politécnico de Bragança, Campus de Santa Apolónia, 5300-253 Bragança, Portugal.

*gabriel.teixeira@ua.pt



Type V deep eutectic systems are non-ionic liquid mixtures that present negative deviations to the ideal behavior, which can lead to remarkably low melting temperatures. These systems are usually composed of mixtures of hydrogen bond donors (HBD) and acceptors (HBA). However, the infinite amount of possible combination suggests the use of modelling tools at least in the preliminary screening stages. This work tests the capabilities of three modelling approaches (GGIC, COSMO-RS and UNIFAC of Dortmund) against a database of non-ionic eutectic systems collected from the literature. Although the GGIC method predicted all the systems, it was the worst performing model with the highest AAD. UNIFAC (Dortmund) resulted in the lowest AAD, however, it was only capable of predicting about two thirds of the systems. Finally, COSMO-RS proved to be the most effective tool to predict Type V DES solid-liquid phase diagrams, with broad applicability and satisfactory predictions.

Introduction

Deep Eutectic Solvents (DESs) are mixtures usually composed of a hydrogen bond acceptor (HBA) and a hydrogen bond donor (HBD), presenting a eutectic temperature below that of an ideal liquid mixture [1]. This eutectic melting temperature depression results from high negative deviations to ideality, that manifest the favourable cross interactions between the HBA and the HBD that are stronger than the interactions present in the pure compounds [2]. As tuneable solvents, the number of combinations of HBAs and HBDs to test for a given application is overwhelming and the trial-and-error experimental approach is highly time-consuming and cost-intensive. To overcome this, modelling techniques can assist the establishment of general guidelines for the prediction of eutectic temperatures for type V DESs, as these would allow an efficient preliminary screening of HBA/HBD combinations.

In this work, the capability of two excess Gibbs energy models (COSMO-RS [3] and UNIFAC of Dortmund [4]) and an empirical group contribution methodology (Hou et al. [5]) to predict the eutectic point of several Type V DESs is explored. Both COSMO-RS and UNIFAC are predictive models that estimate the chemical potential of each component in a liquid mixture. However, COSMO-RS performs these predictions using quantum chemistry descriptors of molecules, while UNIFAC relies on group interaction parameters. Note that the use of these two excess Gibbs energy models is advantageous as they allow for the calculation of activity coefficients, which quantify the non-ideality of DESs. On the other hand, such models must be coupled with solid-liquid equilibrium (SLE) thermodynamics, requiring prior knowledge on the melting properties (temperature and enthalpy) of each precursor. Considering immiscible solid phases, and neglecting the

influence of temperature on heat capacities, and only fusion as the only phase transition, SLE can be described by the following equation,

$$\ln x_i \gamma_i = \frac{\Delta_m H}{R} \left(\frac{1}{T_m} - \frac{1}{T} \right) \quad (1)$$

where γ_i is the activity coefficient of compound i at mole fraction x_i in the liquid phase, $\Delta_m H$ and T_m are its melting enthalpy and temperature, R is the universal gas constant, and T is the absolute temperature.

Empirical group contribution methodologies such as the one proposed by Hou et al. [5] directly estimate the melting temperatures without the activity coefficient intermediate step.

Results and conclusions

More than 100 non-ionic systems were collected from the literature and their precursors were divided into five categories, considering their chemical structure and functional groups, following the definitions proposed by Abranches and Coutinho [2].

The GGIC model was able to describe all systems, but it had by far the worst performance with an average absolute deviation (AAD) in the melting temperature higher than 40 K. On the other hand, COSMO-RS and UNIFAC resulted in similar AAD for their calculations, satisfactorily predicting most of the eutectic systems. However, the UNIFAC of Dortmund was only able to predict around two thirds of the systems, due to the lack of group interaction parameters to describe a few compounds.

Figure 1 presents an overview of the predicted melting temperatures using COSMO-RS, in comparison to the collected experimental data.

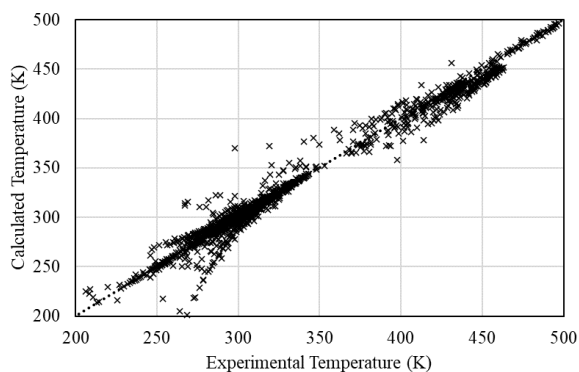


Figure 1. Melting temperatures: experimental versus calculated by COSMO-RS.

Acknowledgements

This work was developed within the scope of the project CICECO-Aveiro Institute of Materials, UIDB/50011/2020, UIDP/50011/2020 and LA/P/0006/2020, and CIMO-Mountain Research Center, UIDB/00690/2020 and LA/P/0007/2020, financed by national funds through the Portuguese Foundation for Science and Technology/MCTES. Gabriel Teixeira thanks FCT for his Ph.D. grant (UI/BD/151114/2021).

References

- [1] M.A.R. Martins et al., *Journal of Solution Chemistry*, 48 (2019) 962-982.
- [2] D.O. Abranches et al., *Current Opinion in Green and Sustainable Chemistry*, (2022) 100612.
- [3] A. Klamt, *Journal of Physical Chemistry*, 99 (1995) 2224-2235.
- [4] A. Fredenslund et al., *AIChE Journal*, 21 (1975) 1086-1099.
- [5] X.J. Hou et al., *AIChE Journal*, (2021) 1-13.

Comparing all the data gathered and estimations of the three models as well as their applicability, this work demonstrates that COSMO-RS is the most effective tool to estimate the SLE phase diagrams of type V deep eutectic solvents. However, in the cases where the group interaction parameters were available, the UNIFAC model of Dortmund performed with similar accuracy to COSMO-RS.

Chemical recycling of poly(ethylene terephthalate) using low-cost ionic liquids

H.L. Judah*, M.Y. Suleman, A. Brandt-Talbot

Department of Chemistry, Imperial College London, London, UK.

*m.suleman18@imperial.ac.uk.



In this work, we report the investigation of protic ionic liquids as dual solvents and catalysts for the hydrolytic depolymerisation of poly(ethylene terephthalate) into terephthalic acid. A variety of protic ionic liquids were screened, with those bearing the acetate anion achieving the highest terephthalic acid yields of up to 82%. After preliminary screening, the optimum hydrolysis reaction conditions were 180 °C for 3 hours. Structural characterization of the main product via IR and NMR spectroscopy confirmed the preparation of terephthalic acid, whilst thermal analysis via DSC and TGA indicated high purity was obtained. This was corroborated using HPLC analysis, which confirmed that product purity of up to 98% was achieved. This work demonstrates that protic ionic liquids are viable low-cost alternatives as reactive solvents for the hydrolysis of poly(ethylene terephthalate) waste, which is promising for the future of the plastic recycling industry.

Introduction

Plastics are a group of materials that have improved the quality of modern life. Owing to their low production cost, light weight and high strength-to-weight ratio, they are used across a broad range of industries. Approximately 40% of plastic is used in packaging, due to efficient transportation and minimization of food waste, which results in cost and energy savings [1]. Consequently, production of plastic has dramatically risen to 367 Mt/year in 2020 [2].

Waste management has not kept pace with production and most plastics do not sufficiently biodegrade, resulting in plastic pollution becoming a global problem [3]. Mortality rates in marine life have risen and microplastics have been detected in animals and humans, with long-term consequences still unclear [4, 5]. There is also a strong link between the plastic and fossil fuel industries which must be weakened.

Plastic is recycled via mechanical recycling, however, the mechanical and optical properties are compromised and mostly downcycling is achieved. Chemical recycling will allow the raw materials in plastic to stay in use, and reduce reliance on fossil feedstocks. Depolymerisation is a promising chemical recycling option for certain polymers. For example, polyesters such as poly(ethylene terephthalate) (PET) (Figure 1).

Hydrolysis is an attractive route due to the production of the industrial monomers used for PET preparation. Various catalysts have been reported, however, problems arise due to contamination with metals, corrosion of equipment with acids and difficulty in terephthalic acid (TPA) isolation. TPA is industrially synthesised via catalytic oxidation of para-xylene in the AMOCO process, in which para-xylene is obtained from petroleum in a highly energy intensive process [6, 7]. Hence, a more sustainable pathway to prepare TPA is needed.

Ionic liquids are a relatively new class of solvents that are composed entirely of ions. They possess interesting solvent

properties that may offer a more sustainable and cost effective method for PET hydrolysis and TPA isolation. Aprotic ionic liquids have demonstrated success in PET depolymerisation. However, it is necessary to explore more cost-effective ionic liquid alternatives, which is the aim of this work.

Objectives

1. Demonstrate that low-cost protic ionic liquids can be used for PET hydrolysis.
2. Optimise the hydrolysis reaction conditions.
3. Determine terephthalic acid purity by developing a HPLC protocol.

Methods and results

During PET hydrolysis, a pressure tube was loaded with 2.0 g of ionic liquid containing 15% water (*w/w*) and 0.1 g of PET. The vessel was sealed and heated in an oven to the desired temperature and time. The post-reaction mixture was basified to pH 10-11 and PET residue filtered and dried. The filtrate was acidified to pH 3-4 and TPA precipitate filtered, dried and isolated yield determined.

The hydrolysis results show that low PET conversion and TPA yields were obtained for protic ionic liquids bearing acidic and neutral anions. This demonstrates that these ionic liquids are not good candidates for PET hydrolysis. However, protic ionic liquids containing the acetate anion achieved much higher conversions and yields of up to 100% and 82%, respectively.

The purity of TPA was determined quantitatively using a HPLC protocol in which samples of crude TPA were prepared with their known masses, and the concentration of TPA determined via calibration graph. Thus, the purity could be determined taking into account any insoluble impurities present. 1,3,5-trimethoxybenzene was used as internal standard.

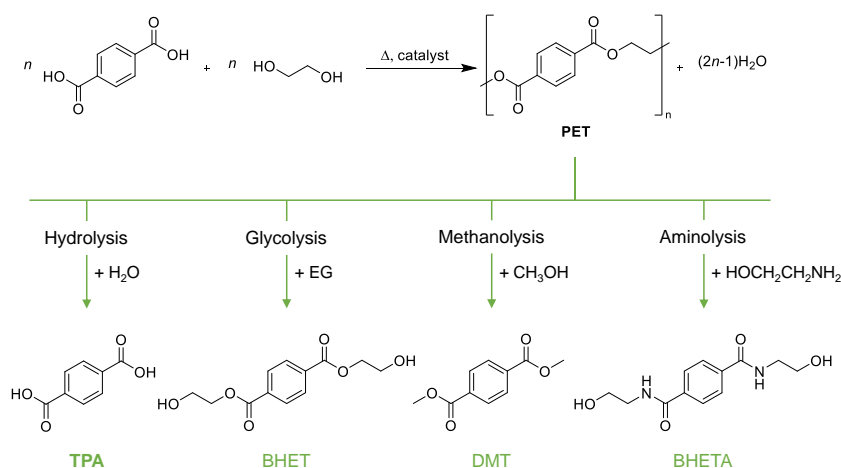
Table 1. HPLC purity results of terephthalic acid.

Terephthalic acid	Ionic liquid	Purity (%)	Std. error (\pm %)
Isolated	[HC ₁ im][OAc]	76.5	0.5
Isolated	[HC ₁ im][OAc] (1:2)	97.7	0.6
Isolated	[HDBN][OAc]	67.2	0.6
Isolated	[C ₂ C ₁ im][OAc]	90.9	0.6

The HPLC purity results in Table 1 demonstrate that the lowest purity was obtained with [HDBN][OAc], which also gave the lowest isolated yield of the acetates (46.8%). The aprotic ionic liquid, [C₂C₁im][OAc] achieved high purity and yield of 93.7%. However, despite [C₁Him][OAc] (1:2) achieving a mid-range yield of 59.2%, it gave the highest purity of nearly 98%.

Conclusions

In this work, a library of low-cost protic ionic liquids were screened for the hydrolysis of PET. The ionic liquids in this study were prepared via addition of acid and base at the desired molar ratio, using a selection of organic and inorganic acids and amines. Protic ionic liquids derived from acetic acid achieved the highest conversion of PET and TPA isolated yield under the optimized conditions. Thermal analysis indicated that TPA was obtained in high purity. This was validated using HPLC analysis, which quantified that crude TPA purity as high as 98% was obtained. This work demonstrates that low-cost protic ionic liquids are promising candidates for achieving chemical recycling of waste PET while preparing TPA without the use of petroleum based feedstocks.

**Figure 1.** Different depolymerisation pathways of PET.

Acknowledgements

We would like to thank the Engineering and Physical Sciences Research Council (EPSRC) for their financial support of this work and the Centre for Rapid Online Analysis of Reactions (ROAR) for their technical support and use of HPLC instrument.

References

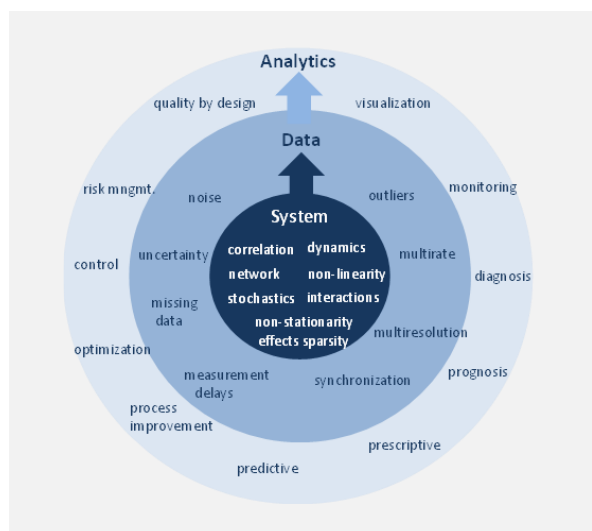
- [1] A.L. Andrady, M.A. Neal, *Philosophical Transactions of the Royal Society B: Biological Sciences*, 364 (2009) 1977-1984.
- [2] PlasticsEurope, *Plastics – the facts 2021: an analysis of European plastics production, demand and waste data*, 2021.
- [3] E.M. Foundation, *The new plastics economy: Rethinking the future of plastics*, 2016.
- [4] A. Anastasopoulou, T. Fortibuoni (2019). *Impact of Plastic Pollution on Marine Life in the Mediterranean Sea. The Handbook of Environmental Chemistry*. doi:https://doi.org/10.1007/698_2019_421.
- [5] H.A. Leslie et al., *Environment International*, [online] 163 (2022) 107199.
- [6] R.A.F. Tomás et al., *Chemical Reviews*, 113 (203) 7421-7469.
- [7] D.-Y. Koh et al., *Science*, 353 (2016) 804-807.

Industrial process analytics: from case-based problem solving to a systematic discipline in chemical engineering

M.S. Reis

Univ Coimbra, CIEPQPF, Department of Chemical Engineering, Rua Sílvia Lima, Pólo II – Pinhal de Marrocos, 3030-790.

marco@eq.uc.pt



The use of data for supporting inductive reasoning, operational management, and process improvement, has been a driver for progress in modern industry. Many success stories exist on the successful application of data-driven methods to address open challenges, across different industrial sectors. Some of them will be shared in this communication. The current and future importance of Industrial Process Analytics is undeniable and is becoming widely considered as a competency that must be internalized in the company's knowledge and skill set. But isolated success stories, even when abundant, are of limited value if the only way to make use of them is by replication on closely related scenarios. It is the mechanisms that led to such successes, not the final solutions themselves, that really matter when it comes to creating sustainable value. For such, a new discipline in the Chemical Engineering curricula should be created, dedicated to Industrial Process Analytics.

The recent advances in Artificial Intelligence & Machine Learning (AI/ML) technology in the fields of image & video analysis and natural language processing (NLP) have generated a plethora of methods and tools, spiking the interest of the research community to explore their application outside these domains, namely in the chemical, food, biotechnological, semiconductor, and pharmaceutical sectors, among others. But this boost in activity has also increased the difficulty of understanding the multiple underlying rationales for applying them, other than the mere curiosity of “seeing what comes out” (still valid, but arguably inefficient). Furthermore, it is often difficult to assess the added value of using these new methods, as many times they are not rigorously compared with conventional solutions presenting state-of-the-art performance.

Therefore, it is now (the) time, we believe, to work on the formal structuring of a discipline of Industrial Process Analytics (IPA), focused on *the ability to generate solutions and value by induction from industrial process data*, and establish a solid methodological ground for research and teaching in this field. This is essential for undergraduate engineering students to learn basic inductive skills and to carry them to industry, where they become naturally part of the company's knowledge lake. When we have achieved that, then the transformative power of IPA will be more than a set of isolated successes, but the result of implementing the principles and methodologies from a consolidated and structured discipline.

In the following paragraphs, I will (i) justify the uniqueness and importance of IPA; (ii) provide some examples of success stories; (iii) discuss the building blocks of a discipline on IPA.

What is unique about Industrial Process Analytics?

Data science and analytics is a fast-growing field, attracting many students with the prospects of well-paid jobs. However, these (future) professionals will certainly face many difficulties if asked to handle real industrial problems, unless they have the

proper background—like Chemical Engineers do. The reason is that underlying every industrial problem, there are two distinct levels of challenges that must be taken into account for delivering an adequate and effective solution: *system-related and data-related challenges*.

System-related challenges are connected to the bare nature of the industrial process where the problem must be solved. Any process for developing a solution should start with a deep understanding of several aspects of the system, such as: the operation mode (continuous, batch, semi-batch), its network causal structure, the degree of non-linearity, presence of (multiscale) dynamics, process delays, stochasticity, the existence of non-stationary phenomena, degree of sparsity of important variables, among others.

Data-related challenges arise from the way data are collected from the system of interest (with the associated complexity, as referred to above) and made available for analysis. These data may present several characteristics that are typical of industrial scenarios, such as: noise, outliers, different levels of uncertainty and quality, different acquisition rates (including irregular sampling), asynchronous registration, missing data, multiple granularities, multiple modalities, clustered data, among others.

These system- and data-related challenges are unique of industrial problems and must be considered when designing the final analytical solution (see graphical abstract). They are, we argue, more adequately handled by *someone with a native background in Chemical Engineering*, complemented with the proper training on IPA. Professionals with no background are prone to miss some of the system/data challenges that must be contemplated, leading to suboptimal or even wrong solutions to the problem.

Some success stories

Many success stories of the application of IPA in different industrial sectors can be referred. Building on our own experience, impacted sectors include: the *Chemical Process Industry*, with new causal-based frameworks for monitoring,

control, and prediction [1-4]; advanced multimodal sensor fusion methods [5], and new hybrid modeling methods for data-intensive environments [6, 7]; *Green economy*, where a federated classification approach was developed for Waste Lubricant Oil management [8], and a new prediction framework for estimating CO₂ emissions in the shipping industry [9]; *Pharmaceutical*, with new methods for retrospective Quality by Design and scalar on function regression [10]; *Microelectronics*, with the development of SPM using Digital Twins [7]; *Chemical & Petrochemical*, with advanced multiresolution frameworks for data analysis [11, 12]; among others developed to these and other sectors, such as *Pulp & Paper*, *Waste Water Treatment Plants*, *Semiconductor*, and *Food*.

Creating the capability for sustaining such success.

Many success stories on the application of IPA can indeed be found in the recently published literature. They result from the increasing efforts and investment of researchers and academia. Their number is only limited by the size of the scientific community, namely the Chemical Engineering community, that is actively involved in pushing forward this field. Clearly, when looking at the industrial impact, despite the current efforts, the bottleneck lies in the dimension of this group of promoters. Therefore, to increase the capacity and move the bottleneck away from academia and R&D, all future Chemical Engineers must have basic training and knowledge on the principles, methodologies, and tools of IPA, to carry them to industry. In this way, IPA becomes internalized in the companies' resident knowledge and skill set. This massive movement of IPA skills and people empowered with the capacity to correctly address data-driven problems will finally lead to the promised transforming impact of data and analytics in industrial settings. Next, we briefly refer to four building blocks of such a discipline on IPA:

1. Understanding the IPA context. As mentioned before, a complete understanding of the context where problems arise and data is collected is fundamental for developing the most adequate analytical solutions. Therefore, the new IPA discipline must provide such background, exploring synergies with industrial partners through seminars, case studies, projects, and industrial visits.

2. A Systematic and Organized Body of Knowledge. Given the plethora of methods currently available, it is critical to find an organized and logical structure for them. In this regard, we propose an hierarchical structure where methodologies are organized in 4 levels: Exploratory – to visualize and monitor variability (e.g., feature engineering, functional data analysis,

PCA, t-SNE, UMAP); Stability – to manage and control variability (statistical process monitoring, fault detection & diagnosis, process control, reinforcement learning); Prediction – to forecast variability (different classes of AI & ML methods, cross-validation, prediction of scalars and functionals); Quality by Design – to optimize/design processes (DOE, Bayesian optimization, Design and Analysis of Computer Experiments, EVOP).

3. A Rigorously Defined Purpose. In order to build the capacity to create new solutions, a clear sense of purpose must be established. Here, we propose adopting the concept of Information Quality (InfoQ), as the guiding principle and target to be maximized. In simple terms, InfoQ is the level of Utility, U , achieved by applying an analytical method, f , to a dataset, X , for achieving a given goal, g :

$$\text{InfoQ}(f, X, g) = U \{f(X | g)\} \quad (1)$$

The InfoQ framework was adapted to the Chemical Processing Industry [13], and will be a valuable resource for future professionals to prioritize and conduct their data-driven activities: the goal of any project should be to maximize the quality of the information generated.

4. Best practices. As the trainees are initiating the learning process and have no experience, they are prone to make errors and overlook possible important aspects of the analysis. Therefore, guidelines and best practices must be shared, along with analytic pipelines for addressing certain activities, e.g., the following sequence steps and how to conduct each one of them: Goal definition → Data collection → Data Integration → Data Cleaning → Feature Engineering → Exploratory Analysis → Model building → Validation → Reporting → Communication.

The Present and the Future

A discipline with this profile has been launched at the Department of Chemical Engineering of the University of Coimbra. The results of this year's survey show that students, irrespectively of their personal preferences and "comfort zones", recognize IPA as a useful skill for their future as professionals, aligning their training with what the Chemical Process Industry is calling for. We, academia and industry, should therefore join efforts in improving the design of this discipline and to better integrate it in the Chemical Engineering curricula, in the continuous effort of preparing the next generations of professionals for their future challenges.

Acknowledgements

Portuguese FCT, project reference UIDB/00102/2020.

References

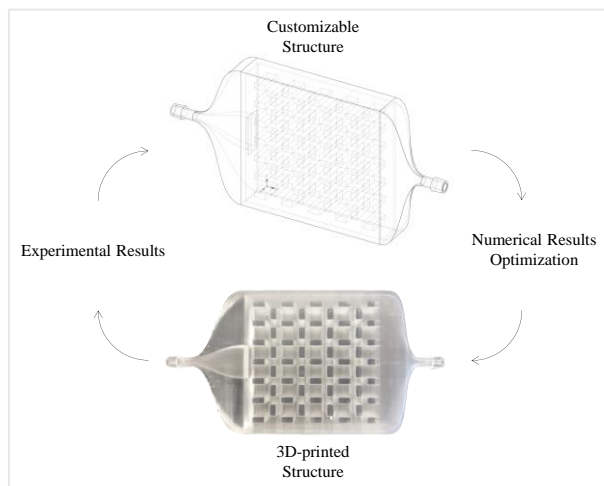
- [1] R. Paredes et al., *Chemical Engineering Science*, 267 (2023), 118338.
- [2] T.J. Rato et al., *Journal of Process Control*, 24 (2014), 905-915.
- [3] M.S. Reis, *AIChE Journal*, 59 (5), (2013), 1570-1587.
- [4] W.-T. Yang et al., *Expert Systems with Applications*, 155 (2020), 113424.
- [5] E. Strelet et al., *IFAC-PapersOnLine*, 54 (3), (2021), 67-72.
- [6] J. Sansana et al., *Computers & Chemical Engineering*, 151 (2021), 107365.
- [7] T.J. Rato et al., *Processes*, 8 (11), (2020), 1520.
- [8] M.S. Reis et al., *Industrial & Engineering Chemistry Research*, 61 (48), (2022), 17544-17556.
- [9] A. Lepore et al., *Quality and Reliability Engineering International*, (2017),
- [10] B.M.A. Silva et al., *International Journal of Pharmaceutics*, 528 (1-2), (2017), 655-663.
- [11] T.J. Rato et al., *Chemometrics and Intelligent Laboratory Systems*, 186 (2019), 41-54.
- [12] G. Gins et al., *Chemometrics and Intelligent Laboratory Systems*, 172 (2018), 150-158.
- [13] M.S. Reis et al., *AIChE Journal*, 64 (11), (2018), 3868-3881.

An integrated approach of numerical topological optimization and 3D printed experimental validation

*J.M.R. Almeida**, *J.B.L.M. Campos*, *J.D.P. Araújo*

CEFT - Transport Phenomena Research Center, Faculty of Engineering, University of Porto, Rua Dr. Roberto Frias, 4200-465 Porto, Portugal; ALiCE – Associate Laboratory in Chemical Engineering, Faculty of Engineering, University of Porto, Rua Dr. Roberto Frias, 4200-465 Porto, Portugal

**up201503251@up.pt*



In the present work, ANSYS® software is used in conjunction with FormLabs® 3D-printer to establish an optimization and prototyping procedure for designing single-phase small reactors. A geometry with rectangular obstacles was assumed, and this topology's hydrodynamic behavior was studied. The values of the most relevant operating conditions (inlet velocity and fluid properties) are set and, afterwards, proceed to the topological optimization step where the effect of the geometrical parameters with higher influence in dispersion, pressure drop, and solid surface area per unit of the total volume of the system was simulated and analyzed. From the results of these simulations and in conjunction with interpolated points, a predictive mathematical model (response surface) was created, which determines the outputs throughout the defined geometrical range. Later, the response surface is evaluated through an established objective function whose goal is to be minimized and includes the combined contribution of dispersion, pressure drop, and surface area terms. Once the enhanced topology is obtained, it is printed in the Form 3+® printer with a see-through resin to allow flow visualization.

Introduction

Innovation entails a trial-and-error process that often leaves large amounts of waste behind. In an era of swift technological development coupled with rising awareness towards a regenerative use of materials, computer-aided engineering software packages emerge as valuable tools in scientific research. These software packages can aid in the modeling and analysis of various engineering systems by means of numerical simulation. Additionally, 3D printing presents itself as a driving tool in fast and cost-effective manufacturing. It can reliably produce complex geometries, which can be used for rapid prototyping [1].

By coupling these two revolutionary technologies, allied with an optimization methodology, a loop procedure of testing reactor geometries is achieved. In this way, a variety of key parameters of a reactor can be studied, such as mass transfer, heat transfer, pressure drop, selectivity, productivity, and reaction kinetics [2].

Objectives

The main objective of this work is to demonstrate the efficiency of conjugating numerical tools with additive manufacturing and subsequent experimental studies. As such, a design was conceptualized, simulated, 3D-printed, and put through experimental evaluation.

Methods

Initially, a structure was modeled in ANSYS® SpaceClaim through IronPython code-based scripting. The finished script allows the generation of domains filled with rectangular obstacles, with an expansion at the inlet and a contraction at the outlet, as shown in the Graphical Abstract. For each of the openings, a male fitting was designed to connect with the clear PVC pipes for the experimental tests. Once a reaction is added to the system, the code is easily adaptable to include additional openings for reactant feed distribution.

Next, a two-dimensional (2D) surface is created by slicing the designated structure through the xOy axis. At the present stage of our work, a 2D approach is being considered for the simulation domain to provide us with a faster proof of concept. Then, the 2D domain is divided into around 10^5 triangular elements with an element size of 2.5×10^{-4} m, as seen in Figure 1.

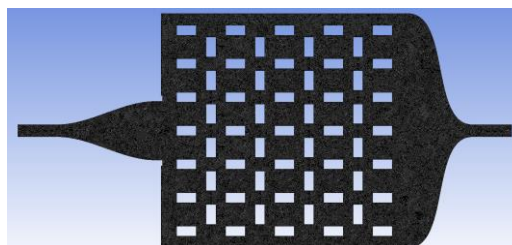


Figure 1. Mesh with around 10^5 triangular elements of size 2.5×10^{-4} m.

Next, the case was set up for simulations in the ANSYS® Fluent software. These simulations were done under single-phase laminar flow and transient conditions and with species transport activated to numerically replicate step input tracer experiments (Danckwerts) [3]. The fluid was assumed with properties similar to liquid water - $\rho = 998 \text{ kg}\cdot\text{m}^{-3}$ and $\mu = 10^{-3} \text{ Pa}\cdot\text{s}$. The boundary conditions were established with zero-gauge pressure at the outlet and no-slip condition at the walls. For the hydrodynamic characterization of the structure, the inlet velocity was varied in the Reynolds number range of 10 to 300. Then, for the optimization step, the Reynolds number was fixed at 50. The adaptive time-advance method was used and based on a Courant number of 0.25. The pressure implicit split operator (PISO) algorithm was employed to deal with the coupling of velocity and pressure.

As aforementioned, the hydrodynamics of the studied systems was inspected for different values of inlet flow velocity. Once

the most interesting inlet velocity was chosen, it was time for the topological optimization step.

The optimizer is the Response Surface Optimization tool in ANSYS® Workbench which uses a set number of simulations with varying geometrical parameters. It formulates a mathematical model that predicts the behavior of the system throughout the given range. Lastly, it was introduced an objective function that evaluates the topology regarding a combined effect of mass and thermal dispersion, pressure drop, and surface area (1):

$$F_{\text{obj}} = w_C \frac{\sum |C_{\text{out}} - \bar{C}_{\text{out}}|}{\bar{C}_{\text{out}}} + w_T \frac{\sum |T_{\text{out}} - \bar{T}_{\text{out}}|}{\bar{T}_{\text{out}}} + w_P (-\Delta p) + w_A \frac{V_{\text{Total}}}{A_s} \quad (1)$$

where the parameters w_C , w_T , w_P and w_A are the weights of each term in the objective function. The different goals are to increase mixing, decrease the pressure drop, and increase the surface area (A_s), which is why the latter is in the denominator. With this objective function, it is intended to comply with these separate goals by minimizing the value of F_{obj} . The term regarding the surface area is specifically useful if one wants to implement this optimization procedure in a catalytic reactor with surface reaction, since a greater surface area of the catalyst would favor the reaction rate.

The optimal geometry is then replicated through additive manufacturing. The 3D-printing was done through stereolithography which operates by virtue of photopolymerization of a liquid resin. The commercial resin used was FormLabs® Clear Resin V4. This resin was chosen for its transparent properties so that the flow could be tracked in order to compare with the numerical results.

Results

With the developed mesh (after the necessary mesh independency studies), the hydrodynamic behavior of the flow passing through the present topology was studied. It was found that for increased Reynolds number, the mass dispersion increased, but at the cost of a larger pressure drop. Furthermore, it was assessed that preferential paths were more pronounced for higher values of inlet velocities (as shown in Figure 2).

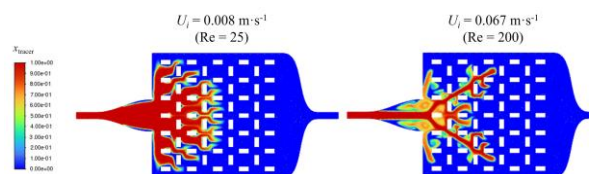


Figure 2. Transient mass fraction of tracer field obtained at $0.3 \cdot \tau$ for $U_{\text{in}} = 0.008 \text{ m} \cdot \text{s}^{-1}$ (left image) and $U_{\text{in}} = 0.067 \text{ m} \cdot \text{s}^{-1}$ (right image).

Once the hydrodynamic behavior was assessed, the most interesting inlet condition ($\text{Re} = 150$) was picked to advance to the optimization phase as it shows a good compromise between a high level of mixing and low-defined preferential paths.

A preliminary study to assess the effectiveness of the optimization method outlined was employed. For now, only two geometrical parameters were subjected to change (length and width of the obstacles). Then, the response surfaces were created, which evaluate the defined outputs relative to the dimensional characteristics through a given range. Once the results were submitted to the evaluation, the optimizer returned new and improved geometrical parameters (see Table 1). A 58.4% decrease in pressure drop was successfully obtained.

It is then possible to proceed to the evaluation of the remaining terms in the objective function and for future work to include more geometric parameters.

Once the optimal structure is reached, the printed structure will be subjected to experimental tests.

Conclusions

It was found that an increase in Reynolds number led to an increase in mass dispersion but also resulted in a larger pressure drop. Additionally, it was noted that higher inlet velocities resulted in more pronounced preferential paths. The study then proceeded to the optimization phase, the response surfaces were created, and the optimizer returned new geometrical parameters, resulting in a 58.4% decrease in pressure drop.

A loop of optimization and prototyping of small reactors was successfully implemented, and it promises to offer many outputs in the future.

Table 1. Input geometrical parameters and output evaluations (pressure drop) for the initial iteration of the structure and the optimized one.

Length of the obstacles (cm)	Width of the obstacles (cm)	Pressure Drop (Pa)
0.500	0.250	0.325
0.258	0.151	0.135

Acknowledgements

This work was financially supported by LA/P/0045/2020 (ALiCE), UIDB/00532/2020 and UIDP/00532/2020 (CEFT), funded by national funds through FCT/MCTES (PIDDAC). J.M.R. Almeida acknowledges the Portuguese Foundation for Science and Technology (FCT) for the PhD grant (UI/BD/151386/2021).

References

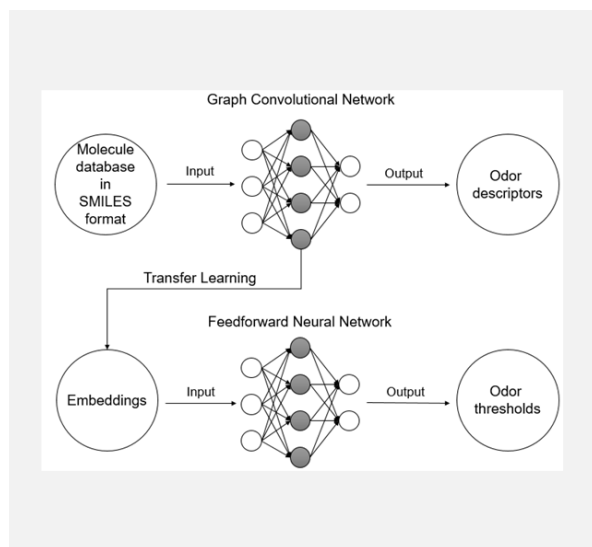
- [1] L.D. Tijjng et al., Applied Materials Today, 18 (2020), 100486.
- [2] B. Jung et al., Chemical Engineering Journal, 424 (2021), 130265.
- [3] T. Gottschalk et al., Chemical Engineering Science, 61 (2006), 6213-6217.

A framework for predicting odor threshold values of perfumes by scientific machine learning and transfer learning

L.M.C. Oliveira^{1,2*}, V.V. Santana^{1,2}, A.E. Rodrigues^{1,2}, A.M. Ribeiro^{1,2}, I.B.R. Nogueira³

¹LSRE-LCM - Laboratory of Separation and Reaction Engineering – Laboratory of Catalysis and Materials, Faculty of Engineering, University of Porto, Rua Dr. Roberto Frias, 4200-465 Porto, Portugal, ²ALiCE - Associate Laboratory in Chemical Engineering, Faculty of Engineering, University of Porto, Rua Dr. Roberto Frias, 4200-465 Porto, Portugal, ³ Chemical Engineering Department, Norwegian University of Science and Technology, Sem Sælandsvei 4, Kjemiblokk 5, Trondheim, Norway.

*up201403344@edu.fe.up.pt



Knowledge of odor thresholds is very important for the perfume industry. This work developed a framework for odor threshold prediction based on scientific machine learning strategies. A transfer learning-based strategy was devised, where information from a graph convolutional network predicting semantic odor descriptors was used as input data for the feedforward neural network responsible for estimating odor thresholds for chemical substances based on their molecular structures. The predictive performance of this model was compared to a benchmark odor threshold prediction model based on molecular structures that did not utilize transfer learning. Furthermore, the prediction was compared to a correlation previously proposed in the literature and a dummy regressor. Results demonstrated that the transfer learning-based strategy displayed a better predictive performance, suggesting this technique can be useful for predicting odor thresholds.

Introduction

Odor thresholds can be divided into two types: odor detection threshold (ODT), the level at which the human olfactory sense can detect a certain smell but not recognize it, and recognition threshold, the level at which that smell can be recognized. Knowledge of thresholds is very important for the industry, not only in terms of process functioning (as in the perfume industry) but also in terms of process safety, as many substances can have severe negative health effects at certain concentrations.

Practical measurement of odor thresholds can have some associated uncertainty, as it requires the usage of human subjects and subjective perceptions. Furthermore, to identify reliable threshold data can be an expensive procedure. Due to these limitations, researching empirical models with the ability to estimate odor thresholds for certain compounds can be an invaluable contribution to this field.

Other models for ODT prediction have been developed in the past. Rodríguez et al. (2011) [1] developed a correlation for predicting ODTs in air, based on the physical properties of the odorants. This model relied on simplifications not necessary in empirical models such as the one envisioned in this work. Hence, in this work, a framework to predict odor thresholds using an empirical model will be proposed. This framework will be based on scientific machine learning strategies, namely Graph Neural Networks, Feed Forward Neural Networks, and Transfer learning.

For this purpose, two databases were built, one composed of several chemical compounds and their respective odor descriptor, and another with the corresponding thresholds. As the literature lacks information regarding ODTs, this work uses Transfer Learning (TL) to develop the proposed models. Therefore, we transfer known and vastly available information to build a model for the ODT.

Methodology

The proposed methodology is based on the capability that certain machine learning models have to learn the correlation between a given chemical structure and a corresponding property of that compound. Several works have been published in other fields demonstrating this [2, 3].

The core part of predicting a property from a molecular structure is the availability of data that provides this information. In the case of ODT, this information is very scarce. Hence, this work uses the transfer learning technique by developing two Artificial Neural Networks. The first one will be used to learn the relationship between a given molecule and its corresponding molecular descriptor, in this case, the odor descriptor. This is done for two main reasons. First, it is necessary to establish a procedure to convert molecular structures into numerical information. For this purpose, the graph neural network is well known. The other reason is the underlying assumption that there should be an unknown correlation between the ODT and the odor descriptor. As it is easier to find the descriptor information than the ODT, the proposed methodology uses transfer learning to leverage this hypothetical correlation. This database is then used to identify a graph convolutional network to model an empirical relationship between chemical structures and different semantic descriptors of odor. The information from the modeled relationship (in the form of embeddings) is used as the input for another artificial intelligence model, which is trained to make predictions of odor threshold values from chemical structures. This methodology is named transfer learning and is the main underlying principle behind the prediction model construction.

Results and Discussion

With all the ANN models identified, it was possible to compare the performance of each strategy in predicting the ODT and evaluate the performance of the proposed method. This was done by using the squared errors for the predictions by both networks. Furthermore, a "dummy regressor" was used to

benchmark the ANN approaches. Hypothetically, in the absence of any prediction model, the best model should be the arithmetic average of the available data. If the ANN models are better than the average, this means that they are the best source of prediction available. Thus, the arithmetic mean is used as a baseline comparison. The arithmetic mean was computed from the database.

The performance of the three approaches for predicting the test data is compared in Table 1, along with examples of ODT predictions for 5 chemical species from the test dataset. These results also include predictions obtained in Rodriguez et al. (2011) [1] for the sake of comparison with an alternative prediction model.

The mean squared error for the specific descriptor network is lower than the generic descriptor network and the average. This outcome confirms this work's main hypothesis: it is possible to transfer learning from a related prediction problem to obtain more accurate prediction results when compared to a network based solely on molecular structures or basic regressors. Furthermore, generic descriptors proved to be a less accurate predictor than even the dummy regressor, since the mean squared error associated with the former's predictions was higher than that of the latter. This suggests that directly relating molecular structures with odor threshold data is not a viable strategy for prediction in this scenario. These results suggest that

the model proposed in this work is a viable prediction model and one that can potentially be developed further and implemented into future works that require the knowledge of odor threshold values, thus eliminating the potential problem of the unavailability of required odor threshold data. Furthermore, the proposed strategy can be improved by generating more training data.

Conclusions

The goal of this work was the creation of a machine learning prediction tool for odor thresholds, an important parameter for the perfume industry. The results demonstrate that the proposed model performs better than the benchmark models, suggesting that the strategy of transfer learning provides an edge in odor threshold prediction when compared to a model based on a direct relationship between molecular structures and odor thresholds. In fact, the benchmark model proved to be more ineffective even when compared to a baseline model of using simple arithmetic mean. Furthermore, our model possesses greater prediction capabilities when compared to predictive models based on simple correlations previously proposed in the literature. Therefore, using transfer learning is a viable technique in odor threshold prediction, with potential for further improvements in potential future works.

Table 1. Examples of odor detection threshold predictions and the mean squared errors for all the prediction models.

Component	Odor detection threshold value (ppm)	Benchmark prediction (ppm)	FNN prediction (ppm)	Arithmetic mean (ppm)	Prediction from Rodriguez et al. (ppm)
2-Methylnaphthalene	0.00069	0.000939	0.004512		3.994×10^{-5}
1-Pentanol	0.0055	0.002288	0.006681		0.003491
Isobutyl Acetate	0.008	0.035267	0.006179	0.007886	0.003614
n-Butyl Alcohol	0.0003	0.007123	0.006734		0.004539
Methyl Isobutyl Ketone	0.03	0.01677	0.01703		0.001986
Mean Squared Error	-	1.77×10^{-4}	6.67×10^{-5}	1.23×10^{-4}	1.65×10^{-4}

Acknowledgements

This work was financially supported by: LA/P/0045/2020 (ALiCE), UIDB/50020/2020 and UIDP/50020/2020 (LSRE-LCM), funded by national funds through FCT/MCTES (PIDDAC), and FCT—Fundação para a Ciência e Tecnologia under CEEC Institucional program. Luís Oliveira acknowledges his Ph.D. scholarship PRT/BD/153091/2021 funded by FEDER funds through NORTE 2020 and by national funds through FCT/MCTES, under MIT Portugal Program.

References

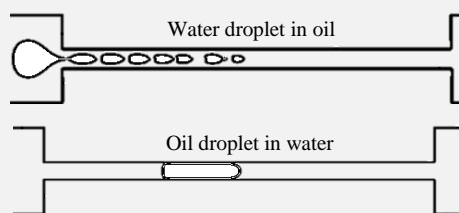
- [1] O. Rodríguez et al., *Flavour and Fragrance Journal*, 26 (2011) 421-428.
- [2] K. Yang et al., *Journal of Chemical Information and Modeling*, 59 (2019) 3370-3388.
- [3] S. Ryu et al., *Chemical Science*, 10 (2019) 8438-8446.

Microdroplets flowing through microfluidic constrictions: experimental and numerical study

A.T.S. Cerdeira*, J.B.L.M. Campos, J.M. Miranda, J.D.P. Araújo

CEFT - Transport Phenomena Research Center, Faculty of Engineering, University of Porto, Rua Dr. Roberto Frias, 4200-465 Porto, Portugal; ALiCE - Associate Laboratory in Chemical Engineering, Faculty of Engineering, University of Porto, Rua Dr. Roberto Frias, 4200-465 Porto, Portugal

*up201811565@edu.fe.up.pt



In recent years, microstructured devices gained an important role in the technological development of several areas. Two-phase flows, and consequently, the presence of droplets is recurring in such devices. Different types and topologies of microscale devices have been addressed and manufactured. In particular, a microfluidic constriction has a simple geometry, but the flow has strong and distinct regions of extensional and shear strains, which can considerably deform the shape of a droplet.

In the present work, experimental and numerical studies concerning the passage of a single microdroplet through a constricted microchannel filled with an immiscible liquid continuous phase are reported. Two pairs of continuous-dispersed fluids were used: 1) mineral oil in water with 2% w/w of SDS; and 2) water in mineral oil with 3% w/w of SPAN[®] 80. Surfactants were added in the continuous phases to obtain monodisperse droplets of small size and to prevent coalescence. The main experimental and numerical results are in good agreement, and the breakup of the water droplet and the non-breaking of the oil droplet when passing through the constriction was verified.

Introduction

The interest in droplets (liquid entities that flow in an immiscible liquid continuous phase) flowing through microfluidic devices (characteristic dimensions below one millimeter) has emerged in the last decades in various fields, including enhanced oil recovery, surface cleaning, medical purposes, and chemical engineering applications [1, 2].

Constrictions are an excellent example of such devices which can fragment droplets with the potential to be applied in microparticle production. The deformation of droplets passing through a constricted microchannel depends on the physical properties and flow rates of dispersed and continuous phases. Reynolds and Capillary numbers, together with the viscosity ratio between dispersed and continuous phases, are the main dimensionless numbers that govern two-phase flows at the microscale [3].

Working fluids

Two different pairs of fluids were used: 1) water with 2% w/w of Sodium Dodecyl Sulfate, SDS, (continuous phase) and mineral oil (dispersed phase); and 2) mineral oil with 3% w/w of SPAN[®] 80 (continuous phase) and water (dispersed phase). The test fluids were characterized regarding some physical properties: i) viscosity (μ) of both Newtonian phases was measured by a rotational rheometer; ii) density (ρ) of both phases was determined with a density probe; and iii) interfacial tension (σ) was obtained in a Du Noüy ring tensiometer. The experimental data for the referred properties are listed in Table 1.

Experimental methods

The microchannel geometry was generated in AutoCAD[®], and the resulting computer-aided design was sent to a specialized laboratory where the geometry was printed into a mask substrate.

Table 1. Physical properties of the two pairs of fluids.

		μ [Pa.s]	ρ [kg/m ³]	σ [N/m]
1)	Water with 2% w/w SDS	0.001	997	0.009
	Mineral oil	0.032	838	
2)	Mineral oil with 3% w/w SPAN [®] 80	0.035	854	0.006
	Water	0.001	998	

The mask was used to produce a SU-8 mould by photolithography [4] with a height of 5h (Figure 1).

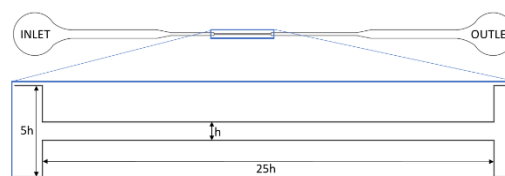


Figure 1. Microchannel constriction used in the experiences.

Microchannel fabrication uses a two-part kit composed of a polydimethylsiloxane (PDMS) pre-polymer, which is a silicone elastomer, chemically inert, thermally stable, hydrophobic and transparent [4-6], and a curing agent [4, 7, 8]. A mixture of PDMS and a curing agent was poured into the SU-8 mould (for channel substrate), and a thin layer of PDMS and curing agent mixture was spread by spin-coating in a glass slide (for sealing channels). Afterwards, the mould filled with PDMS and the coated glass slide were cured in an oven. Then, the cured PDMS was peeled off from the SU-8 mould and sealed to the coated glass slide.

Droplet images were captured via a high-speed camera mounted on an inverted epifluorescence microscope. The fluids were

injected into the microchannel with the help of a dedicated syringe pump.

Numerical methods

The commercial Computational Fluid Dynamics (CFD) package ANSYS Fluent 2021 R2 was used to perform a set of simulations concerning the flow of a single droplet through a microchannel constriction. The simulations were based on a 3D domain with the corresponding dimensions in Figure . To better define the droplets' deformation, a mesh with 732000 hexahedral cells was generated in the referred domain, with finer refinement in the constriction zone (Figure 2).

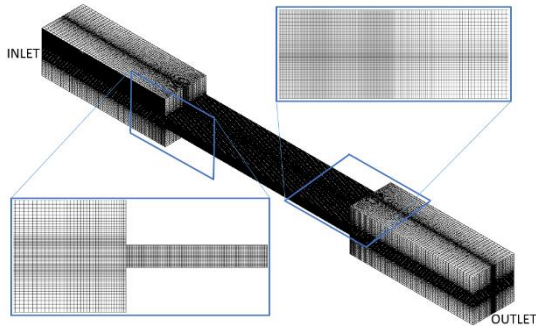


Figure 2. Mesh used in the 3D simulations.

At the inlet, the velocity profile was set uniform, while a pressure-outlet condition was assumed at the exit. A no-slip boundary condition was used at the walls. The physical properties of the fluids tested numerically are listed in Table . A fully non-wetting boundary condition (static contact angle of 180°) was also considered.

The continuity and momentum equations were solved assuming laminar flow conditions. The simulations were performed in the transient state to capture the temporal evolution of the droplet shape. The liquid-liquid interface tracking was based on the Volume of Fluid (VOF) methodology. This method was applied with the geometric reconstruction scheme, which assumes a Piecewise Linear Interpolation Calculation (PLIC) approach to describe the interface between phases. The continuum surface model was chosen to translate the effect of the surface tension at the liquid-liquid interface.

The numerical schemes applied to solve the governing equations were: 1) PISO (Pressure-Implicit with Splitting of Operators) algorithm for pressure-velocity coupling; 2) PRESTO! (PREssure STaggering Option) method was chosen for the pressure interpolations; 3) QUICK (Quadratic Upstream Interpolation for Convective Kinematics) scheme

Acknowledgements

This work was financially supported by LA/P/0045/2020 (ALiCE), UIDB/00532/2020 and UIDP/00532/2020 (CEFT), funded by national funds through FCT/MCTES (PIDDAC). A. Cerdeira also acknowledges the financial support provided by FCT through the PhD Grant 2020.04498.BD.

References

- [1] M. Lee et al., *Soft Matter*, 11 (2015) 2067-2079.
- [2] K. Matsuura et al., *Proc. of MHS 2015 - International Symposium on Micro-NanoMechatronics and Human Science*, Nagoya, Japan, 2015.
- [3] A. Cerdeira et al., *Micromachines*, 11, 2020.
- [4] J. Friend et al., *Biomicrofluidics*, 4 (2010) 26502-26502.
- [5] D. Dendukuri et al., *Advanced Materials*, 21 (2009) 4071-4086.
- [6] A. Mata et al., *Biomedical microdevices*, 7 (2005) 281-293.
- [7] J. Carneiro et al., *Journal of Micromechanics and Microengineering*, 26 (2016).
- [8] Y. Xia et al., *Annual Review of Materials Science*, 28 (1998) 153-184.

was applied to solve the momentum equation; and 4) Green-Gauss Node Based to compute the scalar gradients. Furthermore, an explicit time scheme solved the conservative mass equations with a maximum Courant number of 0.25. The time step applied was variable and determined by the Courant number. In each time step, the convergence criterion assumed was based on the residuals of the momentum and continuity equations, which were monitored and controlled to be kept below 10^{-6} .

Results

The first experiment was performed with an emulsion of mineral oil with 3% w/w of SPAN® 80 and water. The emulsion was injected into the constricted microchannel, and the passage of a single mineral water droplet was captured. A numerical simulation was done to replicate this experiment, i.e., with a droplet of the same size (Figure 3).

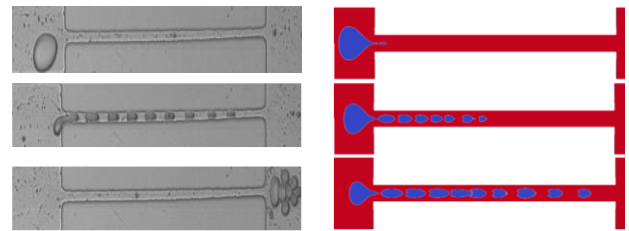


Figure 3. Water droplet in mineral oil with 3% w/w of SPAN® 80: experimental (left); numerical (right).

In a second experiment, an emulsion of water with 2% w/w of SDS and mineral oil was used, and the flow of the mineral oil droplet passing to the constriction was analysed. An analogous simulation was also performed (Figure 4).

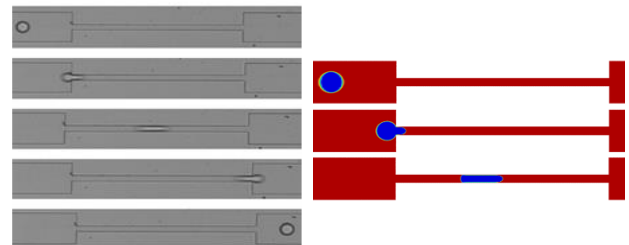


Figure 4. Mineral oil droplet in water with 2% w/w of SDS: experimental (left); numerical (right).

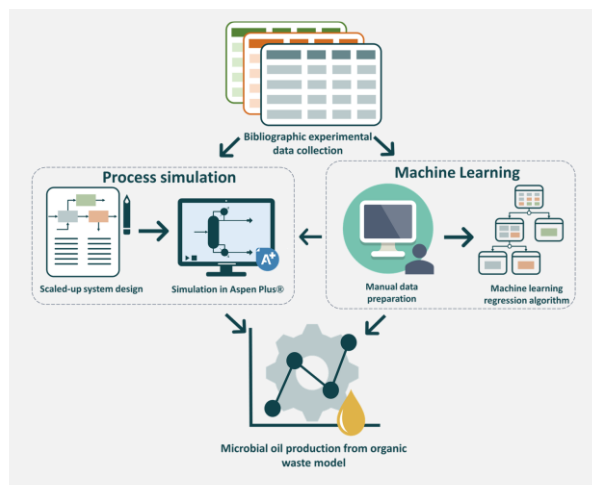
For both scenarios, the experimental and numerical results are in good agreement: 1) the water droplet breaks into slugs within the constriction; and 2) the oil droplet does not break within the constriction.

Understanding the behavior of an integrated process for microbial oil production from organic waste through modelling and simulation

S. Abelleira*, P.L. Cruz, D. Iribarren

Systems Analysis Unit, IMDEA Energy, 28935 Móstoles, Spain; Rey Juan Carlos University, 28933 Móstoles, Spain.

*santiago.abelleira@imdea.org



When produced from organic waste, microbial oil represents a bio-based opportunity to yield high-value products within the circular economy context. The purpose of this work is to develop a model, and analyze the behavior, of an integrated organic waste valorization system for the production of microbial oil.

After a literature review on the different technologies that integrate the process (acidogenic and oleaginous fermentation, and lipid extraction), it is designed and simulated in Aspen Plus®. In particular, literature data concerning oleaginous fermentation under similar conditions to the envisioned system are gathered in a database to build a predictive model through machine learning (ML) algorithms.

The results prove that the ML tool is able to predict the performance of an oleaginous fermenter and, when combined with Aspen Plus®, represents the performance of a semi-continuous biological process, adaptable to different operating and influent conditions.

Introduction

Microbial oil, also known as single-cell oil (SCO), is composed of lipids produced by oleaginous microorganisms such as yeast, microalgae, fungi and bacteria. These oils constitute an alternative to traditional vegetable and fossil-derived oils due to their unique properties and potential applications. SCOs can be produced from a wide range of organic materials, and are even more versatile than vegetable oils produced from biomass crops such as palm, rapeseed or sunflower, as they can be produced independently of seasonal and geographical conditions, in shorter growth times, with lower land and water requirements, and without the need for fertilizers. In fact, SCOs can be produced from organic waste, thereby contributing to avoiding the need for waste disposal. Organic waste options include food waste, agricultural waste, organic industrial waste and the organic fraction of municipal solid waste (OFMSW). Using these waste materials as feedstock, SCOs could be an environmentally-friendly source of energy or oleochemicals, and also cost-competitive as the feedstock is considered critical in the overall cost of the process [1].

Regarding the processes involved in an SCO production system, volatile fatty acids (VFAs) for oleaginous fermentation (OF) can be produced from organic waste through a shortened version of anaerobic digestion, called acidogenic fermentation (AF) or dark fermentation. During AF, all organic matter can be converted into VFAs, which can be then metabolized by oleaginous yeasts to lipids in OF (instead of using sugar-rich organic matter as yeast substrate).

Objectives

Given the novelty of the above-mentioned AF and OF systems, no real data is available from industrial-scale plants to evaluate their behavior and feasibility. In this sense, simulation tools can help design a representative model of an integrated system. Thus, the objective of this work is to develop a model of a scaled-up, integrated organic waste valorization system for the production of SCO, and subsequently analyze its operational behavior.

Methods

The proposed modelling strategy follows the structure shown in the graphical abstract. After literature review, gathered data is used to design the scaled-up system, which is completely simulated in Aspen Plus®. In order to overcome problems concerning the implementation of a biological process in the software, Excel and Fortran subroutines are used to adapt literature data to the simulation environment.

From a process design perspective, three main blocks are defined: AF of organic waste, OF of waste-derived VFAs, and microbial oil extraction from the oleaginous yeasts. As shown in Figure 1, each of the processes requires specific simulation and modelling tools.

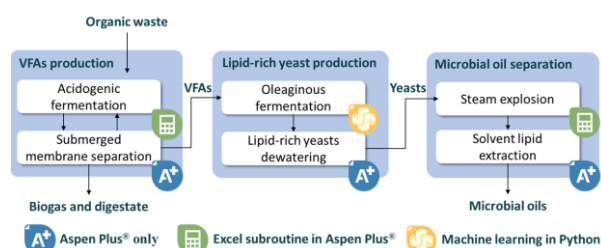


Figure 1. Microbial oil production from organic waste and modelling and simulation tools used in the study.

AF and membrane extraction of the VFA-rich effluent are designed and simulated in Aspen Plus® adapting the parameters of successful experiments described in the literature [2,3].

Due to the difficulty in combining AF and OF in a continuous process, a machine learning (ML) tool is used to predict OF results (biomass and lipid yields and final concentration) from the VFAs influent characteristics and operational parameters. All literature data about OF with similar conditions to the envisioned system is used to construct a database for ML in Python [4-8]. Several regression algorithms (multi-dimensional linear regression, decision tree regression, random Forest regression, neural networks regression, etc.) are tested and their parameters tuned to select the best one. The outcome of the ML is a predictive regression model for OF yield that is then integrated into the Aspen Plus® simulator.

Regarding the design of the products separation and purification section, a steam explosion process (slightly acid medium) is selected as the technique for the lysis of the yeast cells, and an extraction process with n-hexane as solvent is considered to recover lipids from the yeast slurry. The acid steam explosion process was proposed by Kruger et al. [9], and has been described as a cost-effective and scalable lysis technique compared to other options. The selected solvent, n-hexane, has also been reported as a suitable choice compared to other more environmentally-aggressive solvent mixtures (e.g. chloroform-methanol), being able to extract lipid from oleaginous yeasts disrupted slurries with efficiencies higher than 90% [9].

Once the process is completely integrated into Aspen Plus®, a sensitivity analysis is performed to identify how the design parameters, efficiencies and yields affect the chemicals, heat and electricity consumption levels of the system.

Results

Input stream variables and operating conditions identified as relevant to the biomass and lipid yields in the OF process include total and individual VFAs concentration, carbon-to-nitrogen ratio, use of real or synthetic media, and fermentation pH, with a total of 11 variables. 91 data points (actual reported experiments) have all the information for the biomass yield model, while 70 for the lipid yield one. Among the tested ML regression models, decision tree regression is found to be the one with the highest accuracy in this case study, being able to predict the biomass yield of unseen experiments (i.e. those in the test set but not in the training set within the ML exercise) with $R^2=0.88$.

Through the process simulation in Aspen Plus®, the organic loading rate and hydraulic retention time in AF are found to determine the amount of water needed for dilution (Figure 2). Besides water consumption, the dilution ratio affects the cost of downstream heating and separation steps since the volumes increase to produce the same amount of SCO.

Another important parameter is found in the separation steps, such as membrane extraction in the AF and yeast dewatering after OF, which are key in the behavior of the system. Membrane extraction determines not only the quantity of substrate fed to the OF and its concentration in solid sludge, but also the concentration of VFAs and solids in the purge: the higher the concentration of solids after the membrane extraction, the lower the amount of purge needed to prevent sludge accumulation in AF (and therefore the lower the loss of VFA-rich solution). The

Acknowledgements

This work is framed within the OLEOFERM project, which has received funding in the framework of the joint programming initiative ERA CoBioTech, with support from the Spanish Agencia Estatal de Investigación (AEI) and European Union – NextGenerationEU/PRTR with reference number PCI2021-121936, the Ministrstvo za izobraževanje, znanost in šport, Slovenija and the French Agence Nationale de la Recherche.

References

- [1] J. Chopra et al., *Sustainable Energy Technologies and Assessments*, 53 (2022) 102621.
- [2] S. Wainaina et al., *Bioresource Technology*, 274 (2019) 329-334.
- [3] S. Wainaina et al., *Renewable Energy*, 152 (2020) 1140-1148.
- [4] R. Gao et al., *Biotechnology for Biofuels*, 10 (2017) 247.
- [5] R. Gao et al., *Biotechnology for Biofuels*, 13 (2020) 3.
- [6] M. Llamas et al., *New Biotechnology*, 56 (2020) 123-129.
- [7] M. Llamas et al., *Energy*, 206 (2020) 118184.
- [8] S. Morales-Palomo et al., *Journal of Environmental Chemical Engineering*, 10 (2022) 107354.
- [9] J.S. Kruger et al., *ACS Sustainable Chemistry & Engineering*, 6 (2018) 2921-2931.

capability of yeast dewatering before lipid extraction also presents a relevant influence on the process. Even in the most favorable conditions, yeast concentration in OF does not exceed 5% w/w. Such a low concentration involves the need for a centrifuge (with relatively high electricity consumption) or a hydro-cyclone (with relatively low separation efficiency). Also, the lower the concentration of yeast, the higher the steam, acid and solvent requirements, thus hindering the separation steps along the process. Lastly, high VFAs and lipid yields in the fermenters favor oil production.

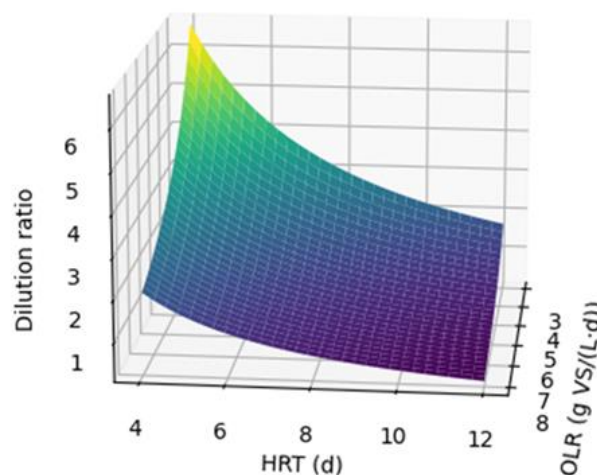


Figure 2. Dilution ratio in AF as a function of the hydraulic retention time (HRT) and the organic loading rate (OLR).

Conclusions

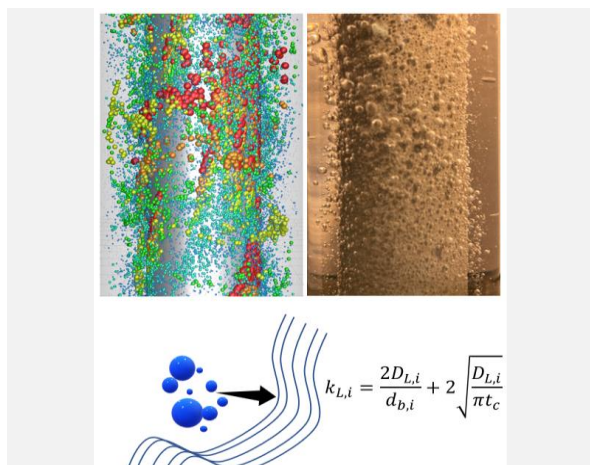
A model of a scaled-up, integrated SCO production process from organic waste was successfully built taking advantage of the combination of machine learning methods, modelling and process simulation. This model allows analysts to understand the behavior of the integrated process as a whole, and it is also expected to be used as a key source of data to subsequently evaluate the sustainability of the system. Throughout this work, design parameters such as OLR, HRT and yeast separation efficiency were identified critical for further research and scaling-up of the process towards industrial implementation.

A novel CFD approach to calculate the ozone mass transfer coefficient (k_L) in a tube-in-tube membrane reactor: coupling numerical and analytical modeling

M.P. Caixeta*, P.H.M. de Oliveira, R.J. Santos, V.J.P. Vilar

¹Laboratory of Separation and Reaction Engineering-Laboratory of Catalysis and Materials (LSRE-LCM), Department of Chemical Engineering, Faculty of Engineering, University of Porto, Rua Dr. Roberto Frias, 4200-465, Porto, Portugal.

*up202003012@up.pt



Ozonation has been widely investigated as an alternative method for water/wastewater disinfection and decontamination. Membrane technology has been employed to enhance gas-liquid contact area, specifically using tube-in-tube configuration. Ozonation was performed in a tangential inlet-outlet tube-in-tube membrane reactor with an upward helical flow. 3D CFD model coupled with a Euler-Lagrange approach and experimental bubble size distribution data was used to simulate gas-liquid multiphase flow. The ozone mass transfer coefficient was calculated using a novel analytical expression, obtained in this work, and inputted in the post-processing step of the CFD simulations. The results achieved with the simulations agreed well with the experimental data and attained a better accuracy compared with other empirical models from literature.

Introduction

Ozone is a powerful oxidant used in water/wastewater treatment, normally injected into the water matrix via bubble diffusers or venturi injectors [1]. However, these conventional methods have limitations including poor mass transfer efficiency, low ozone transfer rates, foam formation and imprecise dosage [2]. Membrane contactors have been identified as an alternative option due to the high interfacial area between the gas and liquid phases [3]. In particular, the tube-in-tube configuration has been investigated for oxidant dispersion and demonstrated to be an interesting alternative to enhance gas-liquid contacting [4]. In this work, a tube-in-tube membrane reactor was used, where gas flows into the membrane's lumen side and permeates through the membrane's pores into the reaction zone, where the gas-liquid contacting process takes place. Millions of micro-sized gas bubbles (~0.4 mm) are formed each second and dragged upward in a helical motion originated by the tangential inlet jet. The main challenge of mass transfer modelling is associated with the determination of the liquid side mass transfer coefficient (k_L), which is the dominant side of the mass transfer resistance [5]. The common method to determine k_L is from empirical correlations, which can offer a good solution but are limited to specific systems and conditions, while analytical solutions can provide a more precise and general solution for the k_L , providing a wider range of application. An analytical expression for k_L was obtained in this work by solving the species diffusion partial differential equation in spherical coordinates, then implemented into a 3D CFD model of a tube-in-tube membrane contacting module. The model was compared with experimental data and with other empirical models available in the literature.

Materials and methods

The tube-in-tube membrane module used in this work is equipped with an inner ceramic tubular membrane (external diameter of 21 mm) and an outer quartz tube (internal diameter of 38 mm) with a useful height of 200 mm. Ozone was generated *in situ* by corona discharge ozonizer and transferred

to a demineralized water matrix, where the dissolved concentration was tracked and used to determine the experimental value of the ozone volumetric mass transfer coefficient ($k_L a$), according to the Eq (1).

$$k_L a = -\frac{1}{\tau} \ln \left(1 - \frac{c_{O_3,L}}{c_{O_3,L}^*} \right) \quad (1)$$

where a is the interfacial gas-liquid contact area per volume (m^{-1}); τ is the liquid passage time (s); $c_{O_3,L}$ is the dissolved ozone concentration ($kg\ m^{-3}$) and $c_{O_3,L}^*$ is the ozone saturation concentration in the water ($kg\ m^{-3}$). A fixed gas flow rate of $45\ Ndm^3\ h^{-1}$ and water flow rates of $30, 70$ and $100\ dm^3\ h^{-1}$ were used to evaluate the influence of the liquid flow rate on the mass transfer. The gas bubbles generated in the tube-in-tube membrane reactor were captured with a high-speed digital camera. The images were treated and processed using the ImageJ software, from where the frequency distribution of the bubble diameters was obtained and the interfacial area (a) could be further calculated to provide the experimental k_L results.

A novel expression to predict the k_L value for a gas species was obtained from the analytical solution of the species transient diffusion equation in spherical coordinates (Eq. (2)):

$$c(r, t) = c_i \frac{R}{r} \left(1 - \frac{2}{\sqrt{\pi}} \int_0^{\frac{(r-R)}{2\sqrt{Dt}}} e^{-\xi^2} d\xi \right) \quad (2)$$

where $c(r, t)$ is the dissolved gas species concentration ($kg\ m^{-3}$) with respect to time t (s) and to radii coordinate r (m); R is the bubble radius (m); D is the species diffusion coefficient in the liquid ($m^2\ s^{-1}$) and ξ is an arbitrary independent variable of the

Gauss error function ($\frac{2}{\sqrt{\pi}} \int_0^{\frac{(r-R)}{2\sqrt{Dt}}} e^{-\xi^2} d\xi$). In this solution, the gas concentration in the bubble surface is (c_i) and diffuses through the coordinate r until the infinite, where it becomes 0 at any instant $t > 0$. Also, the initial concentration ($t = 0$) at any r value is 0. Eq. (2) can be used to solve the species differential flux equation ($J = -D \frac{\partial c}{\partial r} \Big|_{r=R}$) in the bubble's surface,

where the k_L expression automatically appear being the term multiplying the mass transfer driving force (in this particular case, c_i). After some rearrangements to express an average k_L for a fixed contact time between the gas and the liquid phase (t_c), it gets:

$$k_{L,i} = \frac{2D_{L,i}}{d_{b,i}} + 2 \sqrt{\frac{D_{L,i}}{\pi t_c}} \quad (3)$$

where $k_{L,i}$ is the gas species mass transfer coefficient in the liquid side (m s^{-1}); $d_{b,i}$ is the bubble diameter (m) and $D_{L,i}$ is the gas species diffusion coefficient in the liquid phase ($\text{m}^2 \text{s}^{-1}$). Eq. (3) can express the influence of the bubble size and the contact time between the gas and liquid phases in a mass transfer process.

A 3D CFD model was considered to simulate the gas-liquid contacting process using the software ANSYS Fluent through the Discrete Phase Model (DPM), which describes the multiphase flow as a Euler-Lagrange system. To obtain an accurate representation of the gas phase, experimental data for bubble size distribution was inputted into the CFD model. The gas phase physical properties considered for the simulations were: density (ρ_G) of 1.39 kg m^{-3} for an O_2/O_3 mixture, with 0.15 ozone mass fraction, and diffusivity in water (D_{L,O_3}) of $1.76 \times 10^{-9} \text{ m}^2 \text{ s}^{-1}$; while the water properties were: density (ρ_L) of 998.2 kg m^{-3} and viscosity (μ_L) of $1.0 \times 10^{-3} \text{ Pa.s}$. Subsequently, the ANSYS CFD-Post software was used to process the simulation results, where Eq. (3) was inserted and used to calculate the ozone mass transfer coefficient (k_{L,O_3}), based on the simulations data for the bubbles diameter and residence time within reactor.

Results and Discussion

Analyzing the CFD results in Figure 1, the simulations show an increase in k_{L,O_3} when increasing the liquid flow rate coinciding with the onset of helical motion emerging from $70 \text{ dm}^3 \text{ h}^{-1}$ flow rate. Such behavior is expected as the mixture within the annular zone increases, which can be translated to a faster liquid renewal at bubble surface (shorter t_c), leading to a faster mass transfer process (k_L increase).

When compared with other empirical k_L expressions (see Figure 2), the CFD approach used in this work demonstrates a higher level of accuracy in predicting the k_{L,O_3} results for the gas-liquid contacting process in the tube-in-tube membrane reactor.

Acknowledgements

This work was financially supported by: LA/P/0045/2020 (ALiCE) and UIDP/50020/2020 (LSRE-LCM) funded by national funds through FCT/MCTES (PIDDAC); also financially supported by national funds through the FCT/MCTES (PIDDAC), under the project PTDC/EAM-AMB/4702/2020 (OZONE4WATER) and Aquatic/0002/2020 (SERPIC).

References

- [1] K.L. Rakness, *Ozone in Drinking Water Treatment: process design, operation and optimization*, 1st Ed., American Water Works Association, Denver, 2005, 320.
- [2] C. Gottschalk et al., *Ozonation of water and wastewater: A practical guide to understanding ozone and its application*, 2nd Ed., Wiley-VCH, Weinheim, 2008, 189.
- [3] M.J. Berry et al., *Water (Switzerland)*, 9 (2017) 1-18.
- [4] P.H. Presumido et al., *Journal of Environmental Chemical Engineering*, 10 (2022) 108671.
- [5] A. Gabelman, S.T. Hwang, *Journal of Membrane Science*, 159 (1999) 61-106.

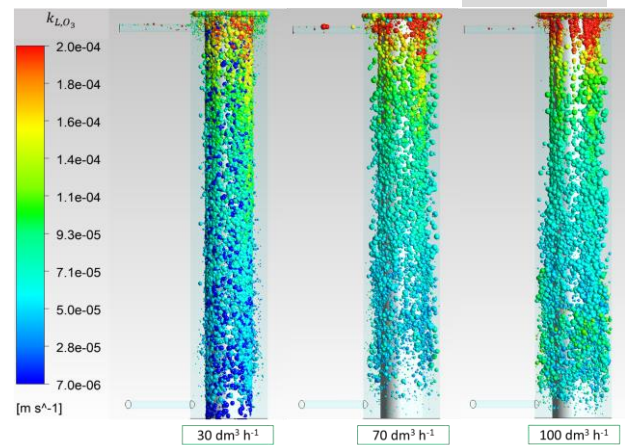


Figure 1. Contours and average value of ozone mass transfer coefficient (k_{L,O_3}) for different water flow rates captured at an instant of 3 times the liquid residence time within the tube-in-tube reactor (τ). Fixed gas flow rate of $45 \text{ Ndm}^3 \text{ h}^{-1}$.

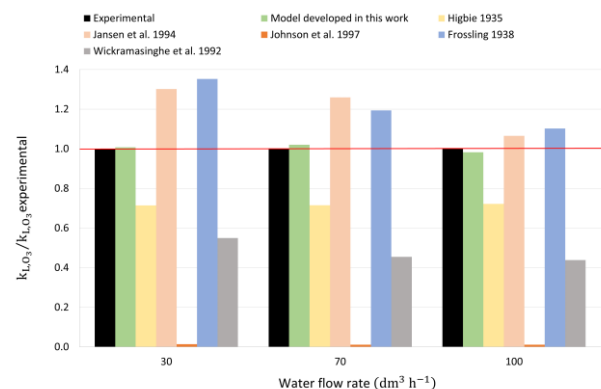


Figure 2. Normalized k_{L,O_3} values calculated from the CFD simulations using different empirical models from literature and comparison with the experimental results from this work.

Conclusions

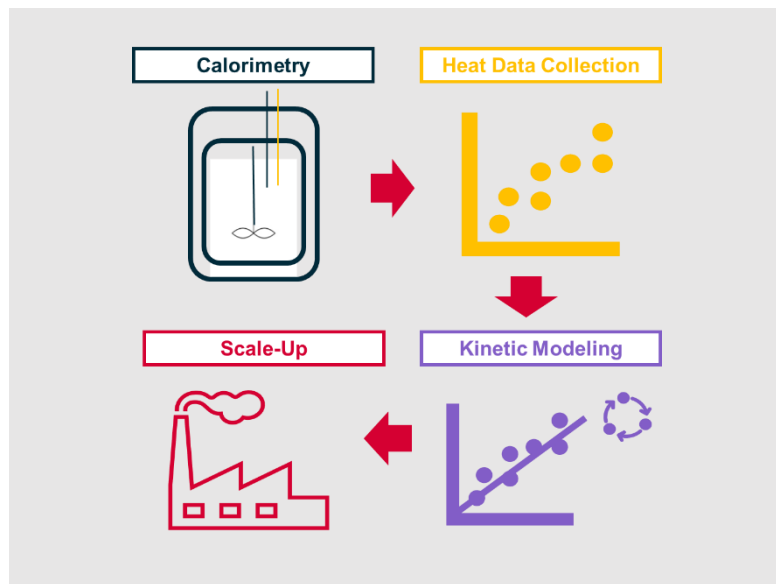
The present work introduces a new approach to predict a gas species mass transfer coefficient using a tube-in-tube membrane reactor for ozonation technology. CFD simulations were coupled with a novel analytical mass transfer coefficient expression to obtain the k_{L,O_3} values in different water flow rates and validated with experimental data. The proposed CFD model showed good potential to be implemented in systems with small bubbles in contact with a liquid.

Kinetic modeling of chemical reactions towards a faster chemical development in the pharmaceutical industry

M.C. Pereira*, N. Lousa

Hovione FarmaCiencia SA, R&D, Sete Casas, 2674-506, Loures, Portugal.

*mcpereira@hovione.com



In the pharmaceutical industry there is a high demand for clinical supplies to be delivered in a timely manner while dealing with complex and new chemical systems within a highly regulated environment. Besides, pharmaceutical process development, optimization and scale-up historically tend to be an iterative approach. This approach entails time and high costs/wastes; therefore, the industry has shifted toward predictability from lab to production. The present work intends to address this gap by kinetic modelling, thus accelerating chemical development, while reducing lab experiments. Towards that end, calorimetric and concentration data are used to build kinetic models yielding safe and robust processes that meet the pharmaceuticals industry needs.

Introduction

In the pharmaceutical industry there is a steady need to ensure that clinical supplies are manufactured and delivered in a timely manner while dealing with complex and new chemical systems within a highly regulated environment. On the other hand, manufacturers are constantly evaluating the best use of the limited financial resources available [1,2].

Besides, pharmaceutical process development, optimization and scale-up historically tend to be an iterative approach. This approach entails time and high costs/wastes; therefore, the industry has been shifting toward predictive approaches from lab to production [3].

The present work is included in the scope of integrated chemical development in the pharmaceutical industry, focused on chemical reaction development. In this framework, the aim is the optimization of the yield, minimization of impurities while simultaneously generating information for safe and robust scale-up.

Mathematical description of chemical phenomena is a powerful tool to approach this issue, as it allows the simulation of the process using lab generated information (modeling approach). Employing this approach, it is possible to find the optimal conditions of a reaction, during early development, while reducing the time and resources invested at the lab.

Methodology explained

In the current work, calorimetry data generated during safety studies of chemical reactions is applied to support kinetic modeling of the chemical synthesis.

Calorimetric data is an output of great importance, as it not only relates to the kinetics but also to the thermodynamic parameters of the chemical transformation, supporting a comprehensive knowledge of the process, including phase changes, heat, and mass transfer phenomena for instance, and supporting safe scale-up of exothermic processes.

In addition, the heat profile of a reaction comprises an advantageous dataset over discontinuous sampling, as it's representative of its progress. Figure 1 shows how reaction heat profile was used to distinguish the reaction mechanism and to determine kinetic and thermodynamic parameters of the an ethanolysis reaction.

Although calorimetry is a powerful tool to assess the kinetic profile, it is a differential kinetic analysis, as it is proportional to the conversion rate. To assess the source of the heat production, it is necessary to feed the model with an integrated dataset. To that end, concentration data should be simultaneously taken during the lab experiment.

Results and Discussion

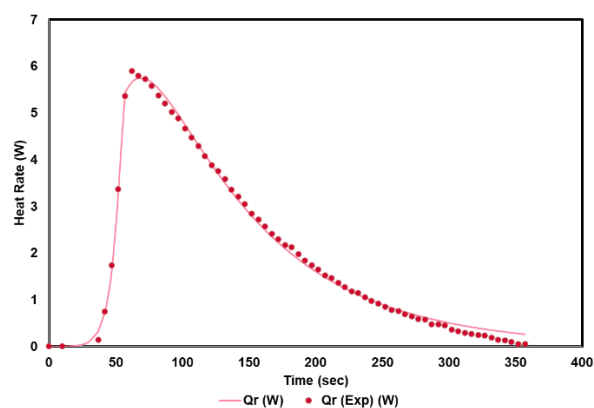


Figure 1. Kinetic modeling of ethanolysis of acetic anhydride using calorimetry data.

Concerning concentration data, several options may be at play. In this work, the impact of the concentration data was similarly assessed in the model development through comparison of discrete sampling versus Process Analytical Technology

(PAT). While PAT reveals to be a more powerful tool to evaluate the reaction progress it is not applicable to all chemical systems and its applicability should be evaluated casewise.

In sum, the present work shows how kinetic modeling of chemical synthesis benefits the pharmaceutical development while meeting industry needs on timeframes, predictability, and quality using calorimetry data.

Acknowledgements

We would like to thank to Dr. Saúl Silva for the support, advice and encouragement. To both, Dr. Filipe Ataide and Prof. Francisco Lemos for the knowledge sharing and attendance during this journey.

References

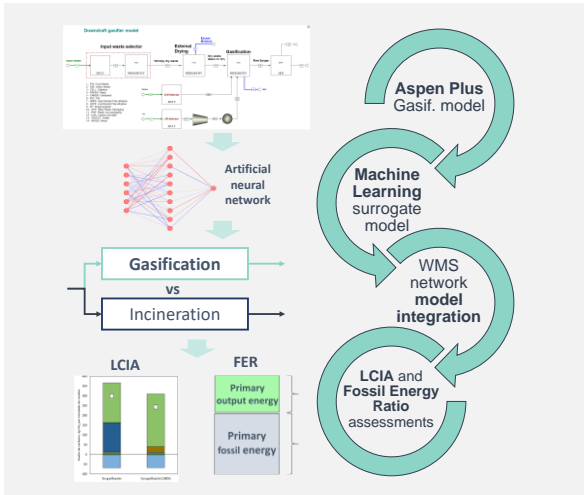
- [1] G.E. Rotstein et al., Computers and Chemical Engineering, 23 (1999) 5883-5886.
- [2] D. Ende, Chapter 1 in Chemical Engineering in the Pharmaceutical Industry: R&D to Manufacturing, D. Ende, 1 Ed., Wiley, 2011, 3-21.
- [3] M.C. Pereira et al., Reaction calorimetry and thermodynamic & kinetic modelling towards a faster chemistry development, Lisbon, Portugal, 2021, 1-10.

Analysis of the role of gasification within a waste management and valorization system using an artificial neural network as surrogate model

*N. Martínez-Ramón**, J.L. Gálvez-Martos, E. Medina-Martos, I.R. Istrate, P.L. Cruz, J. Dufour

Systems Analysis Unit, IMDEA Energy, Avda. Ramón de la Sagra 3, E-28935, Móstoles, Madrid, Spain.

nicolas.martinez@imdea.org



This work aims to elucidate the impact of a gasification system within a municipal solid waste management system. To do so, a set of Aspen plus simulations were developed and transposed into a computationally lighter artificial neural network regression model. This model was integrated within a MATLAB mass flow analysis (MFA) superstructure representative of a modern waste management system. The superstructure is also an LCIA tool capable of providing the performance of the system as a whole. This integrated assessment was elaborated for different scenarios, comparing the performance of incineration and gasification for different energy uses. The fossil energy ratio was also calculated for the different energy products considered (electricity and hydrogen).

Introduction

The European Union has achieved unprecedented levels of prosperity and well-being in recent decades. Its social, health and environmental standards rank among the highest in the world [1].

Maintaining and improving these levels of prosperity while reducing the environmental footprint will certainly require fundamental changes in consumption patterns and use and supply of energy and materials [1].

Circularity, energy valorization from waste and substitution of fossil energy for renewable electricity and hydrogen are key elements to achieve this. Among these, hydrogen production from waste gasification is considered to have an important role in ensuring the total demand for hydrogen, fixed at 10 Mt for 2030 in the EU [2].

The integration of hydrogen production technologies in regional waste management systems can produce low carbon hydrogen, especially in those regions with low land availability for

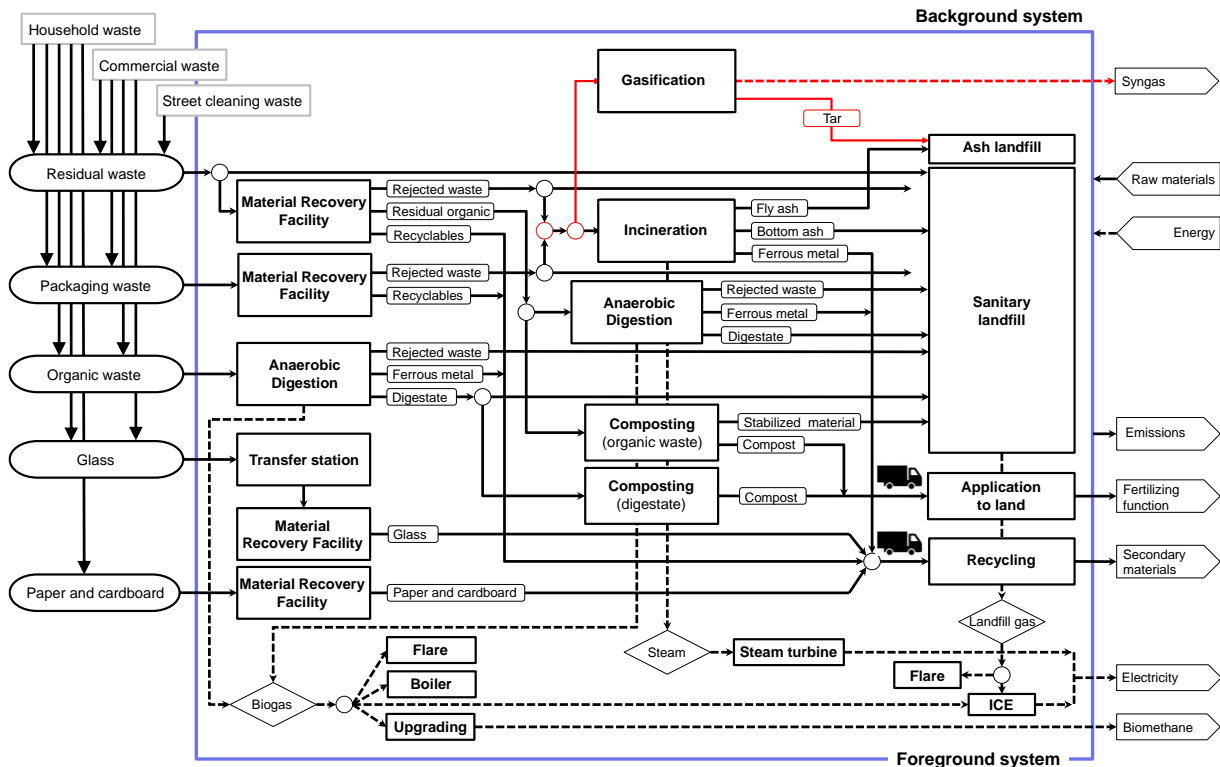


Figure 1. Waste management system material flow scheme with integrated Gasification unit.

renewables (i.e. solar and wind) by geographical and/or economic reasons such as islands or highly populated communities. Whilst the potential of gasification is clear, its widespread commercial and industrial implementation are still limited by process performance and efficiency [3]. It is therefore vital to have system assessment tools to evaluate the real potential of this technology within a particular system.

The objective of this study is to develop an integrated quantitative assessment on the environmental impacts and performance of the introduction of waste gasification as an alternative for incineration within a municipal solid waste (MSW) management system. To do this, surrogate machine learning algorithms from complex simulation models have been implemented.

Methods

The downdraft gasification process was simulated in Aspen Plus® V12. The model was prepared to be flexible and provide synthetic data from a sensitivity analysis for different input conditions such as varying biomass ultimate and proximate compositions, steam to biomass ratio and pressure and temperature of operation in the gasifier. The results of the simulation were used to train an artificial neural network [4]. As these results come from successful simulation runs in Aspen Plus, they are thermodynamically compliant and representative of the natural patterns occurring in the gasification process. To ensure a model with high generalisation capability, a wide range of feedstocks and operating conditions were considered. The main advantage of working with an artificial neural network is the obtention of a computationally light and flexible model which can be integrated in the waste management mass flow analysis (MFA) superstructure in MATLAB, which represents the foreground system. Once integrated, the superstructure was used to assess different scenarios from an LCIA and energy performance point of view. The evaluated scenarios were the following:

- Conventional, in which incineration is used to prevent landfill
- Substitution of incineration for gasification without capacity restriction
- Gasification with capacity restriction and incineration to cover for the remaining fraction

Additionally, the scenarios of syngas to hydrogen and syngas to electricity were compared without capacity restriction to give an

Acknowledgements

Grant PID2021-124705OB-I00 (HYWARE) funded by MCIN/AEI/ 10.13039/501100011033 and “FEDER A way of making Europe”.

References

- [1] EEA, ‘Growth without economic growth — European Environment Agency’, 2020. <https://www.eea.europa.eu/publications/growth-without-economic-growth> (accessed Feb. 17, 2023).
- [2] European Commission and Directorate-General for Energy, ‘Hydrogen’, *A hydrogen strategy for a climate-neutral Europe*, Jul. 08, 2020. https://energy.ec.europa.eu/topics/energy-systems-integration/hydrogen_en (accessed Feb. 27, 2023).
- [3] S. Ascher et al., *Bioresource Technology*, 364 (2022) 128062.
- [4] C.M. de Melo et al., *Trends in Cognitive Sciences*, 26 (2022) 174-187.
- [5] *Directiva (UE) 2018/850 del Parlamento Europeo y del Consejo, de 30 de mayo de 2018, por la que se modifica la Directiva 1999/31/CE relativa al vertido de residuos (Texto pertinente a efectos del EEE)*, vol. 150. 2018. Accessed: Mar. 10, 2023. [Online]. Available: <http://data.europa.eu/eli/dir/2018/850/oj/spa>.

idea of the maximum energy potential of gasification within a modern WMS.

Preliminary results

Gasification has a lower climate change impact per ton of waste than incineration. However, the net performance of the system is highly dependent on the capacity of the gasification plant. If the capacity is not large enough and no alternative is provided, waste has to be disposed of at landfills. Not preventing landfill to its maximum capacity would also damage the LCIA performance of the system as a whole (Figure 2), and this treatment may be avoided if disposal at landfill is higher than 10%, according to the objectives of the European directive 2018/850 [5].

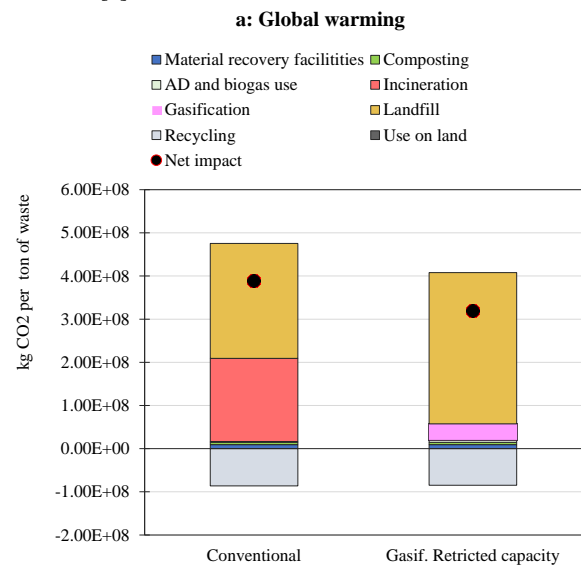


Figure 2. Climate change results for a system with incineration and a system with a gasification unit with treatment capacity of 120,000 tons of waste per year and no incineration.

Preliminary conclusions

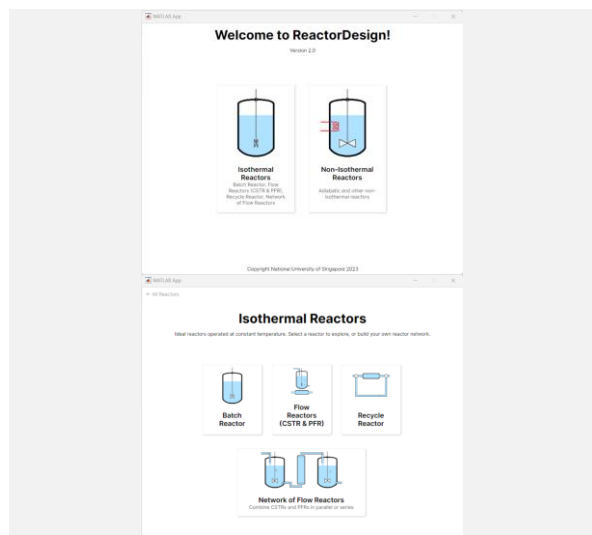
Capacity of the gasification unit is a relevant factor when this technology is evaluated in a systematic assessment of whole MSW management systems. At the same time, gasification towards hydrogen or electricity production from waste has an overall positive impact, reducing the environmental footprint of the waste-to-energy system. However, if capacity is not optimal, it may lead to more waste reaching landfill if the incineration unit has been completely phased out.

ReactorDesign App: An interactive software for self-directed explorative learning

C.W. Lim, N. Yan*

Department of Chemical and Biomolecular Engineering, National University of Singapore, 4 Engineering Drive 4, Singapore 117585, Singapore.

*ning.yan@nus.edu.sg



Reactor Design constitutes the central idea of Chemical Engineering. Despite its importance, the difference in approaches to the subject in university and the industry has led to a widening learning gap as graduates transition from university to the industry. Here, we aim to narrow the gap by developing the interactive ReactorDesign App. It enables students to design reactors involving complex design equations. The concepts covered during lectures are explicitly utilised, allowing students to understand how these fundamental concepts are applied in various reactions. The software leverages the easily accessible MATLAB App platform to encourage self-directed explorative learning, aided by a set of accompanying guiding questions. It is also useful as a tool for solving certain assignment questions that may be too tedious if attempted manually. Our implementation of the technology enhanced learning (TEL) received highly positive feedback from the trial participants.

Introduction

In Chemical Engineering, Reactor Design is widely regarded as one of the most important topics as it relates directly to the chemical transformation of feedstocks into value-added products on the commercial scale. It is therefore essential that Chemical Engineering undergraduates grasp its core ideas well and apply them to design appropriate reactors in their career. However, the teaching of Reactor Design at universities has focused on the manual solution of design equations and use of reference charts, while the industry has evolved to extensively incorporate the use of simulation and monitoring software. Hence, there is often a learning gap as students transition from university to the industry.

Meanwhile, technology has been utilised to improve the learning process in various Chemical Engineering topics, including Process Control [1], Fluid-Solid Systems [2] and Engineering Separations [3]. Specifically, technological tools for innovating the teaching of Reactor Design include the ChemKinetics software [4], MATLAB applications for simple batch reactors and biochemical reactors [5,6] and an IPython software package for heterogeneous catalytic reactions [7]. These existing works appear to focus on the simulation of reactor processes, as opposed to more fundamental ideas of reactor selection and optimisation. Therefore, it seems timely for us to develop an interactive software to enhance the learning of the fundamental concepts of Reactor Design and demonstrate their applications to various reactions.

Objectives

We develop the interactive ReactorDesign App, enabling students to design reactors involving complex design equations. Graphical illustration of the design process will be automatically generated, allowing students to relate to the design procedures taught during lectures. The App leverages the flexibility and efficiency of the MATLAB App platform to enhance the learning process through self-directed explorative learning.

Methods

This study was undertaken at the Department of Chemical and

Biomolecular Engineering, National University of Singapore (NUS) over two academic years (AYs). Here, the Reaction Engineering module is a second-year core module, with a class size of around 190. The ReactorDesign App focuses on the design of ideal reactors under both isothermal and non-isothermal conditions. To maximise the effectiveness of the final product, the most important stakeholder – the students – was involved extensively in all stages of the App development. Firstly, a preliminary version of the App was tested with students in the first AY of the study. This proof-of-concept trial successfully demonstrated the feasibility of our proposed approach. Then, the functions and graphical user interface (GUI) of the App were enhanced significantly, producing the beta version for a small-group testing involving 13 undergraduate students. Their ability to smoothly use various functions of the App was assessed, and any suggestions on improving the usability of the App were also collected. Next, the finalised version of the ReactorDesign App was released to students in the second AY to complement the formal teaching. A set of guiding questions was also provided to encourage students' explorative learning. Several assignment questions were set to examine their understanding of the concepts explored in the App. A series of survey questions was designed to evaluate the effectiveness of the App at achieving its intended objectives.

Results

Upon launching the ReactorDesign App, the welcome page shows animated icons representing the two main sections – Isothermal and Non-Isothermal Reactors (Graphical Abstract, upper image). Clicking on the Isothermal Reactors icon leads the user to its landing page, which further allows for the navigation to various functions for studying the design of ideal reactors, including the batch reactor, single flow reactors (both continuous stirred tank reactor (CSTR) and plug flow reactor (PFR)), recycle reactor and network of flow reactors (Graphical Abstract, lower image). Meanwhile, the Non-Isothermal Reactors section consists of a single functional page. The topics covered by the ReactorDesign App are those typically taught as part of the subject of Ideal Reactor Design at the undergraduate level, making the software a suitable complementary learning

tool. The layout of the functional pages was designed to be consistent to enhance App usability. In general, they contain fields for the user to enter the kinetic and reactor parameters, graphical illustration of the design procedures in the form of a Levenspiel plot, calculation results as well as the chemical equation and rate expression for the reaction (Figure 1). Notably, the user has good flexibility when setting the reaction parameters, allowing a wide range of possible reactions to be explored without the need to go through the manual solution of complicated kinetic and design equations, which is made possible by the computational power of MATLAB. Moreover, the Levenspiel plot on the functional page enables the student to relate to the graphical design procedures taught in the module, avoiding a “black box” style implementation of learning technology which is sub-optimal towards effective learning. The user is also able to customise the displayed plots, allowing for meaningful comparison. For instance, the difference between the space times required for CSTR and PFR is apparent when their corresponding graphical areas are plotted together (dark blue dashed rectangle and yellow shaded region in the Levenspiel plot in Figure 1, respectively). Another App feature helpful for explorative learning is the ability to switch between design and rating modes (using tabs above parameter fields), with the former allowing for the calculation of reactor space time from the specified conversion and the latter enabling the prediction of conversion from the reactor space time.

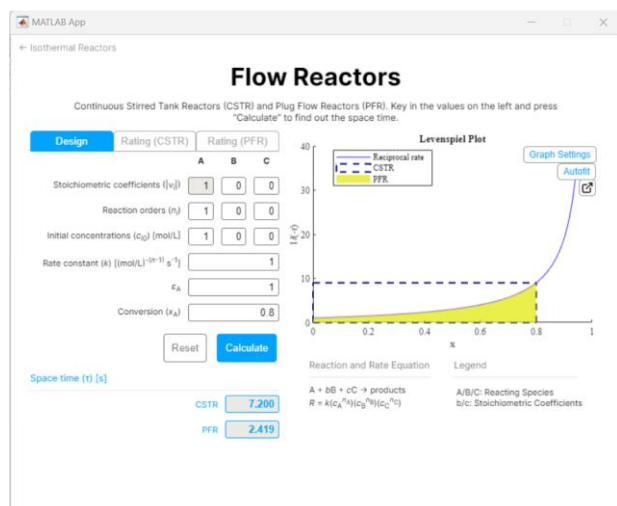


Figure 1. Graphical user interface of the Flow Reactors function for studying CSTR and PFR in the ReactorDesign App.

To encourage explorative learning using the ReactorDesign App, a set of guiding questions has been designed. The questions are organised based on the App functions and, where appropriate, separated into sections for design and rating modes. They are intended to be attempted after the relevant lectures and possibly before solving more in-depth assignment questions, to strengthen conceptual understanding. They are explorative in nature, leveraging the automated calculation characteristic of the

Acknowledgements

This work was supported by a Learning Innovation Fund – Technology (LIFT) grant awarded by the National University of Singapore (NUS) [grant number E-027-00-0010-38].

References

- [1] X. Li, Z. Huang, *Education for Chemical Engineers*, 19 (2017) 1-12.
- [2] E.W.C. Lim, *Education for Chemical Engineers*, 21 (2017) 72-79.
- [3] T. Bánsági, T.L. Rodgers, *Education for Chemical Engineers*, 22 (2018) 27-34.
- [4] S.W. Bigger, *Journal of Chemical Education*, 88 (2011) 244-244.
- [5] R. Molina et al *Education for Chemical Engineers*, 28 (2019) 80-89.
- [6] R. Molina et al., *Education for Chemical Engineers*, 34 (2021) 127-137.
- [7] B. Golman, *Education for Chemical Engineers*, 15 (2016) 1-18.

App to allow students to conveniently investigate various parameters. Some questions also aim to prompt students to think critically about the calculation results, for example by drawing linkages to lecture content or through comparison with answers to other guiding questions. In addition, the ReactorDesign App is useful as a tool for solving assignment questions. Besides speeding up the calculation process, it also generates graphical visualisation in the form of Levenspiel plots, enabling students to learn from the automated solution process.

To assess the effectiveness of the ReactorDesign App, the students were asked to complete a voluntary online survey after using the App for explorative learning (based on supplied guiding questions) and solving selected assignment questions during the semester. The response was positive overall, with the vast majority of respondents agreeing or strongly agreeing that the App helped with understanding the subject of Reactor Design (93%, Figure 2a) and that its graphical visualisation features improved the understanding of reactor design principles (94%, Figure 2b). Most respondents also agreed or strongly agreed that the App enhanced their application of knowledge to design the most optimal reactors (96%, Figure 2c) and that it improved learning flexibility (90%, Figure 2d). Taken together, as a learning tool, the ReactorDesign App was well appreciated by the participating students.

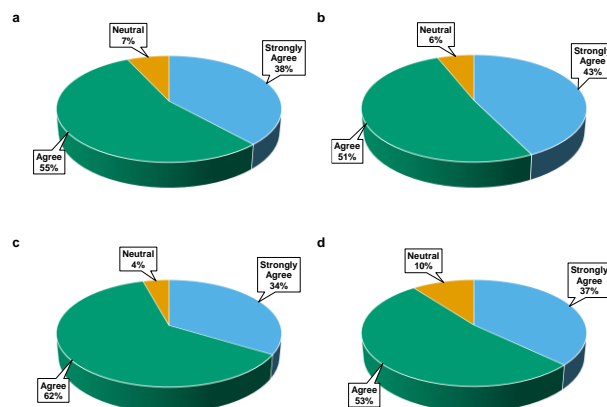


Figure 2. Students' responses to an online survey on the ReactorDesign App. The survey questions are (a) “The ReactorDesign App helps me understand the subject of Reactor Design”, (b) “The graphical visualisation features of the ReactorDesign App enhance my understanding of the design principles of various reactors”, (c) “The ReactorDesign App improves my ability to apply my knowledge to design the most optimal reactor(s) for a given reaction” and (d) “The ReactorDesign App offers learning flexibility, compared to the conventional lecture-tutorial learning framework”.

Conclusions

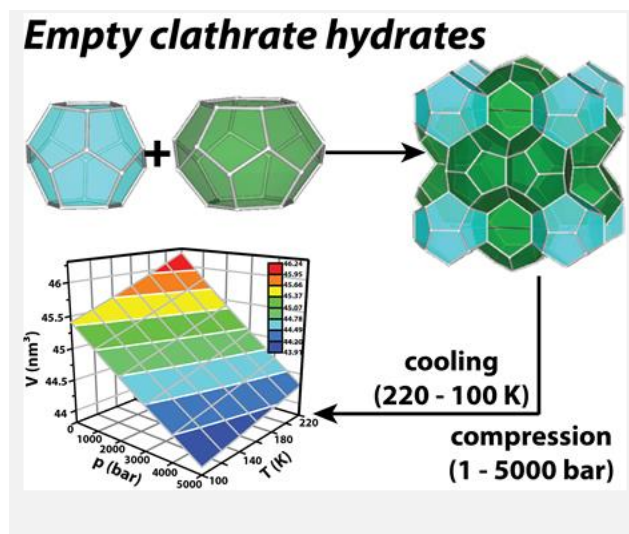
We have developed the interactive ReactorDesign App, which serves as an effective learning aid for encouraging explorative learning as well as a useful tool for problem solving.

Structure and thermodynamics of empty clathrate hydrates below the freezing point of H₂O

F.J.A.L. Cruz*, J.P.B. Mota

LAQV@Requimte, Dept. Chemistry, NOVA University Lisbon, 2829-516 Caparica, Portugal.

*fj.cruz@fct.unl.pt



Simulations are employed to probe empty *sI* and *sII* clathrate hydrates, observing that the volumetric response to an applied $p-T$ gradient is accurately described by the Parsafar and Mason equation of state with an accuracy > 99%. Structural deformation induced upon the crystals is monitored and benchmarked against previous neutron diffraction measurements of ice XVI and hexagonal ice at 1 bar. A critical comparison is established with guest occupied lattices (CH₄, CO₂ and C_nH_{2n+2}), revealing that empty *sII* frameworks are slightly more stable to thermal deformation than their *sI* analogues. Of paramount importance for the oil and natural gas industries, heat capacities obtained are identical for the *sI* and *sII* lattices up to 2000 bar and diverge by ~ 7.3 % at 5000 bar. The canonical tetrahedral symmetry of water-bonded networks is analysed in terms of an angular and a distance order parameters, which are observed to decrease (increase) as pressure (temperature) increases (decreases).

Introduction & Methodology. The thermodynamical phase space of the metastable empty clathrate hydrates (CHs) is probed over broad temperature and pressure ranges ($100 \leq T/K \leq 220$, $1 \leq p/\text{bar} \leq 5000$), using large-scale computer simulations and compared with available experimental data at 1 bar [1, 2]. For that purpose, we employ the fully atomistic and rigid TIP4P-Ice four-charge potential [3] to describe the H₂O lattice of the empty clathrate phases (*sI*, *sII*); this potential was developed to reproduce the experimental melting point of ice *Ih* (272.2 K at 1 bar), and has been successfully employed to study the deformation [1, 2, 4], energetics and decomposition [5, 6], and phase behaviour [7-9] of several CHs. Starting from an initial configuration at the lowest temperature and pressure (100 K, 1 bar), CHs are isothermally pressurised to achieve the desired pressure (1 bar → 100 bar → 500 bar → 1000 bar → 2000 bar → 5000 bar), and the protocol repeated for the next higher temperature (100 K → 120 K → 140 K → 160 K → 180 K → 200 K → 220 K) starting from the corresponding previous equal pressure run. Calculations are run for at least 50 ns in order to obtain statistically consistent data, and the first 5 ns discarded to account for equilibration. Because data collection takes place every 5 ps, each $p-V-T$ state point is obtained from time-averaging an *ensemble* of 9000 data points. The whole $p-V-T$ surface obtained (*cf.* Graphical Abstract) is interpreted using the universal form of the Parsafar and Mason equation of state [10], always with an accuracy better than 99 %.

Results – Structure. Measurements of unit cell length, a , were conducted during the simulations and are here represented in Figure 1a for the room pressure systems, along with data previously obtained for other guest occupied *sII* CHs. A critical comparison is established in terms of the ratio of molecular diameters between the guest molecule, D_G , and cavity diameter, D_C , allowing the parameter (D_G/D_C) to be used as the rationale for unit cell length increase/contraction when the empty crystals become occupied by guest molecules. Furthermore, the solids' isobaric thermal expansivity, obtained in terms of a parabolic line (Fig. 1b), $\alpha_p = [\partial a / (a \cdot \partial T)]_p$, reveals that the empty CHs

exhibit a positive thermal expansion up to a certain temperature threshold, beyond which $[\partial^2 a / (a \cdot \partial T^2)]_p$ becomes negative; the particular temperature at which this phenomenon occurs decreases with applied pressure, and, in the case of the *sII* lattices, starts at 191.5 K@1 bar until finally reaching 161.6 K@5000 bar (Fig.1b).

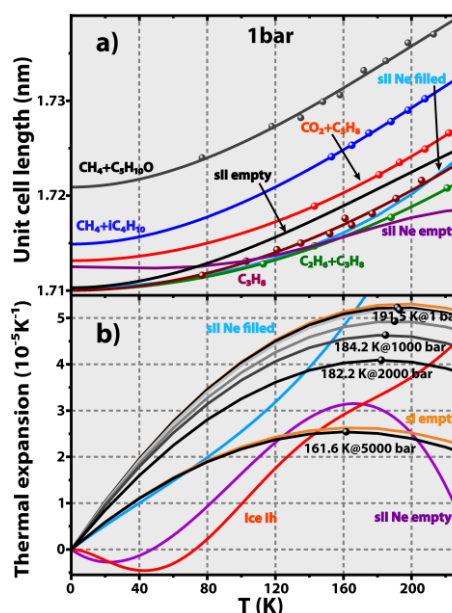


Figure 1. Structural data. *a*) Temperature dependence of unit cell length at 1 bar for *sII* lattices: symbols correspond to experimental measurements of C₃H₈ (dark red), 18.2 % CO₂ + 81.8 % C₃H₈ (light red), 30 % C₂H₆ + 70 % C₃H₈ (green), 87.6 % CH₄ + 12.4 % iC₄H₁₀ (blue) and 95 % CH₄ + 5 % C₅H₁₀O (dark grey). Results obtained in this work for empty *sII* clathrates (black), as well as data for Ne-filled (light blue) and Ne-empty (magenta) *sII* topologies are represented by lines obtained using cubic polynomial fittings. *b*) isobaric thermal expansivities, $\alpha_p = (1/a)(\partial a / \partial T)_p$ obtained using molecular simulations and empty *sII* (black) and *sI* clathrates (dark yellow), and previous atmospheric pressure experimental data for hexagonal ice (red) and Ne-filled and Ne-empty *sII* clathrates (light blue, magenta); values represent the several α_p maxima.

The characteristic tetrahedral structure around oxygen atoms was probed using two order parameters, S_g and S_k , in order to monitor the angular and distance contributions to a canonical tetrahedral symmetry, respectively [11]. Time-averaged distributions reveal that the empty frameworks retain tetrahedral integrity throughout the entire p - T domain, but respond accordingly by slightly distorting the solid lattice. Using Gaussian statistics, it becomes clear that by imposing isothermal conditions whilst increasing pressure, S_g maxima are shifted towards higher values, as a result of the solid contraction and gradual loss of tetrahedral order. For $(p, T) > (2000 \text{ bar}, 200 \text{ K})$, deformation occurs via a mechanism that involves a dominant contribution from angular alterations. The microscopic structure associated with the solids is probed deeper calculating radial distribution functions (g_r), and, in general, both the $g_r(\text{O}-\text{O})$ and $g_r(\text{O}-\text{H})$ curves exhibit two maximum intensity peaks, corresponding to the thickness of the first and second order neighbour shells, centered at $r_{(\text{O}-\text{O})} = (0.27, 0.45) \text{ nm}$ and $r_{(\text{O}-\text{H})} = (0.18, 0.32) \text{ nm}$, revealing that the hydrogen bonds responsible for network integrity are of similar length regardless of the particular (p, T) conditions. A recent neutron diffraction analysis [12] of an empty *sII* hydrate yielded a mean time-space averaged hydrogen bond distance of 0.275 nm, which compares quantitatively with our own average value of $\bar{r}_{(\text{O}-\text{H})} = 0.25 \text{ nm}$.

Results – Thermodynamics. The isobaric heat capacity is obtained using the classical thermodynamic relation $C_p = (\partial H / \partial T)_p$, where H is the solid's molar enthalpy. Figure 2 shows a *quasi*-constant correlation with pressure, at least up to 2000 bar, beyond which C_p becomes a function of the clathrate individual topology. When pressure reaches 5000 bar, the *sII* polymorphs exhibit a C_p that is $\sim 7.3 \%$ larger than the corresponding *sI* crystals, suggesting that the larger cages characteristic of *sII*, when subject to hydrostatic pressure, are better suited to accommodate heat propagation through the lattice thus giving rise to a slightly enhanced C_p as compared to

the *sI* structure. Data obtained for the empty clathrates and also for hexagonal ice have been successfully correlated using Shomate-like equations, $C_p = A + Bp + Cp^2 + Dp^3$ [2].

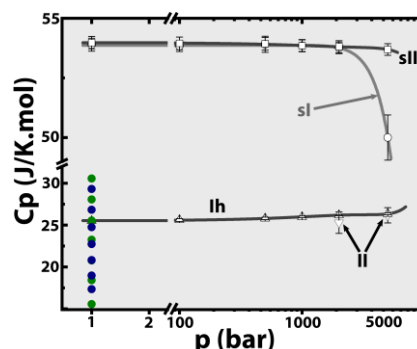


Figure 2. Isobaric heat capacity, C_p . Symbols and error bars correspond to data obtained in the calculations: (\square) empty *sII* clathrates, (\circ) empty *sI* clathrates, (Δ) hexagonal ice *Ih* and (∇) ice *II* and experimental results from Handa and Murray for ice (\bullet) and a THF clathrate (\bullet). Lines correspond to cubic polynomials, $C_p = A + Bp + Cp^2 + Dp^3$. Notice that the C_p scale has been broken in the range 31 – 49.5 J/K.mol.

Handa et al. used a Tian-Calvet heat-flow calorimeter and samples of a tetrahydrofuran CH (THF·16.9H₂O) and H₂O ice, at 85–270 K at room-pressure [13, 14]. Under their experimental conditions, hexagonal ice is the thermodynamically stable form of water, for which the isobaric heat capacity was observed to increase from $C_p = 15.5 \text{ J/K.mol}$ up to $C_p = 30.5 \text{ J/K.mol}$, when temperature climbs from 100 K to 220 K, respectively, giving rise to an average value of $\overline{C_p} = 23 \text{ J/K.mol}$, in satisfactory agreement with our own result of $C_p = 25.5 \text{ J/K.mol}$. For the THF hydrate samples $C_p = 17.4 \text{ J/K.mol}$ (100 K) and 29.3 J/K.mol (220 K). Their complete set of calorimetric data for ice *Ih* and THF·16.9H₂O is graphically represented in Figure 2, together with the results obtained in the present work.

Acknowledgements

This work received support from PT national funds (FCT/MCTES, Fundação para a Ciência e Tecnologia and Ministério da Ciência, Tecnologia e Ensino Superior) through projects UIDB/50006/2020 and UIDP/50006/2020. F.J.A.L.C. gratefully acknowledges FCT/MCTES for funding through program DL 57/2016 – Norma Transitória (Ref. 654/2018-24), and also for funding the Advanced Computing Project 2021.09623.CPCA on Cirrus-A:INCD.

References

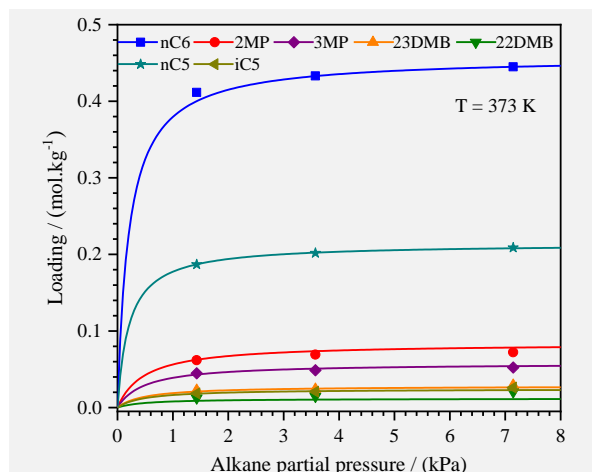
- [1] F.J.A.L. Cruz et al., ACS Earth Space Chemistry, 3 (2019) 789.
- [2] F.J.A.L. Cruz, J.P.B. Mota, Physical Chemistry Chemical Physics, 23 (2021) 16033.
- [3] J.L.F. Abascal et al., Journal of Chemical Physics, 122 (2005) 234511.
- [4] S. Takeya et al., Journal of Physical Chemistry C, 122 (2018) 8134.
- [5] S. Alavi, R. Ohmura, Journal of Chemical Physics, 145 (2016) 154708.
- [6] S.A. Bagherzadeh et al., Journal of Chemical Physics, 142 (2015) 214701.
- [7] H. Tanaka et al., Journal of Chemical Physics, 149 (2018) 074502.
- [8] D. Jin, B. Coasne, Langmuir, 33 (2017) 11217.
- [9] V.K. Michalis et al., Journal of Chemical Physics, 142 (2015) 044501.
- [10] G. Parsafar, E.A. Mason, Physical Review B, 49 (1994) 3049.
- [11] P.-L. Chau, A.J. Hardwick, Molecular Physics, 93 (1998) 511.
- [12] A. Falenty et al., Nature, 516 (2014) 231.
- [13] Y.P. Handa, Canadian Journal of Chemistry, 62 (1984) 1659.
- [14] Y.P. Handa et al., Journal of Chemical Thermodynamics, 16 (1984) 623.

Separation of n/iso-paraffins in a hierarchically structured 3D-printed porous carbon monolith

A. Henrique^{1,2*}, L.F.A.S. Zafaneli^{1,2}, E. Aly¹, H. Stedinger³, J. Gläsel³, A.E. Rodrigues², B.J.M. Etzold³, J.A.C. Silva¹

¹Centro de Investigação de Montanha (CIMO), Instituto Politécnico de Bragança, Campus Santa Apolónia 5300-253, Bragança, Portugal, ²Laboratory of Separation and Reaction Engineering and Laboratory of Catalysis and Materials (LSRE/LCM), Faculty of Engineering University of Porto, Rua Dr. Roberto Frias S/N 4200-465, Porto, Portugal; ³Ernst-Berl-Institut für Technische und Makromolekulare, Technische Universität Darmstadt, Darmstadt, Germany.

*adriano_henrique@ipb.pt



Hierarchically structured 3D-printed porous carbons monoliths were investigated for their applicability in adsorptive n/iso-paraffin separation. Three materials of the same macroscopic shape were employed, which varied in the micro- and mesoporosity by altering the final CO₂ activation step: non-activated and activated at 1133 K for 6 and 12 h, respectively. Chromatographic breakthrough experiments were conducted for pentane and hexane isomer mixtures at industrially relevant separation conditions. Results demonstrated that the initial porosity for the non-activated monolith enables the complete separation of linear paraffins from their branched isomers (slightly adsorbed) via a near molecular sieving effect. The Langmuir isotherm conveniently fitted the adsorption equilibrium data, and a dynamic mathematical model suitably predicted the breakthrough curves. Regarding the CO₂ activated monoliths, both showed adsorption towards all alkanes with practically no selectivity between them.

Introduction

The separation of mixed feedstocks containing pentane and hexane isomers for improving the octane rating of gasoline is a critical topic in the petrochemical industry. The value of a particular paraffin as a component in the gasoline pool is related to its research octane number (RON) assigned. The higher the RON is, the higher the fuel's resistance to auto-ignition [1]. As a general remark, branched alkanes have a superior RON content than their corresponding normal isomers. For example, iso-pentane (iC5; 93.5) has a RON value of nearly 30 numbers above n-pentane (nC5; 61.7). Similarly, the di-branched hexanes 2,2-dimethylbutane (22DMB; 94) and 2,3-dimethylbutane (23DMB; 105) show values at least 64 numbers higher than n-hexane (nC6; 30). The mono-branched hexanes 2-methylpentane (2MP; 74.5) and 3-methylpentane (3MP; 75.5) isomers have similar RON, whose values are about 40 numbers higher than nC6 [1]. Thus, the linear paraffins must be separated from their branched counterparts to achieve high RON blends. Therefore, developing adsorbent materials for optimal process efficiency and easy implementation in large-scale processes is critically important.

Objectives

This work aims to evaluate a series of 3D-printed carbon-based monoliths as adsorbents for the pentane and hexane isomer separation through fixed bed adsorption experiments.

Methods

The monolithic materials, exhibiting cylinder structures composed of tetragonal cubic centred unit cells, were prepared following four main steps [2]: i) resin preparation; ii) photopolymerisation (stereolithographic 3D print); iii) porogen extraction, and iv) thermal treatment. For this study, three monoliths with different degrees of CO₂ activation were evaluated: 1) non-activated (M1-pristine), 2) activated at 1133 K for 6 h (M2-CO₂_6h), and 3) activated at 1133 K for 12 h (M3-CO₂_12h). To assess the materials separation performance, experimental fixed bed breakthrough curves with an equimolar septenary mixture of all C5/C6 alkane isomers were measured with a chromatographic system [3] (373-473 K and total alkane pressure up to 50 kPa). Also, a

general mathematical model, considering the kinetics of mass transfer by the linear driving force model [4], was developed to simulate and analyse the transient adsorption behaviour experimentally observed.

Results

Figure 1 shows the breakthrough curves for the temperature of 373 K and total alkane pressure of 50.0 kPa. The 3D-printed monoliths are expressed in the panels: a) M1-pristine, b) M2-CO₂_6h, and c) M3-CO₂_12h. The real time RON of the product mixture leaving the column is also plotted in the figure.

For the monolith M1-pristine (Figure 1a), the results indicate an adsorption hierarchy order as follows: nC6 > nC5 >>> 2MP > 3MP > 23DMB ≈ iC5 > 22DMB. One can equally observe the ability of the material to separate the linear paraffins from its branched isomers via a near molecular sieving mechanism. All the branched paraffins practically reach the saturation at a total molar amount fed of 0.5 mol.kg⁻¹. This size-selective separation of n/iso-paraffins arises due to the micropore morphology and connectivity of the monolith, where two types of micropores can be present in the material, being defined as open and restricted access [5]. Consequently, the entrance to the restricted pores is narrow enough to allow the passage of the linear molecules, apparently under some diffusional limitations, while getting impassable by their branched counterparts, ultimately resulting in the molecular sieving effect. Regarding the RON values, a plateau at 89 is reached when all branched paraffins leave the column separated from the linear alkanes.

On the other hand, both CO₂ activated monoliths (M2-CO₂_6h and M3-CO₂_12h) do not exhibited such a size-exclusion separation. Figure 1b and 1c reveals that all paraffin isomers were adsorbed, with most of them practically showing a simultaneous elution at a total molar amount fed of 2.0 and 3.0 mol.kg⁻¹, respectively. Moreover, there is a change in the elution order of the components, with the pentane isomers leaving the column first being followed by the hexane isomers (iC5 < nC5 < 22DMB < 23DMB < 2MP < 3MP < nC6). Another interesting remark seen in their breakthrough curves is the high overshoots in concentration, a typical characteristic

of adsorption based on thermodynamically equilibrium competition.

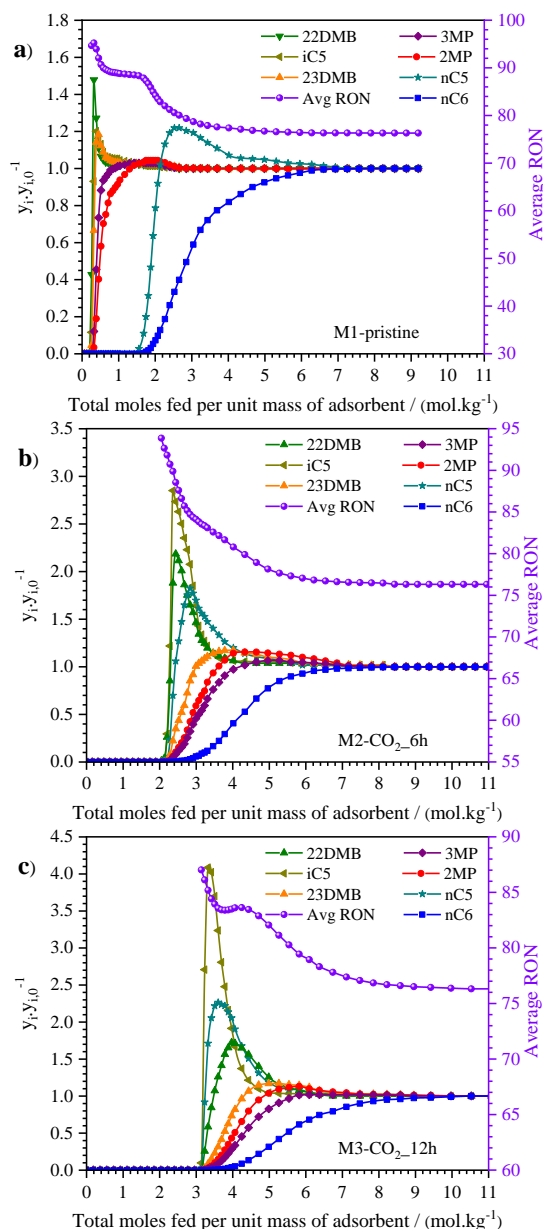


Figure 1. Experimental breakthrough curves for a septenary equimolar mixture of pentane and hexane isomers in 3D-printed monoliths at 373 K and 50.0 kPa: a) M1-pristine, b) M2-CO₂_6h, and c) M3-CO₂_12h.

Comparing the mixture loadings from each material, the adsorption uptake achieved by the monolith M1-pristine (0.85 mol.kg⁻¹) is around three and four times lower than the ones obtained on the monoliths M2-CO₂_6h (2.24 mol.kg⁻¹) and M3-CO₂_12h (3.20 mol.kg⁻¹), respectively. Despite creating

Acknowledgements

The authors acknowledge financial support from: (1) project ref POCI01-0145-FEDER-016517 (PTDC/QEQ-PRS/3599/2014) funded by FEDER funds through COMPETE2020 and FCT; (2) Project PTDC/EQU-EPQ/0467/2020; (3) FCT PhD scholarship to Adriano Henrique (SFRH/BD/148525/2019); (4) Joint financial support from FCT (Portugal) and DAAD (Germany); (5) National funds FCT/MCTES (PIDDAC) to CIMO (UIDB/00690/2020 and UIDP/00690/2020), SusTEC (LA/P/0007/2021), LSRE-LCM (UIDB/50020/2020 and UIDP/50020/2020), and ALiCE (LA/P/0045/2020).

References

- [1] D. Sullivan et al., Part 1 in Handbook of Petroleum Processing, S. A. Treese, P. R. Pujadó, and D. S. Jones, 2 Ed., Springer International Publishing, Switzerland, 2015, 1913.
- [2] H. Stedinger et al., *Advanced Science*, 6 (2019) 1901340.
- [3] A. Henrique et al., *Industrial & Engineering Chemistry Research*, 58 (2019) 378-394.
- [4] S. Sircar et al., *Adsorption*, 6 (2000) 137-147.
- [5] J. Jeromenok et al., *Langmuir*, 29 (2013) 12982-12989.

additional microporosity, in the CO₂ activation process, there are also pore widening and joining of close pores (caused by the removal of the separating walls between them due to mass loss), being these effects more pronounced as temperature and/or activation time increases.

Practically, it can be stated that the monolith M1-pristine represents the most suitable material considering applications for pentane and hexane isomer separation. Thus, the measured data were numerically modulated to gain insights into the governing sorption mechanisms. The Langmuir isotherm was used (continuous lines in the Graphical Abstract), in which the sorption competition of the isomers was divided into two groups: one for the small amounts of branched paraffins in the open pores and the other for the adsorption of linear ones on the pores with restricted access. Then, the obtained parameters were inserted in the mathematical model, and the results are shown in Figure 2. The mass transfer coefficients found to obtain the best fit of the experimental data is around 0.0018 s⁻¹ for the linear paraffins and 0.018 s⁻¹ for their branched counterparts.

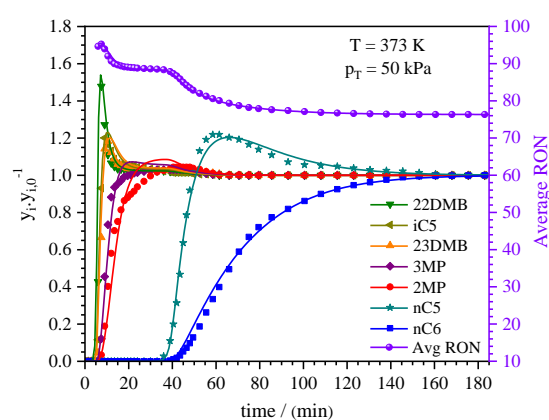


Figure 2. Experimental and numerical breakthrough curves for a septenary equimolar mixture of pentane and hexane isomers in monolith M1-pristine at 373 K and 50 kPa. The continuous lines represent the numerical simulations.

Conclusions

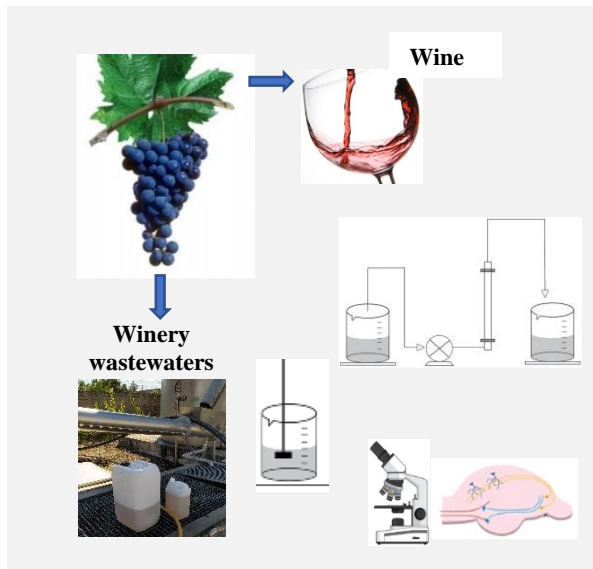
This is the first experimental study on the sorption of pentane and hexane isomers on a series of hierarchically structured 3D-printed porous carbons monoliths. Among the materials, monolith M1-pristine can completely separate linear from iso-paraffins through a near molecular sieving effect, which arises from its micropore morphology and connectivity. To the best of our knowledge, these outcomes have never been reported to such an extent before in any porous solid carbonaceous materials. Concerning the CO₂ activated monoliths, the oxidation and, thus, widening of the pore mouths resulted from the thermal treatment is very likely the main reason for the loss of molecular sieving properties seen in the untreated M1-pristine.

Fenton and ion exchange processes for winery wastewaters treatment

P.M. Reis^{1*}, J.L. Alves^{2,3}, C.M. Matia^{3,4}, M.E. Quinta-Ferreira^{3,5}, L.M. Gando-Ferreira¹, R.M. Quinta-Ferreira¹

¹University of Coimbra, CIEPQPF, Department of Chemical Engineering, Faculty of Sciences and Technology, Pólo II – Rua Sílvio Lima, 3030-790 Coimbra, Portugal; ²Department of Life Sciences, University of Coimbra, P-3004-516 Coimbra, Portugal; ³CNC - Center for Neuroscience and Cell Biology, University of Coimbra, Coimbra, Portugal; ⁴Dep. of Physics, Univ. of Trás-os-montes and Alto Douro, Vila Real, Portugal; ⁵Dep. of Physics, Univ. of Coimbra, Coimbra, Portugal.

*patricia.reis@uc.pt



The large production of wine leads to the generation of sub-products, such as winery wastewater (WW). These waters are seasonal and have significant flow variations, making it challenging to treat them. Real winery wastewater was catheterized at different times, and the Fenton process was applied in order to reduce the chemical oxygen demand (COD) levels. Ion exchange (IE) was applied in this work as a complement to the Fenton process, for the removal of the excess iron present after the Fenton reaction.

For toxicity studies, brain slices incubated with the permeant fluorescent ROS indicator H₂DCFDA were used, in neuronal research, to assess the impact of effluents on neuronal ROS production.

Introduction

Every year large volumes of winery wastewater (WW) are generated throughout the world. These wastewaters have a high organic content which has the potential to cause irreversible environmental impacts [1].

According to the type of wine (red, white, rose, sparkling, etc.), the stage of production (grape harvesting, crushing, fermentation, ageing, filtration, bottling, etc.), the processing operations, and the cleaning procedures, there are significant seasonal variations in the volume and organic load produced throughout the year [2], [3].

Each winery is unique in WW generation and disposal (highly variable volumes, 0,5-14 L per liter of wine, and composition). Thus, due to the significant volume of effluent produced and the seasonal character of this industry, the treatment process has unique challenges and may need to be constantly adapted [4], [5].

The main components of these effluents include resistant high-molecular weight chemicals like polyphenols, tannins, and lignins as well as organic pollutants including organic acids (tartaric, lactic, and acetic), sugars (glucose and fructose), and alcohols (ethanol and glycerol) [2], [6].

Advanced oxidation processes (AOPs) have proved very successful in treating wastewaters including winery wastewaters. These technologies, based on the generation of highly reactive hydroxyl radicals have been increasingly being applied in the treatment of wastewaters. The Fenton method relies on the catalytic breakdown of hydrogen peroxide, which is aided by iron ions, to produce hydroxyl radicals. Indeed, reactive species generated in such systems are capable of oxidizing different organics in wastewater, helping in the depuration of liquid effluents and increasing its biodegradability.

Neurotoxicity assays have recently been offered as an interesting method to evaluate the impact of the effluent treatment on health, being complementary measures to traditional techniques for determining the toxicity of water.

Objectives

The aim of this work was to study the degradation of WW by the Fenton process in order to reduce its organic load until the discharge limit of municipal wastewater treatment plants. Additionally, neurotoxicity studies were carried out assessing optical ROS changes from rat hippocampal slices, perfused with treated or untreated WW. Autofluorescence signals produced by the activity of mitochondrial flavoproteins were taken into account for the determination of the fluorescence signals acquired from the incubated slices.

Methods

The winery wastewater was collected from a wine company located in the center region of Portugal, in different months in order to characterize wastewaters from different stages of the wine process.

Fenton Process was performed in a 1 L glass beaker consisting of 500 ml winery wastewater from red vintage period (end) under constant agitation (200 rpm) in a jar test apparatus. The amount of FeSO₄·7H₂O was added and dissolved under stirring. As the initial pH of the solution was approximately 4, the pH was corrected to 3 with H₂SO₄ solution. The Fenton reaction started immediately after the addition of appropriate amount of hydrogen peroxide (30% w/w). After 1 hour, to stop the reaction the pH was increased to 9-10 with NaOH. To quench the remaining H₂O₂ in the samples, a small amount of a 0.1 g/L solution of catalase (2500 U per mg bovine liver) was used.

The stoichiometric relation (1 g COD = 2.125 g H₂O₂) proposed by Lucas and Peres (2009) served as the basis for

choosing the H_2O_2 concentrations [8]. For this parameter, a concentration of 150% was utilized. The H_2O_2/Fe^{2+} molar ratio of 15 was chosen and the iron amount was 0.04M. After Fenton process, the ion exchange process (IE) was applied to separate iron ions (Fe^{2+}/Fe^{3+}) from the solution.

In neurotoxicity studies, both untreated and treated effluents were used, to evaluate how winery wastewater affected the formation of cellular ROS. According to the method described by Fajardo et al. (2017) [9], reactive oxygen species signals, from brain slices, were detected using the fluorescent ROS indicator H_2DCFDA .

Results

Effluents from the phases of racking, bottling and vintage activities were collected. Table 1 summarizes the main features of five different types of real winery wastewaters generated in a winery located in center region of Portugal. Highly COD values and lower pH are found in racking and red vintage period.

Figure 1 shows the COD and BOD_5 variation at the end of the industrial WWTP. This figure utterly illustrates the seasonal effect of this type of industry, evident in the organic load values. For reasons of confidentiality, values are not presented. The Fenton process applied to the effluent reduced the organic load by 61%, reaching a final COD of $2598 \text{ mg O}_2 \text{ L}^{-1}$.

Ion exchange tests included equilibrium and column experiments.

In addition, the study targeting the effect of this effluent on human health, made by testing its impact on ROS changes in a mammalian neuronal system, allowed a neurotoxicity assessment. ROS generation is better adjusted to normal mitochondrial behavior after an adequate effluent treatment with pollutants removal.

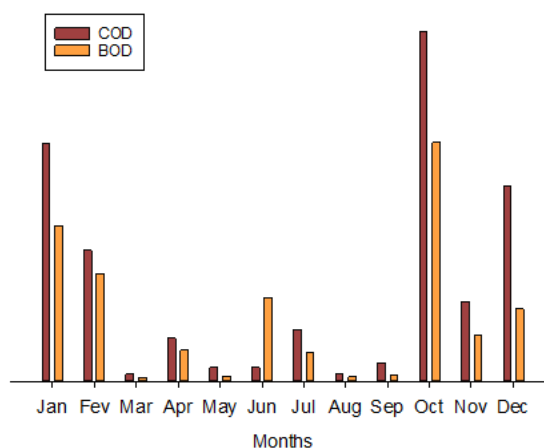


Figure 1. COD and BOD values at the end of the winery wastewater treatment plant in 2022.

Conclusions

Effluents from the wine industry show a wide variability in composition throughout the year, which makes effective treatment very difficult, since treatment characteristics must be constantly updated. The efficiency of Fenton's peroxidation with a real winery wastewater was investigated to evaluate the COD reduction. Under the conditions studied, it was possible to achieve a COD removal efficiency of 61%. In order to remove iron resulting from the Fenton process applied to wine industry effluents, this study analyzed the efficiency of a fixed bed IE process using a strong acid cation exchange resin. The impact on neurotoxicity revealed improved wastewater quality for discharge.

Table 1. Characterization of winery wastewaters used in this work.

	Racking of red winemaking	Pre-season vintage period	White vintage period	Red vintage period (Initial)	Red vintage period (End)
pH	3.7	6.9	5.7	5.1	4.3
COD ($\text{mg O}_2 \text{ L}^{-1}$)	10889.1	1002.2	2136.8	5366.6	6747.1
TN (mg L^{-1})	21.0	3.9	4.3	4.4	2.3
CBO_5 (mg L^{-1})	-	480.4	986.1	2123.6	1739.6
Biodegradability	-	0.48	0.46	0.40	0.26
Tph (mg L^{-1})	70.5	30.6	15.1	57.9	97.2

Acknowledgements

Patrícia Reis acknowledges FCT (Fundação para a Ciência e Tecnologia, Portugal) for the PhD Grant (2021.04553.BD). The neuronal experiments were funded by strategic project UID/NEU/04539/2013.

References

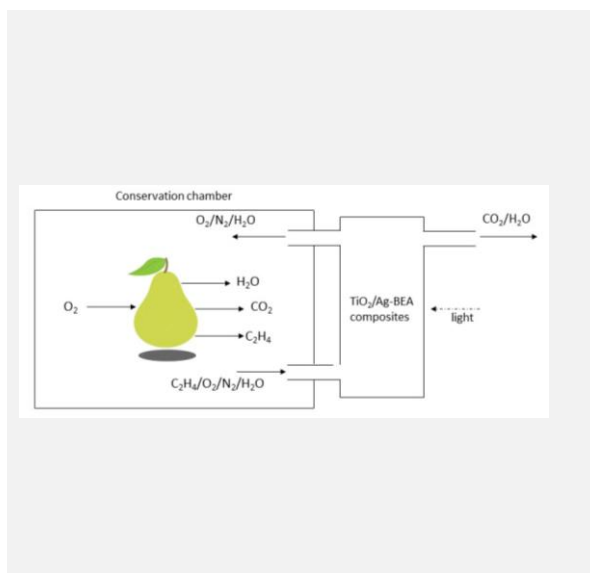
- [1] N. Jorge et al., *Journal of Environmental Management.*, 326 (2022).
- [2] F.C. Moreira et al., *Water Research.*, 75 (2015) 95-108.
- [3] F. Masi et al., *Water Science and Technology*, 71 (2015) 1113-1127.
- [4] L.A. Ioannou et al., *Separation and Purification Technology*, 118 (2013) 659-669.
- [5] L. Marchão et al., *Water Research.*, 203 (2021).
- [6] K.P.M. Mosse et al., *Australian Journal of Grape and Wine Research*, 17 (2011) 111-122.
- [7] J.F. Gomes et al., *Process Safety and Environmental Protection*, 111 (2017) 148-159.
- [8] M.S. Lucas et al., *Journal of Hazardous Materials*, 168 (2009) 1253-1259.
- [9] A.S. Fajardo et al., *Environmental Science and Pollution Research*, 24 (2017) 7521-7533.

TiO₂-silver zeolites composites for ethylene removal and reduction of fruits and vegetable wastes

R. Ferreira^{1,5*}, A. Fernandes¹, J.P. Lourenço^{1,2}, J.M. Silva^{1,3}, I.M. João^{3,4}, S. Morales-Torres⁵, L.M. Pastrana-Martínez⁵, F.J. Maldonado-Hódar⁵, M. F. Ribeiro¹

¹Centro de Química Estrutural, Institute of Molecular Sciences, Instituto Superior Técnico, Universidade de Lisboa, Lisboa, Portugal, ²Faculdade de Ciências e Tecnologia, Universidade do Algarve, Faro, Portugal, ³Instituto Superior de Engenharia de Lisboa, Lisboa, Portugal, ⁴CEG-IST, Universidade de Lisboa, Lisboa, Portugal, ⁵NanoTech – Nanomaterials and Sustainable Chemical Technologies, Department of Inorganic Chemistry, Faculty of Science, University of Granada, Granada, Spain.

*ricardofferreira@tecnico.ulisboa.pt



Every year millions of tons of fruits and vegetables are wasted and climacteric fruits give a huge contribution. One major cause for these losses is the presence of ethylene that is produced during the ripening process. One way to remove the ethylene from the conservation chambers is by a two steps process combining adsorption followed by the photocatalytic combustion of ethylene. The objective of this work is to enable these processes using only one material which is based on composites of TiO₂ and Ag supported in BEA zeolite. The presence of Ag greatly increases the adsorption capacity, while TiO₂ enables the conversion of ethylene through photocatalysis. Several composites with different Ag content (1 to 5 wt.%) were prepared, to reveal how the presence of Ag would affect the photoreaction, as well as the adsorption. The increase of Ag content increases the adsorption but decreases the reaction rate.

Introduction

Fruits and vegetables industry have a significant impact in the Mediterranean countries economy. These industries face a huge problem due the wastes produced every year specially due to post-harvest ripening of climacteric fruits. Ethylene is the compound that initiates the process of ripening (natural hormone), and it is produced during fruits respiration [1]. To decrease those wastes, it is necessary to remove the ethylene from the atmosphere of the conservation chambers. Different technologies have been developed to nullify the ethylene effect such as 1-MCP inhibition, KMnO₄ scrubbing, thermal/photo catalysis and adsorption [2]. A combination of two techniques is also possible, such as adsorption and photocatalysis. Both techniques are cheap and efficient in removing ethylene. Regarding the adsorption, zeolite materials are suitable due to their characteristics (high surface area and porous volume). The possibility to support well dispersed metals is another advantage of zeolites, since metals (such as Ag) can strongly interact with ethylene (π complexation) [3]. The photooxidation of ethylene into CO₂ and H₂O can be performed using a semiconductor with a suitable band gap, such as TiO₂ (the most common photocatalyst used). However, the performance of TiO₂ is limited by its adsorption-desorption behavior of reactants and products [4]. This drawback can be attenuated by supporting TiO₂ on metal-modified zeolite crystals, taking advantage of the large surface area and pore volume and the capability of the metal (such as Ag) to promote the adsorption of ethylene.

Objectives

The objective of this work is to prepare a composite that can simultaneously perform the ethylene removal by adsorption and then convert the ethylene into CO₂. Several composites

with different Ag contents were prepared, to evaluate the influence of Ag presence in the combined adsorption/photocatalysis process.

Methods

Commercial BEA zeolite with Si/Al ratio of 12.5, purchased from Zeolyst, was used as support. The introduction of silver was performed by ion exchange, 24 h in the dark with solution of AgNO₃ [0.01M or 0.03M]. Higher Ag quantities were achieved by performing the ion exchange 3 times. The samples were recovered by filtration then washed with distilled water, dried overnight at 80 °C and then calcined at 500 °C. The introduction of TiO₂ was performed by sol-gel method. The titanium precursor used was titanium isopropoxide that was mixed with the zeolite and a solvent (pure ethanol). TiO₂ concentration introduced in the composite was 30 % (w/w). The adsorption and photocatalytic performance were evaluated in a quartz reactor, in which 25 ml/min of a mixture of C₂H₄/He/O₂/N₂ was passed through 0.45g of sample. Ethylene concentration was 100 ppm. First, breakthrough curves were performed to evaluate the adsorption capacity of the sample, and then a medium-pressure mercury lamp (125 W) was used to perform the ethylene photooxidation. The lamp was cooled using a quartz or glass jacket, depending on the type of experiment (UV-visible radiation or UVA-visible radiation). The lamp was turned on for 3.5 h. The outlet gas stream is then analyzed by an online gas chromatograph with a barrier ionization discharge detector.

Results

The adsorption breakthrough curves (Figure 1) show that the introduction of Ag in the composite greatly increases the adsorption capacity, since the introducing of 1 % of Ag the

ethylene adsorption capacity increases from 2 $\mu\text{mol/g}$ to 290 $\mu\text{mol/g}$. Increasing the Ag content to 3.5 wt.% the adsorption capacity almost doubles to 560 $\mu\text{mol/g}$.

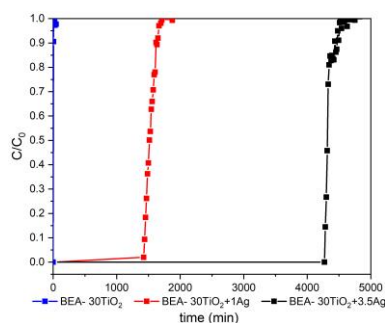


Figure 1. Adsorption breakthrough curves for samples with 0, 1 and 3.5 wt.% Ag.

The increase of Ag is beneficial to ethylene adsorption. However, the zeolite needs to stabilize Ag^+ , since this oxidation state is the one that enables the interaction between Ag and ethylene (π complexation) [3]. H_2 -TPR show that the samples only have one peak at 150 $^\circ\text{C}$, that can correspond to the Ag^+ or Ag_2O reduction [5].

Figure 2 shows that under UV-visible irradiation, all the composites can completely remove the ethylene from the gas stream.

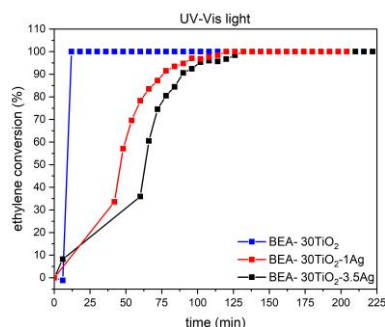


Figure 2. Ethylene conversion for the different composites under UV-visible irradiation.

Figure 3 shows the ethylene conversion under UVA-Visible irradiation. UVA-visible irradiation results show that for 3.5 wt.% of reaction the composites with Ag did not reach 100 % conversion, meaning that these catalysts are less active than the sample without the metal.

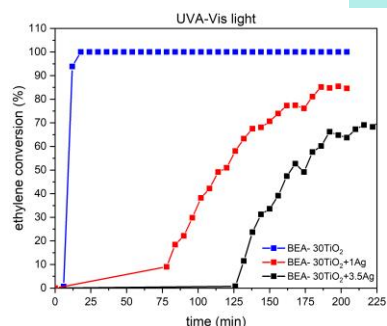


Figure 3. Ethylene conversion of the composites in UVA-visible irradiation.

From XRD patterns (Figure 4) is possible to see that the introduction of silver prior to the introduction of TiO_2 leads to a higher anatase particle size. The higher particle size of the TiO_2 could mean a lower dispersion, decreasing the overall TiO_2 activity present in the composite. From XRD, Ag particles are not shown, by either being too small or by being amorphous. DRS spectra (results not presented) show that the composites absorb light between 200 nm and 375 nm.

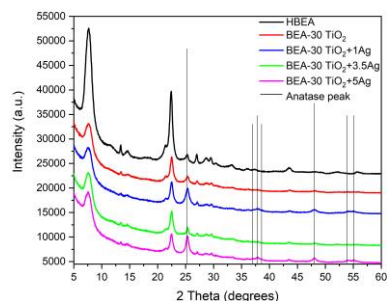


Figure 4. XRD patterns for the Ag- TiO_2 composites.

Conclusions

This work showed that using composites of TiO_2 and Ag supported on a BEA zeolite is possible to adsorb and convert ethylene under different irradiation conditions.

The results showed that the introduction of Ag greatly increases the adsorption of ethylene. However, the Ag present in the zeolite increases the TiO_2 particle size, affecting the photooxidation reaction. The ethylene conversion is higher under UV-visible radiation than under UVA-visible radiation. Overall, the use of a material capable of doing both steps can be beneficial. The use of only one setup capable of adsorption and photocatalysis can reduce the costs of these technologies and decrease the energy costs.

Acknowledgements

Nano4fresh (PRIMA/0015/2019); CQE – FCT (UIDB/00100/2020, UIDP/00100/2020 and 2022.12593.BD); IMS – LA/P/0056/2020. Spanish Project (ref. PCI2020-112045) from MICIN/AEI/10.13039/501100011033 and EU/PRTR. S.M.-T. (RYC-2019-026634-I) and L.M.P.-M. (RYC-2016-19347) are grateful to MICIN/AEI/10.13039/501100011033 and FSE “El FSE invierte en tu futuro” for their Ramon y Cajal research contracts.

References

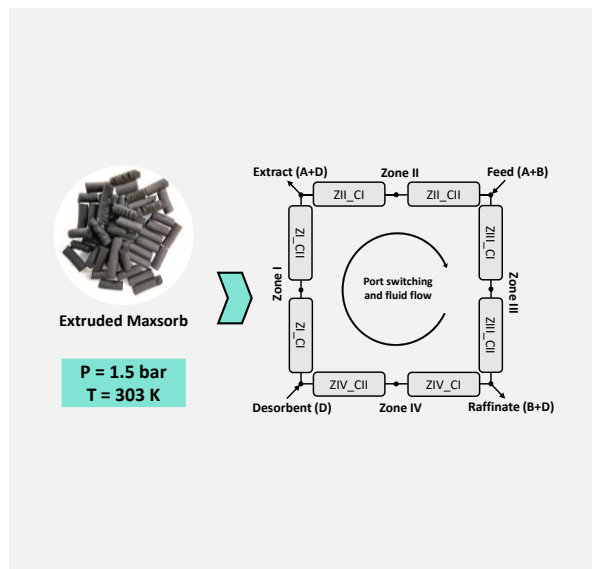
- [1] K. Tripathi et al., Journal of Environmental and Applied Bioresearch, 4 (2015) 27-34.
- [2] N. Pathak et al., Ethylene Removal From Fresh Produce Storage: Current Methods and Emerging Technologies. Elsevier.
- [3] D. Saha et al., Science, 24 (2021) 103042.
- [4] A. Regadera-Macías et al., Catalysis Today, 413-415 (2023) 113932.
- [5] R. Bartolomeu et al., Microporous and Mesoporous Materials, 169 (2013) 137-147.

Methane upgrading on pelletized maxsorb by gas-phase simulated moving bed

R.O.M. Dias*, M.J. Regufe, A.A. Pereira, A.F.P. Ferreira, A.E. Rodrigues, A.M. Ribeiro

LSRE-LCM – Laboratory of Separation and Reaction Engineering – Laboratory of Catalysis and Materials, Faculty of Engineering, University of Porto, Rua Dr. Roberto Frias, 4200-465, Porto, Portugal; ALiCe – Associate Laboratory in Chemical Engineering, Faculty of Engineering, University of Porto, Rua Dr. Roberto Frias, 4200-465, Porto, Portugal.

*rmdias@fe.up.pt



For the study of the separation of methane and nitrogen mixtures by gas-phase simulated moving bed (SMB), maxsorb activated carbon was pelletized by extrusion with 10% binder. Both argon and carbon dioxide were used as potential desorbent gases. The adsorbent performance was evaluated by measuring the adsorption equilibrium data and the dynamic adsorption behavior through fixed-bed experiments. Pure component N_2 , CH_4 , Ar, and CO_2 isotherms were measured at three different temperatures, up to 2.5 bar, using a volumetric method. The results show that CO_2 exhibits the highest affinity to the solid phase followed by CH_4 , N_2 , and Ar. Single, binary, and ternary fixed-bed experiments were performed, allowing the validation of the proposed mathematical model. Two SMB cycles were designed to separate an equimolar CH_4/N_2 mixture using each desorbent gas. The respective separation regions were drawn. Both cycles were able to produce a high purity methane stream with high recovery.

Introduction

With the depletion of the conventional natural gas wells, unconventional methane-rich sources have been explored over the years. These sources are often contaminated with several impurities, among which nitrogen is the most difficult to remove due to the similar properties to those of methane. To meet pipeline specifications, nitrogen is removed when its content is above 3%, to ensure that the calorific value of the stream is not affected by the presence of this inert gas [1]. The main technology used for this purpose is cryogenic distillation, which has very high energy costs associated and is unsuitable for medium and small-scale purification of methane streams [2]. When compared to this technology, adsorption-based processes are very appealing thanks to their easy scalability and lower energy requirements. However, the performance of the solid materials for CH_4/N_2 separation becomes an issue due to their low selectivity [3]. The use of a gas-phase simulated moving bed (SMB) process overcomes this challenge since it can separate mixtures with selectivities close to unity by introducing a desorbent species to displace the adsorbed phase, transforming a difficult separation into two separations that can be easily achieved.

The design and development of a gas-SMB process for separating methane and nitrogen mixtures is the focus of this work, using a pelletized maxsorb with 10% binder as the adsorbent material and two potential desorbent gases – argon and carbon dioxide. The performance of the material was evaluated by measuring the adsorption equilibrium data for the four adsorbates and the dynamic behavior of single and multicomponent adsorption through fixed-bed experiments.

Results and discussion

The pure component isotherms of N_2 , CH_4 , Ar, and CO_2 , presented in Figure 1, were measured at 303, 323, and 343 K in a pressure range of 0 - 2.5 bar using a volumetric apparatus.

The data was successfully regressed with the single-site Langmuir model. The model parameters are presented in Table 1. The results show that CO_2 has the highest affinity to the stationary phase and Ar the lowest, over the entire range of temperature and pressure studied.

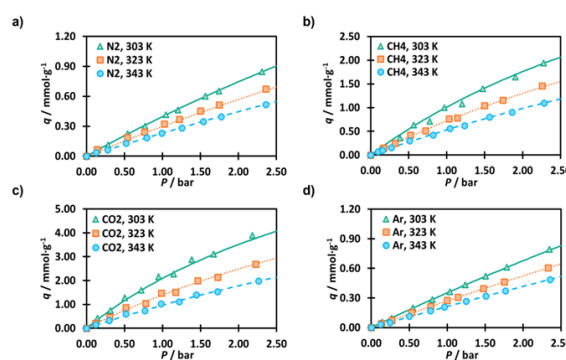


Figure 1. Amount adsorbed of a) N_2 , b) CH_4 , c) CO_2 and d) Ar on Maxsorb pellets at 303 (▲), 323 (■) and 343 K (●). Lines represent the Langmuir fitting.

Table 1. Fitting parameters of the Langmuir model for N_2 , CH_4 , CO_2 and Argon adsorption equilibrium on the maxsorb pellets.

Adsorbate	$q_m / \text{mol} \cdot \text{kg}^{-1}$	$b_0 \times 10^4 / \text{bar}^{-1}$	$-\Delta H / \text{J} \cdot \text{mol}^{-1}$
N_2	6.09	5.79	12049
CH_4	6.80	3.93	15330
CO_2	12.47	0.89	19481
Ar	8.98	5.55	10805

Single, binary, and ternary breakthrough experiments were carried out at 303 K and 1.5 bar, with a total flowrate of 0.2 SLPM. A mathematical model that encompasses mass, energy, and momentum balances was implemented in the gPROMS® software and utilized to predict the observed adsorption dynamics [4]. For example, the breakthrough experiment results with a bed initially saturated with CO_2 and

a feed composition of 25% nitrogen, 25% methane, and 50% carbon dioxide are presented in Figure 2. Analysis of the ternary fixed bed experiment shows that the desorbent is easily displaced by the mixture and is equally able to displace the adsorbed phase, which is an essential step for SMB operation. The simulation results are in good agreement with the experimental data. Similar results were obtained when argon was utilized instead of carbon dioxide, indicating that both gases can be used as desorbents for the SMB process.

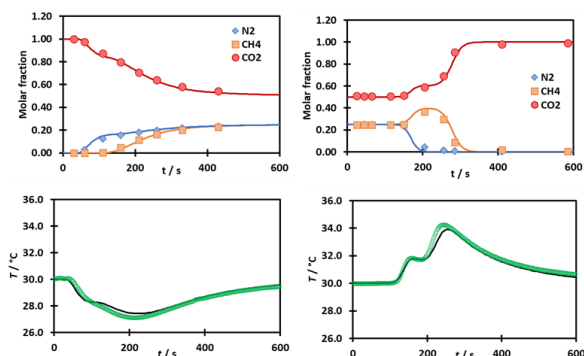


Figure 2. Adsorption of a nitrogen/methane/carbon dioxide mixture (25%/25%/50%) over a Maxsorb fixed bed initially saturated with carbon dioxide. Lines represent the simulation results.

Finally, two simulated moving bed (SMB) cycles were employed to separate an equimolar CH_4/N_2 mixture using each of the desorbent gases to evaluate the impact of the desorbent strength in the process. The experiments were carried out in an open loop, with no desorbent recycle. A 2-2-2-2 four-zone system configuration was considered, with a switching time of 50 s. The SMB unit was operated at 303 K, with the backpressure, located at the end of zone IV, set at 1.5 bar. A feed composition of 50% CH_4 and 50% N_2 was used, with a feed stream of 0.130 SLPM for the argon experiment and 0.070 SLPM for the CO_2 experiment. The internal profiles for each case are presented in Figure 3. In zone II, the more adsorbed species, methane, is retained onto the material, enriching the extract stream, while the less adsorbed species, nitrogen, is carried by the eluent. In section III, the nitrogen content increases as it moves with the fluid phase to the raffinate port. The flow rate in section I is high enough to guarantee that the adsorbent is cleaned, ensuring that section IV is not contaminated after the switch. In section IV, the nitrogen content decreases, with pure desorbent being obtained at the outlet, which can be recycled back into section I when

Acknowledgements

This work was financially supported by LA/P/0045/2020 (ALiCE), UIDB/50020/2020 and UIDP/50020/2020 (LSRE-LCM), funded by national funds through FCT/MCTES (PIDDAC). Rafael Dias acknowledges his PhD scholarship 2020.05095.BD funded by FEDER funds through NORTE 2020 and by national funds through FCT/MCTES.

References

- [1] J.C. Kuo et al., *Journal of Natural Gas Science and Engineering*, 7 (2012) 52-59.
- [2] T.E. Rufford et al., *Journal of Petroleum Science and Engineering*, 94-95 (2012) 123-154.
- [3] D.A. Kennedy et al., *Journal of Chemical & Engineering Data*, 61 (2016) 3163-3176.
- [4] R. Dias et al., *Industrial & Engineering Chemistry Research*, 61 (2022) 12739-12753.

operating in closed loop. The desorbent-free purity for both cycles was very high (100% and 99.3% for the Argon and CO_2 experiment, respectively). A high recovery was also achieved in both cases (> 97%). When argon is used as the desorbent gas, the extract product stream is obtained with a productivity of $14.3 \text{ kg} \cdot \text{m}^{-3}_{\text{ads}} \cdot \text{h}^{-1}$.

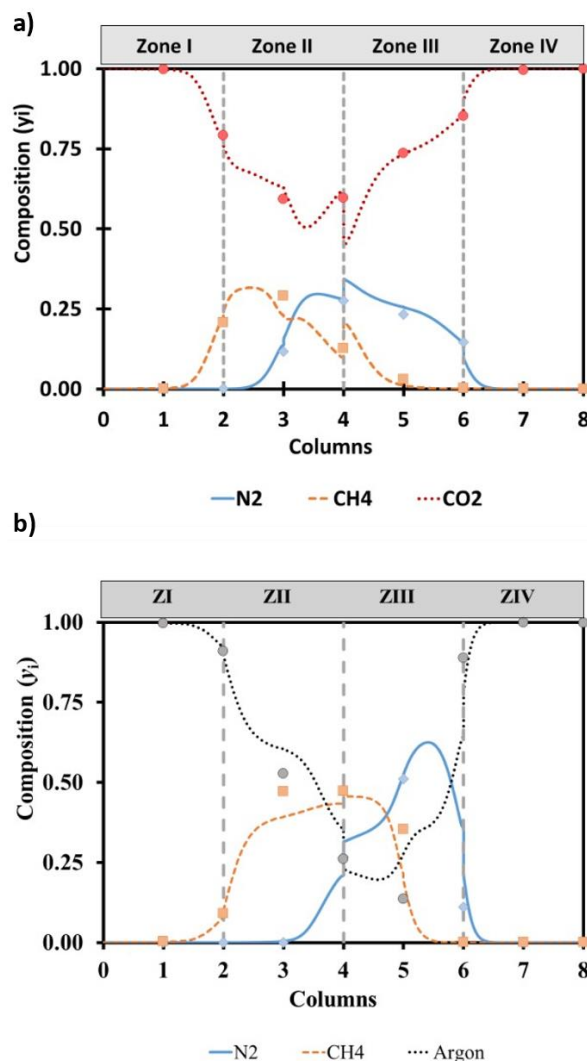


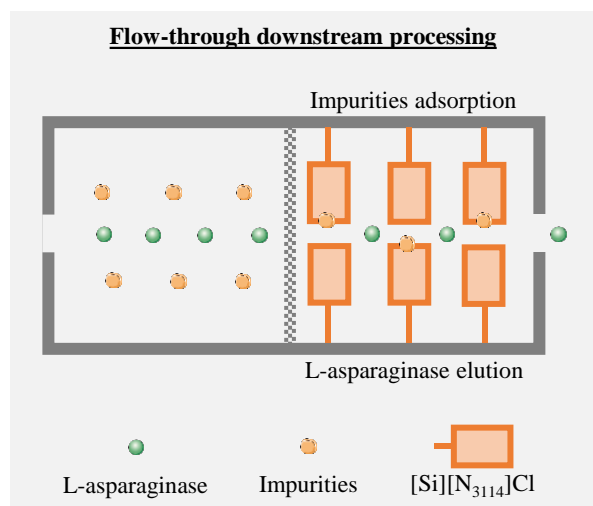
Figure 3. Internal profile in function of the column number for: a) carbon dioxide experiment and b) argon experiment, collected at half switching time. Points represent experimental data and lines represent the simulation results.

Silica-based supported ionic liquid-like phase materials for the flow-through downstream processing of L-asparaginase

J.C.F. Nunes^{1*}, M.R. Almeida¹, G.B. de Paiva², D.B. Pedrolli², V.C. Santos-Ebinuma², M.C. Neves¹, M.G. Freire¹, A.P.M. Tavares¹

¹CICECO - Aveiro Institute of Materials, Department of Chemistry, University of Aveiro, 3810-193 Aveiro, Portugal; ²School of Pharmaceutical Sciences, Department of Bioprocess Engineering and Biotechnology, São Paulo State University (UNESP), Araraquara, São Paulo 14800-903, Brazil.

*jcfn@ua.pt



L-asparaginase (ASNase) is an amidohydrolase enzyme widely distributed in nature, but microorganisms are their preferential source. Nevertheless, high enzyme purity is required by the pharmaceutical industry. Silica-based supported ionic liquid-like phase (SSILLP) materials with different alkyl chain lengths at the cation source and Cl⁻ as the anion source were investigated to purify ASNase. Silica functionalized with dimethylbutylpropylammonium chloride ([Si][N₃₁₁₄]Cl) was selected as the most promising SSILLP material due to the highest purification factor (1.65) attained. The purification operating conditions were optimized through Response Surface Methodology (RSM). Semi-continuous purification of ASNase was carried out under optimized conditions (pH 3 and solid/liquid ratio of 15), attaining a purification factor of 5.15. Thus, SSILLP materials can be applied as simple semi-continuous ASNase purification supports with potential in flow-through downstream processing.

Introduction

L-asparaginase (ASNase) is an enzyme widely distributed in nature, being found in microorganisms, plants, and tissues of various animals [1,2]. Nevertheless, microorganisms are the preferential ASNase source due to their ability to easily grow on inexpensive substrates [1,3]. Bacterial ASNase type II is a potential drug for the treatment of numerous diseases. However, high enzyme purity is required by the pharmaceutical industry, in which downstream processing accounts for up to 80% of total production costs [1]. ASNase downstream processes include enzyme purification through non-chromatographic and chromatographic processes. Ionic liquids (ILs) used in the separation field due to their designer capacity, can improve separation performance and selectivity towards a target compound [4]. This property is displayed in silica-based supported ionic liquid-like phase (SSILLP) materials, since ILs are the functional groups of silica (support to which they are covalently attached), enabling distinct interactions to be established between target compounds and matrix. Regardless of the success of SSILLP materials in biomolecules processing, they were not previously used for enzyme purification. In this work, SSILLP materials with different alkyl chain lengths at the cation source and Cl⁻ as the anion source were applied as alternative supports for the semi-continuous ASNase purification.

Methods

ASNase production was performed using the protocol reported by Bento et al. [5]. SSILLP materials with quaternary ammonium cations and chloride as the counterion were synthesized using an adaptation of the protocol reported by Qiu et al. [6]. The characterization of SSILLP materials was addressed through elemental analysis, zeta potential analysis, Attenuated total reflectance-Fourier-transform infrared (ATR-FTIR) spectroscopy, Brunauer-Emmett-Teller (BET) analysis,

Barrett-Joyner-Halenda (BJH) analysis, and scanning electron microscopy (SEM). The ASNase purification was performed through addition of 1 mL of enzymatic extract to 10 mg of SSILLP materials as detailed by Nunes et al. [7]. The ASNase activity in the supernatants was measured according to the method detailed by Magri et al. [8], and the protein content was determined through spectroscopy at 280 nm. The ASNase purification conditions, namely pH and solid/liquid ratio (S/L ratio), were optimized by Response Surface Methodology (RSM). Semi-continuous purification of ASNase was performed under previously optimized conditions, and protein profiles were analyzed by Sodium dodecyl sulfate-polyacrylamide gel electrophoresis (SDS-PAGE).

Results

The mass of IL per mass of material, point of zero charge (PZC), specific surface area, and BJH adsorption cumulative pore surface area of activated silica and all SSILLP materials are displayed in Table 1. The mass of IL per mass of material of SSILLP materials range from 34.07 to 139.88 mg g⁻¹ and SSILLP materials display higher PZC values (6.5-10.8) than activated silica (3.0) due to the IL cation bound to the silica surface, confirming the successful SSILLP materials' functionalization. The specific surface area (171.7-375.1 m² g⁻¹) and pore surface area (246.2-481.0 m² g⁻¹) of all SSILLP materials were lower than obtained for activated silica (494.2 m² g⁻¹, 553.0 m² g⁻¹), suggesting the IL covalent bound to the silica surface and on the pore walls, further proving the successful SSILLP materials' functionalization.

The highest purification factor (1.65) was obtained using the least hydrophobic SSILLP material, i.e., silica functionalized with dimethylbutylpropylammonium chloride ([Si][N₃₁₁₄]Cl). Hence, [Si][N₃₁₁₄]Cl was selected since it displays a higher affinity to the impurities present in the enzymatic extract over ASNase. The optimal experimental conditions predicted

through RSM to increase the purification factor were a pH value of 3 and S/L ratio of 15. Semi-continuous purification of ASNase was performed under optimized conditions and the purification factor of the purified cell extract fractions ranged from 4.61 to 5.15.

Conclusions

Our simple strategy to enhance the purification of ASNase was efficient since a purification factor of 5.15 was reached in one step with a SSILLP operating in the flow-through like mode.

Table 1. Material, mass of ionic liquid (IL) per mass of material (i.e., silica) (mg g^{-1}), point of zero charge (PZC), specific surface area (S_{BET}), and Barrett-Joyner-Halenda (BJH) adsorption cumulative pore surface area ($\text{m}^2 \text{g}^{-1}$) of activated silica and all SSILLP materials.

Material	IL mass per material mass (mg g^{-1})	PZC	S_{BET} ($\text{m}^2 \text{g}^{-1}$)	Pore surface area ($\text{m}^2 \text{g}^{-1}$)
Silica	—	3.0	494.2	553.0
[Si][N ₃₁₁₄][Cl]	134.74	10.1	212.3 ¹	292.9 ¹
[Si][N ₃₁₁₆][Cl]	139.88	10.8	215.9 ²	304.7 ²
[Si][N ₃₁₁₈][Cl]	126.83	10.6	171.7	246.2
[Si][N ₃₂₂₂][Cl]	49.57	9.3	181.3	259.4
[Si][N ₃₄₄₄][Cl]	34.16	7.1	310.1	418.7
[Si][N ₃₆₆₆][Cl]	34.07	6.8	308.2	410.3
[Si][N ₃₈₈₈][Cl]	41.41	6.5	327.0	442.4
			375.1	481.0

* Before¹ and after² contact with the enzymatic extract.

Acknowledgements

Ana P.M. Tavares and Márcia C. Neves acknowledge FCT for the research contract CEECIND/2020/01867 and CEECIND/00383/2017, respectively. Gabriela B. de Paiva acknowledges the São Paulo Research Foundation (FAPESP) for the PhD fellowship (grant 2021/01284-9). Valéria C. Santos-Ebinuma and Danielle B. Pedrolli thank the National Council of Scientific and Technology Development (CNPq) for the fellowship grant n°312463/2021-9 and 310023/2020-3, respectively. João C. F. Nunes acknowledges SPQ and FCT for the PhD fellowship (SFRH/BD/150671/2020).

This work was developed within the scope of the project CICECO-Aveiro Institute of Materials, UIDB/50011/2020, UIDP/50011/2020 & LA/P/0006/2020, financed by national funds through the FCT/MCTES (PIDDAC). This work was supported by the project POCI-01-0145-FEDER-031268-funded by FEDER through COMPETE2020, and by national funds (OE) through FCT/MCTES, and by FAPESP (2018/06908-8). Valéria C. Santos-Ebinuma acknowledges FAPESP for financial support through the project 2019/15493-9.

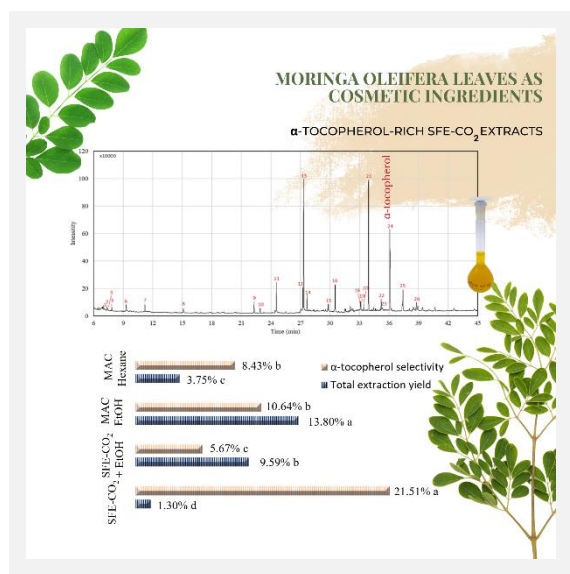
References

- [1] A.M. Lopes et al., *Critical Reviews in Biotechnology*, 37 (2017) 82-99.
- [2] T. Batool et al., *Applied Biochemistry and Biotechnology*, 178 (2016) 900-923.
- [3] N. Verma et al., *Critical Reviews in Biotechnology*, 27 (2007) 45-62.
- [4] E.V. Capela et al., *Separation and Purification Technology*, 305 (2023) 122464.
- [5] H.B.S. Bento et al., *Bioprocess and Biosystems Engineering*, 45 (2022) 1635-1644.
- [6] H. Qiu et al., *Journal of Chromatography A*, 1103 (2006) 265-270.
- [7] J.C.F. Nunes et al., *Separation and Purification Technology*, 315 (2023) 123718.
- [8] A. Magri et al., *Analytical and Bioanalytical Chemistry*, 410 (2018) 6985-6990.

Improving α -tocopherol extraction from *Moringa oleifera* L. leaves using SFE-CO₂J.C. Kessler^{1,2,3,4*}, Y.A. Manrique^{1,2}, I.M. Martins^{1,2}, A.E. Rodrigues^{1,2}, M.F. Barreiro^{3,4}, M.M. Dias^{1,2}

¹LSRE-LCM - Laboratory of Separation and Reaction Engineering–Laboratory of Catalysis and Materials, Faculdade de Engenharia, Universidade do Porto, Rua Dr. Roberto Frias, 4200-465 Porto, Portugal; ²ALiCE - Associate Laboratory in Chemical Engineering, Faculdade de Engenharia, Universidade do Porto, Rua Dr. Roberto Frias, 4200-465 Porto, Portugal; ³Centro de Investigação de Montanha (CIMO), Instituto Politécnico de Bragança, Campus de Santa Apolónia, 5300-253 Bragança, Portugal; ⁴Laboratório para a Sustentabilidade e Tecnologia em Regiões de Montanha, Instituto Politécnico de Bragança, Campus de Santa Apolónia, 5300-253 Bragança, Portugal.

*juliakessler@fe.up.pt



Natural-based products have been used as substitutes for synthetic ingredients in cosmetic formulations. *Moringa oleifera* L. leaves represent an alternative source of an antioxidant agent, the α -tocopherol. The extraction yield and selectivity of α -tocopherol using supercritical fluid carbon dioxide extraction (SFE-CO₂), with and without ethanol as co-solvent, were optimized and compared with results obtained using the conventional maceration methodology (MAC), performed with ethanol (MAC-EtOH) or *n*-hexane (MAC-Hex). The total extraction yield for SFE-CO₂+EtOH was 7 times higher than SFE-CO₂ alone, 9.59% and 1.30%, respectively. The highest total extraction yield (13.80%) and α -tocopherol mass composition (0.47 ± 0.01 mg_{compound}·g_{plant}⁻¹) was obtained for MAC-EtOH, statistically higher than the ones obtained for the other extraction conditions. However, the use of SFE-CO₂ alone resulted to be more selective for α -tocopherol (21.51% relative composition) and, therefore, was selected for future studies.

Introduction

The commercial competitiveness of cosmetic products has attracted industrial's interest in natural bioactive sources. Among the main appeals is the replacement of synthetic ingredients for natural antioxidants, anti-aging, anti-inflammatory and antimicrobial agents [1]. α -tocopherol is recognised as an antioxidant ingredient that reduces the skin's oxidative stress (e.g., photoaging) [2]. This bioactive has been identified in *Moringa oleifera* L. (Mo) leaves [3-5]. Often referred to as the "Tree of Life", Mo presents a rich phytochemical composition and bioactive potential widely studied by the scientific community and has been increasingly used as an ingredient in cosmetic formulations [2].

Recovering α -tocopherol from natural extracts must be performed at operational conditions favouring high efficiency, selectivity, and preservation of the compound's naturalness. Supercritical fluid carbon dioxide extraction (SFE-CO₂) is an environmentally friendly technology that complies with these requirements. The solvent is non-toxic, non-flammable, odourless, and does not remain in the final product [5]. Moreover, the selectivity for target compounds is adjustable by tuning the pressure and temperature, and the total extraction yield can be increased by adding a co-solvent, such as ethanol (EtOH). The SFE-CO₂ products are often compared to extracts obtained by conventional methodologies, such as maceration (MAC).

In a previous work [3], optimisation of SFE-CO₂ extraction of Mo leaves in terms of total extraction yield and phytochemical composition was reported. This work aims to compare the optimised total extraction yield, selectivity or relative composition, and mass composition for α -tocopherol with other methodologies, namely SFE-CO₂ using ethanol as a co-solvent (SFE-CO₂+EtOH) and a conventional methodology, maceration,

using either ethanol (MAC-EtOH) or *n*-hexane (MAC-Hex) as solvents.

Methods

Mo leaves were provided by Moringa del Sur (Malaga, Spain, moringadelsur.com), and sample preparation followed the previously described methodology [3].

SFE-CO₂ extractions were performed under optimised conditions, 195 bar and 55 °C, in triplicate [3]. The co-solvent was added at a continuous flow rate of 0.8 mL·min⁻¹ to the supercritical CO₂ stream at 3.2 mL·min⁻¹ to improve the performance of extracting the target compound from 10 g of sample over 120 min. The entire extracted material was recovered, and the results were compared to those obtained by Kessler et al. [3] using SFE-CO₂ alone. For MAC extraction, the sample was placed in a 250 mL stock flask and filled with EtOH or *n*-hexane (Hex), in a proportion of 1:5 (m/v). The extractions were performed in duplicate for 240 min, at room temperature, under magnetic stirring at 240 rpm.

The volatile compounds were identified and quantified using a gas chromatography-mass spectrometer (GC-MS) (TQ8040 NX Triple Quadrupole, Shimadzu, Japan), following the previously defined analysis procedure [3].

Results

Table 1 shows the results for the total extraction yield, α -tocopherol relative composition (selectivity) and mass composition for the four tested extraction conditions using SFE-CO₂ or maceration.

SFE-CO₂+EtOH extraction has performed significantly better compared to SFE-CO₂ alone ($\alpha = 0.05$), reaching an efficiency of 7 times higher, with total yields of $9.59 \pm 0.17\%$ and $1.30 \pm 0.04\%$ with or without co-solvent, respectively. Previous

works reported similar outcomes, $2.9 \pm 0.7\%$ and $1.6 \pm 0.4\%$ for extraction performed using or not using co-solvent, respectively [4]. EtOH added to the supercritical CO₂ has the tendency to increase the polar affinity of the compounds obtained from the raw material, usually increasing the total extraction yield and changing the selectivity of a target compound [1].

These effects result from the polar and nonpolar characteristics of the solvents, also reflected in the conventional extraction, MAC. Mo leaf extracts presented a significantly higher affinity to ethanol ($\alpha = 0.05$), with $13.80 \pm 0.22\%$ total extraction yield compared to $3.75 \pm 0.09\%$ obtained from MAC-Hex extraction. However, the nonpolar solvent was more efficient in comparison to SFE-CO₂ alone and statistically lower than the yield achieved by SFE-CO₂+EtOH.

The phytochemical profile of Mo leaf extracts revealed the presence of eight different chemical groups (data not shown). The most significant compounds and their activities for cosmetic formulations were reported in a recent paper on the screening of Mo plant parts [3].

SFE-CO₂ alone, SFE-CO₂+EtOH, and MAC extractions have been compared regarding α -tocopherol selectivity and mass composition (Table 1). Significantly higher selectivity was obtained using SFE-CO₂ alone ($21.51 \pm 0.79\%$), followed by MAC-EtOH ($10.64 \pm 0.22\%$), MAC-hex ($8.43 \pm 0.52\%$), and finally SFE-CO₂+EtOH ($5.67 \pm 0.09\%$). On the other hand, the mass composition in α -tocopherol has revealed a different trend. MAC-EtOH reached $0.47 \pm 0.01 \text{ mg}_{\text{compound}} \cdot \text{g}_{\text{plant}}^{-1}$, significantly higher than all the other extraction methodologies. The results

for MAC-Hex and SFE-CO₂+EtOH, $0.30 \pm 0.02 \text{ mg}_{\text{compound}} \cdot \text{g}_{\text{plant}}^{-1}$ and $0.254 \pm 0.003 \text{ mg}_{\text{compound}} \cdot \text{g}_{\text{plant}}^{-1}$, respectively, are also significantly higher than that obtained for SFE-CO₂ alone ($0.20 \pm 0.01 \text{ mg}_{\text{compound}} \cdot \text{g}_{\text{plant}}^{-1}$).

These results exemplify the balance between selectivity and total extraction yield. Although with lower extraction yield, SFE-CO₂ alone has proved to be the most efficient methodology to obtain α -tocopherol enriched extracts. On the other hand, the conventional methodology using a polar solvent (MAC-EtOH) resulted in the richest product in terms of mass but with almost 11% lesser selectivity compared to SFE-CO₂ alone. These differences can be explained by the extraction of different compounds with higher affinity to the EtOH [4], as well as the increased surface contact time between the sample structure and the solvent, improving mass diffusion.

In addition, the main factor influencing the compounds' solubility in the CO₂ solvent may be related to CO₂ density. At the extraction conditions used in this study, 195 bar and 55 °C, the supercritical CO₂ presents $747 \text{ kg} \cdot \text{m}^{-3}$ [6], easily increased by adding EtOH. The co-solvent enhances the solvation power of the mixture due to its higher density ($789 \text{ kg} \cdot \text{m}^{-3}$), and, therefore, improves the solubility of more compounds reducing the extract's selectivity.

Conclusions

The high selectivity of α -tocopherol obtained from Mo leaves by SFE-CO₂ alone leads to choosing this method for future studies aiming at replacing synthetic ingredients in cosmetic formulations.

Table 1. Total extraction yield and α -tocopherol selectivity and mass composition for the extracts obtained from Mo leaves by SFE-CO₂ and maceration.

Mo leaves extracts	SFE-CO ₂ [3]	SFE-CO ₂ , EtOH	MAC-EtOH	MAC-Hex
Total extraction yield (%)	1.30 ± 0.04^d	9.59 ± 0.17^b	13.80 ± 0.22^a	3.75 ± 0.09^c
α -tocopherol selectivity/relative composition (%)	21.51 ± 0.79^a	5.67 ± 0.09^c	10.64 ± 0.22^b	8.43 ± 0.52^b
α -tocopherol mass composition ($\text{mg}_{\text{compound}} \cdot \text{g}_{\text{plant}}^{-1}$)	0.20 ± 0.01^c	0.254 ± 0.003^b	0.47 ± 0.01^a	0.30 ± 0.02^b

α -tocopherol ($y = 1.04 \times 10^{10}x - 7.87 \times 10^6$; $R^2 = 0.9996$; LOD = $6.18 \times 10^{-4} \text{ g} \cdot \text{L}^{-1}$; LOQ = $1.87 \times 10^{-3} \text{ g} \cdot \text{L}^{-1}$). Averages with different letters in the same line indicate significant differences with $\alpha = 0.05$.

Acknowledgements

This work was financially supported by LA/P/0045/2020 (ALiCE), UIDB/50020/2020 and UIDP/50020/2020 (LSRE-LCM), UIDB/00690/2020 and UIDP/00690/2020 (CIMO) and LA/P/0007/2021 (SusTEC), funded by national funds through the Fundação para a Ciência e Tecnologia FCT/MCTES (PIDDAC). Júlia Cristiê Kessler acknowledges her PhD scholarship (ref. 2020.06656.BD) from FCT. Authors thank Moringa del Sur (Malaga, Spain, moringadelsur.com) for providing samples of Mo leaves.

References

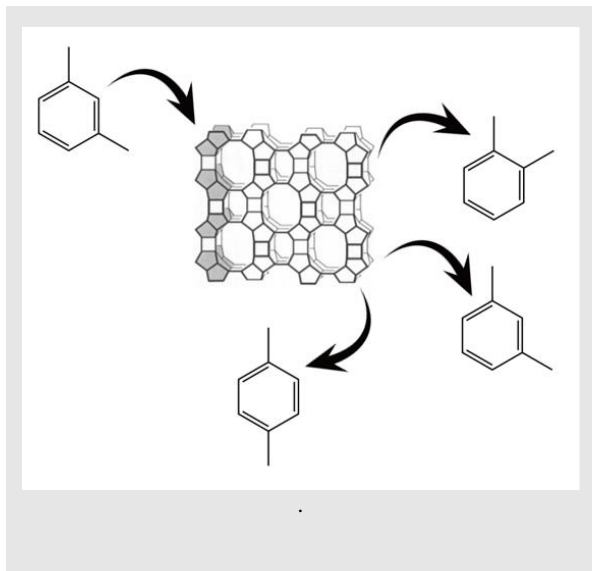
- [1] M. Zorić et al., Sustainable Chemistry and Pharmacy, 27 (2022) 100688.
- [2] S. Athikomkulchai et al., Cosmetics, 8 (2021) 1-18.
- [3] J.C. Kessler et al., Separations, 10 (2023) 210.
- [4] M. da Silva et al., Journal of Food Process Engineering, 45 (2022) e13979.
- [5] S. Zhao and D. Zhang, Separation and Purification Technology, 118 (2013) 497-502.
- [6] NIST, Isothermal Properties for Carbon dioxide, (2022).

Xylene isomerization in the liquid phase by MOR type zeolites

B.A.C. Castro*, A.F.P. Ferreira

LSRE-LCM - Laboratory of Separation and Reaction Engineering – Laboratory of Catalysis and Materials, Faculty of Engineering, University of Porto, Rua Dr. Roberto Frias, 4200-465 Porto, Portugal; ALiCE - Associate Laboratory in Chemical Engineering, Faculty of Engineering, University of Porto, Rua Dr. Roberto Frias, 4200-465 Porto, Portugal.

*up201505452@edu.fe.up.pt



The separation of xylene isomers is an essential step in producing isolated isomers. Nowadays, *p*-xylene can be separated from the other isomers by crystallization and/or adsorption with high purity and recovery rates. However, these technologies only allow the purification of one isomer. Therefore, the other two must be treated in a separate unit to produce additional *p*-xylene through an isomerization reaction. This work evaluated the performance of three zeolites (MOR20, MOR40 and BEA35) in the isomerization of *m*-xylene at 220 °C. MOR40 could convert more *m*-xylene, so it was the chosen catalyst. Afterwards, the kinetics of this reaction was studied for this zeolite at 200, 220, and 240 °C.

Introduction

Xylenes are a group of aromatic compounds usually obtained from crude petroleum. The raw material for producing xylenes is a low-octane naphtha cut converted into high-octane aromatics through catalytic reforming, which results in mixed xylenes, benzene, and toluene (BTX aromatics). On the other hand, toluene disproportionation and transalkylation are also used to produce xylenes. The BTX constituents can be separated by distillation [1].

The limited petroleum sources and the emission of greenhouse gases associated with refining processes drive the growth of alternative solutions to produce these aromatics [2]. The use of renewable sources, namely biomass, as raw material has been studied in the past few years with encouraging results [3].

However, regardless of the raw material used, producing xylenes generally results in an equilibrium mixture of its isomers. The isolation of these three components is a complex process, and its complexity is a direct consequence of their similar physicochemical properties. In fact, the separation of xylene isomers is considered one of the seven world-changing separations [4]. Crystallization and adsorption are the most used processes to obtain *p*-xylene with high purity [5].

Xylene isomerization is used to satisfy the *p*-xylene demand by converting *o*- and *m*-xylene into the desired isomer [6]. This reaction, controlled by the thermodynamic equilibrium, is generally carried out in gas-phase and catalyzed by medium pore zeolites, such as ZSM-5, or large pore zeolites, like mordenite, that will act as acid catalysts [7]. If the mixture contains ethylbenzene, the isomerization is carried out in the presence of hydrogen over bifunctional noble metal acid zeolites to prevent the catalyst deactivation [8, 9].

Zeolites in acid form are widely used at the industrial level as acid catalysts in various hydrocarbon conversion reactions [10]. The mechanism of acid-catalyzed reactions involves the

transfer of a proton from the acid species, which acts as a catalyst, to one of the reactants, as demonstrated in Figure 1 for the isomerization of xylenes:

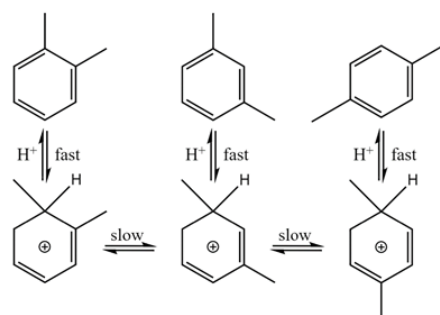


Figure 1. Xylene isomerization: intramolecular mechanism. Adapted from [11].

The strength of the acid sites is an important property that influences the mechanism of the reactions. For instance, strong acid sites favor unimolecular xylene isomerization, while weak acid sites lead to bimolecular reactions. On the other hand, the density of acid sites allows the control of the selectivity for unimolecular or bimolecular reactions. Zeolites that present a low density of Bronsted acid sites facilitate unimolecular reactions while bimolecular reactions occur more readily on catalysts with a high acid sites density [12].

Methods

In this work, the isomerization reaction is carried out in the liquid phase. The batch experiments will be performed in an autoclave (HP pressure vessel 4790; Parr), as represented in Figure 2, starting with pure *m*-xylene and left to react for 5 h to guarantee the equilibrium is reached. To choose the catalyst, the performance of three zeolites (MOR20, MOR40 and

BEA35) was evaluated using the isomerization reaction of *m*-xylene.

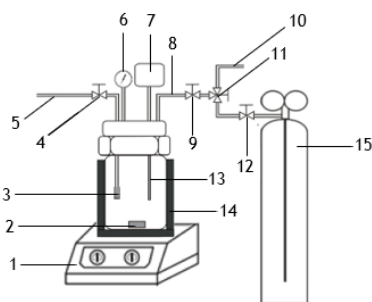


Figure 2. Experimental setup. 1. Heating plate. 2. Magnetic stirrer. 3. Filter. 4. On/off valve. 5. Autoclave outlet tube. 6. Pressure gauge. 7. Temperature controller. 8. Autoclave inlet tube. 9. On/off valve. 10. Vent tube. 11. 3-way valve. 12. N₂ valve. 13. Thermocouple. 14. Thermal jacket. 15. N₂ supply.

Results and Conclusions

The results of the isomerization reaction of *m*-xylene at 220 °C are represented in Table 1.

Table 1. Results of the isomerization reaction of *m*-xylene at 220 °C.

Catalyst	Mass (g)	Conversion (%)	Selectivity pX (%)	Selectivity oX (%)
MOR40	2.006	33.3	50.8	45.3
MOR20	2.006	10.8	51.2	45.6
BEA35	2.007	18.8	58.6	38.5

Conversion is more critical than selectivity because this reaction will co-occur with adsorption.

The adsorption of *p*-xylene causes its concentration in the liquid medium to decrease. Consequently, during the isomerization reaction, *o*- and *m*-xylene are converted to *p*-

Acknowledgements

This work was financially supported by:

FCT grant UI/BD/151076/2021; LA/P/0045/2020 (ALiCE), UIDB/50020/2020 and UIDP/50020/2020 (LSRE-LCM) funded by national funds through FCT/MCTES (PIDDAC).

References

- [1] W.J. Cannella, Xylenes and Ethylbenzene, Kirk-Othmer Encyclopedia of Chemical Technology, John Wiley & Sons, Michigan, 2000.
- [2] *Petroleum Refineries Sector*. Accessed on: 8 February 2022; Available at: www.epa.gov/sites/default/files/2016-11/documents/refineries_2013_112516.pdf.
- [3] Y.T. Kuo et al., *Applied Energy*, 215 (2018) 21-30.
- [4] D.S. Sholl, R.P. Lively, *Nature*, 532 (2016) 435-437.
- [5] Commissaris, S.E., UOP Parex Process, in: R.A. Meyers (Ed.) *Handbook of Petroleum Refining Processes*, McGraw Hill, Boston, 2003, 2.47-2.54.
- [6] M. Guisnet et al., *Microporous and Mesoporous Materials*, 35-36 (2000) 47-59.
- [7] J.C. Gonçalves, A.E. Rodrigues, *Chemical Engineering & Technology*, 39 (2016) 225-232.
- [8] O. Cappellazzo et al., *Industrial & Engineering Chemistry Research*, 30 (2002) 2280-2287.
- [9] A. Corma, A. Cortés, *Industrial & Engineering Chemistry Process Design and Development*, 19 (2002) 263-267.
- [10] G. Busca, *Microporous and Mesoporous Materials*, 254 (2017) 3-16.
- [11] M. Guisnet et al., *Microporous and Mesoporous Materials*, 35-36 (2000) 47-59.
- [12] C.N. Costa et al., *Catalytic Properties of Zeolites*, in: V.J. Inglezakis, A.A. Zorpas (Eds.) *Handbook of Natural Zeolites*, 2012, 103-132.

xylene to restore the thermodynamic equilibrium. Therefore, although BEA35 exhibits a higher selectivity for *p*-xylene, MOR40 showed the highest conversion among the three zeolites, so it was chosen as the catalyst.

After choosing the catalyst for the isomerization, additional experiments were performed to determine the kinetic constant and activation energy for the isomerization of *m*-xylene between 200 and 240 °C. The experimental setup was the same as the one in Figure 1. In this part, experiments had a duration of 0.5, 1, 2, 3, and 5 h for each temperature tested. The results of these experiments are presented in Table 2.

Table 2. Results of the isomerization reaction of *m*-xylene at different temperatures (preliminary results).

Temperature (°C)	Mass (g)	Time (h)	Conversion (%)
200	2.003	0.5	3.3
	2.006	1	6.48
	2.007	2	7.40
	2.005	3	8.59
	2.006	5	9.58
220	2.004	1	5.45
	2.005	2	10.56
	2.005	3	14.0
	2.005	5	16.7
	2.005	0.5	5.83
240	2.003	1	11.9
	2.004	2	16.2
	2.005	3	18.3
	2.007	5	25.7

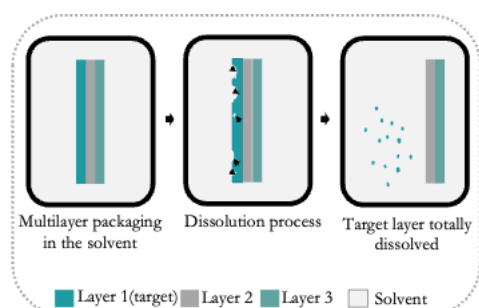
Based on the results presented in this table, it was possible to determine the kinetic constant and the activation energy of this reaction using the gPROMS Model Builder software V7.0.7 (Process System Enterprise, Siemens).

A detailed study on the valorization of multilayer plastic waste based on the dissolution and precipitation technique

A. Cavuquilha^{1*}, C. Maganinho¹, M. Durão¹, A. Dias¹, G. Carreira², I. Portugal¹, C. Silva¹, A. Barros-Timmons¹

¹CICECO - Aveiro Institute of Materials, Department of Chemistry, University of Aveiro, 3810-193 Aveiro, Portugal; ²i9green, Av. D. José Alves Correia da Silva, Edifício Vela Sul 2° D, Rotunda Sul, Cova da Iria, 2495-402 Fátima, Portugal.

*anareth@ua.pt



This work presents a framework for recovering polymers from real mixed multilayer plastic packaging (MPP) waste from a Portuguese plastic recycling facility. This study aimed to identify the materials in the MPP waste and recover the most suitable polymer fraction from the MPP using a dissolution and precipitation-based approach. Additionally, understand the recovered polymer's chemical, thermal, and mechanical behavior, and the blends of this material with a virgin polymer matrix.

Introduction

Multilayer plastic packaging (MPP) is a crucial type of packaging mainly used for food, personal care, and pharmaceutical application and result from the combination of two or more layers in a composite which aims to provide functional and protective properties to the product when they are not reachable by a single type of polymer or with a single layer of the polymer mixture [1]. However, MPP waste represents a prominent fraction of plastic waste in landfills and the environment [2] because MPP complex structure composed of different non-compatible materials does not allow it to be recycled using the conventional mechanical recycling industrial approach, and does not allow the proper separation of the various layers, resulting in poor quality materials [3, 4]. Among alternative methods, selective dissolution and precipitation has been investigated at the laboratory and industrial level and has shown to be a promising approach towards the effective industrialization of MPP waste stream recycling, which is commonly sent to incineration and landfill [4]. As the graphical abstract shows, this technique is based on the dissolution of target layers with selective solvents. Therefore, developing suitable strategies for effectively applying this technique is required.

This work addresses dissolution and precipitation as a strategy for valorizing polymer-based multilayer packaging, dealing with a real MPP waste stream from a Portuguese recycling facility.

Methods

MPP waste previously crushed and washed was donated by a Portuguese recycling facility. Commercial virgin polymers such as LDPE and PET were obtained from Sigma Aldrich and used for comparison in this work. Toluene was pre-selected after Hildebrand solubility parameters analysis and used as the solvent.

MPP waste was dissolved in toluene at a fixed temperature under N₂ atmosphere using a glass three-tabulator round bottom flask equipped with a condenser, under agitation and temperature control. The overall experimental procedure is presented in Figure 1.

Polymer blends of recovered polymer (r-Polymer) and virgin LDPE were prepared by melt mixing in a Plastograph EC Brabender at 120 °C and agitation of 50 to 100 rpm for 10 min.

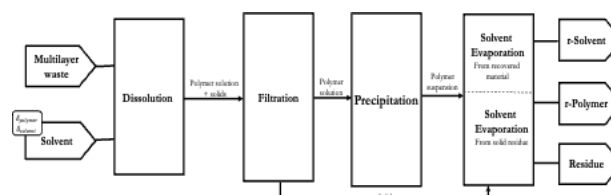


Figure 1. MPP waste dissolution and precipitation experimental procedure flowchart.

The MPP waste, the r-Polymer, and the remaining residue were analyzed using Fourier-transform infrared spectroscopy (FTIR), Differential scanning calorimetry (DSC), and Energy Dispersive Spectroscopy (SEM-EDS). In addition, the r-Polymer/LDPE blends were analyzed by FTIR, DSC, Melt Flow Index (MFI), and tensile tests.

FTIR was performed using a Perkin Elmer system and a universal ATR sampling accessory. The analysis was conducted at room temperature and consisted of 64 scans with a resolution of 4.0 cm⁻¹, and the wave number ranged from 4000 to 400 cm⁻¹. DSC analyses were conducted under nitrogen using steel crucibles in a Perkin Elmer Diamond DSC, in a temperature range from -50 to 300 °C with a 10 °C/min heating rate. The multilayer plastic waste and recovered materials were analyzed in a SU-70 Hitachi SEM equipped with a Bruker QUANTAX 400 EDS accessory. The MFI was determined following the ISO-1133-1 standard using a Model 6 Advanced melt flow system of Ray-Ran, at 190 °C and using a 5 kg piston. Dog bone test specimens for tensile tests were prepared using a Thermo scientific Haake MiniJet II injection molding system at 170 °C and 400 bar. The tensile tests were done using AG-25TA refresh Shimadzu equipment with a load cell of 20 kN at 50 mm/min speed at environmental conditions.

Results

Figure 2 presents the results from FTIR and DSC of the MPP waste. Comparing the FTIR spectra of MPP waste and virgin polymers, there is indication that MPP is composed of high amounts of polyolefins and PET. However, do not discard the possibility of a small quantity of other polymers previously mentioned in the literature, such as PP, EVA, PA, PS and PVC [3]. Melting temperatures measured by DSC confirm the major presence of PE and PET, as well as the presence of PP and PA.

Furthermore, the EDS analysis allowed the identification of the elements present in the sample: besides C and O, which were expected to compose a significant part of the sample, Ca, Si, Al, Ti, and Cl were detected, which can be associated with colorants, aluminum foils, plasticizers, and other plastic additives.

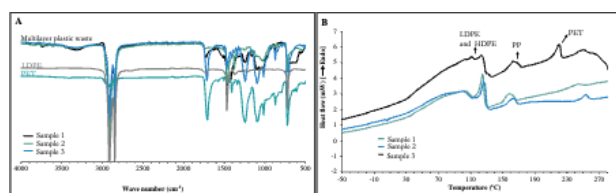


Figure 2. (A) FTIR and (B) DSC of MPP waste.

On average, 42.0 ± 3.2 wt.% of the initial MPP waste is recovered by dissolution and precipitation. Figures 3 and 4 present the FTIR and DSC analysis results of the r-Polymer and residue fraction. The r-Polymer obtained mainly comprises PE, with a small content of PS and PP, as well as plastic additives and colorants contamination. EDS analysis demonstrated the presence of all the initial elements present in the MPP waste in a smaller amount. Concerning the residue fraction, FTIR, DSC (Figure 4), and EDS analysis have shown that it is rich in PET, with a small presence of undissolved polyolefins and the contaminants previously identified.

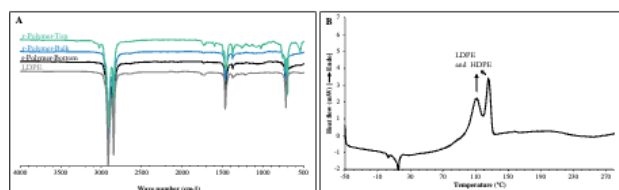


Figure 3. (A) FTIR and (B) DSC of r-Polymer.

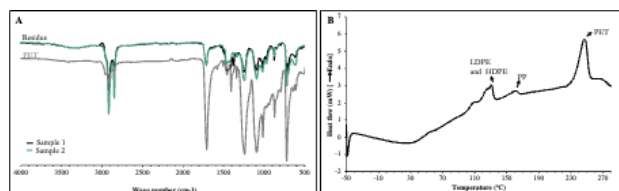


Figure 4. (A) FTIR and (B) DSC of the residue fraction from the dissolution and precipitation of MPP waste.

Table 1. Melting point, MFI, and tensile properties of r-Polymer, LDPE, and polymer blends.

	LDPE	25 % r-Polymer /75 % LDPE	50 % r-Polymer /50 % LDPE	75 % r-Polymer /25 % LDPE	r-Polymer
T_m (°C)	110	126	126	126	126
MFI [190 °C, 5 kg] (g/10 min)	55.95	26.00	17.11	9.43	8.07
Tensile strength at break (MPa)	9.75	11.14	11.37	14.77	17.53
Elongation at break (%)	89.72	90.28	92.07	51.19	23.32
Modulus of elasticity (MPa)	83.40	128.2	205.7	311.4	354.6
Toughness (MPa)	7.98	10.26	11.20	11.22	5.79

Acknowledgements

This work is financed by Portugal 2020 through European Regional Development Fund (ERDF) in the frame of Operational Competitiveness and Internationalization Programme (POCI) in the scope of the project i9rCB, POCI/CENTRO -01-0247-FEDER-070066 and in the scope of the project CICECO-Aveiro Institute of Materials, UIDB/50011/2020, UIDP/50011/2020 & LA/P/0006/2020, financed by national funds through the FCT/MEC (PIDDAC).

References

- [1] J.R. Warner, *Multilayer Flexible Packaging. Technology and applications for the food, personal care, and over-the-counter pharmaceutical industries*, 1Ed., Elsevier Inc., USA, 2010, 201-230.
- [2] C.T. de M. Soares et al., *Resources, Conservation and Recycling*, 176 (2022) 105905.
- [3] M. Rososen et al., *Environmental Science & Technology*, 54 (2020) 13282-13293.
- [4] V. Lahtela et al., *Polymers (Basel)*, 12 (2020) 2517.
- [5] K. Kaiser et al., *Recycling*, 3 (2018) 1.

Polymer blends were done to evaluate and compare the r-Polymer to commercial LDPE in terms of thermal and mechanical behavior and to evaluate the incorporation degree of r-Polymer that does not significantly deteriorate those properties. Table 1 presents the results from the MFI, melting point, and tensile tests for the r-Polymer, virgin LDPE, and blends with 25 % to 75 % of incorporation of r-Polymer. The blends mixed well without visual signs of incompatibility, and as can be seen in Table 1, the melting point of r-Polymer and polymer blends are about 16 °C higher than LDPE. Also, the MFI of r-Polymer is much lower than LDPE, and an incorporation of 25 % leads to a decrease of 53 % in the MFI.

Concerning tensile properties, r-Polymer demonstrates a lower elongation at break and toughness, and higher modulus of elasticity and tensile strength at break. However, blending r-Polymer to LDPE results in higher toughness than the initial materials. According to the results, all the mechanical properties are enhanced by incorporating r-Polymer up to 50 %.

Additional efforts have been dedicated to the characterization of MPP waste, and different approaches for the recovery of polymeric materials, such as multi-step dissolution strategies, delamination, and depolymerization of the PET-rich residue through hydrolysis, have been explored and are aimed to be presented.

Conclusions

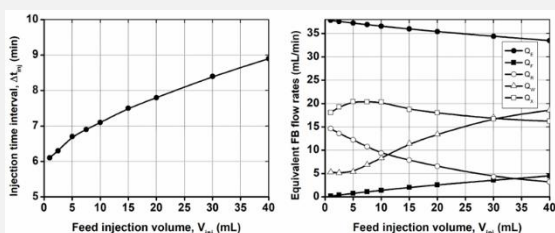
MPP waste comprises mainly PE and PET, with a small presence of PP, PA, and other contaminants such as aluminum, plasticizers, colorants, paper, and other plastic additives. It is possible to recover up to 45.2 wt.% of the total MPP waste, which results in a low contaminated recovered PE. In addition, blends of r-Polymer and LDPE demonstrated that the tensile mechanical properties do not significantly change up to 50 % of r-Polymer incorporation.

Complete separation of nadolol stereoisomers by fixed-bed and simulated moving bed chromatography

R. Arafah^{1,2*}, A. Ribeiro^{1,2}, A. Rodrigues³, L. Pais^{1,2}

¹Centro de Investigação de Montanha (CIMO), Instituto Politécnico de Bragança, Campus de Santa Apolónia, 5300-253 Bragança, Portugal. ²Laboratório para a Sustentabilidade e Tecnologia em Regiões de Montanha (SusTEC), Instituto Politécnico de Bragança, Campus de Santa Apolónia, 5300-253 Bragança, Portugal. ³Laboratory of Separation and Reaction Engineering, Laboratory of Catalysis and Materials (LSRE/LCM), Department of Chemical Engineering, Faculty of Engineering, University of Porto, Rua Dr. Roberto Frias, S/N, 4099-002 Porto, Portugal.

*rarafah@ipb.pt



Effect of the feed injection volume in the injection time interval (left plot) and in the equivalent flow-rates (right plot) for the fixed-bed preparative separation of nadolol racemates.

This work deals with the identification of main experimental strategy for the complete separation of nadolol quaternary mixture into its pure four stereoisomers. Different chiral and achiral adsorbents, with different particle size diameters (5, 10 and 20 μm) as well as several solvents and solvent mixtures (aqueous and organic) are used. The selected global strategy is based on two main steps. The first step is the achiral separation of nadolol racemates (two pairs of enantiomers) by high pH reversed-phase preparative chromatography using C18 adsorbents. Then, the second step is based on two parallel binary chiral separations using Chiralpak IA adsorbents. It is important to notice that both first and second steps can be accomplished by fixed-bed and simulated moving bed (SMB) technologies. The theoretical and experimental results show that SMB technology presents higher preparative performance when compared to the “equivalent” preparative fixed-bed operation.

Highlights

- Strategies for complete preparative separation of nadolol chiral drug.
- Optimization of different solvent compositions using chiral and achiral adsorbents.
- Chiral separation by preparative SMB chromatography.

Introduction

Nadolol is a common prescribed pharmaceutical drug for the relieve of several cardiovascular diseases and represents a very interesting case-study of multicomponent chiral separation since it is composed by four stereoisomers, being two pairs of enantiomers. In this way, it introduces the possibility of alternative strategies, using different kind of preparative separation sequences and techniques, the use of different packings (chiral and achiral stationary phases), and the corresponding mobile phase optimization at both normal and reversed-phase modes.

When considering preparative and multicomponent separation, the complexity deeply increases by introducing the necessity of multi-step separation sequences (or a much more complex multi-region separation process), by opening the possibility to combine chiral and achiral stationary phases (when in presence of stereoisomers instead of just one pair of enantiomers) and to combine different separation techniques (fixed-bed and simulated moving bed (SMB) related processes). The design of the complete preparative separation of nadolol stereoisomers asks for a global experimental and simulation methodology considering both the characterization and optimization of each separation step and its sequences to achieve the four nadolol components pure. New strategies using combinations of achiral and chiral stationary phases and sequences of different separation techniques will be studied. Extensive experimental and simulation results for the complete separation of all the four nadolol stereoisomers using Chiralpak IA (chiral) and different Waters C18 (achiral) stationary phases will be presented.

Methods and materials

For the analytical measurements, an analytical Knauer HPLC was equipped with one Smartline 1050 pump, a 10 mL pump head and two detectors in series: a Smartline UV detector 2520 a polarimeter detector (Chiralser IBZ, Messtechnik, Germany). These measurements were performed using a Chiralpak IA column obtained from Daicel and a XBridge C18 column obtained from Waters. Both columns have the same analytical dimensions (250 mm L × 4.6 mm ID) and packed with 5 μm particle size materials. For the preparative measurements, a preparative Knauer HPLC system equipped with a Smartline UV detector 2520, two Smartline 1050 pumps with 50 mL pump heads, was used. Three different preparative columns (100 mm L × 20 mm ID) were used, a Chiralpak IA (particle size diameter 20 μm), a SiliaChrom XT18 and a XBridge C18 column (both with a particle size diameter of 10 μm). The binary SMB separations of nadolol racemates was performed on a laboratory-scale SMB unit built on the LSRE group, Faculty of Engineering, University of Porto. The SMB unit was operated using a [1-2-2-1] column configuration. The SMB unit was operated with 6 XBridge C18 columns for the binary separation of the two nadolol racemates (1+4)/(2+3) and 6 Chiralpak IA columns for the binary enantiomer separations (1/4) and (2/3). An Azura fixed-bed preparative commercial HPLC system obtained from Knauer was also used for the binary separation of nadolol racemates. This system was equipped with two preparative HPLC pumps P2.1L model with 250 mL/min pump heads, one UV detector UVD2.1L model and a unique Waters XBridge prep C18 column (30 mm ID x 250 mm L) with particle size diameter of 10 μm.

Results and discussion

An extensive set of experimental and simulation results will be presented (see Graphical Abstract, Figure 1, and Figure 2). Results will include the identification of the stereoisomers present in both nadolol racemates by means of using UV and polarimeter detectors in series. Then, a complete methodology developed during the last years by our group will be explained and applied to scale-up the separation process from analytical to preparative scales [1-4].

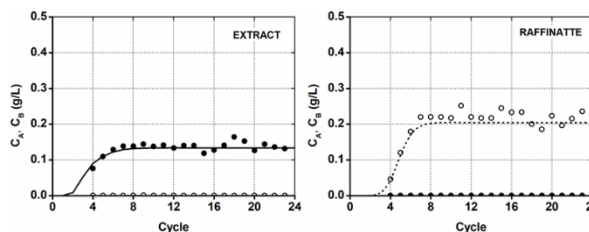


Figure 1. Experimental (points) and predicted (lines) transient evolution (24 full cycles) of the nadolol racemate concentrations in the extract and raffinate SMB outlet streams. Closed circles for the more retained racemate A, open circles for less retained racemate B, for a 2 g/L nadolol feed solution.

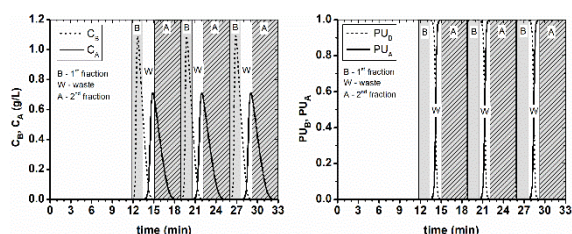


Figure 2. Simulated fixed-bed chromatograms of three consecutive pulses (left plot, dashed line for the less retained racemate B, solid line for more retained racemate A) and purities of B and A (right plot, dashed line for purity of B, solid line for purity of A) of a 9 g/L nadolol feed solution.

Conclusions

The selected and implemented methodology to perform the complete separation of the four nadolol stereoisomers is based on two main steps. The first step is an achiral preparative separation of the two racemates of nadolol (two pairs of enantiomers). The implementation of the first achiral step was done with the separation of nadolol racemates by high pH reversed-phase fixed-bed and simulated moving bed chromatography. Both systems use the Waters XBridge C18

adsorbent of 10 μm particle diameter. The second step is composed of two parallel preparative binary chiral separations of the racemates of nadolol, previously obtained on the first step.

For the first achiral step, an extensive study was carried to select the most promising achiral adsorbent and the more favorable solvent composition. The screening of the mobile phase composition elected the Waters XBridge C18 adsorbent and a 30:70:0.1 (v/v/v) ethanol:water:diethylamine solvent mixture to perform both FB and SMB preparative operations. For FB, using a feed concentration of 9 g/L of an equimolar mixture of the two nadolol racemates, both were recovered almost pure (at least 99.9%), with a global system productivity of 3.06 gfeed/(Lbed.hr) and a solvent consumption of 4.21 Lsolvent/gfeed. For SMB, the pilot unit's pressure drops limits imposed a maximum internal flow-rate of only 5 mL/min and, for a nadolol feed concentration of 2 g/L, both racemates were recovered 100% pure, with a system productivity of 0.13 gfeed/(Lbed.hr) and a solvent consumption of 6.19 Lsolvent/gfeed. Additional simulation results showed that a SMB preparative unit can perform the 9 g/L nadolol racemate separation with a system productivity of 3.61 gfeed/(Lbed.hr) and a solvent consumption of only 1.95 Lsolvent/gfeed using the same average internal flow-rate as in FB operation. Even better SMB productivities can still be obtained using the same feed or solvent flow-rates as in FB operation if the internal SMB flow-rates are allowed and not limited by the system pressure drop.

Concerning the second production step and for racemate A separation, a 25% methanol:75% acetonitrile solvent composition was elected, whereas for racemate B, a 5% methanol:95% acetonitrile was the selected composition. The experimental chiral separation of both nadolol racemates using SMB technology was carried out using the FlexSMB-LSRE unit. For racemate A and using a total feed concentration of 2 g/L, both nadolol stereoisomer (1 and 4) were recovered 100% pure in the outlet streams with a global system productivity of 1.81 g/(L.hr) and a solvent consumption for 2.47 L/g. For racemate B and using a total feed concentration of 2 g/L, both nadolol stereoisomer (2 and 3) were recovered 100% pure in the outlet streams with a global system productivity of 0.87 g/(L.hr) and a solvent consumption for 4.25 L/g.

Acknowledgements

The authors are grateful to the Foundation for Science and Technology (FCT, Portugal) for financial support through national funds FCT/MCTES (PIDDAC) to CIMO (UIDB/00690/2020, UIDP/00690/2020 and SusTEC (LA/P/0007/2021). National funding by FCT, Foundation for Science and Technology, through the individual research grant (SFRH/BD/137966/2018) of R. Arafah is also acknowledged.

References

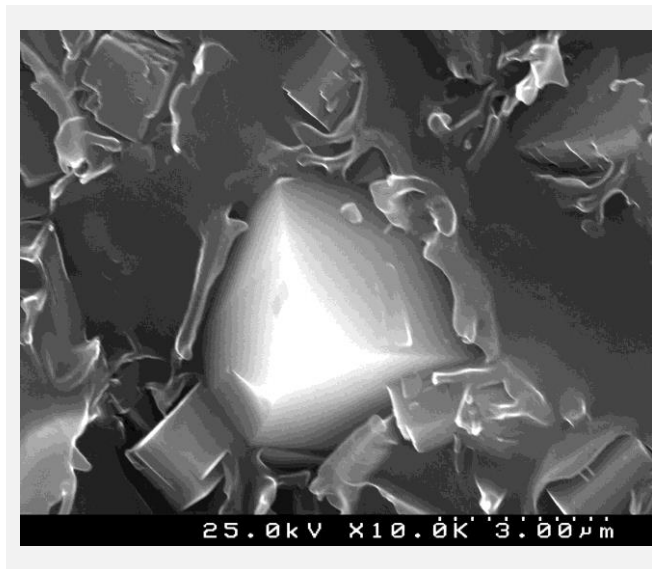
- [1] A. Ribeiro et al., *Chirality*, 25 (2013) 197-205.
- [2] R. Arafah et al., *Chirality*, 28 (2016) 399-408.
- [3] R. Arafah et al., *Chirality*, 31 (2019) 62-71.
- [4] R. Arafah et al., *Separation and Purification Technology*, 233 (2020) 116018.
- [5] R. Arafah et al., *Separation and Purification Technology*, 305 (2023) 122529.

Influence of [emim][Tf₂N] in PES/SAPO-34 mixed matrix membranes for gas separation

J.S. Cardoso^{1*}, Z. Lin², P. Brito³, L. Gando-Ferreira¹

¹CIEPQPF, University of Coimbra, Coimbra, 3030-790, Portugal; ²CICECO, University of Aveiro, Aveiro, 3810-193, Portugal; ³CIMO, Polytechnic Institute of Bragança, Bragança, 5300-253, Portugal.

*jonathancardoso@ipb.pt



Mixed matrix membranes (MMM) are heavily studied and the main concern by researchers is the difficulty to obtain a high selectivity membrane with low defects, mainly interfacial voids due to the poor interaction between polymer matrix and filler. The functionalization of zeolite surface in Poly-EtherSulphone (PES)/Silico-AluminoPhosphate-34 (SAPO-34) led to membranes with higher compatibility. Recently, the use of ionic liquids in the particles surface to improve the gas permeability and separation efficiency has presented advanced results. The aim of this work is to compare the separation efficiency of CO₂ and N₂ in permeance and selectivity criteria. The use of the ionic liquid (IL) [emim][Tf₂N] showed an increase in selectivity and in CO₂ permeance due to promoting a better separation of the dispersant in the polymeric matrix when compared to a film with the same composition without the IL treatment.

Introduction

The silicoaluminophosphates-34 (SAPO-34) appears as one of the main materials in mixed matrix membranes (MMM) for gas separation because of its pore size (0.38nm) is near the kinetic diameter of gases like H₂ (0.29nm), CO₂ (0.33nm), N₂ (0.36nm), CO (0.37nm) and CH₄ (0.38nm). Those materials have been dispersed in a polymeric matrix aiming to obtain membranes with more thermal stability and more selectivity than polymeric membranes, which are more permeable than inorganic membranes. Although PSA, TSA and cryogenic distillation are mostly used industrially in CO₂ separation, the use of MMM with zeolites and other silicate derivatives as constituents of MMM in gas separation, provides lower energy consumption, is modulable and can be connected to traditional processes, besides showing permeability and selectivity above the Robeson upper limit [1-5]. The surface functionalization of inorganic solids arises to improve the zeolite-polymer matrix interaction. ILs are proposed to improve the interaction between those components, increasing the membrane separation performance [6-10].

Materials and Methods

SAPO-34 sample was synthesized using a gel with the molar composition 1.0Al₂O₃; 1.0P₂O₅; 0.6SiO₂; 1.5Morpholine; 0.5Tetraethylammonium hydroxide (TEAOH); 70H₂O. The zeolite was prepared using a dry-gel methodology with 1:1 mass ratio of dry mass/water, heated at 200 °C for 24 h. The produced mixture was then centrifuged, washed, dried at 105 °C in an oven and calcined at 560 °C for 8 h. The samples were characterized via Powder X-Ray Diffraction (PXRD), Dynamic Light Scattering (DLS) and N₂ adsorption and desorption.

20%w/w PES/SAPO-34 membranes were prepared by adding the zeolite in stirring N-Methyl-2-pyrrolidone (NMP) for 1 h and in ultrasonic bath for 4 h. Then a small amount of PES was added to the NMP/SAPO-34 solution and mixed for 1 h at 80

°C. The remaining PES was added and mixed for 3 h at 80 °C, and the solution was stirred overnight at room temperature. The solutions were degassed for 4 h in ultrasonic bath and casted with a knife of 0.3 mm, dried at 80 °C for 2 h and at 200 °C for 20 h under vacuum. The 20%w/w PES/SAPO-34/[emim][Tf₂N] membranes synthesis followed the same procedure using 20%w/w of IL. The samples were characterized by scanning electron microscopy (SEM). Gas permeation experiments were conducted using pure gases to determine their permeability and diffusivity coefficients, and the results were compared to each other in a permeability unit called Barrer ($10^{-10} \text{ cm}^3_{STP} \cdot \text{cm} / \text{cm}^2 \cdot \text{s} \cdot \text{cmHg}$). A schematic of the permeation system is shown in Figure 1 and the permeabilities were obtained according to Eq. 1. The ideal selectivity results (α_{ab}) are represented by the ratio between the permeability (P) of two pure gases, a and b , respectively, measured separately under the same conditions, in the same membrane to evaluate the separation performance, as presented in Eq. 2.

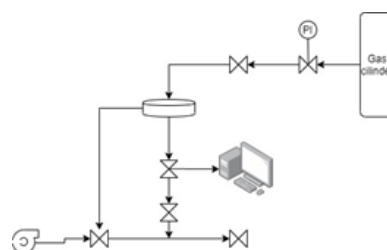


Figure 1. Schematic of the permeation system.

$$P_i = \frac{V_s l}{T_{AMB} \Delta p} \frac{T_{STP}}{P_{STP} A} \frac{dp}{dt} \quad (1)$$

$$\alpha_{a/b} = \frac{P_a}{P_b} \quad (2)$$

Results and discussions

Pure SAPO-34 was synthesized for a reaction time of 24 h using the methodology described and named JS1. The XRD pattern was compared to a standard one. The average particle size obtained was around 0.2 µm, as presented in Figure 3. The

N₂ adsorption-desorption isotherms in Figure 2 exhibited a type I isotherm which is characteristic of microporous structure. The textural properties show that the material presented a high BET area (S_{BET}) and V_{mic} which are comparable to those in literature.

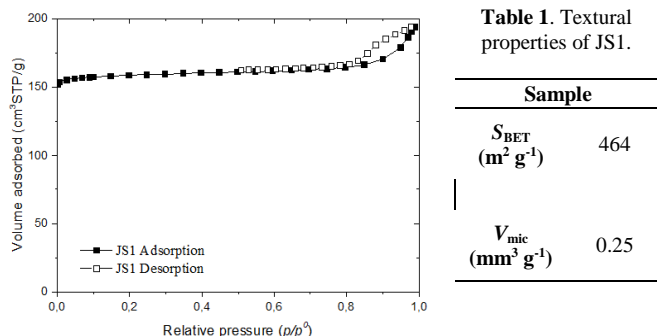


Figure 2. N₂ adsorption-desorption isotherm of JS1.

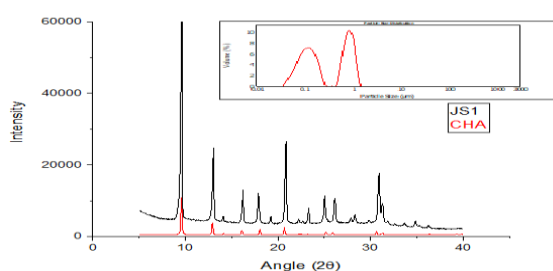


Figure 3. XRD and DLS for JS1 sample.

Fig 4a presents the SEM analysis of PES/SAPO-34 membrane with an agglomeration of crystal along the polymeric matrix. Figure 4b presents the SEM analysis of the PES/SAPO-34/[emim][Tf₂N] membrane with a more disperse crystals in the polymeric matrix. Figure 5 shows that the agglomeration of crystals in (a) presents voids between particles without selectivity, which causes an increase in permeation of all gases with a selectivity reduction. However, the more dispersed crystals presented in (b) are mainly due the use of IL, which helped to involve the crystals reducing agglomeration. This can be noted in CO₂ and N₂ permeability and separation selectivity as presented in the Table 2. The PES/SAPO-34/[emim][Tf₂N] membrane presented a higher CO₂

Acknowledgements

This work was supported by the Strategic Project of CIEPQPF (UIDB/00102/2020), CICECO-Aveiro Institute of Materials (UIDB/50 011/2020, UIDP/50 011/2020 & LA/P/0 06/2020), financed by Fundação para a Ciência e Tecnologia (FCT) through national funds. J.S. Cardoso was funded by the FCT through the PhD grant (SFRH/BD/148170/2019).

References

- [1] L.M. Robeson, *Journal of Membrane Science*, 320 (2008) 390-400.
- [2] S. Li et al., *Advanced Materials*, 18 (2006) 2601-2603.
- [3] M. Usman, *Membranes (Basel)*, 12 (2022) 507.
- [4] H.A. Mannan et al., *Procedia Engineering*, 148 (2016) 25-29.
- [5] N.N.R. Ahmad et al., *International Journal of Energy Research*, 45 (2021) 9800-9830.
- [6] Y. Huang et al., *Journal of Membrane Science*, 487 (2015) 141-151.
- [7] H.A. Mannan et al., *Interfaces in Particle and Fibre Reinforced Composites*, Woodhead Publishing, (2020) 269-309.
- [8] X. Tan et al., *Science*, 378 (2022) 1189-1194.
- [9] N.N.R. Ahmad et al., *Journal of Applied Polymer Science*, 133 (2016) 1-6.
- [10] Y. Liu et al., *Transactions of the Materials Research Society of Japan*, 46 (2021) 39-43.

permeability and higher selectivity when compared to PES/SAPO-34 membrane, showing that the incorporation of [emim][Tf₂N] improved the separation performance.

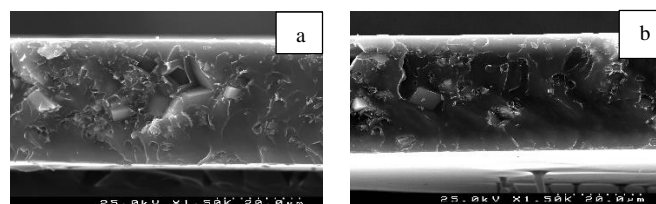


Figure 4. Cross-section of (a) PES/SAPO-34 and (b) PES/SAPO-34/[emim][Tf₂N] membranes.

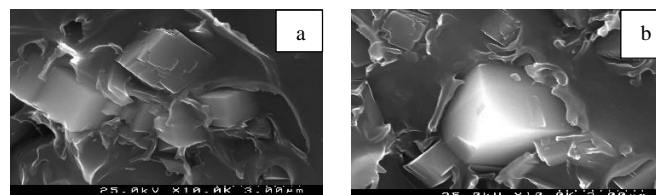


Figure 5. Zoom in particle distribution for (a) PES/SAPO-34 and (b) PES/SAPO-34/[emim][Tf₂N] membranes.

Table 2. Separation performance of PES/SAPO-34 and PES/SAPO-34/[emim][Tf₂N] membranes.

Sample	P _{CO₂} (Barrer)	P _{N₂} (Barrer)	α_{CO_2/N_2}
PES/SAPO-34	0,83	0,04	18,83
PES/SAPO-34/[emim][Tf ₂ N]	2,11	0,05	39,44

Conclusions

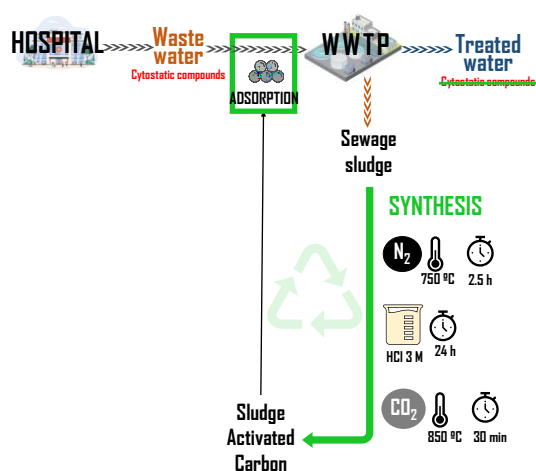
The methodology for nano-sized SAPO01-34 preparation was established as well as the solid with the desired characteristics was used as filler in MMM. The use of the ionic liquid [emim][Tf₂N] promoted an increase in separation performance in PES/SAPO-34 membrane due an increase in the dispersion of the crystals in the polymeric matrix, promoting an improvement in the CO₂ permeation and selectivity of the membranes. Other ionic liquids and deep eutectic solvents are planned to be tested and compared, as a more eco-friendly and less expensive alternatives, in order to understand the effects of those in the separation performance of PES/SAPO-34.

Valorisation of sewage sludge producing an activated carbon as an adsorbent for the removal of cytostatic drugs from water

*E. Portillo**, S. Flores, R. Carrizosa, S. Álvarez-Torrellas, J. Carbajo, V.I. Águeda, J. García

Catalysis and Separation Processes Group (CyPS), Chemical Engineering and Materials Department, Faculty of Chemistry, Complutense University, Avda. Complutense s/n, 28040 Madrid, Spain.

**evaporti@ucm.es*



In this work, several sludge-based activated carbons (SAC), synthesised by physical activation with urban WWTP sludge as a biomass precursor, have been tested as adsorbents in the removal of cytostatic drugs. The synthesis was initiated in all cases with a pyrolysis step with N_2 flow at $750\text{ }^\circ\text{C}$, and two other subsequent steps, one thermal at $850\text{ }^\circ\text{C}$ with CO_2 and an acid washing using a HCl 3 M solution, have been explored to improve the adsorbent SAC properties. SACs are characterised by BET, elemental analysis, FTIR, FRX, and SEM. The activated carbons are used as adsorbents to remove 3 cytostatic drugs: methotrexate (MTX), cyclophosphamide (CYC) and 5-fluorouracil (5FU). The finding highlighted that using acid for rinsing has proven to be a decisive step. Furthermore, placing the thermal activation step with CO_2 after the HCl washing has achieved the material (CN_2HCICO_2 , $S_{BET} = 443\text{ m}^2/\text{g}$) that showed the best adsorption results, with adsorption capacities of 30.6, 24.5 and 210.9 mg/g for 5FU, CYC and MTX, respectively.

Introduction

Sewage sludge is a significant and unavoidable by-product of wastewater treatment plants (WWTP). Historically, it was primarily used in farmland, forestry, incineration and landfill. However, agricultural sludge valorisation is only sometimes feasible due to heavy metal contents and the new legislation surrounding them[1]. In this context, managing sewage sludge in low-cost conditions has become necessary. Additionally, emerging pollutants detected in sewage water have increased in recent years. Specifically, due to the increment of anticancer treatments in our society, cytostatic drugs have been found in hospital and urban wastewater[2]. These compounds entail a high risk due to their mutagenic and teratogenic properties. Thus, they are one of the most dangerous groups of emerging contaminants due to their ability to interfere with DNA[3]. Nowadays, conventional processes in the WWTP cannot efficiently remove these compounds. Therefore, more efficient methods are necessary to prevent their release into the environment. Adsorption is one of the most used methods to eliminate organic pollutants from water because it is economical and easy to accomplish. However, one of this method's drawbacks is the regeneration of the adsorbent. Thus, regeneration methods as the use of solvents or advanced oxidation processes are interesting options[4].

Objectives

The present work aims for two objectives related to the water treatment line. The valorisation of sewage sludge as a biomass resource to produce sludge-based activated carbon (SAC), and, the use of SACs to remove cytostatic compounds from water by adsorption processes.

Methods

The SACs have been prepared with an urban sewage sludge from an urban WWTP, varying the activation route. The process followed is a physical activation with one or two pyrolysis steps and an acid washing. The physical activation occurs under high temperatures in a horizontal furnace, fed continuously with a gas stream. The primary step is pyrolysis at $750\text{ }^\circ\text{C}$ with an N_2 flow of $350\text{--}400\text{ NmL/min}$ for 2.5 h. A CO_2 activation at 150 NmL/min at $850\text{ }^\circ\text{C}$ for 30 min was accomplished as the second

thermal step or as a final step of the synthesis. In addition to the physical activation, HCl washing step was evaluated after or before the CO_2 activation, aiming to unblock the pores and remove ashes from the carbon structure. The wash was performed for 24 h under stirring in a 3 M HCl water solution, followed by a second wash with deionised water. Figure 1 summarises the activation process of the materials studied, specifying the synthesis steps sequence and the nomenclature for each SAC.

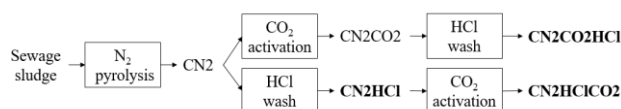


Figure 1. Synthesis sequence and nomenclature of the SACs used for adsorption experiments.

The characterisation of the materials obtained was accomplished by several methods. The specific surface area (S_{BET}) was determined by N_2 adsorption-desorption isotherms studies; Fourier Transformed Infrared spectrometry (FTIR) was used to study the functional groups at the carbon surface, the composition of the materials was determined by micro-elemental analysis and X-ray fluorescence techniques, and finally, the morphological properties were studied by scanning electronic microscopy (SEM).

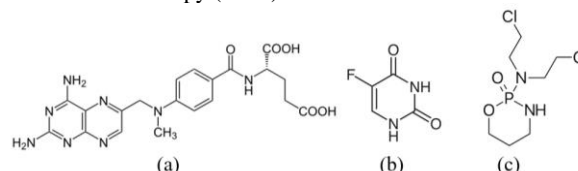


Figure 2. Molecular structure of (a) MTX, (b) 5FU and (c) CYC.

The experimental adsorption tests were assessed using 3 cytostatic compounds: methotrexate (MTX), cyclophosphamide (CYC) and 5-fluorouracil (5FU), with molecular sizes of 24.5, 12.3 and 6.8 \AA , respectively. The molecular structure of the compounds can be seen in Figure 2. Kinetic and isotherm adsorption experiments were carried out at room temperature ($25\pm 1\text{ }^\circ\text{C}$), with orbital oscillation agitation (250 r.p.m.) and an initial concentration of 20 ppm for each pollutant.

The concentration of the pharmaceuticals was followed by High-Performance Liquid Chromatography (HPLC) analysis in a C18 column coupled with a diode array detector.

Results and discussion

Table 2 encompasses the micro-elemental analysis, showing how the activation of the sewage sludge resulted in high carbon content (%C) and how relevant the HCl washing step was to removing the ashes and incrementing the carbon content in the material. CN2HCl is the SAC with the highest carbon content obtained, followed by CN2HCLCO2 and CN2CO2HCl materials.

Table 2. Elemental analysis for the sewage sludge and the synthesised SACs.

Material	C %	H %	N %	S %
Sewage Sludge	40.45	5.05	6.85	0.6
CN2	34.36	1.18	3.17	0.22
CN2CO2	26.87	0.86	1.99	0.18
CN2CO2HCL	48.68	1.5	3.45	0.33
CN2HCLCO2	52.31	1.56	3.75	0.27
CN2HCL	53.47	1.72	5.14	0.28

Figure 3 shows the textural properties analysis results comparing all the synthesis steps. As with the micro-elemental analysis displayed, it can be seen that the HCl washing step significantly impacted the structure of the obtained material. Moreover, pre or post HCl-washing to CO₂ activation will influence highly on the resulting material. Probably due to the CO₂ ability to open the carbon pores and, consequently, activate the carbon material. Thus, if the material already had some porosity, as with CN2HCl, the CO₂ can widen the pores, providing more microporosity to the final adsorbent.

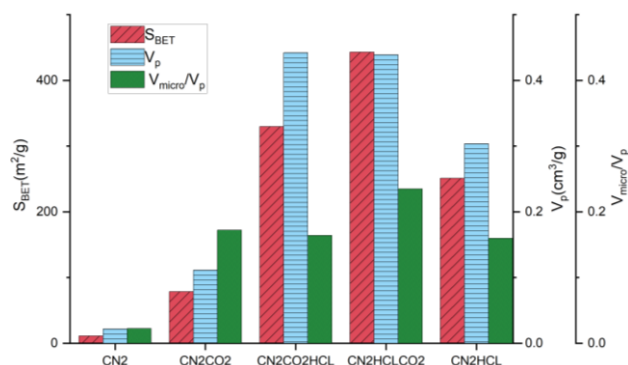


Figure 3. Textural properties characterisation of SACs. V_p : total pore volume (cm³/g); V_{micro}/V_p : relation between the micropore volume and total pore volume; S_{BET} : specific surface area (m²/g).

Based on the characterisation results, CN2HCl, CN2CO2HCL and CN2HCICO2 activated carbons were selected for adsorption experiments. The kinetics tests showed lower equilibrium times for the adsorption of 5FU and CYC, whereas for the MTX molecule, more than 24h is required to reach the equilibrium. However, the MTX adsorption capacity reached the highest values, e.g., 99-99.5 % removal at equilibrium time, for $C_0 = 20$

Acknowledgements

This work has been supported by the MICINN through the CATAD3.0 project PID2020-116478RB-I00. In addition, the authors acknowledge the funding from the *Comunidad de Madrid* (Spain) through the REMTAVARES Network (S2018/EMT-4341) and the European Social Fund. E.P. thanks *Ministerio de Ciencia, Innovación y Universidades*, for awarding her an FPI grant (PRE2021-098466).

References

- [1] M.C. Samolada et al., *Waste Management*, 34 (2014) 411-420.
- [2] P. Hamon, et al., *Journal of Water Process Engineering*, 21 (2018) 9-26.
- [3] L.A. Fernández-García et al., *Environmental Reviews*, 28 (2019) 1-11.
- [4] O. Zanella et al., *Chemical Engineering & Technology*, 37 (2014) 1447-1459.

ppm and an adsorbent dose of 0.3 g/L. These results can be directly related to the molecular sizes and the notable difference in the microporosity of the synthesised activated carbons, resulting in longer kinetic times for the more microporous materials. The adsorption capacities values in the monolayer at equilibrium time can be seen in Table 3. The highest adsorption capacities were reached with CN2HClCO2 material for the 3 compounds; unsurprisingly, the SAC with the highest S_{BET} and microporosity values. Therefore, as shown in the characterisation results, HCl washing before the CO₂ activation step resulted in the most appropriate SAC material.

Table 3. Adsorption capacities in the monolayer for 5FU, CYC and MTX onto the three synthesised SACs.

SAC	Compound	$q_{e_{monolayer}}$ (mg/g)
CN2HCl	5FU	9.7
	CYC	7.1
	MTX	119.7
CN2CO2HCl	5FU	13.6
	CYC	15.9
	MTX	164.8
CN2HCICO2	5FU	30.6
	CYC	24.5
	MTX	210.9

Conclusions

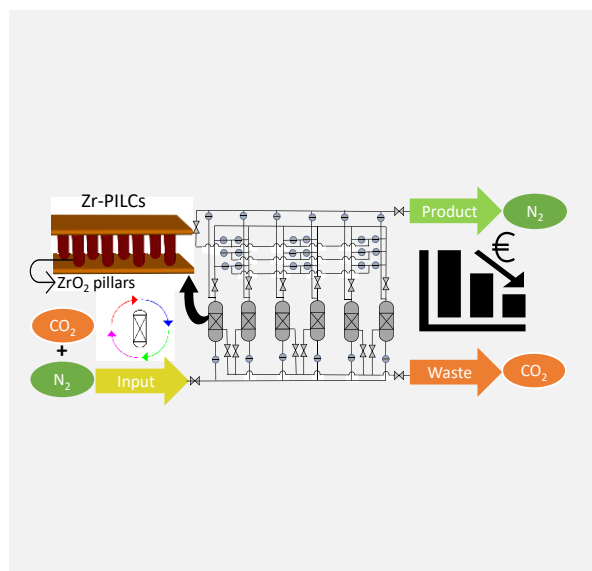
The results of this work have demonstrated the feasibility of using sewage sludge as a precursor of active carbons, which can be effectively applied in the removal of cytostatic compounds from an aqueous solution. Different steps in the physical activation process have been studied, evaluating the HCl washing before and after the CO₂ activation step. Thus, three synthesised activated carbons were selected for the adsorption, e.g., CN2HCl, CN2CO2HCl and CN2HCICO2, that showed S_{BET} values of 250, 330 and 443 m²/g, respectively. Adsorption experiments proved the influence of the molecular size on the kinetic adsorption process, having the smaller molecules, 5FU and CYC, faster kinetics than MTX, but, on the other hand, reaching lower adsorption capacities. From this study can be concluded that HCl washing is an essential step in the carbon synthesis, and applying it before the CO₂ activation could confer higher S_{BET} and greater microporosity to the carbon material. Thus, the highest adsorption capacities were obtained for CN2HCICO2 activated carbon, e.g., 30.6, 24.5 and 210.9 mg/g for 5FU, CYC and MTX, respectively. However, this material extended the required equilibrium times, particularly for the MTX adsorption, due to its higher microporosity and larger molecular size of this compound (24.5 Å). Further research regarding the SAC regeneration will determine the reusability properties of the synthesised SACs and how their different properties will affect their regeneration capacity. For this purpose, it would be interesting to evaluate different regeneration methods and see which one work best and how the textural properties of the SAC affect the regeneration process.

Pillared clays as cost-effective adsorbent for CO₂ capture in the cement industry: experimental and simulation study

A. Al Mohtar^{1*}, T. Frade¹, M. Bordonhos¹, J. Tingelinas¹, C. Saragoça¹, M. Mateus², M.L. Pinto¹

¹CERENA, Departamento de Engenharia Química, Instituto Superior Técnico, Universidade de Lisboa, 1049-001 Lisboa, Portugal; ²Secil SA., Fábrica Secil, Outão, Setúbal, Portugal.

*abeer.mohtar@tecnico.ulisboa.pt



Abstract. Decarbonization of the cement industry is a top priority where many accelerator programs are implemented to meet the sector set objective of meeting the carbon neutrality by 2050.

In the current work, a sustainable adsorbent, pillared clays (PILCs), was considered in the pressure swing adsorption (PSA) processes for carbon dioxide capture from the cement industry. Different process designs were tested where the most efficient process design a six-bed system operating in a 6-1-4 adsorption cycle and a total of 18 steps. Techno-economic analysis was performed where the total annualized costs, considering capital and operational costs, yielded 19.17 €/ton with a 78% of purity and 71.3% of CO₂ recovery, which is significantly lower than the state-of-the-art.

Dynamic adsorption experiments are being considered to validate the adsorption process models and computational fluid dynamics calculations on the heat transfer of these systems are ongoing. These recent studies will also be presented.

Introduction

Solid adsorption is one of the most appealing carbon capture technologies due to its negligible environmental impact with no associated toxic emissions, wastes, or corrosion problems. Nevertheless, this technology is still found at an early industrialization stage with technology readiness level 6 (TRL 6). Solid adsorption is coupled with cyclic processes for continuous operation and regeneration of the adsorbent. The efficiency in these cycles depends on several parameters that can be split into two categories, adsorbent related and process related. Regarding the former, finding the appropriate adsorbent is crucial in the solid adsorption technology. Moreover, process engineering optimizes the system performance and impacts the results significantly. The current work tackles these two aspects by using PILCs that were studied for the first time in PSA separation processes. In addition to exploring different process designs to optimize the system performance, techno-economic analysis was performed, where capital and operational costs were considered.

Materials and Methods

Aluminum and zirconium PILCs (Al-PILC and Zr-PILC) were chosen in the current study since they are known for their stability and simple preparation [1]. Zeolite 13X was chosen as a benchmark. The PILC materials properties considered in the calculations are the reported in the mentioned study [1]. Process simulations was conducted using Aspen Adsorption. First, a two-stage process design was implemented. The considered inlet was composed of 80% N₂ and 20% CO₂. Each stage consisted of two beds operating in a Skarstrom cycle. Later, a more sophisticated design of six beds-PSA operating in 6-4-1 cycle was carried out [2]. The main advantage of the latter is that feed compression is only required once, and thus, the associated operation costs are expected to be significantly

lower. After proving promising results, experimental breakthrough experiments are ongoing using gas mixtures of CO₂ and N₂ with various concentrations. Experiments introducing moisture are also being considered and will be presented. Breakthrough curves fitting is done to validate the mathematical models of the adsorption process via Aspen adsorption.

Computational fluid dynamics (CFD) calculations are being performed using COMSOL Multiphysics upon considering heat transport in porous media to determine the temperature distribution. Where, the heat of adsorption of PILCs is measured and the column dimensions and properties from the large-scale simulator (ASPEN Adsorption) are used.

Table 1. Techno-economic analysis summary Zr-PILC, Zr-PILC and zeolites 13X in two-bed two-stage PSA and Zr-PILC in six-bed PSA [3].

Parameters	Two-bed two-stage PSA			Six-bed PSA
	Zr-PILC	Al-PILC	Zeolite 13X	Zr-PILC
Total annual capital costs (M€/year)	1.59	1.59	1.74	11.18
Total annual operational costs (M€/year)	13.89	13.89	14.79	9.52
Purity (%)	76.6	72.5	50.0	78
Recovery (%)	72.1	62.8	36.6	71.3
Costs per CO ₂ captured (€/ton CO ₂ removed)	25.71	29.5	39.52	19.17

Results and Discussion

Two PSA designs were optimized where PILCs proved to have mild regeneration conditions. In the studied designs,

regeneration (desorption) happened at atmospheric pressure while adsorption at higher pressures (7-10 bars) to reduce the energetic demand. Two PILCs with aluminum and zirconium oxide pillars demonstrated a better performance than the benchmark material, 13X zeolite, under the studied conditions. PILCs presented better performance of purity and recovery of CO₂ (63% recovery and 72% purity for Al-PILC and 72% recovery and 77% purity for Zr-PILC) in comparison to 36.6% recovery and 50% purity for benchmark material, 13 zeolite 13X. For the best case (Zr-PILC), the associated total annualized costs of the process (including operation, investment, and capital costs) were estimated to be 25.71 €/ton CO₂ removed (a much higher value of 39.52 €/ton CO₂ removed was obtained for 13X zeolite, due to the less purity and recovery). The Zr-PILC pillared clay proved very promising where regeneration under mild conditions is possible and thus was selected to be studied in the six-bed-PSA process.

The six-bed-PSA process, although more complex, is much more energy efficient, using only one compression step with several equalization steps, yielding 78% purity and 71.3%

Acknowledgements

This work has received funding from Fundação para a Ciência e a Tecnologia (FCT) in the scope of the projects UIDB/04028/2020 & UIDP/04028/2020 (CERENA). Innovandi, *Global Cement and Concrete Research Network (GCCRN)*, Core Project 2B.

References

- [1] J. Pires et al., *Environmental Science & Technology*, 42 (2008) 8727-8732.
- [2] M.S.A. Baksh, M. Simo, Six Bed Pressure Swing Adsorption Process Operating in Normal and Turndown Modes. US8551217B2, 2011.
- [3] J. Tingelinas et al., *Industrial & Engineering Chemistry Research*, 62 (2023) 5613-5623.

recovery with a total annualized associated cost of 19.17 €/ton CO₂ avoided [3]. These findings are summarized in Table 1 and will be presented. Our study yielded a value for carbon capture costs significantly lower other typically considered carbon capture processes.

Conclusions

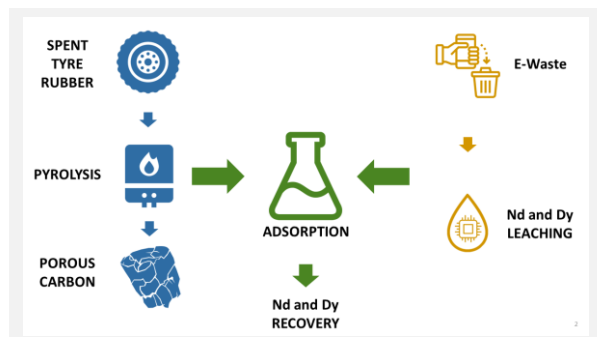
In conclusion, our calculations indicate that the six-bed-PSA process is more efficient for CO₂ capture from the flue gases despite the process's complexity. It is worth mentioning that lowering the CO₂ emissions and energy costs were privileged in this work as the envisaged CO₂ utilization would be toward conversion for other higher value products, such as methanol/methane conversion, where a nitrogen dilution of about 20% can be used and is often convenient. Based on these findings ongoing work on scaling up the synthesis of PILCs is being done. Breakthrough experiments to validate the mathematical modelling of the adsorption process is underway and will be shown. The assumption of isothermal process is being revisited by performing CFD calculation upon considering the heat transfer in porous media

Waste-derived carbon materials for adsorptive recovery of rare earth elements

M. Nogueira^{1*}, M. Bernardo¹, F. Pinto², I. Fonseca¹, N. Lapa¹, I. Matos¹

¹LAQV/REQUIMTE, FCT-NOVA, Caparica, Portugal, ²UB-LNEG, Lisboa, Portugal.

*mf.nogueira@campus.fct.unl.pt



This work explores the adsorption of the rare earth elements (REEs) neodymium (Nd) and dysprosium (Dy) onto waste-derived chars and activated carbons from spent tyre rubber (STR). STR recycling and valorisation are important due to the high environmental threat caused by the improper disposal of ST. Pyrolysis is a promising route for ST valorisation, as it converts waste into high added-value products, such as porous carbon materials that can be used in different industries. Batch and continuous adsorption studies were performed, and the results were fitted to different kinetic and isotherm models, showing that ST-derived activated carbons are effective adsorbents for REEs. This work demonstrates a sustainable and efficient pathway for REEs' recovery from e-waste using waste-derived materials.

Introduction

Rare earth elements (REEs) are a group of 17 chemical elements that present similar characteristics, which include the lanthanide series. They are considered critical raw materials by the European Union (EU) and the USA Department of Energy, due to their high economical and strategic importance, as well as the high risk associated with its supply chain. Nevertheless, REEs play a vital role in the transition to a sustainable, low-carbon, and low-environmental impact economy, due to their unique magnetic, catalytic, and phosphorescent properties [1]. E-wastes are the fastest growing waste stream and require sustainable and efficient pathways for its valorisation as they could provide the opportunity for the recovery of critical raw materials (CRM), as well as the reduction of the dependency of the EU on third-party countries for CRM supply. One promising candidate for e-waste recycling is REE containing permanent magnets. NdFeB magnets have been identified as a key waste flow with a high potential for the recovery of two REEs: neodymium (Nd) and dysprosium (Dy) [2].

Spent tyre, more specifically spent tyre rubber (STR), is a waste stream that represents a huge environmental threat worldwide. The prevision is the increase of this problem as the production rate of new tyres shows a steep increase each year, due to the growing demand from developing countries. Current estimations show that 17 million tons of STR are disposed of each year and their main routes of disposal are landfilling and to a lesser extent energetic valorisation through combustion, both of which imply the loss of the material, as well as the production of highly toxic compounds and emission of greenhouse gases [3]. Considering the aforementioned, STR recycling and valorisation should be strengthened with new solutions and optimization of the current management policies and processes. Pyrolysis demonstrates to be a viable route for STR valorisation, as it effectively converts wastes into high added-value products, such as porous carbon materials that can be used in different industries. Among the many applications of these materials, their unique properties make them highly efficient as adsorbents and ideal supports for catalysts [4].

Although adsorption can be considered a sustainable and green mechanism, the type and nature of the used adsorbent play an important role in the economic and environmental feasibility of this process.

This work will report the adsorption of Neodymium (Nd) and Dysprosium (Dy) onto STR-derived chars and activated carbons, under batch and continuous conditions.

Materials and Methods

The STR used in this work was provided by a company that performs cryogenic recycling of light vehicle tyres. The sample consists of only the rubber fraction of the spent tyres, after the removal of the metal support frame as well as of the fabric present in the tyres. This precursor was named Rubber A.

Batch pyrolysis was performed in a 5 L reactor with continuous stirring. After loading the rubber, the reactor was sealed and purged with N₂ and pressurized at 0.6 MPa. A heating rate of 5 °C.min⁻¹ was applied to a maximum temperature of 405 °C with a hold time of 30 minutes. After cooling, the solid fraction (char) was separated from the liquid fraction (pyrolysis oil). The obtained char was denominated A405.

Activation of the chars was performed in a bench-scale fluidized bed reactor under CO₂. A selected amount of the char was loaded onto the reactor which was then purged with N₂. A heating step with a rate of 5 °C.min⁻¹ was applied until 800 °C. At this point, the N₂ flow was changed to CO₂, and the sample was activated for 8 hours. The resulting activated carbon (AC) was coded A405-CO₂.

The textural and morphological properties of the STR chars and ACs were evaluated by adsorption of N₂ at 77 K, and SEM-EDS. Thermal stability was investigated by TGA. The chemical characterization comprised the following analysis: XPS, FT-IR, Proximate Analysis, Elemental Analysis, pH_{PZC}, mineral content, and XRPD. Bulk density and particle size distribution were also performed.

Batch Nd³⁺ and Dy³⁺ adsorption studies were performed using char A405 and AC A405-CO₂. All assays were performed in 20 mL sealed vials, on a magnetic stirrer at 300 rpm, with a temperature of 25±1 °C, initial concentrations of 10-200 mg.L⁻¹, and contact time of 0.08-72 hours. Nd³⁺ and Dy³⁺ concentrations were determined by ICP-AES. The kinetics for both metals were obtained, and the experimental data were fitted to the pseudo-first-order and pseudo-second-order kinetic models. Adsorption isotherms were also acquired, and the experimental data were fitted to Langmuir and Freundlich

isotherm models. Dynamic adsorption studies were performed with AC 405-CO₂ using a fixed-bed column device, with 100 mg of adsorbent, 1.5 mL.min⁻¹ flow, initial concentrations of 2.5 to 10 mg.L⁻¹, and running time of 180 minutes. The obtained experimental data were fitted to the Thomas model.

Results

Precursor elemental analysis showed that Rubber A had high carbon content (83.4% m/m) and a noticeable sulphur content (2.04% m/m), while its mineral analysis revealed that zinc and calcium were its major constituents with concentrations of 38.6 and 6.38 mg.g⁻¹, respectively. TGA analysis showed that the chosen pyrolysis temperature was suitable for the carbonization of the rubber material as the char presented a very stable thermal behaviour.

Pyrolysis assays revealed a char yield of 51.8%, which resulted in a material with high carbon content (79.1% m/m), a surface area (A_{BET}) of 90 m².g⁻¹ and a predominant mesoporous pore volume. Its mineral analysis showed that the char A405 had a higher content of zinc and calcium than their precursor, which is due to the concentration effect associated with the pyrolysis process. TGA analysis demonstrated that there was a successful carbonization of the rubber and that the char has high thermal stability. Afterwards, the char was activated with CO₂ to expand its structural and chemical properties aiming to improve its efficiency in the recovery of Nd and Dy. Activation of the char had a 15.4% m/m burn-off rate and resulted in activated carbon (A405-CO₂) that has a higher surface area (120.5 m².g⁻¹) and pore volume than its char counterpart.

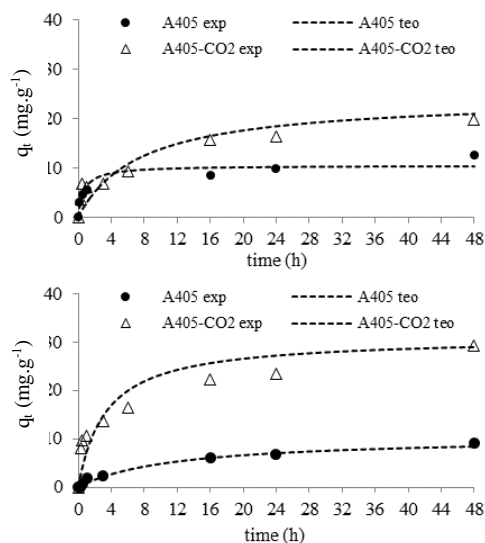


Figure 1. Batch adsorption kinetic curves – Nd³⁺ on top; Dy³⁺ below. Looking at the results from the batch adsorption experiments (Figure 1), it is possible to see that: (i) the behaviour for the adsorption of Nd and Dy is similar; (ii) Char A405 has the same uptake capacity for Nd³⁺ (10.53 mg.g⁻¹) as for Dy³⁺

Acknowledgements

The authors thank Valorpneu for the “Inov.Ação 2018” award. M. Nogueira thanks FCT/MCTES for funding his Ph.D. fellowship (SFRH/BD/147601/2019). This work was also supported by the Associate Laboratory for Green Chemistry – LAQV which is financed by Portuguese funds from FCT/MCTES.

References

- [1] K. Binnemans et al., *Journal of Cleaner Production*, 51 (2013) 1-22.
- [2] Y. Zhang et al., *Metals*, 10 (2020) 1-34.
- [3] I. Jones et al., *Journal of Cleaner Production*, 312 (2021) 20.
- [4] A.M. Sudame et al., *Journal of Physics: Conference Series*, 1913 (2021) 012088.

(10.54 mg.g⁻¹); (iii) when compared to the char A405, the AC 405-CO₂ has better performances for both metals in terms of both kinetics and maximum uptake capacities (Nd – 24.07 mg.g⁻¹; Dy – 30.97 mg.g⁻¹). The data from the batch adsorption studies reveal that the activation of the char did have a significant positive impact on the performances of the AC for the recovery of REEs. Further studies suggested that the main mechanism involved in the adsorption of Nd³⁺ and Dy³⁺ was the ionic exchange, having the zinc present in the adsorbents exchanged with both REEs.

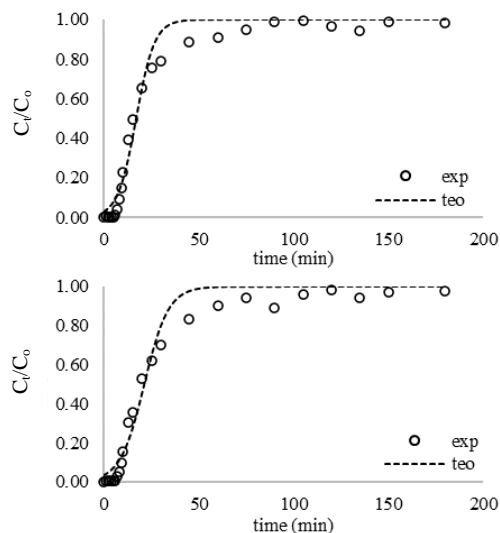


Figure 2. Breakthrough curves for the continuous adsorption assays using AC A405-CO₂ – Nd³⁺ on top; Dy³⁺ below.

Afterwards, the best adsorbent (AC A405-CO₂) was chosen to be used in the next step of this study - continuous adsorption assays. Analysis of the breakthrough curves (Figure 2) demonstrates that AC A405-CO₂ had similar performances for both metals, mirroring the results obtained on the batch experiments. The maximum uptake capacities were 2.9 mg.g⁻¹ for Nd³⁺ and 3.7 mg.g⁻¹ for Dy³⁺, with saturation times, *t*_s (*C*₁/*C*₀ = 0.95), of 74.6 minutes and 102.4 minutes respectively.

Conclusions

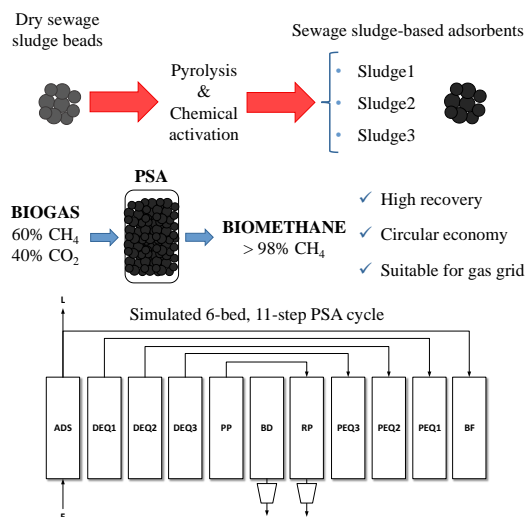
Pyrolysis demonstrated to be a viable route for STR valorisation as it effectively converted STR into a high added-value material that showed to be a suitable adsorbent for the recovery of REEs. Further upgrading of the char into AC has revealed a positive impact on the adsorptive recovery of Nd³⁺ and Dy³⁺, showing maximum uptake capacities of 24.07 mg.g⁻¹ and 30.97 mg.g⁻¹, respectively. Furthermore, the AC 405-CO₂ showed to be a suitable adsorbent to be used in the continuous adsorption of REEs. Overall, the main objective of this work was accomplished as STR was successfully valorised, with the resulting material being used for the recovery of a CRM, demonstrating that pyrolysis and adsorption are suitable pathways for the valorisation of waste streams while reinforcing a circular economy approach to STR management.

Biomethane production by PSA with sewage sludge-based adsorbents

R. Calero-Berrocal*, V.I. Águeda, J.A. Delgado

Catalysis and Separation Processes Group (CyPS), Chemical and Materials Engineering Department, Universidad Complutense de Madrid, 28040 Madrid, Spain.

*rubencal@ucm.es



This study evaluates three sewage sludge-based adsorbents in a pressure swing adsorption (PSA) process to obtain high-purity biomethane from biogas, consisting of 60% CH₄ and 40% CO₂. The adsorption isotherms and kinetic parameters of the adsorbents were obtained experimentally, and simulations of the PSA process were carried out to study the performance of the adsorbents under different cycle configurations. The results show that the sewage sludge-based adsorbents have higher CH₄/CO₂ selectivities than commercial activated carbon, which is helpful in a separation process. The PSA configuration studied achieved high methane recoveries (> 90%), and the biomethane purity obtained in the product complies with the specification to be injected into the gas grid. This study demonstrates that sewage sludge can be used to produce adsorbents suitable for biogas upgrading, contributing to the circular economy and the EU biomethane production targets.

Introduction

In 2022, the European Commission, with the aim of reducing Europe's dependence on Russian energy imports as soon as possible, launched the REPowerEU plan, which sets a target of 35 bcm (billion cubic meters) of biomethane production by 2030 [1]. By the end of 2021, around 3.5 bcm were being produced in the EU-27 [2], making the development of new biomethane production plants necessary to reach the target.

Around 90% of biomethane is produced from raw biogas (which is mainly obtained by anaerobic digestion in biodigesters but can also come from landfill gas recovery systems or wastewater treatment plants) through a post-treatment process called "biogas upgrading", in which carbon dioxide and other contaminants are removed from it, obtaining high-purity methane (> 98%) [3].

The most critical techniques for biogas upgrading are scrubbing with water or other physical solvents, chemical scrubbing, membranes, and pressure swing adsorption (PSA). PSA has already proven to be an effective technology for biogas upgrading under different operating conditions [4], generally with lower energy requirements than other techniques [5]. Several types of adsorbents have been studied for this application, including carbon molecular sieves (CMS), activated carbons, zeolites, metal-organic frameworks (MOFs) and biomass-based adsorbents [6].

Objectives

In this work, the performance of three sewage sludge-based adsorbents in a PSA process to obtain biomethane (CH₄ > 98%) from biogas (CH₄ = 60%, CO₂ = 40%, T = 298 K) is evaluated. For this purpose, the adsorption isotherms and kinetic parameters of the solids are obtained experimentally, and different PSA configurations are studied by simulation.

Materials and Methods

Three carbon-based adsorbents were obtained from dry sewage sludge beads, provided by Sacyr Circular, by applying different pyrolysis and chemical activation treatments. The

adsorption isotherms of CO₂ and CH₄ were measured using a volumetric equipment, BELSORP MAX II, at 298, 313 and 338 K. Using a mathematical model, the kinetic parameters were obtained from the breakthrough curves performed at the same three temperatures in fixed-bed experiments. PSA cycle simulations were carried out using PSASIM®, a program that solves the mass, energy, and momentum balances of the process [7].

Results

The experimental data of the adsorption isotherms were fitted to the Dual Langmuir model. Figure 1 shows the isotherms of CO₂ and CH₄ obtained with one of the solids studied, Sludge1.

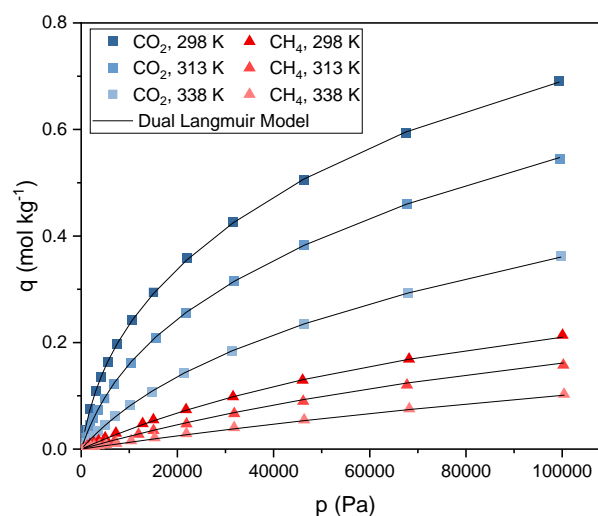


Figure 1. Isotherms of CO₂ and CH₄ on Sludge1 at 298, 313 and 338 K and the Dual Langmuir model.

Compared to commercial activated carbons widely used in gas separation processes, such as BPL (Calgon), which was studied in a previous work [8], the adsorbents based on sewage sludge show lower adsorption capacities. However, the

CH₄/CO₂ selectivities obtained are higher, which is an advantage in the performance of a PSA process.

Breakthrough curves were fitted to the Linear Driving Force (LDF) model to obtain the kinetic parameters. Figure 2 shows the CO₂ and CH₄ breakthrough curves on Sludge1 and the simulated breakthrough curves with the obtained LDF parameters.

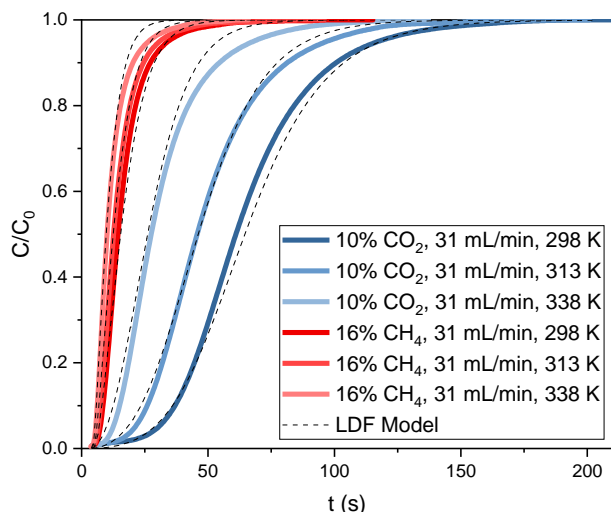


Figure 2. Breakthrough curves of CO₂ and CH₄ on Sludge1 at 298, 313 and 338 K and simulated breakthrough curves with LDF model.

Table 1. Results obtained by simulating a 6-bed, 11-step PSA cycle with Sludge1 or BPL as adsorbent.

Adsorbent	CH ₄ purity (%)	CH ₄ recovery (%)	CH ₄ productivity (mol kg _{ads} ⁻¹ s ⁻¹)	Energy consumption (kJ mol _{CH₄} ⁻¹)
Sludge1	98.08	93.28	2.80E-04	9.65
BPL	98.17	91.44	5.84E-04	9.77

Acknowledgements

Funding from the Centre for the Development of Industrial Technology (CDTI) through project MIG-20201034 (ShineFleet) and from the Spanish Ministry of Economy and Competitiveness through project CTM2017-84033-R is gratefully acknowledged.

References

- [1] European Commission, REPowerEU with clean energy, Publications Office of the European Union, 2022.
- [2] European Biogas Association, Activity Report 2022, Brussels, 2023.
- [3] R. Kapoor et al., Environmental Science and Pollution Research, 26 (2019) 11631-11661.
- [4] C.A. Grande, Chapter 3 in Biofuel's Engineering Process Technology, IntechOpen, 2011.
- [5] A. Mersmann et al., Chemical Engineering & Technology, 23 (2000) 937-944.
- [6] I. Durán et al., Chemical Engineering Journal, 428 (2022) 132564.
- [7] J.A. Delgado, Materiales en Adsorción y Catálisis, 7 (2014) 15-29.
- [8] P. Brea et al., Separation and Purification Technology, 179 (2017) 61-71.

Based on the three adsorbents' experimental equilibrium and kinetic parameters, simulations of the PSA process with different cycle configurations were carried out to maximise the productivity and recovery of methane in the product. In all simulations, a high pressure of 1 bar and a low pressure of 0.1 bar have been considered. Table 1 shows the results of simulations with a 6-bed, 11-step PSA process, whose cycle is shown in the Graphical Abstract, with Sludge1 or BPL as adsorbent.

It is observed that, with the PSA configuration studied, high methane recoveries can be obtained in the product (> 90%), being higher when using Sludge1 as adsorbent. However, the productivity achieved in this case is lower because of its reduced adsorption capacity. The energy consumption due to the compressor is similar.

Conclusions

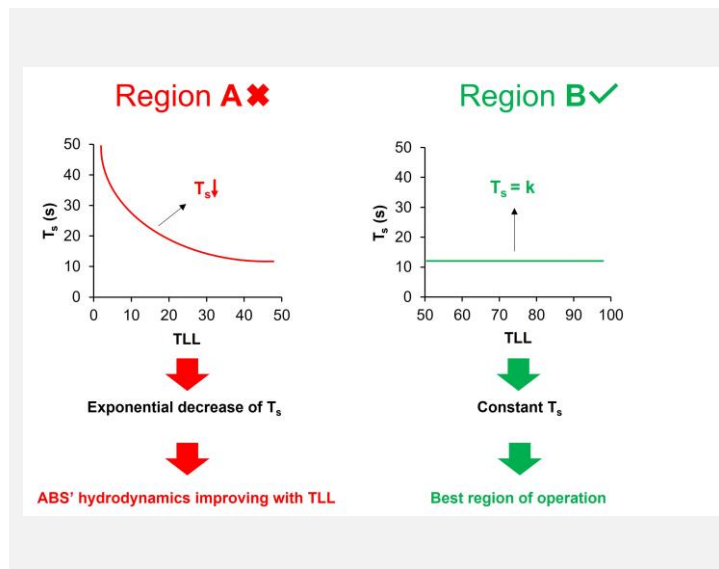
It has been demonstrated that, from sewage sludge, adsorbents as suitable as commercial ones can be obtained for biogas upgrading by employing a PSA process. Moreover, the biomethane produced complies with the specifications to be injected into the gas grid and high recovery is achieved. This study can contribute to the circular economy and to achieving the EU biomethane production targets.

Evaluation of the cholinium chloride-based aqueous biphasic systems (ABS) hydrodynamics

A.M.S. Jorge, J.A.P. Coutinho, J.F.B. Pereira*

University of Coimbra, CIEPQPF, FCTUC, Department of Chemical Engineering, Rua Sílvia Lima, Pólo II - Pinhal de Marrocos, 3030-790 Coimbra, Portugal; ²CICECO – Aveiro Institute of Materials, Department of Chemistry, University of Aveiro, Campus Universitário de Santiago, 3810-193 Aveiro, Portugal.

*jfbpereira@eq.uc.pt



The industrial application of Aqueous Biphasic Systems (ABS) depends on a proper scaling and integration into existing liquid-liquid extraction (LLE) operation units. For that purpose, the phase separation hydrodynamics of three ABS composed of PPG-400/[Ch]Cl, [Ch]Cl/K₃PO₄ and [Ch]Cl/K₂HPO₄ was studied by correlating the mixing time (T_m) and the phase settling time (T_s), at 25 °C and 50 °C. The results showed that T_s is independent of T_m , being very long for the polymer/salt ABS ($T_s > 6$ h) and very fast for salt/salt ABS ($T_s < 150$ s). The enhanced separation hydrodynamics of the salt/salt ABS is directly related with the salting-out effect of the inorganic salt. The phases' density was the most important physicochemical property in ABS' formation. A best biphasic region of operation was defined for [Ch]Cl/salt-based ABS, where the LLE should be designed if aimed the industrial implementation of these types of systems using conventional mixer-settler units.

Introduction

Aqueous Biphasic Systems (ABS) have been extensively studied as an efficient extraction platform for distinct (bio)molecules [1]. Despite all their advantages, the industrial use of ABS is still limited due to the poor understanding of the partition/separation mechanisms, few predictive models, incompatibility with current extraction equipment/facilities, and lack of large-scale studies [2]. Cholinium chloride ([Ch]Cl) is an essential nutrient for various biological functions and it has been largely employed in the formation of ABS. These studies involving [Ch]Cl-based ABS typically include the determination of corresponding phase diagrams and tie-lines, the characterization of some physicochemical properties, and their application for the extraction/separation of several biomolecules [3]. Despite the promising separation results, no studies have been reported on the hydrodynamics of these ABS. Therefore, the aim of this work was to evaluate and compare the hydrodynamics of three [Ch]Cl-based ABS composed of PPG-400 (polymer/salt system), K₃PO₄ and K₂HPO₄ (two salt/salt systems), providing critical insights on phase separation for future scale-up of these LLE processes.

Methods

The phase diagrams of [Ch]Cl/PPG-400, [Ch]Cl/K₃PO₄, and [Ch]Cl/K₂HPO₄ ABS were determined by the cloud point titration method [4] at atmospheric pressure and 25 °C, and for the salt/salt ABS also at 50 °C. The binodal curves of each [Ch]Cl-based ABS were correlated using the Merchuk' equation [4] (Equation 1):

$$Y = A \exp [(B \cdot X^{0.5}) - (C \cdot X^3)] \quad \text{Eq. 1}$$

Where X is the mass fraction of PPG-400, K₂HPO₄ or K₃PO₄ and Y is the mass fraction of [Ch]Cl, both expressed as weight percentages. A, B and C are fitting parameters.

The determination of the TLs was accomplished by using the gravimetric method described by Merchuk et al. [5], with the respective TLL being calculated using Equation 2:

$$\text{TLL} = [(X_t - X_b)^2 + (Y_t - Y_b)^2]^{1/2} \quad \text{Eq. 2}$$

where subscripts "t" and "b" are the "top" and "bottom" phases, respectively.

The determination of physicochemical properties of the coexisting phases of the PPG-400/[Ch]Cl ABS included viscosity and density measurements, while for [Ch]Cl/K₃PO₄ and [Ch]Cl/K₂HPO₄ ABS included measuring of pH, viscosity, density, and surface tension (SFT) of the coexisting phases. For both type of ABS, the hydrodynamics was determined as time required for complete phase separation (T_s) after mixing (T_m) for each ABS. The results were used to obtain correlations for ABS hydrodynamics, by relating T_s with the physicochemical properties of the systems' phases and the characteristics of the phase-forming compounds and respective compositions.

Results

For the system PPG-400/[Ch]Cl, the density values of both phases are similar for all mixture points, *i.e.*, 1.01 g.cm⁻³ and 1.06 g.cm⁻³ for the polymer- and salt-rich phases, respectively. In contrast, the viscosity values between the phases showed significant differences, with the viscosity of the polymer-rich phase being 20x higher than that of the salt-rich phase. The surface tensions are also almost constant (*i.e.*, varying between 60 and 65 mN.m⁻¹.μL⁻¹) for the different TLL and similar for both phases. Due to these phases' properties, a T_s longer than 6 h were obtained for the polymer/salt ABS, which was not adequate for carrying out the hydrodynamics' mixing-settling study. The PPG-400/[Ch]Cl ABS was no longer considered for the remaining work.

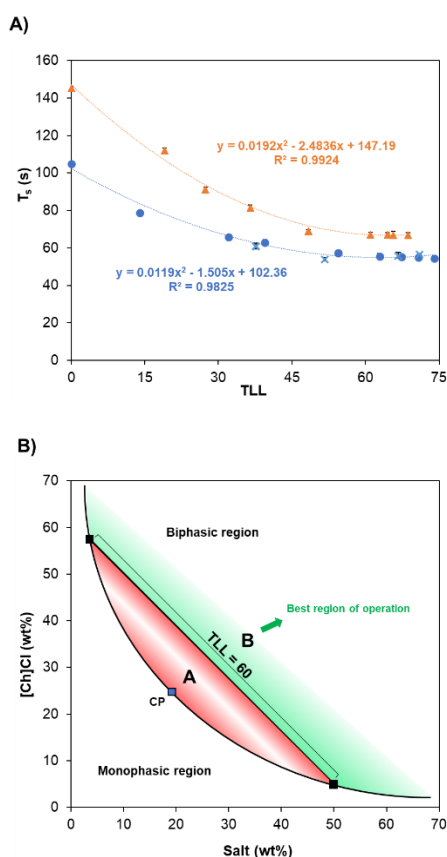


Figure 1. T_s values as a function of TLL at 25 °C (A) (● – mixture points of [Ch]Cl/ K_3PO_4 ; (▲ – mixture points of [Ch]Cl/ K_2HPO_4 ; × – mixture points from Shahrihari et al. [4]; and generic best region of operation for the studied [Ch]Cl-based ABS.

Both salt/salt ABS exhibited considerably faster phase settling times ($T_s < 150$ s) than the polymer/salt ABS. The coexisting phases of these two [Ch]Cl-based ABS exhibited a linear relation between density values and the increase in the TLL, being observed an increase in the densities of the inorganic salt-rich phases and a slight decrease in the densities of the [Ch]Cl-rich phases. This trend suggests that the salt/salt ABS have an easier phase separation compared to the studied polymer/salt ABS, due to the larger density difference ($\Delta\rho$) between the coexisting phases, mainly governed by the salt-rich phase densities. The concentration of the phosphate in the

salt-rich phase modifies the water ratio in the ABS, resulting in a larger difference in density ($\Delta\rho$) between the phases with the increase of salt content and promoting a quicker phase separation of ABS due to a higher rate of phase sedimentation [5]. The viscosity difference between the phases is smaller for the two salt/salt ABS, when compared to the PPG-400/[Ch]Cl system, leading to higher rates of drop coalescence and consequent faster phase separations [5].

T_s is independent of T_m since there are no significant changes of T_s for different T_m . The lower T_s for the system with K_3PO_4 is associated with its higher hydration ability in comparison to K_2HPO_4 , according to the Hoffmeister series [6]. The “stronger” salt being more strongly hydrated, retains more water molecules to the salt-rich phase, enhancing the phase separation and settling. In both salt/salt systems, this behavior results in more distinct phases’ physicochemical properties and a faster phase separation of the ABS [5]. Considering that the increase in TLL increases the salt-rich phase density and, consequently, the $\Delta\rho$ values between the coexisting phases, the distinct T_s registered for each salt/salt system were then correlated with the different salting-out ability of each phosphate salt used [6]. Figure 1.A shows that phase separation for both ABS decrease as the TLL becomes smaller, being maximum T_s at TLL=0 (CP) with an exponential decay from CP until TLL ≤ 60 . For TLL ≥ 60 , T_s becomes constant. These insights allow to establish a best operation region within the biphasic region of [Ch]Cl/salt ABS, *i.e.*, ABS’ hydrodynamics is maximum (region B from Figure 1.B).

Conclusions

In this work, the hydrodynamics of two distinct types [Ch]Cl-based ABS (polymer/salt and salt/salt systems) were compared and related with their phases’ physicochemical properties and characteristics of the phase-forming compounds. The system PPG-400/[Ch]Cl presented very poor hydrodynamics ($T_s > 6$ h), while the systems salt/salt systems presented very short T_s (< 150 s), overcoming one major drawback of conventional ABS. Density was the physicochemical property that most influenced the phase splitting ability of the salt/salt Abs, with the salting-out effect being the main drive-force of the ABS’ separation hydrodynamics. An optimal operation region inside the biphasic region of [Ch]Cl-based salt/salt ABS was defined, enabling their quicker and efficient industrial scale-up.

Acknowledgements

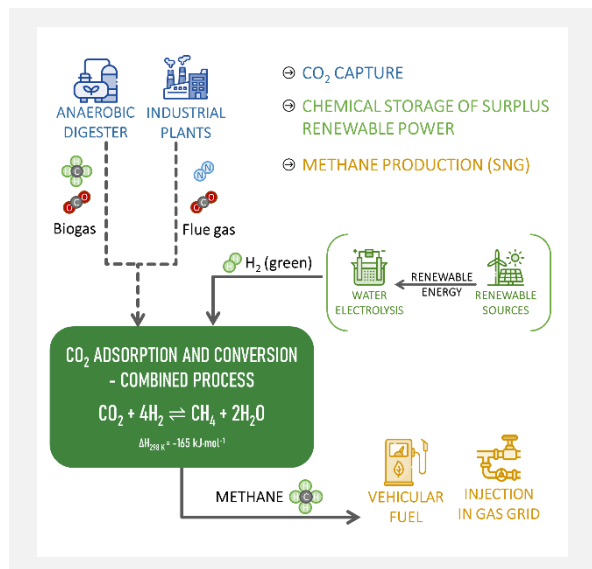
DRI/India/0044/2020 supported by Fundação para a Ciência e a Tecnologia (FCT). CIEPQPF thanks FCT for UIDB/EQU/00102/2020 & UIDP/EQU/00102/2020. CICECO thanks FCT/MEC (PIDDAC) for UIDB/50011/2020, UIDP/50011/2020 & LA/P/0006/2020.

References

- [1] J.F.B. Pereira, J.A.P. Coutinho, Aqueous Two-Phase Systems, in Liquid-Phase Extraction, Elsevier, 2020, 157-182.
- [2] J.F.B. Pereira et al., Fluid Phase Equilibria, 505 (2020) 112341.
- [3] S. Shahriari et al., RSC Advances, 3 (2013) 1835-1843.
- [4] J.C. Merchuket et al., Journal of Chromatography B: Biomedical Sciences and Applications, 711 (1998) 285-293.
- [5] Y.-V. Phakoukaki et al., Chemical Engineering Science, 265 (2023) 118197.
- [6] M.G. Freire, Ionic-Liquid-Based Aqueous Biphasic Systems. Berlin, Heidelberg: Springer Berlin Heidelberg, 2016.

CO₂ capture and valorization to synthetic natural gas – process integrationJ. Martins^{1,2*}, A. Rodrigues^{2,3}, L.M. Madeira^{1,2}¹LEPABE, Rua Dr. Roberto Frias, 4200-465 Porto, Portugal; ²ALiCE, Rua Dr. Roberto Frias, 4200-465 Porto, Portugal; ³LSRE-LCM, Rua Dr. Roberto Frias, 4200-465 Porto, Portugal.

*up201302933@fe.up.pt



The aim of this work is to study and optimize an integrated process for the simultaneous capture of CO₂ and its conversion to renewable CH₄. Two possible CO₂ sources are considered: flue gas streams (in which the CO₂ is diluted in N₂), and raw biogas (composed of CO₂ and CH₄). In a first step, the CO₂-containing stream is fed to an adsorptive reactor that contains two types of materials: a high-temperature CO₂ adsorbent and a methanation catalyst. The integrated process is carried out by periodically switching the inlet stream between i) CO₂-containing stream (adsorption stage), during which the CO₂ is captured, and ii) H₂, which reacts with the previously captured CO₂, simultaneously producing CH₄ and regenerating the adsorbent (reactive regeneration stage). To better understand and optimize the carbon capture and utilization (CCU) process, its performance will be assessed under different operating conditions, such as inlet flow rate, inlet switching time, temperature, pressure, catalyst/adsorbent ratio, amongst others, for each CO₂ source.

Introduction

In the framework of Carbon Capture and Utilization (CCU), carbon dioxide can be catalytically converted to methane through the Sabatier (or methanation) reaction, presented in Eq. (1).



In fact, among the possibilities for CCU, the synthetic natural gas (SNG), CH₄, arises as an attractive product, since it is a high-energy-density gas that benefits from the already existing natural gas distribution infrastructure [1]. From an environmental point of view, this process becomes even more sustainable if, in the context of Power-to-Methane, the H₂ used in the methanation reaction is produced using renewable energy, via water electrolysis (green H₂) [1]. As for the origin of the CO₂, several possibilities arise, for instance flue gas, a gas mixture released at industrial (e.g. cement or steel) and power plants, essentially composed of CO₂ (typically 5-30 % depending on the source) diluted in N₂, and other minor impurities [1]. Raw biogas is also an interesting CO₂-containing stream, generated at sewage treatment plants, landfills, or other sites for industrial and agricultural waste processing, composed of CO₂ (15-60 %) and CH₄ (which can be separated, becoming biomethane) [2].

In this work, the authors study an innovative CCU process in which the CO₂ capture by adsorption (from flue gas or biogas) and its catalytic conversion to SNG are carried out simultaneously and in the same unit, comprising two parallel adsorptive reactors [3,4]. To optimize the process, several operating conditions such as inlet flow rate, inlet switching time, temperature, pressure, and catalyst/adsorbent ratio are varied and their effects are assessed, for each CO₂ source.

Methods

As show in Figure 1, two columns were filled with a layered bed configuration containing two types of commercial materials: a CO₂ adsorbent (K-promoted hydrotalcite) and a methanation catalyst (Ru/Al₂O₃).

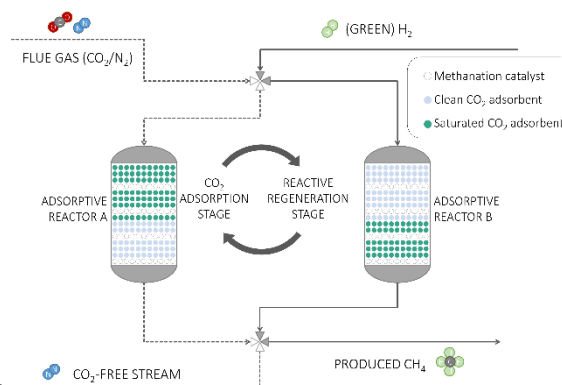


Figure 1. Scheme of the adsorptive-reactive unit using flue gas as feed during CO₂ adsorption stage.

In a first step, herein called CO₂ Adsorption Stage, the CO₂-containing stream (flue gas or biogas) is fed to the column and the CO₂ is retained in the adsorbent, while the remaining components (N₂ for flue gas or CH₄ for biogas) exit the unit. Figure 1 shows a scheme of the process if flue gas is considered as the source of CO₂. In this scheme Adsorptive Reactor A is in the CO₂ Adsorption Stage. As the CO₂ adsorbent approaches saturation, the inlet is switched from the CO₂-containing stream to pure H₂ that reacts with the previously captured CO₂ producing CH₄ (through the Sabatier reaction – Eq. (1)), and simultaneously regenerating the adsorbent, in a step called Reactive Regeneration Stage; in Figure 1, Adsorptive Reactor B is in such stage. To carry out the process the inlet streams are switched periodically, and the

reactors oscillate between the two stages, thus creating a continuous stream of produced CH₄.

In this work several experiments are carried out to study the performance of the cyclic adsorptive-reactive unit under different operating conditions such as inlet composition (flue gas or biogas), inlet flow rate and CO₂ content, switching time, temperature, and pressure amongst others.

The unit is operated until cyclic steady state is reached and the performance under the different conditions is evaluated through several performance indicators, namely CO₂ adsorption capacity, CO₂ conversion, the ratio of H₂ fed per CH₄ produced, and CH₄ purity and productivity, aiming at the process optimization.

Results and Discussion

For brevity reasons, the results presented herein will be focused on the effect of H₂ flow rate using flue gas as the CO₂-containing stream. Figure 2 (top graph) shows that the increase of the inlet flow rate during the Reactive Regeneration Stage has a positive effect on the CH₄ productivity (Prod_{CH₄} – the amount of CH₄ produced per catalyst mass and time unit), which goes from 0.48 to 1.32 mol_{CH₄}·kg_{cat}⁻¹·h⁻¹ as the H₂ flow rate is increased from 50 to 150 mL_N·min⁻¹.

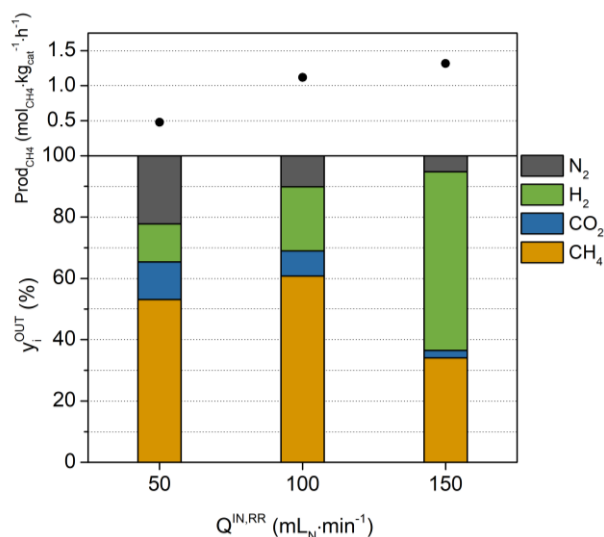


Figure 2. Effect of H₂ inlet flow rate ($Q^{IN,RR}$) on CH₄ productivity (Prod_{CH₄}) and on average outlet fraction components CH₄, CO₂, H₂, and CO during Reactive Regeneration Stage (y_i^{OUT}).

Acknowledgements

This work was financially supported by (i) LA/P/0045/2020 (ALiCE), UIDB/00511/2020 and UIDP/00511/2020 (LEPABE), funded by national funds through FCT/MCTES (PIDDAC) and (ii) Project “HyGreen&LowEmissions - Tackling Climate Change Impacts: the role of Green Hydrogen production, storage and use, together with low emissions energy systems”, with the reference NORTE-01-0145-FEDER-000077, supported by NORTE 2020, under the PORTUGAL 2020 Partnership Agreement, through ERDF. J.A.M. is grateful to the FCT for her Ph.D. grant (DFA/BD/4663/2020), financed by national funds of the Ministry of Science, Technology and Higher Education and the ESF through the POCH. The authors also acknowledge Sasol for supplying the adsorbent material used in this work.

References

- [1] K. Ghaib et al., Renewable and Sustainable Energy Reviews, 81 (2018) 433-446.
- [2] I. Angelidaki et al., Biotechnology Advances, 36 (2018) 452-466.
- [3] L. Madeira, et al., Cyclic adsorptive reactor for upgrade of CO₂/CH₄ mixtures, PCT/IB2022/052657.
- [4] J. Martins, et al., ACS Sustainable Chemistry and Engineering, 10 (2022) 7833-7851.
- [5] K. Coenen, et al., Journal of CO₂ Utilization, 25 (2018) 180-163

The reason for this is related to the influence of the H₂ flow rate on the efficiency of the regeneration of the adsorbent. As it is possible to observe in Eq. (1), the CO₂ methanation reaction produces steam, in addition to CH₄. The presence of H₂O molecules during the regeneration of hydrotalcite-based materials has been reported to significantly facilitate the desorption of CO₂, due to the existence of “exchange sites” in which the removal of the CO₂ molecule can only be achieved by its “substitution” by H₂O, and not by N₂ flushing, for instance [5]. Thus, as the inlet flow rate is increased from 50 to 100 and 150 mL_N·min⁻¹, the amount of CO₂ captured in the adsorbent (assessed by the CO₂ adsorption capacity, data not shown) is also raised from 0.17 to 0.19 and 0.31 mol_{CO₂}·kg_{ads}⁻¹, respectively. Since there is more captured CO₂ and more H₂, the amount of CH₄ produced in the Sabatier reaction is greater, resulting in higher productivity.

Regarding the CH₄ purity ($y_{CH_4}^{OUT}$ – also presented in Figure 2, bottom graph), the increase of the H₂ inlet flow rate is found to be beneficial only up to a certain point. The raise from 50 to 100 mL_N·min⁻¹ of H₂ reduces the fraction of N₂ and CO₂ in the outlet stream, increasing the CH₄ outlet content from 53 to 61 %, for the reasons described above. The further raise of H₂ flow rate causes the severe dilution of the outlet stream in unreacted H₂, decreasing the CH₄ purity to 34 %.

Thus, it is concluded that, in the tested conditions, the raise of H₂ inlet flow rate is beneficial to CH₄ productivity, although, above 100 mL_N·min⁻¹, it is at the expense of CH₄ purity.

The influence of the remaining operating conditions has been and will be further studied, presented and discussed for the case of CO₂ capture and valorization from both flue gas and biogas.

Conclusions

The proposed CCU process for CO₂ adsorption (from both flue gas and biogas) and its catalytic conversion to SNG in the same unit, has been successfully proven.

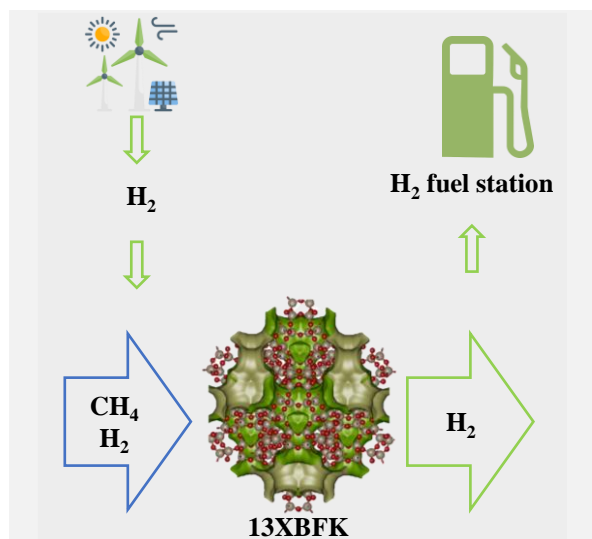
Furthermore, the process is studied under different operating conditions and it is concluded certain variables can have a substantial effect on the performance of the cyclic unit, and thus, should be carefully considered for the subsequent optimization. Methane purities above 70 % were achieved (considering CO₂ capture from flue gas), although it is expected that by optimization and manipulation of the operating conditions, the performance indicators will be further enhanced.

Green hydrogen recovery from natural gas grids by adsorption process

L.F.A.S Zafaneli^{1,2,3,4*}, A. Henrique^{1,2}, E. Aly^{1,2}, A.E. Rodrigues^{3,4}, J.A.C. Silva^{1,2}

¹Centro de Investigação de Montanha (CIMO), Instituto Politécnico de Bragança, Campus Santa Apolónia 5300-253, Bragança, Portugal; ²Laboratório Associado para a Sustentabilidade e Tecnologia em Regiões de Montanha (SusTEC), Instituto Politécnico de Bragança, Campus Santa Apolónia 5300-253, Bragança, Portugal; ³Laboratory of Separation and Reaction Engineering (LSRE), Associate Laboratory LSRE/LCM, Department of Chemical engineering, Faculty of Engineering, University of Porto, 4099-002 Porto, Portugal; ⁴Associate Laboratory in Chemical Engineering (ALiCE), Faculty of Engineering, University of Porto, 4200-465 Porto, Portugal.

*zafaneli@ipb.pt



In this work, the binder-free zeolite 13X was tested to purify green hydrogen injected into natural gas grids. Green hydrogen can be a key factor in meeting global energy demand while contributing to climate goals. In this way, breakthrough curve experiments were performed to assess the equilibrium and kinetic adsorption for H₂ and CH₄ in binder-free zeolite 13X. This work covers the lack of adsorption data and multicomponent breakthrough curves of H₂/CH₄ at low temperatures (until 195 K) which were not available in the literature. The equilibrium data were modeled by using the dual-site Langmuir isotherm model and the multicomponent breakthrough curves were simulated using a mathematical model implemented in MATLAB. Performance parameters based on equilibrium data were discussed. Overall, binder-free zeolite 13X has great potential to separate H₂ from CH₄ based on equilibrium (higher capacity for CH₄ with fast diffusion of both gases).

Introduction

The Green Hydrogen (GH) produced by water electrolysis from renewable sources of energy (e.g., wind, solar, and hydroelectricity) is free of carbon emissions, which can be a key factor in achieving climate goals [1], since it can replace fossil fuel in the mobility sector, for example (see the Graphical Abstract). As the interest in GH grows, the development of its distribution network is a hot topic in the scientific community. One alternative is to inject GH into the existing natural gas (NG) pipelines, to avoid new infrastructure investments [2-4]. One problem concerning the extraction of GH from NG grids relies on the feed concentration that differs greatly from conventional H₂ purification processes (usually H₂ > 70%). In this case, the GH allowed to be injected into the NG grids is limited to 20%. Thus, to improve the conventional purification process, an adsorbent with an increased adsorption capacity towards CH₄ is needed, compared to the ones available.

Methods

In this work, the commercial binder-free beads of zeolite 13X (13XBFK) evaluated were kindly provided by Chemiewerk Bad Köstritz GmbH (Germany). The beads of 13XBFK were manufactured through binder-free synthesis, in which the binder is itself transformed into zeolite matter during the hydrothermal reaction [5]. This procedure overcomes the loss in adsorption capacity associated with the binder composite. The adsorption equilibrium for H₂ and CH₄ were obtained through breakthrough curve experiments in a novel cryogenic fixed bed adsorption apparatus specially designed to screen materials at a wide range of temperatures (77 to 333 K) and pressures up to 4000 kPa [6]. The single and multicomponent breakthrough experiments were performed at 195, 231, and 273 K and pressure up to 1800 kPa. Figure 1 shows the equilibrium data for H₂ and CH₄ in 13XBFK and Table 1 summarized isotherm model parameters.

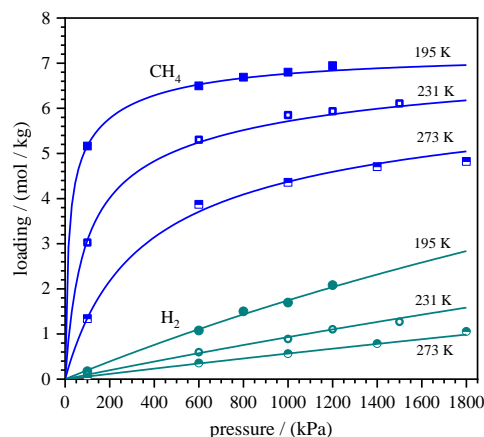


Figure 1. Adsorption equilibrium of H₂ and CH₄ on binder-free zeolite 13X. Symbol = experimental; Lines = model.

Results

According to the adsorption isotherm in Figure 1, the adsorption capacity for CH₄ on 13XBFK is significantly higher than for H₂ at the entire experimental conditions. For example, at 195 K and 100 kPa, the loading obtained for CH₄ is 5.20 mol/kg in contrast with 0.17 mol/kg for H₂, which results in a selectivity of 30 for CH₄ over H₂. These results indicate that 13XBFK has excellent potential for the equilibrium separation of H₂ from H₂/CH₄ by PSA. Lines in Figure 1 show the isotherm model that described very well the experimental data. The loadings of CH₄ were found to be 20% higher in the 13XBFK than the zeolite 13X manufactured by conventional pelletization using inert matter [7]. This result points out an opportunity to reduce the capital and operating costs of an industrial unit. Figure 2 shows the binary breakthrough curve for a mixture of H₂/CH₄ (20/80%) in the 13XBFK at 195 K and 1200 kPa. This experiment starts with a saturated H₂ column. According to

Figure 2, it is possible to obtain an H₂-rich stream (~100 %) in the column outlet for approximately 9 min, when CH₄ starts to leave the column, confirming the separation performance of 13XBFK. The lines in Figure 2 show the mathematical model results that agree very well with the experimental data. The mathematical model was developed based on the mass and energy balances in a fixed-bed adsorption process and was validated in the previous work [6].

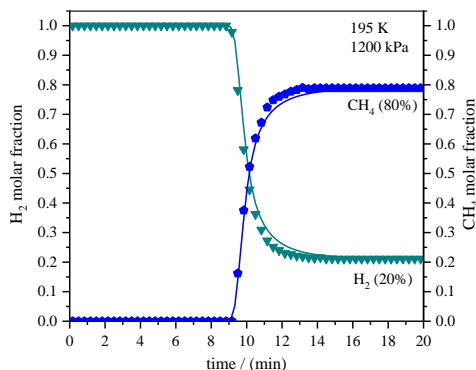


Figure 2. Binary breakthrough curve of CH₄/H₂ on binder-free zeolite 13X at 195 K. Symbol = experimental; Lines = model.

Figure 3 shows the CH₄ working capacity (WC) surface plot estimated taking into account the competitiveness between CH₄ and H₂ to the sites of 13XBFK by the extended dual-site Langmuir isotherm model. The WC is simply the difference between the loading in the adsorption and desorption conditions [8]. For the adsorption condition, it was considered 4000 kPa and 195 K for the mixture ratio of CH₄/H₂ (80/20%). In the case of desorption, it was considered a wide range of temperature (195 to 273 K) and pressure (5 to 500 kPa) for the same mixture ratio. Regarding the surface plot in Figure 3, the CH₄ WC increases as

desorption temperature increases and desorption pressure decreases, as expected.

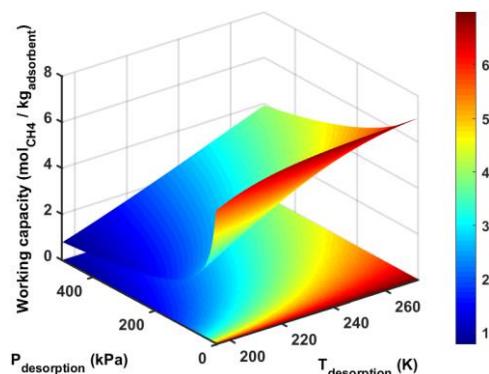


Figure 3. CH₄ working capacity surface plot for binder-free zeolite 13X.

A maximum WC of 7.00 mol of CH₄ per kg 13XBFK is achieved with 5 kPa and 273 K. Note that the desorption pressure has a major impact on the WC since it changes exponentially the WC whereas the desorption temperature seems to affect the WC linearly. This observation points out that 13XBFK is suitable to be used in the pressure swing adsorption process which works cyclically by changing rapidly the pressure between adsorption and desorption steps to obtain high performance of production and regeneration.

Conclusions

Overall, this work covers the lack of equilibrium data for CH₄ and H₂ at low temperatures (until 195 K) obtained through breakthrough curve experiments. Moreover, it was shown that the binder-free zeolite 13X has great potential to purify green hydrogen from natural gas pipelines. The data collected and the models developed are now being used to design a pressure swing adsorption process.

Table 1. Langmuir isotherm model parameters for CH₄ and H₂ on binder-free zeolite 13X.

Species	qm ₁ (mol/kg)	qm ₂ (mol/kg)	b ₁ (kPa ⁻¹)	b ₂ (kPa ⁻¹)	ΔH ₁ (kJ/mol)	ΔH ₂ (kJ/mol)
CH ₄	2.13	5.12	4.10×10 ⁻³	8.04×10 ⁻²	-16.1	-18.0
H ₂	12.65	-	1.60×10 ⁻⁴	-	-7.00	-

Acknowledgments

The authors are grateful to the Foundation for Science and Technology (FCT, Portugal) under project PTDC 2020 * 3599-PPCDTI * Engenharia dos Processos Químicos * project PTDC/EQU- EPQ/0467/2020. Also, through national funds FCT/MCTES (PIDDAC) to CIMO (UIDB/00690/2020 and UIDP/00690/2020), SusTEC (LA/P/0007/2021), ALiCE (LA/P/0045/2020), and LSRE-LCM (UIDB/50020/2020 and UIDP/50020/2020). Additionally, we thank national funding by FCT through the individual Ph.D. research grant SFRH/BD/7925/2020 of Lucas F. A. S. Zafaneli. Moreover, the authors are grateful to Kristin Gleichmann and Chemiewerk Bad Koestritz GmbH for kindly providing the binder-free beads of zeolite 13X studied in this work.

References

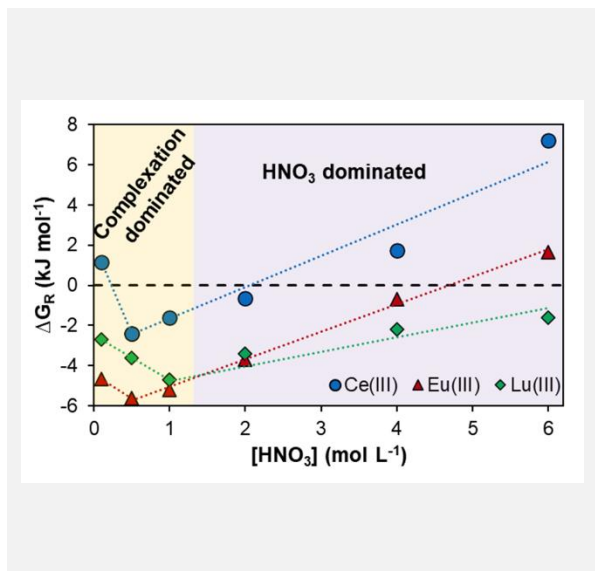
- [1] IRENA, Hydrogen from Renewable Power: Technology outlook for the energy transition. 2018. [Online]. Available: www.irena.org
- [2] IRENA, Hydrogen: a renewable energy perspective, 2nd ed., Tokyo: International Renewable Energy Agency, Abu Dhabi, 2019. [Online]. Available: www.irena.org
- [3] S. van Renssen, Nature Climate Change, 10 (2020) 799-801.
- [4] M.W. Melaina et al., Golden, National Renewable Energy Laboratory (2013).
- [5] K. Gleichmann et al., in Intech (2016) 13.
- [6] L.F.A.S. Zafaneli et al., Separation and Purification Technology, 307 (2023) 122824.
- [7] C.A. Grande, R. Blom, Energy & Fuels, 28 (2014) 6688-6693.
- [8] A.K. Rajagopalan et al., International Journal of Greenhouse Gas Control, 46 (2016) 76-85.

Solvent extraction in non-ideal eutectic solvents – application towards lanthanide separation

U.G. Favero¹, N. Schaeffer^{2*}, H. Passos², K.A.M.L. Cruz¹, D. Ananias², S. Dourdain³, M.C. Hespanhol¹

¹Group of Analysis and Education for Sustainability (GAES), Chemistry Department, Federal University of Viçosa (UFV), Viçosa, MG 36570-900, Brazil; ²CICECO - Aveiro Institute of Materials, Department of Chemistry, University of Aveiro, 3810-193 Aveiro, Portugal; ³Institut de Chimie Séparative de Marcoule, ICSM, CEA, CNRS, ENSCM, Univ Montpellier, BP 17171, Marcoule, 30207, Bagnols-sur-Cèze, France.

*nicolas.schaeffer@ua.pt



In this work, the extraction of lanthanides from nitrate media by the non-ideal hydrophobic eutectic solvent (HES) composed of decanoic acid and trioctylphosphine oxide was determined as a function of the lanthanide cation selection, HES molar fraction, HNO₃ concentration, and temperature. Special emphasis was placed on the determination of the relationship between the HES phase structuration and the extraction performance. All results point towards the need to explicitly consider the HES phase structuration and its compositional changes with solute co-extraction on the Ln³⁺ extraction as no change in the extracted complex speciation was observed across all tested conditions.

Objectives

The mutual separation of Ln³⁺, identified as one of the key separation challenges of the 21st century [1], occurs over 75 counter-current extraction stages and is conservatively estimated to account for 30% of the total associated environmental impacts of Ln³⁺ oxide production [2-3]. This generates substantial volumes of volatile and potentially toxic organic effluents due to relatively dilute operating conditions applied, from ppm levels to approximately 15 g L⁻¹ of target solute. In this context, the development of advanced functional solvents presenting increased efficacy with decreased environmental impacts is highly relevant. Hydrophobic eutectic solvents (HES) emerged as promising substitutes for the traditional apolar phase in SX. HES are low-melting binary mixtures that present interesting properties due to the liquefaction and enhanced solubility provided by the decrease of the melting point of the mixture when compared to those of the starting pure constituents [4]. Extractant molecules can be incorporated as one of the two components of a eutectic systems, acting both as the apolar phase former and chelating agent thereby allowing for greater extractant concentrations and more intensive separation processes. However, HES present a highly structured liquid phase defined by hydrogen-bonded interactions such that intercomponent interactions are expected to play a greater role in SX using HES compared to a diluted extractant solution. In this work, the extraction of lanthanides from nitrate media by the non-ideal solvent composed of decanoic acid (C₁₀OOH) and trioctylphosphine oxide (TOPO) was determined as a function of the lanthanide cation selection, HES molar fraction, HNO₃ concentration, and temperature [4].

Methods

Through the systematic variation of the listed parameters, the delicate balance between complexation and solvent reorganisation and its influence on the extraction and metal selectivity is determined by metal partition experiments, time resolved fluorescence and Raman spectroscopy, and small-angle X-ray scattering (SAXS).

Results

A maximum distribution for all lanthanides was observed for an aqueous phase acidity of 0.5 to 1.0 mol L⁻¹ HNO₃ with a preference for Eu³⁺, resulting in a sharp break in D_{Ln} between the adjacent Eu³⁺ and Gd³⁺ to yield an interesting SF_{Eu/Gd} of 1.8. The D_{Ln} decreased both with increased HNO₃ concentrations and C₁₀OOH content. However, this decrease was more pronounced for the light and middle Ln, allowing for a change in the extraction selectivity and a SF_{Lu/La} of 115 at 4.0 mol L⁻¹ HNO₃. The selectivity could be further tuned through the variation in α_{TOPO} but again at the expense of the maximum achievable D_{Ln}. Overall, the studied HES presented good D_{Ln} values across a range of acidities and exhibited a comparable selectivity to classical SX systems using non-ionic extractants whilst eliminating the need for volatile diluents and phase modifiers. Spectroscopic and SAXS analysis indicate that the change in extraction with α_{TOPO} and/or HNO₃ concentration is due to the modification of the HES phase composition and organisation rather than a change in the extracted complex. A compromise between maximum Ln³⁺ loading and selectivity was observed, driven by the variation in the quantity of weakly hydrogen-bonded TOPO and the change in the configurational entropy of the mixture. The C₁₀OOH+TOPO was used as a model system due as lanthanide extraction using TOPO and carboxylic extractants is well described whilst the phase diagram and properties of the eutectic are reported.

Conclusions

All results point towards the need to explicitly consider the HES phase structuration and its compositional changes with solute co-extraction on the Ln^{3+} extraction, which should vary based on the “depthness” (i.e. strength of intermolecular interaction) of the HES mixture. The derived conclusions are

translatable to other systems and can help guide the design and application of possible HES combinations for SX. Looking beyond the scope of this work, HES appear as promising model solvents to explore the role of H-bonding interactions in complex liquid phases and their link to SX

Acknowledgements

This work was partly developed within the scope of the project CICECO-Aveiro Institute of Materials, UIDB/50011/2020, UIDP/50011/2020, and LA/P/0006/2020, financed by national funds through the FCT/MCTES. This work was supported by the Instituto Nacional de Ciências e Tecnologias Avançadas (INCTAA)/Conselho Nacional de Desenvolvimento Científico e Tecnológico (CNPq) [grant number 465768/2014-8]; Fundação de Amparo à Pesquisa do Estado de Minas Gerais (FAPEMIG) [grant number CEX-PPM-00585-17]; CNPq [grant number 305649/2021-3, 131790/2020-0]; Coordenação de Aperfeiçoamento de Pessoal de Nível Superior (CAPES)/Fundação para a Ciência e Tecnologia (FCT) [grant number 88881.309048/2018-01]; CAPES [grant number 88882.437092/2019-01].

References

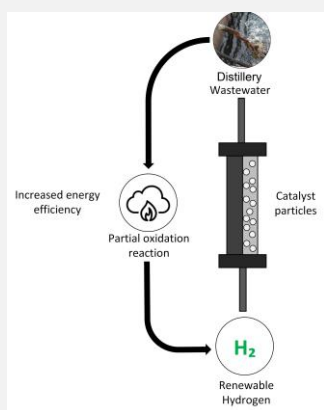
- [1] D.S. Sholl et al., *Nature*, 532 (2016) 435-437.
- [2] F. Xie et al., *Minerals Engineering*, 56 (2014) 10-28.
- [3] E. Vahidi et al, *Environmental Management*, 203 (2017) 255-263.
- [4] M.A.R. Martins, *Journal of Solution Chemistry*, 48 (2019) 962-982.
- [5] U.G. Faveiro et al., *Separation and Purification Technology*, 314 (2023) 123592.

Autothermal reforming of distillery wastewater for renewable hydrogen production

P. Cerqueira^{1,2*}, C. Rocha^{2,3}, M.A. Soria^{1,2}, L.M. Madeira^{1,2}

¹LEPABE, Department of Chemical Engineering, Faculty of Engineering, University of Porto, Rua Dr. Roberto Frias s/n, 4200-465 Porto, Portugal; ²ALiCE – Associate Laboratory in Chemical Engineering, Faculty of Engineering, University of Porto, Rua Dr. Roberto Frias, 4200-465 Porto, Portugal; ³LSRE-LCM, Department of Chemical Engineering, Faculty of Engineering, University of Porto, Rua Dr. Roberto Frias s/n, 4200-465 Porto, Portugal.

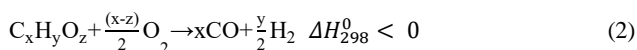
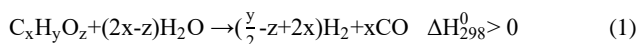
*up201505213@up.pt



The steam reforming and autothermal reforming of wine distillery wastewater were explored in this work, via simulation and experimentally, aiming to solve the problem of such polluted effluents while producing renewable hydrogen. Several synthetic distillery wastewater compositions were considered, based on the typically reported composition of the effluent. The Aspen Plus software was used to simulate the thermodynamic equilibrium conditions. The operating conditions assessed were temperature, pressure, steam-to-carbon (S/C) molar ratio and oxygen-to-carbon molar ratio. The results of the simulations showed optimal hydrogen production for temperatures of around 400-500 °C, pressure of 1 bar and higher S/C ratios for both the steam and autothermal reforming. As for the autothermal reforming, there is an inverse trend between hydrogen production and oxygen fed to the reactor (O₂/C ratio). Experimental validation is expected to follow these results soon.

Introduction

Distillery wastewater (DW) is a problematic effluent of the ethanol and wine spirits industry. It is a pollutant to the soil and water, and is produced in high volumes, with some estimates suggesting that, per liter of ethanol, 5 to 20 liters of wastewater are produced [1]. Solutions to this problem currently employed can be expensive, require multiple steps and are time consuming [2]. In this work, the steam reforming of said waste product is studied, exploring it thermodynamically and then validating the results with experimental data. The steam reforming of DW is an endothermic reaction that produces hydrogen by decomposing the organic oxygenated compounds present in the effluent (C_xH_yO_z) into H₂ and CO (Eq. 1) [3]. Furthermore, this process can be energetically improved by adding a sub stoichiometric amount of O₂ at the reactor inlet, which would promote the partial oxidation of DW (Eq. 2). The partial oxidation reaction still produces hydrogen, and is exothermic, making it possible to achieve thermally neutral operation, in the so-called autothermal reforming [4].



Methods

For the thermodynamic simulations, the Aspen plus software was employed, making use of the RGIBBS reactor. This approach makes use of the Gibbs free energy minimization method, arriving at the equilibrium composition according to the set inlet and operating conditions of the reactor [5]. The DW compositions (Mix 1 to Mix 5, presented in Table 1) were chosen according to the typical components present in the DW and concentrations reported in the literature [1,6].

For the experimental validation of the steam reforming of DW, a Ni and Ru (15 wt.% and 2 wt.%, respectively) based catalyst,

supported on SiO₂ and promoted with La₂O₃ (15 wt.%), was loaded into a fixed-bed reactor. The wastewater is then fed into the reactor, which is kept at high temperatures. Autothermal reforming has the same experimental procedure as steam reforming, but it uses an inlet of oxygen in addition to the DW inlet. Further details about the experimental set-up can be found elsewhere [7].

Table 1. Synthetic distillery wastewater composition in mg/L.

Component	Mix 1	Mix 2	Mix 3	Mix 4	Mix 5
Tartaric acid	5660	2460	2700	1700	7500
Malic Acid	11500	100	4000	500	7500
Succinic acid	11500	6000	4000	1600	2500
Acetic acid	2640	2710	1000	600	10000
Ethanol	130	500	500	300	820
Glucose	3400	4800	1750	1500	13090
D-Galactose	2500	0	1750	1500	0
Fructose	3400	2000	1750	1500	4480
Glycerol	4280	2220	7500	12500	7500
Phenol	600	750	250	500	2225
Gallic acid	600	750	125	250	2225
Caffeic acid	600	750	125	250	2225
Protocatechuic acid	600	750	125	250	2225
Syringic acid	600	750	125	250	2000

Results

The thermodynamic results obtained allowed the comparison of the hydrogen yield for the different DW compositions. Different conditions were also assessed, such as temperature (T= 300 – 1000 °C), pressure (P= 1- 20 bar), steam-to-carbon molar ratio (S/C= 1-60) and oxygen-to-carbon molar ratio (O₂/C= 0-0.3). These simulations revealed optimal hydrogen production for temperatures of around 400-500 °C (Figure 1), pressure of 1 bar and higher S/C for both the steam reforming and autothermal reforming (data not shown for brevity).

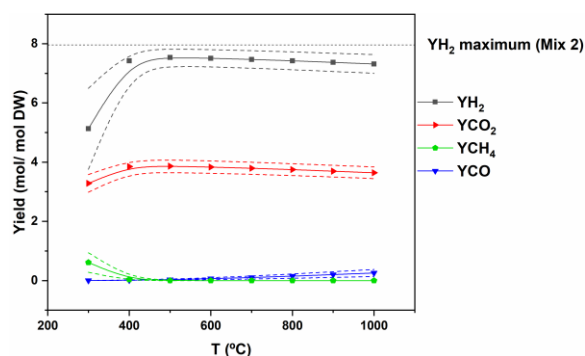


Figure 1. Effect of temperature on the gas products yield. Solid line and symbols show the average yield for all the compositions. Dotted lines show the DW composition with the highest and lowest yield of each product.

As for the autothermal reforming, there is an inverse trend between the hydrogen yield (Y_{H_2} , defined as the moles of H_2 produced per mole of DW fed) and the oxygen fed to the reactor (O_2/C) (Figure 2). The ideal situation for the autothermal reforming is thermally neutral operation, in which the heat from the partial oxidation of DW is enough to overcome the energy requirements of the overall reaction (shown in Figure 2 by the dotted line and symbols).

Further work will be focused on the experimental validation of the concept herein addressed, as done before for the reforming of other oxygenates (e.g. olive oil wastewater [5, 7]).

Acknowledgements

This work was financially supported by LA/P/0045/2020 (ALICE), UIDB/00511/2020 and UIDP/00511/2020 (LEPABE) and UIDB/50020/2020 and UIDP/50020/2020 (LSRE-LCM), funded by national funds through FCT/MCTES (PIDDAC) and by the Project NORTE-01-0247-FEDER-39789, funded by the European Regional Development Fund (ERDF) through the Programa Operacional Regional do Norte (NORTE 2020). This work was also funded by the project HyGreen&LowEmissions (NORTE-01-0145-FEDER-000077), supported by Norte Portugal Regional Operational Programme (NORTE 2020), under the PORTUGAL 2020 Partnership Agreement, through the European Regional Development Fund (ERDF). P. Cerqueira acknowledges the Portuguese Foundation for Science and Technology (FCT) for the PhD grant (2021.04726.BD). M. A. Soria thanks the Portuguese Foundation for Science and Technology (FCT) for the financial support of his work contract through the Scientific Employment Support Program (Norma Transitória DL 57/2017).

References

- [1] L. Fillaudeau et al., *Brewing, winemaking and distilling: an overview of wastewater treatment and utilization schemes (Part IV - Chapter 35), Improving Water and Energy Management in Food Industry*, Woodhead Publishing Limited, 2008.
- [2] T.L. Phuong, M. Besson, *Energies*, 12 (2019) 3974.
- [3] C. Italiano et al., *International Journal of Hydrogen Energy*, 44 (2019) 14671-14682.
- [4] Y.S.M. Camacho et al., *Clean Technologies and Environmental Policy*, 19 (2017) 1437-1447.
- [5] C. Rocha et al., *Journal of the Energy Institute*, 92 (2019) 1599-1609.
- [6] B. Díaz-Reinoso et al., *Chemical Engineering Journal*, 327 (2017) 210-217.
- [7] C. Rocha et al., *Renewable Energy*, 41 (2021) 765-779.

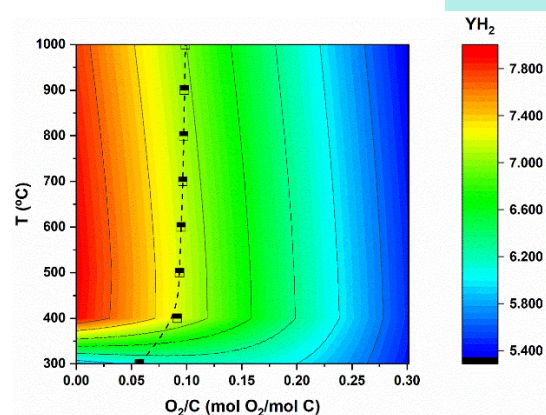


Figure 2. Effect of O_2/C ratio and temperature on hydrogen yield for Mix 2. Dotted line and symbols show thermally neutral operation.

Conclusions

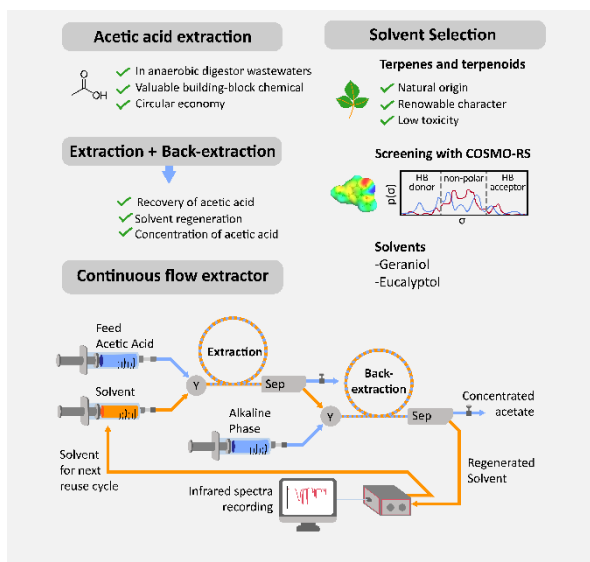
The simulations showed that significant hydrogen production is possible from reforming of DW, revealing the ideal operating temperature, pressure, and S/C. The autothermal reforming was simulated, showing reverse proportionality between the amount of oxygen fed and hydrogen yield; it is possible, however, to achieve thermally neutral operation (heat generated equals heat dissipated) without significant hydrogen loss.

A novel continuous flow multiphase installation for terpene-based extraction of acetic acid from wastewater streams

D. Rodríguez-Llorente^{1*}, J.C. de Mello², J. García¹, M. Larriba¹

¹Catalysis and Separation Processes Research Group (CyPS) of the Complutense University of Madrid, Avda. Complutense s/n, 28040, Madrid, Spain; ²Department of Chemistry, Norwegian University of Science and Technology, Høgskoleringen 5, Trondheim, Norway.

*diegor06@ucm.es



The production of Volatile Fatty Acids in wastewater can be harnessed for a circular economy, with acetic acid being the most abundant. Liquid-liquid extraction is a suitable technique, and terpenes such as geraniol and eucalyptol have been found to be effective solvents. A continuous flow multiphase installation with membrane separators has been used to extract acetic acid and regenerate the solvents with an alkaline solution. Geraniol outperforms eucalyptol in extraction yields, with a 50% yield at a Solvent/Feed ratio of 2.0. Back-extraction achieves complete solvent regeneration, and increasing the back-extraction factor to 40 can concentrate the acetic acid in the alkaline phase up to 6.5 times the initial concentration in the feed. In addition, the stability of the solvents was verified by FTIR.

Introduction

Wastewater treatment plants produce volatile fatty acids (VFAs) as a byproduct of anaerobic digestion, and acetic acid is the most produced VFA. If VFAs can be efficiently recovered from wastewater effluent, they can be used to produce high-value chemicals and reduce the environmental impact of non-renewable petrochemical sources [1,2].

Liquid-liquid extraction (LLE) is a potential method for extracting VFAs, but there is a need for sustainable, low-toxicity solvents. Terpenes and terpenoids are renewable, non-toxic, and have good solvating properties, making them attractive solvents for VFA extraction [4]. Reactive back-extraction (RBE) is an efficient method for separating extracted VFA molecules from the extracting solvent [5].

Objectives

The objectives of this work are to investigate the use of geraniol and eucalyptol as solvents for extracting acetic acid from anaerobic digester effluents, and to develop an integrated flow-based system for VFA extraction and solvent regeneration. Geraniol was chosen due to its effectiveness as an extractant for VFAs, while eucalyptol was selected based on an initial screening of terpenes using the COSMO-RS method. The use of flow chemistry in LLE processes is also explored, as it offers several advantages over traditional batch processes and can be used to optimize the efficiency and cost-effectiveness of extraction processes [6].

Methods

Activity coefficients at infinite dilution of acetic acid in 42 terpenes were calculated at a temperature of 298.2 K using COSMOtherm software. The solvents selected from the molecular simulation were geraniol and eucalyptol.

The fluidic system used in Figure 1 is based on a small number of fluidic components linked together by PTFE tubing. The extraction/back-extraction procedure involved four discrete steps, which included bringing the aqueous source solution into intimate contact with the organic solvent, separating the source solution and the organic phase, bringing the organic phase into intimate contact with an alkaline solution to effect a back-extraction of the target ions into the aqueous phase, and separating the organic phase and the alkaline solution. The separation of the immiscible solvents in the extraction and back extraction steps can be performed using liquid-liquid separators based on porous membranes, exploiting differences in the wettability of the phases. Additionally, an in-line FTIR was added to the solvent outlet to check its stability, as seen in the scheme of the Graphic Abstract.

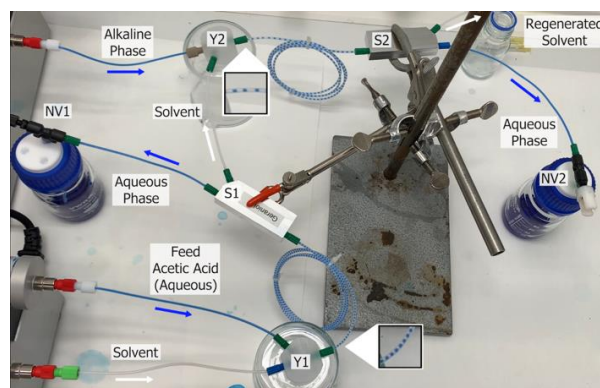


Figure 1. Set-up employed in this work for extraction and back-extraction of acetic acid. Extraction at Solvent/Feed ratio in volume of 1.0. Back extraction at Alkaline Phase/Solvent ratio of 2.0. A blue dye was used in the aqueous phases for visualization.

The aqueous phases were analyzed by HPLC and the water content in the solvents by Karl-Fischer titration.

Results

The results of the back-extraction factor study are shown in Figure 2. This graph shows the ratio of the acetic acid concentration in the alkaline phase (N), and in the raffinate (R), to the initial concentration (C_0) in the feed (F). The C/C_0 ratio in the raffinate (R) will remain constant as the extraction conditions are constant in the system. The higher the extraction rate, the lower these values will be, but the C/C_0 ratio in the alkaline phase (N) will increase. In this case, if it is greater than 1, it would mean that a more concentrated stream of acetate is being obtained, even if the yields are not 100%.

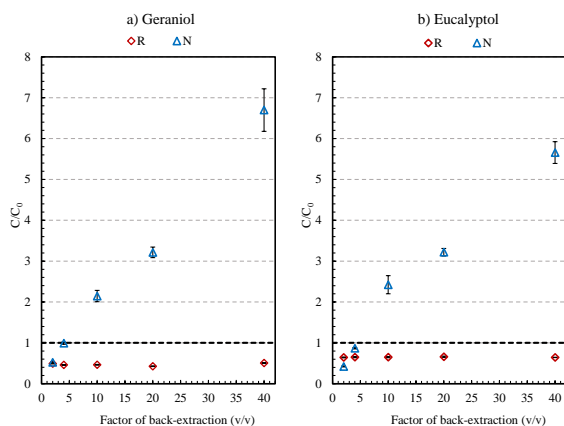


Figure 2. Acetic acid concentration ratio in Raffinate (R) or alkaline phase (N) and initial in Feed (C_0) using geraniol and eucalyptol as a function of the back-extraction factor (Extract/Alkaline Phase) in volume. A total (Solvent (S)+Feed (F)) flow of 200 $\mu\text{L}/\text{min}$, with an S/F ratio of 2.0 and a C_0 of 5 g/L, were employed.

In this study, it was possible to operate with very high back-extraction factors, in this case up to 40, observing a high mass transfer. Geraniol reaches the initial concentration at a back-extraction factor of 5, while eucalyptol still does not exceed it due to lower extraction yields. Interestingly, the results at back-extraction factors of 10 and 20 with eucalyptol are similar to those obtained with geraniol. The advantage of using this system is that it allows regenerating of these renewable solvents and using them again in the extraction process in a cyclic process.

A solvent reuse study was then performed, analysing the stability of the solvents after the back-extraction process. Figure 3 shows the results with geraniol (a) and eucalyptol (b) extraction yields as well as the C_N/C_0 ratio of concentration of acetic acid in the alkaline phase (N), to the initial concentration (C_0) in the Feed (F), at each solvent reuse stage up to a total of 10 stages.

Acknowledgements

The authors thank Comunidad Autónoma de Madrid for the financial support of Projects P2018/EMT-4341 and PR65/19-22441. This work has been supported by the Madrid Government (Comunidad de Madrid, Spain) under the Multiannual Agreement with Complutense University in the line Program to Stimulate Research for Young Doctors in the context of the V PRICIT (Regional Programme of Research and Technological Innovation). Diego Rodríguez-Llorente thanks Ministerio de Ciencia, Innovación y Universidades, for awarding an FPU grant (FPU18/01536). In addition, the Impact Fund of NTNU Nano for HPLC analysis is gratefully acknowledged.

References

- [1] S. Wainaina et al., *Bioengineered*, 10 (2019) 437-458.
- [2] R.J. Jones et al., *Bioresource Technology Reports*, 16 (2021) 100826.
- [3] B.D. Ribeiro et al., *ACS Sustainable Chemistry & Engineering*, 3 (2015) 2469-2477.
- [4] L.M.J. Sprakel, B. Schuur, *Separation and Purification Technology*, 211 (2019) 935-957.
- [5] R. Porta et al., *Organic Process Research & Development*, 20 (2016) 2-25.

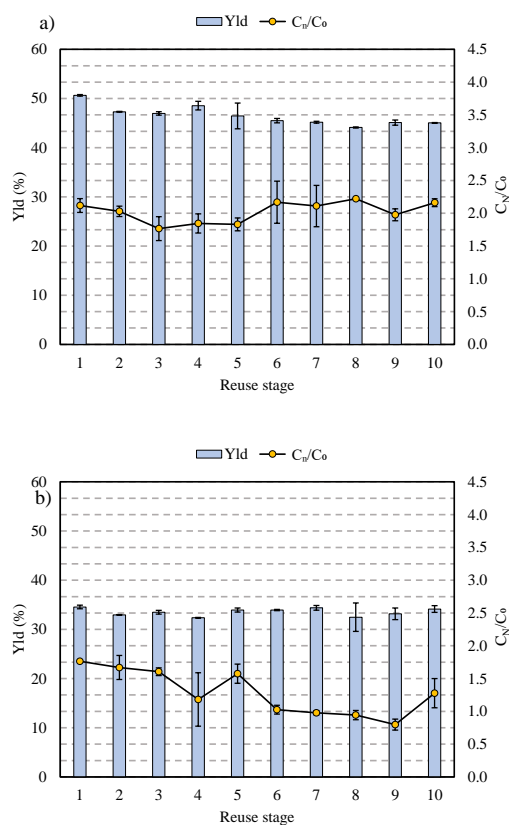


Figure 3. a) Geraniol b) Eucalyptol reuse cycles. Extraction yields and acetic acid concentration ratio between N and initial in Feed (C_0) are presented. A total (Solvent+Feed) flow of 200 $\mu\text{L}/\text{min}$, with an S/F ratio of 2.0, C_0 of 5 g/L, and a back-extraction factor (Extract/Alkaline Phase) in volume of 10 were employed.

Therefore, eucalyptol and, to a greater extent, geraniol are suitable for regeneration and reuse with NaOH 1 M, being stable in the system as it has been proved after 10 cycles of reuse and maintaining extraction and back-extraction yields. In addition, adding HCl to neutralise any alkali that may remain in the solvent before reuse in the extraction process is unnecessary. The stability of solvents was checked with the in-line FTIR.

Conclusions

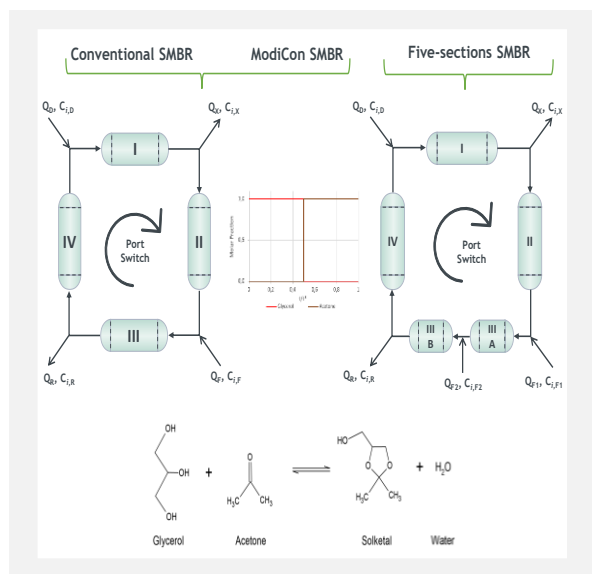
For the first time, a novel continuous flow multiphase installation the extraction and alkaline back-extraction of acetic acid has been experimentally performed. The results show how the continuous flow system of extraction and back-extraction with membranes is stable in the process and allows the coupling of these two operations. The alkaline back-extraction is efficient in the concentration of acetic acid and complete regeneration of solvents, enabling their reuse in solvent reuse cycles.

Enhanced simulated moving bed reactor performance for the synthesis of solketal by implementing the ModiCon strategy

*L. Corrêa**, *R.P.V. Faria*, *A.E. Rodrigues*

Laboratory of Separation and Reaction Engineering - Laboratory of Catalysis and Materials (LSRE-LCM), Rua Dr. Roberto Frias, s/n, Porto, Portugal; ALiCE - Associate Laboratory in Chemical Engineering, Rua Dr. Roberto Frias, s/n, Porto, Portugal.

*up201902799@up.pt



The Simulated Moving Bed Reactor (SMBR) is a sorption-enhanced reactive technology that has been successfully applied to the synthesis of several organic compounds, due to its ability to overcome the thermodynamic limitations associated with reversible reactions. However, the Conventional SMBR for solketal synthesis performs poorly, due to miscibility limitations between the reactants and selectivity issues between the reaction species. This work proposes the implementation of the ModiCon (modulated feed concentration) strategy to enhance the reactants contact and to improve the separation. Due to its industrial relevance, the synthesis of solketal from glycerol and acetone was selected as case-study. The results demonstrate that the new SMBR operating mode can produce solketal with a purity of 97%, reaching a productivity of over $8 \text{ kg}_{\text{Solk}} \cdot \text{L}_{\text{Ads}}^{-1} \cdot \text{day}^{-1}$, proving it is possible to produce solketal in a continuous chromatographic reactor.

Introduction

Solketal is a promising fuel additive that arises as a solution for the glycerol gut generated by the biodiesel industry. Besides improving the quality of the fuel, reinserting solketal in the biodiesel production chain complies with the Circular Economy model, which is of great economic and environmental interest. For solketal synthesis, equimolar amounts of glycerol and acetone react, forming water as by-product. The reaction is reversible, therefore it is thermodynamically limited. The SMBR is a sorption-enhanced Process Intensification (PI) strategy that improves the efficiency of reactive systems by combining separation by adsorption and chemical reaction using a hybrid stationary phase with catalytic activity and adsorption selectivity between the products. This way, by removing the products from the reaction medium, the equilibrium shifts towards product formation.

The Conventional SMBR is constituted of four sections with synchronous time switch (t^*), constant flow rates, and a feed stream composed of glycerol and acetone diluted in ethanol. Solketal production with this operation is limited due to miscibility issues between the reactants, the very different affinities of the reactants with the stationary phase, which gets them separated soon after being fed, and the very similar affinity of acetone and solketal, which makes the raffinate stream prone to contamination [1].

To overcome the issues of the Conventional SMBR, Faria et al. proposed the Five-section SMBR, a non-conventional operating strategy in which the reactants are fed in different positions. This way, Section III of the Conventional SMBR is divided into Section IIIa and IIIb. Due to the different retention of acetone and glycerol with the stationary phase, a counter-current movement between these species is promoted and the overall performance of the unit is enhanced [1].

In the present work, an SMBR with modulated feed stream concentration throughout t^* (ModiCon) was implemented for

the first time to produce solketal. In this alternative SMBR, glycerol is fed in the first fraction of t^* followed then by acetone. This is another non-conventional operating strategy based on the concept of promoting counter-current contact between the reactants, which maximizes their interaction and, consequently, the solketal's output. Since these two non-conventional operations are based on a similar principle to improve the process performance, they are compared with each other and with the Conventional SMBR in terms of productivity, desorbent consumption (DC) and Reactive Separation Region (RSR).

Methods

The SMBR simulation studies were performed considering a pilot unit with eight fixed-bed columns (15 cm in length and 2.12 cm in diameter).

The optimizations of the Conventional and Five-section SMBR were performed following the two steps procedure proposed by Faria et al. The TMBR steady-state model is used to find the feed and extract flowrates, and solid velocity (decision variables) that result in the maximum productivity (objective function), under the purity constraints of 97% (desorbent free) for solketal in the raffinate stream and water in the extract stream. In the first step, the optimal unit configuration (number of columns in each section) was defined. Then, for the best column configuration, a sensitivity analysis was carried out to the safety factor (SF) applied to sections 1 and 4 (solid and liquid regeneration sections) [1].

The ModiCon strategy is a dynamic operation, therefore it requires the equations to be solved dynamically until reaching the cyclic steady state. This makes it unviable to reproduce the same methodology, that relies on the steady-state model. The rigorous SMBR must be used instead. Thus, the column configuration and SFs that achieved the highest productivity in the Conventional SMBR and the t^* that achieved the highest in

the Five-section SMBR were used as inputs for the ModiCon. Then, sensitivity analyses of t^* and of the amount of each reactant fed to the unit (fraction of t^*) were performed to verify how they affect the unit performance.

The model equations were solved using gPROMS®, v. 7.0.7.

Results and Conclusions

The study on the column configuration on the Conventional SMBR reveals that the best productivity is achieved for the 1-2-4-1 configuration. Since acetone is carried in the direction of the fluid flow, most of the reaction takes place in Section III, and this reactant is present in significant amounts only in the column immediately before the feed port, therefore there was no need for more than two columns in Section II. The reaction thermodynamic limitation seems to be what hinders the performance of the Conventional SMBR since it is necessary more columns in the sections assigned for this purpose. As for the regeneration sections, there is no need for more than one column in each section to satisfactorily perform this task.

From the sensitivity analysis to the SF, the combination that achieves the highest productivity in the studied range and that provides a sufficient equivalence between the TMBR and the SMBR is 40% in Section I and 15% in Section IV. At this point, t^* is 25.7 min and the productivity is $1.086 \text{ kg}_{\text{Solk}} \cdot \text{L}_{\text{Ads}}^{-1} \cdot \text{day}^{-1}$ and the DC is $26.24 \text{ L}_{\text{Desorbent}} \cdot \text{kg}_{\text{Prod}}^{-1}$.

The study on the column configuration of the Five-section SMBR reveals that the reaction and the separation of acetone and solketal take place almost exclusively in Section IIIB. Also, the performance is strongly driven by the available reactive region. The only possible configuration to maximize the number of columns in Section IIIB is 1-1-1-4-1.

From the sensitivity analysis to the SF, the combination that achieves the highest productivity in the studied range and that provides a good equivalence between the TMBR and the SMBR models is 40% in Section I and 25% in Section IV. At this point, t^* is 23.14 min and the productivity is $7.03 \text{ kg}_{\text{Solk}} \cdot \text{L}_{\text{Ads}}^{-1} \cdot \text{day}^{-1}$, with a DC of $5.02 \text{ L}_{\text{Desorbent}} \cdot \text{kg}_{\text{Prod}}^{-1}$. It is noteworthy that at this point the reactants feed ratio is 1.03, which results in an excess of acetone of nearly 5%.

For the ModiCon operation, such acetone excess is granted when pure glycerol is fed during 49% of the t^* and pure acetone in the remaining time. The performance of the ModiCon SMBR is slightly superior to the Five-section SMBR. Using the t^* of 23.14 min and a combination of SF of 40% and 25%, the productivity reaches $8.13 \text{ kg}_{\text{Solk}} \cdot \text{L}_{\text{Ads}}^{-1} \cdot \text{day}^{-1}$ with DC of $4.30 \text{ L}_{\text{Desorbent}} \cdot \text{kg}_{\text{Prod}}^{-1}$. The comparison of the RSR provided in Figure 1 shows the larger ModiCon RSR compared to the Five-section and the Conventional. This indicates the first may have a more robust operation.

Acknowledgements

This work was financially supported by LA/P/0045/2020 (ALiCE), UIDB/50020/2020 and UIDP/50020/2020 (LSRE-LCM), funded by national funds through FCT/MCTES (PIDDAC). Isabella Corrêa gratefully thanks the FCT – Fundação para a Ciência e a Tecnologia for the Doctoral Grant (2020.07258.BD) through NORTE2020 – Programa Operacional Regional do Norte from the FSE – Fundo Social Europeu of the UE.

References

[1] R.P.V. Faria et al., Industrial & Engineering Chemistry Research, 61 (2022) 14531-14545.

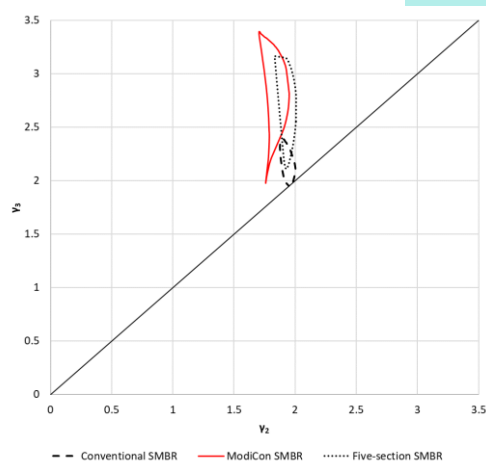


Figure 1. RSR of the Conventional, Five-section and ModiCon SMBR (operational conditions mentioned in the text).

The sensitivity analysis to t^* was performed by varying this variable between 85% and 105% of the optimal t^* . The maximum productivity was achieved for a t^* of 20.4 min ($90\% \cdot t^*$). As for the sensitivity to the fraction of t^* dedicated to the feed of each species, the optimum is achieved in the base case, which means when pure glycerol is fed during 49% of t^* . This proves the system is strongly driven by the chemical reaction thermodynamic equilibrium. The sensitivity analysis to the SFs reveals that the best combinations are 40% and 15%, 40% and 25% and 30% and 15%. Among these results, there is almost no change in productivity, however, when operating with the combination 30% and 15%, the DC is 19% reduced compared to 40% and 25%.

The productivity results of both non-conventional operations are within the range reported for similar processes and prove that solketal can be produced by a continuous chromatographic reactor. The major advantage of using such strategies is the possibility of operating with higher flow rates and, consequently, obtaining better performance parameters.

It is noteworthy that between the proposed non-conventional operation, the ModiCon strategy can achieve a productivity 14% higher due to being able to process an even higher feed flow rate while achieving a DC 14% lower. Also, the ModiCon practical implementation requires fewer modifications to the physical equipment.

The ModiCon SMBR is a non-conventional PI strategy that enhances the efficiency of an already intensified equipment. Using the same unit and the same amount of catalyst, it was possible to process higher feed flow rates even when compared to the Five-section SMBR. Such improvement is due to the enhanced contact of the reactants, which improves the conversion and promotes the better separation of acetone from solketal (withdrawn in the raffinate port).

Optimization of supercritical fluid extraction and reactionsystems for unque application requirements

*J. Carvalho**, *S. Cardoso*

Paralab S.A., Portugal.

**joao.carvalho@paralab.pt*



Supercritical fluids (SCFs), with their unique properties and tunability, are powerful alternatives to traditional organic solvents, enabling a wide range of processes in chemical and biological engineering. They facilitate the selective extraction of valuable or undesirable compounds from solids, the fractionation of liquids, and the impregnation of porous materials. SCFs also support particle formation processes and increase chemical reaction rates with improved selectivity. Their potential to inactivate microorganisms is valuable for sterilization in medical and food applications.

In addition, supercritical CO₂ offers a "green" solution by replacing toxic solvents and minimizing the need for solvent clean-up operations.

By customizing equipment design, we can fully exploit the unique properties of supercritical fluids for specific applications. We have the ability to fine-tune systems to match the scale of operation, desired throughput, and particular compounds in focus. As a result, the inherent versatility of SCFs is used to meet a wide range of application requirements, providing customized, efficient and environmentally sustainable solutions.

RDI at Bondalti

F. Franco

Bondalti Chemicals S.A., Rua do Amoníaco Português nº10 3860-680, Estarreja, Portugal.

filipa.franco@bondalti.com

BONDALTI

TOMORROW MATTERS®

Bondalti is committed to contributing to a better world by creating innovative and sustainable chemistry, in which the energy transition plays a main role in its growth strategy. The company is in the Top 1% of the most sustainable companies in the sector worldwide, according to the EcoVadis global ranking.

Bondalti has industrial facilities in Estarreja (Portugal), Cantabria and Rioja (Spain), logistics facilities in Aveiro, Barreiro (Portugal) and Vigo (Spain), operations in Luanda (Angola) and offices in Lisbon (HQ) and Madrid. The company in 2022 employed around 700 people and recorded a sales volume of around 600 million euros.

Introduction

As a leading chemical industry with a competitive position in the market where it operates, Bondalti core business is the production of Chlor-Alkali (PCA), in the inorganic chemical segment, and Aniline and Derivatives (PAD), in the segment of organic chemicals. Currently Bondalti is the largest Iberian producer of chlorine and hypochlorite and European leader in sales of aniline and mononitrobenzene (MNB), as well as one of the world's leading non-integrated aniline producers. To produce its chemical products, Bondalti relies on two industrial units that are dependent on raw materials such as benzene, salt, ammonia and hydrogen, as well as utilities such as electricity. Bondalti is a national reference in the hydrogen (H₂) value chain, as it is the second largest Iberian producer of H₂ without direct use of natural gas.

Bondalti operates in the Water Treatment solutions market in Portugal, Spain and Angola, as well as globally, exporting solutions all over the world since 2020. In this business area, Bondalti specialises in two large groups of complementary activities:

- Design and Engineering: Design, production, marketing and installation of highly reliable and competitive water and wastewater treatment equipment and solutions.
- Maintenance and Operation: follow-up of each client with an offer of continued support, including comprehensive management, operation, preventive and/or corrective maintenance, while maintaining a close relationship with the client's interlocutors.

Bondalti is developing a green hydrogen project, the "H₂Enable", which was recently recognized as an IPCEI-H₂ project by the European Commission, having also been approved in 2022 for funding under the Recovery and Resilience Plan. The project is in line with the European decarbonisation and reindustrialisation goals, based on advanced, intelligent, and efficient technologies, low environmental impact, orientation towards more qualified products with greater added value, as well as the principles of circularity.

Bondalti seeks to operate in the purification and refining segment, producing lithium hydroxide. The main reason is the possibility for Bondalti to adapt its brine electrolysis technology used in the chlor-alkali sector for several decades,

and replace conventional processes, which have a larger carbon footprint and higher costs, with this process powered by electricity from renewable sources. In addition to lithium hydroxide, this process results in chlorine and hydrogen, by-products that are easily integrated into Bondalti's current value chains.

RDI at Bondalti

Innovation is considered one of the main drivers for sustainable development and increasing competitiveness in the markets where the company operates. Bondalti continuously invests in RDI activities, promoting technological capacity and the active involvement of all employees in continuous improvement.

With a view to respond to future challenges, Bondalti has developed several innovation projects to implement solutions to achieve carbon neutrality in its industrial operations and disruptive projects in line with its business profile.

In 2022 some of these projects led to 8 applications for funding opportunities, within the scope of the Environmental Fund, the Foundation for Science and Technology (FCT) and the Recovery and Resilience Plan (PRR).

Table 1. RDI key results at Bondalti

	2020	2021	2022	Δ (abs)
Expenses and investment in RDI	3.3 M€	2.7 M€	3.2 M€	0.5M€
Employees involved in RDI activities	22%	10%	9%	-
PhD/Post-doc grant projects	3	3	2	-1
Ongoing RDI projects	52	36	39	3
RDI partnerships	24	41	68	27
Patent families*	3	4	4	0
Scientific papers/presentations	1	3	13	10

* Bondalti Chemicals

Monitoring of fermentation processes

E. Monteiro^{1}, R. Rocha¹, H. Lutz²*

¹Bruker Portugal, Lisboa, Portugal; ²Bruker Optik GmbH, Ettlingen, Germany.

**eva.monteiro@bruker.com*



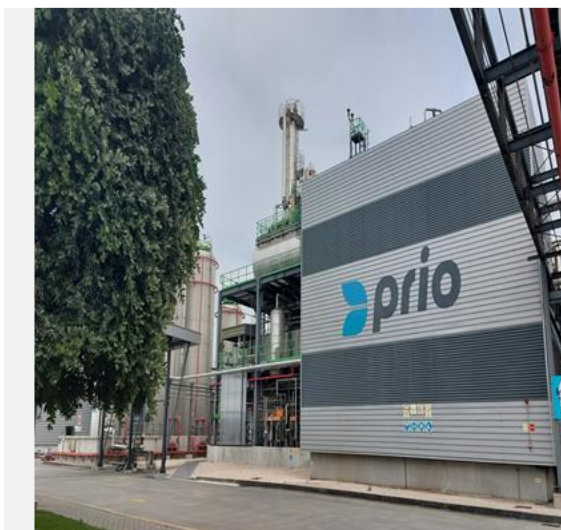
Fermentation is a very complex process and many parameters can affect the final alcohol content and overall yield. In the industry today, most distilleries or fuel ethanol plants use HPLC (high performance liquid chromatography) for fermentation monitoring, including measurements of sugars, acids, glycerol, and alcohol. All these components are interrelated and it is very important to keep track of them at each stage of the fermentation, but there are disadvantages to use HPLC. On the contrary, NIR analysis is fast, can simultaneously determine multiple components per measurement and allow to online monitoring of fermentation processes (continuous control), which is an essential part of the manufacturing process. With FT-NIR each of the steps can be controlled starting from the raw materials over the fermentation and distillation/rectification to the final (bio)ethanol. Especially for the fermentation and the distillation NIR in-line technology is an option which provides best opportunities for real time process control to optimize yield and processing time.

Six Sigma methodology applied in biodiesel production

F. Pereira

PRIO Bio, TGL – Terminal de Granéis Líquidos, Lote D-Porto de Aveiro, 3834-908, Gafanha da Nazaré, Portugal.

filipa.pereira@prio.pt



Since 2006, PRIO has created an integrated value chain that embraces storage, distribution and commercialization of liquid fuels and LPG as well as a biodiesel production plant – PRIO Bio.

The plant operates mainly with residual raw materials, such as used cooking oils and other lipid residues, allowing wastes valorisation and a faster decarbonization in the transportation sector.

Process optimization, when working with residues, is challenging due to the high variability of quality specification in residual feedstock. Therefore, innovation strategies are applied to overcome obstacles and to promote competitiveness.

Focusing on data driven process solving, Six Sigma is one of the methodologies applied in PRIO Bio and was used to predict one of the biodiesel quality parameters – cold filter plugging point (CFPP).

This project allowed to improve the necessary steps to process optimization by supporting rapid decision-making.

In more than 15 years, PRIO has created an integrated value chain that embraces storage, distribution and commercialization of liquid fuels and LPG (having a tank terminal located in Aveiro for stockage and primary logistics), as well as a biodiesel production plant.



Figure 1. PRIO business areas.

PRIO Bio is the biofuel production unit where can be produced more than 100.000 ton/year of biodiesel.

In the plant, mainly residual raw materials, such as used cooking oils and other lipid residues, are used to produce biodiesel. The biofuel produced with residual feedstock permits wastes valorisation and contributes to a faster decarbonization in transportation sector.

Despite the advantages, working with residues to produce biodiesel is, indeed, challenging. The high variability of quality specification in residual feedstock is an additional difficulty for process optimization.

In its genesis, PRIO Bio has always worked with a focus on continuous improvement and sustainable operations.

Therefore, innovation strategies are applied every day to overcome obstacles and to promote competitiveness.

One of the strategies that is applied in PRIO Bio, is the Six Sigma methodology. The integration of this methodology contributes to a process variation decrease, therefore allowing organizations to improve the capability of their business processes.

A Six Sigma project embraces five phases, define, measure, analyze, improve and control, commonly known as DMAIC, as shown in Figure 2.



Figure 2. Six Sigma roadmap methodology.

One project, developed in the plant using Six Sigma methodology, was the prediction of one biodiesel's cold properties quality parameters – cold filter plugging point (CFPP).

This temperature is defined as the lowest at which a biodiesel sample still passes through a defined filter (method complying with international regulations). This quality parameter has its seasonal limits already standardized, depending on the time of the year.

Using raw material and biodiesel quality analysis data, and applying the DMAIC roadmap it was possible to:

- confirm correlations with considerable impact on the production process;
- decrease the amount of time needed to adjust the process upstream in more than 24h;
- create and automatize a feasible mathematical tool to predict the desired quality parameter.

The result of this project permits supporting the daily decision-making, saving time and resources.

PVC – a sustainable material

A. Tomás

Companhia Industrial de Resinas Sintéticas, CIRES, Lda., Rua da CIRES, nº8 / 3860-160 Avanca, Estarreja, Portugal.

Arnaldo.Tomas@Cires.pt



Companhia Industrial de Resinas Sintéticas, CIRES, Lda., was founded in 1960 with five Portuguese and two Japanese companies as shareholders, which constituted the first industrial Portuguese-Japanese joint venture in post-war Europe. In 2009 it became fully integrated into one of its original shareholders, Shin-Etsu Chemical Co.

CIRES consolidated a leading position in the Iberian market, presenting a diversified range of Poly(Vinyl Chloride) polymers-PVC-manufactured by the suspension and emulsion processes.

PVC is one of the most used thermoplastic polymers in the world in the manufacture of materials and products essential to human development.

CIRES is strongly committed to adopting measures aiming a sustainable development within the UN program by 2030. This accounts for all business activities, through the innovation in products and processes towards the provision of key materials for a more sustainable society.

CIRES is a leading producer of a diversified range of PVC polymers manufactured by the suspension process, used in multiple industrial sectors predominantly with relevance in the civil construction segment. At the same time, CIRES also offers a range of specialties with differentiating properties, which include a portfolio of PVC products from the emulsion process to plastisols, in particular for applications in coatings, namely in the automotive sector.

Within the context of Shin-Etsu Chem. Co., CIRES covers the different ESG (Environmental, Social and Governance) aspects in its short, medium and long-term strategic objectives. PVC is the secondly ranked thermoplastic material, with applications of everyday life, ranging from building and construction parts to medical, electric and electronics, sports, automotive and pharmaceuticals.



The manufacture of PVC, like many other production processes, is closely regulated to minimise its impact on human health and in the environment. It is the least energy intensive of all thermoplastics.

Designed for durability, PVC has intrinsically an inherent sustainability characteristic since it's made from rock salt (57%) and oil (43%), by that it contains less carbon than most major thermoplastics.



PVC is a recyclable material and is increasingly being recycled. Depending on the application, PVC can be recycled repeatedly up to 8 times without losing its technical properties. CIRES remains focused on contributing to a better world, investing in a technology to reduce the environmental impact.

As part of this work, by using a renewable and/or circular feedstock with a lower Global Warming Potential (GWP) when compared to fossil fuel sources, the bio-attributed PVC enables a lower carbon footprint that can exceed 70% reduction.

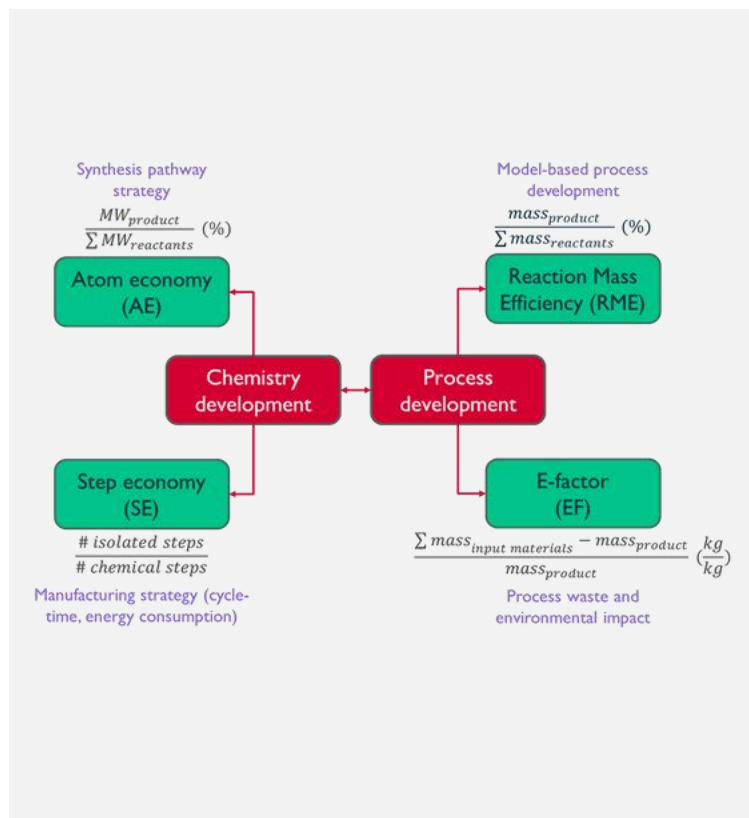
CIRES is supporting and building innovative solutions in a clear commitment and long term vision towards the reinforcement of the planet and society sustainability pillars. costs.

Sustainability at Hovione R&D process chemistry development

N. Pereira

Hovione R&D Center, Process Chemistry Development Estrada Paço do Lumiar, Campus do Lumiar, Edifício R, 1649-038 Lisboa, Portugal.

nlousa@hovione.com



Hovione is a Contract Development and Manufacturing Company dedicated to helping Pharmaceutical Customers bring new and off-patent drugs to market. With more than 60 years of experience and four FDA inspected sites (USA, China, Ireland and Portugal), Hovione offers branded pharmaceutical customers services for the development and compliant manufacture of innovative new drugs including highly potent compounds. We are members of Rx-360, EFCG and a certified B corporation, actively participating in industry quality improvement initiatives to lead new global industry standards. In this context, one paramount goal is the construction of a robust and prosperous business for the long term that serves society by harnessing science and industry. Sustainability practices are therefore fully integrated into the business strategy and specifically at Process Chemistry Development, where we make the best use of science, innovative technologies and digital systems to deliver efficient and environmental friendly manufacturing processes. Our synthetic chemists and chemical engineers are experts in reducing waste-streams, batch-to-batch variability and hazardous substances usage, as well as shortening process cycle-times and optimizing energy and utilities consumption. This work will highlight our current corporate sustainability goals and ongoing initiatives, including some of our team success stories.

Advancing sustainability through gas adsorption and reaction technologies: SYSADVANCE's 20-year journey in gas purification

P. Bárcia

SYSADVANCE, S.A. Rua Comendador Brandão, 461, 4495-375 Póvoa de Varzim, Portugal.

patrick.barcia@sysadvance.com



Figure 1. SYSADVANCE Headquarter in Póvoa de Varzim (Portugal)

Over the last two decades, SYSADVANCE has become a leading innovator in applying the principles of adsorption science and technology to develop industrial processes either for onsite production of nitrogen (N₂) or oxygen (O₂), or for renewable gases purification such as biogas from anaerobic digestion or hydrogen (H₂) from photovoltaic solar or synthetic gas.

This comprehensive technology portfolio has transformed the gas production landscape by significantly reducing energy consumption, carbon footprint, and enhancing industrial gas and energy supply autonomy.

The current geopolitical situation has highlighted the vulnerability of EU's energy system in regards to autonomy and safety. Making our energy use more efficient is one of the most achievable steps we can take towards decarbonisation and improving energy security.

Onsite production of industrial gas

Within this frame, SYSADVANCE deploys a portfolio of adsorptive technologies for gas purification with significant energy saving potential for both industry and medical sectors. The main driver is the decentralization of industrial gas production (O₂ and N₂) combined with a judicious adjustment of the quality grade based on the particular requirements of each application. As an example, tank blanketing operations (often requiring large volumes of N₂ with 98.0 vol% grade) can be supplied by on-site N₂ production plants with a reduction of 75% on the specific power consumption when compared for instance to a pharmaceutical application which generally request higher N₂ purity grade (usually ≥ 99.999 vol%). Decentralized production helps to abate CO₂ emissions associated not only with the production but specially with the gas distribution logistics from the Air Separation Units (ASU) to the final consumption point, improving the sustainability of the industry sector.

Biogas upgrading

Reducing the global economy energy intensity through energetic efficiency is only the first step to achieve the sustainability targets. As the energy transition takes place, it is fundamental to implement and scale-up renewable alternatives that can substitute fossil fuel. The heating value of biomethane is similar to natural gas (HHV > 10.7 kWh/Nm³), being at the same time a fundamental vector of development for a profitable waste valorisation chain. *METHAGEN AD* is a cyclic adsorption process developed by SYSADVANCE for the production of biomethane from biogas. Its new Vacuum-Pressure Swing Adsorption (VPSA) scheme is able to recycle a major fraction of the CH₄ content from the tail-gas increasing then the CH₄ recovery rate. This upgrade allows *METHAGEN AD* to meet the stringent CH₄ emission regulations expected to enter in force by 2025 in some territories like France.



Figure 2. (Left) METHAGEN AD for agricultural waste biogas in Premery, France: biomethane for grid injection; (right) METHAGEN AD for municipal sewage sludge biogas in Boden: biomethane for sustainable Mobility.

Biogenic CO₂ is the tail gas released during the regeneration step of *METHAGEN AD* with an average concentration of 96 vol%. This by-product can be stored or purified for either food & beverage sector, greenhouse production or for a variety of industrial applications. An alternative valorisation pathway for CO₂ consists on its use for renewable energy storage. The SYSADVANCE's *e-METHAGEN* process (currently in final stage of development) promotes the reaction of CO₂ with green H₂, via catalytic methanation. CO₂ reacts at

350°C with H₂ to be converted into CH₄ and H₂O through exothermic reaction. The product is then dried by a thermal regeneration adsorber producing synthetic CH₄ (e-GAS) which can be stored in the grid.

Hydrogen production from syngas and electrolysis

As biomethane, H₂ is also a clean and versatile energy carrier that can help in reducing our reliance on fossil fuels and transition to a low-carbon economy. *METHAGEN Pure* is a VPSA process highly efficient process for purifying H₂ from syngas, and it is used in a variety of applications, including fuel cells, metal treatment, and chemical synthesis. In the VPSA packed bed, strongly adsorbed molecules like carbon monoxide, CO₂, water (H₂O) and methane (CH₄) are trapped in solid phase micropores while the weakly adsorbed H₂ pass through the bed being obtained as high purity grade product. Once saturated, the adsorbent undergoes a regeneration step either by reducing pressure, applying vacuum or performing counter-current purge with a fraction of the raffinate.

Electrolytic H₂, by its turn, is typically saturated with H₂O containing as well residual O₂ which makes it unsuitable for direct use in fuel cells. To overcome this, SYSADVANCE launched recently in the market the *METHAGEN Pure C* which combines catalytic deoxidation and H₂O adsorption steps to produce high purity grade H₂ complying with fuel quality standard SAE J2719:2020 and ISO 14687:2019.

In conclusion, SYSADVANCE's technology portfolio has meaningfully contributed over the last two decades for the transition towards a more sustainable world by transforming gas purification industry landscape.



Figure 3. H₂ deoxidation and drying system



Leading Innovations

We know Vibrational Spectroscopy.

Advanced Research and QA/QC Solutions based on Infrared, Near Infrared and Raman Spectroscopy.

Our selection of near, mid and far infrared and Raman spectrometers is unrivalled across the industry. Our portfolio includes compact, portable routine as well as powerful research spectrometers. Our solutions cover the entire spectral range from near infrared, mid infrared, far infrared to THz applications.

- FT-IR Spectrometers
- FT-NIR Spectrometers
- Raman Spectrometers
- Process Monitoring
- Remote Sensing
- FT-IR Research Spectrometers
- FT-IR Microscopes
- Raman Microscopes
- Dairy Analyzers
- Gas Analyzers
- Silicon Analyzers
- Software Solutions

For more information please visit www.bruker.com/optics



Innovation with Integrity



Empowering Science with Innovation and Integrity

Bruker's unique mass spectrometry solutions are the measure of innovation.

High performance, easy-to-use, expertly supported Highly Differentiated Mass Spectrometry Solutions.

Bruker Applied Mass Spectrometry is pioneering the migration of technology from research to commercial laboratory. The latest product lines reflect this design philosophy to solve the challenges faced by the analysis community in applied markets. We invite you to take a closer look and learn how our products will transform workflows in environmental, food and forensic toxicology analysis.

- GC MS Triple Quadrupole
- LC MS Triple Quadrupole
- LC MS ESI qTOF MS High Resolution
- TIMS TOF – LCMS ESI Ion Mobility qTOF MS
- Target Screener
- CorkScreener
- Maldi TOF MS
- MRMS (FTMS ICR MS)
- PASEF Proteomics
- DIA NN Proteomics

For more information please visit www.bruker.com/daltonics



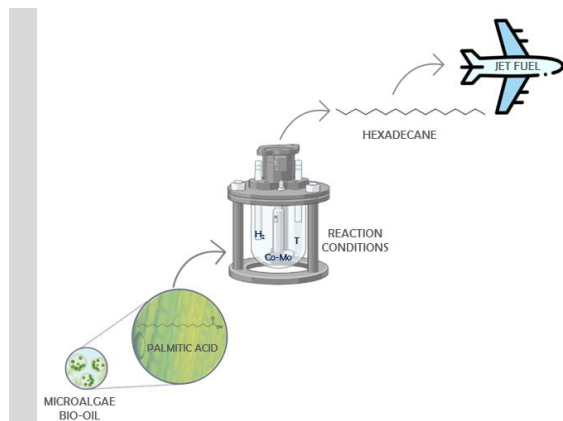
Innovation with Integrity

Sustainable jet fuel production: assessment of reaction conditions in palmitic acid deoxygenation

*K.K. Ferreira**, *L. Ribeiro*, *M.F.R. Pereira*

LSRE - LCM - Laboratory of Separation and Reaction Engineering – Laboratory of Catalysis and Materials, Faculty of Engineering, University of Porto, Rua Dr. Roberto Frias, 4200-465 Porto, Portugal; ALiCE – Associate Laboratory in Chemical Engineering, Faculty of Engineering, University of Porto, Rua Dr. Roberto Frias, 4200-465 Porto, Portugal.

*up202103294@edu.fe.up.pt



Microalgae bio-oil is a renewable resource, which brings a huge opportunity for producing aviation fuel, helping to mitigate the effects of global warming. For its direct application as a jet fuel, deoxygenation reactions are required to enhance some of its physicochemical features. This study seeks to explore the deoxygenation reaction of a model bio-oil compound (palmitic acid) and establish the best reaction parameters using a commercial catalyst (Co-Mo/Al₂O₃). In the performed experiments, 350 °C and 150 rpm were the ideal temperature and stirring rate conditions, resulting in a 79 % conversion of palmitic acid and a 67 % yield of hexadecane. The outcomes also demonstrated that the hydrodeoxygenation route is followed during the fatty acid's deoxygenation.

Introduction

As one of the most significant worldwide economic activities in the modern world, the aviation industry has seen a significant market expansion in the last two decades. Despite the benefits, the combustion of a petrochemical basis aviation fuel increases the emissions of additional pollutants and greenhouse gases [1]. In addition, the price of finished goods has increased due to the depletion of fossil resources and the difficulty in accessing them, further encouraging the use of alternative energies [2].

Using low-carbon emission fuels is the only feasible approach to achieve CO₂ emission reduction targets and accelerate the decarbonization of the aviation industry [2, 3]. Due to their high lipid content in fatty acids (C₁₄-C₂₂), which have a carbon number in the same range as aviation fuel (C₈-C₁₆), microalgae biomass stands out as a renewable source. Thus, employing different cutting-edge technologies, this feedstock has the potential to produce bio-jet fuel [4]. Currently, the most promising method for obtaining liquid hydrocarbons is the hydrothermal liquefaction (HTL) process used to produce bio-oil from microalgae. However, due to its poor physical-chemical properties driven by the presence of oxygenated compounds, its direct application as a fuel is limited [5].

In this context, it is essential to create technologies to improve the physical-chemical characteristics of bio-oil, enabling its use as jet fuel. In hydrotreatment units, catalytic methods for heteroatom removal are frequently used in the petrochemical industry. Even though such processes are well established, research studies are still lacking to determine the ideal conditions for the bio-oil deoxygenation. Thus, this work aims to determine the ideal reaction conditions needed to convert microalgae bio-oil into aviation fuel.

Materials and Methods

Catalytic reactions were carried out in a 100 mL stainless batch reactor (Parr Instruments, USA Mod 4590), using a commercial catalyst Co-Mo/Al₂O₃. Palmitic acid (C₁₆H₃₂O₂), a microalgae model compound, was used as substrate diluted in 50 mL of n-decane to assess deoxygenation reactions. The influence of the experimental conditions was evaluated by varying the temperature (220 – 370 °C), the hydrogen pressure (20 – 60 bar), the reaction time (0.5 – 6 h), the stirring rate (150 – 700 rpm),

the catalyst load (0.1 – 0.4 g) and the palmitic acid concentration (5 – 15 g L⁻¹). The final liquid phase products were analyzed by a Dani GC-FID (model 1000) using a column TRB-5-RTX (30 m × 0.25 mm, 0.25 μm).

Results

Figure 1 shows the outcomes of the assessment of the influence of the temperature.

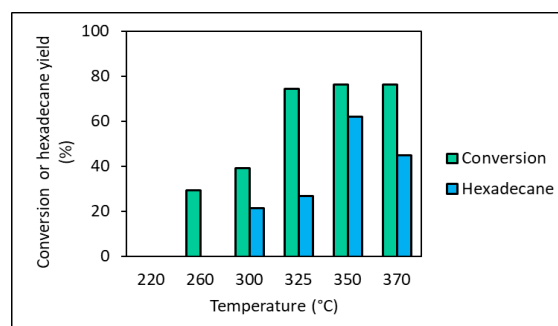


Figure 1. Influence of the temperature on the conversion of palmitic acid and yield of hexadecane after 4 h of reaction. Reaction conditions: 40 bar of H₂, 300 rpm, 0.25 g of Co-Mo/Al₂O₃ and 10 g L⁻¹ of palmitic acid in 50 mL of n-decane.

The conversion of palmitic acid into products was found to begin at 260 °C with the highest value of 76 % at 350 °C. The maximum hexadecane output of 62 % was also noted at this temperature and a small amount of pentadecane (0.3 %) was also produced. According to the results, the deoxygenation mainly followed the hydrodeoxygenation route, resulting in the formation of an alkane with the same carbon number as the fatty acid and water.

The effect of the stirring rate was also investigated over the same conditions at 350 °C. It was observed that experiments performed above 150 rpm have no mass transfer limitations, so that, this stirring rate was chosen to continue the study. Under these conditions, the hexadecane yield was 67 % and the conversion was 79 %. The effect of the remaining parameters described in the Material and Methods section is still being investigated.

Acknowledgements

This work is a result of project Move2LowC - Combustíveis de Base Biológica, with reference POCI-01-0247-FEDER-046117, co-funded by the European Regional Development Fund (ERDF), through the Operational Programme for Competitiveness and Internationalization (COMPETE 2020) and the Lisbon Regional Operational Programme (LISBOA 2020), under the PORTUGAL 2020 Partnership Agreement; and through COMPETE2020LA/P/0045/2020 (ALiCE), UIDB/50020/2020 and UIDP/50020/2020 (LSRE-LCM) funded by national funds through FCT/MCTES (PIDDAC).

References

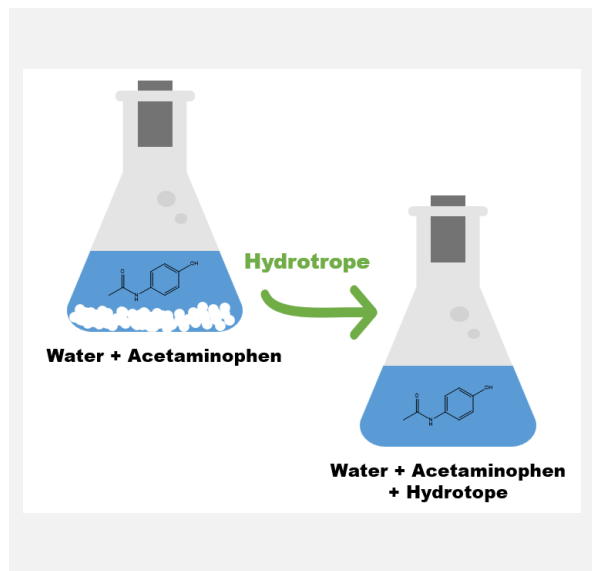
- [1] Y.Y. Lai et al., *Renewable and Sustainable Energy Reviews*, 115 (2021) 111972.
- [2] D. Londoño-Pulgarin et al., *Renewable and Sustainable Energy Reviews*, 143 (2021) 110905.
- [3] M. Wang et al., *Progress in Energy and Combustion Science*, 74 (2019) 31-49.
- [4] G.W. O'Neil et al., *Biofuels from Algae*, Second Edition, Elsevier, 2019, 359-395.
- [5] S. Karatzos et al., *Biofuels, Bioproducts and Biorefining*, 81 (2017) 344-362.

Studies on the hydrotropic enhancement of acetaminophen aqueous solubility

*J. Santos, A. Zambom, M.A.R. Martins, O. Ferreira, S.P. Pinho**

Centro de Investigação de Montanha (CIMO), Instituto Politécnico de Bragança, Campus de Santa Apolónia, 5300-253 Bragança, Portugal; Laboratório para a Sustentabilidade e Tecnologia em Regiões de Montanha, Instituto Politécnico de Bragança, Campus de Santa Apolónia, 5300-253 Bragança, Portugal.

**spinho@ipb.pt*



Hydrotropes are compounds able to enhance the solubility of sparingly water-soluble solutes, for example, active pharmaceutical ingredients. Therefore, hydrotropes may be an eco-friendlier alternative to traditional solvents in drug development and manufacturing processes. This work aims to investigate the solubility enhancement of acetaminophen using different hydrotrope types, and concentrations, and evaluate their effect on the partial molar volume of the molecule. The saturated solutions were prepared by applying the shake-flask method, and the solubility quantified by UV-Vis spectroscopy or gravimetry. Besides, the acetaminophen partial molar volume in the different systems was evaluated through density measurements. Relative solubility was compared between different ionic and non-ionic hydrotropes. Overall, this work provides a more detailed understanding of the role of hydrotropes in improving drug solubility, which could have implications for developing more effective and eco-friendly drug formulations. Insights will also be given on the relation between the partial molar volume change and the solubility increase.

Introduction

Up to 40% of drug candidate failures are due to biopharmaceutical properties, in which poor water solubility plays a role. Furthermore, more than 90% of the commercialized drugs show a very low solubility in water, leading to poor bioavailability, since the compounds are ineffectively absorbed at the administration site, which is a key part of elevated clinical failure due to poor pharmacokinetics [1]. To overcome low solubility issues several techniques have been developed over the past decades, including co-solvency, complexation, cryogenic techniques, crystal engineering, micellar solubilization, microemulsion, pH adjustment, particle-size reduction, supercritical fluid process, solid dispersion and hydrotropy [2]. Among these techniques, hydrotropy stands out as a promising technique if non-toxic, non-flammable, and eco-friendly hydrotropes are used, having shown solubility enhancements over 1000-folds for water-poorly soluble drugs such as rapamycin [3]. Neoteric green solvents as ionic liquids (ILs) or (deep) eutectic solvents (DES) have also been shown as potential hydrotropes of active pharmaceutical ingredients. DES aqueous solutions can enhance the solubility of ciprofloxacin up to 430-fold [4], while enhancements in the order of 11×10^6 -fold have been reported for paclitaxel using choline-based ILs.

In this scenario, acetaminophen (ACP), surprisingly a poorly studied compound, appears as a very interesting solute in the field of hydrotropy. A limited number of hydrotropes was attempted as solubility enhancer of acetaminophen, including organic solvents, biomolecules, salts, ionic liquids, and eutectic mixtures [5]. Among those, the best result was obtained with a mixture of N-methyl pyrrolidone and polyethylene glycol 600, leading to over than 212-fold acetaminophen solubility in water enhancement [6]. Along with solubility data, partial molar volume data may be used to tune computational thermodynamics models used to predict

drug solubility and to understand the interactions between solute-solvent in a system. Only a small set of reports correlating hydrotropes and changes in acetaminophen partial molar volumes have been reported [7-9].

In this work the acetaminophen solubility enhancement in aqueous solutions is studied at 298.15 K by using acetone, ethanol, 1,2-propanediol, glycerol, urea, cholinium chloride or bromide, ammonium sulfate or thiocyanate, and sodium benzenesulfonate, caprylate, salicylate, sulfate, thiocyanate or tosylate, up to 20% (mass fraction). Besides, partial molar volume measurements are underway in different hydrotrope solutions.

Experimental work

Solubility of ACP was obtained using the shake-flask method, in which a small excess of ACP powder was mixed with approximately 5 mL of various aqueous solutions of hydrotropes. The ternary system was stirred at $25 \text{ }^\circ\text{C} \pm 0.5 \text{ }^\circ\text{C}$ for 24 hours using an Eppendorf Thermomixer C, followed by a 12-hour period of rest. After, a liquid sample (0.04 - 1.5 mL) was taken from the saturated solution using a syringe, and filtered through 45 μm Branchia SFNY-145-100 nylon filters. Two different techniques were employed to quantify the ACP solubility at each hydrotrope concentration: UV-Vis Spectroscopy (Pg Instruments T70) or gravimetry.

The use of different techniques was needed due to the characteristics of the substances and their interactions with ACP. Some hydrotropes for example, exhibit absorbance in the UV-Vis absorption range of ACP. Hence, alternative approaches were sought to address this issue. Gravimetry proved to be an effective alternative for measuring the solubility of ACP in systems containing acetone, ammonium thiocyanate, and sodium benzene sulfonate, salicylate, thiocyanate, or tosylate. For the remaining compounds, ACP

solubility was determined using UV-Vis detection at a wavelength of 244.5 nm.

Results and Discussion

The solubility of acetaminophen in pure water at different temperatures was initially measured. As can be seen in Figure 1, data are in good agreement with values from literature ([5], [6], and references therein), validating the experimental setup followed in this work.

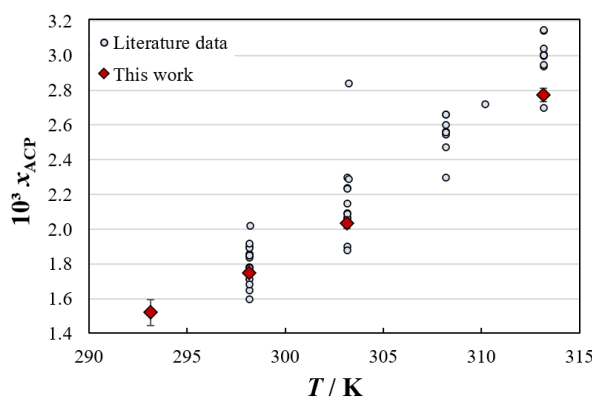


Figure 1. Solubility of ACP in pure water at different temperatures either measured in this work or taken from literature.

The solubility data obtained for aqueous mixtures containing ACP and hydrotropes are shown in Figure 2. The maximum solubility enhancement was obtained with acetone ($S/S_0 > 5.0$), a traditional organic solvent in the pharmaceutical industry. Among the salts, sodium tosylate and sodium salicylate show the higher relative solubilities for low hydrotrope concentration ($w_{\text{hydrotrope}} = 0.05$) being 2.01 and 1.46, respectively, even superior to that one obtained with ethanol at the same concentration. At a higher hydrotrope concentration

Acknowledgments

The authors are grateful to the Foundation for Science and Technology (FCT, Portugal) for financial support through national funds FCT/MCTES (PIDDAC) to CIMO (UIDB/00690/2020 and UIDP/00690/2020) and SusTEC (LA/P/0007/2021). This research was also funded by the European Regional Development Fund (ERDF) through the Regional Operational Program North 2020, within the scope of Project GreenHealth—Digital strategies in biological assets to improve well-being and promote green health, Norte-01-0145-FEDER- 000042, to which A. Zambom is thankful for her grant.

References

- [1] S. Kalepu, V. Nekkanti, *Acta Pharmaceutica Sinica B*, 5 (2015) 442-453.
- [2] K.T. Savjani et al., *ISRN Pharmaceutics*, 22 (2012) 1-10.
- [3] P. Simamora et al., *International Journal of Pharmaceutics*, 213 (2001) 25-29.
- [4] S.N. Pedro et al., *International Journal of Pharmaceutics*, 616 (2022) 121566.
- [5] F. Pourkarim et al., *Physics and Chemistry of Liquids*, 58 (2020) 56-472.
- [6] S. Soltanpour, A. Jouyban, *Journal of Solution Chemistry*, 40 (2011) 2032-2045.
- [7] H. Shekaari et al., *Journal of Molecular Liquids*, 202 (2015) 86-94.
- [8] S. Singh et al., *Journal of Molecular Liquids*, 249 (2018) 815-824.
- [9] D. Warmińska et al., *Journal of Molecular Liquids*, 323 (2021) 114834.

($w_{\text{hydrotrope}} = 0.2$), the scenario changes and acetone and 1,2-propanediol are the best hydrotropes.

The presence of sulfate ion in salts of sodium and ammonium led to a salting-out effect, what is in agreement with the Hoffmeister series (S/S_0 equals to 0.16 for Na_2SO_4 and 0.36 for $(\text{NH}_4)_2\text{SO}_4$).

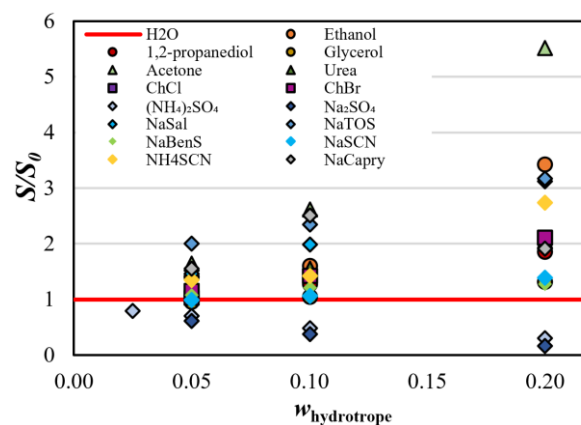


Figure 2. Relative solubility of ACP in low hydrotrope concentration at 298.2 K.

Conclusions

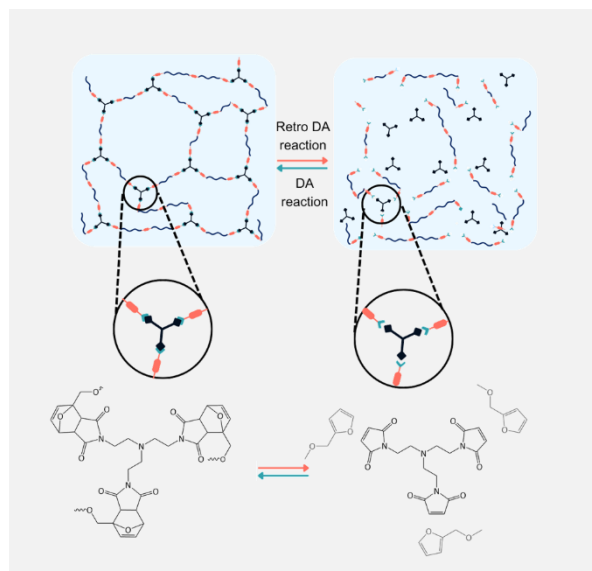
Experimental solubilities enhancements for ACP were obtained using different hydrotropes at temperature of 298.2 K with performance comparable to traditional organic solvents such as acetone and ethanol. Future works will address such analysis at different temperatures, as well as attempts to correlate the ACP solubility with different approaches such as the solvatochromic parameters and COSMO-RS. The overall goal is to be able to *a priori* design hydrotropes to solubilize acetaminophen.

Engineering of a recyclable crosslinked polyurethane with thermally reversible Diels-Alder adduct

A.C. Restrepo, I. Larraza, N. Gabilondo, A. Saralegi, A. Eceiza*

Materials+Technologies' Group (GMT), Chemistry and Environmental Engineering Department, Faculty of Engineering of Gipuzkoa, University of the Basque Country (UPV/EHU), Plaza Europa 1, 20018 Donostia-San Sebastián, Spain.

*arantxa.eceiza@ehu.eus



The maleimide-furan adduct forms covalent bonds at low temperatures, but when heated, these bonds break, splitting the polymer chain into smaller chains and softening the polymer so that it can be reprocessed. As the temperature drops, the maleimide and furan bonds reform and the polymer regains its mechanical properties.

A triol containing the furan-maleimide Diels-Alder adduct has been developed to facilitate the recycling of a crosslinked polyurethane. This triol has been used together with a commercial polymeric isocyanate to synthesize a polyurethane with mechanical properties characteristic of a thermoset. Polyurethane recyclability was subsequently evaluated by breaking it into pellets and reprocessing it by compression.

Recyclability has been demonstrated by mechanical tests, achieving up to 89% of the original properties for the recycled sample.

In recent years, growing environmental concerns are driving the development of more sustainable materials and recyclability already stand out as one of the most promising ways to achieve sustainable circularity [1], [2].

Among polymeric materials, thermosets often have properties superior to those of thermoplastics, but they have the disadvantage that they cannot be recycled or reprocessed. In recent years, research is focusing on the introduction of thermally reversible bonds in the structure of polymers, which allow their recycling or reprocessing [3].

The furan-maleimide Diels-Alder adduct (DA) is one of the most studied thermally reversible covalent bonds [4,5]. At low temperatures, DA bonds are closed, allowing cross-linking in properly designed structures and resulting in materials with improved mechanical properties. At high temperatures, however, the retroDA reaction takes place, which uncouples the DA reactants, facilitating the reprocessing of the crosslinked materials, thus allowing crossing the boundary between thermoplastics and thermosets.

In this work, a partially biobased thermosetting polyurethane plate containing the DA adduct in the structure has been synthesized from a triol containing several DA adduct groups (Triol-DA) and a polymeric isocyanate. The PU obtained has been characterized by different physicochemical, thermal and mechanical techniques, and its recyclability has also been studied. The PU behaves as a thermoset in terms of mechanical properties, but thanks to the Diels-Alder adduct, it can be reprocessed and is suitable for recycling.

First, the Triol-DA was synthesized (Figure 1) and DA reversibility verified by differential scanning calorimetry (DSC) performing several consecutive heating and cooling scans combined with isothermal steps. The DA and retroDA reactions temperatures and times were determined and employed in the recycling of the synthesized polyurethane.

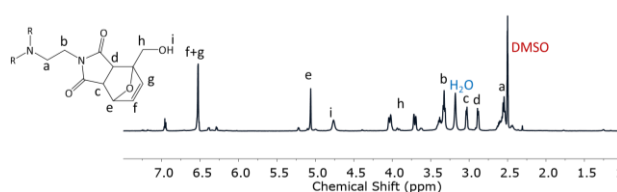


Figure 1. ¹H NMR spectra of the synthesized Triol-DA.

The recyclability of the synthesized PU is performed following the steps shown in Figure 2.

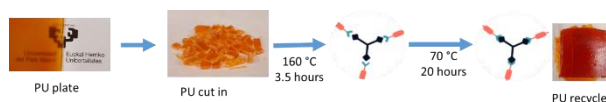


Figure 2. Scheme of recycling process.

The efficiency of bond reformation was assessed performing tensile tests on the original sample (PU) and on the recycled one (rPU). As shown in Table 1, the mechanical properties remain similar after the recycling process. When comparing the ultimate strength values, the recycled polyurethane has a bond reforming efficiency of 89%.

Table 1. Mechanical properties of the original and recycled thermoset polyurethane.

Sample	Young's Modulus (MPa)	Ultimate strength (MPa)	Strain at break (%)
PU	95.4 ± 2.5	12.4 ± 0.7	115.3 ± 2.8
rPU	93.2 ± 8.2	11.0 ± 0.5	84.5 ± 17.6

In conclusion, a new trifunctional triol with dynamic covalent bonds has been successfully synthesised within this work and then used as a crosslinker in the construction of a biobased thermoset polyurethane. The final thermoset polyurethane

presents thermal reversibility given by the Diels-Alder reaction between furan and maleimide. Thus, this thermal reversibility gives the polyurethane the property of recyclability or

reprocessability, which has been demonstrated by mechanical tests, achieving up to 88.7% of the original properties for the recycled sample.

Acknowledgements

Financial support from the Basque Country Government in the frame of Grupos Consolidados (IT-1690-22) and ELKARTEK 2021 (Project NEOMAT KK-2021/00059) is gratefully acknowledged. The authors also acknowledge the Macobehavior-Mesostructure-Nanotechnology SGIker unit from the University of the Basque Country (UPV/EHU). A.C. Restrepo wishes to acknowledge the Materials + Technologies Group for her PhD grant (PIFG21/34).

References

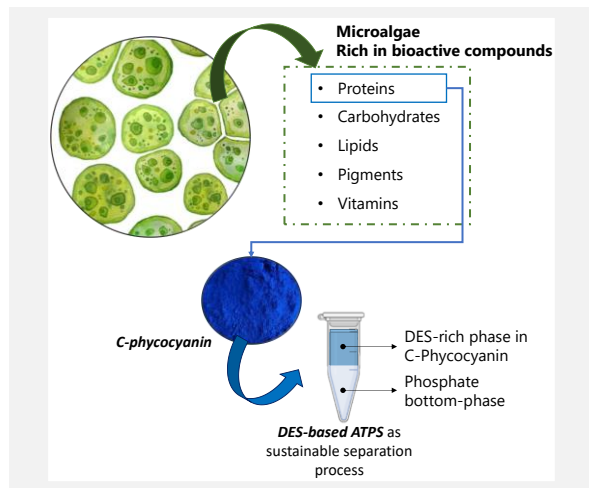
- [1] J. Banik et al., *Waste Management & Research*, 41 (2023) 1063-1080.
- [2] S. Burattini et al., *Chemical Society Reviews*, 39 (2010) 1973-1985.
- [3] C.J. Kloxin, C.N. Bowman, *Chemical Society Reviews*, 42 (2013) 7161-7173.
- [4] A. Gandini et al., *Journal Materials Chemistry*, 19 (2009) 8656-8664.
- [5] B. Willocq et al., *RSC Advances*, 7 (2017) 48047-48053.

Innovative design of a more sustainable technology for microalgae protein recovery

B. Pereira^{1*}, C. Brazinha¹, J.G. Crespo¹, S.P.M. Ventura², C. T. Matos³, L. Costa³

¹LAQV-REQUIMTE, Department of Chemistry, NOVA School of Science and Technology, FCT NOVA, Universidade NOVA de Lisboa, 2829-516 Caparica, Portugal; ²CICECO – Aveiro Institute of Materials, Department of Chemistry, University of Aveiro, 3810-193 Aveiro, Portugal; ³A4F – Algae for future, Estrada do Paço do Lumiar, Campus do Lumiar, Edif. E-R/C, 1649-038 Lisboa, Portugal.

*bad.pereira@campus.fct.unl.pt



Microalgae have been gaining interest due to their ability to produce biomolecules, namely polysaccharides, proteins, and pigments, that can be applied in several fields, namely in feed, food and pharmaceutical industries. However, biorefinery strategies to valorize this biomass through efficient and sustainable processes of extraction and purification in continuous mode are still one of the biggest challenges.

Aqueous two-phase systems (ATPS) appear as one alternative in this work, due to their sustainable features (e.g. simple operation, low energy requirement, and low-cost). From the several types of ATPS previously reported, polymer-salt and deep eutectic solvent-salt were studied in the present work. Several parameters were investigated to improve the stability of the interface between both aqueous phases composing the ATPS, in order to select the optimal system(s) for the purification of C-phycoerythrin.

Introduction

Microalgae and cyanobacteria are versatile organisms rich in several bioactive compounds, namely polysaccharides, biopolymers, phenolics, proteins and pigments, that can be applied in a variety of fields, including nutraceutical, cosmetic and pharmaceutical industries. [1,2] C-phycoerythrin (C-PC) is a blue pigment-protein complex included in the class of phycobiliproteins, which presents beneficial biological activities for human health making it suitable for pharmaceutical, cosmeceutical, and food applications. [2,3]

Traditional strategies for valorizing these photosynthetic organisms are industrially employed, affecting negatively the environment and the overall cost of the production process. [4] Therefore, alternative approaches to purify effectively and in a more sustainable way have been researched. Aqueous two-phase systems (ATPS) have emerged as an innovative technique that comprises advantageous features such as simple operation, low energy requirement, and low-cost operation. [4] From the several types of ATPS, which include polymer-polymer, alcohol-salt, IL-salt, polymer-salt and DES-salt, the latest two were studied in the present work. Several parameters were investigated to improve the stability of the interface between ATPS, assessed by the interfacial tension (IFT) between both aqueous phases, in order to select the ATPS for the purification of C-PC [5,6].

Materials and Methods

In polymer-salt ATPSs, polymers with different molecular weights (MW) were coupled with a wide variety of salt concentrations. The various ATPS prepared seek to explore the effect of polymer MW and salt concentration not only considering the extraction efficiency and partition coefficient of proteins but also their effect on the stability of both phases, assessed by the IFT.

In the deep eutectic solvents (DESs)-based ATPS preparation, different DESs were synthesized, and these were combined with the optimized concentration of salt, previously tested in the

polymer-salt ATPSs. Partition coefficients and extraction efficiency data as well as the interfacial tension between both phases were also determined.

Where the phase volume ratio (V_R) is defined as the ratio of the volume of the top- and bottom-phases (1), and V_T and V_B represent the volume of the top- and bottom-phases, respectively. Partition coefficient (K_P) and extraction efficiency (EE) were determined for the target protein for each ATPS through 2 and 3, respectively,

$$V_R = V_T/V_B \quad (1)$$

$$K_P = C_T/C_B \quad (2)$$

$$EE = \frac{C_T \times V_T}{C_T \times V_T + C_B \times V_B} \quad (3)$$

The equipment used to measure the interfacial tension of the ATPS was a Drop Shape Analyzer (DSA 25B, Kruss GmbH, Germany) through an in-built pendant drop method. The C-PC was quantified by measuring the absorbance at 620 nm using a UV-vis spectrophotometer Cary 100 UV-Vis, Agilent Technologies, Santa Clara, CA, USA.

Results

For polymer-salt ATPSs, the IFT obtained was not measurable, although a visible formation of two phases was observed. The instability of IFT can hinder the fractionation and purification of the target protein (C-PC) when turning the process into a continuous operation mode. Moreover, it was demonstrated that salt concentrations higher than 24 wt% resulted in the C-PC precipitation. Hence, the salt concentration employed for ATPS design was set between 14 wt% and 24 wt%. Table 1 displays the main results.

After studying the polymers-based ATPS, we studied the DES-based ATPSs. The screening of various synthesized DESs were performed, combined with both salt concentrations previously optimized. The selection of DES-based ATPSs was determined again by analysing the protein partition coefficient for the various systems described, which led us to select three ATPSs with measurable and stable IFT (Figure 1).

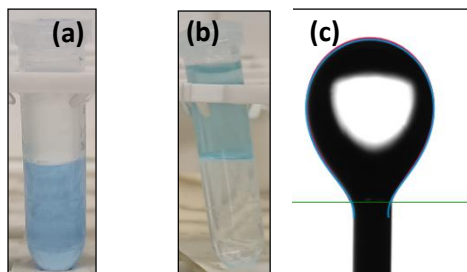


Figure 1. Display of the DES-based ATPS formation and the IFT measurement. (a) Before mixing – addition of the bottom salt phase + C-PC and upper DES phase, (b) After separation of the bottom and upper phases, and (c) IFT of DES in the salt phase.

For the successful ATPSs, the C-PC partition and the extraction efficiency parameters were measured (results in Table 2).

Conclusions

The ATPS interfacial stability is an important feature to take into account when addressing continuous mode operation. According to the results obtained in this study, DES-based ATPSs show to be a promising separation technology for the recovery of C-PC. Meanwhile, future research will focus on improving the parameters with impact on the biomolecule separation in a continuous mode of operation (e.g., pH, viscosity, and temperature) in order to develop a cost-effective and sustainable process.

Table 1. Main results obtained for the polymer-salt ATPS considering the extraction efficiency, and partition coefficient.

Bottom-phase (wt%)	Top-phase (wt%)	Polymer A (16%)				Polymer B (16%)			
		V_R	EE	K_p	IFT (mN/m)	V_R	EE	K_p	IFT (mN/m)
Salt	14	1.1 ± 0.1	0.9 ± 0.0	12.7 ± 2.6	-	1.0 ± 0.0	0.3 ± 0.0	0.4 ± 0.0	-
	19	0.8 ± 0.1	0.8 ± 0.0	7.3 ± 2.6	-	0.7 ± 0.0	0.2 ± 0.0	0.4 ± 0.1	-
	24	0.7 ± 0.1	0.6 ± 0.0	2.8 ± 1.3	-	0.6 ± 0.0	0.2 ± 0.0	0.4 ± 0.2	-

Table 2. Main results of the DES-based-salt ATPSs.

Bottom-phase (wt%)	Top-phase (wt%)	DES A				DES B				DES C			
		V_R	EE	K_p	IFT (mN/m)	V_R	EE	K_p	IFT (mN/m)	V_R	EE	K_p	IFT (mN/m)
Salt	14	0.7	0.7 ± 0.0	2.5 ± 0.1	2.7 ± 0.1	1.0	0.9 ± 0.0	12.9 ± 3.4	5.1 ± 0.1	1.0	0.98 ± 0.0	15.3 ± 0.2	4.8 ± 0.0
	24	0.8	0.9 ± 0.1	7.1 ± 1.5	1.8 ± 0.2	1.0	1.0 ± 0.0	29.4 ± 0.3	7.7 ± 0.1	1.0	0.97 ± 0.1	12.8 ± 0.6	5.5 ± 0.0

Acknowledgements

Bruno Pereira thanks the financial support to Fundação para a Ciência e Tecnologia/Ministério da Educação e Ciência, Portugal, for the PhD Fellow grant SFRH/BD/151221/2021. This work was developed within the scope of the project CICECO-Aveiro Institute of Materials, UIDB/50011/2020, UIDP/50011/2020 & LA/P/0006/2020, financed by national funds through the FCT/MEC (PIDDAC).

References

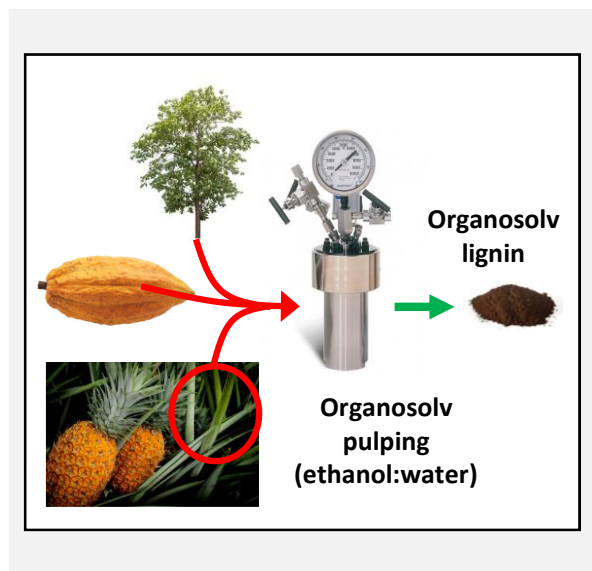
- [1] Â.P. Matos, Journal of American Oil Chemical Society, 94 (2017) 1333-1350.
- [2] J.R. Banu et al., Bioresource Technology, 302 (2020) 122822.
- [3] N.D. Giraldo-Calderón et al., DYNA, 85 (2018) 219-233.
- [4] B.M. Khan et al., ATPS: Critical Reviews in Food Science and Nutrition, 59 (2019) 3165-3178.
- [5] M. Iqbal et al., Biological Proceedings Online, 18 (2016) 1-18.
- [6] Q. Zen et al., Analyst, 139 (2014) 2565-2573.

Organosolv lignin extraction and characterization from three Costa Rican biomasses

A. Valverde-Romero¹, J.M. Mata-Segreda¹; A. Hernández², C.A. Vega-Aguilar^{1*}

¹Escuela de Química, Universidad de Costa Rica. Ciudad Universitaria Rodrigo Facio, San José, Costa Rica; ²Centro de Investigación en Productos Naturales (CIPRONA), Universidad de Costa Rica, San José, Costa Rica.

*carlos.vegaaguilar@ucr.ac.cr



Lignin is present in many biomasses, but its extraction is complex due to its nature. *Organosolv* pulping was performed on three Costa Rican biomasses (teak sawdust, cocoa fruit shell, and pineapple stubble), currently agro-industrial residues. An ethanol-water extraction was performed in a batch reactor, testing different conditions (ethanol concentration, time, and temperature). After the best condition was selected, lignin was extracted and characterized. Finally, methylene blue adsorption tests were performed. The biomasses showed a high total lignin content (up to 45% for teak samples), and good extraction was achieved (up to 45-50% of total lignin). The lignins showed interesting properties, especially for the adsorption of water contaminants, which could provide a promising use shortly.

Introduction

Lignin is a biopolymer present in vegetable biomasses, with a variable structure which depends especially on the plant taxonomy and the extraction method [1]. Currently, the most common pulping method is the *kraft* method, producing strong fibers and an efficient recovery of chemicals, but the lignin ends with a higher condensation, loss of the native structure, and higher sulfur content [2]. Another pulping method is the *organosolv* pulping, where a mixture of water and alcohols at high temperatures and pressures is used to extract lignin with higher purity and a less degraded structure. However, this technique is still under development, and the overall price of the lignin is higher [3].

Costa Rica has an important agro-industry, with world-wide recognized products like bananas, pineapples, and coffee, as well with other products with a lower production, like cocoa beans, wood, and rice. However, several environmental problems appear with the residue's treatment, which contaminates land and water bodies. These residues can reach up to 2 million tons of pineapple stubble, 535 ton of cocoa fruit shell, and 10 735 m³ of unutilized teak sawdust per year [4-6]. As these residues contain high contents of lignin and cellulose, they can be used for pulping and extraction of *organosolv* lignin, which could be converted into added-value products.

This work evaluated three different Costa Rican biomasses that are currently agro-industrial residues, and the corresponding lignin was extracted using the *organosolv* pulping method. The resulting lignin was characterized, and an additional evaluation of the adsorption properties was performed.

Methodology

Three Costa Rican biomasses were evaluated: the cocoa fruit shell (*Theobroma cacao*), pineapple stubble (*Ananas comosus*), and teak (*Tectona grandis*) sawdust. Cocoa and pineapple samples were dried at 60°C to avoid degradation. The teak sample was already dried when received.

The composition was performed on the dried samples using NREL and TAPPI methodology. The following parameters were evaluated: humidity (100°C), ashes (550°C), total lipids (Soxhlet reflux with diethyl ether), total protein (Kjeldahl method), total lignin (Klason lignin + soluble lignin), extractives (water and ethanol) and holocellulose (by difference).

The *organosolv* lignin was extracted using a 3.75 L batch Parr reactor. Different parameters were evaluated in the teak sample, including water-ethanol mixtures (40-60%), temperature (180-200°C) and time (1-2 h). Lignin was separated by adding three volumes of water and then centrifugation at 4000 rpm for 5 min. Lignin was washed using acidified water and dried in a vacuum oven at 50°C overnight.

After the conditions that extracted the highest amount of *organosolv* lignin were selected, the resulting lignins for the three biomasses were characterized by FTIR, TGA and molecular weight (HPLC-GPC).

Additionally, methylene blue adsorption experiments were performed, following the procedure by Zhang [7]. The studied lignins were compared against commercial lignin (Lignol *organosolv* lignin).

Results

The composition analysis of the biomasses is presented in Table 1. Given the woody origin, the highest lignin content was obtained in the teak sample. On the other hand, pineapple stubble showed the lowest lignin content, as it comes from a section of the plant, mainly leaves.

It is also important to note that pineapple and cocoa samples showed higher protein and extractive content percentages. This fact relates to the botanical characteristics of leaves and the external section of the fruit, respectively. Both samples typically present a high sugar content observed in the elevated water extractive percentages.

The best conditions for organosolv extraction methodology were selected using the teak sample with the highest lignin content. The most critical parameter was ethanol concentration, where 60% ethanol showed the best results. Temperature and time showed little influence on the lignin extraction, achieving similar percentages between 180°C and 200°C, and 1 h and 2 h extraction. In the best case, extraction was achieved up to 45-50% based on total lignin content.

It was noted that higher temperatures and longer times caused a charring appearance after the extraction inside the reactor, which could affect the lignin quality and purity. Also, preliminary tests noted that using 100% ethanol was not recommended since separation could not be achieved by adding water.

Lignin characterization showed the typical FTIR peaks for hardwood lignin (for teak samples) and grass lignins (for cocoa and pineapple samples). TGA analysis helped to confirm the purity of the lignin, especially by the presence of cellulose and hemicellulose.

Methylene blue adsorption experiments were performed to evaluate adsorption capacity compared to commercial lignin. It was noted that the teak lignin performed better than the Lignol lignin, with higher adsorption at the same methylene blue concentration in shorter times. These results show a promising use of *organosolv* lignin as an adsorbent for water contaminants while being a renewable and biodegradable material.

Conclusions

The three studied Costa Rican biomasses showed a high percentage of total lignin. *Organosolv* pulping was used to extract this lignin, and after different parameters evaluation, it was possible to remove almost 50% of the total lignin. The produced lignin showed exciting properties, especially when tested for adsorption capabilities. Organosolv pulping showed a promising method for lignin extraction, preserving much of the native lignin properties and allowing the use of the remaining pulp and extractives for further processes.

Table 1. Chemical composition of biomasses (dry basis percentages).

Biomass	Water extractives (%)	Ethanol extractives (%)	Total lignin (%)	Ashes (%)	Lipids (%)	Protein (%)	Holocellulose*
Teak sawdust	2.6 ± 0.3	1.28 ± 0.08	45.63 ± 0.04	1.41 ± 0.05	0.85 ± 0.03	1.12 ± 0.04	47.1 ± 0.3
Cocoa fruit shell	22.3 ± 0.2	3.2 ± 0.7	35.7 ± 0.2	7.68 ± 0.09	0.63 ± 0.03	5.03 ± 0.08	25.5 ± 0.3
Pineapple stubble	21 ± 1	5.5 ± 0.1	25.3 ± 0.7	7.36 ± 0.07	2.63 ± 0.09	7.5 ± 0.3	31.0 ± 0.6

* Holocellulose is calculated by difference.

Acknowledgements

The authors thank Dr. Roger Moya (Escuela de Ingeniería Forestal, Instituto Tecnológico de Costa Rica) for the teak sawdust samples, M.Sc. Lea Wexler (Escuela de Tecnología de Alimentos, Universidad de Costa Rica) for the cocoa samples, and M.Eng. Rodolfo Hernández-Chaverri (Universidad Estatal a Distancia, Costa Rica) for the pineapple stubble samples. The authors also acknowledge Dr. José Vega-Baudrit and LANOTEC for their help with TGA analysis.

References

- [1] B. Kamm et al., *Biorefineries-Industrial Processes and Products: Status Quo and Future Directions*, Wiley-VCH, Weinheim, 2008, 949.
- [2] O.Y. Abdelaziz et al., *Biotechnology Advances*, 34 (2016) 1318-1346.
- [3] C. Nitsos et al., *Energies*, 11 (2017) 1-2.
- [4] V. Arce, *Extracción y caracterización de los flavonoides obtenidos de la cáscara del fruto del cacao (*Theobroma cacao L.*) para su valorización*. Degree Thesis in Food Engineering, Universidad de Costa Rica, San Jose, 2019.
- [5] K. Quesada et al., *Revista Iberoamericana de Polímeros*, 6 (2005) 217-159.
- [6] Ministerio de Ambiente, Energía y Telecomunicaciones (MINAET). *Censo Nacional de la Industria Forestal Primaria de Costa Rica*, MINAET, San José, 2011, 124.
- [7] S. Zhang et al., *Procedia Environmental Sciences*, 31 (2016) 3-11.

Lignin-derived covalent adaptable networks (CANs): a sustainable approach to versatile material design

F.A. Vicente*, G. Tofani, D.B. Tiz, E. Jasiukaitytė-Grojzdek, A.K.B. Likožar

Department of Catalysis and Chemical Reaction Engineering, National Institute of Chemistry, Hajdrihova 19, SI-1000 Ljubljana, Slovenia.

*filipa.andre.vicente@ki.si



Thermoset polymers are strong and durable but lack flexibility and recyclability, while thermoplastics are more flexible and recyclable but not as strong and can melt at high temperatures. Thus, it is of the utmost importance to develop reprocessable thermosets. This can be achieved by the aid of covalent adaptable networks (CANs). CANs have both covalent and non-covalent bonds in their structure, providing stability, strength, and dynamic behavior. These properties make CANs promising for various applications in engineering and materials science. Developing lignin-based CANs is of particular interest as lignin is a renewable and abundant source of material that can be used to produce sustainable thermoset resins. This can help reduce reliance on fossil fuels and lower the carbon footprint of the manufacturing process, while also improving the mechanical properties of composites and reducing production costs. Creating thermoset resins from lignin can contribute to a more sustainable and environmentally friendly industry.

Introduction

Thermoset polymers offer high strength and durability, as they are crosslinked and cannot be remelted or reshaped once they are cured. However, they lack flexibility and have limited recyclability. In contrast, thermoplastics are more flexible and have greater recyclability, but they may not be as strong or durable as thermosets and can soften or melt at high temperatures [1]. For this reason, a lot of effort has been put in creating a bridge between both by developing reprocessable thermosets with the aid of covalent adaptable networks (CANs). CANs are a class of polymeric materials that possess both covalent and non-covalent bonds in their network structure (Figure 1). The non-covalent bonds allow for reversible and dynamic behavior of the material, while the covalent bonds provide stability and strength. This combination of properties enables CANs to exhibit unique and tunable mechanical, thermal, and self-healing properties, making them promising candidates for various applications in engineering and materials science [2].

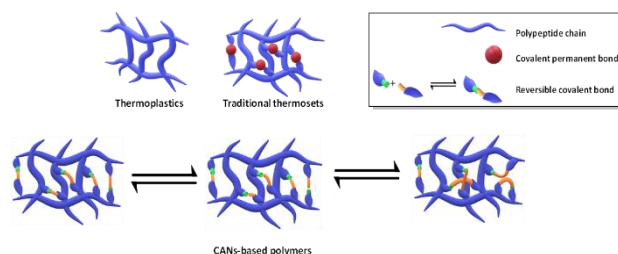


Figure 1. Reversibility of CANs bonds.

It is of particular interest the development of lignin-based CANs considering lignin is a renewable and abundant source of material that can be used to produce sustainable thermoset resins which, in turn, help reduce the reliance on fossil fuels and lower the carbon footprint of the manufacturing process

[3]. Lignin presents a potential alternative source of aromatics due to its composition as a branched phenolic polymer [3]. Furthermore, lignin can be modified to make it compatible for producing epoxy resins with CANs by oxidation. This increases the carbonyl/carboxyl group content and bonds can respond to various stimuli such as heat, light and chemicals, allowing the recycling of the polymer [4], [5]. Additionally, lignin-based thermoset resins have the potential to improve the mechanical properties of composites and reduce the cost of production. Therefore, developing thermoset resins from lignin can contribute to the creation of a more sustainable and environmentally friendly industry [6].

Considering the aforementioned, this work aims at developing lignin-based CANs by firstly functionalize lignin and lignin monomers, which will later form ester and imine bonds and lead to the formation of CANs.

Methods

Herein, two different approaches are considered. In the first case, lignin monomers like vanillin and syringaldehyde were functionalized to present imine and acyl hydrazone bonds. By introducing these bonds on vanillin structure and incorporating them in the final structure of thermosets, the resins' recyclability at the end of its life is ensured. In the second approach, the monomers were replaced by Kraft lignin and an oxygenation step was performed to increase the content of carboxyl groups. These allow the formation of ester bonds and, consequently the development of CANs. To this end, several parameters were considered, namely pH, temperature, pressure and time.

These reactions were followed using SEC, NMR spectroscopy and FTIR.

Results

Considering the use of lignin monomers to prepare CANs, the synthesis of reversible bonds, namely imine and acyl

hydrazone were monitored by NMR (^1H and ^{13}C) and FTIR. As an example, in the case of vanillin, the disappearance of the aldehyde singlet at 9.77 ppm and the newly formed singlet at 8.24 ppm, characteristic for the H proton of imine ($\text{CH}=\text{N}$) confirm the conversion of the aldehyde to imine (Schiff base). The disappearance of the absorption band of aldehydic $\text{C}=\text{O}$ (1662.02 cm^{-1}) and the formation of a new, characteristic band at 1631.30 cm^{-1} for the formation of Schiff base are confirming the transformation.

Regarding the oxygenation studies, the results were also promising with an evident pH drop, which indicated the formation of carboxylic groups. Results of SEC and NMR analysis showed different mechanisms of lignin modifications, such as rearrangements of lignin fragments (Figure 2) and its' depolymerization depending on the oxidation conditions applied.

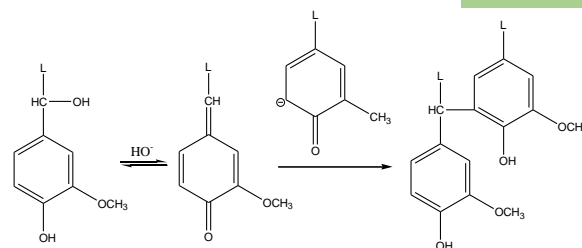


Figure 2. Rearrangement of lignin fragments.

Observed FTIR spectra of the analyzed samples also proved structural changes due to the formation of carboxylic acids from the opening of phenol rings by the action of oxygen. Overall, this data proves the efficiency of the oxidation process for the functionalization of Kraft lignin under the studied conditions.

Acknowledgements

This research was funded by Slovenian Research Agency (P2-0152 and J2-2492) and the European projects ESTELLA (code: 101058371) and HyPELignum (code: 101070302).

References

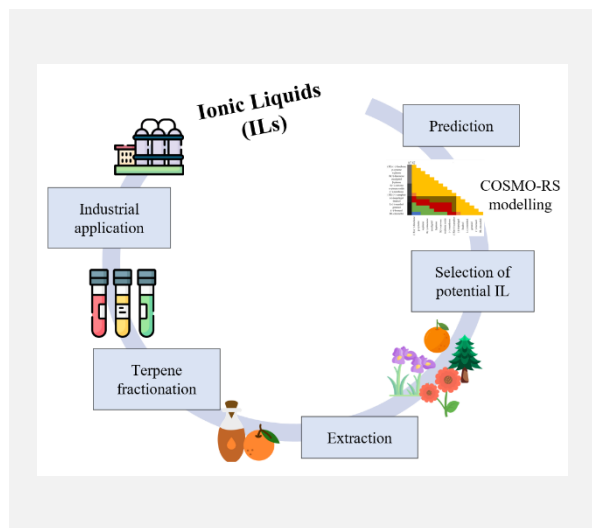
- [1] M.C. Tanzi et al., *Foundations of Biomaterials Engineering*, 1st Ed., Academic Press, 2019, 3-103.
- [2] C.J. Kloxin, C.N. Bowman, *Chemical Society Reviews*, 42 (2013) 7161-7173.
- [3] C. Gioia et al., *Biomacromolecules*, 21 (2020) 1920-1928.
- [4] X.L. Zhao et al., *Green Chemistry*, 24 (2022) 4363-4387.
- [5] C. Xu, F. Ferdosian, *Green Chemistry and Sustainable Technology*, (2017) 1-12. Accessed: Apr. 21, 2023. [Online].
- [6] J.S. Mahajan et al., *ACS Sustainable Chemical Engineering*, 8 (2020) 15072-15096.

Ionic liquids for essential oils processing: terpenes fractionation

A. Zambom^{1,2}, S. Vilas-Boas^{1,2,3}, L.P. Silva³, M.A.R. Martins^{1,2,3}, O. Ferreira^{1,2}, S.P. Pinho^{1,2,*}

¹Centro de Investigação de Montanha (CIMO), Instituto Politécnico de Bragança, Campus de Santa Apolónia, 5300-253 Bragança, Portugal; ²Laboratório para a Sustentabilidade e Tecnologia em Regiões de Montanha, Instituto Politécnico de Bragança, Campus de Santa Apolónia, 5300-253 Bragança, Portugal; ³CICECO-Aveiro Institute of Materials, Complexo de Laboratórios Tecnológicos, University of Aveiro, Campus Universitário de Santiago, 3810-193 Aveiro, Portugal.

*spinho@ipb.pt



Terpenes and their oxygenated forms terpenoids are remarkable compounds widely present in nature and extensively used in many industries such as cosmetics, pharmaceuticals, and food. Despite their abundance they are often available at low concentrations in complex mixtures which difficult their fractionation. This work aims to investigate the potential of ionic liquids (ILs) and their mixtures as entrainers in the separation and purification of terpenes. To do so, the activity coefficients at infinite dilution of terpenes and terpenoids in ILs were measured by inverse gas chromatography in extended temperature ranges. The main goal is to understand the affinity between the solutes (terpenes) and solvents (ionic liquids), allowing the determination of important separation factors, namely selectivity, capacity, and solvent performance index. The experimental results show that ILs can be tailored to be effective mass separation agents in essential oil processing by combining cations and anions of different polarity.

Introduction

The global market for essential oils (EOs) was valued at USD 21.79 billion in 2022 and is expected to expand at a compound annual growth rate of 7.9% from 2023 to 2030 [1]. Terpenes are the main constituents of essential oils, giving them their characteristic scent and flavor. Structurally, they are organic hydrocarbons, whose oxygenated forms are known as terpenoids [2–5].

Although terpene hydrocarbons have significant properties such as antifungal, anticancer, antimicrobial, among others, they contribute very little to the aroma and flavor of EOs. Additionally, terpene hydrocarbons are easily oxidated by the light, heat, or air exposure, producing off-flavors that ultimately deteriorate the essential oil quality. Terpenoids, on the other hand, are more soluble and less prone to oxidation, and are the main responsible for the aroma and antioxidant properties of essential oils [5]. The deterpenation processes – that consists in the separation of terpenes from terpenoids, aiming to improve the final essential oils quality – is thus imperative in many industries to increase the market value of the EO [4].

The most common industrial processes used for deterpenation are vacuum distillation and liquid-liquid extraction [3]. The solvent extraction is preferred, due to its lower energy requirements, while preserving the organoleptic properties of the original oil.

The currently separation methods used for terpenes fractionation have, however, some drawbacks, namely the high toxicity, flammability and/or volatility of the organic solvents used (usually hexane). Therefore, alternative solvents have been investigated to carry out the deterpenation processes and between them, the neoteric ionic liquids (ILs) [2,5–7], and (deep) eutectic solvents (DES) [4,8] can be highlighted due to their promising separation performances and, often, lower environmental impact and higher operational safety.

ILs are liquids made up entirely of ions, which are either organic or inorganic salts that have a low melting point (arbitrarily less than 100°C). They are often referred to as *designer solvents* because their physicochemical properties can be tailored to provide the desired combination of reactivity, solubility, viscosity, polarity, among other characteristics. Therefore, such solvents offer several advantages over the traditional ones. Moreover, ILs have been classified as "green solvents" due to their low volatility, and high thermal and chemical stability [2,5,6,9].

The ILs potential in extraction and separation processes involving terpenes and terpenoids can be evaluated using screening methods [2,5,7]. Those allow to reduce the amount of time-consuming experimental liquid-liquid extractions involving costly solvents. In this sense, solute-solvent interactions, selectivities and capacities can be derived from the activity coefficients at infinite dilution γ_{13}^{∞} , obtained experimentally from retention times using gas-liquid chromatography. Computational prediction tools like the COSMO-RS (COnductor-like Screening MOdel for Real Solvents [10]) that uses only structural information on the molecules can also be used to the same end.

Objectives

This work summarizes our previous findings [2,5–7] on the interactions between terpenes (solutes) and ionic liquids and their mixtures (solvents), using both experimental and quantum chemical modeling methods, namely COSMO-RS. The main goal is to understand the solute-solvent interactions, and to identify suitable ionic liquids for terpene extraction and separation. Overall, it aims to gather tools for the appropriate choice of a solvent for a given separation problem.

Important parameters such as separation factors (selectivities, capacities, and solvent performance indices), gas-liquid partition coefficients, and excess partial molar properties, are

derived from the activity coefficients at infinite dilution, and discussed.

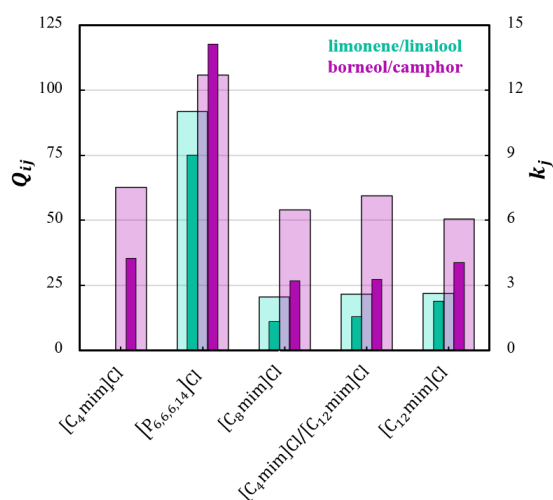


Figure 1. Comparison between the solvent performance indices, Q_{ij}^{∞} , (light colored bars) and capacities, k_j^{∞} , (dark colored bars) at infinite dilution for the separation of limonene/linalool and borneol/camphor at 403.2 K in [C₄mim]Cl [2], [P_{6,6,6,14}]Cl [5], [C₈mim]Cl [7], [C₄mim]Cl/[C₁₂mim]Cl [7], and [C₁₂mim]Cl [7].

Acknowledgements

The authors are grateful to the Foundation for Science and Technology (FCT, Portugal) for financial support through national funds FCT/MCTES (PIDDAC) to CIMO (UIDB/00690/2020 and UIDP/00690/2020) and SusTEC (LA/P/0007/2021). This research was also funded by the European Regional Development Fund (ERDF) through the Regional Operational Program North 2020, within the scope of Project GreenHealth—Digital strategies in biological assets to improve well-being and promote green health, Norte-01-0145-FEDER- 000042, to which A. Zambom is thankful for her grant. S. M. Vilas-Boas thanks FCT and the European Social Fund (ESF) for his Ph.D. grant (SFRH/BD/138149/2018 and COVID/BD/152936/2022). L. P. Silva acknowledges FCT for her Ph.D. grant (SFRH/BD/135976/2018).

References

- [1] Research, G.V. Essential Oils Market Size, Share & Growth Report 2030, 2023, 1-10.
- [2] M.A.R. Martins et al., ACS Sustainable Chemistry Engineering, 4 (2016) 548-556.
- [3] G. Ben Salha et al., Reviews in Chemical Engineering, 37 (2021) 433-447.
- [4] B. Ozturk, Green Processes for Deterpenation of Essential Oils and Extraction of Bioactive Compounds from Orange Peel Waste, The University of Manchester, 2019.
- [5] S.M. Vilas-Boas et al., Journal of Molecular Liquids, 323 (2021) 1-10.
- [6] A. Zambom et al., Molecules, 28 (2023) 1-14.
- [7] Vilas Boas et al., Industrial & Engineering Chemistry Research, 2023, Submitted.
- [8] Z. Qin et al., Journal of Molecular Liquids, 350 (2022) 118524.
- [9] A. Arce et al., Chemical Engineering Journal, 133 (2007) 213-218.
- [10] F. Eckert; A. Klamt, AIChE Journal, 48 (2002) 369-385.

Results

The main results indicate that selected ILs and their mixtures have potential for terpenes fractionation. The best experimental results were obtained for the mixtures of limonene/linalool and borneol/camphor with [P_{6,6,6,14}]Cl, where both, high selectivities and high capacities were attained – Figure 1. The essential oils of plants such as *Citrus* (rich in limonene and linalool) and flowers from *Asteraceae* and *Lamiaceae* families (mainly composed of borneol and camphor) are widely used in flavours, fragrance, and pharmaceutical industries [3,8].

COSMO-RS was evaluated for the description of the selectivities and capacities, showing to be a useful tool for the screening of ionic liquids in order to find suitable candidates for terpenes and terpenoids extraction, and separation.

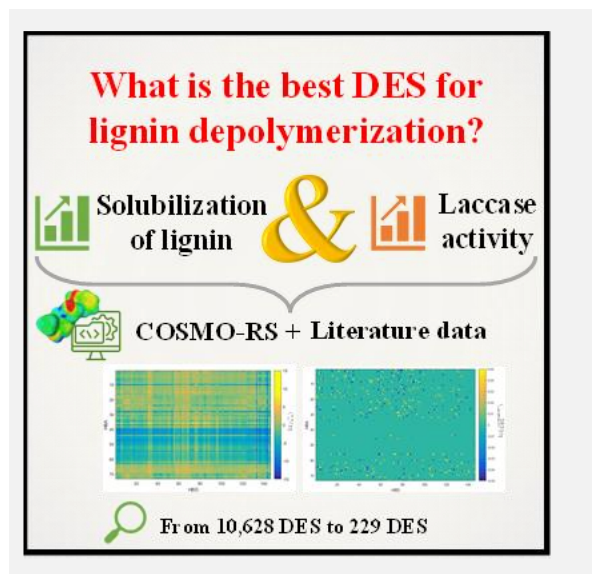
Overall, this work demonstrates the importance of tailoring the polarity of the solvents for specific separation problems involving terpenes and terpenoids.

Using COSMO-RS as a predictive tool to select potential deep eutectic solvents capable of dissolving lignin solubility and enhancing laccase activity

P.V.A. Pontes^{1*}, F.H.B. Sosa¹, J.A.P. Coutinho¹, A.M. da Costa Lopes^{1,2}, J. Andreus³

¹CICECO - Aveiro Institute of Materials, Department of Chemistry, University of Aveiro, 3810-193 Aveiro, Portugal; ²CECOLAB - Collaborative Laboratory Towards Circular Economy, R. Nossa Senhora da Conceição, 3405-155 Oliveira do Hospital, Portugal; ³Department of Chemistry, Universidade Regional de Blumenau (FURB), 89030-903 Blumenau, Santa Catarina, Brazil.

*paulapontes@ua.pt



Lignin is a naturally occurring aromatic polymer that can be used as raw material towards high-value products and applications. However, most of the produced lignin is burned to generate energy in the current scenario. A promising and sustainable approach towards lignin valorization is the enzymatic depolymerization into new biochemicals. Normally this process occurs in aqueous media, but since lignin exhibit hydrophobicity, alternative solvents, such as deep eutectic solvents (DES), capable of dissolving high amount of lignin may provide improvements. In this work, DES aqueous solutions with potential to dissolve a lignin model compound (GG-guaiacylglycerol-beta-guaiacyl ether) without compromising laccase activity on lignin were screened and analyzed by COSMO-RS predictions. The results indicated the existence of promising combinations that could enhance laccase enzymatic activity. The best systems involved halogenated and inorganic salts combined with alcohols, phenols, and carboxylic acids.

Introduction

Lignin, along with cellulose and hemicellulose, is one of the main constituents of lignocellulosic biomass. It is the second most abundant naturally occurring polymer on the planet and is an important source of aromatic compounds [1]. However, currently, most of the produced lignin in industry is burned to generate energy [2]. One of the main challenges in increasing the value of lignin is to overcome its heterogeneity [2]. In this context, obtaining monomers by depolymerization process can be a way to transform lignin into high-value products [2,3]. This can be achieved through various methods, including thermochemical treatment, mechanical treatment, chemical catalysis, or biological treatment [4]. A more sustainable option could be one that falls within the biotechnological scope, such as enzymic processes [5]. Enzymes, whether from fungal or bacterial origin, have been evaluated for their potential to depolymerize both phenolic and non-phenolic components of lignin [3]. Water is the universal solvent for enzyme-based bioprocesses. However, since lignin has limited solubility in water, enzyme depolymerization is often inefficient. Therefore, searching for alternative solvents within the green chemistry sphere towards lignin depolymerization using enzymes is desired [2]. One of the major solvent players that have been studied in processes involving lignocellulosic biomass processing is deep eutectic solvents (DES) [6]. DES are promising eco-friendly solvents to enhance lignin valorization, due to their ability to effectively solubilize lignin [7,8].

Therefore, this study aimed at applying COSMO-RS as a predictive tool for the identification of DES aqueous solutions capable of simultaneously dissolving lignin and maintaining or enhancing the laccase activity towards improved enzymatic lignin depolymerization.

Methods

Owing to the numerous possible combinations of substances to form DESs, COSMO-RS is used as an initial screening tool to select the most promising solvents, avoiding the experimental trial and error methodology. Firstly, the activity coefficients of a lignin model compound (GG-guaiacylglycerol-beta-guaiacyl ether) at infinite dilution ($\ln(\gamma_{GG}^{\infty})$) were calculated using a combination of 73 HBAs (hydrogen bond acceptors) and 146 HBDs (hydrogen bond donors) in an equimolar mixture (total number of 10658 combinations). The activity coefficients at infinite dilution in water ($\ln(\gamma_{DES}^{\infty,water})$) for the same DES combinations were also determined following the rational shown by Pederson et al. [9] who verified that $\ln(\gamma_{DES}^{\infty,water})$ could be used as impactful parameter to predict enzymatic activity in green solvents. Subsequently, the results of $\ln(\gamma_{GG}^{\infty})$ and $\ln(\gamma_{DES}^{\infty,water})$ were combined to select DES with potential of simultaneously dissolving lignin and maintaining or enhancing the laccase activity. All calculations were performed using the software COSMOthermX21 (COSMOlogic GmbH & Co KG, Leverkusen, Germany) with the parametrization BP_TZVP_21.ctd, using COSMO-files. Turbomole program package was used to produce the COSMO-files.

Results

The trend of GG solubility in DES is described in Figure 1, where blue and red colors represent low and high $\ln(\gamma_{GG}^{\infty})$ values, respectively. This means the higher solubility of the compound in DES, the lower is the $\ln(\gamma^{\infty})$ value. From the analysis of Figure 1, it is notorious the higher impact of HBA on defining the best solvent for GG than HBD. The halogenated salts (34-63) as HBAs showed the highest ability to solubilize lignin, because they showed the lowest $\ln(\gamma_{GG}^{\infty})$ values. Among HBDs, the best ones were amides (1-7),

phenols (36-56), alcohols (8-35), carboxylic acids (73-123), amino acids (91-115) and terpenes (139-141).

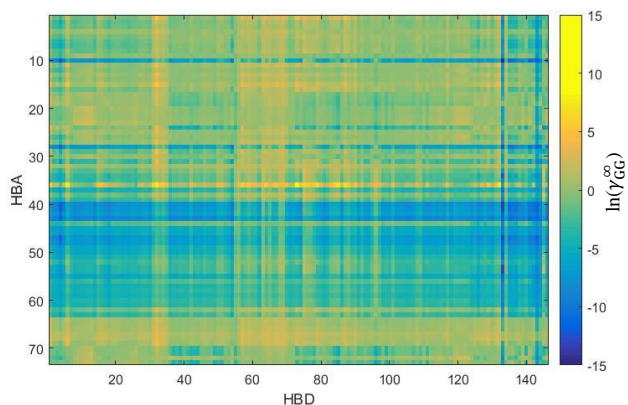


Figure 1. Logarithmic activity coefficients at infinite dilution of GG ($\ln(\gamma_{GG}^{\infty})$) predicted by COSMO-RS in 10658 possible HBA and HBD combinations in equimolar mixture at 25 °C.

However, DES with high potential to dissolve lignin might not be suited for enzyme activity. Therefore, it is also necessary to evaluate whether this possible HBA and HBD combinations impact on the enzymatic activity of laccase. Toledo et al. [10] evaluated the impact of DES aqueous solutions on the enzymatic activity of laccase. DES were prepared with inorganic salts, halogenated salts and amino acids as HBAs, while alcohols were used as HBDs. Based on the results reported by Toledo et al. [10], a correlation between $\ln(\gamma_{DES}^{\infty,water})$ with the enzymatic activity of laccases in these solvents can be found. When water activity coefficients of DES were close to zero, higher laccase activities were achieved. In this sense, $\ln(\gamma_{DES}^{\infty,water})$ were calculated and screened for those close to zero for all the combinations proposed in this work as well. As shown in Figure 2, HBA exhibited the highest impact on defining the best solvent. The best HBA candidates were amides (1-3), amino acids (04-16), and sugars (64-69), while the most effective HBD were amides

(1-7), alcohols (8-35), phenols (36-56), sugars (57-72), and carboxylic acids (73-123).

Through the analysis of the results and their trends obtained by COSMO-RS, it was possible to selected the best possible combinations of HBA:HBD (1:1) that might potentiate the enzymatic activity of laccase and simultaneously dissolve lignin. Therefore, from a range of 10,658 possibilities, 229 possible combinations of DES were found based on halogenated and inorganic salts as HBAs, and alcohols, phenols, and carboxylic acids as HBDs. The next step of this study is to measure laccase activity in some of DES combinations found in this study for validation.

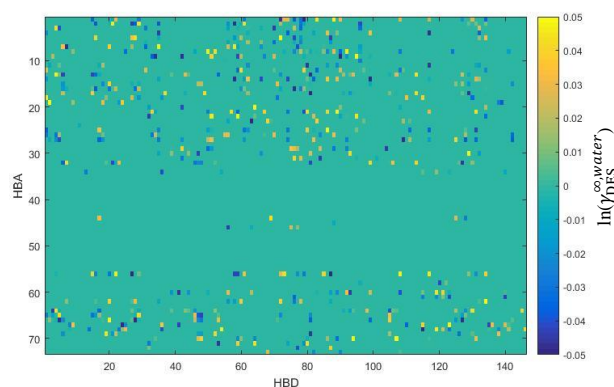


Figure 2. Logarithmic activity coefficients at infinite dilution ($\ln(\gamma_{DES}^{\infty,water})$) of water in 10658 possible HBA and HBD combinations in equimolar mixture predicted by COSMO-RS at 25 °C.

Conclusions

The use of adjusted data from the literature combined with the prediction of activity coefficients by COSMO-RS to screen a wide range of DES towards improved enzymatic depolymerization of lignin shows great potential. The obtained results indicated that the most suitable DES combinations of HBA and HBD might comprise halogenated and inorganic salts with alcohols, phenols, and carboxylic acids, which should be tested experimentally on laccase activity.

Acknowledgements

This work was developed within the scope of the project CICECO-Aveiro Institute of Materials, UIDB/50011/2020, UIDP/50011/2020 & LA/P/0006/2020, financed by national funds through the FCT/MEC (PIDDAC). Filipe H. B. Sosa acknowledge FCT – Fundação para a Ciência e a Tecnologia, I.P. for the researcher contracts CEECIND/07209/2022 under the Scientific Employment Stimulus - Individual Call 2022. Paula V. A. Pontes acknowledge the funding received from the Brazilian Science and Research Foundation – CNPq (grant number: 200768/2022-0). André M. da Costa Lopes thanks his research contract funded by FCT and project CENTRO-04-3559-FSE-000095 - Centro Portugal Regional Operational Programme (Centro2020), under the PORTUGAL 2020 Partnership Agreement, through the ERDF.

References

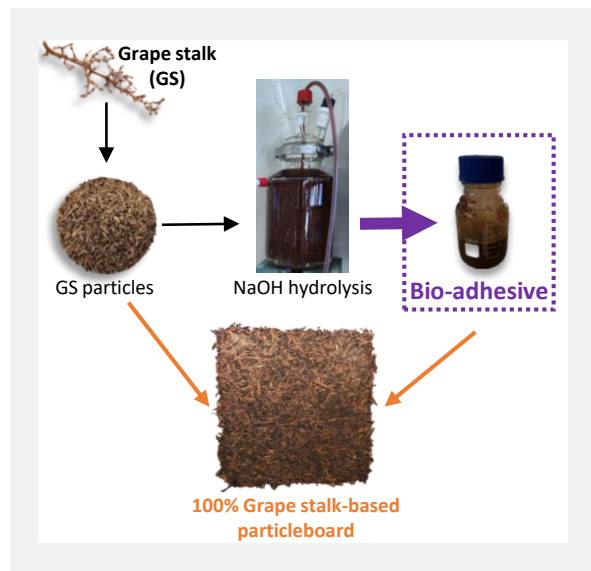
- [1] J.J. Bozell et al., Top value-added chemicals from biomass: Volume II - Results of screening for potential candidates from biorefinery lignin. Pacific Northwest National Laboratory (PNNL), Richland, 2007, 79.
- [2] M. Zhou et al., Bioresources and Bioprocessing, 10 (2023) 1-22.
- [3] L. Zhao et al., Industrial Crops & Products, 188 (2022) 115715.
- [4] C. Chio et al., Renewable and Sustainable Energy Reviews, 107 (2019) 232-249.
- [5] D.W.S. Wong, Applied Biochemistry and Biotechnology, 157 (2009) 174-209.
- [6] A.M. da Costa Lopes, Acta Innovations, 40 (2021) 64-78.
- [7] P. Li et al., RSC Advances, 13 (2023) 3241-3254.
- [8] F.H.B. Sosa et al., ACS Sustainable Chemistry & Engineering, 8 (2020) 18577-18589.
- [9] J.N. Pedersen et al., Scientific Reports, 9 (2019) 17479.
- [10] M. Toledo et al., ACS Sustainable Chemistry & Engineering, 7 (2019) 11806-11814.

Grape stalks of *Vitis vinifera* L.: a renewable source for bio-based adhesives

R.A. Fernandes^{1,2,3*}, N. Ferreira¹, S. Lopes¹, A.K. Barreto⁴, J. Santos^{1,2,3}, J.M. Martins^{2,3,4}, L.H. Carvalho^{2,3,4}

¹ARCP - Associação Rede Competências em Polímeros, UPTEC - Asprela II, 4200-355 Porto, Portugal; ²LEPABE - Faculty of Engineering, University of Porto, Rua Dr. Roberto Frias, s/n 4200-465 Porto, Portugal; ³ALiCE - Associate Laboratory in Chemical Engineering, Faculty of Engineering, University of Porto, Rua Dr. Roberto Frias, 4200-465 Porto, Portugal; ⁴DEMad - Department of Wood Engineering, Instituto Politécnico de Viseu, Campus Politécnico de Repeses, 3504-510 Viseu, Portugal.

*raquel.fernandes@arcp.pt



The wine industry is one of the major contributors for world economy, but also a great producer of by-products, with no valorization process associated. Grape stalks are a great source of chemical molecules that may be applied in several industries. In the present work, grape stalk particles were extracted with an aqueous solution of sodium hydroxide (NaOH) in order to obtain a concentrated extract with bonding properties.

It was founded that NaOH concentration has a positive impact on the extraction efficiency, increasing the recovering of phenolic compounds. Moreover, all extracts presented interesting bonding capacity, with high potential to be improved through the addition of additives and/or hardeners.

The cure process of the bio-adhesive requires lower temperatures (up to 140 °C), which may be an industrial advantage to their application. The panel produced using grape stalk particles and grape stalk-based extract evidenced promising physical-mechanical properties.

Introduction

The wine industry is one of the major contributors for world economy. According to the International Organization of Vine and Wine (OIV), in 2022, Portugal occupies the 10th place in the world ranking, of wine production, with ca. 7.3 million hL [1].

During the winemaking process, a high amount of by-products is produced, both liquid (washing waters) and solid (stalk (5-7%), pomace (20-25%) and lees (2-6%)) [2]. In fact, for producing 100 L of wine, ca. 31 kg of solid and 50-140 L of liquid by-products are generated [2], revealing an opportunity to increase the value of this sector.

Up to now, these types of residues are applied in animal feed and land fertilization. However, their high content of organic matter, rich in phenolics, tannins, flavonoids, and sugars, may turn them in an environmental concern [2].

In the last years, efforts have been made by academic and industrial researchers to develop and improve technologies to valorize winery by-products for food, health, energy and, also, particleboard (PB) manufacturing [3, 4].

In the case of PB manufacturing, wine residues can be studied both as raw material and as substrate for bio-adhesive production [4], which can be an interesting alternative to the use of synthetic resins.

In this way, the present work aims to study the impact of NaOH concentration on the extraction efficiency and bonding properties of the bio-adhesive obtained from grape stalks from red pomace *Vitis vinifera* L.

Methods

Dried grape stalks were grounded and sieved and particles with size between 500 µm and 2 mm were selected.

For the extraction, solid particles were mixed with NaOH aqueous solutions (0.0, 1.0, 5.0 and 10.0 g L⁻¹), in a solid:liquid ratio of 1:3 (w/w). The extraction was carried out in a

borosilicate reactor for 1 h at 70°C. After this time, the extract was collected and filtered. Extraction yield was calculated in terms of amount of solid extract/amount of grape stalks. Total phenolic content (TPC) was quantified through Folin-Ciocalteu method, using gallic acid as standard [4].

The adhesive properties of the extracts were accessed at 120 °C through Automated Bonding Evaluation System (ABES), according to the standard method ASTM D7998-19 [4]. Additionally, the impact of NaOH concentration in the curing kinetics at different temperatures (60 to 160 °C) was also evaluated, fixing the pressing time at 60 s.

For the manufacturing of the panel, the following conditions were adopted: target density of 700 kg/m³, 10% of adhesive in mixture (w/w), thickness of 3 mm, 140 °C and 5 minutes of pressing. The physical mechanical properties were performed in triplicate and followed the standard methods for PB (density – EN 323, Moisture content – EN 322, Internal bond – EN 319 and Thickness swelling – EN 317), using samples of 50×50 mm.

Results

As observed in Table 1, increasing the concentration of NaOH leads to an increased extraction yield (EY). In fact, using adding no NaOH to the solution (EXT0, Table 1), it was reached a solid content of 1.02 %, which represents ca. 0.87% of EY. With the addition of NaOH, the solid content of the extracts increases up to six times (EXT10, Table 1), as well as the EY. This finding can be explained by the effect of the pH on the extraction, once that several phenolic compounds commonly present in the grape stalks' extract, as condensed tannins, stilbenes, and aromatic polyphenols, are more soluble in alkaline conditions.

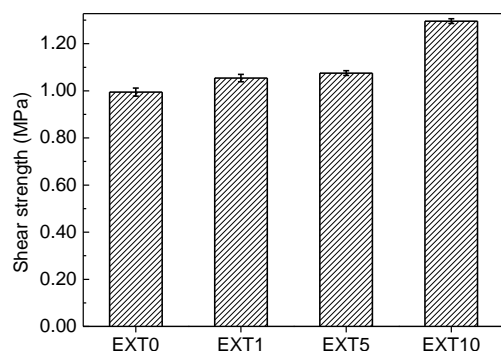
Table 1. NaOH concentration, extraction yield (*EY*) and total phenolic content (TPC) of all extractions.

Codification	[NaOH] (g/L)	Extraction yield, <i>EY</i> (%)	TPC (mg GAE/g dried extract)
EXT0	0.0	0.87	31.5 ± 0.4
EXT1	1.0	1.49	33.7 ± 0.1
EXT5	5.0	2.36	130.4 ± 3.5
EXT10	10.0	5.19	207.6 ± 4.2

Additionally, alkaline hydrolysis of lignocellulosic materials is an easy, cheap and effective method to recover valuable compounds, by partial or total solubilization of long chain polymers, as cellulose, hemicellulose and lignin. In fact, a high amount of polyphenols are originated by the breaking of these macromolecules, which indicate that harder conditions of extraction, namely in pH and temperature, allow to obtain highly efficient processes.

The impact of NaOH concentration in the total phenolic content (TPC) of extracts was also evaluated (Table 1). A higher amount of NaOH leads to a higher removal of phenolic compounds from grape stalk particles. In the case of EXT10, TPC was about 200 mg GAE/g of dried extract, indicating that EXT10 is composed by 20% of phenolic compounds. This observation is in agreement with the previous results of *EY*, reinforcing the relevance of NaOH in the extraction process.

The extracts were studied as potential bio-adhesive to use on the manufacturing of PBs. For that reason, it is extremely important to access their mechanical resistance to shear. In this way, all extracts were evaluated through ABES, pressing for 60 s at 120 °C (Figure 1).

**Figure 1.** ABES shear strength (MPa) of grape stalk extracts' pressed at 120°C for 60 s.

As observed, the extracts present an interesting bonding capacity, with shear strength ≥ 1 MPa after 60 s of pressing at 120 °C (Figure 1). Although this value was low, the possibility of adding other bio-substances that can act as hardeners or

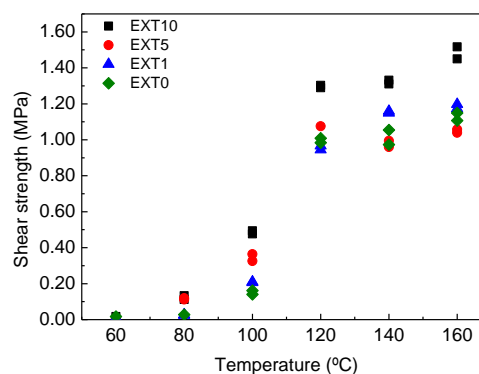
Acknowledgements

The authors gratefully acknowledge the funding by: LA/P/0045/2020 (ALICE) and UIDB/00511/2020—UIDP/00511/2020 (LEPABE) funded by national funds through FCT/MCTES (PIDDAC) and Project “INOVC+: Smart Innovation Ecosystem of Centro Region of Portugal” (project number CENTRO-01-0246-FEDER-000044), partially supported by the FEDER (Fundo Europeu de Desenvolvimento Regional), through the Regional Operational Programme of Centre (CENTRO 2020) of the Portugal 2020 Partnership Agreement.

References

- [1] OIV, World Statistics, 2022.
- [2] S. Prozil et al., *Industrial Crops and Products*, 35 (2012) 178-184.
- [3] A. Nanni et al., *Polymers*, 13 (2021) 381.
- [4] J. Santos et al., *Polymers*, 14 (2022) 1137.

additives to improve the bonding performance of these extracts. In this way, grape stalk-based adhesive may have great potential to PB manufacturing. The effect of NaOH concentration in the curing behavior of the extract is shown in Figure 2.

**Figure 2.** Impact of NaOH concentration (g/L) and pressing temperature (°C) on the shear strength of the extracts (EXT0 – green diamond; EXT1 – blue triangles; EXT5 – red circles; EXT10 – black squares).

Conclusions

According to the results, NaOH concentration may have a positive contribution to improve the performance of the grape stalk extracts' as bio-adhesive. In fact, the maximum shear strength is reached by EXT10 (ca. 1,50 MPa). On the other hand, the temperature of pressing seems to accelerate the cure of the bio-adhesive up to 140 °C for all extracts. The pressing conditions are determinant to the industrial application of adhesives in PB manufacturing, once that high temperatures and/or long pressing times not only requires great energy input, but also may decrease the productivity. In order to confirm the applicability of these extracts on the PB manufacturing, it was produced a composite panel using grape stalk particles as raw material and EXT1 as adhesive. The physical mechanical properties of the panel were evaluated and results are shown in Table 2.

Table 2. Physical-mechanical properties of composite panel.

Parameters	
Density (kg/m ³)	654 ± 22
Moisture (%)	9.36 ± 0.03
Internal bonding (MPa)	0.17 ± 0.01
Thickness swelling (%)	67.8 ± 6.0

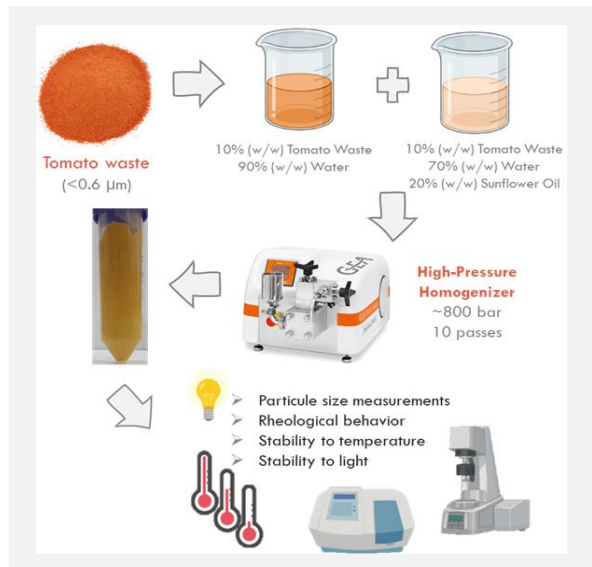
As conclusion, the use of grape stalks as raw material for the production of bio-adhesives for PB manufacturing opens up a possibility of adding value to the wine industry through the valorization of this by-product.

Lycopene cream obtained by high-pressure homogenization of tomato waste

H. Ribeiro^{1*}, B. Schuur², J.F.B. Pereira¹

¹University of Coimbra, CIEPQPF, Department of Chemical Engineering, Rua Sílvio Lima, Pólo II – Pinhal de Marrocos, 3030-790, Coimbra, Portugal; ²University of Twente, Faculty of Science and Technology, Green Energy Initiative, Sustainable Process Technology Group, PO Box 217, 7500 AE Enschede, The Netherlands.

*helenaribeiro270@gmail.com



Tomato processing by-products are rich in bioactive compounds that can be recovered and/or processed for different applications, bringing economic and environmental benefits. In this work, high pressure homogenization (HPH) was used for recovering compounds from tomato waste, using water and sunflower oil aqueous solutions as solvents. The HPH treatment reduced the particle size in both suspensions. The addition of sunflower oil increased the apparent viscosity and emulsion consistency index. The lycopene stability at temperature and light was higher in the emulsions containing sunflower oil. Since the biomass contains lipids/oils, it was possible of forming emulsions only with water after a HPH treatment. The proposed technology only requires water and tomato waste to achieve pigmented and colored emulsions, making this process attractive in terms of sustainability for future industrial applications.

Introduction

Food waste valorization, through the recovery and production of valuable products in a biorefinery concept, improves the sustainability and economic competitiveness of agro-food industries. Tomato waste is one representative example, in which 20-40% of its fresh weight is discarded (including peels, pomace and seeds), still containing highly valuable biological active compounds, such as carotenoids, lipids, crude fibers, carbohydrates and crude proteins [1, 2]. Lycopene is the major carotenoid present, mainly found in (72–92%) in the skin fraction of the tomatoes [3, 4]. This tomato fraction is, thus, of upmost interest since peels are one of main residues of tomato-processing industries. However, the selection of the extraction method for the recovery of added-value compounds is still the most challenging step, especially, due to the complexity and presence of several physicochemical obstacles in these food materials [5]. Considering the hydrophobicity of carotenoids, extraction procedures commonly use toxic and non-ecofriendly volatile organic compounds (VOCs). The use of process intensification, including thermal or mechanical treatments, has been applied to reduce the mass transfer resistances of cell walls and membranes, and/or to reduce the use of organic solvents [6]. Among these, high-pressure homogenization (HPH) has been pointed as a fast and effective method to micronize plant tissue in suspension and to release the bioactive compounds entrapped in cells, enhancing high extraction yields [7]. This mechanical processing technique is suitable for industrial applications due to simple operation, scalability, reproducibility, and high throughput [8].

Methods

In this work, we evaluated the extraction of bioactive compounds, namely lycopene, from the tomato waste, using high-pressure homogenizer (HPH) from suspensions of tomato waste. Solutions containing 10 wt% of tomato waste and water and water + sunflower oil (20% w/w) solutions were prepared and submitted to a HPP treatment (800 bar) for up to 10 passes. Samples (40 mL) were taken after different passes (1, 3, 5, 7,

and 10) for further analyses. The particle size measurement, rheological behavior, lycopene stability to light and thermal stability were evaluated.

Results

The HPH treatment resulted in a formation of homogeneous emulsions. The increase of the number of passes reduced the size of the tomato waste particles, being the small sizes obtained in the water-sunflower oil suspensions. Relatively to the rheological behavior, both suspensions presented a pseudoplastic behavior ($n < 1$). The viscosity has an abrupt increase after one HPH pass, a value that increased with the increase of the number of passes. The addition of sunflower oil resulted in higher emulsion consistency index (K) and viscosity values compared to the solution containing only water. The addition of sunflower oil improved the lycopene thermal (at 37 °C and 55 °C) and light stabilities, in comparison with the water suspensions.

Conclusions

The type of tomato waste used in this work, composed mainly by peels and seeds, allowed the formation of stable emulsions using only water due to the lipid content present in the tomato seeds. This work also demonstrated that a HPH treatment of the tomato waste using water and water + sunflower oil as solvents is enough for the recovery of bioactive compounds from tomato waste and the formulation of bio-based emulsions. The use of HPH contributes for the intensification of the process, guaranteeing high recovery yields and the integration of extraction-formulation in a single processing stage, making the process more attractive for a future industrial application. The development of efficient, simple, and economical cell disruption operations with bio-based solvents (such as water and sunflower oil) will not only allow the development an effective rupture of the cell wall, but also the solubilization and maintenance of the biological activities of the intracellular solutes, which still represents a major challenge in the recovery of bioactive compounds from food waste.

Acknowledgements

CIEPQPF is supported by the Fundação para a Ciência e Tecnologia (FCT) through the projects UIDB/EQU/00102/2020 and UIDP/EQU/00102/2020. Helena Ribeiro acknowledges to FCT for PhD Grant (UI/BD/150909/2021).

References

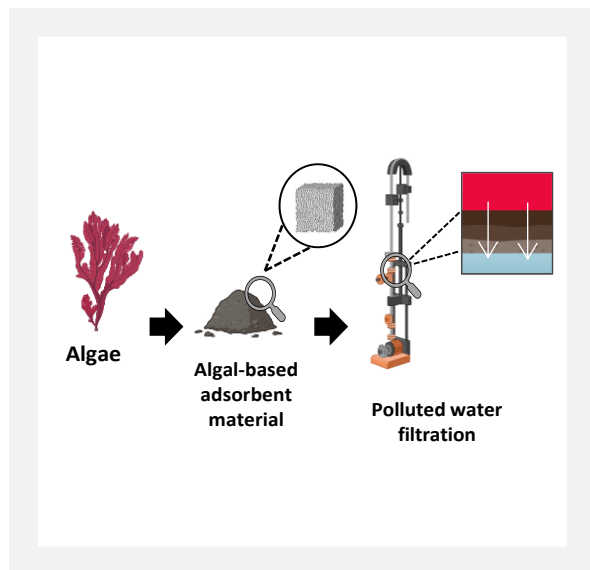
- [1] D.D. Adi et al., “Biological and Microbial Technologies for the Transformation of Fruits and Vegetable Wastes,” in *Byproducts from Agriculture and Fisheries: Adding Value for Food, Feed, Pharma, and Fuels*, 2020, 403-420.
- [2] R.K. Saini et al., *Food Research International*, 108 (2018) 516-529.
- [3] C. Fritsch et al., *Sustainability*, 9 (2017) 1-46.
- [4] Y.P.A. Silva et al., *Waste and Biomass Valorization*, 10 (2019) 2851-2861.
- [5] B.J. Allison, C. W. Simmons, *Biomass and Bioenergy*, 105 (2017) 331-341.
- [6] S. Jurić et al., *International Journal of Food Science & Technology*, 56 (2021) 4907-4914.
- [7] W. Mustafa et al., *Journal of Food Engineering*, 236 (2018) 9-18.
- [8] S. Schultz et al., *Chemical Engineering Technology*, 27 (2004) 361-368.

Development of polymeric adsorbent materials from the agar industry for removal of organic dyes in wastewaters

M. Carpintero, I. Marcet, M. Rendueles, M. Díaz*

Department of Chemical Engineering and Environmental Technology, University of Oviedo, Oviedo, Spain.

**mrenduel@uniovi.es*



The purpose of the present study is to investigate and develop a cost-effective method for removing organic dyes from water using biopolymers recovered from a by-product of the agar industry. Acidified liquid byproduct was centrifuged and the solid part, which is rich in proteins and polysaccharides, was recovered and lyophilized. The biosorption of safranin as dye component in wastewaters was studied with in a batch reactor system, varying parameters such as adsorbent dose, dye concentration, contact time and pH. It was found that the pseudo-second order model was well-fitted to the experimental data, indicating that the adsorption mechanism was controlled by different chemisorption processes, not only by intra-particle diffusion and physisorption. The results of the continuous column studies showed that the adsorption capacity of the developed materials for safranin was 70-75 mg/g of dry material. Desorption studies were performed using chlorohydric acid to study the reuse of the material.

Introduction

The textile dyeing industry is known to be one of the most contaminating manufacturing industries, as it consumes large quantities of energy, water and chemical resources and generates tons of hazardous effluents. The presence of dyes in these industrial wastewaters causes an important risk to the environment, especially aquatic ecosystems, as it interferes with photosynthesis, reduces the dissolve oxygen level, and can be toxic for the aquatic flora and fauna [1]. In this sense, safranin is one of the most widely used cationic and azine dyes in the textile industry for staining cotton, bast fibres, wool, silk, leather and paper [2]. Due to its adverse properties, wastewaters containing this synthetic dye require a proper treatment before its discharge.

Among the possible wastewater treatment methods, adsorption is considered as one of the best procedures for removing organic and inorganic pollutants from water due to its low-cost, simple operation and absence of reaction intermediate generation [3]. In this sense, in last years low-cost materials such as agro-food residues have been extensively studied as adsorbents for the removal of pollutants from water. In this research, the solid part recovered of a liquid by-product stream from the agar industry was employed to develop porous biomaterials for the adsorption of organic contaminants.

Methods

Agar industry wastewater was acidified to pH 2 and centrifuged to recover the solid part. The retrieved solid was lyophilized, characterized (in proteins, carbohydrates, phenols, inorganic salts content) and milled to obtain the coarse fraction then used in the adsorption experiments. Safranin adsorption assays were conducted in batch, with varying parameters such as adsorbent dosage, dye concentration, contact time and pH. Once optimal parameters were determined, continuous column assays (Figure 1) were performed to assess the maximum adsorption capacity of the

algae adsorbate for each dye. Finally, different desorption experiments using pH changes were performed to study material reuse.

Furthermore, the algae-based adsorbent material was characterized using scanning electron microscopy (SEM) and Fourier-transform infrared (FTIR) spectrum. Additionally, parameters such as point of zero charge (pH_{pzc}), surface area, pore volume and average pore size were also determined.



Figure 1. Column for continuous adsorption assays.

Results

The characterization of the algae-based adsorbent material reveals that the solid material recovered from the agar industry wastewaters contains a significant percentage of proteins and polysaccharides. These polymers have functional groups with varying charges at different pH values, which could interact with dye molecules present in water, retaining them.

The adsorption tests carried out indicate that the adsorption capacity of these algae-based materials for safranin was 70-75 mg/g of dry material.

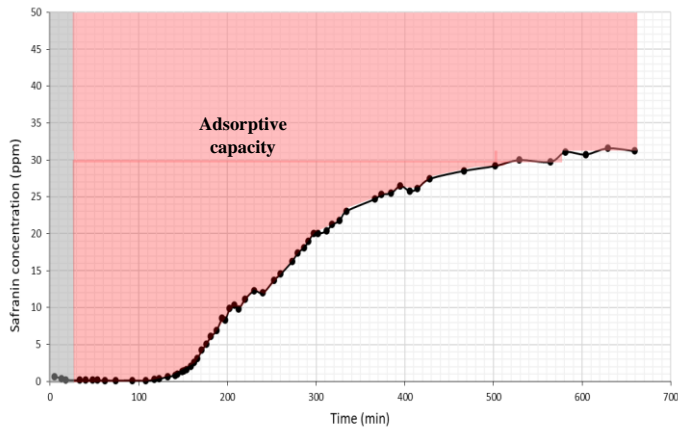


Figure 2. Adsorption capacity graphical representation.

Regarding the kinetics (Table 1), the adsorption process follows a pseudo-second order model. This suggests that the adsorption mechanism is not only due to intra-particle diffusion and physisorption, but also controlled by different chemisorption processes.

Acknowledgements

The authors are grateful for the financial support from the Spanish Ministry of Science and Innovation through project MCIU-19-RTI2018-094218-B-I00.

References

- [1] N. Oke, S. Mohan, *Journal of Hazardous Materials*, 422 (2022) 126864.
- [2] S. Kaur et al., *Journal of Industrial and Engineering Chemistry*, 22 (2015) 19-27.
- [3] Q. Liu et al., *Journal of Hazardous Materials*, 382 (2020) 121040.

Table 1. Kinetic parameters for the removal of safranin onto algae porous adsorbent.

Kinetic model	Parameter	Values
Pseudo-first order	q_e exp (mg/g)	8.12
	q_e cal (mg/g)	13.21
	k_1 (min^{-1})	0.00829
	R^2	0.9635
Pseudo-second order	q_e exp (mg/g)	8.12
	q_e cal (mg/g)	8.86
	k_2 ($\text{g mg}^{-1} \text{min}^{-1}$)	0.00087
Intra-particle diffusion	R^2	0.9557
	k_p ($\text{mg g}^{-1} \text{min}^{-1/2}$)	0.23880
	C (mg/g)	0.57
Elovich model	R^2	0.9055
	α (mg/min)	0.4194
	β (g/mg)	0.8360
	R^2	0.8256

Conclusions

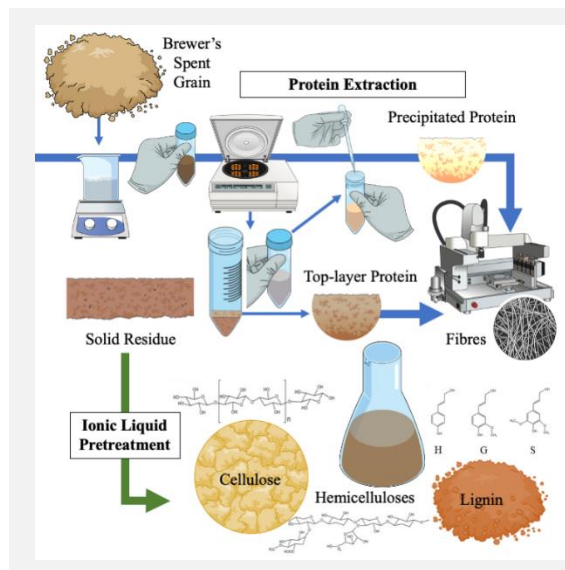
The prepared adsorbent obtained from the solids of a liquid by-products of agar industry has shown good retention properties for retention of safranin. The retention capacity is over 75 mg/g of solid and the kinetics follows the pseudo-second order model. This cheap material could be an alternative to more expensive adsorbents used in the dye industries wastewaters treatments.

Building a spent grain biorefinery using ionic liquids - with a focus on the extraction and valorisation of protein

P. Kumar*, P.Y.S Nakasu, A. Brandt-Talbot, J.P Hallett

¹Department of Chemical Engineering, Imperial College London, South Kensington, London SW7 2AZ, United Kingdom.

*p.kumar20@imperial.ac.uk



Brewer's spent grain, a waste biomass from the beer brewing industry is utilised as a feedstock in a two-step biorefinery design: firstly, using an alkali-based sequential extraction technique to generate two protein products (defined as precipitated and top-layer protein), followed by a pretreatment stage which employs ionic liquids, to further fractionate and recover the cellulose, lignin, and hemicellulose derivatives from the spent grain. By exploring and evaluating the biomaterial and bio-based chemical product options from these BSG fractionates, the possibility of BSG as a feedstock for a high-value output, second-generation biorefinery in support of a circular biorefinery is established. In particular, reported here is the extraction process, its optimisation, product characterisation and application of the proteins, with the targeted aim of producing protein-polymer composites in the form of extrudable fibres for air filtration products. Results showed that a multi-step extraction boosted precipitated protein yields by three-fold but decreased its purity to 72%. The top-layer protein yields and purities stayed consistent, benefiting from a well distributed amino-acid profile in comparison the precipitate. Both protein products show steady degradation curves through thermogravimetric analysis and are extrudable in the form of fibres (up to 15 wt%).

Introduction

Brewer's Spent Grain (BSG) is the most abundant, yet underutilised, waste biomass produced by the brewing industry with a potential for providing renewable chemicals, materials, and protein as a value-added product. Annually, more than 3 million tonnes are produced in Europe [1] which aside from direction to landfill, is sold as low-value animal feed where its nutritional value lies solely in its protein content. Due to its year-round availability, fairly simplistic preservation and storage requirements, it presents itself as the perfect feedstock for a second-generation biorefinery. More of such feedstocks are required if we are to truly sever our dependence on fossil resources and progress towards sustainable, biobased processes, thus supporting long-term economic growth in the form of a circular bioeconomy [2].

BSG is type of lignocellulosic biomass comprised of a high protein content (up to 31%), and predominantly non-starch polysaccharides, cellulose and hemicelluloses, some of which are lignified [3]. Traditional process methods have been employed in the past to extract proteins from BSG, such as chemical pre-treatments, which are commonly followed by enzymatic hydrolysis to convert its polysaccharides to sugars [4]. However, in order to overcome the recalcitrance of the lignocellulosic material in BSG which hinders the performance of these enzymes, the typical pretreatment conditions used are harsh, leading to recovered protein of poor quality and yields.

As of late, research has focused on the recovery of these proteins, along with one or two other by-products (such as arabinoxylans, a type of hemicellulose [5]) in efforts to utilise BSG in a more circular fashion. But those reported pose questions on the economies of scale-up, due to the large volumes of solvents required during operation and waste generated. In recent years, novel recyclable solvents called Ionic Liquids (ILs) and defined as liquid salts at ambient temperatures [6], have gained interest for the processing of different lignocellulosic biomass types. They can successfully break down the biomass by selectively extracting the hemicelluloses and lignin, to produce a cellulose-rich pulp [7]. This process known as the ionicSolv process, was developed at Imperial College and is

under commercialisation by its spin-out company, Lixea. Yet, it has not been optimised for protein-rich lignocellulosic biomass such as BSG.

Aim and Objectives

The first objective of this study is to design a process for the extraction, recovery, and purification of BSG proteins, while maximising the quality of the other biopolymer fractions present: cellulose, hemicellulose, and lignin. Secondly, it is to employ ILs to fractionate and recover these other biopolymer components from the remaining protein depleted BSG residue. Once this two-step biorefinery process is established, the BSG fractions can be valorised to create a variety of bio-derived chemicals and materials. The aim is to demonstrate their viability through the production of biofuels, fibres, hydrogels and ionogels, as well as protein-enriched products, showcasing the true potential of BSG in support of a circular bioeconomy.

Methods

BSG was air-dried and milled before storage at room temperature. Prior to the protein extraction, the grains were Soxhlet extracted with ethanol to ensure the removal of lipids and other extractable residues (i.e. acids, sugars) from the brewery process.

Proteins were extracted using dilute sodium hydroxide with 10 wt% BSG loading at room temperature for 1 hour, followed by isoelectric precipitation at pH 3.5 through the dropwise addition of hydrochloric acid to the liquid phase (supernatant) of the extract slurry after centrifugation. The 'precipitated' protein was then washed (with DI water) and centrifuged three times before freeze-drying. Similarly, the solid residue was repeatedly washed and centrifuged before freeze-drying. Once dried, the 'top-layer protein' was separated from the solid residue, yielding two distinct protein products (referred to precipitated and top-layer protein). After separation, the remaining protein depleted BSG residue undergoes IL pretreatment.

For the IL pretreatment, the following cholinium-based ILs are being screened: cholinium hydrogen sulfate [Ch][HSO₄],

trifluoroacetate, [Ch][TFA], methanesulfonate, [Ch][MeSO₃] and acetate [Ch][OAc]. As benchmarks, N,N,N-dimethylbutylammonium hydrogen sulfate, [DMBA][HSO₄], which is an IL commonly used in the IonoSolv pretreatment solvent, and choline chloride, a salt, was also selected. The effectiveness of pretreatment will be studied by varying pretreatment time, temperature and BSG solids loading then quantified by calculating the cellulose pulp and lignin yields.

Results and Conclusions

Initial optimisation experiments proved that the time and temperature of the protein extraction is not as impactful as the NaOH concentration. Thus, 1 hour at room temperature was selected as the extraction conditions. Further exploration of the NaOH concentration yielded that 0.1M was the best in terms of both protein purities and yields. In addition, a sequential extraction technique was introduced, with two additional NaOH extraction steps for 30 mins, due to its ability to increase the total protein yield above 50% (Figure 1a). With the addition of each extra extraction step, the overall purity of the total precipitated protein decreased from 89 to 74% but the purity of top-layer protein remained fairly consistent (approx. 41%) (Figure 1b). Mass balance calculations proved that the precipitated protein yield of each individual extraction step follows a steady downwards trend (Figure 2).

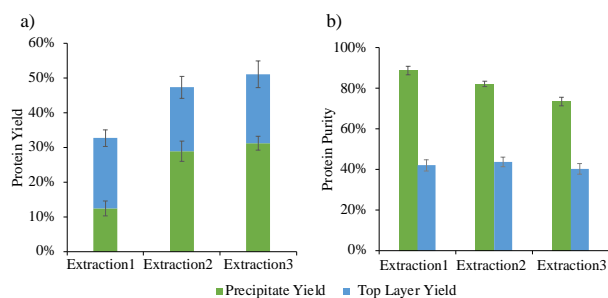


Figure 1. Total protein yields (a) and purities (b) of precipitated and top-layer proteins with 1 extraction (Extraction1), 2 extraction steps (Extraction2) and 3 extraction steps (Extraction 3).

The precipitated protein is a fine beige powder whereas the top-layer protein is of a darker colour but fluffier consistency. Thermogravimetric analysis (TGA) revealed both protein products follow similar degradation profiles, as shown in Figure 3, for the precipitated and top-layer protein, respectively. Through amino acid profiling, differences in the composition of the proteins extracted were revealed. As expected, both have a

Acknowledgements

We would like to acknowledge alumnus Mark Richardson for generously supporting this project.

References

- [1] Z. Qazanfarzadeh et al., *Journal of Cleaner Production*, 385 (2023) 135726.
- [2] A. Zeko-Pivač et al., *Frontiers in Bioengineering and Biotechnology*, 10 (2022) 870744.
- [3] E. Piercy et al., *Green Chemistry*, 25 (2023) 808-832.
- [4] K.M. Lynch et al., *Journal of Industrial Brewing*, 122 (2016) 553-568.
- [5] E. Vieira et al., *Industrial Crops and Products*, 52 (2014) 136-143.
- [6] R.D. Rogers, G.A. Voth, *Accounts of Chemical Research*, 40 (2007) 1077-1078.
- [7] F.J.V. Gschwend et al., *Journal of Visual Experiments*, 114 (2016) e54246.

strong presence of glutelin, but the amino acids are more evenly distributed for top-layer protein in comparison to that of the precipitated, which contains more proline.

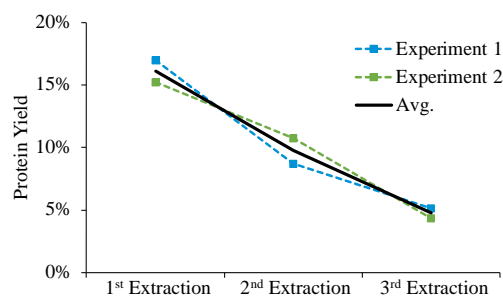


Figure 2. Isolated precipitated protein yields of each sequential extraction step.

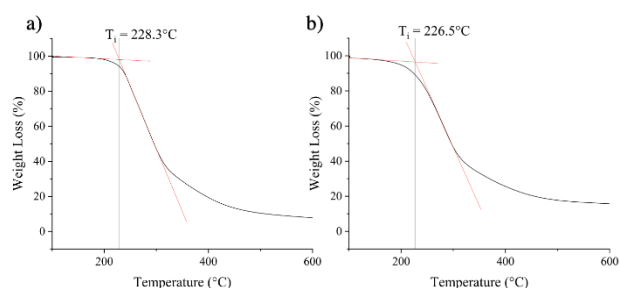


Figure 3. Thermogravimetry curves of the precipitated (a) and top-layer (b) protein.

Application of these proteins in the formation of sustainable, biodegradable, multifunctional fibres are being explored, chiefly as replacement for conventional non-degradable air filters. Initial testing has proven the extrudability of these proteins (up to 15 wt %) in various protein-polymer blends, such as polylactic acid (PLA), polyethylene oxide (PEO) and silicone, in the form of non-brittle fibres demonstrating that the BSG proteins are a promising co-polymer.

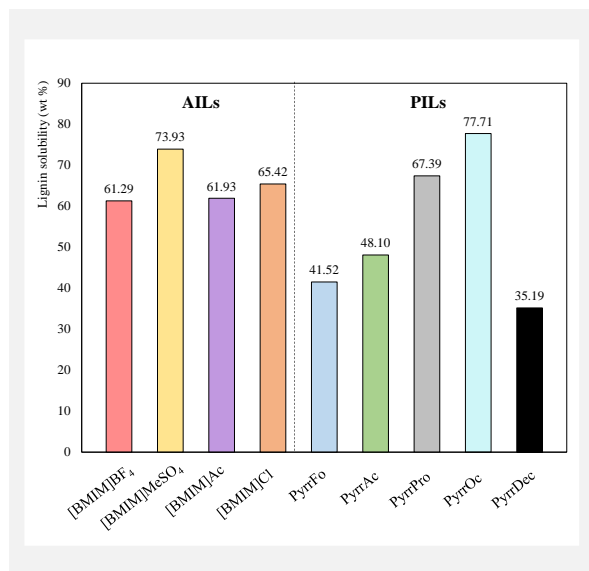
To conclude, the development of the first stage of this two-step BSG biorefinery process was successful – through the extraction of two unique protein products through a multistep alkali-based extraction technique with encouraging material applications. The development of the second stage (IL pretreatment) for the recovery of the cellulose, lignin and hemicellulose products is currently underway, with latest results from the IL screening to be included in this poster.

Determination of Kraft lignin solubility in aprotic and protic ionic liquids aqueous solutions

R.M. Dias^{1*}, S.M. Vilas-Boas², M.C. Costa²

¹Chemical Institute (IQ) – Federal University of Goiás – UFG, Campus Samambaia, 74001-970, Goiânia, Brazil; ²School of Chemical Engineering (FEQ), University of Campinas – UNICAMP, 13083-852, Campinas, Brazil.

*rafael.macedo2@ufg.br



In the last decade, Ionic Liquids (ILs) have been reported as good solvents for the fractionation, dissolution, and depolymerization of lignin, one of the main goals of the biorefinery concept. In this scenario, determining lignin solubility in this class of solvents is crucial for developing new strategies for lignin valorization. In this study, the Kraft lignin solubility in Aprotic Ionic Liquid (AIL) and Protic Ionic Liquid (PIL) aqueous solutions were determined at 323.15 K and ambient pressure. The AIL 1-butyl-3-methylimidazolium methyl sulfate ([BMIM]MeSO₄) was capable of dissolving more than 73.9 wt% of lignin, while the PIL pyrrolidinium octanoate (PyrOc) dissolved 77.7 wt%. The ILs tested could dissolve large amounts of lignin, reaching results comparable to other solvents, such as Deep Eutectic Solvents or traditional organic solvents.

Introduction

Lignin is a macromolecule widely found in the cellular wall of lignocellulosic biomass. This biomolecule has been attracting the attention of researchers due to its complex structure. It is a polyphenolic biomolecule and can be converted into fine and high-value chemicals, such as vanillin, ketones, and alcohols. However, lignin presents a highly irregular polymeric structure and poor reactivity, and it is usually burned as low-value fuel [1]. Within the biorefinery context, lignin valorization plays a key role. In this context, the first step to address lignin's valorization is finding a good solvent capable of dissolving large amounts of this macromolecule; therefore, determining lignin solubility in various solvents is essential.

Over the years, Ionic Liquids (ILs) have shown to be promising alternative solvents for the fractionation, dissolution, and depolymerization of lignin [2]. ILs are organic salts composed of organic cations and organic/inorganic anions and exist in a molten state at temperatures below 100 °C. The strong ionic interactions between ions normally result in appealing properties, such as negligible vapor pressure, high chemical and thermal stabilities, low melting point, and non-flammability. These distinguished characteristics make ILs extensively studied and applied in many areas [3].

ILs are frequently divided into two classes: Aprotic Ionic Liquids (AILs) and Protic Ionic Liquids (PILs). AILs are a class that consists of ions that do not have liable protons in their structure, which means that a positive cation charge is generally durable, and the cation is not in chemical equilibrium with its precursor. The production of AILs often involves multiple steps, which makes AILs usually expensive, and their price impairs their application in industrial processes. On the contrary, PILs present anions and cations in equilibrium with their acid and base precursors and are formed by proton transfer from Brønsted acid to a Brønsted base [4]. They are easier synthesized than AILs, being produced in a single-step reaction. For this reason, PILs are considerably cheaper than AILs, and have been pointed out as an alternative to traditional AILs. This work investigates the lignin solubility in imidazolium-based AILs and pyrrolidinium-based PILs aqueous solutions at 323.15 K and

ambient pressure, aiming at identifying the most promising options for lignin dissolution and fractionation.

Objectives

This work evaluates the Kraft lignin solubility in AILs and PILs aqueous solutions at 323.15 K and ambient pressure. The low temperature selected for the experimental assays (313.15 K) was chosen to preserve the lignin structure and avoid water evaporation from the aqueous phase. The effect of water on the ability of ILs to dissolve lignin is important to be addressed since ILs are naturally hygroscopic, and it is also expected to find humidity in biomass and organic compounds such as the Kraft lignin used in this study.

Methods

Five PILs were synthesized according to the procedure described by Dias et al. [5], and they were named as follows: pyrrolidinium formate (PyrFo), pyrrolidinium acetate (PyrAc), pyrrolidinium propionate (PyrPro), pyrrolidinium octanoate (PyrOc), and pyrrolidinium decanoate (PyrDec). Four AILs (1-butyl-3-methylimidazolium methyl sulfate ([BMIM]MeSO₄); 1-butyl-3-methylimidazolium acetate ([BMIM]Ac); 1-butyl-3-methylimidazolium chloride ([BMIM]Cl); 1-butyl-3-methylimidazolium tetrafluoroborate ([BMIM]BF₄)) were used as bought, without any further purification step.

Results

The Kraft lignin solubility values achieved by the AILs (61.29 – 73.93 wt%) and PILs (35.19 – 77.71 wt%), at 313.15 K, demonstrates that these ILs were capable of dissolving large amounts of lignin compared to the literature results [6,7]. The effect of water on the ability of AILs to dissolve Kraft lignin is shown in Figure 1, where the Kraft lignin solubilities in AILs aqueous solution, at 313.15 K, are presented.

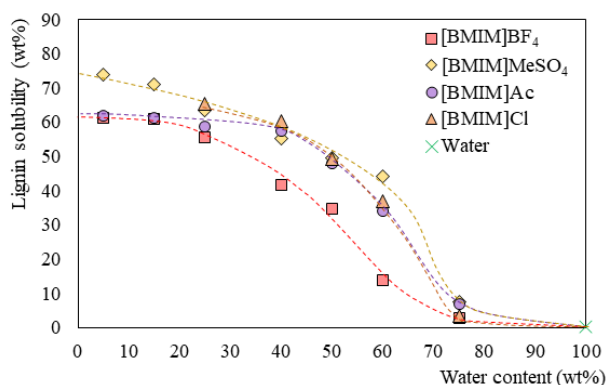


Figure 1. Kraft lignin solubility in AIL aqueous solutions at 323.15 K.

The Kraft lignin solubility curve in imidazolium-based AIL aqueous solutions presented an S-shape and pursued a linear middle section similar to the profile obtained by Protz et al [8]. In this study, at higher concentrations of water, the lignin solubilities remained lower than 7 wt%, in solutions up to 25 wt% of imidazolium-based AILs. Then, the solubilities sharply increased (in solutions within 25 – 75 wt% of AIL content) and, from about 75 wt% of AIL content, the curves remained close to a constant. To most of the range of water content, the same trend is still observed concerning the ability of AIL aqueous solutions to dissolve Kraft lignin: [BMIM]MeSO₄ > [BMIM]Cl > [BMIM]Ac > [BMIM]BF₄. This behavior may be related to the capacity to establish hydrogen-bonds and the electronegativity of the anionic part of the AIL [9].

The effect of water on the ability of PILs to dissolve Kraft lignin was deeply addressed, and the Kraft lignin solubilities in PILs aqueous solutions, at 313.15 K, are presented in Figure 2.

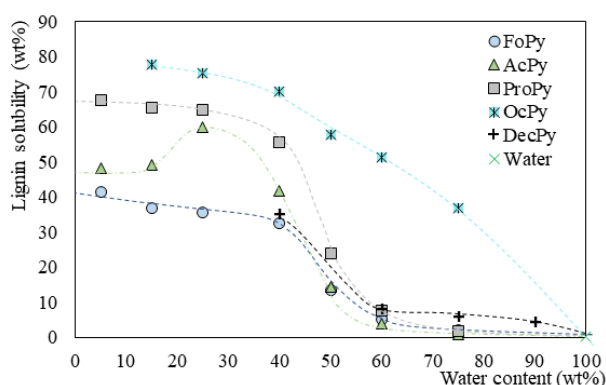


Figure 2. Kraft lignin solubility in PIL aqueous solutions at 323.15 K.

Acknowledgements

The authors thank CNPq [163506/2020-5, 306666/2020-0], FAPESP [2014/21252-0] and FAEPEX/UNICAMP for financial support.

References

- [1] F.S. Chakar et al., *Industrial Crops Products*, 20 (2004) 131-141.
- [2] M. Peng et al., *Fuel*, 335 (2023) 126960.
- [3] J. Plotka-Wasyłka et al., *Microchemical Journal*, 159 (2020) 105539.
- [4] A. Mirjafari et al., *RSC Advances*, 3 (2013) 337-340.
- [5] R.M. Dias et al., *Industrial and Engineering Chemistry Research*, 59 (2020) 18193-18202.
- [6] Y. Pu et al., *Journal of Wood Chemistry and Technology*, 27 (2007) 23-33.
- [7] R.M. Dias et al., *Industrial Crops Products*, 143 (2020) 111866.
- [8] R. Protz et al., *Carbohydrate Polymer Technologies and Applications*, 2 (2021) 100041.
- [9] H. Lateef et al., *Journal of Chemical Technology & Biotechnology*, 84 (2009) 1818-1827.
- [10] T. Rashid et al., *Industrial Crops Products*, 84 (2016) 284-293.

The curves observed when PyrrFo and PyrrPro aqueous solutions were applied to dissolve Kraft lignin are similar to those reported in our previous study [5]. A sharp decrease in the solubility is revealed with the addition of water in the solutions: this behavior is highly accentuated to solutions between 40 wt% to 60 wt% of water content. The addition of water in this concentration range strongly decreased the capacity of the PIL aqueous solution to solubilize Kraft lignin, proving that water has a strong role as an antisolvent to these PIL solutions, as previously demonstrated when pyridinium formate aqueous solutions were evaluated by Rashid et al. for lignin dissolution [10]. To water contents higher than 60 wt%, the PIL aqueous solutions presented poor capacities to dissolve lignin, except for PyrrOc. The results revealed that PyrrOc could dissolve large amounts of Kraft lignin even with higher water contents. Unlike the other PIL aqueous solutions, a progressive and continuous ability to dissolve Kraft lignin is observed for PyrrOc, without abrupt decreases in its profile, as observed in the other analyzed cases. The results obtained in this work demonstrate that both AIL and PIL aqueous solutions could dissolve Kraft lignin, and are promising options to be applied in the biorefinery concept for lignin valorization purposes.

Conclusions

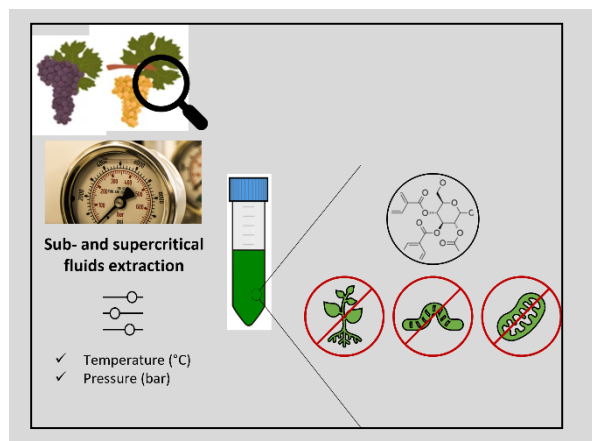
The Kraft lignin solubility values obtained for the AILs (61.29 – 73.93 wt%) and PILs (35.19 – 77.71 wt%) in this study, at 313.15 K, indicate that they are capable of dissolving large amounts of lignin compared to the literature results. In general, the results obtained in the AILs and PILs aqueous solutions agreed with the literature concerning the role of water in Kraft lignin dissolution task: usually, water acts as an antisolvent in ILs aqueous solutions. For most cases reported in the literature, water presents a poor ability to dissolve lignin which is related to lignin structure (hydrophobic) and the properties of water. The ability to solubilize Kraft lignin is presented as follows: PyrrOc (77.71 wt%) > [BMIM]MeSO₄ (73.93 wt%) > PyrrPro (67.39 wt%) > [BMIM]Cl (65.42 wt%) > [BMIM]Ac (61.93 wt%) > [BMIM]BF₄ (61.29 wt%) > PyrrAc (48.10 wt%) > PyrrFo (41.52 wt%) > PyrrDec (35.19 wt%).

Winery waste streams as potential natural pesticides

J.P. Baixinho^{1,2*}, F.B. Gaspar^{1,2}, P.J.A. Madeira³, M.R. Bronze^{1,2,4}, N. Fernández¹

¹IBET, Instituto de Biologia Experimental e Tecnológica, Apartado 12, 2781-901 Oeiras, Portugal; ²Instituto de Tecnologia Química e Biológica António Xavier, Universidade Nova de Lisboa, Av. da República, 2780-157 Oeiras, Portugal; ³Ascenza Agro SA, Edifício Lumnia, R. Centieira 61 5b 1800-056 Lisboa - Portugal; ⁴FFULisboa, Faculdade de Farmácia da Universidade de Lisboa, Av. das Forças Armadas, Lisboa, Portugal.

*jbaixinho@ibet.pt



This work is part of a major project in which one of the main goals is to develop an exploitation strategy to convert the current winemaking process waste streams into valuable products by exploring their potential as natural pesticides. Within this context, a series of solid waste streams from white and red wine production (namely grape stems and grape pomace) will be processed and characterized regarding their fungicide activity. Different strategies involving green extraction techniques (supercritical fluids extraction) were used for the recovery of bioactive fractions. The obtained extracts were evaluated as potential fungicides against the filamentous fungi *Aspergillus brasiliensis* and *Botrytis cinerea*.

Food waste is one of the most challenging issues humankind is facing. Grape is an important agro-economic activity with more than 78 Mton produced worldwide in 2019. The International Organisation of Vine and Wine estimated that 270 million hL of wine were globally produced in 2016 [1] and it is estimated that 14.5 million tons of grape by-products (Figure 1) are generated annually in Europe [2,3]. The disposal and treatment of these organic materials is a problem of ecologic and economic impact. One of the European Commission targets for 2030 is to reduce the use and risk of chemical and hazardous pesticides by 50%. Traditional pesticides are used to improve and protect crops yield by fighting diseases and pests. However, they present long term hazard to the environment and humans through their persistence in nature and body tissues [4]. To overcome these challenges, actions have been taken to replace synthetic pesticides by chemicals of natural sources [5].

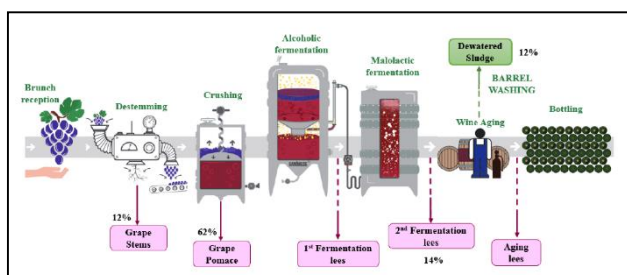


Figure 1. Overall schematic diagram of the wine production, identifying the main residues generated and their quantities along the different stages of the vinification process.

The extraction of bioactive compounds largely depends on the effectiveness of the selected extraction methods. With a growing demand for green alternatives, the applications of sustainable extraction technologies have been widely studied to diminish the use of organic solvents and energy consumption to ensure economic viability while ensuring environmental and consumers' health protection. Supercritical fluids extraction (SFE) is one of the strategies already applied to recover fatty acids and polyphenols from grape skins and seeds [6-7]. The aim of this work is to build a strategy to extract natural bioactive compounds from winery residues with potential

antifungal activity. A sustainable extraction of high-added-value compounds from agroindustry by-products will contribute to building sustainable consumption and production patterns. Biomass from the winemaking industry, namely vine pruning residues (shoots and leaves) and pomace of red (Aragonez) and white (Arinto) wine production from *Vitis vinifera* were characterized for its bioactive content [8-9]. Grape-identified compounds include flavonoids: flavonols, flavones, flavan-3-ols, flavanones and anthocyanidins. The non-flavonoids comprise stilbenes and phenolic acids.

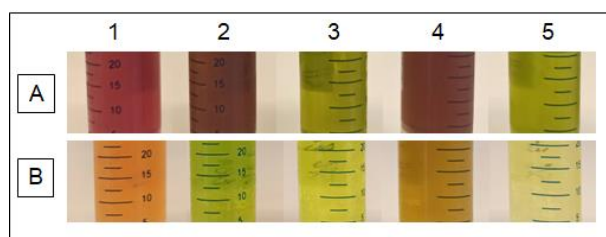


Figure 2. Different types of compounds obtained after conventional extraction methods and supercritical CO₂ extraction. A and B represent two different raw materials, red and white grape stems, respectively. The numbers correspond to different types of solvents: 1, Water; 2, Ethanol; 3, Ethyl acetate; 4, Methanol:Acetone:Water (60:30:10 v/v); 5, Supercritical CO₂.

Solid-liquid extractions were performed for comparison with Supercritical CO₂ results. Briefly, the freeze-dried grape by-products were extracted with different types of solvents or mixtures (raw material:solvent 1:20 (w/v)) for 2 hours at room temperature. Supercritical CO₂ was evaluated as an environmentally friendly technique for extracting bioactive compounds from the above-mentioned by-products. Operational parameters included temperature (40 °C), pressure (35 MPA) and extraction ratio solvent/co-solvent (CO₂, 10% water /or ethanol) (Figure 2).

Grape variety revealed a key parameter of phenolic composition. Phenolic compounds have been found in several parts of grape berries such as skins, pulp, and seeds (grape pomace). Anthocyanins found in the skin are directly responsible for the color of red grapes cultivars. Due to its positive characteristics,

extraction of these compounds is performed with large amounts of organic solvent, ethanol, or water, at low temperatures. The main flavonols and hydroxycinnamic acids obtained are quercetin-3-O-glucuronide, quercetin-3-O-galactoside, quercetin-3-O-glucoside, quercetin-3-O-galactoside, procyanidin B1, procyanidin B2, procyanidin C1. In the seeds, flavan-3-ols (monomeric catechins and proanthocyanidins) are the main polyphenolic compounds. White grape seeds presented higher amounts of phenols than red grape samples. Water and ethanol were revealed to be the solvents which extracted more compounds with an extraction yield of 32 %. Non-polar solvents were revealed to be more selective with yields of 7 %. Stilbenoids fraction present in the extracts more promising.

To evaluate the antifungal potential of the obtained extracts antifungal susceptibility testing assays were performed. This

characterization of the extracts was accomplished with the standardized method to determine the susceptibility of nondermatophyte filamentous fungi using disk diffusion testing, as described by the CLSI [10].

Aspergillus brasiliensis CECT 2574 was used as a quality control for the correct execution of the assay and *Botrytis cinerea* CECT 20973 was used as a representative target of filamentous fungi with the ability to attack vineyards.

The work is aligned with the concept of zero waste production chains applying the extracted bioactives for new bio-based pesticides, promoting residue valorisation and the development of novel products with a high social and economic interest to reduce the use and risk of chemical and hazardous pesticides.

Acknowledgements

This work was funded by Fundação para a Ciência e Tecnologia/Ministério da Ciência, Tecnologia e Ensino Superior (FCT/MCTES, Portugal) through national funds to iNOVA4Health (UIDB/04462/2020 and UIDP/04462/2020), the Associate Laboratory LS4FUTURE (LA/P/0087/2020) and Fundação para a Ciência e Tecnologia PhD Studentships (2021.06269.BD). We also acknowledge the financial support from Portugal 2020 to the Portuguese Mass Spectrometry Network (LISBOA-01-0145-FEDER-402-022125) and Sogrape Vinhos, SA for the support and raw material.

References

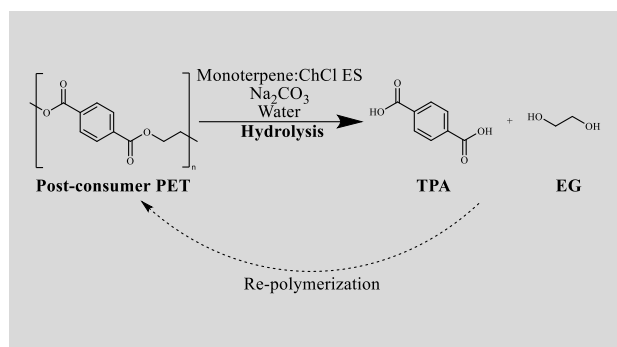
- [1] International Organization of Vine and Wine, "OIV Statistics," 2016. Available: <https://www.oiv.int/en/statistiques/recherche>.
- [2] A. Teixeira et al., International Journal of Molecular Sciences, 15 (2014) 15638-15678.
- [3] M. Bordiga et al., International Journal of Molecular Sciences, 54 (2019) 933-942.
- [4] M.S. Khan, M.S. Rahman, "Pesticide residue in foods: Sources, management, and control", (2017) 1-200.
- [5] G.M.W. Lengai et al., Scientific African, 7 (2020) e00239.
- [6] D.P. Makris, Current Opinion in Green and Sustainable Chemistry, 13 (2018) 50-55.
- [7] C. Da Porto, A. Natolino, Journal of Supercritical Fluids, 130 (2017) 239-245.
- [8] V. Silva et al., Food Control, 92 (2018) 516-522.
- [9] G. Simonetti et al., Molecules, 25 (2020) 3748.
- [10] Clinical and Laboratory Standards Institute (CLSI). *Method for antifungal Disk Diffusion Susceptibility Testing of Nondermatophyte Filamentous Fungi; Approved Guideline*. CLSI document M51-A (ISBN 1-56238-725-1). Clinical and Laboratory Standards Institute, 940 West Valley Road, Suite 1400, Wayne, Pennsylvania 19087-1898 USA, 2010.

Recycling of poly(ethylene terephthalate) waste by efficient hydrolytic depolymerization with bio-based eutectic solvents

V. de Paula^{1*}, A.J.D. Silvestre¹, A.F. Sousa^{1,2}

¹CICECO—Aveiro Institute of Materials, Department of Chemistry, University of Aveiro, 3810-193 Aveiro, Portugal; ²Centre for Mechanical Engineering, Materials and Processes, Department of Chemical Engineering, University of Coimbra, Rua Sílvio Lima – Polo II, 3030-790 Coimbra, Portugal.

*vgmp@ua.pt



The present work presents a highly efficient and *greener* alternative route for recycling one of the most consumed polymers today - poly(ethylene terephthalate) (PET). The process consists in the hydrolytic depolymerization of PET into terephthalic acid (TPA) using terpenoid-based eutectic solvents (ES) under alkaline conditions. It was demonstrated that PET depolymerization can only occur due to the synergistic effect of the ES components and the base. Structural characterization by ATR-FTIR and NMR analyses proved the purity of the recovered TPA as well as of the residual PET. Finally, depolymerization conditions were optimized using a design of experiments (DoE) approach, enabling TPA isolation with yields higher than 90 %.

Introduction

Polymers started a new era supporting the development of modern society due to their unique properties. In this regard, polymers have been widely used in packaging applications, owing to a set of properties that includes low density, flexibility, transparency, impermeability, mechanical resistance, and durability [1]. Despite these, their main advantage also become a major problem because most of the routinely used polymers are not biodegradable nor recycled. As a result, they tend to accumulate in landfills or in natural environments. Thus, the development of new *green* technologies for the effective recycling of polymers, in a more circular economy perspective, is of utmost importance for the sustainable development of our society. Poly(ethylene terephthalate) (PET), one of the most consumed polymers worldwide, can be mechanically recycled. However, this, besides involving only pure monostream waste, typically leads to downcycling due to an interplay of factors, including the decreasing of molecular weight and ensuing properties. On the other hand, within chemical recycling of PET, hydrolytic depolymerization often involves the treatment of the polymer with aqueous NaOH or H_2SO_4 at high temperatures [2-6], ensuing high energy demands and harsh reaction conditions. Recently, several studies have demonstrated the potential of eutectic solvents (ES) as a more sustainable approach for polyesters depolymerization as demonstrated in our recent study [7]. Thus, following our interest in this domain, the present work aims at the development of an innovative and more sustainable method for the chemical recycling of PET, using a combination of ESs and a base as catalysts.

Methods

Alkaline depolymerizations of post-consumer waste PET (pcPET) obtained from commercial PET bottles were conducted using choline chloride (ChCl) as the HBA and Thymol (Thy), a phenolic monoterpene, as HBD for the ES preparation, alongside Na_2CO_3 as a milder base for the depolymerizing mixture. Reactions were conducted under different temperatures range and time as disclosed below. Experiments using only Thy were also conducted to prove that the synergistic effect between the ES and Na_2CO_3 was essential to promote PET depolymerization. Moreover, experiments using only the ES

were also performed to prove the key role of the base in the reaction.

Results and discussion

The first set of experiments, performed at 180 °C for 2 h, allowed to obtain a first insight into the depolymerization of PET, based on PET weight loss. These showed that PET depolymerization takes place with the selected ES/ Na_2CO_3 , enabling the recovery of pure terephthalic acid (TPA), as confirmed by ATR-FTIR and NMR spectroscopy, with 99.17 % PET weight loss, and a high TPA yield of 79.31 %. Furthermore, the experiments using only Thy, with or without the base, showed that, in this case, PET is dissolved but not depolymerized, whereas the ES without Na_2CO_3 does not dissolve or depolymerize PET, demonstrating that the synergistic effect of the ES and Na_2CO_3 is essential in this depolymerization approach. Based on previous group experience [7], a range of temperatures between 120 and 180 °C and reaction times between 2 and 8 h were chosen for a design of experiments (DoE) using the Central Composite Design methodology. The experimental data was then fitted to a quadratic model (Figure 1).

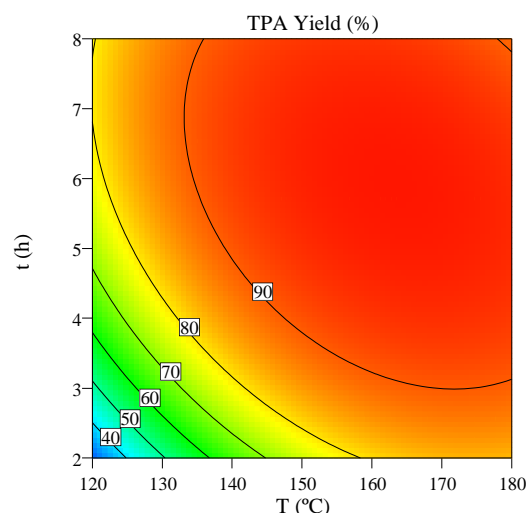


Figure 1. Contour plot of the effects of temperature and reaction time on the TPA yield for the ES/ Na_2CO_3 system.

Finally, the optimal conditions for minimizing the temperature and reaction time for the ES system, while maximizing TPA yield, was determined to be 4.5 h at 147 °C, with a predicted TPA yield of 91.5 %, based on the computed model.

Conclusions

This work demonstrates that $\text{ChCl}:\text{Thy}$ combined with sodium carbonate is a promising system for PET depolymerization, enabling efficient TPA recovery in high yields with a simple purification step.

Research on other bio-based ESs and their ability to depolymerize PET and other polyesters, as well as on the recycling of the ES, is currently ongoing.

Acknowledgements

This work was developed within the scope of the CICECO—Aveiro Institute of Materials (UIDB/50011/2020 & UIDP/50011/2020) & LA/P/0006/2020, financed by national funds through the FCT—Fundação para a Ciência e a Tecnologia/MEC (PIDDAC). This research is also sponsored by FEDER funds through the program COMPETE—Programa Operacional Factores de Competitividade—and by national funds through the FCT under the project UID/EMS/00285/2020. The FCT is also acknowledged for the research contract under Scientific Employment Stimulus to AFS (CEECIND/02322/2020). This publication is supported by COST Action FUR4Sustain—European network of FURan based chemicals and materials FOR a Sustainable development, CA18220, supported by COST (European Cooperation in Science and Technology).

References

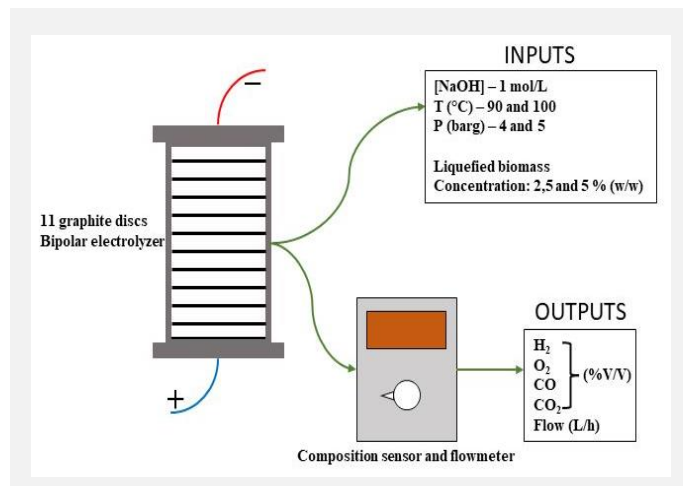
- [1] J. J. Klemeš et al., *Energy Sources, Part A: Recovery, Utilization, and Environmental Effects*, 43 (2021) 1549-1565.
- [2] E. Langer et al., Chapter 5 in *Plasticizers Derived from Post-Consumer PET*, William Andrew Publishing, 1st Ed., Elsevier, Norwich, 2019, 127-171.
- [3] S. D. Mancini et al., *Polymer-Plastics Technology and Engineering*, 46 (2007) 135-144.
- [4] T. Yoshioka et al., *Industrial & Engineering Chemistry Research*, 40 (2001) 75-79.
- [5] A. Al-Sabagh et al., *Egyptian Journal of Petroleum*, 25 (2016) 53-64.
- [6] E. Barnard et al., *Green Chemistry*, 23 (2021) 3765-3789.
- [7] B. Agostinho et al., *Green Chemistry*, 24 (2022) 3115-3119.

Liquefied biomass utilization in water co-electrolysis for synthesis gas production

D.M. Martins^{1}, T.M. Cabrita², J.C. Rodrigues², J.F. Puna^{1,3}, J.F. Gomes^{1,3}*

¹Instituto Superior de Engenharia de Lisboa, Instituto Politécnico de Lisboa, R. Conselheiro Emídio Navarro 1, 1959-007 Lisbon, Portugal; ²GSyF, Lda, R. S. Sebastião, 11 2500-064 Fanadia, Caldas da Rainha, Portugal; ³CERENA – Centro de Recursos Naturais e Ambiente, Instituto Superior Técnico, Universidade de Lisboa, Av. Rovisco Pais, 1, 1949-001, Lisbon, Portugal.

*a43720@alunos.isel.pt



Developed within the scope of an R&DT project by the start-up GSYF, Lda, this 1 kW pilot unit aims at the recovery of previously liquefied biomass from lignocellulosic forest residues, which was later used as a carbon source in a co-electrolysis process, intended for the production of synthesis gas (H₂, CO, CO₂), also known as syngas. In turn, this syngas will be transformed into other value-added products, namely synthetic biofuels such as methane, methanol or biodiesel. This prototype unit consists of an electrolyte reservoir, a set of pressure and temperature sensors, a transport pump, a radiator with fan (in order to control the temperature of the process), a heating resistance, a moisture adsorption column and an electrolyzer consisting of a stack of 11 spaced graphite discs [2,3].

Introduction

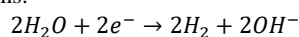
Over the last decades the continuous increase in the world's energy needs resulted in growing consumption of non-renewable fuel sources (oil, natural gas, among others) and, consequently, greater environmental impacts. For this same reason, there is an increasing commitment to the development of alternative sustainable energy sources (biomass, solar and wind energy, among others) [1].

Developed within the scope of an R&DT project by the start-up GSYF, Lda, this 1 kW pilot unit aims at the recovery of previously liquefied biomass from lignocellulosic forest residues, which was later used as a carbon source in a co-electrolysis process, intended for the production of synthesis gas (H₂, CO, CO₂), also known as syngas. In turn, this syngas will be transformed into other value-added products, namely synthetic biofuels such as methane, methanol or biodiesel. This prototype unit consists of an electrolyte reservoir, a set of pressure and temperature sensors, a transport pump, a radiator with fan (in order to control the temperature of the process), a heating resistance, a moisture adsorption column and an electrolyzer consisting of a stack of 11 spaced graphite discs [2,3].

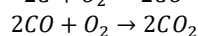
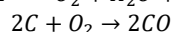
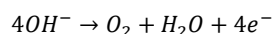
Process theory

The production of synthesis gas via electrochemical means is based on the following reactions[2]:

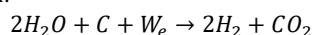
Cathode reactions:



Anode reactions:



Global reaction:



Objectives

Current experimental work focuses on carrying out optimization tests to determine the ideal conditions for the production of syngas to be in the future used as feedstock for methane

production. For this specific purpose, the syngas produced aims for oxygen concentrations as low as possible (to minimize the risk of catalyst deactivation during methanation) and a CO₂:H₂ ratio ideally close to the one associated with the conversion of CO₂ into methane (1:4) [3].

Two different biomasses were tested at two different concentrations (2.5 and 5% (W/W)) to compare with each other and the performance without using any liquefied biomass. In all tests the electrolyte was a 1M solution of NaOH.

Methods

Three different groups of tests were executed, one without adding liquefied biomass, one using a liquefied sample of acacia biomass and another using a sample of non-specified composition designated as evergreen. Each sample was diluted in the electrolyte solution at 2.5 and 5% (W/W) and each was tested within an interval of pressure (4 and 5 bar gauge) and temperature (100 and 110 °C).

The tests themselves were executed over 3 hours with data such as temperature, and pressure current applied among others, being collected in intervals of 15 minutes. For simpler presentation the average of the 3 last collections in the stationary state was collected and presented as the shortened results for each test.

Results

As an example of the data collected, the following table presents a comparison of performance for the conditions of 4 bar gauge and 100 °C:

Table 1. Test results for the conditions of 4 bar gauge and 100 °C.

Biomass used	O ₂ (%)	CO (%)	CO ₂ (%)	H ₂ (%)	F (L/H)	CO ₂ :H ₂ RATIO
Without Biomass	4.1	1.8	25.4	68.7	46.84	2.71
2.5% Acacia	3.9	2.0	34.5	59.6	67.53	1.72
5% Acacia	3.3	2.0	54.9	39.7	63.21	0.72
2.5% Energreen	6.2	2.0	40.6	51.2	56.83	1.26
5% Energreen	4.1	2.0	40.6	53.3	67.68	1.31

Conclusions

From the data obtained through experimental work it can be concluded that the additions of liquefied biomass cause significant increase in the CO₂ content in the gas outlet, resulting in a lower CO₂:H₂ ratio. Additionally, the higher CO₂ productions also requires more O₂ consumption, generating syngas with lower O₂ concentration. Focusing on the production of syngas specifically for future use in methanation, the

addition of biomass, specifically Acacia shows favored results in the production of a syngas mixture while lowering its O₂ content. On the other hand, CO₂:H₂ ratios as expected are farther from the ideal value when compared to the ideal 0,25. Although, this can be easily resolved either by later addition of H₂ or alternatively the partial removal of its CO₂ (with this still being an easier approach compared to removing the O₂).

Acknowledgements

The authors would like to thank the Fundação para a Ciência e Tecnologia (FCT, I.P.) for funding granted through the project "CLEANFOREST", ref. PCIF/GVB/0167/2018.

References

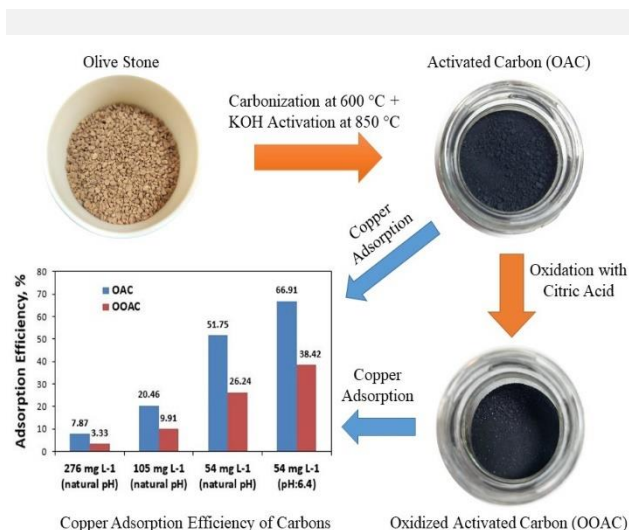
- [1] X. Ma, Q. Fu, International Journal of Environmental Research and Public Health, 17 (2020) 1428.
- [2] L. Guerra et al., Journal of Environmental Chemical Engineering, 6 (2018) 604-609.
- [3] L. Guerra et al., Journal of Environmental Chemical Engineering, 6 (2018) 671-676.

Olive stone-based chemically modified carbon adsorbents for copper adsorption

V. Rahimi, D. Gómez-Díaz, M.S. Freire, J. González-Álvarez*

Department of Chemical Engineering, School of Engineering, Universidade de Santiago de Compostela, Rúa Lope Gómez de Marzoa s/n. 15782, Santiago de Compostela, Spain.

*julia.gonzalez@usc.es



Carbon adsorbents fabricated from biomass precursors can be extensively used for the removal and recovery of heavy metal ions from aqueous solutions on account of low cost, availability and easy regeneration. In this research, in a first stage, a chemically activated carbon from olive stones was synthesized using KOH (OAC). Then, citric acid was applied to oxidize the surface chemistry of the activated carbon (OOAC) to investigate the effect of acid treatment on the adsorption efficiency of copper from aqueous solutions. The carbons were characterized using different analytical techniques such as FTIR, SEM, BET analysis, potentiometric titration and point of zero charge determination. Batch adsorption experiments demonstrated that treatment of the KOH-activated carbon with citric acid adversely influenced the copper adsorption efficiency resulting in a reduction of 50% at initial concentrations of 54 and 105 mg L⁻¹ and 58% at 276 mg L⁻¹ using natural pH compared to OOAC. Moreover, the highest adsorption efficiency (66.91%) was obtained for OAC at 54 mg L⁻¹ and an initial pH of 6.4.

Introduction

Copper is the most abundant metal present in waste printed circuit boards (WPCBs) (as the main component of waste electrical and electronic equipment) so that WPCBs are considered as prominent secondary copper resources and its recovery from WPCBs has very high economic and environmental advantages [1, 2]. Moreover, with the rapid growth and development of industrialization and urbanization, water pollution by toxic heavy metals has become a worldwide environmental problem [3]. Among these metals, copper is extensively used in different industries such as mining, metallurgical, refining, and electroplating. These industries produce a lot of wastewater containing a high concentration of copper which can be hazardous to the environment and human health. Therefore, it is required to remove copper from wastewater. The adsorption process using activated carbon fabricated from biomass resources is a promising approach to remove and recover copper from WPCBs and wastewater due to its low operational cost, easy performance, high efficiency, low sludge production, and easy regeneration of adsorbents [4, 5]. Activated carbon is extensively used to remove different pollutants from wastewater owing to its great surface area, high pore volume and adsorption capacity [6]. It has been found that citric acid has a high affinity for copper ions modifying the surface chemistry of a commercially available granular activated carbon to improve the adsorption capacity of copper from aqueous solutions [7]. However, to our knowledge, no studies were carried out on the effect of citric acid treatment on the surface chemistry of chemically activated carbons for copper adsorption. Therefore, in this work an activated carbon derived from olive stones as a biomass waste was initially fabricated using potassium hydroxide (KOH) followed by a surface oxidation using citric acid in order to investigate the influence of acid treatment on the copper adsorption efficiency of KOH-activated carbon.

Materials and Methods

After carbonization of olive stones as precursor at 600 °C for 1 hour, potassium hydroxide was used as an activating agent to fabricate activated carbon with a carbon/KOH ratio of 1:2 (w/w) at 850 °C for 2 hours (OAC). Then, the acid oxidation using 1 M citric acid solution was carried out with a solid/liquid ratio of 160 g L⁻¹ at room temperature under shaking for 30 min (OOAC) to evaluate the effect of acid treatment on the copper adsorption efficiency. Both prepared carbons were characterized using scanning electron microscopy (SEM), Fourier transform infrared spectroscopy (FTIR), nitrogen adsorption-desorption at -196 °C and carbon dioxide adsorption at 0 °C analyses, elemental analysis, potentiometric titration, and point of zero charge (pH_{pzc}) determination. Furthermore, batch experiments were performed by adding 50 mg of carbon into 50 mL of copper solutions (54, 105 or 276 mg L⁻¹) and using an orbital water bath shaker at a rate of 250 rpm and a pH of roughly 5.2 (natural pH) at room temperature for 72 hours. The effect of pH on the copper adsorption efficiency was investigated by carrying out two additional experiments at a pH of 6.4. Sodium hydroxide (NaOH) solution with a concentration of 0.1 M was used to adjust the pH value. All the experiments were replicated and the mean value was determined.

Results and Discussion

FTIR spectrum of OOAC showed a peak at 1724 cm⁻¹ due to the presence of carboxylic functional group (COOH) as a result of the treatment of surface chemistry (Figure 1). This is in agreement with the slight difference between the concentration of surface functional groups (C_{esf}) obtained from the potentiometric titration for both carbons (11.67 mmol g⁻¹ for OOAC compared to 10.50 mmol g⁻¹ for OAC). The peaks observed at 1001 and 1403 cm⁻¹ in OAC could be assigned to C-N stretching. Moreover, the peak at 1549 cm⁻¹ in OAC and 1585 cm⁻¹ in OOAC could be related to stretching vibration of -C=O or -NH. The broad peak at 3424 cm⁻¹ for both carbons is

attributed to vibration from amine groups (-NH) and hydroxyl groups (-OH).

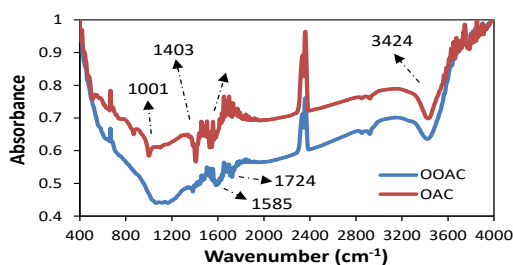


Figure 1. FTIR spectra of the carbons.

The first derivative of the titration curve for OOAC shows surface acidity owing to the presence of two hydrogen ions in comparison with OAC which is related to the presence of two equivalence points and two dissociation constants as a result of creating two different forms of citric acid dissociation (Figure 2). This effect can be also deduced from the pH_{pzc} of the carbons (3.5 for OOAC compared to 8.1 for OAC). In addition, the steepest slope in the first derivative curve represents the equivalence point for each carbon to determine the concentration of surface functional group. After citric acid treatment, the hydrogen and oxygen contents increased from 0.794 and 27.63% to 1.814 and 30.18%, respectively as shown in Table 1. As the hydrogen and oxygen amounts increased, the amount of carbon decreased while there was a little decrease in the content of nitrogen. This probably indicates that the acid treatment led to the introduction of more oxygen-containing functional group (carboxylic) and a reduction in the nitrogen-containing functional group (amine) on the surface of the KOH-activated carbon.

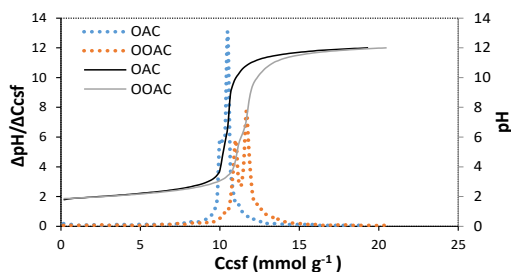


Figure 2. Titration curves (solid) and first derivative curves (dotted) for the carbons.

SEM images of the carbons (Figure 3) demonstrated no significant difference in the surface morphology which is in agreement with the amount of surface area and pore volume determined for both carbons with no considerable change (1760

$m^2 g^{-1}$ and $0.825 cm^3 g^{-1}$ for OOAC compared to $1708 m^2 g^{-1}$ and $0.818 cm^3 g^{-1}$ for OAC).

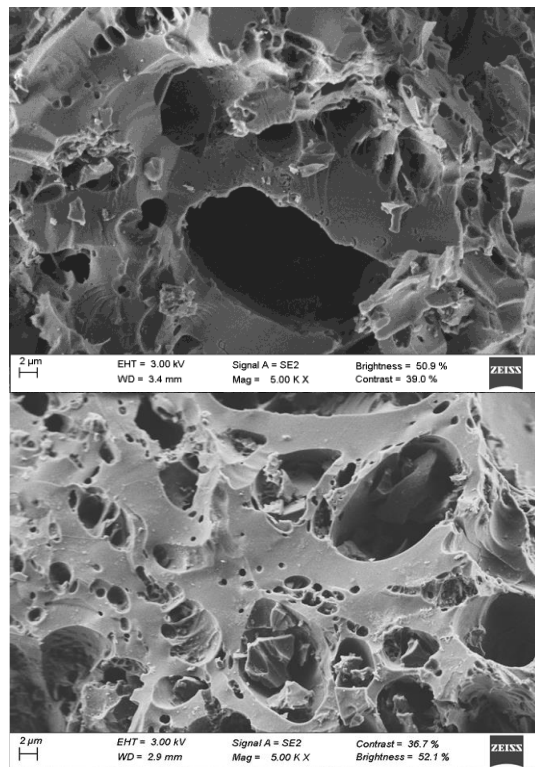


Figure 3. SEM images of the carbons: (a) OAC (b) OOAC.

Table 1. Elemental analysis of the carbons

Adsorbent	Element (%)				
	Nitrogen	Carbon	Hydrogen	Oxygen*	Sulfur
OAC	0.264	71.312	0.794	27.63	-
OOAC	0.213	67.793	1.814	30.18	-

* Calculated by difference $[100 - (N + C + H)]$

Batch adsorption experiments demonstrated that olive stone-based KOH-activated carbon without citric acid treatment is able to adsorb 51.75% of copper at $54 mg L^{-1}$ and natural pH compared to 26.24% for OOAC. As the initial pH increased to 6.4, a higher adsorption efficiency was obtained for both carbons (66.91% for OAC in comparison to 38.42% for OOAC). Moreover, increasing the copper concentration led to a reduction in the adsorption efficiency of both carbons (20.46% and 7.87% for OAC and 9.91% and 3.33% for OOAC at 105 and $276 mg L^{-1}$, respectively). This reduction in the adsorption efficiency of copper after citric acid oxidation could be related to that those functional groups that could interact with copper ions [8] as amine groups diminished, while other as the carboxylic groups increased only slightly

Acknowledgements

This work is part of I+D+i project Reference PID2021-122923NB-I00 financed by MCIN/AEI /10.13039/501100011033 / FEDER, UE.

References

- [1] M.L.F. Gameiro et al., Journal of Hazardous Materials, 183 (2010) 165-175.
- [2] E.-Y. Kim et al., Minerals Engineering, 21 (2008) 121-128.
- [3] H.K. Sharma et al., Chapter 3 in Biostimulation Remediation Technologies for Groundwater Contaminants, IGI Global, City, 2018, 50-79.
- [4] H. Demiral, C. Güngör, Journal of Cleaner Production, 124 (2016) 103-113.
- [5] L.S. Queiroz et al., Journal of Environmental Management, 270 (2020) 110868.
- [6] A. M. El-Wakil et al., Journal of Analytical & Bioanalytical Techniques, 5 (2014) 187.
- [7] J.P. Chen et al., Carbon, 41 (2003) 27-35.
- [8] C.I. Orozco et al., Sustainable Chemistry and Pharmacy, 32 (2023) 101016.

Effect of activation conditions of carbons derived from pine sawdust on wood dye removal

C.H. Pimentel, M.S. Freire, D. Gómez-Díaz, J. González-Álvarez*

Department of Chemical Engineering, School of Engineering, Universidade de Santiago de Compostela, Rúa Lope Gómez de Marzoa s/n, 15782 Santiago de Compostela, Spain.

*julia.gonzalez@usc.es



The toxic effects of dyes on humans and the aquatic environment are serious concerns. For this reason, an important research aim is the recovery of this type of substances by the development of suitable separation operations. Thus, one biochar and two activated carbons derived from pine sawdust (PS) were prepared as low-cost adsorbents for the removal of an acid wood dye from aqueous solutions in batch mode. The carbon activated with KOH at high temperature (ACPS-850) had the highest surface area ($2864.5 \text{ m}^2 \text{ g}^{-1}$), mainly due to micro and mesopores, and a high adsorption capacity (1660.4 mg g^{-1}) was achieved at an initial concentration of 500 mg L^{-1} . Optimum dye uptake at 25°C was recorded for an initial dye concentration of 500 mg L^{-1} at natural pH (9.32) and carbon dosage (0.3 g L^{-1}) for ACPS-850 and for an initial dye concentration of 100 mg L^{-1} at natural pH (8.10) and carbon dosage (0.5 g L^{-1}) for ACPS-600. Regarding the activated carbons equilibrium data were well fitted to the Langmuir model and generally adsorption kinetics was satisfactorily explained by the pseudo-second order kinetic model.

Introduction

Nowadays, a significant worldwide concern is the environmental pollution caused by dye-containing wastewaters from several industrial sources. The discharge of highly coloured wastes to water streams impedes light penetration which disturbs the biological processes taking place. Additionally, as most dyes are of synthetic origin, they present toxicity and sometimes mutagenic and carcinogenic effects and their removal from wastewaters becomes necessary [1]. There are several biological, chemical and physical techniques to remove dyes from wastewaters, but the adsorption operation has comparatively exceptional advantages for eliminating contaminants from liquid wastes due to its high efficiency, simplicity and safety. Activated carbons (ACs) are among the most widely used adsorbents but their high cost limits their use. Then, to overcome this limitation, the development of cost-effective ACs is imperative. Many studies have been focused on the development of low-cost renewable ACs being lignocellulosic materials the most common precursors [2-4]. Particularly, sawdust, an abundant and low-cost sawmill waste, is an interesting precursor for AC production as meets the dual purpose of waste management and sustainability [2, 5]. Normally, the production of AC comprises pyrolysis, in which the biomass is thermochemically decomposed at elevated temperatures in the absence of oxidants, and chemical activation with agents such as ZnCl_2 , HNO_3 or KOH , etc. to improve the AC specific surface area and textural properties providing binding sites and improving the sorption capacity [3-5]. In this study, one biochar (BC) and two activated carbons were prepared from pine (*Pinus radiata*) sawdust (PS) and used for the removal of a red wood dye (Red for wood GRA-200%) from aqueous solutions.

Materials and methods

PS was provided by a regional sawmill (Lugo, Spain) and after air-drying it was sieved and the fraction between 0.5 and 1 mm was selected for use.

Carbonization was carried out in a horizontal tubular furnace under an inert atmosphere provided with nitrogen (10 mL min^{-1}). PS was heated up at a rate of 5°C min^{-1} to reach the desired temperature of 600°C and maintained for 1 h. Then, the BC was mixed with KOH at a BC/ KOH mass ratio of 1:4 (w/w) and the mixture was heated at 5°C min^{-1} to the desired temperature, 600°C (ACPS-600) or 850°C (ACPS-850), under nitrogen atmosphere (10 mL min^{-1}) for 2 h. After activation the obtained AC was washed with 0.1 M HCl , subsequently, with distilled water to neutralize the pH [6], and finally dried at 105°C for 24 h. The materials were characterized by the point of zero charge (pH_{PZC}), BET specific surface areas (SSA) determined from N_2 and CO_2 sorption isotherms, Fourier-transform infrared spectroscopy (FTIR) and scanning electron microscopy with energy dispersive X-ray analysis coupled (SEM-EDX) before and after adsorption.

Adsorption studies were carried out in batch mode at 25°C . The effect of operating parameters such as time (up to equilibrium), initial dye concentration ($5\text{-}500 \text{ mg L}^{-1}$), adsorbent dose ($0.1\text{-}0.5 \text{ g L}^{-1}$) and pH (2-12) on adsorption performance was investigated and the best conditions were selected.

Results and Discussion

As seen in Table 1 the activation temperature strongly influenced the textural properties of the carbons.

To study the adsorption process, firstly, the effect of the initial dye concentration was evaluated using an adsorbent dose of 0.5 g L^{-1} , and for the lowest concentration (5 mg L^{-1}) the removal efficiency for both activated carbons was close to 100% at all pH assayed. However, the removal efficiency was significantly reduced using BC as adsorbent. As BC was not able to completely remove the red dye at 5 mg L^{-1} , the study at higher

concentrations was only carried out with the ACs. ACPS-850 was found to be very effective in removing the dye and removal percentages close to 100% were achieved in the pH range from 2 to 12. Regarding ACPS-600, adsorption efficiency depended significantly on pH and dye initial concentration. At 500 mg L⁻¹ the maximum uptake was 35.5% at pH 2 but reducing initial concentration to 100 mg L⁻¹ the dye was completely removed at natural pH (8.1) and pH 2.

In a second stage, at the initial concentrations for which total dye removal was achieved, the effect of the adsorbent dose at natural pH was studied for the ACs in the range 0.1-0.5 g L⁻¹. For ACPS-850, a 100% removal efficiency was attained reducing the adsorbent dose to 0.1 g L⁻¹ at the lowest concentration (5 mg L⁻¹) and to 0.3 g L⁻¹ at the highest one (500 mg L⁻¹). On the contrary for ACPS-600, adsorbent dose could only be reduced at the lowest initial dye concentration. The results at the selected conditions for both ACs are shown in Figure 1.

Kinetic studies performed under the conditions selected showed that the adsorption process generally follows the pseudo-second order kinetic model with $R^2 > 0.98$. The adsorption equilibrium data were best fitted by the Langmuir adsorption isotherm with $R^2 > 0.95$.

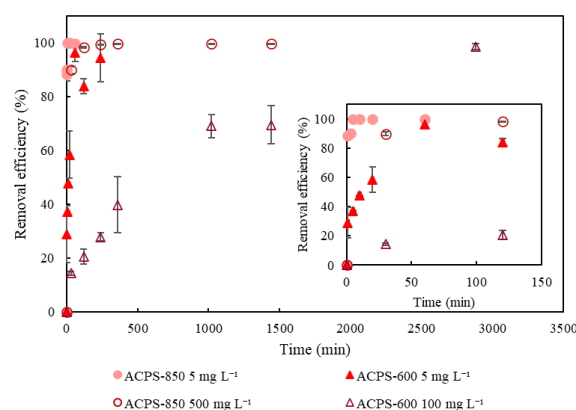


Figure 1. Effect of contact time on red wood dye adsorption at different initial concentrations for the selected conditions (natural pH: 4.09 (5 mg L⁻¹), 8.10 (100 mg L⁻¹) and 8.66 (500 mg L⁻¹); adsorbent dose: at 5 mg L⁻¹ for both AC 0.1 g L⁻¹; at 500 mg L⁻¹ for ACPS-850 0.3 g L⁻¹ and at 100 mg L⁻¹ for ACPS-600 0.5 g L⁻¹).

Conclusions

This study demonstrated the potential of pine sawdust waste biomass as an economical and efficient raw material to produce activated carbons with high surface area for dye removal from aqueous solutions.

Table 1. Characterization of the materials.

Materials	SSA N ₂ -196°C (m ² g ⁻¹)	SSA CO ₂ 0°C (m ² g ⁻¹)	pH _{PZC}	EDX* (%)
BC	293.3±7.7	254.8±1.3	6.7	C (91%); O (8%)
ACPS-600	2437.2±5.6	1354.2±21.8	4.0	C (84%); O (13%); F (1%)
ACPS-850	2864.5±0.9	588.1±25.9	7.2	C (43%); O (37%); K (15%); Al (5%)

*for atomic percentage > 1%.

References

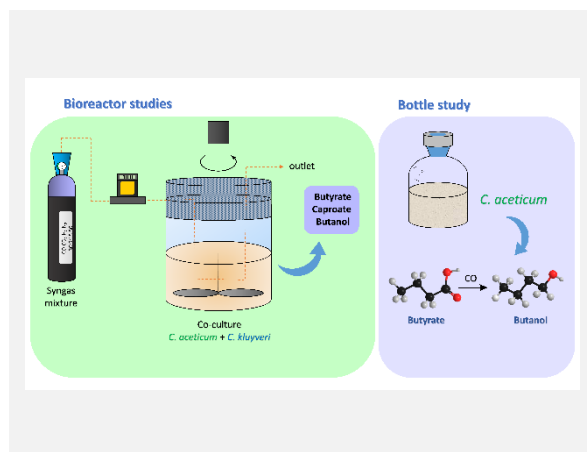
- [1] M.N. Mahamad et al., *International Biodeterioration and Biodegradation*, 102 (2015) 274-280.
- [2] R. Chikri et al., *Journal of Chemistry*, 2020 (2020) 1-17.
- [3] U. Tezcan Un et al., *International Journal of Environmental Science and Technology*, 16 (2019) 899-908.
- [4] J. Wang et al., *Applied Surface Science*, 530 (2020) 147187.
- [5] M.M. Pandey et al., *Spectrochimica Acta - Part A: Molecular and Biomolecular Spectroscopy*, 115 (2013) 887-890.
- [6] O.E. Eleri et al., *Electrochimica Acta*, 362 (2020) 137152.

Medium chain fatty acids production from syngas by a co-culture of *Clostridium aceticum* and *Clostridium kluyveri*

*C. Fernández-Blanco, M.C. Veiga, C. Kennes**

Chemical Engineering Laboratory, Faculty of Sciences and Centro Interdisciplinar de Química e Bioloxía (CICA), BIOENGIN Group, University of A Coruña, E-15008, A Coruña, Spain.

*Kennes@udc.es



One of the main drawbacks of combining syngas fermentation and chain elongation technology is the pH discrepancy between acetogens and chain elongating microorganisms. Despite this, the suitability of a co-culture of *C. aceticum* and *C. kluyveri* metabolizing syngas at near neutral pH in stirred tank bioreactors has been proven with this work. Two experiments were performed. In the first one, maximum concentrations of butyrate and caproate of 7.0 and 8.2 g/L, respectively, were produced. In the second bioreactor experiment, with a different pH strategy, besides carboxylic acids accumulation, considerable amounts of butanol were also produced because of the reduction, by *C. aceticum*, of the butyrate already formed in the broth. In both experiments, ethanol was used as an exogenous electron agent to some extent. Furthermore, batch bottle assays were carried out with a pure culture of *C. aceticum* grown on CO in presence of butyrate to assess and confirm its capability of producing butanol, reaching concentrations up to 951 mg/L.

Introduction

A promising technology to produce biocommodities such as alcohols and carboxylic acids in a sustainable way is syngas fermentation, since it employs acetogenic bacteria as autotrophic biocatalysts that utilize CO and CO₂ through the Wood-Ljungdahl pathway. Nevertheless, the distillation of these highly water-soluble end-products is rather expensive since it is an energy-intensive process. An alternative is to convert the produced short chain acids from syngas into MCFAs (Medium Chain Fatty Acids), such as caproic acid (C₆), through a second fermentation step. MCFAs are more hydrophobic, have a higher added-value and a higher energy density which makes them more suitable for the biofuels/bioproducts market. Likewise, this second bioconversion is performed through a biochemical process called chain elongation based on the reverse β -oxidation pathway.

However, to undertake this approach in a single reactor, one of the major challenges to be addressed is the pH incompatibility between most acetogens and chain elongating microorganisms. While acidic conditions promote solventogenesis (i.e., ethanol production) in acetogens, this is harmful to the survival of *C. kluyveri*, especially below pH 4.5 [1].

In *C. aceticum*, solventogenic phase starts at a pH around 6.9 rather than more acidic pH values [2]. It would therefore be interesting to combine this strain with *C. kluyveri*, taking advantage of the fact that ethanol production in *C. aceticum* takes place at a pH close to the optimum for *C. kluyveri*. So, the aim of the present work was to study the optimal operational conditions and the MCFAs and alcohols resulting from a formerly non-reported co-culture of *C. aceticum* and *C. kluyveri* fed syngas in bioreactors.

Materials and Methods

The exact composition of the medium used has been reported in recent literature [3]. The experiments were performed in 2 L Eppendorf BIOFLO 120 bioreactors, with a working volume of 1.2 L, and at a constant temperature of 30°C. After cooling down to room temperature, the reactor medium was flushed with pure

N₂ through a microsparger for 1 h and a half, while stirring at 250 rpm. Thereafter, the N₂ supply was stopped, and syngas feed was started using a constant flow rate of 10 mL/min, regulated by means of a mass flow controller. The CO:CO₂:H₂:N₂ ratio in the syngas mixture was 30:5:15:50. Next, the pH was adjusted to 7.5 and a seed inoculum of *C. aceticum* (10% v/v, 120 mL) in early exponential growth phase and a vitamins solution were also introduced in the reactor. The pH was monitored on-line and adjusted, when needed, through the addition of HCl or NaOH 1 M solutions connected to peristaltic pumps. In all the experiments, once the desired ethanol concentration was reached, after the solventogenic stage, 160 mL of *C. kluyveri* inoculum, with the corresponding vitamins, were added to the fermentation broth. On a daily basis, one or two liquid samples were withdrawn from the bioreactors with a sterile syringe for subsequent optical density measurements at $\lambda = 600$ nm and analysis of metabolites. Occasionally, 1 mL gas samples were taken from the outlet of the bioreactors for H₂, CO and CO₂ determinations.

Results and Discussion

In the first bioreactor experiment, exponential growth was reached after 62 h and acetate production was observed, so pH regulation was stopped to allow acidification and stimulate solventogenesis (Figure 1). The OD_{600nm} and acetate concentration reached then 0.87 and 1 g/L, respectively. In the following days, the pH dropped to 6.58 (t = 134 h), with an acetate concentration of 4.6 g/L at that pH. In order to avoid any possible inhibitory effect, the pH was adjusted to 6.9 at this point. This new pH value was maintained for 4 days, during which OD_{600nm} slowly declined from 1.97 to 1.70, and the acetate concentration continued to increase steadily up to 9 g/L after 230 h. Since no ethanol production was observed, the pH was decreased to 6.8 and an increase in ethanol concentration was then noticed, up to 329 mg/L, at t = 305 h. The pH was then further lowered in search of a value at which higher ethanol productivity could occur without compromising the biomass concentration. The ethanol concentration reached 3.2 g/L at t = 542 h and pH 6.5; however, the OD_{600nm} dropped

significantly from 1.6 to 1.3, so the pH was slightly increased again to 6.6, to circumvent further biomass decay. Though OD_{600nm} had been gradually increasing again, reaching a maximum of 2.6, at $t = 407$ h; from this point onwards, it followed a declining trend, a behavior previously reported with this strain at low pH [2]. On the other hand, acetate, which had reached a maximum concentration of 15.9 g/L, decreased for the first time to 15.4 g/L, at $t = 496$ h, while an increase of 0.9 g/L in ethanol concentration was observed at the same time. This indicated that acetate was being converted to ethanol at a faster rate than its *de-novo* synthesis.

Next, at $t = 593$ h, 160 mL of a *C. kluyveri* culture in early exponential phase was inoculated in the reactor, when the acetate and ethanol concentrations were 14.7 and 3.2 g/L, respectively. At some point, it was even necessary to supply exogenous ethanol three times upon its depletion. These three additions increased the ethanol concentration up to 4 g/L, 6.7 g/L and 5.8 g/L, respectively. Owing to the renewed availability of the electron donor, butyrate and caproate continued to accumulate via chain elongation, reaching final caproate and butyrate concentrations of 8.2 g/L and 7.0 g/L, respectively. Also, after inoculation of *C. kluyveri*, H_2 production was continuously detected, at trace levels, until the end of the experiment.

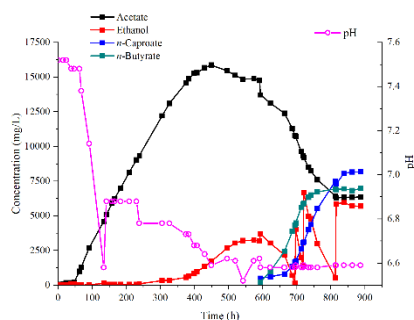


Figure 1. Metabolites concentrations in the culture broth with the co-culture (left axis) and the working pH (right axis) versus time (h) during the 1st bioreactor experiment [3].

Based on these data, a second bioreactor was started-up in which the pH was maintained at 6.6 immediately after natural acidification. This was expected to favor earlier ethanol production and avoid excessive accumulation of acetate found in the previous assay.

By doing this, biomass decay was observed, and, at this stage, acetate concentration started to decrease, while ethanol concentration increased. Just before inoculating 160 mL of *C. kluyveri* seed culture into the bioreactor, the concentrations of acetate and ethanol, at $t = 310$ h, were 3.9 g/L and 1.5 g/L, respectively (Figure 2), corresponding to an ethanol:acetate molar ratio of 0.5, which was indeed higher than the ratio of 0.28 of the previous described experiment, as successfully planned with this new pH-strategy. Nonetheless, at the same time, this led to lower net total concentrations of the electron donor and

Acknowledgements

This research was funded through the Spanish Ministry of Science and Innovation and European FEDER funds (PID2020-117805RB-I00). CFB thanks Xunta de Galicia for her doctoral contract (ED481A-2020/ 028). The authors, belonging to the BIOENGIN group, thank Xunta de Galicia for financial support to Competitive Reference Research Groups (ED431C 2021/55).

References

- [1] R. Ganigué et al., *Frontiers in Microbiology*, 7 (2016) 702.
- [2] K. Arslan et al., *Bioresource Technology*, 292 (2019) 121941.
- [3] C. Fernández-Blanco et al., *Journal of Environmental Management*, 302 (2022) 113992.

the electron acceptor than in the previous experiment, due to the earlier pH drop. At this point, OD_{600nm} started decreasing dramatically, attributed to the decay of *C. aceticum*. Several attempts were made in order to try to reactivate the strain by raising the pH again. On the other hand, according to the consumption and production profiles, the activity of *C. kluyveri* started 7 days after its inoculation (at $t = 480$ h), with an increase in butyrate concentration and ethanol consumption. From this point onwards, the concentration of butyrate remained higher than caproate, reaching maximum values of 1.96 g/L and 1.14 g/L, respectively. Finally, unexpectedly, considerable amounts of butanol were first found at $t = 900$ h, reaching a maximum concentration of 719 mg/L.

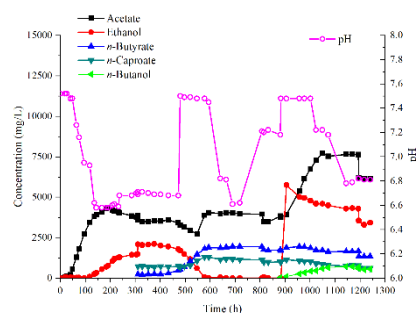


Figure 2. Metabolites concentrations in the culture broth with the co-culture (left axis) and the working pH (right axis) versus time (h) during the 2nd bioreactor experiment [3].

To confirm that indeed, *C. aceticum* is the microorganism responsible for the reduction of butyrate, previously formed by *C. kluyveri* into butanol, a study was carried out in CO pressurized bottles with a pure culture of *C. aceticum*. The strain was inoculated in a medium containing 2.3 g/L butyrate (Table 1), which was converted to 951 mg/L butanol, after 400 h, with a conversion efficiency of 96%. Thus, the ability of *C. aceticum* to reduce carboxylates to their corresponding alcohols is proven.

Table 1. Experimental conditions of the bottle assay with *C. aceticum*. (Concentrations are shown in mg/L).

[Butyrate] _{in}	[Butyrate] _{end}	[BuOH] _{max}	[Acetate] _{max}
2319	1135	951	1417

Conclusions

This research demonstrated the suitability to combine syngas fermentation and chain elongation technologies in one single bioreactor to produce MCFAs and bioalcohols. For this purpose, a co-culture consisting of *C. aceticum* and *C. kluyveri* was successfully used in a pH range of 6.6–7.5. This work used *C. aceticum* for the first time as a new acetogenic bacterium able to co-exist with *C. kluyveri* at pH values close to neutrality, which had never been tested before, thus contributing to progress beyond the state of the art. Also, the ability of *C. aceticum* to reduce butyrate to butanol, in presence of syngas, was demonstrated.

Response surface methodology approach for keratin recovery using a bio-based ionic liquid

C. Polesca^{1,2}, A. Al Ghatta², H. Passos¹, J.A.P. Coutinho¹, J.P. Hallett², M.G. Freire^{1*}

¹CICECO - Aveiro Institute of Materials, Department of Chemistry, University of Aveiro, Aveiro, Portugal; ²Laboratory of Sustainable Chemical Technology, Department of Chemical Engineering, Imperial College London, South Kensington Campus, London, United Kingdom.

*maragfreire@ua.pt



Chicken is one of the most consumed meats in the world. Consequently, a large amount of feathers waste is generated, highlighting the requirement to develop sustainable ways of waste valorization. Although keratin recovery from chicken feathers has been reported in the literature using imidazolium-based ionic liquids (ILs), bio-based ILs were not investigated yet. In this work it was used cholinium acetate as a bio-based IL for keratin dissolution from chicken feathers waste. A response surface methodology approach was used to identify optimal keratin dissolution and recovery operating conditions. The IL recovery and reuse were successfully evaluated, and a techno-economic assessment was performed. The results obtained in this work demonstrate that bio-based ILs are attractive solvents for keratin dissolution, opening the door for their use in this field and the development of more sustainable recovery processes.

Introduction

Chicken industrial processing results in a high amount of feather waste, corresponding to around 7 wt % of the total mass of an adult chicken [1], [2]. The highest component present in feathers is keratin (± 90 wt %) [1] a fibrous protein with applications in cosmetics and biomedical field [2], [3]. Keratin presents low solubility in organic solvents due to the inter- and intramolecular disulfide bonds in sulfur-containing amino acids [4]-[6] making its recovery a difficult process. To overcome this, researchers have reported the use of ionic liquids (ILs) as efficient solvents to dissolve biomass rich in keratin [4], [7]. ILs are salts with low melting temperatures compared to inorganic salts because they are composed of large organic cations and organic or inorganic anions [8].

In 2005, 1-butyl-3-methylimidazolium chloride ($[\text{C}_4\text{C}_{1\text{im}}]\text{Cl}$) was used for the first time to dissolve wool and recover keratin [9]. Since then, ILs have demonstrated excellent results when well-designed, highlighting the good performance of acetate-based ILs due to its stronger hydrogen-bonding acceptor ability [4]. More recently, our research group optimized keratin recovery from chicken feathers using 1-butyl-3-methylimidazolium acetate ($[\text{C}_4\text{C}_{1\text{im}}][\text{C}_1\text{CO}_2]$). Despite the efficient effect of this IL, imidazolium-based ILs can present some environmental and biocompatibility concerns [10], [11]. To overcome this issue, ILs derived from renewable feedstock (e.g. amino acids and natural sugars) can be used, aimed to present lower toxicity and higher biocompatibility [12], [13]. In this work [14] we investigated the use of a bio-based and low-cost IL, namely cholinium acetate ($[\text{N}_{111}(\text{2OH})][\text{C}_1\text{CO}_2]$), for chicken feathers dissolution. In addition, considering the challenges regarding the industrial application of ILs (their cost and requirement for recovery and reuse) [8], we evaluated $[\text{N}_{111}(\text{2OH})][\text{C}_1\text{CO}_2]$ recycling (4 cycles) and performed a techno-economic assessment of the developed keratin recovery process.

Methods

Following our previous work [2], chicken feathers were dissolved in an aqueous solution of $[\text{N}_{111}(\text{2OH})][\text{C}_1\text{CO}_2]$ (80 wt%) in a solid:liquid (chicken feathers:solvent) weight ratio of 1:20 w/w, at 100 °C, 650 rpm for 4 h. Keratin precipitation was optimized through central composite planning using the RSM 2³, investigating coagulant solvent, time and solution:coagulant ratio. The solution was centrifugated for 20 min at 25 °C and 4000 rpm in a refrigerator centrifuge. Keratin was collected and washed with water to improve IL removal, and then dried at 50 °C in an air oven for 48 h. The keratin recovery yield ($\text{Ker}_{\text{RY}}\%$) was obtained according to the mass of keratin recovered (m_{keratin}) and mass of chicken feathers (m_{feathers}), considering the amount of protein present in the feathers (90 wt %) [2] according to Equation 1:

$$\text{Ker}_{\text{RY}}\% = \left(\frac{m_{\text{keratin}}}{m_{\text{feathers}} \times 0.9} \right) \times 100 \quad (1)$$

The recovery and reuse of $[\text{N}_{111}(\text{2OH})][\text{C}_1\text{CO}_2]$ was evaluated by removing the volatile compounds from the solution obtained after precipitation and washing steps, using a rotatory evaporator. The purity of the IL was determined by determining the water content in the obtained IL. The mass of IL recovered (m_{R}), the mass of IL used at the dissolution step (m_0) and the purity of IL (%IL) were used to determine the IL recovery yield ($\text{IL}_{\text{RY}}\%$):

$$\text{IL}_{\text{RY}}\% = \left(\frac{m_{\text{R}} - \% \text{IL}}{m_0} \right) \times 100 \quad (2)$$

Concerning the techno-economic assessment, a process simulation was carried out at Aspen Plus V11 for process modelling with the integrated Aspen Economics package for the estimation of the purchased and installed costs of the plant,

following the principles reported in the literature for other biomass processes [15].

Results

The results obtained with RSM (Figure 1) indicate that keratin yield increases when the ethanol concentration is low (around 20.25 wt%), revealing that water is better at creating H-bonds with $[N_{111(2OH)}][C_1CO_2]$, enabling protein precipitation.

The optimal conditions for keratin recovery are 20.25 wt % of ethanol in water, 5 h, and solution:coagulant ratio of 1:1.45 w/w, achieving a keratin yield of (93 ± 4) wt %.

Regardless of the feasibility of the keratin recovery process using an aqueous solution of IL, $[N_{111(2OH)}][C_1CO_2]$ was recovered and reused for 4 cycles. The higher amount of recovered IL (~88 wt %) proceed from the precipitation step, followed by the first washing (~5 wt %), while the subsequent washings correspond to only ~1 wt %.

Aiming to develop a sustainable process, the economic and environmental impact of $[N_{111(2OH)}][C_1CO_2]$ recycling was also evaluated. According to our process simulation, the process has a positive CO_2 emission of about $4.04 \text{ kgCO}_2 \cdot \text{kg}_{\text{keratin}}^{-1}$, mainly due to the unavailability of heat sources in the process in contrast

to typical biomass-based approaches. The minimum selling price achieved for keratin is $22 \text{ \$} \cdot \text{kg}^{-1}$, calculated taking into consideration the total productivity of $350 \text{ tons}_{\text{keratin}} \cdot \text{year}^{-1}$, making this process suitable for cosmetics and biomedical applications.

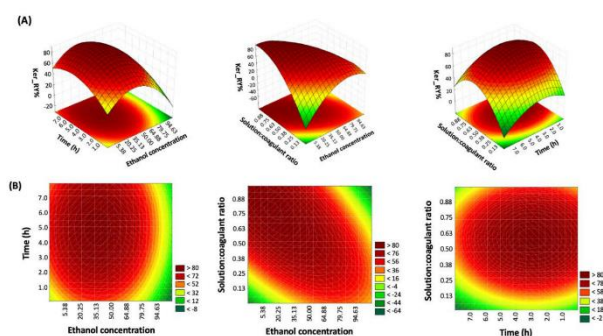


Figure 1. Surface graphs (A) and contour graphs (B) of the interactions of different variables in the keratin recovery: (i) time and ethanol concentration, (ii) solution:coagulant ratio and ethanol concentration, and (iii) solution:coagulant ratio and time.

Acknowledgements

This work was developed within the scope of the project CICECO-Aveiro Institute of Materials, UIDB/50011/2020, UIDP/50011/2020 & LA/P/0006/2020, financed by national funds through the FCT/MCTES (PIDDAC). C. Polesca acknowledges FCT - Fundação para a Ciência e a Tecnologia for the Ph.D. grant with the reference UI/BD/151282/2021. H. Passos acknowledges FCT, I.P., for the researcher contract CEECIND/00831/2017, under the Scientific Employment Stimulus-Individual Call, 2017.

References

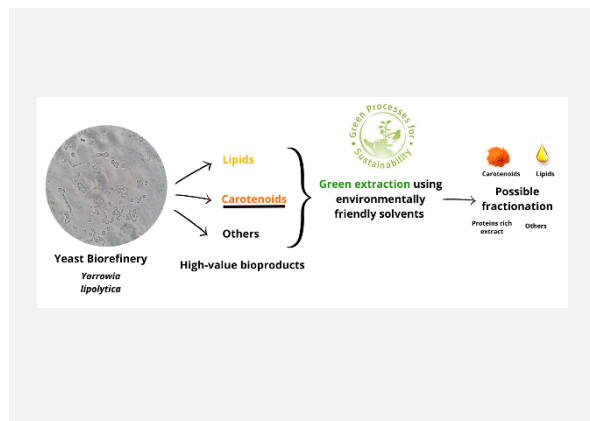
- [1] T. Tesfaye et al., *Sustainable Chemistry and Pharmacy*, 8 (2018) 38-49.
- [2] C. Polesca et al., *Green Chemistry*, 25 (2023) 1424-1434.
- [3] R.-R. Yan et al., *Applied Microbiology and Biotechnology*, 106 (2022) 2349-2366.
- [4] X. Liu et al., *ACS Sustainable Chemistry & Engineering*, 6 (2018) 17314-17322.
- [5] E.M. Nuutinen et al., *RSC Advances*, 11 (2021) 27512-27522.
- [6] R.K. Donato et al., *Polymers*, 12 (2020) 1-64.
- [7] R. Li et al., *Journal of Applied Polymer Science*, 127 (2013) 2648-2653.
- [8] C. Polesca et al., *Current Opinion in Green and Sustainable Chemistry*, 37 (2022) 100675-100683.
- [9] H. Xie et al., *Green Chemistry*, 7 (2005) 606-608.
- [10] A. Tarannum et al., *International Journal of Biological Macromolecules*, 209 (2022) 498-505.
- [11] J. Flieger et al., *International Journal of Molecular Sciences*, 21 (2020) 6267-6308.
- [12] D. Mondal et al., *Green Chemistry*, 18 (2016) 6071-6081.
- [13] J.M. Gomes et al., *ACS Sustainable Chemistry & Engineering*, 8 (2020) 13507-13516.
- [14] C. Polesca et al., Submitted for publication, 2023.
- [15] A. Al-Ghatta et al., *ACS Sustainable Chemistry & Engineering*, 7 (2019) 16483-16492.

Recovery of carotenoids from *Yarrowia lipolytica* using biosolvents

C. Naveira-Pazos^{1,2*}, M.C. Veiga¹, C. Kennes¹, J.F.B. Pereira²

¹University of A Coruña, Chemical Engineering Laboratory (BIOENGIN group), Faculty of Sciences and Center for Advanced Scientific Research (CICA), E-15008, A Coruña, Spain; ²University of Coimbra, CIEPQPF, Department of Chemical Engineering, Faculty of Sciences and Technology, Rua Sílvio Lima, Polo II, Coimbra, Portugal.

*cecilia.naveira@udc.es



The production of natural microbial pigments is of great industrial interest due to their use in different industrial sectors. *Yarrowia lipolytica* has the ability to synthesize several compounds of high added value, among which carotenoids (β -carotene) and lipids stand out. In this study, the yeast strain was grown on glucose for accumulation and subsequent recovery of intracellular carotenoids. This yeast strain accumulated carotenoids, which were then extracted using mixed biosolvents, without the need of organic chemical solvents and energy intensive mechanical approaches. The maximum recovery yields of carotenoids (from 50-100%) were achieved using four successive SLE (Solid-Liquid Extraction) operations, when these are integrated with a subsequent SLLS (Solid-Liquid-Liquid Extraction). The proposed biosolvents-based extraction process if combined with other downstream processing units can allow the fractionation of the different intracellular products.

Introduction

The production of carotenoids is currently a very important topic mainly in the nutraceutical and food industries. Microbes appear to be the most promising sources of these types of metabolites, with yeasts demonstrating a high capacity for the synthesis of antioxidant carotenoids, such as β -carotene. However, the traditional recovery of carotenoids, since these are biosynthesized intracellularly by different yeasts, involves the use of energy intensive mechanical methods and/or volatile organic compounds. These processes are highly efficient but also have disadvantages in terms of sustainability, such as high consumption of energy and the hazardous nature of some solvents to both humans and the environment [1].

It is now crucial to develop more biocompatible and environmentally-friendly extraction processes that protect human health and environment. Therefore, much attention is being paid to the development of extraction platforms that use less toxic solvents of biological origin, such as ethanol, isopropanol, water, among others. Mussagy et al., (2020) demonstrated that it was possible to recover different types of carotenoids and lipids from wet *R. glutinis* CCT-2186 biomass using a mixture of ethanol, ethyl acetate and water [2]. EtOH (ethanol) and water are two environmentally-friendly solvents that are widely used in industry [3]. Besides, EtOAc (ethyl acetate) can also be considered as a biosolvent as it can be obtained from the conversion of bioethanol [4].

Considering this, the main goal of this work was to recover carotenoids accumulated in the wet biomass of the oleaginous yeast *Yarrowia lipolytica*, evaluating the efficiency of these bio-based solvents on another type of yeast strain and compare it to *R. glutinis*. *Y. lipolytica* is considered a very suitable microorganism for biofuel production, as it can accumulate lipids very efficiently [5]. Further studies could focus on the possible fractionation of the products obtained (as shown in the Graphical Abstract), carrying out the saponification of the extract, and thus separating lipids from carotenoids. This integrated approach constitutes a truly interesting technology even at an industrial level.

Material and methods

Strain and aerobic fermentation

An engineered strain of *Y. lipolytica* was used to produce carotenoids, among other bioproducts (e.g., microbial oils).

Aerobic yeast cultivation

The yeast cultivation was carried out in aerobic conditions in 500 mL flasks and using glucose as sole carbon substrate. The cultivation was carried out for 7 days, until most of the initial substrate was consumed.

Biomass determination

Microbial growth was determined spectrophotometrically (Hitachi, Model U-200, Pacisa & Giralt, Madrid, Spain) by measuring the optical density at a wavelength of 600 nm, following the protocol described previously [6].

Glucose analysis

The amount of glucose present in the fermented medium was measured by using a high-performance liquid chromatograph (HPLC) (HP1100, Agilent Co., USA).

Determination of carotenoids content

The quantification of β -carotene was determined by measuring the visible-light absorption spectra (V-550/560/570 Spectrophotometer). The calibration curves at 455 nm were established using a β -carotene standard solution, and the total carotenoid concentrations were quantified as β -carotene equivalent.

Solid-Liquid Extraction (SLE) of carotenoids using mixtures of biosolvents

The β -carotene equivalent content was determined following the SLE method described by Mussagy et al., (2021) [7]. Briefly, the SLE experiments were carried out in 20 mL capped glass tubes. 1.125 mL of pure acetone (as control) and a ternary mixture of EtOH, EtOAc and H₂O was added to a given amount of wet biomass. The tubes were homogenized using a magnetic stirrer hot plate mixer (IKA C-MAG HS7) for 1 h at 65 °C and with agitation. Afterwards, the samples were centrifuged (3800

rpm) for 10 min, and the cell lysate supernatants recovered, stored, and used for the determination of carotenoids content. Successive SLE were performed until the supernatants were colourless, determining the total amount of β -carotene equivalent of the samples and the respective extraction profiles.

Solid-Liquid Extraction (SLE) followed by Solid-Liquid-Liquid extraction (SLLE) for phase separation

SLE under different initial proportions of each of the biosolvents were carried out. After mixing for 1 h at 65 °C the mixtures, additional amount of water and ethyl acetate was added to shift the equilibrium to the biphasic region. The samples were then vortexed for 5 min and centrifuged (3800 rpm) for 10 min. The phases were separated and the carotenoids in the upper phase quantified.

Results and Discussion

The yeast cultivation with glucose showed that, for an initial substrate concentration of 36.6 g/L, large amounts of the carbon source were consumed after seven days of growth, achieving a maximum OD₆₀₀ of 22 on day 6.

After the yeast cell cultivation, the wet biomass was recovered and subjected to following extractions for the recovery of intracellular carotenoids. The first step was to evaluate the capacity of mixed biosolvents, in a ternary mixture, for the recovery of carotenoids (and other metabolites) from *Y. lipolytica* wet biomass. Different solvent ratios and different amounts of starting biomass were used to determine the best conditions for efficient carotenoids' extraction. Different proportion of solvents were evaluated and successive SLEs were carried out until the extracts became colourless. The total amount of β -carotene equivalent present in the samples were determined and compared with the extraction profile obtained with acetone, as control. Although the profiles obtained with acetone and the biosolvent mixture were similar, the concentration of carotenoids (as β -carotene equivalent) extracted using biosolvents was higher than that obtained with acetone.

The next step was to carry out different SLE, with different initial proportions of biosolvents and then integrated it with a following SLLE at the biphasic region. In that case, independently of the initial proportion of mixed solvents, a same

ternary composition of mixed biosolvents was obtained in all trials (*i.e.*, achieving the same SLLE biphasic mixture). It was found that, with the integration of SLE and SLLE operations, the carotenoid recovery reached yields of up to 100% after only four consecutive extractions. This is an impressive result when compared with the 15 SLE required to obtain the complete recovery of the carotenoids. As shown in Figure 1, β -carotene equivalent recovery yields increased as the composition of EtOAc increases, and the water ratio decreases in the mixtures used in the SLE.

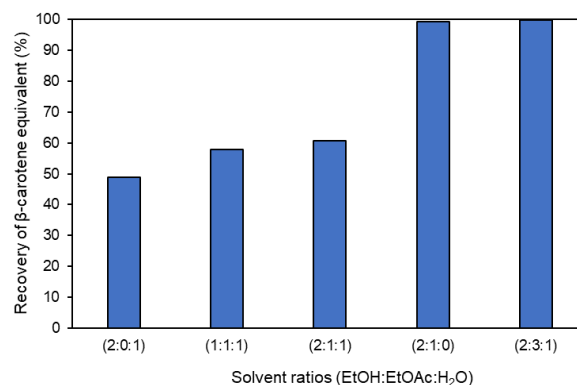


Figure 1. Recovery yields (%) of carotenoids (β -carotene equivalent) in different mixtures of ethanol, ethyl acetate and/or water.

Conclusions

In this work, the recovery of carotenoids from *Y. lipolytica* wet biomass was successfully achieved using biosolvents. SLE followed by a SLLE step significantly enhanced the recovery of these pigments, contributing for decreases the processual costs. This work also revealed that the efficiency of the extraction process of these pigments can be achieved by increasing the amount of EtOAc and decreasing the amount of H₂O in the extraction mixture, increasing the extraction yield by up to 2-fold. The potential of biosolvents for pigment recovery as a sustainable and economical alternative to conventional solvents was demonstrated, as well as the possibility of integrating SLE and SLLE processes for the recovery of other metabolites biosynthesized by microorganisms.

Acknowledgements

Cecilia Naveira Pazos thanks Inditex-UDC 2023 grants for financial support of her short-term visit to University of Coimbra. Part of this research was financed by the Spanish Ministry of Science and Innovation (PID2020-117805RB-I00). The BIOENGIN group at UDC, thanks Xunta de Galicia for financial support to Competitive Reference Research Groups (ED431C 2021/55). CIEPQPF is supported by the Fundação para a Ciência e Tecnologia (FCT) through the projects UIDB/EQU/00102/2020 and UIDP/EQU/00102/2020.

References

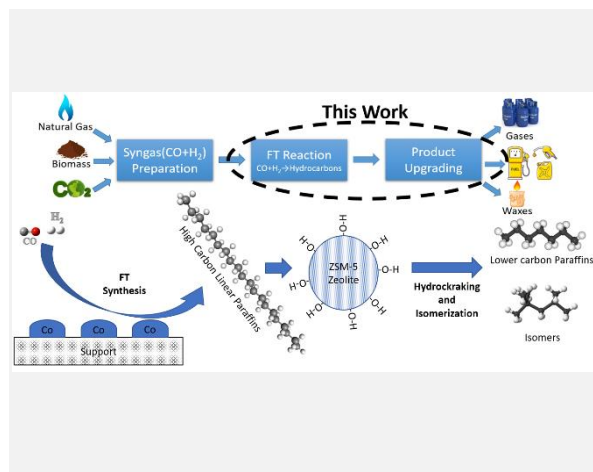
- [1] C.U. Mussagy et al., *Green Chemistry*, 24 (2022) 118-123.
- [2] C.U. Mussagy et al., *Green Chemistry*, 22 (2020) 8478-8494.
- [3] D. Prat et al., *Green Chemistry*, 18 (2016) 288-296.
- [4] J.A. Posada et al., *Bioresource Technology*, 135 (2013) 490-499.
- [5] S. Yook et al., *Renewable Energy*, 132 (2019) 61-67.
- [6] C. Naveira-Pazos et al., *Bioresource Technology*, 360 (2022) 127649.
- [7] C.U. Mussagy et al., *Separation and Purification Technology*, 266 (2021) 118548.

Obtaining liquid fuels by applying bifunctional catalysts in the Fischer-Tropsch process

D. Costa^{1*}, J. Joaquim¹, E. Falabella², C.M. Magalhães^{3,4}, B.F. Machado⁴, M.F. Ribeiro¹

¹Centro de Química Estrutural, Instituto Superior Técnico, Universidade de Lisboa, Av. Rovisco Pais, Lisboa 1049-001, Portugal; ²Department of Organic Processes, School of Chemistry, UFRJ – CT, Bloco E, Cidade Universitária, Ilha do Fundão, Rio de Janeiro, RJ 21941-909, Brazil; ³LSRE-LCM, Faculty of Engineering, University of Porto, 4200-465 Porto, Portugal; ⁴CoLAB Net4CO₂ - Network for a Sustainable CO₂ Economy, 4200-355 Porto, Portugal.

daniel.pereira.costa@tecnico.ulisboa.pt



Fischer-Tropsch (FT) process, which transforms syngas (H₂ and CO) into liquid fuels, appears as a possible solution to decrease CO₂ emissions. Bifunctional catalysts combining metal and acid properties to promote simultaneously the FT synthesis and upgrading (hydrocracking and isomerization) can contribute to a decrease in the overall costs of the process.

In this work different bifunctional cobalt-based catalysts were tested. These bifunctional catalysts comprise supported catalysts based on microporous ZSM-5 zeolites with different Si/Al ratios, hierarchical ZSM-5 zeolites prepared through desilication with different conditions and core-shell catalysts using ZSM-5 shell and different supports (Al₂O₃, SiO₂ and ZSM-5 zeolite) as core. After comparison, we concluded that the textural properties of the hierarchical zeolite are important to maximize the yield towards gasoline-range hydrocarbons and isomer content of the final product.

Introduction

CO₂ emissions prices have been increasing in the last decades due to environmental politics, boosting the research for more sustainable processes in order to achieve a carbon neutral economy [1]. The Fischer-Tropsch (FT) process can be a good solution to produce sustainable fuels since the technology is already very well developed [2]. However, the FT process usually is a 3 steps process (graphical abstract) which increases the overall costs. Bifunctional catalysts comprising metal and acid sites can be used to reduce the number of steps needed and decrease the costs [3].

The most common FT catalysts are based on cobalt and iron, generally supported on Al₂O₃ or SiO₂. Cobalt catalysts present both higher activity than iron ones and lower activity for the water gas shift reaction and hydrogenation, forming less CH₄. In this work, a cobalt-based catalyst was used. The acid sites from bifunctional catalysts can be provided by zeolites [3]. These metal zeolite-based catalysts can be obtained as physical mixtures, core-shell or supported catalysts. Using bifunctional catalysts, FT leads to the formation of hydrocarbons, which can then suffer hydrocracking and isomerization.

In recent years the application of hierarchical zeolites, having both meso and micropores, have shown advantages when compared with normal zeolites. Hierarchical zeolites can improve the dispersion of the metal phase in supported catalysts, increase the overall activity of the catalyst, decrease the selectivity to methane by reducing the diffusion limitations of the reactants, and increase the accessibility to acid and/or metal sites [4].

Objectives

The objective of this work was to evaluate the performance of different bifunctional catalysts in order to understand potential structure-activity correlations and maximize the yield towards liquid fuels.

Methods

Catalysts Preparation

All the supported catalysts were prepared by incipient wetness impregnation using cobalt nitrate as precursor. The reference FT catalyst, prepared at Universidade Federal do Rio de Janeiro (UFRJ) has 10 wt.% cobalt and 0.5 wt.% Re supported in γ -Al₂O₃. The other supported catalysts have 10% cobalt loading supported in different microporous and hierarchical zeolites.

The core-shell catalysts were prepared by synthesizing a ZSM-5 zeolite using general recipes but adding the cobalt based supported catalysts to the synthesis solution. The zeolite crystallizes and grows around the supported catalyst (core) forming a shell. γ -Al₂O₃, SiO₂ and a hierarchical ZSM-5 zeolite were used as supports.

The parent zeolites used in this work were acquired from *Zeolyst* with Si/Al ratios of 25 and 40. A sequential alkaline-acid treatment was applied for both zeolites to generate mesopores. The alkaline treatment was performed using NaOH or TPAOH to promote different textural properties.

Characterization

All catalysts were characterized by Inductively Coupled Plasma Optical Emission Spectroscopy chemical analysis, powder X-ray diffraction, N₂ physisorption, thermogravimetric analysis, NH₃ temperature programmed desorption, adsorption of pyridine followed by FTIR spectroscopy and H₂ temperature programmed reduction.

Catalytic tests

The catalytic tests were performed in a bench-scale fixed-bed down-flow stainless steel reactor (Microactivity Efi, *PID Eng&Tech*). The catalyst was reduced *in situ* with a 120 mL·min⁻¹·g_{cat}⁻¹ pure hydrogen at 1 bar during 10 h at 400 °C (heating ramp of 2 °C·min⁻¹). The catalysts were then tested at 20 bar, 240 °C, GHSV = 4 m³·kg_{cat}⁻¹·h⁻¹ and H₂/CO = 2. The gases were analyzed using an online gas chromatograph while the liquid organic fraction was analyzed using an offline gas chromatograph.

Results

From Table 1 it is possible to observe that the alkaline treatment has successfully created mesopores in all hierarchical samples, leading to an increase of mesopore volume in the range of 200 to 600 %. The largest increase was observed for the sample obtained from an MFI zeolite with Si/Al = 40, ZSM5 40, after desilication with NaOH (ZSM5 40 NaOH), since a lower concentration of Al in the framework allows a higher destruction of the pore structure. On the other hand, the sample obtained from an MFI zeolite with Si/Al = 25, ZSM5 25, after alkaline treatment with TPAOH (ZSM5 25 TPAOH) presented the lowest mesopore volume increase, and the highest surface area due to the effect of TPAOH as pore-directing agent by hindering the mesopore formation. The samples obtained from MFI zeolite with Si/Al = 25 after desilication with NaOH and TPAOH presented similar Si/Al ratio and amounts of Brønsted acid sites when compared with the parent zeolite, suggesting that desilication led to some Al removal or that some Al atoms were removed from the framework during the mild acid treatment. The other desilicated sample, NaZ40AIC, has a Si/Al ratio and acid properties similar to PZ25C, instead of the respective parent zeolite, PZ40C. This unexpected reduction of Si/Al ratio obtained after alkaline treatment and mild acid treatment suggests that in the case of NaZ40AIC more Al remained in the framework. From the H₂ temperature programmed reduction results, an increase of the reduction temperatures for the zeolite supported catalysts was observed, due to the higher metal-support interaction. This effect was stronger for microporous zeolites.

From Table 2 it is possible to observe that the zeolite-supported catalysts presented a lower CO conversion, since there are evidence of a lower cobalt dispersion and reducibility in such type of catalysts when compared to the reference Al₂O₃-supported catalyst. This behavior is not observed for the

Co/ZSM-5 40 catalyst. The zeolite supported catalysts also evidenced an increase in CH₄ selectivity that can be related with hydrocracking of α -olefins or hydrogenolysis, as well as an increase of C₂₋₄ and C₅₋₁₂ hydrocarbons due to the hydrocracking and isomerization promoted by the zeolite. The hierarchical zeolites increased the CO conversion due to lower diffusion limitations of the reactants. The hierarchical samples also showed a higher selectivity towards C₅₋₁₂ range and presented a higher content of isomers in the liquid products. The increase in C₅₋₁₂ selectivity can be due to an increase of accessibility of the acid sites, which promoted even more hydrocracking and isomerization. This higher acid site accessibility also increases the isomer generation. On the other hand, the higher surface area of hierarchical samples could promote the key-lock mechanism favoring even more the isomer formation. Between the hierarchical samples, the catalyst Co/ZSM5 25 TPAOH presented the highest amount of isomers in the liquid products.

Conclusions

This work showed that it is possible to generate hierarchical ZSM-5 zeolites with different textural properties through sequential alkaline and acid treatments by just changing the base used in the alkaline treatment and the parent zeolite. From the catalytic tests it was proven that zeolites can increase the quality and yield of liquid products and that the one-step production of liquid fuels through FT process is possible using bifunctional catalysts. Finally, hierarchical zeolites are important to increase the process since this type of material not only increase the quality and selectivity of liquid fuels, but also maximizes CO conversion.

All the core-shell catalysts will be tested in similar conditions to the supported catalysts in order to understand the effect of adding a zeolite “shell” on the catalytic performance.

Table 1. Textural and acid properties of the zeolitic samples.

Sample	Surface Area (m ² g ⁻¹)	Pore Volume (cm ³ g ⁻¹)	Brønsted acid sites (μmol g ⁻¹)		Si/Al
			150 °C	450 °C	
ZSM5 25	482	0.36	305	79	27.5
ZSM5 40	472	0.24	208	32	36.9
ZSM5 25 NaOH	583	0.89	311	117	25.7
ZSM5 25 TPAOH	660	0.73	307	90	25.0
ZSM5 40 NaOH	556	0.71	323	86	27.5

Table 2. Catalytic Properties of the supported catalysts.

Catalysts	CO Conv. (%)	CH ₄	CO ₂	Selectivity (%)			C _{Iso}
				C ₂₋₄	C ₅₋₁₂	C ₁₂₊	
CoRe/Al ₂ O ₃	63.1	12.5	0.9	3.2	-	-	0.05
Co/ZSM5 25	43.0	18.8	0.5	4.7	60.0	16.0	0.16
Co/ZSM5 25 NaOH	49.3	14.4	0.6	4.7	69.6	10.7	0.25
Co/ZSM5 25 TPAOH	55.8	14.6	0.8	4.6	68.6	11.4	0.40
Co/ZSM5 40 NaOH	70.4	17.1	1	6.1	66.4	9.4	0.20

Acknowledgements

The authors thank CQE and FCT for funding through project UIDB/00100/2020, funding program under the Recovery and Resilience Plan (Missão Interface N.º 01/C05-i02/2022) and project Cat4GtL (POCI-01-0247-FEDER-069953), co-funded by ERDF through COMPETE 2020 under PORTUGAL 2020.

References

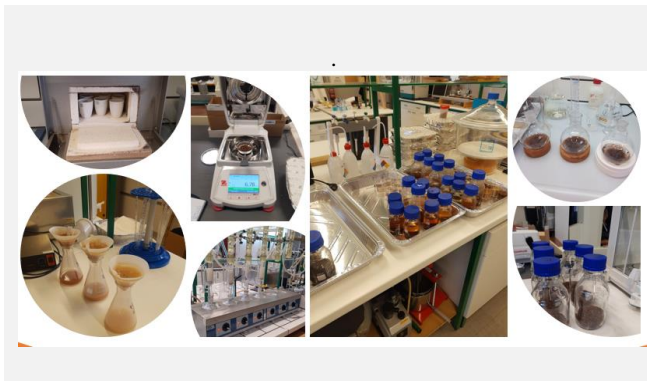
- [1] British Petroleum, “Energy Outlook 2020 edition explores the forces shaping the global energy transition out to 2050 and the surrounding that,” BP Energy Outlook 2030, Stat. Rev. London Br. Pet., (2020) [Online]
- [2] A.P. Steynberg, Introduction to Fischer-Tropsch technology, vol. 152, Elsevier B.V., Sasolburg, 2004, 5-63
- [3] D.X. Martínez-Vargas et al., Industrial and Engineering Chemistry Research., 58 (2019) 15872-15901.
- [4] S. Sartipi et al., Journal of Catalysis, 305 (2013) 179-190.

Impact of storage conditions on the chemical composition of wine industry by-products

A.K. Barreto¹, R.A. Fernandes^{2,3,4}, J. Santos^{2,3,4}, P. Magalhães⁵, J.M. Martins^{1,3,4}, I. Brás^{1,6}, L.H. Carvalho^{1,3,4}

¹ESTGV - Polytechnique University of Viseu, Campus Politécnico, 3504-510, Viseu, Portugal; ²ARCP-Associação Rede de Competência em Polímeros, Rua Dr. Júlio de Matos, 828/888, 4200-355 Porto, Portugal; ³LEPABE - Faculty of Engineering, University of Porto, Rua Dr. Roberto Frias, s/n 4200-465 Porto, Portugal; ⁴ALiCE - Associate Laboratory in Chemical Engineering, Faculty of Engineering, University of Porto, 4200-465 Porto, Portugal; ⁵Tintex Textiles SA, Zona Industrial, Polo 1, Campos, 4924-909 Vila Nova de Cerveira, Portugal; ⁶CISeD - Centre for Research in Digital Services, Polytechnique University of Viseu, 3504-510, Viseu, Portugal.

*pv22182@alunos.estgv.ipv.pt



Grape pomace is one of the major by-products of the wine production industry. Understanding its chemical composition is essential to evaluate the potential of obtaining added-value compounds/products from it. The reuse of industrial by-products currently attracts the interest of both academic and industrial research to reduce the environmental impact of manufacturing processes by reducing/eliminating the residues that needed to be disposed. The present study aims to access the effect of conditioning on chemical properties of the grape pomace, to identify possible sustainable routes of valorization. The high content of holocellulose and lignin indicate that grape pomace can be a great source of polyphenols, sugars and other important molecules.

Introduction

The wine production sector in Portugal is one of the most representative sectors of the agricultural economy, with a production of more than seven hundred million liters, being the fourth largest wine producer in the European Union (EU) in 2021 [5]. However, this industrial process generates a large quantity of by-products, and it is fundamental to develop routes of valorization of these by-products, since they represent a great loss of resources.

Wine by-products do not represent a hazardous waste, but their high content of organic matter and their seasonal production can contribute to potential pollution problems [6]. The most relevant by-products are vine strains, vine shoots and grape pomace (composed by grape stalk, skins and seeds), which is the main residue generated during wine production [3].

The use of these by-products as raw material, for instance in the textile industry, to produce added-value compounds may be an excellent way to increase the value of wine industry and also to reduce its environmental impact.

Objectives

The main objective of this work was to evaluate the effect of storage conditions on chemical composition and on the main structural characteristics of the macromolecular components of grape pomace.

Methods

Grape pomace supplied by Quinta do Soalheiro was stored under three different conditions (0 - no conditioning, 6A - 6 weeks in open containers and 6C - 6 weeks in closed containers both at ambient conditions) and reduce to powder using a RETSCH SM300 cutting mill and sieved in a sieve shaker RETSCH S200 (<500 μm). These by-products were characterized in terms of ash content, moisture, extractives (in dichloromethane, ethanol and water), tannins, pH, moisture, Klason lignin, holocellulose, α -cellulose and hemicelluloses.

The ash content was determined by the Weende method, the process consists of incinerating 2 g of sample in crucibles, which remain in the muffle for three hours at a temperature of 525 $^{\circ}\text{C}$

and then the total minerals present in the sample are quantified, as described in the Tappi standard T211 om-02.

The content of extractives in dichloromethane, ethanol and water were determined via Soxhlet extractions according to the Tappi standard T 204 cm-97.

Moisture was measured by a moisture analyzer OHAUS (MB120). For the pH determination, samples were subjected to hot water extraction and the obtained liquid extract was analyzed using an immersion electrode.

For tannins' determination, samples were mixed with a 1% NaOH solution and placed in an ultrasonic bath at 60 $^{\circ}\text{C}$ for 1 hour. The extracted material was filtered and dried at 40 $^{\circ}\text{C}$ until constant weight.

For the determination of Lignin content, the standard Klason Lignin method was used, where two hydrolysis were carried out, one with 72% acid for 1 hour and the other with 3% acid for 4 hours. The standard Klason method consisted of combining the methods for determining insoluble lignin content (Tappi standard T222om-02) and soluble lignin content (T UM 250).

For holocellulose, the chlorite/acetic acid method was used, which allows solubilization of lignin, obtaining an insoluble residue after filtration in a filtering crucible. For the extraction of α -cellulose and hemicellulose, 0.5 g of dry holocellulose were weighed and 2.5 ml of 17.5% NaOH were added in a thermostatic bath at 20 $^{\circ}\text{C}$ for about 1.5 hours.

Results and Conclusions

The major results obtained are shown in Table 1.

The analysis revealed the existence of a high amount (w/w) of holocellulose (46,38%), lignin (13,05%), α -cellulose (33,05) and hemicellulose (18,55%) (Table 1) in the initial sample (0). These main macromolecular constituents of the cell wall had similar values reported in literature for the chemical composition of hardwoods and similar [7,14].

Table 1. Chemical composition of grape pomace.

	Initial sample (0)	Sample 6 weeks Open (6A)	Sample 6 weeks Closed (6C)
Ashes (%)	7,07± 0,07	6,90±0,03	8,83±0,20
Moisture (%)	5,49±0,45	6,86±0,05	7,45±0,10
pH	3,94±0,02	4,50±0,06	6,42±0,07
Extractives			
Dichloromethan (%)	8,63±0,4	11,80±0,1	12,01±0,1
Ethanol (%)	12,04±0,3	6,56±0,3	6,50±0,2
Water (%)	19,90±0,3	19,72±0,1	19,44±0,3
Klason lignin (%)	13,05±1,5	22,52±2,4	23,69±3,5
Holocellulose (%)	46,38±0,0	39,37 ±0,7	38,37±0,6
α -Cellulose (%)	33,05±0,2	20,00±0,1	8,88±0,1
Hemicellulose (%)	18,55	5,75	14,76
Tannins (%)	24,24± 1,5	24,65± 0,7	24,06± 0,7
Phenols (%)	9,97	4,94	4,57

Holocellulose content had a reduction after six weeks in both in 6A (39,37%) and 6C (38,37%) conditions, as well as hemicellulose content, which was 5,75% and 14,76% for 6A and 6C, respectively. These results are explained by several authors due to the degradation of wood by hydrolysis that leads to the depolymerization of hemicelluloses, the most thermally unstable component of wood [10].

The macromolecular components of the vine (cellulose, lignin and hemicelluloses) have potential added value. Cellulose and lignin are valued mainly for non-food purposes, such as in the paper, nanocellulose, adhesives, materials, and furniture industries, among others [1]. However, holocellulose, α -cellulose and hemicellulose degrade over the weeks, regardless of their conservation (Table 1).

The ash content in the initial sample (7,07%) is in accordance with the ones reported on literature [9]. The variation over the 6 weeks kept open and kept closed is very slight (6A - 6,90%; 6C - 8,83%). According to the literature, the enrichment of potassium, calcium, iron, sodium, and magnesium components is irregular, although these components are accumulated in the grape berry, as maturation occurs, there is a reduction [2].

The initial sample has a more acidic pH (3,94) than samples 6A and 6C. According to the literature, during herbaceous growth there is an increase in the concentration of tartaric acid due to

cell multiplication and the concentration remains stable throughout the vine maturation phase. pulp cells, these two acids being the ones that maintain the acidity of the vine [2]. However, acidic compounds degrade over time, reducing its concentration and, consequently, increasing the pH.

Regarding extractives content, in dichloromethane (non-polar solvents), initial sample (8.63%), 6A (11.80%) and 6C (12.01%), where lipophilic fractions (diterpenes, sterols and fatty acids) were extracted [9]. On the other hand, the extractives content of water or polar solvents (ethanol) are obtained from the extraction of hydrophilic fractions. Ethanol extractives are compounds of colored pigments, phlobaphenes, flavonoids, anthocyanins. The content of ethanolic extractives on the initial sample is almost twice (12.04%) of open (6.56%) and closed samples (6.50%). This difference in values is possibly caused by the degradation of these compounds. According to the literature, vine sugars are the result of photosynthesis carried out by the green organs, for this reason in the initial sample it was possible to remove a greater amount of these compounds [3]. Hot water extractives include salts, simple sugars, polysaccharides, and some phenolic substances. In the initial sample the content of extractives in water was (19.90%) and in samples 6A and 6C they were respectively 19.72 and 19.44% the content like the initial sample was maintained [7]. Tannins constitute the primary components of woody tissues [4]. In the tannin content, the value obtained (24.24%) was much higher compared to the tannin content [8]. This difference can be explained by the variation in the origin of the stalks, as well as the contribution of condensed tannins soluble in alkaline solution with high molecular weight and hydrolysable tannins that are easily degraded in alkaline conditions. These phenolic compounds are found in the fibers, the skin of the grape and give it its purple color [3].

Currently, several technological solutions for the full use of by-products from grape processing into wine are available, and the possibility of transforming these by-products has become of interest to industries. For the productive sector, the adoption of these agro-industrial waste recovery technologies based on the generation of high added value products should be encouraged, since they represent relevant business opportunities from an economic and environmental point of view [3].

Acknowledgements

The authors gratefully acknowledge the funding by: Project TRUEHUE (SI I&DT-Projects in co-promotion, POCI-01-0247-FEDER-047183) in the scope of Portugal 2020, co-funded by FEDER (Fundo Europeu de Desenvolvimento Regional) under the framework of POCI (Programa Operacional Competitividade e Internacionalização); LA/P/0045/2020 (ALiCE) and UIDB/00511/2020-UIDP/00511/2020 (LEPABE) funded by national funds through FCT/MCTES (PIDDAC).

References

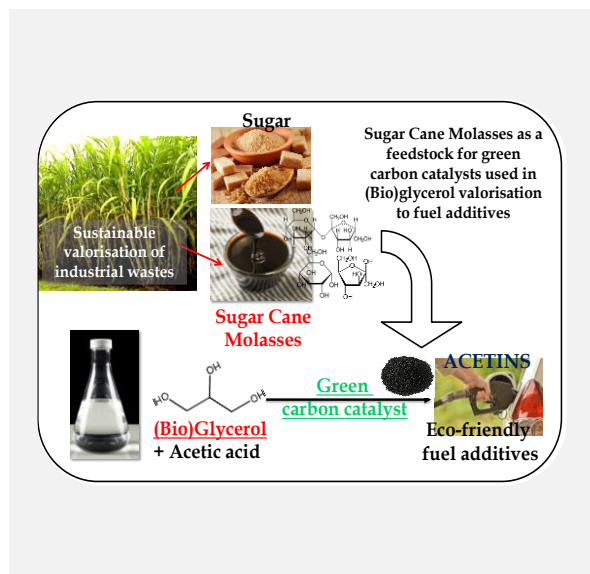
- [1] C. Beres et al., Waste Management, 68 (2017) 581-594.
- [2] J. Dias, Tenth intensive winemaking course, (2006).
- [3] L. Semiarido, P. de Souza, Production System - Vine Cultivation. 1, 2a Edition, (2010). ISSN 1807-0027, Electronic Version.
- [4] P. Hernes et al., Geochimica et Cosmochimica Acta, 68 (2004) 1293-1307.
- [5] IVV - Institute of Wine and Vine (a), Evolution of World Wine Production (2023). Series 2000 to 2021[cited 2023 March 21]; Available from :<<https://www.ivv.gov.pt/np4/6953.html>>.
- [6] IVV - Institute of Wine and Vine (b), Evolution of National Wine Production by Wine Region (2023). Series 2009/2010 to 2021/2022. [cited 2023 March 21]; Available from: <<https://www.ivv.gov.pt/np4/163.html>>.
- [7] U. Klock et al., Wood chemistry (2013). Federal University of Paraná, Department of Engineering and Forestry Technology.
- [8] L. Ping et al., Industrial Crops and Products 33 (2011) 200-204.
- [9] G. Spigno et al., Bioresource Technology, 99 (2008) 4329-4337.
- [10] J. Stamm, Wood and Cellulose Science. Ronald Press, New York, USA (1964).

Towards sustainable valorization of industrial waste - catalysts derived from sugar cane molasses for upgrading glycerol to fuel additives

K.M. Eblagon^{1,2}, A. Malaika^{3*}, K. Ptasińska³, M. Kozłowski³, J.L. Figueiredo^{1,2}

¹LSRE-LCM - Laboratory of Separation and Reaction Engineering – Laboratory of Catalysis and Materials, Faculty of Engineering, University of Porto, Rua Dr. Roberto Frias, 4200-465 Porto, Portugal; ²ALiCE - Associate Laboratory in Chemical Engineering, Faculty of Engineering, University of Porto, Rua Dr. Roberto Frias, 4200-465 Porto, Portugal; ³Faculty of Chemistry, Adam Mickiewicz University in Poznań, Poznań, Poland.

*anna.malaika@amu.edu.pl



Industrial sugar cane molasses (SCM) was used as a feedstock for producing bio-carbon catalysts suitable for upgrading glycerol waste to eco-friendly fuel additives (i.e., di- and triacetins, DA, and TA, respectively). Two methods of carbon preparation were compared, namely: one-step partial carbonization (PC) and two-step hydrothermal carbonization (HTC) followed by functionalization with sulfuric acid. It was found that SCM can be easily transformed into carbonaceous products using both methods. However, the final bio-carbons differed in their textural and chemical features, giving the facile PC method advantage. All the catalysts worked effectively in the esterification of glycerol to acetins, and the best catalysts yielded about 74 % of DA and TA after only 2 h of the reaction. A clear correlation between the content of $-SO_3H$ groups present on the PC catalyst and the formation of TA was found. The positive impact of oxygen functionalities on the catalytic performance was also established.

Introduction

Sustainable valorization of industrial wastes alleviates environmental concerns caused by waste disposal, limits reliance on fossil-based resources, and potentially decreases the production cost of bio-products using cheap carbon sources. The sugar industry worldwide produces large volumes of sugar cane molasses (SCM), mostly used for cattle feed or bioethanol production [1]. Alternatively, SCM residue can serve as a renewable feedstock to produce carbon materials for various applications, including catalysis. This approach can provide additional revenue for agricultural industries.

On the other hand, in biorefinery, glycerol is the main by-product, representing around 10 % of biodiesel production. The significant increase in biodiesel production in recent years has highlighted the need for effective glycerol valorization to minimize the glut in the glycerol market [2].

Herein, we report the synthesis of carbon materials from sugarcane molasses (SCM) *via* different preparation routes, both low-temperature ones, i.e., partial or hydrothermal carbonization, followed by sample functionalization. As shown in the Graphical Abstract, the obtained bio-carbons were applied as solid acid catalysts for the esterification of glycerol to produce acetins. It is important to underline that the present work is a first attempt to join waste valorization from the sugar industry and biodiesel production.

Experimental

Industrial grade sugar cane molasses (SCM, syrup) was supplied by RAR Portugal (RAR, Refinarias de açúcar reunidas, S.A.) SCM as received was used as a substrate to produce carbon catalysts containing sulfonic and oxygen functionalities. Two environmentally friendly synthesis approaches were compared: partial carbonization (PC) and hydrothermal carbonization (HTC). In the PC method, involving carbonization and functionalization in-situ, SCM was heated with the addition of

concentrated sulfuric acid at 180 °C for 0.5 h, which resulted in a PC-C-SO₃H sample. Alternatively, a two-step method, involving carbon formation *via* classical HTC, followed by post-functionalization was applied. In the HTC, a solution of SCM syrup was heated at 180 °C under autogenous pressure for 8 h, which resulted in HTC-C. Subsequently, HTC-C was functionalized by treatment with concentrated sulfuric acid, resulting in the HTC-C-SO₃H sample. The physicochemical properties of the prepared bio-carbons were characterized in detail using: EA, XPS, SEM-EDS, N₂ physisorption, and potentiometric titration.

Glycerol esterification with acetic acid was carried out in a three-necked bottom flask with a reflux condenser under Ar flow. Acetic acid (28.9 cm³) and a catalyst (0.7 g) were first heated in a flask to 110 °C. When the desired temperature was reached, glycerol (7.75 g) was added to the mixture, and the reaction time was started. Small aliquots of the reaction mixture were taken periodically and analyzed using a gas chromatograph equipped with an Intercap WAX capillary column (length = 30 m, diameter = 0.53 mm, film thickness = 1 μm) and FID detector.

Results

It was found that both preparation methods used (i.e., HTC and PC) were convenient techniques for upgrading molasses to high-value carbonaceous products. The materials obtained by both techniques showed low specific surface areas (S_{BET}), which were 15 m²/g for HTC-C-SO₃H and 18 m²/g for PC-C-SO₃H, and poorly porous structures. These textural features of the samples resulted from the presence of only larger pores, i.e., macro- and mesopores. HTC and PC methods produced hydrochars with abundant functional groups. However, the PC-C-SO₃H showed acidic O- and S-functionalities generated in one step, whereas HTC-C required additional post-functionalization to anchor the

-SO₃H moieties onto the carbon surface. The EA results showed that PC-C-SO₃H contained around 34 % of oxygen and 3.6 % of sulfur. On the other hand, sulfonation of HTC-C resulted in the introduction of 2.8 % of sulfur and an increase in oxygen content from 30.5 % (in HTC-C) to 36.5 % (in HTC-C-SO₃H). According to XPS results, S-functionalities found on these samples' surfaces were mostly in the form of sulfonic groups. Concerning the results of the total acidity (A_{tot}) measured by potentiometric back titration, both PC-C-SO₃H and the initial hydrothermal carbon, i.e., HTC-C, showed very high total acidities of 3.93 and 1.45 mmol H⁺/g, respectively. These results are typical for carbonaceous materials prepared from sugars at relatively low temperatures. Importantly, the acidity shown by PC-C-SO₃H and HTC-C resulted from different factors. In the case of HTC-C, the high A_{tot} was due to surface oxygen groups of acidic properties, such as carboxyl or phenolic functionalities (as shown by the results from EA and XPS). In the case of the PC-C-SO₃H sample, presenting high oxygen and sulfur contents (as mentioned above), the high total acidity was related to the presence of oxygen groups and S-containing functionalities introduced into the carbon matrix during the preparation stage. Moreover, sulfonation of HTC-C resulted in an increase in A_{tot} from 1.45 to 3.76 mmol H⁺/g.

SCM-derived bio-carbons were tested in glycerol esterification to fuel additives. Without the catalyst, the glycerol conversion was around 64 % after 2 h and increased with time to ~ 93% recorded after 24 h. The observed autocatalytic effect was due to the presence of acetic acid in the reaction, which can act as a catalyst for esterification. The transformation of glycerol to acetins was facilitated by the addition of the produced catalysts, as shown in Table 1. As seen from this table, all samples showed

significantly improved glycerol conversion and higher combined yields of di- and triacetins compared to a blank test.

Table 1. Catalytic performance of SCM-derived carbon catalysts in glycerol esterification to acetins at 110 °C after 2h. Conv- conversion, Y-yield, Gly-glycerol, MA-monoacetins, DA-diacetins, and TA-triacetin.

Catalyst	Conv Gly	Y MA	Y DA	Y TA
Blank	64.5 %	46.6 %	16.8 %	1.1 %
HTC-C-SO ₃ H	96.4 %	23.8 %	55.1 %	17.4 %
PC-C-SO ₃ H	96.5 %	22.8 %	53.8 %	19.8 %

Furthermore, the catalysts retained their activities in subsequent reaction cycles, which made them a promising alternative to expensive commercial solid acids. It was found that the catalytic performances of SCM-derived bio-carbons resulted mainly from the presence of -SO₃H functionalities. In addition, it was found that the oxygen groups enhanced the catalytic performance by aiding in the adsorption of the reagents and improving the access of the substrates to the catalyst's active sites.

Conclusions

Overall, both preparation methods studied allowed for transforming SCM into valuable solid-acid catalysts. However, considering the carbon preparation conditions, the complexity of the preparation method, process feasibility, and environmental impact, partial carbonization (PC) was indicated as a promising option for converting sugar wastes to cheap active bio-catalysts. These carbons were proved to be very active catalysts for glycerol acetylation, giving high yields of DA and TA in a short time.

Acknowledgements

This work was financially supported by LA/P/0045/2020 (ALiCE), UIDB/50020/2020 and UIDP/50020/2020 (LSRE-LCM), funded by national funds through FCT/MCTES (PIDDAC). KME is grateful to FCT for Junior Researcher Grant (grant no.2021.00535.CEECIND). AM acknowledges financial support from AMU (ID-UB Project: Excellence Initiative—Research University, grant No 018/07/POB3/0012).

References

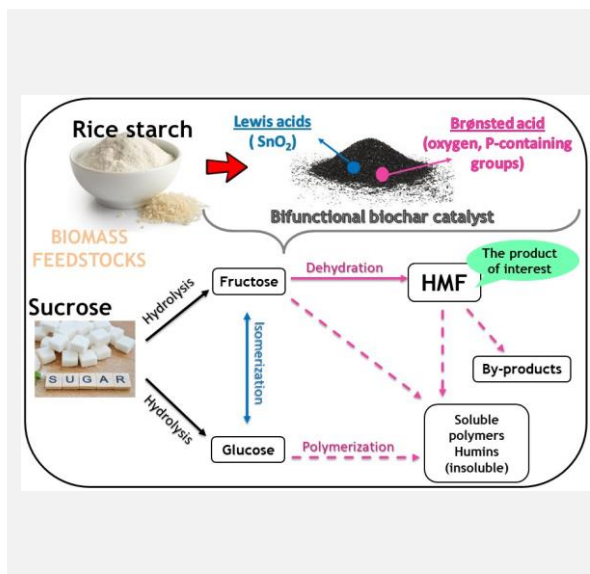
- [1] J. Howard et al., ACS Sustainable Chemistry & Engineering, 6 (2018) 4531-4538.
- [2] M.H. Moklis et al., Sustainability, 15 (2023) 1-30.

Production of 5-hydroxymethylfurfural from table sugar in water using bifunctional biochar catalysts

A. Malaika^{1*}, K.M. Eblagon^{2,3}, M.A.C. Bravo^{1,2,3}, M. Kozłowski¹, J.L. Figueiredo^{2,3}

¹Faculty of Chemistry, Adam Mickiewicz University in Poznań, Poznań, Poland; ²LSRE-LCM - Laboratory of Separation and Reaction Engineering – Laboratory of Catalysis and Materials, Faculty of Engineering, University of Porto, Rua Dr. Roberto Frias, 4200-465 Porto, Portugal; ³ALiCE - Associate Laboratory in Chemical Engineering, Faculty of Engineering, University of Porto, Rua Dr. Roberto Frias, 4200-465 Porto, Portugal.

*anna.malaika@amu.edu.pl



5-Hydroxymethylfurfural (HMF) is a key platform bio-compound for producing many high-value fine chemicals, biopolymer precursors, pharmaceuticals, and biofuels. In the present work, the bifunctional catalyst, which contained phosphorous and oxygen functionalities as Brønsted acid sites (BA) and SnO₂ as Lewis acid sites (LA), was produced from rice starch using hydrothermal carbonization. The impact of the catalyst preparation method (one-pot hydrothermal process vs. impregnation with H₃PO₄) and the effect of carbonization and the addition of different active sites on the catalyst performance were studied in the conversion of sucrose to HMF in water. Reaction modeling was carried out to understand the influence of the type of atmosphere (air, CO₂, or N₂) or pressure (1-2 bar) on the rate constants of the intermediate reactions (shown in the graphical abstract). It was found that *in situ* addition of surface groups yielded better catalytic results than step-wise impregnation with acid. Very promising selectivity to HMF of 23.7 % with almost 100 % conversion of sucrose was obtained by a bifunctional catalyst prepared by HTC in one pot. The study of the reaction atmospheres revealed that similar selectivities to HMF were obtained in CO₂ and air, however, more humin was produced under the former conditions.

Introduction

The conversion of biomass to value-added platform chemicals has gained increasing attention nowadays. HMF has a unique position among biomass-derived molecules due to its multifunctionality resulting from its structure comprising a furan ring with alcoholic and aldehyde groups. As a result, HMF can be transformed into high-value chemicals and biofuel products, such as 2,5-furan dicarboxylic acid, levulinic acid, and other environmentally friendly substitutes for existing petrochemicals.

5-HMF is generally produced through the dehydration reaction of fructose with the presence of a catalyst in order to achieve high conversion and selectivity; however, this process is hindered by the high production cost and limited accessibility of fructose. On the other hand, table sugar (sucrose) is a widely available and cheap carbohydrate that gives an equimolar mixture of glucose and fructose upon heating in water in the presence of a Brønsted acid catalyst. This processability makes sucrose a more versatile feedstock as compared to lignocellulosic biomass. Unfortunately, the conversion of sucrose to HMF has not been investigated extensively due to the complexity of the process and additional reaction steps which decrease the overall yield of the desired product.

The production of HMF from sucrose is a cascade process involving thermal hydrolysis of sucrose to C₆ sugars, isomerization of glucose to fructose, and finally, dehydration of fructose to HMF. As a result, a suitable bifunctional catalyst for this reaction is recommended, i.e., the system including Lewis acid or basic sites to facilitate isomerization, and Brønsted sites to catalyze the final dehydration of fructose to HMF [1].

In general, the conversion of sucrose to HMF has been studied by applying homogenous catalysis using toxic mineral acids as catalysts, mostly diluted H₂SO₄ [2], costly ionic liquids [3], or a combination of p-toluenesulfonic acid as Brønsted acid (BA)

catalyst and chromium chloride as Lewis acid (LA) catalyst [4]. However, a suitable and environmentally friendly heterogeneous catalyst for the cascade conversion of sucrose to HMF has not yet been found. Thus, the present work is focused on developing a biomass-derived carbon catalyst containing a combination of active sites for cascade conversion of sucrose to HMF in water. Water was chosen as an optimal solvent for the mass production of HMF mainly because of the good solubility of the substrates, zero toxicity, easy availability, and low cost.

Experimental

Bifunctional catalysts were prepared using the hydrothermal method, applying rice starch as a carbon source, and diluted H₃PO₄ and SnCl₂·H₂O as precursors of phosphorous groups (BA sites) and SnO₂ phase (LA centers), respectively.

To prepare a carbon catalyst containing SnO₂, 15 g of rice starch was mixed with 2.1 g of SnCl₂·H₂O in 20 mL of DI water. The mixture was transferred to an autoclave and hydrothermally carbonized in an oven at 180 °C for 5.5 h. Subsequently, the material was filtered and washed several times with hot DI water (until neutral pH of the filtrate was obtained), followed by ethanol. The as-prepared material was dried in a laboratory oven at 110 °C overnight and abbreviated C_starch_Sn. In the final step, the sample was thermally treated at 550 °C in the flow of N₂ (100 ml/min) to obtain C_starch_Sn_550. For comparison, a reference catalyst was prepared following the same preparation steps as used for C_starch_Sn_550, but without adding SnCl₂·H₂O prior to the HTC process. This catalyst was abbreviated C_starch_550.

To prepare a bifunctional catalyst, 1 g of C_starch_Sn was immersed in 20 mL of 2M H₃PO₄ and left under stirring at room temperature for 12 h. Subsequently, the catalyst was washed with DI water and dried at 110 °C overnight. Finally, the catalyst was calcined at 550 °C as described above. The as-prepared material was abbreviated C_starch_Sn_imp_PA_550. For

comparison, a bifunctional catalyst was prepared in one step using HTC. The same preparation steps were followed as those used for obtaining C_starch_Sn_550, but starch and the precursor of SnO₂ were added to 20 mL of 2M H₃PO₄ instead of DI water. Subsequently, the material was washed, dried in an oven, and thermally treated at 550 °C as described above. The final sample was abbreviated C_starch_Sn_PA_HTC_550.

For the sake of comparison, starch was also hydrothermally carbonized without P- or Sn- precursors (C_starch sample) and treated at high temperature (C_starch_550 sample) according to the previous preparation method.

The catalysts were characterized using various techniques, including elemental analysis, Scanning Electron Microscopy-Energy-Dispersive X-ray Spectroscopy (SEM-EDX), Thermogravimetric (TG) method, Fourier-Transform Infrared (FT-IR) analysis, X-ray Diffraction (XRD) technique, Inductively Coupled Plasma (ICP) method, and X-ray Photoelectron Spectroscopy (XPS).

The catalytic testing was conducted in a Parr-type reactor using 10 ml of 5 wt.% sucrose in water as a substrate and 0.03 g of the produced biochar as a catalyst. The reactor was heated up to 180 °C and kept under these conditions for 30 min under autogenous pressure. Additional testing was carried out changing the air atmosphere for N₂ (1-2 bar) or CO₂. After the reaction was completed, the reactor was cooled down, and the solution was analyzed using HPLC. In addition, a simple reaction model was successfully applied to the experimental results to evaluate the impact of reaction atmosphere (i.e., Air, CO₂, or N₂) and pressure (1-2 bar), according to the method described in [5].

Results

The as-prepared C_starch showed a low specific surface area of 4 m²/g, typical for carbons obtained from sugars by HTC. The carbonization of C_starch at 550 °C increased its surface area to 457.2 m²/g, which was the highest value obtained for all the catalysts. After adding the SnCl₂ to the starch precursor before HTC, the S_{BET} of the final C_starch_Sn_550 sample decreased to 375.9 m²/g. Interestingly, comparing bifunctional catalysts, larger S_{BET} was obtained by a catalyst impregnated with H₃PO₄ compared to the one produced in the one-pot method. The elemental analysis showed high amounts of oxygen present in the prepared samples. Considering the bifunctional carbons, higher amounts of oxygen were found in C_starch_Sn_PA_HTC_550 (i.e., 15.8 wt.%) as compared to C_starch_Sn_imp_PA_550 (i.e., 10.5 wt.%).

The catalytic results shown in Table 1 demonstrated that all of the catalysts showed ~100 % conversion of sucrose. In addition,

the carbonization of C_starch at 550 °C increased the selectivity to HMF but decreased the conversion of glucose. This can be due to removing some of the oxygen functionalities during the thermal treatment of the C_starch sample. These functionalities probably catalyzed side reactions of sugars. As shown in Table 1, adding SnO₂ further increased the selectivity to HMF. However, the best result was obtained by bifunctional catalysts prepared in one pot *via* HTC. This catalyst showed impressive 23.7 % selectivity to HMF. On the other hand, its counterpart prepared by impregnation showed only 15.7 % selectivity toward HMF.

Table 1. The catalytic performance of the biochars in sucrose conversion to HMF.

Catalyst	Conv. (%)	Sel. (%)		
		Glucose	Fructose	HMF
C_starch	100.0	29.5	22.3	12.8
C_starch_550	100.0	44.1	29.9	13.8
C_starch_Sn_550	97.3	46.7	25.7	18.5
C_starch_Sn_imp_PA_550	98.6	45.8	27.1	15.7
C_starch_Sn_PA_HTC_550	98.6	42.3	23.8	23.7

The kinetic study revealed that the lowest proportion of unwanted side products was obtained when the reaction was carried out in the air, which was due to the high rate constant of fructose dehydration to HMF and the low rate constant of fructose degradation to humin. Also, in air, the reaction can occur *via* isomerization of glucose to fructose as well as directly from glucose to HMF. On the other hand, in N₂ and CO₂, the reaction takes place solely *via* isomerization of glucose to fructose followed by fructose dehydration to HMF, and the rate constants for fructose polymerization to side products were higher than in air.

Conclusions

A very active bifunctional catalyst was prepared by a one-step hydrothermal carbonization method of starch in the presence of the tin oxide precursor and diluted phosphoric acid. The best catalyst contained BA in the form of oxygen functionalities and LA in the form of SnO₂ and showed 98.6 % conversion of sucrose with 23.7 % selectivity to HMF. It was also revealed that *in-situ* incorporation of BA and LA sites allowed for obtaining higher yields of HMF than the step-wise preparation involving impregnation. The modeling of the reaction kinetics showed that air atmosphere favored selectivity to HMF by minimizing the degradation of fructose to humins. time.

Acknowledgments

This work was financially supported by LA/P/0045/2020 (ALiCE), UIDB/50020/2020, and UIDP/50020/2020 (LSRE-LCM), funded by national funds through FCT/MCTES (PIDDAC). KME is grateful to FCT for Junior Researcher Grant (grant no.2021.00535.CEECIND). AM acknowledges financial support from AMU (ID-UB Project: Excellence Initiative—Research University, grant No 038/04/NŠ/0024).

References

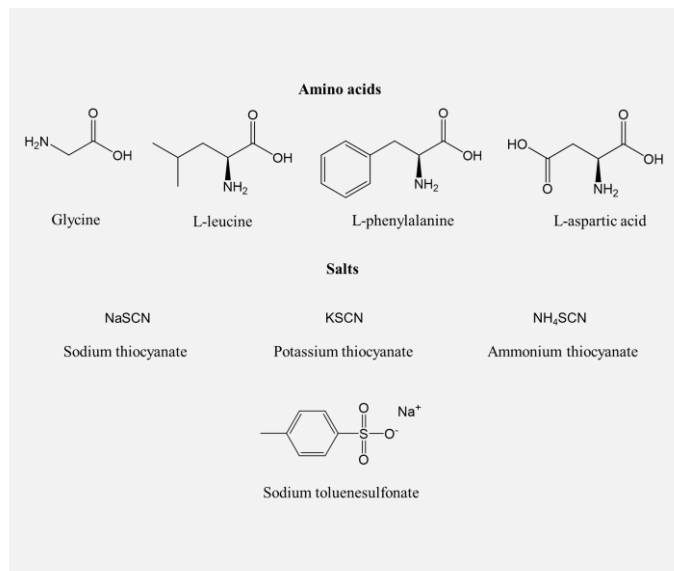
- [1] K. Morawa Eblagon et al., *Nanomaterials* 10 (2020) 1685.
- [2] S. Bower et al., *Bioresource Technology*, 99 (2008) 7354-7362.
- [3] P.V. Rathod et al., *Catalysis Letters*, 149 (2019) 672-687.
- [4] S. Mulk et al., *Journal of Environmental Chemical Engineering*, 10 (2022) 106613.
- [5] K. Morawa Eblagon et al., *Applied Catalysis B: Environmental*, 184 (2016) 381-396.

Solubility of amino acids: the effect of chaotropic anions

M. Aliyeva^{1,2,3*}, P. Brandão³, J.A.P. Coutinho³, O. Ferreira^{1,2}, S.P. Pinho^{1,2}

¹Centro de Investigação de Montanha (CIMO), Instituto Politécnico de Bragança, Campus de Santa Apolónia, 5300-253 Bragança, Portugal; ²Laboratório para a Sustentabilidade e Tecnologia em Regiões de Montanha, Instituto Politécnico de Bragança, Campus de Santa Apolónia, 5300-253 Bragança, Portugal; ³CICECO – Aveiro Institute of Materials, Department of Chemistry, University of Aveiro, 3810-193 Aveiro, Portugal.

*alyeva.m@gmail.com



This work addresses the effect of chaotropic anions (thiocyanate and tosylate) on the solubility of glycine, L-leucine, L-phenylalanine, and L-aspartic acid in aqueous solutions at 298.2 K. The salts used were NaSCN, KSCN, NH₄SCN, and NaC₇H₇SO₃ (sodium tosylate), with salt concentrations ranging from 0 to 2 molal. The pH of the saturated solutions was registered, and solid-phase studies were also performed. All the thiocyanate salts and sodium tosylate induced a salting-in effect, except in the systems composed of glycine in aqueous sodium tosylate solutions at 0.5 and 1 molal. For L-leucine, L-phenylalanine, and L-aspartic acid the salting effect of anions followed the order tosylate > thiocyanate > nitrate > chloride, in good agreement with the behavior predicted by the Hofmeister series. Differently, the relative solubility of glycine in aqueous nitrate solutions was higher than in those containing thiocyanate, followed by the chloride and, closing the rank, the solutions containing the tosylate anion, suggesting that the solubility change in this case is achieved by a different mechanism.

Introduction

The knowledge of amino acids (AA) solubility in aqueous salt solutions is relevant for different technical applications. For example, during the production of L-aspartic acid (L-Asp) by chemo or enzymatic synthesis, after the extraction steps, impurities, such as inorganic salts, acids, and alkalis, are still present in the system. Thus, the knowledge of the solubility of L-Asp in these aqueous salt solutions is necessary to optimize the crystallization process [1]. On the other hand, a hot topic still under debate is what may be referred to as contemporary Hofmeister solvation science [2], where ion-protein and ion-ion interactions at the protein surface and in the aqueous medium must be taken into account. An original picture establishing the line between simple chaotropes, such as thiocyanate or perchlorate, and structure-disrupting ions like sulfonates or phenolates, which act as hydrophobic/hydrotropic ions, was discussed by Leontidis [3]. More recently, using solubility, tensiometry, calorimetry data, and COSMO-RS calculations, a two-dimensional space diagram based on the nature of the anion headgroup and the hydrophobicity of the anion apolar moiety was proposed to clarify the so-called expanded Hofmeister series of ionic groups in amphiphilic molecules [4]. Essential oils (EOs) are the most abundant sources of terpenes and terpenoids [1], which are the sources of the oil's pleasant aromas and biological and pharmacological properties [2]. Among the different EOs, those extracted from citrus species are one of the most commercially attractive options, especially due to their wide use as natural fragrances and flavors [3]. Besides, CEOs present numerous appealing properties, such as antioxidant, antibacterial, antidiabetic, antifungal, and insecticidal activities [4].

To fill the gap identified for systems containing thiocyanate-based salts, in this work, the solubilities of glycine (Gly), L-leucine (L-Leu), L-phenylalanine (L-Phe), and L-aspartic acid (L-Asp) in aqueous NaSCN, KSCN, and NH₄SCN solutions were measured. Besides the reasons mentioned above, the

thiocyanate anion was also selected because it is located at the right end of the Hofmeister series (strong salting-in agent for proteins), and it is very interesting to discuss and compare the effect of thiocyanate anion to that of chloride, nitrate or sulphate. In addition, after investigating the impact of inorganic salts on the solubility of AA, the study was extended to the sodium salt with an organic anion, tosylate.

Solubility measurements

The so-called shake-flask method has been applied. The experimental setup includes the thermostatic water bath that guarantees a temperature uncertainty of 0.1 K and magnetic plates for stirring. The binary (salt and water) solutions with the molalities 0.5, 1, and 2 molal were prepared by gravimetry (Denver Instrument, ± 0.0001 g). The saturated solution was prepared by adding a slight excess of AA into the equilibrium cell and a known amount of binary solution. After, it was placed into the water bath at 298.2 K and stirred for around 30 hours to reach equilibrium. The mixing speed was between 500-700 rpm in all the experiments. After the stirring period, the solutions rested for at least 12 hours to precipitate the undissolved AA particles. The amino acid content of the saturated solutions was found by the refractive index method of analysis, and the pH of the saturated solution also measured. Additionally, the solid phase of the pure AA as received from the supplier and the solids in equilibrium with the saturated solutions, after vacuum filtration and drying at room temperature, were analyzed by powder and single-crystal X-ray diffraction.

Results and discussion

Figure 1 shows the relative solubilities of the studied AA in different aqueous salt solutions at 298.2 K. All the thiocyanate salts induced a salting-in effect over the whole salt concentration range for all the AA, matching the expected trend from the Hofmeister series.

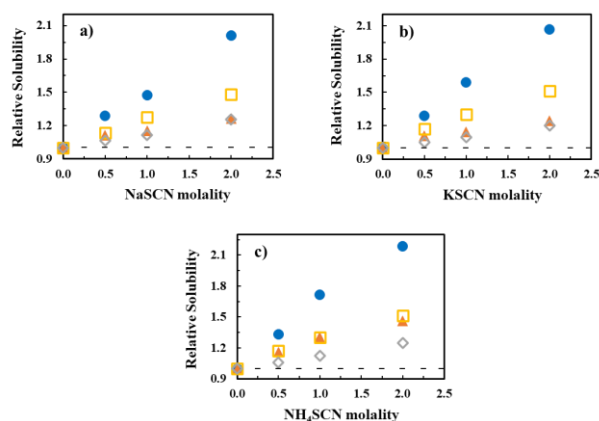


Figure 1. Relative solubility of \diamond , glycine; \blacktriangle , L-leucine; \square , L-phenylalanine, and \bullet , L-aspartic acid in aqueous a) NaSCN; b) KSCN, and c) NH_4SCN solutions with different molalities at 298.2 K.

To evaluate the effect of the anions on the solubility of the studied amino acids, the salts with the sodium cations were chosen. Figure 2 shows the relative solubility of glycine, L-leucine, L-phenylalanine, and L-aspartic acid in aqueous NaCl, Na_2SO_4 , NaNO_3 , NaSCN, and Na-tosylate solutions at 298.2 K. Thus, the relative solubilities of L-leucine, L-phenylalanine, and L-aspartic acid followed the same order: tosylate > thiocyanate > nitrate > chloride, showing that the anion effect on the solubility of these amino acids is in agreement to the Hofmeister series. Even if the increase in the solubility with sodium tosylate is not significant, meaning that it does not act as an efficient hydrotrope for L-aspartic acid, due to its small apolar region and its significant polarity, it is the salt with the most relevant effect, showing the importance of the hydrophobic parts of both solute and hydrotrope, but also the much higher effect of the interaction between the apolar part of the AA with the anions.

For glycine, the tosylate anion presents a completely reversed effect, inducing a very weak salting-in and even a salting-out at 0.5 and 1 molal. The reason for this can be the smaller side-chain group in glycine and the fact that glycine from the supplier used in the analysis with Na-tosylate was α -form, and not a mixture of α and γ form, as in all other systems, showing the importance of identifying the solid phase present in solubility measurements. The thiocyanate anion, which is the strongest inorganic salting-in anion in the Hofmeister series, for glycine induced a salting-in effect with a lower magnitude than the nitrate and even sulphate anions. Although the sulphate anion is a strong salting-out agent in the Hofmeister series, it induces a salting-in effect in very small amino acids like glycine. The solubility ranking observed is thus nitrate > sulphate > thiocyanate > chloride > tosylate.

Acknowledgments

This work was developed within the scope of the project CICECO-Aveiro Institute of Materials, UIDB/50011/2020, UIDP/50011/2020 and LA/P/0006/2020, and CIMO-Mountain Research Center, UIDB/00690/2020 and LA/P/0007/2020, financed by national funds through the Portuguese Foundation for Science and Technology (FCT)/MCTES. Mehriban Aliyeva thanks FCT and the European Social Fund (ESF) for her Ph.D. grant (SFRH/BD/139355/2018).

References

- [1] J. Wang et al., *Journal of Chemical Engineering Data*, 55 (2010) 1735-1738.
- [2] P. Jungwirth, and P.S. Cremer, *Nature Chemistry*, 6 (2014) 261-263.
- [3] E. Leontidis, *Current Opinion on Colloid and Interfacial Science*, 23 (2016) 100-109.
- [4] J. Mehringer et al., *Physical Chemistry Chemical Physics*, 9 (2021) 1381-1391.

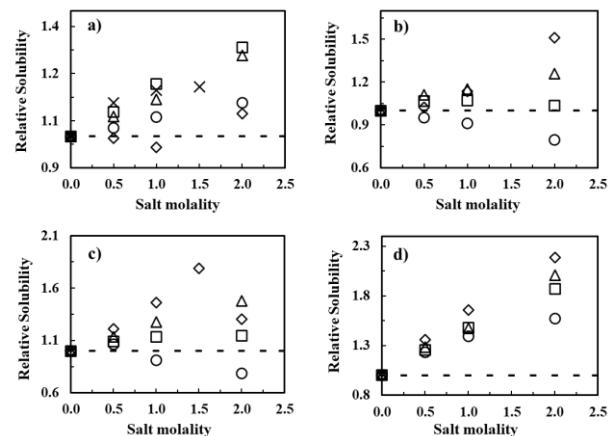


Figure 2. Relative solubility of a) glycine; b) L-leucine; c) L-phenylalanine, and d) L-aspartic acid in aqueous \circ , NaCl; \square , NaNO_3 ; \blacktriangle , NaSCN; \times , Na_2SO_4 and \diamond , Na-tosylate solutions with different molalities at 298.2 K.

Conclusions

The solubilities of glycine, L-leucine, L-phenylalanine, and L-aspartic acid were studied in aqueous NaSCN, KSCN, and NH_4SCN solutions at 298.2 K. The salts with the thiocyanate anion induced a salting-in effect with all the AA following the ranking Asp > Phe > Leu > Gly. The relative solubility of Gly was very close to Leu in aqueous solutions of salts with the sodium or potassium cation, while in aqueous NH_4SCN solution, this similarity was found between Leu and Phe.

Furthermore, the solubilities of these four amino acids were studied in aqueous Na-tosylate solutions. Up to concentrations of 1 molal, the order observed was the same as for the thiocyanate solutions, and excepting glycine, all the AA showed a salting-in effect. Surprisingly, a solubility decrease was observed for phenylalanine at higher Na-tosylate concentrations. The analysis of the phenylalanine crystals taken after the solubility studies at 2 molal showed changes in the structure of the solid phase. Na-tosylate increased the solubility of L-leucine, L-phenylalanine, and L-aspartic acid more than any of the studied inorganic salts.

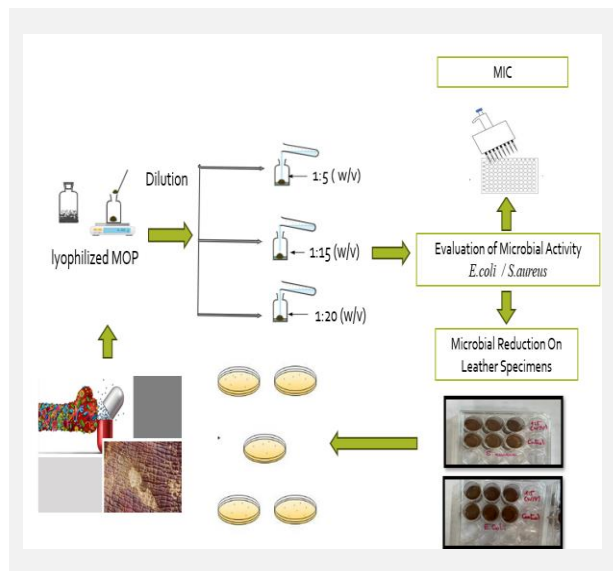
To evaluate the anion effect on the solubility of glycine, L-leucine, L-phenylalanine, and L-aspartic acid, the corresponding relative solubilities in aqueous solutions of NaCl, NaNO_3 , NaSCN, and Na-tosylate were compared. Excepting glycine, the relative solubility followed the order tosylate > thiocyanate > nitrate > chloride, in agreement with the Hofmeister series. For glycine, the order was nitrate > sulphate > thiocyanate > chloride > tosylate.

Olive pomace extracts as antimicrobial agents for leather treatments

K. Kebaili^{1,2,3*}, *H.H.S. Almeida*^{1,2}, *A.E.K. Benhlima*³, *M.F. Barreiro*^{1,2}, *P.J.L. Crujeira*^{1,2}

¹Centro de Investigação de Montanha (CIMO), Instituto Politécnico de Bragança, Campus de Santa Apolónia, 5300–253, Bragança, Portugal; ²Laboratório Associado para a Sustentabilidade e Tecnologia em Regiões de Montanha (SusTEC), Instituto Politécnico de Bragança, Campus de Santa Apolónia, 5300–253, Bragança, Portugal; ³University of Saida, Dr. Moulay Tahar Faculty of Science and Technology.

*kkhadidja.kebaili@gmail.com



The leather industry suffers significant losses due to antimicrobial resistance, resulting in issues such as discolouration, unpleasant odours, and decreased performance. Antimicrobial resistance has far-reaching implications for public health and society, leading to increased rates of illness and death. However, the olive oil industry has the opportunity to harness the valuable compounds found in moist olive pomace, specifically bioactive polyphenols, as eco-friendly, safe, and natural antimicrobial agents. This study aimed to assess the antimicrobial capacity of moist olive pomace (MOP) and its potential application in leather treatment. Three MOP extracts were obtained using different concentrations and optimised extraction conditions. The antimicrobial effects of the extracts on *Escherichia coli* and *Staphylococcus aureus* were evaluated using microdilution and colourimetric assays. The most effective concentration of MOP inhibited both bacteria at 31.3 mg/mL, resulting in a remarkable microbial reduction of 90.22% for *S. aureus* and 85.45% for *E. coli*. Moreover, this concentration exhibited bactericidal activity on leather specimens. These findings underscore the potential of MOP extracts as antimicrobial agents across diverse industries, including leather.

Motivation

The leather industry suffers substantial losses from antimicrobial resistance, resulting in problems such as discolouration, odours, and reduced performance [1]. This multi-faceted issue has far-reaching implications for public health and society, contributing to higher morbidity and mortality rates [2]. However, the olive oil industry's disposal of moist olive pomace with its valuable bioactive polyphenols creates a remarkable opportunity to harness these compounds as environmentally friendly, secure, and inherent antimicrobial agents [3]. By capitalising on this potential, the challenges the leather industry faces can be addressed while promoting sustainable and natural solutions for combating antimicrobial resistance. In this context, this work aimed to assess the antimicrobial efficacy of moist olive pomace (MOP) and explore its potential integration into the sustainable production chain by examining its effects on leather specimens.

Experimental Methods

Three MOP extracts were prepared using water as the solvent at different MOP-to-water ratios (1:5, 1:15, and 1:20 w/v) and studied. The antimicrobial activity was assessed by determining the minimum inhibitory concentration (MIC) against *Staphylococcus aureus* ATCC 6538 and *Escherichia coli* ATCC 8739. Additionally, the effectiveness of the extracts in reducing microbial growth on leather specimens was quantified by counting the colony-forming units (CFU) after performing a specific experimental methodology, as shown in Figure 1.

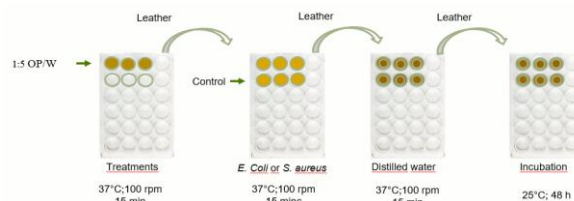


Figure 1. The scheme illustrates the evaluation of antimicrobial activity on leather specimens.

Results and Discussion

Regarding the antimicrobial activity, the 1:15 (MOP to water ratio) extract demonstrated the lowest MIC value of 31.3 mg/mL, effectively inhibiting both *E. coli* and *S. aureus*. These findings highlight the strong antimicrobial activity of the MOP extracts. Compared to [4] and [3], the MIC values for *E. coli* were lower, indicating a more potent inhibitory effect. Similarly, the MIC values for *S. aureus* were also lower, suggesting enhanced antimicrobial activity potential. The complete results are shown in Table 1.

Significantly, the findings, as shown in Figure 2, reveal an exceptional 100% reduction in microbial count using the MOP extract at the prescribed MOP to water ratio (1:5). This notable outcome underscores the potent microbicidal properties of the extract against both *E. coli* and *S. aureus*. Moreover, the histograms shown in Figure 3 vividly illustrate the percentage reduction in the leather specimens, offering compelling evidence of the extract's remarkable efficacy ($p < 0.0001$) in significantly reducing the microbial load.

Table 1. Minimum inhibitory concentration (MIC) of different OP ratio extracts on gram-negative bacteria (*Escherichia coli* ATCC 8739) and gram-positive bacteria (*Staphylococcus aureus* ATCC 6538).

Bacteria	MIC (mg/ml)		
	1:5 (w/v)	1:15 (w/v)	1:20 (w/v)
<i>Staphylococcus aureus</i> ATCC 6538	64	31.3	NI
<i>Escherichia coli</i> ATCC 8739	32	31.3	24

NI: No Inhibition

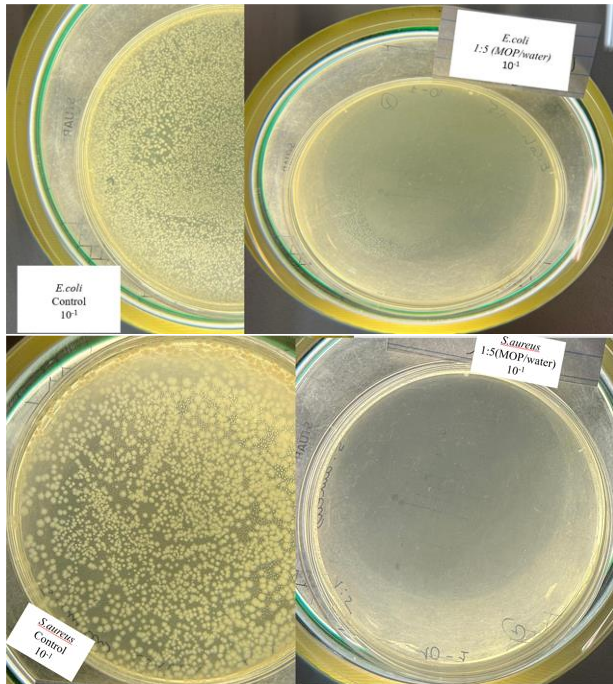


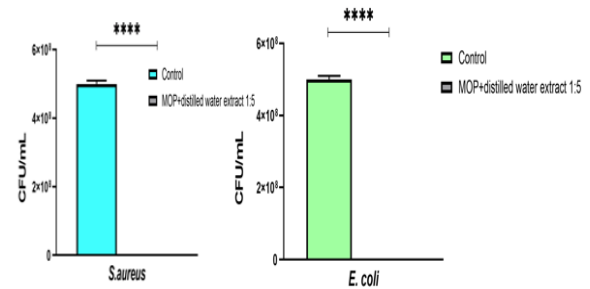
Figure 2. Microbial reduction in leather specimens against *E. coli* and *S. aureus*.

Acknowledgements

Project RARISS – Raças Autóctones, rastreabilidade, inovação e soluções sustentáveis (POCI-01-0247-FEDER-069810). FCT/MCTES for the financial support to CIMO (UIDB/00690/2020 and UIDP/00690/2020) and SusTEC (LA/P/0007/2021). Pedro Crueira thanks OleaChain (NORTE-06-3559-FSE14 000188) for the researcher contract. FCT for the SFRH/BD/148124/2019 research grant of H.H.S. Almeida.

References

- [1] C. Costa et al., U.Porto Journal of Engineering, 6 (2020) 86-97.
- [2] WHO Global Strategy for Containment of Antimicrobial Resistance, (2001) 11.
- [3] I. Gómez-Cruz et al., Antioxidants, 10 (2021).
- [4] M.A. Nunes et al., Pharmaceuticals, 14 (2021) 3-4.



**** $p < 0.0001$; ** $p < 0.01$; * $p < 0.05$; ns = not significant

Figure 3. Histogram representing the percentage microbial reduction in leather against *S. aureus* and *E. coli*.

Conclusions

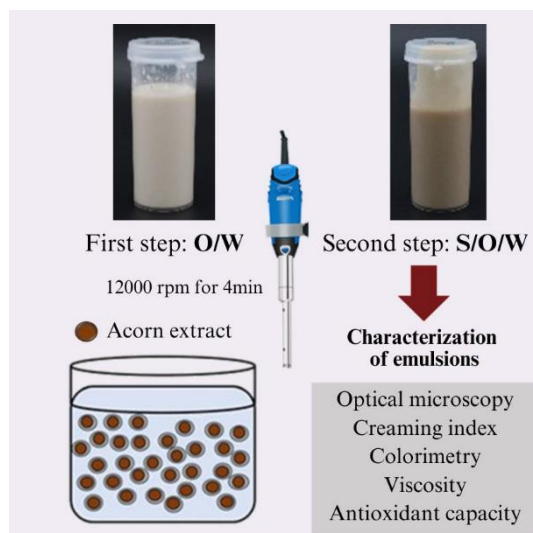
Olive pomace extracts exhibited significant antimicrobial activity against Gram-negative (*Escherichia coli*) and Gram-positive (*Staphylococcus aureus*) bacteria, varying with extract concentration. The 1:5 (w/v) extract demonstrated the highest activity, followed by the 1:15 (w/v) extract, while the 1:20 (w/v) extract showed lower efficacy against *S. aureus*. Leather specimen evaluation confirmed complete microbial reduction. These findings provide valuable insights into extraction ratios, antimicrobial potential, and the effectiveness of moist olive pomace in preventing microbial deterioration of leather. Future research should be devoted to optimising extraction methods, exploring applications and health benefits, and investigating the composition activity.

Development of acorn shell extract solid-in-oil-in-water (S/O/W) emulsion-based carriers envisaging cosmetic applications

L.F. Fernandes^{1,2}, L.G. Teixeira^{1,2,3}, G. Colucci^{1,2,3,4}, M.P. Sousa⁵, P.S. Babo⁶, A. Santamaria-Echart^{1,2}, R.F. Canadas^{5,6,7}, M.F. Barreiro^{1,2*}

¹Centro de Investigação de Montanha (CIMO), Instituto Politécnico de Bragança, Bragança, Portugal; ²Laboratório Associado para a Sustentabilidade e Tecnologia em Regiões de Montanha (SusTEC), Instituto Politécnico de Bragança, Bragança, Portugal; ³Laboratory of Separation and Reaction Engineering (LSRE-LCM), Faculdade de Engenharia, Universidade do Porto, Porto, Portugal; ⁴Associate Laboratory in Chemical Engineering (AliCE), Faculdade de Engenharia, Universidade do Porto, Porto, Portugal; ⁵Tech4MED, R. 25 de Abril, Ronfe, Guimarães, Portugal; ⁶LANDRATECH, Largo do Esteiro n° 6, Azambuja, Portugal; ⁷FMUP—Faculdade de Medicina, Universidade do Porto, Alameda Prof. Hernâni Monteiro, Porto, Portugal.

*barreiro@ipb.pt



Using natural extracts as active ingredients in cosmetics is increasingly demanded by consumers, primarily supported by sustainable principles and clean-label trends. To reach effective products, an essential step is the development of suitable carriers to load and deliver the target active principles. In this context, the present work is focused on the development of a solid-in-oil-in-water (S/O/W) system targeting the production of acorn shell-based cosmetic products. With this strategy, it is possible to incorporate a solid extract as a part of an O/W emulsion taking advantage of the effectiveness of these systems for topical applications. The process design comprised, in the first stage, the development of a stable O/W system. Thereafter, in the final complete process, the solid extract is finely dispersed in the oil phase followed by the dispersion of this phase in water. The best results were obtained using an O/W ratio of 30/70 (v/v) with 30% of Arabic gum (w/v, water-basis) and 2% of Tween 80 (w/v, oil-basis) added to the aqueous phase. To achieve the final S/O/W, 5% of PGPR (Polyglycerol polyricinoleate) (w/v, oil-basis), was added to the oil phase to disperse the extract (1%, w/v, oil-basis). The best system was characterized concerning stability, color attributes, viscosity, and antioxidant capacity.

Introduction

Nowadays, consumers are increasingly concerned about their health, demanding, and advocating the incorporation of natural bioactive or functional ingredients in cosmetics and other formulations to improve their health status [1].

For a long time, *Quercus* species have been used in traditional medicine in various countries and tribes. The bark, fruit, and leaves of *Quercus* genus species have been reported to possess a wide spectrum of biological effects such as antioxidant, antidiabetic, anticancer, anti-inflammatory, and antibacterial [2,3,4]. Thus, due to the high content of phenolic compounds, its extracts can be applied in various areas such as pharmaceuticals, cosmetics, and food [3,4]. In this context, the extract of the acorn by-product has revealed great commercial potential, even for the cosmetic industry, especially biological cosmetics. Moreover, it is a by-product and, therefore, the reuse of waste, decreasing the environmental impact, is arousing a deeper academic interest in the research and qualification of this by-product [5].

For the development of a cosmetic formulation, an important step is the development of an effective carrier. According to recent literature, the so-called solid-in-oil-in-water (S/O/W) double emulsions are increasingly proposed for incorporating hydrophilic solid extracts. By choosing adequate dispersing systems, e.g., emulsifiers or polymers, the solid particles can be finely dispersed and retained in the oil phase, forming what is designed by solid-in-oil (S/O) dispersion. Upon the dispersion of this first emulsion in water, the S/O/W emulsion is formed. In the S/O dispersion, adding a hydrophobic polymer or hydrophobic emulsifier is needed to stabilize the internal phase of the emulsion [6]. Another important aspect

to circumvent in this type of product is to achieve a suitable viscosity level for topical applications, which needs to be controlled by adding adequate hydrophilic polymers and emulsifiers to stabilize the O/W emulsion.

The present study aimed to develop solid-in-oil-in-water (S/O/W) emulsion-based carriers for acorn shell extract envisaging cosmetic applications.

Materials and methods

For the O/W emulsion, water, sweet almond oil, Tween 80 (emulsifier), and Arabic gum (stabilizer) were used. Different O/W ratios (10/90, 20/80, 30/70, v/v), Tween 80 (2% w/v, oil-basis), and Arabic gum (3%-35% w/v, water-basis) were tested. For the S/O dispersion, the acorn extract was dispersed using 5% of PGPR (w/v, oil-basis) as a stabilizer. The acorn extract was supplied by Tech4Med company corresponding in the liquid form being dried by lyophilization. The used content in the S/O/W emulsion (1%, w/v, oil-basis) was based on the maximum content giving rise to a homogeneous oil dispersion. To produce the S/O/W, the extract was firstly dispersed in the oil using an Ultra-turrax® system at 12000 rpm for 4 min. This dispersion was incorporated in the water phase and stirred using the previously referred conditions. The produced emulsions were kept refrigerated (4 °C) until characterization. The S/O/W emulsions were characterized concerning stability (creaming index), particle size, color, viscosity, and antioxidant activity. Antioxidant capacity was measured by the photo colorimetric DPPH (2,2-diphenyl 1-picrylhydrazyl) method.

Results

For the O/W emulsion, the best results (Figure 1) were obtained using an O/W ratio of 30/70 (v/v), 30% of Arabic gum (w/v, water-basis), and 2% of Tween 80 (w/v, oil-basis) added to the aqueous phase. The final S/O/W comprised 5% of PGPR (w/v, oil-basis), and 1% of extract (w/v, oil-basis).

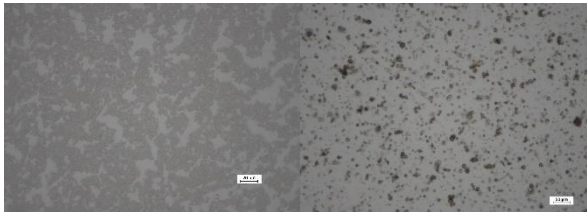


Figure 1. Optical microscopy (200X) of: a) O/W emulsion with 30% of Arabic gum (w/v, water-basis) and 2% of Tween 80 (w/v, oil-basis); and b) S/O dispersion with 5% of PGPR (w/v, oil-basis).

The results showed that the S/O/W emulsion exhibited long-term stability, with a creaming index equal to zero for the first 15 days, followed by slight phase separation (< 5%). By analyzing Figure 2, a slight increase in the volume-mean droplet size can be observed.

This is due to the destabilization phenomena, although a macroscopically uniform emulsion remains. In addition, it is noted that the droplets are heavily agglomerated due to the high viscosity of Arabic gum [7].

The S/O/W emulsion color did not show any perceptible change during the studied period ($\Delta E \leq 1$), as shown in Table 1.

Table 1. Results obtained for the color analysis of the S/O/W emulsion.

Sample	L*	a*	b*	RGB color
t0	64.87±0.51	2.02±0.15	14.48±0.33	
t7	65.06±0.12	1.94±0.03	14.13±0.05	
t15	64.57±0.40	1.98±0.02	14.25±0.10	
t30	65.20±0.13	2.16±0.10	13.74±0.17	

The viscosity was measured for 0, 7, 15, and 30 days, using a viscosimeter. The upward flow curves were modeled using the Oswald-de Waele ($\tau = -K_c \dot{\gamma}^n$, where τ is the shear stress (mPa), k is the consistency index ((Pa.s)ⁿ), $\dot{\gamma}$ is the shear rate (s⁻¹), and n is the flow behavior index (dimensionless)).

The viscosity studies showed non-linear responses. The emulsion S/O/W exhibited non-Newtonian pseudoplastic

Acknowledgments

The authors are grateful to the 'la Caixa' Foundation, Promove Program, for the support to the Acorn4MED project (PV20-00038). The authors are grateful to the Foundation for Science and Technology (FCT, Portugal) for financial support through national funds FCT/MCTES (PIDDAC) to CIMO (UIDB/00690/2020 and UIDP/00690/2020) and SusTEC (LA/P/0007/2021). National funding by FCT, P.I., through the institutional scientific employment program contract of A. Santamaria-Echart. FCT for the Ph.D. research grants of L. G. Teixeira (2020.08803. BD) and G. Colucci (2021.05215. BD).

References

- [1] A. Idris et al., *Biogerontology*, 21 (2020) 293-310.
- [2] T. Mehdi et al., *Evidence-Based Complementary and Alternative Medicine*, 2020 (2020) 20.
- [3] B. Ema et al., *Forests*, 11 (2020) 904.
- [4] V. Ana et al., *Comprehensive Reviews in Food Science and Food Safety*, 15 (2016) 947-981.
- [5] B. Ani et al., *Cosmetics*, 2 (2015) 82-92.
- [6] S. Anali et al., *AAPS PharmSciTech*, 22 (2021) 199.
- [7] X. Huang et al., *Food hydrocolloids*, 15 (2001) 533-542.
- [8] S. Ping et al., *Carbohydrate Polymers*, 135 (2016) 27-34.
- [9] D. Fransiska et al., *IOP Conference Series: Earth and Environmental Science*, 715 (2021) 012050.

(shear-thinning) behavior ($n < 1$). The maximum viscosity detected for the S/O/W was 8907 mPa/s, which conforms with the viscosity range for cosmetics is 2000-50000 mPa/s [9]. The inhibitory concentration (IC₅₀) obtained for S/O/W emulsion was 2.19 mg/mL (for the O/W emulsion, 8.99 mg/mL), corroborating the impact of the acorn extract.

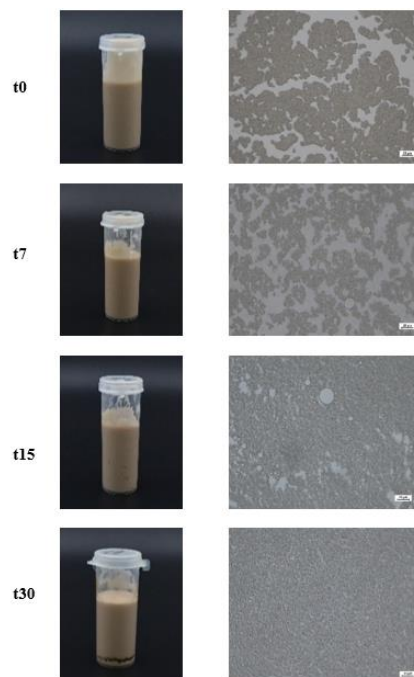


Figure 2. S/O/W emulsions visual aspect and optical microscopy analysis (200X).

Conclusions

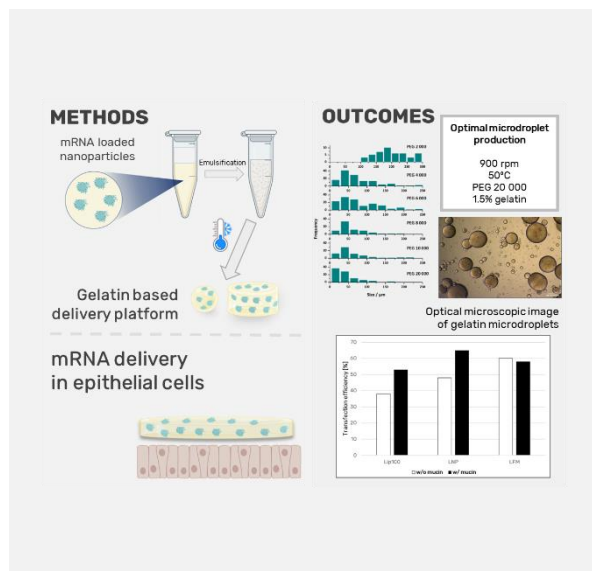
It was concluded that the proposed system was appropriate for incorporating the acorn shell extract potentiating cosmetic formulation development. Emulsions remained stable during 30 days of storage at 4°C. Furthermore, no noticeable color changes were observed, and pseudoplastic (shear-thinning) behavior was detected. In addition, the extract and the formulation revealed antioxidant capacity. Further studies of this ongoing study will consider the characterization of the encapsulation efficiency and skin permeation studies using Franz cells.

Gellable aqueous biphasic systems as a novel strategy for mRNA nasal delivery

B. Kopilovic¹, N. Laroui², J.A.P. Coutinho¹, C. Pichon^{2*}, M.G. Freire^{1*}

¹CICECO - Aveiro Institute of Materials, Department of Chemistry, University of Aveiro, 3810-193 Aveiro, Portugal; ²Centre de Biophysique Moléculaire (CBM), UPR 4301 CNRS, University of Orléans, 45071 Orléans, France.

*maragfreire@ua.pt and chantal.pichon@cnrs.fr



Biopharmaceuticals have become indispensable for treating diseases that traditional pharmaceuticals cannot address, such as cancer, autoimmune disorders, and genetic diseases. Recent advances in nanotechnology have revolutionized vaccine development, enabling the production of high-quality nucleic acids and efficient lipid-based delivery systems in vivo. In vitro transcribed messenger ribonucleic acid (IVT-mRNA), also known as "third-generation vaccines", offer significant potential to address unmet clinical needs. In this study, we developed an aqueous biphasic system (ABS) composed of biopolymers with gelling properties to deliver biopolymer-modified nanocarriers with improved delivery across the mucosal layer of the nasal epithelial. The chosen ABS, composed of gelatin, is safe for human use and has been proven to improve the mucosal passage of nanoparticles. The use of biopolymers in this novel delivery system has resulted in a remarkable transfection rate of 90% in upper airway epithelial cells, while delivery via the gelatin carrier has achieved up to 70%, suggesting the significant clinical potential of these nanoparticles and their delivery approach.

Introduction

Recent advances in mRNA-based therapies have demonstrated considerable potential for treating a variety of disorders. However, the successful distribution of mRNA to their intended places in the body is still challenging.¹ The use of hydrogels as a delivery mechanism for mRNA-based therapies has attracted interest in this area. Hydrogels, with their water-swollen three-dimensional network that resembles the original extracellular matrix, have unique benefits for mRNA delivery, such as increased stability, controlled release, and high payload concentrations. For a better biodistribution across the nasal epithelial mucosal layer, an innovative technique based on the use of aqueous biphasic systems (ABS) comprised of biopolymers, namely polyethylene glycol and gelatin, were used. This novel delivery technology has shown excellent transfection rates and substantial therapeutic promise. These advances in mRNA delivery offer potential options for the creation of effective and tailored treatments for a variety of disorders and age spans.

Methods

The methods employed in the mRNA ABS hydrogel preparation involved the determination of the phase diagram, microsphere size, encapsulation efficiency and assessment of biological activity on epithelial cells. The ABS phase diagram

was determined to establish the appropriate composition for optimal encapsulation and delivery across the mucosal layer of the nasal epithelium. Microsphere size determination was conducted to ensure uniformity and control in the delivery system. Encapsulation was confirmed using fluorescence microscopy to visualize the amount of biopharmaceutical effectively encapsulated within the hydrogel carriers. Additionally, the biological activity of the mRNA was evaluated using epithelial cells to determine the effectiveness of the delivery approach in transfecting the target cells.

Conclusions

In conclusion, this study highlights the significant advancements and promising potential of ABS-based delivery systems for mRNA therapeutics. Our data show that ABS hydrogels is an appealing option to deliver mRNA in a specific location. The unique physicochemical properties of hydrogels, mimicking the native extracellular matrix, enable the maintenance of mRNA activity, controlled release, and targeted delivery. The assessment of in vivo delivery will be the next step of our study. Overall, hydrogels represent a promising path for future research and development in biopharmaceutical therapeutics, offering new possibilities for treating a wide range of diseases and revolutionizing the field of biomedical applications.

Acknowledgements

This work was developed within the scope of the project CICECO-Aveiro Institute of Materials, UIDB/50011/2020, UIDP/50011/2020 & LA/P/0006/2020, financed by national funds through the FCT/MEC (PIDDAC). This work was developed within the scope of the EIC-Pathfinder YSCRIPT project with reference 101047214, supported by the budgets of the Horizon Europe Program. Bojan Kopilovic acknowledges the FCT for the PhD grant SFRH/BD/06481/2020.

References

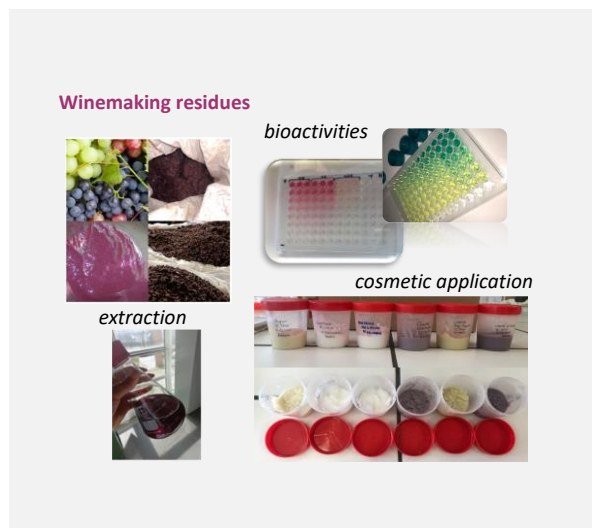
[1] E.C. Lavelle, R.W. Ward, Nature Reviews Immunology, 22 (2022) 236-250.

Exploiting winemaking residues as ingredients for cosmeceutical applications

C.N. Duarte^{1,2,3}, A. dos Santos^{1,2}, T. Oludemi^{1,2,4}, C. Santos-Buelga³, R.C.S. Dias^{1,2}, L. Barros^{1,2}, J.S. Amaral^{1,2*}

¹Centro de Investigação de Montanha (CIMO), Instituto Politécnico de Bragança, Campus de Santa Apolónia, 5300-253 Bragança, Portugal; ²Laboratório Associado Para a Sustentabilidade e Tecnologia em Regiões de Montanha (SusTEC), Instituto Politécnico de Bragança, Campus de Santa Apolónia, 5300-253 Bragança, Portugal; ³Grupo de Investigación en Polifenoles (GIP-USAL), Facultad de Farmacia, Universidad de Salamanca, E-37007 Salamanca, Spain; ⁴Nutrition and Bromatology Group, Department of Analytical Chemistry and Food Science, Faculty of Science, University of Vigo, E-32004 Ourense, Spain.

*jamaral@ipb.pt



Grape pomace and their components (mainly skins and seeds) have been widely studied concerning its chemical composition and bioactivity since there is considerable interest from the food, cosmetic and pharmaceutical industries to turn this by-product rich in bioactive compounds into innovative ingredients. However, other residues from the winemaking process, such as the wine lees and the diatomaceous earth used for wine filtration are less studied and underexploited products. In this work, in addition to the most known residues from red wine processing, residues from white wine production, wine lees and diatomaceous earth were studied for their content in total phenolics, antioxidant activity and capacity of inhibiting collagenase and tyrosinase, two skin enzymes frequently involved in skin aging process. Moreover, extracts were evaluated for their eventual cytotoxicity in skin cells (fibroblasts and keratinocytes). Aiming to evaluate its potential to be used for cosmeceutical applications, two extracts were selected and added to a base formulation of a cream, with or without commercial preservatives. The antioxidant activity of the 6 creams was measured and preliminary results concerning produced antimicrobial activity of the creams were obtained.

Introduction

Over the last years, there has been a growing interest and trend in valorizing different by-products from the agri-food industry towards a circular economy. These by-products are frequently rich in bioactive compounds, particularly polyphenols, that can be further exploited by other industries such as pharmaceutical, cosmetic and food. The winemaking industry is amongst the ones that generate many by-products, mainly grape pomace, but also wine lees and other undervalued residues, such as diatomaceous earth used in wine filtration. While grape seeds can be used to produce grapeseed oil and the pomace can further undergo distillation or be used as a fertilizer or as animal feed, the stems, lees, and diatomaceous earth are generally discarded and perceived as an environmental problem. So far, most works on the chemical characterization and bioactive properties of extracts obtained from wine industry by-products have focused on grape pomace while studies on wine lees, particularly from white grapes, and on diatomaceous earth are still very scarce. Therefore, in this work, these underexploited residues were evaluated and compared with the more widely studied grape pomace, skins and seeds. Hydroethanolic extracts were prepared and evaluated for their total phenolics content, antioxidant activity, cytotoxicity in fibroblasts (HFF-1) and keratinocytes (HaCaT) cell lines, and the capacity of inhibiting enzymes associated with skin aging (tyrosinase and collagenase). Finally, a base formulation of a cream was produced, added with different extracts and submitted to challenge test assay.

Methods

Samples: Winemaking by-products (red grape pomace, grape stems, red wine lees, white wine pomace and lees, diatomaceous earth used in red wine filtration) were supplied by Caves Campelo S.A. (Portugal). The seeds and skins were manually separated from the red grape pomace. The red lees

were centrifuged to separate the liquid from the solid phase. A total of 5 g of each sample was extracted with 100 mL of hydroethanolic solution (80%, v/v) by sonication for 5 min followed by stirring for 1h, at ambient temperature and protected from light.

Cream base-formulation: the base cream was prepared by using the following ingredients: water (74%), glycerin (5%), sweet-almond oil (15%), Olive M 1000 (6%). The formulation was also prepared with the addition of the commercial preservative Sensidin DO (0.5%) and/or antioxidant (tocopherol, 0.3%) and/or with red or white pomace extract, with the quantity of water used adapted. A total of 6 different creams were prepared.

Total phenolics: were determined by spectrophotometry using the Folin-Ciocalteu reagent and a calibration curve constructed using gallic acid as standard (0.005–0.5 mg/mL) [1].

Antioxidant Activity: assays were performed as previously described, namely DPPH radical-scavenging activity [1], reducing power [2] and lipid peroxidation inhibition in porcine brain [1]. Results were expressed as EC₅₀ values, corresponding to the sample concentration providing 50% of antioxidant activity or 0.5 of absorbance in the reducing power assay.

Antibacterial Activity: based on the results previously obtained that evidenced antimicrobial activity for the extracts obtained with the winemaking residues under study [3], the antimicrobial activity of creams incorporated with extract from white and red grape pomace was further evaluated. The prepared creams were subjected to the challenge test procedure using the Gram-positive bacteria *S. aureus* and Gram-negative *P. aeruginosa*, with determinations being carried out at day 0, 1, 7 and 30.

Cytotoxicity Assay in Skin Cell Lines: the cytotoxic activity of the extracts (50 µg/mL) was investigated in fibroblasts (HFF-1) and keratinocytes (HaCaT) by the Sulforhodamine B (SRB) assay.

Enzymes inhibition: collagenase inhibition was evaluated using the colorimetric assay kit from Sigma-Aldrich (MAK293), and tyrosinase inhibition using L-3,4-dihydroxy-phenylalanine (L-DOPA) as substrate and 3-methyl-2-benzothiazolinone-hydrazonehydrochloride (MBTH) as a chromogenic stabilizing agent, as previously described [4].

Results and discussion

Table 1 shows the obtained results for total phenolics, antioxidant activity and inhibition of collagenase and tyrosinase. Diatomaceous earth presented the second highest amount of total phenolics and demonstrated to be a potential source of bioactive compounds, evidenced by its antioxidant capacity, highlighting the best results in the reducing power assay. In general, the safety of the extracts for skin cells was demonstrated by the absence of toxicity in HFF-1 and HaCaT cells.

Overall, the extracts of grape pomace, seeds, skins, and stems, were able to inhibit collagenase and tyrosinase, two enzymes involved in skin aging process, with best results observed for the red grape pomace and seeds. However, a low or even absent inhibition was observed for the lees and diatomaceous earth. Table 2 shows the results of the antioxidant activity and challenge test performed with the prepared creams.

The high antioxidant activity of red grape pomace is evidenced by results of creams 1 and 2. Cream 3, added with white pomace extract, showed better results than creams 4 and 6, which may be due to the additive/synergistic action of tocopherol. Preliminary results of the challenge test suggest an antimicrobial activity of red pomace extract when added to the cream, while white pomace extract seems to present a synergetic effect with the commercial preservative Sensidin DO. Nevertheless, more assays are needed assuring a better homogenization of the inoculum in the cream and including a negative control.

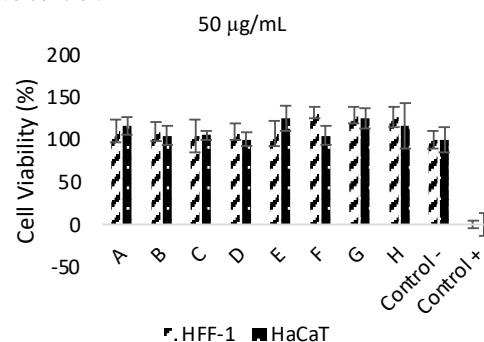


Figure 1. Cell viability effects of residues extracts (50 µg/mL) on HFF-1 and HaCaT cells. A: Red Wine Lees (Solid Phase); B: Red Grape Pomace; C: White Wine Lees; D: Diatomaceous Earth; E: Red Wine Lees (Liquid Phase); F: Seeds; G: Skins; H: Stems.

Table 1. Total phenolic compounds, antioxidant activity and enzymes inhibition activity of extracts obtained from winemaking residues.

Sample	Total phenolic compounds (mg GAE/mL)	Antioxidant activity EC ₅₀ (mg/mL)			Collagenase inhibition (%)	Tyrosinase inhibition (%)
		DPPH	Reducing Power	TBARS		
Red grape pomace	111 ± 2	0.123 ± 0.007	0.17 ± 0.004	0.03 ± 0.02	89 ± 2	28.2 ± 0.1
Skins	73 ± 1	0.217 ± 0.005	0.24 ± 0.004	0.018 ± 0.005	75 ± 7	34.55 ± 0.05
Seeds	146.6 ± 0.6	0.081 ± 0.005	0.11 ± 0.007	0.021 ± 0.003	87 ± 8	45.3 ± 0.1
Stems	63.7 ± 0.7	0.21 ± 0.005	0.41 ± 0.004	0.110 ± 0.007	82 ± 3	29.93 ± 0.02
White grape pomace	72 ± 5	0.411 ± 0.005	0.326 ± 0.003	0.094 ± 0.0003	ND	ND
White wine lees	19.7 ± 0.4	0.93 ± 0.08	0.83 ± 0.09	0.38 ± 0.02	NA	NA
Red wine lees (Liq. phase)	26.7 ± 0.5	0.578 ± 0.005	0.78 ± 0.001	0.35 ± 0.02	NA	0.61 ± 0.02
Red wine lees (Sol. phase)	37.6 ± 0.5	0.506 ± 0.007	0.68 ± 0.002	0.609 ± 0.005	NA	1.22 ± 0.03
Diatomaceous earth	126.9 ± 0.9	0.17 ± 0.01	0.11 ± 0.004	0.20 ± 0.03	18 ± 3	NA

NA: no activity; ND: not determined.

Table 2. Challenge test results (UFC/ml, mean of 2 determinations).

Cream	DPPH EC ₅₀ (mg/mL)	<i>S. aureus</i> (UFC/ml)				<i>P. aeruginosa</i> (UFC/mL)			
		T0	T1	T7	T30	T0	T1	T7	T30
1 (with RPE)	0,04 ± 0,001	8.50x10 ³	5.10x10 ⁴	6.50x10 ²	6.50x10 ²	3.90x10 ⁴	7.75x10 ⁵	1.39x10 ⁵	1.00x10 ¹
2 (with RPE + SenS)	0,05 ± 0,001	4.00x10 ³	1.99x10 ⁵	1.05x10 ³	6.50x10 ²	3.05x10 ⁴	5.85x10 ⁴	1.37x10 ⁵	1.05x10 ¹
3 (with WPE + SenS + Toc)	0,04 ± 0,001	2.45x10 ⁵	7.85x10 ³	2.50x10 ²	4.65x10 ²	<10UFC in 1/1000	<10 UFC in 1/100	<10 UFC in 1/100	<10UFC in 1/10
4 (with WPE + SenS)	0,23 ± 0,05	6.45x10 ⁵	1.05x10 ⁴	4.50x10 ¹	2.10x10 ²	6.00x10 ³	1.00x10 ¹	5.50x10 ¹	7.20x10 ²
5 (-cont, without SenS+Toc)	0,12 ± 0,002	4.90x10 ⁵	2.40x10 ⁵	1.87x10 ⁵	1.85x10 ⁴	1.35x10 ⁵	2.98x10 ⁶	4.50x10 ⁶	4.90x10 ⁶
6 (+cont, with SenS)	0,14 ± 0,004	3.15x10 ⁴	2.10x10 ²	2.50x10 ¹	2.10x10 ²	4.90x10 ⁵	4.90x10 ⁵	4.90x10 ⁵	4.90x10 ⁵

RPE: red pomace extract; WPE: white pomace extract; SenS: commercial preservative Sensidin DO; Toc: tocopherol.

Acknowledgements

This work was financially supported by project "BacchusTech - Integrated Approach for the Valorization of Winemaking Residues" (POCI-01-0247-FEDER-069583) and by COMPETE 2020, under the PORTUGAL 2020 Partnership Agreement, through ERDF and FCT and national funds FCT/MCTES (CIMO: UIDB/00690/2020, UIDP/00690/2020, SusTEC: LA/P/0007/2020). To COST Action 20133 FULLRECO4US, supported by COST (European Cooperation in Science and Technology). To Campelo for supplying the winemaking residues. L. Barros thanks the national funding by FCT, P.I., through the institutional scientific employment program-contract. The GIP-USAL thanks to Spanish "Ministerio de Ciencia and Innovación" (PID2019-106167RB-I00) and "Junta de Castilla y León" (SA093P20 and CLU-2018-04).

References

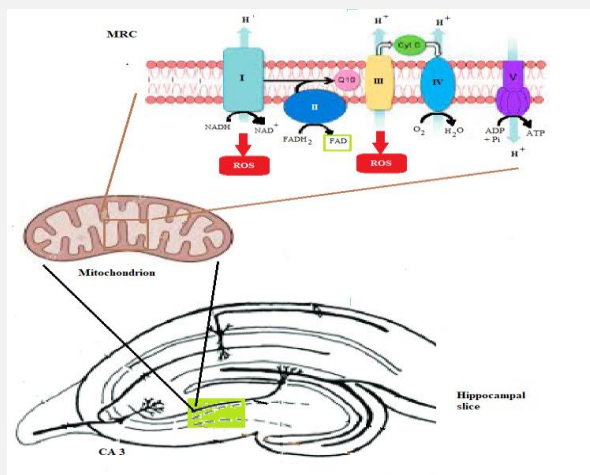
- [1] J.H. Iyda et al., Food Research International, 121 (2019) 714-722.
- [2] V. Silva et al., Antioxidants, 9 (2020) 178.
- [3] C.N. Duarte et al., Cosmetics, 10 (2023) 58.
- [4] O. Taofiq et al., Food and Chemical Toxicology 108 (2017) 139-147.

Potassium evoked ROS signals in mitochondria

J.L.R. Alves^{1,2}, M.S. Sousa^{1,3}, P.M. Reis⁴, R.M. Quinta-Ferreira⁴, M.E. Quinta-Ferreira^{1,5}, C. M. Matias^{1,6*}

¹CNC, Univ. Coimbra, P-3004-504 Coimbra, Portugal; ²Dept. Life Sciences, Univ. Coimbra, P-3004-516 Coimbra, Portugal; ³ESS, Inst. Pol. do Porto, P-4200-072 Porto, Portugal; ⁴CIEPQPF, Dept. Chemical Engineering, Univ. Coimbra, P-3030-790 Coimbra, Portugal; ⁵Dept. Physics, Univ. Coimbra, P-3004-516 Coimbra, Portugal; ⁶UTAD, Dept. Physics, 5000-911 Vila Real, Portugal.

*cmatias@utad.pt



Effluents, mainly from agricultural and industrial activities, contain often an excessive concentration of potassium, which may have a negative impact in the soil-plant-microorganisms system. High levels of potassium consumed by animals and humans may cause multiple undesired physiological changes, such as in mitochondria, the organelles that provide cellular energy. In particular, neuronal autofluorescence and the production of reactive oxygen species (ROS) of mitochondrial origin can be important indicators of the mitochondrial respiratory chain (MRC) function. In this study, effects of the blockers of the I- and III- MRC complexes, rotenone and myxothiazol, respectively, were studied in brain slices. It was observed that autofluorescence and ROS signals, detected with the indicator H₂DCFDA and evoked by potassium depolarization (20 mM KCl), under hypoxic conditions (40% O₂), were enhanced and abolished, respectively, by the combined application of those blockers. This suggests that the I- and III- MRC complexes mediate potassium induced ROS production under hypoxic conditions.

Introduction

Effluents from domestic origin have a relatively low potassium content (10 – 30 mg L⁻¹). In contrast, a variety of agricultural and industrial wastewaters, including those from olive oil, lactic acid, pig and wine processing industries, contain high levels of potassium (1,000 - 20,000 mg L⁻¹) [1]. The use of these enriched wastewaters for irrigation may have both beneficial (increased organic matter and soil fertility) and harmful (higher soil salinization and unwanted pH) consequences [1]. Long time exposures to these wastewaters have been shown to lead to higher potassium content of crops and, consequently, of biological tissues and fluids. In neurons, high extracellular potassium concentration causes membrane depolarization and the activation of several ionic channel mechanisms [2] that may lead to changes in the mitochondrial function. This can be evaluated through the autofluorescence, i.e. the intrinsic fluorescence of flavoprotein origin, and by the production of reactive oxygen species (ROS) [3]. In excess, these compounds are considered to be involved in diseases and in the degeneration of the central nervous system [3]. The aim of this work was to study potassium induced-autofluorescence and ROS changes under hypoxia (40% O₂), which causes higher ROS signals. The role of the mitochondrial complexes I and III in ROS production was evaluated, by means of the simultaneous application of their blockers, rotenone (2 μM) and myxothiazol (2 μM), respectively. For this purpose, rat hippocampal slices were perfused with a solution of artificial cerebrospinal fluid (ACSF) and incubated with the cell-permeant fluorescent ROS indicator H₂DCFDA (10 μM). This indicator is fluorescent at wavelengths between 460 and 490 nm, which is also the range of fluorescence of the coenzyme flavin adenine dinucleotide (FAD) [4]. For this reason, the ROS fluorescence signals were obtained subtracting the FAD-linked autofluorescence changes, recorded from uncubated slices, from the total fluorescence signals measured from slices containing the ROS indicator. In order to evaluate the effect

of the mitochondrial respiratory chain (MRC) in ROS production, the mitochondrial inhibitors rotenone (2 μM) and myxothiazol (2 μM), were applied. Neuronal activity was stimulated by 20 mM KCl, evoking the potassium ion (K⁺), at that concentration, a rise of about 20 mV in the plasma membrane resting potential and, thus, neuronal depolarization [2]. Thus, the role of the referred complexes was assessed by comparing ROS and autofluorescence signals, in the absence and in the combined presence of the mentioned mitochondrial blockers.

Experimental methods

Hippocampal slices (350 μm thick) were obtained from Wistar rats (12 – 16 weeks old). In the experimental chamber, the slices were perfused, at a rate of 1.5–2 ml/min, with oxygenated ACSF or a drug-containing medium, at 30–32 °C. ACSF contained (in mM): NaCl 124.0; KCl 3.5; NaHCO₃ 24.0; NaH₂PO₄ 1.25; MgCl₂ 2.0; CaCl₂ 2.0 and glucose 10.0. In order to evoke membrane depolarization, a modified ACSF, composed of NaCl 107.0; KCl 20; NaHCO₃ 24.0; NaH₂PO₄ 1.25; MgCl₂ 2.0; CaCl₂ 2.0 and glucose 10.0 was applied. The NaCl concentration was reduced to maintain the osmolarity of the solution. The normal oxygenation condition consisted in the use of a gas mixture of 95% O₂/ 5% CO₂. Hypoxia was evoked by the use of a different gas mixture (40% O₂/ 55% N₂/ 5% CO₂). The drugs rotenone (2 μM) and myxothiazol (2 μM) were applied simultaneously, in the perfusion media, throughout the experiment. The detection of the optical signals was performed using a transfluorescence microscope (Zeiss). The preparation was illuminated by an halogen light source (12 V, 100 W), being the incident light selected by means of an excitation filter (470 ±10 nm) and the emitted light by a high-pass filter (> 500 nm). The light was collected from the *stratum lucidum* of the hippocampal CA3 area and focused on a silicon photodiode (1 mm², Hamamatsu). The signal was converted by a 16-bit I/V converter and analyzed using the

Signal Express® platform from National Instruments. For the observation of the ROS signals, the hippocampal slices were incubated, during 1 hour, in a solution of ACSF containing the permeant indicator H₂DCFDA (10 μ M), continuously oxygenated with 95% O₂/ 5% CO₂. The optical ROS data consist of fluorescence values (F) after subtracting from the total fluorescence (F_T), collected from incubated slices, the autofluorescence component (F_A), measured at an equivalent region of indicator free slices. The measurements are presented as mean \pm s.e.m. Statistical significance was tested using the Mann-Whitney *U* test, *p* < 0.05 were considered significant.

Results and discussion:

In the situation of hypoxia, the cell depolarization evoked by the application of KCl (20 mM) caused an increase in both the FAD-linked autofluorescence and the ROS signals. The amplitude of the autofluorescence records increased to $106 \pm 3\%$ (mean \pm s.e.m., *n* = 3) with respect to baseline (first ten minutes), at 35-40 min after the beginning of the experiment. On the other hand, the ROS signals, obtained using the same stimulation protocol, rose to $113 \pm 3\%$ (*n* = 3) at the same period of time. As expected, both the autofluorescence and ROS changes decreased during the removal of KCl. However, while the FAD-linked fluorescence decreased to values below the baseline, the ROS signals remained potentiated after washout (Figure 1a). In the presence of both mitochondrial blockers rotenone (2 μ M) and myxothiazol (2 μ M), applied throughout the experiments, the depolarizing agent KCl (20 mM) caused a higher enhancement of autofluorescence (compared with control), which reached an amplitude of $116 \pm 2\%$ of the baseline values (mean \pm s.e.m., *n* = 3, *p* < 0.05). In contrast, the referred drugs completely blocked the KCl-induced rise of the ROS changes (Figure 1b,c). The formation of ROS, which increases with cell depolarization and depends on the intensity of hypoxia, is normally related with mitochondrial activity, namely with the MRC function [5]. It was previously shown that, in ischemic conditions, the activation of complexes I- and III- of MRC [6] evokes ROS production. These results confirm the role of those complexes in ROS production, which was abolished in the presence of the applied blockers. Moreover, the FAD-linked autofluorescence, which is related with the mitochondrial activity, increased in the presence of the same blockers, i.e. rotenone and myxothiazol. The results may be due to the blockade of complex I by rotenone, which disrupts the electron chain, affecting complex II, which is responsible for the reduction/oxidation of FAD [7], modifying, consequently, its fluorescence.

Acknowledgements: Patrícia Reis acknowledges FCT (Fundação para a Ciência e Tecnologia, Portugal) for the PhD Grant (2021.04553.BD). The experiments were funded by strategic project UID/NEU/04539/2013.

References

- [1] M. Arienzo et al., *Journal of Hazardous Materials*, 164 (2009) 415-422.
- [2] V. Bancila et al., *Journal of Neurochemistry*, 90 (2004) 1243-1250.
- [3] M.C.W. Oswald et al., *FEBS Letters*, 592 (2018) 679-691.
- [4] O.I. Kolenc, K.P. Quinn, *Antioxidants and Redox Signaling*, 30 (2019) 875-889.
- [5] L.L. Dugan et al., *Journal of Neuroscience*, 15 (1995) 6377-6388.
- [6] N.S. Chandel et al., *Proceedings of the National Academy of Sciences*, 95 (1998) 11715-11720.
- [7] P.R. Rich, A. Maréchal, *Essays in Biochemistry*, 47 (2010) 1-23.

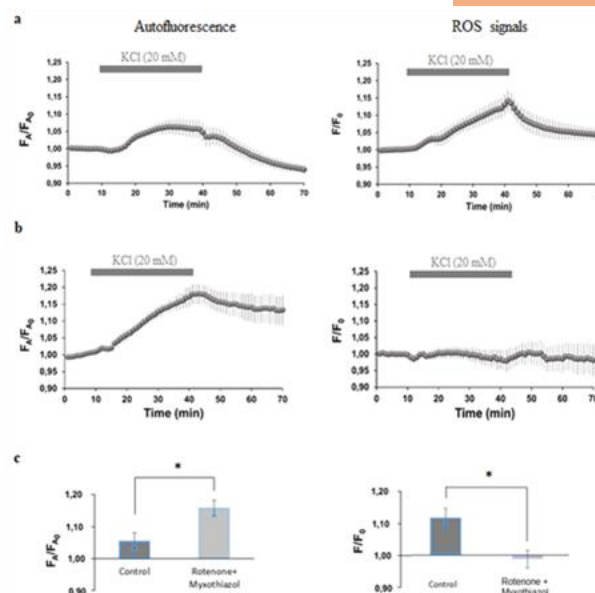


Figure 1. Autofluorescence and ROS signals evoked by KCl under hypoxia in the absence and the presence of rotenone and myxothiazol. **a.** Effect of the application of 20 mM KCl (indicated by the bar) in autofluorescence (left) and ROS signals (right), from slices perfused with ACSF oxygenated with 40% O₂ (hypoxia). **b.** Similar recordings performed in the presence of a mixture of rotenone (2 μ M) and myxothiazol (2 μ M). **c.** Bar graphs representing the values of autofluorescence (left) and ROS signals (right) measured in the last five minutes (35-40 min) of the application of KCl, comparing the control signals (panels a) with those obtained in the presence of rotenone and myxothiazol (panels b). The results are presented as mean \pm s.e.m. The brackets represent the significance of the effect of these agents, calculated using the Mann-Whitney *U* test (* - *p* < 0.05). F – ROS fluorescence; F_A - autofluorescence; F₀ and F_{A0} – basal ROS fluorescence and basal autofluorescence.

Conclusions

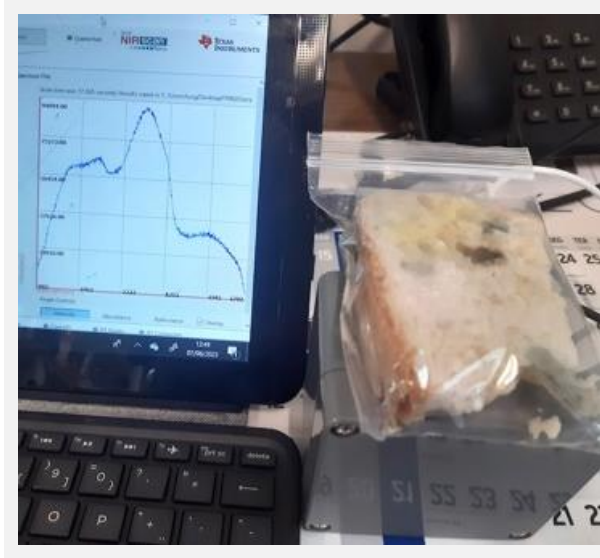
Many effluents, from various agricultural and industrial sources, contain excess potassium that may affect soils, crops and animals, when they are used for long-term irrigation. This study shows that in high extracellular potassium (20 mM KCl), and under hypoxic conditions (40% O₂), the inhibition of mitochondrial complexes I- and III- of MRC, by rotenone and myxothiazol, respectively, leads to an enhancement of autofluorescence and to the blockade of ROS formation. The latter finding is in agreement with the idea that the production of mitochondrial ROS, which is enhanced in the presence of high extracellular potassium, is mediated by the mentioned complexes.

Near-infrared spectroscopy analysis of bread: study of shelf life and correlation with microbiological analysis

*D. Amendoeira**, A. Teixeira, L.G. Dias, L. Estevinho

Centro de Investigação de Montanha (CIMO), Instituto Politécnico de Bragança, Bragança, Portugal; Laboratório Associado para a Sustentabilidade e Tecnologia em Regiões de Montanha (SusTEC), Instituto Politécnico de Bragança, Campus de Santa Apolónia, 5300-253 Bragança, Portugal.

**dianapaulo2014@gmail.com*



Near-Infrared (NIR) is a promising technique for the analysis of bread in order to assess its quality and shelf life. The NIR spectrum can be used to measure properties such as moisture, protein, starch, sugars, fats, among others, which can help predict the bread's shelf life.

In this study, NIR spectra were measured and microbiological analyses were performed on bread over a period of two weeks. The correlation between these data will allow to define NIR as an assessment tool for quality and, consequently, for the analysis of the product's shelf life. Currently, the relationship between NIR spectra and microbiological analyses is being studied using multivariate statistical methods, aiming to develop a non-destructive technique for evaluating bread quality.

As a result, it is intended for this technique to be applied in situ in food companies, aiming to improve the efficiency of the food chain and ensure food safety for consumption.

Introduction

Proper and balanced nutrition plays a crucial role in promoting health and well-being. Bread, as one of the staple foods in the human diet, plays a fundamental role in this context by providing essential nutrients for the body. It is therefore essential to have fast, accurate, and precise analytical tools to assess bread quality.

NIR is a rapid and non-destructive technique that can be used to measure the composition of food products, such as moisture, protein, starch, sugars, fats, among others. It can also enable the evaluation of microbial contamination [1]. Therefore, the intent was to use this instrumental analysis method to assess the shelf life of bread by establishing a relationship between NIR spectra and microbial contamination levels [2], through the application of chemometric tools (Figure 1).

The development of NIR methods that assess the quality of a food product is highly advantageous and applicable in the industry [1,3], as it can quickly identify changes in product quality and take corrective measures to ensure that bread meets the required quality standards. With an accurate estimation of the bread's shelf life, the industry can inform consumers, assess microbiological safety, and detect possible contaminations early on, thereby ensuring food safety and protecting the company's reputation [4].

Materials and methods:

In this study, wheat bread (Rio Maior bread) purchased from a commercial establishment in Bragança was used. The samples of bread were sliced and analyzed at 8 different time points to evaluate the microbial evolution of the bread, specifically to determine its shelf life. Sampling was conducted at 0, 2, 4, 6, and 8 days. Three different bread preparation procedures were performed in duplicate:

- Sliced bread was placed individually on an open surface, exposed to ambient air conditions.
- Sliced bread was individually placed in properly sealed plastic bags.
- The crumb of sliced bread was ground and individually placed in properly sealed plastic bags.

All analyzed samples were exposed to sunlight and kept at room temperature. At the specified time points, each sample was tested for the presence of Salmonella sp., total coliforms, Escherichia coli, mesophilic aerobic microorganisms, as well as mold and yeast counts. All bread samples were analysed by NIR (from Texas Instruments) in the range of 900 to 1900 nm, using the free software DLP NIRscan Nano GUI v2.1.0 (Figure 1).



Figure 1. NIR from Texas Instruments

In addition, moisture analyses were conducted to correlate its content with NIR spectra. These evaluations provide valuable

information regarding the microbiological safety and chemical characteristics of bread, contributing to ensuring the quality and safety of food products.

Currently, multivariate statistical tools are being applied to establish a relationship between spectra and microbial composition using the opensource R software.

Acknowledgements

CERTRA - Development of Traditional Cereal Value Chains for Sustainable Food in Portugal, Investment RE-C05-i03 - Research and Innovation Agenda for the Sustainability of Agriculture, Food, and Agro-Industry, No. 12/C05-i03/2021 - PRR-C05-i03-I-000161, R&D+I ; Projects - Sustainable Food Research and Innovation Projects. Action Line 1.2 – Products

References

- [1] K.B. Beć et al., *Foods*, 11(2022) 1465-1517.
- [2] N. El-Morsy et al., *Journal of Food and Dairy Sciences*, 5 (2014) 33-44.
- [3] S. Grassi, C. Alamprese, *Current Opinion in Food Science*, 22 (2018) 17-21.
- [4] A.M.K. Pedro, M.M.C. Ferreira, *Applied Spectroscopy*, 63 (2009) 1308-1314.

Conclusions

In summary, the results of this study using NIR can bring significant advantages to the industry in estimating the shelf life of bread. This contributes to reducing waste, improving product quality, optimizing the supply chain, and ensuring food safety.

Analysis of bread using potentiometric electronic tongue: importance for quality control

A. Teixeira*, D. Amendoeira, L. Estevinho, L.G. Dias

Centro de Investigação de Montanha (CIMO), Instituto Politécnico de Bragança, Bragança, Portugal; Laboratório Associado para a Sustentabilidade e Tecnologia em Regiões de Montanha (SusTEC), Instituto Politécnico de Bragança, Campus de Santa Apolónia, 5300-253 Bragança, Portugal.

alexandrateixeira99@hotmail.com



This study aimed to evaluate the electronic tongue's ability to distinguish between different types of bread based on cereal compositions (wheat, rye, and corn). This has significant implications for bread quality control, ensuring consistency and detecting adulterations. The potentiometric electronic tongue, with 20 sensors using polymeric membranes, successfully discriminated the bread types. The device was connected to a multiplexer and controlled by software for signal acquisition. The sensor profile data was treated with multivariate statistical methods using the opensource R software. Bread samples were prepared, extracted, and analyzed using the electronic tongue. Results demonstrated the system's value, offering non-destructive, simplicity, and adaptability. The study's innovation lies in applying this technique to bakery products, enhancing quality control and adulteration detection.

Objectives

The aim of this study was to evaluate the electronic tongue's ability to distinguish between different types of bread based on their cereal compositions (wheat, rye, and corn). The significance of this work for bread quality control is substantial. The ability to distinguish between different types of bread based on their cereal compositions can be used to ensure product quality consistency (by verifying if each batch of bread produced conforms to its cereal composition specifications). Additionally, the technique can be used to detect adulterations in bread (by confirming the presence of lower quality ingredients or adding undeclared ingredients).

Potentiometric ETongue device and analysis

The potentiometric ETongue was an all-solid multi-sensor device that included 20 sensors prepared with polymeric membranes obtained by mixing 32% of polyvinyl chloride as polymeric matrix, 65% of one plasticizer compound and 23% of one membrane additive. The additive compounds were long carbon chain with different functional groups, being non-specific, presenting low selectivity and cross-sensitivity to the different species in the samples (both inorganic and organic, ionic and non-ionic) [1,2]. The multi-sensor device was built in a cylindrical piece of acrylic with an architecture already described in previous work [3]. This device together with a double junction Ag/AgCl reference electrode was connected to a multiplexer Agilent Data Acquisition/Switch Unit model 34970A, which was controlled by the Agilent BenchLink Data Logger software, installed in a PC computer, for the sensor signals acquisition.

ETongue analysis of each solution was performed after a period of stabilization of 3 minutes, after which the 20-signal profile was obtained. Between sample analysis, the system was washed with deionized water and cleaned with absorbent paper.

Bread samples and preparation for analysis

The bread samples used were of wheat, corn, mixture of wheat and rye (33%) and commercial white and integral bread. The bread samples' crumb was crushed and extracted with a hydrochloric-ethanol solution for three hours with agitation (5-10 g of bread and 20 ml of solution). After filtration and dilution of 10 mL of extract into 50 mL with deionized water (Figure 1). Solutions were analyzed with the electronic tongue. The obtained signal profiles were processed with R software.



Figure 1. Breads in the hydrochloric-ethanol solution.

Conclusions

Results showed that the potentiometric electronic tongue is a valuable tool for the analysis of bread with different cereal compositions, as it was possible to correctly discriminate all types of bread. The advantages of this analytical system include non-invasiveness, simplicity, and rapidity, as well as the ability to be easily adapted for other applications. The innovation of this work lies in the application of the technique in bakery products, and its importance for bread quality control is significant, helping to ensure product quality consistency and to detect adulterations.

Acknowledgements

CERTRA - Desenvolvimento de Cadeias de Valor de Cereais Tradicionais para uma Alimentação Sustentável em Portugal, Investimento RE-C05-i03 – Agenda de investigação e inovação para a sustentabilidade da agricultura, alimentação e agroindústria, N.º 12/C05-i03/2021 – PRR-C05-i03-I-000161, Projetos I&D+I Projetos de Investigação e Inovação - Alimentação Sustentável. Linha de ação 1.2 - Produtos.

References

- [1] Y. Kobayashi et al., *Sensors*, 10 (2010) 3411-3443.
- [2] L.A. Dias et al., *Sensors & Actuators: B. Chemical*, 136 (2009) 209-217.
- [3] A. Jarboui et al., *Talanta*, 208 (2020) 120364.

Optimization of phenolic compounds extraction from mountain ash fruit pulp

G. Vergara^{1,2*}, N.L. Seixas^{1,2}, N.P. Mira^{3,4}, L. Estevinho^{1,2}, L.G. Dias^{1,2}

¹Centro de Investigação de Montanha (CIMO), Instituto Politécnico de Bragança, Bragança, Portugal; ²Laboratório Associado para a Sustentabilidade e Tecnologia em Regiões de Montanha (SusTEC), Instituto Politécnico de Bragança, Campus de Santa Apolónia, 5300-253 Bragança, Portugal; ³iBB, Institute for Bioengineering and Biosciences, Department of Bioengineering, Instituto Superior Técnico, Universidade de Lisboa, Avenida Rovisco Pais, 1049-001 Lisbon, Portugal; ⁴Associate Laboratory i4HB—Institute for Health and Bioeconomy at Instituto Superior Técnico, Universidade de Lisboa, Av. Rovisco Pais, 1049-001 Lisboa, Portugal.

gaah.valentina@hotmail.com



Currently, consumers are seeking healthier foods, which has encouraged the development of natural products without the addition of chemical preservatives. In this context, Tramazeira pulp (*Sorbus aucuparia*), due to its content of substances such as quercetin, ascorbic acid, tocopherols, vitamins, and fibers, can potentially serve as an alternative to replace the chemical additives currently used in yogurt preservation. Additionally, the biological properties evaluated in the pulp showed possible applications as a food additive, contributing to enhancing the bioactivity of the product. The overall objective of this study is to assess the effect of fermented and non-fermented extracts from Tramazeira fruit pulp on the preservation and bioactivity of yogurt.

Introduction

The *Sorbus aucuparia*, known as the Mountain Ash, is a native tree of Europe and Asia Minor commonly found in exposed, rocky, and steep locations. It belongs to the Rosaceae family and is recognized for its remarkable properties. The fruits contain sorbitol, tannins, malic acid, and sorbate, sugars, pectin, and toxic to humans, requiring its removal when preparing the fruit pulp. It is common to use fruits to produce jams, sauces, and other culinary products. In some regions of Europe, through fermentative processes, liqueurs and vinegars are made using the fruits of *Sorbus aucuparia*.

Recently, it was reported that the antioxidant activity of some Sorbus fruits was related to polyphenolic compounds [1,2]. Several authors have conducted studies to verify the antioxidant potential of phenolic acids with the aim of replacing synthetic antioxidants, widely used in the preservation of lipidic foods, as they can increase the shelf life of many products by 15 to 200% [3].

Objectives

This work involves the study of the pulp of the *Sorbus aucuparia* fruit from the "Trás-os-Montes" region in terms of physical-chemical, microbiological, and biological properties, as it is a valuable source of phenolic compounds, which can be beneficial to human health and have potential for use in the food, cosmetic, and pharmaceutical industries.

Acknowledgements

TRAMONTE - Valuation of biological resources in the northern interior: the Transmontana Mountain Ash as a case study, FCT Project and "la Caixa" - Promote 2022, Promote Program: Mobilizing R&D Projects. The future of the interior. Polytechnic Institute of Bragança.

References

- [1] A.T. Hukkanen et al., Journal of Agricultural and Food Chemistry, 54 (2006) 112-119.
- [2] A. Termentzi et al., Food Chemistry, 98 (2006) 599-608.
- [3] R.M. Duran, R.B. Padilla, Grasas e Aceites, 44 (1993) 101-106.

vitamin C. The flowering of the Mountain Ash usually occurs from May to July, and its fruits ripen in late September. In general, they are acidic and slightly bitter. The seed, in turn, contains cyanogenic glycosides, which, when in contact with water, generate hydrocyanic acid, highly

Methods

A central composite experimental design was performed to optimize the extraction of phenolic compounds by RSM, with percentage of ethanol (ranging from 24% to 95.4% ethanol) and the pH value (ranging from 0.88 to 5.12) in the hydro-ethanolic solvent extractor as factors. The results of the determinations of total phenolic compounds, total flavonoids, antioxidant potential and individual sugar contents were used as responses.



Figure 1. The fruit extract (2023).

Results

In Figure 1, we can observe the Tramazeira's fruit, the fruit pulp, and the freeze-dried pulp, where the yield was measured. It was found that 354 g of fruit produces 168 g of pulp (47% of the fruit), and, subsequently, 49 g of freeze-dried pulp (14% of the fruit).

Extraction of phenolic compounds from *Sorbus aucuparia* tree leaves for use in food

H.F. Rodrigues^{1,2*}, N.L. Seixas^{1,2}, N.P. Mira^{3,4}, L.G. Dias^{1,2}, L.M. Estevinho^{1,2,3}

¹Centro de Investigação de Montanha (CIMO), Instituto Politécnico de Bragança, Bragança, Portugal; ²Laboratório Associado para a Sustentabilidade e Tecnologia em Regiões de Montanha (SusTEC), Instituto Politécnico de Bragança, Campus de Santa Apolónia, 5300-253 Bragança, Portugal; ³iBB, Instituto de Bioengenharia e Biociências, Departamento de Bioengenharia, Instituto Superior Técnico, Universidade de Lisboa, Avenida Rovisco Pais, 1049-001 Lisbon, Portugal; ⁴Laboratório Associado i4HB - Instituto de Saúde e Bioeconomia em Instituto Superior Técnico, Universidade de Lisboa, Av. Rovisco Pais, 1049-001 Lisboa, Portugal.

*hellenrodrigues@ipb.pt



This study aims to optimize the extraction of phenolic compounds from the leaves of *Sorbus aucuparia* tree, for its potential use as a natural food additive. The leaves were harvested in Polis, Portugal, and dried in an oven. A response surface methodology was used to determine the optimal hydro-ethanolic solution composition. Factors such as ethanol percentage and pH were investigated, and response variables including total phenolic content, total flavonoid content, and antioxidant activity were analyzed. Thin-layer chromatography revealed differences in the extracts, emphasizing the need for optimization. The findings will contribute to understanding the potential application of *Sorbus aucuparia* phenolic compounds in food products. Further research is required to evaluate their efficacy.

Introduction

Sorbus aucuparia, commonly known as the rowan tree or mountain ash, is a deciduous tree belonging to the genus *Sorbus* in the Rosaceae family [1]. In favorable conditions, it can grow to a height ranging between 15 and 20 meters. The tree features unique odd-pinnate leaves, measuring approximately 10-25 cm in length, composed of 9-19 pairs of elongated leaflets ranging from 2 to 6 cm. These leaves lack a noticeable petiole, possess a sharp apex, serrated margins, and exhibit a dark green color that transforms into a vibrant orange hue during the autumn season [2]. The rowan leaves contain various chemical compounds, including phenolic compounds, which confer therapeutic properties to the leaves, with antioxidant, anti-inflammatory, antimicrobial, and hypoglycemic effects [1,3]. However, scientific evidence is still limited, and further research is needed to evaluate the efficiency and effectiveness of therapeutic applications.

The current study aims to optimize the extraction of phenolic compounds from *Sorbus aucuparia* leaves, thus harnessing their potential for use as a natural additive in a food product such as yogurt.

Methodology

The leaves were harvested in Polis, in the city of Bragança, Portugal, in November 2022. The samples were dried for 3 days in an oven at a temperature of 40°C, conducting sample weighing until a constant weight was achieved.

To optimize the composition of the extractive hydro-ethanolic solution, a response surface methodology was applied using a central composite experimental design of 14 different assays to study the influence of the percentage of ethanol and (Table 1 and Figure 1). The pH ranged from 0.87 to 5.14 (fixed with different concentrations of hydrochloric acid), while the percentage of ethanol varied from 60 to 95.4%.

Table 1. Experimental design to test the composition of the extractive hydro-ethanolic solutions

Assays	Ethanol (%)	Measured pH
1	60	3,01
2	60	3,01
3	85	4,50
4	60	3,01
5	35	1,50
6	35	4,50
7	85	1,50
8	60	3,01
9	24	3,01
10	95,4	3,01
11	60	0,87
12	60	5,14
13	60	3,01
14	60	3,01

As response variables, the results obtained in the experimental design solutions by applying the total phenolic content, total flavonoid content and antioxidant (DPPH) analytical methods were used.

Data treatment using response surface methodology (RSM) was performed with R software to determine the optimal point for the studied factors.

Thin-layer chromatography was applied to verify the differences within the extracts. It was used a TLC silica gel 60 aluminum sheet and an eluent with chloroform – methanol – water (3:6:1). All extraction samples were applied into the silica sheet, using 3 µL measured in a syringe of 5 µL. After analysis, the silica sheet was visualized at UV radiation of wavelength of 365 nm (Figure 2).

As can be seen, there were differences between the extractive solutions, which justifies the optimization of the phenolic content extraction.



Figure 1. Samples after extraction with hydro-ethanolic solutions defined by the experimental design.

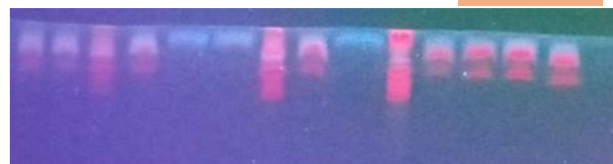


Figure 2. TLC analysis of the hydro-ethanolic visualized at 365 nm.

Acknowledgements

TRAMONTE-Valorization of the biological resources of the north interior: the Tramazeira Transmontana as a case study, FCT and "la Caixa" - Promove 2022, Promove Program: Mobilizing R&D Projects. The future of the interior. Polytechnic Institute of Bragança.

References

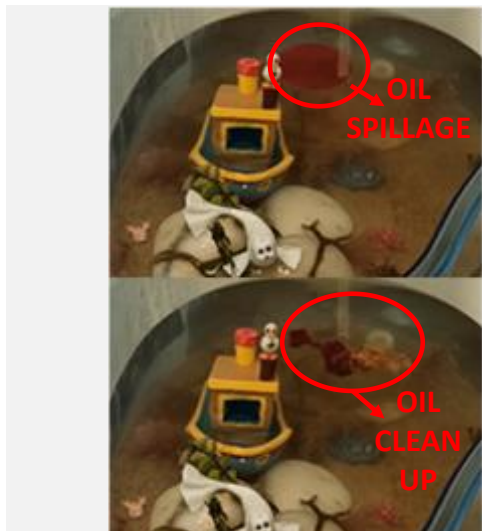
- [1] A. Sołtys et al., *Phytochemistry Reviews*, 19 (2020) 491-526.
- [2] M. Rätty et al., "Sorbus aucuparia in Europe: distribution, habitat, usage and threats". *European Atlas of Forest Tree Species*. Publ. Off. EU, Luxembourg, 2016.
- [3] V. Sarv et al., *Antioxidants*, 9 (2020) 813.

Laccase mediated grafting of pine sawdust for oil spill recovery

N. Miguez^{1,2}, A. Sanromán¹, D. Moldes¹*

¹BioSUV Group, Department of Chemical Engineering, University of Vigo, 36310 Vigo, Spain; ²Autonomous University of Madrid, 28049 Cantoblanco, Madrid, Spain.

*diego@uvigo.gal



Accidental oil spillage in water vessels can have important consequences for the environment as well as human health. Thus, the importance of developing economic and eco-friendly strategies for oil recovery. In this work, pine sawdust was transformed into a recyclable, low cost, biodegradable oil selective sorbent. Hydrophobic pine sawdust was obtained through lauryl-gallate grafting, employing the laccase-guaiacol system. The prepared sorbent was characterized in terms of hydrophobicity (contact angle up to 130.24°), water sorption capacity (negligible) and oil sorption capacity (in the range of 5 to 5.3 g/g).

Introduction

Oil leakage into oceans and other bodies of water has become a serious threat to aquatic ecosystems and human health. In the last decade, approximately 24,000 tons of oil have been spilled by tankers worldwide [1]. In addition, remediation of oil spills has been reported as one of the most expensive [2], thus having significant economic repercussions.

Generally, treatments for oil leakage include in-situ burning, chemical dispersion, mechanical removal, bioremediation and use of sorbents [3]. Among these different approaches, the application of sorbents is usually a quite efficient and convenient method with minimum ecological impact and relatively low costs [4].

According to literature [5], sorbent materials are classified into three major groups: (a) inorganic mineral materials, (b) organic synthetic sorbents and (c) organic vegetable products. Inorganic mineral sorbents include perlite, vermiculite, zeolite, diatomite, graphite, sorbent clay or volcanic ash. These materials are readily available and recyclable but their use has been hindered by their poor buoyancy and low adsorption capacity. Synthetic organic products, such as, polypropylene, polyester, rubbers or polyurethane foams possess high sorption capacities but their cost and poor biodegradability make them economically and environmentally non-friendly. Natural-based materials have aroused great interest due to their abundance, renewability, high availability, low cost, and biodegradability. However, they have poor buoyancy, scarce oleophilic properties and their oil sorption capacity is inferior compared to several synthetic materials. Commonly, these materials are hydrophilic in nature, thus favoring water sorption over the absorption of oil [6].

Nevertheless, the hydrophobicity of these products can be increased by different techniques, such as, thermal and hydrothermal modification, mercerization, acetylation, benzylation and grafting [7].

Enzymatic grafting is an eco-friendly alternative that can be used to successfully modify a target surface by forming covalent bonds between said surface and a chosen

hydrophobic molecule [8]. Laccases are ecofriendly biocatalysts capable of modifying lignocellulosic materials and have been previously employed in laccase mediated grafting of paper, wood, kraft pulp and cornstalk [9].

In this work, laccase mediated grafting was used to improve hydrophobic/oleophilic properties of pine sawdust. The performance of the novel pine sawdust sorbent was evaluated in terms of hydrophobicity, water sorption capacity, oil sorption capacity, sorption time and type of oil.

Materials and methods

Pine sawdust grafted with lauryl-gallate (PSLG) was prepared by mixing laccase (LAC), guaiacol, lauryl-gallate (LG) and pine sawdust in 100 mM sodium citrate buffer (pH 4.6) at 50 °C. First, 2 g of pine sawdust were oxidized with 5 mM guaiacol and 100 U/g of LAC during 2 h. Then, 700 mg of LG and 100 U/g of LAC were added and the grafting reaction was completed overnight.

The hydrophobicity/oleophilicity of the obtained sorbent was investigated and compared to a control sample of pine sawdust (PS). A contact angle measuring instrument (MobileDrop GH11, Krüss) was employed for this goal. Each contact angle assay was carried out by dropping a distilled water droplet onto the sorbent surface (previously pressed). Samples were tested at least 3 times and the average contact angle was calculated. In addition, both PSLG and PS samples were weighted to study their sorption capacity in water, oil and oil/water systems. Materials were immersed in a beaker containing 90 mL of water, diesel oil or sunflower oil at room temperature for 15 min or 24 h. When the selected contact time was up, materials were weighted again. Their sorption capacity was determined by the following equation:

$$S = \frac{m_f - m_i}{m_i}$$

Where S is the sorption capacity (g/g); m_f is the mass of sawdust saturated with liquid (g); and m_i is the initial mass of sawdust (g).

The oil sorption capacity in a mixed oil/water system was investigated at different diesel oil concentrations (3% - 17 %). For this experiment, 500 mg of sorbent were immersed in a beaker containing seawater and diesel oil for 15 min. Materials were weighed before and after the immersion. Then, a Soxhlet extraction with hexane was performed to study the diesel oil adsorbed by the materials. Also, the remaining liquid was mixed with 20 mL of hexane and put through a decanting funnel to separate the oil fraction. The obtained fractions were concentrated by rotary evaporation and Gas Chromatography (GC) was used to determine diesel oil content.

Results

The hydrophobicity/oleophilicity of the novel sorbent was analyzed using contact angle measurements. Surfaces with a water contact angle under 90° are considered hydrophilic while materials with contact angles greater than 90° are seen as hydrophobic [10]. Figure 1 shows water droplets being placed onto the surface of a control sample of pine sawdust (PS) and the modified sorbent (PSLG). As displayed in Figure 1A, the water droplet rapidly penetrates the surface of the raw material, preventing the measurement of the contact angle. This behavior indicates very poor hydrophobic attributes, which complicate its application as a sorbent in oil clean up. In contrast, Figure 1B shows a significant improvement in the hydrophobic properties of the treated sawdust (PSLG), presenting a water contact angle of 130.24° .

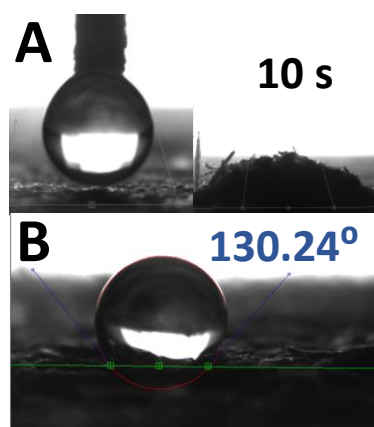


Figure 1. Water contact angle of (A) PS and (B) PSLG.

Acknowledgements

N. Miguez is funded by a Margarita Salas postdoctoral fellowship (CA1/RSUE/2021-00513) provided by the Spanish Ministry of Universities and Universidad Autónoma de Madrid (Spain).

References

- [1] S. Nurliyana Che Mohamed Hussein et al., *Materials Today: Proceedings*, 19 (2019) 1382-1389.
- [2] B. Singh et al., *Environmental Science: Water Research & Technology*, 6 (2020) 436-463.
- [3] N. Kumar et al., *Green Chemistry Letters and Reviews*, 14 (2021) 634-641.
- [4] A. Bayat et al., *Chemical Engineering & Technology*, 28 (2005) 1525-1528.
- [5] H.M. Choi et al., *Environmental Science & Technology*, 26 (1992) 772-776.
- [6] Y. Shin et al., *ACS Omega*, 4 (2019) 412-420.
- [7] M. Zamparas et al., *Molecules*, 25 (2020).
- [8] W.D.H. Schneider et al., *ACS Sustainable Chemistry & Engineering*, 7 (2019) 13418-13424.
- [9] M. Fernández-Fernández et al., *Journal of Wood Chemistry and Technology*, 35 (2014) 156-165.
- [10] T. Yu et al., *Chemical Engineering Journal*, 384 (2020) 123339.

Tables 1 and 2 show the water and oil sorption capacities of both the untreated sawdust (PS) and the modified material (PSLG). Table 1 corroborates the results obtained in the contact angle measurements, presenting the control sorbent as substantially hydrophilic. Moreover, the grafted material showed an almost insignificant water sorption capacity even after 24 h.

Table 1. Water sorption capacity at different times (g/g).

	Water sorption in 15 min (g/g)	Water sorption in 24 h (g/g)
PS	7.43 ± 0.49	6.69 ± 0.60
PSLG	0.16 ± 0.11	0.38 ± 0.12

Table 2 presents the oil sorption capacity of the materials tested (PS and PSLG) for two kinds of oil: diesel oil and sunflower oil. Both sorbents neglected to show significant differences between the investigated oils. The blank material (PS) displays good oil sorption capacity but it is considerably lower than its water sorption ability. This implies that in a mixed oil/water system, water sorption will be favored and, thus, the material will sink in the water column.

Contrastingly, PSLG showed a significantly higher oil sorption compared to water sorption, consequently enhancing the performance of the material in oil recovery.

Table 2. Oil sorption capacity after 15 min (g/g).

	Diesel oil sorption (g/g)	Sunflower oil sorption (g/g)
PS	2.59 ± 0.05	2.99 ± 0.09
PSLG	5.32 ± 1.54	5.03 ± 0.88

The Graphical Abstract shows a simulation of oil recovery from a contaminated water vessel. As it can be observed, the prepared material is capable of selectively adsorbing oil as well as staying afloat for a posterior recovery.

Conclusions

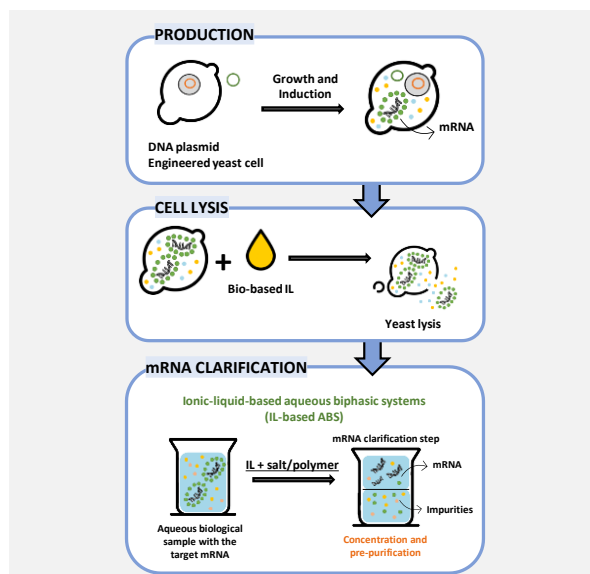
In conclusion, laccase mediated grafting can be used to confer hydrophobic properties to lignocellulosic materials such as pine sawdust. Moreover, this study presents a novel sorbent with adequate selectivity towards oil and good oil sorption capacity that can be obtained through a low cost and eco-friendly approach.

Development of an integrated process for the recovery and purification of recombinant messenger RNA vaccines resorting to bio-based ionic liquids

A.S.C. Marques^{1*}, A.Q. Pedro¹, C. Gonçalves², A.P.M. Tavares¹, C. Pichon², M.G. Freire¹

¹CICECO – Aveiro Institute of Materials, Department of Chemistry, University of Aveiro, Portugal; ²Centre de Biophysique Moléculaire, CNRS, Orléans, France.

*anascm10@ua.pt



Messenger RNA (mRNA) based-vaccines played a key role in fighting the COVID-19 pandemic, representing a promising alternative to conventional vaccines. However, its widespread use is still challenged by the lack of efficient large-scale manufacturing technologies. It becomes thus imperative the development of scaled-up technologies, guaranteeing simultaneously mRNA with high integrity, purity, and biological activity. Therefore, this work aims the development of a cost-effective and integrated extraction-purification of mRNA bioproduced from yeasts resorting to bio-based ionic liquids (ILs). IL-mediated lysis allowed the recovery of intracellular recombinant mRNA, being then clarified using aqueous biphasic systems, formed by the addition of an inorganic salt. Overall, this robust and self-sufficient mRNA downstream process will contribute to reduce the costs of these vaccines, being essential to support the ever-growing market demands while helping to meet future societal challenges.

Introduction

Messenger RNA (mRNA) based-vaccines represented a giant step in the fight against COVID-19 pandemic and provided a solution to this global crisis. Compared to traditional vaccines (e.g., subunit, live attenuated, and DNA-based), mRNA presents improved safety and efficacy profiles, respectively, due to their non-infectious and non-integrating nature that eliminates the risk of infection, as well as due to the possibility of being modified for improved stability and translatability [1]. Typically, mRNA production is achieved by *in vitro* transcription (IVT). However, the generation of mRNA by IVT at large scale and under current good manufacturing practice (cGMP) conditions remains challenging [2]. It relies on a complex supply chain and the availability of large amounts of these materials is limited and purchasing costs are high [2]. Moreover, the complex and multi-step mRNA purification process encompassing deoxyribonuclease digestion, precipitation, chromatography and tangential flow filtration steps contributes to increase the cost of mRNA products [2,3]. For this reason and considering the relevant market size of mRNA (USD 39.90 billion in 2021) [3], a robust and self-sufficient production process for mRNA, that comes along with a simplified manufacturing process and reduced cost of goods is essential to support future market demands [2]. As eukaryotic organisms and generally recognized as Safe (GRAS) for humans, yeasts are promising alternatives as recombinant microfactories for mRNAs, being currently under investigation for this purpose [4]. However, as mRNA is produced intracellularly, it is necessary to develop an integrated extraction-purification process. Ionic liquids (ILs) are molten salts comprising organic ions and well-known as designer solvents, allowing to cover a wide hydrophilicity-hydrophobicity range. These compounds have been widely used as a tool to concentrate, stabilize, extract, and purify biopharmaceuticals [6-9].

Therefore, this work aims the development of a cost-effective and integrated extraction-purification of mRNA bioproduced from yeasts resorting to bio-based ILs.

Methods

For this purpose, new bio-based ILs were identified, synthesized and characterized (chemical structure by NMR spectroscopy and water content by Karl Fischer titration) [6]. The mRNA of interest was biosynthesized resorting to a modified yeast strain, which was cultivated according to a previously optimized protocol [4]. Yeast cells were recovered by centrifugation and incubated with specific concentrations of ILs, after which the released intracellular mRNA was precipitated and recovered. The integrity of the extracted mRNA was evaluated using agarose gel electrophoresis, the concentration using UV spectroscopy and the identity using *in vitro* translation. In addition, the effect of ILs on mRNA stability was also investigated. The mRNA samples were dissolved in aqueous solutions of the different ILs. The mixtures were incubated for different periods, 1, 15 and 22 days at 25 °C and at 4 °C. After the incubation, mRNA was precipitated, recovered and its integrity evaluated using agarose gel electrophoresis.

Results

Results revealed that some ILs were able to promote yeast cell lysis and mRNA extraction from specific intracellular compartments and simultaneously maintain the mRNA stability. Ongoing work focus the optimization of IL-mediated yeast lysis envisaging to increase the yields of extracted mRNA. Parameters such as the amount of biomass, temperature, IL concentration, agitation, will be optimized. After lysis, the ability of these ILs to create an ABS with distinct salts and biocompatible polymers will be investigated, envisaging to concentrate the target mRNA and remove main impurities,

allowing to combine lysis and mRNA clarification in a single step.

Conclusions

Overall, this study highlights the potential of bio-based ILs as an effective method for lysing yeast cells and extracting mRNA, however, the process needs to be optimized. The successful

development of this work will advance the current state of the art of mRNA manufacturing and will allow a cost reduction of mRNA biopharmaceuticals, contributing to a wide access of the general society to this cutting-edge and fast-growing class of biopharmaceuticals. Thus, it will have high impact on the economy as well as on human well-being and health and therefore will help meet future societal challenges.

Acknowledgements

This work was developed within the scope of the project CICECO-Aveiro Institute of Materials, UIDB/50011/2020, UIDP/50011/2020 & LA/P/0006/2020, financed by national funds through the FCT/MCTES (PIDDAC). This work was additionally funded by the EIC-Pathfinder YSCRIPT project with reference 101047214, supported by the budgets of the Horizon Europe Program. Augusto Q. Pedro and Ana P. M. Tavares acknowledge FCT, respectively, for the research contracts CEECIND/2020/02599 and CEECIND/2020/01867.

References

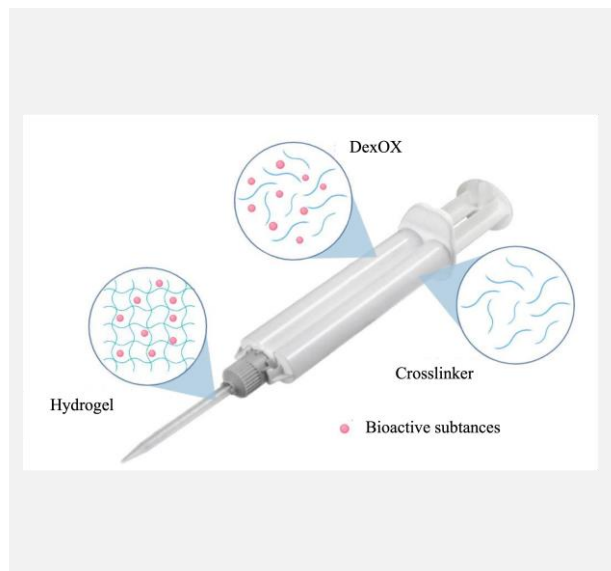
- [1] C. Zhang et al., *Frontiers in Immunology*, 10 (2019) 594.
- [2] S.S. Rosa et al., *Vaccine*, 39 (2021) 2190-2200.
- [3] Grand view research, "mRNA Therapeutics Market Size, Share & Trends Analysis Report by Application (Infectious Diseases, Oncology), By Type (Prophylactic Vaccines, Therapeutic Drugs), By End-use, By Region, And Segment Forecasts, 2022 - 2030." [Online]. Available: <https://www.grandviewresearch.com/industry-analysis/mrnatherapeutics-market-report>.
- [4] "Yscript - Yeast cell factory for mRNA bioproduction." [Online]. Available: <https://www.yscript.eu/>. [Accessed: 31- Mar-2023].
- [5] S.P.M. Ventura et al., *Chemical Reviews*, 117 (2017) 6984-7052.
- [6] S. De Santis et al., *Physical Chemistry*, 17 (2015) 20687-20698.
- [7] A.Q. Pedro et al., *ACS Sustainable Chemistry & Engineering*, 6 (2018) 16645-16656.

Dextran-based hydrogel composites for tissue engineering

P. Alves¹, A.F. Simões¹, M.F.P. Graça², I.J. Correia^{1,2}, P. Ferreira^{1,3}*

¹University of Coimbra, CIEPQPF – Chemical Engineering Process and Forest Products Research Center, Rua Sílvia Lima Polo II 3030-790, Coimbra, Portugal; ²CICS-UBI, Health Sciences Research Center, University of Beira Interior, P-6200 506 Covilhã, Portugal; ³Department of Chemical and Biological Engineering, Coimbra Institute of Engineering, Rua Pedro Nunes 3030-199, Coimbra, Portugal.

*paves@eq.uc.pt



Bone infections caused by diseases or injuries are a major health issue. In addition, the conventional therapeutic approaches used to treat bone present several drawbacks. Therefore, the focus of this work was the development of scaffolds for bone regeneration, which could be applied in the form of injectable hydrogels, that circumvent the use of invasive procedures, despite allowing the bone regeneration.

Throughout this work, injectable hydrogels were developed based on a natural polymer, dextran, along with the use of two inorganic compounds, calcium β -triphosphate and nanohydroxyapatite, that were aimed to reinforce the mechanical properties of the 3D mesh. The materials were chemically characterized and considering the requirements for the intended application, the swelling capacity, degradation in a simulated physiological environment as well as compression tests were performed. Furthermore, Vancomycin was also incorporated into the polymeric matrices to assist in the regeneration process, and the scaffolds drug release profile was assessed. The cytotoxic profile of the hydrogels was assessed by performing an MTS assay, using osteoblasts as model cells.

Introduction

The development of injectable scaffolds, which allow the incorporation of active substances, becomes promising, constituting an alternative to implants and grafts, managing to overcome the problems of lack of bone donors, rejection of prostheses and their associated effects. It also avoids the need to resort to invasive procedures and consequently brings advantages in the decreased recovery period and surgical risks and even in improved aesthetic results for the patient. In addition, it is also a versatile alternative, as it adapts to the lesion, being able to assume the morphology of the defect, however irregular it may be. It also allows an easy incorporation of active substances during its preparation and reduces the risk of infections [1]. The present work aims at the production of injectable hydrogels based on dextran for bone regeneration. These hydrogels are intended to fill defects in bone tissue to promote its regeneration. Dextran, a polysaccharide and therefore a natural polymer, provides some inherent advantages, namely its biodegradability and biocompatibility.

Synthesis of oxidized dextran (DexOx)

The procedure used to obtain oxidized dextran (dexOx) was based on previous works [2] according to the scheme in Figure 1.

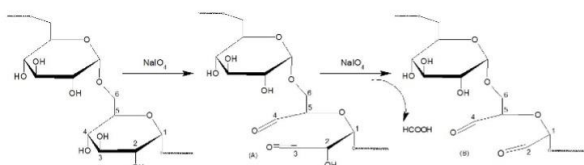


Figure 1. Representative scheme of the oxidation of Dex through reaction with sodium periodate. (A) First oxidation, introduction of aldehyde groups at C3 and C4. (B) Second oxidation, introduction of the aldehyde group at C2 and release of formic acid.

Synthesis of DexOx/ADD scaffolds

After the introduction of the aldehyde groups into the dextran structure (DexOx), it can be crosslinked with AAD. Chemical crosslinking occurs due to the formation of a Schiff base, [2,3] through the reaction of the aldehyde groups with the hydrazide groups of AAD, thus forming hydrazone bonds, as seen in Figure 2.

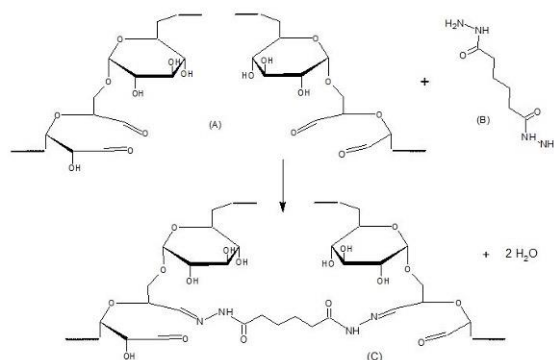


Figure 2. DexOx crosslinking with AAD. (A) DexOx. (B) AAD. (C) Crosslinked DexOx, hydrazone bond formation.

In addition, 1% (w/v) inorganics compounds (β -TCP and nHAp), were also mixed in the DexOx solution. Table 1 summarizes the compositions of the hydrogels that were prepared, varying the amount of crosslinker and the presence of inorganics, in order to assess their influence in the final properties of the prepared materials.

Table 1. DexOx e AAD hydrogels' composition.

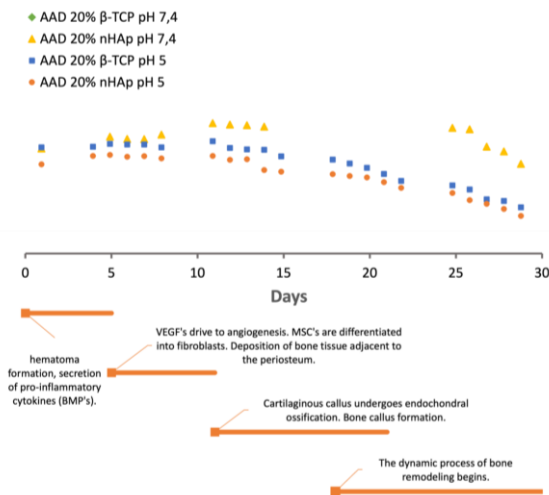
Compounds	H1	H2	H3	H4	H5	H6
Dex % (m/v)	20	20	20	20	20	20
AAD (%)	10	20	10	10	20	20
β -TCP % (m/v)	-	-	1	1	-	-
nHAp % (m/v)	-	-	-	-	1	1

Drug incorporation

A 5% (w/v) vancomycin aqueous solution was added to the AAD solution which was then added to the DexOx solution according to the compositions in Table 1.

Results

ATR-FTIR and ^1H NMR analysis allowed not only to chemically characterize the samples through the identification of characteristic bonds, but also to verify whether the oxidation and cross-linking processes were successful. Figure 3 shows the degradation profiles obtained at pH 7.4 and 5 in parallel with the timeline of the bone healing/regeneration process. The samples chosen for this analysis were the samples with 20% AAD and with the presence of inorganic compounds since they present the best results.

**Figure 3.** Timeline of the bone healing/regeneration process.

Hydrogels presented Young's modulus values between 200 and 300 kPa. Analyzing the differences between the various compositions, it is possible to verify that by increasing the crosslinking percentage, the samples become more resistant, which is translated into a higher Young's modulus.

Controlled release of vancomycin was carried out for the different compositions of the hydrogels and the cumulative release profiles obtained are shown in Figure 4.

The cytocompatibility of the different hydrogels was evaluated using hOB cells (as cell model), through MTS assay. As can be seen in Figure 5, after 1 and 3 days of incubation with the samples, the cells presented cell viabilities superior to 70%, demonstrating that the cells remain viable.

Acknowledgements

This research was funded by Strategic Research Center (CIEPQPF) Project UIDB/00102/2020 supported by FCT - Fundação para a Ciência e a Tecnologia I.P. And by national funds from FCT - Fundação para a Ciência e a Tecnologia, I.P., within the project 2022.02495.PTDC.

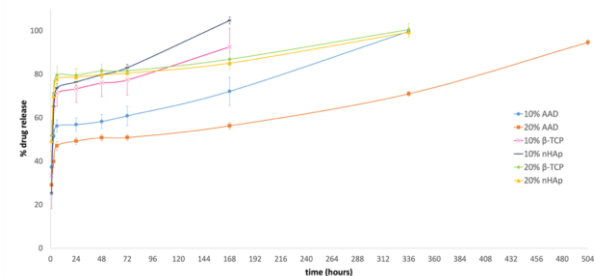
References

- [1] B. Chang et al., *Materials Science and Engineering: R: Reports*, 111 (2017) 1-26.
- [2] J. Maia et al., *Polymer*, 46 (2005) 9604-9614.
- [3] A. Lisman et al., *Journal of Biomaterials Applications*, 28 (2014) 1386-1396.
- [4] S.J. Kim et al., *Journal of Applied Polymer Science*, 92 (2004) 1731-1736.

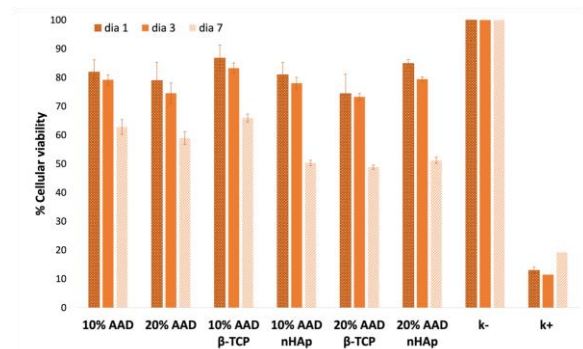
Table 2. Young's modulus and maximum compressive stress results obtained for each hydrogel.

	Young's Modulus (kPa)	Maximum compressive stress*
H1	206 ± 33	121 ± 24
H2	250 ± 39	73 ± 2
H3	240 ± 24	120 ± 28
H4	243 ± 18	57 ± 4
H5	283 ± 77	73 ± 2
H6	277 ± 40	61 ± 12

* Maximum compressive stress reached before failure.

**Figure 4.** Cumulative controlled vancomycin release profiles for the different hydrogel compositions.

However, the results of the day 7 showed a decrease of the viabilities to lower than 70%, which was not intended. These results may be related to the presence of AAD and agree with some works of the literature [4,5].

**Figure 5.** Cell viability of osteoblasts after 1, 3 and 7 days of contact with the hydrogels.

Conclusions

In general, the hydrogels presented a suitable degradability, about one month, which are in line with the average time of the bone regeneration process. The compression tests gave favorable values for Young's modulus (200-300 kPa). The drug release profile showed an initial burst release of around 50-80%, which makes longstanding treatment difficult, but it can facilitate the prevention of infections in the initial period. Regarding the material's biocompatible, the results obtained showed some cytotoxicity which could be associated with AAD.

Valorization of brewery spent grain to produce volatile fatty acids through acidogenic fermentation

L. Ferreiro*, M.C. Veiga, C. Kennes

Chemical Engineering Laboratory, Faculty of Science and Interdisciplinary Centre of Chemistry and Biology (CICA), University of A Coruña, Rua da Fraga 10, E-15008, A Coruña, Spain.

*laura.ferreiro.santos@udc.es



This work explores the production of volatile fatty acids through the anaerobic digestion of brewery spent grain. The first part of the experiment consists in carrying out a pre-treatment of acid hydrolysis (3% H₂SO₄, 121°C, 20 min) to promote the digestion.

Finally, the performance of a continuous reactor was demonstrated at laboratory scale using the pre-treatment product as a substrate. In this, the effect of the different hydraulic retention times (15 to 3 days), the effect of the presence of solid retention times and variations in the organic loading rate (1 to 6 g COD L⁻¹ d⁻¹) were studied. The maximum degree of acidification of the reactor at scale was 73% at 37°C with a hydraulic retention time of 15 days at pH of 5-5.10.

Introduction

Each year, over 3.4 million tonnes of brewery spent grain (BSG) are produced in the European Union [1]. Bagasse constitutes 85% of the total waste produced in the brewing industry [2], which is composed of 70% in fibers, such as cellulose, hemicellulose and lignin, 30% in proteins and some minerals and lipids [3].

One of the methods used for the valorization and use of waste is anaerobic digestion (AD). Methane was considered the final product of AD but in recent years volatile fatty acids (VFA) have gained increased attention. VFA are acids made up of five or fewer carbon atoms (acetic acid, propionic acid, butyric acid and valeric acid) [4].

The complex structure of the brewery spent grain hinders the hydrolysis step in anaerobic digestion, in addition the high lignin content prevents the formation of VFA due to it acts as an inhibitor of acidogenic microorganisms responsible to produce VFA.

The acid hydrolysis pre-treatment allows the extraction of sugars, proteins and other nutrients contained in the BSG to a liquid medium easily assimilated by microorganisms, while lignin and indigestible fibers precipitate in the mixture, so they are easy to separate. The pre-treatment consists of two stages of acid hydrolysis with 3% sulfuric acid for 20 min at 121°C, with a centrifugation and filtration steps to separate both phases.

The product resulting from the BSG pre-treatment is liquid rich in simple sugars (glucose, fructose, xylose, cellobiose and arabinose), proteins and other nutrients favourable to produce VFA through anaerobic digestion (Table 1).

Table 1. Composition of the pre-treatment of brewery spent grain

COD (mg COD/L)	Sugar content (mg COD/L)	Protein content (mg/L)	Ammonium content (mg/L)	Phosphate content (mg/L)
19660,57	17499,97	702,90	112,46	68,78

Materials and Methods

A continuous stirred tank reactor of 2L was inoculated using an inoculum from a brewery located in A Coruña, which was previously heat treated (3h at 100°C) to inhibit the activity of methanogenic microorganisms. The substrate used was the product of the acid hydrolysis pre-treatment of BSG. The reactor temperature was kept constant at 37°C with a stirring of 100 rpm and a pH at 5.00-5.10. During this experiment we studied the influence of the different hydraulic retention times (HTR), the effect on the variation of the organic loading rate (OLR) and the influence of the solids retention time (SRT). The operational scheme of the reactor is shown in Figure 1

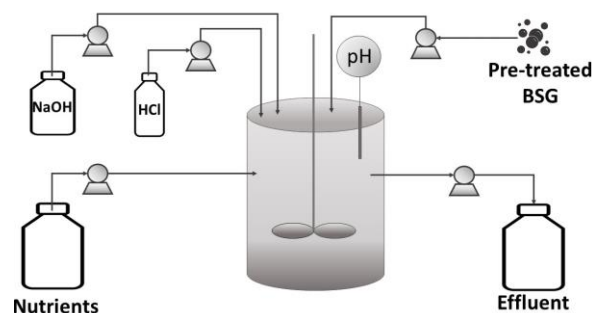


Figure 1. Diagram of the operation of the reactor.

Results and Conclusions

The degree of acidification (DA) of the reactor has been maintained under all conditions between 59 and 73%. The highest degree of acidification was obtained with an HRT of 15 days, an OLR of 1.2 g COD L⁻¹ d⁻¹, but without the presence of SRT, which prevented its long-term operation due to loss of biomass. Therefore, the presence of SRT was a key factor for the development of the experiment. The second highest degree of acidification obtained was 71%, for SRT values of 31 days, HRT of 3 days and with an OLR of 6 g COD L⁻¹ d⁻¹. The profile of VFA was dominated by acetic, propionic and butyric acids in all conditions. The different

operational parameters along with their influence are shown in Table 2.

Table 2. Reactor operating conditions.

VCO (mg COD/L d)	HRT	SRT	AGV (mg COD/L)	DA%	SV (g SV/L)
1259,50	15	-	19508,02	73	5,05
3053,33	6	17	11317,63	59	4,95
3053,33	6	41	12142,28	64	15,10
6011,25	3	31	13468,00	71	14,80

Acknowledgements

I thank my tutors Dra. Maria del Carmen Veiga Barbazán and Dr. Christian Kennes for the opportunity to carry out my doctoral thesis within the BIOENGIN research group, as well as being able to attend this congress as a form of learning and experience.

References

- [1] S. Sobek et al., Renewable Energy, 199 (2022) 157-168.
- [2] M. Hu et al., Energy Conversion and Management, 118 (2016) 118.
- [3] E.C. Guarda et al., Applied Science, 11 (2021) 3222.
- [4] R. Iglesias-Iglesias et al., Environmental Technology, 42 (2021) 3889-3899.

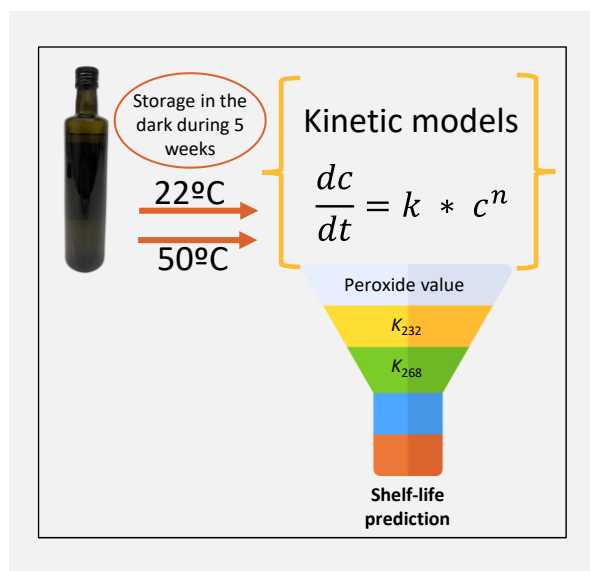
Predicting the shelf-life of extra virgin olive oil during storage at 22 and 50°C, using a kinetic modelling approach

N. Ferreiro^{1,2,3*}, J.A. Pereira^{1,2}, N. Rodrigues^{1,2}, A.M. Peres^{1,2}

¹Centro de Investigação de Montanha (CIMO), Instituto Politécnico de Bragança, Campus Sta Apolónia, Bragança, Portugal;

²Laboratório associado para a sustentabilidade e tecnologia em regiões de montanha (SusTEC), Campus Sta Apolónia, Bragança, Portugal; ³Universidad de León, Departamento de Ingeniería Agrária, Av. Portugal, nº41, León, 24071, Espanha.

*nuno.ferreiro@ipb.pt



Olive oil (OO) is a high-value food due to its appreciated sensory attributes and health benefits. The shelf life (SL) of an OO is a key parameter, being influenced by the olive cultivar, agro-climatic, extraction and storage conditions. So, kinetic models were developed for 3 physicochemical quality parameters (peroxide value and the extinction coefficients at 232 and 268 nm), to estimate the SL, based on a Time to Reach the legal Upper Limit (TRUL) approach. For that, a ripe EVOO, stored in amber glass bottles, in the dark and during 5 weeks, at 22 and 50°C, was used. Zero-, first-, and second-order kinetic models were evaluated, and the best correlations were achieved for the zero-order model. Based on this model, the SL of the stored EVOOs were predicted to be 47-210 days and 35-80 days at 22 and 50°C, respectively. As expected, the SL decreased for the higher storage temperature, being the lowest values predicted for K_{232} and K_{268} , data, for 22 and 50°C, respectively.

Introduction

Only extra virgin or virgin olive oils (EVOOs or VOOs), can be commercialized, being their classification dependent on the fulfillment of a set of legal thresholds [1]. EVOO is a key ingredient of the Mediterranean cuisine [2] and its intake was associated to several health benefits recognized by nutritional and health claims [3,4]. However, olive oil is prone to lipid oxidation due to its richness in unsaturated fatty acids, which is responsible for degrading the chemical and sensory quality of EVOO leading to the appearance of unpleasant off-flavors, obliging a quality grade re-classification to VOO or even lampante oil, which cannot be commercialized.

Thus, besides monitoring the oil quality through the extraction line, the olive oil industry is urged to guarantee the label information authenticity from packaging, during storage and transportation, until purchased by the end-consumer. Several strategies have been proposed aiming to establish accurate models for predicting the olive oil shelf-life (SL) [5], which can be defined as the time-period under normal storage conditions within which no off-flavors are developed and the quality parameters are within the legal limits [6]. Two types of shelf-life prediction models are available: kinetic and empirical [5,7-11].

In this study, classical kinetic models were applied aiming to describe in a straightforward way the complexity of the oxidation reactions and related oil quality degradation.

Materials and Methods

Ripe EVOO samples, from the crop year of 2022, were collected and further used. The oil was stored in amber glass bottles (100 mL) with a plastic cap. In total, 40 bottles were used, being 20 stored at 22°C and the other 20 bottles stored at 50°C, all of them protected from light exposure. Bottles were stored during 5 weeks, being 4 bottles picked from each storage condition, each week for analysis. Before storage, the quality parameters of the

olive oil (free acidity, peroxide value and extinction coefficients at 232 and 268 nm) were assessed, following the procedures described in the Commission Delegated Regulation (EU) 2022/2104, allowing confirming the EVOO classification (FA = 0.28%; PV = 5.8 mEqO₂/kg oil; K_{232} = 1.87, and K_{268} = 0.13). The total phenols content (TPC) and total carotenoids content (TCC) of the initial EVOO were also determined, by spectrophotometry, being equal to 245 ± 24 mg GAE/kg and 8.0 ± 0.2 mg/kg. At each sampling date (7, 14, 21, 28, and 35 days) the quality parameters of the stored oils were evaluated following the EU guidelines, being further used to establish the kinetic models, which were then applied to estimate the SL of the olive oils in terms of commercial grade.

The evolution of the PV, K_{232} and K_{268} data at each storage temperature studied (22 and 50°C), were used to calculate the thermal rate constants due to the oxidation process that took place during the storage time-period. Since the FA was almost constant along the storage time, this parameter was not considered, in terms of kinetic modelling. Three reaction orders were considered (zero-, first- and second-order kinetic models, Equation (1)), being selected the kinetic model that allowed the best mathematical fit of the experimental data:

$$\frac{dP}{dt} = k \times P^n \quad (\text{Eq. 1})$$

where, P refers to the parameter under study (PV, K_{232} , or K_{268}), t is the storage time-period (in days), and k is the rate constant and n is the reaction order (equal to 0, 1 or 2 for zero-, first- and second-order kinetic models, respectively).

Results and Discussion

The results showed that the zero-order kinetic model allowed the best fitting of the experimental data for the three quality parameters, which was slightly superior compared to the first- and second-order kinetic models. Table 1 shows the rate

constants ($k \pm$ standard error [SE]) and the correlation coefficients (R) obtained assuming the zero-order kinetic mechanism for the thermal degradation of the EVOO quality due to the natural oxidation process at 22 and 50°C, during the 5 weeks of storage.

Table 1. Rate constants ($k \pm$ standard error [SE]) and correlation coefficient (R) for olive oils stored during 5 weeks at 22 or 50°C, obtained assuming a zero-order kinetic model.

Variable	22°C		50°C	
	$k \pm$ SE	R	$k \pm$ SE	R
PV	0.14±0.03*	0.928	0.18±0.04*	0.945
K_{232}	0.013±0.003*	0.935	0.011±0.003*	0.920
K_{268}	0.0004±0.0002*	0.866	0.0026±0.0002*	0.994

* k units for PV: $\text{mEq.O}_2 \times \text{kg}^{-1} \times \text{day}^{-1}$; k units for K_{232} and K_{268} : day^{-1}

Taking into account the maximum legal limits [1] for EVOO grade classification ($\text{PV} \leq 20$ $\text{mEq.O}_2/\text{kg}$ oil; $K_{232} \leq 2.50$, and $K_{268} \leq 0.22$) and using the zero-order kinetic models previously established, based on the experimental data collected during the 5 weeks of storage at 22 or 50°C, it was possible to estimate the SL (i.e., the Time required to Reach the Upper Legal Limit, TRUL) for the studied oil, considering the initial values determined for the oil before storage. Table 2 shows the SL determined according to each parameter and storage temperature, predicted using the zero-order fitting. The SL values were slightly greater than those reported by Gomez-Alonso et al. [12], based on the time to reach the upper limit of PV or of the extinction coefficients, for purified olive oil, stored at 25 and 50°C (48-104 days, and 5-24 days, respectively). However, the predicted SL were lower than those reported for monovarietal EVOO from cv. Cornicabra stored at 25°C (238-686 days) and of the same order of magnitude of those determined at 50°C (15-59 days) [13], which were estimated using zero- or first-order kinetic models developed for the same three quality parameters. On the other hand, for monovarietal EVOO from cv. Coratina, significantly greater SLs were

Acknowledgements

NF acknowledges his PhD scholarship (2022.10072.BD), from the Portuguese Foundation of Science and Technology (FCT). This study was supported by FCT under the scope of the strategic funding of CIMO (UIDB/00690/2020 and UIDP/00690/2020), and Associate Laboratory SusTEC (LA/P/0007/2020).

References

- [1] European Commission Regulation EC No 2568/91, Official Journal of the European Union, L248 (1991) 1-82.
- [2] V. Gkotsamanis et al., *Maturitas*, 159 (2022) 33-39.
- [3] European Commission Regulation (EU) No 432/2012, Official Journal of the European Union, L136 (2012) 1-40.
- [4] Regulation (EC) No 1924/2006 of the European Parliament and of the Council, Official Journal of the European Union, L404 (2006) 9-25.
- [5] X. Li et al., *Journal of Food Quality*, 2018 (2018) 1639260.
- [6] C. Guillaume et al., *Journal of Chemistry*, 2016 (2016) 6393962.
- [7] R. Aparicio-Ruiz et al., *Grasas y Aceites*, 68 (2017) e219.
- [8] M.G. Di Serio et al., *Journal of Food Processing Preservation*, 42 (2018) e13663.
- [9] L. Conte et al., *Foods*, 9 (2020) 295.
- [10] A. Serrano et al., *LWT*, 136 (2021) 110257.
- [11] V. Mancebo-Campos et al., *Antioxidants*, 11 (2022) 539.
- [12] S. Gomez-Alonso et al., *European Journal of Lipid Science and Technology*, 106 (2004) 369-375.
- [13] V. Mancebo-campos et al., *European Journal of Lipid Science and Technology*, 110 (2008) 969-976.

reported in the literature (377 and 61 months for 25 and 50°C, respectively) [9]. This variability may be tentatively attributed to the expected differences in the chemical composition of each olive oil, which greatly depend on the cultivar, agro-climatic conditions, olive maturation index at harvest, and extraction conditions.

Table 2. Shelf-life (SL, in days) calculated using the zero-order kinetic model.

Variable	Shelf-life (days)	
	22°C	50°C
PV	100	80
K_{232}	47	56
K_{268}	210	35

As can be inferred from Table 2, in general, the SL decreases when the storage temperature increases (with the exception of the results for K_{232}). Moreover, the correctness of the EVOO label for the studied olive oil, stored at 22°C, mimicking the usual temperature of oil's storage, could only be ensured for 47 days, which is a rather low SL, taking into account that olive oils are often stored for 10-12 months.

Conclusions

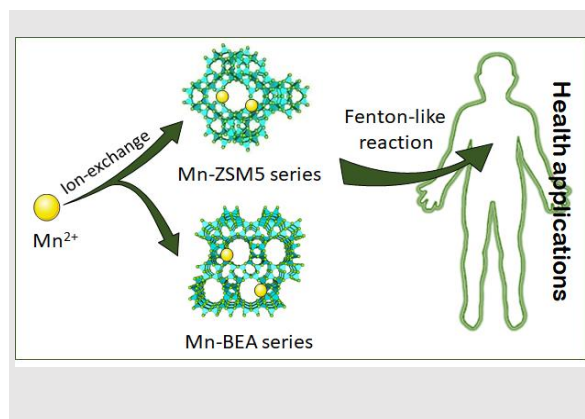
The study performed allowed confirming that zero-order kinetic models can be used to estimate the SL of olive oils, based on the TRUL of three quality parameters (PV, K_{232} , and K_{268}) used to establish the commercial grade of olive oil, in-line with the literature. Moreover, it also highlighted that, from the referred parameters, the extinction coefficients were those that would suffer a faster raise, being those that should be used to estimate the SL of olive oils. Finally, from our results and those previously reported, it is clear that the SL prediction is greatly dependent of the olive oil under study. Besides, the study also points out that the classical kinetic models alone can hardly describe the complexity of the oxidation reactions and related oil chemical-sensory degradation.

Metal-ion zeolites obtained by chemical and mechanochemical methods as Fenton-like catalysts for health applications

J.T. Costa¹, V. Ivasiv^{2,3,4}, A.R. Bertão^{2,3,4}, N. Nunes^{1,5}, A.S. Mestre^{5,6}, A.P. Carvalho^{5,6}, A.M. Fonseca^{2,9}, F. Baltazar³, J.N. Moreira^{7,8}, I.C. Neves^{2,9}, A. Martins^{1,5*}

¹DEQ, Instituto Superior de Engenharia de Lisboa, Lisboa, Portugal; ²CQUM-Centre of Chemistry, Department of Chemistry, Universidade do Minho, Braga, Portugal; ³Life and Health Sciences Research Institute (ICVS), School of Medicine, University of Minho, Braga, Portugal; ⁴ICVS/3B's - PT Government Associate Laboratory, Braga/Guimarães, Portugal; ⁵Centro de Química Estrutural, Faculdade de Ciências, Institute of Molecular Sciences, Universidade de Lisboa, Lisboa, Portugal; ⁶Departamento de Química e Bioquímica, Faculdade de Ciências Universidade de Lisboa, Lisboa, Portugal; ⁷CNC - Center for Neurosciences and Cell Biology (CIBB), University of Coimbra, Portugal; ⁸Univ Coimbra - University of Coimbra, CIBB, Faculty of Pharmacy, Portugal; ⁹CEB - Centre of Biological Engineering and LABBELS - Associate Laboratory, University of Minho, Portugal.

*amartins@deq.isel.ipl.pt



One of the critical steps for the development and health applications of inorganic nanoparticles is to exhibit high efficiency without inducing toxicity. In this work, metal-ion zeolites were developed to be used as Fenton-like catalysts for health applications. ZSM-5 and BEA zeolites were modified through chemical and mechanochemical methods to obtain nanomaterials with tuned particle size and texture. Characterization data showed that the modified materials kept the crystal structure although some textural modifications occurred. Upon Mn^{2+} loading, the catalytic behavior was evaluated by Fenton-like reaction using physiological and mild acidic conditions (37 °C, pH=7.4 and 6.4 and 50 μM H_2O_2), since these conditions are relevant to various pathological environments. MnBEA series showed the best results by Fenton-like reactions, revealing the great potential of metal-zeolite nanomaterials for health applications.

Introduction

Zeolites are inorganic materials with high thermal and mechanical stability, organized porosity, and intrinsic acidity [1]. These nanomaterials have been widely used as adsorbents and catalysts. In addition, they present a high stability in biological environments making them good candidates for medical and healthcare applications [2,3]. The development of these nanomaterials as heterogeneous catalysts for health applications is appealing, since some pathological conditions exhibit mild acidity and overproduction of hydrogen peroxide (H_2O_2), important characteristics for the Fenton reaction [4]. However, some limitations as the crystal size and acidity cause some constraints [5]. So, the design of zeolite nanomaterials through chemical methods, such as desilication, or mechanochemical is a possible strategy to produce nanomaterials with optimized properties to transport and react in biological medium, envisaging further application for biomedical purposes.

The aim of this work is to modify ZSM-5 and BEA zeolites by chemical and mechanochemical methods for optimize the catalytic behavior of Mn-ion zeolites by Fenton-like reactions through physiological and mild acidic experimental conditions for future medical applications.

Methods

Commercial powder zeolites, from Zeolyst International, ZSM5 (Si/Al=15) and BEA (Si/Al=12.5) were submitted two types of treatments: i) chemical, and ii) mechanochemical using a ball mill. The chemical modification consisted in an alkaline treatment with NaOH (0.6 or 0.1 M for ZSM5 and BEA, respectively), at 65 °C for 30 min, followed by an acid treatment with HCl (0.1 M) at 70 °C for 3 h. The solids were recovered by centrifugation, dried, and calcined at 550 °C overnight under air flow. The samples were named ZEO_[NaOH]D for the alkaline treated samples, followed by "AT" for acid treated materials The

mechanochemical procedure was made in a shaker mill (VWR Star-Beater). The materials were ~~and~~ milled for the required time and frequency using five 3 mm steel balls. The samples were labeled as ZEO_ F_t , where F is the frequency (Hz) and t is the milling time (min). Structural characterization of the pristine and modified zeolites was made through the X-ray diffraction patterns obtained in 2θ range between 5 and 40° in a Pan'Analytical PW3050/60X'Pert PRO. Textural analysis was achieved by low temperature N_2 adsorption isotherms (Micromeritics ASAP 2010) obtained after a previous treatment at 300 °C for 3h under vacuum. Particle size distribution was evaluated by light scattering experiments (Malvern, Master3000) and TEM microscopy using JEOL JEM-2100-HT (Cryo & Tomography) working with an accelerating voltage of 200 kV. To conduct the TEM analysis, a drop of an aqueous dispersion of the sample was placed onto a 400-mesh copper grid coated with carbon film. The grid was then dried under vacuum before being viewed under the microscope. The metal ion (Mn^{2+}) was introduced on the zeolite nanomaterials by ion exchange method (1 mM of Mn^{2+}) using a procedure describe in [2]. The metal ion zeolite catalysts were evaluated using methylene blue (MB) as model molecule by Fenton-like reaction in a semi-batch reactor at atmospheric pressure under stirring using physiological and mild acidic conditions: $T = 37$ °C, $pH = 7.4$ and 6.4 , $[H_2O_2] = 50$ μM , $t_r = 90$ min. The reactor was loaded with methylene blue solution (5 ppm) and the catalyst dose was 400 mg L^{-1} .

Results

The Mn-ion zeolites nanomaterials were prepared with ZSM5 and BEA as pristine zeolites, and with the modified zeolite nanomaterials by chemical and mechanochemical treatments. The average size of particles and morphologies of pristine zeolites were analyzed by TEM, as shown in the Figure 1.

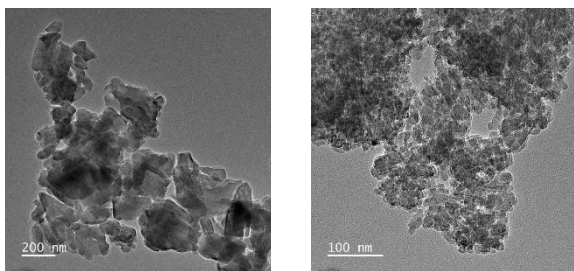


Figure 1. TEM images of pristine zeolites: ZSM5 (left) and BEA (right).

The two different commercial zeolites, ZSM5 and BEA display different average particle sizes. ZSM5 zeolite exhibits irregular particles, with large aggregates, medium and small particles (308, 115 and 30 nm, respectively), and BEA show small particles with an average size of 20 nm, which form large aggregates.

The crystallinity and textural parameters of the pristine and chemically modified materials are presented in Table 1 revealing that the crystal structures of the zeolites were kept but some loss of crystallinity occurs, especially in the case of BEA series. The textural parameters show the development of microporosity, especially in the case of ZSM5 series.

All these samples were submitted to ion exchange procedure with the same concentration of Mn^{2+} for obtain Mn-ion zeolite catalysts. Figure 2 shows the results obtained with these catalysts for the Fenton-like reaction using MB as probe molecule. The data show that the MB was degraded under physiological and mild acidic conditions in the presence of Mn-ion zeolite catalysts. The degradation of the MB molecule by Fenton-like reaction at $pH = 7.4$ was achieved (data not shown) and the best catalytic results were obtained with the Mn-ion BEA series. However, as expected, the degradation was enhanced in the $pH = 6.4$ with $[H_2O_2] = 50 \mu M$ at $37^\circ C$. It must be noted that there is a significant difference between the MnZSM5 and the MnBEA series, as all the catalysts prepared with BEA series samples are more efficient in degrading the MB molecule. In fact, both MnBEA_0.1D and MnBEA_0.1D/AT are very active under mild acidic conditions ($pH = 6.4$ and $H_2O_2 = [50 \mu M]$). In fact, with these samples total MB degradation was achieved while in the case of ZSM5 derived catalysts the maximum degradation attained was only 60%.

Acknowledgements

V.I. and A.R.B. thank for the PhD grants, UI/BD/152219/2021 and SFRH/BD/141058/ 2018, respectively. ASM thanks FCT for the Assistant Researcher contract CEECIND/01371/2017 (Embrace Project). This work was supported by FCT (Foundation for Science and Technology, Portugal) by the projects: UIDB/00100/2020, UIDP/00100/2020 and LA/P/0056/2020, CQ/UM (UID/QUI/0686/2020), CEB (UIDB/04469/2020) and LABELS (LA/P/0029/2020), and Instituto Politécnico de Lisboa (IPL) through Project IPL/2022/ZeoMed ISEL.

References

- [1] F.R. Ribeiro, M. Guisnet, Les zeolites: un nanomonde au service de la catalyse. EDP Science, Les Ullis, 2006.
- [2] L. Ferreira et al., Colloids and Surfaces B: Biointerfaces, 142 (2016) 141-147.
- [3] N. Vilaça et al., Materials Science and Engineering: C, 120 (2021) 111721.
- [4] Z. Tang et al., Chemical Reviews, 121 (2021) 1981-2019.
- [5] A. Carvalho et al., Hierarchical Zeolites: Preparation, Properties and Catalytic Applications, Nova Science Publishers, New York, 2015.

Table 1. Crystallinity and textural parameters of starting and chemically modified samples.

Sample	C_{XRD}^a (%)	V_{micro}^b ($cm^3 g^{-1}$)	V_{meso}^c ($cm^3 g^{-1}$)	A_{ext}^b ($cm^2 g^{-1}$)
ZSM5	100	0.15	0.07	43
ZSM5_06D	65	0.12	0.29	78
ZSM5_06D/AT	64	0.11	0.20	106
BEA	100	0.14	0.53	250
BEA_01D	53	0.08	0.52	203
BEA_01D/AT	47	0.08	0.56	205

^aCrystallinity percentage using parent zeolites as reference material; ^b V_{micro} and A_{ext} quantified through the application of $f \alpha_s$ method; ^c $V_{meso} = V_{total} - V_{micro}$ where V_{total} corresponds to the amount of N_2 adsorbed a $p/p^0 \approx 0.95$

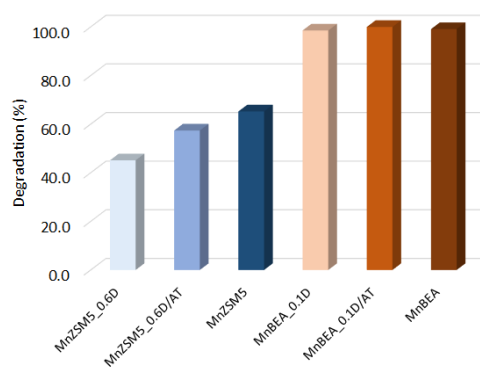


Figure 2. Degradation efficiency of the Mn-ion catalysts prepared with the pristine zeolites and the modified nanomaterials by chemical methods. Conditions of reaction: 25 mL buffer solution $pH = 6.4$ MB (5 ppm); 10 mg catalyst; $H_2O_2 = [50 \mu M]$, $t = 90$ min and $T = 37^\circ C$.

The control with the pristine zeolites and in the presence of the physiological and mild acidic conditions are not enough to trigger the reaction, which confirm that the reaction occurs by a typical Fenton process.

The study will continue testing the catalysts prepared with mechanochemically modified samples that preserved more than 80 % of the crystallinity of the starting sample.

Conclusions

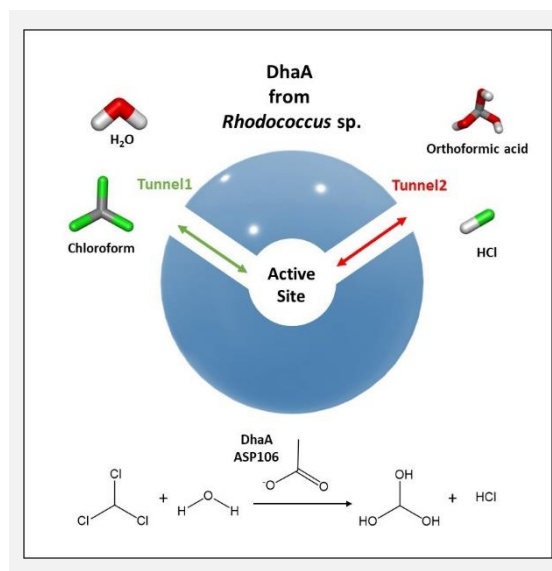
Chemical and mechanochemical methods were utilized to obtain several Mn-zeolite nanomaterials, which were tested for their ability to degrade MB using the Fenton-like reaction at mild acidic and physiological conditions. All the Mn-zeolite nanomaterials displayed catalytic activity under these experimental conditions, indicating their potential as Fenton-like catalysts for health applications

Computer-aided identification of trihalomethane degradation by haloalkane dehalogenase DhaA from *Rhodococcus* sp.

M.M. Pereira*, R.C. Martins

University of Coimbra, CIEPQPF – Chemical Engineering Processes and Forest Products Research Center, Department of Chemical Engineering, Faculty of Sciences and Technology, Rua Silvio Lima, Polo II, 3030-790 Coimbra, Portugal.

*matheus@eq.uc.pt



The work aims to investigate the potential of DhaA from *Rhodococcus* sp. as biocatalyst for trihalomethanes (THMs) removal from drinking water. For this, a computational protocol for enzymatic tunnel/access prediction and molecular docking analysis of substrates/products was carried out. The three-dimensional structure of DhaA was analyzed using CaverWeb 1.0 to identify the most promising tunnels for ligand transport. The identified tunnels were analyzed and the ligand transport capacity using ligand energy analysis of substrates/products was evaluated. The binding energies of each ligand (water, chloroform, dichloromethane, chloromethanediol, hydrochloric acid, and orthoformic acid) were calculated based on the sequence of complete dehalogenation with DhaA as a biocatalyst. According to the binding energies profiles, Tunnel 1 exhibited the highest ligand transport capacity. The higher bottleneck radius allows a lower energy barrier, promoting an efficient substrate and product transport. Overall, the obtained results demonstrate that DhaA from *Rhodococcus* sp. as a promising and sustainable biocatalyst for chloroform full dehalogenation, contributing to the development of novel approaches for THMs removal from drinking water.

Introduction

During the last century, progress on safe drinking water distribution were remarkable and chlorine-based disinfection played a crucial role on this achievement [1]. However, the reactive disinfectant (chlorine) in contact with natural organic matters (NOM) produces a hazardous class of pollutants, disinfection by-products (DBPs) [2]. Trihalomethanes (THM) is the most identified class of DBP in water treated with chlorine, been firstly detected in drinking water in middle 70 of last century [2]. Despite the benefits of chlorine disinfection (effective elimination of pathogens and low operational costs), the presence of THMs in drinking water has raised significant environmental and health concerns. Several processes have been applied for the removal of THMs from water, including physical-chemical and biological-based techniques [3]. Among these methods, bioremediation represents a sustainable and effective approach for the removal of THMs after they are formed. *Rhodococcus* sp. is a genus of actinomycetes (gram-positive bacteria) that display the ability to treat effluents contaminated by THMs with high efficiency while performing more eco-friendly operations (with reduced production of residues and by-products) [4]. The *Rhodococcus* sp. mechanism of THMs removal is promoted by Haloalkane dehalogenase DhaA, which is a highly active enzyme for halogenated substrates in bacterial metabolic pathways [5]. Therefore, *Rhodococcus* sp. can be a viable and sustainable source of biocatalysts that allow the removal of THMs from drinking water. Thus, this study aim identifies the potential of DhaA from *Rhodococcus* sp. as biocatalyst for THMs removal from drinking water. For this, a computational protocol using enzymatic tunnel/access prediction and molecular docking analysis of substrate/products was applied.

Methods

The three-dimensional structure of DhaA from *Rhodococcus* sp. was obtained from the Protein Data Bank (PDB: 1bn6) and uploaded to the CaverWeb 1.0 web server [6] for the identification of tunnels. The tunnels were identified using the

default configuration, and then filtered based on their bottleneck radius (Å) and length (Å). The most promising tunnels were selected for ligand transport analysis. The binding energies of each ligand (water, chloroform, dichloromethane, chloromethanediol, hydrochloric acid and orthoformic acid) were calculated using the reaction sequence of a complete dehalogenation using DhaA as biocatalyst (THM and subproducts) (Figure 1).

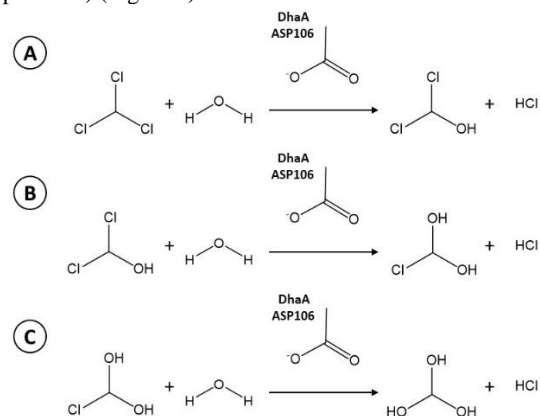


Figure 1. Chloroform catalytic dehalogenation using DhaA from *Rhodococcus* sp. as biocatalyst.

Results

The identification of enzymatic tunnels in the DhaA structure was carried out, aimed at determining the efficiency of enzymatic dehalogenation of chloroform. DhaA presented four possible tunnels that extend from the enzyme surface to the catalytic site (ASP106, GLU130 and HIS272). However, two of these tunnels displayed unfavorable characteristics for substrate and product transportation (e.g., long length that hindered substance transport). The most favorable tunnels for ligand transport are described in Figure 2. The identified tunnels display similar lengths ($\approx 13\text{Å}$). However, tunnel 1 exhibited the highest substance transport capacity due to higher bottleneck

radius (1.8Å). In fact, tunnels in different DhaAs were previously studied using molecular dynamics simulations [5]. According to the authors, DhaAs have two predominant tunnels: the main tunnel, responsible for substance entry and exit, and the slot tunnel, which supports product release in the reaction.

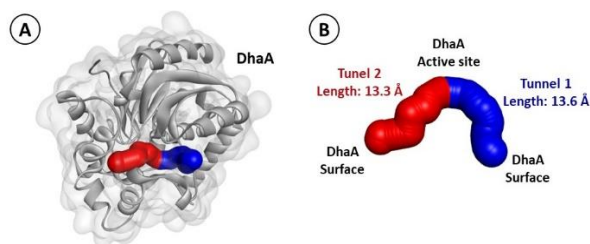


Figure 2. Tunnels in the crystal structure of DhaA: (A) Overall structure of DhaA with two predominant tunnels, (B) DhaA main tunnel (blue) and slot tunnel (red).

The dehalogenation reaction occurs through the nucleophilic attack of ASP106 on chloroform in the presence of water. Therefore, the identification of the binding energies chloroform and water through Tunnels 1 and 2 was performed. Figure 3 depicts the trajectory of chloroform and water from the DhaA surface to the active site. The transport of chloroform and water was accomplished with lower energetic barriers through Tunnel 1.

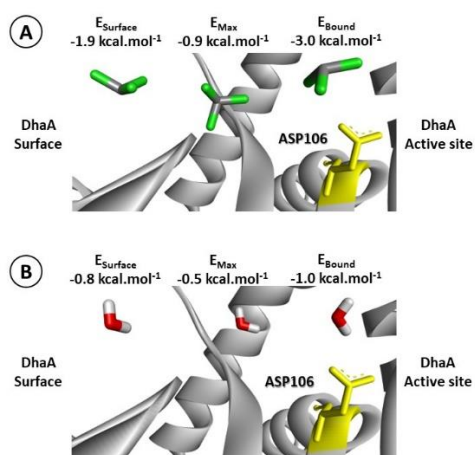


Figure 3. Ligand trajectory from DhaA surface into the active site using tunnel 1: (A) Chloroform and (B) Water.

In the second reaction step, the product formed (dichloromethanol) is hydrolyzed, and chloromethanediol is formed. Thus, a binding energy analysis was performed for these two compounds only at the active site, as the reaction occurs in a sequence and the products are not released until full dehalogenation is achieved. Based on the results, the binding energy of the substrates studied on the active site of DhaA

Acknowledgements

The work was developed within the scope of the project H2OforAll financed by the European Union, under the Grant Agreement GA101081953. The authors acknowledge the funding for CIEPQPF supported by the FCT through the projects UIDB/EQU/00102/2020 and UIDP/EQU/00102/2020.

References

- [1] X. Li et al., *Environmental Science & Technology*, 52 (2018) 1681-1689.
- [2] T. Bellar et al., *Journal AWWA*, 66 (1974) 703-706.
- [3] R. Sinha et al., *Journal of Environmental Chemical Engineering*, 9 (2021) 106511-106536.
- [4] D. Frascari et al., *Applied Microbiology and Biotechnology*, 73 (2006) 421-428.
- [5] M. Klvana et al., *Journal of Molecular Biology*, 392 (2009) 1339-1356.
- [6] J. Stourac et al., *Nucleic Acids Research*, 47 (2019) 414-422.

increased in the following order: chloromethanediol < dichloromethanol < chloroform. The presence of more halogen atoms increases the binding energy to the enzyme active site. After complete dehalogenation, the products formed are orthoformic acid and hydrochloric acid. Therefore, the trajectory of these compounds from the active site of DhaA to the enzyme surface was investigated using tunnels 1 and 2. Figure 4 displays the energy profile of orthoformic acid and hydrochloric acid trajectory from DhaA active site to enzyme surface using tunnel 1. The results obtained show the same behavior observed for the chloroform and water. Tunnel 1 allows a lower energy barrier and facilitates the transport of substrate and product from dehalogenation.

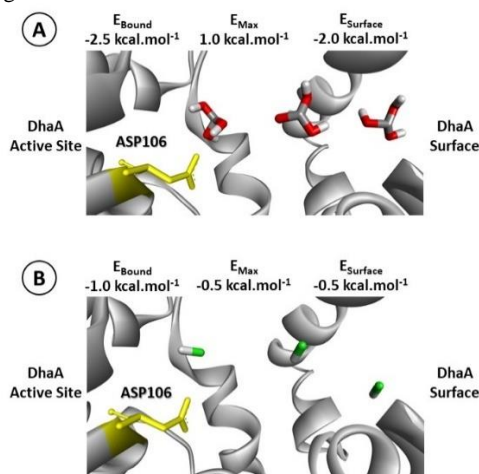


Figure 4. Ligand trajectory from DhaA active site to enzyme surface using tunnel 1: (A) Orthoformic acid and (B) Hydrochloric acid.

Conclusions

The enzymatic tunnels of DhaA from *Rhodococcus* sp. were identified and the efficiency of enzymatic dehalogenation of chloroform was evaluated. According to DhaA structure analysis, four possible tunnels provide access to small molecules from the enzyme surface to the catalytic active site. However, only two (the main tunnel and the slot tunnel) were favorable for ligand transport due to their shorter length and higher bottleneck radius. Molecular docking simulations showed that Tunnel 1 allows chloroform and water transport with lower energetic barriers. The binding energy analysis of products formed by each dehalogenation reaction step into DhaA active site shown that the presence of more halogen atoms increases the binding energy (more stability of an enzyme-substrate complex). Finally, the trajectory analysis of orthoformic acid and hydrochloric acid displayed a lower energy barrier for transport through Tunnel 1. The results obtained reveal that DhaA from *Rhodococcus* sp. is a promising biocatalyst for complete dehalogenation of THMs, that could be further applied for removal of THMs from drinking water.

Ultrasound-assisted synthesis of inulin esters with antimicrobial and anti-inflammatory activities

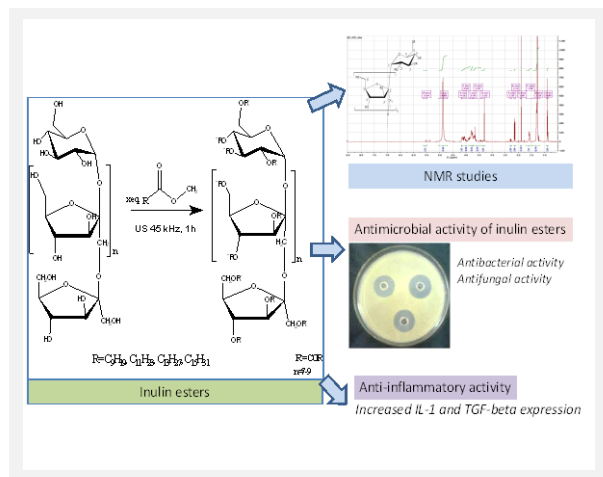
L. Hambarliyska^{1*}, *N. Petkova*¹, *Y. Tumbarski*², *D. Vassilev*³, *M. Brazkova*⁴, *A. Krastanov*¹, *I. Ivanov*¹, *P. Denev*¹, *I. Gotova*⁵, *Z. Dimitrov*⁵

¹Department of Organic Chemistry and Inorganic Chemistry, University of Food Technologies, 26 Maritza Blvd., Plovdiv, 4002, Bulgaria; ²Department of Microbiology, University of Food Technologies, 26, Maritza Blvd., Plovdiv, 4002, Bulgaria;

³Department of Mathematics, Informatics and Natural Sciences, Technical University of Gabrovo, Gabrovo, 5300, Bulgaria;

⁴Department of Biotechnology, University of Food Technologies, 26 Maritza Blvd., Plovdiv, 4002, Bulgaria; ⁵LB-Bulgarcicum PLC, R&D Center, 1000 Sofia, Bulgaria.

**vanya.hambarliyska@gmail.com*



Short-chain inulin was synthesized via transesterification, using fatty acid methyl esters (C10, C12, C14 and C16), NaOMe as a catalyst and ultrasonic irradiation. Inulin esters were characterized by physical-chemical and spectral methods. For the first time the antimicrobial activity of inulin middle and long fatty chain acid esters were tested against Gram-positive and Gram-negative bacteria, yeasts, and fungi. The most pronounced antimicrobial effect against Gram-positive microorganisms, *Escherichia coli*, and yeasts showed medium-chain inulin esters. The strongest antimicrobial activity against yeast and fungi was shown by inulin caprate, while inulin laurate was the most active against Gram-positive and some Gram negative microorganisms (Table 1). Three particular cytokines (IL-1 β , IL-8, TGF- β) were used to evaluate the *in vitro* anti-inflammatory activity of inulin esters. The addition of esters to the probiotic strain *Lactobacillus gasseri* led to increased induction of IL-1, but resulted in a reduction in IL-8 induction (Table 2). Inulin myristate and caprate used alone increased TGF-beta expression.

Table 1. Antimicrobial activity of inulin esters in concentration 10 mg/mL.

Tested microorganism	Type	Inulin caprate DE = 0.03	Inulin laurate DE = 0.17	Inulin myristate DE = 0.76	Inulin palmitate DE = 0.55	Str	Amp	Nys
1. <i>Bacillus subtilis</i> ATCC 6633	Gram positive	28	26	15	-	28***	21***	n/a
2. <i>Bacillus cereus</i>		22	25	-	-	25***	40***	n/a
3. <i>S. aureus</i> ATCC 25923		16	21	8	-	25***	40***	n/a
4. <i>L. monocytogenes</i> ATCC 8632		14	22	-	-	23***	33***	n/a
5. <i>Salmonella enteritidis</i>	Gram negative	10	13	23	11	18**	38***	n/a
6. <i>Escherichia coli</i> ATCC 25922		26	23	8	-	26***	40***	n/a
7. <i>Proteus vulgaris</i> ATCC 6380		-	-	-	-	24***	38***	n/a
8. <i>P. aeruginosa</i> ATCC 9027		21	24	25	19	23***	-	n/a
9. <i>Candida albicans</i> NBIMCC 74	Yeasts	19	15	-	-	n/a	n/a	13
10. <i>Saccharomyces cerevisiae</i>		12	8	-	-	n/a	n/a	-
11. <i>Aspergillus niger</i> ATCC 1015	Fungi	16	12	-	-	n/a	n/a	-
12. <i>Aspergillus flavus</i>		11	12	8*	-	n/a	n/a	8*
13. <i>Penicillium</i> sp.		14	13	-	-	n/a	n/a	9*
14. <i>Rhizopus</i> sp.		13	12	-	-	n/a	n/a	10*
15. <i>Mucor</i> sp.		13	-	-	-	-	-	-
16. <i>F. moniliforme</i> ATCC 38932		11	10	-	-	n/a	n/a	-

Positive controls: Amp – Ampicillin (10 μ g/mL); Str – Streptomycin (30 μ g/mL); Nystatin (40 μ g/mL), n/a – not applied, *low inhibitory effect, **moderate inhibitory effect, ***strong inhibitory effect, - absent

Table 2. The anti-inflammatory activity of inulin esters in concentration 0.2 % in 2% DMSO

N $^{\circ}$	Inulin ester	IL-1	IL-1 with addition of <i>L.gasseri</i>	IL-8	IL-8 with addition of <i>L.gasseri</i>	TGF-beta	TGF-beta with addition of <i>L.gasseri</i>
1	Inulin caprate DE = 0.03	19.8 \pm 1.7	228.3 \pm 18.2	4.5 \pm 0.5	13.0 \pm 1.1	919.2 \pm 83.6	1611.0 \pm 127.3
2	Inulin laurate DE = 0.17	46.5 \pm 4.1	244.2 \pm 26.6	43.7 \pm 3.9	82.6 \pm 7.7	172.9 \pm 15.3	1656.5 \pm 130.4
3	Inulin myristate DE = 0.76	33.7 \pm 2.9	315.0 \pm 29.0	21.9 \pm 1.8	83.5 \pm 6.9	1383.5 \pm 112.1	1720.2 \pm 157.9
4	Inulin palmitate DE = 0.55	28.5 \pm 2.0	277.1 \pm 27.8	162.6 \pm 12.4	46.3 \pm 4.1	564.3 \pm 49.2	11169.2 \pm 911.6
5	Control	0.0	92.6 \pm 7.9	1691.3 \pm 126.4	168.4 \pm 14.3	-	-

Acknowledgements

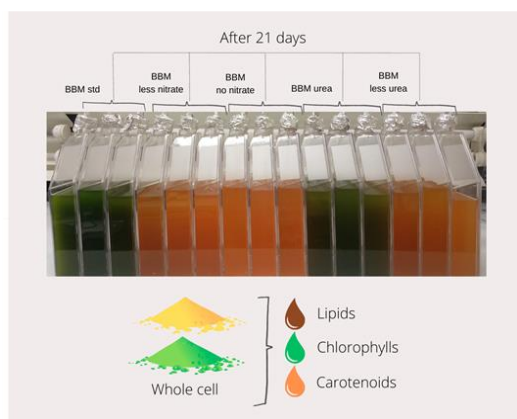
This study was financially supported by the National Science Fund “Competition For Financial Support For Fundamental Research - 2016”, Project Code ДН 06/11, Ministry of Education and Science, Bulgaria.

Urea as an alternative source of nitrogen for microalgae cultivation: effect on growth and biomass composition

P.S. Corrêa^{1*}, M.M.A. Freitas¹, N.S. Caetano^{1,2,3}

¹CIETI, Center for Innovation in Engineering and Industrial Technology, School of Engineering, Polytechnic Institute of Porto, Portugal; ²LEPABE, Laboratory for Process Engineering, Environment, Biotechnology and Energy, University of Porto, Portugal; ³ALiCE, Associate Laboratory in Chemical Engineering, University of Porto, Portugal.

*prisa@isep.ipp.pt



The species *Chromochloris zofingiensis* was cultivated in five different media with respect to nitrogen concentration and source. Higher carotenoids content was observed in biomasses cultivated with higher nitrogen concentration, BBM (U) and BBM std, 1.24 and 1.17 mg·g⁻¹, respectively. Being the highest chlorophyll accumulation found in the control condition (10.32 mg·g⁻¹). In contrast, when the nitrogen concentration was reduced, the carotenoids content was almost threefold higher using urea as nitrogen source (0.71 as opposed to 0.22 mg·g⁻¹). Moreover, higher lipids accumulation was observed in tenfold nitrogen-reduced media, 45.1 and 40.8 % (BBM (-) and BBM (U-), respectively). Nevertheless, there was no statistical difference between the results of lipids content obtained in NaNO₃ and urea media with same nitrogen concentration. Finally, replacing sodium nitrate with urea did not improve the final biomass concentration.

Introduction

Microalgae have been extensively investigated as a rich source of several biomolecules, e.g., pigments, lipids, proteins, carbohydrates, among others. *Chromochloris zofingiensis*, for instance, is particularly known as potential source of astaxanthin, a xanthophyll with interesting antioxidant properties. The imposition of abiotic stress during cultivation of microorganisms (i.e., by changing temperature, pH, nutrients, etc.) can affect their growth and promote metabolic changes that directly influence the production of various biomolecules, modifying the biomass composition [1]. In particular, the effect of nitrogen starvation has been widely studied in the literature [2-4]. As for the nitrogen source, sodium nitrate is the most common in microalgae culture media, however, urea can be used as a cheaper alternative reagent. Studies conducted by Hsieh and Wu [5] in *Chlorella sp.* suggested that in certain amounts urea can effectively increase lipids production, especially in semi-continuous cultures. Restiawaty et al. [6] tested the supplementation of Beneck's medium with low amounts of urea, observing a faster specific growth rate by supplementation with 30 mg·L⁻¹. However, the induction of lipid production was higher with 10 mg·L⁻¹ supplementation. In the present work, five conditions were tested.

Objectives

The main objective of the present work was to investigate the potential of urea, as BBM nitrogen source, considering its effect on growth and biomass composition of *C. zofingiensis*.

Methods

In addition to the control experiment (BBM std, standard Bold's Basal Medium) and the medium replacing NaNO₃ with urea with same nitrogen concentration (BBM (U)), the concentration of nitrogen was reduced tenfold (BBM (-) and BBM (U-)) and completely removed from the medium (BBM (x)). Cellular growth was measured by optical density at 750 nm and correlation curve: Biomass (g·L⁻¹) = (O.D._{750nm} - 0.0607)/2.3299, R² = 0.9981, for 21 days. Pigments extractions

were performed according to Fernandes and Cordeiro [7] with some modifications (instead of ultrasonicing the samples for 90 min, they were ultrasonicated for 30 min three times). Total of carotenoids and chlorophylls were determined according to Wellburn [8]. Lipid extraction and quantification were performed according to Byreddy et al. [9], with some modifications. Briefly, samples were filtered on PTFE syringe filters before drying at 65 °C.

Results

When comparing cultures with the same nitrogen concentration, the replacement of sodium nitrate by urea impaired cell growth after 3 days of cultivation (Figure 1). As shown in Tab. 1, the highest final biomass concentration (1.77 g·L⁻¹) was found in control condition (BBM std), while the lowest was observed in the absence of nitrogen source (0.19 g·L⁻¹), as expected.

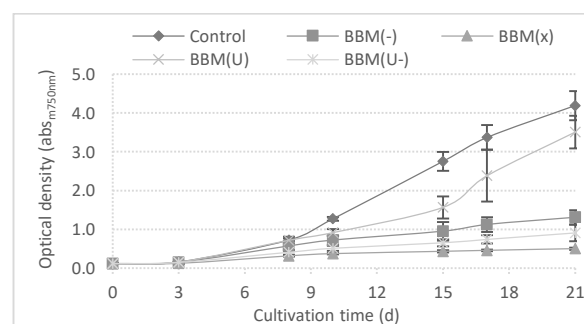


Figure 1. *C. zofingiensis* cell growth in five different media for 21 days.

Regarding the pigments production, the conditions with higher nitrogen concentration, BBM std and BBM (U), showed no statistically significant difference in carotenoids production, 1.17 and 1.24 mg·g⁻¹, respectively. However, the chlorophyll accumulation was higher in the control condition (BBM std), 10.32 compared to 8.90 mg·g⁻¹ (BBM (U)). Additionally, the reduction of urea concentration in the medium had less impact on carotenoid production (0.71 mg·g⁻¹) when compared to the

medium with less sodium nitrate BBM (-) ($0.22 \text{ mg}\cdot\text{g}^{-1}$) and without nitrogen source ($0.39 \text{ mg}\cdot\text{g}^{-1}$). Nevertheless, chlorophyll production showed no statistical difference in these three conditions. Concerning the lipid content, the reduction of nitrogen in the medium led to the highest accumulations of this compound, 40.8 and 45.1 % (BBM (U-) and BBM (-), respectively), even higher than in the absence of nitrogen (33.1 %) (Tab. 1). In contrast, the conditions with ten times more nitrogen, produced almost half of the best results, 23.1 and 25.9 % (BBM (U) and BBM std, respectively). These results suggest that reduction of nitrogen can induce lipids accumulation and that urea can substitute NaNO_3 as a nitrogen source without impair the production of total carotenoids and lipids.

Conclusions

Although urea did not increase biomass accumulation, it did not impair pigment and lipid production. Moreover, the higher nitrogen concentration in the medium led to higher amounts of carotenoids ($1.24 \text{ mg}\cdot\text{g}^{-1}$, BBM (U)) and chlorophylls ($10.32 \text{ mg}\cdot\text{g}^{-1}$, BBM std). On the other hand, a tenfold reduction in nitrogen almost doubled the lipid content, 45.1 % compared to 25.9 %, in BBM (-) and BBM std, respectively. Furthermore, statistical analysis showed no difference in lipid accumulation comparing the medium with NaNO_3 and urea with the same nitrogen concentration. However, a slight increase of almost two- threefold in carotenoid production was observed in the media supplied with urea when nitrogen concentration was reduced, $0.71 \text{ mg}\cdot\text{g}^{-1}$ compared to $0.39 \text{ mg}\cdot\text{g}^{-1}$ (BBM (X)) and $0.22 \text{ mg}\cdot\text{g}^{-1}$ (BBM (-)). Therefore, the results achieved in this work reinforce urea as a suitable source of nitrogen for *C. zoofingensis* cultivation.

Table 1. Biomass concentration, pigments, and lipids production of *C. zoofingensis* cultivated under five different conditions.

Cultivation condition	X ($\text{g}\cdot\text{L}^{-1}$)	Car _T ($\text{mg}\cdot\text{g}^{-1}$)	Chl _T ($\text{mg}\cdot\text{g}^{-1}$)	Total lipids (%)
BBM std	$1.77 \pm 0.16^{\text{d}}$	$1.17 \pm 0.13^{\text{e}}$	$10.32 \pm 1.07^{\text{j}}$	$25.9 \pm 3.2^{\text{k}}$
BBM (-)	$0.54 \pm 0.08^{\text{b}}$	$0.22 \pm 0.05^{\text{e}}$	$0.56 \pm 0.09^{\text{b}}$	$45.1 \pm 2.5^{\text{m}}$
BBM (x)	$0.19 \pm 0.01^{\text{a}}$	$0.39 \pm 0.04^{\text{e}}$	$0.22 \pm 0.04^{\text{b}}$	$33.1 \pm 1.4^{\text{l}}$
BBM (U)	$1.48 \pm 0.18^{\text{c}}$	$1.24 \pm 0.19^{\text{e}}$	$8.90 \pm 0.40^{\text{i}}$	$23.1 \pm 0.1^{\text{k}}$
BBM (U-)	$0.36 \pm 0.09^{\text{a,b}}$	$0.71 \pm 0.05^{\text{f}}$	$1.14 \pm 0.06^{\text{b}}$	$40.8 \pm 1.3^{\text{m}}$

X: biomass concentration; Car_T: Total carotenoids concentration; Chl_T: Total chlorophylls concentration. Same superscript letter means no significant difference between values, with 95 % of confidence level.

Acknowledgements

The authors would like to acknowledge the financial support of Fundação para a Ciência e Tecnologia (FCT), through grants UI/BD/151529/2021, UIDB/04730/2020 (CIETI), LA/P/0045/2020 (ALiCE) and UIDB/00511/2020 - UIDP/00511/2020 (LEPABE).

References

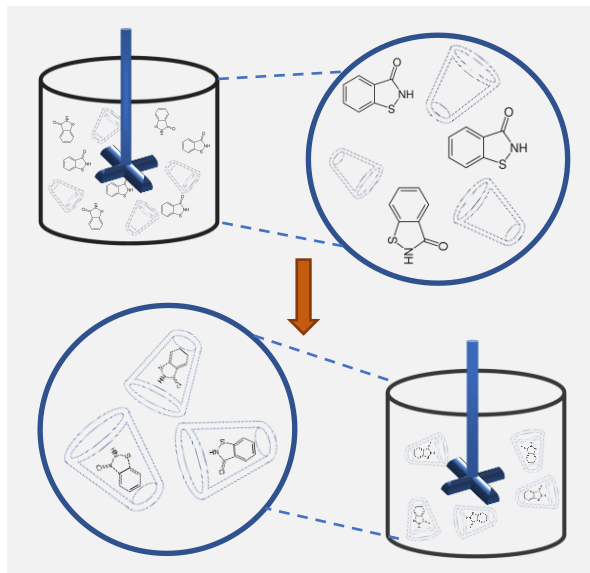
- [1] P.S. Corrêa et al., Algal Research, 67 (2022) 102859.
- [2] X. Li et al., Bioresource Technology, 263 (2018) 555-561.
- [3] X. Wang et al., Frontiers in Marine Science, 6 (2019) 00095.
- [4] C. Latsos et al., Frontiers in Marine Science, 7 (2020) 563333.
- [5] C.-H. Hsieh, W.-T. Wu, Bioresource Technology, 100 (2009) 3921-3926.
- [6] E. Restiawaty et al., Indian Chemical Engineer, (2023) 1-12.
- [7] T. Fernandes, N. Cordeiro, Journal of Applied Phycology, 34 (2022) 757-775.
- [8] A.R. Wellburn, Journal of Plant Physiology, 144 (1994) 307-313.
- [9] A.R. Byreddy et al., Journal of Microbiological Methods, 125 (2016) 28-32.

Microencapsulation of biocide benzisothiazolinone: a promising technique for the improvement of its aqueous solubility

V.F.M. Silva¹*, E.M.P.J. Garrido², F. Borges³, J.M.P.J. Garrido²

¹CIETI, School of Engineering (ISEP), Polytechnic of Porto, Rua Dr. Antonio Bernardino de Almeida, 431, 4249-015 Porto, Portugal; ²CIQUP-IMS, Department of Chemical Engineering, ISEP, Polytechnic of Porto, Rua Dr. Bernardino de Almeida 431, 4249-015 Porto, Portugal; ³CIQUP-IMS, Department of Chemistry and Biochemistry, Faculty of Sciences, University of Porto, Rua do Campo Alegre, s/n, 4169-007 Porto, Portugal.

*vfmsi@isep.ipp.pt



Benzisothiazolinone (BIT) is an antimicrobial agent used to preserve a wide number of products. However, its low water solubility, reduced bioavailability, and concerns raised about its inherent sensitization potential and allergic contact dermatitis have limited the industrial application of this biocide.

Microencapsulation with cyclodextrins can overcome some of these limitations by the formation of inclusion complexes. Three cyclodextrins were tested. The results showed that the complexation with cyclodextrin increases the solubility of BIT, thus significantly reducing the amount of active substance to be incorporated into the products, reducing the use, and enhancing the activity of this biocide.

Introduction

Benzisothiazolinone (BIT) is known as one of the isothiazolinone agents extensively applied as preservative in numerous industrial water-based solutions, and household cleaners [1]. Despite its antimicrobial activity and enormous potential applications, case reports of allergic contact dermatitis have made the use of BIT a critical issue worldwide [2-3]. In addition, its limited physicochemical properties (poor bioavailability and low water solubility) restrict its application and induces the use of higher concentrations to achieve a good biological activity.

The development of cost effective and environmentally friendly microencapsulation technologies offers a good opportunity to overcome these limitations. Enclosing biocides in microcapsules can not only extend their lifetime but also facilitate their handling, enhance biocidal activity, and minimize the need for higher concentrations [4].

Cyclodextrins (CD) are cyclic oligosaccharides of glucopyranose units with a truncated cone design of different sizes. The CD molecules are water soluble, have a hydrophilic outer wall and a hydrophobic inner wall, and can form inclusion complexes with lipophilic substances, which increases their water solubility [5].

Therefore, the aim of this work was to evaluate the effects of cyclodextrin complexation on the water solubility of BIT.

Methods

Phase solubility studies were performed using three cyclodextrins: β -CD, 2-hydroxypropyl- β -CD, and methyl- β -CD (Figure 1). The measurement was based on the phase solubility technique proposed by Higuchi and Connors [6], which evaluate the increasing water-soluble property of BIT during its

interaction with the cyclodextrins. Considering the highest stability constant obtained, the inclusion complex was prepared in the solid state by two methods: physical mixing and kneading. Analytical techniques were used to evidence the cyclodextrin inclusion, such as Fourier-Transform Infrared (FTIR) spectroscopy, Differential Scanning Calorimetry (DSC), Thermogravimetry (TG) and Nuclear Magnetic Resonance spectroscopy (NMR).

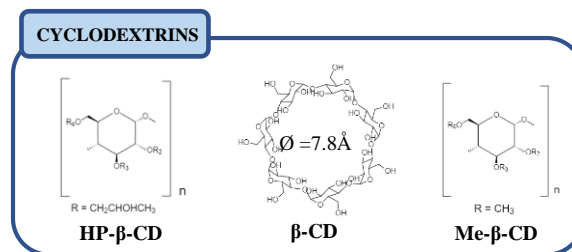


Figure 1. Cyclodextrins.

Results

The results indicated that BIT forms inclusion complexes with CDs showing improved physicochemical properties compared to free BIT. The microencapsulation increased BIT solubility threefold, compared to the native biocide solubility, and shows a 1:1 (CD:BIT) stoichiometry ratio for all the cyclodextrins. The stability constants BIT/ β -CD = 196.4M⁻¹, BIT/ HP- β -CD = 197.2M⁻¹, and BIT/ Me- β -CD = 204.2M⁻¹ suggest a similar interaction of all cyclodextrins with BIT. Thus, different techniques used to characterize the inclusion complex confirmed the encapsulation and the improvement of the physicochemical characteristics of BIT.

Conclusions

The encapsulation approach with cyclodextrins offers an effective solution to the solubility of scarcely water-soluble Benzisothiazolinone molecules. As a result, these inclusion

complexes of BIT with CD favor the biocide dose reduction, reducing the necessity of repeated applications, and enhancing the activity of the selected biocide.

Acknowledgements

This work was supported by national funds through Foundation for Science and Technology (FCT) (Project UIDB-04730-2020).

References

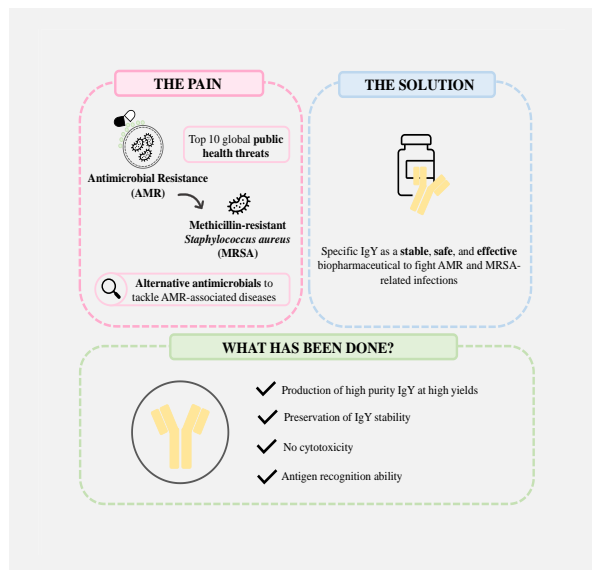
- [1] V. Silva et al., *Molecules*, 25 (2020) 991.
- [2] R.M. Novick et al., *Food and Chemical Toxicology*, 56 (2013) 60-66.
- [3] M. Goodier et al., *Dermatitis*, 29 (2018) 332-338.
- [4] H. Yow et al., *Soft Matter*, 2 (2006) 940-949.
- [5] S. Wupper et al., *Biomolecules*, 11 (2021) 401.
- [6] T. Higguchi et al., *Advanced Analytical Chemistry of Instrumentation*, 4 (1965) 117-212.

In vitro evaluation of avian immunoglobulin Y (IgY) antibodies to fight infectious illnesses caused by methicillin-resistance *Staphylococcus aureus* (MRSA)

C. Almeida, M.C. Neves, M.G. Freire*

CICECO-Aveiro Institute of Materials, Department of Chemistry, University of Aveiro, 3810-193 Aveiro, Portugal.

*maragfreire@ua.pt



Due to antibiotic misuse, bacteria are becoming resistant to these medicines, known as Antimicrobial Resistance. Biopharmaceuticals, such as antibodies, can be viable therapeutic alternatives to tackle this worrisome scenario. Polyclonal IgY is a promising antibody for the treatment of several infectious diseases, such as the ones caused by MRSA. However, its widespread use as biopharmaceutical still faced challenges regarding their recovery at high purity and yields, as well as their preservation. The present work aims to evaluate the potential of IgY as biopharmaceutical to tackle MRSA-related diseases, by assessing their stability, toxicity, and activity. Promising stabilizers for IgY were found. IgY is non-toxic towards Caco-2 cells and specific IgY can recognize PBP2a of MRSA. Overall, the potential of IgY as biopharmaceutical to tackle MRSA-related infectious diseases was confirmed, allowing to reduce the economic, societal, and health burdens.

Introduction

Owing to the intensive use of antibiotics in the last decades, bacteria undergo continuous mutations and become resistant to these medicines, making infections difficult to treat [1,2]. This phenomenon is known as Antimicrobial Resistance (AMR). AMR is considered one of the most serious public health threats worldwide, with Methicillin-resistant *Staphylococcus aureus* (MRSA) being one of the most problematic virulent bacteria [3-5]. Therefore, the prevention and control of MRSA are currently public health priorities in the European Union [4]. Notwithstanding the relevance of antibiotics to treat a wide range of microbial infections, these medicines are progressively becoming less efficient [6]. Thus, there is an urgent need to find effective alternative therapeutics to tackle the AMR worrisome scenario, for instance biopharmaceuticals.

Immunoglobulins, also termed antibodies, are glycoproteins produced by jawed vertebrates conferring immunity towards numerous foreign agents, for instance bacteria, viruses, among others [7]. Within the panoply of immunoglobulins classes available, avian immunoglobulin Y (IgY) is a promising antibody to be applied as biopharmaceutical. Contrarily to its mammalian equivalent Immunoglobulin G (IgG), IgY antibodies are recovered by non-invasive methods at high titers from hen's egg yolk, being the latter a relevant alternative and more sustainable source of antibodies [8,9]. By being polyclonal antibodies, IgY can recognize numerous epitopes on an antigen, which is extremely advantageous for the treatment of several microbial infectious diseases, including the ones caused by MRSA [8,9]. Nonetheless, the extensive use of IgY as biopharmaceutical is yet constrained by the complex nature of their source, i.e., egg yolk, which imposes a challenge for their recovery at high purity and yields, as well as their preservation. To surpass the first drawback, the team involved in this project, already developed a low-cost and fast purification technology based on liquid-

liquid extraction processes using Aqueous Biphasic Systems (ABS) that allows to obtain high purity (>98%) IgY antibodies at high yields.

Objectives

Accordingly, this work aims to evaluate the potential of IgY antibodies as biopharmaceutical to tackle infectious diseases caused by MRSA, by assessing their stability, toxicity, and activity towards this multiresistant bacteria.

Methods

Thus, IgY antibodies were recovered from the egg yolk of commercial and hyperimmune hens previously immunized with the recombinant Penicillin-binding protein 2a (PBP2a) of MRSA and purified according to the previously mentioned purification platform. Afterwards, the stability of the IgY antibodies obtained from the egg yolk of commercial hens was evaluated by Circular Dichroism (CD) Spectroscopy for a period of 1-3 weeks of storage with sugars and polyols, and after 1 month of storage formulated with amino acids at different thermal conditions. Moreover, the percentage of aggregates formed during storage under the previously described conditions, was evaluated through Size Exclusion-High Performance Liquid Chromatography (SEC-HPLC), as well as the protein profile unveiled resorting to Dodecyl Sulphate Polyacrylamide Gel Electrophoresis (SDS-PAGE). Regarding the safety of IgY antibodies, their toxicity towards human colon epithelial (Caco-2) cell lines was assessed. The ability of specific IgY against PBP2a to recognize the antigen was evaluated through Dot-Blot and Enzyme-Linked Immunosorbent Assay (ELISA).

Results

Novel bio-based compounds were found to have a great potential as stabilizers to preserve IgY stability, paving the way for their use as excipients in potential IgY therapeutic

formulations. IgY poses no toxicity towards Caco-2 cells and specific IgY can recognize PBP2a protein of MRSA.

Conclusions

This evidence confirms the potential of IgY as biopharmaceutical to tackle infectious diseases caused by MRSA, while allowing to reduce the associated economic, societal, and health burdens.

Acknowledgements

This work is financed by Portugal 2020 through European Regional Development Fund (ERDF) in the frame of CENTRO2020 in the scope of the project AntYmicrob, CENTRO -01--0145-FEDER-181219 and in the scope of the project CICECO – Aveiro Institute of Materials, UIDB/50011/2020, UIDP/50011/2020 & LA/P/0006/2020, financed by national funds through the FCT/MEC (PIDDAC). M.C. Neves acknowledges FCT, I.P. for the research contract CEECIND/00383/2017 under the CEEC Individual 2017.

References

- [1] B. Aslam et al., *Infection and Drug Resistance*, 11 (2018) 1645-1658.
- [2] N.D. Friedman et al., *Clinical Microbiology and Infection*, 22 (2016) 416-422.
- [3] F. Prestinaci et al., *Pathogens and Global Health*, 109 (2015) 309-18.
- [4] R Köck et al., *Euro Surveillance*, 15 (2010) 19688.
- [5] B.A. Alghamdi et al., *Saudi Journal of Biological Sciences*, 30 (2023) 103604.
- [6] C. Llor, L. Bjerrum, *Therapeutic Advances in Drug Safety*, 5 (2014) 229-241.
- [7] Y. Sun et al., *Journal of Animal Science and Biotechnology*, 3 (2012) 1-5.
- [8] J. Kovacs-Nolan, Y. Mine, *Avian and Poultry Biology Reviews*, 15 (2004) 25-46.
- [9] E.P.V. Pereira et al., *International Immunopharmacology*, 73 (2019) 293-303.

Extraction study of bioactive compounds from ginger by ultrasound and analysis of antioxidant action

S.S. Bernardoni^{1*}, B.L. Schneider², D.A. Nardino³, R.M. Suzuki⁴, C.C. Sipoli^{1,5}

¹Federal Technological University of Paraná, R. Marcílio Dias - 635, Apucarana, Brazil; ²Federal Technological University of Paraná, R. Marcílio Dias - 635, Apucarana, Brazil; ³State University of Maringá, Av. Colombo - 5790, Maringá, Brazil; ⁴Federal Technological University of Paraná, R. Marcílio Dias - 635, Apucarana, Brazil; ⁵Federal Technological University of Paraná, R. Marcílio Dias - 635, Apucarana, Brazil.

*sosobernardi@gmail.com



Brazil is recognized worldwide for its rich flora, especially the use of its vegetables in the treatment of diseases. In this sense, ginger has gained visibility in terms of disease prevention, as it has bioactive compounds such as terpenes, gingerols, shogaols and paradols, which have antioxidant action in the human body.

Thus, the present work proposed different extraction conditions using ultrasound, at different temperatures of 20, 50 and 70°C and times of 15, 30, 45 and 60 minutes, in order to evaluate the antioxidant activity of ginger by the methods of sequestration of the DPPH and ABTS radicals.

After DPPH and ABTS analyses, it was statistically analyzed by the Anova and Tukey tests that the best extraction condition was at 70°C and 45 minutes.

Introduction

Brazil is recognized worldwide for its flora, and having the greatest biodiversity in the world. Associated to this fact, since the first contacts with the indigenous people of the Americas, it was possible to recognize that they enjoyed the plants, highlighting their use for healing and treatment of diseases [1]. In humans, oxygen can be toxic, since this factor is associated with the formation of oxygen radicals, being an oxidizing agent. Medicinal plants with antioxidant properties can be used as preventive medicines, in order to avoid the oxidative process. Therefore, ginger (*Zingiber officinale*) when seen as a plant of phytotherapeutic potential has bioactive compounds with antioxidant, antidiabetic, anti-inflammatory, antitumor and antiviral properties [2].

This rhizome is a source of many antioxidants, and plays a vital role in reducing lipid peroxidation, inhibiting the pathogenesis of several diseases [3]. The biological activity of ginger can be associated to the presence of bioactive compounds such as terpenes and phenolic compounds, highlighting gingerols, shogaols and paradols [4], which are then associated with a decrease in the production of free radicals [3].

The extraction of these bioactive compounds can be performed using different techniques, with emphasis on ultrasound associated with solvent. Solvent extraction has advantages when it comes to productivity, yield and selectivity, moreover to mitigating the need for heat supply or the use of chemical substances [5].

These are several methods that can determine the antioxidant activity in compounds, however, one of the most uses is by scavenging the free radical DPPH (2,2-diphenyl-1-picrylhydrazyl) and ABTS (2,2-azino-bis(3-ethylbenzothiazolin)-6-

sulfonic) [6]. With the spectrophotometer, it is possible to monitor the decrease in absorbance.

So, the present work aims to study the characterization of ginger bioactive compounds, likewise your antioxidant action in an effort to be possible in future studies to encapsulate these extracts in drugs and foods.

Methods

Ginger samples obtained from a local trade in the city of Apucarana – PR were peeled and cut into strips. Subsequently, the ginger was taken to an oven with air circulation, at a temperature of 80°C for 24 hours. After weight stabilization, the dry samples were crushed in a conventional blender (Arno Power Mix Plus Lq20). The sample was stored in a plastic bag, protected from light and under refrigeration.

In 100 mL erlenmeyers, 0.5 g of sample was added with EtOH:H₂O 70:30 (v/v). The recipients were added in an ultrasound (Schustr L200), respecting the chosen temperatures (20, 50 and 70°C) and times (15, 30, 45 and 60 minutes). After filtration, the volumes were adjusted with ethanol in a 50 mL volumetric flask, at last, stored under refrigeration (4°C) in amber flasks.

For the analysis of DPPH radical scavenging in ginger, each sample received a blank (0.5 mL of sample and 2.5 mL of MeOH). The replicates were composed o 0.5 mL of sample and 2.5 mL of DPPH, while the control was made with 0.5 mL of MeOH and 2.5 mL of DPPH. After 30 minutes in the spectrophotometer (Agilent Technologies Cary 60 UV-Vis model), at 517 nm. Antioxidant activity was calculated in percentage of control inhibition as shown in the equation below.

$$\% \text{ inhibition of DPPH} = \left\{ \frac{Ac - (Aa - Ab)}{Ac} \right\} * 100$$

Where Ac is the absorbance of the control, Aa is the absorbance of the sample and Ab the absorbance of the blank [7].

For the ABTS analysis, a solution with 0.192 g of ABTS and 50 mL of distilled water was prepared, simultaneously, a solution was made with 0.3784 g of potassium persulfate and 10 mL of distilled water. The ABTS^{•+} radical cation formation was prepared with 5 mL of ABTS solution and 88 µL of potassium persulfate solution, where it was kept in an amber flask at ambient temperature for 16 hours before use. On the day of analysis, 1 mL of formed radical was diluted in EtOH with sufficient amount to obtain an absorbance close to 0.700, which was read in a spectrophotometer at a wavelength of 734 nm. For the blank of each sample, 150 µL of sample in 3 mL of EtOH was used, the control 150 µL of EtOH in 3 mL of ABTS radical solution, and the replicates 150 µL of sample in 3 mL of ABTS radical solution, the readings were performed after 6 minutes of rest. Antioxidant activity was obtained similarly the DPPH analysis. The results obtained were qualified through the analysis of variance Anova (n=3) and Tukey test (p<0.05) using Statistica® 8.0.

Results and Discussion

Two independent variables were evaluated in the extraction process, temperature and time. Table 1 represents the results obtained to evaluate the antioxidant activity of the DPPH and ABTS analysis.

For the ABTS radical reduction test, the results varied between 72.42 ± 0.14% and 98.75 ± 0.17%, exposing that for the hydroalcoholic extract of ginger it presents a high reduction action of the ABTS^{•+} radical, so, the highest percentage was obtained under conditions of 20°C and 45 minutes. The results of the present study were superior compared to that of Nardino [4], where the maximum percentage was 29.88%. This difference can be explained by the extraction method, which in the author's case extraction was performed in the shaker and in the current work in ultrasound, the amount of sample in the test and the cultivation conditions (planting and harvesting carried out at different times). For the DPPH radical reduction analysis, the condition that showed the best response was 70°C and 45 minutes. The results obtained indicate an effective extraction of antioxidant action of ginger, reaching approximately 94.90% of reduction of the formed radical. When compared with the data obtained by Nardino [4], in the present work some of the percentages were higher than those found by the author, this factor can be explained by different extraction methodology.

To continue the experiments, the extraction conditions that showed the best response for both antioxidant tests were the extract prepared at 70°C and 45 minutes.

Conclusions

It was possible to propose the method of extraction by ultrasound as an efficient technique for the extraction of bioactive compounds present in ginger. Considering the times and temperatures evaluated, the best condition was 70°C and 45 minutes, showing 94.90% and 98.75% reduction of DPPH and ABTS radicals, respectively.

Table 1. Results of antioxidant activity (% inhibition) by different methods

Test	Temperature (°C)	20	50	70
	Time (min)	Average values		
ABTS	15	72,45 ± 0,14 ^d	86,97 ± 0,30 ^d	96,89 ± 0,10 ^b
DPPH		83,05 ± 0,20 ^c	84,48 ± 0,75 ^b	92,50 ± 0,51 ^b
ABTS	30	90,94 ± 0,46 ^c	88,25 ± 0,3645 ^c	95,97 ± 0,61 ^{a,b}
DPPH		82,89 ± 0,37 ^b	86,35 ± 0,24 ^a	92,35 ± 0,63 ^b
ABTS	45	98,75 ± 0,17 ^b	91,76 ± 0,76 ^b	97,88 ± 0,37 ^a
DPPH		80,00 ± 0,65 ^b	87,92 ± 0,93 ^a	94,90 ± 0,48 ^{a,b}
ABTS	60	88,26 ± 0,38 ^a	84,82 ± 0,27 ^a	97,35 ± 0,30 ^a
DPPH		86,64 ± 0,05 ^a	87,57 ± 0,24 ^a	93,95 ± 0,81 ^a

The data obtained represent the average of the samples (n=3). In the same column, values with equal letters do not differ significantly (p<0.5).

Acknowledgements

To UTFPR Campus Apucarana, to professors Caroline Casagrande Sipoli and Rúbia Michele Suzuki and the multi-user laboratory (LAMAP).

References

- [1] C. Brito, A história da saúde indígena no Brasil e os desafios da pandemia de Covid-19. FIOCRUZ, 2020. Disponível em: <http://coc.fiocruz.br/index.php/pt/todas-as-noticias/1779-a-historia-da-saude-indigena-no-brasil-e-os-desafios-da-pandemia-de-covid-19.html>. Acesso em: 08 de ago. 2022.
- [2] H. Rostamkhani et al., Journal of Functional Foods, 94 (2022) 105111.
- [3] K. Barbosa et al., Revista de Nutrição, 23 (2010) 629-643.
- [4] D.A. Nardino et al., Otimização do processo de extração de compostos bioativos do zingiberofficinale (gingibre) para incorporação em lipossomas e estudo do potencial em aplicações farmacêuticas. 2021. Dissertação de Mestrado. Universidade Tecnológica Federal do Paraná.
- [5] C.O. Bernardo et al., Ciência Rural, 46 (2016) 739-746.
- [6] N.R. Sucupira et al., Journal of Health Sciences, 14 (2012) 4.
- [7] M. Boroski et al., Antioxidantes - Princípios e Métodos Analíticos. 1ª Ed. Curitiba, 2015.

Validation of a prototype of a miniaturized near infrared spectrometer on complex organic samples

L.L. Monteiro^{1*}, P. Zoio^{1,2*}, B.B. Carvalho³, L.P. Fonseca¹, C.R.C. Calado²

¹Institute for Bioengineering and Biosciences (iBB), Instituto Superior Técnico (IST), Universidade de Lisboa (UL), Av. Rovisco Pais, 1049-001 Lisboa, Portugal; ²CIMOSM—Centro de Investigação em Modelação e Optimização de Sistemas Multifuncionais, ISEL—Instituto Superior de Engenharia de Lisboa, Instituto Politécnico de Lisboa, R. Conselheiro Emídio Navarro 1, 1959-007 Lisboa, Portugal; ³Instituto de Plasmas e Fusão Nuclear, Instituto Superior Técnico (IST), Universidade de Lisboa (UL), Av. Rovisco Pais 1, 1049-001 Lisboa, Portugal.

*luis4lopesmonteiro@gmail.com (L.L.M.); cecilia.calado@isel.pt (C.R.C.C.)

Fourier Transform Infrared (FTIR) spectroscopy focused on the near infrared (NIR) region has become crucial for quality control on diverse areas, from energy to biomedical applications, by enabling *in-situ* and in real time analysis of samples with complex organic compositions [1,2]. The development of portable and miniaturized NIR spectrometers (miniNIR) can further extend NIR spectroscopy applications [3,4], thus this work compares *in-situ* analysis based on a FT-NIR benchtop spectrometer with a miniNIR prototype to detect and quantify contaminants in biodiesel, such as vegetable oils, methanol, and glycerol. Good models based on principal component analysis-linear discriminant analysis of FT-NIR spectra were obtained, predicting contaminants with accuracies between 75 to 95%, while the miniNIR prototype's delivered models with accuracies between 66 to 86%, showing the device's potential for preliminary quality control of biodiesel, with the added advantages of low cost and portability.

Introduction

For a long time now, quality control of products across multiple industries has been performed with well-established techniques such as liquid and gas chromatography, which while efficient and adequate, are time-consuming, generate a large amount of toxic waste, and are usually operated off-line [5]. This has created a need for quick analytical procedures that operate which allow for *in-situ* monitoring of samples and processes, such as infrared spectroscopy.

Infrared (IR) spectroscopy is quickly becoming a popular technique for quality analysis, as the wavelength accuracy and spectral quality of the spectrometers can provide detailed information on complex organic samples [6]. For example, in the biodiesel industry, infrared spectroscopy focused on the near infrared (NIR) range has been used to monitor biodiesel synthesis and contaminant detection with great results.

The application of this technique has been further expanded thanks to the utilization of miniaturized and portable NIR spectrometers, pocket-size devices with lower utilization costs than regular spectrometers and that are used to perform at-line analysis of samples [7]. This work aimed to evaluate the performance of a prototype of a portable miniaturized NIR (miniNIR) spectrometer and compare it to the performance of a benchtop FT-NIR spectrometer with a transfection probe, based on spectral regions focusing on part of the vibration combination and the first overtone regions, in the simultaneous *in-situ* analysis of vegetable oil, used cooking oil, methanol, and glycerol in biodiesel.

Materials and Methods

Biodiesel blends with one contaminant each (rapeseed oil, two different types of used cooking oil, methanol, and glycerol) were prepared and analyzed with a benchtop FT-NIR spectrometer, using a NIR transfection fiber optic probe and operating in the

9000 – 4000 cm^{-1} region of the spectrum, and with a prototype of a miniNIR spectrometer (pictured in Figure 1), with a matrix of six independent LED covering the 7700 – 4700 cm^{-1} region of the spectrum.

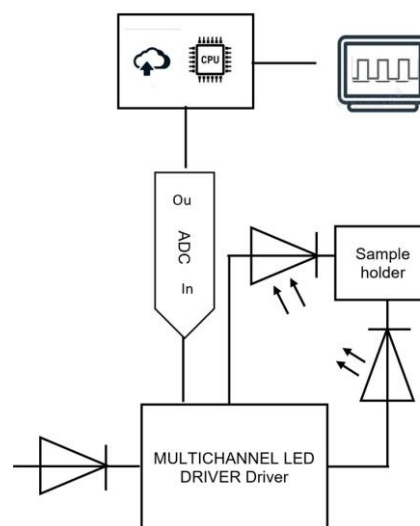


Figure 1. Schematic representation of the prototype of the miniaturized and portable NIR spectrometer used.

Different spectra preprocessing methods were used on the obtained data before conducting a principal component-linear discriminant analysis (PCA-LDA) to predict the presence of contaminants in biodiesel, and building the partial least square (PLS) regression models to quantify the contaminants in the samples.

Results and Discussion

The PCA-LDA models with the best accuracies obtained from FT-NIR spectral data and miniNIR data to predict the presence of contaminants in biodiesel are shown in Table 1.

Table 1. Accuracies of the best PCA-LDA analyses based on FT-NIR and miniNIR data

Target contaminants	Accuracy based on FT-NIR analysis/%	Accuracy based on miniNIR analysis/%
All	75	78
Rapeseed and used cooking oils	95	72
Rapeseed oil	84	86
Used cooking oil	79	74
Methanol	91	68
Glycerol	78	79

Although not as high as the models based on FT-NIR data, the accuracies of the PCA-LDA models based on miniNIR data are considered reasonable, showing the prototype's potential to detect different contaminants.

As for the PLS models built to quantify the contaminants in the biodiesel, the models based on the miniNIR prototype data

showed poor prediction abilities, with low R-Squared values (between 0.50 and 0.85) and high values of root mean square error of prediction (RMSEP), while the models based on FT-NIR data showed very good predictive ability. The discrepancy in results can most likely be attributed to the LED set-up of the prototype, which is different from the miniaturized NIR devices already commercially available, and could potentially be corrected by using LEDs with a higher resolution.

Conclusions

Portable and miniaturized NIR spectrometers are a more economical alternative to benchtop spectrometer which allow for a quick *in-situ* analysis of complex samples, which could increase quality control. Compared to the benchtop FTIR spectrometer, the miniaturized and portable prototype showed good predictive ability of target contaminants, but didn't allow for their quantification. In the future, other LED set-ups could be evaluated to see how the performance of the prototype is affected. As it is now, thanks to its low-cost and small dimensions, the prototype could be used in primary assessments of organic samples, which could then be analyzed by more sophisticated techniques.

Acknowledgements

This research was funded by grants DSAIPA/DS/0117/2020, UIDB/04565/2020 and UIDP/04565/2020 from FCT, and NproMD/ISEL/2020 from Instituto Politécnico de Lisboa.

References

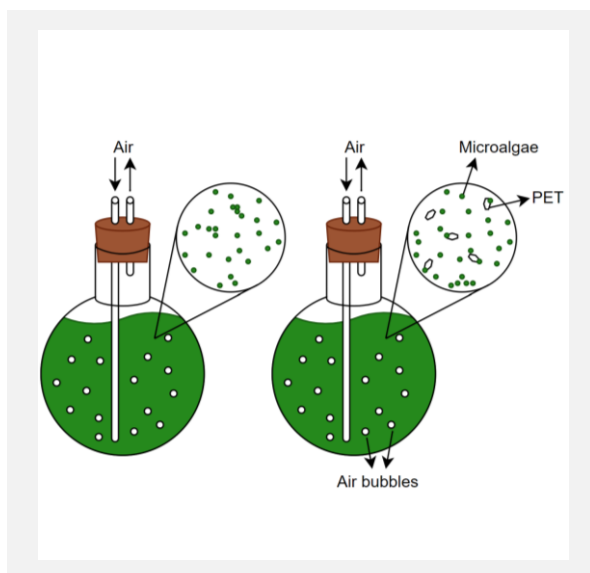
- [1] K.C. Sales et al., *Applied Spectroscopy*, 69 (2014) 760-772.
- [2] E.K. Gelinski et al., *Open Chemical Engineering Journal*, 12 (2018) 95-110.
- [3] M. Alcalà et al., *Journal of Near Infrared Spectroscopy*, 21 (2014) 445-457.
- [4] K.B. Beč et al., *Foods* 11 (2022) 1465.
- [5] G.O. Ferrero et al., *Renewable and Sustainable Energy Reviews*, 150 (2019) 128-135.
- [6] S.J. Mazivila, *Talanta*, 180 (2018) 239-247.
- [7] R.F. Kranenburg et al., *Forensic Chemistry*, 30 (2022) 100437.

Interaction between *Chlorella vulgaris* and microplastic (PET) particles examined by optical and nuclear microscopy

S.A. Vaz^{1,3,4*}, T. Pinheiro², L.P. Monteiro¹, S.M. Badenes¹, R.C. Martins³, H.M. Pinheiro⁴

¹A4F - Algae For Future SA, Campus do Lumiar, Edifício E - R/C, Estrada do Paço do Lumiar, 1648-038 Lisboa, Portugal; ²iBB—Institute for Bioengineering and Biosciences and Department of Engineering and Nuclear Sciences, Instituto Superior Técnico, Universidade de Lisboa, Av. Rovisco Pais 1, 1049-001 Lisboa, Portugal; ³University of Coimbra, CIEPQPF, Department of Chemical Engineering, FCTUC, Pólo II, 3030-790 Coimbra, Portugal; ⁴iBB—Institute for Bioengineering and Biosciences and Department of Bioengineering, Instituto Superior Técnico, Universidade de Lisboa, Av. Rovisco Pais, 1049-001 Lisboa, Portugal.

*sofia.anibal.vaz@tecnico.ulisboa.pt



The continuous development of our society, with its underlying industry and consumer products profile, is leading to an increase in waste production which results in higher concentrations of pollutants in receiving media, namely microplastics, that the natural ecosystems cannot process effectively. In this study, the interaction between microalgae (*Chlorella vulgaris*) cultures and microplastic (PET) particles is examined to determine the possible fate and effects of the latter in the context of adding a microalgae cultivation step to the treatment process of domestic wastewater. Comparative cultivation runs were carried out in the presence and absence of microplastic. Using optical microscopy coupled to a fluorescence module and nuclear microscopy, it was possible to confirm the formation of algae-microplastic aggregates. These results indicate that biomass harvesting techniques will likely remove the microplastic simultaneously, improving the final quality of treated wastewater.

Introduction

The emergence of microplastics in the aquatic and terrestrial ecosystems is a growing concern that is leading to the development of new technologies aiming to remove these pollutants from the wildlife compartments. Microplastics are materials with particle sizes below 5 mm that are derived from all the plastic containing products nowadays used and discarded. These materials have bioaccumulation properties that higher their role as potential carriers of toxic substances, whether these are collected throughout their course in the environment or are already present from their manufacture. Therefore, microplastics pose a great threat to human and wildlife health, even more so because they are rapidly invading the environment due to their reduced size. They are easily disseminated in the aquatic environment, show an ability to enter the food chain, and their degradation is slow and challenging, rendering them very persistent [1-2].

Microalgae cultivation systems have been widely studied for the treatment of domestic wastewater, with many works having already been published confirming the microalgae capacity to remove various pollutants, especially nitrogen and phosphorus compounds, from different wastewater treatment effluents [3-5]. In addition, the use of microalgae for the bioremediation of domestic wastewater enables a sustainable strategy in the global wastewater treatment industry. The microalgae use of CO₂ as a carbon source and release of O₂ in photosynthesis, allows the mitigation of the negative effects caused by excessive concentration of CO₂ in the atmosphere, and the reduction of energy consumption for aeration. The recovery of microalgae biomass from wastewater treatment

systems and its use to produce added value products can also render the process more economically feasible [6].

Regarding the use of microalgae cultivation for microplastic removal from wastewater, information is still scarce but some studies have shown great promise from this technology [1,7].

Objectives

The aim of this study was to contribute for a better understanding of the possible removal mechanisms of microplastics particles using microalgae cultivation systems. To examine the interaction between the microalgae *Chlorella vulgaris* and PET microparticles, a microplastic typically present in domestic wastewater, different microscopy techniques were assessed.

Methods

Chlorella vulgaris Ma016 was obtained from the A4F – Algae for Future SA Culture Collection of Algae, PT. In these experiments autoclaved tap water supplemented with a macro/micronutrients and vitamins mix, with nitrate as the nitrogen source, was used as cultivation media. The cultivation was performed in sterile conditions, in 2-L glass flasks with a 1.8-L working volume, bubbled with air enriched with 0.5 % (v/v) CO₂ at a rate of 0.5 L min⁻¹, filtered with a 0.22 μm membrane filter. The cultures were maintained under continuous illumination from a LED system with a light intensity between 100 and 140 μmol m⁻² s⁻¹ and with the temperature varying between 23 and 26 °C. Each flask was inoculated with an initial biomass concentration of 0.2 g L⁻¹ in cell dry weight. The fed medium contained microplastic particles, polyethylene terephthalate (PET) powder, particle

size < 300 μm , purchased from Goodfellow Cambridge Ltd., UK, at concentration of 0.1 g L^{-1} . Parallel control experiments were run in the absence of microplastic. The experiments had a duration of 21 days, with 90 % medium volume renovations on the 7th and 14th cultivation days.

Microalgae growth was measured through optical density measurements at 600 nm on whole culture samples and the nitrate concentration was measured through the ultraviolet spectrophotometric screening method on the supernatant of centrifuged samples [8]. Two replicates and three controls were run in parallel, and the results are presented as mean \pm standard deviation.

The interaction between microalgae and microplastic was followed by examination of whole culture samples using optical microscopy on an Olympus BX53 fluorescence microscope (Evident, Japan), and through nuclear microscopy on centrifuged and distilled-water washed biomass samples using the nuclear microprobe (Oxford Microbeam, UK) installed at the Centro Tecnológico e Nuclear of Instituto Superior Técnico, Portugal. PIXE (Particle Induced X-ray Emission), RBS (Rutherford Backscattering Spectroscopy) and STIM (Scanning Transmission Ion Microscopy) were used simultaneously, allowing the examination of morphology and the retrieval of quantitative elemental distribution data.

Results

The average biomass productivity achieved during the three 7-day cycles was 0.61 ± 0.10 and 0.63 ± 0.11 $\text{OD}_{600\text{nm}} \text{day}^{-1}$ and the nitrate consumption was 1.51 ± 0.25 and 1.52 ± 0.20 mM day^{-1} , for the controls and the tests, respectively. Therefore, the effect of the presence of microplastic particles on microalgae growth and nitrogen uptake is apparently not significant.

Microscopic examination evidenced the accumulation of cells on the surface of the microplastic particles (e.g., Figures 1a and 1b). Quantitative analyses were carried out with spectra from points (e.g., Figure 1d) with an area close to that of the nuclear microbeam (ca. 3 μm^2), which were selected in each sample from the PET, PET+microalgae and microalgae zones. The obtained elemental signature for PET ($\text{C}_{15}\text{O}_2\text{H}_{16}$) matches the one normally attributed to this plastic material and it was

possible to quantify a microalgae signature (including P, S, Cl, Ca and a little Fe). The latter signature also appeared covering the microplastic particles (e.g., Figures 1e and 1f for P and S, respectively) indicating the presence of a microalgae biofilm, as it is also apparent in Figure 1b.

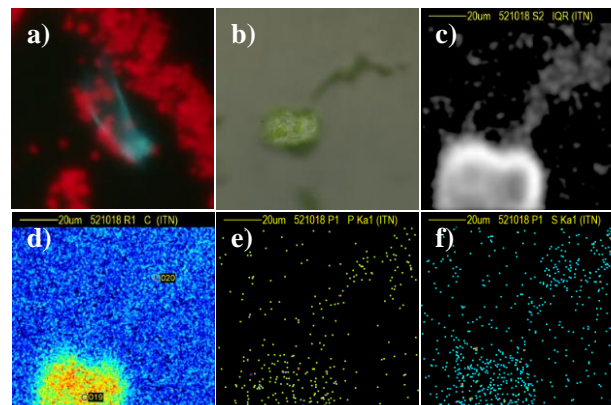


Figure 1. a) fluorescence microscopy image of a microplastic (light blue/green) and microalgae (bright red) aggregate (40 \times magnification); b) optical reflection microscopy image under bright field of a microplastic particle (light green) and microalgae (dark green) aggregate; c) STIM density map of a zoom in of image b), showing a microplastic particle (light grey/white) with attached microalgae (dark grey); d) RBS map for carbon of image c), with the locations of the points used for quantitative elemental analysis; e) PIXE map for phosphorus of image c); f) PIXE map for sulfur of image c).

Conclusions

These results indicate that the introduction of a microalgae cultivation step in domestic wastewater treatment may enhance not only the removal of pollutants such as nitrogen and phosphorus, but also that of microplastic particles, due to the formation of their co-aggregates with algae cells. These can then be recovered through optimized physico-chemical processes. Also, this study shows that combined optical and nuclear microscopy techniques can be powerful tools to monitor and characterize microalgae cultivation in the presence of microplastics.

Acknowledgements

S.A. Vaz acknowledges the doctoral grant with the reference PRT/BD/152859/2021 from FCT - Fundação para a Ciência e a Tecnologia, I.P. The authors acknowledge further support from FCT through institutional grants (UIDB/EQU/00102/2020, UIDB/04565/2020, UIDP/04565/2020, LA/P/0140/2020).

References

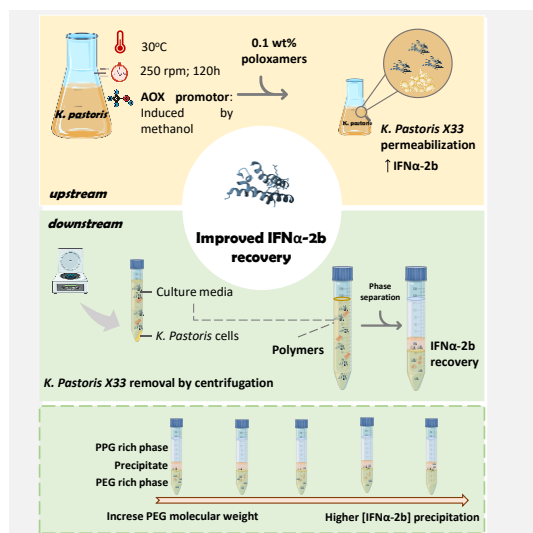
- [1] Y.R. Cheng, H.Y. Wang, *Chemical Engineering Journal*, 435 (2022) 135079.
- [2] S. Miri et al., *Chemosphere*, 286 (2022) 131670.
- [3] E. Geremia et al., *Environments*, 8 (2021) 136.
- [4] A. Guldhe et al., *Journal of Environmental Management*, 203 (2017) 299-315.
- [5] S.F. Mohsenpour et al., *Science of the Total Environment*, 752 (2021) 142168.
- [6] R. Sharma et al., *Bioresource Technology*, 344 (2022) 126129.
- [7] C. Cunha et al., *Environmental Pollution*, 249 (2019) 372-380.
- [8] R.B. Baird, A.D. Eaton, E.W. Rice, *Standard methods for the examination of water and wastewater*, 23rd Ed, American Public Health Association, American Water Works Association, Water Environment Federation (2017).

Polymer-based aqueous biphasic systems as a tool for the recovery of protein-based biopharmaceuticals

*L.S. Castro**, *A.Q. Pedro*, *M.G. Freire*

CICECO – Aveiro Institute of Materials, Department of Chemistry, University of Aveiro, Campus Universitário de Santiago, 3810-193 Aveiro, Portugal.

**l.castro@ua.pt*



The increment in life expectancy coupled with climate change, and rapid urbanization lead to an increase in the number of chronic and infectious diseases. To mitigate such prospects, one promising strategy is the application of biopharmaceuticals, which are effective in the clinical treatment of a broad range of diseases, such as infectious diseases and cancer. Despite their multiple advantages, biopharmaceuticals manufacturing remains time-consuming and expensive, and thus not widely accessible worldwide, especially for low- and middle-income countries. In this work, polymer-based aqueous biphasic systems were applied for the recovery of recombinant therapeutic proteins directly from the culture media of *Komagataella pastoris*. Overall, we found that by tailoring the molecular weight of the polymers used as agents for the formation of the biphasic system, the preferential partition of the target protein is selectively changed, offering improved and customizable approaches for their extraction and purification from biological media.

Introduction

Over the last decades, the development of innovative medicines such as protein-based biopharmaceuticals improved human lifespan and general health, providing novel treatments for chronic disorders. Among them, interferon alpha-2b (IFN α -2b), which is a 17 kDa protein that has been used in the treatment of chronic hepatitis C has had a considerable impact on the global therapeutic proteins market for the last 30 years [1,2]. Despite the multiple advantages of biological products over traditional pharmaceutical products such as higher sensitivity and low side effects, their use is not widespread, especially for middle- and low-income countries. One of the biggest hindrances to the application of biopharmaceuticals is their high cost, usually associated with expensive manufacturing technologies [3]. The manufacturing process can be divided into two main stages the upstream stage involving the expression of the desired product and the downstream stage where the recovery and purification occur [4]. Since both the upstream stage and the downstream stage are connected, the choice of host for protein expression is of great importance.

Methods and Results

In this sense, during the development of this work, we proceeded to the application of *Komagataella Pastoris* X-33 harboring the pPICZ α vector coupled with the alpha-mating factor signal for the secreted expression of IFN α -2b. The results showed that the application of 0.1% of poloxamers and polysorbates can significantly increase the levels of secreted IFN α -2b, when compared with the results for the media without any additives.

Acknowledgements

This work was developed within the scope of the projects CICECO-Aveiro Institute of materials, UIDB/50011/2020, UIDP/50011/2020 & LA/P/0006/2020, financed by national funds through the FCT/MEC (PIDDAC). Leonor S. Castro and Augusto Q. Pedro acknowledge FCT, respectively, for her PhD grant 2020/05090/BD and for the research contract CEECIND/02599/2020 under the Scientific Stimulus – Individual Call.

However current downstream processing strategies for biopharmaceuticals are still responsible for a significant part of its manufacturing costs.

Over the years, several attempts have been made to improve the downstream processing of biopharmaceuticals such as the use of aqueous biphasic systems (ABS). First proposed by Albertson, ABS are a well-known liquid-liquid extraction methodology that has been widely applied for the recovery and purification of several biomolecules including proteins, nucleic acids, and biomarkers, being recognized by their highly biocompatible nature due to its high-water content. In this work, polymer-polymer aqueous biphasic systems composed of polyethylene glycol (PEG) with different molecular weights and polypropylene glycol 400 g/mol (PPG400) were applied for the recovery of IFN α -2b directly from the culture media.

Conclusions

The results show that depending on the PEG molecular weight and the respective mixture compositions, the protein is selectively partitioned with high yield to the phase enriched in PEG, or precipitates at the interface, offering novel and customized routes for the recovery of protein-based biopharmaceuticals.

Overall, this work demonstrates the importance of optimizing both the nature of ABS components and the respective mixture compositions to improve the recovery of biopharmaceuticals, ultimately leading the way to advance their overall manufacturing process.

References

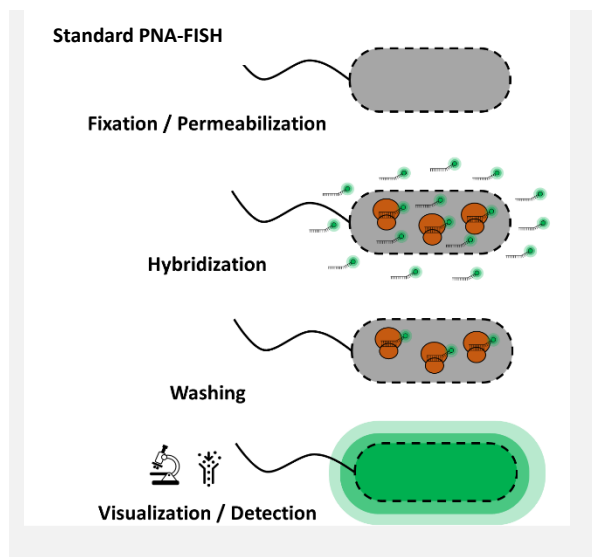
- [1] L.S. Castro et al., *Vaccines*, 9 (2021) 328.
- [2] G. Walsh, E. Walsh, *Nature Biotechnology*, 40 (2022) 1722-1760.
- [3] A.C. Szkodny, K.H. Lee, *Annual Review of Chemical and Biomolecular Engineering*, 13 (2022) 141-165.
- [4] S.C. Hock et al., *Generics and Biosimilars Initiative Journal* 9 (2020) 52-60.

Application of PNA-FISH based-methods for bacterial detection and localization in biofilms

A. Barbosa^{1,2}, D. Goeres³, N.F. Azevedo^{1,2}, L. Cerqueira^{1,2*}

¹LEPABE - Laboratory for Process Engineering, Environment, Biotechnology and Energy, Faculty of Engineering, University of Porto, Rua Dr. Roberto Frias, 4200-465 Porto, Portugal; ²ALiCE - Associate Laboratory in Chemical Engineering, Faculty of Engineering, University of Porto, Rua Dr. Roberto Frias, 4200-465 Porto, Portugal; ³Center for Biofilm Engineering, Montana State University, Bozeman, MT 59717-3980, USA.

*lcerqueira@fe.up.pt



Legionella contamination of water systems represents a serious social problem that can lead to severe diseases that manifest as both Pontiac fever and Legionnaires' disease (LD).

We established a new PNA-FISH method that has been successfully designed for the specific detection of the *L. pneumophila* by optimizing a peptide nucleic acid (PNA) sequence based on fluorescently selective binding to specific bacterial rRNA sequences.

Under the scope of ERA Chair project e.Biofilm, we will present a preliminary model for the use of mRNA PNA-FISH to study the regulatory network of *L. pneumophila* that is useful for clarifying the organizational and functional development of biofilms and understanding the role that spatial and temporal heterogeneity plays in *L. pneumophila* virulence in water systems under different physicochemical conditions, disinfection treatments, and in the presence of diverse microbial consortia.

Introduction

Legionella pneumophila represents a particular concern and remains one of the most tracked agents in most anthropogenic water systems, being considered an opportunistic waterborne pathogen. Close surveillance and the use of diagnosis methods in water management are critical to effectively reduce the public risk caused by *Legionella*. Despite excellent developments in the area of identification, the current technologies do not fully answer the needs of industrial entities for *Legionella* monitoring.

Nucleic acid mimics fluorescence *in situ* hybridization (NAM-FISH) is a molecular assay where fluorescently labelled NAMs, such as peptide nucleic acids (PNA), are used to penetrate microbial cells and hybridize with specific rRNA sequences [1]. In earlier work, we reported the design of several PNA probes, targeting specific pathogens in food, clinical and environmental samples (e.g. *Helicobacter pylori*, *Salmonella* spp., *Aspergillus fumigatus*) [2-6]. Additionally, under the scope of the ERA Chair e.Biofilm project, we want to explore the use of PNA probes for *Legionella* biofilm studies. One of the advantages of the NAM-FISH is that, in addition to the detection of microorganisms, it allows us to locate individual cells in multispecies and multistrains biofilms, hence enabling for the study of their three-dimensional spatial distribution [7]. PNA probes provide an advantage over standard FISH because their neutrally charged, synthetic nature and shorter length can contribute to improved diffusion of the probe through the biofilm matrix and to a better signal-to-noise ratio of the probe due to a stronger affinity of PNA to the target sequences [8,9]. In here we will explore the development of PNA probes for the detection of *L. pneumophila* in water samples. We will demonstrate that adapting PNA-FISH to target mRNA and combining it with spectral imaging using high-resolution CLSM will allow us to

study gene expression in single cells both in suspension and in biofilms thereby combining spatial and functional information of the cells *in situ*.

Methods

ISO protocol 11731:2017 for the identification of the bacteria will be adapted in order to achieve an optimized Limit of Detection for the detection of the bacteria in water samples following probe design and the optimization of hybridization conditions [10]. To assess the probe's specificity and sensitivity values, 22 *L. pneumophila* strains and 24 non-*L. pneumophila* strains were tested.

Results

It was possible to observe that all the target strains had a positive fluorescence signal (100% sensitivity) but none of the non-target strains were positive (100% specificity) (Figure 1). Currently, the filtration/centrifugation protocols for water sample treatment prior to hybridization are being performed to optimize and simplify the detection protocols when low concentrations of bacteria are present.

Finally, we will present a preliminary model for the use of mRNA PNA-FISH to study the regulatory network of *L. pneumophila* that is used to provide information about gene expression in single cells either in the planktonic or sessile state, recording both spatial and functional information.

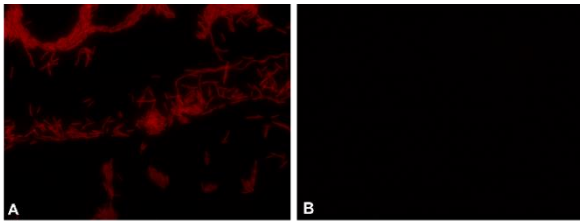


Figure 1. A. *L. pneumophila* in water samples using the developed PNA probe; B. *E. coli* samples using the PNA probe (negative control).

Acknowledgements

This work was financially supported by: LA/P/0045/2020 (ALiCE), UIDB/00511/2020 and UIDP/00511/2020 (LEPABE), funded by national funds through the FCT/MCTES (PIDDAC); Project e.Biofilm – “Creation of a group of Excellence on Engineered Biofilms”, Grant Agreement number 101087568, financed by the European Commission in the scope of the Horizon Europe Framework Programme. PhD fellowship 2022.11840.BD supported by national funds through FCT – Fundação para a Ciência e a Tecnologia. The acknowledgements should be written here.

References

- [1] M. Nácher-Vázquez et al., *Microbiological Research*, 262 (2022) 127086.
- [2] L. Cerqueira et al., *Journal of Clinical Microbiology*, 51(6) (2013) 1887-93
- [3] C. Almeida et al., *International Journal of Food Microbiology*, 161(1) (2013) 16-22.
- [4] C. Almeida et al., *Applied and Environmental Microbiology*, 79(20) (2013) 6293-300
- [5] R. Rocha et al., *Food Microbiology*, 80 (2019) 1-8
- [6] L. Cerqueira et al., *Microorganisms*, 8(12) (2020) 1950.
- [7] C. Almeida et al., *Plos One*, 6(3) (2011) e14786
- [8] L. Cerqueira et al., *Biofouling*, 29(7) (2013) 829-840.
- [9] H. Stender et al., *Journal of Microbiological Methods*, 48 (2002) 1-17
- [10] M. Nácher-Vázquez et al., *Microorganisms*, 10 (2022) 1409.

It is well known that *L. pneumophila* presents a biphasic life cycle, alternating between transmissive (motile, virulent) and replicative (non-virulent) states. The transition from the replicative to the transmissive phase is governed by a well-known list of genes. We have been designing PNA probes specific for these targets.

Conclusions

Rethinking current *Legionella* research and management paradigms are critical to provide additional insight into *Legionella* proliferation and control strategies.

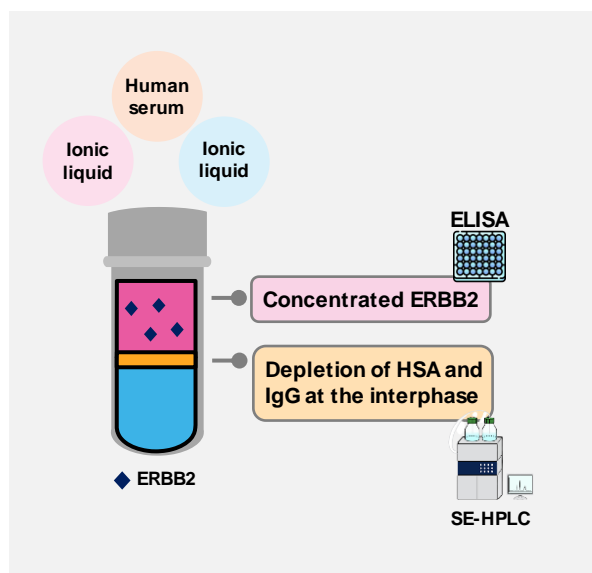
Development of efficient platforms for breast cancer biomarkers extraction resorting to ionic liquid-based aqueous biphasic systems

M.S.M. Mendes^{1*}, M.C. Souza¹, J.P. Conde^{2,3}, M.G. Freire¹, F.A. e Silva¹

¹CICECO - Aveiro Institute of Materials, Department of Chemistry, University of Aveiro, 3810-193 Aveiro, Portugal.

²Instituto de Engenharia de Sistemas e Computadores-Microsistemas e Nanotecnologias (INESC MN), Rua Alves Redol 9, Lisbon, 1000-029, Portugal ; ³Department of Bioengineering, Instituto Superior Técnico, Universidade de Lisboa, Av. Rovisco Pais 1, Lisbon, 1049-001, Portugal.

*msilvinamm@ua.pt



High abundance serum proteins, especially human serum albumin (HSA) and immunoglobulin G (IgG), represent a critical barrier for the accurate quantification of cancer biomarkers. To reduce the interfering effects caused by these proteins, a prior sample pretreatment and biomarker extraction step may be necessary. Here, ionic liquid-based aqueous biphasic systems (IL-based ABS) are foreseen as tunable and efficient alternatives for the pretreatment of human serum and the extraction of epidermal growth factor receptor 2 (ERBB2) – an important biomarker to improve the clinical management of breast cancer. Within this framework, this work aims to investigate a new class of IL-based ABS composed of two ILs for the one-step removal of high abundance proteins and extraction of ERBB2 from human serum. The most efficient IL-IL ABS achieved the complete removal of IgG and 69% of HSA, while extracting 93% of ERBB2 in the top phase in one step. As compared to more usual ABS comprising IL-salt, polymer-salt and polymer-IL combinations, IL-IL ABS can be more easily adjusted to improve serum pretreatment and biomarker extraction.

Introduction

Breast cancer diagnosis is currently performed resorting to techniques such as mammography, magnetic resonance imaging (MRI) and biopsy [1]. Despite the undeniable benefits in managing breast cancer, these methods are limited for early-stage diagnosis, which is crucial to improve the disease outcome and prolong patient survival [1]. The analysis of biomarkers in human serum such as human epidermal growth factor receptor 2 (ERBB2) is a promising tool to shift towards an earlier detection of breast cancer [2]. However, the presence of high abundance serum proteins, especially human serum albumin (HSA) and immunoglobulin G (IgG), limits the accurate and reliable quantification of cancer biomarkers [3]. Therefore, biomarker analysis can be preceded by a sample pretreatment and biomarker extraction step in order to achieve more accurate results [3]. The most conventional serum pretreatment techniques are solid-phase extraction, which is highly sensitive, but expensive, and protein precipitation that despite the low cost provides low biomarker yields [3]. Due to their water-rich and tunable nature, aqueous biphasic systems (ABS) can overcome the main challenges of conventional techniques, while keeping high selectivity and cost-efficiency [4]. Despite promising results have been achieved in the field of biomarkers, conventional polymer-based ABS present limited polarity range and high viscosity, which limits the applicability, selectivity and efficiency of biomarker extraction and analysis [5]. To overcome these limitations and maximize the potential of ABS in the biomarker analysis field, ionic liquids (ILs) have been proposed as a class of phase-forming agents that allows a more tailored polarity range between the two phases, a quicker phase separation and higher extraction efficiencies [4]. To date, however, the application

of IL-based ABS to assist biomarker analysis remains seldom investigated.

Objectives

This work aims to develop novel human serum pretreatment and biomarker extraction strategies using IL-based ABS, particularly composed IL-IL combinations, and compare their performance with conventional IL-salt, polymer-salt and polymer-IL ABS.

Methods

Different ABS were evaluated in terms of their performance to remove the high-abundance serum proteins HSA and IgG at the interphase and extract the breast cancer biomarker ERBB2 in one of the aqueous phases in one step. The concentration of HSA and IgG in each phase of the ABS was quantified using size exclusion high-performance liquid chromatography (SE-HPLC), allowing to determine the depletion efficiencies. The ability to extract ERBB2 was further evaluated using enzyme-linked immunosorbent assays (ELISAs) to quantify the concentration of ERBB2 in the aqueous phases.

Results and discussion

To evaluate the ability of each ABS to deplete HSA and IgG at the interphase, a mixture composition in the biphasic region was chosen based on the analysis of previously determined phase diagrams. Regarding the ABS performance to promote the depletion of HSA and IgG at the interphase, depletion efficiencies ranged from 3% to 100% for IgG, and from 30% to 100% for HSA depending on the IL structure or the pair of phase-forming agents. ABS containing two ionic liquids achieved a maximum depletion of 100% of IgG and 69% of

HSA at the interphase, outperforming most conventional ABS. Based on the depletion efficiencies obtained, studies on the extraction ERBB2 from human serum in one of the aqueous phases were then performed using the best performing systems. Remarkably, while keeping its ability to deplete HSA and IgG, one of the best previously identified IL-IL ABS also

allowed the extraction of 93% of ERBB2 in the top phase in one step. Overall, IL-IL ABS were shown to be more efficient than conventional ABS as sample pretreatment and biomarker extraction tools, bringing new perspectives for the analysis of breast cancer biomarkers.

Acknowledgements

This work was developed within the scope of the project CICECO-Aveiro Institute of Materials, UIDB/50011/2020, UIDP/50011/2020 & LA/P/0006/2020, financed by national funds through the FCT/MEC (PIDDAC). This work was developed within the project PTDC/EMD-TLM/3253/2020 (ILSurvive), funded by national funds (OE), through FCT/MCTES. M.S.M.M. acknowledges FCT for the doctoral grant 2022.11229.BD. F.A.eS. acknowledges FCT for the researcher contract CEECIND/03076/2018 under the Scientific Employment Stimulus – Individual Call 2018.

References

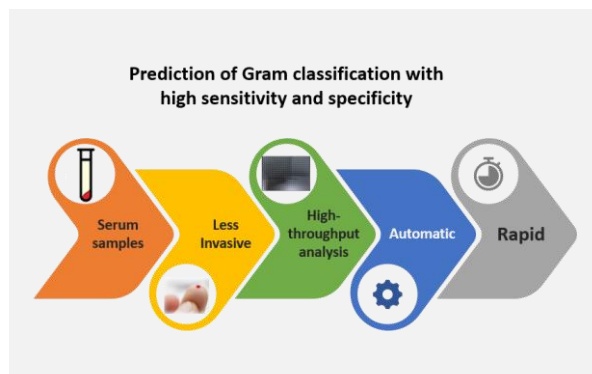
- [1] A.B. Chinen et al., *Chemical Reviews*, 115 (2015) 10530–10574.
- [2] J.A. Ludwig, J.N. Weinstein, *Nature Reviews Cancer*, 5 (2005) 845–856.
- [3] P.Y. Lee, J. Osman, T.Y. Low, R. Jamal, *Bioanalysis*, 11 (2019) 1799–1812.
- [4] M.M. Pereira et al., *Scientific Reports*, 10 (2020) 1–8.
- [5] J. Kim et al., *PLoS One*, 10 (2015) 1–16.

Streamlining bacterial infection dDiagnosis: rapid Gram classification using FTIR Spectroscopy

R. Araújo^{1,2*}, L. Ramalhe^{2,3}, T. Fonseca⁴, C. von Rekowski⁴, L. Bento^{1,2,5}, C. Calado^{4,6}

¹CHRC, R. Câmara Pestana 6, Lisbon, Portugal; ²NMS, R. Campo dos Mártires da Pátria 130, Lisbon, Portugal, ³IPST, Alameda das Linhas de Torres, Lisbon, Portugal, ⁴ISEL, R. Conselheiro Emídio Navarro 1, Lisbon, Portugal, ⁵CHULC, R. José António Serrano, Lisbon, Portugal, ⁶CIMOSM, R. Conselheiro Emídio Navarro 1, Lisbon, Portugal.

*rubenalexandredinisaraujo@gmail.com



Short abstract: In a hospital setting, diagnosing infections typically involves a complex process that includes the collection of biological samples and growing a culture for organism isolation, followed by its characterization. However, these methods are slow, require multiple steps and are often limited by the need of specialized equipment and skilled personnel. In this preliminary study, it was analysed the serum, by FTIR spectroscopy, of 29 critically ill COVID-19 patients in an ICU. It was analysed the effect of varied pre-processing methods and spectral sub-regions on t-SNE. Through the optimization of SVM models, it was possible to achieve a very good gram predictive model with a sensitivity and specificity of 90 and 89% respectively. As an accurate classification of bacterial strains is crucial to guide effective antimicrobial therapy and prevent the spread of multidrug-resistant bacteria, FTIR spectra, acquired in a simple, economic, and rapid mode, presents therefore the potential for development of new classification methods that would greatly enhance the ability to manage bacterial infections.

Introduction

Gram classification is of the utmost importance in hospitals, in order to properly diagnose bacterial infections and determine the appropriate treatment [1]. However, correctly identifying the Gram classification of a bacterial infection can be challenging due to potential misinterpretation of staining results, overlapping cell morphology, and emerging antibiotic-resistant bacteria [2]. Therefore, accurate and timely Gram classification is crucial for guiding appropriate antibiotic therapy, preventing infection spread and to help minimize antibiotic resistance [3]. These challenges only serve to highlight the importance of rapid, economic, and reliable diagnostic methods in a clinic or hospital environment, a critical step to effectively treat and prevent serious complications and life-threatening events for the patients. Spectroscopy [4], especially FTIR spectroscopy present itself as a technique that can enable this goal, as it is can acquire the metabolic status of the biological system in a high sensitivity and specificity mode. Indeed, FTIR spectroscopy, especially in the mid-infrared region (MIR), from 400 to 4000cm⁻¹, has been widely used in biomedicine applications, from discrimination between B and T-lymphocytes [5], infection processes [6], capturing the human physiological state through serum and plasma analysis [7], as well as for medical diagnosis, prognosis [8], among many others.

Objectives

This work aims to evaluate if Fourier Transform Infrared (FTIR) spectroscopic analysis of human serum, would allow for the prediction and correct gram classification in critically ill patients in an ICU environment.

Methods

Biological Assay

Peripheral blood was collected in a serum tube with no anticoagulant VACUETTE®, using standard blood collection procedures. Samples were maintained at 4°C until blood centrifugation at 3000 rpm for 10 minutes (Micro 220T, Hettich, Tuttingen, Germany). Serum samples were kept at -20°C until FTIR spectra acquisition. A total of 29 patients, with COVID-19 and bacteraemia, and admitted to the ICU of Hospital São José, Centro Hospital Universitário Lisboa Central, were considered. All participants provided a signed

informed consent before enrolment in the study approved by the Hospital's Ethics Committee.

FTIR spectra acquisition

Triplicates of 25 µL of serum diluted at 1/10 in water were transferred to a 96-wells Si plate and then dehydrated for about 2.5 h, in a desiccator under vacuum (ME 2 pump, Vacuubrand, Wertheim, Germany). Spectral data was collected using a FTIR spectrometer (Vertex 70, Bruker, Germany) equipped with an HTS-XT (Bruker, Germany,) accessory. Each spectrum represented 64 coadded scans, with a 2cm⁻¹ resolution, and was collected in transmission mode, between 400 and 4000 cm⁻¹. The first well of the 96-wells plate did not contain a sample and the corresponding spectra was acquired and used as background. Medians of triplicate spectra were used.

Spectra pre-processing and processing

All spectra were submitted to atmospheric correction, using OPUS® software, version 6.5 (Bruker, Germany, Billerica, USA). A baseline correction was also performed. Second derivative spectra (based on a Savitzky-Golay filter, and a 2nd order polynomial over a 15-point window) and unit vector normalization and spectra processing were conducted by Orange 3 Data Mining Toolbox (Faculty of Computer and Information Science, University of Ljubljana, Slovenia). Spectra processing included t-distributed stochastic neighbour embedding (t-SNE) and Support Vector Machine (SVM) models optimization.

Results

A total of 29 COVID-19 patients, all hospitalized at the ICU, were considered, all presenting bacteremia, as based on microbiological analysis. Patients, between the two groups, i.e., gram positive and gram negative, did not present significant differences concerning gender, age, and body mass index (p>0.1).

Among the many pre-processing tested (Table 1), from non-derivative to derivative spectra (data not shown), it was the atmospheric correction spectra with a normalized (unit vector normalization) second derivative (Table 1D, Figure 1), which proved to be the most effective at separating the two groups of patients. This was possible due to the minimization effect that normalization has on the spectra, regarding the impact of sample quantity under analysis. Also, the second derivative

contributes to a superior differentiation of groups, as it resolves superimposed bands, therefore increasing the information retrieved from the spectra. As derivatives also increase noise, care must be taken however, as any region that might decrease the signal-to-noise ratio should, therefore, be removed.

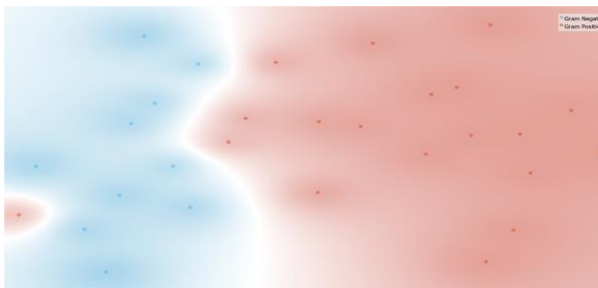


Figure 1. t-SNE of patients with gram negative (blue) and gram positive (red) bacteria, based on serum spectra after a normalized second derivative between 1040-1045 cm^{-1} , 1345-1350 cm^{-1} , 2190 to 2195 cm^{-1} and 2965-2970 cm^{-1} .

Having identified the best pre-processing through means of the spectra t-SNE with the best scores separation between the two groups of patients, SVM models were developed to predict Gram classification, based on non-derivative spectra and second derivative spectra, based on the whole spectra, or select sub-regions. For that, 80% of patient's data were used for model training and the remaining 20% used for an independent dataset for model validation. A total of 100 models were built for each spectra pre-processing model and regions evaluated, based on random selection of data for the model's training and validation. The various model's performance, for each pre-processing, can be observed in Table 1.

The best predictive model was achieved based on the spectra with atmospheric correct and normalized second derivative, on the spectral sub-regions 1040-1045 cm^{-1} , 1345-1350 cm^{-1} , 2190 to 2195 cm^{-1} and 2965-2970 cm^{-1} (Table 1D), highlighting the relevance of the regions $\approx 1045 \text{ cm}^{-1}$, to the stretching vibrations of the C-O bond in cyclic ethers such as tetrahydrofuran and oxirane, $\approx 1350 \text{ cm}^{-1}$ associated with the

Acknowledgements

This work was supported by the project grant DSAIPA/DS/0117/2020 supported by *Fundação para a Ciência e a Tecnologia*, Portugal and by the project grant NepromD/ISEL/2020 financed by *Instituto Politécnico de Lisboa*.

References

- [1] N. Tripathi and A. Sapra, *Gram Staining*. Treasure Island (FL), 2022. <http://www.ncbi.nlm.nih.gov/pubmed/14925025>
- [2] L.P. Samuel et al., *Journal of Clinical Microbiology*, 54 (2016) 1442-1447.
- [3] S. Vasoo et al., *Mayo Clinic Proceedings*, 90 (2015) 395-403.
- [4] S. Berezin et al., *Scientific Reports*, 7 (2017) 3810.
- [5] L. Ramalhete et al., *Vibrational Spectroscopy*, 111 (2020) 103177.
- [6] R. Araújo et al., *Metabolites*, 12 (2022) 92.
- [7] R. Araújo et al., *BioTech*, 11 (2022) 56.
- [8] L. M. Ramalhete et al., *Proteomes*, 10 (2022) 24.
- [9] G. Larrouy-Maumus, *Current Medicinal Chemistry*, 26 (2019) 1924-1932.

bending vibrations of the C-H bond in the CH₃ group, $\approx 2195 \text{ cm}^{-1}$, associated with the stretching vibrations of the C≡N bond in nitriles. This absorption is typically very strong and narrow and can be used to identify nitrile functional groups in various molecules. The $\approx 2970 \text{ cm}^{-1}$ region associated with the stretching vibrations of the C-H bond in methyl (CH₃) groups. This absorption can be used to identify the presence of methyl groups in various molecules, including lipids and other organic compounds. The relevance of these regions, cannot be overstated, for example, changes in the position or intensity of the absorption bands at 1030-1070 cm^{-1} can be indicative of changes in the molecular composition of lipids and carbohydrates, which are common in many infectious agents [9]. These regions relevance is highlighted by the very good prediction model developed (Table 1D), which resulted in a sensitivity and specificity of 90% and 89%, respectively.

Table 1. SVM models' performance to predict Gram classification on spectra from serum of 29 patients with atmospheric and baseline correction (A), complete spectra normalized second derivative (B), and select sub-regions (C), normalized second derivative between 1040-1045 cm^{-1} , 1345-1350 cm^{-1} , 2190 to 2195 cm^{-1} and 2965-2970 cm^{-1} (D), and normalized second derivative between 600-1800 and 2800-3100 cm^{-1} (E) as well as select sub-regions (F).

	AUC	CA	Precision	Sensitivity	Specificity
A	0.487	0.643	0.460	0.643	0.324
B	0.460	0.662	0.443	0.662	0.331
C	0.950	0.892	0.892	0.892	0.868
D	0.969	0.897	0.898	0.897	0.883
E	0.906	0.797	0.797	0.797	0.658
F	0.904	0.880	0.879	0.880	0.815

Conclusions

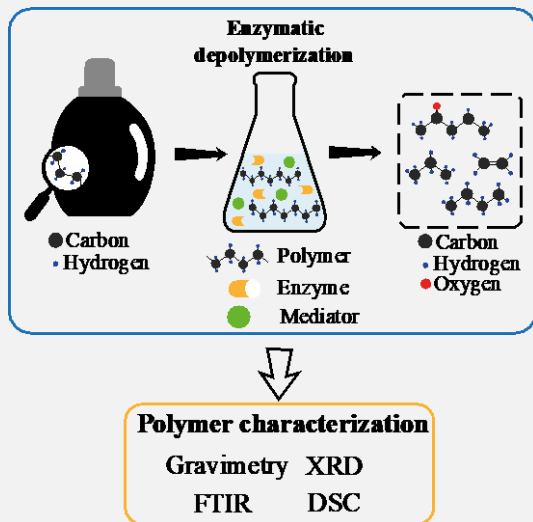
The present work points to an alternative technique to classify, using FTIR spectroscopy, between positive and negative Gram bacteria in the blood stream, through a simple, rapid, and economic mode, in ICU patients. This allows adequate treatment to critically ill patients, leading to fast infection detection rates, and individually concocted course of antibiotics, at the same time avoid its unnecessary use, which ultimately would ease the metabolic burden on the patients.

Enhancing plastic waste recycling: investigating the impact of additives on polymer degradation via laccase from *Trametes versicolor*

M.I.S. Aguiar*, A.F. Sousa, A.P.M. Tavares, A.M. Ferreira

CICECO – Aveiro Institute of Materials, Department of Chemistry, University of Aveiro (UA), 3810-193, Aveiro, Portugal.

*m.aguiar@ua.pt



Plastics i.e. synthetic polymers, are ubiquitous in our daily lives and their annual production exceeds 350 million tons. However, only a small fraction of the polymers produced annually are (bio)degradable or recycled.

Therefore, the aim of this work is to achieve a recycling process based on an enzymatic depolymerization process for high-density polyethylene (HDPE) packaging waste. For this end, the enzyme laccase from *Trametes versicolor* was used, and three different approaches were evaluated: (i) biocatalytic media, (ii) mediators and (iii) HDPE with and without additive (orange pigment 64, PO64). The extent of the reactions was evaluated gravimetrically, FTIR, DSC and XRD.

The most effective system was HDPE without additive and treated with buffer, laccase and ABTS. This system resulted in a weight loss of 32.90%, new bands in the FTIR spectrum (e.g. carbonyl band) and a higher diffraction angle in XRD. Further studies to optimize the process are underway.

Introduction

Plastics are ubiquitous synthetic polymers typically produced from fossil-based resources in a still highly linear manner, yet indispensable in daily life and many industrial applications [1,2,3].

Environmental pollution from synthetic plastics has been reported since the 1970s [4]. The accumulation of plastics is due to their massive production combined with their recalcitrant nature, as the hydrophobicity, degree of crystallinity, very stable carbon-carbon bonds, and surface topography lead to an extremely slow rate of degradation [5]. In addition, the techniques of plastic recycling are not ideal as the physical properties of the recycled material deteriorate significantly compared to virgin polymers, resulting in their use in the market with lower quality requirements.

Therefore, the main objective of this work was to achieve a recycling process based on the concept of circular economy by developing an enzymatic depolymerization process for packaging waste consisting of commonly produced high-density polyethylene (HDPE). Laccase from *Trametes versicolor* was used as the enzyme, and three different approaches were tested as described below.

Methodology and Results

First, two different solutions were evaluated as biocatalytic media: a citrate-phosphate buffer with a pH of 4.5 and an aqueous mixture of a deep eutectic solvent (DES - cholinium dihydrogen citrate: xylitol at 50 (w/w)%). The results indicate that, contrary to expectations, DES did not enhance the laccase's activity [6], with the enzyme's activity being almost zero after 24 h of incubation. In fact, the HDPE (with additive) weight losses observed were three times higher when buffer was used as biocatalytic medium than when DES was used.

In the second approach, two different mediators were tested (2,2'-azinobis-(3-ethylbenzothiazoline-6-sulfonic acid, ABTS and 1-hydroxybenzotriazole, HBT). The weight loss of HDPE (with additive) using ABTS was more than double that when using HBT as mediator, indicating that ABTS is the best option

was mediator for this purpose. Additionally, the FTIR spectra showed a slightly more intense carbonyl band for the ABTS systems than for the HBT system.

The third approach aimed to determine whether removing the additives from polymers enhances the enzymatic reaction. Additives are often incorporated into polymers to improve their properties, but they can difficult waste management. For instance, additives such as pigments can interact with the active site of enzymes preventing them from attacking the polymer [7]. Therefore, it was compared the performance of HDPE with and without color-additive (i.e., orange pigment 64, PO64). The experimental results demonstrated that the enzymatic depolymerization of HDPE was significantly more efficient for HDPE without additive, particularly when using laccase as enzyme in conjunction with ABTS as mediator and buffer as biocatalytic medium. This approach yielded a remarkable weight loss of 32.90%, in contrast to the 2.87% observed for HDPE with additive. The FTIR spectra for HDPE without additive were possible to see new carbonyl and hydroxyl related bands, especially for the best system (HDPE without additive + laccase + ABTS + buffer). The DSC results show that pretreatment to remove additives from HDPE [8], leads to a less crystalline polymer and that enzymatic treatment of this polymer leads to an increase in its crystallinity, especially when treated with laccase in the presence of ABTS and buffer. Therefore, the DSC results suggest that the amorphous domains were being preferentially attacked by the enzyme. The results of XRD also suggested that the enzyme is attacking the amorphous domain.

Conclusions

Overall, the results indicate that enzymatic oxidation has occurred, preferentially attacking the amorphous domain in HDPE polymers without additives. These findings highlight the potential of enzymatic depolymerization as a promising solution for recycling HDPE and promoting sustainable polymers use. However, additional research is necessary to comprehend the alterations in the polymer and enhance the

process's efficacy to attain the most favorable recycling outcomes.

Acknowledgements

This work was developed within the scope of the project CICECO-Aveiro Institute of Material, UIDB/50011/2020, UIDP/50011/2020 & LA/P/0006/2020, financed by national funds through the FCT/MCTES (PIDDAC). AFS, APT and AMF acknowledges FCT for the research contract CEECIND/02322/2020, CEECIND/2020/01867 and CEECIND/00361/2022, respectively. This publication is supported by COST Action FUR4Sustain- European network of FURan based chemicals and materials FOR a Sustainable development, CA18220, supported by COST (European Cooperation in Science and Technology).

References

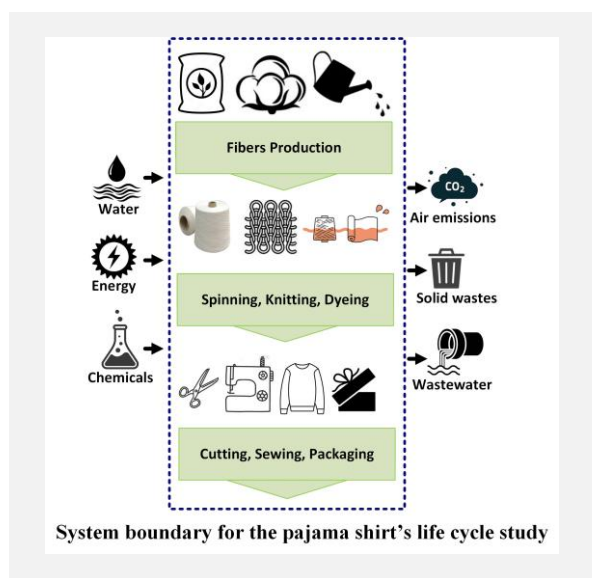
- [1] Sonnendecker et al., *ChemSusChem*, 15 (2022) e202200696.
- [2] Jiang et al., *Polymers*, 13 (2021) 2730.
- [3] Schyns and Shaver, *Macromolecular Rapid Communications*, 42 (2021) 1-27.
- [4] Qin et al., *ChemSusChem*, (2021) 3975.
- [5] Wei and Zimmermann, *Microbial Biotechnology*, 10 (2017) 1308-1322.
- [6] Toledo et al., *ACS Sustainable Chemistry & Engineering*, 7 (2019) 11806-11814.
- [7] Pande et al., *Journal of Biomolecular Structure and Dynamics*, (2021) 1-11.
- [8] Ferreira et al., *Molecules*, 27 (2022) 98.

Life cycle environmental impact assessment of a pajama shirt

A.A. Martins^{1*}, R. Lapa¹, B. Mota¹, S. Maia¹, J.C.G.E. da Silva², C. Soares³, T.M. Mata^{4*}

¹University of Porto - Faculty of Engineering / LEPABE — Laboratory for Process Engineering, Environment, Biotechnology and Energy / ALICE — Associate Laboratory in Chemical Engineering, Portugal; ²Chemistry Research Unit (CIQUP), Institute of Molecular Sciences (IMS), DGAOT, Faculty of Sciences of University of Porto (FCUP), Rua do Campo Alegre s/n, 4169-007 Porto, Portugal; ³IMPETUS Portugal-têxteis SA, Estr. da Praia 1755, 4740-696 Barqueiros, Portugal; ⁴LAETA—INEGI, Associated Laboratory for Energy and Aeronautics — Institute of Science and Innovation in Mechanical and Industrial Engineering, Portugal.

*aamartins@fe.up.pt; tmata@inegi.up.pt



The textile industry is widely recognized as one of the most polluting industries in the world. It generates significant environmental impacts throughout its supply chain, from raw materials production to manufacturing, distribution, and disposal of textile products. Thus, understanding the environmental impacts of textiles helps identify areas for improvement and allows consumers, businesses, and policymakers to make informed decisions regarding sustainable and responsible consumption. Hence, this work evaluates the life cycle environmental impacts of a nightwear shirt on a “cradle-to-gate” approach. For the environmental impacts’ evaluation both the SimaPro LCA software and the Higg Index webtool were used, considering the same data and five impact categories. The results revealed that the life cycle stages that contribute most to the impacts are organic cotton production and spinning, elastane production and spinning, and dyeing. Although both LCA tools are useful to provide textile companies with reasonable estimates of the environmental impacts of their products, SimaPro allows geographically specific data to be defined, which in certain situations can mean significant differences in the assessment performed.

Introduction

The textile and fashion industry are among the most relevant industrial sectors in the European Union (EU) in terms of employment and added value created. Due to its intensive consumption of materials, chemicals and energy, and the generation of significant amounts of waste and emissions throughout the supply chain, significant environmental impacts result from the textile industry activities [1]. Thus, the EU has defined a specific strategy to improve this sector sustainability, considering all steps of the supply chain and the products life cycle.

In order to improve the environmental performance of the textile industry it is necessary to objectively evaluate the current life cycle impacts of the production systems on a “cradle-to-grave” perspective (i.e. from raw materials extraction to the end of life). In this context, it is important to ensure that all relevant aspects of the production system, including the supply chain, are considered [2]. Such analysis can be done using the LCA methodology [3]. Due to the complexity of its application, in particular in industrial practice, LCA software (e.g., SimaPro) and web-based tools (e.g., Higg Index) were developed for specific sectors and/or industries [4]. Although simplifying the application of LCA in practice it is unclear how credible are the results obtained by these tools.

Methodology

The LCA methodology was used for this study, in accordance with the ISO 14040 [5] and 14044 standards [6]. The functional unit chosen is 1 pajama shirt, size medium (M) as shown in Figure 1.



Figure 1. Pajama shirt, size M.

The study geographical coverage is Portugal, since the electricity mix, transport conditions, among others, considered are the Portuguese as much as possible. The LCA study is “cradle-to-gate”, which means that the life cycle stages included go from raw materials production/cultivation to the pajama shirt packaging and ready to leave the Portuguese textile company.

The system boundaries for the knit fabric and pajama shirt production, with the indication of the background and foreground processes, is shown in Figure 2.

Primary data from the industrial processes was used, as much as possible, complemented with data from the EcoInvent life cycle inventory database and the literature whenever necessary.

The same data and information and the same environmental impacts were considered for the calculations with Simapro V 8.5.2. and the Higg index. The impact categories considered in the LCA study include: eutrophication (ET), climate change (CC), water use (WU), freshwater ecotoxicity (FE=chemistry) and resource depletion – fossil fuels (AD).

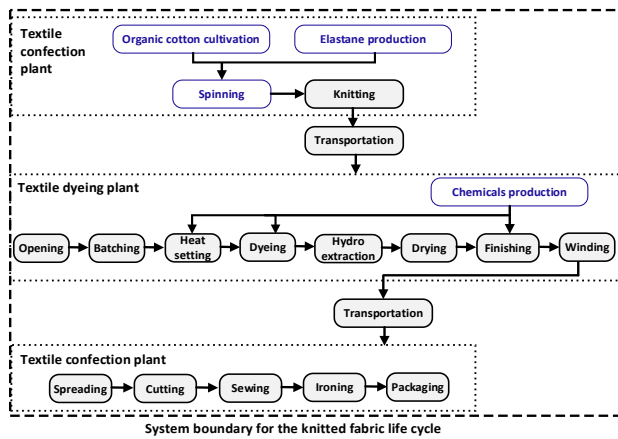


Figure 2. System boundaries for knitted fabric and pajama shirt production, with the background processes in blue and the foreground in black.

Results and Discussion

The relative importance of each life cycle stage, calculated using SimaPro for this LCA study, is presented in Figure 3.

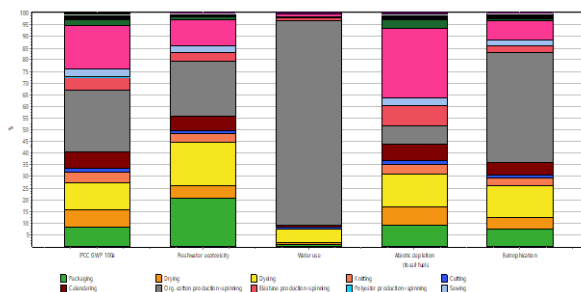


Figure 3. Contribution of the life cycle processes to the pajama shirt environmental impact categories studied.

It can be seen that the overall environmental impacts are controlled by few life cycle stages, in particular the production and spinning of organic cotton, elastane production and spinning, and dyeing. They correspond to the life cycle stages in which there is larger consumption of chemicals and energy, and in which efforts should be made first to reduce the overall environmental impacts. The remaining stages are less important, even though their relative importance depends on the environmental impact category. Thus, a focus should be given

Acknowledgements

This work was financially supported by base Funding of the following projects: IJUP2021- Impetus - 6, funded by IMPETUS Portugal-Têxteis SA, and LA/P/0045/2020 (ALiCE), UIDB/00511/2020 (LEPABE), UIDB/50022/2020 (LAETA), UIDB/50020/2020 and UIDP/50020/2020 (LSRE-LCM), funded by national funds through FCT/MCTES (PIDDAC). António Martins gratefully acknowledges the Portuguese national funding agency for science, research and technology (FCT) for funding through program DL 57/2016 – Norma transitória. Teresa Mata gratefully acknowledges the funding of Project NORTE-06-3559-FSE-000107, cofinanced by Programa Operacional Regional do Norte (NORTE2020), through Fundo Social Europeu (FSE).

References

- [1] S. Patwary, *Textile & Leather Review*, 3 (2020) 158-173.
- [2] K.J. Watson, S. G. Wiedemann, *Sustainability*, 11 (2019) 0-16.
- [3] H. Baumann, A.M. Tillman, *The Hitch Hiker's Guide to LCA - An orientation in life cycle assessment methodology and application*. 2004.
- [4] E. Chun et al., *Journal of Global Scholars of Marketing Science Bridging Asia and the World*, 31 (2021) 437-452.
- [5] ISO 14040, *Environmental management - Life cycle assessment - Principles and framework*. International Organization for Standardization, 2006.
- [6] ISO 14044, *Environmental management - Life cycle assessment - Requirements and guidelines*. International Organization for Standardization, 2006.
- [7] APREN, "Electricity Generation by Energy Sources in Mainland Portugal in 2022," 2022. <https://www.apren.pt/en/renewable-energies/production> (accessed Mar. 08, 2023).
- [8] H. Ritchie, M. Roser, "Electricity Mix," 2008. <https://ourworldindata.org/electricity-mix> (accessed Mar. 08, 2023).

to use fibers and dyeing methods with lower environmental impact.

In Table 1 the results from both SimaPro and Higg Index are presented, for the 5 environmental impact categories considered. It can be seen that larger values for climate change and resource depletion – fossil fuels are obtained for Higg index than for SimaPro, around two times larger, which can be explained by the different electricity mixes used in both LCA tools. In particular, SimaPro allows using the Portuguese electricity mix for the calculations, while the Higg Index considers for electricity the world average, which has a lower percentage of renewable energy than the Portuguese mix [7,8].

Table 1. Comparison between the SimaPro and Higg Index results.

Environmental Impact Category	SimaPro	Higg Index
Climate change (kg CO ₂ eq)	1.468	2.404
Eutrophication (kg PO ₄ eq)	0.00269	0.00232
Water use (m ³)	6.416	3.856
Resource depletion-fossil fuels (MJ)	14.318	27.212
Freshwater ecotoxicity/ Chemistry * (PAF.m ³ .day /units)	5029.5	5.375

*The Freshwater ecotoxicity/Chemistry impact categories were not compared since they are calculated differently with SimaPro and Higg Index, which also explains the different magnitude in the results obtained with both LCA tools.

Conclusions

This work performed an evaluation of the life cycle environmental impacts of a pajama shirt production. Results showed that organic cotton production and spinning, elastane production and spinning, and dyeing are the dominant life cycle steps in the overall pajama life cycle environmental impacts, depending their relative importance on the environmental impact category under consideration.

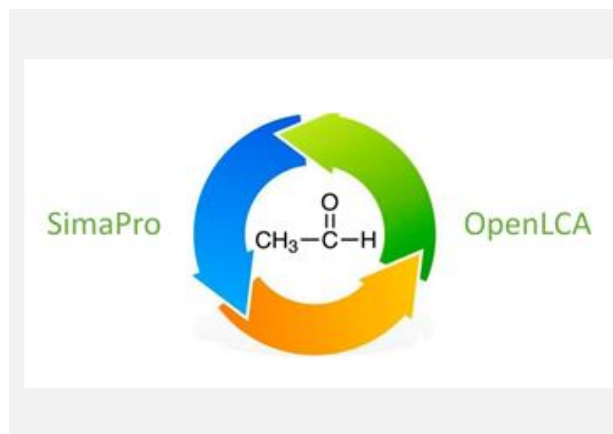
Regarding the comparison between the results obtained using the Higg index and the SimaPro LCA software, the results were similar for the ET category, but around two times larger for CC and AD categories. It can be concluded that Higg index is helpful in providing companies with reasonable estimates of the environmental impacts of their textile products. However, as certain choices are not available in this webtool, as for example, the location-specific electricity mix values or options for specific processes, the prediction could be far from reality, potentially penalizing companies that are, for example, investing strongly in using renewable energy.

Life cycle assessment: a comparison of different tools using an academic case study

R.N. Dias^{1*}, N. Stamatopoulou¹, R.M. Filipe^{1,2}, H.A. Matos¹

¹CERENA, Instituto Superior Técnico, Av. Rovisco Pais 1, 1049-001 Lisboa, Portugal; ²Instituto Superior de Engenharia de Lisboa, Instituto Politécnico de Lisboa, R. Conselheiro Emídio Navarro 1, Lisboa 1959-007, Portugal.

ricardo.n.dias@tecnico.ulisboa.pt



Every current project must have a feasibility study, that takes into consideration environmental impacts, and not just the economic viability. The introduction to design and modelling of chemical equipment poses a perfect opportunity to introduce sustainable development tools, such as LCA. In this paper, an approach to LCA through an open access LCA tool (OpenLCA) is proposed and the results corroborated using the commercial software SimaPro. Firstly, four alternatives of the process were modelled in Aspen Plus, and then implemented in SimaPro and OpenLCA. This implementation sequence follows a possible introductory course to the subjects of modelling and LCA. The four case studies intend to demonstrate the importance of optimised process conditions, energy integration and material recirculation, through quantitative analysis, using energy and material consumption and LCA.

Introduction

In the early 1980's the concept of sustainable development got momentum [1], and so did life cycle assessment (LCA), a methodology that intends to study the environmental impact of a given product in the society. LCA considers the complete life cycle of a product, from the material extraction from nature (cradle) to the disposal in a landfill or incineration, where its life ends (grave). LCA methods follow a set of guidelines from ISO 14040 [2] and ISO 14044 [3], which makes then a standardized method and can be relied on for environmental assessments.

Every current project must be assessed and supported by a feasibility study that takes into consideration not only the economic viability, but also its environmental impact. Training future engineers able to address sustainable process design is now a major concern. It is crucial that engineering students have a solid base upon which they feel comfortable working on, and simple and clear case studies are valuable to achieve this purpose. One such case study is the acetaldehyde production from the ethanol dehydration [4]. This case study can be implemented in any modelling tool and allows for an introduction to reactor and distillation column modelling. The introduction to the design and modelling of chemical process equipment is an opportunity to introduce sustainable development tools, such as LCA. After using a modelling tool to design and assess process alternatives, students can use a LCA analysis to further validate and support its results.

In this paper, an approach to LCA using an open access LCA tool (OpenLCA) is proposed, and the results are corroborated using SimaPro. Firstly, four alternatives of the process were modelled in Aspen Plus, and then implemented in SimaPro and OpenLCA. This implementation sequence follows a possible introductory course to the subjects of modelling and LCA. The four case studies intend to demonstrate the importance of

optimised process conditions, energy integration and material recirculation, through quantitative analysis, using energy and material consumption and LCA.

Methods

The acetaldehyde production from the dehydrogenation of ethanol was modelled using Aspen Plus. A representation of the base case modelled can be found on **Error! Reference source not found.1**. The ethanol is initially compressed, heated, and fed to the reactor, where the dehydrogenation reaction occurs. After exiting the reactor, the resulting stream is compressed, and the gaseous phase removed. The liquid phase is then expanded and fed to a distillation column, where the product is separated from the other components of the liquid stream. A set of alternative designs resulting from improvements to the base case, namely energy integration, recirculation of the unreacted ethanol, and a combination of both, was created. A total of four alternatives was used, as shown on Table 1.

Table 1. Brief description of the alternatives evaluated.

ALTERNATIVE	DESCRIPTION
V0	Base alternative
V1	Energy integration (EI)
V2	Recirculation (R)
V3	EI and R

This case study, with the different alternatives, was implemented in SimaPro and OpenLCA where the LCA analysis was carried out, using the Aspen Plus modelling results. The frontiers were set as the plant borders, and therefore, a gate-to-gate analysis was performed. The functional unit was defined as 1 kg of acetaldehyde production and the EF method [5] was used, following the European Union recommendation.

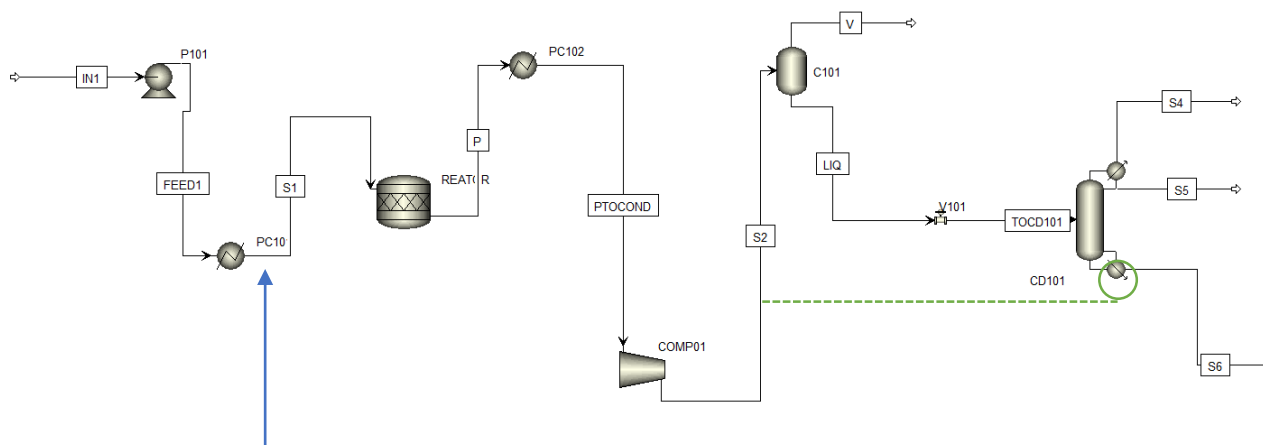


Figure 1. Flowsheet of the V0 alternative of the case study.

Results and discussion

The main results obtained with SimaPro and OpenLCA can be found on Table 2. It is possible to observe that the alternative V2 is the more sustainable, rather than V3, which was the one expected to be more sustainable, since it features energy and mass integration. This might be caused by the fact that to achieve convergence on the V3 simulation, there is ethanol and acetaldehyde that is lost on the gaseous purge stream, V on **Error! Reference source not found.** 1.

Table 2. Single score results for the acetaldehyde case study, and ranking classification.

ALTERNATIVE	SIMAPRO (RANK)	OPENLCA (RANK)
V0	1.52 (4)	0.952(3)
V1	1.51 (3)	0.953(4)
V2	0.96 (1)	0.247(1)
V3	0.99 (2)	0.305(2)

Table 2 also shows that the final decision on which is the more sustainable alternative is the same for both tools. This was expected since both tools use the same databases and the same evaluation method, although the Ecoinvent database used in OpenLCA is not up to date.

Acknowledgements

The present work was financed by the Portuguese Foundation for Technology and Science (FCT) PTDC/EAM-PEC/32342/2017 and CERENA strategic project FCT-UIDB/04028/2020. This support is gratefully appreciated.

References

- [1] A.F. Mimoso et al., Journal of Cleaner Production, 90 (2015) 128-141.
- [2] The International Standards Organisation, ISO 14040:2006.
- [3] International Organization for Standardization (ISO), "ISO 14044 Environmental Management-Life Cycle Assessment Requirements and Guidelines," 2006, Accessed: Mar. 07, 2023. [Online]. Available: <https://www.iso.org/standard/37456.html>
- [4] P. Khamhaeng, P. Kim-Lohsoontorn, IOP Conference Series: Materials Science and Engineering, 2020.
- [5] European Commission, "Recommendations on the use of the Environmental Footprint methods to measure and communicate the life cycle environmental performance of products and organisations", Official Journal of the European Union, 2021.

The more influential indicators were determined to be the land use on SimaPro and Photochemical ozone formation on OpenLCA.

Conclusions and future work

LCA analysis is nowadays a requirement for a growing number of projects, and therefore there is a need for LCA outreach. Most of the current LCA tools are paid, which limits the access of many people to it. OpenLCA is a free platform that anyone can use, making it easier for engineering students to engage with LCA. In this work, a well-known academic case study was used to implement an LCA analysis both with SimaPro and OpenLCA.

Four alternatives were created by implementing variations of the original process with the aim of increasing the efficiency, as well as the sustainability of the process. SimaPro was used to provide a well-established and reference analysis for comparison with the OpenLCA analysis that was also implemented.

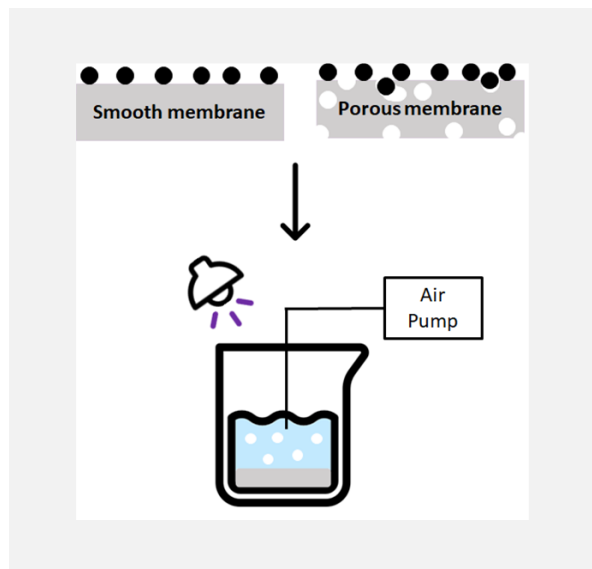
The results obtained with OpenLCA are comparable to the ones obtained with SimaPro, with the ranking results being the same. We conclude that this is an interesting case study for LCA analysis and that the use of the free OpenLCA tool is an attractive option, particularly for academic purposes

Porous PDMS membranes as P25 supports for the photocatalytic degradation of parabens

M.J. Silva¹*, R. Alves¹, P. Alves¹, J. Gomes¹, P. Ferreira^{1,2}, R.C. Martins¹

¹University of Coimbra, CIEPQPF – Chemical Engineering Process and Forest Products Research Center, Rua Sílvio Lima Polo II 3030-790, Coimbra, Portugal; ²Department of Chemical and Biological Engineering, Coimbra Institute of Engineering, Rua Pedro Nunes 3030-199, Coimbra, Portugal.

*mariaj@eq.uc.pt.



Heterogeneous photocatalysis is a suitable technology for the removal of contaminants of emerging concern from waters and wastewaters, such as parabens. However, usually photocatalysis is performed with the photocatalyst in suspension, which requires time-consuming and costly supplementary separation processes. As such, heterogeneous supported photocatalysis has gained interest in the scientific community. To develop a suitable supported photocatalyst, commercial TiO₂ (P25) powder was immobilized in polydimethylsiloxane (PDMS) membranes either in their surface or matrix. To enhance the membranes' stickiness and surface area, by increasing their porosity, solvents were added to the membranes' formulation and, to improve their hydrophilicity, a plasma process was applied. It was concluded that the immobilization on the surface is the most effective methodology, and that the addition of solvents needs to be optimized, to obtain the targeted results. The smooth membranes with the photocatalyst on their surface were able to remove ~55% of paraben, while with the porous membranes just ~33% of removal was obtained.

Introduction

Recently, contaminants of emerging concern, which possess a risk to environmental and human health, have been detected in waters and wastewaters [1,2]. These pollutants are persistent and hard to degrade by conventional treatment technologies, inevitably ending up in natural water resources [2,3].

Advanced oxidation processes are effective in the oxidation of numerous pollutants [3]. Photocatalysis stands out due to its advantages: simplicity, cost-efficiency and promising approach for full scale use [4,5]. But, as typically the photocatalyst is used in suspension, expensive and time-consuming processes are necessary for its recovery [4,6]. As such, a promising technology is supported photocatalysis. Among the supports, polymeric materials, such as polydimethylsiloxane (PDMS), are an encouraging option [4,6]. PDMS has been studied given its sticky surface, transparency, stability under irradiation, flexibility, chemical stability against the corrosive effect of photocatalysts and thermal resistance [4, 7]. Yet, PDMS is hydrophobic, showing low affinity towards water [5], which compromises the contact between the pollutants and the photocatalyst.

In this work, PDMS was selected as the substrate for P25, which was immobilized in the polymer matrix, by entrapping the photocatalyst, or in the surface, through a grafting process. This work aims to boost the characteristics of the membranes, for use in wastewaters treatment. Thus, as PDMS is hydrophobic, a plasma treatment was applied to improve its hydrophilicity and, to enhance the membranes' stickiness and surface area (by increasing the porosity), a solvent was added to the formulation.

Materials and Methods

The synthetic wastewater contained 1 mg/L of each paraben: methylparaben (MP), ethylparaben (EP) and propylparaben (PP). P25 was chosen as the photocatalyst. Sylgard® 184, a PDMS kit, that contains the prepolymer and curing agent, was used.

In the present study, smooth and porous membranes, without and with photocatalyst were prepared. To produce (i) smooth PDMS membranes, protocol I was applied, (ii) smooth P25/PDMS membranes, protocols II and III were followed, (iii) porous PDMS membranes, protocol IV was implemented and (v) porous P25/PDMS, protocols V and VI were used. The membranes were named after the protocol utilized. Table 1 explains the conditions used to produce the different membranes. Protocol I, II, IV and V: The compounds presented in Table 1 were mixed. The mixture was later degassed, cured, washed with acetone and plasma treated. Protocol III and VI: The compounds presented in Table 1 were mixed. The mixture was later degassed, cured and plasma treated. Later, the membranes were subjected to a grafting process, washed with distilled water and dried at room temperature, until constant weight.

For the photocatalytic experiments, 50 ml of the wastewater were used and mixed by bubbling air. The membranes were placed at the bottom of the reactor and on top of the reactor was placed a UV-A lamp with an irradiance of 0.014 mW/cm² and which main wavelength peak emission was at 365 nm. The reactor was placed in a box with a reflective interior surface. The experiments were performed for 2 h and in duplicate.

The parabens concentration was followed through high performance liquid chromatography, with a C18 column, at 40 °C and 255 nm. The injection volume of the samples was 100 µL and the mobile phase (1 mL/min) consisted in a 50:50 (v/v) mixture of methanol and 0.1 w/w% H₃PO₄ aqueous solution.

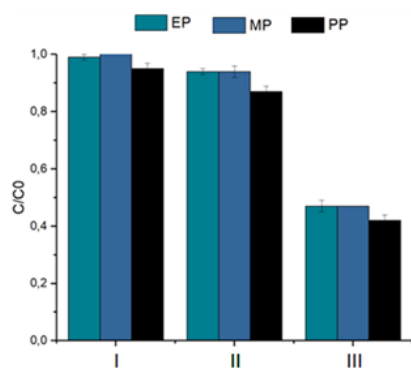


Figure 1. Photocatalytic degradation achieved by smooth membranes.

Results

The performance results of smooth and porous membranes in the photocatalytic degradation of parabens are illustrated in Figures 1 and 2, respectively. It is worth stating that no adsorption was verified for the different membranes. By analyzing Figures 1 and 2, it can be seen that the introduction of a photocatalyst in the formulation of the membranes allows to attribute them photocatalytic activity. In addition, it is also verified that in both scenarios, the immobilization of the photocatalyst on the surface is the most effective methodology, which can be speculated to be a consequence of a higher amount of photocatalyst available for the wastewater treatment process. In the future, to verify this hypothesis, the membranes should be characterized by SEM_EDS. Comparing Figures 1 and 2, it can be concluded that the introduction of ethanol in the membrane formulation did not have the desired effect, since

porous membranes have a lower photocatalytic performance. However, this may be improved if the following parameters were optimized: (i) the selected solvent, (ii) the amount of solvent used, (iii) the amount of photocatalyst added and (iv) the plasma process conditions.

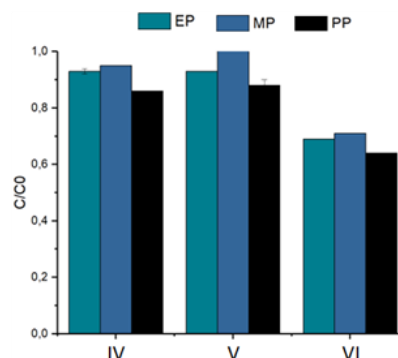


Figure 2. Photocatalytic degradation achieved by porous membranes.

Conclusions

From this study it was concluded that (i) PDMS is an adequate support for P25, (ii) the introduction of P25 conferred photocatalytic activity to the membranes, (iii) the immobilization on the surface is the most effective methodology and (iv) the use of porous membranes is an interesting technology, but requires further optimization. Additionally, characterization tests, such as WCA, AFM and SEM_EDS, need to be conducted to better understand and compare the photocatalytic performance of the different membranes.

Table 1. Conditions for the preparation of the membranes.

Preparation Conditions	Protocol I	Protocol II	Protocol III	Protocol IV	Protocol V	Protocol VI
Reagents	3 g prepolymer 0.3 g curing agent	3 g prepolymer 0.3 g curing agent 3.81 mg P25	3 g prepolymer 0.3 g curing agent	3 g prepolymer 0.3 g curing agent 3 g ethanol	3 g prepolymer 0.3 g curing agent 3 g ethanol 3.81 mg P25	3 g prepolymer 0.3 g curing agent 3 g ethanol
Degassing Step	Under vacuum 30 min	Under vacuum 30 min	Under vacuum 30 min	Ultrasound bath 10 min	Ultrasound bath 10 min	Ultrasound bath 10 min
Curation Step	65 °C ; 4 h	65 °C ; 4 h	65 °C ; 4 h	Room temperature 3 days	Room temperature 3 days	Room temperature 3 days
Plasma Treatment Grafting Process parameters	100 W; 0.6 mbar Argon ; 4 min	100 W; 0.6 mbar Argon ; 4 min	100 W; 0.6 mbar Argon ; 4 min Membrane placed in a UV chamber (0.63 mW/m ²) for 1 h and immersed in P25 aqueous dispersion (30 mL ; 210 mg/L)	100 W; 0.6 mbar Argon ; 4 min	100 W; 0.6 mbar Argon ; 4 min	100 W; 0.6 mbar Argon ; 4 min Membrane placed in a UV chamber (0.63 mW/m ²) for 1 h and immersed in P25 aqueous dispersion (30 mL ; 210 mg/L)

Acknowledgements

This research was funded by the European Union through the European Fund for Regional Development (FEDER) within the framework COMPETE 2020 by the financial support of the project POCI-01-0247-FEDER-047545 (PhotoSupCatal – Development of supported catalytic systems for wastewater treatment by photo-assisted processes). The authors Maria João Silva and João Gomes gratefully acknowledge Foundation for Science and Technology Portugal for the PhD Grant (2022.09787.BD) and for the financial support (CEECIND/01207/2018), respectively. Thanks are due to FCT/MCTES for the financial support to CIEPQPF (UIDB/00102/2020).

References

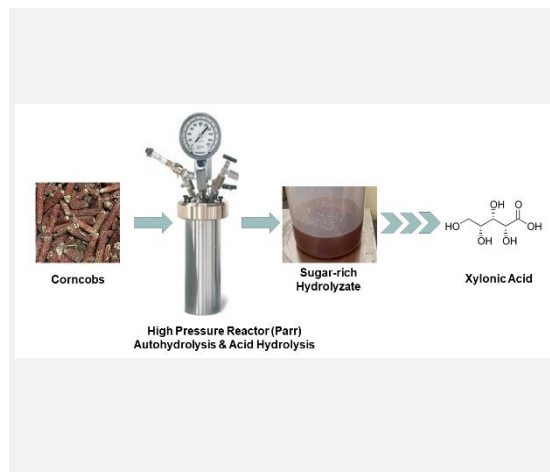
- [1] J. Lincho et al., Applied Sciences, 11 (2021) 2307.
- [2] N. Bolong et al., Desalination, 239 (2009) 229-246.
- [3] J. Rivera-Utrilla et al., Chemosphere, 93 (2013) 1268-1287.
- [4] M.J. Silva et al., Water, 14 (2022) 825.
- [5] H.O. Gomes et al., Journal of Water Process Engineering, 46 (2022) 102458.
- [6] H.S. Zakria et al., RCS Advances, 11 (2021) 6985.
- [7] I.M. Sosnin et al., Reactive and Functional Polymers, 158 (2021) 104781.

Catalytic conversion of hemicellulose-derived pentoses into sugar/aliphatic acids

V. Van-Dúnem^{1,2*}, L.C. Duarte¹, L.M.D.R.S. Martins², F. Carvalheiro¹

¹Unidade de Bioenergia e Biorrefinarias, LNEG – Laboratório Nacional de Energia e Geologia, Estrada do Paço do Lumiar, 22, 1649-038 Lisboa, Portugal; ²Centro de Química Estrutural, Institute of Molecular Sciences, Departamento de Engenharia Química, Instituto Superior Técnico, Universidade de Lisboa, Av. Rovisco Pais, 1049-001 Lisboa, Portugal

*vanmira.vandunem@lneg.pt



Xylose is the second most abundant carbohydrate in nature and its efficient utilization is a prerequisite and a crucial factor in achieving the high-value utilization of lignocellulosic biomass resources.

In this work, we studied the application of a palladium (IV) $[\text{Pd}(\text{C}_{12}\text{H}_{14}\text{N}_5\text{O})]@\text{SiO}_2$ and C-scorpionate gold(III) $[\text{AuCl}_2(\text{HCpz}_3)]\text{Cl}$ (pz = pyrazolyl)catalysts on the oxidation of D-xylose into value-added sugar acids/aliphatic acids under mild conditions. This strategy was applied to both D-xylose solutions and to pentose-rich hydrolysates obtained from corncobs fractionation, both by mild direct dilute acid hydrolysis and autohydrolysis followed by dilute acid post-hydrolysis.

Data obtained show that both catalysts can effectively catalyze pentose oxidation reactions under mild ($<100\text{ }^\circ\text{C}$) conditions. Reaction yields, selectivity, and kinetics are comparable for both catalysts, with $[\text{Pd}(\text{C}_{12}\text{H}_{14}\text{N}_5\text{O})]@\text{SiO}_2$ exhibiting slightly better kinetic performance and $[\text{AuCl}_2(\text{HCpz}_3)]\text{Cl}$ complex slightly better selectivity to xyloonic acid.

Introduction

The use of biomass resources to achieve sustainable economic growth relies on the development of the biorefinery concept. Biomass is composed of three main polymers, cellulose, hemicellulose, and lignin. In contrast to cellulose, for which many applications have already been found, hemicelluloses, namely their derived pentoses conversion, still need to be studied. Xylose is the second most abundant carbohydrate in nature and its efficient utilization is a prerequisite and a crucial factor in achieving the high-value utilization of lignocellulosic biomass resources.

Within the biorefinery, the (bio)chemical platform is considered the best option to produce value-added compounds from biomass, which can be developed based on the use of fermentation processes or alternative chemical pathways, which are faster and with potential economic advantages. In this framework, xylose can be converted into various chemicals, including xyloonic acid, lactic acid, formic acid, acetic acid, and xylitol, via redox reactions [1].

Considering the high value of sugar acids, a new route that consists of the catalytic conversion of pentoses to sugar acids/aliphatic acids using innovative palladium and C-scorpionate gold catalysts was studied. This included the application of those catalysts in the oxidation of D-xylose into value-added sugar acids. These studies were developed using both D-xylose solutions and pentose-rich hydrolysates obtained from the hydrolysis of corncobs, a xylan rich-material, and a relevant agriculture byproduct highly available worldwide at low cost.

Objectives

The aim of this work is the development of new processing routes that enable the selective valorization of lignocellulosic biomass-derived pentose sugars into innovative value-added chemicals within the biorefinery framework.

The upgrade strategy encompasses the recovery of monomeric pentoses from corncobs using two alternative routes [2]:

- Autohydrolysis (A) followed by Dilute Acid Post-hydrolysis (B)
- Mild Direct Dilute Acid Hydrolysis (C)

Followed by their conversion into the corresponding sugar acids/aliphatic acids using C-scorpionate complexes as green catalysts through chemical oxidation.

Methods

Corncobs were kindly provided by Estação Nacional de Melhoramento de Plantas (Elvas, Portugal), dried, milled ($<6\text{ mm}$), and stored in closed plastic containers. Its chemical characterization according to NREL protocols [3] yielded the following composition (expressed on a dry mass basis): 32% glucan, 32% xylan, 5.0% arabinan, 4.0% acetyl groups, 17.0% total lignin, and others (10.0%).

Pentose-containing hydrolysates were obtained by autohydrolysis and very dilute acid hydrolysis of corncobs in a 600 mL reactor (Parr, USA) as optimized before [3]. Both processes were carried out under non-isothermal conditions up to a final temperature of $200\text{ }^\circ\text{C}$. A liquid-to-solid ratio (LSR) of 8 (g/g) was used in both cases, either with water or a 25 mM H_2SO_4 solution.

The production of monomeric pentoses from autohydrolysis liquors was carried out through dilute acid post-hydrolysis at $121\text{ }^\circ\text{C}$, for 60 min, and a catalyst concentration of 1% H_2SO_4 , as also previously optimized [2].

The selective oxidation of pentose sugars was studied using $[\text{Pd}(\text{C}_{12}\text{H}_{14}\text{N}_5\text{O})]@\text{SiO}_2$ or $[\text{AuCl}_2(\text{HCpz}_3)]\text{Cl}$ (pz = pyrazolyl) as catalysts. The experiments were carried out using either a D-xylose aqueous model solution (40 mmol/L) or the hydrolysates diluted to similar xylose concentration, 20 μmol of catalyst, 10 mmol of H_2O_2 . The influence of temperature was studied in the range of $20\text{ }^\circ\text{C}$ to $100\text{ }^\circ\text{C}$ and in the presence or absence of a base (Na_2CO_3 , 0.1 mmol).

The identification and quantification of monosaccharides (xylose, arabinose, and glucose), formic and aliphatic acids were carried out by HPLC, equipped with a refractive index (RI) detector and a diode array detector (DAD), using an Aminex HPX-87H column (Bio-Rad, Hercules, USA) at a flow rate of 0.6 mL/min.

Results

The chemical composition of hemicellulosic hydrolysates obtained from autohydrolysis (A), autohydrolysis + dilute acid post-hydrolysis (B) and very diluted hydrolysis of corncobs is shown in Table 1.

Table 1. Composition (g/L) of the liquors obtained from A: autohydrolysis, B: autohydrolysis followed by dilute acid post-hydrolysis, and C: very diluted acid hydrolysis of corncobs.

Component	A	B	C
Glucooligosaccharides	1.71	--	0.70
(Arabino)xylooligosaccharides	29.28	--	0.12
Glucose	0.20	1.71	2.82
Xylose	1.26	33.40	36.18
Arabinose	1.25	3.02	3.59
Acetic Acid	1.28	4.24	4.22
Formic Acid	0.27	0.57	--
Furfural	0.37	0.90	3.40
Hydroxymethylfurfural	0.09	0.10	0.31

Hydrolysates obtained by the autohydrolysis process were rich in pentoses, containing 29 g/L oligomeric pentoses (of which 28 g/L are xylooligosaccharides, XOS) and low concentration of monomeric pentoses. Very diluted acid hydrolysis was the best method to obtain a high concentration of monomeric pentoses, producing 36 g/L of xylose. As corncobs hemicelluloses are moderately acetylated, acetic acid was also found, although its concentration is higher for hydrolysates obtained under acidic conditions.

The hydrolysates obtained by autohydrolysis, and by autohydrolysis followed by dilute acid post-hydrolysis contain

very low concentrations of furans, the most relevant sugar degradation products under acidic conditions, reaching in total < 1g/L, with furfural being the most relevant single furan present. Conversely, the hydrolysates obtained by very diluted acid hydrolysis contain a higher amount of furans, from which furfural represents almost 10% of the pentoses present.

The oxidation of D-xylose was examined over the palladium catalyst and C-scorpionate Gold (III) complex.

With the palladium catalyst, the best results were achieved after 24 h at 20 °C. Under these conditions, a relevant conversion of xylose into sugars acids, namely xylonic acid, occurred (yield *ca.* 30%).

When the reaction was performed using the C-scorpionate gold complex the maximum yield was obtained after 48 h, at 80 °C without the presence of base (Na₂CO₃). Under these conditions, there was also a significant conversion of xylose into aliphatic acids, namely formic acid. Oxidation reactions of D-xylose using corncobs hydrolysates obtained from different treatments were evaluated. Data obtained are being analyzed compared with those obtained with pure D-xylose solutions.

Conclusions

All the fractionation methods tested were highly selective towards corncobs hemicellulose. High recovery of XOS could be obtained under relatively mild autohydrolysis conditions whereas very dilute acid hydrolysis favours the production of monomeric pentoses at a high yield.

Regarding acids production, both catalysts ([AuCl₂(HCpz₃)]Cl and [Pd(C₁₂H₁₄N₅O)]@SiO₂) enable the production of xylonic acid, with the latter exhibiting a slightly faster kinetic.

Acknowledgements

This work was carried out at the Biomass and Bioenergy Research Infrastructure (BBRI), Centro de Química Estrutural, (CQE) and Institute of Molecular Sciences (IMS). BBRI is funded by the BBRI-LISBOA-01-0145-FEDER-022059 project that is supported by the Operational Programme for Competitiveness and Internationalization (PORTUGAL2020), by Lisbon Portugal Regional Operational Programme (Lisboa 2020) and by North Portugal Regional Operational Programme (Norte 2020) under the Portugal 2020 Partnership Agreement, through the European Regional Development Fund (ERDF). Centro de Química Estrutural (CQE) is a Research Unit funded by Fundação para a Ciência e Tecnologia through projects UIDB/00100/2020 and UIDP/00100/2020. IMS is an Associate Laboratory funded by FCT through project LA/P/0056/2020. Vanmira Van-Dúnem gratefully acknowledges the Ph.D. grant from FCT (2020.05991.BD).

References

- [1] D. Ji et al., Fuel, 14 (2022) 122773.
- [2] V. Van-Dúnem et al., Poster EUBCE 2022 – European Biomass Conference & Exhibition, Online & Marseille.
- [3] A. Sluiter et al., NREL Laboratory Analytical Procedures: Determination of Structural Carbohydrates and Lignin in Biomass. NREL/TP-510-42618 (2012).

Analysis of energy transition scenarios in industry, using RETScreen

B. Moreira¹, C.G. Braz^{2*}, M.C. Fernandes¹

¹CERENA, Department of Chemical Engineering, Instituto Superior Técnico, Universidade de Lisboa, Av. Rovisco Pais 1, Lisboa, Portugal, Portugal; ²Industrial Process and Energy Systems Engineering (IPESE), École Polytechnique Fédérale de Lausanne, Lausanne, Switzerland.

*catarina.braz@epfl.ch



Energy management has become a crucial strategic priority for industries, particularly considering the volatile nature of resource prices and the increasingly urgent need to address the current climate situation, as it enables companies to optimize energy efficiency, reduce energy costs and carbon emissions, thus ensuring long-term sustainability and competitiveness in a rapidly changing economic and environmental landscape.

RETScreen Expert is a tool used to study energy management. The program allows tracking all stages in project development, from goal setting to feasibility studies, and to compare the actual project performance with calculated estimates.

A textile plant was studied to define potential modifications to improve energy efficiency and reduce energy costs and emissions. Solar panels, biomass and electric boilers were some of the projects analyzed.

Introduction

The objective of this work is to explore the potential of the RETScreen Expert program in the Portuguese industry, more specifically in the textile industry, as a medium sized facility in the northern Portugal. The case under study is a textile factory capable of performing all stages of the production process. Therefore, a comprehensive understanding of the entire process is necessary to perform a proper energy assessment, with that in mind, the company required an energy audit for the year 2021 [1]. Starting from the definition of the base scenario of the studied factory, the intention is to analyze from both an environmental and financial point of view, not only the current situation of the installation but also the implementation of measures that improve the unit's energy efficiency. To establish the actual energetical outlook the main source of data is the energy audit that not only describes the energy consumption, but also desegregates it, so it is possible to identify the major consumptions and elaborate improvements.

The results obtained should guide those responsible regarding the measures to be adopted to improve the factory's energy management. The opportunities studied can be divided into two types of measures: process optimization, and replacement of equipment with updated versions. Normally, special attention is given to optimization measures, since the replacement of equipment, considering only the improvement in energy efficiency, may not be justified due to the high initial investment.

RETScreen Methodology

Over the past decade, several studies and analyses have been conducted using the RETScreen software. Although the program's advantages are undeniable, there is still room for improvement. The software is governed by input/output methods, which means that the more accurate and detailed the data provided by the user, the more exhaustive and reliable the output generated. One of the system's greatest advantages is the thoroughness of the economic analysis, which provides the user with extensive data and several comparison tools [2].

However, some of the weaknesses are: the time-step of the program, which is monthly and does not allow the user to analyze hourly data; the difficulty in sharing information; the inability to perform more advanced calculations [3] and the fact that the software does not provide an optimization tool [4]. Nevertheless, this software is used globally to execute financial assessments of systems generating renewable energy [3].

As represented in the visual abstract, the workflow of the RETScreen software is divided into three main analyses.

Benchmark

The first step is defining that the facility is located in Barcelos, after that the program gathers the meteorological data from the nearest weather station, then once the facility type is defined as industrial textiles, the program calculates the project's benchmark. All calculations performed by the software are developed using the values on the several databases integrated.

Feasibility Analysis

The feasibility analysis is essential to describe the facility and segregate all the costs and consumptions. Beginning with the energy method, the fuels being used were defined along with their prices for the first quarter of 2023 and also the working schedules of the three different production stations, in this specific. The last information needed to describe the energy outlook is the segregation of the energy end-use, including the description of all the equipment used and the process heat, and the steam production and use.

If the purpose of using the software is to analyze a specific change, on all the steps mentioned so far, it is possible to add a proposed case and specify the details of the new equipment, or in case the change is the optimization of the fuels' supply, there is the option to simulate the generation of heat and power through different sources.

The following analysis is the costs associated with the project. It is possible to discriminate the annual costs, the annual savings, and if it applies, the periodic costs. The depth of the costs' description depends on the level chosen, with level 1 being the simplest and level 3 being the most thorough. The

same happens in the emission analysis, where, in level 3, it is possible to define the greenhouse gases' emission factors, the electricity generation efficiencies, and the transport and distribution losses. Finally, there is a financial analysis that, being provided with the company's financial parameters and annual revenues, generates the yearly cash flows, and calculates all the indicators needed to evaluate the financial viability of the project. The last and optional step of the feasibility analysis is the financial sensitivity and risk analysis.

Performance

As previously mentioned, the third main analysis is focused on evaluating the project's performance by comparing the estimates generated by the program with actual user-provided data. After manually inputting all relevant data, the program provides a range of graphs for data comparison and an option to establish a baseline. The methodology employed for this study aligns with the aforementioned process.

Factory Presentation

The industrial unit to be analyzed is responsible for several stages of the textile process, starting with weaving, followed by modeling, cutting, confection, printing, laundry, dyeing, and finally packaging, Figure 1. The manufacturing is the only process that is outsourced.

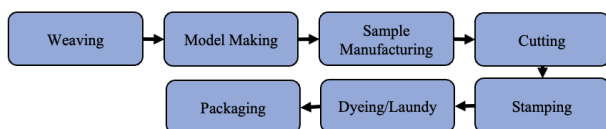


Figure 1. Production process flowchart.

The company positions itself in the international market, exporting 100% of its production. In 2021, almost 2.5 million pieces of clothing were produced. The facility being assessed is composed by an office area, the production zone, the loading dock, the parking area, and the wastewater treatment plant, currently employing 72 workers.

Currently, the factory uses three fuels that cover the energy consumption of the entire organization, namely electricity, natural gas, and diesel, Figure 2. Regarding the final application of energy in this sector, the main electrical consumption is associated with the dyeing/washing and printing processes, representing almost 45% of the total consumption, with the former heating the water used through a heat transfer with the steam produced on-site. The consumed steam comes from two boilers, which operate alternately, their consumption corresponds to 98,9% of the natural gas used annually. The company's fleet is responsible for all diesel consumption.

Currently, among the three energy sources, almost 90% of the emissions result from natural gas burning. The factory has already been in the process of energy transition for several years, and as such, some energy improvement measures have

Acknowledgements

The authors gratefully acknowledge the support of the CERENA (strategic project FCT-UID/ECI/04028/2019).

References

- [1] B.F. Peixoto, Relatório de Auditoria Energética e PREN, 2022.
- [2] M. Weiwu et al., Energy, 159 (2018) 385-409
- [3] S. Sinha, S.S. Chandel, Renewable and Sustainable Energy Reviews, 32 (2014) 192-205
- [4] L. Kyoung-Ho et al., Energy, 47 (2012) 83-96

already been implemented. However, there is still ample room for improvement, with the main focus of the studied measures being the reduction of fuel consumption and of the energy invoice.

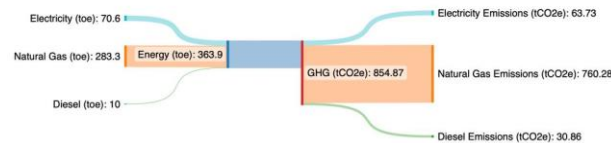


Figure 2. Energetical description of the industrial unit.

Results and Conclusions

Regarding the use of natural gas, the alternative analyzed is the replacement of equipment. As for the thermofixation oven, which uses the burning of natural gas to obtain heat, there are already equipment available on the market that perform the same process, using only electricity as fuel. Using the program to simulate the substitution of the existing equipment for a 100% electric equivalent the fuel consumption would decrease from 62,6 MWh per year to 50,5 MWh, which corresponds to a 19,2% reduction. In terms of emissions, the new equipment would be responsible for the emission of 9,8 tCO₂e per year, provoking a reduction of 22,5% when compared to que 12,6 tCO₂e of the current scenario. Calculating the cost of the fuel in both scenarios, using the prices for the first quarter of 2023, the substitution of natural gas for electricity would reflect on a 26,8% decrease.

In the case of steam boilers, there are alternatives such as electric and biomass boilers, however an energy, economic and environmental analysis is necessary to conclude whether the replacement is viable and which alternative is best.

Even though same measures such as replacement of the lightning and wastewater heat recovery can be implemented, reducing electricity usage is an extremely challenging goal, given that it is an industry. Consequently, the scenario of renewable energy production on site and possible models for its implementation are analyzed.

Finally, reducing diesel consumption can only be achieved by replacing the fleet, however, within the scope of this measure, different approaches can be followed, and the chosen one will certainly be the one that presents the best long-term results, according to the resources currently available.

Several alternatives presented would contribute greatly to the reduction of the unit's emissions, which is simultaneously one of the goals in an energy transition.

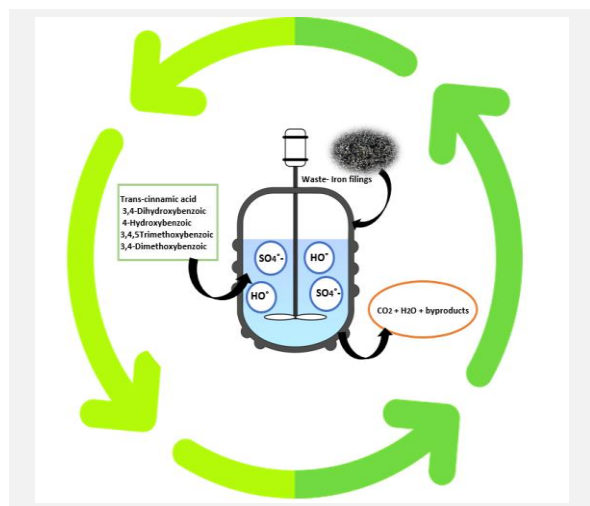
The measures mentioned above were analyzed using the software under study, and it is possible to conclude that, despite some limitations in the level of detail that can be provided for the current scenario, it is a tool capable of performing a first feasibility analysis of singular measures. Therefore, the program can be used by those responsible when deciding whether a more detailed study is advantageous.

Persulfate process activated by heterogeneous catalyst for synthetic olive mill wastewater treatment

T. Vaz*, M. Quina, R. Martins, J. Gomes

CIEQPQF—Chemical Engineering Processes and Forest Products Research Center, Department of Chemical Engineering, Faculty of Sciences and Technology, University of Coimbra, Rua Silvio Lima, 3030-790 Coimbra, Portugal.

*telma@eq.uc.pt



Water is an essential resource for sustaining life. Nonetheless, it is one of the most threatened resources in the world, either for its increasing consumption, climate change, or due to its lack of quality. The Mediterranean countries are the largest producers of olive oil, an industry that consumes large amounts of water and produces effluent with high organic load, olive mill wastewater (OMW). In addition, these countries suffer from severe droughts, which turns urgent to treat this effluent to be reused or recycled into water courses. Bearing in mind the concept of circular economy, this work focuses on the treatment of a synthetic effluent composed of five common phenolic compounds present in OMW using sulfate radical-based advanced oxidation processes (Persulfate-PS) activated by an industrial waste, iron filings. Removal of 59% was achieved with a persulfate dosage of 750 mg/L and pH of 3 after 3 hours of reaction.

Introduction

In the last years, freshwater sources have been threatened by the introduction of insufficiently treated and untreated water resulting from the growth of industrialization and urbanization. The olive oil industry is a relevant key in the economic development of Mediterranean countries, but it is responsible for large consumptions of water and the production of problematic effluents, the olive mill wastewater (OMW). According to International Olive Council (IOC), in 2020/2021, world production of olive oil was about 3 Mt, with Mediterranean countries being responsible for the production of about 97% of world production [1-3]. Although the OMW is produced seasonally and in smaller quantities compared to other waste, the adverse this effluent on the environment are high. Some studies indicate that about 1 m³ of OMW can be equivalent to 100–200 m³ of domestic wastewater [4-5]. Dark color, acid pH (~5), high chemical oxygen demand-COD (30-318 g/L), total phenolic compounds-TPh (1-10 g/L), and biological oxygen demand-BOD (35-132 g/L) are some characteristics that make the treatment of this effluent difficult and make its disposal a serious environmental problem [6]. In the EU, there is no common policy that regulates the discharge of this effluent, and each country is responsible for its own norms. A common practice is its storage in lagoons followed by evaporation under natural convection [2,7]. Thereby, it is urgent to develop technologies for the treatment of OMW to guarantee efficient reuse in agriculture, especially in the Mediterranean region, where the water crisis is increasing. Over the last few years, several researchers have studied the best treatment, from the most conventional treatments (e.g. adsorption, filtration, and biological processes) to the most current ones, such as advanced oxidation processes (AOPs) [8]. Fenton's process appears as one of the most desirable for industrial-scale application. However, there is still the need to combine it with other treatments for the effluent to meet discharge requirements. Sulfate radical-based advanced oxidation processes (SR-AOPs) have been the subject of recent investigations to overcome some disadvantages of Fenton's process. Persulfate (PS, S₂O₈²⁻) and

Peroxymonosulfate (PMS, HSO₅⁻) are the two most commonly used oxidant agents for environmental applications, that when activated (e.g. by transition metals, heat and radiation) produced hydroxyl and sulfate radicals (HO[•] and SO₄^{•-}, respectively) that allows oxidizing the organic pollutants present in the aqueous matrices in harmless molecules such as CO₂, H₂O, and inorganic ions [9-10].

In this way, this work aims to treat synthetic OMW using persulfate (PS) activated by an iron waste, referred to as iron filings. For this, the best treatment conditions will be determined using a design of experiences (DoE).

Materials and methods

The solution of synthetic OMW is constituted of five phenolic compounds (Trans-cinnamic acid, 3,4-Dihydroxybenzoic, 4-Hydroxybenzoic, 3,4,5-Trimethoxybenzoic, and 3,4-Dimethoxybenzoic) dissolved in ultrapure water with a concentration of 100 mg/L (approximately 800 mgO₂/L of COD). A DoE was performed using the *software* JMP Statistical Discovery from SAS, and the variables considered are persulfate dosage (500, 750, and 1000 mg/L) and pH (3, 5, and 7) at room temperature for 3 h of reaction time. The iron filings dosage was kept constant, 1 g/L. The tests are performed in a mechanical stirrer reactor and the reaction starts when the iron filings are added after the addition of PS and respective pH adjustment. At regular intervals of time, samples of 1.2 mL were extracted, quenched with 0.3 mL methanol, and filtered with 0.45 μm cellulose acetate syringe filter [10]. The samples were analyzed utilizing high-performance liquid chromatography (HPLC) for determining the concentration of phenolic compounds in each sample. To evaluate the iron filings leaching, the liquid samples iron concentration was measured using atomic absorption (ContraAA 300, Analytik Jena).

Results

Figure 1 shows the removal efficiencies of phenolic compounds for the different pHs and PS dosages under study.

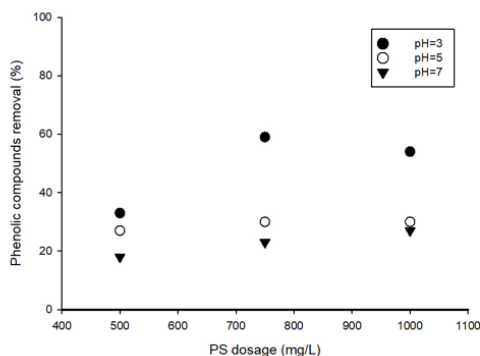


Figure 1. Influence of pH and PS dosage in phenolic compounds removal after 3 h.

A PS dosage of 750 mg/L and pH of 3 proved to be the most favorable conditions for the treatment of synthetic OMW using 1g/L of iron filings, obtaining the removal of 59% of phenolic compounds. Using the *software* JMP Statistical Discovery from SAS, a linear model was obtained for the removal of phenolic compounds within the range of values of the studied variables $500 < \text{PS dosage (mg/L)} < 1000$ and $3 < \text{pH} < 7$, Equation 1.

$$\text{Phenolic compounds (\%)} = 32.56 + 6.83 \left(\frac{\text{PS dosage} - 750}{250} \right) - 11.67 \left(\frac{\text{pH} - 5}{2} \right) \quad (1)$$

However, throughout this treatment, there was leaching by the iron filings, about 39 mg/L. Therefore, it will be necessary to

Acknowledgements

T. Vaz and J. Gomes acknowledge Foundation for Science and Technology Portugal for the fellowship Ph.D. grant (2022.14237.BD) and for the financial support (CEECIND/01207/2018), respectively, Thanks are due to FCT/MCTES for the financial support to CIEPQPF (UIDB/00102/2020).

References

- [1] IOC (International olive council), Available online: www.internationaloliveoil.org/wpcontent/uploads/2021/12/IOC-Olive-Oil-Dashboard-1.html#production-2 (accessed on 22/04/23).
- [2] P. Paraskeva, E. Diamadopoulos, *Journal of Chemical Technology & Biotechnology: International Research in Process, Environmental & Clean Technology*, 81 (2006) 1475-1485.
- [3] R.C. Martins et al., *Environmental Technology*, 31 (2010) 1459-1469.
- [4] A. Al-Bsoul et al., *Science of the Total Environment*, 700 (2020) 134576.
- [5] K. Bampalioutas et al., *Journal of Chemical Technology & Biotechnology*, 94 (2019) 265-275.
- [6] F. Görmez et al., *SN Applied Sciences*, 2 (2020) 1-11.
- [7] T.M. Koutsos et al., *Science of the Total Environment*, 622 (2018) 942-953.
- [8] A. Kirmaci et al., *Aksaray University Journal of Science and Engineering*, 2 (2018) 52-62.
- [9] S. Giannakis et al., *Chemical Engineering Journal*, 406 (2021) 127083.
- [10] K. Lalas et al., *Science of The Total Environment*, 846 (2022) 157378.

implement a subsequent treatment to remove the iron, because according to Portuguese Decree-Law N°. 236/98, it must be fulfilled a limit of 2 mg/L of dissolved iron into water sources. In future studies, in addition to iron removal, the influence of temperature on PS activation for treating this effluent will also be studied. Throughout this study, it was verified that 3,4-Dihydroxybenzoic acid is the most prone compound to degradation under these conditions (Figure 2).

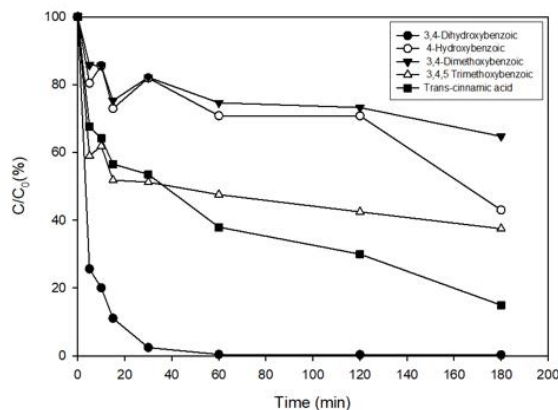


Figure 2. Individual degradation of phenolic compounds present in the synthetic effluent over time with PS dosage of 750 mg/L, 1g/L of iron filings, and pH of 3.

Conclusions

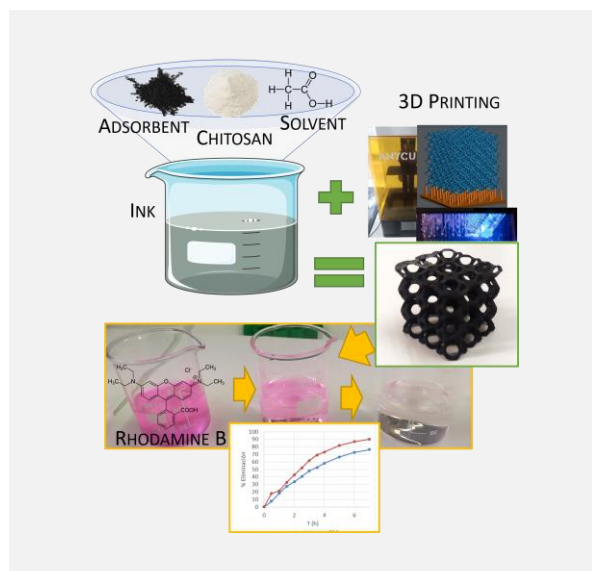
The optimization study of the operating conditions, PS dosage, and initial pH using iron filings for the treatment of synthetic OMW allowed the removal of 59% of phenolic compounds. However, due to the significant leaching of the iron filings, subsequent treatment is required for the removal of the dissolved iron or another partial addition of PS to use the dissolved iron.

Self-supported 3D-printed plate-lattices with chitosan-based ink adsorbents for the removal of pollutants

*S. Fernández-Davila**, M.A. Sanromán, E. Rosales

CINTECX, Universidade de Vigo, Department of Chemical Engineering, Campus Universitario As Lagoas—Marcosende, 36310 Vigo, Spain.

sergio.fernandez.davila@alumnos.uvigo.gal



The enhancement of the adsorption treatments and improvement of the adsorbents for their use in flow systems and facilitating the recycling process are still required. This work is aimed at the production of a composite by the deposition of a well-known adsorbent, activated carbon, on 3D-printed plate-lattices. To do that, different inks based on chitosan or PVDF were tested and their fixation on different 3D printed plate-lattices studied through different parameters (solvent composition, temperature). The best results were attained with chitosan-based inks which proved a better fixation and stability through time. The so-developed adsorbents were assessed using a model dye, Rhodamine B. The dye removal efficiency attained levels comparable to the base adsorbent alone. The system followed pseudo-first order kinetics with removal values of 100%. The use of the supported composites revealed a good performance of the adsorption system attaining high adsorption levels.

Introduction

On the road to environmentally sustainable development, both constant research on the presence, fate and impact of known and new pollutants in the environment as well as the implementation of effective technologies for the remediation of this contamination, play fundamental roles. The treatment of surface and groundwater is a practice which carried on since ancient times, nowadays is fundamental to maintaining our quality of life. The increasing demand of society for the remediation of contaminated water from different sources is embodied in increasingly strict regulations.

Most detected contaminants species are recalcitrant organic compounds of high toxicity generated in different activities and, the impact of certain sectors (mining, iron and steel, textile...). Once the contaminants are retained in the environment, their distribution and behaviour are governed by different factors such as pH, organic matter content, redox properties, microbiological activity, etc. which difficult their treatment. The generated pollutants are discharged directly into the soil or in receiving water bodies and subsequently sink down to the soil. Any contaminant present in a soil matrix may affect public health and lead to contamination and groundwater and, consequently, avoid their expected use.

Therefore, the elimination of the pollutants that are generated as a consequence of different human activities is a problem of big dimensions and difficult to tackle, which nevertheless needs the adoption of urgent and effective measures in our task of safeguarding in time the environment. There are many treatment techniques with a long tradition and, obviously, they have been greatly improved in their knowledge and design over the years. The implementation of new sustainable or improved technologies for the preservation of the environment, which combine efficiency and economy, is now a requirement, taking into account the existing discharge and the growing presence of contaminants.

One of the most widely used techniques for the decontamination of organic components is adsorption, which is based on the retention of the contaminant on the surface of adsorbent material. The materials most commonly used as adsorbents are carbonaceous materials (activated carbon, biochar, hydrochars) that have a small particle size in addition to a large pore density, since these parameters determine a large specific surface area. The powder state of most of the adsorbents limits their reusability, including the recovery, and may cause secondary pollution. To overcome this problem, the immobilization of the adsorbent material on a surface has been extensively studied and has provided satisfactory results.

An interesting approach is the generation of composite based on a carbonaceous ink and supported on complex structures with tunable ordered shapes as adsorbent [1]. The ink contains a carbonaceous material, a binder intended to immobilize the material and a solvent. This ink, once included in the composite would allow the immobilization of the material in the support, preventing its release during the adsorption process. The production of complex structures is also a matter of concern due to their complexity and on-demand requirements of shapes and sizes. Additive manufacturing and more precisely 3D-printing technology is a cheap, feasible and versatile technology that enables the fabrication of this support. The combination of ink and support allows for the limitation of secondary pollution and easy recovery stated before.

The aim of this work is the removal of a model pollutant, Rhodamine B, using different composites based on self-supported 3D-printed plate-lattices and carbonaceous (activated carbon) inks. Two different inks were evaluated and several parameters affecting the preparation of the composite were studied.

Material and methods

Reagents: Flake activated carbon, powdered active carbon, superconducting carbon, acetic acid, chitosan, polyvinylidene (PVDF) and N-methyl-2-pyrrolidone (NMP).

Composite support structures: several structures used as supports involving different geometries were printed using a Resin 3D printer.

Carbonaceous PVDF-based ink: the following proportions were used for the preparation of the ink (w/w): 85% active carbon, 10% PVDF and 5% superconducting graphite [2]. Once mixed, they were dissolved in 14.7 mL of NMP/g of activated carbon and stirred for 30 min. For the preparation of the composite, the selected structure was immersed in the ink and subjected to drying at 70°C for 6 h.

Carbonaceous Chitosan-based ink: the chitosan was dissolved in a mixture of water:acetic acid ratio (1.14:1) per gram of chitosan and kept in agitation for 24 h. Then, 12.5 ml of chitosan solution for each gram of active carbon was added and the mixture stirred for 30 min. Similarly to the other ink, the composite was prepared by immersion the structure in the ink and drying it at 70°C for 6 h.

Adsorption assays: To carry out the adsorption tests, 50 mL of a solution containing rhodamine B 10 mg/L and the generated composites were used. The system was magnetically stirred at 250 rpm during the process and samples were periodically taken and measured spectrophotometrically.

Results and discussion

Selection of composite 3D-printed supports

The selection of the complex structures was assessed: 6 different types of structures (Figure 1 a-d ordered by increasing surface area) were selected according to their geometry, tunable ordered structure, available surface area and feasibility to be used as support in different treatment alternatives.

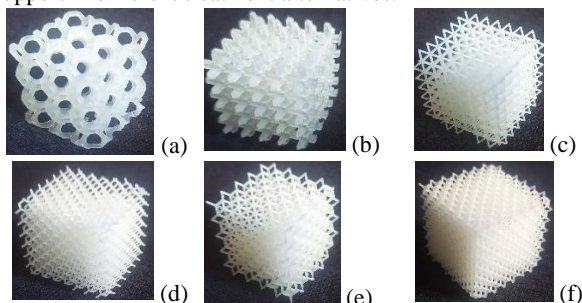


Figure 1. Structures selected for the composite supports.

Considering the requirements, initially, the generation of the composite was studied for Figure 1a and later on, the generation of the other composites was considered.

Composite generation

- **Selection of the adsorbent material:** for the development of the composited activated carbon was selected as model carbonaceous material in two different forms (powder and flakes). Moreover, their integration in two different inks was also evaluated (PVDF- and chitosan-based inks).

Acknowledgements

This research was funded through the projects TED2021-129590A-I00, funded by MCIN/AEI/10.13039/501100011033 and European Union Next Generation EU / PRTR and project ED431C 2021-43 funded by Xunta de Galicia, and the European Regional Development Funds.

References

- [1] H.S. Far et al., ACS Applied Materials & Interfaces, 14 (2022) 44488-44497.
- [2] V. Poza-Nogueiras et al., Journal of Environmental Chemical Engineering, 10 (2022) 107506.

It was observed that the inks that used active carbon in the form of flakes could not properly be added to both inks reducing the amount that can be fixed on the surface of the selected support and showing a heterogeneous distribution of the carbonaceous material.

On the other hand, inks that used active carbon powder did leave a homogeneous layer on the surface of the structures, so these were the ones selected for evaluation purposes and adsorption tests were developed.

During the adsorption tests, it was found that the composite with chitosan-based ink achieved a higher removal and uptake than those with PVDF-based inks, attaining a removal of 100% after 24 h. Even so, a small release of the ink was observed and the modification of the inks formulation was required.

- **Ink formulation and composite preparation:** the formulation of the ink was modified by increasing the viscosity of the inks, concentration of active carbon and the possibility of adding two layers of the inks.

The preparation of the composites using two layers of ink was discarded. Even though the release of the compound to the water was reduced, it clogged the support and thus, reducing the adsorption capability. With the double concentration of active carbon (2x) the adsorption uptake capacity was improved and as before a better performance of the chitosan-based ink could be verified without release, so the use of PVDF-based ink was discarded.

Once the chitosan-based ink was selected, the decrease in the viscosity of the chitosan to facilitate the ink fixation was evaluated. Operating in this way, improved the behaviour of the composite resulting in a viable alternative to increase the amount of carbonaceous material (2x) attaining a higher uptake probably due to overcome the diffusion limitations that can be caused by the resulting layers that difficult the access to the carbonaceous material. For this reason, the ink with the lower viscosity and amount of carbonaceous material was selected as the ink formulation for the scale-up.

Scale up: Once the ink formulation was attained the composites based on all the selected supports indicated in Figure 1 were prepared and evaluated.

All the generated composites showed an almost complete removal of the dye in 2h (90%) with those generated over the structures (Figure 1e) and (Figure 1f) achieving total removal. The uptake values were quite similar to those obtained for the removal. These composites attained uptakes values of 7.746 and 9.791 mg/g, respectively. The reuse of the adsorbents was successfully assayed in four cycles proving the feasibility of the selected composites to be reused.

Conclusions

These results demonstrate the importance of the selection of a proper geometry in the design of the composite which affect their behaviour and also allowed obtaining viable composites for the removal of pollutants that can be applied

Renewable energy production in marine natural caves using Wells turbines

T.F. Tavares^{1}, C.I.C. Pinheiro², R.M. Filipe^{3,4}*

¹Universidade de Cabo Verde, Campus de Palmarejo, Cabo Verde; ²Centro de Química Estrutural, Institute of Molecular Sciences, Instituto Superior Técnico, Universidade de Lisboa, Av. Rovisco Pais 1, 1049-001 Lisboa, Portugal; ³Instituto Superior de Engenharia de Lisboa, Instituto Politécnico de Lisboa, R. Conselheiro Emídio Navarro 1, 1959-007 Lisboa, Portugal; ⁴Centro de Recursos Naturais e Ambiente, Instituto Superior Técnico, Universidade de Lisboa, Av. Rovisco Pais 1, 1049-001 Lisboa, Portugal.

**tomas.tavares@docente.unicv.edu.cv*



This work addresses the generation of energy from sea waves in a Marine Natural Cave, installed in Cidade Velha, Santiago Island, Cabo Verde, using Wells turbines. Specifically, the aerodynamic influence of a fixed blade Wells turbine is investigated using experimental data collected onsite and numerical simulation. The challenging operating conditions require an efficient control scheme. To this aim, a dynamic model of the process is being developed and will be used to investigate different control strategies. The preliminary plan intends to address three alternatives to maximize the wave generated power by optimizing the turbine operating conditions, and it will involve: (i) manipulation of the turbine inlet flow, (ii) manipulation of a control valve that splits the excess flow to a secondary Wells turbine and (iii) manipulation of the turbine blades pitch angle.

The inevitable depletion of oil reserves, associated with environmental problems, such as global warming, have driven the search for alternative energy sources [1]. Within the proposed options are wind energy, solar energy and wave energy. In the framework of hydro energies, the energies produced by sea waves, received increased attention due to its contribution, as a clean energy, in, insofar as its use constitutes one of the ways to mitigate the greenhouse effects caused by carbon emissions [2]. Ormaza et. al [4] considers wave energy as one of the candidates for the reduction of greenhouse effect problems, if we consider the size of the oceans and their dynamic characteristics, still unexplored as a source of energy on earth. Other preliminary studies show that wave energy has sufficient potential to supply future energy needs [4].

Wave energy is a particularly promising renewable energy source for green hydrogen production. Green hydrogen is produced by using renewable energy sources to electrolyze water into hydrogen and oxygen. The resulting hydrogen can be stored and transported for use in a variety of applications. This process produces no greenhouse gas emissions, making it a truly sustainable fuel source. Producing green hydrogen from wave energy can also create economic opportunities for cities. The production of green hydrogen requires significant infrastructure, such as electrolysis plants and storage facilities. This infrastructure can be built in urban areas, creating new jobs and boosting the local economy.

There are some challenges to producing green hydrogen from wave energy, such as the high cost of building wave energy converters, the harsh operating conditions for the equipment and the potential impact on marine life.

According to Falcão & Henriques [3] there is a wide variety of technologies for the transformation of wave energy into mechanical energy for electricity production, namely the

Oscillating Water Column (OWC), Oscillating Bodies and Overtopping [3]. The energy produced through the OWC appears as an alternative to the energy produced from oil and its derivatives in two perspectives: a) from the point of view of the cost of its exploitation, because it is cheaper and with few negative effects on the environment and the atmosphere [5]; b) from the point of view of ease of use, both for home use and for mobility purposes, including the replacement of fossil fuels in means of transport.

Regarding mobility issues, although electric vehicles are gaining popularity, the challenges of autonomy and long charging time put into question their efficiency. These obstacles can be overcome with new technologies, including the development of green hydrogen-powered vehicles, which can be produced from electricity generated by sea waves. The production of green hydrogen from renewable wave energy has the potential to revolutionize the transportation sector in Cabo Verde. It is a sustainable, zero-emissions fuel source that can significantly reduce air and noise pollution. Producing green hydrogen from wave energy can also create economic opportunities for Cabo Verde, and it is a key step towards reducing the reliance on fossil fuels.

This innovation can represent a strong alternative to the dependence on fossil fuel imports, for a country that imports almost 100 % of the energy it consumes. In this sense, the production of green hydrogen from wave energy may lead to an added value to the sustainable development of the country, by reducing fuel purchases and creating economic opportunities through local technological developments and job creation.

In this work the generation of energy from sea waves in a Marine Natural Cave, installed in Cidade Velha, Santiago Island, Cabo Verde, using Wells turbines is simulated based on experimental data collected onsite. The variability of the wave height poses

challenging operating conditions and require an efficient control scheme. This work aims to address this issue using a dynamic model to investigate different control strategies. Three alternatives to maximize the wave generated power are investigated: (i) manipulation of the turbine inlet flow, (ii) manipulation of a control valve that splits the excess flow to a secondary Wells turbine and (iii) manipulation of the turbine blades pitch angle.

In the context of Cabo Verde, the use of renewable energy is fundamental to environmental and economic sustainability in order to overcome the problem of energy dependency by 80 % and eliminate the high cost of imports.

As an archipelagic country, surrounded by sea and with a climate that favors sun and wind throughout the year, it has the basic conditions to produce renewable energy from these resources. Currently, Cabo Verde still produces 20 % of the energy it consumes, 18 % from wind and 2 % from solar. It is predicted that the production will reach 30 % in 2025 and 50 % in 2030, according to government data. Although wave energy is not yet used in the country, it has great potential to increase energy efficiency and sustainability in the archipelago due to the large area of sea that surrounds the islands. The first approach in this regard is that reported by Monteiro et al. [5], and the development and application on a larger scale could be a positive alternative, both for the purpose of satisfying energy needs and for the production of green hydrogen, facilitating the mobility of means of transport in the country.

According to Monteiro et al. [5] all the material used in the construction of the Wells turbine was purchased at Cape Verdean market. The design and characteristics took into account issues related to material acquisition and manufacture costs, as well as the characteristics of the maritime environment where the turbine operates, and the environmental policy. The turbine was then built with PVC pipe material, being fully coated with fiberglass and resin, to increase its mechanical strength and improve its resistance in aggressive environmental conditions such as the sea. PVC is the second most consumed thermoplastic in the world. It demonstrates an excellent cost-benefit ratio when compared to other materials such as wood, metals and ceramics. It is a material with high resistance to impacts, water, weathering, chemical products and corrosive environments. It has good electrical insulation properties and good dimensional stability at room temperature [6]. Figures 1 and 2 depict some steps of the manufacture process of a Wells turbine and Figure 3 shows three newly manufactured turbines already finished with different pitch angles.

Previous studies shown that the Cidade Velha Cave has the potential to produce renewable electricity [5]. However, the turbine that was installed has proved to be inefficient when the operating conditions are characterized by moments of strong sea

turbulence. There are sea wave energy peaks that can be almost eight times higher than those manageable by the aforementioned Wells turbine. Within this context, future work will address the development of an advanced control strategy to optimize the recovery of the waves' energy in the Cave.



Figure 1. Wells turbine manufacture (I).



Figure 2. Wells turbine manufacture (II).



Figure 3. Finished Wells turbines.

As a first step, within the scope of an ongoing project funded by PNUD, ONU, new turbines are being developed to be installed onsite. The data collected from the natural sea cave in Cidade Velha by Monteiro et al. [5] and new data collected onsite with the new turbines will be used as input data for the development and validation of a dynamic mathematical model. This model for the simulation of the oscillating water column and the Wells turbines behavior, will be used for the development of control strategies aiming to maximize wave energy recovery efficiency.

Acknowledgements

The financial support from FCT under projects UIDB/00100/2020, UIDP/00100/2020, UIDB/04028/2020 and UIDP/04028/2020 is gratefully acknowledged.

References

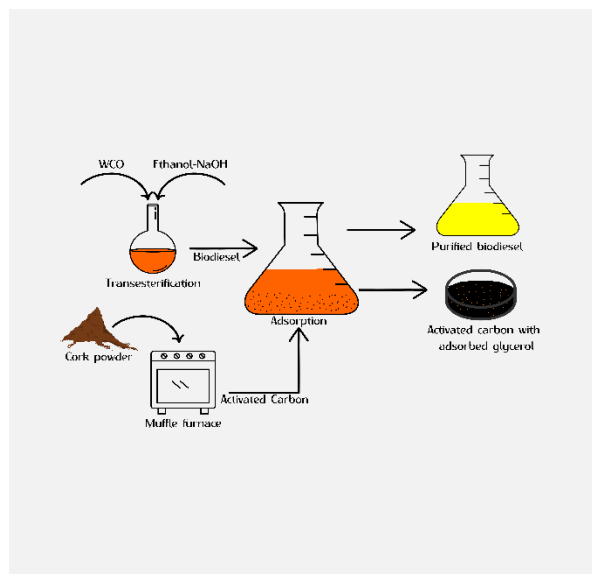
- [1] M. Gharibi et al., *International Journal of Hydrogen Energy*, 44 (2019) 25428-25441.
- [2] J. Lekube et al., *6th International Conference on Power Science and Engineering*, St. Petersburg, Russian Federation, 2017.
- [3] A. Falcão et al., *Renewable Energy*, 3 (2015) 1-34.
- [4] M. Ormaza et al., *Joint 48th IEEE Conference on Decision and Control and 28th Chinese Control Conference*, Shanghai, China, (2009) 7315-7320
- [5] W. Monteiro et al., *Journal of Ocean Engineering and Marine Energy*, 7 (2021) 327-337.
- [6] F. Júnior et al., *II Semana Nacional de Ciência e Tecnologia do IFPE*, Pernambuco, Brasil, 2011.

Biodiesel production from residual cooking oils and its purification through adsorption processes using activated carbon prepared from cork waste

M.L.L. Garção^{1,2,3*}, A.M. Queiroz^{1,2}, P. Brito^{1,2}, A.E. Ribeiro^{1,2}, M.C.S. Gomes³

¹Centro de Investigação de Montanha (CIMO), Instituto Politécnico de Bragança, Campus de Santa Apolónia, 5300-253 Bragança, Portugal; ²Laboratório para a Sustentabilidade e Tecnologia em Regiões de Montanha (SusTEC), Instituto Politécnico de Bragança, Campus de Santa Apolónia, 5300-253 Bragança, Portugal; ³Universidade Tecnológica Federal do Paraná, R. Marçílio Dias, 635, Jardim Paraíso, 86812-460, Apucarana, Brazil.

*m.limagarcao@gmail.com



Biodiesel is a renewable fuel that can be produced from waste cooking oil mainly through transesterification. However, from its production results a contaminant called glycerol, which must be removed. Wet washing is the most common method for biodiesel purification, but it has several drawbacks, including high costs and the generation of large amounts of aqueous effluent. This study proposes using activated carbon obtained from industrial cork waste in adsorption as an alternative method for glycerol removal. This approach could potentially reduce the environmental impact and cost of producing biodiesel, while also providing an alternative for the valorization of industrial cork waste. The highest value of removal of 89% of glycerol occurred with a cork chemically activated carbon with KOH at a load of 2% wt at 25°C for 6 hours of contact. After the biodiesel washing using adsorption process, the remaining glycerol content was 0.016%wt, below the maximum value of 0.02%wt specified by the EN14214:2012 standard.

Introduction

Global energy consumption has increased in recent decades, and the International Energy Agency predicts a 50% increase in demand for energy by 2030. As the supply of fossil fuels is limited and has environmental problems, researchers are exploring alternative energy sources. Biofuels, such as biodiesel, are promising renewable energy sources with lower carbon emissions that can be made from a variety of resources, including waste cooking oil, oily sludge from factories, and discarded animal fats [1].

Biodiesel is renewable, biodegradable, non-toxic, sulfur-free, and aromatic carcinogen-free, making it a more environmentally friendly option compared to petroleum-derived diesel. The cost of biodiesel is currently higher than petroleum diesel, but using waste cooking oil as a feedstock can reduce the cost since it is 25% to 40% of the price of edible oil. Biodiesel is produced mainly through transesterification, a process that converts oils or free fatty acids into alkyl esters and glycerol [2].

The properties of biodiesel depend on the feedstock used, and it must meet certain standards, such as the European Biodiesel Standard EN 14214:2012, which defines characteristics that determine the behavior of biodiesel combustion in an engine and the methods used to determine those parameters. To meet these specifications, the biodiesel produced must undergo a purification process to remove impurities such as glycerol, which, according to the standard, must be a maximum of 0.02% wt [3].

Several studies related to the purification of biodiesel by adsorption have been carried out. Materials such as silicates, clays, and polymers, among others, are widely used as adsorbents. In this work, activated carbon from cork residue was investigated as a potential adsorbent due to the high porosity and large surface area of the material [4].

Materials and methods

The first stage of the work was to optimize biodiesel production, using temperatures of 30, 45 and 60°C and oil:alcohol molar ratios of 1:6, 1:7.5 and 1:9. The catalyst used was NaOH and its load was fixed in 1%wt, since it is a concentration suitable for obtaining high ester yield in biodiesel.

After biodiesel production, four types of activated carbon were produced to be used as adsorbent in purification using a two-step carbonization process with chemical activation with solid KOH. Cork powder was first carbonized at 550°C for 1 and 2 hours, resulting in CC1 and CC2, respectively. These materials were then mixed with solid KOH in a weight proportion of 1:5 and carbonized again at 750°C for 2 hours, resulting in the final products CCB1 and CCB2. These materials were washed with HCl (0.1M) and distilled water until neutral pH and dried in an oven at 100°C. Posteriorly, all materials, including cork powder, were characterized by their surface area at 77 K using Quantachrome NOVATOUGH LX², elemental composition with a CHNS analyzer Flash 2000 (Thermo Fisher Scientific, Massachusetts, USA), pH_{PZC} using the methodology from Rovani (2015) [5] and thermogravimetric analysis using a TGA-50 Shimadzu equipment.

The last experimental stage was the adsorption process. First, a preliminary study was made to determine which materials had the highest potential in glycerol removal, and then the selected ones were used to study adsorption kinetics and equilibrium in the temperatures of 25, 35, and 45°C and adsorbent load from 0.1 to 3%wt. The experimental data was fitted to kinetic and equilibrium models.

Results and discussion

The studies showed that the best Fatty Acid Ethyl Ester's yield of 88.26%, was achieved with a reaction temperature of 30°C,

1%wt catalyst load, and 1:9 oil:alcohol molar ratio. The activated carbon production resulted in a carbonization process yield of approximately 20% and the activation process yielded around 50%. Some results are shown in Table 1.

Table 1. Adsorbents characterization results.

Material	S_{BET} (m ² /g)	C/H ^a	pH _{PZC}
Cork	5.16	0.65	4.64±0.15
CC1	203.65	3.07	10.47±0.05
CC2	64.41	3.18	10.40±0.02
CCB1	2057.25	11.21	9.76±0.00
CCB2	1687.22	11.40	8.71±0.02

^aC/H molar ratio obtained from the elemental composition analysis.

The surface area of the prepared cork activated carbon materials was similar to those reported in the literature, with the highest surface area (S_{BET}) of 2057.25 m²/g observed for CCB1. The analysis of the elemental composition and the increase of the calculated ratios (C/H) indicated the high efficiency of the carbonization process. Thermogravimetric analysis showed that the most significant weight variation is the loss of moisture, except for cork, which showed significant losses during the degradation of cellulose and suberin.

The pH_{PZC} value for cork was consistent with the literature, being an acid pH value. Other materials had a basic PZC due to decreased oxygen content from carbonization and the strong base used in chemical activation. The chemically activated materials were washed until neutral pH, decreasing PZC.

In the preliminary adsorption studies, it was shown that the best materials for glycerol removal were original cork and CCB1. The first was effective because of its acid pH_{PZC}, which increases the affinity with glycerol, and CCB1, despite its basic pH_{PZC}, has a very high surface area, increasing the removal efficiency.

The adsorption kinetics was studied using 2 and 3%wt adsorbent concentrations. It was shown that the increase in the temperature decreased adsorption capacity, disfavoring the washing process. Due to the low density of the materials, causing relatively large sample volumes to be handled, the increase in adsorbent load also negatively impacted the adsorption, generating agglomerations of adsorbent and reducing its contact area with the adsorbate.

The equilibrium time was similar for all kinetic studies, around 6 hours, and using 2%wt of CCB1 at 25°C the biodiesel was purified until the amount required in the European standard. The obtained adsorption profile and glycerol content are presented in Figure 1.

The data were fitted to pseudo-first order and pseudo-second order models. The second one represented better the experimental profile in most of the cases, and the highest adsorption capacity reached was 66.25 mg/g using 2%wt of CCB1 at 25°C.

Lastly, the equilibrium adsorption was studied. The tests were made with concentrations from 0.1 to 3%wt of adsorbent at the

temperatures of 25, 35, and 45°C. The adsorption profile presented an unfavorable behavior, which indicates that the adsorption is more significant in higher adsorbate concentrations.

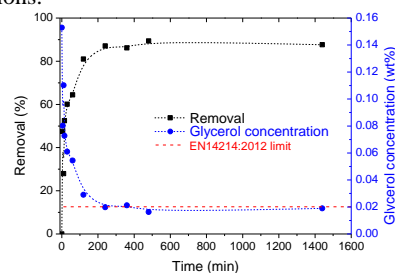


Figure 1. Adsorption profile of glycerol in biodiesel using 2% CCB1 as adsorbent at 25°C

The data were fitted to the Freundlich and Langmuir models, but only the first one could represent the adsorption. The estimated parameters confirmed the unfavorable adsorption behavior.

As in kinetic studies, the highest removal value was obtained with CCB1 at 25°C. The variation of glycerol removal and its content in relation to the adsorbent concentration is shown in Figure 2.

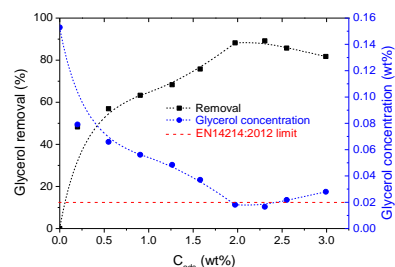


Figure 2. Glycerol removal and content for biodiesel purified with CCB1.

It is possible to confirm that the glycerol removal decreases with the increase of adsorbent concentrations when it is above 2.3%wt. In both kinetics and equilibrium studies, it was possible to remove more than 89% of glycerol from biodiesel, achieving a final concentration of approximately 0.016%wt, below the requirements of EN14214:2012.

Conclusions

Based on the objectives of this work, the optimization of biodiesel production and its purification through adsorption using cork waste, and its activated carbons as an alternative method to washing with water, were studied. Therefore, it can be concluded that the carbon in cork residues chemically activated with KOH has great potential in removing glycerol. This process can replace the water washing process, contributing to the reduction of effluent generation and to the reuse of a large-scale residue produced by Portuguese cork industry.

Acknowledgements

The authors are grateful to the Foundation for Science and Technology (FCT, Portugal) for financial support through national funds FCT/MCTES (PIDDAC) to CIMO (UIDB/00690/2020 and UIDP/00690/2020) and SusTEC (LA/P/0007/2020).

References

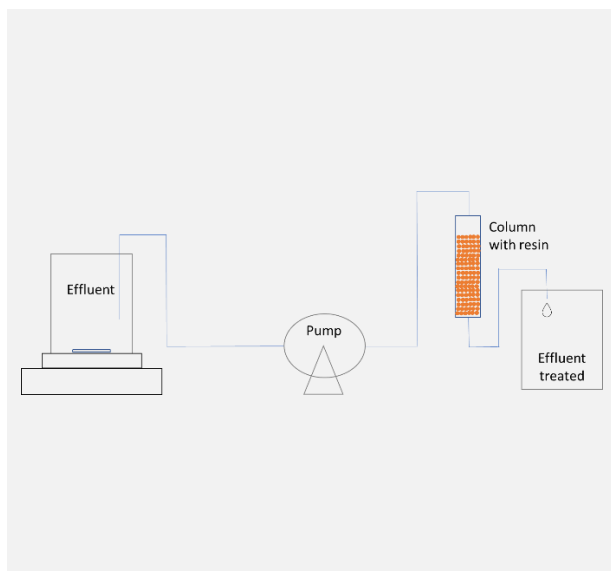
- [1] S. N. Gebremariam, J. M. Marchetti, *Energy Conversion and Management*, 168 (2018) 74-84.
- [2] L. Liu et al., *Journal of Cleaner Production*, 278 (2021) 123799.
- [3] M. Carmona-Cabello et al., *Bioresource Technology*, 323 (2021) 124597.
- [4] H. Bateni et al., *Biofuel Research Journal*, 4 (2017) 668-690.
- [5] S. Rovani, *Preparo e caracterização de carvão e carvão ativado a partir de resíduos agroindustriais e aplicação na remoção de estrogênios*, PhD Thesis, Universidade Federal do Rio Grande do Sul, Porto Alegre, 2015.

Recovery of phenolic compounds from olive mill wastewater using ion exchange process

M.J. Fernandes, J. Gomes, R.C. Martins*, E. Domingues

University of Coimbra, CIEPQPF, Department of Chemical Engineering, Faculty of Sciences and Technology – Pólo II, Rua Sílvio Lima, 3030-790 Coimbra, Portugal.

*martins@eq.uc.pt



The production of olive oil leads to high amounts of olive mill wastewater (OMW) that needs to be treated before discharging it into the environment. The treatment of these streams can be done using advanced oxidation processes with the degradation of the organic compounds. However, these effluents are rich in added-value compounds such as phenolic acids with interest in markets such as pharmaceutical and cosmetic. In this context, it would be interesting to consider the possibility of recovering as much as possible these compounds before degrading the remaining organic matter by oxidation processes. The pre-treatment of the effluent using an ion exchange process may enable the recovery of phenolic compounds. This study focuses on the removal of phenolic acids from synthetic OMW using Amberlite®HPR1100 as adsorbent. The resin has proven to be more selective for 3,4-dimethoxybenzoic acid when compared with the adsorption of other phenolic acids. Globally, around 38.2% of the phenolic acids feed to the adsorption system were adsorbed on the resin. Finally, a reduction of 34% of the initial COD of the effluent was possible with this treatment. The selection of suitable conditions for the phenolic acids removal from the resin was also tested in this work.

Introduction

The production of olive oil in the European Union represents about 68% of global production worldwide, producing around 2 million tons of olive oil per year [1]. The production of olive oil requires large amounts of water that ends up contaminated, producing large amounts of olive mill wastewater (OMW). This effluent has a high concentration of phenolic compounds, which give it high phytotoxic and antimicrobial properties. So, their treatment is important to prevent further environmental damage [2]. These compounds have interesting antioxidant properties that make them interesting for pharmaceutical and cosmetic applications, for example.

There are many studies involving different technologies for the treatment of OMW, in particular, advanced oxidation processes like Fenton [3]. Their efficiency is high, but, as there is a degradation of most phenolic compounds, a recovery of those molecules after these processes is limited [4]. So, a pre-treatment of the OMW aiming to recover phenolic compounds can be economically attractive due to their high added-value. Besides, such approach contributes to a circular economy. Adsorption is a technique that may be used to remove phenolic compounds from wastewater without using a solvent allowing their recovery.

A study developed by Cifuentes-Cabezas et al. [5] focused on the recovery of phenolic compounds from a real and synthetic effluent using Purolite non-ionic resins. The resin that showed higher removal efficiency for phenolic compounds was MN200 with a dosage of 40 g/L. The desorption was also better when MN202 was employed with a mixture of 50% ethanol and 50% water. Finally, ~91% of the total phenolic content was recovered from the initial solution under optimal conditions. Savarese et al. [6] tested a pilot-scale process whose objective is to treat OMW and recover phenolic extract. The process has seven filtration steps, and the nanofiltration concentrate goes to the adsorption step using resins to recover the antioxidant extract (mainly polyphenols). To remove the

polyphenols from the polymeric resins, ethanol is used as solvent. This process was able to 27 kg of extract when 10 m³ of effluent was treated.

Vavouraki et al. [7] studied the removal of phenolic compounds from a synthetic effluent that simulated real OMW. The resins used in this study were Amberlite XAD4, XAD16, and FPX66. The initial effluent was diluted, and a ratio of 20% resin was employed. The recovery of phenolic compounds was at its maximum (75%) when Amberlite FPX66 was used and 40% of the phenols adsorbed into the resin were recovered.

Objectives

This study proposes the recovery of a mixture of phenolic compounds (synthetic effluent, SW), before any treatment, using a cationic resin, Amberlite®HPR1100.

Methods and materials

The resin used as adsorbent agent is Amberlite®HPR1100 and their properties are shown in Table 1 [8]. In this study, 71 g of resin (dry mass) were entered in a column (height = 50 cm; diameter = 4.9087 cm). The resin was activated using 3 cycles of cleaning with sulfuric acid (1 M), sodium hydroxide (1 M), and water between them, for 6 hours. Then the resin was stored with sulfuric acid 1.5 M overnight.

Table 1. Characteristics of Amberlite®HPR1100 [8].

Appearance	Amber
Copolymer	Styrene-divinylbenzene
Functional group	Sulfonic acid
Ionic Form as Shipped	Na ⁺
Particle diameter (µm)	585±5
Surface area (m ² /g)	0.673
Average pore diameter (nm)	2.595
Pore volume (cm ³ /g)	0.0004
Real density (g/cm ³)	1.227

To simulate a real OMW, a solution with 100 mg/L of four phenolic acids (3,4-dimethoxybenzoic, 3,4,5-trimethoxybenzoic, 3,4-dihydroxybenzoic, and 4-hydroxybenzoic acid) was used. The effluent is introduced into the column at a flow rate of 4 mL/min at the top of the column. A total of 4 L of effluent was used. Samples were taken from the bottom of the column and stored to analysis.

For the synthetic effluent, the phenolic content was evaluated by HPLC. The column used was C18 (SilicaChrom) at 40°C with a flow rate of 0.5 mL/min (50% methanol and 50% acidified water). To detect the compounds, a wavelength of 255 nm needs to be employed. To determine the COD of the effluent, the standard method 5220D was employed [9]. The tubes with the effluent, acid, and digestion solution will be placed in the thermoreactor (ECO25, Velp Scientifica, Taufkirchen, Germany) for 2 hours at 150°C. The absorbances were measured using a multiparameter photometer with COD (Hanna, HI83399; Póvoa de Varzim, Portugal).

Results and discussion

To evaluate the removal of phenolic acids from the effluent along time, samples were collected over time and analyzed using HPLC. As can be seen in Figure 1, the resin presents different affinities towards the removal of the different phenolic compounds. The curves show that after around 700 min, the column was almost saturated with phenolic compounds since their removal reaches a plateau. After 1050 min, 38.2% of the total phenols were removed from the effluent using the resin. Higher removal efficiencies (48%)

Acknowledgements

Thanks are due to FCT/MCTES for the financial support to CIEPQPF (UIDB/00102/2020). J. Gomes gratefully acknowledges FCT by the financial support (CEECIND/01207/2018).

References

- [1] "European Commission | Agri-food data portal | Agricultural markets | Olive oil and table olives." <https://agridata.ec.europa.eu/extensions/DataPortal/olive-oil.html> (accessed Apr. 25, 2023).
- [2] "Environmental Impact of Olive Oil Processing | EcoMENA." <https://www.ecomena.org/olive-oil-wastes/> (accessed Apr. 25, 2023).
- [3] P. Cañizares et al., *Chemosphere*, 67 (2007) 832-838.
- [4] M. Kallel et al., *Chemical Engineering Journal*, 150 (2009) 391-395.
- [5] M. Cifuentes-Cabezas et al., *Separation and Purification Technology*, 298 (2022) 121562.
- [6] M. Savarese et al., *International Journal of Food Science and Technology*, 51 (2016), 2386-2395.
- [7] A. I. Vavouraki et al., *Waste Biomass Valorization*, 12 (2021) 2271-2281.
- [8] E. Domingues et al., *Water*, 14 (2022) 706.
- [9] R. B. Baird, A. D. Eaton, and E. W. Rice, "Standard Methods for the Examination of Water and Wastewater," American Public Health Association: Washington, DC, USA, 2017.

were achieved for the 3,4-dimethoxybenzoic acid. The COD of this mixture was also analyzed to assess the COD reduction, and 34% of the initial COD was removed using only the resin.

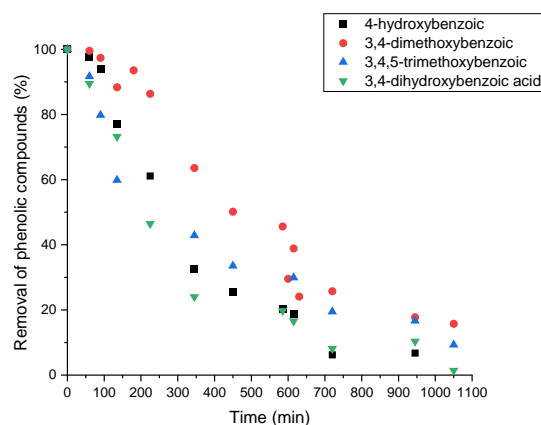


Figure 1. Removal of phenolic acids over time.

Conclusions

The removal of phenolic compounds using Amberlite HPR1100 is possible. Further studies need to be conducted to evaluate the removal of the phenolic compounds from the resin. Batch experiments can also be done to determine the best ratio between the volume of effluent to be treated and the mass of resin used, in addition to the determination of the adsorption isotherms and their parameters to further optimize the continuous process.

Novel photocatalysts for pharmaceuticals removal from wastewater: a literature survey and a perspective for healthy freshwater ecosystems

F. Rodrigues^{1,6*}, M.J. Feio¹, A.R. Calapez¹, N. Simões², A.M.P.T. Pereira³, L.J.G. Silva³, A. Freitas^{4,5}, L. Durães⁶

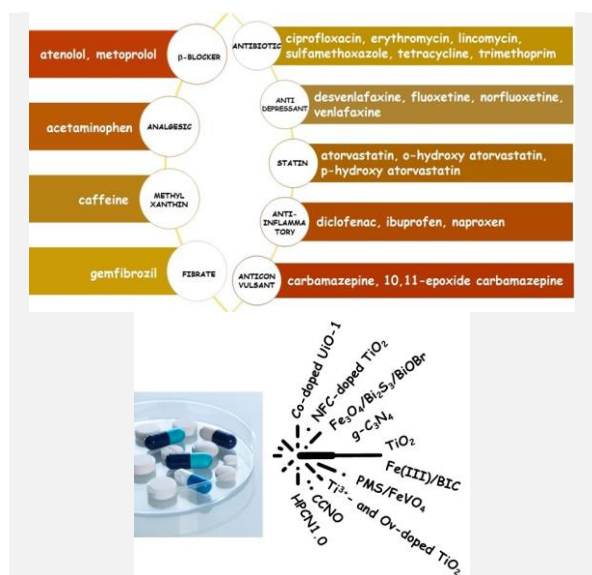
¹University of Coimbra, MARE, Department of Life Sciences, Largo Marquês de Pombal, 3004-517 Coimbra, Portugal;

²University of Coimbra, INESC, Department of Civil Engineering, Rua Luis Reis Santos, 3030-788 Coimbra, Portugal;

³University of Coimbra, LAQV/REQUIMTE, Faculty of Pharmacy, Azinhaga de Santa Comba, 300-548 Coimbra, Portugal;

⁴LAQV/REQUIMTE, Rua Dom Manuel II, Apartado 55142, 4051-401 Porto, Portugal; ⁵INIAV, I.P., Avenida da República, Quinta do Marquês, 2780-157 Oeiras, Portugal; ⁶University of Coimbra, CIEPQPF, Department of Chemical Engineering, Rua Sílvio Lima, 3030-790 Coimbra, Portugal.

*fernanda.rodrigues@student.uc.pt



Pharmaceuticals are Contaminants of Emerging Concern (CECs) because they persist in freshwater ecosystems due to inefficacy of wastewaters treatment processes for their removal, and lead to multidrug-resistant microorganisms, constituting risk factors for the health of humans, animals and plants, especially in urban areas. Thus, a wide scientific literature review was done to search for new photocatalysts able to clean that kind of pollutants and increase the health of freshwater ecosystems. The database used was Web of Science and a final list of articles related to wastewater/river water matrices enumerated 10 different types of photocatalysts tested in the last 5 years. Among all these photocatalysts, 3 achieved *ca.*100% until 60 min of contact with wastewater and 2 were considered for the removal of ciprofloxacin and diclofenac, detected in urban streams water samples. Therefore, these solutions are very relevant options for treatment of pharmaceuticals-contaminated wastewater.

Introduction

The pharmaceuticals are being widely used for human and veterinary purposes in modern society. These compounds and their metabolites are present in wastewaters, and if they are not appropriately treated, they are discharged in urban streams and rivers causing environmental impacts to freshwater ecosystems. Therefore, pharmaceuticals have been considered Contaminants of Emerging Concern (CECs).

Objectives

The objective of the present work was to address the state-of-art of scientific literature about the novel photocatalysts used to remove pharmaceuticals present in wastewater. Another goal was to analyse the potential of such catalysts to improve the water quality of urban streams through the removal of the pharmaceuticals found in collected samples, and therefore reduce risks for the ecosystem and human health.

Methods

To elucidate which photocatalysts have been tested to treat wastewaters containing pharmaceuticals, the literature review was done by searching ("urban stream*" OR "urban river*" OR river*) AND (drug* OR pharmac* OR medic*) AND (WWTP* OR STP* OR ETP* OR "wastewater treatment plant*" OR "sewage treatment plant*" OR "effluent treatment plant*" OR wastewater* OR sewage* OR effluent*) AND (photocataly* OR aerogel*) in Web of Science (WoS), on march 2023.

The original list returned by WoS (List 1) consisted of 158 articles and covered the literature from 2005 to 2023. Then, a second list of 95 pre-selected articles (List 2) was filtered manually, considering those of the previous list that were actually related to the theme (photocatalysis treatment,

mentioning the concern about pharmaceuticals in wastewater discharges to freshwater ecosystems – surface waters).

A more refined selection was done generating a third and final filtered list of 10 articles (List 3), considering the period of publication from 2018 to 2023 (the last 5 years) and those that really reported tests with photocatalysts (excluding articles that only cited works of other authors) in the matrices wastewater and river water (many studies test the photocatalysts in ultrapure, deionized, drinking and tap water, but not in those complex matrices). This decision to study the most recent published articles was a result of List 2 analysis to check the accumulated number of articles over the years, as shown in Table 1. It was calculated that in the last 5 years there were 165% more articles published about the theme than in the previous 13 years.

Table 1. Articles of List 2.

Period	Number	%
2005 to 2017	26	27
2018 to 2023	69	73
TOTAL	95	100

Information about the studied pharmaceuticals (human use) and their categories, type of photocatalyst and radiation, as well as efficiency and time of pharmaceutical removal were analysed. Finally, original results of a water sampling campaign conducted by the authors of this work in November 2022, in urban streams of Coimbra, Portugal, were used to evaluate the potential of the tested photocatalysts described in literature to remove the same pharmaceuticals detected in the streams water.

Results

Table 2 shows important information reported by the authors [1-10], corresponding to the 10 analysed articles (List 3), and a scheme of the pharmaceuticals and their categories are shown in the Graphical Abstract.

A total of 23 pharmaceuticals, belonging to 9 drug categories, were studied, being sulfamethoxazole and antibiotic, respectively, the most frequent ones. The photocatalysts studied were all different, but some have the same origin, for example TiO₂ (NFC-doped TiO₂, TiO₂ and Ti³⁺- and oxygen vacancy-doped TiO₂) and g-C₃N₄ (HPCN1.0 and g-C₃N₄). Also, in the case of PMS/FeVO₄, the study was conducted only in association with another treatment process (peroxymonosulfate activation). The radiation sources used were visible light [2,3,4,7,8,9,10], ultraviolet [5], UV-VIS [6] and sunlight (simulated) [1]. About the target matrices, some tests used domestic [2,3,4,5,9,10], others hospital/medical [8,6,7], and few pharmaceutical/industrial wastewaters [1,2], but almost all used natural river waters [1,3,4,6,7,8,9,10] in parallel to check the efficiency of the new photocatalysts. In relation to the removal efficiency of pharmaceuticals, 3 ranges were observed: *ca.* 100% [2,4,5,7,10], 75-90% [1,6], 50-70% [3,8,9]. In terms of removal time, 3 ranges were registered: 30-60 min [1,4,6,7,8,10], 120-240 min [3,5] and 420-600 min [2,9]. As a general evaluation for wastewaters, the photocatalysts studied by authors [4,7,10], respectively, g-C₃N₄, PMS/FeVO₄, HPCN1.0, seem to be considered options to their treatment because they had very good removal efficiencies in a shorter time, but a deeper study still should be carried out.

Among 16 water samples of Coimbra's urban streams collected during the autumn of 2022, only two of them detected

pharmaceuticals studied by the literature review authors: US10 (Arregaça, 40°11'51.9"N, 8°25'03.8"W) and US11 (São Miguel, 40°13'39.1"N, 8°26'15.3"W). The pharmaceuticals detected were the antibiotic ciprofloxacin (5.228 ng/L – US10; 2.067 ng/L – US11) and the anti-inflammatory diclofenac (29.291 ng/L – US10; 8.214 ng/L – US11). The photocatalyst used by [6] was the only one tested for the removal of ciprofloxacin from river water (76.49% in 60 min), while [3,4] tested photocatalysts to remove diclofenac from the same water matrix (55.65% in 240 min, and *ca.* 100% in 60 min, respectively). Therefore, considering also the good removal efficiency to the same pharmaceuticals from wastewater, it can be inferred that effluents with these pollutants could be previously treated with Fe(III)/BIC [6] and g-C₃N₄ [4], in order to improve the freshwater ecosystems of the stream/river that receives it.

Conclusions

Pharmaceuticals are present in wastewater, but part of them are not appropriately removed by the main technologies used nowadays. In the literature review done in this work 10 articles about novel photocatalysts were analysed in terms of removal of pharmaceuticals in complex matrices. Three photocatalysts presented excellent removal efficiency and time, *ca.* 100% up to 60 min, an important result to reduce costs, since large amounts of wastewater need to be treated. Also, two efficient photocatalysts were indicated to specifically treat ciprofloxacin and diclofenac. Therefore, they can be considered good options to avoid contamination or improve the water quality of urban streams and rivers, although further tests are needed. In addition, new technologies are lacking for other pharmaceuticals present in the urban freshwater ecosystems.

Table 2. List of articles analysed in this work (List 4).

Author	Year	Ref.	Pharmaceutical	Photocatalyst	Efficiency	
					Wastewater	River water
Cao <i>et al.</i>	2018	[1]	tetracycline	Co-doped UiO-1	87.1%	88.5%
Ata and Töre	2019	[2]	erythromycin, ciprofloxacin, sulfamethoxazole	NFC-doped TiO ₂	<i>ca.</i> 100%	-
Li <i>et al.</i>	2019	[3]	diclofenac, ibuprofen	Fe ₃ O ₄ /Bi ₂ S ₃ /BiOBr	54.9%, 58.9%	55.65%, 68.66%
Barros <i>et al.</i>	2021	[4]	diclofenac metoprolol	g-C ₃ N ₄	<i>ca.</i> 100%	<i>ca.</i> 100%
Fattahi <i>et al.</i>	2021	[5]	lincomycin desvenlafaxine atorvastatin, o-hydroxy atorvastatin, p-hydroxy atorvastatin naproxen ^a	TiO ₂	<i>ca.</i> 100%	-
Li <i>et al.</i>	2021	[6]	ciprofloxacin	Fe(III)/BIC	84.71%	76.49%
Zhang <i>et al.</i>	2021	[7]	sulfamethoxazole	PMS/FeVO ₄	97.5%	95.6%
Chen <i>et al.</i>	2022	[8]	tetracycline	Ti ³⁺ - and Ov-doped TiO ₂	52.68%	70.76%
Wang <i>et al.</i>	2022	[9]	naproxen	CCNO	60.9%	64.8%
Tan <i>et al.</i>	2023	[10]	sulfamethoxazole	HPCN1.0	<i>ca.</i> 99%	<i>ca.</i> 99%

^a Other pharmaceuticals, by categories, with different efficiency removals: sulfamethoxazole, trimethoprim | fluoxetine, norfluoxetine, venlafaxine | diclofenac, ibuprofen | carbamazepine, 10,11-epoxide carbamazepine | atenolol | acetaminophen | caffeine | gemfibrozil.

Acknowledgements

This study had the support of: Fundação para a Ciência e Tecnologia, I. P. (FCT), under the studentship reference number 2022.14367.BD, and the strategic projects UID/EQU/00102/2020, UIDB/04292/2020, UIDP/04292/2020, LA/P/0069/2020, UIDB/00308/2020, and a PI CEEC contract (MJF); POCI-01-0145-FEDER-006910; European Regional Development Fund (ERDF), through COMPETE 2020; and European Commission, Horizon Europe program (OneAquaHealth project, GA: 101086521).

References

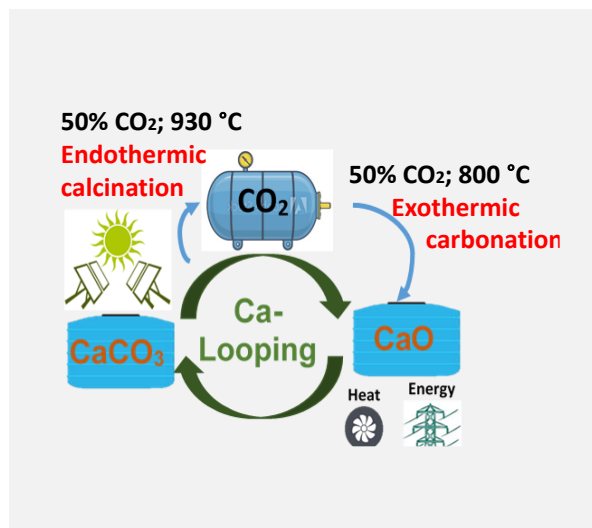
- [1] J. Cao *et al.*, Chemical Engineering Journal, 353 (2018) 126-137.
- [2] R. Ata and G. Töre, Journal of Environmental Management, 233 (2019) 673-680.
- [3] S. Li *et al.*, Chemical Engineering Journal, 378 (2019) 122169.
- [4] M. Barros *et al.*, Journal of Environmental Chemical Engineering, 9 (2021) 104747.
- [5] A. Fattahi *et al.*, Catalysts, 11 (2021) 576.
- [6] S. Li *et al.*, Applied Surface Science, 566 (2021) 150658.
- [7] J. Zhang *et al.*, Chemical Engineering Journal, 403 (2021) 126384.
- [8] X. Chen *et al.*, Chemical Engineering Journal, 427 (2022) 130945.
- [9] Y. Wang *et al.*, Separation and Purification Technology, 296 (2022) 121425.
- [10] C. Tan *et al.*, Chemosphere, 310 (2023) 136686.

Effect of steam on a fluidized-bed calcium lopping process using natural and waste resources

A.C. Ferreira, P. Teixeira, C.I.C. Pinheiro*

Centro de Química Estrutural, Institute of Molecular Sciences, Departamento de Engenharia Química, Instituto Superior Técnico, Universidade de Lisboa, Avenida Rovisco Pais 1, 1049-001 Lisboa, Portugal.

carla.pinheiro@tecnico.ulisboa.pt



The Calcium Lopping (CaL) is a reversible process [$\text{CaO (s)} + \text{CO}_2 \text{ (g)} \leftrightarrow \text{CaCO}_3 \text{ (s)}$] that allows the use of the same material over several cycles, and a sustainable use of abundant and cheap mineral resources, with high energy density (1790 kJ/kg of CaCO_3).

In this work, different calcium-based materials from Portuguese natural geological and waste sources (Limestones and Marbles) were selected and evaluated as sorbents on the CaL cycle process for thermochemical energy storage in a lab-scale fluidized bed reactor. All materials tested show a deactivation along the cycles. The best materials have a constant heat release efficiency of 263-366 kJ/kg of CaCO_3 , from the 6th cycle.

The steam addition on the calcination/carbonation multicycles improved the calcination step, by decreasing the temperature needed to reach the same calcination efficiency and increasing the material's stability. The addition of 5% steam concentration in gaseous feed flow led to the best result at 915 °C in the calcination step.

Introduction

The Calcium Lopping (CaL) is a reversible process [$\text{CaO (s)} + \text{CO}_2 \text{ (g)} \leftrightarrow \text{CaCO}_3 \text{ (s)}$] that allows the use of the same material over several cycles, and a sustainable use of abundant and cheap mineral resources, such as limestone and dolomite [1, 2] and higher energy density (1790 kJ/kg of CaCO_3). Higher temperatures used in the CaL process led to drawbacks correlated with pore plugging and sintering of particles originating a substantial drop in the multicycle CaO conversion derived from natural calcium-based materials. [3] To overpass these drawbacks, several approaches have been proposed to enhance the multicycle activity and stability such as hydration, thermal activation, and mechanical grinding. [4, 5]

The steam introduction in the gas flow has been reported as an effective way to reduce the high temperatures used in the CaL process, thus contributing to increasing the calcination rate. Some studies point out that in the presence of water vapor, the operating temperatures can decrease by about 40 °C. [6] Water vapor is believed to accelerate the decomposition of CaCO_3 through catalysis, which weakens the CaO- CO_2 bond and thus lowers the incipient calcination temperature. [7]

The main objective of this work is to study different calcium-based materials from Portuguese natural and waste sources (Limestones and Marbles) and evaluate their performance on the CaL cycle process for thermochemical energy storage in a lab-scale fluidized bed reactor. The addition of different steam concentrations (2.5%, 5%, 10% steam) in the gaseous feed flow was optimized for the calcination step and evaluated in the calcination/carbonation multicycles of the CaL process.

Materials and Methods

All limestone and waste marble materials were dried at 105 °C, crushed and sieved in order to separate the fraction between 355-500 μm used during the CaL experiments.

The elemental content (Ca, Mg, Si, Al, Fe, Na, K) of materials was determined by ICP-OES, in an independent accredited laboratory. The textural properties of fresh and used materials (i.e., after the carbonation-calcination experiments) were

assessed by N_2 sorption at -196 °C (Quantachrome Model Autosorb IQ apparatus). The samples were outgassed under vacuum at 90 °C for 1 h and then at 120 °C (fresh materials) or 350 °C (spent materials) for 5 h. The total pore volume (V_p) was calculated from the adsorbed volume of nitrogen for a relative pressure (p/p_0) of 0.97. The BET equation was applied to estimate the specific surface area (S_{BET}) and the pore size distribution (PSD) was obtained by using BJH model (desorption branch). The powder X-ray diffraction (PXRD) patterns of fresh and used materials were obtained using the X-Ray diffractometer (Bruker, AXS-D8 Advance) using $\text{Cu K}\alpha$ ($\lambda = 0.15406 \text{ nm}$) radiation operating at 40 kV and 30 mA (2θ angle range: 20–80°, step size: 0.03°, step time: 0.5s). Crystallography open database (COD) was used to identify the crystalline phases. The morphology and particle distribution of fresh and used materials were assessed by scanning electron microscopy (Hitachi S2400 with Bruker light elements EDS detector).

The CaL reactivity and stability of the natural and waste materials were assessed in a fluidized-bed laboratory scale unit. Approximately 5 g of material were loaded into the quartz reactor and pre-activated at 930 °C for 7 min, under 50 % of CO_2 flow (CO_2 from Air Liquide, $\geq 99.998 \%$) balanced with air (v/v) (reconstituted air, Air Liquide). After this step, the reactor temperature was cooled down to 800 °C, and the carbonation step was conducted in the same gas mixture. This procedure was repeated along ten carbonation-calcination cycles. The steam flow was introduced by passing the dry gas stream (air and CO_2) through a water bubbler system that includes a saturator (gas washing bottle) filled with distilled water and submerged in a thermostatic bath. The Antoine equation was used to calculate the required saturator temperatures, and the volumetric fraction of steam in the overall gas flow was verified using a humidity sensor. Figure 1 shows a schematic representation of the experimental setup.

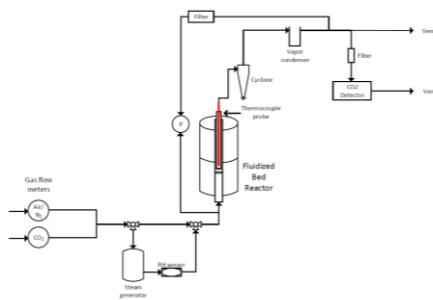


Figure 1. Lab Scale fluidized-bed reactor scheme.

Results and Discussion

Characterization

The limestone and waste marble (WM) materials were characterized by elemental analysis to evaluate the distribution of the constituents. The Ca content is very similar (32.80 and 39.24 wt.%) for all materials, which correspond to purities between 81.9 and 98.0 % of CaCO_3 . As expected the natural materials presented some impurities like Si, Mg, Al, or Fe (major ones) and Na, K (residual ones). The surface areas of the materials are inferior to $2 \text{ m}^2/\text{g}$.

XRD analysis was performed to identify the crystalline phases of limestone and marble materials (Figure 2). The identified peaks correspond to the calcium carbonate phase in the form of calcite (the polymorph with more thermodynamic stability). It is also possible to identify peaks of quartz. The crystallite size of materials was estimated using Scherrer's equation ($D = k\lambda/b\cos\theta$), D is the crystallite size (nm), b is full width at half maximum (FWHM) of the XRD peak, λ is the wavelength (0.15406 nm), θ is the Bragg angle (degree) and K is the Scherrer constant ($K = 0.9$, assuming spherical particles). The crystallite sizes were around 70 ± 10 nm, normally higher for waste marbles than limestones.

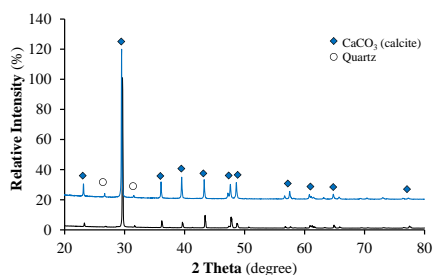


Figure 2. Representative XRD patterns of limestone (blue line) and waste marble (black line) materials.

Limestone or waste marble materials are mainly composed of agglomerated semi-cubic non-uniform particles that are nonporous (Figure 3a). The grain size distribution confirms that

more than 50-60% of particles are between 355-500 μm (Figure 3b).

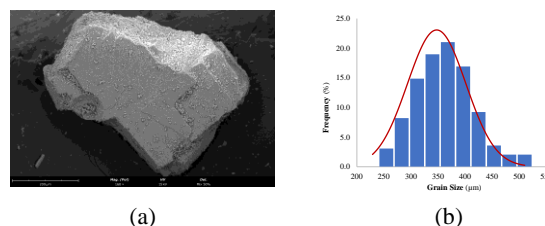


Figure 3. Morphological characterization of waste marble material (a) SEM image (x160); (b) Grain size distribution.

CaL experiments

After 10 cycles, all materials tested show a significant deactivation along the cycles. Figure 4 presents the results obtained from one limestone and one waste marble. The best materials present a CaO carbonation conversion of around 14-20 %, which corresponds to a heat release efficiency of 263-366 kJ/kg of CaCO_3 , from the 6th cycle.

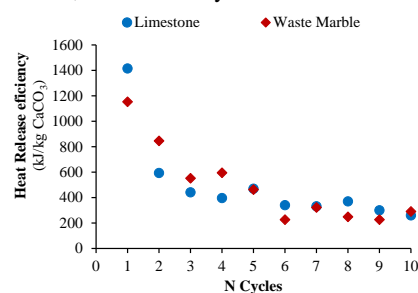


Figure 4. HSD of limestone and WM materials through 10 carbonation-calcination cycles.

To improve the performance of these materials the study of steam introduction on the gas flow was carried out. The optimization of the steam addition on the gas flow was carried out firstly on the calcination step with different fractions (% , v/v) of steam (2.5%, 5%, and 10%) and reaction temperatures (890, 905, 915 and 930 $^{\circ}\text{C}$). Independently of steam fraction (% , v/v), at the two lower temperatures the calcination step does not finish in 7 min. At 915 and 930 $^{\circ}\text{C}$ for 7 min, 2.5% of steam was enough to accelerate the calcination reaction. Preliminary results show that the addition of steam accelerated the CaCO_3 decomposition, decreasing the temperature needed to reach the same calcination efficiency. Also, the characterization of the materials after the CaL experiments points out that along the cycles the presence of steam reduces the diffusion resistance through the carbonate layer, and small pores are generated, which increase the efficiency and stability of the material.

Acknowledgments

Authors thank FCT in Portugal for funding the following projects: "Solar-driven Ca-Looping Process for Thermochemical Energy Storage" (PTDC/EAM-PEC/32342/2017); Centro de Química Estrutural (UIDB/00100/2020 and UIDP/00100/2020), the Institute of Molecular Sciences (LA/P/0056/2020).

References

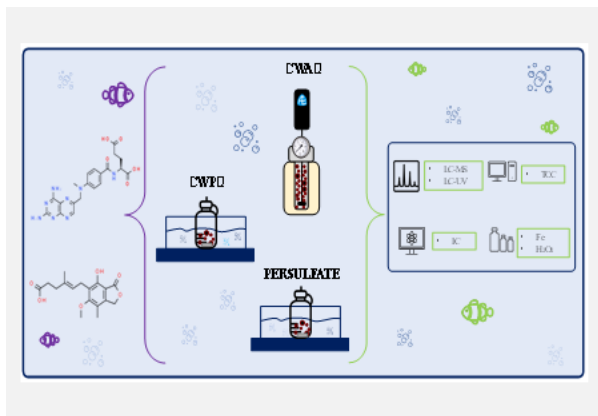
- [1] P. Teixeira et al., Separation and Purification Technology, 235 (2020) 116190.
- [2] Y. Yang et al., Energies, 14 (2021) 6847.
- [3] L. André, S. Abanades, Energies, 13 (2020) 5859.
- [4] K. Wang et al., Chemical Engineering Journal, 390 (2020) 124163.
- [5] A. Coppola et al., Separation and Purification Technology, 189 (2017) 101-107.
- [6] A.K. Burnham et al., Fuel, 59 (1980) 871-877.
- [7] S. Guo et al., Energy Fuels, 29 (2015) 7572-7583.

Removal of cytotoxic contaminants through advanced oxidation processes with a catalyst derived from sewage sludge

*D. Huber-Benito**, M. Martín-Martínez, M. Larriba, V.I. Águeda, J. García

Catalysis and Separation Processes Group (CyPS), Chemical Engineering and Materials Department, Faculty of Chemistry, Complutense University of Madrid, Avda. Complutense s/n, 28040 Madrid, Spain.

dihuber@ucm.es



Traditional disposal methods of sewage sludge are becoming less significant, making it necessary to develop economically viable and environmentally friendly technologies to recycle this residue. Sludge derived carbons can be used as catalysts in advanced oxidation processes to remove emerging pollutants. The presence of methotrexate and mycophenolic acid in wastewater treatment plants effluents suggests conventional treatments are ineffective, requiring more efficient methods. This study involves synthesizing a catalyst from sewage sludge and comparing its effectiveness in advanced oxidation processes, such as CWAO, CWPO, and persulfate, to eliminate cytostatic compounds.

Introduction

Sewage sludge is considered a potential source of secondary environmental contamination due to the presence of various pollutants such as organic contaminants, pathogens, and heavy metals [1], that causes a potential risk to human health and the environment. Traditional management techniques for sewage sludge disposals, such as incineration, fertilizer, or composting are decreasing in significance. Thus, it is crucial to create novel economically viable and environmentally friendly technologies, to recycle the resource and energy present in sludge, while also removing pollutants. One way of using this residue is manufacturing sludge-derived carbons (SDCs). These materials are versatile owing to the effects of surface functional groups, the existence of microporous and mesoporous structures as well as metal ions [2].

SDCs can work as catalysts in advanced oxidation processes to facilitate the generation of sulfate radicals, superoxide radicals, and hydroxyl radicals with low energy requirements and transition metals for degrading refractory pollutants. This may be attributed to the presence of many nutrients (N and P), metals (Ni, Zn, Mg, Ca, Ti, Cu, Fe, and Al), O, Si, S, and carbon which have always been involved in the preparation of different heterogeneous carbonaceous catalysts [3]. Thus, SDCs have been used in some catalytic systems, like the persulfate decomposition for bisphenol A degradation [4] or the degradation of m-cresol by catalytic wet peroxide oxidation (CWPO) [5].

The presence of methotrexate and mycophenolic acid in the wastewater treatment plants (WWTP) effluents suggests the low removal of these compounds through conventional treatments [6, 7]. Therefore, new and more efficient processes are necessary to prevent their release into the environment. Over the years, numerous studies have suggested advanced methods such as ozonation, electrooxidation, or photocatalysis for removing these types of compounds. However, the use of a sewage sludge-derived catalyst in heterogeneous oxidation has not yet been examined for eliminating them.

Methods and Results

This study involves synthesizing a catalyst through pyrolysis, followed by acid treatment using HNO_3 . To ensure proper washing, water treatment at 97°C is conducted. More details on the treatment of sewage sludge are presented in Figure 1. The resulting material exhibits a S_{BET} of $387\text{ m}^2/\text{g}$. Figure 2 displays the FTIR spectrum. This spectrum exhibits a prominent peak at 1050 cm^{-1} , related to the silicon content of the materials. The band at 1500 cm^{-1} can be attributed to carbonyl ($\text{C}=\text{O}$) groups. Finally, the broad band at 3500 cm^{-1} is characteristic of $-\text{OH}$ and $-\text{NH}$ surface functional groups.

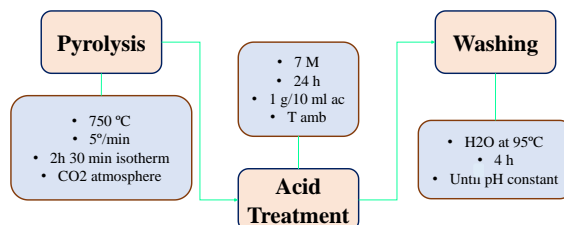


Figure 1. Steps and conditions for the synthesis of the catalyst.

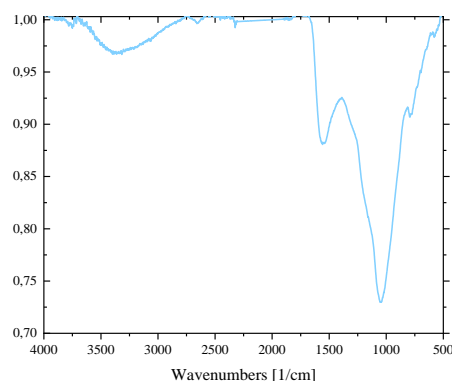


Figure 2. FTIR spectra of the catalyst synthesized.

Finally, the catalyst has been used in different advanced oxidation treatments of cytostatic compounds, particularly catalytic wet air oxidation (CWAO), CWPO, and persulfate-

based advanced oxidation. The capacity of the catalyst to produce the needed oxidation radicals for each process has been evaluated.

Acknowledgements

This work has been supported by the MICINN through the CATAD3.0 project PID2020-116478RB-I00. In addition, the authors acknowledge funding from the Comunidad de Madrid (Spain) through the REMTAVARES Network (S2018/EMT-4341).

References

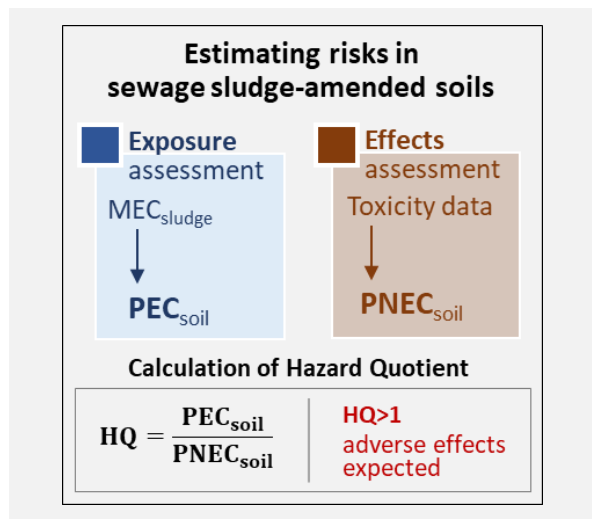
- [1] L. Feng et al., *Science Technology*, 49 (2015) 4781-4782.
- [2] L. Yua et al., *Desalination and Water Treatment*, 202 (2020) 169-182.
- [3] N. Ruiz-Gómez et al., *Waste Management*, 59 (2017) 211-221.
- [4] C. Huang et al., *Journal of Materials Chemistry A*, 6 (2018) 8978-8985.
- [5] Y.M. Wang et al., *Journal of Hazardous Materials*, 326 (2017) 36-46.
- [6] N. Negreira et al., *Science of the Total Environment*, 497-498 (2014) 68-77
- [7] M.S.F. Santos, *Science of the Total Environment*, 645 (2018) 1264-1272.

Sewage sludge as agricultural fertilizer - a screening of environmental risk assessment for PAHs, PCBs, synthetic musks and volatile methylsiloxanes

*F. Rocha**, *V. Homem*

LEPABE - Laboratory for Process Engineering, Environment, Biotechnology and Energy, Faculty of Engineering, University of Porto, Rua Dr. Roberto Frias, 4200-465 Porto, Portugal; ALiCE - Associate Laboratory in Chemical Engineering, Faculty of Engineering, University of Porto, Rua Dr. Roberto Frias, 4200-465 Porto, Portugal.

**ficrocha@fe.up.pt*



Although there are obvious economic and environmental advantages to the agricultural valorization of sewage sludge, further research is needed to determine if the contaminants loading in this matrix poses a risk to the sustainability of agricultural soil and the safety of farm goods. The reported levels of polycyclic aromatic hydrocarbons (PAHs), polychlorinated biphenyls (PCBs), synthetic musk compounds (SMCs), and volatile methylsiloxanes (VMSs) in sewage sludge were surveyed literature over the past decade. The collected data was used to estimate the environmental risk of these contaminants in sludge-amended agricultural soils. PCBs occurrence was rare, while individual PAHs were often detected in sewage sludge at significant amounts. Galaxolide and tonalide were the predominant musks and cyclic siloxanes D5 and D6 the most prevalent contaminants of their class. A risk assessment evaluation reported the highest risk for 9 PAHs and 1 SMC, with the remaining targets presenting a HQ < 1.

Introduction

Sustainability of agricultural production needs a paradigm shift on how to handle the problem of farmland nutrients depletion. Farmers still heavily rely on chemical mineral-based fertilizers (N, P, K), whose production requires energy-intensive processes and is dependent on geographically rare and limited ore deposits [1]. Policymakers are committed to promote waste recycling towards a circular economy model, and closing nutrient loops by reusing biodegradable wastes, such as sewage sludge, might minimize this dependency [1,2].

Sewage sludge is high in organic matter and macro and micronutrients that promote plant development. In fact, its application on farmland has been related to benefit soil fertility, in addition to improving the physical and structural properties of the soil [1,2]. On the other hand, concerns about sewage sludge unpleasant odor and the presence of pathogens, heavy metals, and numerous chemical contaminants in its composition have prevented its use [2-4]. To ensure the safety of the soil compartment and farmed goods, several countries already implemented legislation to regulate sewage sludge application to farmland. In the European Union (EU), for instance, the Council Directive 86/278/EEC sets limits for heavy metals in sewage sludge and receiving soils, and some Member States went farther, establishing limit levels for pathogens and some organic micropollutants, such as PAHs, PCBs, dioxins, and furans [4]. This EU regulation is currently under review to meet recent scientific findings and align with the current EU green policy landscape, with one of the topics under discussion being the establishment of thresholds for contaminants of emerging concern in sewage sludge.

Assessing the occurrence and the environmental risks of such contaminants in sewage sludge, especially when its use in farmland is considered, is of the utmost importance. The state of the art on this topic is well described for a few chemical species (e.g. heavy metals, PAHs, and PCBs), whose levels have been monitored for a longer time, and for which mitigation measures such as their prioritization on watchlists and the establishment of legislated limits are already in place [4]. But further research

is needed to address the situation regarding a wide range of other potentially hazardous contaminants, including pharmaceuticals and those used in cosmetics and toiletries [3,5].

The purpose of this work is to outline recent studies on the occurrence of PAHs, PCBs, SMCs, and VMSs in sewage sludge, in order to estimate the environmental risk of these organic contaminants in sludge-amended agricultural soils. PAHs and PCBs constitute 2 classes of persistent and legacy contaminants, whose incidence in sewage sludge and potential threat to the soil compartment shall still be monitored. SMCs, used as fragrances, and VMSs, used as additives to ease the application of personal care products, are both massively used worldwide and continuously released to wastewater treatment plants (WWTPs), accumulating in sewage sludge [5]. Recent studies have monitored their levels in this matrix, and due to their environmental persistency and bioaccumulation potential, their possible risks for the soil compartment should be evaluated.

Methodology

Scientific literature from 2010 onwards was reviewed to obtain a snapshot of the levels of PAHs, PCBs, SMCs, and VMSs in sewage sludge samples from municipal WWTPs worldwide. The prevalent compounds reported at higher concentrations were considered for the environmental risk assessment study, carried out following the approach proposed by the European Union Technical Guide Document on Risk Assessment [6]. The measured concentrations in sewage sludge were used to estimate the predicted environmental concentrations in soil (PEC_{soil}), considering a rate of sludge application of 0.5 kg_{dw}/m².y (approximately 5.5 ton/ha) and standardized agricultural soil mixing depth (0.20 m) and bulk density (1700 kg/m³) parameters. PEC values were then compared to the predicted no-effect concentrations (PNEC_{soil}), established based on assessment factors and toxicological data. Hazard quotients (HQ_s = PEC_{soil}/PNEC_{soil}) were then calculated and used for the prioritization of the target compounds in sludge-amended soil (HQ > 1 indicates that adverse effects may occur, since the exposure concentration exceeds the PNEC).

Results and Conclusions

A total of 68 studies reporting the levels of at least one of the classes of compounds under analysis in sewage sludge were reviewed. PAHs were the most frequently targeted, followed by PCBs, musks, and siloxanes (Table 1). Reported concentrations vary considerably, depending on numerous factors such as the features and processes employed in WWTPs, type of sludge samples analyzed (primary, activated, or digested), source of effluents treated (domestic, industrial, agricultural), and geographical areas served. Nonetheless, it was possible to identify some trends regarding the frequency and the relative levels of the studied compounds. Concerning the analysis of PAHs in sewage sludge, most work has focused on 16 of these chemicals, all of which are frequently detected in most samples, notably 4- and 5- ring PAHs, and some 3-ring ones. Average total concentrations ranged between 2.4 $\mu\text{g}/\text{kg}_{\text{dw}}$ and 86 $\text{mg}/\text{kg}_{\text{dw}}$. Higher levels were frequent in samples from WWTPs located in densely populated areas also treating industrial effluents (up to 280 $\text{mg}/\text{kg}_{\text{dw}}$). In the case of PCBs, most studies focused on the monitoring of 6 or 7 congeners (nos. 28, 52, 101, 118, 153, 138, 180). This class of contaminants were the least detected, or present only at very low concentrations. These findings are consistent with the fact that these chemicals have been banned or heavily regulated worldwide. Even so, significant amounts of these legacy pollutants were reported in a few samples from WWTPs processing industrial effluents, with total values up to 7 $\text{mg}/\text{kg}_{\text{dw}}$.

Regarding SMCs, polycyclic musks are more frequently detected, with galaxolide and tonalide representing more than

90% of all musks content in most studies. Nitromusks were also assessed, but their occurrence and levels were minimal when compared to the polycyclic ones. Macrocyclic musks were the least targeted group of synthetic fragrances. As for VMSs, their occurrence was reported in all studies, primarily the cyclic ones (D5 and D6 were those found at highest concentrations, >90% of total content), which goes in line with their use in toiletries formulations. For both SMCs and VMSs, the total mean and median levels were the highest of all classes of contaminants targeted (Table 1), which underlines the need to further monitor and study the potential environmental hazards of these chemicals in sewage sludge. The risk assessment for individual contaminants was performed using reported average amounts and, for a worst-case-scenario, the maximum stated values found in each study. An $\text{HQ}>1$ was consistently found for PAHs (9 of these compounds), for which $\text{PNEC}_{\text{soil}}$ values were relatively low (0.29 – 29.6 $\mu\text{g}/\text{kg}_{\text{dw}}$) due to their high toxicity for terrestrial organisms. No PCBs reported a $\text{HQ}>1$, but the individual amounts were often not disclosed (with its sum being reported instead), which hinders the risk assessment for individual congeners. Tonalide was the only musk with a $\text{HQ}>1$ (in 4 different studies), while HQ values for all individual VMSs were below 1. For these contaminants of emergent concern, the lack of experimental ecotoxicity data for terrestrial organisms may hinder the results of their potential hazard evaluation, since future data indicating higher toxicity may alter this assessment due to the consistently high reported concentrations for some of these chemicals.

Table 1. Overview of reported levels of PAHs, PCBs, SMCs, and VMSs in scientific literature, and their risk assessment highlights.

Class	Literature overview	Reported Average concentrations (Σ) ($\mu\text{g}/\text{kg}_{\text{dw}}$)	Reported maximum concentrations (Σ) ($\mu\text{g}/\text{kg}_{\text{dw}}$)	Compounds with $\text{HQ} > 1$ (n= number of studies)
PAHs	35 studies covered in 18 countries (16 compounds)	Range: 2.4 – 86000 Mean: 8300 Median: 2534	Range: 138 – 280000 Mean: 17115 Median: 4000	BaP (n=18), Pyr (n=18), BaA (n=6), B(bjk)F (n=6), Chry (n=6), Fl (n=2), DBaH A (n=2), BghiP (n=1), Ace (n=1)*
PCBs	20 studies covered in 14 countries (7 compounds)	Range: 0.5 – 2405 Mean: 396 Median: 89	Range: 16.4 – 6987 Mean: 1032 Median: 112	$\text{HQ} < 1$
SMCs	16 studies covered in 10 countries (18 compounds)	Range: 1744 – 83883 Mean: 19241 Median: 7223	Range: 4496 – 129926 Mean: 37408 Median: 15980	Tonalide (n=4)
VMSs	14 studies covered in 8 countries (7 compounds)	Range: 522 – 77870 Mean: 22947 Median: 16845	Range: 2360 – 113906 Mean: 32442 Median: 21703	$\text{HQ} < 1$

*BaP – benzo(a)pyrene; Pyr – pyrene; BaA – benzo(a)anthracene; B(bjk)F – benzo(b+j+k)fluoranthene; Chry – chrysene; Fl – Fluoranthene; DBaH A – dibenzo(a,h)anthracene; BghiP – benzo(ghi)perylene; Ace – acenaphthene.

Acknowledgements

This work was financially supported by: i) LA/P/0045/2020 (ALiCE) and UIDB/00511/2020 -UIDP/00511/2020 (LEPABE) funded by national funds through FCT/MCTES (PIDDAC); ii) Project PTDC/ASP-PLA/29425/2017 - POCI-01-0145-FEDER-029425, funded by FEDER funds through COMPETE2020 – Programa Operacional Competitividade e Internacionalização (POCI) and by national funds (PIDDAC) through FCT/MCTES; iii) Project "S4Hort_Soil&Food - Sustainable practices for Soil health & horticultural products quality improvement in the Entre Douro e Minho Region", with reference NORTE-01-0145-FEDER-000074, supported by Norte Portugal Regional Operational Programme (NORTE 2020), under the PORTUGAL 2020 Partnership Agreement, through the European Regional Development Fund (ERDF); iv) Project "HealthyWaters – Identification, Elimination, Social Awareness and Education of Water Chemical and Biological Micropollutants with Health and Environmental Implications", with reference NORTE-01-0145-FEDER-000069, supported by Norte Portugal Regional Operational Programme (NORTE 2020), under the PORTUGAL 2020 Partnership Agreement, through the European Regional Development Fund (ERDF); v) PhD Studentship 2020.09041.BD (Filipe Rocha), financed by FCT with funds from the State Budget and by the European Social Fund (ESF), within the framework of PORTUGAL2020, namely through NORTE 2020; vi) V. Homem thanks national funds through FCT, under the Scientific Employment Stimulus—Individual Call - CEECIND/00676/2017.

References

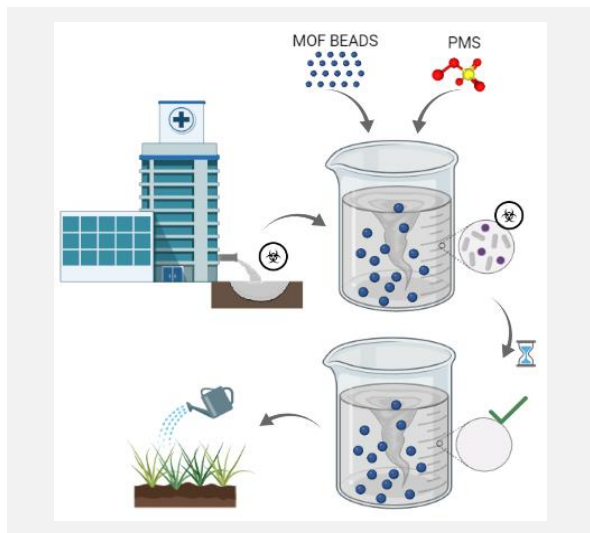
- [1] K. Chojnacka et al., *Bioresource Technology*, 295 (2020) 122223.
- [2] A.E. Kanteraki et al., *Science of the Total Environment*, 839 (2022) 156270.
- [3] K. Fijalkowski et al., *Journal of Environmental Management*, 203 (2017) 1126-1136.
- [4] M.C. Collivignarelli et al., *Sustainability*, 11 (2019) 6015.
- [5] V.S. Thomaidi et al., *Science of the Total Environment*, 548-549 (2016) 280-288.
- [6] J. de Bruijn et al., *Technical Guidance Document on Risk Assessment. Part 1. Part 2. EUR 20418 EN. 2002. JRC23785.*

New copper-based solid heterogenous catalyst for peroxymonosulphate activation for disinfection of wastewater

A. Giraldez*, M.A. Sanromán, M. Pazos

BIOSUV Research Group, CINTECX, University of Vigo, As Lagoas Marcosende s/n, Vigo, Spain.

*alba.giraldez.rodiguez@uvigo.gal



In order to provide solutions to the current global water problem, this study attempts to apply an effective treatment to reuse wastewater with a high amount of pathogens, mainly.

This study focuses on the application of an Advanced Oxidation Processes (AOPs) process based on the generation of sulphate radicals, using peroxymonosulphate activated with a heterogeneous catalyst. As a catalyst, a Metal Organic Framework (MOF) is used, which is a novel porous material formed by the union of transition metal ions through organic bridges. In particular, the MOF Basolite C-300[®] is used, which is characterised by being based on copper.

According to the results obtained, it is demonstrated that the catalyst can be immobilised in polyacrylonitrile beads to improve the handling of the MOF. Furthermore, it was observed that the catalyst can be easily recovered and thus reused in numerous disinfection processes, maintaining its disinfectant efficacy and without significant changes in the structure.

Introduction

At present, one of the biggest challenges is to treat the wastewater generated, in order to be able to reuse it and reduce the demand for new potable water for different actions in households as well as in industry. One of the main problems is found in the treatment of wastewater from hospitals because it contains a high quantity of organic matter, solvents, medicines, antibiotics, pathogenic microorganisms (*Escherichia coli*, *Enterococcus*, *Pseudomonas aeruginosa*, *Klebsiella sp.*, ...) virus and waste from radiation and x-rays, among others [1,2]. Traditional methods used in wastewater treatment plants (WWTPs) such as filtration with subsequent biochemical treatment are inefficient systems for these wastes and can even cause microorganisms to develop resistance to emerging contaminants, such as active pharmaceutical ingredients (APIs), present in wastewater [1].

On the other hand, AOPs do not have these limitations and could replace traditional treatments due to their proven effectiveness in degrading recalcitrant toxic compounds [3]. The most commonly used AOPs include ozonation, ultrasound, as well as hydroxyl radical and sulphate radical-based processes.

Sulphate radicals-based AOPs can be carried out using persulphate (PS) or peroxymonosulphate (PMS) as a precursor [3]. In the specific case of this study, the sulphate radicals are generated by activating PMS with heterogeneous catalysts via electron transfer from transition metals to PMS.

Furthermore, in this research, MOFs are used as heterogeneous catalysts. These compounds are recently developed multifunctional materials with large surfaces multiple active sites, and high stability, which are among their most distinctive features [4]. Besides, the most common form in which these MOFs are found is in powder form, which makes it difficult to handle them at the laboratory level, as well as to use them on an industrial scale in the future. This is due to the fact that recovery requires the use of filters of very few microns and losses are very common. Therefore, this study assessed the feasibility of immobilising it.

Objectives

The aim of this study is to evaluate the disinfectant power of PMS activated with a heterogeneous catalyst, specifically with the MOF Basolite C-300[®]. Moreover, it is to analyse if the disinfection power is maintained when the catalyst is immobilised- in polyacrylonitrile beads, in order to facilitate the reuse of the catalyst and to avoid the possible metal leaching after the treatment. In this study, *Escherichia coli* (*E. coli*) is used as the reference pathogen, which is one of the main pathogens present in these wastewaters.

Methods

The proliferation of the microorganism: to use the microorganism (*E. coli* CECT 102 from the *Colección Española de Cultivos Tipo*), it must be cultivated in a Meat Peptone Broth (MPB) medium by inoculation at 1% (v/v) and incubated in an orbital shaker (180 rpm, 37°C and without light) for 20 h (around 10¹⁰ colony-forming units (CFU/ml)). For the purpose to eliminate the interference of the culture medium, the culture in the stationary phase was centrifuged and the obtained cell pellet was washed with saline solution (0.9% w/w), concentrating it 10 times. This cell suspension was the initial suspension in the assays.

Immobilisation of catalyst: to improve the handling of MOF in heterogeneous reaction systems, it was decided to encapsulate the MOF Basolite C-300[®] in polyacrylonitrile (PAN) beads and to test if it presented advantages over the powered MOF phase. For the synthesis process of the MOF-PAN beads (MOF beads), the reported procedure was followed [5].

Disinfection tests: to evaluate the disinfection power of PMS activated with the MOF Basolite C-300[®] free or immobilised, flask-scale tests were performed using 100 mL of synthetic water (0.268 g/L (NH₄)₂SO₄, 0.06 g/L MgSO₄·7H₂O, 0.006 g/L MnSO₄·H₂O, 0.0003 g/L FeCl₃·6H₂O, 0.006 g/L CaCl₂·2H₂O and 1 g/L glucose anhydrous). Two flasks were incubated, one with only synthetic water and the pathogen (inoculated at 1% (v/v) 10¹⁰ CFU/mL; control assay) and the other with synthetic

water, the concentration of PMS, the catalyst tested and the pathogen (inoculated at 1% (v/v) 10^{10} CFU/mL). Both cultures were incubated in an orbital shaker (80 rpm, 25°C and without light). A sample (1 mL) was taken from each flask at 5, 15, 30, 60 mins and 24 h. The samples were seeded in a Petri dish with MPB medium, diluting the sample in the necessary serial dilutions of buffered peptone water solution or a neutralizing solution (4% w/v $\text{Na}_2\text{S}_2\text{O}_3$ diluted in 0.25 M KH_2PO_4), in order to obtain a CFU valid count. These plates were incubated in a culture chamber at 37°C for 24 h. After this time, if cell growth was obtained in the plates with samples from the flask with PMS and the catalyst, it indicated that the used concentration was not toxic to the microorganism.

Also, it is important to note that the number of colonies obtained per Petri dish had to be between 20 and 300 colonies for the result to be considered valid.

Cu leaching: to determine the amount of copper released into the water after the disinfection test, an ICP-analysis was carried out. For this purpose, at the end of the disinfection test, the medium (synthetic water) was filtered (using a 0.45 μm filter) and a 5 mL sample was stored in a glass tube at 4°C until subsequent measurement.

Results

Disinfection tests: firstly, different tests were carried out to evaluate the disinfecting power of MOF as powder and PMS alone. From these results it was observed that with a concentration of 2 mM MOF, a reduction in cell growth was achieved, but not removed completely after 24 h. The same was also achieved when a concentration of 0.1 mM of PMS alone was used.

Therefore, different concentrations of PMS catalysed by the MOF were evaluated until the optimum was obtained (2 mM PMS + 2 mM MOF; 0.1 M PMS + 0.03 mM MOF; 0.1 M PMS + 0.1 mM MOF and 0.1 M PMS + 0.17 mM MOF), achieving complete elimination of cell growth after 30 minutes using a concentration of 0.1 mM PMS and 0.1 mM MOF Basolite C-300[®].

MOF immobilisation: according to the procedure described previously, beads of the MOF Basolite C-300[®] were produced. They were made using a ratio of 30% MOF to PAN, as well as 8%, 60% and 80%, all these percentages based on weight. Physical and chemical characterization were done, and the obtained MOF beads were shown to be more resistant to mechanical stress with increasing MOF concentration. Furthermore, the MOF beads with a ratio of 30% (w/w) and 60% (w/w) showed a more homogeneous encapsulation of the MOF Basolite C-300[®].

Disinfection test with immobilised MOF: these optimum disinfection conditions were then tested using the immobilised MOF as a catalyst. In these tests, the 8% (w/w) MOF beads were unable to eliminate cell growth completely after 24 h. In contrast, the remaining MOF beads before 24 h were able to

eliminate all the pathogens. Therefore, it was analysed whether these characteristics were maintained when reused and whether the beads underwent any structural modification. The results after 24 h were as expected for the 30% (w/w) and 60% (w/w) MOF beads, with losses of less than 20% in weight for both beads.

Figure 1 shows a graphical summary of several tests performed in this study, evaluating the disinfection using MOF, as powder or immobilised, as catalyst for sulphate radical production.

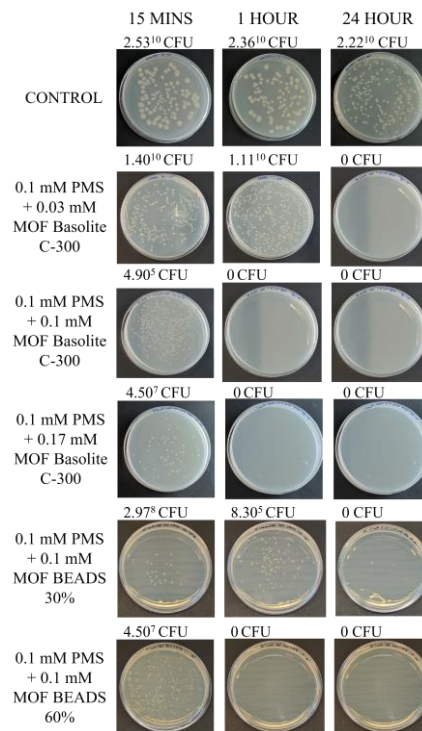


Figure 1. *E. coli* grown in MPB medium Petri dishes during the tests performed.

Cu leaching in the tests: From the results, it was observed that around 45% of copper was released in the tests using the MOF Basolite C-300[®] in powder form and around 2% for each use of the MOF beads.

Conclusions

Consequently, it can be concluded that the MOF Basolite C-300[®] is a multifunctional material because it has disinfectant powder and at the same time it is a great heterogeneous catalyst. As a result of the immobilization of the MOF in beads, their recovery and subsequent reuse are facilitated, and the MOF maintain their disinfectant power after numerous serials uses with leaching around 2%. In addition, the process has great potential for application in environmental remediation with the possibility of large-scale implementation.

Acknowledgements

This research has been financially supported by Project PDC2021-121394-I00 funded by MCIN/AEI/10.13039/501100011033 and by the European Union Next Generation EU/PRTR, Project PID2020-11GBI00 funded by MCIN/AEI/10.13039/501100011033 and Xunta de Galicia and the European Regional Development Fund (ED431C 2021-43).

References

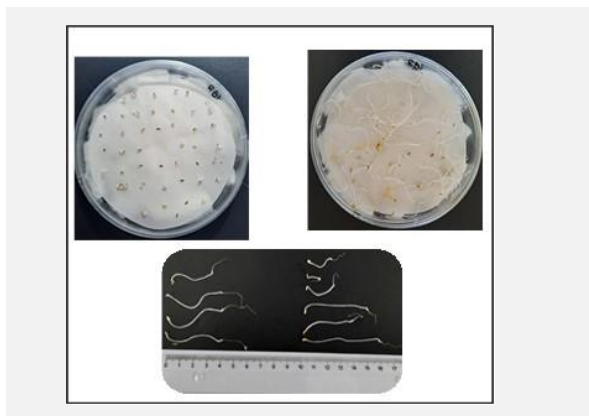
- [1] J. Scaria, P.V. Nidheesh, Environmental Research, 217 (2023) 114786-114794.
- [2] B. Pratap et al., Chemosphere, 313 (2023) 137547-137561.
- [3] S. Giannakis et al., Chemical Engineering Journal, 406 (2021) 127083-127103.
- [4] Y. Xun et al., Chemical Engineering Journal, 462 (2022) 142021-14043.
- [5] B.J. Riley et al., ACS Applied Materials and Interfaces, 12 (2020) 45342-45350.

Study of nanoplastics impact on seed germination of *Lactuca sativa*

A.M. Barreiros^{1*}, D.P. Varela¹, E.B. Moura¹, L.R. Araújo¹, M. Barrocas¹, H. F. Silva^{1,2}, J. Coelho^{1,3}, S. Piçarra^{3,4}, M. Matos^{1,5}, N. Silva^{1,2}, C. Oliveira²

¹DEQ-ISEL-IPL, Dep. de Engenharia Química do ISEL/IPL, R. Conselheiro Emídio Navarro 1, 1959-007, Lisboa, Portugal; ²CQE, Institute of Molecular Sciences, Dep. de Química e Bioquímica, FCUL, Campo Grande, 1749-016 Lisboa, Portugal; ³EST do Barreiro, IPS, Rua Américo da Silva Marinho, 2839-001 Lavradio, Portugal; ⁴CEQ, Institute of Molecular Sciences, Dep. de Engenharia Química, IST/UL, Av. Rovisco Pais 1, 1049-001 Lisboa, Portugal; ⁵IT – Instituto de Telecomunicações, IST/UL, Av. Rovisco Pais 1, 1049-001, Lisboa, Portugal.

*ana.barreiros@isel.pt



Water is a natural resource vital for the survival of humanity and all species on earth, however, it is a limited resource. Water reuse enables circular water use and can contribute to a reduction of freshwater usage and promote agriculture and water sustainability. Nevertheless, it also has the potential of polluting both surface water and groundwater and may have negative effects on soil and plant.

The main aim of this study is to evaluate the effect of treated wastewater (TWW) containing nanoplastics (either alone or combined with toxic metals, (Cd, Cr, Pb and Ni) on lettuce seed generation test.

The result point to different direction, namely from a strong combined effect of nanoplastic and toxic metals in lettuce growth.

Introduction

Freshwater resources are scarce and increasingly under pressure. Water reuse can limit abstractions from surface waters and groundwater and promote a more efficient management of water resources [1]. Reutilization of treated wastewater (TWW) further contributes for minimizing the use of fertilizers since TWW contains an acceptable concentration of nitrogen and phosphorus. But TWW may also contain other pollutants, such as metals or nanoplastics (Np), the latter originating either from natural degradation of micro and/or macroplastics or from products such as cosmetics, paints, electronic devices, among others [2].

Nanoparticles are tiny particles with a size range between 1 and 100 nanometers, and they have unique physicochemical properties that can lead to enhanced reactivity, increased surface area, and altered toxicological effects. Due to their small size, they can easily penetrate cell membranes and interact with biological systems, which can potentially lead to adverse health effects.

However, the behavior and impact of Np can be highly dependent on the type of Np, the environmental conditions, and the exposure duration and concentration. For example, some studies have shown that Np can bind with organic molecules, such as proteins or lipids, which can reduce their toxicity or alter their biodistribution in the body. In other cases, Np may increase the toxicity of organic molecules or cause oxidative stress, inflammation, or genotoxicity [3,4].

Therefore, it is essential to consider the context of exposure when assessing the impact of Np, and further research is needed to understand the complex interactions and mechanisms of Np toxicity. Regulatory agencies also monitor the use of Np in consumer products and industrial applications to ensure their safety and minimize potential risks to human health and the environment [5].

This study aims to analyze the impact of using TWW containing nanoplastics (either alone or combined with toxic metals, (Cd, Cr, Pb and Ni) on lettuce seed generation test. The germination test is a simple method of environmental biomonitoring [6].

Materials and Methods

Spheric nanoparticles of polymethylmethacrylate (PMMA) with a mean diameter of 132 nm (st. dev. 25 nm) were produced by microemulsion and characterized by both Light Diffraction (Mastersizer, Malvern) and Transmission Electron Microscopy (Hitachi H8100 Electron Microscope). These particles were used to simulate the Np, as PMMA is one of the nanoplastic found in waters [7, 8, 9]. Seven pairs of twin solutions (in tap water / TWW) were prepared: 5 pairs with Np in decreasing concentrations, a pair of control solutions (water / TWW only) and an extra pair containing Np plus the above mentioned toxic metals (at the maximum concentrations allowed by law in Annex XVIII of Decree-Law 238/96) [10]. Lettuce seeds were let to germinate inside petri dishes, in the dark, at an average temperature of 21 °C. Each 3 petri dishes were poured every two days with one of the above mentioned waters. After a week, parameters as the germination ratio, average root length, average seedling length and total mass were determined and analyzed.

Results

At figure 1 it is possible to observe that there were no significant differences in the germination ratios of lettuce seed poured with Np containing waters when compared to the controls. Despite the increased Np concentration and the presence of toxic metal, germination of the lettuce seeds seems quite tolerant to the presence of Np in the pouring water. This might be related to the barrier effect of the seed coat, that may prevent Np and metals from meeting the embryo.

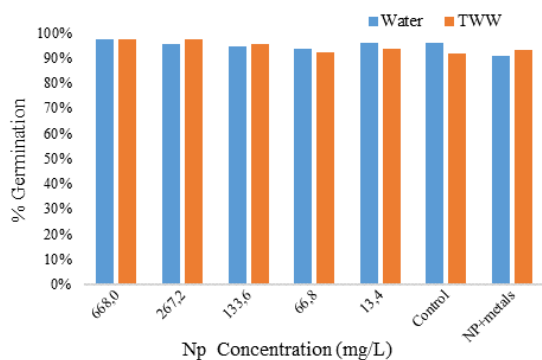


Figure 1. Germination rate variation for the tested conditions.

Acknowledgements

We would like to thank Instituto Politécnico de Lisboa as the entity promoting and financing the project (Project IPL IDI&CA 2022, with the acronym NpRiskH2O) and the participation of Erasmus students Julia Kozak and Bruno Caruso.

References

- [1] EEA (2023) <https://www.eea.europa.eu/ims/use-of-freshwater-resources-in-europe-1>.
- [2] C.C. Gaylarde et al., *Environmental Pollution*, 272 (2021) 115950.
- [3] T. Wu, M. Tang, *Journal of Applied Toxicology*, 38 (2018) 25-40.
- [4] Wided Najahi-Missaoui et al., *International Journal of Molecular Sciences* 22 (2021) 385.
- [5] J. Allan et al., *Regulatory Toxicologies and Pharmacology*, 122 (2021) 104885.
- [6] W. Wang, P.H. Ketri, *Water, Air and Soil Pollution*, 52 (1990) 369-376.
- [7] Y. Li et al., *Environmental Research* 204 (2022) 112134.
- [8] V.V. Annenkov et al., *Environmental Pollution* 278 (2021) 116910.
- [9] S. Singh et al., *Chemosphere* 290 (2022) 133169.
- [10] Decreto-Lei n.º 236/98 de 1 de agosto, N.º 176/1998, Série I-A, 3676-3722.

Combined results of the average root length, average seedling length and total mass obtained after the same germination time point to a different direction, namely from a strong combined effect of Np and toxic metals in lettuce growth.

Conclusions

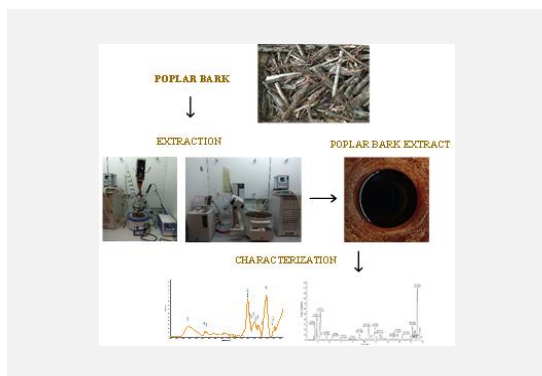
The results reported here display an alternative towards the valorization of compost derived from MSW. Active catalysts were prepared from compost, which allowed to remove up to 47 and 51% of TOC and COD, respectively, as well as the color, depending on the chosen conditions, of highly polluted leachate waters obtained in mechanical and biological treatment units.

Evaluation of potential applications for poplar bark, a byproduct from food packaging

S. Oliveira^{1*}, S. Monteiro^{1,2,3}, J. Santos^{1,2,3}, R.A. Fernandes^{1,2,3}, B. Freitas¹, N. Ferreira^{1,4}, I. Ferreira⁵, C. Vieira⁵, F.D. Magalhães^{2,3}, J.M. Martins^{2,3,4}, L.H. de Carvalho^{2,3,4}

¹ARCP - Associação Rede de Competência em Polímeros, Rua Júlio de Matos, 828/882, 4200-355 Porto, Portugal; ²LEPABE – Laboratório de Engenharia de Processos, Ambiente, Biotecnologia e Energia, Faculdade de Engenharia da Universidade do Porto, Rua Dr. Roberto Frias, 4200-465 Porto, Portugal; ³ALiCE - Associate Laboratory in Chemical Engineering, Faculdade de Engenharia da Universidade do Porto, Rua Dr. Roberto Frias, 4200-465 Porto, Portugal; ⁴DEMad – Departamento de Engenharia de Madeiras, Instituto Politécnico de Viseu, Campus Politécnico, 3504-510 Viseu, Portugal; ⁵FWFI - Freshwood Forms Industry, Lote 7, Zona Industrial da Vieira de Leiria, 2430-600 Vieira de Leiria, Portugal.

*susana.oliveira@arcp.pt



Poplar wood food-packaging products are a good alternative to the conventional fossil-based solutions. However, the process adopted in the industrial wood processing generates a great amount of by-products, as Poplar bark.

This work studied the potential valorization of poplar bark through alkaline extraction.

The obtained extract was characterized by FTIR-ATR spectroscopy, and HPLC-MS chromatography techniques. The chemical properties were also accessed through total phenol content, antioxidant activity, and Stiasny number. The results obtained of characterization of poplar bark extract showed that extract has potential to be used in the development of products with added value like adhesives, biopolymers, or components for the pharmaceutical or food industry.

Introduction

According to Propopulus, there are around 450.000 hectares of production-oriented poplar forests in the European Union. France, Spain, and Italy are the most relevant countries [1].

Poplar is widely used in the production of panels, paper, or for energy purposes by the wood processing industries [1].

Regarding to plywood production, Poplar is the main raw material in most countries due to its good properties, such as lightness, color, great homogeneity, and ease of processing [1,2].

During the industrial wood processing, particularly in the debarking step, a large quantity of bark is obtained, which is known to have a high content of extractives, namely polyphenols [2,3].

Due to the interesting properties of phenolic compounds, as anti-UV and antioxidant properties, their application as an additive in medicine, pharmaceutical or cosmetic industry has been widely studied [2,3]. In addition, the application of polyphenolic compounds in formulation of bio-adhesives or biopolymers have been also a hot-spot for scientific research [3,4].

The aim of this work is to evaluate the potential application of poplar bark extract as bio-adhesive in the manufacturing of food packaging solutions.

The chemical composition of the extracts was accessed by FTIR-ATR spectroscopy, HPLC-MS, antioxidant activity, the total phenol content, and the Stiasny number.

Methods

Hybrid poplar (*Populus x canadensis* Moench.) subproducts (vener cuts and bark) were supplied by Freshwood Forms Industry. Firstly, poplar bark was grounded in a cutting mill (Retsch, Haan, Germany) and the materials were oven-dried at 60 °C until attaining the equilibrium moisture content. Then, they were sieved by a vibratory sieve shaker (Retsch, Haan, Germany). The particle sizes between 500 µm and 2 mm were selected as raw material to obtain the extracts.

Extraction

The extract from poplar bark was obtained under alkaline conditions. The alkali extraction was performed with 1% NaOH, 80 °C, and 60 minutes. Solid/liquid ratio was fixed at 1/10, on dry basis.

After that, the material was filtered under vacuum using a Buchner funnel, and the extract was concentrated in a rotary evaporator (BUCHI).

The extraction yield was calculated based on the difference between material mass before and after drying, on dry basis, and expressed in percentage.

Total phenols content

The total phenols content was determined by the Folin-Ciocalteu method [5,6,7]. The phenols content was calculated as a gallic acid equivalent from the calibration curve of gallic acid standard solutions (2-40 µg/mL). Results were expressed as mass of gallic acid equivalent (GAE) as a function of 100g of extract, on dry basis.

Antioxidant activity

The antioxidant activity of the extract was determined by the FRAP (ferric reducing/antioxidant power). The relative antioxidant activity of the poplar bark extract was calculated from the calibration curve of L-ascorbic acid (0.1-0.2-0.3-0.4-0.5-0.6 mmol/l). The results were expressed as nmol of ascorbic acid equivalent (AAE) as function mg of extract, on dry basis.

Stiasny number

The Stiasny number of the poplar bark extract was determined according to the proposed by Yazaki and Hillis [4,7]. The Stiasny number was calculated from the ratio of the mass of the precipitate to the total dissolved solid content of the tannin extract. The result is expressed as a percentage.

Fourier Transform Infrared Spectroscopy (FTIR)

The infrared spectra were recorded using a VERTEX 70 FTIR spectrometer (BRUKER) in transmittance mode with a high sensitivity DLATGS detector at room temperature. Samples were measured in ATR mode, with a A225/Q PLATINUM ATR Diamond crystal with single reflection accessory. The

spectra were recorded from 4000 to 500 cm^{-1} with a resolution of 4 cm^{-1} .

HPLC-MS chromatography

Liquid chromatography analysis was conducted using a Vanquish HPLC (Thermo Scientific). Chromatographic separation was performed in an Atlantis T3 column 2.1×100 mm, 3 μm (Waters, Milford, MA USA). The LC equipment was coupled to an Orbitrap Exploris 120.

Results and Conclusions

The main properties of the extract were characterized and are present in Table 1.

Table 1. Extraction Yield and characterization of poplar bark extract.

Extraction Yield (%)	Total phenols content (g GAE/100 g extract)	Stiasny number (%)
11.14±0.58	43.86±1.95	37.04±1.26

GAE: Gallic acid equivalent.

Extraction yield obtained is similar to the values obtained for other interesting lignocellulosic by-products like eucalyptus or pine bark. Concerning the total phenol content in the aqueous poplar bark extract, it is lower than the value obtained by Diouf et al. [8] for aqueous Trembling Aspen Bark extracts. However, it is slightly higher than that obtained previously by other authors for Eucalyptus bark extracts (21.9 g GAE/100 g extract) using similar extraction conditions [8]. The authors demonstrated that the extract presents a high proportion of polyphenolic components. The Stiasny number was lower than the minimum Stiasny value to produce high-quality adhesives of 65% indicated by Yazaki and Collins [7]. The identification of chemical compounds from poplar bark by FTIR-ATR is shown in Figure 1.

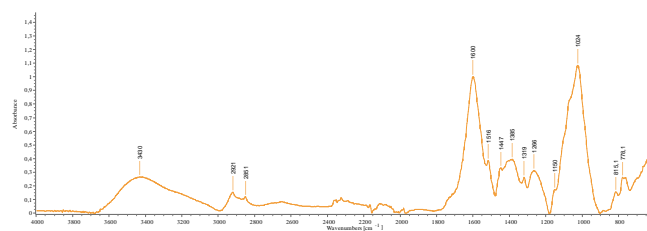


Figure 1. FTIR spectra of poplar bark extract (4000-500 cm^{-1}).

The most relevant peaks and groups of the extract are shown in Table 2.

Acknowledgements

The authors gratefully acknowledge the funding by: LA/P/0045/2020 (ALiCE) and UIDB/00511/2020—UIDP/00511/2020 (LEPABE) funded by national funds through FCT/MCTES (PIDDAC); Project Embalagem do Futuro®, Agenda Verde for Business Innovation, investment project n° 59, financed by the PRR, NextGenerationEU.

References

- [1] Propopulus - The European Poplar Initiative. Available online: European poplar, a local, sustainable, efficient choice - Propopulus (accessed on 12 april 2023).
- [2] E. Autor et al., *Biomolecules* 12 (2022) 539.
- [3] R.K. Devappa et al., *BioEnergy Research*, 8 (2015) 1235-1251.
- [4] E. Araujo et al., *Journal of Cleaner Production*, 280 (2021) 124324.
- [5] M. Cruzado et al., *Revista de la Sociedad Química del Perú*, 79 (2013) 57-63.
- [6] G. Vázquez et al., *Wood Science Technology*, 46 (2012) 443-457.
- [7] G. Vázquez et al., *Industrial Crops and Products*, 29 (2009) 364-370.
- [8] P.N. Diouf et al., *Wood Science Technology*, 43 (2009) 457-470.

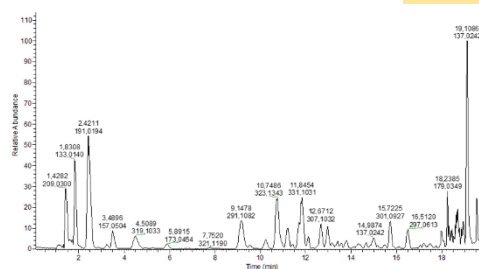


Figure 2. HPLC-MS chromatogram.

Table 2. FTIR peak of poplar bark extract.

Peak (cm^{-1})	Range (cm^{-1})	Group
3430	3336	-OH stretch
2921	2916-2936	-CH ₂ - asymmetric stretch
2851	2843-2863	-CH ₂ - symmetric stretch
1600	1500-1600	C=C (polyphenols)
1516	1510	C=C symmetric stretching aromatic (polyphenols)
1447	1450-1455	C-H bending
1385	1380-1400	C-C stretching
1319	1260-1350	CHR-OH deformation
1266		
1150	1155	C-O stretching (C-OH, C-O-C)
1024	1025-1035	C-O, C-C, and C-C-O bending
815	810-850	C-O-C symmetric stretching
778	720-750	C-C skeletal vibrations

The intensity of the main bands of the FTIR spectra indicate that the most abundant components in the poplar bark extract are hydrolysable tannins. In lower amount are condensed tannins, and sugars. This is in agreement with the low Stiasny number obtained (due to the lower reactivity of hydrolysable tannins towards formaldehyde), and the considerably high total phenol content.

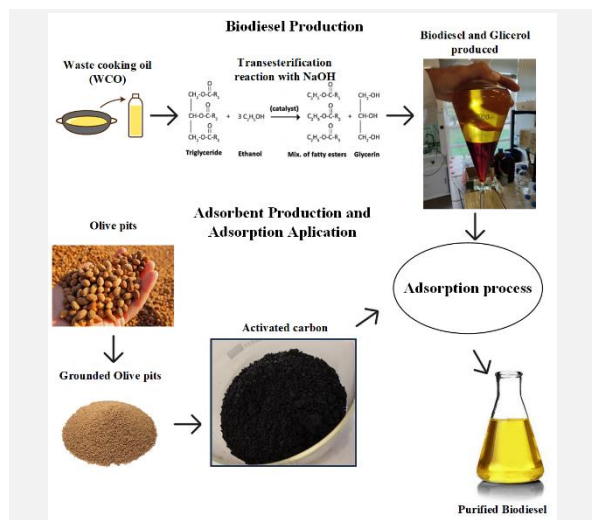
The monomeric components of the extract were identified by HPLC-MS. The resulting signal was processed by the base peak method, and the chromatogram obtained is presented in Figure 2. In the extracts, it was detected that hydroxybenzoic acids, catechin, epicatechin (from condensed tannins) and ellagic acid structures (hydrolysable tannins) were the most important monomers. Regarding the results obtained, the valorization of poplar bark by alkaline extraction was an interesting way to obtain extracts with the potential to be used in the development of value-added products, like adhesives, biopolymers or components for the pharmaceutical or food industry.

Study of biodiesel production from waste cooking oil by ethyl transesterification and its purification with the use of natural adsorbents

G.L. Camilo^{1,2,3*}, M.C.S. Gomes³, A. Queiroz^{1,2}, A. Ribeiro^{1,2}, P. Brito^{1,2}

¹Centro de Investigação de Montanha (CIMO), Instituto Politécnico de Bragança, Campus de Santa Apolónia, 5300-253 Bragança, Portugal; ²Laboratório para a Sustentabilidade e Tecnologia em Regiões de Montanha (SusTEC), Instituto Politécnico de Bragança, Campus de Santa Apolónia, 5300-253 Bragança, Portugal; ³Universidade Tecnológica Federal do Paraná, Jardim Paraíso, 86812-460, Apucarana, Brasil.

*glaminocamilo@gmail.com



Biodiesel production from waste cooking oil (WCO) has become an economic opportunity and an environmental strategy to help address the global challenges of renewable energy production. Considering classical industrial processes for biodiesel production, adsorption and ion exchange technologies are the most commonly used alternatives for crude biodiesel purification. These methods, also known as dry cleaning methods, use an appropriate adsorbent to selectively remove certain impurities from the liquid biodiesel phase through contact with the surface of the adsorbent. Dry cleaning offers several advantages, including simple integration into an existing industrial plant, shorter purification time, lower water consumption, and lower effluent generation. In this work, the main goals are the optimization of ethylic biodiesel production from WCO, followed by the study of its purification by adsorption, applying various types of previously characterized natural adsorbents, physically and chemically activated, which were obtained from residual biomass (olive pits), with a specific focus on glycerol removal.

Introduction

In recent years, a collective effort is being made in search of alternative forms of energy through renewable and friendlier to the environment sources. Currently, about 80% of the world consumption of energy comes from fossil fuels. The environmental problems associated with the use of these non-renewable fuels include air pollution and global warming [1]. In this scenario, biodiesel presents itself as a renewable fuel, environmentally friendly and with similar characteristics to common diesel. The cost of conventional biodiesel production is higher than the production of diesel from petroleum. Since it is produced mainly from high quality virgin oils, it is estimated that 70 to 80% of the total cost of biodiesel production is associated with the cost of their raw materials [2]. With this perspective, biodiesel production from waste cooking oil (WCO) has become an economic opportunity and an environmental strategy to help address global renewable energy challenges and contribute to a sustainable society [3]. Transesterification is the most used method to reduce the viscosity of vegetable oils, and the most accessible and available alcohols for this reaction include methanol and ethanol. The use of ethanol for production adds an even more sustainable character to the process, due to its world production being mainly through sugar cane plantations. Among the purification processes for crude biodiesel, the wet wash method, which uses water to purify the esters, is the most frequently used. On average, for each liter of purified biodiesel, the amount of water needed for purification varies from 0.2 to 10 liters. Wet washing is also energy and time consuming and economically inefficient. The literature indicates that effluent treatment costs account for 0.09 to 3.8% of the total cost of production [4]. Adsorption and ion exchange are the most commonly used affinity separation processes worldwide, which are also known as dry washing methods. Dry cleaning offers several advantages over wet

cleaning, including ease of integration into an existing plant, shorter purification time, lower water consumption and lower effluent generation [5].

Activated Carbon (AC), activated fiber (carbon fiber) and activated alumina are among the most usual adsorbents in industrial applications. AC, which shows a large porous volume and high surface area, can be manufactured from any organic material rich in carbon, such as: sawdust, wood, coal, peat, fruit nuts, bituminous coal, lignite, coconut husks and olive pits [5].

Objectives

The main objectives of this work are the optimization of biodiesel production from waste cooking oil by alkaline transesterification using ethanol and the purification of the biofuel produced using activated carbon adsorbents produced from ground olive pits, focusing on the removal of free glycerol from biodiesel.

Methods

Initially, an optimization of the production of biodiesel from WCO by the ethylic transesterification route is sought. The optimization was carried out by a response surface methodology based on a Box-Behnken design for the study of 3 parameters: alcohol:oil molar ratio, reaction temperature and catalyst concentration. Subsequently, the synthesis of several adsorbent materials based on natural sources, such as olive pits, was implemented. The procedure employed for zinc chloride activation was adapted from [6] and the procedure for the physical activation at 800°C was carried out in a muffle furnace for 1 hour, with a heating rate of 10°C/min. The N₂ adsorption-desorption experiment were conducted at 77K using a commercial surface area and pore size analyzer (Quantachrome Instruments – Model Novatouch LX4). The samples were degassed at 120°C for 16 hours. The surface area

was obtained using the BET model (Brunauer-Emmett-Teller) and the pore size distribution was assessed by the DFT method (Density Functional Theory).

For the determination of free glycerol content in the biodiesel produced, the methodology developed by [7] was followed. Adsorption kinetics was evaluated at temperatures of 25°C, 35°C and 45°C. For each batch, 80g of biodiesel, adsorbent concentration equal to 5%wt was used, and contact times of 5, 10, 15, 30, 60, 120, 240, 360, 1380 and 1440 min.

Results

The two most impacting parameters in the percentage of fatty acid ethyl esters (%FAEE) in the biodiesel produced are the alcohol:oil ratio and the temperature. The percentage of catalyst was not able to have an impacting influence on the yield. Below, in Figure 1, the contour surface for the study of the two parameters of greatest influence on the %FAEE.

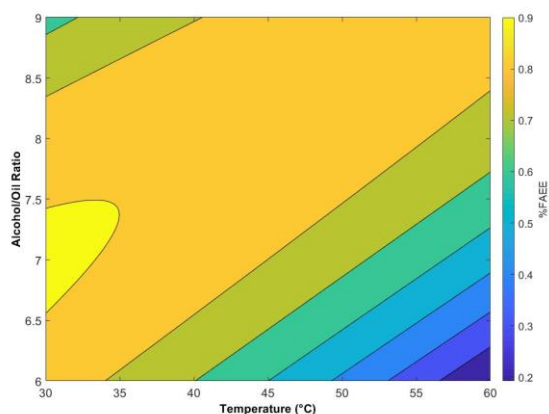


Figure 1. Contour Plot of %FAEE vs. Alcohol:Oil ratio vs. Temperature.

It was possible to observe the possibility of using waste cooking oil for the production of biodiesel. The optimal conditions for biodiesel production were determined as being 30°C, 7.5 alcohol/oil ratio and 1%wt of catalyst.

Table 1 shows the results of the analysis of the surface area for the activated carbons produced and the precursor used, olive pit. The production of activated carbons demonstrates promising textural properties, with two materials with surface areas greater than 300 m²/g.

Table 1. Some textural properties of the adsorbents.

Adsorbent	Surface area (m ² /g)	Pore diameter (nm)
Precursor	1.3798	2.7436
H ₃ PO ₄ - 500°C	171.7740	0.7742
KOH - 800°C	61.1832	1.5381
Physical - 800°C	374.5070	0.8260
ZnCl ₂ - 500°C	936.9390	2.1684

Acknowledgements

The authors are grateful to the Foundation for Science and Technology (FCT, Portugal) for financial support through national funds FCT/MCTES (PIDDAC) to CIMO (UIDB/00690/2020 and UIDP/00690/2020) and SusTEC (LA/P/0007/2021).

References

- [1] E. Arenas et al., *Processes*, 9 (2021) 1-12.
- [2] R. Ahmed et al., *Journal of Industrial and Engineering Chemistry*, 110 (2022) 1-14.
- [3] C. Chen et al., *Energy Reports*, 7 (2021) 4022-4034.
- [4] M. Catarino et al., *Chemical Engineering Journal*, 386 (2020) 123930.
- [5] H. Bateni et al., *Biofuel Research Journal*, 4 (2017) 668-690.
- [6] A.R. Hidayu et al., *Procedia Engineering*, 148 (2016) 106-113.
- [7] P. Bondioli et al., *European Journal of Lipid Science and Technology*, 107 (2005) 153-157.

The activated carbons with the highest areas were physically activated at 800°C and chemically activated with zinc chloride, both were selected for further adsorption studies.

In Figure 2, it is possible to observe some results of the adsorption kinetics study, carried out at 3 different temperatures for physically activated carbon at 800°C. An equilibrium time close to 4 hours of adsorption was observed. An increase in the adsorption capacity according to temperature was also observed, which can be explained by the better mass transfer due to the decrease of biodiesel viscosity.

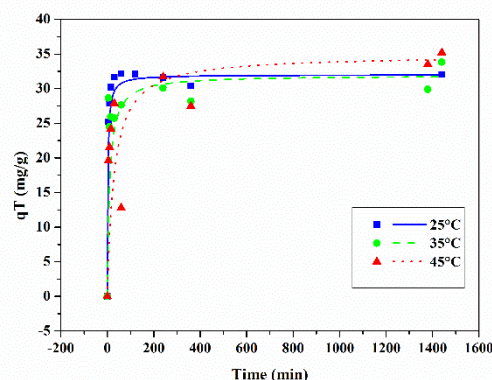


Figure 2. Kinetic study of 800°C-AC with 5% adsorbent concentration.

The pseudo-second order model (lines) was found to better fit to the experimental kinetic data (points). The obtained results are presented in Figure 2, and the related estimated kinetic parameters are shown in Table 2.

Table 2. Kinetic constants values.

T (°C)	q _e (mg/g)	K (g/mg.min)	R ²
25	32.01	0.01276	0.9998
35	31.94	0.00314	0.9942
45	34.86	0.00099	0.9946

Conclusions

The adsorption tests and analyzes demonstrated a good adsorption capacity for these materials, a moderate equilibrium time and therefore enabling the reduction or, with further studies, the complete avoidance of the use of water for the purification of the product, reducing the generation of effluents inherent to the conventional purification process. More research for the development of techniques can be carried out in the future, such as the study of adsorption in a continuous regime using a column packed with the adsorbent, and even a mixture of washing procedures with adsorption, in order to seek a drastic reduction on the consumption of water, and a simultaneous valorization of a residue as an adsorbent material.

Energy rationalization plan of a road transport company: elaboration and monitoring

P. Pereira^{1}, T. Santos^{1,2}, J. Puna^{1,3}*

¹Department of Chemical Engineering, Instituto Superior de Engenharia de Lisboa, Instituto Politécnico de Lisboa, 1959-007 Lisboa; ²CERNAS - Research Center for Natural Resources, Environment and Society, Coimbra, Portugal; ³CERENA - Centro de Recursos Naturais e Ambiente, Instituto Superior Técnico, Universidade de Lisboa, 1949-001 Lisboa, Portugal.

*tsantos@deq.isel.ipl.pt



The road transport sector is one of the main sources of atmospheric pollutants and contributor to the increase of greenhouse gases due to its high energy intensity and consumption of fossil fuels. In this sense, global policies are working to develop decarbonisation strategies aimed at sustainable transport, including measures for the use of alternative fuels. This study aims to support a company linked to the logistics sector within its commitments to energy efficiency and to achieve its sustainable development purposes. To achieve that, an energy performance of the company will be done within the scope of its road haulage activity and as a fleet owner. Afterwards, an energy audit will be carried out followed by an Energy Rationalisation Plan based on it. Results from emissions calculations and reporting can inform business decisions and actions that lead to emission reductions. This work is still under development.

Introduction

Global policies face major challenges in the field of energy and climate change, namely in the use of fossil fuels as a primary energy source for various sectors, including transport. The European Green Pact and other proposed policy documents are the strategy for the European Union (EU) to achieve climate neutrality by 2050 and an interim target of 55% greenhouse gas (GHG) emissions reduction by 2030 compared to 1990 [1].

The transport sector represents one of the main consumers of petroleum products, thus contributing decisively to energy dependence, and to GHG emissions and other pollutants [2]. It was observed that the total GHG emissions by transports in the EU Member States (EU27) increased around 33.5% in the past three decades (Figure 1). In particular, the GHG emissions from road transport increased 27.8% [3], which was quite significant in comparison with other activity sectors (Figure 1).

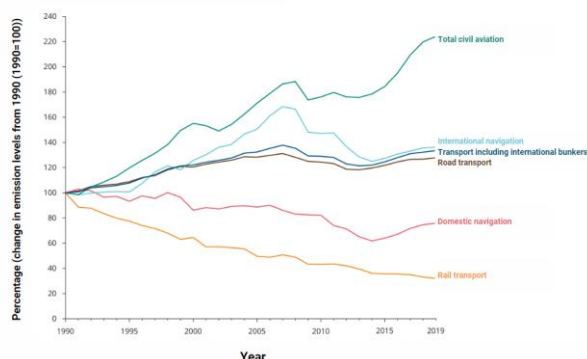


Figure 1. Trends in GHG emissions by transport mode in the EU-27, 1990-2019 [3]. Reference value of 100% for 1990.

This sector is also the most energy-intensive and with the greatest indirect contribution to primary energy imports and associated energy dependence [4].

Particularly in Portugal, transport represents an important part of final energy consumption, being the road transport responsible for almost all of that consumption. In this case, it is urgent to adapt appropriate policies to achieve carbon neutrality [2].

The challenges to be faced are essentially linked to solutions for other forms of mobility, and the underlying technological developments to ensure alternatives in forms of mobility. To achieve carbon neutrality, it will be necessary to evolve from a linear economic model sustained by fossil fuels to a circular and carbon neutral model [5].

This project aimed to assess and improve the energetic and environmental performance of the company TIEL - Transporte e Logística, S.A. in the scope of its activity of Goods Road Transport.

Methodology

The present work has as a case study the company TIEL. The TIEL Group is focused on its core business, which is the road transport of goods, and within this sector it consistently seeks to focus on the sub-sector of specialised transport, namely energy and chemicals. The company firmly believes that it has the capability to adapt to any future changes in the energy paradigm. It is confident that hybrid solutions will dominate for at least ten to fifteen years, during which time the primary energy sources will still be commercialized by the current oil companies and transported by land, particularly in tanker vehicles (such as biofuels, natural gas, and hydrogen).

The company is a fleet owner, with an annual energy consumption higher than 500 tonnes oil equivalent(tonne)/year, complying with the Ordinance n° 228/90 of the 7th of April, which approves the Regulation of the Management of Energy Consumption for the Transport Sector (RGCE Transports) [6]. In this context, and aligned with the measures set out in Directive N°2012/27/EU of the European Parliament and

Council, of 25 October 2012 [7], an energy audit was carried out on the consumption recorded by the company in the transport of goods by road in order to reduce the GHG emissions and promote the use of renewable energy sources.

The company has a diversified fleet adjusted to its needs in relation to the markets where it operates and the clients it serves. To carry out the energy audit, a series of data related to road haulage was selected and analysed, including key items for the sector (energy prices, fleet characteristics, energy sources consumed, Euro emission control standards, engine power). In line with the literature, several parameters were also assessed, namely final energy consumption (FEC), distance travelled, GHG emissions and energy class of the tyres used in the fleet [8].

Results

From the result of the energy audit to the transport process, referring to 2022, it is registered that TIEL owns 168 motorised transport units out of which 95% are powered by diesel and 5% by liquefied natural gas (LNG). The vehicles have the most varied types, brands and models and have around 6.8 years old.

From the collected and processed data, it was verified that the company has an energy-intensive fleet with an energy consumption of 3,671.2 toe in 2022. It was also observed a specific energy consumption of 283 goe/Vkm (Figure 2), in the form of fuel consumption by the means of transport, namely using diesel and LNG. More in detail, in the year 2022 it was possible to verify a slight improvement in the performance of fuel consumption (Diesel and LNG) per unit of distance travelled. This fact was considered a good record in view of the worsening performance in 2021 (Figure 2). There was also a 3.3% increase in specific energy consumption, measured in GHG/Vkm, in 2021, 6.5% above the forecasted in the Energy Rationalization Plan (ERP) for 2022 (Figure 3), returning the values of this indicator to levels of energy efficiency similar to 2018 as shown in Figure 2.

Acknowledgements

The authors acknowledge the Administration of TIEL for the information availability and for the support along the development of this study.

References

- [1] Europarl, 2022; <https://www.europarl.europa.eu/factsheets/pt/sheet/68/politica-energetica-principios-gerais>
- [2] APA, 2022, Relatório do estado do ambiente – Transporte de mercadorias; <https://rea.apambiente.pt/content/transporte-de-mercadorias?language=pt-pt> e.pt
- [3] EEA, 2022; Transport and environment report 2021 Decarbonising road transport - the role of vehicles, fuels and transport demand; European Environment Agency; <https://www.eea.europa.eu/publications/transport-and-environment-report-2021>
- [4] RP, FA, APA; 2019; Roteiro para a Neutralidade Carbónica 2050; República Portuguesa, Fundo Ambiental, Agência Portuguesa do Ambiente; <https://descarbonizar2050.apambiente.pt/>
- [5] Europarl, 2023; <https://www.europarl.europa.eu/news/pt/headlines/society/20190926STO62270/como-a-ue-podera-atingir-a-neutralidade-carbonica-ate-2050>
- [6] Ordinance n° 228/90 of the 7th of April; Official Gazette N°72/1990, Series N°I, Ministry of Industry and Energy.
- [7] Directive N°. 2012/27/EU, of the European Parliament and of the Council, of 25 October 2012.
- [8] T. Sofia et al., Transportation Research Part A, 170 (2023) 1-25.

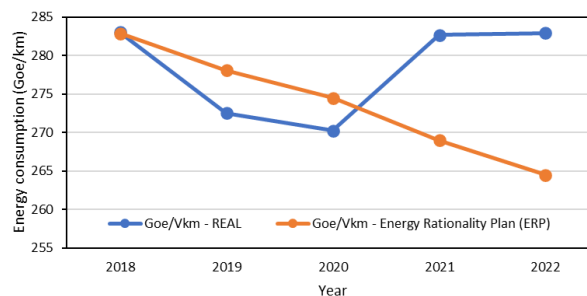


Figure 2. Comparison between the real and estimated (by the ERP) specific energy consumption over the years.

It was also noticed a reduction in the CO₂ emissions for each litre of fuel (diesel and/or LNG) consumed. This fact derives from the constant introduction of vehicles powered by LNG, and their maximum occupation and allocation to services that travel long distances, thus promoting the adoption of less polluting fuels.

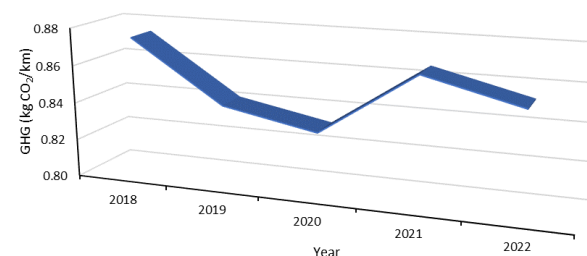


Figure 3. GHG emissions between 2018 to 2022.

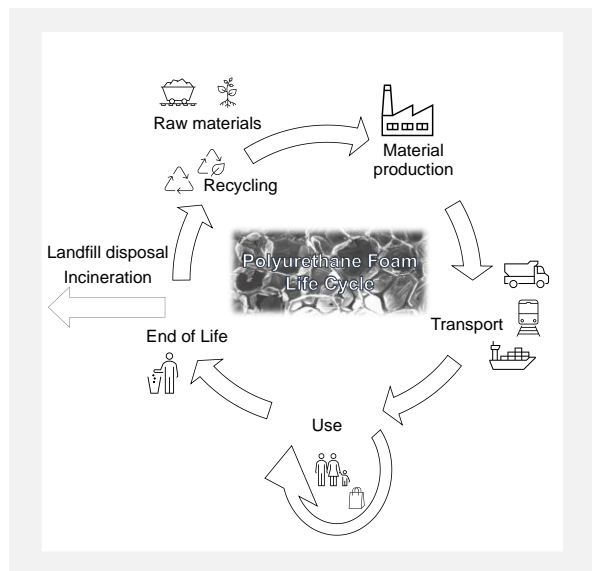
Still regarding the previous point, due to the fact that the percentage of the fleet powered by LNG is not significant, there is no improvement in CO₂ emissions per unit of distance travelled, which can be seen by the identical shapes of Figures 2 and Figure 3. In a second phase, the work plan will consist in defining a set of measures and commitments that will allow the energy consumption reduction of the company and will actively contribute to the rationalization of energy consumption in the sector in accordance with the regulatory obligations of RGCE Transports. This will be achieved through the identification of operational and behavioural measures for a rational economy of consumption and viable technical solutions to subsequently define the ERP.

Comparison of environmental assessments of polyurethane foams

R. Silva^{1*}, A. Barros-Timmons¹, P. Quinteiro²

¹CICECO - Aveiro Institute of Materials and Department of Chemistry, University of Aveiro, Campus Santiago, 3810-193 Aveiro, Portugal; ²Centre for Environmental and Marine Studies (CESAM), Department of Environment and Planning, University of Aveiro, Campus Universitário de Santiago, 3810-193 Aveiro, Portugal.

*raquelasilva@ua.pt



Polyurethane (PU) is one of the most useful polymers, being PU foams (PUF) circa 50% of its global market. As PUF production is mainly dependent on fossil feedstocks the increasing environmental concerns, have been promoting the development of greener alternatives. Yet, the possible green benefits need to be assessed and compared to conventional process. This study covers the results from a systematic literature analysis about life cycle assessment (LCA) studies on PUF produced using a variety of feedstocks. Emphasis is given to the methodological choices followed, and the need to harmonize results in order to establish comparisons and understand their effect. Specifically, for the most evaluated life cycle impact category, global warming (GW), the results fall in the 2.95 to 7.67 kgCO₂eq/FU range, depending on the feedstocks used.

Introduction

PU is one of the most versatile polymers, its global market is predicted to grow to 27,61 million metric tons in 2026. PUF represent approximately 50% of the global PU market and are generally classified as flexible, semi-rigid and rigid according to their structure and subsequent properties. This variety of properties is the main reason for their use in several distinct industrial applications.

The conventional raw materials of PUF production, isocyanates, and polyols, are fossil-based and in the case of isocyanates, rather hazardous. To address the central point of the European Green Deal which aims at reducing greenhouse gas (GHG) emissions and decoupling economic growth from resource use significant changes must be considered to find alternative raw materials and optimization of manufacturing processes. Hence, both academia and industry have been developing strategies to replace or reduce them with renewable and safer products that ensure, at least the main properties of conventional products.

LCA is a standardized and widely recognized methodology that evaluates the potential environmental impacts associated with a product by compiling and evaluating inputs (e.g., energy and raw materials), outputs (emissions to air, water, and soil) and corresponding impacts over the product' life cycle [1].

LCA has been applied to study the environmental performance of fossil-based PUF, namely for thermal insulations purposes [2] and of alternatives used in its production such as the use of chemically recycled polyols, bio polyols, and polyols obtained by CCU (carbon capture and utilization). Quinteiro et al. [3] carried out a study to compare the environmental performance of fossil-based PUF with bio-based PUF incorporating different ratios of fossil and bio-based polyols, including the production of PUF using waste cooking oils (WCO) -based polyol. In fact, the assessment of the environmental impacts of PUF is so important that some companies and associations regularly report the performance of PUF in Environmental Product Declarations (EPD) based on LCA methodology.

This work provides the first systematic review on LCA-based studies of PUF published in peer-reviewed journals, to evaluate to what extent have environmental effects on PUF already been addressed and quantified, and to understand whether PUF based on renewable resources are effectively more environmentally friendly than the fossil based PUF.

Material and methods

The procedure followed to conduct the literature review of published works referred to the environmental assessment of PUF. The literature search has been conducted by searching the Scopus database for relevant studies published or in press in peer-reviewed journals up to September 2022.

The following combined search terms: “polyurethane” and “life cycle assessment”; “polyurethane” and “life cycle analysis”; “polyurethane” and “carbon footprint”, and “polyurethane” and “circular economy”, were considered on titles, abstracts, and keywords.

A final sample of 10 articles published in peer-reviewed journals was obtained yet, only 8 allowed harmonization of GW results. In addition, EPD were also considered. Within this sample, each case study may involve different scenarios (i.e., different formulations of PUF, alternative raw materials, etc.), which were expressed as “occurrences”. Therefore, the sample encompasses 69 occurrences.

Results and discussion

Figure 1 shows the types of feedstocks of occurrences to produce PUF and PUF-based products, 4 types of feedstocks can be distinguished: i) fossil polyols; ii) bio-based polyols; ii) recovered fossil polyols, and iv) recovered biobased polyol, including polyol recovered from WCO.

Considering the approaches of the occurrences, 75% followed a cradle-to-grave, 18% a cradle-to-gate, and 7% a gate-to-gate approach.

Among life cycle impact assessment methods, CML-IA (developed by the Institute of Environmental Sciences of the University of Leiden) was the most widely used, representing 53% of the reviewed articles considered.

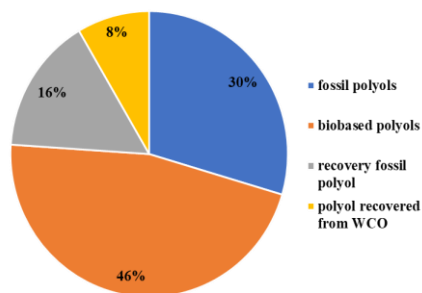


Figure 1. Type of feedstock of occurrences.

The ILCD (International life cycle data system), the IPCC (Intergovernmental panel on climate change), the IMPACT 2002+, and the TRACI (Tool for reduction and assessment of chemicals and other environmental impacts), were also methods used in the LCA studies considered. Additionally, more recent assessment impact assessment methods, such as Product Environmental Footprint (PEF; developed by the European Commission), were applied in two of the reports reviewed. The methodological choices contribute to the variation range among the study's results. To compare the impact assessment results, a harmonization of the results, by harmonizing the functional unit (FU), and declared unit for EPD, was performed by expressing the GW impact per 1 kg of PUF. The comparison of the total environmental results focusses on the GW because of its relevance for the evaluation of global climate change effects and it is the only impact category addressed in all the reviewed publications. The harmonization of the results presented should not be interpreted as a correction of the results found in the original publications, but rather as harmonized results that allow comparisons between different LCA studies. This harmonization makes it possible to distinguish ranges of useful values for comparing PUF studies and carrying out benchmarking. Figure 2 shows the harmonized results for GW of 69 occurrences from 8 articles and 7 EPD. It is clear that the values span through a wide range: fossil-based PUF present a variation between 2.95 kgCO₂eq/FU to 7.60 kgCO₂eq/FU; bio-based PUF between 3.10 kgCO₂eq/FU to 6.95 kgCO₂ eq/FU; the recovery fossil polyol -based PUF GW results vary between 5.43 kgCO₂eq/FU to 7.67 kgCO₂eq/FU, and WCO based PUF between 4.68 kgCO₂eq/FU to 5.51 kgCO₂eq/FU. This wide variation occurs mainly because of the use of different feedstocks to obtain PUF.

Acknowledgements

The authors would like to acknowledge the Portuguese Foundation for Science and Technology (FCT)/MCTES for the financial support to CICECO-Aveiro Institute of Materials, UIDB/50011/2020, UIDP/50011/2020 & LA/P/0006/2020, financed by national funds through the FCT/MEC (PIDDAC) and CESAM (UIDP/50017/2020+UIDB/50017/2020 + LA/P/0094/2020), through national funds. Paula Quinteiro also thank FCT/MCTES for contract CEECIND/00143/2017.

References

- [1] ISO, "Environmental Management – Life Cycle Assessment – Principles and Frameworks. ISO 14040.," International Organization for Standardization, Geneva, Switzerland, 2006.
- [2] H. Jang et al., *Journal of Marine Science and Engineering*, 9 (2021) 1099.
- [3] P. Quinteiro et al., *Journal of Cleaner Production*, 371 (2022) 133554.

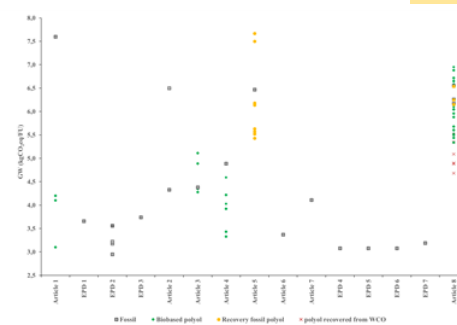


Figure 2. Harmonized GW per 1 kg of PUF.

In the biobased-PUF group the occurrences associated with higher GW impacts were observed for soybean-based scenarios, mostly due to the higher variations in carbon stocks associated with changes in land use compared to other crops [3]. In the recovery fossil polyol -based PUF, a smaller variation range is observed because they are all related to polyol recovery via the chemically breaking down of polyurethane scraps which were converted back into a reactive raw material. In the WCO based PUF only a small variation range is observed, since the variations are related to the same raw materials, with small changes in the formulation, comparing two different EoL (End of Life) [3].

Additionally, it was also concluded that overall, regardless the feedstock used and PUF formulation, the isocyanate is the main hotspot when addressing the GW of PUF (responsible for more than 50%). This is attributed to the production of intermediates, nitric acid and toluene, required to produce toluene diisocyanate (TDI), or aniline required to produce methylene diphenyldiisocyanate (MDI).

Conclusions

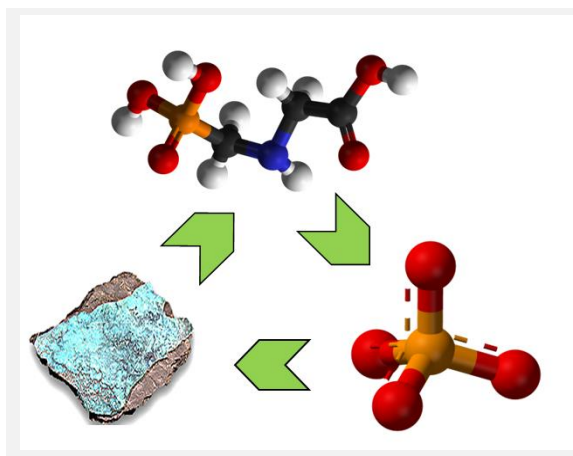
The bio-based polyols are the most studied type of feedstock with 44% of the occurrences. Overall, the higher values for GW are associated with the use of recovered fossil-based polyol mainly because extra energy and isocyanate are required. It could also be perceived that the ranges of the harmonized GW results for the fossil-based and bio-based feedstocks are very similar. The need for more consistent data and consensus LCA impact assessment methods between studies must be emphasized. Indeed, this worked has demonstrated the need for a consistent and robust framework for the harmonization of LCA results for all impact categories found in literature. Clearly this should be developed for PUF, as well as for LCA studies for alternative synthetic routes involving the synthesis of Non-isocyanate PU and/or the recently marketed green isocyanate, because the main hotspot identified comes from isocyanate feedstock.

Electrochemical recovery of phosphorus from aqueous solutions

C. Afonso*, A. Fernandes, L. Ciriaco, M.J. Pacheco, A. Lopes

FibEnTech-UBI and Universidade da Beira Interior, Av. Marquês D'Ávila e Bolama, 6201-001 Covilhã, Portugal.

*cesar.afonso@ubi.pt



In the last centuries, the food scarcity has boosted the use of synthetic fertilizers in agriculture, leading to environmental problems, like the exhaustion of raw materials, such as phosphate rock, and a higher release of nutrients into water bodies. In this work, the electrochemical oxidation of glyphosate, an herbicide, and the posterior removal of phosphorus from solution, have been studied as a technology capable of reducing the need for phosphorous raw materials and decreasing the phosphorus release into water bodies. Tests were conducted in galvanostatic and potentiostatic modes, using a boron-doped diamond anode and a titanium cathode. The highest glyphosate degradation rate was attained in galvanostatic mode, at the highest applied current density, with total organic carbon and nitrogen removals of about 80%. However, the highest phosphorus removal from solution was achieved in the potentiostatic mode, at low current. These results show that an optimization of the system is needed, to find the best conditions to, simultaneously, reduce organic load and recover phosphorus.

Introduction

Phosphorus is a key component of life, used in the growth and reproduction of many species [1]. It is also used extensively in agriculture and farming industries, in fertilisers and herbicides, such as glyphosate. However, the overuse of these treatments has led to critical levels of phosphorus in wastewater, which can promote eutrophication of water bodies and other major consequences [2], such as heavily affecting certain ecosystems, as is the case of glyphosate that is toxic to aquatic life and is thought to be carcinogenic to humans. Therefore, several new technologies for the removal and subsequent recovery of phosphorus from wastewater have been studied. One of such technologies with major potential involves electrochemical processes [3,4].

Objectives and Methodology

This study aimed the degradation of organic phosphorus and the recovery of phosphorus-containing compounds, from aqueous solution, by electrochemical processes. For that, glyphosate solutions, containing 10 mg L^{-1} of phosphorus, were treated in a one-compartment electrochemical cell, using a BDD anode and a Ti cathode. Tests duration varied from 1 to 6 h, and were either current-controlled (5, 10, and 30 mA cm^{-2}) or potential-controlled (5.0 V). Calcium chloride was added to the solution, to increase electrical conductivity and to supply the solution with calcium, to facilitate the formation of a precipitate. Several parameters were analysed to follow the electrochemical experiments: total organic carbon (TOC) and total nitrogen (TN), using a TOC/TN analyser; total phosphorus (P_{total}) and orthophosphates (P-PO_4^{3-}), through a spectrophotometric method; calcium (Ca^{2+}), chloride (Cl^-), chlorate (ClO_3^-) and perchlorate (ClO_4^-) ions, through ion chromatography.

Acknowledgements

This research was funded by project Carb2Soil (PRR-C05-i03-I-000030), through Plano de Recuperação e Resiliência (PRR), BI grant (project Carbo2Soil) awarded to C. Afonso, and by Fundação para a Ciência e a Tecnologia, FCT, project UIDB/00195/2020, and contract awarded to A. Fernandes.

References

- [1] D.M. Karl, Nature, 406 (2000) 31-33.
- [2] J. Elser, E. Bennett, Nature, 478 (2011) 29-31.

Results and Conclusions

It was found that the organic phosphorus was oxidized to phosphate, which was latter removed by cathodic precipitation. For the current-controlled assays, those conducted at the current density of 10 mA cm^{-2} (potential difference of $\approx 10 \text{ V}$), for 2 h, were the most efficient at removing phosphorus from solution, although the highest mass precipitated was attained at 30 mA cm^{-2} , with higher precipitate yields obtained at 6 h duration assays. However, the experiments conducted with potential control, at 5.0 V, showed the highest P_{total} removal, but low precipitate yields. These results indicate that phosphorus is removed in the first 2 h of the assays and at lower applied potentials. TOC and TN analysis showed a consistent decrease of total carbon and nitrogen throughout the assays, with higher reduction ($\approx 80\%$) at 30 mA cm^{-2} and 6 h. These results show the efficacy of the anodic oxidation process in the degradation of the glyphosate molecule and in the reduction of the organic load. The decrease in P_{total} concentration, observed in all experiments, indicated the degradation of the organic phosphorus in the solution. The increase in P-PO_4^{3-} concentration showed that the organic phosphorus was oxidised to phosphate. Ion chromatography data revealed a reduction in both chloride and calcium ions across all experiments. The decrease in Cl^- is due to its oxidation to ClO_3^- and ClO_4^- , visible on the chromatograms. The decrease in Ca^{2+} concentration, also detected by ion chromatography, is due to the salt precipitation at the cathode.

Although the two main objectives were attained, the best experimental conditions to simultaneously fulfil those objectives must be more worked out.

- [3] Y. Wang et al., Water Research, 209 (2022) 117891.
[4] Y. Ren et al., Environmental Functional Materials, 1 (2022) 10-20.

Removal of estrogens from water using activated carbon adsorbent materials prepared from olive stones

E.C. Milani^{1,2,3*}, M.L. Menezes³, J.L. de Tuesta⁴, A.E. Ribeiro^{1,2}, P. Brito^{1,2}, A. Queiroz^{1,2}

¹Centro de Investigação de Montanha (CIMO), Instituto Politécnico de Bragança, Campus de Santa Apolónia, 5300-253 Bragança, Portugal; ²Laboratório para a Sustentabilidade e Tecnologia em Regiões de Montanha (SusTEC), Instituto Politécnico de Bragança, Campus de Santa Apolónia, 5300-253 Bragança, Portugal; ³Universidade Tecnológica Federal do Paraná (UTFPR-AP), 86812-460 Apucarana, PR, Brasil; ⁴Department of Chemical and Environmental Technology, ESCET, Rey Juan Carlos University, Tulipán s/n, 28933 Móstoles, Madrid, Spain.

*eduriqueerick@gmail.com



Estrogens are a type of hormones that are continuously released to environment presenting several undesirable effects on aquatic species and human health even when present at very low concentrations. With the present work we will present an extensive set of experimental results that presents the valorization of olive stones residues to prepare activated carbons to be used as adsorbent for the removal of estrogens by adsorption from water. Five different adsorbents were produced and characterized. The carbonization yield, the pH at point of zero charge, BET surface area of the carbonaceous materials were measured. Additionally, FTIR analysis was also performed. The simultaneous removal of the three estrogens from water was evaluated for all five prepared adsorbents. For the adsorbent with the best removal performance, a kinetic study was carried out. The obtained results show that olive stones exhibit potential for the production of activated carbons with high surface area used to remove estrogens from water.

Introduction

Estrogens belong to the class of water micropollutants named as endocrine disrupting chemicals and are considered persistent substances in the environment. Estrogens are a type of hormones that are continuously released to environment presenting several undesirable effects on aquatic species and human health even when present at very low concentrations (trace levels) [1, 2]. Additionally, it is known that traditional sewage and drinking water treatment plants are not able to remove or degrade these compounds and additional treatments are required [3, 4].

Activated carbons (ACs) are low-cost carbonaceous materials with a high surface area. ACs undergo an activation process in order to increase its adsorption performance. Activation can be performed by physical treatment, in which the organic material is thermal treated with an atmosphere of air, CO₂, and water vapor, or also by applying some chemical treatments using generally, strong acids, chloride salts or strong bases [5].

As carbon source for ACs preparation, many precursors have been tested, mainly biomass wastes (olive stones, rice husk, coconut shell, among others). According to the Instituto Nacional de Estatística (INE), in 2021, Portugal produced more than 1.3 million tons of olives and it is estimated that more than 500,000 tons of residues were generated per year [6]. Currently, there is an effort to produce bio-based adsorbents that are able to remove efficiently a wide range of micropollutants from water [7].

Objectives

The main objective of this work is to prepare and characterize different types of adsorbents from olive stones. The selection of the better material is based on the highest removal performance of estrone (E1), 17 β -estradiol (E2) and 17 α -ethinylestradiol (EE2) from water matrices using adsorption process.

Methods

Five different adsorbents were produced, namely powdered olive stone (OS), physical activated at 800°C for 1h, with a heating rate of 10°C/min with N₂ flow of 20 cm³ min⁻¹ (CF), carbonized at 500°C for 1.5h with a heating rate of 10°C min⁻¹ in a sealed crucible (CC), chemical activated using phosphoric acid (CA) and chemical activated with sodium hydroxide (CB). The carbonization yield was calculated and the pH at point of zero charge (pH_{PZC}), BET surface area (S_{BET}) of the carbonaceous materials were determined (see Table 1). FTIR analysis of all materials was performed (Figure 1). The simultaneous removal of the three estrogens (E1, E2 and EE2) from water was evaluated for all the five prepared adsorbents. For the adsorbent with the best removal performance, a kinetic study was also carried out.

Results

The carbon production method significantly influences the carbonization yield. Acid activation was the method that allowed the highest yield (57.45%). The adsorbent's production method also has a significant impact on the adsorbents' pH_{PZC}, which is shown by the fact that the acid activation provides the material with the lowest pH_{PZC} (3.84). Acid activation was also the one that promoted the greatest increase in surface area with S_{BET} of 590 m² g⁻¹.

Table 1. Some surface properties and estrogen removal using five olive stone adsorbents.

Adsorbents	Yield (%)	pH _{PZC}	S _{BET} (m ² /g)	Total estrogens removal (%)
OS	-	5.43	4	24.2
CF	23.0	8.64	14	24.9
CC	26.9	8.46	67	51.2
CA	57.5	3.84	590	96.4
CB	33.9	8.92	27	36.6

In Figure 1, the band at 3438 cm^{-1} indicates the O-H stretching of alcohol and phenols [4]; the activated carbons suffered a drastic reduction in relation to the OS, due to the high temperatures (500 and 800°C) submitted. The band located at 2923 cm^{-1} indicates the stretching and bending of the C-H of the OS carbon chain [4]; activated carbons did not obtain a visible band in this region, showing that the carbonization process promoted the thermal decomposition of the C-H bonds and formation of carbon structures.

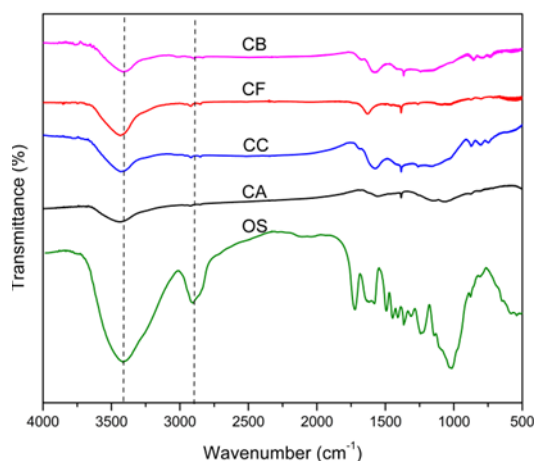


Figure 1. FTIR analysis of the five prepared adsorbents.

The adsorbent selection was performed by simultaneous adsorption of E2, EE2 and E1 at 25°C for 24h with an initial concentration of 2 mg L^{-1} of adsorbents at pH 7. Removal was proportional to surface area, thus the adsorbent with greater removal was the CA with 96.4% removal and was chosen to perform a kinetic study.

The kinetic study was carried out at temperatures of 25 , 35 and 45°C . Pseudo-first order, pseudo-second order and Elovich models were used to fit to experimental results obtained for the removal of total estrogens, as presented in Figure 2.

The equilibrium time was found to be 1800 min. The adsorption capacity at the equilibrium increased with the increase of temperature. The models that best fit to the experimental data was first the Elovich model, then the pseudo-second order and finally the pseudo-first order. This indicate that the adsorption of estrogens in this adsorbent occurs by a chemisorption process,

Acknowledgements

The authors are grateful to the Foundation for Science and Technology (FCT, Portugal) for financial support through national funds FCT/MCTES (PIDDAC) to CIMO (UIDB/00690/2020 and UIDP/00690/2020) and SusTEC (LA/P/0007/2021). J.L. Diaz De Tuesta acknowledges the financial support of "Comunidad de Madrid" (Spain) for the individual research grant 2020-T2/AMB-19836.

References

- [1] P. Bhatt et al., *Journal of Environmental Chemical Engineering*, 10 (2022) 107598.
- [2] D. Guerrero-Gualan et al., *Water*, 15 (2023) 353.
- [3] M. Gavrilescu et al., *New Biotechnology*, 32 (2015) 147-156.
- [4] F. Fadzail et al., *Materials Today: Proceedings*, 57 (2022) 1108.
- [5] M. Gayathiri et al., *Chemosphere*, 294 (2022) 133764.
- [6] Instituto Nacional de Estatística, <https://www.ine.pt/>. Accessed September 2022.
- [7] J.L. Diaz de Tuesta et al., *Journal of Environmental Chemical Engineering*, 9 (2021) 105004.

since the Elovich and the pseudo-second order models describe a chemical adsorption process.

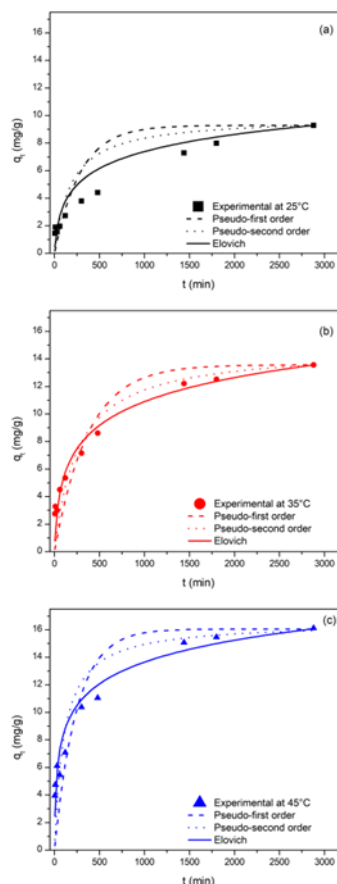


Figure 2. Adsorption kinetics of total estrogens for 15 mg of AC activated charcoal from 5 to 2880 min, with stirring at 150 rpm in 50mL of solution with an initial concentration of 2 mg L^{-1} of each estrogen at pH 7.0. Temperature of 25°C (a), 35°C (b) and 45°C (c).

Conclusions

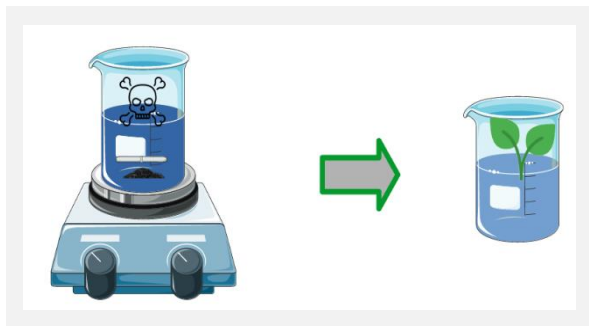
The results obtained show that acid activation (AC) prepared material is the adsorbent presenting the better removal performance. The overall results, confirm that olive stones exhibit potential for the production of adsorbents with high surfaces used to remove estrogens from water.

Application of commercial activated carbon for removal of copper (II) ions from aqueous media

R.S. Antônio*, M. de Souza

State University of Maringá, 5790 - Colombo Avenue, Maringá, Brazil.

*z.rodriigo.antonio@gmail.com



The present work aims to study the adsorption process as a separation technique for the removal of copper metal ions from aqueous media. Commercial activated carbon was used as adsorbent material. The microscopy analysis of the adsorbent material used showed great irregularities and cavities on the surface of the material suggesting high specific area. The kinetic model used was the Langmuir kinetic model.

Introduction

Water is fundamental for life on our planet. However, the scientific community has been issuing several warnings, through specialized literature, about the quality of liquid water, compromised due to the presence of numerous chemical constituents [1]. The chemical constituents present in water bodies are called emerging contaminants [2].

Although emerging contaminants are present in small amounts, the presence of these chemical constituents in water has been proven to affect the quality of life of living beings [3]. Moreover, studies prove that the amount of metals present in water bodies has been increasing over the years [4].

Thus, in view of the potential problems that can be generated by emerging contaminants, the adsorption process has been shown to be efficient in removing these contaminants from aqueous media [5].

Thus, the objective of this work is to study the application of bituminous activated carbon to remove copper (II) ions from aqueous medium as proposed in the graphical abstract.

Materials and Methods

For characterization of the material a Scanning Electron Microscope (SEM, QUANTAFEI-250) was used. The adsorption process was carried out in batch mode. For this, 1.5 g of activated carbon and 2 L of copper solution at a concentration of 7.5 mg L⁻¹ were used. Aliquots of 5 mL were collected during approximately 10 h, at determined time intervals and in such a way that the total collected volume of sample did not exceed 5% of the total volume of solution contained in the beaker. The experimental procedure was carried out at a constant temperature of (25 ± 2) °C and collected samples were read in an atomic absorption spectrophotometer (Varian SpectraAA 50B). The Qtiplo® software was employed to adjust the mathematical model studied, using the Scaled Levenberg-Marquardt algorithm.

The adsorption capacity of the material was determined using Equation (1):

$$q = \frac{(C_0 - C_t) * V}{m} \quad (1)$$

Where C_0 is the initial concentration and C_t is the concentration at a given instant of time (mg L⁻¹), V is the volume of solution (L) and m is the mass of adsorbent (g) and q is the adsorption capacity of the material (mg g⁻¹).

The adsorption kinetics was determined according to the Langmuir Equation (2):

$$\frac{dq}{dt} = k_1 * C_0 * (q_{max} - q_t) - k_2 * q_t \quad (2)$$

Where k_1 and k_2 are adsorption kinetic constants with units of (L mg⁻¹min⁻¹) and (min⁻¹) respectively. Being q_{max} the maximum adsorption capacity of the material previously determined.

Results and Discussions

In Figure 1 it is possible to observe that the adsorbent material presents irregular surface and full of cavities. These characteristics suggest that the material may possess high specific area, which is desirable for an adsorbent material. In Figure 2, it can be observed that the fit of the kinetic model proposed by Equation 2 did not present good statistical parameters (r^2 and χ^2). This result can be attributed to several factors, such as the small mass of adsorbent material used in relation to the total volume of solution used in the experiment, which impaired the reading in the atomic absorption spectrophotometer, generating an irregular reading and without a characteristic of a trend curve. Another hypothesis is the choice of the iteration algorithm chosen in the software used to adjust the model studied.

The evidence that the model is not suitable can be seen in the parameters obtained in Table 1, where the deviations of the model parameters found are relatively high when compared to the order of magnitude. In addition, the statistical parameter r^2 was not high, although the χ^2 value is desirable.

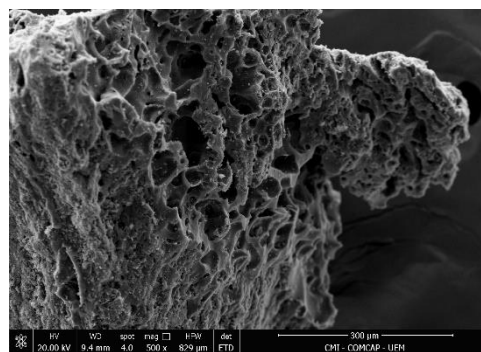


Figure 1. SEM image of the adsorbent material.

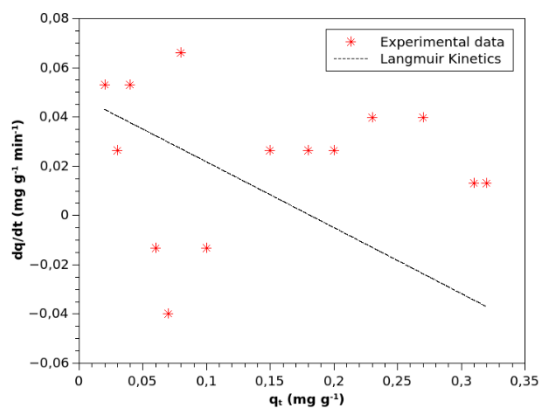


Figure 2. Langmuir kinetic model fitted to experimental data.

Table 1. Parameters obtained by adjusting the Langmuir kinetics model.

Parameters	Value
k_1	0.0065 ± 0.0013
k_2	0.21 ± 0.18
r^2	0.38
χ^2	0.23

Conclusions

With the results obtained with the experiments performed, it can be concluded that the adsorbent material used can be used for the removal of copper (II) ions from aqueous media. The microscopy image of the material shows that it has an irregular surface and cavities, suggesting a high surface area. However, the experimental procedure needs to be improved, so that there is less noise in the reading of the aliquots collected during the kinetics. Another factor that may have impaired the lack of fit of the kinetic model studied was the choice of the iteration algorithm employed in the software that was used for fitting the Langmuir model.

Acknowledgements

The authors thank the Coordenação de Aperfeiçoamento de Pessoal de Nível Superior (CAPES, Financing Code 001), Conselho Nacional de Desenvolvimento Científico e Tecnológico (CNPq), the Complex of Research Support Centers (COMCAP), and Chemical Engineering Department of the State University of Maringá (DEQ - UEM) and Alpha Carbo® Company.

References

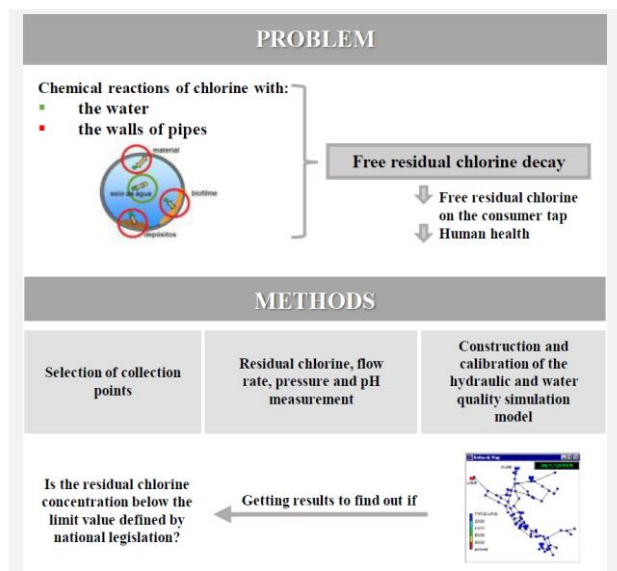
- [1] R. Meffe, I. de Bustamante, *Science of the Total Environment*, 481 (2014) 280-295.
- [2] F. Riva et al., *International Journal of Hygiene and Environmental Health*, 221 (2018) 451-457.
- [3] M.D. de Almeida et al., *Aquatic Toxicology*, 194 (2017) 86-93.
- [4] B. Qu et al., *Marine Pollution Bulletin*, 135 (2018) 318-331.
- [5] E.M. Mistar et al., *Sains Malaysiana*, 48 (2019) 719-725.

Chlorine decay in water treatment and distribution

P. Fernandes, M.T. Santos, T. Trindade*

Departamento de Engenharia Química, Instituto Superior de Engenharia de Lisboa, Instituto Politécnico de Lisboa, R. Conselheiro Emídio Navarro 1, 1959-007, Lisboa, Portugal.

**patricialexandrasf@gmail.com*



Chlorination is the most used disinfection process of drinking water. In order to ensure the quality of water that reaches consumers taps, the amount of chlorine added to the water must be kept within a standard range. However, there are values of residual chlorine disinfectant in the consumer tap below the minimum limit, begin a potential public health risks. In this way, the importance and necessity of carrying out a study of the decay of chlorine in the treatment and distribution of water is verified. This research work aims to study chlorine decay in the water distribution network of the Instituto Superior de Engenharia de Lisboa. To achieve this goal, water sampling and laboratorial quantification of flow, temperature, and residual chlorine are carried out. Additionally, it will be built and calibrated a numerical hydraulic water quality model water distribution network is used as a methodology. This work is still under development.

Introduction

Chlorination is the most widely used drinking water disinfection process. The main goal of chlorination is to prevent the proliferation of harmful microorganisms [1]. Chlorine is mainly used due to its low relative costs, ease of use and ability to remain in the drinking water distribution network, preventing the proliferation of microorganisms from water treatment plants to the consumers tap [2].

In order to ensure the quality of water that reaches consumers taps, the amount of chlorine added to the water must be kept within a standard range. The effective amount of chlorine that must be available at any point in the drinking water distribution network is defined as free residual chlorine [2]. However, during chlorination are generated various health damaging disinfection by-products, such as trihalomethanes [1]. According to the Portuguese legislation, in order to contribute to the promotion of public health, the disinfection process must be complete, ensuring the existence of a residual chlorine concentration between 0,2 and 0,6 mg/L [3].

However, after leaving the water treatment plant and before arriving to a customers' tap, numerous reactions occur that reduces the concentration of free residual chlorine, presenting potential public health risks. These reactions are related to the chemical, microbiological and physical characteristics of the water, as well as the materials that make up the pipe through which the water flows. There are many factors that have been considered among the literature that may directly or indirectly influence disinfectant residual stability such as, temperature, pH, nutrients, organic matter, dissolved oxygen, the presence of other potentially interacting species (bromide, iodide and corrosion products), water age, hydraulic condition, pipe materials, and applied disinfectant residual type and concentration [4].

According to the Annual Report of Water and Waste Services in Portugal [5], in 2021, the values of residual chlorine disinfectant in the consumers' tap showed that 6.61% of the water samples

are below the minimum limit, recommended by the Portuguese legislation. In this way, the importance and necessity of carrying out a study of the chlorine decay in the treatment and distribution of water is verified.

Since the 1990s, several researchers' have used the software EPANET to evaluate the chlorine that remains in the water distribution system after chlorination [6]. EPANET is a free software that performs an extended period numerical simulation of water hydraulic behavior and quality in pressurized pipe networks [7].

Aim

This research work aims to study chlorine decay in the water distribution network of the Instituto Superior de Engenharia de Lisboa (ISEL). It is planned to monitor different points along the network through water sampling and laboratory quantification of selected parameters. Additionally, it is proposed to develop a kinetic model for the decay of chlorine in the network using the EPANET software.

Through the construction and calibration of a hydraulic and water quality model of the distribution system, it is intended to conclude whether the water supplied to ISEL has the adequate residual chlorine concentration according to portuguese standards.

Methods

For the development of the research work, the following steps are presented:

- Analysis of ISEL water distribution network and export from AutoCad or in plants;
- Selection of monitoring points in the water distribution network with different hydraulic conditions, namely, points of higher and lower consumption, ends of the network and intermediate control;
- Measurement of flow, temperature, and residual chlorine;
- Construction and calibration of a numerical model for hydraulic simulation and water quality of the ISEL water distribution network.

The laboratory quantification of the samples will be carried out using the following analytical methods:

- Residual chlorine, by applying the DPD Colorimetric Method with spectrophotometer readings;
- Flow rate, by measuring volume and time;
- pH, by applying the electrochemical method;
- Temperature, using a digital thermometer.

This research work is being developed as part of a dissertation to obtain a Master's Degree in Quality and Environmental Engineering. This work is still under development.

References

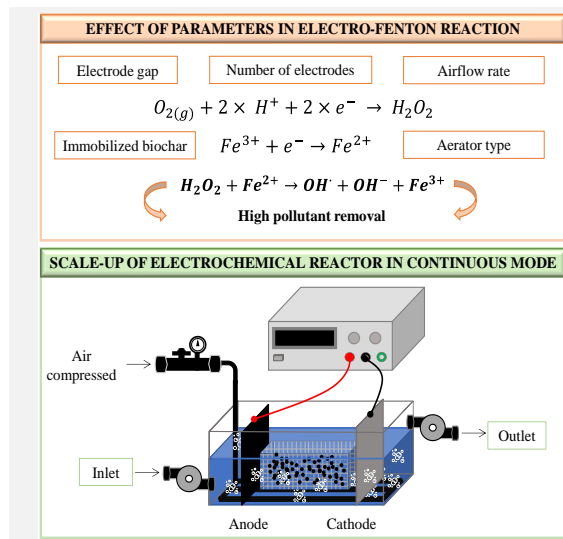
- [1] D. Stefán, et al., *Microchemical Journal*, 149 (2019) 104008.
- [2] S. Javadinejad e al., *Modeling Earth Systems and Environment*, 5 (2019) 1015-1023.
- [3] Decreto-Lei n.o 306/2007, de 27 de Agosto, *Diário da República*, N.o 164, Série I-A.
- [4] R.A. Li et al., *Water Research*, 153 (2019) 335-348.
- [5] A. Martins et al., Volume 2 – Controlo da qualidade da água para consumo humano In *Relatório Anual dos Serviços de Águas e Resíduos em Portugal (2022)*, Entidade Reguladora dos Serviços de Águas e Resíduos, Lisbon, 2022, 64.
- [6] N.S. Muhammad et al., *International Journal of Integrated Engineering*, 13 (2021) 94-99.
- [7] L. Rossman et al., *EPANET 2.2 User Manual*, U.S. Environmental Protection Agency, Washington, DC, 2020, 1.

Optimization of electro-Fenton process parameters and subsequent reactor design for continuous flow treatment

N. Bernárdez*, B. Lomba, M. Pazos, E. Rosales, M.A. Sanromán

University of Vigo, Department of Chemical Engineering. Campus As Lagoas-Marcosende, Vigo, Spain.

*nuria.bernardez@uvigo.gal



The present work has focused on the design of an easily scalable reactor for electro-Fenton treatment of wastewater. Initially, in the electrochemical reactor at small scale, several variables were evaluated in order to optimize conditions to produce the maximum hydrogen peroxide. In addition, the possibility of incorporating biochar to provide the required iron to catalyse the formation of hydroxyl radicals has been analysed. By the combination of electro-Fenton and adsorption was possible to achieve the elimination of Methylene Blue close to 97 % in 90 min, compared to 54 % obtained in anodic oxidation.

Based on the previous results, a reactor which allows working in continuous mode was designed in Solidworks. Then, its application has been tested in two new comparative trials of anodic oxidation and electro-Fenton treatment. Under these conditions, the removal of 82 % of the pollutant was achieved in 15 min with electro-Fenton, compared to 43 % obtained in anodic oxidation.

Introduction

Conventional wastewater treatment through biological processes cannot address current problems associated with the presence of toxic and non-biodegradable compounds present in industrial effluents [1], such as pharmaceuticals, pesticides, dyes and phenolic compounds [2].

Within this framework, Advanced Oxidation Processes have been presented as an effective and sustainable technology for the removal of recalcitrant pollutants, highlighting electrochemical processes, among which is electro-Fenton [3]. This technique, based on the continuous electro-generation of H₂O₂ combined with the uninterrupted regeneration of Fe²⁺ to produce hydroxyl radicals, allows reaching an almost total mineralization of contaminants mentioned [4].

Heterogeneous catalysis has been exposed as an effective way to incorporate iron into the medium [3]. In the present study, a biochar was used as an adsorbent and catalyst due to this material provides the necessary iron for to electro-Fenton take place. In order to facilitate the operation in continuous mode, biochar was immobilized in an alginate matrix to prevent complications with dust.

Objectives

The purpose of this work resides in the optimization of limiting parameters of the electro-Fenton reaction, such as the production of H₂O₂ and the contribution of iron to the system on a small scale, for a subsequent design and application in a reactor of greater volume, which allows the effluents treatment in continuous mode.

Materials and methods

Configuration of the electro-Fenton reactor

Trials have been performed in a rectangular methacrylate reactor with a capacity of 1 L and a working solution volume of 0.87 L, using Na₂SO₄ as electrolyte (0.01M). The electric field was delivered by applying a fixed potential variation of 10 V between electrodes, monitoring intensity variations throughout the treatments. The continuous bubbling of oxygen on the

cathode surface provided the oxygen required for H₂O₂ production.

Regarding the electrodes, graphite and nickel foam were used as anodic and cathodic materials respectively, with submerged surface of 23.5 cm² in all cases.

Experiments for optimization of H₂O₂ production

The main parameters studied in the influence of H₂O₂ production were the number of electrodes used, with anode-cathode and cathode-anode-cathode configurations, and the distance between electrodes.

Concerning the aeration system, two different aeration models were tested: a rectangular rigid diffuser and a cylindrical ductile tube. The influence of airflow supplied has also been analysed, varying between 1, 1.5 and 3 L/min.

H₂O₂ production levels were quantified using the Titanium Oxalate method [5]. To do this, 0.25 mL of H₂SO₄ (0.5 mM) was added to 2 mL of the sample, followed by 0.2 mL of Titanium Potassium Oxalate and 0.05 mL of distilled water. The mixture was then shaken and measured after 5 min by a UV-Vis spectrophotometer (Thermo Fisher Genesys M-150) at 400 nm.

Synthesis of alginate-biochar-spheres

A biochar provided by Ibero Massa Florestal S.A (UL-Oliveira de Azeméis, Portugal) was used in the alginate spheres. For its immobilization process, a 2% w/v concentration of biochar was retained in a 1% w/v alginate spherical matrix, using a CaCl₂ solution as hardening solution.

Degradation of Methylene Blue

The efficiency of the system based on previous results was evaluated on a small scale, using Methylene Blue as a model pollutant with a concentration of 7 ppm. The working volume was reduced to 0.5 L and potential drop was maintained at 10 V using the electrodes and their configuration determined previously. Electro-Fenton treatment combined with adsorption by addition of 54 g of alginate-biochar-spheres was compared with anodic oxidation tests at pH 3 and 6. Handling of spheres was facilitated by adding them to the system in a rectangular mesh adapted to the geometry of the cell. Dye concentration was quantified by spectrophotometry methodology measuring the samples at 661 nm.

Reactor scaling

Based on the hydrodynamic simulation studies performed, a reactor design with 1 L capacity which allows working both continuously and with recirculation was designed in Solidworks. Finally, this reactor was studied by comparative tests of anodic oxidation and heterogeneous electro-Fenton treatment to confirm its proper functioning.

Results

Previous studies have reported that graphite and nickel foam electrodes produce a high rate of H_2O_2 [6]. This part of the work has centred on evaluating the electrodes arrangement and the aeration system choice to maximize the hydrogen peroxide generation in a way which can be cost-effective on a large scale. The evolution of H_2O_2 concentration over time is shown in Figure 1. As can be seen, there was a significant improvement when electrodes were placed at shorter distances, since the field average intensity increased (40 mA for 9.4 cm and 20 mA for 19.2 cm) increasing, in turn, reactions on the electrode surface.

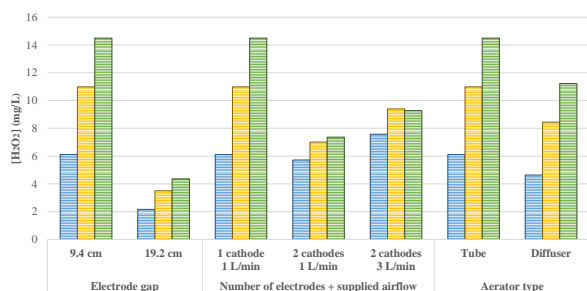


Figure 1. Parameters studied in the production of H_2O_2 after 30 min (blue), 60 min (yellow) and 90 min (green) of treatment.

The number of cathodes effect has been studied together with the variation of airflow. For these tests, a continuous increase in H_2O_2 generation when using a single cathode *versus* a rise and subsequent stabilization when adding a second is shown. This could be again due to an increase in the number of reactions in the medium, but in this case, the intensity effect has led to the steady state when two cathodes were used (40 mA for 1 cathode and 1 L/min, 70 mA for 2 cathodes and 1 L/min, 60 mA for 2 cathodes and 3 L/min), reaching this earlier when airflow was increased to 3 L/min.

However, although at short times the H_2O_2 production speed increased with the use of two cathodes and a higher aeration flow rate, the improvement was not significant enough to be profitable. In addition, the use of lower flow rates avoids other operational problems, such as splashing or solution evaporation. Finally, concerning the aerator used, the tube type was chosen, since in addition to improving peroxide production, it allows greater adaptability to the system.

Acknowledgements

This research was funded through Project PCI2022-132941 and PDC2021-121394-100 funded by MCIN/AEI /10.13039/501100011033 and Xunta de Galicia, and the European Regional Development Fund (ED431C 2021-43).

References

- [1] A. Hadj et al., *Chemosphere*, 202 (2018) 111-118.
- [2] S. Anisah et al., *Journal of Water Process Engineering*, 40 (2021) 101952.
- [3] V. Poza-Nogueiras et al., *Journal of Electroanalytical Chemistry*, 895 (2021) 115475.
- [4] O. Ganzenko et al., *Chemosphere*, 253 (2020) 126659.
- [5] R. Sellers, *Analyst*, 105 (1980) 950-954.
- [6] E. Bocos et al., *Process Safety and Environmental Protection*, 101 (2016) 34-44.

For the electro-Fenton reaction to take place through the electro-generated H_2O_2 , a biochar containing iron and other metals such as manganese has been used as a heterogeneous catalyst for the Fenton-like reaction.

Since the purpose of the system is to work with a continuous flow, biochar was immobilized in an alginate matrix to avoid operational problems that could be caused by dust. Likewise, working with a larger particle size also facilitated the catalyst incorporation and recovery before and after the process.

Dye removal rates for the different tests were evaluated using different configurations. In Table 1, several of the performed tests are shown. The adjustment corresponds to pseudo-first-order kinetics, being k the kinetic coefficient.

Table 1. Kinetic parameters of small-scale treatments.

Treatment	k (min^{-1})	R^2
Anodic oxidation (pH 6)	0.0079	0.993
Anodic oxidation (pH 3)	0.0199	0.988
Electro-Fenton + Adsorption	0.0471	0.998

As the H_2O_2 production is favoured in acidic media, the improved degradation rate for anodic oxidation at pH 3 appears consistent. However, both tests showed a decrease in their degradation rates compared to trials in which alginate-biochar-spheres have been added. This could be justified for two reasons: on the one hand, the material provided the system with the necessary iron to catalyse the H_2O_2 reaction and generate OH^\bullet radicals so that the pollutant was degraded, and on the other hand, adsorption mechanisms could be taking place on the biochar surface that favoured the Methylene Blue removal.

Given the promising results obtained on a small scale, a reactor design that can operate at higher volumes has been carried out. This new reactor was made of PVC, with an inlet at the bottom and an overflow outlet. A series of slots were incorporated on the sides to facilitate the placement of the electrodes.

At this scale, the obtained results are shown in Table 2. Once again, the best degradation rate was obtained with the electro-Fenton treatment in combination with biochar adsorption.

Table 2. Kinetic parameters of the larger-scale reactor.

Treatment	k (min^{-1})	R^2
Anodic oxidation (pH 3)	0.0363	0.995
Electro-Fenton + Adsorption	0.1095	0.991

Conclusions

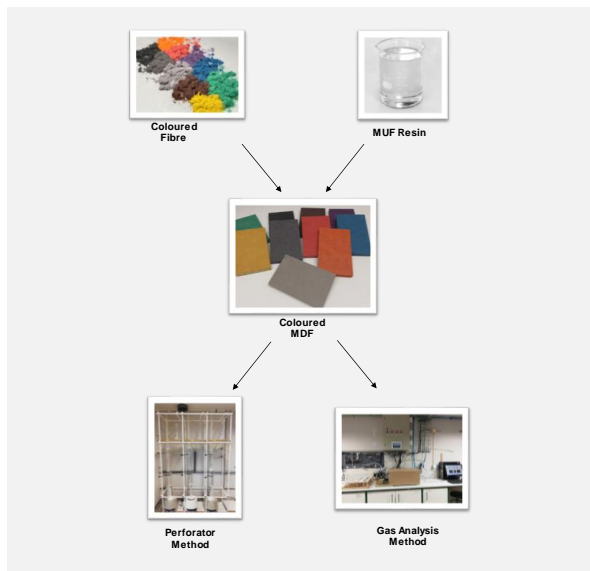
In view of the results, it was determined that electro-Fenton treatment application under the H_2O_2 optimized production, combined with the dual activity (adsorbent and catalyst) of biochar, allows an almost total elimination of Methylene Blue, both on a small scale as in a reactor designed to work continuously.

Comparison of test methods to assess formaldehyde emissions in coloured MDF

M.L. Almeida^{1,2,3*}, C. Coelho^{1,2,3}, J.M. Martins^{1,2,3}, R.M. Ramos⁴, F.M. Magalhães^{2,3}, L.H. Carvalho^{1,2,3}

¹Wood Engineering Department, ESTGV – Polytechnic University of Viseu, Campus Politécnico, 3504-510 Viseu, Portugal; ²LEPABE – Laboratory for Process Engineering, Environment, Biotechnology and Energy, Faculty of Engineering, University of Porto, Rua Dr. Roberto Frias, 4200-465 Porto, Portugal; ³ALiCE – Associate Laboratory in Chemical Engineering, FEUP, 4200-465 Porto, Portugal; ⁴LAQV-REQUIMTE, Department of Chemistry and Biochemistry, Faculty of Sciences, University of Porto, Rua do Campo Alegre s/n, Porto, 4169-007, Portugal.

*malmeida@fe.up.pt



The use of amino resins, such as Urea-Formaldehyde (UF) and Melamine-Urea-Formaldehyde (MUF) resins, as bonding adhesives for the manufacture of Wood-Based Panels (WBP) is the primary contributing factor to the Formaldehyde (FA) release problem from these panels. For many years, WBPs, such as Particleboard (PB), Medium Density Fibreboard (MDF) and Oriented Strand Board (OSB), have been produced using UF or MUF resins, due to its low cost, easily adaptable to a variety of curing conditions, homogeneity and water solubility that facilitate their industrial handling. Beyond the formaldehyde-based resins used in WBP, wood itself emits FA. Furthermore, the strategy followed by the producers of increasing the use of recycled wood, which also includes rejected boards, has increased the sources of FA. Formaldehyde Emissions (FE) were determined by the two most common methods (Perforator and Gas analysis) and relationships between the two were established.

Introduction

Formaldehyde (FA) is a chemical compound classified as carcinogenic and toxic by the International Agency for Research on Cancer (IARC) since 2006. It is a colourless, pungent-smelling gas and its presence in indoor air is harmful to human health. Sources include environmental tobacco smoke and other combustion sources; pressed wood products – such as Particleboard (PB) and certain textiles, foams and glues [1]. Due to its classification as a carcinogenic air pollutant, FA has been subject to many research and regulations through the years. This substance is soluble in water, ethanol, diethyl ether and acetone [2].

Wood-Based Panels (WBP) industry uses mainly formaldehyde-based resins, such as: urea-formaldehyde (UF), melamine-formaldehyde (MF) or melamine-urea-formaldehyde (MUF), due to its low cost, fast curing and good mechanical properties. In comparison to MF and MUF, UF resins have lower price and higher reactivity which allows for shorter press times. However, they have lower moisture resistance due to the reversibility of the aminomethylene link and hence the susceptibility to hydrolysis [3].

Particleboard (PB), Medium Density Fibreboard (MDF) and Oriented Strand Board (OSB) are the most used WBP, mostly in construction and furniture applications. During WBP service life, Formaldehyde Emissions (FE) comes mainly from two sources, the unreacted FA and the reversibility of reactions (hydrolysis) [3].

For the determination of FA release in WBP, there are different test methods available, following European standards, such as: Chamber Method – EN 717-1, Gas Analysis Method – EN ISO 12460-3, Flask Method – EN 717-3 and Perforator Method – EN ISO 12460-5. The Desiccator Method, determined by the Japanese standard JIS A 1460, is also used.

Objectives

In this study it is intended to compare two of the different test methods available for the determination of FA release in WBP – EN ISO 12460-3 and EN ISO 12460-5 – and apply them to MDF Valchromat® produced with different thicknesses and colours.

Methods

Coloured MDF was provided by Valbopan, S.A. and several tests were carried out by applying the two methods to the same sample of industrially produced dry-processed fibreboards – MDF. One of the main problems in this study is the impact of unrelated properties such as thickness, density, moisture content and colour of the MDF on the relationship between Formaldehyde Emissions (FE) and Formaldehyde Content (FC). Therefore, the collected samples represent a wide range of values for those properties, including black, brown, grey, yellow, orange and green colours and 8, 10, 12, 16, 19, 30 mm as thicknesses.



Figure 1. Perforator apparatus – EN ISO 12460-5.

The FC was determined using the perforator method – EN ISO 12460-5 (Figure 1). This method runs for a total of three hours and the equipment is relatively inexpensive. It involves the use of boiling toluene (119 °C) for 2 hours to extract FA from small pieces in a glass apparatus, called perforator. FE was determined using EN ISO 12460-3 (Figure 2), under accelerated conditions (temperature of 60 °C, 4 hours). A known-area specimen is put in a sealed space where the temperature, relative humidity, airflow and pressure are all maintained at predetermined levels. In both methods, the FA is absorbed in water and the FC of this aqueous solution is determined photometrically by the acetylacetone method.



Figure 2. Gas analysis chamber – EN ISO 12460-3.

Results

The results from this study are presented in the following figures (Figure 3 and 4). In Figure 3, it can be observed the results from the relationship between FE and FC values in different thicknesses of coloured MDF. In Figure 4 we can observed the relationship between FE and FC values in different colours of coloured MDF.

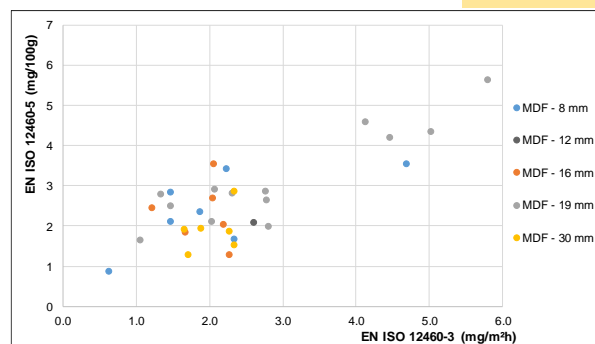


Figure 3. Relationship between FE and FC values in different thicknesses of coloured MDF.

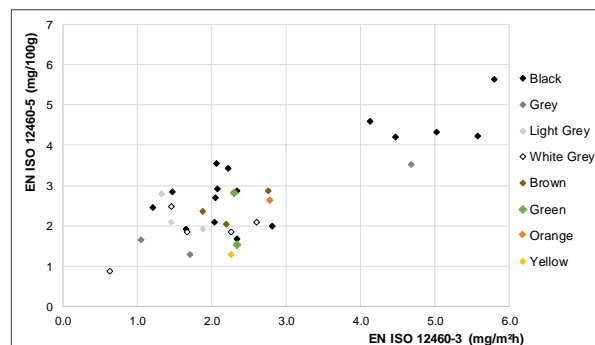


Figure 4. Relationship between FE and FC values in different colours of coloured MDF.

Conclusions

It can be seen that the relationship between the values of the perforator and gas analysis methods, show a strong dependence on both thickness and colour of the product. Work is in progress to establish a mathematical model relating the FE and FC and integrating the influence of colour and thickness.

Acknowledgements

RMR thanks FCT (Fundação para a Ciência e Tecnologia) for funding through program CEECIND/04259/2017. This work was financially supported by: LA/P/0045/2020 (ALiCE), UIDB/00511/2020 and UIDP/00511/2020 (LEPABE), funded by national funds through FCT/MCTES (PIDDAC); project PTDC/CTM-PAM/1348/2021 funded by FEDER funds through COMPETE2020 – Programa Operacional Competitividade e Internacionalização (POCI) and by national funds (PIDDAC) through FCT/MCTES.

References

- [1] U.S. Environmental Protection Agency, “An introduction to indoor air quality (IAQ): Volatile organic compounds (VOCs)”. Washington DC, 2021.
- [2] T.S. Salthammer et al., Chemical Reviews, 110 (2010) 2536-2572.
- [3] M. Dunky, International Journal of Adhesion and Adhesives, 18 (1998) 95-107.
- [4] N.A. Costa, Wood Science and Technology, 47 (2013) 1261-1272.

Catalytic hydrodechlorination of 4-chlorophenol in water

C. Lopes*, J. Restivo, C.A. Orge, M.F.R. Pereira, O.S.G.P. Soares

Laboratory of Separation and Reaction Engineering - Laboratory of Catalysis and Materials (LSRE-LCM), Faculdade de Engenharia, Universidade do Porto, Rua Dr. Roberto Frias, 4200-465 Porto, Portugal; ALiCE - Associate Laboratory in Chemical Engineering, Faculty of Engineering, University of Porto, Rua Dr. Roberto Frias, 4200-465 Porto, Portugal.

*catarinalopes@fe.up.pt



Chlorophenols are a class of persistent organic pollutants frequently found in wastewater. These compounds present high stability and consequently, they degrade very slowly in nature. Therefore, the study of methodologies to remove or degrade this class of compounds is of utmost importance. Catalytic hydrodechlorination (HDC) is an important technique that can be employed for the disposal of chlorophenol. This methodology requires less energy compared with other methodologies and reduces significantly the toxicity of the effluents. The main goal of this work was to study the catalytic activity of different catalysts. The catalytic tests allowed us to conclude that the support of the catalyst plays a key role in the chlorophenol's reduction, and multi-walled carbon nanotubes (CNT) presented a higher reduction rate.

Introduction

Chlorophenols are a group of pollutants widely found in several important industrial processes such as the production of germicides, algacides, fungicides, herbicides, dyes, wood protectors, and plant growth regulators [1]. As a result, they are widespread environmental contaminants. This class of compounds is classified as persistent contaminants, and they present high toxicity and low biodegradability [2]. The European Union and the US Environmental Protection Agency have classified the majority of chlorophenols as priority contaminants and banned their use and discharge [3]. Moreover, the World Health Organization (WHO) has set guidelines for some chlorophenols [3]. Hence, the development of efficient remediation techniques is crucial for removing these contaminants from water. Some conventional techniques, such as thermal or biological treatments, can be employed, but they present some limitations, namely the possible formation of highly toxic dioxins and the requirement of high temperatures in the first mentioned technique, whereas biological treatments are slow and are affected by chlorophenols toxicity [2]. Catalytic hydrodechlorination (HDC) emerges as an environmentally friendly method for the degradation of chlorophenols. This method can be performed under mild conditions with high efficiency. The non-chlorinated equivalents formed, namely phenol, are often significantly less harmful [4]. Previous studies investigated the reduction of chlorophenols in the aqueous phase with different catalysts, pressures, and temperatures, and also with different pH values. Several metallic supported catalysts have also been explored and precious metals, in particular palladium, have displayed good activity results [2].

Therefore, the main goal of this work was to study the hydrodechlorination of 4-chlorophenol in an aqueous solution, using catalysts impregnated in different supports, namely alumina (Al_2O_3), activated carbon (AC) and multi-walled carbon nanotubes (CNT) catalysts.

Methods

For this study, different catalysts were synthesized using the incipient wetness impregnation method. An aqueous solution of palladium chloride (II), PdCl_2 , was impregnated to reach the desired palladium content in the following supports: Al_2O_3 , AC and CNT. The particle diameter of all supports was selected between 0.1 and 0.3 mm before the impregnation process. After, the samples were dried at 100 °C for 24 h and then they were calcinated at 200 °C in a N_2 atmosphere for 1 h, followed by a reduction with H_2 flow for 3 h.

Textural characterization of the synthesized catalysts was performed through N_2 adsorption isotherms at -196 °C determined in a Quantachrome NOVA 4200e multistation with previous sample degasification at 150 °C for 3 h.

The catalytic reduction experiments were carried out in a semi-batch reactor. In a typical experiment, 400 mL of 2 mM of NaOH was introduced in the reactor together with hydrogen at a flow rate of 100 $\text{cm}^3 \text{min}^{-1}$ (STP) and a catalyst loading of 200 mg with a stirring velocity of 700 rpm for 15 min. Then, 10 mL of a 4-chlorophenol solution was added to obtain an initial pollutant concentration of 100 ppm. The experiments were carried out at atmospheric pressure and ambient temperature for 5 h. After predefined intervals, samples were taken in order to quantify 4-chlorophenol and chloride concentrations. These samples were analysed by high-performance liquid chromatography (HPLC) using a Hitachi Elite Lachrom apparatus equipped with a diode array detector to quantify 4-chlorophenol. The stationary phase was a Hamilton PRP-X100 column (150 mm x 4.1 mm) working at room temperature, under isocratic conditions. The mobile phase was a solution of water/methanol (1:4 v/v) and 30 mM of H_3PO_4 with a flow rate of 1 mL min^{-1} . The chloride ions concentration was quantified using ionic chromatography in a Metrohm 881 Compact IC Pro apparatus, equipped with a Metrosep A Supp 7 anionic exchange column (250 mm x 4.0 mm).

Results

Some catalytic studies were performed for various catalysts, but only the results with 5% Pd/Al₂O₃, 5% Pd/AC and 5% Pd/CNT are presented here.

The specific surface areas (S_{BET}) obtained using the Brunauer-Emmett-Teller method from nitrogen isothermal adsorption data at -196 °C of the prepared catalysts are summarized in Table 1.

Table 1. BET surface area (S_{BET}) for different catalysts, 5% Pd/Al₂O₃, 5% Pd/AC and 5% Pd/CNT.

Sample	($S_{\text{BET}} \pm 5$) / m ² g ⁻¹
5%Pd/Al ₂ O ₃	49
5%Pd/AC	1274
5%Pd/CNT	197

Among the three studied catalysts, 5% Pd/AC presented the highest S_{BET} and 5% Pd/Al₂O₃ the lowest.

Figure 1 shows the results obtained for the hydrodechlorination reactions over the 5% (wt.) Pd catalysts supported on the different supports. In order to assess the effect of the reducing agent (hydrogen), a blank test utilizing only this gas was conducted, and it was shown that 4-chlorophenol is not reduced under these circumstances. For all tested catalysts, the reduction of 4-chlorophenol was completed in 240 min, which demonstrated that all studied catalysts are efficient in the hydrodechlorination of 4-chlorophenol. 5% Pd/Al₂O₃ presented the slowest degradation rate, whereas the catalyst composed of palladium supported on CNT (5% Pd/CNT) presented the fastest degradation rate, achieving the complete degradation in 10 min.

Acknowledgements

This work was financially supported by NanoCatRed (NORTE-01-0247-FEDER-045925) (ERDF — COMPETE 2020, – NORTE 2020 and – FCT under UT Austin Portugal) and national funds through the FCT/MCTES (PIDDAC) under the project 2022.03874.PTDC - F-CAT. This work was also financially supported by LA/P/0045/2020 (ALiCE), UIDB/50020/2020 and UIDP/50020/2020 (LSRE-LCM), funded by national funds through FCT/MCTES (PIDDAC).; CAO acknowledges FCT funding under DL57/2016 Transitory Norm Programme. OSGPS acknowledges FCT funding under the Scientific Employment Stimulus - Institutional Call CEECINST/00049/2018.

References

- [1] X. Ma et al., Applied Catalysis B: Environmental, 165 (2015) 351-359.
- [2] Z.M. de Pedro et al., Applied Catalysis B: Environmental, 103 (2011) 128-135.
- [3] Z. Zhao et al., Environmental Research, 210 (2022) 113004.
- [4] E.S. Lokteva et al., Mendeleev Communications, 32 (2022) 249-252.

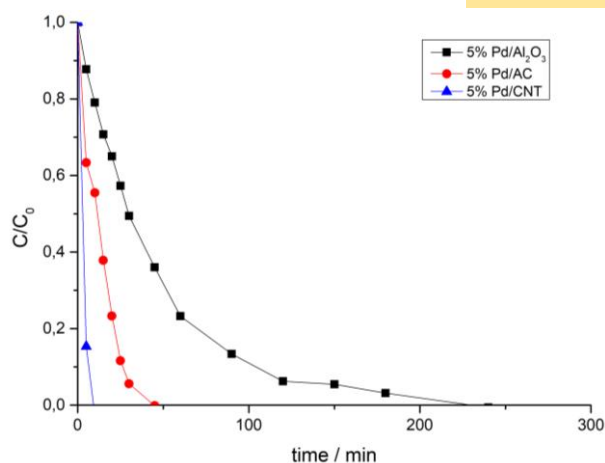


Figure 1. Concentration profile of 4-chlorophenol for different catalysts, 5% Pd/Al₂O₃, 5% Pd/AC and 5% Pd/CNT.

The chloride ions concentration was measured during all catalytic tests, and it was concluded that the 4-chlorophenol degradation is mainly due to dechlorination.

Conclusions

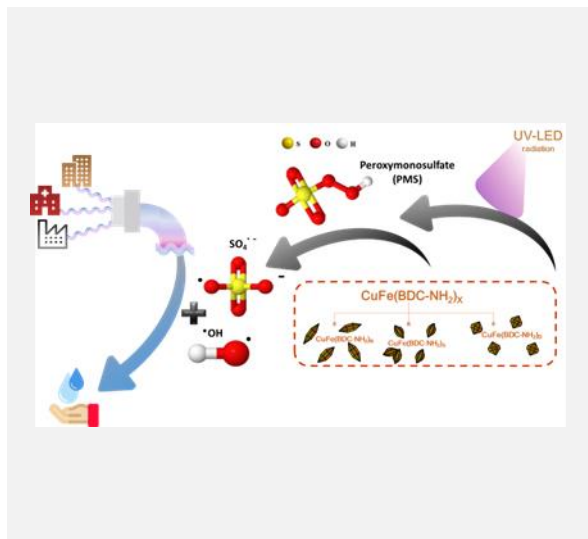
This work aimed to evaluate the catalytic activity of catalysts synthesized using different noble metals and supports in the reduction of 4-chlorophenol. The obtained results showed that the reduction of 4-chlorophenol is highly dependent on the support of the catalyst, with the best test achieving the complete degradation in 10 minutes.

Influence of FeCu-MOF morphologies on peroxymonosulfate activation for rhodamine B degradation

A. Fdez-Sanromán*, B. Lomba-Fernández, M. Pazos, E. Rosales, M.A. Sanromán

CINTECX, Universidade de Vigo, Department of Chemical Engineering, Campus Universitario As Lagoas—Marcosende, 36310 Vigo, Spain.

*antia.fernandez.sanroman@uvigo.gal



In this study, by means of a solvothermal process, several bimetallic CuFe-MOFs have been synthesized by changing the ratio of the solvents (DMF/ethanol/water), metal salts, or reaction temperature. The result is three MOFs with different physical-chemical and morphological properties: rod-like form, CuFe(BDC-NH₂)_R; spindle-like form CuFe(BDC-NH₂)_S; and diamond-like form, CuFe(BDC-NH₂)_D. Their catalytic activity has been ascertained by the activation of peroxymonosulfate (PMS) for the degradation of a model dye, Rhodamine B. The effect of several variables (initial pH, PMS concentration and catalyst dosage) were assessed. Operating under optimal conditions, the dye was completely removed in less than 1 h using CuFe(BDC-NH₂)_R and CuFe(BDC-NH₂)_S. Moreover, coupling UV-LED irradiation enhanced the production of sulfate radicals for CuFe-MOFs/PMS system degradation. The presence of two metals improves matter's catalytic activity, which can be applied to persistent contamination removal.

Introduction and objectives

Synthetic dyes are widely used to color many different products such as textiles, paper, cosmetics, and drugs. The direct discharge of these colored compounds in the environment can cause serious problems to the environment due to their contribution of high organic loading and toxicity. Conventional wastewater treatment plants cannot degrade the majority of these pollutants and generate large volumes of sludge, thus, causing secondary loading of environmental pollutants [1]. This situation has prompted the search for more effective water treatment techniques to ensure high-quality water. Effective water treatment techniques include advanced oxidation processes (AOPs), since the bonds of pollutant molecules can be break by *in-situ* generation of non-selective radicals with high oxidizing power, such as hydroxyl and sulfate radicals [2]. Among them, it can be highlighted the generation of sulphate radicals by peroxymonosulfate (PMS) activation, which can be carried out using heat, ultrasound, light and transition metals. For this last activation method, nowadays, the use of heterogeneous catalysts stands out because it facilitates their use and reuse in continuous processes. Metal-organic frameworks (MOF), which are highly ordered structures composed of organic and inorganic components, are noteworthy and attracting great interest. MOFs stand out because they provide physicochemical properties of significant interest, such as large surface area and structural variety [3]. However, the most interesting property of MOFs is their enormous flexibility that allows them to easily modify their structure. So, in a way, it is possible to obtain tailor-made materials with a certain pore size and catalytic activity. Moreover, according to the literature, MOFs show catalytic properties to activate PMS, especially when they have two or more metals, due to the abundance of active sites and oxygen valences.

In this work it is aimed to synthesize an iron-copper bimetallic MOF (CuFe-MOF) by a solvothermal synthesis in which the ratios of solvents, precursor metal salts and reaction

temperatures have been varied. In order to prove the feasibility of the synthesis procedure for obtaining CuFe-MOFs with different properties, their characterization and analysis of their catalytic activity have been carried out. Their catalytic activity has been studied by removal of a model dye such as Rhodamine B, which is a xanthene dye, used as a water tracer fluorescent and colorant in textiles and food stuffs. For this reason, its use is extensive, and it is detected into the environment.

Materials and methods

Materials:

Synthesis CuFe(BDC-NH₂)_x: N, N-dimethylformamide (DMF), ethanol, 2-aminoterephthalic acid (NH₂BDC), iron (II) sulfate heptahydrate, copper (II) acetate, copper (II) chloride hexahydrate and iron (III) chloride hexahydrate. All the chemicals mentioned were purchased from Sigma Aldrich.

Model pollutants: Rhodamine B supplied by Sigma Aldrich.

Synthesis of CuFe(BDC-NH₂)_x and Cu(BDC-NH₂)_R: The procedure for the synthesis of CuFe(BDC-NH₂)_R is based on the work of Fu et al. [4], CuFe(BDC-NH₂)_D on the work of Khosravi et al. [5]. However, CuFe(BDC-NH₂)_S synthesis is carried out as CuFe(BDC-NH₂)_D, but the metal salts have been changed with 0.4 g of copper (II) acetate and 0.556 g of iron (II) sulfate heptahydrate being used in this case. Analogously to CuFe(BDC-NH₂)_R, Cu(BDC-NH₂)_R was synthesized using 0.4 g of copper (II) acetate as precursor.

Experimental set-up:

Rhodamine B degradation: Initially, the catalytic activity of the three CuFe-MOFs is evaluated in various AOPs such as Fenton-like, photo-PMS, and photocatalysis. First, the influence of the initial pH, which is evaluated between 3 and 9, the CuFe-MOF concentration, between 0.125 and 0.5 g/L, and PMS, whose values are from 0.1 to 1 mM are studied. For the best conditions for the Fenton-like process, light irradiation has been added to the treatment system. For these tests (photo-PMS and photocatalysis), a 30 W UV-A LED lamp operating at 365 nm is

used as a light source. The samples were measured by a UV-Vis spectrophotometer. All experiments were carried out in 100 mL individual cylindrical cells with an operating volume of 50 mL, containing 10 mg/L of Rhodamine B.

Results

The morphology and surface differences between the synthesized CuFe-MOFs have first been evaluated using TEM and SEM as shown in Figure 1. The left image reveals CuFe(BDC-NH₂)_R, equivalent to its rod shape, the middle image reveals CuFe(BDC-NH₂)_S, equivalent to its spindle shape, and the right image reveals CuFe(BDC-NH₂)_D, equivalent to its diamond shape.

Subsequently, the improvement of the bimetallic's catalytic activity against Cu(BDC-NH₂)_R with Rhodamine B degradation is evaluated. From this study, an increase in degradation was observed, since after 60 min, the Cu(BDC-NH₂)_R-PMS system degrades 20%, whereas with CuFe(BDC-NH₂)_R-PMS, 45%. However, when compared to CuFe(BDC-NH₂)_D and CuFe(BDC-NH₂)_S the degradation is higher than 90%. Therefore, the inclusion of iron improves the degradation of the Rhodamine B. As seen from the characterization of these materials, the differences found between the three CuFe-MOFs can be explained by their different morphology and hence their composition.

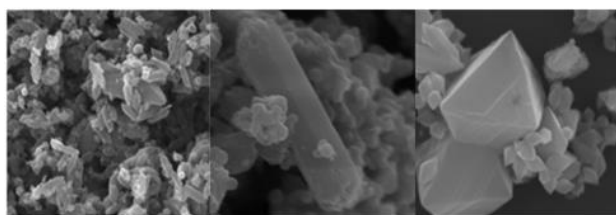


Figure 1. SEM images of the three synthesised FeCuMOF, from left to right, CuFe(BDC-NH₂)_R, CuFe(BDC-NH₂)_S and CuFe(BDC-NH₂)_D.

After verifying the improvement of iron incorporation in the catalyst, the influence of the initial pH, PMS and catalyst concentration on the Fenton-like process is analyzed. In general terms, for these three catalysts, the same behavior has been found for each parameter. First, in the analysis of the influence of the initial pH, slight changes in degradation have been denoted, being better under more acidic conditions. Since the

Acknowledgements

This research has been financially supported by MCIN / AEI /10.13039/501100011033 (Project PID2020-113667GB-I00 and PDC2021-121394-I00) and by the European Union Next Generation EU / PRTR and Xunta de Galicia, and the European Regional Development Fund (ED431C 2021-43). Antía Fdez-Sanromán thanks Ministerio de Ciencia e Innovación (PRE2021-098540) for her predoctoral fellowship.

References

- [1] C.A. Martínez-Huitle, E. Brillas, *Applied Catalysis B: Environmental*, 87 (2009) 105-145.
- [2] E. Rosales et al., *Journal of Hazardous Materials*, 213-214 (2012) 369-377.
- [3] A. Fdez-Sanromán et al., *Applied Sciences*, 10 (2022) 7810.
- [4] A. Fu et al., *Chemosphere*, 297 (2022) 134257.
- [5] F. Khosravi et al., *Applied Organometallic Chemistry*, 36 (2022) e6749.

differences are less than 5%, natural pH conditions are used to avoid acidification and basification of the solution and its subsequent treatment. As for the catalyst concentration, the differences in degradation at 60 min between 0.125 g/L and 0.25 g/L of CuFe(BDC-NH₂)_S and CuFe(BDC-NH₂)_R, are less than 15%, while CuFe(BDC-NH₂)_D, are over 40%. However, if 0.25 g/L and 0.5 g/L are compared, the differences are less than 10% for these three FeCu-MOF. Finally, the PMS concentration is analyzed from 0.1 mM to 1 mM. In this study, it was found that Rhodamine B degradation increases more than 40% between both PMS concentrations. For this reason, the optimum conditions for the Fenton-like process, for the three CuFe-MOF, are 0.25 g/L catalyst, 1 mM PMS and an initial pH value of 6. Subsequently, CuFe-MOF's capacity as a photocatalyst was evaluated and an increase in the degradation rate was detected, being CuFe(BDC-NH₂)_D the one with the highest degradation rate, 0.191 min⁻¹. Concerning CuFe(BDC-NH₂)_S, there was a slight increase in the degradation rate, from 0.0650 to 0.0941 min⁻¹ with UV radiation. However, CuFe(BDC-NH₂)_R shows practically no increase in the degradation rate of Rhodamine B. In addition, for the last mentioned system, reuses of CuFe(BDC-NH₂)_S and CuFe(BDC-NH₂)_R have been carried out to evaluate their stability. From these experiments, it has been concluded that, after 5 cycles, Rhodamine B removal efficiency has not been affected. This is because of the stability and high efficiency of the catalyst allowing that the attained removal has not been reduced by even 5%. Therefore, it can be said that these FeCu-MOF have high stability and reusability, which makes them of great interest for future continuous processes to treat contaminated water.

Conclusions

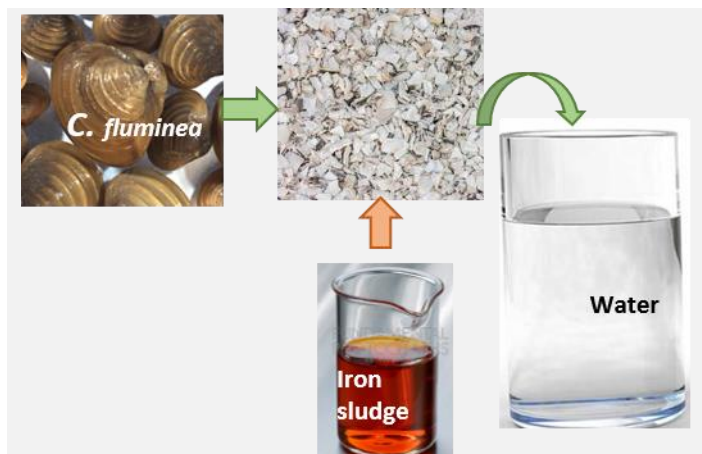
Three CuFe-MOF with different morphologies and properties have been successfully synthesized. It has been demonstrated that bimetallic MOFs improve PMS activation compared to monometallic MOFs. Moreover, within bimetallic, it has been possible to design catalysts with ideal properties to degrade recalcitrant pollutants. In addition, it was proved that the combination system PMS/CuFeMOF/UV is the most effective system due to the radiation improving the generation of the hydroxyl and sulfate radicals.

Integrating Fenton's process with adsorption using *C. fluminea* shells: an iron recovery strategy

E. Domingues^{1*}, T. Vaz¹, P. Mazierski², J. Gomes¹, R.C. Martins¹

¹University of Coimbra, CIEPQPF – Chemical Engineering Processes and Forest Products Research Center, Department of Chemical Engineering, Faculty of Sciences and Technology, Rua Silvio Lima, Polo II, 3030-790 Coimbra, Portugal; ²University of Gdansk, Faculty of Chemistry, Department of Environmental Technology, 80-308 Gdańsk, Poland.

*evadomingues@eq.uc.pt



In this study, clam shells from the invasive species *C. fluminea* were used as a raw material to prepare an adsorbent. The adsorbent was used for iron removal from water that was previously treated by homogeneous Fenton's process. The promising results show that the integration between Fenton's process and adsorption with clam shells may be a suitable way to address the environmental associated to this invasive species while overcoming Fenton's process drawback associated to iron sludge production.

Introduction

Advanced oxidation processes (AOPs), combined with other techniques, have gained some notoriety regarding water treatment. AOPs produce reactive species that allow the degradation and mineralization of pollutants in aqueous medium. They are based in hydroxyl radicals ($^{\circ}\text{OH}$) production. These moieties present a non-selective profile, high reactivity and oxidation potential (E_0 of 2.80 V) [1,2,3]. Fenton's process is one of the most studied AOPs. This technology is based in the reaction between hydrogen peroxide (H_2O_2) and iron ions source. Fenton's is an inexpensive and environmentally friendly process, operates under moderate conditions (room temperature), uses easy to handle reagents, as well as the high elimination rates reached are the main advantages of this method. However, it has some disadvantages since it operates in a narrow pH range and leads to the formation of iron sludge since the dissolved iron used as catalyst must be removed from solution. This is usually done by pH increase of the media leading to $\text{Fe}(\text{OH})_3$ precipitation. Nonetheless, due to its high efficiency Fenton's is often used for the treatment of agro-industrial effluents, in particular olive mill wastewater (OMW) [4]. In Portugal, according to the DL 236/98, the total iron concentration allowed for disposal of treated wastewater in aquatic environments and public water source is 2 mg/L [2, 5, 6]. Thus, the need for an underlying step to Fenton's process that allows the reduction of iron is crucial.

Objectives

The goal of this work is to study the possibility to remove iron after Fenton's process for treatment of the OMW using the shell of the adult clam *Corbicula fluminea*. The *C. fluminea* is freshwater infauna bivalve commonly known as the Asian clam. This species, native from Southeast Asia, suffered over the last century a great global expansion being present in different areas of the planet. *C. fluminea* is an invasive pest that constitutes a serious problem, both economic and ecological. This species is responsible for establishing dense populations in underwater structures and equipment, resulting in their degradation. The strategy comprises the implementation an iron recovery step after Fenton's process, using clam shell. In a first phase, the iron adsorption capacity of the shell is evaluated using a synthetic

solution and after, the same capacity was studied with treated OMW after the Fenton's reaction. As far as we know, this is the first time that iron removal has been carried out using the shell of an invasive species, the *C. fluminea*.

Methods

Batch adsorption experiments

Batch tests were performed by contacting 40 mL of iron solution ($[\text{Fe}^{2+}] = 2 \text{ g/L}$) with different amounts and diameters of shells (0.2-3 g and $>420 - <841 \mu\text{m}$, respectively). Initial pH was measured and kept without any change. In the studies after Fenton process, the initial pH value was 3 (characteristic pH of the Fenton reaction). The sealed vials were continuously stirred (50 rpm) in a thermostatic bath during the desired time at constant temperature (25°C) until equilibrium was settled.

Analytical techniques

The zeta potential analysis was carried by electrophoretic light scattering in a Malvern Zetasizer Nano ZS (ZEN3600, Malvern Instruments Ltd, United Kingdom). Dissolved iron was determined by atomic adsorption.

Results and discussion

Adsorbents, in general, develop charges at the solid-liquid interface due to dissociation or adsorption of ions from the solution. The pH range in which the net surface charges of the adsorbent are null is referred to as Load Point Zero (pH_{ZPC}) of the adsorbent. The pH_{ZPC} value of the adsorbent was obtained from the construction of a graph of the net surface charge of the adsorbent depending on the pH, as shown in Figure 1.

Analyzing Figure 1, it is observed that the net surface charge of the adsorbent decreases with increasing of the pH. In the pH 1-2, the surface charge of the adsorbent is zero. This range is defined as the pH_{ZPC} of the adsorbent. The adsorption of cations is favored at a pH greater than pH_{ZPC} , since, in this case, the net charge of the adsorbent surface is negative ($\text{pH} > 2$) [7]. The initial iron solution has a pH of 3, but when the clam shell is added, the pH rises to 6-7, due to the shells composition of calcium carbonate. The pH increase will favor the adsorption of the cation.

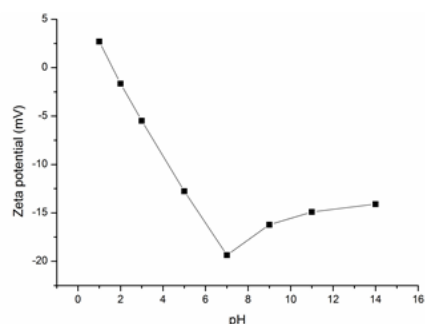


Figure 1. Zeta potential as function of pH.

The potential of porous shells as a naturally abundant low-cost sorbent for the removal of iron in aqueous solutions was investigated in a batch study. In Figure 2 the effect of the shells diameter and the contact time in iron removal from the aqueous solution can be observed. The evaluation of the distribution particle size measurement of adsorbent was carried out by sieving.

Shell particles show high affinity for iron leading to interesting removal rates. The mixture of particles with smaller diameters leads to higher surface of contact between the adsorbent and the iron which is translated to higher removals in shorter contact times. Of the same shape, larger particles, showed the longer time required for iron retention due to their smaller contact surface.

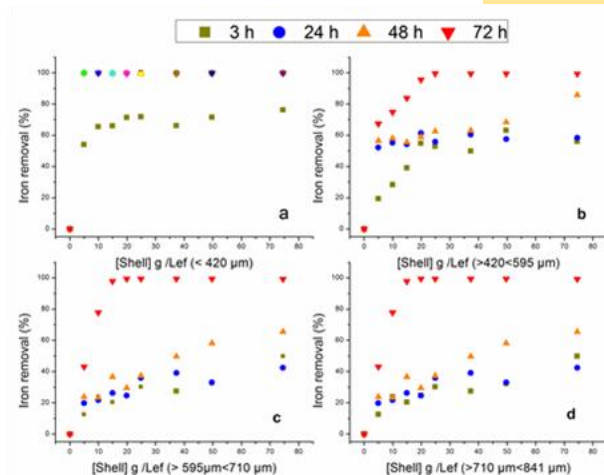


Figure 2. Shell diameter effect on iron adsorption.

Conclusions

Biosorbents, such clams' shells, are highly attractive for removing metals due to their low-cost and abundant supply from natural biomineralization. With the main objective of developing a low-cost sorbent, this study shows that *Corbicula fluminea* shells have a high iron adsorption capacity. Thus, this low-cost material can be used post-Fenton's process for iron removal and potential recovery

Acknowledgements

Thanks are due to FCT/MCTES for the financial support to CIEPQPF (UIDB/00102/2020). The author J. Gomes gratefully acknowledges Foundation for Science and Technology – FCT (Portugal) by the financial support (CEECIND/01207/2018).

References

- [1] K. Fedorov et al., *Chemical Engineering Journal*, 432 (2022) 134191.
- [2] E. Domingues et al., *Water*, 14 (2022) 706.
- [3] M.P. Rayaroth et al., *Chemical Engineering Journal*, 430 (2022) 133002.
- [4] E. Domingues et al., *Science of The Total Environment*, 832 (2022) 155029.
- [5] B. Volesky, *Hydrometallurgy*, 59 (2001) 203-216.
- [6] Yi. Zhang et al., *Acta Physiologiae Plantarum*, 33 (2011) 683-689.
- [7] M. Canle et al., *Current Opinion in Green and Sustainable Chemistry*, 6 (2017) 101-138.

Water disinfection using UVC diodes that emit light at different wavelengths

M.E. Martins^{1,2*}, J. Sérgio^{1,3}, C. Santos¹, A.P. Marques¹, M.T. Crespo^{1,3}, V.J. Pereira^{1,3}

¹iBET, Instituto de Biologia Experimental e Tecnológica, Portugal; ²Faculdade de Ciências e Tecnologia, Universidade do Algarve, Portugal; ³Instituto de Tecnologia Química e Biológica António Xavier, Universidade Nova de Lisboa, Portugal.

*maria.martins@ibet.pt



The development of effective disinfection treatment processes will be crucial to help the water industry cope with the inevitable challenges resulting from the increase in human population and climate change.

Three single small light emitting diodes that emit light at different wavelengths (255nm, 265nm, 260nm, 270nm, 280nm and their combinations) proved to be extremely effective to inactivate gram-negative (*Escherichia coli*) and gram-positive (*Enterococcus faecium*) bacteria that are routinely monitored as fecal contamination indicators of water quality.

The use of light emitting diodes may prove to be a sustainable alternative to the conventionally used low pressure mercury lamps to guarantee effective disinfection in water treatment utilities.

Introduction

Ultraviolet (UV) treatment using low pressure mercury lamps, that emit monochromatic light at 254nm, is widely applied to achieve disinfection of water due to the proven effectiveness of this treatment process against a wide range of waterborne pathogens. In addition to its disinfection effectiveness, UV can also degrade organic compounds by direct photolysis of photolabile compounds as a consequence of light absorption.

The use of UV light emitting diodes (LEDs) for disinfection recently emerged as a disinfection alternative due to their advantages: they are mercury free and therefore don't lead to the production of mercury waste, compact, robust, have longer lifetimes, do not need stabilization time, lead to a low energy consumption and can be constructed with a diversity of wavelengths. So, if proven effective, they can replace low pressure mercury lamps.

Some studies have already reported the use of different LED systems for the inactivation of different microorganisms in water sources [1-4]. These effective disinfection systems could still be improved using a combination of wavelengths that ensure damages in the microbial DNA and RNA, affect proteins, the enzymatic activity, membrane permeability, cell wall and biological processes of the different microorganisms with no or minimum dark and light repair possibilities.

Gaining a deep understanding of the mechanisms of inactivation of LEDs that emit light at different wavelengths would allow the development of alternative effective water disinfection systems. In this work, LEDs that emit light at different wavelengths (255nm, 265nm, 260nm, 270nm, 280nm and different combinations of wavelengths) were tested in terms of their potential to inactivate gram-negative (*Escherichia coli*) and gram-positive (*Enterococcus faecium*) bacteria that are routinely monitored as fecal contamination indicators of water quality.

Results

Inactivation assays were conducted in phosphate buffer and real water matrices using culture collection strains (*E. coli* DSM 18039 and *E. faecium* DSM 109923) and bacteria isolated from

real surface water matrices using selective media (RAPID[®] *E.coli* 2 and *Enterococcus faecium* ChromoSelect Agar).

The results obtained show that extremely high levels of inactivation were achieved after 1 minute exposure to three small LEDs that emit light at the different wavelengths – 260, 270 and 280nm (Figure 1). The inactivation results obtained for the target bacteria (*E. coli* and *E. faecium*) were extremely similar.

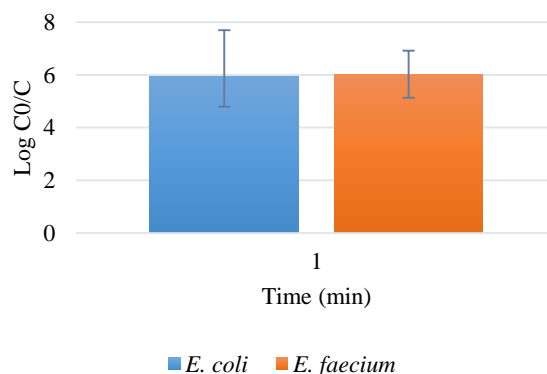


Figure 1. Inactivation of *E. coli* and *E. faecium* using a combination of LEDs that emit at 260nm, 270nm and 280nm.

After determining the UV fluences of LEDs that emit at different wavelengths needed to achieve 4 log inactivation of different target microorganisms in real matrices, the mechanisms of inactivation were addressed (by monitoring changes in cell morphology, membrane permeability, enzymatic activity as well as DNA damage) and the potential photoreactivation and dark repair was studied to define the best inactivation conditions that prevent reactivation.

Conclusions

LEDs that emit at different wavelengths (255nm, 265nm, 260nm, 270nm, 280nm and different combinations of wavelengths) were found to be extremely effective to inactivate

gram-negative (*Escherichia coli*) and gram-positive (*Enterococcus faecium*) bacteria that are routinely monitored as fecal contamination indicators of water quality. Future work

should confirm the effectiveness of the proposed solution for the inactivation of virus. The use of LEDs may become a sustainable alternative to the conventionally used mercury lamps.

Acknowledgements

This research was funded by Fundação para a Ciência e a Tecnologia through the project PTDC/EAM-AMB/1561/2021. iNOVA4Health (UIDB/04462/2020, UIDP/04462/2020) and LS4FUTURE Associated Laboratory (LA/P/0087/2020), a program financially supported by Fundação para a Ciência e Tecnologia/Ministério da Ciência, Tecnologia e Ensino Superior through national funds, is also acknowledged.

References

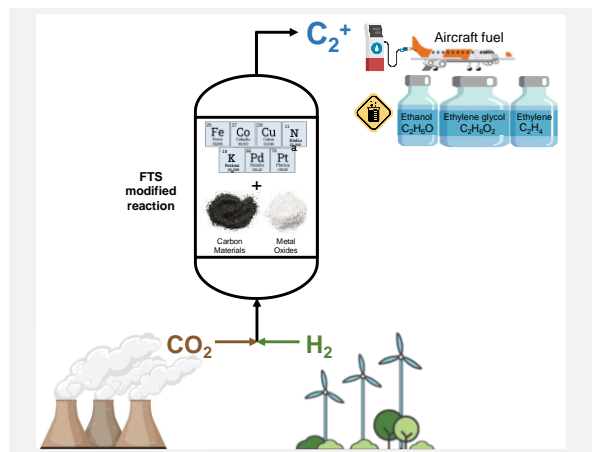
- [1] K. Song et al., *Water Research*, 94 (2016) 341-349.
- [2] S. Rattanakul, K. Oguma, *Water Research*, 130 (2018) 31-37.
- [3] B.R. Oliveira et al., *Water Research*, 168 (2020) 115108.
- [4] B.R. Oliveira et al., *Environmental Pollution*, 287 (2021) 117553.

Catalysts screening for the CO₂ hydrogenation reaction in C₂₊ products

M.B.S. Felgueiras, M.F.R. Pereira, O.S.G.P. Soares*

LSRE-LCM – Laboratory of Separation and Reaction Engineering - Laboratory of Catalysis and Materials, Faculty of Engineering, University of Porto, Rua Dr. Roberto Frias, 4200-465 Porto, Portugal; ALiCE – Associate Laboratory in Chemical Engineering, Faculty of Engineering, University of Porto, Rua Dr. Roberto Frias, 4200-465 Porto, Portugal.

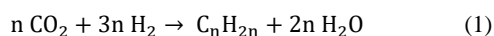
*mbsf@fe.up.pt



Carbon dioxide (CO₂) is one of the main drivers of climate change. The development of technologies to transform excess CO₂ into valuable chemicals and fuels is crucial to protect the environment and reduce dependence on fossil fuels. In this work, the most suitable catalyst supports and metallic active phases for the CO₂ valorization reaction in C₂₊ products (products with 2 or more C atoms) were assessed. The catalysts were texturally characterized, and catalytic tests for the CO₂ hydrogenation reactions were carried out at 200–350 °C, 15–20 bar and under H₂, CO₂ and N₂ flows. AC-supported catalysts recorded the lowest and the CNT-supported catalysts showed the highest CO₂ conversion values. Although Na catalysts demonstrate the highest CO₂ conversion, Fe catalysts are more selective for C₂₊ products.

Introduction

Carbon dioxide (CO₂) is the most common greenhouse gas, accounting for about 76% of these gases [1]. Most of this pollutant comes from the residential or commercial buildings. The increase in these emissions results in global warming, which triggers climate change and has consequences such as shortages of fresh water, rising floods and rising sea levels, which influence livestock, agriculture, and the global food system [2]. The hydrogenation of CO₂ is a versatile route capable of producing various chemicals and C₂₊ hydrocarbons (Equation 1) [3].



The production of C₂₊ products (compounds with 2 or more C atoms) by the hydrogenation of CO₂ would be highly desirable from the viewpoint of utilizing CO₂ as a carbon feedstock to produce chemical products. However, the selectivity for C₂₊ products is still low in most of the reported catalysts, so more fundamental studies are needed to develop an efficient catalyst for this purpose. The most used catalysts in the CO₂ hydrogenation reaction through a modified Fischer-Tropsch synthesis (FTS) are essentially metal oxides (ZrO₂, CeO₂, Al₂O₃, Fe₂O₃) and carbon materials: carbon nanotubes (CNT) and activated carbon (AC). Fe and Co based catalysts with alkali metal promoters (especially Na and K) are highly active with selectivity up to 57% for C₂–C₄ hydrocarbons and 40–60% CO₂ conversion [4]. Both the support and the promoter metal may affect the activity and the selectivity of the catalysts [3].

Objectives

This work aims to find the most suitable supports and combinations of metals for both CO₂ conversion and selectivity to C₂₊ products.

Materials and Methods

Commercial multi-walled carbon nanotubes (CNT), activated carbon (AC), and aluminum oxide (γ -Al₂O₃) were used as support for the metallic phases. The metallic catalysts were

prepared through incipient impregnation using the following metallic precursors: iron nitrate, cobalt nitrate, cerium nitrate, potassium nitrate, sodium carbonate, manganese acetate and ammonia molybdate. The total amount of impregnated metal corresponds to 20–37% (wt.%) and the subscript numbers in the elements represents the mass loadings of the metals: Fe₂₀, Fe₁₅K₁₀, Fe₁₇Mn₁₂, Fe_{6.67}Co_{3.33}K₁₀, Fe₁₇Mn₁₂K₈, Fe₁₇Mn₁₂Ce₂, Na₂Co₂₀ and Na₁Co₂₀Mo₁. In all catalysts, the metallic precursor solution was impregnated in support solution and left for 1.5 h at room temperature in the ultrasonic bath. Finally, the sample was placed in the oven for 24 h at 100 °C.

The thermal treatment of the synthesized materials was carried out at 400 °C under a flowrate of N₂ (1 h) and H₂ (3 h) of 100 cm³ min⁻¹ at a heating rate of 10 °C min⁻¹.

The textural properties of the synthesized materials were determined by N₂ adsorption-desorption equilibrium isotherms at -196 °C. The specific surface area (S_{BET}) was calculated by the BET method and the specific surface area of mesopores (S_{meso}) and the specific volume of micropores (V_{micro}) by the t-method.

The performance of the catalysts for the CO₂ hydrogenation was evaluated on a Microactivity-Reference (PID) unit. A mass of 200 mg of catalyst and filler (Carborundum) were mixed to make a bed of 2 cm³ and placed in a continuous-flow fixed-bed steel tubular reactor. All the catalysts were reduced under 80% (vol.%) H₂ - 20% (vol.%) N₂ flow rate (37.5 cm³ min⁻¹ at 400 °C for 4 h with a heating rate of 10 °C min⁻¹ at ambient pressure. Catalytic evaluation was performed under the reaction conditions of 200–350 °C, 15–20 bar and a 50% (vol.%) H₂, 16.7% (vol.%) CO₂ and 33.3% (vol.%) N₂ flow rate (30 cm³ min⁻¹) for 1.5 h with a heating rate of 3 °C min⁻¹.

Analysis of products was conducted using the Micro GC Fusion® Gas Analyzer chromatograph equipped with a packed Porapak Q column (length of 1 m) followed by a packed 5 Å molecular sieve column (5 m) connected to a thermal conductivity detector (TCD).

Results

AC presents the highest specific surface areas ($394 - 966 \text{ m}^2\text{g}^{-1}$) whereas Al_2O_3 the lowest ($70 - 205 \text{ m}^2\text{g}^{-1}$). The pore volume is higher in the catalysts supported on CNT.

Table 1 shows the CO_2 conversion results obtained for the maximum reaction temperature, 350°C .

Table 1. CO_2 conversion results obtained at the maximum reaction temperature, 350°C .

CNT	$x_{\text{CO}_2} / \%$	Al_2O_3	$x_{\text{CO}_2} / \%$	AC	$x_{\text{CO}_2} / \%$
NaCo	95	NaCo	85	NaCo	90
NaCoMo	89	NaCoMo	73	NaCoMo	57
Fe	47	Fe	34	Fe	6
FeCoK	43	FeCoK	46	FeCoK	22
FeK	42	FeK	37	FeK	21
FeMnK	37	FeMnK	20	FeMnK	13
FeMn	35	FeMn	33	FeMn	15
FeMnCe	23	FeMnCe	36	FeMnCe	3

It is notable that the AC supported catalysts recorded the lowest CO_2 conversion values, revealing that is not an adequate support for these reactions. Among the catalysts supported on CNT and Al_2O_3 , only FeCoK and FeMnCe showed slightly better results when supported on Al_2O_3 . Therefore, in the next catalytic tests, AC-supported catalysts will not be included. CNT-supported

catalysts have shown to be promising for the reaction under study and will be our focus in the next developments of this work.

The reaction products obtained for Fe-impregnated catalysts were carbon monoxide (CO), ethylene (C_2H_4), ethane (C_2H_6), propylene (C_3H_6), propane (C_3H_8) and at least six more C_2+ products. On the other hand, catalysts with Na, although presenting higher CO_2 conversions, were less selective to C_2+ products, obtain only CO, methane (CH_4), C_2H_6 , C_3H_8 and pentane (C_5H_{12}).

Conclusions

The main objective of this study was assess which support was most suitable for the CO_2 valorization reaction in C_2+ products and which combinations of metals would be more favorable for the CO_2 conversion and the selectivity of C_2+ products.

AC-supported catalysts recorded the lowest CO_2 conversion values. The catalysts supported on CNT showed to be promising for the reaction under study and will be our focus in the next developments of this work. Fe-impregnated catalysts were selective for at least 11 C_2+ products. On the other hand, catalysts with Na, although presenting a greater capacity to obtain higher CO_2 conversions were selective to only 5 C_2+ products. Therefore, the next catalysts will be synthesized using combinations of Fe and Na to find a balance between conversion and selectivity to the CO_2 hydrogenation reaction.

Acknowledgements

This work was financially supported by LA/P/0045/2020 (ALiCE), UIDB/50020/2020, and UIDP/50020/2020 (LSRE-LCM), funded by national funds through FCT/MCTES (PIDDAC) Mariana B. S. Felgueiras acknowledges the PhD research grant from FCT (2022.09616.BD), funded by national funds and by the European Union (EU) through the European Social Fund (ESF). O.S.G.P.S. acknowledges FCT funding under the Scientific Employment Stimulus – Institutional Call CEECINST/00049/2018.

References

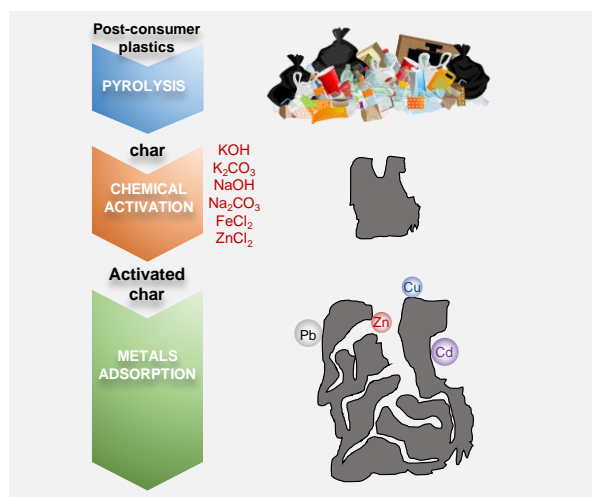
- [1] Global Emissions Available online: <https://www.c2es.org/content/international-emissions/>.
- [2] William D. Fletcher, C.B.S. Introduction. In *Reaching Net Zero: What It Takes to Solve the Global Climate Crisis*; Candice Janco, 2020; 1-8.
- [3] J. Wang et al., *Catalysis Today*, 215 (2013) 186-193.
- [4] R.-P. Ye et al., *Nature Communications*, 10 (2019) 5698.

Removal of heavy metals from aqueous solution using as adsorbent char derived from the pyrolysis of post-consumer plastic waste

L. Pereira, M. Calero*, R.R. Solís, A. Pérez, M.J. Muñoz, M.A. Martín-Lara

Chemical Engineering Department, University of Granada, Avda. Fuentenueva, s/n 18071 Granada, Spain.

*mcalero@ugr.es



The presence of heavy metals in wastewater is one of the problems of many industrial processes. Adsorption is one of the most widely used technologies for the treatment of these effluents. In addition, the use of low-cost materials as precursors to obtain solid adsorbents has shown great interest in recent years. In this work, the use of a char produced from the pyrolysis of a mixture of post-consumer plastic waste as a heavy metal adsorbent has been studied. For this, the pyrolysis char has been activated with different chemical agents. The activated char has been characterized and subsequently used as an adsorbent for heavy metals. The results have shown that the adsorption capacity depends on the characteristics of the adsorbent solids and the adsorbed metal. The material treated with Na_2CO_3 has slightly higher adsorption capacity values and the best results are obtained for Pb adsorption with all the materials. The adsorption capacity of Pb reaches values close to 40 mg/g when char treated with Na_2CO_3 is used.

Introduction

One of the problems derived from industrial activity is the generation of wastewater containing heavy metals. This type of aqueous effluent is produced by industries such as chemicals, mining, metallurgy or electronics and can contain a multitude of metals such as cadmium, lead, zinc, nickel, cobalt, copper, chromium or mercury. Some of these elements are considered highly toxic, and can cause significant problems for living beings and the environment.

Heavy metal removal can be carried out using various technologies such as precipitation, filtration, reverse osmosis, ion exchange, electrodialysis, oxidation or adsorption. Adsorption is one of the most widely used technologies. In addition, various innovative, economical and environmentally friendly materials have been developed. In this sense, in recent years interest has been shown in the use of carbonaceous materials as low-cost adsorbents for the treatment of wastewater containing metals. An example of a carbon-rich material proposed for this use is the char generated by thermochemical treatments of different types of raw materials such as biomass or plastics. The adsorption capacity of these materials is mainly determined by their surface properties that depend on the raw material used and the operating conditions of the thermochemical process and subsequent activation of the char obtained.

In this work, the use of a char produced from the pyrolysis of a mixture of post-consumer plastic waste as a heavy metal adsorbent has been studied.

Methodology

Once produced, the char has been subjected to an activation process with different chemical agents. The activated char has been characterized and subsequently used as an adsorbent for heavy metals (Cu, Ni, Zn, Pb and Cd). For this, discontinuous tests have been carried out, using different initial metal concentrations, a solid/liquid ratio of 0.5 g/L and a contact time of 2.5 h. Figure 1 shows a diagram of the char preparation process used.

Results

Figure 2 shows some of the main characteristics of the materials.

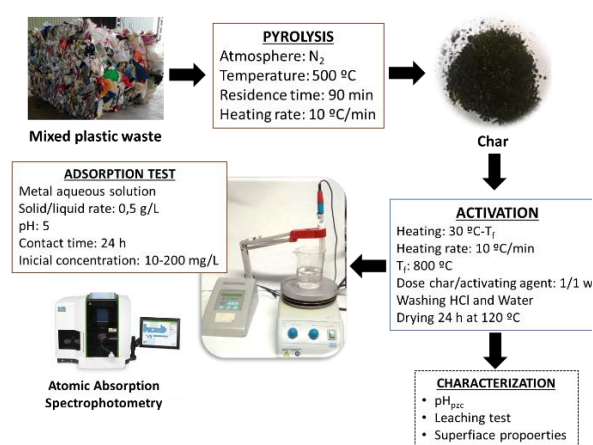


Figure 1. Graphical scheme of methodology.

Table 1 shows the results of the maximum adsorption capacity of the different activated materials, using aqueous solutions with an initial metal concentrations of 10 mg/L. Likewise, as an example, Figure 3 shows the Pb adsorption isotherms obtained with the activated materials that have shown the best adsorption capacity.

Table 1. Preliminary evaluation of adsorption capacity of chemically-developed materials.

Material	Pb mg/g	Cu mg/g	Ni mg/g	Zn mg/g	Cd mg/g
KOH-char	5.0	3.8	2.7	1.9	2.7
K_2CO_3 -char	4.5	3.9	3.6	1.7	1.6
NaOH-char	5.1	3.8	2.4	2.2	3.1
Na_2CO_3 -char	5.2	4.0	2.5	2.9	3.7
FeCl_3	0.7	0.0	0.5	0.5	0.0
ZnCl_2	4.2	0.8	0.5	0.0	0.4

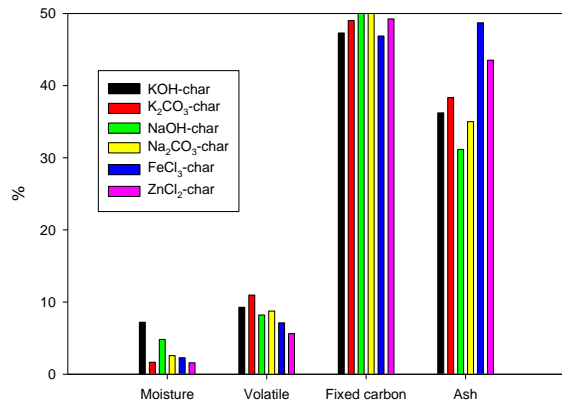


Figure 2a. Immediate analysis of chemically-developed materials

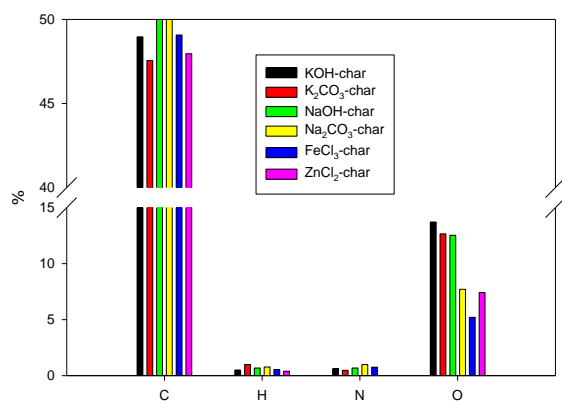


Figure 2b. Elemental analysis of chemically-developed materials

The results show that the adsorption capacities obtained vary depending on the type of activating agent and the adsorbed metal. This is mainly because the adsorption capacity depends on the surface characteristics of the adsorbent, such as its surface area (see Figure 2c), its surface charge or the type of functional groups present on the solid surface. Likewise, the adsorption capacity depends on the characteristics of the metal, such as its ionic state in solution, the ionic radius, its charge, etc.

Acknowledgements

Grant TED2021-130157B-I00 funded by MCIN/AEI/10.13039/501100011033 and by the “European Union NextGenerationEU/PRTR” and Grant PID2019-108826RB-I00/AEI funded by State Research Agency/10.13039/501100011033.

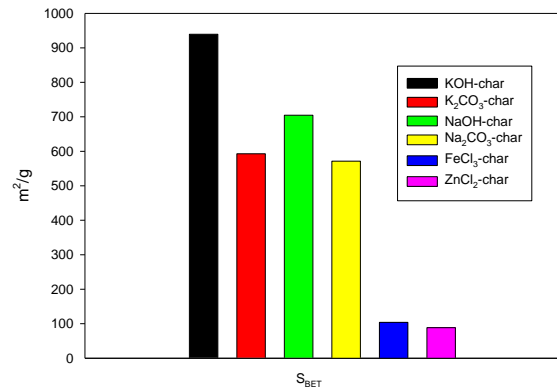


Figure 2c. Textual analysis of chemically-developed materials

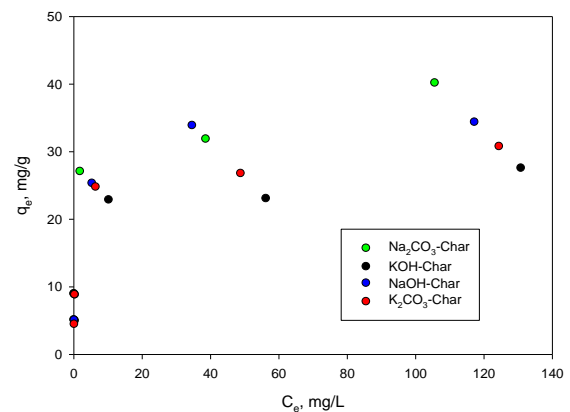


Figure 3. Adsorption isotherms of Pb.

Conclusions

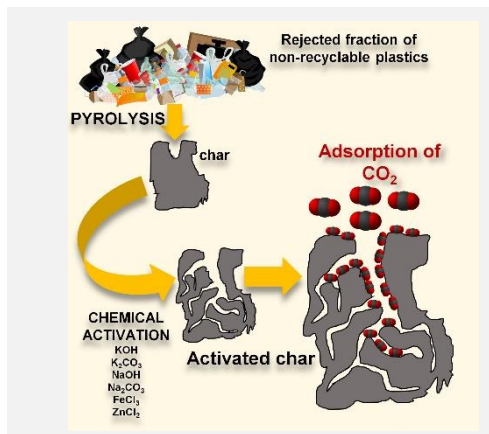
In this case, it has been found that, in general, the material treated with Na₂CO₃ has slightly higher adsorption capacity values than the other treatments for most metals and that the best results are obtained for Pb adsorption with all the materials. In this sense, the adsorption capacity of Pb reaches values close to 40 mg/g when char treated with Na₂CO₃ is used.

Development of low-cost adsorbent materials from char of pyrolysis of post-consumer mixed plastic waste and its application to effluent purification (CARBOPLASTIC project)

L. Pereira, R.R. Solís, M. Calero, G. Blázquez, M.A. Martín-Lara*

Chemical Engineering Department, University of Granada, Avda. Fuentenueva, s/n 18071 Granada, Spain.

*marianml@ugr.es



Plastic materials, in addition to consuming energy and resources for their production, cause a significant environmental problem due to the waste they generate. The CARBOPLASTIC project evaluates the development and application of adsorbent materials derived from the char of pyrolysis of post-consumer mixed plastic waste. The main objective of the project is to develop new scientific knowledge technology and commercial products for waste plastics derived materials. The project covers all aspects in a circular economy from precursors to processing, conversion and refining and application of advanced produced materials in several sustainable technologies such as CO₂ capture and pollutants removal from wastewaters. In our opinion, the results of the project can support authorities in the design and implementation of reforms that help combat environmental pollution by plastics mainly about the definition of national and municipal waste management policies or the preparation of action plans and strategies for the circular economy.

Introduction

The global plastic production has increased over years due to the important applications of plastics in many sectors. However, the continuous demand of plastics has caused the plastic wastes accumulation in the landfills and causing a major environmental problem. In addition, the increased demand for plastic materials poses another problem, the high dependence on petroleum because that is the main raw material in plastics production.

To mitigate these problems, some alternatives that have been developed to manage plastic wastes are mechanical recycling and energy recovery. However, there are some drawbacks of these methods such as the high cost of the efficient separation process of the materials or the emission of pollutants that can reduce the sustainability of the process.

Objectives

Therefore, the general objective of this project is to be able to contribute to the recycling of plastic waste, which would help reduce environmental pollution, limit the use of raw materials and fight against climate change, recognizing the potential of plastic as a valuable resource. At the end of their life, dirty non-recyclable mixed plastics from municipal solid waste are still very valuable resources that will be transformed by pyrolysis into new chemical feedstock (from liquid product) and into valuable adsorbent materials (from solid product).

The research project evaluates the performance of adsorbent materials derived from char of pyrolysis of post-consumer mixed plastic waste in biogas upgrading to biomethane and wastewater treatment. It covers all chemical engineering aspects from precursors (the nature of plastic waste) to processing (thermochemical conversion, porosity development, chemical functionalization) and application (CO₂ capture and removal of pollutants from wastewater).

The specific objectives of the project are:

- Objective 1: Study the pyrolysis of post-consumer mixed plastic waste to produce valuable products (Figure 1).
- Objective 2: Screen properties of char byproduct (Figure 2).
- Objective 3: Upgrade properties of char for developing novel low-cost adsorbent materials through a unique set of functionalization protocols (Figure 2).

- Objective 4: Evaluate the resulting materials in advanced applications as adsorbents (biogas upgrading and pollutants removal in aqueous phase) (Figure 2).
- Objective 5: Assess the socio-economic and environmental impact of char production, upgrading and application.

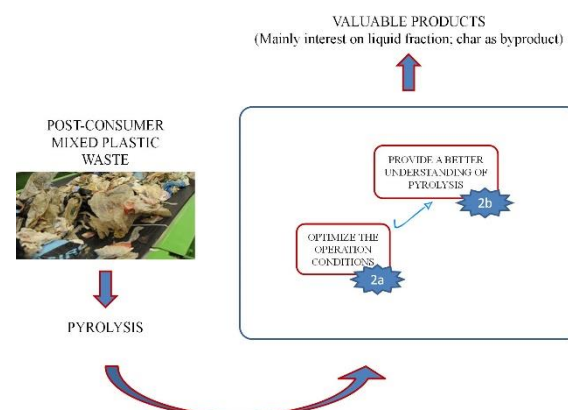


Figure 1. Graphical scheme of objective 1.

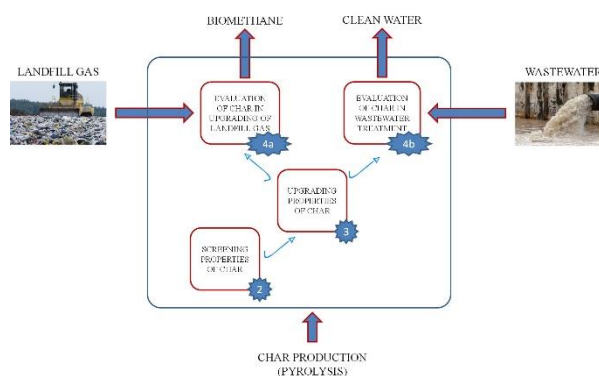


Figure 2. Graphical scheme of objectives 2, 3 and 4.

Preliminary results

Until now, adsorbents that have been developed by chemical activation of char and has been deeply characterized. Also, these developed materials have been preliminarily evaluated as adsorbents of CO₂. Main results are summarized in Table 1 and Figure 3.

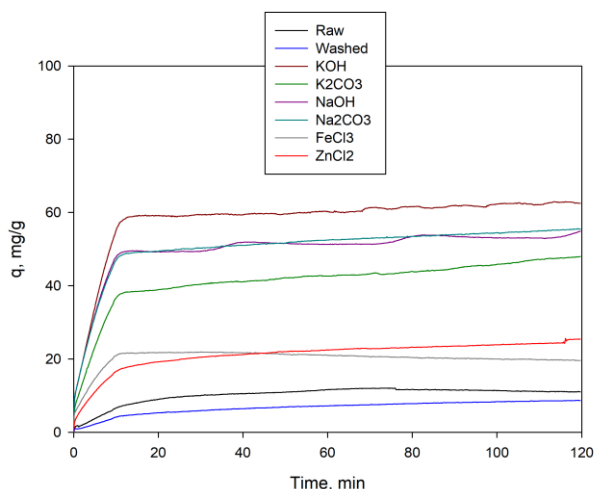


Figure 3. CO₂ adsorption performance of chemically-developed materials in function of time.

Table 1. Summary of characterization of chemically-developed materials.

	Analysis	Raw char	Washed char	KOH char	K ₂ CO ₃ char	NaOH char	Na ₂ CO ₃ char	FeCl ₃ char	ZnCl ₂ char
Elemental	C, %	36.97	52.19	48.96	47.55	54.96	55.54	49.07	47.96
	H, %	2.36	5.14	0.50	0.99	0.68	0.77	0.54	0.39
	N, %	1.02	1.45	0.61	0.47	0.68	0.98	0.75	0.00
	S, %	0.00	0.00	0.00	0.00	0.00	0.00	0.73	0.71
	O*, %	19.86	5.28	13.71	12.65	12.53	7.71	5.20	7.41
Immediate	Moisture, %	2.93	1.61	7.20	1.66	4.82	2.57	2.28	1.59
	Volatile, %	29.96	31.97	9.28	10.97	8.20	8.76	7.12	5.63
	Fixed carbon, %	28.32	30.48	47.30	49.03	55.83	53.66	46.88	49.25
	Ash, %	39.79	35.94	36.22	38.34	31.15	35.00	43.71	43.53
Textural	S _{BET} , m ² /g	2.60	3.30	939.40	592.80	704.50	571.30	104.00	88.40
	S _{MP} , m ² /g	0.00	0.00	821.80	457.40	552.50	425.40	57.70	41.00
	V _T , cm ³ /g	0.01	0.01	0.65	0.52	0.56	0.54	0.19	0.16
	V _{MP} , cm ³ /g	0.00	0.00	0.40	0.23	0.29	0.22	0.02	0.07

Acknowledgements

Grant TED2021-130157B-I00 funded by MCIN/AEI/10.13039/501100011033 and by the “European Union NextGenerationEU/PRTR” and Grant PID2019-108826RB-I00/AEI funded by State Research Agency/10.13039/501100011033.

Conclusions

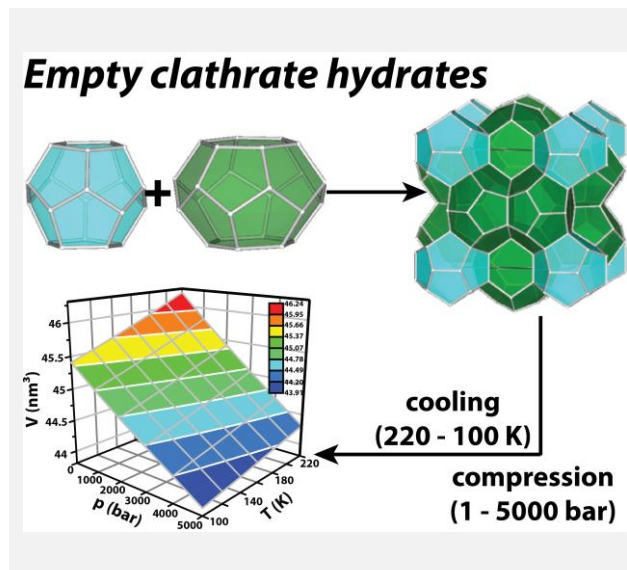
Solid char from pyrolysis of dirty non-recyclable mixed plastics from municipal solid waste can be converted into a value-added material, which can treat effluents containing CO₂. This transformation of char into high-value adsorbent materials could represent an attractive means to mitigate the global waste plastic problem, whilst simultaneously contributing to CO₂ removal.

A molecular simulation study of the structure and thermodynamics of empty clathrate hydrates below the freezing point of H₂O

F.J.A.L. Cruz*, J.P.B. Mota

LAQV@Requimte, Dept. Chemistry, NOVA University Lisbon, 2829-516 Caparica.

*ff.cruz@fct.unl.pt



Simulations are employed to probe empty *sI* and *sII* clathrate hydrates, observing that the volumetric response to an applied $p-T$ gradient is accurately described by the Parsafar and Mason equation of state with an accuracy $> 99\%$. Structural deformation induced upon the crystals is monitored and benchmarked against previous neutron diffraction measurements of ice XVI and hexagonal ice at 1 bar. A critical comparison is established with guest occupied lattices (CH₄, CO₂ and C_nH_{2n+2}), revealing that empty *sII* frameworks are slightly more stable to thermal deformation than their *sI* analogues. Of paramount importance for the oil and natural gas industries, heat capacities obtained are identical for the *sI* and *sII* lattices up to 2000 bar and diverge by $\sim 7.3\%$ at 5000 bar. The canonical tetrahedral symmetry of water-bonded networks is analysed in terms of an angular and a distance order parameters, which are observed to decrease (increase) as pressure (temperature) increases (decreases).

Introduction & Methodology

The thermodynamical phase space of the metastable empty clathrate hydrates (CHs) is probed over broad temperature and pressure ranges ($100 \leq T/K \leq 220$, $1 \leq p/\text{bar} \leq 5000$), using large-scale computer simulations and compared with available experimental data at 1 bar [1, 2]. For that purpose, we employ the fully atomistic and rigid TIP4P-Ice four-charge potential [3] to describe the H₂O lattice of the empty clathrate phases (*sI*, *sII*); this potential was developed to reproduce the experimental melting point of ice *Ih* (272.2 K at 1 bar), and has been successfully employed to study the deformation [1, 2, 4], energetics and decomposition [5, 6], and phase behaviour [7-9] of several CHs. Starting from an initial configuration at the lowest temperature and pressure (100 K, 1 bar), CHs are isothermally pressurised to achieve the desired pressure (1 bar \rightarrow 100 bar \rightarrow 500 bar \rightarrow 1000 bar \rightarrow 2000 bar \rightarrow 5000 bar), and the protocol repeated for the next higher temperature (100 K \rightarrow 120 K \rightarrow 140 K \rightarrow 160 K \rightarrow 180 K \rightarrow 200 K \rightarrow 220 K) starting from the corresponding previous equal pressure run. Calculations are run for at least 50 ns in order to obtain statistically consistent data, and the first 5 ns discarded to account for equilibration. Because data collection takes place every 5 ps, each $p-V-T$ state point is obtained from time-averaging an *ensemble* of 9000 data points. The whole $p-V-T$ surface obtained (*cf.* Graphical Abstract) is interpreted using the universal form of the Parsafar and Mason equation of state [10], always with an accuracy better than 99 %.

Results – Structure

Measurements of unit cell length, a , were conducted during the simulations and are here represented in Figure 1a for the room pressure systems, along with data previously obtained for other guest occupied *sII* CHs. A critical comparison is established in terms of the ratio of molecular diameters between the guest molecule, D_G , and cavity diameter, D_C , allowing the parameter (D_G/D_C) to be used as the rationale for unit cell length

increase/contraction when the empty crystals become occupied by guest molecules. Furthermore, the solids' isobaric thermal expansivity, obtained in terms of a parabolic line (Figure 1b), $\alpha_p = [\partial a / (a \cdot \partial T)]_p$, reveals that the empty CHs exhibit a positive thermal expansion up to a certain temperature threshold, beyond which $[\partial^2 a / (a \cdot \partial T^2)]_p$ becomes negative; the particular temperature at which this phenomenon occurs decreases with applied pressure, and, in the case of the *sII* lattices, starts at 191.5 K@1 bar until finally reaching 161.6 K@5000 bar (Figure 1b).

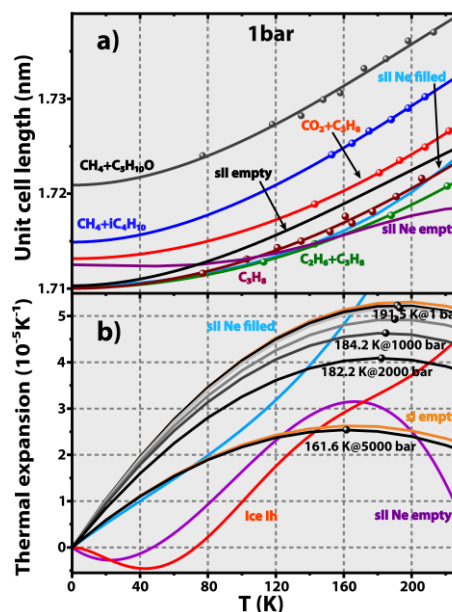


Figure 1. Structural data. *a*) Temperature dependence of unit cell length at 1 bar for *sII* lattices: symbols correspond to experimental measurements of C₃H₈ (dark red), 18.2 % CO₂ + 81.8 % C₃H₈ (light red), 30 % C₂H₆ + 70 % C₃H₈ (green), 87.6 % CH₄ + 12.4 % iC₄H₁₀ (blue) and 95 % CH₄ + 5 % C₅H₁₀O (dark grey). Results obtained in

this work for empty *sII* clathrates (black), as well as data for Ne-filled (light blue) and Ne-empty (magenta) *sII* topologies are represented by lines obtained using cubic polynomial fittings. **b)** isobaric thermal expansivities, $\alpha_p = (1/a)(\partial a/\partial T)_p$ obtained using molecular simulations and empty *sII* (black) and *sI* clathrates (dark yellow), and previous atmospheric pressure experimental data for hexagonal ice (red) and Ne-filled and Ne-empty *sII* clathrates (light blue, magenta); values represent the several α_p maxima.

The characteristic tetrahedral structure around oxygen atoms was probed using two order parameters, S_g and S_k , in order to monitor the angular and distance contributions to a canonical tetrahedral symmetry, respectively [11]. Time-averaged distributions reveal that the empty frameworks retain tetrahedral integrity throughout the entire p - T domain, but respond accordingly by slightly distorting the solid lattice. Using Gaussian statistics, it becomes clear that by imposing isothermal conditions whilst increasing pressure, S_g maxima are shifted towards higher values, as a result of the solid contraction and gradual loss of tetrahedral order. For $(p, T) > (2000 \text{ bar}, 200 \text{ K})$, deformation occurs via a mechanism that involves a dominant contribution from angular alterations. The microscopic structure associated with the solids is probed deeper calculating radial distribution functions (g_r), and, in general, both the $g_r(\text{O}-\text{O})$ and $g_r(\text{O}-\text{H})$ curves exhibit two maximum intensity peaks, corresponding to the thickness of the first and second order neighbour shells, centered at $r_{(\text{O}-\text{O})} = (0.27, 0.45) \text{ nm}$ and $r_{(\text{O}-\text{H})} = (0.18, 0.32) \text{ nm}$, revealing that the hydrogen bonds responsible for network integrity are of similar length regardless of the particular (p, T) conditions. A recent neutron diffraction analysis [12] of an empty *sII* hydrate yielded a mean time-space averaged hydrogen bond distance of 0.275 nm, which compares quantitatively with our own average value of $\bar{r}_{(\text{O}-\text{H})} = 0.25 \text{ nm}$.

Results – Thermodynamics

The isobaric heat capacity is obtained using the classical thermodynamic relation $C_p = (\partial H/\partial T)_p$, where H is the solid's molar enthalpy. Figure 2 shows a *quasi*-constant correlation with pressure, at least up to 2000 bar, beyond which C_p becomes a function of the clathrate individual topology. When pressure reaches 5000 bar, the *sII* polymorphs exhibit a C_p that is $\sim 7.3 \%$ larger than the corresponding *sI*

crystals, suggesting that the larger cages characteristic of *sII*, when subject to hydrostatic pressure, are better suited to accommodate heat propagation through the lattice thus giving rise to a slightly enhanced C_p as compared to the *sI* structure. Data obtained for the empty clathrates and also for hexagonal ice have been successfully correlated using Shomate-like equations, $C_p = A + Bp + Cp^2 + Dp^3$ [2].

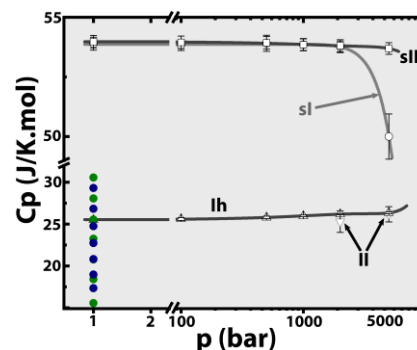


Figure 2. Isobaric heat capacity, C_p . Symbols and error bars correspond to data obtained in the calculations: (\square) empty *sII* clathrates, (\circ) empty *sI* clathrates, (Δ) hexagonal ice *Ih* and (∇) ice *II* and experimental results from Handa and Murray for ice (\bullet) and a THF clathrate (\bullet). Lines correspond to cubic polynomials, $C_p = A + Bp + Cp^2 + Dp^3$. Notice that the C_p scale has been broken in the range 31 – 49.5 J/K·mol.

Handa et al. used a Tian-Calvet heat-flow calorimeter and samples of a tetrahydrofuran CH (THF·16.9H₂O) and H₂O ice, at 85–270 K at room-pressure [13, 14]. Under their experimental conditions, hexagonal ice is the thermodynamically stable form of water, for which the isobaric heat capacity was observed to increase from $C_p = 15.5 \text{ J/K}\cdot\text{mol}$ up to $C_p = 30.5 \text{ J/K}\cdot\text{mol}$, when temperature climbs from 100 K to 220 K, respectively, giving rise to an average value of $\bar{C}_p = 23 \text{ J/K}\cdot\text{mol}$, in satisfactory agreement with our own result of $C_p = 25.5 \text{ J/K}\cdot\text{mol}$. For the THF hydrate samples $C_p = 17.4 \text{ J/K}\cdot\text{mol}$ (100 K) and $29.3 \text{ J/K}\cdot\text{mol}$ (220 K). Their complete set of calorimetric data for ice *Ih* and THF·16.9H₂O is graphically represented in Figure 2, together with the results obtained in the present work.

Acknowledgements

This work received support from PT national funds (FCT/MCTES, Fundação para a Ciência e Tecnologia and Ministério da Ciência, Tecnologia e Ensino Superior) through projects UIDB/50006/2020 and UIDP/50006/2020. F.J.A.L.C. gratefully acknowledges FCT/MCTES for funding through program DL 57/2016 – Norma Transitória (Ref. 654/2018-24), and also for funding the Advanced Computing Project 2021.09623.CPCA on Cirrus-A:INCD.

References

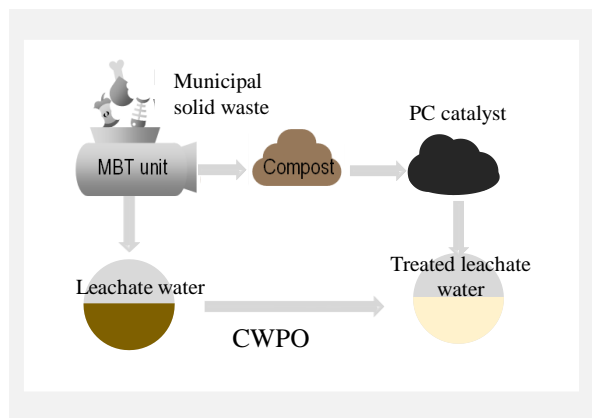
- [1] F.J.A.L. Cruz et al., ACS Earth Space Chemistry, 3 (2019) 789.
- [2] F.J.A.L. Cruz, J.P.B. Mota, Physical Chemistry Chemical Physics, 23 (2021) 16033.
- [3] J.L.F. Abascal et al., Journal of Chemical Physics, 122 (2005) 234511.
- [4] S. Takeya et al., Journal of Physical Chemistry C, 122 (2018) 8134.
- [5] S. Alavi, R. Ohmura, Journal of Chemical Physics, 145 (2016) 154708.
- [6] S.A. Bagherzadeh et al., Journal of Chemical Physics, 142 (2015) 214701.
- [7] H. Tanaka et al., Journal of Chemical Physics, 149 (2018) 074502.
- [8] D. Jin, B. Coasne, Langmuir, 33 (2017) 11217.
- [9] V.K. Michalis et al., Journal of Chemical Physics, 142 (2015) 044501.
- [10] G. Parsafar, E.A. Mason, Physical Review B, 49 (1994) 3049.
- [11] P.-L. Chau, A.J. Hardwick, Molecular Physics, 93 (1998) 511.
- [12] A. Falenty et al., Nature, 516 (2014) 231.
- [13] Y.P. Handa, Canadian Journal of Chemistry, 62 (1984) 1659.
- [14] Y.P. Handa et al., Journal of Chemical Thermodynamics, 16 (1984) 623.

Compost-derived catalyst for wet peroxide oxidation of leachate waters

F.F. Roman^{1,2}, G.F. Batista^{1,2,3}, A.S. Silva^{1,2}, J.L. Diaz de Tuesta⁴, R.V. Mambrini³, H.T. Gomes^{1,2*}

¹Centro de Investigação de Montanha (CIMO), Instituto Politécnico de Bragança, Campus de Santa Apolónia, 5300-253 Bragança, Portugal; ²Laboratório Associado para a Sustentabilidade e Tecnologia em Regiões de Montanha (SusTEC), Instituto Politécnico de Bragança, Campus de Santa Apolónia, 5300-253 Bragança, Portugal; ³Departamento de Química, Centro Federal de Educação Tecnológica de Minas Gerais (CEFET-MG), Campus I, Belo Horizonte 30421-169, Brazil; ⁴Department of Chemical and Environmental Technology, Rey Juan Carlos University, Calle Tulipán s/n., 28933 Móstoles, Spain.

*htgomes@ipb.pt



Municipal solid waste (MSW) is a major contributor to the waste generated in Europe, and anaerobic digestion is a common treatment in mechanical and biological treatment (MBT) units, generating two byproducts: compost and leachate waters. Catalytic wet peroxide oxidation (CWPO) is an alternative process for wastewater treatment where carbon-based materials have displayed proper catalytic activity. This work aims to valorize waste materials from the anaerobic digestion of MSW (compost) into a value-added carbon-based catalyst, highlighting its applicability in the CWPO of highly polluted wastewater (leachate waters).

Introduction

Municipal solid waste (MSW) represents around 10% of all waste generated, reaching up to 502 kg per person per year in Europe [1]. Anaerobic digestion is a common treatment for MSW, resulting in digestate and highly polluted leachate waters. The digestate is mostly valorized by composting for agriculture purposes, yet there are several limitations to using this compost. At the same time, leachate waters have a complex composition, including recalcitrant organic compounds to biological treatments [2]. In this sense, catalytic wet peroxide oxidation (CWPO) emerges as promising low-cost process and it allows for attaining high removal rates of organic compounds [3]. CWPO is based on the catalytic decomposition of hydrogen peroxide into hydroxyl radicals, requiring proper catalysts [3]. Carbon-based materials have shown promising activity in CWPO reactions [4-6]. Thus, this work aims at the valorization of the compost obtained from the anaerobic digestion of MSW into carbon-based catalysts for further application in the treatment by CWPO of the leachate waters generated in mechanical and biological treatment units.

Methodology

The compost and the leachate waters were supplied by Resíduos do Nordeste, the company responsible for MSW management in the northeast region of Portugal. The leachate waters were filtered with a paper filter and characterized, as in a previous work [2].

The compost was used as carbon precursor for the synthesis of pyrochar at 800 °C (PC) and characterized, as described elsewhere [7]. The oxidation reactions were carried out at 80 °C, considering a varying catalyst loading of 1.8 – 7.2 g L⁻¹, initial pH (*pH*₀) = 3.0, and H₂O₂ concentration to mineralize the TOC content ([H₂O₂]₀ = 86 g L⁻¹), added in 5 intervals, one addition each hour in the first 4 h of reaction (0, 1, 2, 3, and 4 h). A pre-treatment consisting of an adsorption step with exchange-ion resins was also applied, aiming at decreasing the content of scavenging ions that may decrease the efficiency of the process. 150 mL of leachate waters at pH 9.5 was mixed with 3 g of a

cationic exchange resin (Lewatit TP207, Sigma-Aldrich) and stirred for 48 h. The resulting effluent was subsequently treated by CWPO, considering the conditions described above.

Results

The main characteristics of the PC catalyst and the original compost are described in Table 1. As can be observed, the increase in the C/H ratio indicates the successful carbonization of the compost. Furthermore, PC has a strong base character, with a low concentration of acidic functionalities, likely removed at the high temperature heat treatment that was subjected [2]. The basic functionalities likely arise from the alkali and alkaline-earth metals composing PC's ashes. Additionally, PC displays an intermediate surface area, in agreement with surface areas obtained by pyrolysis of other residual sources [6].

Table 1. Characteristics of the compost and the PC catalyst.

Parameter	Compost	PC catalyst
C/H ratio	9.2	44
Acidity (mmol g ⁻¹)	-	0.9
Basicity (mmol g ⁻¹)	-	2.5
pH _{pzc}	-	11.0
S _{BET} (m ² g ⁻¹)	-	77
Ashes (%)	55.5	81.5

The main characteristics of the leachate waters are described in Table 2, and the results of CWPO are displayed in Figure 1. At the lowest catalyst concentration (1.8 g L⁻¹), barely any COD or TOC are removed in 24 h of reaction (2.1 and 8.3%, respectively). By increasing to 3.5 g L⁻¹, the removals of COD and TOC are increased, achieving 30 and 26%, respectively. Finally, increasing the catalyst concentration to 7.2 g L⁻¹, 35% of COD and 41% of TOC were removed. The CWPO treatment was also very effective in removing the color of the effluent (Figure 2).

Table 2. Characteristics of the leachate waters under treatment.

Parameter	Value
COD	60 g L ⁻¹
TOC	27 g L ⁻¹
Chlorides	5 g L ⁻¹

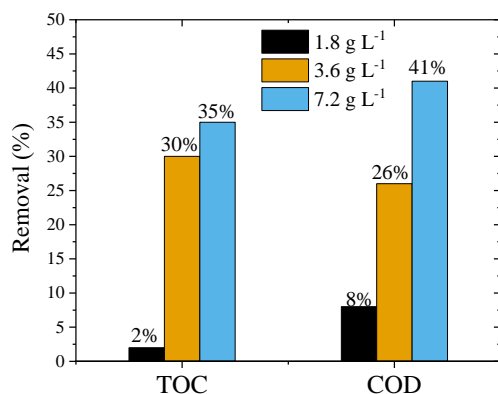


Figure 1. Removal of COD and TOC considering different catalyst loads by CWPO. Conditions: $[\text{COD}]_0 = 60 \text{ g L}^{-1}$, $[\text{H}_2\text{O}_2]_0 = 86 \text{ g L}^{-1}$, $\text{pH}_0 = 3.0$, $T = 80 \text{ }^\circ\text{C}$, $C_{\text{catalyst}} = 1.8\text{-}7.2 \text{ g L}^{-1}$.

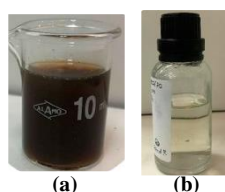


Figure 2. Color of the leachate waters (a) before and (b) after CWPO. Conditions: $[\text{COD}]_0 = 60 \text{ g L}^{-1}$, $[\text{H}_2\text{O}_2]_0 = 86 \text{ g L}^{-1}$, $\text{pH}_0 = 3.0$, $T = 80 \text{ }^\circ\text{C}$, $C_{\text{catalyst}} = 1.8\text{-}7.2 \text{ g L}^{-1}$.

Nevertheless, the TOC and COD content remains high after the CWPO treatment, likely due to the scavenging effect of chlorides and other ions that mainly act as scavengers of the hydroxyl radicals [2, 8]. Thus, the combination of a pre-treatment step followed by CWPO was explored, and the results can be observed in Figure 3. The pre-treatment improved the

results in terms of TOC and COD removals. But the main improvement was in the efficiency of H_2O_2 consumption ($\eta_{\text{H}_2\text{O}_2}$), calculated as $X_{\text{TOC}}/X_{\text{H}_2\text{O}_2}$. At the same time, the treatment by CWPO resulted in an $\eta_{\text{H}_2\text{O}_2}$ of 41%, the combination of both treatments allowed to increase in the efficiency to 65%.

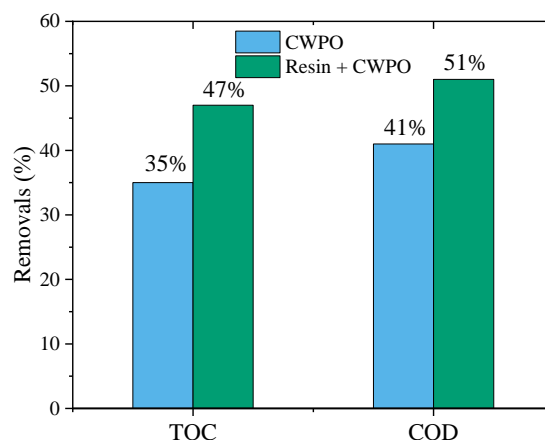


Figure 3. Removal of COD and TOC considering only CWPO and a combination of a pre-treatment with a cationic resin and CWPO. Conditions: $[\text{COD}]_0 = 60 \text{ g L}^{-1}$, $[\text{H}_2\text{O}_2]_0 = 86 \text{ g L}^{-1}$, $\text{pH}_0 = 3.0$, $T = 80 \text{ }^\circ\text{C}$, $C_{\text{catalyst}} = 7.2 \text{ g L}^{-1}$.

Conclusions

The results reported here display an alternative towards the valorization of compost derived from MSW. Active catalysts were prepared from compost, which allowed to remove up to 47 and 51% of TOC and COD, respectively, as well as the color, depending on the chosen conditions, of highly polluted leachate waters obtained in mechanical and biological treatment units.

Acknowledgements

This work was financially supported by LA/P/0045/2020 (ALiCE), UIDB/50020/2020 and UIDP/50020/2020 (LSRE-LCM) funded by national funds through FCT/MCTES (PIDDAC); CIMO (UIDB/00690/2020) and by project “VALUECOMP - Valorización de compost procedente de residuos municipales mediante la obtención eficiente de productos de valor añadido”, with reference 0765_VALUECOMP_2_P, through FEDER under Program INTERREG. Fernanda F. Roman acknowledges FCT and FSE for the individual research grant (SFRH/BD/143224/2019). Adriano S. Silva was supported by the doctoral grant SFRH/BD/151346/2021 financed by FCT with funds from NORTE2020, under MIT Portugal Program. Jose L. Diaz De Tuesta acknowledges the financial support through the program of *Atracción al Talento* of *Comunidad de Madrid* (Spain) for the research grants 2020-T2/AMB-19836 and 2022-T1/AMB-23946.

References

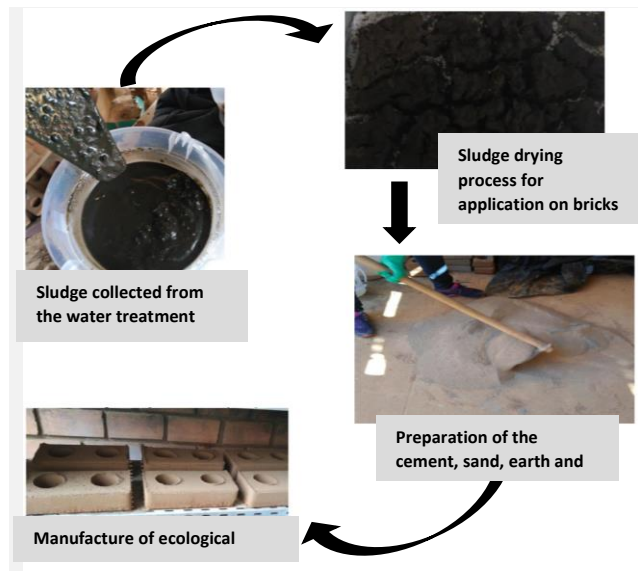
- [1] Eurostat - statistics explained, Municipal waste statistics, 2021. Available at https://ec.europa.eu/eurostat/statistics-explained/index.php?title=Municipal_waste_statistics. Accessed on March 27th, 2023.
- [2] G.F. Batista et al., *Catalysts*, 12 (2022) 238.
- [3] R.S. Ribeiro et al., *Applied Catalysis B: Environmental*, 187 (2016) 428-460.
- [4] F.F. Roman et al., *Catalysis Today*, in press, (2023). DOI: 10.1016/j.cattod.2023.01.008
- [5] R.S. Ribeiro et al., *Journal of Environmental Management*, 308 (2022) 114622.
- [6] J.L. Diaz de Tuesta et al., *Journal of Environmental Chemical Engineering*, 9 (2021) 105004.
- [7] J.L. Diaz de Tuesta et al., *Environmental Technology & Innovation*, 24 (2021) 101984.
- [8] R.S. Ribeiro et al., *Applied Catalysis B: Environmental*, 219 (2017) 645-657.

Water treatment station sludge with application in the production of ecological bricks

R.M. Cabral^{1*}, C. Akamatsu², N.C.M. Ross², R.J.E. Martins¹, M.T.A. Pietrobelli²

¹Instituto Politécnico de Bragança, Campus de Santa Apolónia 5300-253 Bragança, Portugal; ²Universidade Tecnológica Federal do Paraná, R. Doutor Washington Subtil Chueire, 330, Ponta Grossa, Brazil.

*rafaelarmc@hotmail.com



Accelerated urban growth increases the demand for natural resources, especially water. In Brazil, treatment plants use the conventional process for water treatment, transforming water that is unfit for consumption into drinkable water. However, this process generates sludge, a residue that has chemical elements in its composition that, if disposed of incorrectly, negatively affect human life and the environment. As an alternative to solve this problem, it is the use of sludge generated in industrial applications, such as civil construction, which is the focus of this work. The present work seeks to evaluate the partial replacement of sludge in the soil in the manufacture of ecological bricks, consisting then of sand (gravel), soil, sludge and cement. Test specimens were manufactured based on the literature and these were evaluated in accordance with the Brazilian regulations, succeeding the tests of resistance to compression and absorption. According to the NBR 8491:2012 standard, the bricks showed high water absorption, however, with the results within the limit, however they did not reach the minimum compressive strength established by a specific standard.

Introduction

According to the Brazilian Institute of Geography and Statistics - IBGE, the population of the city of Ponta Grossa has increased by approximately 25% since 2010, consequently leading to a growing demand for water resources. Currently the 65th most populous city in Brazil.

The Water Treatment Stations (WTS) in Brazil use a conventional process for water treatment, however with the generation of WTS sludge which is a residue of this process. The sludge is made up of organic and inorganic materials, with a high moisture content, and may contain several chemical elements which, when discarded in an erroneous manner, generate negative impacts on human life and the environment [1].

Several studies have been carried out regarding the destination of WTS sludge, including its use in civil construction, with its incorporation in the manufacture of bricks [2].

With these points presented, the present work aims to study the incorporation of WTP sludge in the manufacture of bricks acting as a partial substitute for soil.

Methods

The sludge samples from the Water Treatment Station, the soil with a reddish color and clayey appearance, the sand (a gravel from hail deposits with a yellowish color and sensorially coarse particles), all these materials were collected/acquired in the city of Ponta Grossa – PR, in Brazil.

Initially, the analysis of total solids of the sludge was carried out using the gravimetric method, following the NBR 10664/1989 standard [3], in which a homogenized portion of the sample was transferred to an evaporation capsule in a water bath and then dried in an oven. The difference between the mass of the capsule containing the dry residue and the mass of the empty capsule corresponds to the total residue.

In the manufacture of the ecological brick, the methodology used was described in the Booklet for the Production of Soil-cement Brick of the Technology Foundation of the State of Acre

(FUNTAC, 1999) and with the parameters of NBR 10833: 2012 on the use of a hydraulic manual press in the manufacture of soil-cement brick [4].

For the initial preparation, the soil and sludge, separately, were dried at 110 °C for 48 hours and the gravel was dried with the aid of a frying pan (due to low humidity) and then sieved in a 4.8 mm mesh. Portland cement (NBR 10833:2012) CP-II-F-32 from the Cauê brand was used, with four mixtures being carried out with different concentrations of earth-sludge, which are described in Table 1. The ready mixes were transferred to the manual press silo, to shape the brick (Figure 1) [5].

Table 1. Proportion of mixtures under analysis.

Mixture	Cement (%)	Sand (%)	Soil(%)	Sludge(%)
0	10,00	63,00	27,00	0,00
1	10,00	63,00	25,75	1,25
2	10,00	63,00	24,50	2,50
3	10,00	63,00	22,00	5,00



Figure 1. Bricks store for healing.

For bricks to be considered suitable for use, they must have “sharp edges and cannot show cracks, fractures or other defects that could compromise the settlement, resistance and durability of the masonry” [6]. Also having compressive strength between 1.7 Mpa and 2.0 Mpa and water absorption values between 20% and 22%, with a minimum age of seven days, according to NBR 8492:2012. Following this norm, compression and absorption tests were carried out, using seven and three bricks of each type of mixture, respectively.

In the first test, the bricks were cut in half, and then the respective faces were glued together with Portland cement paste and then immersed in water for 6 hours. After this period, the surfaces of the bricks were dried and transferred to the testing machine. The applied load was gradually increased at a rate of 500 N/s until failure occurred. With the results obtained through the equation:

$$ft = \frac{F}{S} \quad \text{Eq. 1}$$

where:

ft is the simple compressive strength, MPa

F is the breaking load of the specimen, N

S is the load application area, mm²

In the second test, the bricks were dried at a temperature of around 105 °C to a mass, in grams, constant (m_1), then immersed in a water tank for 24 hours. After this period, the brick surfaces were dried with a slightly damp cloth and then weighed (m_2) again. With the results obtained through the equation:

$$A = \frac{m_2 - m_1}{m_1} * 100 \quad \text{Eq. 2}$$

where:

A is the water absorption, %

m_1 is the mass of dry brick, g

m_2 is the mass of the saturated brick, g

Results and Conclusions

This work is of fundamental importance in the study of the feasibility of applying ETA sludge in civil construction, through the manufacture of ecological bricks. The lots showed high water absorption (Table 2) due to high porosity, but still meeting the specifications imposed by the standard. This can be due to the use of sand in the manufacture of bricks, since lumps are formed in the mixture, especially those containing sludge. With this also influencing the results of resistance to depression (since

the test is carried out after the blocks submerged in water) shown in Table 3.

Table 2. Water absorption for each mixture (average).

Mixture	Water absorption at 28 days (%)
0	18
1	20
2	20
3	20

The drop in resistance in the bricks together with the increase in the percentage of sludge can be explained due to the granules (Figure 2) of sludge, that is, when there is addition of a material with little resistance, in case of comparison to the other components of the mixture, leads to loss of strength in the final product.

Table 3. Values of compressive strength for each mixture (average).

Mixture	Breaking Load (N)	Compressive Strength (Mpa)
0	14031,69	0,975
1	7945,26	0,552
2	10085,84	0,701
3	6869,51	0,477

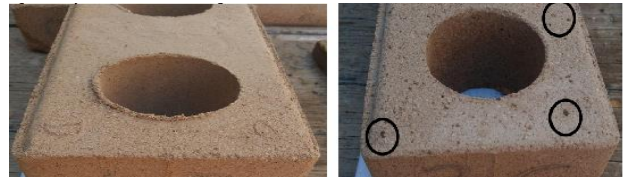


Figure 2. Visible slime granules.

In general, the bricks do not meet the specifications of NBR 8491: 2012, requiring further studies to improve them. Studies focused on improving the homogenization of the mixtures or testing different types of soils and compositions in the mortar, with the aim of bringing the mixture closer to the ideal one in this type of application.

Acknowledgements

We thank Sanepar for providing the sludge for this study. UTFPR-PR for the structure provided, especially Prof. Sandra Mara Kaminski Tramontin responsible for the Destructive and Non-Destructive Testing Laboratory (LabENS). This work had financial support of Project NORTE-01-0247-FEDER-072124. Bagaço+Valor - Tecnologia Limpa para a Valorização dos Subprodutos do Bagaço na Indústria Extratora de Azeite. funded by the European Regional Development Fund (ERDF).

References

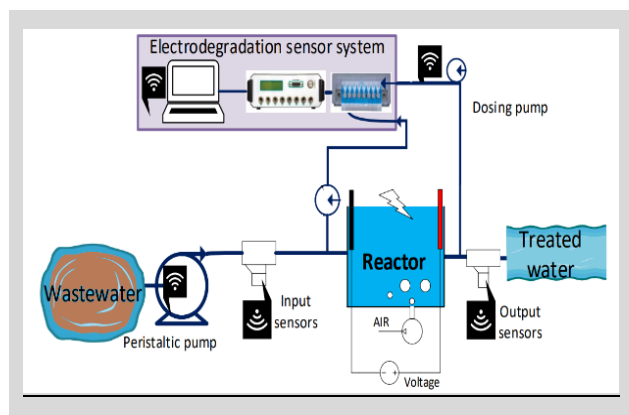
- [1] R. Tartari et al., *Cerâmica*, 57 (2011).
- [2] C. Hoppen et al., *Química Nova*, 29 (2006).
- [3] ABNT (Associação Brasileira de Normas Técnicas). NBR 10664: Determinação de resíduos (sólidos) – Método Gravimétrico. Rio de Janeiro, 1989.
- [4] FUNTAC. Cartilha para produção de tijolo solo cimento. Rio Branco, AC. 1999.
- [5] ABNT (Associação Brasileira de Normas Técnicas). NBR 10833: Fabricação de tijolo e bloco de solo-cimento com utilização de prensa manual ou hidráulica. Rio de Janeiro, 2012.
- [6] ABNT (Associação Brasileira de Normas Técnicas). NBR 8492: Tijolo de solocimento – Análise dimensional, determinação da resistência à compressão e da absorção de água – Método de ensaio. Rio de Janeiro, 2012.

Development and evaluation of an automatic monitoring and measurement system for electrodegradation processes

M.R. Pereira¹*, E. González-Romero², M. Pazos¹, E. Rosales¹, M.A. Sanromán¹

¹Department of Chemical Engineering, University of Vigo, Isaac Newton Building, Campus As Lagoas Marcosende 36310, Vigo, Spain; ²Department of Analytical and Food Chemistry, University of Vigo, Campus As Lagoas-Marcosende, 36310, Vigo, Spain.

*mario.rua@uvigo.es



A portable monitoring system and fast online data acquisition allows users to obtain and monitoring different analyte concentration data from wastewater in an automatic and configurable way. The system was developed by using a set of sensors that measure water properties such as pH, conductivity and temperature and the corresponding controller. The evolution of the electrodegradation processes can be monitored remotely on a data collection system based on an internet platform associated to the process, which provides a real-time analysis of the results and, depending on the needs, the system can be adapted to evaluate different drugs of interest. The automation of this monitoring system also optimizes the data collection time and eliminates the need of human intervention to perform the measurements and facilitate the on-time decision making.

Introduction

The current environmental and social context gives priority importance to water, as the vital resource that it is. United Nations sets ambitious objectives to ensure that this resource reaches the entire global population in the best conditions of quality and quantity according to the 2030 Agenda for Sustainable Development adopted in 2015 [1].

Water pollution caused by industrial activities is an increasingly accentuated phenomenon, which manifests itself especially in an increase in the concentration of micropollutants, both in surface and groundwater, with the consequent loss of quality of these water resources. Conventional wastewater treatment plants (WWTP) are not designed for the treatment of these complex compounds resulting in an important source of their entry into the environment [2]. In addition, most of the pharmaceuticals are poorly metabolized in the human body, with the parent compounds being excreted and often transported to WWTP. Therefore, the current landscape of water sources is worrying. As example for 2030, in Spain, is expected a reduction in water availability by 5-14% to 20-22% in arid and semi-arid areas [3]. However, water scarcity is a global problem which is not only limited to traditional dry areas. Thus, this situation generates a growing demand for water reuse, which is increasingly inaccessible to the population. For this reason, tailor-made systems for industrial WWTP are demanded that establish new standards on wastewater management. In all these new systems, it is necessary the implementation of monitoring systems that allow a fast online data acquisition.

The study presents the construction and evaluation of a real-time and representative monitoring system for a wastewater treatment plant with the control of critical parameters of the process as pollutant concentration, flow or aeration, as well as the temperature, conductivity, pH and level of the flow at the inlet and outlet of the reactor.

Materials and methods

The graphical abstract illustrates how the effluent is driven by the peristaltic pump towards the reactor's inlet sensors, then deposited inside the reactor for the duration of the process, and then dislodged toward the outlet after a period of residence. The

water circuit consists of probes and pipes connected in line so that liquid circulates through them while measurements are taken. It has been necessary to adapt the pipes to the sections of the probes as well as to the inlet and outlet of the reactor.

At the same time, the system is coupled with a dosing pump that is connected to both the reactor's inlet and outlet. The dosing pump sends the flow through a designed cell to the detection of pollutants in water by differential pulse voltammetry techniques. Additionally, this cell is attached to a potentiostat for performing on-line measurements of water pollutants. The potentiostat and the cell must be connected in the manner shown in graphical abstract for the potentiostat to be able to measure the flow. Finally, the potentiostat must be connected to a computer in order to set up the software of measurement.

The physical-chemical parameters from the water flow like pH, temperature, conductivity and level of liquid must be monitored before and after the reactor. To do this, industrial probes for pH and conductivity were used and placed in the system such as showed in Figure 1.

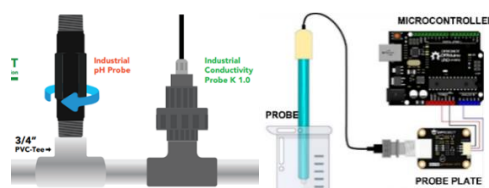


Figure 1. Example of placement of the probes in the reactor outlet pipe (left) and architecture of the connection circuit of the probe to the microcontroller (right).

The information obtained from these measurements will be transmitted to the microcontroller, in whose memory the necessary programming has been included to allow the interpretation of the signal from each probe. Some of the probes already include their own board that converts the signal from analog to digital before sending it to the microcontroller.

All these probes must satisfy the following needs: to be powered individually, to be able to send the obtained readings to the cloud and to have a way of communication between them, to ensure

we can compare the readings obtained before and after the reactor.

The selected microcontroller is the ESP32 because this microcontroller includes a WiFi module suitable for sending data and communicating. The voltage obtained from the sensors is transformed into the in the microcontroller using the appropriated code developed in the Arduino® IDE, a well-known programming software. Every sensor has its own ESP32 connected (Figure 2). The ESP32 works independently measuring the water properties but they also work together. Using one of the ESP32 dedicated only to receive all the data generated in the other ESP32, the system will work in a slave-master configuration where the master can compare the data from the other ESP32 slaves and to act in consequence if need. The online monitoring system consists of eight development KIT for ESP32 microcontrollers, one of them acts as said before like a master receiving signals from the other seven microcontrollers that are individually coupled with a set of devices. The entire system must be connected to a WiFi network for operation (Figure 2).



Figure 2. Structure of the control system with a example of programming recorded in the memory of the microcontroller.

The graphical interface represents the evolution over time of the physicochemical properties of water. In the case of the experiments carried out, the sensors presented results every 10 seconds, with stable values and the analyte concentration measurements every 15 min. The data obtained during the process carried in the electrodegradation reactor, under different electrochemical was recorded and reported (Figure 3).

Acknowledgements

This work was financially supported by LA/P/0045/2020 (ALiCE), UIDB/50020/2020 and UIDP/50020/2020 (LSRE-LCM), and UIDB/00511/2020 - UIDP/00511/2020 (LEPABE) funded by national funds through FCT/MCTES (PIDDAC), and the doctoral scholarship 2020.05252.BD from FCT.

References

- [1] A.S. Myerson et al., Handbook of industrial crystallisation, 3rd Ed., Cambridge University Press, 2019, 313-345.
- [2] J.W. Mullin, Crystallization, 4th Ed, Elsevier Science, 2001, 1-46.
- [3] C. Costa et al., Introdução à cristalização: princípios e aplicações, 1^a Ed, EdUFSCar, 2011, 1-17.
- [4] A.S. Foust et. al., Principles of Unit Operations, Wiley, 1980.
- [5] A.M.A. Ferreira et al., Modular Oscillatory Flow Plate Reactor, EP3439773 (B1).
- [6] A.M.A. Ferreira et. al., Apparatus for mixing improvement based on oscillatory flow reactors provided with smooth periodic constrictions, EP3057694 (B1).
- [7] P. Cruz et al., CrystEngComm, 20 (2018) 829-836.
- [8] J.C.B. Lopes et al., Network mixer and related mixing process, PCT/IB2005/000647, US 8434933, EP 1720643, PT 103072.
- [9] J.C.B. Lopes et al., Network heat exchanger device, method and uses thereof, PCT/IB2018/052463, US 11 484 862.
- [10] A.C.G. Moreira et al., Industrial & Engineering Chemistry Research, 59 (2020) 18510-18519.
- [11] P.J. Gomes et al., Journal of Nanoscience and Nanotechnology, 9 (2009) 3387-3395.

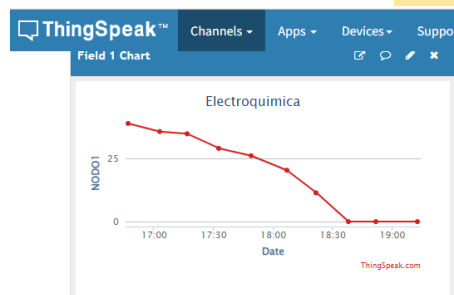


Figure 3. Obtained data from node #1 on potentiostat.

The graphic shows a continued decrease of the pollutant concentration measurements taken every 15 min. Under the effect of the electric field, a degradation of 80% of the contaminant was detected compared to the initial detection peak (40 to 8 ppm) after 90 min of the experiment. The measurements were taken automatically by a configuration of the Microsoft® automation software (Power Automate©) with the mentioned interval of 15 min.

After a comparative study, the mentioned application for the cloud ThingSpeak™, is chosen. This IOT application can gather information from the CSV exported by the potentiostat's software and store it in different channels. Every channel has an associated graphical interface that prints all the received data over the time. This IOT platform also allows printing the incoming data from the monitoring sensors after programming all the ESP32 connected to each one.

Conclusions

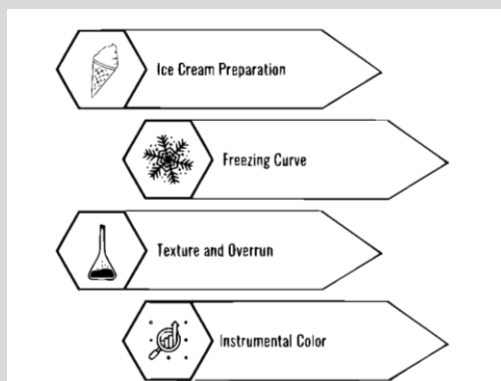
This on-line monitoring system, built as a portable system with low energy consumption, has allowed a satisfactorily measurement and monitoring of flow, temperature and pH in real time. Operating the system allowed attaining results with high reproducibility, stability and robustness in the acquisition of data. Thus, the system can be articulated to evaluate parameters in different processes related to water quality or the monitoring of degradative processes. It can be also concluded that the system is able to monitor process conditions and act if required to correct deviations. The communication protocol between microcontrollers is stable and without loss of information, confirming the reliability of the system. This system could reduce the economic and energy costs of the process since the influence of each parameter under study is known in real time.

Application of *Spirulina platensis* biomass and protein as an alternative emulsifier in the production of ice creams

P. de Paula^{1,2,3*}, S. Silva^{1,2}, P. Rodrigues⁴, D. Drunkler³, M. Barreiro^{1,2}, E. Ramalhosa^{1,2}

¹Centro de Investigação de Montanha (CIMO), Instituto Politécnico de Bragança, Campus de Santa Apolónia, 5300–253, Bragança, Portugal; ²Laboratório Associado para a Sustentabilidade e Tecnologia em Regiões de Montanha (SusTEC), Instituto Politécnico de Bragança, Campus de Santa Apolónia, 5300–253, Bragança, Portugal; ³Universidade Tecnológica do Paraná, Av. Brasil, Medianeira, Brasil; ⁴Research Centre in Digitalization and Intelligent Robotics (CeDRI), Instituto Politécnico de Bragança, Campus de Santa Apolónia, Bragança, 5300-253, Portugal.

*a54153@alunos.ipb.pt



This study aimed to develop ice creams using *Spirulina platensis*-based emulsifiers and assess their physical and sensory properties. Two emulsifiers were used: powdered *Spirulina platensis* biomass and protein extract, alongside a commercial emulsifier as a control. Ice creams with different formulations were prepared, namely by varying the percentage of the new emulsifiers. The freezing curves of the produced ice creams were similar. *Spirulina* addition affected the color but not the meltability and overrun. Ice creams with *Spirulina* biomass were softer and less resistant to cutting, while those with protein concentrate showed a variable texture behavior. Sensory analysis involving 50 participants revealed that the control ice cream ranked highest in the overall appearance, flavor, and general appreciation. However, the three ice creams were similarly rated in terms of texture. The control ice cream was preferred by 43.8% of the tasters, followed by the ice cream using *Spirulina* concentrate (31.3%). In conclusion, the study provides important insights for developing healthier and more sustainable ice creams in line with consumer preferences.

Introduction

Microalgae have been extensively researched due to their high protein content (50-70%), essential amino acids, vitamins (especially B12), minerals, as well as pigments (carotenoids, phycocyanins, and chlorophylls), polyunsaturated fatty acids, including omega-3 fatty acids, and other biologically active compounds [1]. Among the various microalgae, *Spirulina platensis* stands out for its high protein content. Although it has been used as a food component for centuries, its cultivation for food purposes has only been developed in the past few decades [2]. Several studies have been conducted with the aim of using both the biomass and the extracted proteins from this algae, albeit this last point to a lesser extent.

With the population's growing concern for healthier foods, research on natural alternatives to replace synthetic additives used in the food industry has increased. Consumers seek innovative and high-quality products with characteristics similar to or better than traditional ones. Developing products that meet this demand is important to the industry [3].

Concerning ice creams, they need to have balanced ingredients, and among them, emulsifiers play an important role as they are added to smooth out the texture and ensure the complete distribution of air cells [4].

In this context, this work aims to evaluate the effects of using *Spirulina platensis* biomass and protein concentrate as emulsifiers on the physicochemical and sensory characteristics of ice creams.

Experimental procedure

Different ice cream formulations were prepared, as indicated in Table 1. All the tests were performed in triplicate.

Table 1. Ice cream formulations

Ice cream	Milk (mL)	Sugar (g)	Stabilizer ¹ (g)	Emulsifier ² (g)	Biomass (g)	<i>Spirulina</i> (g)
0%	300.00	75.00	3.00	3.00	0.00	0.00
25%	300.00	75.00	3.00	2.24	0.74	0.56
50%	300.00	75.00	3.00	1.50	1.50	1.13
75%	300.00	75.00	3.00	0.74	2.24	1.69
100%	300.00	75.00	3.00	0.00	3.00	2.26

¹Stabilizer: "Super Liga Neutra" from Selecta, stabilizer for edible ice creams manufactured by "Duas Rodas Industrial Ltda" in Brazil.

²Emulsifier: "Emustab" from Selecta, a neutral emulsifier and stabilizer for ice creams, manufactured by "Duas Rodas Industrial Ltda" in Brazil

The ice creams were prepared by mixing all ingredients, except the emulsifier, in a blender for 3 minutes. Then, they were frozen in a horizontal freezer for 3 hours. Subsequently, the emulsifier was added, and the mixture was blended again for an additional 5 minutes-period before being transferred to plastic containers that were transferred to the horizontal freezer.

Ice Cream Freezing Curves

Temperature sensors were introduced in the plastic containers and were used to acquire the temperature decrease of the ice creams, with a sampling time of one minute. The data was recorded in a Google spreadsheet to produce the temperature curve profiles for each formulation.

Evaluation of meltability, overrun, and texture

To evaluate the meltability of the ice creams, the tests were conducted in an oven with a controlled temperature of 25 °C. The volume of melted ice cream collected in the graduated cylinder was recorded every 10 minutes.

Overrun (air incorporation) was calculated according to Equation 1.

$$\text{Overrun (\%)} = (V_{\text{final}} - V_{\text{initial}}) / V_{\text{initial}} \times 100 \quad (\text{Eq 1})$$

where: V_{final} is the volume of the aerated product, and V_{initial} is the initial volume of the non-aerated mixture.

The texture analysis was conducted using the TA.XT Plus Texture Analyzer. Two tests were performed. The first one measured the compressive strength by using the Knife Edge (HDP/BS) cutting cell, and the second assessed ice cream spreadability. Data acquisition and integration were carried out using the Texture Exponent TPA32 software.

Instrumental Color Measurement

The color was determined using a Konica Minolta colorimeter (Chroma Meter CR 400), employing the CIE*Lab* color scale system. Calibration was performed using a standard white plate following the manufacturer's instructions. The results were expressed in L^* (lightness), a^* (*red-green hue), b^* (*yellow-blue hue), C^* (chroma or color intensity), and h (hue angle or color purity).

Sensory Analysis

The sensory analysis was conducted at the Polytechnic Institute of Bragança, involving 50 untrained evaluators aged between 16 and 60 years. The samples provided included a control ice cream, ice cream with 100% *Spirulina platensis* biomass, and ice cream with 100% *Spirulina platensis* protein concentrate as emulsifiers. All ice creams were evaluated for acceptability regarding overall appearance, color, texture, flavor, and general appreciation using an unstructured hedonic scale. After tasting the three ice creams, the evaluators were asked to indicate their preference (Preference Test).

Results and Discussion

The results obtained from the freezing curves demonstrated that the presence of *Spirulina* biomass and protein concentrate did not significantly affect the freezing rate of the ice creams.

Regarding meltability, ice creams with *Spirulina* biomass and protein concentrate showed a progressive melting behavior similar to the control ice cream, indicating that adding these ingredients did not impact the resistance to melting. Similar results were observed for the overrun (Table 2), indicating that the presence of *Spirulina* biomass and protein concentrate did not significantly affect the air incorporation in the ice creams.

However, adding *Spirulina* biomass and protein concentrate impacted the color of the ice creams (Table 2). Ice creams with biomass displayed a greener shade, while those with protein concentrate showed a bluer shade. Nevertheless, these color changes did not negatively affect the sensory acceptance of the ice creams. Regarding texture, ice creams with *Spirulina* biomass were smoother and less resistant to cutting compared to the control ice cream.

The sensory analysis revealed that ice creams with *Spirulina* biomass and protein concentrate were visually appealing to the evaluators. However, the flavor was lower rated compared to the control ice cream. Some of the evaluators mentioned a pronounced *Spirulina* taste in the ice creams with these ingredients. Nevertheless, the overall appreciation of the ice creams was positive, indicating a generally favorable perception.

Conclusions

In conclusion, adding *Spirulina* biomass and protein concentrate affected some physical properties and sensory characteristics of the ice creams, such as color and flavor. However, these changes did not compromise the overall quality and sensory acceptance of the ice creams. Therefore, replacing the emulsifier with *Spirulina* biomass and protein concentrate may be a viable strategy for producing ice creams with distinct nutritional and visual features, meeting consumers' preferences for more natural and healthy products.

Table 2. Color, overrun and texture results of the ice creams.

	L^*	a^*	b^*	C^*	h	Overrun	Shear (g)	Firmness (g)	Work of Shear (g.s)	Stickiness (g)	Work of Adh. (g.s)
Control	75.22	-2.91	2.26	3.75	143.33	105.56	2100.23	55166.73	79656.17	-3844.30	-354.31
25% Biomass	56.83	-9.77	-0.91	9.83	185.55	100.00	1589.94	17479.00	24491.00	-2844.00	-268.00
50% Biomass	51.62	-8.18	-0.89	8.27	187.79	94.07	1686.32	40640.92	62757.12	-1818.67	-242.16
75% Biomass	45.96	-4.70	-2.36	5.27	207.14	87.27	1094.94	42467.15	66602.91	-3440.74	-492.51
100% Biomass	41.92	-6.91	-3.09	7.63	204.42	77.78	783.3	34087.46	50854.00	-2842.75	-299.83
25% Conc.	48.21	3.35	-23.58	23.88	278.04	125.93	1010.67	60835.68	94772.57	-859.00	50.00
50% Conc.	38.11	9.36	-25.44	27.11	290.16	90.91	586.33	46900.56	65202.16	-1776.82	-35.00
75% Conc.	37.73	10.42	-24.00	26.19	293.72	76.67	1462.18	55892.75	74156.27	-333.39	-15.00
100% Conc.	35.80	13.39	-31.94	34.71	292.84	90.00	862.24	47722.68	74856.00	-4353.57	-370.43

Acknowledgements

This work was developed within the scope of CIMO-Mountain Research Center (UIDB/00690/2020 and UIDP/00690/2020) and SusTEC (Associate Laboratory for Sustainability and Technology in Mountain Regions) (LA/P/0007/2020), funded by national resources through Fundação para a Ciência e Tecnologia (FCT/MCTES) (PIDDAC). We also extend special thanks to Algiky - Algae-based Solutions S.A for donating the *Spirulina* biomass and protein extract.

References

- [1] M.A. Borowitzka, Chapter 3 - Biology of Microalgae. In *Microalgae in Health and Disease Prevention*, (2018) 23-72.
- [2] A.L. Lupatini et al., *Journal of the Science of Food and Agriculture*, 97 (2016) 724-732.
- [3] E. Vendruscolo et al., *British Food Journal*, 122 (2019) 693-707.
- [4] Q.A. Syed et al., *Journal of Nutritional Health & Food Engineering*, 8 (2018) 422-435.

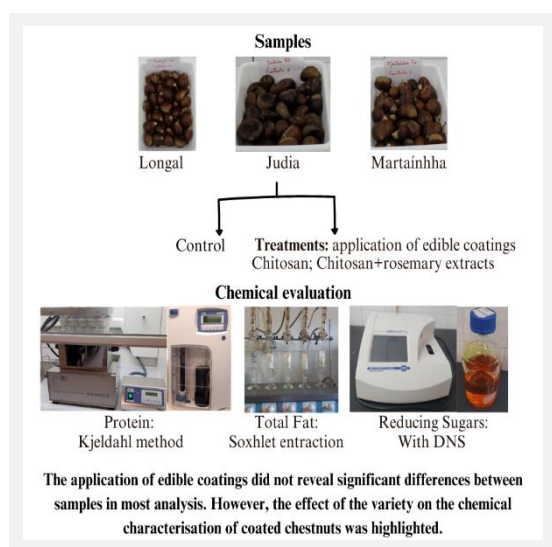
Effect of edible coatings on the chemical properties of chestnuts

J. Correia^{1*}, Y. Zbiss^{2,3}, F. Lema^{2,3}, L. Fernandes⁴, I. Braga⁴, A. Gonçalves⁴, M. do C. Fidalgo⁵, J. Moreira⁶, E. Ramalhosa^{2,3}

¹Escola Superior da Saúde, Instituto Politécnico de Bragança, Campus de Santa Apolónia, 5300-253 Bragança, Portugal ;

²Centro de Investigação de Montanha (CIMO), Instituto Politécnico de Bragança, Campus de Santa Apolónia, 5300-253 Bragança, Portugal; ³Laboratório Associado para a Sustentabilidade e Tecnologia em Regiões de Montanha (SusTEC), Instituto Politécnico de Bragança, Campus de Santa Apolónia, 5300-253 Bragança, Portugal; ⁴MOREColab, Edifício do Brigantia Ecopark, Avenida Cidade de Leon, 506, 5300-358 Bragança, Portugal; ⁵Escola Superior Agrária, Instituto Politécnico de Bragança, Campus de Santa Apolónia, 5300-253 Bragança, Portugal; ⁶Sortegel - Produtos Congelados, S.A., Rua S. Mamede Nr. 25, 5300-903 Sortes, Bragança, Portugal.

*julianaalexandra01@live.com.pt



The perishability of chestnuts corresponds to the loss of weight and quality due to the molds' growth, resulting in significant economic losses. The use of edible coatings may be a potential strategy for the future to reduce these losses. Thus, the primary goal of this study was to assess the effect of adding edible coatings based on chitosan and rosemary extracts on specific chemical parameters (protein, total fat and reducing sugars) of chestnut during its three-week storage at ambient temperature. The results showed that the control and the coatings with chitosan and with rosemary extract did not exhibit any significant differences.

Introduction

Chestnut is a perishable fruit that easily loses weight and it may lose quality due to mold growth, which causes important economic losses. The application of edible coatings may be a promising technique to be applied in the future in order to minimize these losses [1]. The chitosan coating has been shown to improve the quality of chestnuts at the microbiological level, suggesting that it is a possible alternative to improve preservation and may be an effective method to solve the problem of microbial growth [2]. Thus, the main objective of the present work was to evaluate the effect of applying edible coatings based on chitosan and rosemary extracts on some chemical properties of chestnut, throughout its storage at room temperature for 3 weeks.

Experimental part

Three varieties of chestnuts were evaluated namely, Longal, Judia and Martainha. All fruits were subjected to the following treatments: chitosan and chitosan+rosemary extracts. In parallel, fruits without edible coatings were analysed as control. The chemical properties determined were protein, total fat and reducing sugars. Protein was determined by Kjeldahl method,

the total fat through Soxhlet extraction with petroleum ether and reducing sugars by the dinitrosalicylic acid (DNS) method.

Results and Discussion

Regarding protein, some significant differences were determined between the beginning and after 3 weeks of storage. Judia was the variety that showed the highest protein content (6.33 to 8.31%, d.w.). For the fat content, similar results were obtained between time 0 and after 3 weeks, varying between 2.02 and 3.52 % d.w. However, between varieties some differences were highlighted, showing Judia the lowest values (2.02 to 2.69 % d.w.). Regarding reducing sugars, Martainha and Longal showed a similar profile, with a slight increase at 21 days of storage. On the contrary, for Judia, a slight decrease was observed.

Conclusions

In conclusion, chitosan is one of the most widely studied edible coating. However, in relation to its effect on protein, fat and reducing sugars contents, no differences were observed in a very evident manner in relation to the control and to the coating with rosemary extract.

Acknowledgements

The authors are grateful to the Foundation for Science and Technology (FCT, Portugal), which gave financial support through national funds FCT/MCTES (PIDDAC) to CIMO (UIDB/00690/2020 and UIDP/00690/2020) and SusTEC (LA/P/0007/2021). The authors also thank the financial support given by the European Regional Development Fund (ERDF) for financial support to the project RevestCast (POCI-01-0247- FEDER-049276).

References

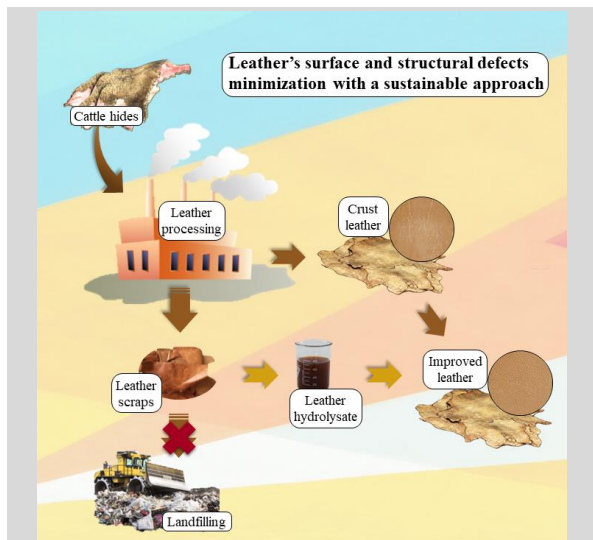
- [1] R.K. Dhall, Food Science and Nutrition, 53 (2013) 435-450.
- [2] L. Fernandes et al., Scientia Horticulturae, 263 (2020) 109105.

Leather's surface and structural defects minimization with a sustainable approach

M.J. Penayo^{1,2,3}, J.D. Rivaldi⁴, S.E. Arantzazu^{1,2}, M.F. Barreiro^{1,2*}

¹Centro de Investigação de Montanha (CIMO), Instituto Politécnico de Bragança, Campus de Santa Apolónia, 5300-253 Bragança, Portugal; ²Laboratório Associado para a Sustentabilidade e Tecnologia em Regiões de Montanha (SusTEC), Instituto Politécnico de Bragança, Campus de Santa Apolónia, 5300-253 Bragança, Portugal; ³Universidad Nacional de Asunción, Av. Mcal López 3492, 2169 San Lorenzo, Paraguay; ⁴Departamento de Aplicaciones Industriales y Bioprocesos de la Facultad de Ciencias Químicas, Universidad Nacional de Asunción, Paraguay.

*barreiro@ipb.pt



Pursuing a greener future, the European Union and the United Nations encourage industries to adopt new practices based on sustainability principles and circular economy strategies. The waste produced by the leather industry takes part in this initiative by proposing a sustainable approach to minimizing leather's defects. This work aims to minimize defects of discarded leather by employing hydrolysate from discarded leather (LH) with transglutaminase (TG) in low-quality leather and simultaneously improve its mechanical properties. Adding LH and TG resulted in lighter and smoother leather without a significant dimensional variance. The statistical analysis (ANOVA) revealed that TG's concentration significantly influences the elongation percentage of leather. In contrast, LH demonstrated a weak, yet significant, influence on the tensile strength. This work showed the applicability of LH and TG in leather defects' minimization and mechanical properties enhancement.

Introduction

In 2015, the Portuguese government, alongside countries of the European Union and the United Nations, decided to take a step towards a sustainable future by adopting a strategy based on sustainability principles, centering on promoting the model of reducing, reusing, and recycling residues, contributing to the preservation of the environment and at the same time decreasing their impact on climate change [1].

The leather industry was one of the industries affected by this new course of action. According to the literature, 20% of a metric ton of wet salted hides is converted to leather [2]. From all produced leather, a significant fraction is rejected due to defects on their surface and low structural integrity caused by mechanical stress during processing, resulting in insufficient aesthetic appealing attributes and inferior mechanical properties to meet quality standards and being labeled as low-quality [3]. Defects in leather can be translated into an absence of collagen fibers in the leather fabric. This alters the loading capacity of the collagen fibers surrounding the area where the defect is located, leading to an uneven stress distribution throughout the material and, subsequently, a poorer mechanical performance [4].

A sustainable approach to leather waste treatment involves reintroducing its proteins as reinforcement elements in the leather. This can be done with the help of exogenous cross-linkers such as transglutaminase (TG), which has been reported as an effective binder in leather and other collagen-based materials, enhancing physical properties and thermal resistance [5], [6].

Objectives

In view of quality improvement, appearance, and mechanical properties of discarded leather by the minimization of its defects and simultaneously reducing the quantity of leather destined to waste, the current work aimed to obtain a leather with reduced defects employing by-products obtained from solid leather residues (leather hydrolysate) and TG to induce an enzymatic cross-linking between leather fibers and the hydrolysate.

Methods

The wet-white leather hydrolysate was used at 25% and 50% concentrations. The cross-linker, TG, was used at 10% and 15% contents. The leather was first soaked at 30°C for 60 minutes under continuous stirring (150 rpm). Then the hydrolysate and TG were added, and the temperature rose to 50°C to induce TG cross-linking reaction. After the treatments, the samples underwent characterization by Optical (OM) and Scanning Electron microscopy (SEM), followed by organoleptic analyses and physical evaluations.

The most promising samples were subjected to a flexural strength test (Bally method) under dry conditions (ISO5402-1-2017). A rotational central composite design 2² with 3 central points was employed to evaluate the influence of the additives over the mechanical properties of the leather, conditioning the samples in accordance with the standard ISO 2419:2012 for mechanical testing based on ISO 3376:2020.

Results

Leathers treated with 50% hydrolysate and 10% and 15% TG resulted in slightly stiffer samples, indicating excessive crosslinking. For the leather treated with 25% hydrolysate, both concentrations of TG delivered similar characteristics, giving no significant difference on their surface (Figure 1 a and b). The organoleptic analyses revealed that leathers treated with 10% TG and 25% and 50% hydrolysate were smoother, and mildly thicker, and a noticeable minimization of its defects was achieved. These effects can be attributed to the addition of leather hydrolysate since similar results have been reported in the literature [7]. A greater weight reduction was recorded in leather treated with 25% hydrolysate compared to the one treated with 50% hydrolysate.

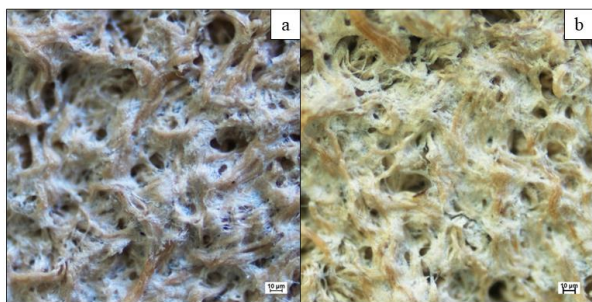


Figure 1. Microscopic analysis of leather samples (with 40x magnification) treated with 25.0% leather hydrolysate and 10.0% and 15.0% of transglutaminase, respectively in a and b. Source: Own elaboration.

The Bally test demonstrated that the integrity of the treatment was maintained, pointing out a slight presence of defects (grade 1) on the leather before running the test, and getting grade 2 after applying 100.000 flexing cycles.

The average values of the mechanical properties of untreated leather correspond to a maximum tensile strength of 18.63 ± 1.79 MPa, and elongation percentage at maximum tension of $37.53 \pm 3.63\%$. In the selected study region (Table 1), the elongation percentage is the response that proves to be improved the most, with the highest achieved value (60.60%) with 30.00% of leather hydrolysate and 17.07% of TG, while the maximum tensile strength achieved was of 17.09 MPa after adding 51.21% of leather hydrolysate and 10.00% of TG.

The statistical analysis ANOVA in Table 2 shows the significant influence of the leather hydrolysate over the tensile strength of leather, while only the influence of transglutaminase resulted significant for the elongation percentage.

After analyzing the values in Table 1 and Table 2, it can be stated that the lower the quantity of leather hydrolysate and TG incorporated in the leather, the lower the tensile strength and elongation percentage values, respectively. The addition of these additives has been reported in the literature as mechanical

properties' enhancers in collagen-based materials, supporting the results obtained in this work [5], [7].

Predictive models were only successfully obtained for the elongation percentage with a correlation coefficient of 67.60%, while for the tensile strength, the same coefficient was only of 37.32%, indicating a lack of correlation among the experimental values and the values estimated with the model.

Table 1. Mechanical properties of treated leather according to the experimental matrix.

Run	Variables		Mechanical properties	
	Leather hydrolysate (%)	Transglutaminase (%)	Tensile strength (MPa)	Elongation Percentage (%)
1	-1 (15)	-1 (5)	8.89	36.80
2	1 (45)	-1 (5)	13.55	46.29
3	-1 (15)	1 (15)	12.76	43.10
4	1 (45)	1 (15)	12.71	50.87
5	- α (8.78)	0 (10)	12.60	46.80
6	+ α (51.21)	0 (10)	17.09	50.78
7	0 (30)	- α (2.92)	13.05	26.69
8	0 (30)	+ α (17.07)	11.74	60.60
9	0 (30)	0 (10)	11.30	47.44
10	0 (30)	0 (10)	13.58	42.71
11	0 (30)	0 (10)	11.25	50.07

Conclusions

The reduction of superficial defects was achieved under the studied conditions, highlighting the treatment of faulty leather at 50.0 °C for 1 hour and constant stirring with 25.0% (OHV) of leather hydrolysate and 10.0% (OLW) of TG, giving a lighter, smoother, and elastic leather without a significant dimensional variance.

The statistical analysis of the results revealed a significant effect of the concentration of TG over the elongation percentage of leather. In contrast, the leather hydrolysate demonstrated a weak yet significant influence over the tensile strength.

The minimization of leather defects was accomplished, yet the optimization of the treatment conditions and the effect of additive concentration is still under development

Table 2. ANOVA of additives influence over the tensile strength and elongation percentage considering a linear model.

Factors	Tensile strength			Elongation percentage		
	Sums of Squares	Mean Square	<i>p</i> -value	Sums of Squares	Mean Square	<i>p</i> -value
Model	15.02	15.02	0.0459	432.58	216.29	0.0110
A-Leather hydrolysate	15.02	15.02	0.0459	65.54	65.54	0.1504
B-Transglutaminase	---	---	---	367.04	14.16	0.0055
Lack of fit	21.71	3.10	0.4099	180.30	2.22	0.3423
Pure error	3.53	1.77	---	27.03	13.51	---
Standard deviation	1.67	---	---	5.09	---	---
Variation coefficient (%)	13.29	---	---	11.09	---	---

Acknowledgements

This work was made possible thanks to the Foundation for Science and Technology (FCT, Portugal) for financial support through national funds FCT/MCTES (PIDDAC) to CIMO (UIDB/00690/2020 and UIDP/00690/2020), and SusTEC (LA/P/0007/2021). This work was developed within the scope of the project GreenShoes 4.0 (POCI-01-0247-FEDER-046082). National funding by FCT, P.I., through the institutional scientific employment program contract of A. Santamaria-Echart.

References

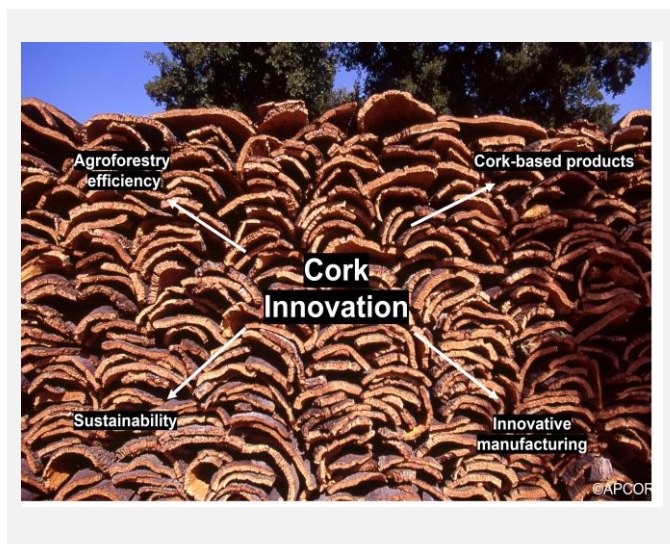
- [1] European Commission, "European Commission 2020 - New circular economy action plan", 2020.
- [2] D. Masilamani et al., *Journal of Cleaner Production*, 113 (2016) 338-344.
- [3] S. Prabakar et al., "The Effect of Cloisite ® Na⁺ Nanoclay Filler on the Morphology and Mechanical Properties of Loose Leather", 2016.
- [4] K.M. Nalyanya et al., *Journal of AQEIC*, 69 (2018) 59-68.
- [5] S. Cheng et al., *Food Chemistry*, 271 (2019) 527-535.
- [6] C. Baozhen, C. Jing, *Journal of the American Leather Chemists Association*, 110 (2015).
- [7] Y. Dilek et al., *Society of Leather Technologists and Chemists*, 103 (2019) 129-134.

Innovation in cork: state of the art and future research possibilities

R.N. da Silva

Cork Technological Centre, Rua Amelia Camossa, Santa Maria de Lamas, Portugal.

rsilva@ctcor.com



Cork is a naturally renewable material with unique properties that make it versatile and with economic value.

Over the past decades, the cork industry and cork researchers have undergone a constant process of innovation, exploring new applications, more efficient processes, and developing added sustainable products.

We examine recent developments in cork-based products, manufacturing processes and applications across different fields. Additionally, we identify key challenges and propose potential research directions that can drive innovation and unlock new opportunities for cork-based industries.

This communication aims to present the state of the art of cork innovation, highlighting the main areas of research and future possibilities of investigation in this field, with focus on the most recent research on chemical innovations.

Introduction

Cork products have been in use for centuries due to their versatility, sustainability, and unique properties. Cork is obtained from the bark of the cork oak tree, primarily found in Mediterranean regions such as Portugal, Spain, and Italy. These trees can live for several hundred years, and their bark can be harvested without causing any harm, making cork a highly renewable and eco-friendly material.

Cork has a cellular structure composed of tiny air-filled pockets, which give it its characteristic lightweight and buoyant properties. It is also highly compressible, flexible, and resistant to moisture, rot, and fire. These features make cork an excellent choice for a wide range of applications.

Beyond wine stoppers, cork finds applications in various industries. In construction, cork is used as insulation material, as it provides excellent thermal and acoustic properties. Cork flooring is another popular choice due to its durability, comfort, and natural aesthetics. Cork is also utilized in gaskets, seals, and vibration dampening products in automotive and manufacturing sectors.

Cork has gained recognition as an eco-friendly alternative to leather and synthetic materials in fashion and accessories. Cork fabric is lightweight, water-resistant, and soft to the touch, making it suitable for bags, wallets, and footwear. Its natural grain patterns give each product a unique appearance. The market for cork products continues to expand as more industries and consumers recognize the benefits of this versatile material. Innovation and research are driving the development of new applications and product designs. As sustainability becomes a key consideration across various sectors, cork's renewable nature and unique properties position it as a desirable material for the future.

Additionally, cork has found its way into the world of design and decoration. It can be used to make wall and ceiling coverings, bulletin boards, and furniture. Its natural texture and warm tones add a touch of elegance to interior spaces.

The cork industry has seen steady growth over the years, driven by increased environmental awareness and the demand for sustainable materials. Portugal is the largest producer of cork, accounting for a significant share of the global market. However, other countries, such as Spain, Italy, and Morocco, also contribute to cork production.

Cork research goes from different forms of innovation covering a wide variety of scientific fields, with a strong emphasis on chemistry and chemistry related fields. Over the literature it is possible to find innovation examples that goes from product innovation, design and aesthetics, manufacturing, efficiency and optimization, advanced-materials, digitalization, business model, marketing and even value chain integration innovation.

But it is in chemistry area that the most differentiative research has been taken. It goes from better technical performing products - by exploring creation of innovative cork-based products, such as lightweight composites, bio-based materials, and smart cork applications -; to innovative manufacturing techniques including high-performing disinfection procedures and advanced molding processes; and even agroforestry efficiency to efficient waste reduced operations in a sustainable perspective.

Composites and byproducts

Cork composites are typically created by combining cork particles, layers, powder or granulates with a binder or matrix material, such as rubber, thermoplastics, or thermosetting resins. The cork particles act as reinforcement, providing lightweight, compressibility, and insulations properties, while the matrix material adds strength and stability to the composite. Many examples can be found of new cork composites. Studies have shown that cork composites exhibit improved thermal insulation compared to other conventional materials. These composites can contribute to energy efficiency by reducing heat transfer and noise transmission in

buildings in mobility sector by reducing vibration and noise transmission in vehicle structures [1].

Besides cork itself, the bark of the cork oak tree yields various extracts that have valuable biological properties and needs more research [2]

An emerge line of research is de developments around micro- and nanotechnology and functionalization of cork. Several example can be found in the literature from the improvement of antimicrobial properties, mechanical, thermal, and hydrophobic properties [3].

High-performing manufacturing

Hugh-performing manufacturing in the cork industry involves the utilization of advanced techniques and technologies to enhance the quality, efficiency, and precision of cork production processes.

These manufacturing advancements ensure that cork products meet rigorous standards and fulfill the requirements. Several examples can be found on the literature around the development or best-performing production of cork products from Sustainable extraction and processing techniques, streamlining cork extraction, and processing and implementing smart manufacturing techniques, to Automation and digitalization in cork production implementing robotics and AI in cork production, even to quality control and optimization methods [4].

Agroforestry research

Due to preliminary yet highly promising recent results on the effects of irrigation [5] on reducing the initial cycle of cork production, further development in this area soon is expected. Combining with smart and possibly AI assisted management of irrigation water aiming at maximizing productivity but specially to create a system with a strong resilience to extreme drought.

Acknowledgements

This work was funded by SIAC2021: Scientific and technological interface. Cork industry (POCI-01-0246-FEDER-181298), CTCOR—Innovation and Technological Centre—CTI basal funding (AAC n° 03/C05-i02/2022), and Agenda PRODUTECH R3. R. Nunes da Silva thanks her Researcher contract by PORNorte (NORTE-06-3559-FSE-0000112).

References.

- [1] A. Cherki et al., *Construction and Building Materials*, 54 (2013) 202.
- [2] J. Azevedo et al., *Food Chemistry*, 367 (2022) 130607.
- [3] F.R. Oliveira et al., *Advances in Materials Science and Engineering*, (2014) 685829.
- [4] M.K. Taylor et al., *Journal of Agricultural and Food Chemistry*, 48 (2000) 2208.
- [5] C. Camilo-Alves et al., *Forests*, 11 (2020) 88.
- [6] M.T. Martínez et al., *Horticulturae*, 9 (2023) 692.
- [7] J.A. Paulo et al., *Modelling Earth Systems and Environment*, 9 (2023) 3329-3342.
- [8] M.A. Carneiro et al., *Journal of Water Process Engineering*, 50 (2022) 103291.
- [9] J.R. Silva et al., *Journal of Environmental Chemical Engineering*, 10 (2022) 107750.

Further developments are also expected in terms of disease control – testing and improving resistance to fungi such as *Phytophthora cinnamomi* [6].

Also of importance is increasingly more accurate modelling and prediction of cork quality as well as the most efficient time for debarking, whilst avoiding sampling or other destructive methods [7].

Environmental improvements and applications

The pathway for net zero requires the development and application of novel solutions to meet environmental requirements. In the cork sector, conversion of existing gas-powered boilers as well as other heating equipment to non-fossil fuel is a relevant field of study – through combination of increases in heat use efficiency and novel fuels such as hydrogen, new research to investigate optimal application are required.

Additionally, to further move towards to an even more circular economy, research on new products based on waste material, particularly cork powder, are extremely important. In particular, the use of cork granulates to produce biochars for water treatment has demonstrated potential but requires further study [8].

Yet another research field is water and wastewater and reuse – novel methods for cork boiling wastewater treatment [9] as well as its reuse within the production facility are necessary improvements due to increasing limitations of this resource.

Conclusions

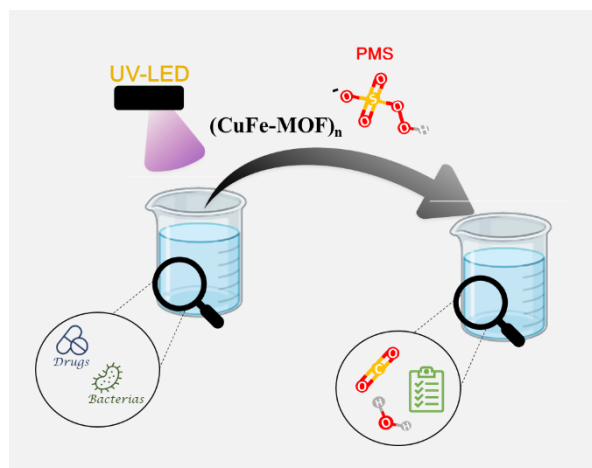
In line with the current state of the art research and proposing future research directions, this communication aims to highlight and to inspire new research and guide future research efforts and contribute to the continued growth and development of the cork industry.

Application of different CuFe-MOFs for reduction of the environmental and sanitary impact of hospital effluents

B. Lomba-Fernández*, A. Fdez-Sanromán, M. Pazos, E. Rosales, M.A. Sanromán

CINTECX, Universidade de Vigo, Department of Chemical Engineering, Campus Universitario As Lagoas—Marcosende, 36310 Vigo, Spain.

*barbara.lomba.fernandez@uvigo.gal



In this work, three CuFe-MOFs were obtained by solvothermal method. Two temperatures (90, 150°C) were tested and different metallic salts were used in the synthesis of the different CuFe-MOFs. Their characterization showed different morphologies and properties of the materials with different Cu/Fe ratio. These MOFs were named as CuFe-MOF_n, being n=1 for the highest ratio and 3 for lowest value. Their catalytic properties for peroxymonosulfate (PMS) activation were tested with different emerging pollutants, like Sulfamethoxazole (SMX), Antipyrine (ANT), and *Escherichia coli* (*E. coli*). The synthesized CuFe-MOFs showed remarkable catalytic activity to induce the oxidation process with sulfate radical generated from PMS to efficiently remove SMX and ANT. Moreover, a synergistic role of photocatalytic activation of PMS by UV-LED irradiation was detected. A high antibacterial activity was also attained with the system CuFe-MOF₁/PMS due to the high copper content concerning the others.

Introduction and objectives

Nowadays, water is widely recognized as a natural resource that is limited and extremely valuable. Due to overpopulation and industrial activity, many organic pollutants, known as emerging pollutants, and pathogens have appeared in recent years. Thus, drugs consumption has increased worldwide in recent decades, both among animals and humans. According to the World Health Organization, only in 2021, US\$ 1170 billion was spent on global pharmaceuticals, demonstrating the widespread use of pharmaceuticals by veterinarians and doctors [1].

Effluents from pharmaceutical manufacturing, hospitals, and houses are the primary source of entry to the environment (containing both the parent compound and metabolites excreted by animals and humans), with a minor contribution from the inappropriate disposal of expired medicines. In addition, different types of pathogens may enter wastewater systems from a variety of sources, including human waste, decontamination wastewater, animal farming effluents, hospital effluents, and surface water runoff following wide-area biological incidents.

These pollutants have led to water contamination and has become a global problem. This situation has prompted the search for more effective water treatment techniques to ensure high-quality water [2].

Among the current alternatives to the conventional technologies, Advanced Oxidation Processes (AOPs) are highlighted due to their eco-friendliness and high ability to disinfect and degrade persistent emerging and dangerous pollutants. The AOPs use non-selective radicals of high oxidizing power, such as hydroxyl (HO[•]) and sulfate (SO₄^{•-}) radicals, oxidize organic pollutants until their mineralization (CO₂, H₂O and inorganic compounds) and cause membrane rupture in microorganisms.

Nowadays, the activation of PMS has received considerable attention to produce SO₄^{•-}. These radicals from the activation of PMS possess much higher redox potential and greater adaptive capability contrast to other reactive species such as

HO[•]. Therefore, their use resulting in superior degradation performance for organic pollutants. [3]

The activation of PMS can be possible by different methods; however, the use of transition metals is considered as good option due to its facility and effective manner to produce reactive oxygen species.

Metal-organic frameworks (MOFs), an assembly of metal ions and organic ligands, have been widely used as metal activator/catalyst and adsorbent. In addition, they are synthesized by facile procedures with rational design of the structure and composition. Conventional synthesis of MOFs is carried out either by solvothermal or hydrothermal methods. In this method, the soluble MOF precursors are subjected to a temperature gradient, which in turn leads to a concentration gradient and once the critical concentration is reached self-assembled nucleation and crystal growth are initiated, resulting in the formation of crystalline porous MOF. By modification of these conditions is possible to obtain a MOFs of different characteristics [4].

For this reason, this study was focused on the synthesis of several CuFe-MOFs by solvothermal method operating at different condition to obtain materials with different properties. Moreover, their catalytic activity has been studied by decontaminating water polluted with different emerging pollutants, such as, SMX or ANT, for pharmaceuticals and *E. coli*, for pathogens which were selected as model contaminants.

Materials and methods

Synthesis CuFe-MOF_n: Synthesis of CuFe-MOFs was carried out by solvothermal methods (Figure 1). After the mixture of metallic salts and ligands, the solution was introduced in a sealed autoclaves that were used to heat the reactants under autogenous pressure above or near the solvent boiling point. The reaction conditions are described in Table 1. These MOFs were named as CuFe-MOF_n, being n=1 for the highest ratio and 3 for lowest value.

CuFe-MOFs characterization: Synthesized CuFe-MOFs were characterized by TEM, SEM, EDX, XRD, and FT-IR analysis, using the equipment available in the C.A.C.T.I. of University of Vigo.

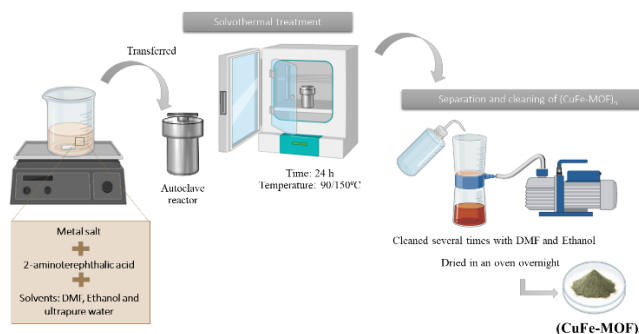


Figure 1. General scheme with the steps followed to perform the synthesis of the three CuFe-MOF. DMF:dimethylformamide

Table 1. Essential parameters for synthesis, including metallic salts, solvents ratio and temperature.

	Metallic salts	Solvent ratio* (DMF:EtOH:H ₂ O)	T ^a (°C)
MOF₁	FeSO ₄ · 7H ₂ O (50 mM) Cu(CH ₃ COO) ₂ · H ₂ O (50 mM)	1:1:8	90
MOF₂	FeSO ₄ · 7H ₂ O (66.5 mM) Cu(CH ₃ COO) ₂ · H ₂ O (66.5 mM)	7:1:0	150
MOF₃	CuCl ₂ · 6H ₂ O (66.5 mM) FeCl ₃ · 6H ₂ O (66.5 mM)	7:1:0	150

*DMF:EtOH:H₂O = dimethylformamide:ethanol:water

Experimental set-up:

Degradation of the drug mixture: Experiments to eliminate the drug mixture were carried out under the conditions of 1mM PMS, 0.25 g/L concentrations of the three CuFe-MOF and neutral pH. Fenton-like, photo-PMS, photolysis, photoadsorption and photocatalysis processes were used. To determine the concentration of the drug mixture, a high-performance liquid chromatography (HPLC), an Agilent instrument equipped with a Diode Array Detector at two wavelengths: 242 nm for ANT and 263 nm for SMX, was applied. For the chromatographic separation, it was employed a ZORBAX Eclipse XDB-C8 column (dimensions of 4,6 x 150 mm; 5 µm).

Disinfection: *E. coli* CECT 102 inactivation experiments were carried out at 0.1 mM PMS and 0.25 g/L concentrations of the three CuFe-MOFs. The mixtures were kept in an incubator at

80 rpm and 25°C for 5 and 15 min. The evaluation was made through the Colony Forming Units per mL(CFU/mL) method. After that, the liquid samples were spread into an agar plate and incubated for 24 h in an oven at 37 °C [5].

Results

CuFe-MOFs characterization:

SEM and TEM images depicted the surface structure morphology of prepared bimetallic CuFe-MOFs, pointing to three types of morphology, including spindle and octahedron morphology. In addition, their elemental composition was determined by EDX analysis to show the incorporation of both metals in the synthesized framework. The analysis indicated in several cases a lower amount of Cu in the MOFs sample with respect to the employed amount in its preparation. That could be due to the observed tendency of carboxylate groups to form strong bonds with iron.

Degradation of the drug mixture and disinfection of *E. coli*: After their characterization, it was proceeded to analyse its catalytic and disinfection capacity with a mixture of contaminant such as drugs, SMX and ANT, and pathogens, *E. coli*.

First, the catalytic capacity to degrade the drugs was analyzed operating at natural pH and catalyst dosage of 0.25 g/L. Based on this testing, it was found that both CuFe-MOF₂ and CuFe-MOF₃ have a high catalytic capacity. Particularly in the UV/PMS/CuFeMOF and PMS/CuFeMOF systems the drugs degradation achieved around the 80% in 30 min. Furthermore, the degradation was confirmed by the detection of short-chain carboxylic acids (oxalic, succinic, and acetic) and the reduction in toxicity values.

However, when disinfecting *E. coli*, CuFe-MOF₁ was the only catalyst that allows the complete elimination of this pathogen in less than 1 h, while the other two catalysts cannot degrade more than 50%. The reason for this is that CuFe-MOF₁ has a much higher copper content than the others, since copper can disrupt bacterial cell envelopes.

Conclusions

Bimetallic CuFe-MOFs catalyst has been designed in view of their application in the activation of PMS. Their characterization confirmed the differences among them. These properties allow a different application. Thus, the materials with high iron content had better results in the drugs degradation while the ones with high copper content increase the disinfection rate. Finally, these CuFe-MOFs could be easily recycled and reused in consecutive times without any decrease in catalytic activity.

Acknowledgements

This research was funded through the join 2019-2020 Biodiversa & Water JPI joint call for research proposals, under the BiodivRestore ERA-Net COFUND programme with the Project PCI2022-132941 funded by MCIN/AEI /10.13039/501100011033 and PID2020-113667GBI00, funded by MCIN/AEI/10.13039/501100011033 and Xunta de Galicia, and the European Regional Development Fund (ED431C 2021-43).

References

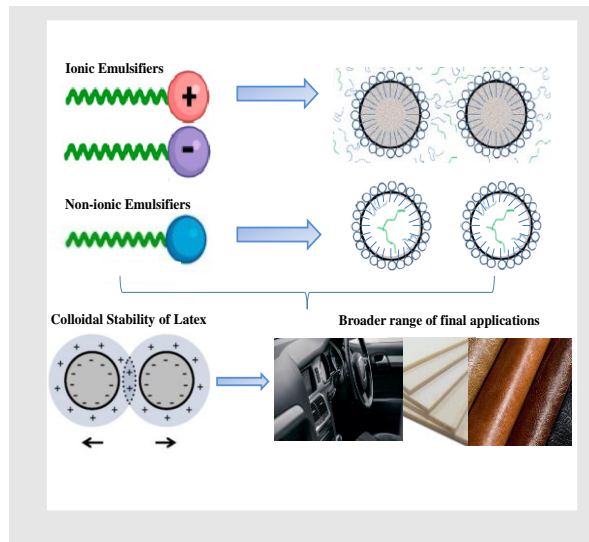
- [1] S.-H. Lee et al., Journal of Water Process Engineering, 31 (2019) 199828.
- [2] A.J. dos Santos et al., Current Opinion in Electrochemistry, 26 (2021) 100674.
- [3] J.M. Peralta-Hernández, E. Brillas, Chemosphere, 313 (2023) 137411.
- [4] A. Fdez-Sanromán et al., Applied Sciences, 12 (2022) 8240.
- [5] A. Fdez-Sanromán et al., International Journal of Environmental Research and Public Health, 19 (2022) 6852.

Development of new PVC based products through emulsion process

L. Lameiras^{1,2,3*}, J. Marques¹, A.M.V. Barros-Timmons², F.D. Magalhães³, A. Tomás¹

¹Companhia Industrial de Resinas Sintéticas, CIRES, LDA, Rua da Cires N°8, 3960-160 Avanca, Portugal; ²CICECO-Aveiro Institute of Materials, Departamento de Química, 3810-193, Universidade de Aveiro, 3810-187 Aveiro, Portugal; ³LEPABE, Departamento de Engenharia Química, Universidade do Porto, Rua Dr. Roberto Frias, 4200-465 Porto, Portugal.

*liliana.lameiras96@gmail.com



The aim of this work is to develop new poly(vinyl chloride) products using the emulsion process. Based on the production technology known by CIRES, LDA, several trials were performed in a pilot-scale to study a new system of ionic/non-ionic emulsifiers, which can improve the colloidal stability of PVC latex. This could allow for a more efficient removal of the residual monomer. Simultaneously, the target is to reduce the fogging index and VOCs associated with the final article. The improvement of these parameters is important for applications in the automotive industry. Simultaneously, operation conditions of the free radical emulsion polymerization process were manipulated, in order to obtain different particle size distributions that could allow a greater control of plastisol rheology. Overall, this will offer a broader range of final applications. These purposes align with the sustainable development of the PVC European Industry.

Introduction

Poly(vinyl chloride), commonly known as PVC, is the second most consumed polymer in the world after polyethylene. Its properties and its cost make this product very competitive, hence its constant development being so relevant. From 2022 to 2023 its compound annual growth rate (CAGR) was of 7.9 %. It is expected that the market of the poly(vinyl chloride) should have an annual growth rate of 7.6 % by 2027 [1]. Three methods of PVC production can be identified: Emulsion, Bulk and Suspension [2]. The emulsion technique was the first to be used at industrial level and it involves the application of vinyl chloride (VCM) as monomer and water as a dispersant agent, which usually uses anionic emulsifiers for the particle size control [3]. In the case of emulsion polymerization, the average particle size is in the range of 0.1 to 1 μm , and since it is free radical polymerization, the initiators are soluble in the aqueous phase [4]. In the conventional emulsion polymerization of VCM, particle formation is predominantly started by micelle nucleation, thus, the type and concentration of emulsifier end up defining the final distribution of particle sizes, as well as the properties of the final product. In addition, the emulsifiers are responsible for the colloidal stabilization of the polymer particles formed [5,6].

The study of the interaction of PVC resin with the plasticiser, in the final plastisol system, is of great importance. The final application of the plastisol in the rotational moulding processes, glove manufacture, superficial coatings, etc., is normally determined by its rheological behaviour [2]. Therefore, the presence of particles with higher average diameter is essential for manipulating this behavior in order to prepare low viscosity plastisols, for example. For this, wide particle size distributions are necessary which can be obtained using the seeded emulsion polymerization process [2,7]. This “seed” has the objective of promoting the widening of the size distribution specifically the bimodal size distributions, as seen in Figure 1.

This new particle size distribution, with a wider range of particle sizes, allows to improve packing and brings advantages at a rheological level [4]. Nevertheless, the micelle nucleation is

associated with emulsion systems considered “ideal”, i.e. systems in which the monomer is not soluble in water.

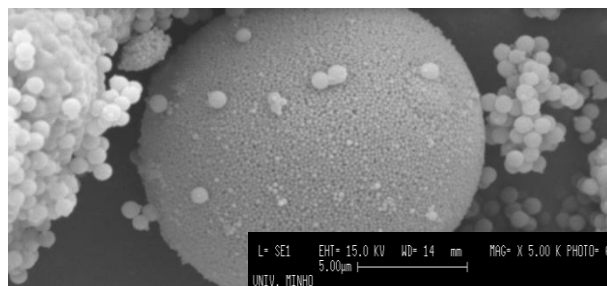


Figure 1. Representative SEM micrograph of bimodal latex sample.

In the case of the VCM, which presents some solubility in water, the aqueous phase could represent the main site for the initiation and propagation of the reaction in detriment of the micelle core. Therefore, the emulsifier plays a more relevant role in the colloidal stability. This type of nucleation is usually designated as homogeneous or secondary nucleation [7]. This work, studies how certain parameters, such as the nature of the emulsifier and the surface coverage of seed particles, affect the formation and stabilization of the particles.

Methodology

The experimental work was performed in a pilot plant of CIRES, LDA, in a cylindrical reactor with 5 L of capacity with a stirring system and reaction temperature control, equipped with tanks and pumps for the water charge, VCM and emulsifiers. Throughout the studies for the preparation of new polymers, conventional recipes were used in semi-continuous operation with an initial DW-deionized water charge, initiator and buffer. Before adding the monomer and emulsifier, the reactor was closed and the oxygen was removed from the reactor.

Results

The fogging index is one of the parameters to consider in the characterization of obtained polymers, and it represents the quantity of volatile compounds emitted by a polymer sample at

high temperatures over a specific time. The emulsifiers used during polymerization help stabilize the polymer particles formed, but the emulsifier residues present in the final product contribute to the formation of the fogging index.

In this part of the study, the values of the fogging index of three ionic emulsifiers were compared. Three batches were prepared: B1, B2 and B3 with the same ratio of emulsifier in relation to the quantity of VCM and the fogging index was measured. The results are shown in Table 1.

Table 1. Batches with different emulsifier: Fogging index.

	B1	B2	B3
Emulsifier	Ammonium Laurate	Sodium Laurate	Sodium Decylbenzenesulfonate
Fogging index (mg)	48.1	28.8	18.7

From Table 1, it was possible to conclude that the fogging index decreased drastically when ammonium laurate was replaced by sodium laurate, even though they have the same hydrophobic chain. This proves that the ammonium ion has a strong contribution to the fogging index. Using sodium decylbenzenesulfonate it is possible to achieve an even more significant reduction in the fogging index. The higher boiling point of this emulsifier associated with the aromatic ring limits its migration to the polymer surface. The objective of this part of the study was to explore how the HLB parameter of the emulsifiers and the process parameters affect the formation and stabilization of particle size distribution.

Hydrophilic-Lipophilic Balance (HLB)

At this stage of the study, the application of the HLB concept was explored in the selection of emulsifiers for the polymerization of VCM. Six non-ionic emulsifiers were selected and identified as EA to EF. A stable solution was prepared using a mixture of sodium laurate (LS) and these non-ionic emulsifiers using a 70:30 ratio. The results are shown in Figure 2.

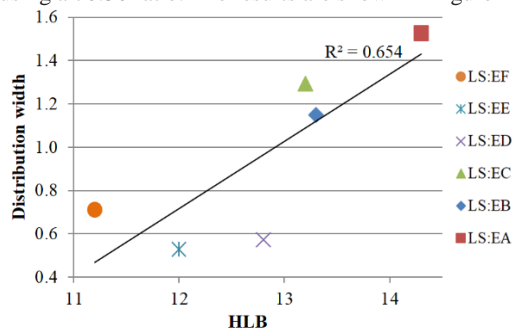


Figure 2. Variation of distribution width with HLB.

Acknowledgements

The financial support of FCT is gratefully acknowledged.

References

- [1] The Business Research Company, "Poly-Vinyl Chloride Global Market Report," The Business Research Company, 2023.
- [2] Y. Saeki, T. Emura, *Progress in Polymer Science*, (2002) 2055-2131.
- [3] R. Hohenadel et al., "PVC Polymerization with metered addition of emulsifiers". United States Patent 6,242,541, 5 June 2001.
- [4] J.H. Ko et al., "Polyvinyl chloride resin and method of preparing the same". United States Patent 9,902,817, 27 February 2018.
- [5] M. Pourmehr, A. Navarchian, *Journal of Applied Polymer Science*, 111 (2008) 338-347.
- [6] E.G. Barroso et al., *Journal of Applied Polymer Science*, 109 (2008) 664-673.
- [7] T. Mckenna et al., *Chemical Engineering Technology*, 36 (2013) 1179-1186.

Emulsifiers with a higher HLB value have a stronger affinity with water. It was noted that with the increase of the emulsifiers HLB it was possible to manipulate the particle size distribution (PSD) of the obtained polymers, given that the width of the particles distributions increases. This way, the homogeneous nucleation was favoured in detriment of the micelle nucleation.

Surface Coverage of the seed particles

The objective in this part of the study was to evaluate the role played by the slow addition of the emulsifier, as well as its influence on the stabilization of the particles. Delaying the dosage of emulsifier compared to the standard recipe will cause the system to reach the fractional surface coverage of particles later. Thus a larger volume fraction of large particles are obtained. To achieve this, the growth of the seed particles was manipulated, Figure 3(a), and they were subsequently used in a new polymerization process. This resulted in a bimodal particle size distribution with a significant increase in particle size, as shown in Figure 3(b).

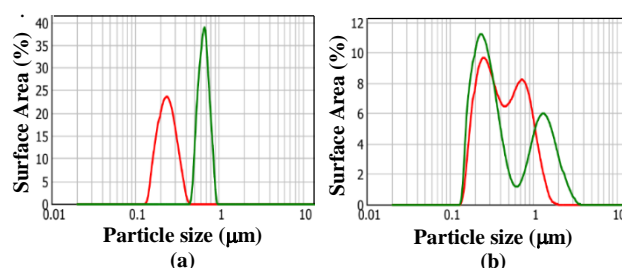


Figure 3. Particle size distributions: (a) monomodal seed; (b) bimodal distribution.

Conclusions

It was concluded that in batches prepared using the same emulsifiers dosages, changing only the type of emulsifier used, has a significant impact in the reduction of the fogging index of a determined sample.

The use of a specific emulsifier, selected based on its HLB parameter, was found to promote homogeneous nucleation in the VCM polymerization process. As the HLB value of the emulsifier increases, its affinity to water also increases, resulting in formation of larger particles.

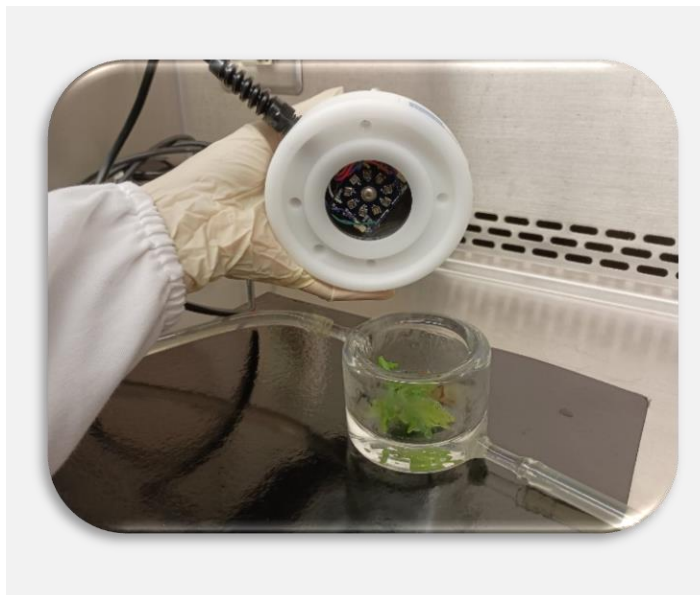
Delaying the dosage of the coverage emulsifier makes it possible to achieve better control over the volume fraction and formation of larger particles. The lack of emulsifier results in a very small formation of new micelles inside the reactor, and the particle population that is formed at the beginning of the process tends to grow through homogeneous nucleation mechanisms

Evaluate the effectiveness and effects of ultraviolet light-emitting diodes for food production, preservation, and microbiological safety

K. Luz^{1,2*}, M.T. Crespo^{1,3}, V.J. Pereira^{1,3}, A.P. Marques¹

¹Instituto de Biologia Experimental e Tecnológica, Apartado 12, 2780-901, Oeiras, Portugal; ²NOVA School of Science and Technology, 2829-516 Caparica, Portugal; ³Instituto de Tecnologia Química e Biológica António Xavier, Universidade Nova de Lisboa, Av. da República, 2780-157, Oeiras, Portugal.

*katia.luz@ibet.pt



Fresh fruits and vegetables are essential to a healthy diet. Three single small light emitting diodes that emit light at different wavelengths (260 nm, 280 nm, and their combination) were extremely efficient for the inactivation of *Salmonella enterica* Typhimurium and *Listeria monocytogenes*, that have been associated with foodborne outbreaks.

Introduction

In the last decade, the market of fresh fruits and vegetables had a high consumption increase [1,2]. However, uncooked products may also be a common source for various microorganisms, including pathogenic and spoilage bacteria. Moreover, outbreaks of foodborne illnesses associated with the consumption of fresh produce have increased [3]. The World Health Organization estimates that food contaminated with microorganisms and/or chemical contaminants is responsible for more than 200 diseases. Every year foodborne diseases cause: almost 1 in 10 people to fall ill, resulting in the loss of 33 million healthy life years.

Data indicates that about 1.3 billion tons of food suitable for human consumption is wasted every year, with 44% attributed to fruits and vegetables. Food losses and wastes present critical concern at a global level. Therefore, the United Nations agenda has initiatives with development investments towards preventing and reducing postharvest losses [5].

Disinfection has been described as the most important processing step to guarantee the quality, safety, and shelf-life of fresh fruits and vegetables ready-to-eat. Even though chlorine has been widely applied due to its efficacy, relatively low price, and easy application, it is known to produce hazardous disinfection by-products [6]. Light emitting diodes (LEDs) appear to be a promising disinfection alternative compared to mercury lamps due to their sustainability, longer lifetimes, lower costs, energy consumption and maintenance, compact size, and wavelength diversity [7].

This study aims to explore the use of UV-C LEDs as an alternative disinfection method to inactivate bacteria associated with foodborne outbreaks (*Salmonella enterica* Typhimurium and *Listeria monocytogenes*) on fresh products.

Results

Phosphate buffer spiked with *Salmonella enterica* Typhimurium or *Listeria monocytogenes* were used to test the inactivation efficiency of three single small UV-C LEDs that emit light at different wavelengths (260 nm, 280 nm, and their combination). Lettuce leaves spiked with *Salmonella enterica* Typhimurium were exposed in both sides, for 10 minutes, to UV-C light emitting diodes that emit at 260, 280 nm and their combination. Photoreactivation and dark repairs assays were performed after UV-C LEDs exposure to ensure that *Salmonella enterica* Typhimurium were not able to reactivate.

An evaluation of the effect of UV-C LEDs on genetic damage was also carried out.

The preliminary results obtained show that three single small LEDs that emit light at 260 nm, 280 nm, and their combination were extremely efficient for the inactivation of bacteria associated with foodborne outbreaks.

Conclusions

The results show that this disinfection system could be a promising approach to be applied on food to achieve effective inactivation of microorganisms present in salads and bacteria associated with foodborne disease.

The time needed to achieve a certain level of inactivation will decrease if a higher number of LEDs, higher intensity and/or shorter distance is used

Acknowledgements

This research was funded by Fundação para a Ciência e Tecnologia/Ministério da Ciência, Tecnologia e Ensino Superior (FCT/MCTES, Portugal) through the Exploratory Research Project SafeFood (Reference 2022.01340.PTDC), National funds to iNOVA4Health (UIDB/04462/2020 and UIDP/04462/2020) and the Associate Laboratory LS4FUTURE (LA/P/0087/2020). We also thank Professor Paula Teixeira from Escola Superior de Biotecnologia, Universidade Católica Portuguesa for providing the bacterial strains used on this study.

References

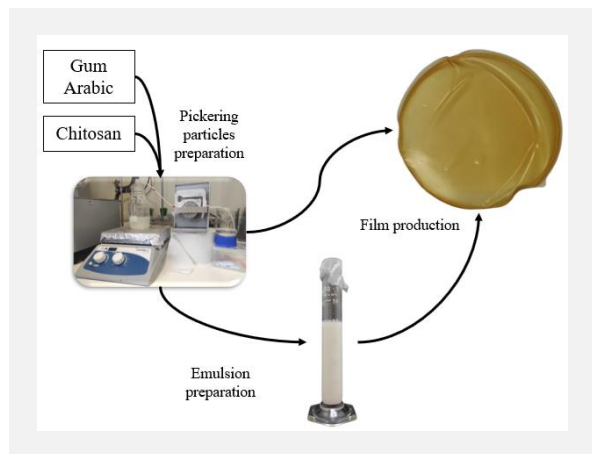
- [1] O. Esua et al., *Processes*, 8 (2020) 1433.
- [2] R. Betts, *International Food Hygiene*, 23 (2014) 9-12.
- [3] R.M. Callejón et al., *Foodborne Pathogens and Disease*, 12 (2015) 32-38.
- [4] World Health Organization (WHO), *Food Safety* (Access: March 1, 2021): <http://www.who.int/en/news-room/fact-sheets/detail/food-safety>.
- [5] FAO. 2018. *Food loss and waste and the right to adequate food: making the connection*. Rome. 48 pp. Licence: CC BY-NC-SA 3.0 IGO. <https://www.fao.org/food-loss-and-food-waste/flw-data>
- [6] J. Gadelha et al., *EFSA Journal*, 17 (2019) e170913.
- [7] A. Meireles et al., *Food Research International*, 82 (2016) 71-85.

Development of chitosan/gum arabic films using Pickering emulsions envisaging hydrophobic compounds incorporation

J.F.R. Vicente^{1,2,3*}, T.L.B. Schreiner^{1,2}, C.C. Sipoli³, A. Santamaria-Echart^{1,2}, M.F.F. Barreiro^{1,2}

¹Centro de Investigação de Montanha (CIMO), Bragança, Portugal; ²Laboratório Associado para a Sustentabilidade e Tecnologia em Regiões de Montanha (SusTEC), Bragança, Portugal; ³Universidade Tecnológica Federal do Paraná (UTFPR), Apucarana, Brasil.

*jefersonrio28@gmail.com



The production of biobased films incorporating hydrophobic components is a challenge due to the compatibilization production methods. Pickering emulsions (PEs), specifically oil-in-water emulsions, offer a solution. Using chitosan/gum Arabic particles as stabilizers, hydrophobic components can be incorporated into films, added to the PEs. In this work, the content of the emulsion and film-forming solution was optimized, along with the addition of glycerol, as a plasticizer. A stable emulsion formulation was obtained at 10/90 (oil/water) with a particle concentration of 4.0% w/v and 0.5% w/w of the hydrophobic compound. An emulsion/aqueous dispersion ratio of 05/95 with 20% w/w glycerol was defined as optimum for the films. The effective addition of TE into the films was validated by the uniformity of the color and homogeneous surface of the films. These findings demonstrate the potential of Pickering emulsions for producing biobased films with incorporated hydrophobic components.

Introduction

Polymers and their applications are subjects of extreme importance in the environmental context, primarily due to their profound impact [1]. Particularly, biobased polymers, derived from biological sources, have emerged as promising alternatives to synthetic counterparts owing to their biodegradability and desirable properties [2]. However, these materials, predominantly hydrophilic matrixes, imply a challenge when hydrophobic components are used to be functionalized, in the area of functional films, as an example [3]. In this context, novel strategies to enable the compatibilization of these components are needed, highlighting the use of emulsions, particularly Pickering emulsions (PEs) [2,4]. PEs are emulsions that use solids particles as stabilizers, that allow the use of different raw materials, such as polysaccharides, thus generating particles of the same nature or more compatible with polymer matrices commonly used in the preparation of natural-based films [4]. Based on these concepts, this work aimed to develop a stable Pickering emulsion based on chitosan (Ch) and Arabic gum (GA) particles, incorporated with turmeric extract (TE), and its subsequent compatibility in the preparation of Ch and GA-based films.

Methodology

Emulsions were prepared following Sharkawy et al. [4] methodology, involving mixing chitosan solution (in acetic acid) and Arabic gum solution in water, forming the Pickering particles by coacervation. The oil was added to the particles' containing aqueous phase and homogenized at 13500 rpm in an Ultraturrax. Films were prepared using the casting method, with the film-forming mixture consisting of a combination of an emulsion/aqueous dispersion. The aqueous dispersion included the Ch/GA particles dispersion and glycerol (as a plasticizer). The prepared emulsions were evaluated in terms of oil ratio (ϕ), particle concentration, and emulsion stability, while in the film properties, the impact of the emulsion/aqueous dispersion ratio on the film formation was availed.

Results and discussion

Firstly, emulsions with ϕ of 0.50 and 0.40 were prepared, evaluating their stability according to the formation of the phase separation calculated by the creaming index (CI) (calculated by the volume of the separated phase in relation to the total volume). At the same time, films with these emulsions were prepared in order to validate the product formed under these conditions. Figure 1 shows the emulsions obtained at t_0 (time of preparation) and t_7 (seven days after preparation), as well as the obtained films (emulsion/dispersion ratio of 100/0). Lower stability was observed at a lower oil ratio, due to the decrease in viscosity, which, favors the mobility of the droplets, allowing greater coalescence between them [5]. Brittle films with oil excess were obtained.

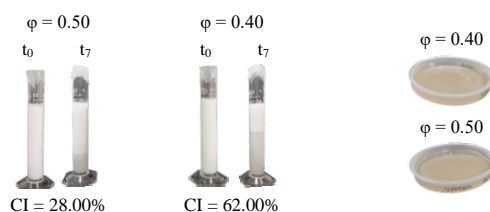


Figure 1. Emulsions and films prepared using neutral olive oil, 1.5% w/v Ch/GA particles at different times, and ϕ .

Considering the oil excess of the films, the emulsion/aqueous dispersion ratio was modified in the film-forming mixture. Concurrently, the emulsion formulation was varied, increasing the concentration of Ch/GA particles to obtain stable emulsions over time. Using different Ch/GA particle concentrations ranging from 1.5 to 4.0% w/v at a fixed ϕ of 0.30, the emulsions shown in Figure 2 were prepared.

The increase in particle concentration provided greater stability to emulsions considering the greater quantity of particles to stabilize the oil droplets in the system [6]. The optimum emulsion formulation was established at $\phi = 0.10$ and 4.0% w/v Ch/GA particles. For the films, a formulation containing an

emulsion/aqueous dispersion ratio of 05/95, with the addition of 20% of glycerol (film total dry mass basis) as a plasticizing agent, was defined.

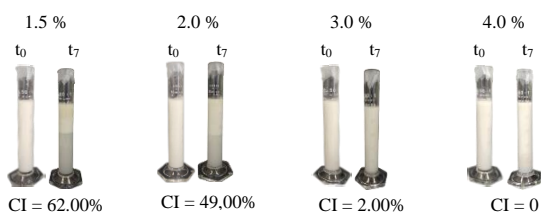


Figure 2. Emulsions prepared using sweet almond oil, $\phi = 0.30$, and at different Ch/GA particles concentration.

Having determined the most promising emulsions and film formulations, TE was incorporated into the oil phase of the emulsion at a concentration of 0.5% w/w. In order to validate the incorporation of TE, the base emulsion, film, and the corresponding incorporated with TE were compared, as shown in Figure 3.

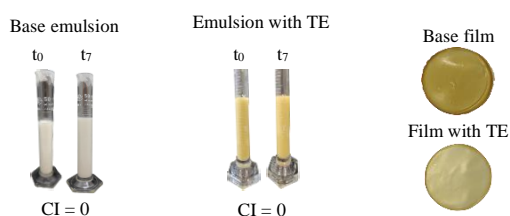


Figure 3. Base emulsion, base film and the corresponding systems added with TE.

For both emulsions and films, color differences were appreciated, as confirmed by colorimetric analysis, presented in Table 1.

The emulsions morphology and average droplet size (ADS) was analyzed by optical microscopy, shown in Figure 4. Both emulsions presented a spherical shape, and an ADS of $3.56 \pm 1.36 \mu\text{m}$ and $2.88 \pm 0.70 \mu\text{m}$ for the base and TE-added emulsions, respectively, at t_0 . These values showed that the TE reduced the ADS of the particles.

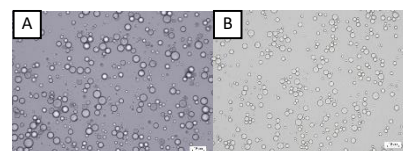


Figure 4. Optical microscopy with 400x magnification for (A) emulsion base and (B) emulsion with TE.

Both, the base film and the corresponding added with TE, were analyzed by Fourier Transform Infrared Spectroscopy (FTIR) (Figure 5). It was not possible to observe variations in the peaks, indicating the complete incorporation of the TE or that the low concentration was not enough for its identification.

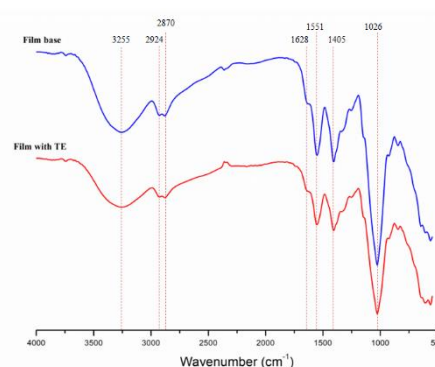


Figure 5. FTIR spectra of the base film (blue) and the film containing the TE (red).

Conclusions

In this study, a hydrophilic film incorporating TE, a hydrophobic component, was successfully developed. An emulsion with $\phi = 0.10$, 4.0% w/v Ch/GA particles, and 0.5% w/w TE was used. The resulting emulsion presented a yellowish coloration with spherical droplets, presenting an ADS of $3.05 \pm 0.78 \mu\text{m}$. From this emulsion, a yellowish film was formed with a composition of 05/95 emulsion/aqueous dispersion and 20% glycerol (relative to the total dry mass of the film). The film effectively incorporated the emulsion, leading to homogeneous systems. Further research is required to validate the relationship between the extract concentration and emulsion and film properties. Additionally, it is recommended to conduct tests to explore the potential applications of this material in the pharmaceutical, food, and cosmetic industries.

Table 1. Colorimetric parameter according to the CIELAB system for emulsions and films at t_0 .

Material	L*	a*	b*	RGB Color
Base emulsion	81.83 ± 0.07	-1.32 ± 0.01	2.77 ± 0.02	
Emulsion with TE	71.81 ± 0.05	-2.00 ± 0.07	40.46 ± 0.06	
Base film	87.40 ± 0.31	-7.34 ± 0.16	44.15 ± 0.62	
Film with TE	85.52 ± 0.10	-8.35 ± 0.04	58.49 ± 0.16	

Acknowledgements

The authors are grateful to the Foundation for Science and Technology (FCT, Portugal) for financial support through national funds FCT/MCTES (PIDDAC) to CIMO (UIDB/00690/2020 and UIDP/00690/2020), and SusTEC (LA/P/0007/2020). To Red Cytel ENVABIO100 121RT0108.

References

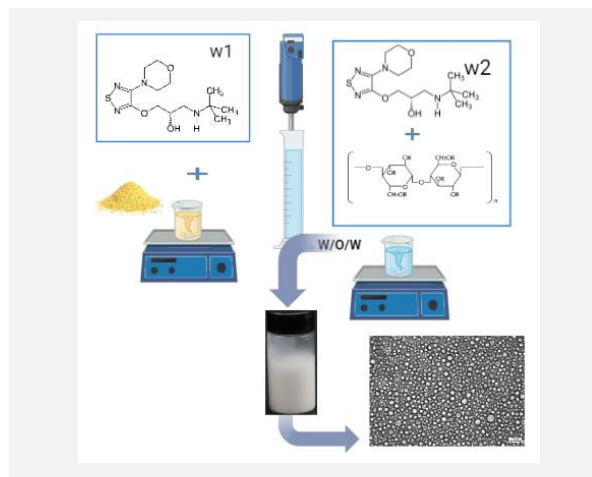
- [1] Ibrahim et al., *Coatings*, 11 (2021) 1423.
- [2] Jiménez-Saelices et al., *Carbohydrate Polymers*, 242 (2020) 116366.
- [3] Sun et al., *International Journal of Biological Macromolecules*, 159 (2020) 696-703.
- [4] Sharkawy et al., *Carbohydrate Polymers*, 224 (2019) 115190.
- [5] Ren et al., *LWT*, 162 (2022) 113468.
- [6] Mwangi et al., *Food Hydrocolloids*, 60 (2016) 543-550.

Emulsion-based drug carriers for timolol maleate envisaging glaucoma treatment

A.R. Teixeira¹, L.G. Teixeira^{2,3,4,5}, A. Santamaria-Echart^{2,3}, G.R. Silva¹, M.F. Barreiro^{2,3*}

¹Universidade Federal de Ouro Preto, Rua Professor Paulo Magalhães Gomes, 122 - Bauxita, Ouro Preto - MG, 35400-000, Brasil; ²Centro de Investigação de Montanha (CIMO), Instituto Politécnico de Bragança, Campus de Santa Apolónia, 5300–253, Bragança, Portugal; ³Laboratório Associado para a Sustentabilidade e Tecnologia em Regiões de Montanha (SusTEC), Instituto Politécnico de Bragança, Campus de Santa Apolónia, 5300–253, Bragança, Portugal; ⁴Laboratory of Separation and Reaction Engineering (LSRE-LCM), Portugal; ⁵Associate Laboratory in Chemical Engineering (ALiCE), Portugal.

*barreiro@ipb.pt



The present study involves developing and characterizing a new carrier system for ocular treatment based on a double emulsion system ($W_1/O/W_2$) for timolol maleate incorporation. The emulsification process was carried out in two steps. The first emulsion (W_1/O) was produced using a water-to-mineral oil ratio of 30:70 (v/v), and soy lecithin (4%, v/v) as emulsifier. Metolose/chitosan particles produced at a 1:1 (v/v) ratio were used as Pickering stabilizers in the second emulsion. Timolol maleate, when applied, was incorporated in the first water phase (W_1) at a content of 2.5 mg/mL. The obtained emulsions were characterized by an average droplet diameter of $1.95 \pm 0.004 \mu\text{m}$ (25°C) and $1.88 \pm 0.003 \mu\text{m}$ (4°C), and a pH of 4.8. Moreover, an encapsulation efficiency (EE) of 99.84% and a high viscous product were achieved. The developed system aims to improve precorneal retention time and drug bioavailability. The double emulsions have been shown to be a stable and efficient system for delivering timolol, making it a potential candidate for future research as an alternative treatment for open-angle glaucoma.

Introduction

Colloidal dispersions are important systems for drug incorporation, enabling controlled and sustained release [1]. Double emulsions ($W_1/O/W_2$) are widely used in the pharmaceutical field for encapsulating hydrophilic drugs [2]. However, these systems often face physical stability issues, such as coalescence, flocculation, and gravitational separation [3]. Pickering emulsions, which are characterized to be stabilized by solid particles, eliminate the need for conventional surfactants [4]. Moreover, they can produce very stable systems, preventing emulsion droplet coalescence [5]. The particles used in these emulsions can comprise polymers such as chitosan, which is utilized in ophthalmic preparations due to its bio-adhesiveness properties to the corneal surface [6]. Another widely used polymer is hydroxypropyl cellulose (HPMC), which has been shown to enhance the physiological performance of bioactive compounds [7]. Thus, combining these desired effects, a double emulsion was prepared to protect a hydrophilic compound (timolol maleate), incorporated in an aqueous internal phase, envisaging an action in a hydrophilic medium (cornea) but with good advisedness. Searching for stable formulations, the second emulsion was stabilized using Pickering particles based on chitosan and HPMC, exploiting their intrinsic properties.

Methodology

Strategy for the production of the 1st emulsion

Considering obtaining a stable double emulsion ($W_1/O/W_2$), the first objective was to reach a stable W_1/O primary system to retain the hydrophilic drug in the internal phase. Various formulations were tested based on previously published methodologies [8]. Different emulsifiers, namely a mixture of Span 80 + Tween 80 (3:1, v/v), and soy lecithin, were tested to stabilize a mineral oil/water emulsion. Different W_1/O (20/80, 30/70, and 40/60, v/v) were tested with emulsifier contents ranging from 0.5 to 5% (emulsifier: Span 80 + Tween 80, 3:1 v/v ratio) and 2 to 4% (emulsifier: lecithin).

When analyzing the produced emulsions, the ones stabilized with the mixture Span 80:Tween 80 revealed an almost prompt formation of a serum layer. The stability increases with lecithin, with only a slight serum layer appearing after 24 hours. For that reason, the study progressed with using the first emulsion based on lecithin and the preparation of the second emulsion right after the preparation of the primary one. The objective was to achieve a final stable double emulsion.

Strategy for the production of the 2nd emulsion

To increase the stability of the system, Pickering particles composed of HPMC (trade name: Metolose SH) and chitosan at a 1:1 (v/v) ratio were produced and used to stabilize the second emulsion (2% v/v). The primary emulsion/water ratio ($(W_1/O)/W_2$) was 1/1. The emulsions were stored at 25°C and 4°C . After 7 days, the emulsions using a primary emulsion with a W_1/O of 20/80 and 30/70 and 3 and 4% lecithin remained stable at both tested temperatures. Considering the advantages of privileging the internal water phase (W_1) amount to maximize the incorporation of timolol maleate, the emulsion using 30/70 W_1/O ratio and 4% lecithin was chosen (coded as E23). From here, the work proceeded by substituting the internal water phase with a timolol maleate solution comprising 2.5 mg/mL concentration.

Characterization of the double emulsion

The creaming index was determined for the sampling periods 7, 15, and 30 days, also accompanied by optical analysis and determination of the average droplet diameter using Dynamic Light Scattering (DLS). Moreover, pH and viscosity were also measured. Encapsulation efficiency was determined using the indirect method described by Hemar et al. (2010) with quantification by spectrophotometry at $\lambda = 294 \text{ nm}$.

Results

The developed emulsions were stored, and the emulsified phases and creaming index were measured. Among those with a creaming index of zero, E23 (4% soy lecithin), which remained stable for 40 days, exhibited higher viscosity, an important parameter for ophthalmic formulations [9]. Only the

emulsion stored at a temperature of 25°C and containing the drug exhibited a creaming index of 3.3%. The recorded pH measurement of the system was 4.8. It is widely accepted within

the field that a pH range of 4 to 8 is considered suitable for ocular applications [10]. The images in Figure 1 depict spherical droplets with similar sizes and monodispersity. These findings are consistent with the values obtained by the dynamic light scattering (DLS) technique, as shown in Tables 1 and 2 and Figure 2, indicating a unimodal distribution with a narrow peak.

Table 1. Droplet size expressed as Dv50, D4.3 and span (μm) for the studied of emulsions stored at 25°C

Sample	Dv 50 (μm)	D 4.3 (μm)	Span
E23- control	1.91 \pm 0.002	3.49 \pm 0.01	4.50 \pm 0.03
E23- loaded with timolol	1.95 \pm 0.004	3.27 \pm 0,03	3.867 \pm 0.04

Table 2. Droplet size expressed as Dv50, D4.3 and span (μm) for the studied of emulsions stored at 4°C.

Sample	Dv 50 (μm)	D 4.3 (μm)	Span
E23- control	1,88 \pm 0.004	3.53 \pm 0.008	4.70 \pm 0.03
E23 – loaded with timolol	1,88 \pm 0.003	2.59 \pm 0,01	2.38 \pm 0.002

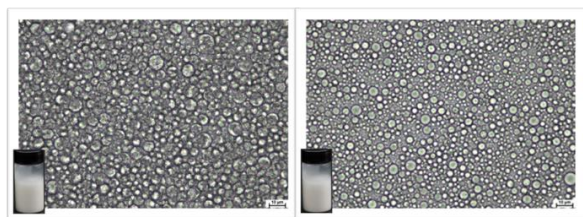


Figure 1. Optical microscopy images of the emulsions without timolol maleate (left) and loaded with it (right).

These values demonstrate that there was no change in the behavior of the droplets when the timolol maleate was added. The apparent viscosity of the double emulsion loaded with

Acknowledgements

Conselho Nacional de Desenvolvimento Científico e Tecnológico, Doutorado Sandwich no Exterior Processo: 200727/2022-2. Programa de Pós-Graduação em Ciências Farmacêuticas. Universidade Federal de Ouro Preto, Brasil. FCT/MCTES (PIDDAC) to CIMO (UIDB/00690/2020 and UIDP/00690/2020) and SusTEC (LA/P/0007/2021). National funding by FCT, P.I., through the institutional scientific employment program contract of A. Santamaria-Echart and L.G. Teixeira grant (2020.08803. BD).

References

- [1] M. Cang et al., *Journal of Dispersion Science and Technology*, 41 (2019) 479-494.
- [2] J. Liu et al., *Journal of Food Engineering*, 273 (2020).
- [3] D. Sungai et al., *Journal of Controlled Release*, 295 (2019) 31-49.
- [4] S. Asma et al., *Journal of Molecular Liquids*, 355 (2022).
- [5] E. Dickinson, *Food Hydrocolloids*, 68 (2017) 219-231.
- [6] E. Ribeiro et al., *Food Hydrocolloids*, 119 (2021).
- [7] A. Oluwatyin, *International Journal of Pharmaceutics: X*, 1 (2019).
- [8] M.L. Almeida et al., *Journal of Dispersion Science and Technology*, 38 (2017) 82-88.
- [9] F.D. Battistini et al., *European Journal of Pharmaceutical Sciences*, 105 (2017) 188-194.
- [10] R. Bachu et al., *Journal of Ocular Pharmacology and Therapeutics*, 34 (2018) 312-324.

timolol maleate exhibited a gradual decrease with increasing shear rate (0 to 12 s^{-1}), as depicted in Figure 3, reflecting a non-Newtonian behavior [4].

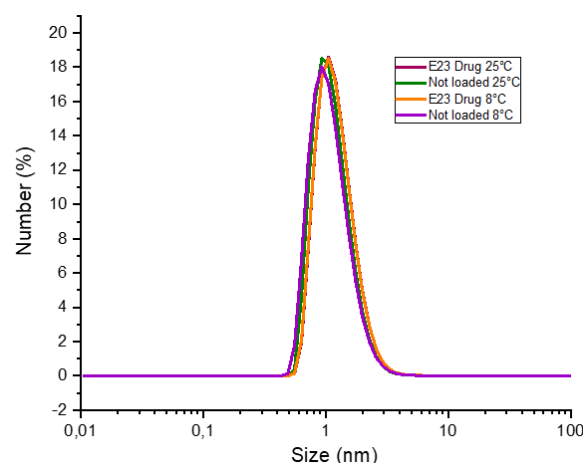


Figure 2. Droplet size distribution of the double emulsion stored at 25°C and 8°C.

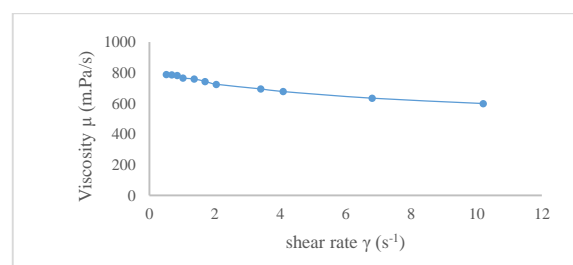


Figure 3. The rheological profile of the double emulsion.

Conclusions

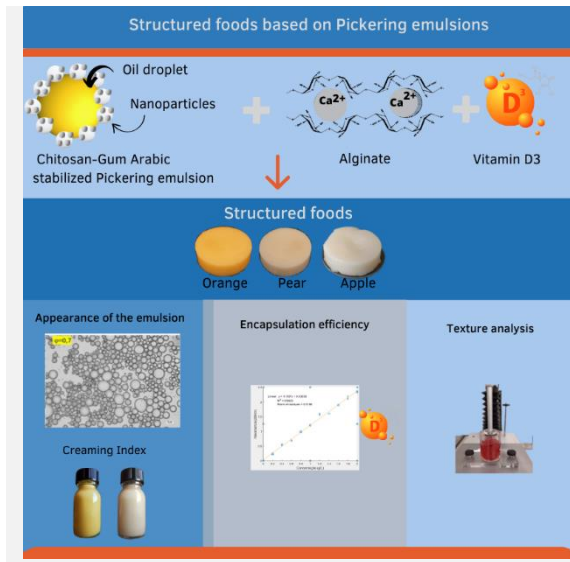
In this study, a stable and efficient double emulsion (W1/O/W2) system for timolol maleate delivery was developed. This ongoing work will proceed with the proof of concept for glaucoma treatment.

Structured foods based on Pickering emulsions as vitamin D3 vehicles

L.S. Iwamura^{1,2,3*}, L.C. Ghirro^{1,2}, E. Ramalhosa^{1,2}, B.D. Junior³, A. Santamaria-Echart^{1,2}, M.F. Barreiro^{1,2}

¹Centro de Investigação de Montanha (CIMO), Portugal; ²Laboratório Associado para a Sustentabilidade e Tecnologia em Regiões de Montanha (SusTEC), Portugal; ³Universidade Tecnológica Federal do Paraná (UTFPR), Campus Campo Mourão, Brasil.

*iwamura@alunos.utfpr.edu.br



Pickering emulsions (PEs) use solid particles as stabilizers. They offer advantages such as low toxicity, improved stability, and enhanced functionality incorporation. This project focuses on developing Chitosan/Gum Arabic nanoparticles for PEs and their application in structured foods. Results showed the potential of Chitosan/Arabic gum nanoparticles with Pickering action as promising systems for new food matrices. Two stable O/A formulations (E-1.5%-0.5 and E3.0%-0.7) were obtained but lacked a gel appearance. To improve gel appearance, alginate was added to the formulation, resulting in stable emulsions suitable for structured food development. Emulsions with gel-like characteristics remained stable for 28 days, and structured foods with encapsulated vitamin D3 were successfully developed. Texture analysis revealed similarities of the developed products with gelatin and flan products. In conclusion, structured foods based on Pickering emulsions using Chitosan/Gum Arabic nanoparticles are promising for the food industry, with the potential for encapsulating lipophilic vitamins (e.g., vitamin D3).

Introduction

Pickering emulsions (PEs) are characterized by using solid particles as stabilizers. Compared to conventional emulsions, they are less toxic, and present greater stability and improved capacity to incorporate functionalities [1]. Using these systems as structuring materials offers high potential, particularly for developing structured foods taking advantage of their predominantly elastic behavior and gel structure.

Objectives

In this context, this project aims to develop Chitosan/Gum Arabic nanoparticles, their use in developing PEs and subsequent testing in the design of structured foods. Usually, many structured food solutions are produced by the addition of hydrocolloids, being proposed in this work an innovative alternative for their production. The solution proposed here as also has the advantage to act as a delivery system of lipophilic vitamins.

Methods

Chitosan/gum Arabic nanoparticles were prepared in a 1:1 ratio. Pickering emulsions were prepared using the stator rotor method with nanoparticle concentrations of 1.5%, 3% and 4% (w/v) and Mygliol 812 oil volume fractions of $\phi=0.3$, $\phi=0.5$, $\phi=0.7$.

For the development of the structured food, PEs were produced combined with Ca-alginate hydrogel by ionotropic gelation method. Pickering emulsions were then prepared with a concentration of 1.5% Chitosan/Arabic gum particles at an oil fraction of $\phi=0.5$. The system was therefore tested by incorporating orange, apple, and pear-flavoured juices by water substitution, and incorporating vitamin D3 at a concentration of 0.1% (1 g L^{-1}) dissolved in the oil. The alginate (2% w/v) was dissolved in the juices under stirring. The prepared Pickering emulsion was mixed with an equal volume of the alginate solution, and the mixture homogenized. Subsequently, the mixture was allowed to stand and poured into molds. Gelation

occurred by injecting CaCl_2 solution (2% w/v) into the mixture. The samples were characterized by optical microscopy, creaming index analyses (IC) and texture profile analysis (TPA). The Encapsulation Efficiency of vitamin D3 was analyzed by ultraviolet-visible spectrophotometry (UV-vis) at 265 nm.

Results

The results indicated the feasibility of using the Chitosan/Arabic gum nanoparticles with Pickering action as promising systems for developing new food matrices. According to the creaming index (IC) and optical microscopy, as shown in Figure 1 and Figure 2, the process resulted in two O/W formulations with good concentration stability of 1.5% with volumetric oil fractions of $\phi=0.5$ (E-1.5% -0.5) and 3.0% with $\phi=0.7$ (E-3%-0.7). However, despite this stability, 18 and 15 days, respectively, these emulsions lacked gel appearance as shown in Figure 3.



Figure 1. Appearance of emulsions.

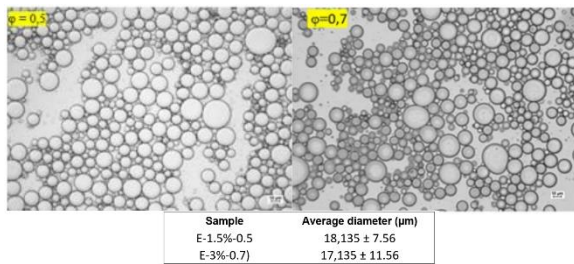


Figure 2. Mean droplet diameter of samples E-1.5%-0.5 and E-3%-0.7.

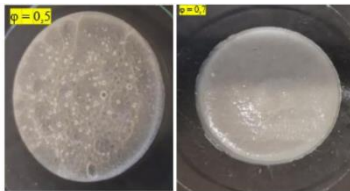


Figure 3. Aspect of the emulsions of samples E-1.5%-0.5 and E-3%-0.7.

New emulsions were produced using alginate as an alternative for improving the gel appearance of the emulsions to make the system suitable for structured food development. From sample E-1.5%-0.5, with the use of alginate in the formulation and three types of juices (Orange, Pear, and Apple), it was possible to develop structured food with emulsions with gel-like characteristics that remained stable during the 28 days, according to the evaluation of the creaming index as shown in Figure 4.



Figure 4. Samples produced using in the formulation and three types of juices (Orange, Pear, and Apple).

Acknowledgements

FCT – Fundação para a Ciência e a Tecnologia, I.P., for the financial support through national funds FCT/MCTES (PIDDAC) to CIMO (UIDB/00690/2020 and UIDP/00690/2020) and SusTEC (LA/P/0007/2020). FCT – Fundação para a Ciência e a Tecnologia, I.P., for the institutional scientific employment program contract of Arantzazu Santamaria-Echart, and PhD research grant of L. Ghirro (2022.13765.BD). FCT – Fundação para a Ciência e a Tecnologia, I.P., under the project 2022.01308.PTDC (NutriPick3D).

References

[1] W. Shi et al., Food Hydrocolloids, 52 (2016) 253-264.

Developing the structured food encapsulated with vitamin D3 was possible, showing good encapsulation efficiency (85.42% 89.70% and 88.42%), presenting a potential benefit in protecting hydrophobic compounds.

Comparing the developed samples with existing market substitutes, according to texture analysis as shown in Figure 5 the samples were similar to gelatin (sample L1) and flan (sample M1) products, as shown in Table 1.



Figure 5. Texture analysis of structured foods and similar products (flan and gelatin).

The samples containing Pear and Orange juice originated higher values in the texture properties (firmness, consistency, cohesiveness, and viscosity), probably due to the viscosity of the juices. The apple sample showed similar behavior to flan regarding firmness, consistency, cohesiveness, and viscosity. Orange Sample showed different behavior in relation to flan and gelatin. Still, it has a texture profile closer to gelatin, despite demonstrating head-to-head results superior in relation to firmness (182.47 g) and showed smaller viscosity (120.90 g·sec).

Conclusions

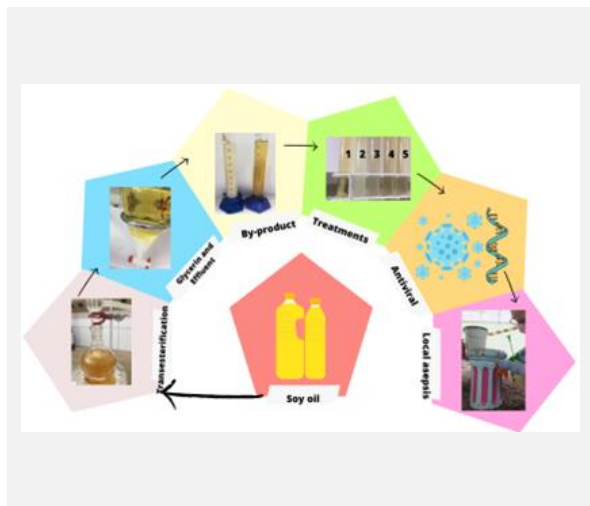
Developing structured food based on Pickering Emulsion was conducted successfully, using chitosan/gum Arabic nanoparticles as solid particles. The developed system is promising for the food industry due to the possibility of encapsulating vitamin D3, which can be further combined with other bioactive compounds, both hydrophilic and hydrophobic types, searching for synergistic effects. Printability is also a feature to explore.

Low-cost sanitizers derived from the biodiesel process: a study developed during the Covid-19 pandemic

A.C.C.M. da Silva¹, B.K.F. Pussi², C.C.R.L. Santos², D.T.O.S. Romeiro², E.E.P. Céleri¹, F.H.C.N. Abreu², G.V.L. Júnior¹

¹Universidade Federal do Espírito Santo (UFES), Vitória/ES, Brazil, ²Universidade Federal da Grande Dourados (UFGD), Dourados/MS, Brazil.

*carmemcenos@gmail.com



SARS-CoV-2 is highly spreadable and superficially adherent. The study aimed to present biodiesel by-products as sanitizing agents. From the transesterification of soybean oil, glycerin (G) and effluent (E) were obtained, separated into treatments. The volatile content was evaluated, (FTIR) fourier transform infrared spectroscopy, (TG) thermogravimetry and surface asepsis were simulated. The treatments were compared with the controls: 70% alcohol and 1% hypochlorite, in two times: 5 and 10 minutes against the virus. RNA was extracted and subjected to quantitative reverse transcriptase in polymerase chain reaction for 4 virus analytes. Treatment 2, presented a higher volatile content in relation to the others, contrary to Treatment 1, the others presented results proportional to their composition of E and G. A composition of glycerol, water, soaps and ethanol was observed by FTIR and TG; There was a decrease in the amount of viral RNA. When compared to 1% hypochlorite, Treatment 1, 4 and 5 also decreased viral cells within 10 minutes. When compared to 70% alcohol, all treatments showed better results in the amount of viral RNA.

Introduction

SARS-CoV-2, a virus of the *Coronaviridae* family, has a high potential for transmissibility, infection and adherence to different surfaces and materials [1]. The main route of transmission of the virus is through direct contact with mucous membranes, droplets from coughing and sneezing [2]. However, other forms of contagion were studied during the pandemic and a study pointed out that the virus survives deposited on surfaces for periods of 2 hours to 9 days, thus allowing indirect contamination [3].

Objectives

This study aimed to present an economical and effective alternative in the use of a by-product and a residue (effluent) from the biodiesel process, as sanitizing agents, mainly related to SARS-CoV-2.

Methods

From commercial soybean oil, ethyl transesterification was carried out, obtaining glycerin as a by-product and, through purification of the esters, the effluent. A combination of these materials was used for different Treatments (T): T1 (only glycerin), T2 (only effluent), T3 (70% Glycerin + 30% effluent), T4 (50% Glycerin + 50% effluent) and T5 (30% Glycerin + 70% effluent). The five treatments were analyzed in triplicate through the volatile content at 105 °C, density, dynamic viscosity, kinematic viscosity at 40 °C. Fourier FTIR and TG were also performed. During the pandemic, a simulation of local asepsis was carried out with treatments and a spray pump. The 5 treatments with samples of SARS-CoV-2 were tested, for comparison 70% alcohol and 1% hypochlorite were used as controls, it was tested in two times: 5 and 10 minutes, after this time the RNA extraction was immediately started. The extraction was performed with the "QIAamp® Viral RNA mini" extraction kit (QIAGEN), according to the manufacturer's protocol, positive control (positive sample for SARS-CoV-2) and negative control (water) were added in the extraction

shipment. After extraction, the RNA was sent for RT-qPCR with Kit All plex™ 2019-nCovAssay kit

Results

The reactional synthesis used presented a yield for the glycerin phase of 20.05±0.29%, according to the stoichiometry presented in the literature [4]. The effluent obtained in the purification of biodiesel presented a yield of 23.75±1.47%. It was extremely important to evaluate the visual appearance of the samples that would later be studied as potential sanitizing agents in the inactivation of SARS-CoV-2. All treatments were clear and free of solid impurities at 20 °C, as can be seen in Figure 1.

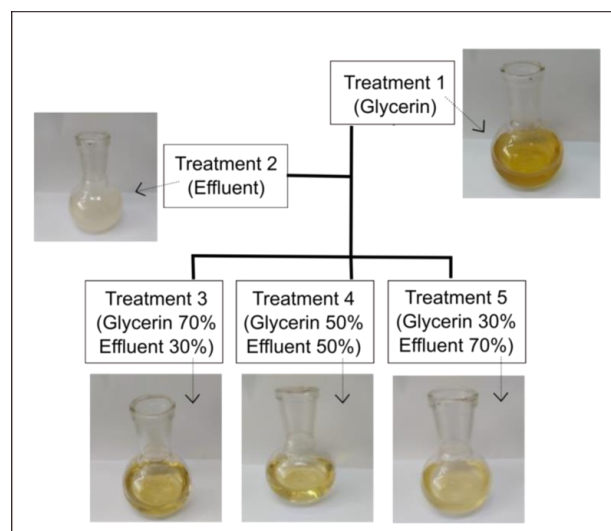


Figure 1. Evaluation of the visual appearance of the treatments.

T2 had a higher volatile content compared to the others, contrary to treatment T1, T3, T4 and T5 showed results proportional to their composition of effluent and glycerin. The physical-chemical results pointed to a cleaning procedure without problems due to the low fluidity, as the simulation of asepsis

actually resulted. FTIR (Figure 2) and TG (Figure 3) signaled a composition basically of glycerol, water, soaps and ethanol. The treatments were compared with the controls: 70% alcohol and 1% hypochlorite, in two times: 5 and 10 minutes against the virus. RNA was extracted and subjected to RT-qPCR for 4 virus analytes. There was a decrease in the amount of viral RNA. When compared to 1% hypochlorite, T1, T4 and T5 also decreased viral cells within 10 minutes. When compared to 70% alcohol, all treatments showed better results in the amount of viral RNA.

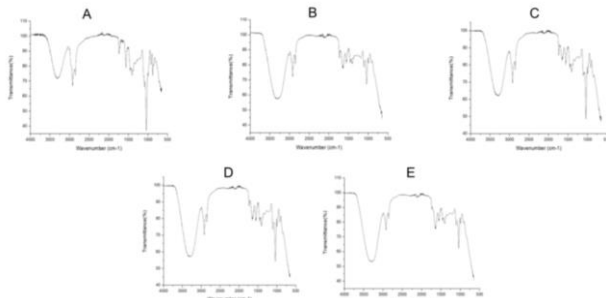


Figure 2. Spectrum of treatments. (A) T1 100% Glycerin. (B) T2 100% Effluent. (C) T3 70% Glycerin + 30% effluent. (D) T4 50% Glycerin + 50% effluent. (E) T5 30% Glycerin + 70% effluent.

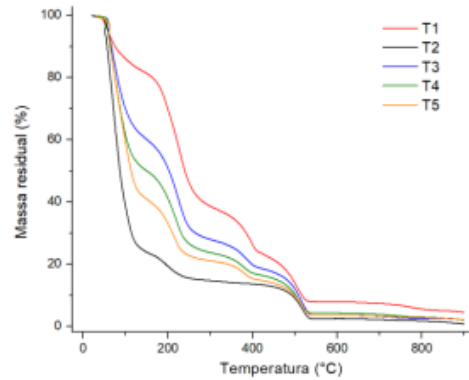


Figure 3. Thermogram of treatments. (A) T1 100% Glycerin. (B) T2 100% Effluent. (C) T3 70% Glycerin + 30% effluent. (D) T4 50% Glycerin + 50% effluent. (E) T5 30% Glycerin + 70% effluent.

Conclusions

The treatments were able to inactivate the virus, presenting superiority when compared to alcohol 70%. Among the 5 treatments, 3 also showed greater efficacy in relation to hypochlorite 1%, proving its effect as a sanitizer.

Acknowledgements

FAPES (Espírito Santo Research Support Foundation); LABPETRO (Laboratory for Research and Development of Methodologies for Petroleum Analysis at UFES); Federal University of Espírito Santo (UFES); Federal University of Grande Dourados (UFGD); State University of Mato Grosso do Sul (UEMS).

References

- [1] T. Acter et al., *Science of The Total Environment*, 730 (2020) 138996.
- [2] J. Reza et al., *Food and Chemical Toxicology*, 145 (2020) 111702.
- [3] L.G. Costa et al., *Química Nova*, 43 (2020) 723-728.
- [4] A. Núñez-Delgado, *Science of the Total Environment*, 727 (2020) 138647.

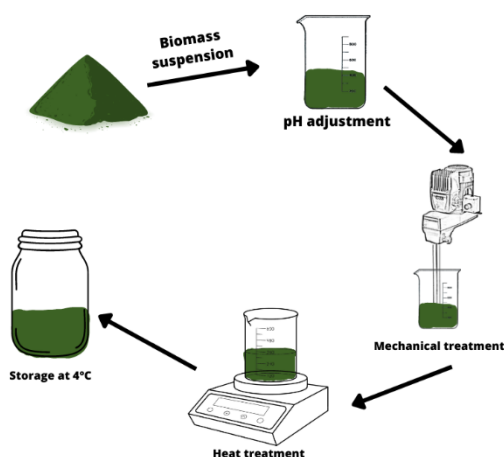
Hydrogel formation from *Spirulina platensis* biomass: screening of process variables

L.L. Aquino^{1,2,3*}, S.C. Silva^{1,2}, E. Colla³, E. Ramalhosa^{1,2}, A.Santamaria-Echart^{1,2}, M.F. Barreiro^{1,2}

¹Centro de Investigação de Montanha (CIMO), Instituto Politécnico de Bragança, Campus de Santa Apolónia, 5300-253 Bragança, Portugal; ²Laboratório Associado para a Sustentabilidade e Tecnologia em Regiões de Montanha (SusTEC), Instituto Politécnico de Bragança, Campus de Santa Apolónia, 5300-253 Bragança, Portugal; ³Universidade Tecnológica do Paraná, 85884-000, Medianeira, Brasil.

*leandroaquino@alunos.utfpr.edu.br

Production scheme of the hydrogel



Spirulina platensis is a microalgae widely used in several industrial fields, e.g., in food, pharmaceuticals and cosmetics. It has a high nutraceutical potential, namely a protein content of 60-70% (dry weight basis). The interest in seaweed use is growing due to its technological and functional potential and the ability to enhance the nutritional properties of final products when added as the whole biomass. This has led to studies exploring the possibilities of incorporating seaweed into various products. The aim of this work is to identify specific variables impacting the development of physically crosslinked (heating-induced) hydrogels based on *Spirulina platensis* biomass. A Fractional Factorial Design (FFD) 2^{6-2} was carried out to assess the effects of six (6) variables (temperature, pH, heating time, stirring time, stirring speed, and concentration of the whole biomass) against the following responses: firmness (g) and consistency (g.sec) of the gels. The results allowed the selection of two variables with significant effects (biomass concentration and pH) which will be studied to optimize the preparation process. These results can help in future works for developing and incorporating these hydrogels in several final products directed to different industries.

Introduction

The change in society's habits in the search for healthier foods and eco-friendly products has grown, and, consequently, studies on the topic have increased. In this sense, microalgae emerge as an option, being currently used as a food supplement marketed mainly in powder form and capsules. A great emphasis is on algae, which have high levels of proteins and compounds of interest, such as antioxidants, being the most produced genus in the world, *Spirulina* and *Chlorella* [1].

Spirulina or *Arthrospira platensis* is a blue-green unicellular microalgae [2], which has compounds that arouse interest in the food, pharmaceutical, and cosmetic industries, such as the presence of vitamins and minerals, photosynthetic pigments (phycobiliproteins), antioxidant compounds, and polyunsaturated fatty acids [3,4].

The components present in *Spirulina* biomass have several nutritional and therapeutic activities that make it attractive for food supplements and a potential source for preventing and treating various diseases [5]. In addition to the great nutritional highlight, microalgae can compose product formulations with various technological properties, such as foaming, gelling, emulsifying properties, and others [6].

The versatility of hydrogel applications becomes a factor that drives this study since it is important for several areas, such as food (adding nutritional value), pharmaceutical (serving as a vector for the distribution of drugs), and cosmetics (as a carrier of bioactive compounds).

A Fractional Factorial Design (FFD) strategy was used to study the hydrogel formation, a statistical method employed in experimental designs to efficiently study the effects of multiple variables on an outcome. This involves selecting a subset of factor combinations from a full factorial design, reducing the number of experiments required while providing information on the significant variables of the studied process.

Objective

This work aims to study the formation of hydrogels based on *Spirulina platensis* through physical crosslinking by heating, using a Fractional Factorial Design as a tool, obtaining a final product of interest for food, pharmaceutical, or cosmetic industries.

Methods

To study the hydrogel formation process based on the microalgae *Spirulina platensis*, an FFD 2^{6-2} was developed. The studied variables were temperature (x1), pH, (x2), heating time (x3), stirring time (x4), stirring speed (x5), and the concentration of the whole biomass (x6). The coded and real values of the variables are presented in Table 1.

Table 1. Real and coded values of the FFD variables.

Variables/Levels	-1	0	1
Temperature (°C)	85	90	95
pH	6	8	10
Heating time (min)	30	45	60
Homogenization time (min)	5	10	15
Homogenization speed (rpm)	6500	8000	9500
Biomass concentration (%)	12	16	20

The evaluated responses included the gels' firmness (g) and consistency (g.sec). This study enabled to determine the significant variables by analyzing the effects.

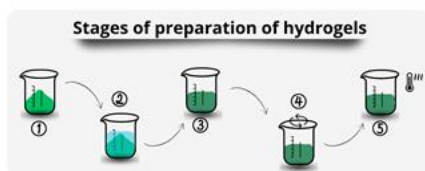


Figure 1. Hydrogel preparation steps.

The suspensions were prepared as presented in Figure 1. In step 1, the percentage of *Spirulina* was weighed based on 100 ml of distilled water. In step 2, 100 ml of distilled water were added. Step 3 involved adjusting the pH, step 4 involved homogenization in the Ultraturrax (CAT Scientific, Unidrive X1000D Homogenizer Drive, Germany), and step 5 heating the microalgae suspension. After these steps, the samples were left at room temperature and stored at 4°C until analysis.

From the formed gels, texture profile analysis (TPA) was performed to obtain the response of gel firmness and consistency. An A/BE probe – D 35 Back Extrusion Rig 35 mm disc was used, at a speed of 1 mm/s and with the probe's distance to the sample set at 70 mm.

Results and discussion

The data for the effects on the firmness and consistency responses are presented in Tables 2 and 3, respectively.

Table 2. Estimation of the effects on the firmness of the gels.

Factors	Firmness (g)			
	Effect	Standard Error	t (11)	p-value
Average	75,61	7,89	9,58	0,00*
x1	8,59	16,74	0,51	0,62
x2	-37,74	16,74	-2,26	0,05*
x3	-2,12	16,74	-0,13	0,90
x4	11,76	16,74	-0,70	0,50
x5	15,66	16,74	0,94	0,37
x6	65,88	16,74	3,94	0,00*

x1 – Temperature (°C), x2 – pH, x3 – heating time (min), x4 – homogenization time (min), x5 – homogenization speed (min), x6 – biomass concentration (%).

*Significant effects (p<0.05)

Acknowledgements

The authors are grateful to the Foundation for Science and Technology (FCT, Portugal) for financial support through national funds FCT/MCTES (PIDDAC) to CIMO (UIDB/00690/2020 and UIDP/00690/2020) and SusTEC (LA/P/0007/2020). National funding by FCT- Foundation for Science and Technology, through the institutional scientific employment program contract with Arantzazu Santamaria-Echar. Federal Technological University of Paraná - Medianeira Campus.

References

- [1] V.O. Galarza, Brazilian Journal of Food Technology, 22 (2019) e2019043.
- [2] X. Ai et al., International Journal of Biological Macromolecules, 231(2023) 1483-96.
- [3] Y. Yang et al., Marine Drugs, 18 (2020) 148.
- [4] H. Nakata et al., Journal of Functional Foods, 77 (2021) 104344.
- [5] M. Ambrosi et al., Revista de Ciências Farmacêuticas Básica e Aplicada, (2009) 29.
- [6] S. Benelhadj et al., Food Chemistry 196 (2016) 1056-1063.

In Table 2, it can be observed that the significant variables were pH (x2) and biomass concentration (x6). The negative pH effect indicated that lower pH values formed firmer and more consistent gels. The effect of biomass concentration was positive, indicating firmer systems at higher biomass concentrations.

Table 3. Estimation of the effects on the consistency of the gels.

Factors	Consistency (g.sec)			
	Effect	Standard Error	t (11)	p-value
Average	1268.86	136.85	9.27	0.00*
x1	99.92	290.31	0.34	0.74
x2	-680.62	290.31	-2.34	0.04*
x3	-36.76	290.31	-0.13	0.90
x4	242.64	290.31	0.84	0.42
x5	279.20	290.31	0.96	0.36
x6	1172.91	290.31	4.04	0.00*

x1 – Temperature (°C), x2 – pH, x3 – heating time (min), x4 – homogenization time (min), x5 – homogenization speed (min), x6 – biomass concentration (%).

Table 3 presents the data of the effects on consistency parameter, showing that the effects of x2 (pH) and x6 (biomass concentration) were significant. The pH had a negative effect, and the biomass concentration had a positive effect, demonstrating that more consistent formulations were formed at higher biomass concentrations and lower pH levels.

In this sense, the pH had a negative effect, since, at high pH values, the gelification ability of *Spirulina platensis* biomass is not favored, as well as at pH close to the protein isoelectric point (pH 3.0). In addition, the biomass concentration effect was also positive because increasing the protein content in the suspension, together with carbohydrates and lipids, favors the crosslinking process.

Future works

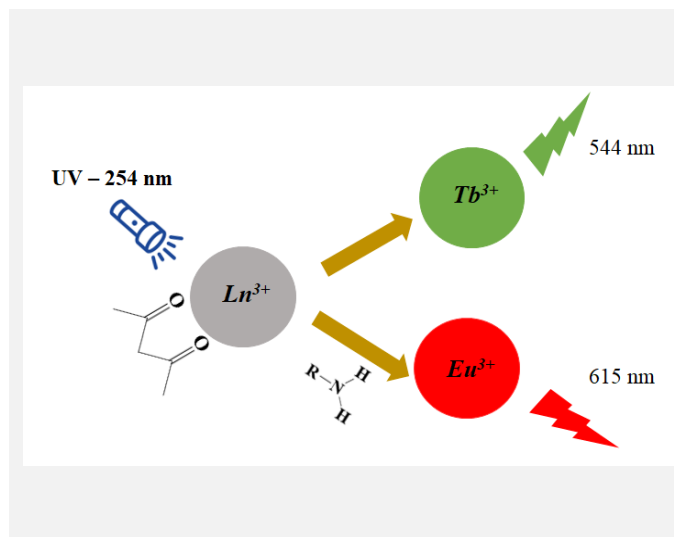
The significant effects will be subjected to a complete factorial design in future studies. In the end, the best formulations will be characterized in terms of stability, viscosity, and gel texture. Moreover, functional properties, e.g., antioxidant, will be determined.

Luminescent responsive lanthanide-doped silica films for biogenic amines recognition

C.M.R. Almeida^{1,2*}, J. Pina³, J.M.S.C. Magalhães², M.F. Barroso⁴, L. Durães¹

¹University of Coimbra, CIEPQPF, Department of Chemical Engineering, 3030-790, Coimbra, Portugal; ²LAQV-REQUIMTE, Departamento de Engenharia Química, Faculdade de Engenharia, Universidade do Porto, Rua Dr. Roberto Frias, 4200-465, Porto, Portugal; ³University of Coimbra, CQC-IMS, Department of Chemistry, Rua Larga, 3004-535 Coimbra, Portugal; LAQV-⁴REQUIMTE, Instituto Superior de Engenharia do Porto, Instituto Politécnico do Porto, Rua Dr. António Bernardino de Almeida 431, 4200-072 Porto, Portugal.

*claudio@eq.uc.pt



The development of a ratiometric fluorescent sensor based on co-doped Tb³⁺/Eu³⁺ silica film onto paper substrate was reported. The sensor was obtained by the sol-gel process, using tetraethylorthosilicate and methyltriethoxysilane as silica co-precursors and incorporating the lanthanides (sensor elements) and acetylacetone as the (antenna molecule). Different variations on the ratio between intensity emission bands of Tb³⁺ and Eu³⁺ were obtained after exposure to different amines. The sensor showed a high selectivity for primary aliphatic amines (biogenic amines). The prepared sensor was also tested as a food freshness indicator in meat and fish samples during the food degradation. Significant changes were observed, especially after one week, corresponding to the deterioration of foods. The emissions of chosen lanthanides in the visible region allows the “naked-eye” observation of the processes without analytical instrumentation.

Introduction

Amines are a class of relevant molecules in sectors such as biology, pharmaceuticals, cosmetics and food industry. These compounds present unique properties such as basicity, polarity and hydrogen bonding capacity [1]. Among them, biogenic amines, which are formed during food spoilage through decarboxylation reactions of the amino acid precursors, represent a problem in the food industry, since some of them can cause serious problems to human health [4, 5].

In this way, strong demand for cost-effective and reliable analytical devices able to detect and quantify amines has been verified [2]. Optical sensors, essentially those that explore the visible region (400 – 700 nm), present several advantages for on-site inspection operations, mainly because they offer instantly reliable and important information without the need for complex analytical instruments. Until now, most of optical sensors for amines have poor selectivity and resolution [3]. Other aspect which can represent an issue on amines sensor development, is based on the fact that these compounds do not have optical activity.

In this work, we report a co-doped Tb³⁺ and Eu³⁺ silica films, as a ratiometric sensor for the detection and discrimination of amines vapors. The sensor displays different values in the relative emission intensity ratio (I_{Eu}/I_{Tb}) induced by the amine vapors, which can be used to discriminate amines based on their chemical properties, such as pKa.

Results

The exposure of developed sensors to amine vapors produces a well-defined color response as shown in Figure 1. The sensors exhibit different colors when exposed to different amine vapors, such as dimethylamine, putrescine and cadaverine.

Each amine gives a different response pattern, with significant changes measured either by visual and spectroscopic tools. Some amines increase the europium emission intensity which is responsible for the orange-red color observed.

Regarding the intensity ratio variations (Eu³⁺/Tb³⁺), the significant changes observed for the biogenic amines, indicates that the energy transfer process is favored in the presence of such amines.



Figure 1. Visual response of lanthanide-silica films under UV light after exposure to different amine vapors.

Regarding the long-term stability of the sensors, in general, even after 4 months, the sensors kept their ability to visually and spectroscopically detect and distinguish different amines. Despite it was noted that the intensity emission bands decrease over time, especially in the first 2 weeks after sensors production, the decrease on the intensity ratio in the presence of the amine samples is less significant.

During food spoilage, several compounds are released including alcohols, ketones and biogenic amines, among others [6]. In an attempt to use the developed sensor system in food spoilage control, samples of meat and fish were monitored for 15 days, regarding the color variation under UV light (Figure 2).

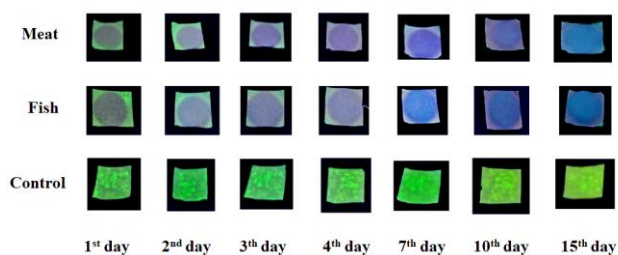


Figure 2. Visual response of lanthanide-silica films under UV light after exposure to different amine vapors.

After day 7, significant changes in the color parameters were verified, either for fish or meat samples. However, since the food decomposition results in a variety of compounds,

Acknowledgements

Cláudio M.R. Almeida acknowledges the PhD grant SFRH/BD/150790/2020 by Fundação para a Ciência e a Tecnologia (FCT, Portugal) funded by national funds from MCTES (Ministério da Ciência, Tecnologia e Ensino Superior) and, when appropriate, co-funded by the European Commission through the European Social Fund. This work was also supported by the European Regional Development Fund (ERDF), through COMPETE 2020 – Operational Programme for Competitiveness and Internationalization, combined with Portuguese National Funds, through Fundação para a Ciência e Tecnologia, I.P. [POCI-01-0145-FEDER-006910; UID/EQU/00102/2020; NORTE-01-0145-FEDER-31968; PTDC/NAN-MAT/31968/2017, UIDB/50006/2020; UIDP/50006/2020]. The CQC - IMS is supported by the FCT through the projects UIDB/00313/2020 and UIDP/00313/2020.

References

- [1] J.L. Klockow et al., *Fluorescent Sensors for Amines in Book Reference Module in Chemistry, Molecular Sciences and Chemical Engineering*, 2nd ed.; Elsevier, 2017; Vol. 8, 447-467.
- [2] Y. Li et al., *TrAC Trends in Analytical Chemistry*, 113 (2019) 74-83.
- [3] C.M.R. Almeida et al., *Journal of Materials Chemistry C*, 10 (2022) 15263-15276.
- [4] W. Ahmad et al., *Critical Reviews in Analytical Chemistry*, 50 (2020) 485-500.
- [5] Y. Özogul, F. Özogul, *Occurrence and Toxicity*, (2019) 1-17.
- [6] D. Mayr et al., *Applied and Environmental Microbiology*, 69 (2003) 4697-705.

including more and less volatile species, the color variations cannot be fully attributed to a specific compound.

Conclusions

Differentiated colour changes under UV light were observed after sensor exposure to amine vapours. The changes can be correlated with the amines properties such as chemical structure and pKa.

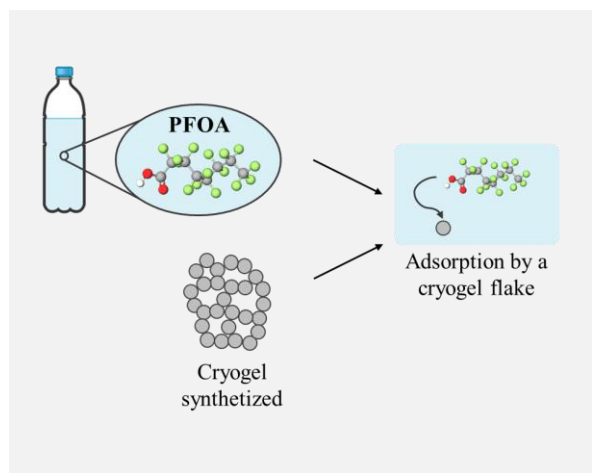
The observed increased emission intensity of europium bands after exposure to biogenic amines, proves that these amines increase the energy transfer from acetylacetone molecules to the Eu^{3+} ions, resulting in a increased emission bands intensity ratio. As a result, the observed variations can be used to discriminate different amines.

Development of a silica-based cryogel for the adsorption of perfluorooctanoic acid (PFOA) in water

*M.I. Roque**, V. Rocha, E. Domingues, R.C. Martins, L. Durães

University of Coimbra, CIEPQPF, Department of Chemical Engineering, Rua Silvio Lima, 3030-790 Coimbra, Portugal.

*inesroque@eq.uc.pt



Water quality has been a major concern in recent years, given the increase of industrialization and globalization. The presence of per- and polyfluoroalkyl substances (PFAS) in water is an increasing concern. This work aimed at developing a silica-based material, by the sol-gel process, with an affinity for the perfluorooctanoic acid (PFOA), to remove it from water. The synthesized material was characterized by SEM, and by its water contact angle and zeta potential. The adsorption capacity of the synthesized material to adsorb the PFOA was analyzed and, from this test, removal rates from 69.4% to 91.7% were obtained, depending on the initial concentration of the pollutant. In this sense, this material shows to be a suitable candidate for the removal of PFOA present in water. Furthermore, the adsorption isotherm proved to be better described by the Freundlich model.

Introduction

The increase of industrialization and globalization over the past years has taken a toll on the water quality. The consequent presence of several water pollutants has led to more careful water quality analysis and the imposition of stricter water quality regulations, including the creation of regulatory limits for new substances. The presence of PFAS in water has been a concern as they are toxic, persistent and are accumulating in the organisms [1].

Silica-based materials have shown to be good adsorbents aiding in water pollutant removal, as a result of their porous structure and easy characteristics' tailoring, by making several changes to the sol-gel method (*e.g.*, surface modification, drying method, *etc.*) [2].

Objectives

The objective of this work is to synthesize a silica-based adsorbent with affinity for one PFAS, the PFOA, so to remove efficiently this pollutant from water.

Methods

A silica-based adsorbent was synthesized by the sol-gel method, using tetraethyl orthosilicate, methyltrimethoxysilane and 3-aminopropyltriethoxysilane (25:70:5 (mol%), respectively) as the reaction precursors. Ethanol was used as the solvent. For this process, oxalic acid and ammonium hydroxide were used as sol-gel catalysts. The drying method employed in the synthesis of the material was freeze drying.

The quantification of the PFOA was performed according to the METTLER TOLEDO© procedure which relies on a colorimetric method for the extraction of the PFAS-methylene blue complex, onto chloroform, which can then be analyzed by a UV-Vis spectrophotometer.

Results

The cryogel synthesized by the sol-gel process was characterized by the determination of its water contact angle, zeta potential and by analysis of its surface by means of scanning electron microscopy (SEM).

The analysis of the water contact angle showed the material to be slightly hydrophobic, according to Anderson et al., as it

presented a water contact angle of 91° [3]. It was also verified how this characteristic changed over time, and by day two the water contact angle could no longer be measured, which in turn is beneficial for the purpose of this work, as the contact with water improves. Furthermore, it was also verified if this characteristic did not lead to a degradation of the material over time. To this end, the behavior of this material in water was analyzed over 3 weeks. This test showed that the material could be maintained in water during this time.

To assess the possibility of the synthesized material's ability to be used to adsorb the PFOA, an analysis of its surface charge was performed. This analysis showed that the material is positively charged, having a zeta potential of 25.9 mV.

A SEM study was also performed, to evaluate the structure of the material (Figure 1), showing the presence of an aerogel-like ramified and porous structure, being the very high porosity crucial for the extensive adsorption of the pollutant.

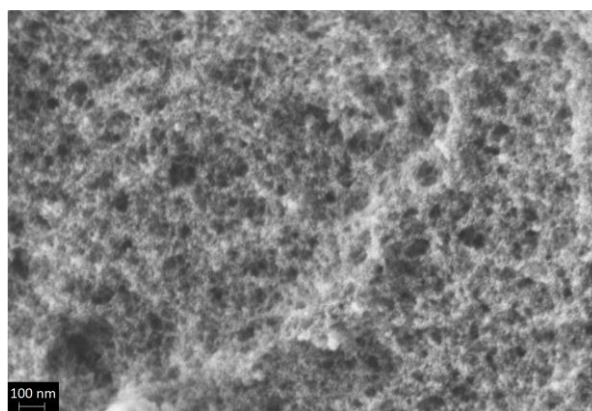


Figure 1. SEM performed to the synthesized adsorption material.

A calibration curve for the PFOA was created by measuring the absorbance of solutions with different pollutant concentrations (from 2.07 mg/L to 30 mg/L), at 650 nm (Figure 2).

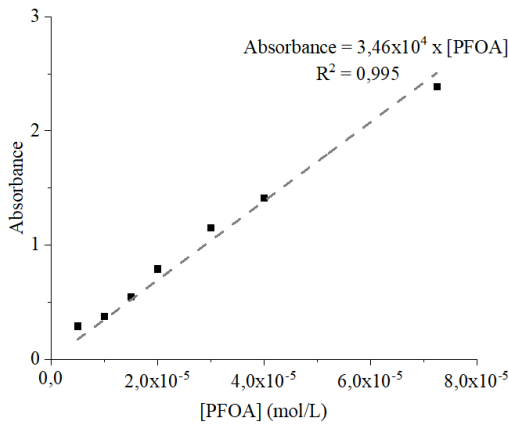


Figure 2. Calibration curve for the PFOA.

For the adsorption isotherm, 15 mL of different PFOA solutions with various concentrations were placed in contact with 0.03 g of the cryogel, over 24 h. After, the extraction of the PFOA was performed and its quantification was conducted by UV-Vis spectrophotometry. The equilibrium capacity (q_e) (mg/g) was then obtained by Equation 1, where C_i is the initial concentration (mg/L), C_e is the equilibrium concentration (mg/L), m is the mass of the adsorbent (g) and V the volume of the solution (L) [4]. The C_i , C_e , and q_e values obtained for the PFOA adsorption by the cryogel are present in Table 1.

$$q_e = \frac{(C_i - C_e)V}{m} \quad (1)$$

The removal of the pollutant by the cryogel was obtained by Equation 2 [4]. The results for this removal are also represented in Table 1.

$$R (\%) = \frac{100(C_i - C_e)}{C_i} \quad (2)$$

Table 1. Equilibrium capacity, initial and equilibrium concentrations, and removal achieved by the adsorption of the PFOA by the cryogel.

C_i (mg/L)	C_e (mg/L)	q_e (mg/g)	Removal (%)
5	1.53	1.74	69.4
10	2.60	3.70	74.0
15	4.17	5.41	72.2
20	5.15	7.43	74.3
30	7.81	11.1	74.0
50	10.3	19.8	79.4
100	12.2	43.9	87.8
200	16.7	91.7	91.7

From the previous results it is possible to observe that a considerable removal of the PFOA pollutant was achieved and

Acknowledgements

Funded by the European Union, under the Grant Agreement GA101081953 attributed to the project H2OforAll - Innovative Integrated Tools and Technologies to Protect and Treat Drinking Water from Disinfection Byproducts (DBPs). This research was co-funded by the European Regional Development Fund (ERDF). The researchers from CIEPQPF were supported by Portuguese Foundation Science and Technology (FCT), under project UIDB/EQU/00102/2020.

References

- [1] J.N. Meegoda et al., International Journal of Environmental Research and Public Health, 19 (2022) 16397.
- [2] A. Lamy-Mendes et al., Molecules, 24 (2019) 3701.
- [3] A.M. Anderson et al., Chapter 3 in Aerogels Handbook, M. and M. Editors, 1st Ed., Springer, New York, 2011, 57-62
- [4] M. Tang et al., Colloids and Surfaces A, 602 (2020) 125009.
- [5] P. Pourhakkak et al., Chapter 1 in Adsorption: Fundamental Processes and Applications, M. Editor, 1st Ed., Academic Press Inc., San Diego, California, 2021, 1-70.

that for higher initial PFOA concentrations, higher removal rates were also obtained.

The experimental results were then compared with the Langmuir and Freundlich models, Equations (3) and (4), respectively (Figure 3). In the Langmuir model, q_m represents the maximum adsorption capacity (mg/g) and K_L is the adsorption model constant (L/mg); in the Freundlich model, K_F is the adsorption model constant (mg/g), and n is the adsorption strength [4].

$$\frac{C_e}{q_e} = \frac{1}{q_m K_L} + \frac{C_e}{q_m} \quad (3)$$

$$\ln q_e = \ln K_F + \frac{1}{n} \ln C_e \quad (4)$$

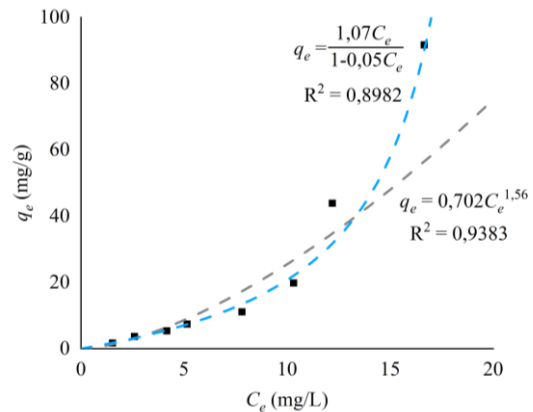


Figure 3. Experimental data adjusted by the Langmuir (blue) and Freundlich (gray) models.

From Figure 3 it is possible to verify that the experimental results are better described by the Freundlich model isotherm. According to Pourhakkak et al., this is an indicative of a non-uniform adsorbent surface with exponentially expanding adsorption energy and interactions between active sites and soluble molecules [5]. The SEM analysis, previously performed, confirmed the ramified, porous structure with many active sites, favoring the PFOA adsorption.

Conclusions

With this work, a silica-based material, with a potential for the adsorption of PFOA, was developed. The adsorption of the pollutant by the cryogel was evaluated by the analysis of the adsorption isotherm, which can be described by the Freundlich model. The removal values obtained ranged from 69.4% to 91.7%, proving to be a viable alternative for the adsorption of PFOA from water.

Ethosomes: an approach for bioactive plant extract preservation envisaging cosmetic applications

P. Plasencia^{1,2,3*}, A. Santamaria-Echart^{1,2}, S. Heleno^{1,2}, G. Colucci^{1,2}, P. Garcia³, L. Barros^{1,2}, M.F. Barreiro^{1,2}

¹Centro de Investigação de Montanha (CIMO), Instituto Politécnico de Bragança, Campus de Santa Apolónia, 5300-253 Bragança, Portugal; ²Laboratório Associado para a Sustentabilidade e Tecnologia em Regiões de Montanha (SusTEC), Instituto Politécnico de Bragança, Campus de Santa Apolónia, 5300-253 Bragança, Portugal; ³Departamento de Ciências Farmacéuticas, CIETUS-IBSAL, Universidad de Salamanca, Campus Miguel de Unamuno, 37007; Salamanca, Spain.

*marina@ipb.pt



The present work is focused on upgrading the commercial potential of berry crop by-products by encapsulating them into liposomes to preserve their bioactivity. The extracts have been obtained with an ethanol-water mixture using ultrasound-assisted extraction, and the most promising ones were encapsulated in ethosome system. To achieve this goal, ethosomes were prepared using the cold method. Ethosomal suspensions were characterized concerning particle size distribution by laser dispersion, differential scanning calorimetry, infrared Fourier-transform spectroscopy, encapsulation efficiency, and morphological analysis using optical, scanning electron, and transmission electron microscopy. These results indicate that ethosomes are an appropriate method to encapsulate hydroethanolic bioactive plant bioresidue extracts and a good option to preserve them for further use in industrial applications, such as cosmetics. Future work will include optimizing the process and proof of concept by developing a cosmetic application.

Introduction

Returning to ancient cosmetic raw materials is a trend. The use of natural extracts has been growing since the beginning of the XXI century, mostly with those plants that have evolved various photo-adaptive mechanisms, including the production of antioxidants and UV-absorbing compounds, by being exposed to intense radiation in their environmental conditions [1]. The waste biomass derived from berry crops is a new focus of study, since producers are increasingly interested in its valorization, namely through the production of high-added-value products. In this context, the leaves and other aerial parts are good examples of waste biomass that can be exploited for several applications in cosmetic formulations since these residues possess interesting chemical compositions and consequent bioactive properties. On the other hand, plant extracts are not stable for useful periods without adding preservatives, and European regulations are very restrictive for those types of cosmetic formulation additives. Studies showed that encapsulation results in the preservation of the plant's extract, like hyssop, also concluding that this process is an effective way to increase the antioxidant activity of the extract and, if added to edible oils with natural antioxidants, increasing their shelf-life [2]. The ethosome system has several advantages, including greater drug permeability, increased drug entrapment, and better drug delivery [3], [4]. Ethosomes are simple to make, stable, and safe to use. This kind of ultradeformable vesicles has already proved their potential to transmit medicinal chemicals via the skin without negative effects two decades after their development. Examples like antiaging and hyperpigmentation, hair tonics for hair growth, or topical cellulite cream, have been on the cosmetic market. The use of ethosomes with appropriate vehicles such as creams, gels, and patches improve skin permeability and therapeutic benefits [5].

Objectives

The main objectives of this work was to encapsulate hydroethanolic extracts previously obtained from berry plant cropping waste through innovative technologies, that are expected to provide more stable ethosomes, preserve the bioactive and antioxidant properties of the extracts, while enhancing skin permeation, improve drug delivery, and increase drug entrapment efficiency.

Methods

Classical liposomes have been used as an option to encapsulate lipophilic compounds. In the present work, the used extracts are a mixture of compounds with a predominantly hydrophilic profile, so ethosomes were used as an alternative. The cold process of encapsulation was employed. Briefly, the aqueous extract solution is added while stirring to the mixture of organic ethanol and soy phosphatidylcholine once full dissolution has been achieved [6]. The study started with producing five distinct ethosomal suspensions, with different ethanol contents, from 20 to 40%, and miglyol replacing the extract. The ethosomes were analyzed by optical microscopy and laser dispersion to determine their shape and particle size distribution. Following, the extract was encapsulated using the formulation that best suited the intended use, using 35% of ethanol in the organic phase. Laser dispersion, differential scanning calorimetry, infrared Fourier-transform spectroscopy, encapsulation efficiency, and morphology using optical, scanning electron, and transmission electron microscopy were used to characterize the extract-loaded ethosomal suspension.

Results

Since the used extract had a significant amount of hydrophilic components, it was possible to dissolve in the aqueous phase. Irregular surface morphology and the three-dimensional nature of ethosomes were further confirmed by SEM, suggesting the

vesicular ultra-deformability characteristics possessed by these novel kinds of carriers [7] (Figure 1). TEM morphology analysis techniques showed us the formation of a lipidic shell with an aqueous core, in which both fractions were encapsulated [8]. Osmium tetroxide is fixed by the phospholipidic layer, revealing a darker tone. It is used to give contrast to lipidic chains. It is also possible to observe the particles' irregular shape (Figure 1).

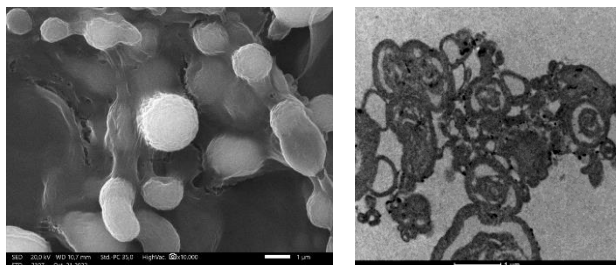


Figure 1. SEM and TEM (scale= 1 µm).

The particle size obtained for extract-loaded ethosomes is above the desired for the intended application (Figure 2). Overall, the mygliol-loaded ethosomes' size in volume increased with an

increase in the ethanol fraction. The size distributions of blueberry extract-loaded ethosomes also increase compared with mygliol-loaded ethosomes (see data in Table 1).

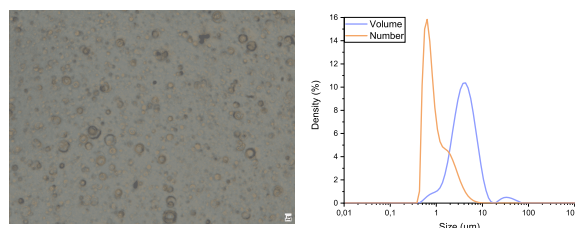


Figure 2. OM analysis (400x magnification, scale= 1 µm), size distributions blueberry extract loaded ethosomes (35% in ethanol).

Conclusions

It is feasible to encapsulate hydrophilic extracts using the current approach. With ethosomes, the achieved particle size was greater than expected for the intended use. Generally, the size and volume of mygliol-loaded ethosomes increase with the ethanol content in the organic-phase mixture. The size distributions of blueberry extract-loaded ethosomes increase as compared to mygliol-loaded ethosomes.

Table 1. Statistical analysis (D10, D50, and D90) of size distributions (in number and volume), blueberry extract (BB), and mygliol (Mg) loaded ethosomes

Variable	Sample	D10 Size (nm)	(±) std	D50 Size (nm)	(±) std	D90 Size (nm)	(±) std	SPAN Text	D4:3 Size (nm)	(±) std
in number	Et_35_BB	529	0,44	802	1,77	2350	2,41	2,27	-	-
	Et_35_Mg	634	7,66	1040	6,69	2130	5,84	1,44	-	-
in volume	Et_35_BB	1760	9,03	3960	24,00	8240	109,00	1,64	5210	94,97
	Et_35_Mg	1240	0,99	2560	0,52	4910	2,34	1,43	2860	0,00

Acknowledgments

The authors are grateful to the Foundation for Science and Technology (FCT, Portugal) for financial support through national funds FCT/MCTES (PIDDAC) to CIMO (UIDB/00690/2020 and UIDP/00690/2020) and SusTEC (LA/P/0007/2020), and for the research contract of A. Santamaria-Echart and PhD grant of G. Colucci (2021.05215.BD). We thank the Electron Microscopy Facilities-NUCLEUS of the University of Salamanca for SEM and TEM images.

References

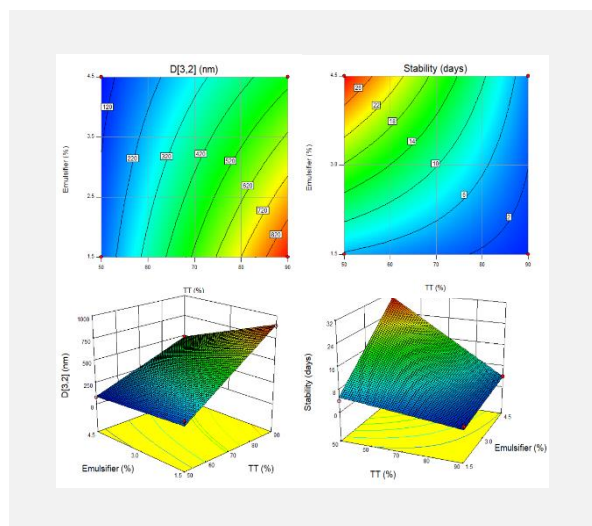
- [1] J. Rojas et al., *International Journal of Pharmacy and Pharmaceutical Sciences*, 8 (2016) 13-23.
- [2] N. R. Savadkouhi et al., *Food Science and Nutrition*, 8 (2020) 1264-1271.
- [3] E. Touitou, B. Godin, *Journal of Drug Delivery Science and Technology*, 17 (2007) 303-308.
- [4] E. Touitou et al., *Journal of Controlled Release*, 65 (2000) 403-418.
- [5] N. Nainwal et al., *Journal of Liposome Research*, 29 (2019) 103-113.
- [6] A. Ascenso et al., *International Journal of Nanomedicine*, 10 (2015) 5837-5851.
- [7] D. Mishra et al., *European Journal of Pharmaceutical Sciences*, 33 (2008), 424-433.
- [8] X. Q. Niu et al., *International Journal of Pharmaceutics*: X, 1 (2019) 100027.

Formation and stabilisation of oil-in-water nanoemulsions using binary emulsifier mixtures of *Tribulus terrestris* extract and *Quillaja* bark saponin

T.B. Schreiner^{1,2,3,4}, A. Santamaria-Echart^{1,2}, A.M. Peres^{1,2}, M.M. Dias^{3,4}, S.P. Pinho^{1,2}, M.F. Barreiro^{1,2*}

¹Centro de Investigação de Montanha, Instituto Politécnico de Bragança, Campus de Santa Apolónia, 5300-253 Bragança, Portugal; ²Laboratório Associado para a Sustentabilidade e Tecnologia em Regiões de Montanha (LA SusTEC), Instituto Politécnico de Bragança, Campus de Santa Apolónia, 5300-253 Bragança, Portugal; ³Laboratory of Separation and Reaction Engineering – Laboratory of Catalysis and Materials (LSRE-LCM), Faculty of Engineering University of Porto, Rua Dr. Roberto Frias, S/N, 4200-465 Porto, Portugal; ⁴Associate Laboratory in Chemical Engineering (ALiCE), Faculdade de Engenharia, Universidade do Porto, R. Dr. Roberto Frias, S/N, 4200-465, Porto, Portugal.

*barreiro@ipb.pt



Emulsifiers are used in many industrial fields, with the natural origin ones gaining increasing relevance. Identifying diversified sources as natural emulsifiers is a pertinent topic for sustainability principles. Saponin-rich extract *Tribulus terrestris* (TT) was evaluated as a viable alternative to *Quillaja* bark saponin (QS). An experimental design using binary emulsifier mixtures of TT with QS was carried out by varying their composition, content, and processing conditions (HPH cycles). Emulsions were characterised by zeta potential, morphology, droplet size, and stability. Zeta potential indicated stable emulsions; even creaming was observed in samples with a low emulsifier and high TT%. Diameter of emulsions was between 78-921 nm, with smaller sizes agreeing with the higher stability. Statistical analysis revealed an optimum composition range of emulsifier (3.9-4.5% wt.) and TT content (50-56% wt.) to reach stable products. Overall, TT can provide an effective solution combined with QS.

Introduction

Nanoemulsions are colloidal dispersion systems comprising two immiscible phases and an emulsifier resulting in a single macroscopic phase. They have small-sized droplets and can be kinetically stable over long time scales. The emulsifier is the main ingredient responsible for maintaining the stability and performance of emulsified products [1]. However, most commercialised products use synthetic emulsifiers. Nevertheless, consumers' appetite to buy more sustainable, natural, and environmentally friendly ingredients is increasing due to environmental and social awareness and healthy habits [2]. In this context, saponins are a class of natural surface-active substances versatile in terms of physicochemical and biological properties. Most studies address saponins from the *Quillaja* Saponaria Molina tree (QS). Although it proved to be an excellent emulsifier, there is a current need to identify and apply alternative saponin sources mainly due to sustainability, cost, and prevention of plant overexploitation. The saponin-rich extract *Tribulus terrestris* (TT) from puncture vine can be highlighted as a promising alternative, presenting a critical micelle concentration (CMC) of 0.59 g/L, circa 30% lower than other studied extracts, and superior emulsifying capacity/stability and foaming capacity/stability [3].

Objectives

This work aims to study the effect of combining TT saponin-rich extract with *Quillaja* bark saponin in forming (and stabilising) nanoemulsions applying an experimental design methodology. A nanoemulsion characterisation comprising particle size, zeta potential, morphology by optical microscopy, and storage stability (30 days) was carried out.

Methods

A series of oil-in-water (O/W) nanoemulsions were prepared using a fixed O/W ratio (w/w) of 10/90. For the preparation, the oil and water phases were mixed using an Ultraturrax at 11000 rpm for 3 min. This coarse emulsion was after subjected to high-pressure homogenisation (HPH) at 100 MPa. The prepared nanoemulsions were fully characterised. A 2k full factorial design was performed with three factors and three replicates at the central point. Three independent factors were evaluated, namely the TT content in the emulsifier mixture (X_1 , 50-90 % wt.), the emulsifier content in the emulsion (X_2 , 1.5-4.5 % wt.), and the number of HPH cycles (X_3 , 5-15 cycles), whose effects were studied on selected responses (droplet diameter, $D[3,2]$, (Y_1 , nm), and stability (Y_2 , days)).

Results

The collected data are shown in Table 1. Excepting TQ6 all nanoemulsions appeared milky-like without phase separation. That specific samples showed a CI value of 2% right after preparation. This fact could be associated with the lower emulsifier content (1.5% wt.) and the higher TT content (90% wt.) of the used emulsifier mixture. The zeta potential ranged from -47 to -41 mV, indicative of sample stability. However, some prepared samples did not remain stable for a 30 days-period, even when presenting highly negative initial zeta potential values. Although this parameter is generally a suitable indicator of stability, other factors, such as macroscopic inspection, must be conducted to guarantee highly stable emulsions. In this work, such stability parameters were monitored over time. The samples corresponding to the central point (samples TQ1, TQ5, and TQ7) presented a slightly higher emulsifier content (3.0% wt.) and a lower TT content (70% wt.), revealing intermediate stability (10 days). This behaviour

indicates that stability is favoured when the emulsifier content increases and TT content decreases (a CI of only 6% was determined after 30 days). The maximum CI value (10%) was observed for TQ6 and TQ10. Both presented large droplet diameters, which according to Stokes' law, caused stability to decrease.

Table 1. Zeta Potential, droplet diameter, stability, and CI for the 11 samples (TQ1-TQ11) of the experimental design.

	Zeta Potential (mV)	Droplet Diameter (nm)	Stability (days)	CI 30 days (%)
TQ1	-44.0	215	11	6
TQ2	-43.5	78	30	0
TQ3	-41.1	103	30	0
TQ4	-46.6	112	7	8
TQ5	-44.0	197	10	6
TQ6	-46.4	921	0	10
TQ7	-43.9	169	10	6
TQ8	-41.2	493	4	8
TQ9	-46.8	210	4	8
TQ10	-43.6	493	4	10
TQ11	-45.4	892	2	8

The morphology of the emulsions was analysed by optical microscopy. Generally, on the first day, most samples showed droplets of round shape and high homogeneity. The sample TQ3 presented one of the minor droplet diameters, making its visualisation difficult. This morphological aspect was maintained even after 30 days, in accordance with the observed high stability (CI of 0% after 30 days). By contrast, the sample TQ7, which showed a small droplet diameter after production, evidenced considerable growth over time. This effect is reflected in a CI of 6%. One of the most unstable samples, TQ11, which promptly resulted in two separated phases after production, has shown an upper phase rich in oil, characterised by large oil droplets (original dispersed phase) dispersed in water.

Table 2. Regression parameters (β 's coefficients) of the optimal Multiple Linear Regression Models were established for the droplet diameter (nm) and stability with time (days) using a stepwise variable selection method for the 2^3 experimental design and respective model quality parameters.

Source	Droplet diameter D[3,2](nm)		Stability (days)	
	β 's coefficients (coded factors)	P-value	β 's coefficients (coded factors)	P-value
Model	----	<0.0001	----	<0.0001
Intercept	+412.80	<0.0001	+10.13	<0.0001
X_1 – <i>Tribulus terrestris</i> (%)	+286.95	<0.0001	-7.62	<0.0001
X_2 – Emulsifier (%)	-120.95	<0.0001	+6.88	<0.0001
X_3 – Number of cycles	-	n.s.	-	n.s.
X_1X_2	-85.80	0.0003	-5.38	<0.0001
Curvature	----	<0.0001	----	0.7877
Lack of fit	----	0.2992	----	0.1774
Quality parameter	Values		Values	
Adequate Precision	36.5		39.4	
R^2	0.9922		0.9934	
R^2_{adj}	0.9882		0.9901	
R^2_{pred}	0.9709		0.9746	

Acknowledgements

The authors are grateful to FCT for financial support through national funds FCT/MCTES (PIDDAC) to CIMO (UIDB/00690/2020 and UIDP/00690/2020), SusTEC (LA/P/0007/2021), LSRE-LCM (UIDB/50020/2020 and UIDP/00690/2020), and ALiCE (LA/P/0045/2020). FCT for the PhD research grant of T.B. Schreiner (2020.05564.BD). National funding by FCT, P.I., through the institutional scientific employment program contract of A. Santamaria-Echart.

References

- [1] Y. Yang et al., *Food Hydrocolloids*, 30 (2013) 589-96.
- [2] D.J. McClements et al., *Advances in Colloid and Interface Science*, 234 (2016) 3-26.
- [3] T.B. Schreiner et al., *Colloids and Surfaces A: Physicochemical and Engineering Aspects*, 623 (2021) 126748.

The experimental droplet size measurements enabled the analysis of the effect of the obtained formulations. The TQ2 and TQ3 samples showed the lowest values, 78 and 103 nm, respectively, favouring the stability of the emulsions against aggregation and creaming since the droplets' rate movement was proportional to the square of their radius, according to Stokes' law [2]. The triplicates of the central point presented similar values, with an average of 194 nm, reflecting the excellent reproducibility of the experiments. The less stable samples (TQ6, TQ8, TQ10, and TQ11) reached the largest diameters, where samples TQ6 and TQ11 have a size around 900 nm, again in agreement with Stokes' law. The statistical regression parameters are shown in Table 2. The analysis pointed out that for both dependent variables (i.e., D[3,2] and stability), the number of cycles did not have a significant effect, nor did none of the respective second and third-order parameters (P-value > 0.05). So, these terms were not included in the final models. X_1 and X_2 parameters, also shown in Table 2, significantly influence emulsions' mean droplet diameter, TT content being the most relevant variable. The size reduction was observed as the emulsifier increased and the TT content decreased. Stability was also selected to evaluate the emulsions' potential, and their variability within all the tested parameters was small. The highest stability occurs at higher emulsifier percentages (4.5%) and when the TT content reaches 50%, as shown in the Graphical Abstract.

Conclusions

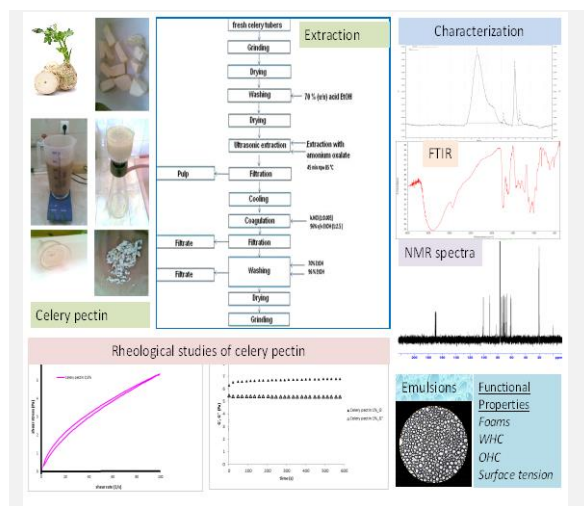
Nanoemulsions were successfully produced using emulsifier mixtures of TT extract with QS. The most stable samples (CI of 0% for 30 days) were achieved using an emulsifier mixture comprising TT at 50% wt. and a content of 4.5% wt. The samples were produced using 5 (TQ2) and 15 HPH (TQ3) cycles, achieving 78 and 103 nm droplet diameters, respectively. The performed design of experiments using as responses the droplet diameter and stability pointed out that the optimum samples need emulsifier contents between 3.9 and 4.5% wt., and emulsifier mixtures with 50 to 56% wt. of TT content.

Physicochemical characterization and functional properties of a pectic polysaccharide fraction isolated from celery tubers

N. Petkova¹, D. Vassilev^{2*}, M. Ognaynov³, D. Yaneva², M. Krystijan⁴, M. Todorova⁵, I. Vasileva¹, I. Petrova⁶, P. Denev¹

¹Department of Organic Chemistry and Inorganic Chemistry, University of Food Technologies, Technological Faculty, 26 Maritza Blvd, 4002 Plovdiv, Bulgaria; ²Department of Mathematics, Informatics and Natural Sciences, Technical University of Gabrovo, 4 Hadji Dimitar str., Gabrovo, 5300, Bulgaria; ³Laboratory of Biologically Active Substances, Institute of Organic Chemistry with Centre of Phytochemistry, Bulgarian Academy of Sciences, 139 Ruski Blvd, 4000 Plovdiv, Bulgaria; ⁴Department of Carbohydrates Technology, Faculty of Food Technology, University of Agriculture in Krakow, Balicka Street 122, 30-149 Krakow, Poland; ⁵Department of Organic Chemistry, Faculty of Chemistry, University of Plovdiv, 4000 Plovdiv, Bulgaria; ⁶Department of Tourism and Gastronomy Management, University of Food Technologies, Faculty of Economics, 26 Maritza Blvd, 4002 Plovdiv, Bulgaria.

*dvassilev@tugab.bg



Low-methyl-esterified pectic polysaccharide from celery tubers (*Apium galvolean*s) was isolated by ultrasonic extraction and further characterization of the composition and functional properties was performed. Anhydrouronic acid content was 60.2 g/100 g, as glucuronic and galacturonic acid were the main sugars together with arabinose. Infrared and nuclear magnetic resonance spectroscopy showed typical signals for pectin structure. The celery pectin consisted of two fraction different molecular weight populations in the range of 27–912 kDa. The obtained pectin demonstrated promising surface tension, emulsifying and foaming properties at concentration 0,5%. The functional properties indicated that celery pectin possessed promising water- and oil-holding capacity and non-Newtonian liquid behavior. Celery pectin at 0.5% pectin solution were characterized by poor thixotropic properties, while 1% pectin solution demonstrated a more stable system. Therefore, due to its chemical and functional properties celery pectin could be successfully applied in food, cosmetics and pharmaceutical preparations.

Introduction

Pectins from alternative sources as a vegetable (celery, leek, tomatoes, and potatoes) deserve attention due to its improved functional properties. The current study aimed to isolate pectic polysaccharide from celery tubers (*Apium galvolean*s) and further characterization of the composition and functional properties to be performed.

Results

Celery pectin was isolated by ultrasonic extraction with 0.8% (w/v) aqueous ammonium oxalate. The pectin was evaluated as low-methyl-esterified (46.0%) with a degree of acetylation of 2%. The sugar composition indicated that galacturonic acid, galactose, arabinose, and rhamnose were the main constituents (Table 1). Infrared and nuclear magnetic resonance spectroscopy confirmed the pectin nature and structure of polysaccharides. The functional properties indicated that celery pectin possessed promising water- and oil-holding capacity and non-Newtonian liquid behavior (Table 2 and Fig 1). The celery pectin demonstrated significant foaming ability and promising emulsifying properties in a concentration of 1%.

Conclusions

The isolated polysaccharide fraction from celery tubers could be successfully applied as an emulsifier and stabilizer and foaming agent in cosmetics, food products, and pharmaceutical supplements.

Table 1. Yield and chemical characterization of celery pectin.

Characteristics of celery pectin	Values
Yield (g/100 g dw)	29.0
Protein, %	1.9
Hyp, %	3.4
Total phenols, mg/g	0.1
Anhydrouronic acid content, g/100 g dw (mol%)	60.2(87.5)
Glucuronic acid	2.1
Galacturonic acid	3.7
Neutral sugars, mol%	
Rhamnose	0.5
Galactose	2.7
Arabinose	7.9
Glucose	0.3
Mannose	0.0
Fucose	1.0
Xylose	0.0
Degree of methylation, %	46.0
Degree of acetylation, %	1.6

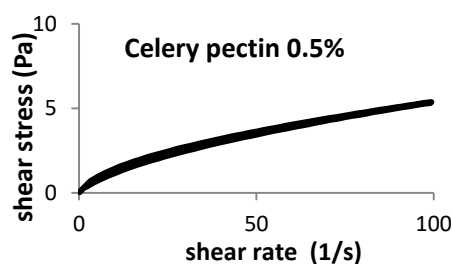


Figure 1. Flow curve of 0.5% pectin solution.

Table 2. Rheological parameters of 0.5% pectin solution.

Sample	Ostwald de-Waele model			Area of hysteresis loop (Pa/s)	
	K (Pa.sn)	n (-)	R ²	Thixotropy	Antithixotropy
Celery pectin	0.376±0.010 ^a	0.580±0.013 ^d	0.999±0.001	22.14±1.12 ^a	0.00±0.00 ^c

Parameters in columns denoted with the same letters (a, b, etc.) do not differ statistically at the level of confidence p=0.05

Acknowledgements

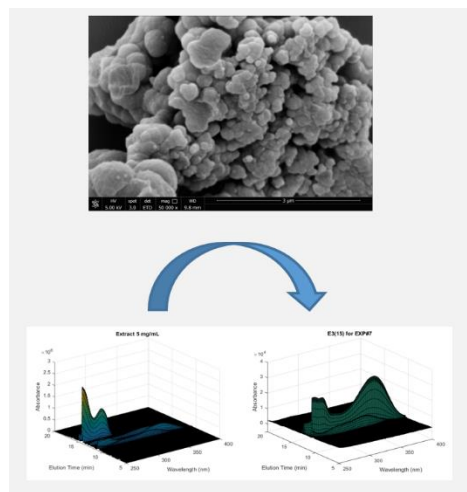
This study was financially supported by the Project BG05M2OP001-1.002-0023 "Competence Center "Intelligent Mechatronics, Eco- and Energy-Saving Systems and Technologies", financed by the Operational Program "Science and Education for Smart Growth", co-financed by the European Union through the European Structural and Investment Funds.

Design of functional polymers and sorption/desorption processes for the valorization of bioactive compounds in olive leaf

A. Almeida^{1*}, C. Martins¹, C.P. Gomes¹, R.C.S. Dias¹, M.R.P.F.N. Costa²

¹Polytechnic Institute of Bragança-Mountain Research Center (CIMO), Bragança 5300-253, Portugal; ²LSRE-LCM-Laboratory of Separation and Reaction Engineering—Laboratory of Catalysis and Materials Faculty of Engineering-University of Porto, Porto 4200-465, Portugal.

*ayssata@ipb.pt



Novel polymeric materials to be used in sorption/desorption processes aiming at the valorization of olive leaf contained compounds were designed and synthesized at the gram scale. The designing of the developed polymer networks was made considering the targeting of different kinds of molecules in olive leaf, namely secoiridoids, flavonoids, lignans and triterpenoids. Molecular imprinting with diverse templates and selection of different kinds of functional monomers were considered within this purpose. The tailored polymers were synthesized through particular working conditions concerning the kind of initiator and initiation mechanisms (e.g. thermal polymerization and photo UV polymerization), polymerization temperature (in the range 25 to 60 °C) and reactants concentrations for manipulation of the morphology and size of the produced particles.

The tailored adsorbent particles were packed in preparative columns (e.g. up to ~ 80 mL bed volume and adsorbent mass up to ~ 40 g) and used in sorption/desorption processes with olive leaf extracts at high concentration in low water content mixtures (e.g. 5 mg/mL in ethanol/water 80/20). The ability for the fractionation of the mixture of compounds in the initial complex extracts is demonstrated with generation of high-added value products with relevance for circular bio-economy.

Introduction

A huge amount of olive leaf containing economically exploitable bioactive compounds is currently discarded each year. Indeed, in spite of the considerable quantities of secoiridoids (e.g. oleuropein), flavonoids (e.g. luteolin glycosides) or triterpenoids (erythrodiol, oleanolic acid, etc) contained in olive leaf, around 4.5 million tons of this biomass (by-product of the olive and olive-oil production) are nowadays mostly burned or used for animal feed. It is well known that the different kinds of polyphenols and triterpenoids in olive leaf present important bioactive effects and therefore a high potential for application in the food, feed, chemical, nutraceutical, cosmetic and pharmaceutical sectors [1].

Irrespective to the method used to get the bioactive compounds in olive leaf (hydroalcoholic, organic solvents, SCCO₂, etc), a mixture of diverse compounds is obtained at the end.

Therefore, separation and purification steps should be implemented to get individual molecules or mixtures suitable for practical applications, namely technological approaches based on sorption/desorption processes [2]. Functional and molecularly imprinted polymers (MIPs) are candidates to play an important role in the purification of such complex extracts [3-6].

Results and Discussion

The tailoring of new adsorbents leads to potentially improved sorption/desorption processes concerning the loading capacity and selectivity towards target compounds [3-6]. Here, we

present results with novel synthesized materials which design encompasses the change of template molecules in molecular imprinting, the kind of functional monomers and their polarity as well as the polymerization conditions (concentration, temperature, etc) with impact on the size/morphology of the particles (see Table 1).

An example for the outcomes obtained with the processing of olive leaf extracts with the developed functional particles is presented in Figure 1. The HPLC-DAD analyses put into evidence the production of a flavonoid rich fraction from a complex olive leaf extract using a sorption/desorption process with the MIP particles (Figure 1 - left). Note that the initial olive leaf extract is rich in oleuropein while the flavonoids are minority compounds (see Figure 1 - right). Figure 2 highlights the use of the synthesized tailored adsorbents and the designing of solvent-gradient and temperature-swing sorption/desorption processes for the fractionation of different kinds of compounds in olive leaf (secoiridoids, phenolic acids, phenyl alcohols, glycosylated flavonoids and aglycone flavonoids). Fractions rich in phenyl alcohols and phenolic acids were produced with aqueous solvents, secoiridoids were fractionated when increasing the ethanol content while flavonoids were isolated using high organic content solvents. Other case studies are presented in this work, also with triterpenoids rich olive leaf extracts, demonstrating the performance of the developed materials and processes with the generation of high-added value compounds with relevance in circular bio-economy.

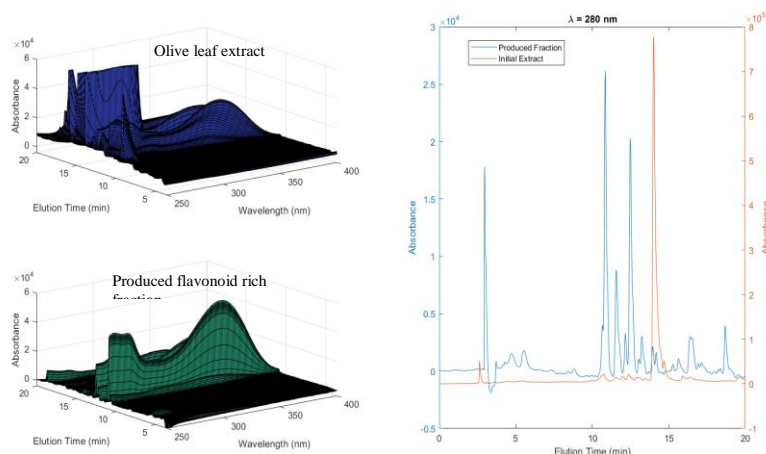


Figure 1. HPLC-DAD analyses showing the production of a flavonoid rich fraction from an olive leaf extract with high oleuropein content through a sorption/desorption process with the developed MIP particles.

Table 1. Representative set of functional polymers prepared for the valorization of bioactive compounds in olive leaf.

Material	Template	Funct. M1	Funct. M2	Crosslinker	Initiator	Init. Mechanism	T (°C)
#1	Oleuropein 70%	<i>N</i> -vinylpyrrolidone	-	MBAm	VA044	Thermal	40
#2	Oleuropein 70%	Acrylamide	-	EGDMA	AIBN	Photo UV	25
#3	Quercetin	4-vinylpyridine	-	EGDMA	AIBN	Thermal	60
#4	Oleanolic Acid	2-(dimethylamino)ethyl methacrylate	Styrene	MBAm	VA044	Thermal	40

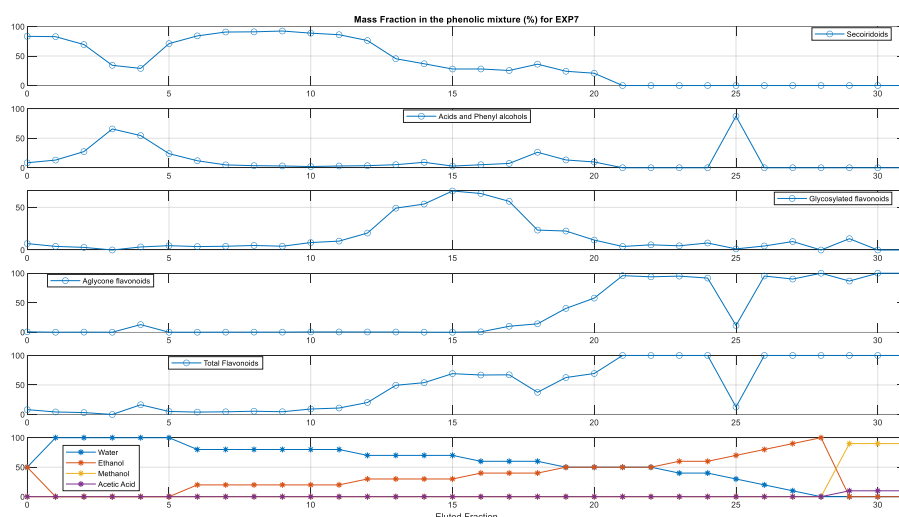


Figure 2. Mass fraction (%) of different phenolic families in fractions collected by desorbing MIP particles pre-loaded with an olive leaf extract. The different fractions were generated through a solvent gradient process (from water to methanol/acetic acid 9/1) combined with temperature change (sorption at room temperature and desorption at 40 °C).

Acknowledgements

We acknowledge the support through the OLEAF4VALUE project. This project has received funding from the Bio-Based Industries Joint Undertaking under the European Union's Horizon 2020 research and innovation programme under grant agreement n° 101023256. Catarina Gomes acknowledges to FCT for the PhD scholarship 2020.06057.BD. We also thank to NATAC for providing the olive leaf extracts and the aid with the identification by LC-MS of compounds there contained. Rolando Dias is grateful to the Foundation for Science and Technology (FCT, Portugal) for financial support through national funds FCT/MCTES (PIDDAC) to CIMO (UIDB/00690/2020 and UIDP/00690/2020) and SusTEC (LA/P/0007/2020). Mário Rui Costa acknowledges the support by LA/P/0045/2020 (ALiCE), UIDB/50020/2020 and UIDP/50020/2020 (LSRE-LCM), funded by national funds through FCT/MCTES (PIDDAC).

References

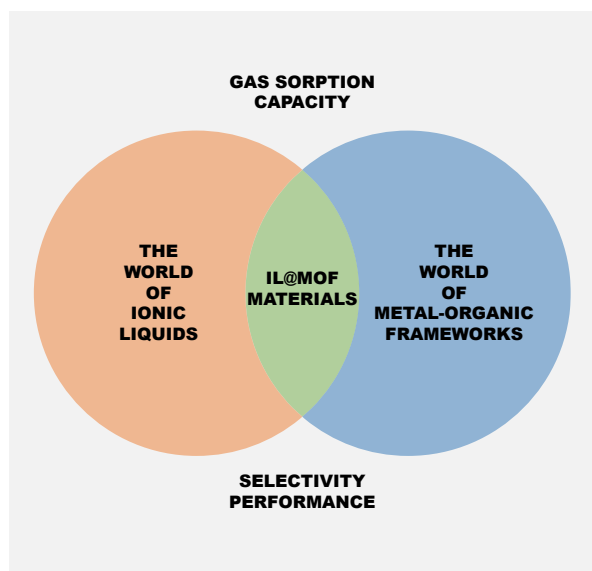
- [1] OLEAF4VALUE, Olive leaf multi-product cascade based biorefinery. Accessed March 2023. <https://oleaf4value.eu>
- [2] P. Pérez-Larrán et al., *Current Opinion in Food Science*, 23 (2018) 165-172.
- [3] C.P. Gomes et al., *Chromatographia*, 82 (2019) 893-916.
- [4] C.P. Gomes et al., *Chromatographia*, 83 (2020) 1539-1551.
- [5] C. Didaskalou et al., *Green Chemistry*, 19 (2017) 116-3125.
- [6] C.P. Gomes et al., *Macromolecular Reaction Engineering*, 17 (2023) 2300011.

Impregnating ionic liquids into a MOF: assessment of the cationic and anionic effects and their impact on sorbent properties

T.J. Ferreira¹, A.T. Vera¹, B.A. de Moura¹, C. Cabral¹, L.M. Esteves¹, T.O. Carvalho¹, J. Pais¹, L.P.C. Silva², M. Tariq¹, P.M. Reis¹, J.M.S.S. Esperança¹, I.A.A.C. Esteves^{1*}

¹LAQV/REQUIMTE, Department of Chemistry, NOVA School of Science and Technology, FCT NOVA, 2829-516 Caparica, Portugal; ²Departamento de Engenharia Química e de Petróleo, Universidade Federal Fluminense, Niterói, 24210-240, Brasil.

*i.esteves@fct.unl.pt



Metal-Organic Frameworks (MOFs) and Ionic Liquids (ILs) are promising alternatives to more traditional materials for carbon dioxide (CO₂) separation, given their physical and chemical properties and their affinity towards this gas. In this work, several combinations of IL@MOF composites, where the IL was impregnated into the MOF ZIF-8 structure, were produced to determine the impact of the cationic and anionic structures on sorbent properties such as gas sorption capacity and selectivity performance. The cationic structure can be tailored to improve ideal selectivity between 0-1 bar, with long side-alkyl chains being favored for this purpose. Synergistic effects can be promoted with an appropriate anion, such as carboxylate-based ones. These anions led to composites that had higher CO₂ sorption capacity than pristine ZIF-8 between 0-1 bar.

Introduction

Anthropogenic carbon dioxide (CO₂) emissions have increased the mean global temperature of planet Earth. This gas is the main contributor to global warming and, consequently, to climate change [1]. Efforts have been made to develop environmentally-friendly chemical processes to mitigate CO₂ emissions to the atmosphere.

Gas adsorption-based processes are low-energy demanding, cost-effective, and make use of adsorbent materials with high capacities for the species to be captured or separated [2]. One of the key aspects of gas adsorption-based processes is the chosen adsorbent. A novel type of porous material, Metal-Organic Frameworks (MOFs), have appeared and are a potential alternative to more traditional adsorbents.

MOFs consist of metal atoms or small metallic clusters linked to organic functional groups, thus possessing a high degree of tunability in their composition and shape, and appealing properties for adsorption processes, such as very high specific surface area and porosity, as well as high thermal and chemical stabilities [3].

MOF-based composites have been considered to improve sorbent properties such as the gas sorption capacity and selectivity performance of its precursor [4]. Ionic liquids (ILs) are a class of materials that have been used for CO₂ capture. They are conventionally defined as salts with low melting point (below 373 K) and consist of organic, asymmetric cations and organic or inorganic anions. ILs exhibit unique properties such as negligible vapor pressure, nonflammability, and high thermal and chemical stabilities and some show high CO₂ solubility [5]. The high level of tunability of both cation and/or anion can be used to enhance CO₂ solubility. The impregnation of an IL into the structure of a MOF should desirably lead to synergistic effects that improve sorbent properties.

Objectives

The main objective of this work was the assessment of the sorption capacities of CO₂, CH₄, and N₂ in the produced composites compared with the pristine MOF. The implications of the cationic and anionic structures in sorbent properties were determined from the obtained isotherms.

Methods

ILs of different cationic families and with distinct anions were impregnated into MOF ZIF-8 by the wet impregnation method. The characterization techniques used for these composites include Helium Pycnometry, N₂ Sorption-Desorption at 77 K, Fourier Transform Infrared Spectroscopy (FT-IR), Powder X-Ray Diffraction (PXRD), Scanning Electron Microscopy (SEM), and Transmission Electron Microscopy (TEM). CO₂, CH₄, and N₂ adsorption-desorption equilibrium isotherms were obtained between 0-16 bar and at 303 K using a previously reported standard static gravimetric method [6].

Results

Characterization results indicate that IL impregnation was successful and did not affect the crystalline structure of the MOF. The textural properties of the composites were inferior to the pristine ZIF-8 ones due to the partial occupation/blockage of pores by the IL.

The incorporation of an IL into ZIF-8 generally led to an increase in ideal CO₂/CH₄ and CO₂/N₂ selectivities, particularly between 0-1 bar. The selectivity of the composite could be tailored by the chosen cation, with longer side alkyl chains being favorable to increase this property. At higher pressures than 1 bar, longer side-alkyl chains were unfavorable in terms of gas sorption capacity.

Regarding the anionic effect, these structures were the main ones responsible for the sorbent properties of IL@ZIF-8 materials.

Many anions were screened and carboxylate-based ILs were found to promote synergistic effects. This is because their respective composites sorbed more CO₂ than pristine ZIF-8

between 0-1 bar. The enhanced sorption of this gas led to higher ideal CO₂/CH₄ and CO₂/N₂ selectivities at this pressure range.

Acknowledgements

The authors thank Fundação para a Ciência e Tecnologia, FCT/MCTES (Portugal), for financial support through PhD grants SFRH/BD/139627/2018 and COVID/BD/152969/2023 (T. J. F.), PhD grant 2021.07148.BD (T.O.C.), FCT Investigator contract (2021.00511.CEECIND – P. M. R), projects PTDC/CTM-CTM/30326/2017, PTDC/EQU-EQU/32050/2017 and 2022.03931.PTDC, and Material Characterization Laboratory (LAMATE/UFF) for enabling N₂ sorption-desorption equilibrium measurements. Additionally, the work was also partially supported by the Associate Laboratory for Green Chemistry, LAQV, which is funded by national funds from FCT/MCTES (UIDB/50006/2020, UIDP/50006/2020 and LA/P/0008/2020). The NMR spectrometers are part of The National NMR Facility, supported by FCT/MCTES (Grant RECI/BBB-BQB/0230/2012).

References

- [1] Intergovernmental Panel on Climate Change (IPCC), Climate Change 2013: The Physical Science Basis. Contribution of Working Group I to the Fifth Assessment Report of the Intergovernmental Panel on Climate Change, Cambridge University Press, Cambridge, United Kingdom and New York, NY, USA.
- [2] A. Bonilla-Petriciolet, D. I. Mendoza-Castillo, H. E. Reynel-Ávila, Adsorption Processes for Water Treatment and Purification, Springer, 2017, 2.
- [3] H.-C. Zhou et al., Chemical Reviews, 112 (2012) 673-674.
- [4] I. Ahmed, S. H. Jung, Materials Today, 17 (2014) 136-146.
- [5] Z. Lei et al., Chemical Reviews, 114 (2014) 1289-1326.
- [6] B.C.R. Camacho et al., Separation and Purification Technology, 141 (2015) 150-159.

Wet-spinning of lignin-nanocomposite fibres for stronger carbon fibres using low-cost ionic liquids

Z. Kamora*, A. Brandt-Talbot, M. Shaffer

Imperial College London, White City, W12 0BZ, London, United Kingdom.

*zk520@ic.ac.uk

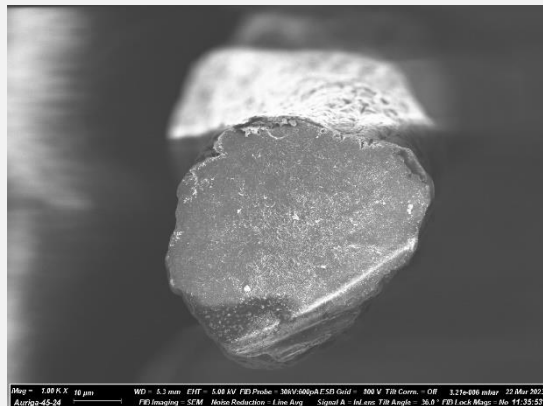


Figure 1. Scanning electron microscope image of cross-section of carbonised lignin nanocomposite fibre shows distribution and preservation of nanotubes (scale, 10 µm)

This investigation reports on a three-component system for the fabrication of lignin nanocomposite fibres (LNCF) (diameter 55-60 µm), *via* wet-spinning. Lignin was isolated by the low-cost and easy to prepare ionic liquid, dimethyl butyl ammonium hydrogen sulphate [DMBA][HSO₄]. Well dispersed single-walled nanotubes (SWNTs) in the same solvent, [DMBA][HSO₄], have been incorporated as the polymer additive to improve the mechanical performance and fibre integrity. The lignin biopolymer provided stabilisation in the single walled nanotube dispersion leading to consistent extrusion of structured fibres containing a > 94 % of lignin and > 3 % of SWNTs. The addition of SWNTs improved the carbon yield of the fibres by 10-15 % from the former fibres that contained PVA and lignin. SWNTs may improve the overall graphiticity of the carbonised fibres and well-aligned nanotubes will greatly enhance the fibre strength properties [1].

Introduction

Carbon fibre reinforced composites are an interesting material in military/aerospace engineering, automotive industries and in sporting equipment due to their low density and high strength to weight ratio [2,3]. However, the manufacture of carbon fibre is unsustainable as it is derived from polyacrylonitrile (PAN) which is a petrochemical resource and expensive because it requires high carbonisation temperatures. The precursor accounts for 50 % of the cost of carbon fibre [2,3,4].

Lignin may pose as a suitable replacement precursor as it is a biopolymer with a high carbon content and readily available as annual extraction is over 60 million tonnes [3,4]. Delignification occurs with ionic liquids and is the highlighted process for this study [4].

Dimethyl butylammonium hydrogen sulfate ([DMBA][HSO₄]) is the ionic liquid (IL) of interest. It is derived from low-cost starting materials and relatively easy to prepare. Lignin can be extracted by [DMBA][HSO₄] *via* the ionosolv process [4].

Lignin is not spinnable alone due to its low molecular weight and amorphous structure [3,4]. A co-polymer with a high molecular weight is added to the dope (spinning liquid) to aid fibre formation.

At present, the tensile properties of lignin carbon fibres (LCFs) fall below the industrial requirements for vehicle manufacture (172 GPa strength and Young's modulus 1.72 GPa respectively). Lignin carbon fibres also result in low carbon yield [5]. Therefore, it is necessary to explore alternative materials that can be incorporated to improve the spinnability and mechanical properties of lignin carbon fibres.

Single walled nanotubes (SWNTs) are recognised for their high electrical conductivity, thermal stability, Young's modulus and tensile strength [6]. SWNTs can add

graphitisation and alignment to fibres. These benefits can be displayed if SWNTs are dispersed individually. Carbon nanotubes (CNTs) have proven difficult to disperse due to the low affinity of the sp² hybridised atoms along the surface of a carbon nanotube [6].

There is a lack of research into alkyl ammonium ILs to disperse SWNTs [6]. Therefore, the effectiveness of [DMBA][HSO₄] as a dispersive solvent for SWNTs was tested as well as the spinnability of the lignin nanocomposite dope was examined.

Objectives

1. To identify the prime concentration of SWNTs that can be dispersed in [DMBA][HSO₄] containing 5.02 % water. Purity of the SWNTs is the main factor affecting a quality dispersion in [DMBA][HSO₄]
2. Wet-spin fibres continuously for tensile characterisation and elemental analysis
3. Prove that the addition of SWNTs may provide structure, aid fibre formation, and improve graphitisation in lignin nanocomposite fibres (LNCF)

Methods and results

A spinning dope is prepared by dissolving lignin in [DMBA][HSO₄] and then dispersing the SWNTs with this solution using a pestle and mortar. The composite dope is wet-spun into a coagulation bath containing water to enable diffusion of the solvent within the fibres. The ionic liquid can also be recycled. The fibres are collected, dried, thermally stabilised and carbonized for further processing.

Optical micrographs (Figure 2) identified that the composite dope retained an adequate dispersion of SWNTs as shown by the reduced particle size 1-2 µm. Polarized images show signs of birefringent SWNTs represented by the lighter sections of the images. Aligned nanotubes are identifiable through

birefringence. Obtaining a homogenous dispersion is vital for spinning consistent fibres with minimal defects. The fibres were wet spun successfully with nearly circular cross sections and could be suspended with a small weight to dry overnight.

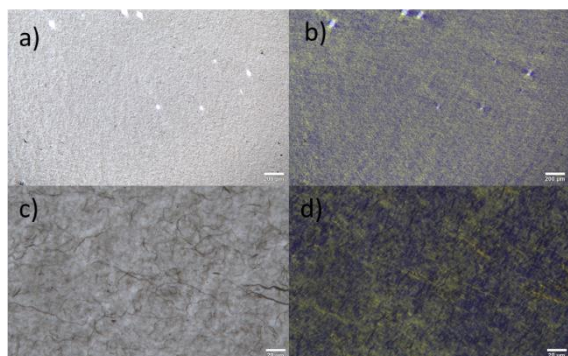


Figure 2. Composite dope, 0.5 wt. % SWNTs mixed for 60 min. in [DMBA][HSO₄] containing lignin. a) 200 μm b) polarized 200 μm c) 20 μm d) polarized 20 μm

The thermogravimetric analysis (TGA) data shows a remarkable increased carbon yield for the LNCF of 54 % in Figure 3 after the addition of SWNTs. Previous carbon yield for lignin/PVA ranged from 32-36 % yield. The increase in carbon yield may be attributed to the addition of SWNTs.

Acknowledgements

I would like to thank the supervisors of this project, Agnieszka Brandt-Talbot and Milo Shaffer for continued support and intellectual input.

References

- [1] Z. Kamora et al., 2022, Carbon fibres from lignin and carbon nanotubes, Patent no. 11332.
- [2] X. Huang, *Materials*, 2 (2009) 2369-2403.
- [3] E.A. Adeshiyan, *Sustainable Lignin for Carbon Fibers: Principles, Techniques, and Applications*, 1, Springer Nature Switzerland AG, 2019, 51-58.
- [4] A. Brandt et al. *Green Chemistry*, 15 (2013) 550-583.
- [5] J. Jin et al., *ACS Sustainable Chemistry & Engineering*, 6 (2018) 14135-14142.
- [6] J.P. Lu, *Journal of Physics and Chemistry of Solids*, 58 (1997) 1649-1652.

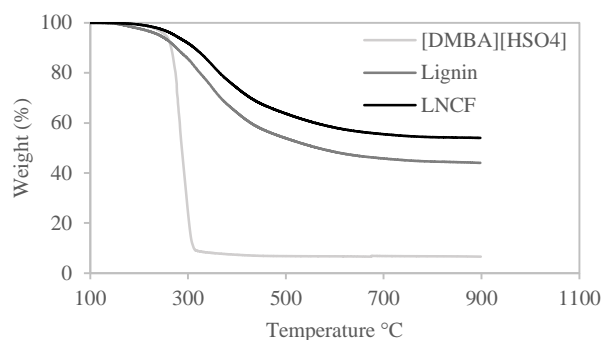


Figure 3. Imitation of carbonisation using thermogravimetric analysis of lignin nanocomposite fibres and its respective starting reagents to estimate carbon yield

Conclusions

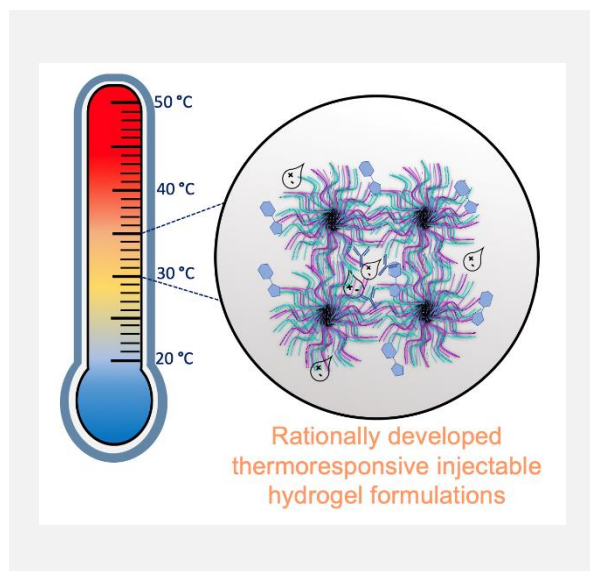
This investigation proved that lignin nanocomposite carbon fibres can be produced efficiently with the three components in a homogenous dope. Fibres were wet-spun using the low-cost ionic liquid as a multifunctional solvent and SWNTs to enhance fibre mechanical properties. Continuous structured fibres formed after SWNTs were added and enabled carbonised fibres with a high carbon content > 94 %. The low-cost ionic liquid was functional for both the dissolution of lignin and to disperse the carbon nanotubes. SEM images proved retainment of the SWNTs within the fibre. Future work will involve tensile testing and structural analysis *via* XRD.

Rationally developed injectable choline chloride-based hydrogel formulations for controlled and local therapeutic delivery applications

T.A. Shmool^{1*}, A.P. Constantinou², T.K. Georgiou², J.P. Hallett¹

¹Department of Chemical Engineering, Imperial College London, Imperial College Road, London SW7 2AZ; ²Department of Materials, Imperial College London, Exhibition Road, London SW7 2AZ, United Kingdom.

*t.shmool20@imperial.ac.uk



Herein, we overcome the limitations of conventional therapeutic carriers and develop a series of injectable hydrogel formulations for localised and controlled therapeutic delivery applications. We integrate choline chloride with our in-house synthesised polymer OEGMA300₂₀-*b*-BuMA₂₂-*b*-DEGMA₁₁, to produce thermoresponsive hydrogels which can be injected in liquid form and gel in the body. We demonstrate that incorporating traditional pharmaceutical excipients can suppress the aggregation and increase the stability of the model therapeutic immunoglobulin G and the hydrogel. Our hydrogel platforms exhibit enhanced mechanical strength compared to the traditional hydrogel formulation and show great promise for effectively protecting, targeting and locally delivering therapeutics in a controllable fashion.

Introduction

The greatest limitations of conventional therapeutic carriers is achieving effective controlled and localised delivery of the therapeutics. Hydrogels are water swollen three-dimensional networks that can be engineered to provide precise spatiotemporal control over the release of diverse therapeutics [1]. Injectable hydrogels can be delivered via syringe-needle injection, offering minimally invasive delivery in a controlled manner. However, injectable hydrogels suffer from poor physical stability and relatively low mechanical strength [1]. In addition to overcoming delivery barriers, hydrogels must cope with the inherently high aggregation propensity of the loaded therapeutics [1]. Thus, further work is required for hydrogels to be effectively deployed for controlled and localised therapeutic delivery.

Objectives

In this work, we overcome the limitations of existing hydrogel delivery systems. We engineer injectable, thermoresponsive stable hydrogel platforms, designed to exist as aqueous solutions at 25 °C for injection and follow a sol-gel transition in the body. Developed systems will be designed to protect and locally deliver therapeutics in a controlled fashion.

Methods

We rationally integrate our recently developed thermoresponsive polymer OEGMA300₂₀-*b*-BuMA₂₂-*b*-DEGMA₁₁ (OBD) with choline chloride ([Cho][Cl]) to create injectable [Cho][Cl]-hydrogels [2,3]. We use 20 w/w% OBD and 15 w/w% [Cho][Cl], shown to promote gelation processes and improve the stability of biomolecules [2,4]. We design three formulation buffers for the [Cho][Cl]-hydrogels, each containing excipients at proportions previously found favorable for suppressing protein aggregation in aqueous solutions [5-7]. The formulation buffers include F1 containing arginine (0.39

w/w%), histidine (0.15 w/w%) and sucrose (2.7 w/w%); F2 containing trehalose (5.0 w/w%), histidine (0.29 w/w%) and glycerol (0.25 w/w%); and F3 containing sucrose (4.2 w/w%), histidine (0.64 w/w%) β -cyclodextrin (6.7 w/w%) and polyvinylpyrrolidone (PVP) (3.0 w/w%). We also produce a control system containing the hydrogel in phosphate buffered saline (PBS), a conventional buffer. In each formulation we also include the model therapeutic immunoglobulin G (IgG) at 1:1.4 w/w% IgG: formulation buffer.

Results

We performed dynamic light scattering measurements to determine the aggregation propensity of each formulation. We found that the [Cho][Cl]-hydrogel in F1, F2 and F3 exhibited significantly lower hydrodynamic diameter values (46 ± 0.06 , 41 ± 0.3 and 41 ± 0.4 nm, respectively) compared to the hydrogel in PBS (67 ± 0.3 nm). This indicated that our formulations served to suppress IgG and hydrogel aggregation; however, aggregation was enhanced for the control formulation. Next, we performed temperature variable rheology experiments to determine the gelation temperature (T_{gel}) and strength of each hydrogel. For each formulation, at 25 °C, the storage modulus (G') was lower than the loss modulus (G''), confirming liquid state at room temperature (Figure 1), critical for injectability. We observed that the hydrogel in PBS presented a T_{gel} of 40 °C. In contrast, the [Cho][Cl]-hydrogel in F1, F2 and F3 exhibited T_{gel} values of 33, 30 and 31 °C, respectively, within the biologically relevant regime (below 37 °C). We found that the [Cho][Cl]-hydrogels were stronger compared to the control. Specifically, we found maximum storage modulus of 290, 250, 330 Pa for the [Cho][Cl]-hydrogel in F1, F2 and F3, respectively; and 260 Pa for the control. This demonstrates that our excipient matrix strongly modulates the T_{gel} value and strength of each hydrogel platform.

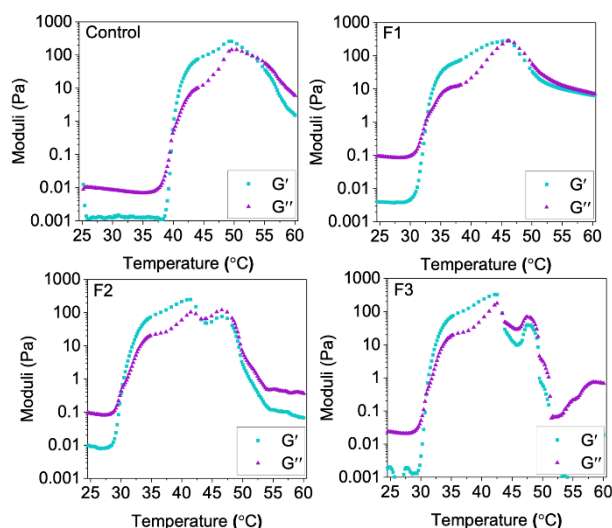


Figure 1. Storage (G' , cyan squares) and loss (G'' , purple triangles) moduli as a function of temperature for the control hydrogel in PBS, and for [Cho][Cl]-hydrogel in F1, F2 and F3.

Discussion

It has previously been shown that the addition of traditional excipients, including sugars and polyols, can increase T_{gel} , reduce gel strength and result in destabilisation [8,9]. However, when combining such excipients with the [Cho][Cl]-hydrogel, we observed that for each formulation the T_{gel} was lower and the mechanical strength was higher compared to the hydrogel in PBS. This highlights the role of [Cho][Cl] in tuning the thermoresponsive and mechanical properties of the hydrogel, achieving the desired outcome. We suggest that macromolecular confinement effects strongly regulate T_{gel} , G' and the stability of

the [Cho][Cl]-hydrogels. Likely, [Cho][Cl] promoted strong hydrogen bonding and electrostatic interactions and molecular confinement effects, serving to stabilise the hydrogel network [4,10]. Additionally, we propose that for each formulation, the integration of the excipients with the [Cho][Cl]-hydrogel, contributed to the formation of intricate hydrogen bonding networks, lacking for the hydrogel in PBS. Specifically, glycerol and arginine could form strong hydrogen bonds with the hydroxyl groups of sucrose and trehalose, respectively [5,6]; thereby increasing the stability of the IgG and the [Cho][Cl]-hydrogel network. Additionally, the highest stability found for [Cho][Cl]-hydrogel in F3 can be attributed to the formation of strong hydrogen bonds between β -cyclodextrin, sucrose and PVP, resulting in a more stable matrix, confining the [Cho][Cl]-hydrogel and preventing IgG and hydrogel aggregation. Thus, the electrostatic, hydrophobic networks and hydrogen bond formation ability of [Cho][Cl] and the excipients [10] provide an important contribution to IgG and hydrogel stability, and serve to hinder aggregation, lower T_{gel} , and raise G' compared to the conventional formulation of the hydrogel in PBS.

Conclusions

We consider that hydrogels with T_{gel} higher than body temperature would be unsuitable for sustained and controlled injectable delivery. Similarly, a hydrogel with T_{gel} and gelation window well below 37 °C would not readily form a gel in the body following administration. Given that our stable [Cho][Cl]-hydrogels presented T_{gel} values between 30 to 33 °C and aggregation of the therapeutic and hydrogel was prevented, these offer innovative advanced injectable platforms to be explored for localised, controlled and targeted delivery applications.

Acknowledgements

This research is funded by the Department of Health and Social Care using UK Aid funding and is managed by the Engineering and Physical Sciences Research Council (EPSRC, grant number: EP/R013764/1). The views expressed in this publication are those of the authors and not necessarily those of the Department of Health and Social Care. A.P.C. acknowledges support from the Department of Materials at Imperial College London, the EPSRC Doctoral Prize Fellowship (EP/M506345/1) and the EPSRC Impact Acceleration Grant (EP/R511547/1).

References

- [1] J. Li et al., Nature Reviews Materials, 12 (2016) 16071.
- [2] A.P. Constantinou et al., Macromolecules, 54 (2021) 1943-1960.
- [3] T.A. Shmool et al., Polym. Chemistry, 13 (2022) 2340-2350.
- [4] T.A. Shmool et al., Chemical Science, 12 (2021) 196-209.
- [5] M. Batens et al., Physical Chemistry Chemical Physics, 22 (2020) 17247-17254.
- [6] T.A. Shmool et al., European Journal of Pharmaceutics and Biopharmaceutics, 144 (2019) 244-251.
- [7] C. Haeuser et al., Journal of Pharmaceutical Sciences, 109 (2020) 807-817.
- [8] J. Tang et al., Carbohydrate Polymers, 44 (2001) 197-209.
- [9] K. Nishinari et al., Thermochemica Acta, 206 (1992) 149-162.
- [10] T.A. Shmool et al., Chemical Science, 12 (2021) 9528-9545.

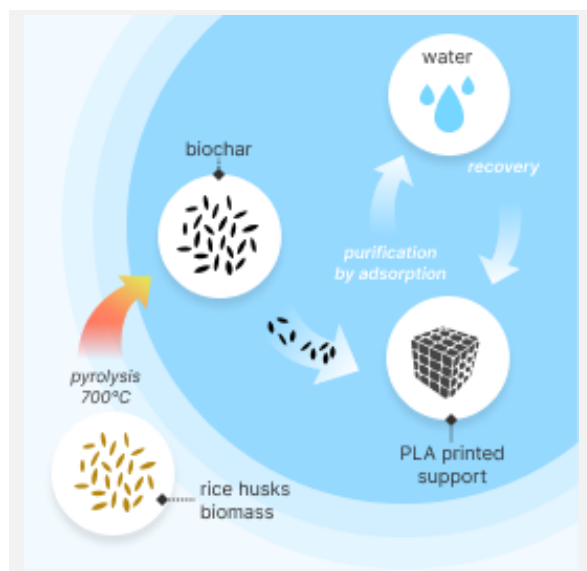
Rice husks biochar as adsorbent for removal water pollutants: the use of porous 3D printed supports

D.S. Gamarano¹, V.S. Guedes², F.C.C. Moura², M.L.B. Almeida², E. Ayres^{1*}

¹Universidade do Estado de Minas Gerais (UEMG), Rua Gonçalves Dias, 1434, Belo Horizonte – 30140-091, Brazil;

²Universidade Federal de Minas Gerais (UFMG), Avenida Antônio Carlos, 6627, Belo Horizonte - 31270-901, Brazil.

*eyres.pu@hotmail.com



Water is the most basic need and one of the crucial concerns for human beings. With the growth of new techniques and variety of materials, 3D printing is becoming more competitive in the field of water treatment. In this study, the use of a 3D printed support coated with rice husks biochar was proposed as sorbent for water pollutants removal. Surface area of this rice husks derivative varies with the previous treatment suffered by the biomass. Preliminary results have indicated that, acid pretreatment gives rise to a significant increase in surface area. The adsorption capacity of the supports can be linked to the 3D printing parameters, such as infill pattern and infill percentage. Moreover, the supports might provide a good reusability and recycling performance during repeated sorption-desorption cycles. These experiments are ongoing and will be presented soon. Here in, it is posed a preliminary proposition and discussion about the advantages and disadvantages of such supports.

Introduction

The growth of industrialization and urbanization favors a rise in the diversity of pollutants in water [1]. Comparatively to others, adsorption is a simple process with high efficiency and low cost [1]. Agricultural byproducts biomass that are available in large quantities have potential as low cost adsorbents [2]. Rice husk (RH) is an abundantly available and inexpensive agro waste, which has been widely modified and used in different applications [3]. RH has been converted into several adsorbents, such as activated carbon, biochar, silica, composite, and hydrogel, for water purification [3]. Biochar (BC) is a form of charcoal, and it is produced after a controlled thermal treatment such as pyrolysis. Rice husk-based biochar was evaluated as adsorbent to remove chlorpyrifos from domestic water. The BC demonstrated performance of adsorption practically identical to activated carbon [4]. On the other hand, regeneration and reuse of powdered adsorbents often involves capital and energy and can be a source of secondary pollution [5]. An interesting alternative to improve this step is the incorporation of the porous material on functional supports. To this end, additive manufacturing (3D printing) has attracted considerable attention, as it enables the design and fabrication of three-dimensional (3D) complex lattices [6]. The use of 3D printed supports overcomes the limitation of the secondary pollution and facilitates the recycling of powder adsorbents without any elaborate separation procedure [7]. The aim of this work is the design and fabrication of different 3D-printed supports, in which their porous structures will be uniformly decorated with BC derived from RH. Experiments comparing the efficiency of free powder adsorbent with that achieved by the various coated supports are ongoing.

Methods

Rice husk (RH) untreated and RH, refluxed with HCl (6N) for 3 hours to leach metallic impurities, were used to produce biochar

(BC). For the pyrolysis process samples were placed into a tubular oven, where temperature and heating rate were adjusted to 700 °C and 10 °C min⁻¹, respectively, and residence time of 2 h. The supports were 3D printed with poly(lactic acid) (PLA) filament using FDM technology. The parts were printed using infills with different patterns and percentages. The coating of the 3D devices followed the protocol reported by others [6]. Briefly, BC was dispersed in acetone by sonicating for 30 min. After that, the suspension was mixed with polyvinylidene fluoride (PVDF) dissolved in DMF (7.5 wt%) and sonicated for another 30 min. To obtain a concentrated ink, the acetone was evaporated. Finally, the obtained ink was sprayed onto the 3D devices with an airbrush and dried at room temperature (Figure 1). The specific surface area of BC derived from untreated and treated RH was determined by nitrogen adsorption, from the N₂ adsorption and desorption isotherms, at 77 K, using the Quantachrome equipment (NovaWin2 model). The specific surface area was calculated by applying the equation derived by Brunauer, Emmett and Teller (multipoint method BET).

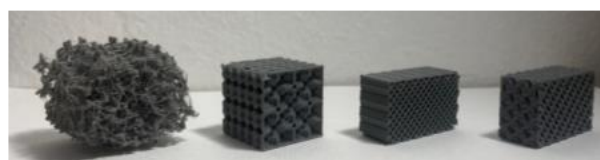


Figure 1. 3D printed supports coated with BC from treated RH.

Results

Chemical methods have been efficiently adopted to modify crop straws in order to improve their pore and surface properties and to enhance their performance for adsorption purposes [8]. The main role of acid modification is to enhance the content of acidic functional groups by the removal of mineral impurities [8]. Real et al. [9] reported the strong interaction between the silica and the potassium contained in the rice husks. According to them, if the K⁺ cations are not removed prior to the heat treatment they might cause a dramatic decrease of the surface area in the

derived products. Table 1 presents the surface area of RH derivatives: untreated BC and treated BC.

Table 1. Surface area of RH biochar.

Sample	Surface area (m ² /g)
Untreated BC	5.58
Acid treated BC	121,7

Okoya et al. [4] found a BET surface area of RH biochar of 97.20 m²/g. This value is in accordance with the value of treated BC, as shown in Table 1. Interesting, these authors carried out the treatment with HCl after the pyrolysis. Yakout and colleagues [11] have prepared a series of modified biochars derived from rice straw. They reported values of BET surface areas from 46.9 to 179.7 for biochar treated with H₂SO₄ and KOH, respectively. Herein, the value of surface area is suitable for the proposed application. The other side of the work is the manufacture of 3D printed supports with the surface functionalization with adsorbents. In the case of this work, this is achieved with the deposition of adsorbent particles onto the surface of the support. Fagundes et al. [11] have published a complete review on this subject. According to them, new research opportunities, among others, can arise in the functionalization approaches of the 3D

printed supports, in order to avoid the leaching of the adsorbent particles. In the case of the present research, this issue is also a concern. But the main focus is on the relationship between support geometry and adsorption efficiency. About that, another comprehensive review Ghosal et al. [12] reported a 3D-printed PLA filter coated with Fe(III) oxide for arsenite removal. According to the citation, 3D printing enables modulation of surface area and volume, which have direct effect in removal efficiency. The filter in question has shown 129.87 mg g⁻¹ adsorption capacity of arsenite.

Conclusions

The pyrolysis conversion of biomass agriculture waste into value-added biochar is an attractive approach. Biochar is a suitable porous material to be used as adsorbent in adsorption process of water pollutants. The regeneration and reuse of adsorbents has economic and environmental benefits in terms of avoiding the use of a new adsorbent and preventing the arise of secondary pollution. An interesting alternative to circumvent this drawback is the coating of the porous material onto functional supports. 3D printed porous supports can provide high and tunable surface areas with direct influence over the adsorption capacity. In this sense, more detailed studies are ongoing in our laboratory.

Acknowledgements

The authors thank Minas Gerais State Research Support Foundation (FAPEMIG), Coordination for the Improvement of Higher Education Personnel (CAPES) and National Council for Scientific and Technological Development (CNPq) for funding research.

References

- [1] A. da S.V. de Almeida et al., *Journal of Environmental Chemical Engineering*, 9 (2021) 104891.
- [2] M. Ahmaruzzaman, V.K. Gupta, *Industrial & Engineering Chemistry Research*, 50 (2011) 13589-13613.
- [3] S.K. Shukla, Chapter 6 in *Green Materials for Wastewater Treatment*, (ECSW, volume 38), 1st Ed., Springer, Cham, 2020, 366 pages.
- [4] A.A. Okoya et al., *Current Journal of Applied Science and Technology*, 39 (2020) 1-11.
- [5] D. Saidulu et al., *Journal of Environmental Management*, 306 (2022) 114461.
- [6] M. del Rio et al., *Applied Materials Today*, 24 (2021) 101130.
- [7] H.S. Far et al., *ACS Applied Materials & Interfaces*, 14 (2022) 44488-44497.
- [8] M.J. Ahmed et al., *Journal of Molecular Liquids*, 330 (2021) 115616.
- [9] C. Real et al., *Journal of the American Ceramic Society*, 79 (1996), 2012-2016.
- [10] S.M. Yakout et al., *Environmental Engineering & Management Journal (EEMJ)* 14.2 (2015) 473-480.
- [11] A.P. Fagundes et al., *Journal of Environmental Chemical Engineering*, 10 (2022) 108049.
- [12] P. Ghosal et al., *Advanced Sustainable Systems*, 6 (2022) 2100282.

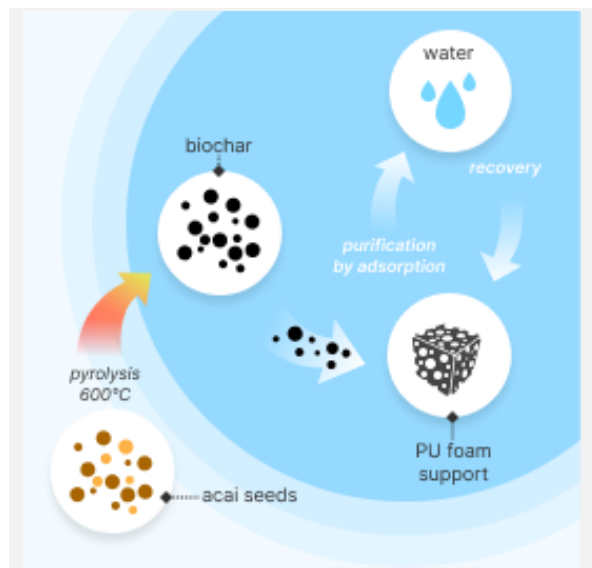
Activated biochar from acai seeds (*Euterpe oleracea* Mart): the use of polyurethane foam as adsorbent device for water treatment

M.L.B. Almeida^{1*}, E.H.M. Nunes¹, B.R. Barrioni², L.A.F.P. Cohen³, E. Ayres³

¹Universidade Federal de Minas Gerais (UFMG), Avenida Antônio Carlos, 6627, Belo Horizonte, 31270-901, Brazil;

²Universidade Federal dos Vales do Jequitinhonha e Mucuri (UFVJM), Avenida 1, Janaúba, 39440-000, Brazil; ³Universidade do Estado de Minas Gerais (UEMG), Rua Gonçalves Dias, 1434, Belo Horizonte, 30140-091, Brazil.

*marys@denc.ufmg.br



The acai (*Euterpe oleracea* Mart.) production chain is one of the most important for the North region of Brazil. Its importance is linked to the cultural identity and the health benefits that the consumption of the fruit promotes. However, the high production of residues derived from industrial processing is responsible for environmental, social and economic problems in the main cities of the region. The biochar generated by pyrolysis of the original biomass demonstrated an enormous increase of surface area, especially when alkali activated. In the present work, the first results of the use of biochar as adsorbent is presented. Here in the cells of polyurethane foam are decorated with the biochar. Thus, the foam serves as support for the biochar. This enables to reuse the adsorbent, avoiding secondary pollution when it is applied in water treatment. This approach is in line with current environmental worries and also with the issue of adding value to wastes.

Introduction

The valorization of bio-based wastes and by-products, inserting them in the circular economy paradigm, is a new development strategy to circumvent the drawbacks caused by the accumulation of waste and its improper disposal [1]. These bio-based wastes and by-products include several different wastes from the food and agriculture industries [2,3]. One of these bio-based wastes is the acai seed (*Euterpe oleracea*), the waste of acai pulp production [4]. These residues accumulate, in large amounts, over the urban regions of the main cities in Amazon region (Figure 1). Biochar commonly has large volume of pores and high surface area. This material has been used as an adsorbent for removing contaminants from aqueous solutions [5]. This work aimed to investigate the use of acai seed, through the production of biochar by pyrolysis with subsequent chemical activation. The alkali treatment increases the specific surface area due to improvement in the structure of biochar. The more common used alkalis for modification are sodium hydroxide and potassium hydroxide [4,6]. An important issue during the adsorption of contaminants using porous materials, especially when using powdered solids, is the recovery of the adsorbent. In this context, an interesting alternative is the use of porous polyurethane (PUF) as a support to facilitate the sorbent recovery [7].



Figure 1. Acai seeds accumulated over Amazon urban regions.

Methods

The acai seeds, as the pulp extraction residues, were collected on the streets of Belem city (north of Brazil). The material was dried for 12 h in an oven at 100 °C and manually scraped to remove any fiber adhered to the seed. For the pyrolysis process samples were placed into a tubular oven, where temperature and heating rate were adjusted to 600 °C and 10 °C min⁻¹, respectively, and residence time of 2 h. The biochar activation was carried out by mixing it with KOH (3:1). The protocol followed reference [4]. The specific surface area was determined by nitrogen adsorption, from the N₂ adsorption and desorption isotherms, at 77 K, using the Quantachrome equipment (NovaWin2 model). The specific surface area was calculated by applying the equation derived by Brunauer, Emmett and Teller (multipoint method BET). The PUF to serve as support was synthesized following the procedure previously reported by this research group [7]. The coating was prepared according to reference [6]. In short, BC was dispersed in acetone by sonicating for 30 min. After that, the suspension was mixed with polyvinylidene fluoride (PVDF) dissolved in DMF (7.5 wt%) and sonicated for another 30 min. To obtain a concentrated ink, the acetone was evaporated. Finally, cubic sample of PUF (3 x 3 cm) was immersed into the dispersion and kept at room temperature for 1 h. After removing the excess of dispersion, the coated foam was dried at 60 °C for 24 h. (Figure 2).



Figure 2. PUF coated with acai seeds activated biochar.

The morphologies of PUF and PUF coated with activated biochar were captured through X-ray microtomography

(Skyscan 1174, Aartselaar, Belgium) with an X-ray source voltage of 35 kV, a current of 800 μ A, and a three dimensional (3D) spatial resolution of 8.05 μ m. The 3D models were assembled with CTAn v.1.15.4.0 (Bruker-microCT, Belgium). In addition, CTVol v.2.3.1.0 (Skyscan, Bruker-microCT, Belgium) was used to visualize the 3D images.

Results

The presence of adsorbent onto the PUF surface, instead of incorporated in the form of composite, significantly increases the adsorption efficiency. Our research group reached 83% of adsorption efficiency removing Trifluralin from aqueous solution [8]. Pure adsorbent removed 95.3%, however, its use is not feasible due to the difficulty of recovering [8]. The specific surface area is one of the properties that have a significant effect on the adsorptive characteristics of a material, and consequently on its potential for industrial application [9]. The values of surface area are presented in Table 1.

Table 1. Evolution of surface area values.

Samples	Surface area ($\text{m}^2 \text{g}^{-1}$)
Acai seeds	0,693
Biochar	720
Activated biochar	1039

The values showed in Table 1 are in accordance with the literature, where acai seeds activated biochars, produced via pyrolysis at 400 and 600 $^{\circ}\text{C}$, gave rise to surface areas of 1150 and 929 g m^{-2} , respectively [4]. Figure 3 presents the images of the 3D structures obtained through microtomography of PUF and coated PUF.

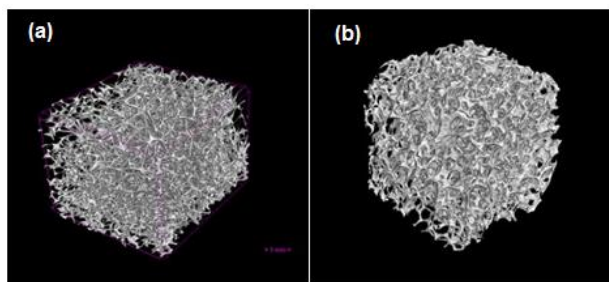


Figure 3. Microtomography 3D images of (a) PUF and (b) coated PUF.

Acknowledgements

The authors thank Minas Gerais State Research Support Foundation (FAPEMIG), Coordination for the Improvement of Higher Education Personnel (CAPES) and National Council for Scientific and Technological Development (CNPq) for funding research.

References

- [1] T.-L. Chen et al., *Science of the Total Environment*, 716 (2020) 136998.
- [2] M. Vicente et al., *Mix Sustentável*, 5 (2019) 85-96.
- [3] C. Maraveas, *Materials*, 13 (2020) 262.
- [4] A.S.V. Almeida et al., *Journal of Environmental Chemical Engineering*, 9 (2021) 104891.
- [5] S.F. Lütke et al., *Journal of Environmental Chemical Engineering*, 7 (2019) 103396.
- [6] M.J.B.H.H. Ahmed, E.H. Hummadi, *Journal of Molecular Liquids*, 330 (2021) 115616.
- [7] M.L.B. Almeida et al., *Journal of Hazardous Materials*, 346 (2018) 285-295.
- [8] M.L.B. Almeida et al., *Journal of Polymers and the Environment*, 28 (2020) 2511-2522.
- [9] N.I.A. Acevedo et al., *Brazilian Applied Science Review*, 5 (2021) 39-57.
- [10] K. Uram et al., *Materials*, 14.19 (2021) 5616.

Some morphological characteristics of these samples were taken from the microtomography analysis. The open porosity of PUF and coated PUF is 84.03 and 80.69, respectively. Moreover, total porosity corresponds exactly to the open porosity. Thus, the total porosity slightly diminished due to the presence of biochar, less than expected. The behavior of average cell (pore) size was also observed (Figure 4). It is possible to perceive a wider pore size distribution in the coated sample (b).

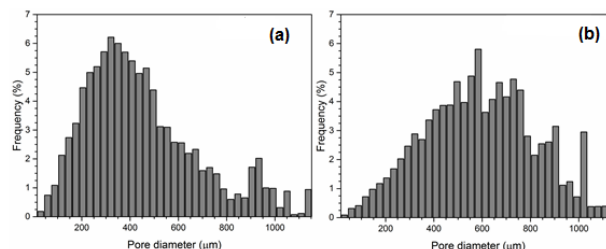


Figure 4. Pore size distribution obtained by microtomography: (a) PUF and (b) coated PUF.

There is a study of the influence of biochar on the morphology of the cells of polyurethane foam [10]. However, in this case the biochar was introduced to the polyol. Thus the biochar had direct effect in the foaming process. Here in, the biochar was added onto the surface of the polyurethane already foamed. It was a physical process. In view of this, the change in the pore size distribution might be attributed to the lack of homogeneity of the biochar in the foam cells.

Conclusions

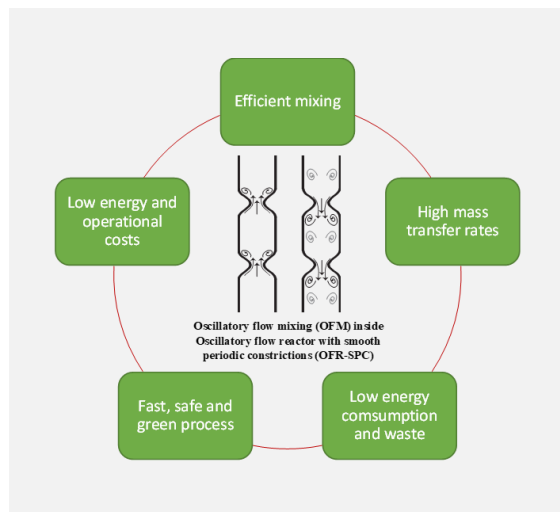
In this study, the use of biochar derived from waste acai seeds (*Euterpe oleracea*) has been purposed as adsorbent. The use of polyurethane foam as support will be explore. This enables the developed device to be reused. The goal is to make the adsorption process for the water treatment more environmentally friendly, avoiding secondary pollution. We are presenting the first results with this kind of biomass, the experiments are still ongoing. Our research group has already proven successful in using polyurethane foams as a support for adsorbents for the decontamination of aqueous solutions.

Continuous oscillatory flow reactor: effect of liquid flow rate on gas-liquid mass transfer in a gas-liquid-solid system

F. Almeida*, F. Rocha, A. Ferreira

LEPABE - Laboratory for Process Engineering, Environment, Biotechnology and Energy, Faculty of Engineering, University of Porto, Rua Dr. Roberto Frias, 4200-465 Porto, Portugal; ALiCE - Associate Laboratory in Chemical Engineering, Faculty of Engineering, University of Porto, Rua Dr. Roberto Frias, 4200-465 Porto, Portugal.

*up201202863@edu.fe.up.pt



In this work, the effect of the liquid flow rate on gas-liquid mass transfer was studied for the first time in a gas-liquid-solid system in an oscillatory flow reactor provided with smooth periodic constrictions (OFR-SPC). For that different superficial gas velocities (u_G) and oscillatory conditions (amplitude (x_0), frequency (f)), operating in co and counter-current modes were used. For each liquid flow rate the volumetric liquid-side mass transfer coefficient ($k_L a$) and gas holdup (ϵ_G) were determined. The results show that increasing liquid flow rate in counter-current mode increase $k_L a$ and ϵ_G . When a solid phase is present, the liquid recirculation allows the fluidization of particles, solving the common mass transfer problems at low oscillations ($x_0 < 9$ mm $f < 2$ Hz). These results are very promising, the liquid flow rate imposed on the OFR-SPC in counter-current proved to be a crucial parameter, since it improved gas-liquid mass transfer without compromising power consumption, which is important for chemical and bioprocess intensification.

Introduction

Nowadays it is vital for the chemical industry to develop sustainable and eco-efficient processes. Process intensification is a promising field that can effectively tackle the process challenges and at the same time offer the potential for a “clean processing” in order to diminish the environment impact of the chemical industry. The intensification of a gas-liquid process is a challenge, mainly when a solid phase is present since the solids significantly affect the mass transfer process. Recently, some authors have proposed the oscillatory flow reactor provided with smooth periodic (OFR-SPC) to enhance gas-liquid mass transfer of several chemical processes, even with a moderate power consumption [1–4]. The OFR is a column provided with periodic baffles and it is characterized by the oscillatory movement imposed on the liquid, controlled by oscillation amplitude and frequency [4]. So far, all the studies published were conducted only without liquid recirculation (co-current and counter-current). Therefore, the present study intends to evaluate the liquid recirculation, for the first time in an OFR-SPC, on gas-liquid mass transfer in presence of solids (up to 30% (v/v)). The volumetric liquid-side mass transfer coefficient ($k_L a$) and gas holdup (ϵ_G) were evaluated.

Materials and Methods

Experimental setup and operating conditions

Mass transfer experiments were performed in an OFR-SPC mounted vertically and operated in semi-batch mode at pressure of 1.013×10^5 Pa and at temperature of 298.15 K. The O_2 mass transfer was evaluated by controlling the following variables: (i) oscillation amplitude (4, 9 and 19 mm) and frequency (1, 2, 3 and 4 Hz); (ii) superficial gas velocity (0.49 to 9.8 mm s^{-1}); (iii) solid's load (0, 10 and 30% (v/v)) polystyrene (EPS) ($d_p = 1.1$ mm); (iv) liquid flow rate (Q) (230, 505 and 728 ml min^{-1}). A rotational motor (Cat R100 C, United States) was attached to a piston at the tube to oscillate

the liquid according to a set of oscillation amplitudes (x_0) and frequencies (f), thus providing a sinusoidal oscillation.

Different values of superficial gas velocity (u_G) (4.9×10^{-4} to 9.8×10^{-3} m s^{-1}) obtained from gas flow rate controlled by a gas flow meter (Alicat Scientific, United States). The liquid flow rate was controlled through a pump (RX200 Y2, United States) and operated in co-current and counter current.

Mass transfer experiments

To evaluate the O_2 mass transfer in distilled water the dynamic method was used and performed as follows. Firstly, before each experiment, the liquid was deoxygenated by injecting N_2 into the bottom of the reactor (stripping process) by a needle with an inner diameter of 0.3 mm, until the dissolved oxygen concentration reaches zero. At this point Air (79% N_2 and 21% O_2) was injected into the reactor by the same needle (absorption process) and controlled by the flow controller. The dissolved oxygen concentration in the liquid was continuously measured using a fibre optic oxygen meter (OXR50-HS, Pyroscience) introduced at the top of the OFR-SPC and connected to the FireSting O_2 instrument (Pyroscience). The variation of the O_2 concentration over the time was recorded in a computer through the FireSting Logger software for further processing. Afterwards, the volumetric liquid-side mass transfer coefficient ($k_L a$) was calculated from the measurement of the O_2 concentration with time.

Results and Discussion

Figure presents the volumetric liquid-side mass transfer coefficient ($k_L a$) and gas holdup (ϵ_G) values determined in a liquid phase of distilled water, as function of the superficial gas velocity (u_G) ranging from 0.49 to 9.8 mm s^{-1} for 230 ml min^{-1} (Figure 1A) and for 505 ml min^{-1} (Figure 1B) under different oscillation frequencies varying from 1 to 4 Hz, and oscillation amplitudes ranging from 4 to 19 mm.

According to these data the $k_L a$ is influenced by the superficial gas velocity (u_G) and oscillatory conditions

applied to the liquid. Increasing the u_G from 0.49 to 9.8 mm s^{-1} the $k_L a$ increased an average of 8 – fold. The increase in $k_L a$ with u_G was expected, since typically, the increase in u_G promotes an increase in gas holdup and in specific interfacial area, as a consequence of the high number of bubbles injected per unit of time.

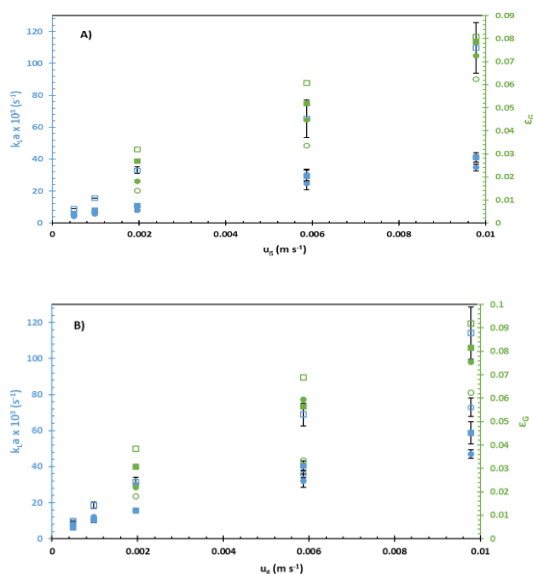


Figure 1. Effects of oscillatory conditions on $k_L a$ ($x_0 = 4$ mm: ● - $f = 1$ Hz, ○ - $f = 4$ Hz; $x_0 = 19$ mm: ■ - $f = 1$ Hz, □ - $f = 4$ Hz) and ε_G ($x_0 = 4$ mm: ● - $f = 1$ Hz, ○ - $f = 4$ Hz; $x_0 = 19$ mm: ■ - $f = 1$ Hz, □ - $f = 4$ Hz) for all range of u_g in counter-current mode: A) $Q = 230$ ml min^{-1} ; B) $Q = 505$ ml min^{-1} .

In what concerns to the oscillatory conditions, both amplitude and frequency influenced the $k_L a$. According to Figure 1 an increase in the oscillation frequency from 1 to 4 Hz led to an increase in the $k_L a$, an average of 1.5-fold. This increase is moderate at low oscillation frequencies ($f = 1$ and 2 Hz), being more pronounced at higher oscillation frequencies ($f = 3$ and 4 Hz). This effect of the oscillation frequency in the $k_L a$ was markedly enhanced, around 2-fold, with the increase in the oscillation amplitude from 4 to 19 mm. This way, the oscillation amplitude demonstrated the greatest effect on $k_L a$, as it rules the length of the eddies along the OFR-SPC, and, therefore, the bubble behaviour inside it. Therefore, this enhancement in the O_2 mass transfer in response to those oscillatory conditions may be a result of the oscillatory flow mixing in radial (oscillation frequency) and axial (oscillation amplitude) directions, which generates the formation and

Acknowledgements

This work was financially supported by LA/P/0045/2020 (ALiCE), UIDB/00511/2020 and UIDP/00511/2020 (LEPABE), funded by national funds through FCT/MCTES (PIDDAC). F. Almeida would wish to thank to FCT for PhD scholarship 2020.05246.BD.

References

- [1] A. Ferreira et al., Chemical Engineering Science, 170 (2017) 400-409.
- [2] A.L. Gonçalves et al., Journal of Environmental Chemical Engineering, 9 (2021) 106505-106517.
- [3] A. Ferreira et al., Chemical Engineering Journal, 262 (2015) 499-508.
- [4] F. Almeida et al., Chemical Engineering Science, 263 (2022) 118048-118066.

dissipation of strong eddies and their interaction with the SPC. This behaviour increases bubble residence time, reduces bubble size and the film thickness around the bubbles (resistance to mass transfer), created by the convection phenomena of the fluid oscillations around bubbles.

Regarding the gas holdup, it decreased an average of ~ 1.3 - fold at low oscillation amplitude ($x_0 = 4$ mm) as frequency increased from 1 to 4 Hz. This decrease in ε_G is the result of the low intensity of the eddies' propagation and their rapid dissipation. Thus, bubbles did not become trapped inside the vortices, consequently, bubble rise velocity ($2\pi f x_0$) increased, and ε_G reduced (Figure 1). On the other hand, increasing oscillation amplitude from 4 to 19 mm and oscillation frequency from 1 to 4 Hz, ε_G values increased an average of ~ 1.5 -fold (Figure 1). Under high oscillatory conditions ($x_0 > 9$ mm $f > 2$ Hz) the formed eddies occupied all the area within each SPC cavity, resulting in bubbles' breakup and their trap inside the eddies. These phenomena are responsible for the changes in the bubbles' trajectories, thus, increasing the bubble's residence time and gas holdup.

Relatively the effect of liquid flow rate it evidenced an increase on $k_L a$ and ε_G ~ 1.5 -fold and ~ 1.3 -fold, respectively, when operating in counter current mode. This increase is a consequence of the changes in bubbles behaviour, reducing their size (high mass transfer rates) and their residence time (high gas holdup). In the presence of EPS particles, the liquid recirculation allowed the fluidization of particles solving the common mass transfer problems at low oscillations ($x_0 < 9$ mm $f < 2$ Hz). Experiments in co-current mode were not possible to perform as it was impossible to keep the liquid volume inside OFR-SPC constant.

Conclusions

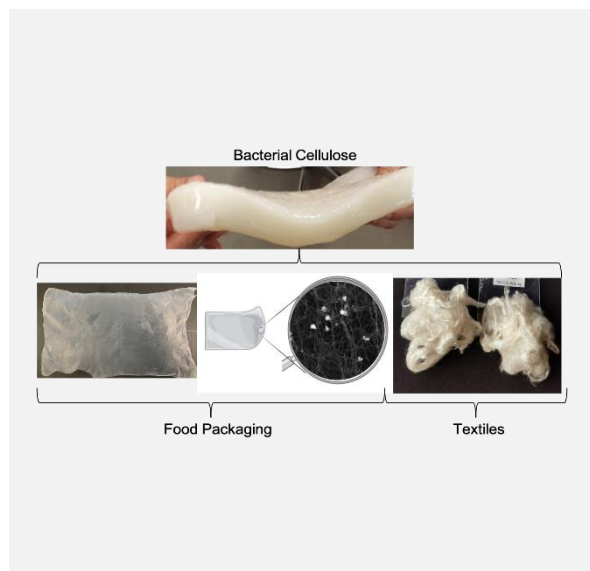
This study demonstrated that oscillatory conditions increase $k_L a$, consequence of the bubble's size decrease. The increase found in ε_G as oscillation amplitude and frequency increased was the result of an increase in bubble residence time, except at lower amplitudes where ε_G tended to decrease as frequency increased, which may be due to the oscillatory velocity imposed on the liquid. An increase in liquid flow rate resulted in a ε_G and $k_L a$ increase. A negligible influence of solids loading was found on $k_L a$ and ε_G , at low oscillations. Considering these promising results, the liquid flow rate imposed on the OFR-SPC in counter-current proved to be a crucial parameter, since it improved gas-liquid mass transfer without compromising power consumption, which is important for chemical and bioprocess intensification.

Development of bacterial cellulose composites for food packaging and textiles

F.A.G.S. Silva^{1*}, F. Dourado¹, M. Hummel², F. Poças³, M. Gama¹

¹Centre of Biological Engineering, University of Minho, Campus de Gualtar 4710-057 Braga, Portugal; ²LABELS - Associate Laboratory, 4710-057 Braga, Portugal; ³Department of Bioproducts and Biosystems, Aalto University, P.O Box 16300, 00076 Aalto Espoo, Finland; ⁴Universidade Católica Portuguesa, CBQF-Centro de Biotecnologia e Química Fina – Laboratório Associado, Escola Superior de Biotecnologia, Rua Diogo Botelho 1327, 4169-005 Porto, Portugal.

*francisco.agss@gmail.com



Most of all petroleum-based materials are used for a short period of time but then take centuries to degrade. Food packaging and textile are examples of industries that are truly dependent of synthetic materials. Therefore, there is an increasing interest on seeking alternatives to these materials. Plant nanocellulose (PNC) has been actively studied, yet the high demand may arise environmental issues such deforestation and wood processing. An alternative source is bacterial cellulose (BC), produced by bacteria of the genus *Komagataeibacter*, through fermentation. BC has a great potential due to great mechanical performance, despite some drawbacks such high water affinity (for food packaging) and high molecular weight (for textiles). Different approaches were used with the attempt to reduce water vapor permeability and functionalize BC based composite for Food packaging. For textiles, highly performing fibres were developed after using adapted Lyocell and Ioncell technologies.

Challenges of Food Packaging and Textiles

Most of all petroleum-based materials are used for a short period of time but then take centuries to degrade. About 21% of global production are accumulated in landfills and waterways [1]. These may release microplastics that have harmful effects to both terrestrial and marine ecosystems [2].

Food packaging and textile are examples of industries that are truly dependent of synthetic materials. The plastic packaging market has been expanding with a growth rate of 20–25% per year [3]. Regarding the textile industry, synthetic fibres have dominated the market representing up to 60 % of the global fibre production [4]. The most used synthetic fibre is polyester, with a market share of around 50 % of total global fibre production, followed by Cotton with 25 % of total global fibre production [4]. Cotton also raised environmental concerns due to a measureless water consumption [5]. The development of sustainable or renewable polymeric materials is an active research area, yet the overall performance of renewable polymers is often inferior when compared to traditional petroleum-based polymers [6]. Plant nanocellulose (PNC) is seen as an alternative for the production of high-performance bio-based materials. Yet the high demand for bio-based materials (such PNC), may lead to intensive deforestation for PNC extraction, as well as wood (chemical based) processing. An alternative is bacterial cellulose (BC), a cellulose produced by bacteria of the genus *Komagataeibacter*, through fermentation. BC offers interesting properties such as high porosity, biocompatibility, non-toxicity and biodegradability [7]. Either for food packaging and textile industries, BC has a great potential due to the great mechanical performance. Yet some limitations need to be surpassed, such the high-water affinity (for food packaging) as well as the high degree of polymerization (for textiles) [8,9].

BC application on Food Packaging

The first task was to develop a layered biodegradable composite based on a plasticized BC (either with glycerol or polyethylene glycol) and poly (3-hydroxybutyrate-co-3-hydroxyvalerate) (PHBV), as an attempt to improve the water vapour permeability. The PHBV coating on plasticized BC reduced significantly the water vapour permeability (from 0.990 to 0.032 $\text{g}\cdot\mu\text{m}\cdot\text{m}^{-2}\cdot\text{day}^{-1}\cdot\text{Pa}^{-1}$) and increased the hydrophobicity (contact angle from 10-40° to 80-90°). The mechanical and barrier properties of the obtained layered composite met the requirements for food packaging.

Although the results obtained being important for food packaging, its commercial use is still far off due to production costs and low production capacity, especially when compared to PNC [6]. Nevertheless, BC is a proven material to support substances that play an active/intelligent role in food packaging, with ability to carry and release active substances [10,11].

BC application on Active Food Packaging

A functionalized BC film was developed, by *in situ* incorporating zinc oxide nanoparticles (ZnO). BC_{ZnO} composites were developed and characterized, and the Zn migration assessed using food simulants (ethanol 10, 20 and 50% v/v) and chicken skin as a food model. Finally, the antimicrobial properties of BC_{ZnO} on chicken skin were also investigated. Small ZnO nanoparticles (≈ 144 nm) with low polydispersity index (≈ 0.139) were successfully produced, with high ZnO incorporation (27% $\text{m}_{\text{ZnO}}/\text{m}_{\text{BC}_{\text{ZnO}}}$) and homogeneous distribution inside BC, by the dropwise addition of NaOH, to a $\text{Zn}(\text{CH}_3\text{COO})_2\text{-PVOH}$ solution with an immersed BC membrane, followed by drying. Low Zn migration levels were observed using both food simulants and chicken skin at 4 °C (being temperature and pH dependent). Using chicken skin as a food model, the BC_{ZnO} film was effective against *Escherichia*

coli, Salmonella spp. (0.5-1.0 log reduction) and Campylobacter spp. (2.0 log reduction), showing promising results as an alternative film for active packaging.

BC application on Textiles

In order to seek an alternative sources of textile fibres, the development of man-made cellulosic fibers (MMCF) using BC was considered. Lyocell and Ioncell technologies (with collaboration of Thuringian Institute for Textile and Plastics Research and the Department of Bioproducts and Biosystems, Aalto University) were adopted to assess cellulose dissolution (using *N*-methylmorpholine-*N*-oxide (NMMO) and 1,5-

diazabicyclo [4.3.0] non-5-enium acetate ([DBNH][OAc]) as well as the spinnability of the obtained dopes. Successful spinning trials were achieved after BC dissolution on the aforementioned solvents. The resulting filaments offered competitive mechanical performance, with improved stiffness (breaking tenacities: 56 cN.tex⁻¹ BC_{Lyocell} and 60 cN.tex⁻¹ for BC_{Ioncell}) and competitive elasticity (Elongation: 8.29 % BC_{Lyocell} and 12 % for BC_{Ioncell}). These results showed that BC is a promising bio-based material that textile industry may benefit from.

Acknowledgements

This study was supported by the Portuguese Foundation for Science and Technology (FCT) under the scope of the strategic funding of UID/BIO/04469/2013 unit, BIOPROTECT - Development of Biodegradable Packaging Material with Active Properties for Food Preservation POCI-01-0247-FEDER-069858, COMPETE 2020 (POCI-01-0145-FEDER-006684) and BioTecNorte operation (NORTE-01-0145-FEDER-000004) funded by the European Regional Development Fund under the scope of Norte2020 - Programa Operacional Regional do Norte.” The authors also acknowledge the financial support of the FCT (ESF) through the grant given to Francisco A.G.S. Silva (SFRH/BD/146375/2019). The authors also thank all the support given by the Thuringian Institute for Textile and Plastics Research (TITK) and the department of Bioproducts and Biosystems at Aalto University. The authors also thank the support of Aquitex - Acabamentos Químicos Têxteis, S.A.

References

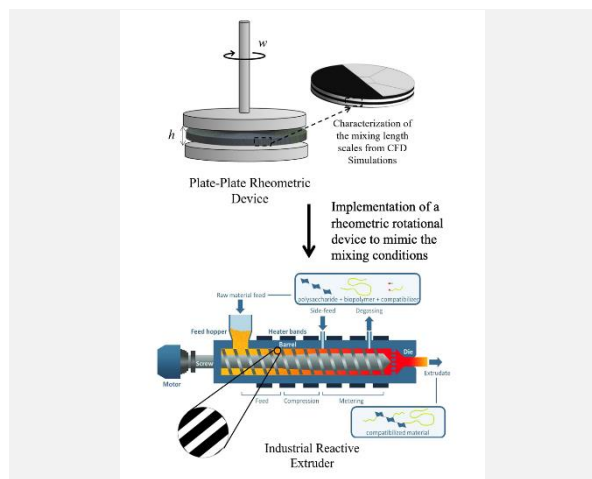
- [1] A.A. Souza Machado et al., *Global Change Biology*, 24 (2018)1405-1416.
- [2] R. Geyer et al., *Science Advances*, 3 (2017) 25-29.
- [3] J. Huang et al., *Nanocellulose: from fundamentals to advanced materials*, John Wiley & Sons, 2019.
- [4] Textile Exchange. *Preferred Fiber & Materials: Market Report*, (2022) 1-118.
- [5] L. Shen et al., *Resources Conservation & Recycling*, 55 (2010) 260-274.
- [6] F.A.G.S. Silva et al., *Nanomaterial*, 10 (2020) 1-29.
- [7] A.F. Jozala et al., *Applied Microbiology Biotechnology*, 100 (2016) 2063-2072.
- [8] F. Meister et al., *Nordic Pulp & Paper Research Journal*, 30 (2015) 112-120.
- [9] S. Paunonen, *BioResources*, 8 (2013) 3098-3121.
- [10] C. Vilela et al., *Trends Food Science Technology*, 80 (2018) 212-222.
- [11] P. Cazón et al., *Food Hydrocolloids*, 113 (2021) 106514.

Modelling of reactive extrusion process by mixing two similar fluids in the extruder

E. Delvar^{1,2}, M.S.C.A. Brito^{1,2}, A. Santamaria-Echart³, M.F. Barreiro³, C.G. Silva^{1,2}, R.J. Santos^{1,2*}

¹ALiCE - Associate Laboratory in Chemical Engineering, Faculty of Engineering, University of Porto, Rua Dr. Roberto Frias, 4200-465 Porto, Portugal, email; ²Laboratory of Separation and Reaction Engineering – Laboratory of Catalysis and Materials (LSRE-LCM), Faculty of Engineering, University of Porto, Rua Dr. Roberto Frias, 4200-465 Porto, Portugal; ³Laboratório Para a Sustentabilidade e Tecnologia em Regiões de Montanha, Instituto Politécnico de Bragança, Campus de Santa Apolónia, 5300-253 Bragança, Portugal.

*rsantos@fe.up.pt



This work focused on developing reactive extrusion process by combining rotational devices (plate-plate or cone-plate rheometer) and Computational Fluid Dynamics (CFD) tools to introduce a process for sustainable performance in the footwear industry. An experimental protocol to assess the reactive polymerization has been developed from CFD simulations and linked to the conditions in an industrial reactive extruder. To analyze the kinematics of deformation, the results show that the interfacial area and striation thickness in rheometric flows are quantified by the stretching of a material element. The main purpose of this work is a protocol connecting the process conditions for BIOTPUs at a laboratory scale using small quantities of raw materials to industrial extrusion processes.

Introduction

Among the extensive range of polymers employed in footwear, polyurethanes are the most utilized because they have various versatile properties, such as resistance to degradation, durability, strength, and lightness. Biobased polyols, isocyanates, and chain extenders are the most common components in the TPUs formulation. Reactive extrusion (REX) is one of the processing technologies that is being assessed for the large-scale incorporation of biobased thermoplastic polyurethanes (BioTPUs) in the footwear industry. REX is a significant production and processing method with several applications in polymers' processing, modification or functionalization, and recycling. Designing extruders for REX systems requires data on the rheology of raw materials, the reactive mixture, and the kinematics of polymerization. REX enables the mixing control, reaction time, and temperature for reactive mixtures of melted polymers with high molecular weights. The development of product formulations for REX industrial processes typically occurs at the laboratory scale. However, replicating the intricate mixing conditions found in industrial settings poses a significant challenge. This work focuses on studying a rotational device that creates a laminar flow, which is significant for the manufacturing industry. The flexibility of processing conditions in the rheometer enables the assessment of a wide range of equipment designs and operational conditions. The rheometric method offers notable advantages, including reduced raw material requirements, shorter testing times, and the evolution of viscosity build-up, which enables the kinetic process (rheokinematic method).

Mixing of Similar Fluids

Ottino et al. (1978) considered that mixing occurs by stretching and folding in a laminar flow, giving rise to a lamellar structure of two fluids – the lamellar model [1]. The formation of a lamellar structure in laminar flow is sketched in the graphical abstract. The mixing degree is then quantified by the evolution of the interfacial area between the phases being mixed ($\alpha'(t)$)

and the lamellae thickness thinning over time ($s(t)$) by the stretching mechanisms under the laminar flow regime.

CFD model – Single Screw extruder

Low-temperature physical crosslinking biobased thermoplastic polyurethane (TPU) formulations are set as the basis for the development of this work. So, the viscosities of both phases are set to 1 Pa·s, the densities of the phases to 1 kg m⁻³, and the process time window in the scale of one minute, which are typical parameters for reactive polymerization of BioTPUs. The development of a formulation methodology is based on CFD simulations of the rheometric flow devices and REX. The flow Reynolds numbers are low (≤ 1), and creep flow conditions for the rheometric and extruder flows enable steady-state hydrodynamic simulations. The mixing is simulated from the dynamic simulation of the transport of a tracer over the steady flow field. The geometry of the single screw extruder used in this project consists of one screw that is rotating inside one cylinder, as shown in Figure 1. The screw walls are set to angular velocity ω , and the tangential velocity at each position of the extruder wall is $v = \omega R_{screw}$, where R_{screw} is the distance of the extruder surface to the rotation axis. The cylinder enclosing the extruder screw is stationary.

Results and Discussion

Figure 1 shows the pathlines in the screw extruder obtained from a 3D CFD simulation. The pathlines show a flow that resembles the Taylor-Couette flow between concentric rotating. Although, in this case, there is an axial velocity component due to screw geometry. Figure 1 also shows the tracer mass fraction map that displays the creation of an interfacial area in a binary mixture in this flow. The two phases were initially side by side. The maximum and minimum shear rates in each section might be described by:

$$\dot{\gamma}_{max} = \frac{\omega R_{ext}}{R_{ext} - (R_{screw} + r/2)}$$

and

$$\dot{\gamma}_{min} = \frac{\omega R_{ext}}{R_{ext} - (R_{screw} - r/2)}$$

where r is the distance to this axis.

An average value is considered for all domain as,

$$\dot{\gamma} = \frac{\omega R_{ext}}{R_{ext} - R_{screw}}$$

The mixing mechanisms shown in Figure 1 are based on the shear rate field that was well-approximated in the assumptions leading to the screw-extruder equations for $\alpha'(t)$ and $s(t)$ in Table 1.

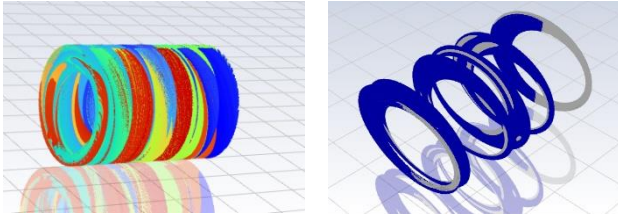


Figure 1. (left) Pathlines in the extruder and (right) mass fraction maps of a binary mixture.

Product development parameters

The parameters for the rheokinematic formulation are determined by matching the interfacial area generation and striation thickness thinning in the extruder and in the rheometric flows, in this case the cone-plate or plate-plate with two fluids set side-by-side. The interfacial area and the striation thickness for plate-plate and cone-plate are described in Table 1. The

complete development of the equations for the rheometric flows is found in Brito et al. [5]. The rheometric flows are steady, but the mixing scales evolve in each location with time, while in the extruder, the evolution occurs in space along the axial direction. The relation between time and the position in the extruder, z , is given by

$$t = z/v_z$$

The rotational speed imposed to the cone-plate system is given by

$$\omega = \frac{\omega_{ext} R_{ext} \beta}{R_{ext} - R_{screw}}$$

And for the plate-plate, it is given by

$$\omega = \frac{\omega_{ext} R_{ext} h_p}{(R_{ext} - R_{screw}) R_p}$$

where h_p is the gap between the top and bottom plate, R_p is the radius of the plates, and β is the angle between the cone and the plate.

Conclusions

This study used a rotational rheometric device to develop polymeric materials in reactive extrusion, matching the evolution of mixing scales in fluids with similar viscosity. CFD results show a similar evolution of homogeneous lamellar structures in the extruder and the rheometric flows. As a result, the rheometric rotational devices are viable methods for high throughput development methodology, enabling them to accurately replicate the mixing scales observed in pilot machines at a laboratory scale.

Table 1. Mixing scales length obtained in topology.

Topology	Contour Maps of phases	Interfacial Area	Striation Thickness
Plate-plate		$\alpha'(t) = \sqrt{1 + \left(\frac{\omega R_p t}{h_p}\right)^2}$	$s(t) = \frac{s_0}{\sqrt{1 + \left(\frac{\omega R_p t}{h_p}\right)^2}}$
Cone-plate		$\alpha'(t) = \sqrt{1 + \left(\frac{\omega t}{\beta}\right)^2}$	$s(t) = \frac{s_0}{\sqrt{1 + \left(\frac{\omega t}{\beta}\right)^2}}$
Screw-extruder		$\alpha'(t) = \sqrt{1 + \left(\frac{\omega_{ext} R_{ext} t}{R_{ext} - R_{screw}}\right)^2}$	$s(t) = \frac{s_0}{\sqrt{1 + \left(\frac{\omega_{ext} R_{ext} t}{R_{ext} - R_{screw}}\right)^2}}$

Acknowledgements

This work was financially supported by LA/P/0045/2020 (ALiCE), UIDB/50020/2020, UIDP/50020/2020 (LSRE-LCM), LA/P/0007/2021 (LA SusTEC), UIDB/00690/2020 and UIDP/00690/2020 (CIMO), funded by national funds through FCT/MCTES (PIDDAC); BioShoes4All (PRR - 000011), supported by PRR - Plano de Recuperação e Resiliência - Bioeconomia.

References

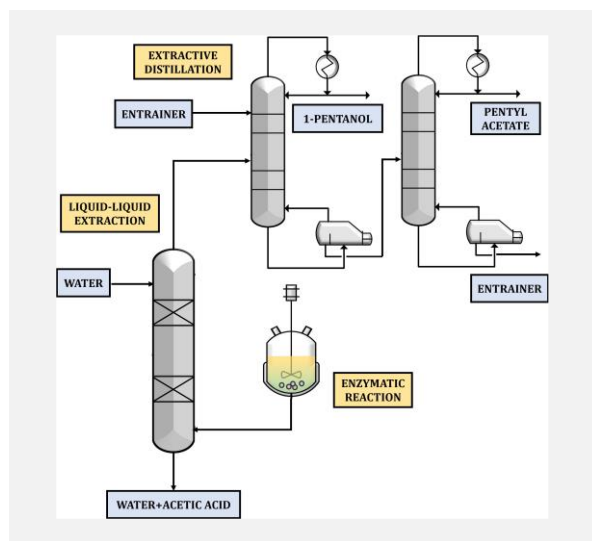
- [1] J.M. Ottino et al., Chemical Engineering Science, 34 (1978) 877-890.
- [2] W.D. Mohr et al., Industrial & Engineering Chemistry Research, 49 (1957) 1857-1862.
- [3] W.E. Ranz, AIChE Journal, 25 (1979) 41-47.
- [4] B. Imré et al., Carbohydrate Polymers, 209 (2019) 20.
- [5] M.S.C.A Brito et al., AIChE Journal, 68 (2022) e17597.

Integration of a reaction-purification process to obtain pentyl acetate

L. Domínguez*, B. Lorenzo, J. Ortega, L. Fernández

Division of Thermal Engineering & Instrumentation (IDeTIC), 35017-University of Las Palmas de Gran Canaria, Spain.

*leandro.dominguez@ulpgc.es



In this work the integration of solvent-free enzymatic synthesis of pentyl acetate with a set of separation processes is analyzed to achieve the highest degree of purification of the ester, which has applications in different industrial sectors, such as food and pharmaceuticals. A methodology has been used that allows to manage, in a more rigorous way, the experimental information to finally design processes with real quality data.

The idea raised here is to propose a more sustainable process for producing pentyl acetate achieving the maximum purity, using real experimental data and mathematical models to describe the esterification kinetics, phase equilibria and mixing properties. In summary, the ester is separated from the acid by liquid-liquid extraction with water, and then the organic phase is separated by an extractive distillation process. The results show that the proposed sequence of operations is valid to recover the pentyl acetate obtained by esterification.

Introduction

In order to achieve a more sustainable chemical industry, the investigations have been addressed in the direction of increasing the interest in carrying out the enzymatic catalysis for the production of certain chemicals, since this synthesis route consumes less energy and the enzymes can be obtained from renewable resources. In this context, solvent-free systems (SFS) are also increasing their use because they reduce the waste generation. However, the development of such alternatives requires a complete reconsideration of the production process, including the reaction and separation stages, as the reactor product and operating conditions differ from traditional processes.

Short-chain esters are used in different industrial sectors and they are feasible alternatives to replace hydrocarbons in many applications. Furthermore, many of them are biodegradable and can be produced from biomass. Fischer esterification is the usual process to produce esters, but strong inorganic acids are required in industry to catalyze the reaction, so enzymatic catalysis combined with SFS represents a much more sustainable alternative for their production.

Pentyl acetate is an ester that can be produced enzymatically by Fischer esterification, as demonstrated in a recent work [1]. The authors concluded that it is possible to obtain pentyl acetate under solvent-free conditions with the Lipozyme[®]435 catalyst, reaching high conversions (>80%) after 8 hours, using a batch-reactor. Obviously, the presence of the ester in the final product is not finalist, since its purity is around 45% (w/w). Therefore, to complete the goal and the process to be taken to a major scale, it is necessary to implement a series of separation stages to purify the pentyl acetate, taking into account the problems that arise in its purification. A priori that refine require the use of specific techniques, because of mainly to the formation of an azeotrope in the pentyl acetate/pentan-1-ol binary.

Methodology

Following a methodology proposed by our research group [2], based on the sequence of tasks {experimentation↔ modeling/checking→simulation} (Figure 1), in this work the integration of the mentioned processes has been studied. First, the enzymatic reaction to produce pentyl acetate and then the separation and/or the purification of said ester. By means of experimentation, the kinetic information previously known [1] is complemented with phase equilibrium data (vapor-liquid and liquid-liquid) and the corresponding mixing properties. The information obtained is correlated with suitable models and the quality of the experimentation is verified by a thermodynamic point of view. The generated models are implemented in a chemical engineering simulator to design the production process.

Results

The results show that it is possible to purify the pentyl acetate using a sequence of operations similar to that shown in the graphical abstract. The reactor outlet stream is treated with water to remove the unreacted acetic acid and an aqueous phase is separated from an organic phase due to the immiscibility between water and ester. Then, the organic phase, consisting mainly of pentyl acetate and pentan-1-ol, is separated by extractive distillation to break the azeotrope mentioned above. To the best of our knowledge, the integration of the enzymatic synthesis of pentyl acetate with the subsequent separation process is not reported in the literature, so this study represents a contribution to the development of a set of chemical processes, making it more sustainable.

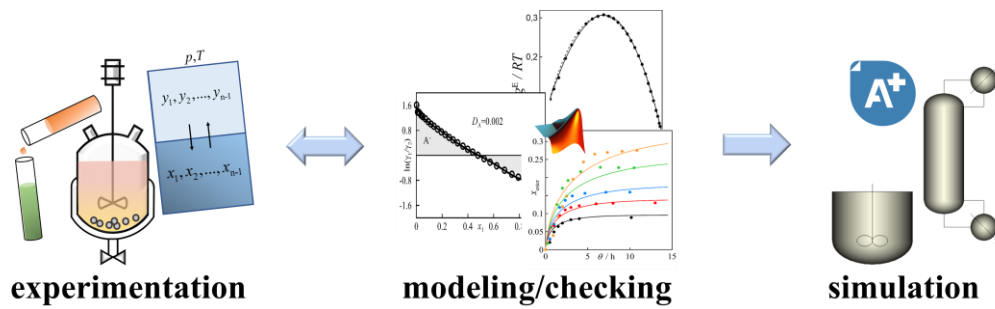


Figure 1. Methodology for the rigorous treatment of kinetic-thermodynamic information.

Acknowledgements

Authors are thankful to the Spanish Ministry of Science and Innovation for the grant number PID2021-127970OB-I00. B.L. thanks her predoctoral contract (PRE2019-087401) from the Spanish Ministry of Science and Innovation.

References

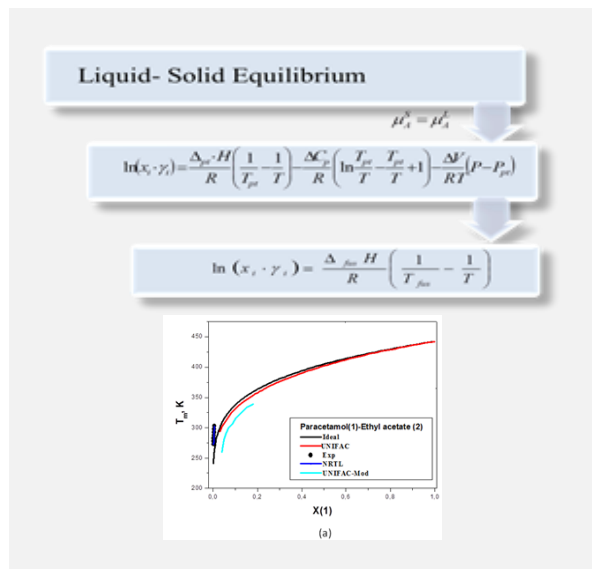
- [1] B. Lorenzo et al., *Processes*, 11 (2023) 1640.
- [2] J. Ortega et al., *Industrial & Engineering Chemistry Research*, 59 (2020) 8346-8360.

Prediction of solubility and phase diagram of some pharmaceutical substances

K. Bitchikh^{1*}, N. Smakghi², A. H. Meniai³

¹Laboratoire des Sciences et Techniques de L'Environnement, Ecole Nationale Polytechnique, Alger, Algérie ; ²Laboratoire de Recherche Sciences de l'Eau, Ecole Nationale Polytechnique, Alger, Algérie ; ³Laboratoire de l'Ingénierie des Procédés de l'Environnement, Université Salah Boubendir, Constantine 3, Algérie.

*karima.bitchikh@g.enp.edu.dz



The present study deals with the modeling of solid-liquid equilibrium for binary systems in different solvents at different temperatures by means of various thermodynamic models such as NRTL and UNIFAC.

Two solutes, namely Benzoic acid and Paracetamol were considered in different solvents like Ethyl Acetate, Acetone, Water, Acetic Acid, Octanol, Ethanol, Propanol and Butanol.

The use of the NRTL model requires interaction parameter values which are not always available. Therefore, this work was an opportunity to compute these parameters for the different systems considered

Introduction

Generally Solid-liquid equilibria (SLE) are less considered, comparatively to Vapour-Liquid and Liquid-Liquid equilibria (VLE and LLE, respectively) and the great majority of the relevant models, particularly for the calculation of the activity coefficient, concern the last two types, although their use has been extended to handle SLE due to major applications like crystallization where the knowledge of the solubility of a given solute in solvents and mixtures of solvents is essential for the design and calculation of such process.

All these factors motivated and encouraged the present study, were considered in various solvents like Ethyl Acetate, Acetone, Water, Propanol and Butanol.

Methods

Most of the proposed approaches are based on rigorous and robust thermodynamic models taking into account the non ideality which prevails in the great majority of systems. They differ by the way they propose to express the excess free Gibbs energy function (GE) in term of the concentration at a constant temperature for non-ideal liquid mixtures.

A variety of activity coefficient models is reported and well described in the literature ranging from the oldest and simplest ones due to Van Laar and Margules which are rather devoted to binary systems [1], to relatively more recent and more elaborated ones like the Wilson, NRTL, UNIQUA1C and UNIFAC models which are more involved with multicomponent systems [2]. However before describing each model, it may be useful to discuss the ideal solubility case which can be assumed to prevail when the solute and the solvent have a great similarity in chemical nature, properties and molecular interactions, hence an activity coefficient equal to unity to lead to the following ideal solubility expression:

$$\ln \frac{1}{x_1} = \frac{\Delta h^m}{RT_m} \left(\frac{T_m}{T} - 1 \right) - \frac{\Delta C_p}{R} \left(\frac{T_m}{T} - 1 \right) + \frac{\Delta C_p}{R} \ln \frac{T_m}{T} \quad (1)$$

with x_1 the solute solubility, T_m the solute melting temperature, Δh^m the melting enthalpy, ΔC_p the difference between the solute and solvent heat capacities and R the universal gas constant.

Results and discussion

The solubilities of Benzoic acid and Paracetamol in different solvents were also considered using the different thermodynamic models.

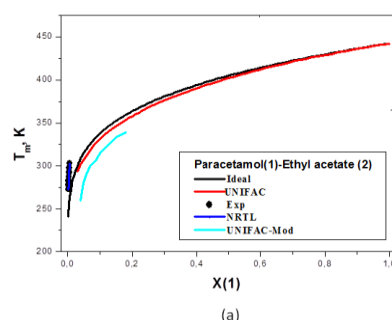


Figure 1. Solubility of paracetamol in ethyl acetate.

Conclusions

With regard to Paracetamol, it is found that it is not very soluble in the various solvents used and this for temperatures not exceeding 30°C.

The same observation as paracetamol was repeated for benzoic acid, which was found to be poorly soluble in the various solvents used and at a temperature not exceeding 50°C with a maximum value of 30%.

References

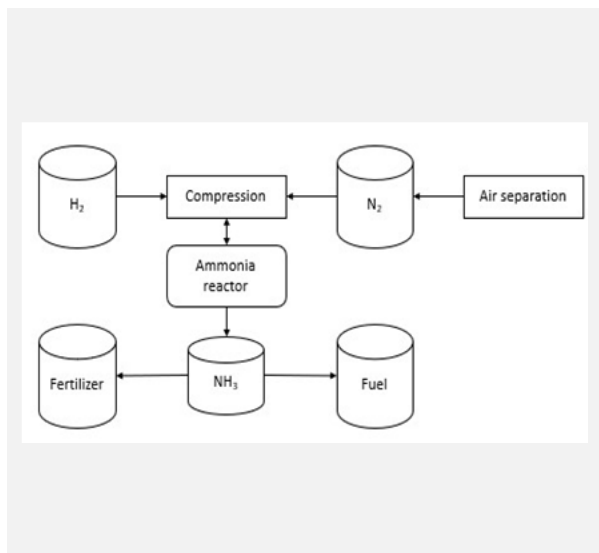
- [1] H. Van Ness et al., Introduction to Chemical Engineering Thermodynamics, 8th Ed., McGraw Hill Education, 2017.
- [2] R.C. Reid et al., The properties of gases and liquids, 4th Ed., McGraw Hill Book Company, 1987.

Heat integration of the Haber Bosch process for the production of green ammonia

J. Leitão¹, C.G. Braz², H.A. Matos^{1*}

¹Centro de Recursos Naturais e Ambiente, Instituto Superior Técnico, Universidade de Lisboa, Av. Rovisco Pais 1, 1049-001 Lisboa, Portugal; ²Industrial Process and Energy Systems Engineering (IPESE), École Polytechnique Fédérale de Lausanne, Lausanne, Switzerland.

*henrimatos@tecnico.ulisboa.pt



Ammonia is an important compound in the agricultural industry due to its large application in nitrogen-based fertilisers. The most common ammonia production pathway is the Haber – Bosch process, in which hydrogen from natural gas and nitrogen react. As natural gas prices keep rising and the decarbonisation of the chemical industry is required, it is important to start implementing large-scale green ammonia production processes [1].

A large-scale ammonia synthesis simulation was performed in *Aspen Plus*, which can be divided into two parts. An air separation unit that includes a compressor and two distillation columns to separate nitrogen from air, and a reactor for ammonia synthesis, which is separated from its reactants through two separators. An energy analysis was then performed in *Aspen Energy Analyzer*, with seven different types of utilities being used, and a heat exchanger network was created, in order to reduce the utilities spent and carbon emitted.

The results indicate process viability, with further optimization of the simulation and study of different ammonia synthesis techniques to be done in future work.

Introduction

The aim of this work was to simulate a large-scale ammonia production plant (500 thousand tonnes of ammonia per year) that improves upon the high energetic expenses related to the Haber – Bosch process. The simulation encompasses two different segments, an air separation unit and a reactor. An energy analysis for this process was made and optimization of the heat exchanger network was done through heat integration using *Aspen Energy Analyzer*. As one of the goals is to reduce environmental problems associated with the Haber – Bosch method, the simulated process' carbon emissions were also looked into before and after heat integration. The results will bring light to the viability of this alternative and the improvements to be made in order to maximize efficiency and minimize energy consumption.

Simulation

Air separation unit

The first module of this simulation is the air separation unit, where air enters at atmospheric pressure and temperature, and is compressed to 7 bar with further cooling to -200 °C. These conditions guarantee that the air is fully liquified and ready to be separated into its components. Thus, two distillation columns were used sequentially to maximize separation efficiency, where nitrogen leaves as liquid distillate and oxygen as the bottoms product, with the nitrogen streams from each distillation column being mixed afterwards, as seen in the next Figure 1.

The columns were firstly simulated as DSTWU models, in order to obtain their reflux ratio and distillate to feed ratio. Then, the RADFRAC model was used and the main parameters were optimized through a sensitivity analysis, to maximize the separation efficiency.

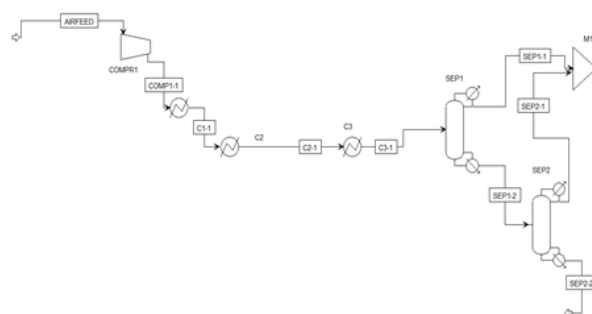


Figure 1. Diagram of the air separation unit.

Ammonia synthesis system

Furthermore, an independent hydrogen stream was mixed with the nitrogen obtained previously, which was then compressed to 128 bar through a series of compressors with coolers in between. This stream was then inserted into the reactor, where the ammonia formation reaction occurs.



At 450 °C and 128 bar, a conversion rate of 30% was considered for the ammonia production [2], and the reactor outlet was then cooled back to -30 °C. Additionally, the cold stream was then separated into ammonia and the rest of the reagents, using two different flash separators, the first working at 128 bar, and the second at 17 bar.

The top stream of each separator is then mixed back before the reactor inlet, whilst guaranteeing that the mixture conditions are adequate, using multiple compressors and coolers to achieve the pre-reactor conditions. A purge is also necessary to guarantee that the air impurities are kept at a safe quantity. The full ammonia synthesis system is shown in Figure 2.

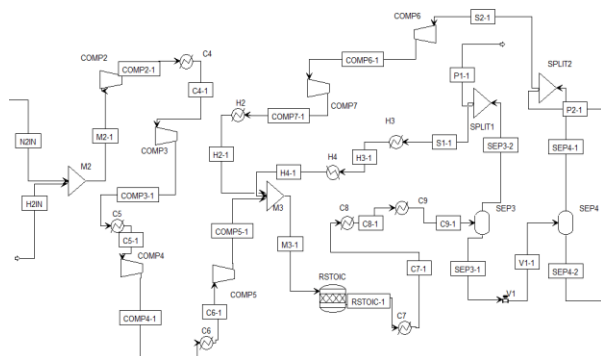


Figure 2. Diagram of the ammonia synthesis section.

Energy analysis

As mentioned previously, it is important to assess the energetic consumption of this process in order to understand its viability. Heat duties were obtained for each equipment and the electric consumption of pumps and compressors was calculated. Then, heat integration was performed in *Aspen Energy Analyzer* to create a heat exchanger network (HEN) that minimizes energy expenses and carbon emissions.

Results and conclusions

The simulation model presented in Figures 1 and 2 complied with the process specifications, producing 500 thousand tonnes of ammonia per year, with a molar purity of 98.3% and a global yield of 89.7%. The main parameters for the air separation unit are also presented in the table below.

Table 1. Main parameters of the distillation columns.

	SEP1	SEP2
Reflux ratio	1.37	6.00
Distillate to feed ratio	0.75	0.10
Number of stages	25.0	20.0
Feed stage	10.0	10.0
Efficiency (%)	96.0	99.7

Depending on the necessities of potential buyers, product purity could be improved upon, as well as total process yield, although at an increase in energy expended, which could be evaluated in the future.

An energy analysis of the process was also done, having utilized seven different types of utilities, which may be unnecessary and improved upon further. The heat exchanger network and the energy analysis's main results are described in Figure 3.

Acknowledgements

The authors acknowledge the financial support by CERENA (strategic project FCT-UIDB/UIBD/04028/2020).

References

- [1] IRENA and AEA, *Innovation Outlook: Renewable Ammonia*, International Renewable Energy Agency, Abu Dhabi, Ammonia Energy Association, Brooklyn, 2022.
- [2] G.R. Maxwell, *From Synthetic Nitrogen Products: A Practical Guide to the Products and Processes*, Kluwer Academic Publishers, New York, 2005.
- [3] E.R. Morgan et al., *ACS Sustainable Chemistry and Engineering*, 5 (2017) 9554-9567.

Table 2. Energy analysis main results.

	Simulation
Total heat duty (MW)	407.6
Electrical consumption (MW)	65.8
Recoverable heat duty (MW)	108.1
Total utilities (GW)	284.2
Utilities after heat integration (GW)	133.3
Carbon emissions (kg/hr)	10490
Carbon emissions after heat integration (kg/hr)	-17970

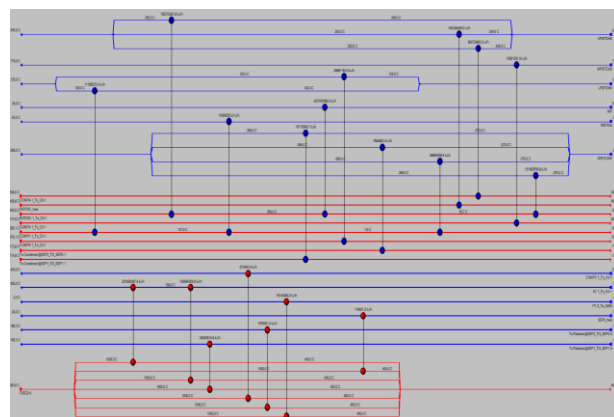


Figure 3. Diagram of the heat exchanger network.

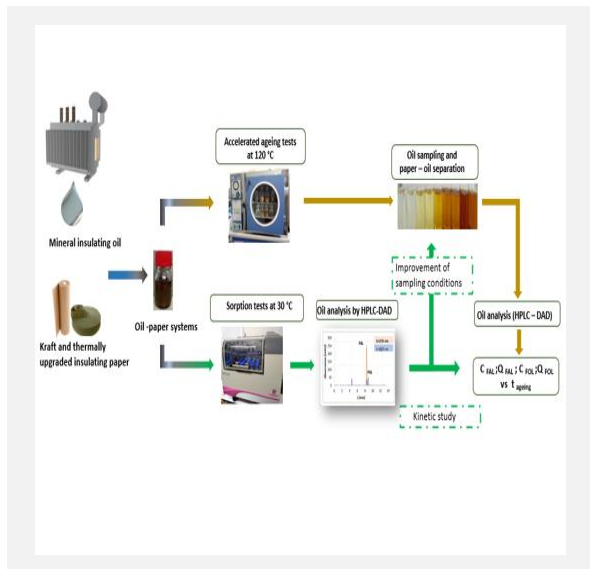
These results are according to expectation, since the process is energetically intense and, according to Morgan et al. [3], a plant that produces 100 thousand tonnes of green ammonia per year has a heat requirement of around 150 MW. It is important to note that, after heat integration, the carbon emissions become negative, since there are three different types of steam being generated, whose impact is accounted for as avoided CO₂ emissions, and thus counts as negative emissions. Further investigation of this impact should be done in future work through life cycle assessment, to ensure that all sources of impact are being considered. Although water electrolysis has not been included in this simulation, its addition to the process in the future could be beneficial for research purposes. Different ammonia synthesis methods should also be investigated in order to maximize process efficiency and minimize energy consumption.

Sorption assays of furanic compounds in transformers insulation oil and paper systems

M.A.J. Teixeira^{1*}, S.Y. Matharage², Z. Wang², M.M.Q. Simões³, I. Portugal¹, C.M. Silva¹

¹CICECO – Aveiro Institute of Materials, Department of Chemistry, University of Aveiro, Aveiro, Portugal; ²Department of Engineering, Centre for Smart Grid, University of Exeter, Exeter, United Kingdom; ³LAQV- REQUIMTE, Department of Chemistry, University of Aveiro, Aveiro, Portugal.

*ma.teixeira@ua.pt



The wellness of transformers insulation, constituted by cellulosic materials and insulating oil is crucial for its operation, highlighting the monitoring and knowledge of degradation processes by lab ageing tests. Among monitored markers, furanic compounds are associated to cellulosic materials. However, their detection in oil may be affected by temperature and time. Ageing tests at 120 °C of two different papers (Kraft and thermally upgraded paper) in mineral oil, indicated furfural (FAL) and furfuryl alcohol (FOL) as compounds of interest in oil by analysis using high-performance liquid chromatography with diode array detection. Therefore, sorption tests were performed with these two compounds in oil-paper systems at 30 °C, 100 rpm for 168 h with initial furanics concentration from 2 to 196 ppm. Regarding the results, these compounds showed different kinetics, having papers more affinity for FOL and apparent linear correlations between total concentration in oil and papers.

Introduction

Transformers are indispensable equipment of power grids to electrical supply which demands is increasing nowadays. Although they are designed to operate for several decades, the lifetime of transformer is dependent of its insulation status. An adequate and timely monitoring will contribute for the detection of transformers faults extending promoting necessary interventions for the extension of their operating life. In this line, the performance of accelerated ageing tests in a laboratory environment are beneficial in this context, because it allows the analysis of the behaviour of different solid insulating materials and insulating oils under controlled conditions and permitting the development of models to explain their degradation processes.

Several degradation markers have been associated to different insulation faults, such as furanic compounds which are typically associated to deterioration of cellulosic materials (furfural, furfuryl alcohol, 5-hydroxymethylfurfural, 5-methylfurfural, and 2-acetylfuran) [1-2]. Among these, furfural content in oil has been largely explored in order to correlate with cellulose degree of polymerization [1]. However, sampling conditions, such as temperature and time, may have impact on its concentration [3].

In this study sorption tests of two furanic compounds - furfural (FAL) and furfuryl alcohol (FOL) - in oil-paper systems were prepared for a better understanding of their distribution under equilibrium at controlled conditions.

Material and methods

For the preparation of accelerated ageing tests Kraft paper and thermally upgraded crepe paper (TUP) and a mineral uninhibited mineral oil Nynas Nytro Taurus were used in a ratio of 1 g of wet paper (6,4 % of moisture) for 10 mL of oil in 100 mL bottles. The addition of 54 cm² of copper was also tested. These oil-paper systems were placed at 35 °C for 24 h under vacuum for

impregnation. After, the samples bottles were closed and aged at 120 °C. Periodical samples were collected during 5 to 7 weeks. Then, oil-paper samples were leaven at room temperature before analysis.

In case of sorption test, the oil-paper ratio was 8:80 g/mL. The concentrations ratio of FAL and FOL in the oil was *ca.* 1 and total furanic concentrations between 2 and 200 mg/kg. These oil solutions were then added to the Kraft and TUP paper and plated inside an orbital shaker at 30 °C for 168 h to reach equilibrium. After equilibration the furans in the oil were analyzed by high-performance liquid chromatography with diode array detection (HPLC-DAD), and their concentration in the paper was calculated by mass balance.

Results

The performance of accelerated ageing tests evidenced the presence of furfural as the furanic compound with most relevance in the case of Kraft paper, while systems with TUP showed concentrations closed to the quantification limit of 0.05 ppm. Moreover, the results for furfuryl alcohol indicated a peak during the first weeks in oil-Kraft paper systems. For oil-TUP systems furfuryl alcohol seemed to be the furanic compound with most presence, but no clear tendencies were observed.

Preliminary sorption tests of FAL and FOL in oil indicated for samples with initial furanics concentration of 10 ppm, the equilibrium concentrations were reached after 72 h (kraft paper) and 26 h (TUP). However, when oil with initial overall furanics concentration of 196 ppm samples collected after 72 h and 168 h indicated that the equilibrium in oil paper systems was not reached. In this case, FAL and FOL in oil reduction after 168 h was 31.1 and 78.1 % for Kraft, and 25.8 and 77.3 % for TUP, respectively. These results indicate a higher paper affinity for FOL in comparison to FAL.

With the definition of 168 h period of time to reach equilibrium, oil mixtures samples of both systems were analyzed and the experimental data for the individual and total furanics showed an apparent linear distribution between their concentrations in oil and paper.

Conclusions

Regarding the results of sorption tests of furfural and furfuryl alcohol mixtures in oil-paper systems, it has been concluded that these compounds have different kinetics. Furfuryl alcohol showed higher affinity than furfural in this operating conditions. This study helped for a better understanding of these degradation markers partitioning in typical transformer insulation systems, although more tests at different conditions should be carried out for the development of robust sorption models.

Acknowledgements

This work is financed by Portugal 2020 through European Regional Development Fund (ERDF) in the frame of Operational Competitiveness and Internationalization Programme (POCI) in the scope of the projects number 39906 NEXTRA- Enabling the NEXT Generation of Smarter TRAnsformers, (POCI -01-0247-FEDER-039906). This work is also in the scope of the project CICECO – Aveiro Institute of Materials, UIDB/50011/2020 & UIDP/50011/2020 & LA/P/0006/2020, financed by national funds through the FCT/MEC (PIDDAC). The work developed with LAQV received financial support from PT national funds (FCT/MCTES, Fundação para a Ciência e Tecnologia and Ministério da Ciência, Tecnologia e Ensino Superior) through the project UIDB/50006/2020 | UIDP/50006/2020. Miguel Teixeira thanks FCT for a PhD grant (UI/BD/151139/2021)

References

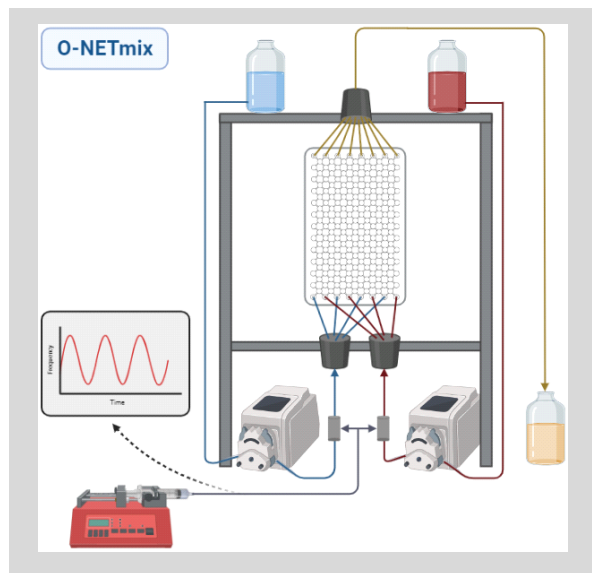
- [1] L. Cheim et al., IEEE Electrical Insulation Magazine, 27 (2011) 29-42.
- [2] J. Scheirs et al., Journal of Applied Polymer Science, 69 (1998) 2541-2547.
- [3] L. Yang et al., IEEE Transactions on Dielectrics and Electrical Insulation, 23 (2016) 1393-1401.

Introducing the O-NETmix - a novel technology for continuous crystallisation

A.F. Freitas^{1,2,3*}, Y.A. Manrique^{1,3}, J.C.B. Lopes^{1,3,4}, R.J. Santos^{1,3}, A. Ferreira^{2,3}, M.M. Dias^{1,3}

¹LSRE-LCM – Laboratory of Separation and Reaction Engineering – Laboratory of Catalysis and Materials, Faculty of Engineering, University of Porto, Rua Dr. Roberto Frias, 4200-465 Porto, Portugal; ²LEPABE – Laboratory of Process Engineering, Environment, Biotechnology and Energy, Faculty of Engineering, University of Porto, Rua Dr. Roberto Frias, 4200-465 Porto, Portugal; ³ALiCE – Associate Laboratory in Chemical Engineering, Faculty of Engineering, University of Porto, Rua Dr. Roberto Frias, 4200-465 Porto, Portugal; ⁴Colab NET4CO2 – A Network for a Sustainable CO2 Economy, Rua Júlio de Matos, 828-882, 4200-355 Porto, Portugal.

*affreitas@fe.up.pt



The evolution of crystallisation processes has been determined by a growing understanding of the physical and chemical processes involved, as well as the development of new techniques and technologies that have improved its efficiency and accuracy. This work explores the development of a new technology, the oscillatory NETmix (O-NETmix), for continuous crystallisation. This device combines the NETmix structure for controlled and efficient mixing with the best features of the oscillatory flow crystalliser (OFC), most notably its ability to deliver high residence times vital for crystal growth. Experimental studies were carried out on calcium phosphates production, with and without oscillation. The effect of the oscillation was reflected in a variation in the particle size.

Introduction

Crystallisation is recognised as one of the main purification processes in the chemical industry [1]. It is described as the conversion of a substance or substances from a gaseous, liquid or amorphous solid state to a crystalline state [2,3]. The crystallisation process becomes increasingly important in the industry for obtaining a wide range of products, from the most basic, which can be called commodity products, to those with high added value. Many production processes in the pharmaceutical, food and chemical industries include a crystallisation step, regardless of whether the objective is separating or purifying the compounds [3]. The final characteristics of the crystals can vary in size and shape depending on the course of their formation during the process; the presence of impurities in the solution also influences and can result in changes in the particle characteristics [4]. Continuous oscillatory crystallisers offer a promising solution for crystal production, potentially achieving higher yields and improved product quality compared to traditional crystallisation methods. Oscillatory flow crystalliser (OFC) is an internationally patented mixing technology developed at LEPABE/FEUP that exhibits several advantages, including controlled mixing; heat and mass transfer intensification; reduced induction time; narrower metastable zone width and crystal size distribution; predictable scale-up; and the possibility to operate in batch or continuous mode [5,6]. OFC is a tube or channel provided with periodic sharp constrictions (baffles) operating under oscillatory flow mixing (OFM) [7]. NETmix is an internationally patented mixing technology developed at LSRE-LCM/FEUP, particularly suitable for complex and fast kinetic reactions since mixing and heat transfer can be efficiently controlled [8,9]. It consists of a

network of mixing chambers interconnected by transport channels. The network is generated by repeating unit cells composed of one chamber and two inlet and two outlet channels oriented at a 45° angle from the main flow direction. When fluids flow through this network, at Reynolds numbers above 150, mixing becomes chaotic and quite intense, and the hydrodynamics evolve to a self-sustained oscillatory laminar flow regime inside the chambers inducing local strong laminar mixing.

Objectives

The main objective of this work is to introduce a new technology, the oscillatory NETmix (O-NETmix) as new concept for continuous crystallisation. Production on calcium phosphate crystals is presented as a first case study.

Methods

The oscillation of the inlet flow streams in NETmix leads to more flexible control and operation of this device. For this purpose, an experimental set-up was assembled, with a flow oscillation system coupled to the structure of an existing LabNETmix reactor [10]. The oscillation system was built with components described below according to the circuit shown in Figure 1. The variable-frequency drive SINAMICS G110 from Siemens (1, Figure 1) was connected to the electric motor JM63B-4-B14 from SEIPEE (2, Figure 1). The motor was linked to a shaft with a flexible spring shaft at its extremities (3, Figure 1) through a V-belt (4, Figure 1); that transmitted rotation to two flexible spring shafts, the position of the shafts can be set to different phase angles: $\pi/2$, π and $3\pi/2$. These shafts are connected to two Iso cylinder ESNU-8-25-P-A from FESTO (5, Figure 1). The coupling of this system

to the LabNETmix was made through a tube connecting the Iso cylinder to the tube between the pump outlet and the distributor inlet of each reagent. The Iso cylinder acts as a piston, and the fluid moves inside the reactor, promoting oscillatory action.

For the synthesis of calcium phosphate, solutions of calcium chloride (0.20M) and of orthophosphoric acid (0.12M) were used as reactants; sodium hydroxide was added to the orthophosphoric acid solution for pH adjustment [11]. All the materials were commercially obtained and used as received without further purification. The solvent used for both solutions was distilled water. The solutions were fed to the O-NETmix reactor by gear pumps (Imastec™ BVP-Z) at $Re=100$ and $37^{\circ}C$.

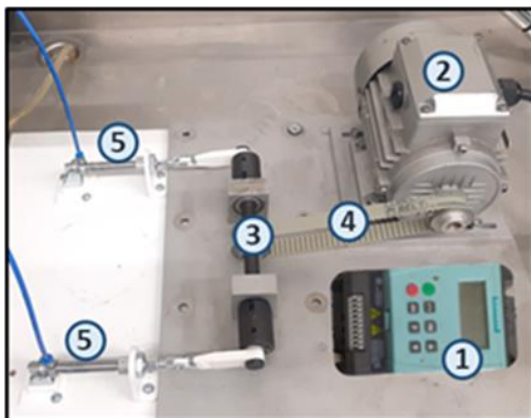


Figure 1. The oscillatory system used in the experimental set-up: 1- variable-frequency drive; 2- electric motor; 3- shaft with a flexible spring shaft at its extremities; 4- V-belt; 5- Iso cylinder ESNU-8-25-P-A.

Acknowledgements

This work was financially supported by LA/P/0045/2020 (ALiCE), UIDB/50020/2020 and UIDP/50020/2020 (LSRE-LCM), and UIDB/00511/2020 - UIDP/00511/2020 (LEPABE) funded by national funds through FCT/MCTES (PIDDAC), and the doctoral scholarship 2020.05252.BD from FCT.

References

- [1] A.S. Myerson et al., Handbook of industrial crystallisation, 3rd Ed., Cambridge University Press, 2019, 313-345.
- [2] J.W. Mullin, Crystallization, 4th Ed, Elsevier Science, 2001, 1-46.
- [3] C. Costa et al., Introdução à cristalização: princípios e aplicações, 1^a Ed, EdUFSCar, 2011, 1-17.
- [4] A.S. Foust et al., Principles of Unit Operations, Wiley, 1980.
- [5] A.M.A. Ferreira et al., Modular Oscillatory Flow Plate Reactor, EP3439773 (B1).
- [6] A.M.A. Ferreira et al., Apparatus for mixing improvement based on oscillatory flow reactors provided with smooth periodic constrictions, EP3057694 (B1).
- [7] P. Cruz et al., CrystEngComm, 20 (2018) 829-836.
- [8] J.C.B. Lopes et al., Network mixer and related mixing process, PCT/IB2005/000647, US 8434933, EP 1720643, PT 103072.
- [9] J.C.B. Lopes et al., Network heat exchanger device, method and uses thereof, PCT/IB2018/052463, US 11 484 862.
- [10] A.C.G. Moreira et al., Industrial & Engineering Chemistry Research, 59 (2020) 18510-18519.
- [11] P.J. Gomes et al., Journal of Nanoscience and Nanotechnology, 9 (2009) 3387-3395

Results

Synthesis of calcium phosphate preliminary results carried out with and without oscillation are shown in Table 1. The average diameter was obtained Laser diffraction (Coulter LS 230) and the calcium to phosphate ratio was determined by Energy Dispersive Spectroscopy (EDS). From experiments L3 and L4, respectively without and with oscillation, it appears that oscillation decreases the average diameter of the particles. However, experiments L4 and L5 indicate that an increase in frequency increases the average diameter of the particle. The results of EDS are qualitative and intended to verify only the existence of the calcium and phosphorus elements in the material analysed. X-ray diffraction analyses are being carried out to categorise the calcium phosphates produced.

Table 1. Summary of the synthesis of calcium phosphate in LabNETmix reactor with and without oscillatory system and main results.

ID	Oscillation	Average diameter (μm)	Ratio Ca/P
L3	-	10.3	1.52
L4	6 Hz	9.0	1.43
L5	20 Hz	12.4	1.48

Conclusions

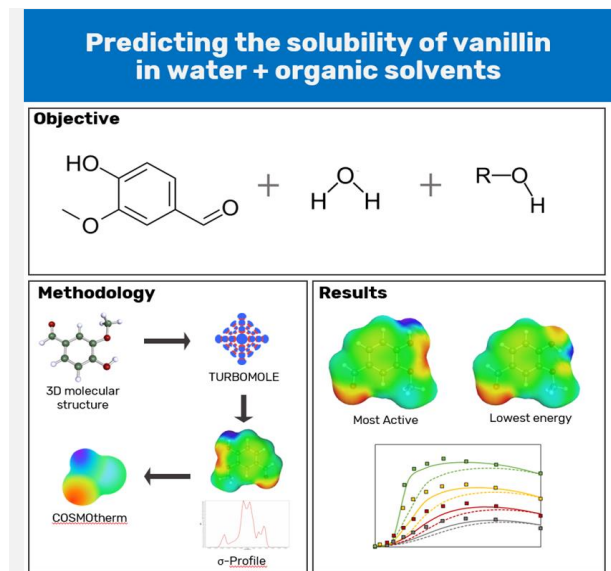
The main objective of this work was to use assess inlet flow oscillation as a mean to control continuous crystallisation in NETmix. The experimental set-up was assembled successfully, and the first studies in producing calcium phosphate were carried out. Oscillation is demonstrated as an operational variable that can control crystallisation in NETmix. Further tests are being conducted to draw a complete picture of the impact of flow oscillation on crystallisation.

Application of COSMO-RS to predict the phase equilibria of vanillin in aqueous mixtures

I.W. Cordova^{1,2,3}, G. Teixeira³, D.O. Abranches³, S.P. Pinho^{1,2}, O. Ferreira^{1,2}, J.A.P. Coutinho^{3*}

¹Centro de Investigação de Montanha (CIMO), Instituto Politécnico de Bragança, Campus de Santa Apolónia, Bragança, Portugal; ²Laboratório para a Sustentabilidade e Tecnologia em Regiões de Montanha, Instituto Politécnico de Bragança, Campus de Santa Apolónia, Bragança, Portugal; ³CICECO, Aveiro Institute Of Materials, Complexo de Laboratórios Tecnológicos, Aveiro University, Campus Universitário de Santiago, Aveiro, Portugal.

*jcoutinho@ua.pt



The poor water solubility of hydrophobic compounds can hinder their application in different fields (e.g., pharmaceutical, cosmetic or food industries). The addition of a co-solvent or hydrotrope is a common approach to address this issue, although the molecular-level mechanisms that induce the increase of the solubility are still not entirely understood. This work presents a methodology to predict and interpret the solubility enhancement of vanillin in mixtures of water with organic solvents (methanol, ethanol, and 1-propanol), using the Conductor-like Screening Model for Real Solvents (COSMO-RS). The effect of using different conformers, dependent on the solvent composition, was studied. It was found that this option allowed a better description of the solubility curves compared to the default distribution of conformers or the use of a single conformer. This work demonstrates the potential of COSMO-RS to predict the solubility of vanillin in pure and mixed solvents, as well as the liquid-liquid equilibria of the binary vanillin/water, and the importance of the selected conformers set on the quality of the predictions.

Introduction

Vanillin is a phenolic compound classified as an aromatic aldehyde (3-methoxy-4-hydroxybenzaldehyde), being a widely recognized flavour obtained from pods of *Vanilla planifolia* [1,2]. In addition to its organoleptic properties, vanillin and its derivatives present antioxidant activity, preventing oxidative damage to membranes and human cells [3]. Recent studies have shown that vanillin also presents anti-inflammatory effects [4].

The solubility of vanillin in water is much lower when compared to the values reported in several organic solvents [5]. Increasing its aqueous solubility could be beneficial to achieve a more sustainable extraction and purification from its natural source, and also to promote its incorporation into water-based products in the pharmaceutical and food industries. In this sense, hydrotropes could be used to achieve this solubility enhancement. Hydrotropes are a class of amphiphilic compounds that usually present high solubility in water, being either ionic or neutral compounds.

In this work, the Conductor-like Screening Model for Real Solvents (COSMO-RS), a model based on quantum chemistry and statistical thermodynamics [6-7], was used to predict the solubility of vanillin in pure solvents and mixtures of water and organic solvents (acting as hydrotropes or cosolvents), and the solid-liquid and liquid-liquid equilibria of the binary mixture of vanillin and water.

Acknowledgements

The authors are grateful to the Foundation for Science and Technology (FCT, Portugal) for financial support through national funds FCT/MCTES (PIDDAC) to CIMO (UIDB/00690/2020 and UIDP/00690/2020) and SusTEC (LA/P/0007/2020) and CICECO-Aveiro Institute of Materials, UIDB/50011/2020 & UIDP/50011/2020. I. W. Cordova is grateful to FCT for her contract 2022.12407.BD. Gabriel Teixeira is grateful to FCT for his Ph.D. grant (UI/BD/151114/2021).

Methods

Two vanillin conformers were optimized in the software package TURBOMOLE V7.4 2019 [8] using DFT with the BP-86 functional, the triple- ζ valence polarized basis set (TZVP-FINE), and the COSMO solvation model with infinite permittivity. To better predict the solubility curves, the conformer distribution was fitted to the experimental solubility data of vanillin in the pure solvents (water or organic solvents). For the mixed solvents, the conformer weights were calculated using a linear regression considering the conformers distribution already fitted for the pure solvents.

Results and conclusions

The default conformer set of COSMO-RS can qualitatively describe the solubility enhancement of vanillin by adding the co-solvent, though it systematically underpredicts the solubilities curves of vanillin when plotted against the composition of the mixed solvents. In this work, the predictions with the fitted conformers distribution showed an improved description of the solubility curves (in water + organic solvents) and of the liquid-liquid equilibria (water + vanillin), demonstrating the strong impact of selecting different conformers sets on the results.

References

- [1] S.S. Arya et al., *Advances in Traditional Medicine*, 21 (2021) 1-17.
- [2] G. Banerjee et al., *Journal of the Science of Food and Agriculture*, 99 (2019) 499-506.
- [3] L. Blaikie et al., *Bioorganic & Medicinal Chemistry Letters*, 30 (2020) 1-6.
- [4] H.M. Cheng et al., *Journal of Agricultural and Food Chemistry*, 65 (2017) 10233-10242.
- [5] F. Shakeel et al., *Food Chemistry*, 180 (2015) 244-248.
- [6] A. Klamt, *Journal of Physical Chemistry*, 99 (1995) 2224-2235.
- [7] BIOVIA COSMOtherm, Release (2021); Dassault Systèmes.
- [8] S.G. Balasubramani et al., *Journal of Chemical Physics*, 152 (2020) 184107.

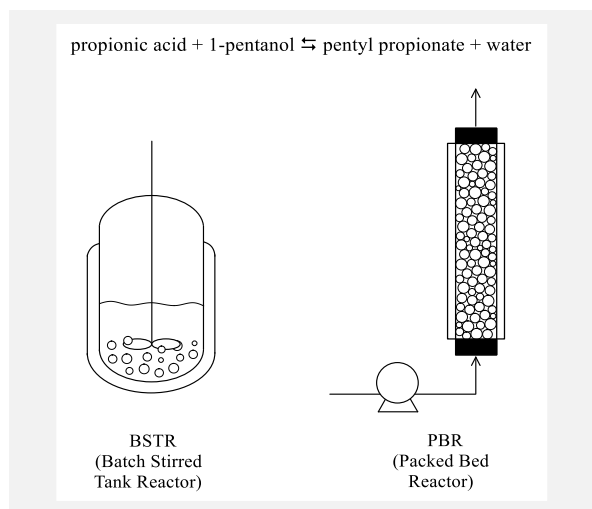
Solvent-free enzymatic esterification of pentyl propionate. Comparison of results using two types of reactors: BSTR and PBR

B. Lorenzo¹*, A. González², E. Martín², L. Domínguez¹, L. Fernández¹, J. Ortega¹

¹Division of Thermal Engineering & Instrumentation (IDeTIC), 35017-University of Las Palmas de Gran Canaria, Spain;

²Chemical Engineering Department, 37008-University of Salamanca, Spain.

*beatriz.lorenzo@ulpgc.es



This paper addresses the solvent-free esterification of pentan-1-ol with propionic acid to produce pentyl propionate, using Lipozyme®435 as catalyst. A batch stirred tank reactor (BSTR) and a packed bed continuous reactor (PBR) are tested and compared in technical and economic terms. The effect of some variables such as temperature, reagents proportion, catalyst load and flow rate is analyzed.

High conversions can be achieved in both reactors, evidencing the technical feasibility of the solvent-free reaction in both batch and continuous operation. Enzyme deactivation occurs as a result of the synergic effect of high temperatures (>70 °C) and low alcohol/acid ratio. At equal reaction conditions, enzyme deactivation is much stronger in the batch reactor, indicating a higher enzyme stability in the packed bed reactor.

Introduction

Biocatalysis has great potential for industrial-scale applications, but its use in the current industry is limited by the unfeasibility of such processes, taking into account certain metrics of an economic nature, as achievable product concentration, the performance of the product in relation to the substrate (mol product/mol substrate), yield considering space-time, or volumetric yield (mass product/(time×reactor volume), and biocatalyst yield (mass product/mass biocatalyst) [1]. These limitations can be overcome by adopting certain bioprocess intensification strategies, such as enzyme immobilization, solvent-free reaction systems and continuous flow enzymatic reactors [2,3], among others.

Despite these guidelines for achieving feasible processes for industrial applications, so far only a few articles have been published on immobilized enzyme esterification of short- and mid-chain carboxylic acids with alcohols in continuous flow reactors. In addition, the authors are not aware of any publication showing experiences under solvent-free conditions, nor using acetic acid as an acyl donor.

This work presents the results of an investigation on solvent-free esterification of pentan-1-ol with propionic acid to produce pentyl propionate using the immobilized commercial enzyme Lipozyme®435. The effect of temperature, reagents ratio, catalyst concentration and flow rate are studied and compared when using a batch-stirred-tank-reactor (BSTR) and a packed-bed-reactor (PBR), the latter operating in continuous flow.

Results

The observed behavior is complex and not regular. The effect of the temperature for the synthesis when using the ratio alcohol/acid=1 in BSTR, is an increase in the reaction rate and in the conversion until reaching 60 °C; then, these parameters strongly decrease at higher temperatures. However, in PBR a regular increase in the conversion and reaction rate is observed at temperatures up to 70 °C, and decreases when 80 °C is

reached, this negative variation being softer than in BSTR (Figure 1). This indicates that the stability of the enzyme is higher in PBR than in BSTR. On the other hand, for a ratio of alcohol/acid=2 a regular increase in both conversion and reaction rate is observed as the temperature increases in both reactors. This leads us to think that the deactivation of the enzyme is a result of the combination of several factors: high temperatures (>70 °C) and low alcohol/acid ratio.

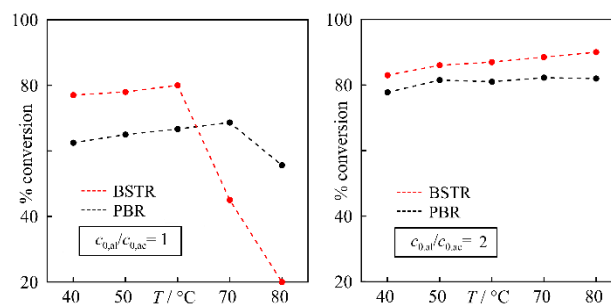


Figure 1. Reaction conversion at several temperatures for pentyl propionate synthesis in BSTR and PBR at alcohol/acid = 1 and 2.

The economical metrics calculated for the optimal conditions in each type of reactor indicate that the PBR is more suitable for industrial production of pentyl propionate (Table 1).

Table 1. Economical metrics calculated for pentyl propionate synthesis.

	Conversion (%)	$g_{ester}/(g_{cat} \times h)$	g_{ester}/g_{cat}	$g_{ester}/(L \times h)$
BSTR	80.4	4.2	618	27.2
PBR	80.0	3.7	295	791

The PBR showed good stability for the operation time tested in this work (3 h). According to a previous work [4] in which the enzyme has been reused in 10 successive 8-hour cycles without deactivation, PBR is expected to be stable for more than 80 hours.

Acknowledgements

The authors thank the Spanish Ministry of Science and Innovation for the grant number PID2021-127970OB-I00, and Novozymes© for providing the catalyst used in this work. B.L. is grateful for her predoctoral contract (PRE2019-087401) from the Spanish Ministry of Science and Innovation.

References

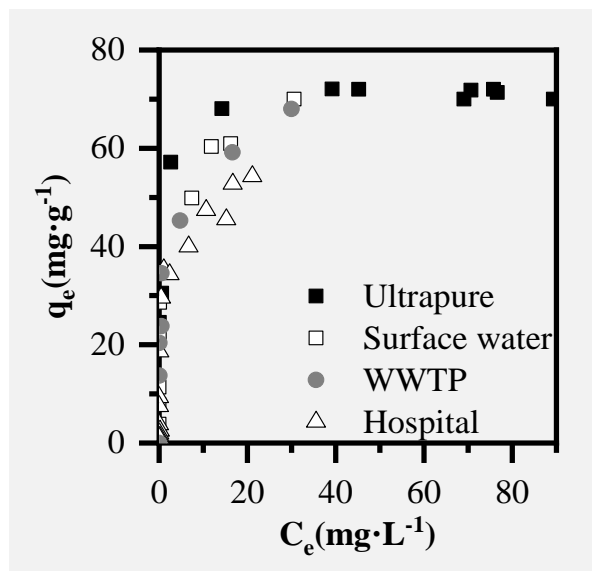
- [1] M. Meissner et al., *Nature Catalysis*, 5 (2022) 2-4.
- [2] H.M. Salvi et al., *Catalysis Science and Technology*, 11 (2021) 1994-2020.
- [3] R. Rodrigues Sousa et al., *Catalysis Science and Technology*, 11 (2021) 5696-5711.
- [4] B. Lorenzo et al., *Processes*, 11 (2023) 1640-1653.

High-adsorption-performance carbon material for removal of fluoroquinolone from wastewater

A.B.H. Abreu, S. Álvarez-Torrellas, V.I. Águeda, J.A. Delgado, J. Carbajo*, J. García

Catalysis and Separation Processes Group (CyPS), Chemical Engineering and Materials Department, Faculty of Chemistry, Complutense University, Avda. Complutense s/n, 28040 Madrid, Spain.

*jcarbajo@ucm.es



In this work, the adsorption of a fluoroquinolone on a new carbon xerogel (RFX) has been studied. Stirred tank adsorption experiments have been carried out in order to evaluate the kinetics and the adsorption equilibrium, obtaining an equilibrium time of 24 h and an equilibrium adsorption capacity of 0.072 kg kg⁻¹. In addition, the influence of pH and the nature of different real aqueous matrices were studied, concluding that both parameters affect the adsorption process of ciprofloxacin. On the other hand, fixed bed adsorption experiments were carried out, studying several operating parameters. Also, the regeneration of the adsorbent was evaluated in a satisfactory way. Finally, a mathematical model based on conservation equations was proposed by means of which the experimental breakage curves were satisfactorily fitted and the matter transfer coefficients of the process were estimated.

Introduction

Antibiotics are one of the most widely used types of drugs today, instrumental in combating many infectious diseases in humans and animals. As a consequence of incomplete metabolism and direct elimination of unused antibiotic residues, these compounds have been frequently detected in the aquatic environment. In recent decades, this situation has gained much attention because antibiotics can cause resistance in bacterial populations, rendering them ineffective in the treatment of many diseases [1].

The aim of this work is to evaluate the removal of the antibiotic ciprofloxacin (CPX) in water on a carbon xerogel by stirred tank and fixed bed adsorption. The kinetics, the adsorption equilibrium, the influence of the pH of the solution and the nature of the aqueous matrix on the adsorption of CPX have been studied. The effect of different operating variables on the continuous adsorption process was also analysed and the regeneration of the adsorbent was investigated. Finally, a mathematical model based on conservation equations has been used to determine the matter transfer coefficients necessary to design an industrial scale adsorption unit.

Materials and methods

Materials

Ciprofloxacin (CPX) ($\geq 98\%$) and formaldehyde (36.5-38% in water and stabilised with 10-15% methanol) were supplied by Sigma-Aldrich. Resorcinol ($\geq 99\%$), sodium hydroxide (98%) and methanol ($\geq 99\%$) were supplied by Fluka, Panreac and Fischer Chemical, respectively.

Adsorbent synthesis

The xerogels (RFX) were synthesized following the procedure described by Job et al [2]. The reaction of resorcinol (R) and formaldehyde (F) was carried out in aqueous medium under the following conditions: molar ratio R: F=0.5, and pH=5.8. Then, the dried solid was pyrolyzed under inert atmosphere ($N_2 = 100$

cm³ min⁻¹) at 800°C for 2 h. Finally, the resulting material was ground and sieved.

Characterisation of the adsorbent

The RFX material was characterised by N₂ adsorption-desorption isotherms at -196°C using a Micromeritics ASAP 2020. Also, the isoelectric point (pH_{PIE}) of the RFX material was determined by determining the zeta potential as a function of pH using a Nano-ZS90 Zetasizer (Malvern Instruments, Ltd.).

Stirred tank adsorption experiments

In order to study the kinetics and equilibrium of adsorption of CPX on RFX, stirred tank adsorption experiments were carried out by placing 25 mL of a CPX solution ($C_0 = 0.1$ kg m⁻³) in contact with different adsorbent masses (0.001-0.1 g) at 25±1 °C and a stirring speed of 250 rpm. Batch experiments were carried out using different real matrices (hospital effluent, surface water and WWTP effluent) and initial solutions with different pH (4, 6, 7, 10) prepared with buffer solutions, using an initial concentration of 0.03 kg m⁻³. The concentration of CPX in the samples was analysed on a Varian Prostar HPLC chromatograph using a Perkin Elmer C18 column (220 mm x 3.6 mm; 5µm). Acetonitrile-water (25/75 v/v) ($Q = 0.5$ mL min⁻¹) and a wavelength of 278 nm were used as mobile phase.

Fixed bed adsorption experiments

In the continuous adsorption experiments, the concentration of CPX in the effluent was measured continuously in a UV-Vis detector (Varian 9050 model) at a wavelength of 295 nm. All experiments were carried out at constant temperature (25±1 °C) using ultrapure water solutions. The influence of the volumetric flow rate (Q), the initial CPX concentration (C₀) and the mass of RFX (m_{RFX}) on the breakthrough and saturation times, the shape of the breakthrough curves and the matter transfer parameters were investigated.

Modelling of fixed bed adsorption experiments

The matter transfer between the liquid phase and the adsorbent is described by the Homogeneous Solid Diffusion Model (HSDM) [3,4] using the Linear Driving Force (LDF) approximation [5]. Two series resistances to matter transfer have been considered: the external matter transfer coefficient in the liquid film (k_f) and in the adsorbed phase (K_s). The resulting Ordinary Differential Equation (ODE) system was integrated using the ODEPACK package.

Results and Discussion

The N_2 adsorption-desorption isotherm of RFX can be classified as a Type-I isotherm, suggesting that the material has a high degree of microporosity with a large contribution of macropores. The results about the influence of pH on the CPX adsorption revealed that the adsorption capacity showed a high decreasing at pH = 10, due to the occurrence of repulsive interactions between the negatively charged adsorbent surface and the adsorbate, which is in its anionic form at pH 10 (Figure 1). On the other hand, a slight decrease in the CPX removal could be observed in the adsorption experiments accomplished with both surface water and WWTP effluent, while a much more drastic decrease (23%) was found with the hospital effluent (Figure Graphical abstract). Moreover, several fixed-bed adsorption experiments were carried out at different values of volumetric flow rate ($Q = 0.2, 0.5, 1.0 \text{ mL min}^{-1}$), initial CPX concentration ($C_0 = 0.005, 0.02, 0.04 \text{ kg m}^{-3}$), and mass of adsorbent ($m = 0.01, 0.05 \text{ g}$), in order to study their influence on the breakthrough curves. As flow rate increased, besides of a shorter breakthrough time, a higher slope of the curve was observed, which is indicative of a decreasing of the external mass transfer resistance. Thus, when the initial concentration increased, the breakthrough of the bed occurred faster. Besides, for a higher mass of adsorbent, the breakthrough time increased; additionally, for a fully-developed concentration profile in the bed, at different column length values, parallel breakthrough curves could be expected [6,7]. In addition, regeneration studies of the adsorbent using methanol were accomplished; only a decreasing of 16% in the adsorption capacity was measured after 3 consecutive adsorption-desorption cycles. Finally, a mathematical model based on conservative equations was used for the fitting of the experimental breakthrough curves. By this way, both the external mass transfer coefficients in the adsorbed

phase (K_s) and in the liquid boundary layer (k_f) could be calculated. Thus, K_s value was found of $1.51 \cdot 10^{-4} \text{ s}^{-1}$, and k_f were of $5.34 \cdot 10^{-5}$ and $9.62 \cdot 10^{-6}$, for volumetric flow rates of 0.5 and 0.2 mL min^{-1} , respectively.

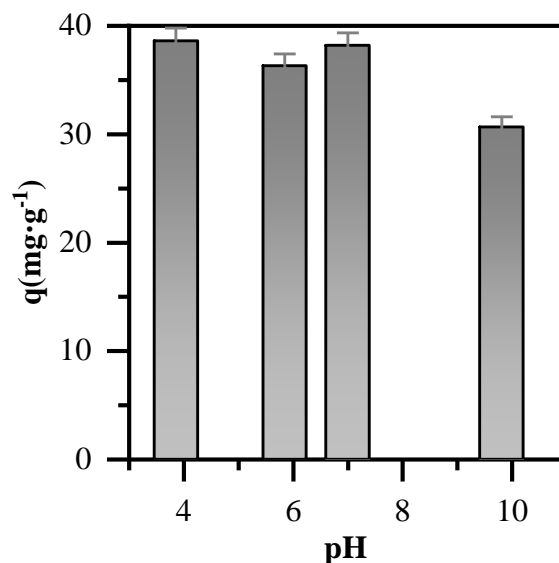


Figure 1. Batch adsorption experiments. Influence of the pH of the solution on the adsorption of CPX on RFX.

Conclusions

In this work, the removal of CPX on a carbon xerogel (RFX) was studied by means of stirred tank and fixed bed adsorption processes. The batch experiments revealed that pH and organic matter content are factors that significantly affect the adsorption capacity of CPX and can lead to a decrease in adsorption capacity. On the other hand, a high degree of adsorbent regeneration was achieved after 3 adsorption-desorption cycles, using methanol as regeneration agent. Finally, the experimental breakage curves were satisfactorily adjusted by means of a mathematical model based on conservative equations, obtaining the matter transfer coefficients in the adsorbed phase (K_s) and in the liquid film (k_f), observing that k_f increases with increasing volumetric flow rate.

Acknowledgements

This work has been supported by the Spanish MICINN through the project CATAD3.0 PID2020-116478RB-I00. In addition, the authors thank the financial support from the Comunidad de Madrid (Spain) through the Industrial PhD projects (IND2017/AMB-7720 and IND2019/AMB-17114), REMTAVARES Network (S2018/EMT-4341) and the European Social Fund.

References

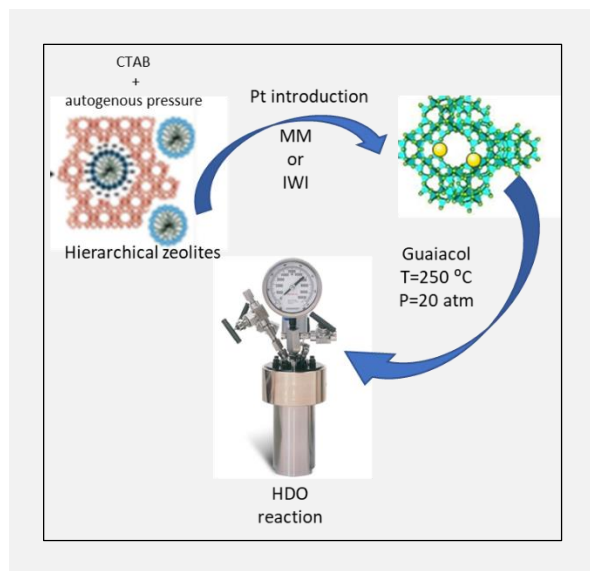
- [1] Z. Movasaghi et al., *Industrial Crops & Products*, 127 (2019) 237-250.
- [2] N. Job et al., *Carbon*, 42 (2004) 619-628.
- [3] T.W. Weber, R.K. Chakraborti, *Journal of American Institute of Chemical Engineers*, 20 (1974) 228-238.
- [4] V. Meshko et al., *Water Resources*, 35 (2001) 3357-3366.
- [5] Z. Xu et al., *Journal Zhejiang University Science A*, 14 (2013) 155-176.
- [6] A. Spaltro et al., *Journal of Contaminant Hydrology*, 218 (2018) 84-93.
- [7] A.B. Hernández-Abreu et al., *Applied Surface Science*, 552 (2021) 149513.

Design of hierarchical Pt/zeolite catalysts for the hydrodeoxygenation of biomass-derived oxygenated molecules

M. Matos¹, L.C. Silva¹, M. Araújo¹, N. Horta¹, B. Amaro¹, A.P. Carvalho^{2,3}, N. Nunes^{1,2}, J. Coelho^{1,4}, A. Martins^{1,2*}

¹DEQ, Instituto Superior de Engenharia de Lisboa, Instituto Politécnico de Lisboa, Lisboa, Portugal, ²Centro de Química Estrutural, Faculdade de Ciências, Institute of Molecular Sciences, Universidade de Lisboa, Lisboa, Portugal, ³Departamento de Química e Bioquímica, Faculdade de Ciências Universidade de Lisboa, Lisboa, Portugal; ⁴Centro de Química Estrutural, Instituto Superior Técnico, Institute of Molecular Sciences, Universidade de Lisboa, Lisboa, Portugal.

*amartins@deq.isel.ipl.pt



New energy sources, such as biomass, are being explored as an alternative to fossil fuels. However, the transformation of biomass into bio-oils fuels yields high oxygen content products, which is not a satisfactory outcome. To counter this, an hydrodeoxygenation (HDO) reaction can be performed in the presence of bifunctional catalysts. In this study commercial Y and ZSM-5 zeolites or respective hierarchical zeolites, prepared by soft templating method, were used as acid supports. The metal function (Pt) was immobilized through mechanical mixture (MM) or incipient wetness impregnation (IWI). The catalytic behavior was studied in a high-pressure batch reactor using guaiacol as a model oxygenated molecule at 250 °C and 20 atm. Preliminary results showed the influence of structure and acidity of the zeolite support as well as the effect of the hierarchical porosity. It was also found that mechanical mixture is a simple and effective method to prepare the bifunctional catalysts for HDO reaction.

Introduction

To overcome the environmental issues raised by fossil fuels, new energy sources, such as biomass, are being explored. Biomass can be transformed into bio-oil which, however due to the high oxygen content of this product, it doesn't present the adequate properties of a fuel. [1] To make it suitable, hydrodeoxygenation (HDO) reaction is generally performed. Catalytic HDO is carried out in presence of a bifunctional (metal and acid) catalyst. Metal loaded zeolites are among the most studied catalyst for HDO reactions [2]. Nonetheless, the strong acidity of these materials as well as its intrinsic microporosity may lead to deactivation phenomena, despite the presence of the metal function. A possible solution is the use of hierarchical zeolites with tuned acidity and porosity [3]. One of the strategies to produce hierarchical zeolites is the surfactant templated method, proposed by Garcia-Martinez et al. where a post synthesis alkaline treatment in the presence of a surfactant followed by a thermal heating under autogenous pressure produces material with ordered micro + mesoporosity. (Figure 1) In this study, the potentialities of commercial and hierarchical zeolites prepared by soft templated method are explored. The obtained materials are loaded with Pt through mechanical mixture or incipient impregnation method. The catalytic behaviour is studied in the hydrodeoxygenation of oxygenated model molecules, such as guaiacol.

Methods

Commercial zeolites NH₄ZSM-5 (Si/Al=15) and NaY (Si/Al=5.1), both from Zeolyst were used as starting materials. Parent HZSM-5 was obtained through calcination (550°C under dry air) of the parent material in ammonium form. NaY was used as received and submitted to ion exchange with 2 M

NH₄NO₃ at 80 °C for 6 h, followed by calcination at 550 °C. Both parent zeolites were modified through the surfactant templated method using previously optimized procedures [5,6].

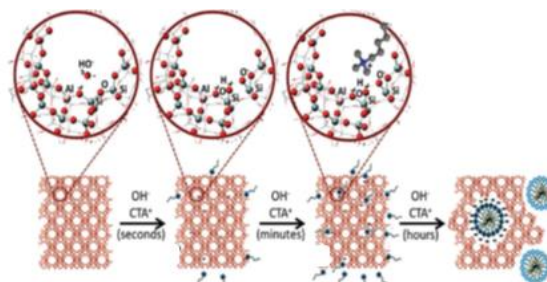


Figure 1. Surfactant-templated method [4].

The metal function (Pt) was introduced using two distinct procedures: mechanical mixture (MM) with commercial PtAl₂O₃ using an agata mortar and incipient wetness impregnation (IWI), mixing the zeolite samples with the minimum aqueous solution of H₂PtCl₆.xH₂O. In both cases the Pt content on the zeolites is 1 (wt.%). The produced samples were named following the code: Pt/ZEO_ST_MM/IWI, where ZEO is the name of the zeolite, ST was used in the case of Soft Templated hierarchical materials, and MM or IWI is the method used for Pt addition.

The HDO catalytic experiments were performed in a 50 mL batch Parr reactor (Figure 2) using 200 mg of bifunctional catalyst and 25 ml of reaction mixture (5 vol. % guaiacol in *n*-heptane), heated at 250 °C, pressure of 20 atm and 350 rpm stirring. Upon heating the reaction mixture, samples were withdrawn after 15-, 30- and 60-min reaction. The samples were analysed using a gas chromatograph (Perkin Elmer, Auto

System) equipped with FID detector and a 30 m capillary column DB5-MS.



Figure 2. Parr 4843 batch reactor.

Results

In this study bifunctional catalysts prepared from two zeolitic matrixes (Y and ZSM-5), were studied and several parameters were evaluated: i) influence of the mode of Pt introduction (mechanical mixture *vs* incipient wetness impregnation); ii) effect of the different pore sizes and topology for the two zeolite structures; iii) acidity of the zeolitic support in the case of Y zeolite (NaY *vs* HY); iv) effect of hierarchical porosity for both zeolite structures. For all catalysts the reaction conditions were kept constant. The zeolite matrixes were previously characterized by powder X-ray diffraction, showing the original diffraction patterns were kept although some loss of crystallinity was observed in the case of hierarchical materials. The textural properties were evaluated through low temperature N₂ adsorption isotherms, denoting the presence of micro+mesoporosity in the case of hierarchical materials. The total conversion of guaiacol for all the bifunctional catalysts at 250 °C and 20 atm is presented on Figure 3.

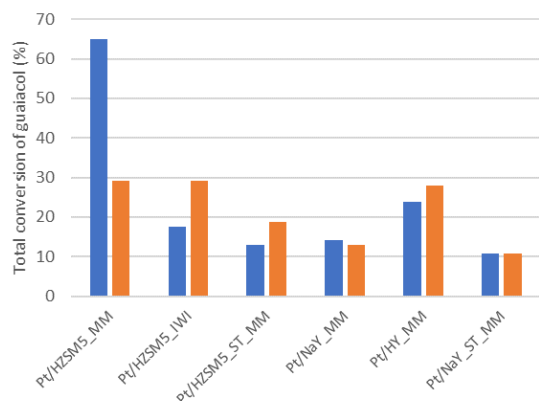


Figure 3. Total conversion of guaiacol after 15 min (blue) and 60 min (orange) reaction time at 250 °C and 20 atm.

Acknowledgements

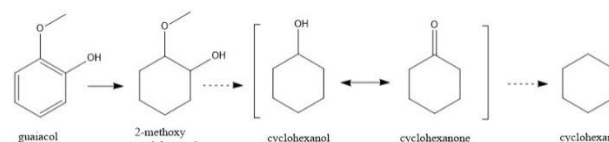
This research was funded by Fundação para a Ciência e Tecnologia (FCT) through UIDB/00100/2020, UIDP/00100/2020 and LA/P/0056/2020.

References

- [1] S. Kim et al., *Green Chemistry*, 21 (2019) 3715.
- [2] R.F. Nunes et al., *Molecules*, 28 (2023) 2245.
- [3] A. Carvalho et al., *Hierarchical Zeolites: Preparation, Properties and Catalytic Applications*, Nova Science Publishers, New York, 2015.
- [4] M.J. Mendoza-Castro et al., *Advanced Materials Interfaces*, 8 (2020) 1-23.
- [5] A. Talebian-Kiakalaieh, S. Tarighi, *Journal of Industrial and Engineering Chemistry*, 88 (2020) 167.
- [6] A. Martins et al., *Microporous and Mesoporous Materials*, 323 (2021) 1111167.
- [7] C.R. Lee et al., *Catalysis Communications*, 17 (2012) 54.

The method used for the introduction of the metal function (MM *vs* IWI) was evaluated for HZSM-5 based catalysts, being Pt/HZSM-5_MM the sample where the highest conversion was obtained, thus, this method was selected to prepare all the other catalysts. When confronting the catalysts with distinct zeolite structures one can see that in the presence of Pt/HZSM-5_MM the conversion is substantially higher when compared with Pt/HY_MM, probably because the medium pore size of HZSM-5 does not allow the formation of high amounts of bulky intermediates. On the other hand, the role of the support acidity (NaY *vs* HY) shows that the presence of protonic acid sites in Pt/HY_MM samples leads to almost double conversion when compared with Pt/NaY_MM. Finally, the behaviour of hierarchical materials (ST samples) shows for the samples prepared so far, catalytic conversions lower than the ones obtained from the respective parent materials.

The product distribution for all catalysts agrees with the reaction pathways for the HDO reaction proposed by Lee et al. [7] for the reaction that occur on noble metals catalysts with acid support (Scheme 1). However, the detection of phenol and benzene in some cases can indicate the occurrence of the reaction pathways on solely acid sites.



Scheme 1. HDO reaction pathway on the noble metal catalysts with acid supports (dashed lines represents the reaction steps on the acid sites and continuous lines are for the reactions on the noble metal sites) [7].

Conclusions

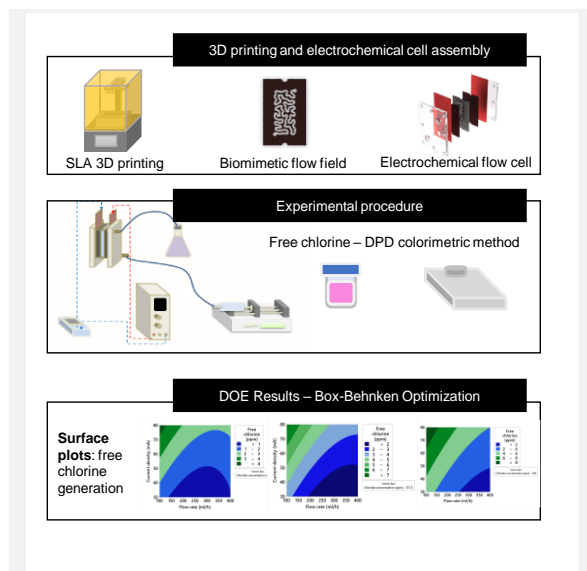
The preliminary results in this study allow us to understand the effects of several parameters, namely, the zeolite structure, acidity, texture, and Pt mode of incorporation, for the chosen reactions conditions in the HDO reaction. This study will continue with the optimization of soft templated hierarchical zeolites as well as improvements on the mechanical mixture, using a ball mill.

3D printed biomimetic flow fields for the electrochemical generation of free chlorine

I. García-López*, V.I. Águeda, A. Garrido-Escudero

Research Group Catalysis & Separation Processes (CYPS), Department of Chemical Engineering, Universidad Complutense de Madrid, 28040, Madrid, Spain.

*inmgarci@ucm.es



Access to clean drinking water to remote locations in developing countries still represents a challenge. Electrochlorination has appeared as an efficient and adaptable alternative for in-situ water disinfection. However, most electrochlorinators rely on the replenishment of sodium chloride to produce free chlorine efficiently. In this work, a new 3D printed biomimetic flow field was developed to enhance the mass transfer inside the electrochemical cell, to convert the chlorides naturally present in water into free chlorine, avoiding the addition of salt. A Box-Behnken Design of Experiments (DOE) was carried out to analyze the influence of three operative parameters (chloride concentration, water flow rate and applied current) into the response variable (free chlorine). In all the tested conditions, the free chlorine generation exceeded 0,5 mg/L, achieving a maximum of 7,55 mg/L. These operative conditions could be adjusted in the future to the water requirements depending on the location.

Introduction

Chlorination is the most widely extended disinfection method due to its killing efficiency against pathogens. To avoid the handling and dosing of the hazardous chlorine, electrochlorination is becoming more and more extended nowadays. Electrochemical flow cells allow an efficient conversion of chlorides in water into free chlorine [1], especially at low chloride concentrations [2]. The flow field plays an important role in mass transport. Differential growth shapes, present in numerous systems in nature like the human intestine, have demonstrated to increase the mass transfer in electrochemical cell in a very compact volume [3]. In this work, we propose to apply this biomimetic geometry to the free chlorine generation, relying only in the chlorides present in water. To extract the maximum information in a very short number of experiments, the Design of Experiments (DOE) methodology was employed.

Materials and methods

The biomimetic channel was designed parametrically using the software Rhinoceros and its extension Grasshopper. More details regarding the geometry generation can be found elsewhere [4]. The flow field containing the channel space, which also served as a gasket, was 3D printed in a commercial SLA 3D printer (Anycubic Photon Mono) with an ABS-like resin. Then, it was cleaned with isopropyl alcohol 99% and cured with UV 405 nm light.

The flow field was assembled in a filter-press like configuration, according to the description defined in [3]. Graphite was used as anode and stainless-steel 304 as cathode. The electrochemical cell was connected to a power supply, which allowed the applied current regulation.

The water containing chlorides was injected to the flow cell by a syringe pump. After the electrochemical treatment, this water was collected in a flask, from where 10 ml were taken. To measure the free chlorine contained in the sample, a DPD (N,N-

diethyl-p-phenylenediamine) pill reagent (Lovibond) was added to the 10 ml of water. The color intensity was measured by a photometer and related to the total free chlorine concentration. A Box-Behnken (BB) response surface design was employed. In this design, each variable was evaluated over three levels with equally spaced values (coded as -1, 0, +1). The range of the operative parameters were flow rate, 100-400 ml/h; applied current, 30-80 mA; chloride concentration, 25-250 mg/L. The total number of experiments with the matrix generated by the Minitab software was 15.

Results

The model statistical significance and its validity were tested through the analysis of variance (ANOVA). The model robustness was evaluated by the coefficient of determination (R^2) and the adjusted coefficient of determination (adjusted R^2), which were 0,983 and 0,954, respectively. The three independent variables were significant (p value < 0,05), and the interaction of flow rate and chloride, and the quadratic interaction of flow rate.

Two-dimensional response surface plots are drawn in Figure 1 to visualize the interaction effects between applied current and flow rate over free chlorine production, for each chloride concentration. The maximum free chlorine generation corresponds to the regions of low flow rate and high current density. At low flow rate, the residence time inside the reactor increases, and so the conversion of chlorides into chlorine. High current also increases conversion into products according to Faraday's law.

The typical concentration of residual free chlorine in drinking water after disinfection is 0,2-1 mg/L. According to the chloride concentration of the water to be treated, the operative conditions can be adjusted in the electrochlorinator to achieve the desired disinfectant concentration.

Conclusions

In this work, a novel 3D printed biomimetic electrochemical flow cell was developed. This design allows obtaining up to 7,55

mg/L of free chlorine in a very compact volume. It represents an opportunity to be installed in remote locations where access to centralize disinfection systems is difficult or not possible.

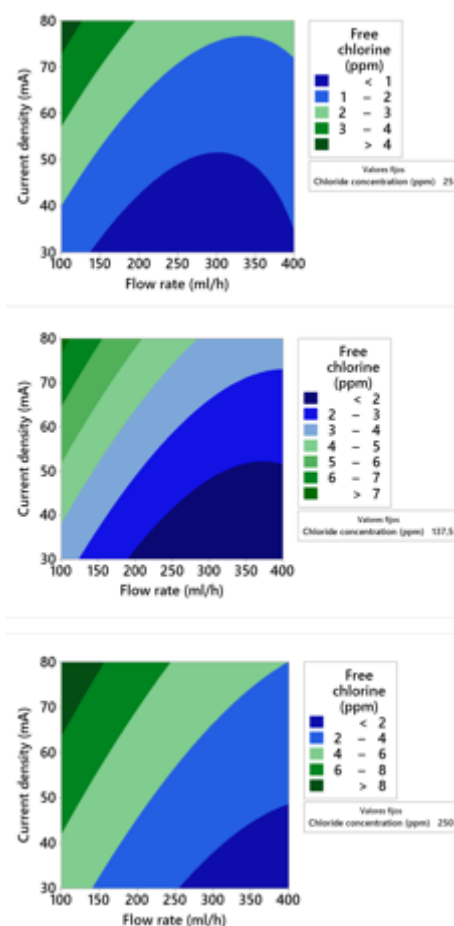


Figure 1. Free chlorine surface responses at three chloride concentrations.

Acknowledgements

Funding from the Centre for the Development of Industrial Technology (CDTI) through project MIG-20201034 (ShineFleet) and from the MICINN through the CATAD3.0 project PID2020-116478RB-I00 are gratefully acknowledged.

References

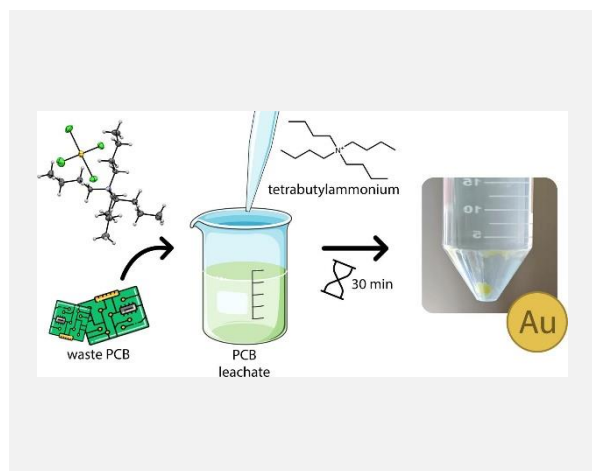
- [1] E. Chinello et al., *Journal of The Electrochemical Society*, 166 (2019) E336.
- [2] D. Ocasio, D.L. Sedlak, *ACS ES&T Engineering*, 2 (2022) 1933-1941.
- [3] I. García-López et al., *Reaction Chemistry & Engineering*, 8 (2023) 1776-1784.
- [4] I. García-López et al., *Chemical Engineering Journal Advances*, 13 (2023) 100438.

Selective precipitation of gold from an aqua regia leachate of e-waste using a quaternary ammonium ionic liquid

A.F.M. Nogueira¹, A.R.F. Carreira¹, S.J.R. Vargas^{1,2}, H. Passos¹, N. Schaeffer^{1*}, J.A.P. Coutinho¹

¹CICECO - Aveiro Institute of Materials, Department of Chemistry, University of Aveiro, 3810-193 Aveiro, Portugal; ²Purdue University, West Lafayette, IN 47907, United States.

*nicolas.schaeffer@ua.pt



E-waste is a source of valuable base and precious metals, making its exploration a key step in reducing the environmental impact of modern electronics. Gold is present in e-waste in greater concentrations than the primary ores from which it is mined, providing a strong incentive for its recycling. In this work, the use of a quaternary ammonium ionic liquid (IL) as a precipitating agent for the selective recovery of gold from an aqua regia leachate of printed circuit boards was investigated. A suitable IL was selected considering the cation's apolar volume and geometry as well as counter-anion selection. Optimized precipitation conditions were applied to a leachate sample, resulting in a gold salt with a metallic content of over 90% gold. The technique presented herein allows for the selective separation of gold using relatively simple materials and techniques with a lower reagent use than what is required with other gold separation techniques employing ILs.

Introduction

E-waste is a source of valuable base and precious metals, making its exploration a key step in reducing the environmental impact of modern electronics and establishing a circular market for critical and rare materials [1], [2]. Gold is one of such materials present in e-waste in greater concentrations than the primary ores from which it is mined, providing a strong justification for its recycling [3]. Precipitation processes, if selective, present a simple and economical alternative for the recovery of critical metals from primary and secondary ores including electronic wastes.

Objectives

In this work, the recovery of gold by precipitation from both mono-elemental solutions and real CPU leach solution is demonstrated using hydrophilic quaternary ammonium salts. A simple precipitation procedure is proposed that minimizes the use of organic solvents whilst eliminating the need for complex synthesis and post modification [4].

Methods

Gold, tin, platinum, iron, nickel and copper solutions were prepared by dissolution of the corresponding chloride salts in distilled water. Quaternary ammonium ($[N_{xxxx}]^+$, $2 \leq x \leq 5$), 1-methyl-1-methylpiperidinium ($[C_4mpip]^+$) and 1-butyl-3-methylimidazolium ($[C_4mim]^+$) solutions were prepared by dissolution of the corresponding chloride, bromide or nitrate salts in distilled water. The CPU leachate was obtained by two successive leaching steps using nitric acid and aqua regia following a previously described protocol [5].

Precipitation was assessed by measuring the concentration of metals in solution before and after addition of the ionic liquid (IL) solutions by Total Reflection X-Ray Fluorescence (TXRF). Precipitate structure was assessed by X-Ray Diffraction (XRD) and Raman spectroscopy.

Results

A suitable IL was selected considering the cation's apolar volume and geometry as well as counter-anion selection. The precipitation was optimized in regard to time, the IL to Au molar ratio, temperature and aqua regia dilution. IL to gold ratio and dilution were found to be the key factors driving the precipitation. The gold precipitation yield is shown to be dependent on the apolar volume of the precipitant, with the addition of tetrabutylammonium-based salts resulting in the recovery of over 90 % of gold from synthetic solutions. The origin of gold precipitation selectivity relative to common metal ions upon addition of tetrabutylammonium nitrate ($[N_{4444}][NO_3]$) was assigned by X-ray crystal structure to the formation of size selective apolar cavity between neighbouring $[N_{4444}]^+$ cation and the $[AuCl_4]^-$ anion.

Following optimisation as a function of the gold to precipitant molar ratio, aqua regia concentration and time, approximately 70 % of gold could be recovered from waste CPU leach solution with a final purity of 91.4 % (mol/mol). In various leachate conditions, $[N_{4444}][NO_3]$ demonstrated its versatility as a gold extractant. It can be effectively utilized within an acidic aqueous biphasic system, particularly when higher aqua regia concentrations lead to decreased precipitation yields. This ensures a selective gold recovery approach.

Conclusions

The $[N_{4444}]^+$ cation was proven to be a selective towards Au against Cu, Ni or Pt under a variety of conditions, allowing the disclosed methodology to be applied to a range of relevant and/or difficult separations.

A tetrabutylammonium tetrachloroaurate salt is obtained by following the procedure described herein. Tetrabutylammonium salts are widely used in numerous applications, including as phase transfer catalysts [6]. The disclosed results improve the circularity of gold, offering a straightforward method for its recycling.

Acknowledgements

This work was developed within the scope of the project CICECO-Aveiro Institute of Materials, UIDB/50011/2020, UIDP/50011/2020 & LA/P/0006/2020, financed by national funds through the FCT/MEC (PIDDAC). H. Passos and A.R.F. Carreira acknowledge FCT, under the Scientific Employment Stimulus Individual Call (CEECIND/00831/2017) and Ph.D. grants SFRH/BD/143612/2019, respectively. N. Schaeffer acknowledges the national funds (OE), through FCT in the scope of the framework contract foreseen in the numbers 4, 5 and 6 of the article 23, of the Decree-Law 57/2016, of August 29, changed by Law 57/2017, of July 19.

References

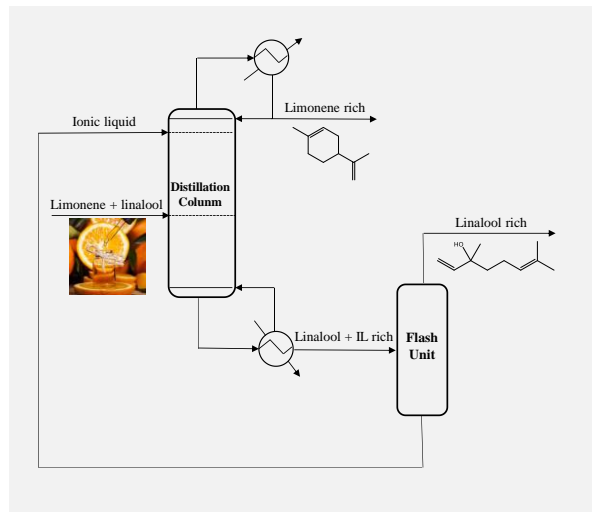
- [1] J. Cui, L. Zhang, *Journal of Hazardous Materials*, 158 (2008) 28-256.
- [2] V. Forti et al., 'The Global E-waste Monitor 2020', *U. N. Univ. UNU Int. Telecommun. Union ITU Int. Solid Waste Assoc. ISWA BonnGenevaRotterdam*, 120, 2020.
- [3] G.J. Hutchings et al., *Chemical Society Reviews*, 37 (2008) 1759.
- [4] A.F.M. Nogueira et al., *Separation and Purification Technology*, 316 (2023) 123797.
- [5] M.C. Hespanhol et al., *Journal of the Taiwan Institute of Chemical Engineering*, 115 (2020) 218-222.
- [6] B.K. Banik et al., *Molecules*, 25 (2020) 5918.

Fractionation of citrus essential oil through extractive vacuum distillation using imidazolium-based ionic liquids as entrainers

S.M. Vilas-Boas^{1,2,3,4*}, F.R.M. Batista⁵, R.M. Dias⁶, J.A.P. Coutinho³, Q. Ferreira^{1,2}, M.C. da Costa⁴, S.P. Pinho^{1,2}

¹Centro de Investigação de Montanha (CIMO), Instituto Politécnico de Bragança, Campus de Santa Apolónia, 5300-253 Bragança, Portugal; ²Laboratório para a Sustentabilidade e Tecnologia em Regiões de Montanha, Instituto Politécnico de Bragança, Campus de Santa Apolónia, 5300-253 Bragança, Portugal; ³CICECO – Aveiro Institute of Materials, Department of Chemistry, University of Aveiro, 3810-193 Aveiro, Portugal; ⁴School of Chemical Engineering (FEQ), University of Campinas (UNICAMP), 13083-852 Campinas, Brazil; ⁵Department of Chemical Engineering, School of Engineering of Lorena, University of São Paulo - USP, Lorena, 12602-810, SP, Brazil; ⁶Chemical Institute (IQ), Federal University of Goiás – UFG, Campus Samambaia, 74001-970, Goiânia, GO, Brazil.

*sergiomboas@ipb.pt



Removing the hydrocarbon fraction from the oxygenated terpenic fraction of citrus essential oils (CEOs) is a crucial step to improve the stability and preserve the sensorial properties of the final product. One of the most common separation processes used to fractionate CEOs at the industrial level is vacuum distillation. This work evaluates the use of two imidazolium-based ionic liquids (ILs), [C₄mim][OAc] and [C₄mim]Cl, as entrainers for the fractionation of CEO in a process composed by an extractive distillation column and a flash separator unit. As commonly found in CEO profiles, a mixture of limonene (hydrocarbon) and linalool (alcohol) was used to model the CEO. Vapor-liquid equilibrium (VLE) measurements of the limonene/linalool and limonene/linalool/IL mixtures were carried out at 5 kPa, and the obtained data were considered in the process simulation. The results suggest that [C₄mim]Cl is more effective than [C₄mim][OAc] in improving the linalool purity in the final product.

Introduction

Essential oils (EOs) are the most abundant sources of terpenes and terpenoids [1], which are the sources of the oil's pleasant aromas and biological and pharmacological properties [2]. Among the different EOs, those extracted from citrus species are one of the most commercially attractive options, especially due to their wide use as natural fragrances and flavors [3]. Besides, CEOs present numerous appealing properties, such as antioxidant, antibacterial, antidiabetic, antifungal, and insecticidal activities [4].

Although hydrocarbon terpenes are frequently the major constituents of citrus EO, they contribute little to the flavor and fragrance associated with the final product. The hydrocarbon part is poorly soluble in water and alcohol, interfering with the yield of the extraction process. Moreover, monoterpenes and sesquiterpenes are easily oxidized in off-flavors, deteriorating the essential oil's flavor and aroma [5]. Therefore, separating the hydrocarbon from the oxygenated fraction, a process known as deterpenation, is crucial to improve commercial essential oils' stability, solubility, and storage requirements [6]. At the industrial level, deterpenation is a key step to produce high-quality CEOs. The most common separation processes applied in industry to fractionate CEOs are liquid-liquid extraction or vacuum distillation [5]. The latter is often preferred since it usually delivers higher purities for the final product.

In the present work, isobaric vapor-liquid equilibrium measurements were carried out for limonene/linalool and limonene/linalool/IL mixtures at 5 kPa. Then, the acquired VLE data were considered in the process simulation composed of an extractive distillation column and a flash separator unit.

Experimental procedure for the VLE measurements

The VLE experiments were conducted using a dynamic recirculation ebulliometer (Fischer GmbH, 0602) coupled to a thermostatic bath (Nova Ética, NT 281), a vacuum pump

(Edwards, RV5), and a pressure control unit (Fisher system M101). The experiments were performed at 5 kPa to avoid temperature ranges where the organoleptic properties of the CEOs can be compromised [7]. The ebulliometer operates under continuous recirculation of the liquid and vapor phases until reaching the equilibrium, assumed after (30-40) min at constant temperature and pressure. For each reported data, two samples with volumes between (0.1-0.5) cm³ were collected from the liquid and condensed vapor phases with a gas-tight syringe through sampling nozzles covered by silicone seals. The phase composition was determined by refractometry (Mettler Toledo, RE40D). For the limonene + linalool + IL systems, the standard solutions had a constant mass fraction of IL of (0.050 ± 0.001).

Process simulation

The process simulation was conducted in the Aspen Plus V11 commercial software. A binary mixture of limonene + linalool (mass fraction $w_{\text{limonene}} = 0.90$) was chosen to represent the citrus essential oil. A two-phase fractionation column (REDFRAC model) and a two-outlet flash tank (FLASH2 model) were selected to simulate the distillation column and the flash unit, respectively. The use of ILs ([C₄mim][OAc] or [C₄mim]Cl) as entrainers to facilitate the deterpenation of the model CEO was tested. In this scenario, the IL fed to the distillation column and the terpeneless CEO are recovered in the bottom stream. Then, the distillation column outlet bottom stream is sent to the flash unit, where the terpeneless CEO is separated from the IL, the latter being recycled to the distillation column. The CEO feed flow (F) is 1000 kg·h⁻¹, at 298.2 K and 101.3 kPa. The flash unit temperature is 363.2 K, while pressures of 5 Pa and 100 Pa for the simulations performed with [C₄mim][OAc] and [C₄mim]Cl, respectively, were selected. The ILs are in Aspen Plus User-Defined components, and their thermophysical data (i.e., heat capacities, enthalpies of vaporization, and vapor pressures) were retrieved from the literature. A reflux ratio of 1.0 was considered

in the distillation column to perform the simulations, and the number of stages (n) varied between 5 and 60. Moreover, ionic liquid/CEO (S/F) feed ratios of 0.050 and 0.075 were studied, and the CEO was fed at the column's middle stage ($n/2$).

Results and Discussion

The VLE data obtained for the binary limonene/linalool mixture and the ternary limonene/linalool/[C₄mim][OAc] and limonene/linalool/[C₄mim]Cl mixtures are shown in Figure 1.

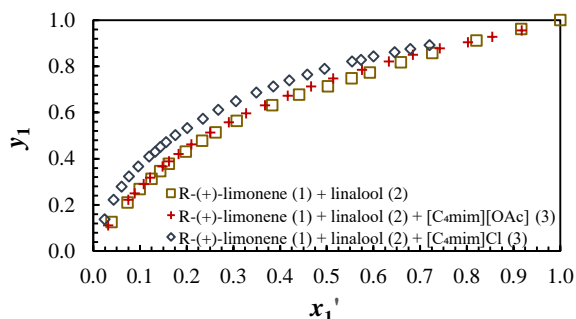


Figure 1. Experimental VLE data for limonene/linalool, limonene/linalool/IL ([C₄mim][OAc] or [C₄mim]Cl) mixtures. The mass fraction of the ILs in the mixtures were kept at 5%.

The presence of [C₄mim][OAc] (5% in mass fraction) slightly increases the relative volatility of the limonene/linalool mixtures for $x_1' < 0.8$. Nevertheless, [C₄mim]Cl delivers a much stronger increase in the relative volatilities of the terpenic mixture, particularly when low amounts of limonene are present in the liquid phase, suggesting that the presence of the chloride IL favors the separation of the limonene/linalool mixture.

The results for the process simulation are exhibited in Figure 2, where the required number of stages in the distillation column is presented for different target linalool purities in the terpeneless CEOs (bars). The achieved limonene purity in the distillate is also included in Figure 2 (circles).

As shown in Figure 2, higher linalool purity in the final product requires more stages in the distillation column. Also, the limonene purities in the distillate increase as the target linalool increases, though purities superior to 98% are found in all scenarios.

Acknowledgements

This work was developed within the scope of the project CICECO-Aveiro Institute of Materials, UIDB/50011/2020, UIDP/50011/2020 and LA/P/0006/2020, and CIMO-Mountain Research Center, UIDB/00690/2020 and LA/P/0007/2020, financed by national funds through the Portuguese Foundation for Science and Technology (FCT)/MCTES. The work was also funded in part by The Brazilian National Council for Scientific and Technological Development (CNPq), grants 163506/2020-5 and 306666/2020-0, and in part by the São Paulo Research Foundation (FAPESP), grant 2014/21252-0. Sérgio M. Vilas-Boas thanks FCT and the European Social Fund (ESF) for his Ph.D. grant (SFRH/BD/138149/2018 and COVID/BD/152936/2022).

References

- [1] S. Baptista-Silva et al., Journal of Essential Oil Research, 32 (2020) 279-295.
- [2] F. Perri et al., Journal of Multidisciplinary Sciences, 3 (2020) 195-214.
- [3] M. Sawamura, Citrus essential oils: flavor and fragrance, 1st Ed, Wiley, 2010, 398.
- [4] H. Bora et al., Plants, 9 (2020) 357.
- [5] A. Arce et al., Tree and Forestry Science and Biotechnology, 2 (2008) 1-9.
- [6] B. Ozturk et al., Journal of Chemical & Engineering Data, 63 (2018) 2384-2393.
- [7] G. Ben Salha et al., Reviews in Chemical Engineering, 37 (2021) 433-447.

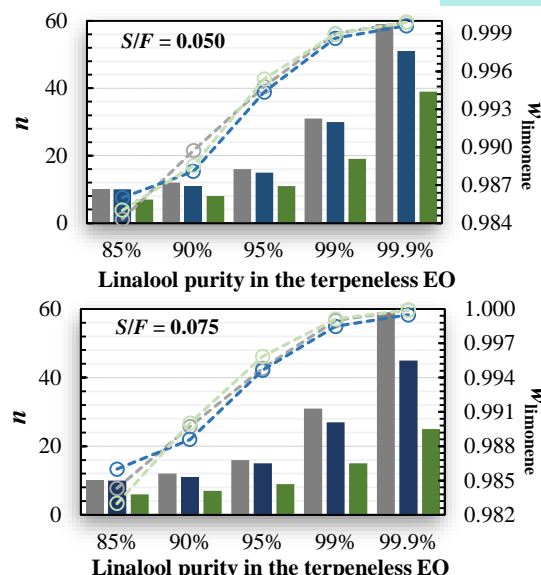


Figure 2. Overview of required stages (n) to obtain the target linalool purities in the terpeneless CEO from the process free of IL (gray bars), with [C₄mim][OAc] (blue bars), and [C₄mim]Cl (green bars). The circles represent the limonene mass fraction obtained in the distillate. Dashed lines are guide for the eyes.

An increase in the IL/CEO feed ratios from 0.050 to 0.075 leads to fewer stages in the distillation column, particularly when linalool purities higher than 99% are desired. This effect is more pronounced for the process with [C₄mim]Cl, where columns containing at least 66% fewer stages are required to achieve the target linalool purities compared to the IL-free process.

Conclusions

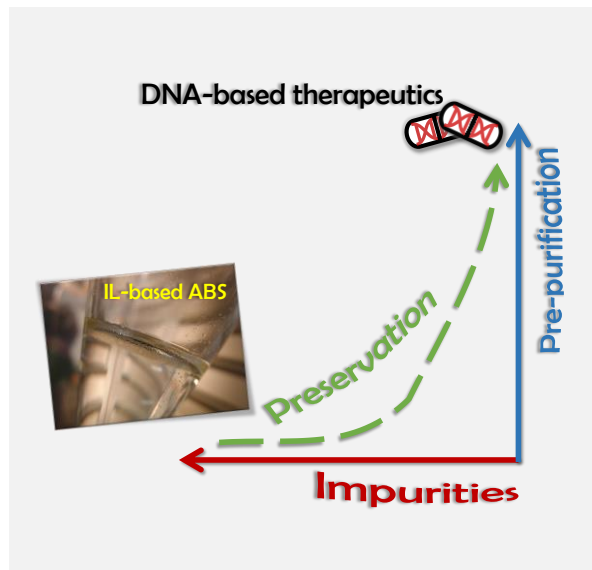
In this work, experimental VLE data were obtained for the limonene/linalool and limonene/linalool/IL ([C₄mim][OAc] or [C₄mim]Cl) mixtures at 5 KPa. Moreover, a process composed of an extractive distillation column and a flash separator unit is proposed to fractionate CEOs. The VLE data and the simulation results reveal that both ILs favor the fractionation of the CEOs, with [C₄mim]Cl performing better than [C₄mim][OAc].

DNA simultaneous extraction, purification, and preservation with ionic liquid-based aqueous biphasic systems

A.I. Valente^{1*}, T.B.V. Dinis², A.P.M. Tavares¹, F. Sousa³, M.G. Freire¹

¹CICECO – Aveiro Institute of Materials, Department of Chemistry, University of Aveiro, Campus Universitário de Santiago, 3810-193 Aveiro, Portugal; ²LSRE-LCM - Laboratory of Separation and Reaction Engineering-Laboratory of Catalysis and Materials, Department of Chemical Engineering at Faculty of Engineering, University of Porto, Rua Dr Roberto Frias s/n, 4200-465 Porto, Portugal; ³CICS-UBI – Health Sciences Research Center, University of Beira Interior, Av. Infante D. Henrique, 6200-506 Covilhã, Portugal.

*anaivalente@ua.pt



The production of deoxyribonucleic acid (DNA) as therapeutic has several challenges. An effective downstream process is highly demanding, as it should be capable of extracting, purifying, and preserving DNA integrity, by reducing its degradation by endonucleases. When properly designed, aqueous biphasic systems (ABS) based on ionic liquids (ILs) is a promising technique. In this work, double-stranded DNA (dsDNA) was separated from deoxyribonuclease I (DNase I) endonuclease through the application of a three-phase partitioning system (TPP) formed by an ABS composed of biocompatible cholinium-based ILs. dsDNA was completely extracted to the IL-rich phase, while DNase I was precipitated at the ABS interface. The system composed of [Ch][Gly] and PEG 400 allows the dsDNA simultaneous extraction, purification, and preservation in the long term, paving the way for their application in the bioprocessing of DNA-based therapy products.

Introduction

Gene therapy requires the development of an efficient large-scale upstream/downstream process, in which high quantities of DNA with high purity levels may be produced [1,2]. DNA must be recovered from a complex lysate media containing critical impurities with similar chemical, physical and structural properties, posing additional challenges to the downstream process [2].

The selective partition of plasmid DNA (pDNA) from other nucleic acids (ribonucleic acid (RNA) and genomic DNA (gDNA)) through the control of conventional ABS parameters [3,4], while cell debris and contaminant proteins can be accumulated at the interphase was already demonstrated. However, until now, no attempt has been made to apply an IL-based ABS with DNA.

Taking that into account, in this work IL-based ABS/TPP systems were designed for the simultaneous extraction, pre-purification and preservation of DNA.

Methods

A screening of ABS composed of several cholinium-based ILs and polymers was initially carried out to optimize the enrichment of dsDNA into the IL-rich phase. The studied ILs were: cholinium bromide ([Ch]Br), cholinium chloride ([Ch]Cl), cholinium dihydrogen phosphate ([Ch][DHP]), cholinium acetate ([Ch][Ace]) and cholinium glycolate ([Ch][Gly]). The polymers were: Poly(ethylene glycol) (PEG) of 400 and 600 g·mol⁻¹ (PEG 400 and PEG 600, respectively) and

Poly(propylene glycol) (PPG) of molecular weight of 400 g·mol⁻¹ (PPG 400).

The structural stability of dsDNA was evaluated in a solution of each compound before the partition behavior evaluation and after the application of the ABS through circular dichroism spectroscopy. The partition behavior was studied first separately and then with both molecules (dsDNA and DNase I) in the ABS.

Results

As already reported in our work [5], in all the studied systems, dsDNA partitioned to the IL-rich phase. For the endonuclease, DNase I precipitated at the ABS interphase with PEG in their composition.

Finally, the best ABSs for the partition of the individual biomolecules, were appraised to simultaneously separate dsDNA and DNase I through the precipitation of the protein at the interphase and preserve the dsDNA at the IL-rich phase. The selected systems were the ones containing the ILs [Ch][Gly] and [Ch][DHP].

Conclusions

Due to its biocompatible features, [Ch][Gly] fulfills the aim of this work at ensuring the technical viability of IL-based ABS/TPP for the “one-pot” extraction, purification and preservation of dsDNA, as experimentally demonstrated, whose results are expected to be transposed to other DNA types as advanced therapy products.

Acknowledgements

This work was developed within the scope of the project CICECO-Aveiro Institute of Materials, UIDB/50011/2020, UIDP/50011/2020 & LA/P/0006/2020, financed by national funds through the FCT/MEC (PIDDAC) and CICS-UBI projects UIDB/00709/2020 & UIDP/00709/2020 financed by national funds through the FCT/MCTES. Ana P.M. Tavares acknowledges the FCT for the research contract CEECIND/2020/01867 and Ana I. Valente acknowledges the FCT PhD grant (SFRH/BD/08352/2021).

References

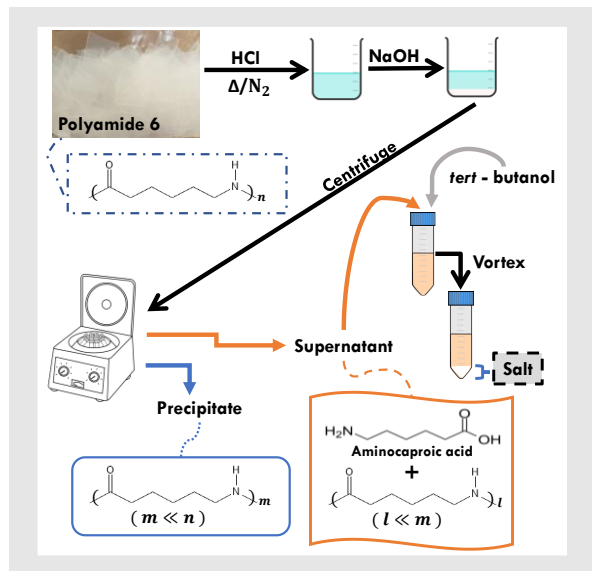
- [1] J. Ohlson et al., *Drug Discovery Today*, 25 (2020) 1891-1893.
- [2] X. Wang et al., *Genes & Diseases*, 8 (2021) 298-306.
- [3] S.C. Ribeiro et al., *Biotechnology and Bioengineering*, 78 (2002) 376-384.
- [4] A. Frerix et al., *Biotechnology and Applied Biochemistry*, 42 (2005) 57-66.
- [5] T.B.V. Dinis et al., *Separation and Purification Technology*, 315 (2023) 123646.

Polyamide chemical recycling processes: preliminary studies

J. Araújo*, N. Gama, A. Cavuquila, C.M. Silva, A. Barros-Timmons

CICECO - Aveiro Institute of Materials, Department of Chemistry, University of Aveiro, Campus Universitário de Santiago 3810-193, Aveiro, Portugal.

*jessica.araujo@ua.pt



Polyamide (PA) is a class of polymer whose use has been increasing year after year due to the wide range of applications. This contributed to environmental problems, hence, its recycling, in particular chemical recycling, has attracted increasing attention.

Following the interest of enhancing the sustainability of polymers, in this work, a preliminary study of the chemical recycling of PA 6 is presented. PA 6 was depolymerized into its monomers and oligomers using hydrochloric acid and the salt formed upon neutralization was efficiently removed using the non-ionic kosmotrope, *tert*-butanol.

Introduction

PA 6, also known as Nylon 6, is one of the most used nylons worldwide, having important applications in fibers, molded parts for the automotive industry, and other uses, namely in bearings, gears, bushings, handles, coatings for wires and cables, clothing, networks fishing gear, reinforcing materials for tires, parachutes, and conveyor belts. During the manufacturing of these fibers as well as after use of the ensuing textiles, a large amount of non-biodegradable waste is generated, causing serious environmental problems. Hence, the deposition of this waste in landfills has become increasingly unreasonable, due to the high cost associated and to the decrease of the raw materials' availability. In addition, the legislative pressure and public opinion related to environmental protection, especially in the developed countries, contributed to the implementation of recycling programs for this type of waste. [1]

One simple approach to recycle these wastes is mechanical recycling. This methodology consists in milling the polymer wastes, followed by melt extrusion. Yet, this option is not the optimal long-term solution, since the repeated melting and processing of the polymer can lead to the degradation of the material. Consequently, it results in the deterioration of its properties, decreasing the value of the ensuing material. Alternatively, chemical recycling allows the recovery and reuse of monomers. Some routes for the chemical recycling of PA are: hydrolysis, which requires water or steam; ammonolysis, which uses ammonia; or glycolysis, which uses glycols. [1]

Methods

PA 6 (Goodfellow) was dissolved in HCl (37 %) under reflux. To optimize the recycling conditions, different reaction parameters, such as temperature and reaction time, were tested. Upon the set reaction times the reaction mixtures were cooled down using an ice bath, and then neutralized [2]. For this purpose, the required volume of a 5 M sodium hydroxide aqueous solution was added, being the ensuing mixture centrifuged three times at 3500 rpm, for 15 minutes, to separate the supernatant obtained and replaced by distilled water, to

remove any salt formed. Finally, the precipitate obtained was dried at 70 °C.

Aiming the efficient removal of the high amount of salt formed during neutralization, the methodology patented by Ferreira et al. [3] was used as reference. The first supernatant, which contained a higher amount of salt, was mixed with *tert*-butanol in a proportion of 1:5 (w/w), in a vortex at room temperature. Next, the liquid and solid phases formed were separated, and the *tert*-butanol recovered using a rotary evaporator.

As an alternative to the neutralization process, the monomer separation was carried out by adding distilled water, used as anti-solvent [4]. Using this methodology, at the end of reaction, 20 mL of distilled water was added to the mixture, followed by 30 minutes of stirring, after which it was left at 0 °C overnight. The obtained solution, containing soluble compounds, such as monomers and oligomers, was subjected to a treatment with the ion exchange resin Dowex® 50WX2 (cationic resin).

To the contents of the various reaction products, *i. e.*, the precipitate and supernatants recovered were characterized by Fourier transform infrared spectroscopy (FTIR) (PerkinElmer Spectrum BX) performed in the 500 to 4000 cm⁻¹ range. The crystals obtained from the solution treated with the ion exchange resin were analyzed by proton nuclear magnetic resonance (¹H NMR) using a Bruker Avance III Nuclear Magnetic Resonance spectrometer operating at 300 MHz and deuterated dimethyl sulfoxide as a solvent.

Results

The reaction conditions and corresponding solid yield are summarized in Table 1. As it can be observed, as the reaction time increased, the yield in terms of solid collected decreased and the amount of water-soluble species, such as monomer and oligomers, increased. This can be associated with the increase of extension of the depolymerization reaction, resulting in higher degradation of PA. In fact, with the increase of temperature, a further degradation of the polyamide was observed, with the solid yield decreasing to the point where no precipitate was obtained. This was the case for the reaction that took place at 100 °C, for 4 hours.

Table 1. Solid yield upon depolymerization reaction of PA 6 for different temperatures at times.

Exp.	Temperature (°C)	Reaction time (h)	Solid yield (%)
1	80	1	92.2
2	80	3	77.5
3	80	4	72.0
4	90	4	51.3
5	100	4	0

Figure 1 illustrates the FTIR spectra of PA 6 and of the precipitates obtained for the reactions that took place at 80 and 90 °C. Being the three spectra obtained identical, it can be deduced that the precipitate obtained mainly consisted in non-depolymerized PA.

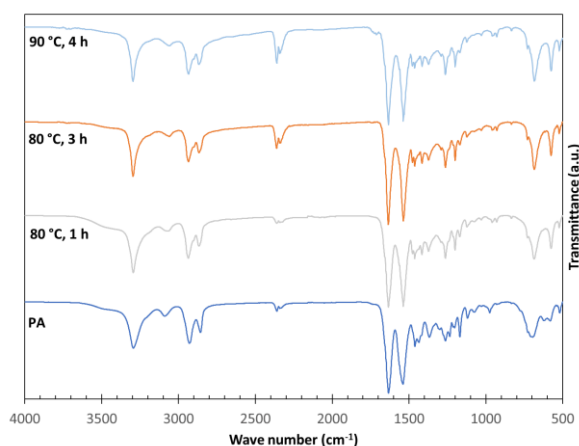


Figure 1. FTIR spectra of PA 6 and precipitates obtained.

Additionally, in Figure 2, the spectra for the supernatants collected after the first centrifugation for the above-mentioned reactions are presented. The bands centered at 1640 and 1540 cm^{-1} , attributed to amide I (C=O stretching vibrations) and amide II (N-H stretching vibrations), respectively, are present, albeit less defined, with a broad peak also visible at 3450 cm^{-1} , denoting the presence of the -OH- carboxylic group. The differences found in the spectra obtained suggest that some water-soluble species, with lower molecular weight, such as monomers and oligomers, might be present in the supernatant.

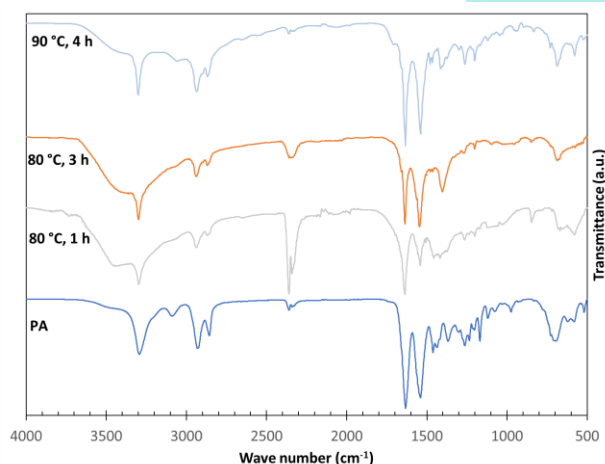


Figure 2. FTIR spectra of PA 6 and supernatants obtained.

From the ^1H NMR analysis (Figure 3) of the solution obtained after 4 h of reaction at 100 °C, which was treated with the ion exchange resin, the presence of species that could be attributed to oligomers and even monomers (*i. e.*, aminocaproic acid) was detected.

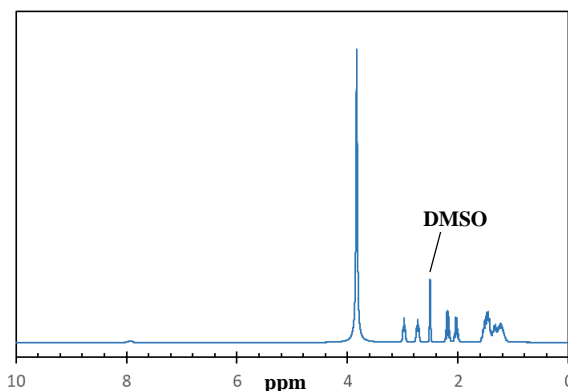


Figure 3. ^1H NMR spectrum of the product obtained at 100 °C.

Conclusions

The results obtained demonstrated that the depolymerization of PA 6 is a complex system which requires a temperature of at least 100 °C, for 4 h, to yield extensive breakdown of the chains. Using milder reaction conditions affords significant amounts of the precipitate (mainly PA, as per the FTIR spectra analyzed). Nonetheless, to understand if the desired monomer is indeed present further characterization of the reaction products is still required. The use of *tert*-butanol proved very efficient to remove the salt formed.

Acknowledgements

This work was developed within the scope of the project CICECO-Aveiro Institute of Materials, UIDB/50011/2020, UIDP/50011/2020 & LA/P/0006/2020, financed by national funds through the FCT/MCTES (PIDDAC). A.C. acknowledges the PhD grant financed by I9GREEN. The authors are grateful to the Chemical Engineering 4th year students who have broken the preliminary ground of this study (B. Graça, B. Neves, D. Mota, M. Morais)

References

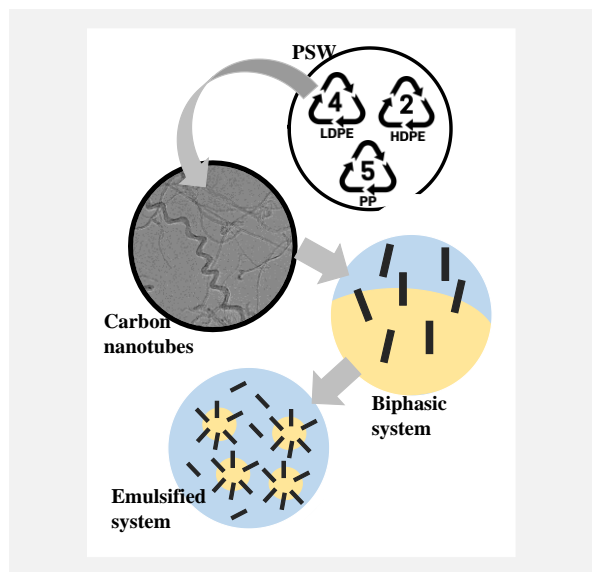
- [1] M. Chanda, *Advanced Industrial and Engineering Polymer Research*, 4 (2021) 133-150.
- [2] S.P. Khuntia et al., *Polymers for Advanced Technologies*, 33 (2022) 411-426.
- [3] A.J. De Faria Ferreira et al., "Crude glycerol purification process," WO 2017/001892 A1, Jan. 05, 2017 [Online]. Available: <https://patents.google.com/patent/WO2017001892A1/pt>
- [4] S.R. Shukla et al., *Journal of Applied Polymer Science*, 100 (2006) 186-190.

Oxidative desulfurization of a simulated fuel using plastic waste-derived carbon nanotubes: a Pickering interfacial catalysis approach

F.F. Roman^{1,2,3,4,*}, J.L. Diaz de Tuesta⁵, A.M.T. Silva^{3,4}, J.L. Faria^{3,4}, H.T. Gomes^{1,2}

¹Centro de Investigação de Montanha (CIMO), Instituto Politécnico de Bragança, Campus de Santa Apolónia, 5300-253 Bragança, Portugal; ²Laboratório Associado para a Sustentabilidade e Tecnologia em Regiões de Montanha (SusTEC), Instituto Politécnico de Bragança, Campus de Santa Apolónia, 5300-253 Bragança, Portugal; ³LSRE-LCM - Laboratory of Separation and Reaction Engineering - Laboratory of Catalysis and Materials, Faculty of Engineering, University of Porto, Rua Dr. Roberto Frias, 4200-465 Porto, Portugal; ⁴ALiCE - Associate Laboratory in Chemical Engineering, Faculty of Engineering, University of Porto, Rua Dr. Roberto Frias, 4200-465 Porto, Portugal; ⁵Department of Chemical and Environmental Technology, Rey Juan Carlos University, Calle Tulipán s/n., 28933 Móstoles, Spain.

*roman@ipb.pt



The presence of sulfonated and nitrogenated compounds in fuels is associated with environmental and health issues, and legislation has been limiting the content of S in fuels to 10 ppm. Due to drawbacks of conventional processes, alternatives to achieve deep desulfurization have been sought and oxidative desulfurization stands out. Similarly, the humankind has been facing issues with plastic waste accumulation; and plastic waste can be easily converted into carbon-based materials. This work aims at the oxidative desulfurization of a simulated fuel containing thiophene, as a model compound, considering a biphasic system using carbon nanotubes derived from plastic solid waste. The reactions were conducted with and without previous sonication during 10 mins, to assess the effect of emulsifying the system, increasing the interfacial area between oxidant phase (H_2O_2) and fuel.

Introduction

With increasing urbanization, humankind has experienced an escalating dependence on energy, and oil and petroleum-based products are the main resource for energy supply [1]. Specially, the transportation sector relies heavily on petroleum-derived products, mainly gasoline (23%) and diesel (64%) [1]. Crude oil is composed by several hydrocarbons, with some inherent heteroatoms, such as nitrogen (0.1-1.8 wt.%) and sulfur (0.1-8.0 wt.%) [2]. The presence of sulfonated and nitrogenated compounds in fuels is associated with a series of environmental and health issues due to the formation of SO_x and NO_x gases upon combustion. The release of these toxic gases has driven legislation to limit the content of S in fuels [2] down to the currently allowed limit of 10 ppm of S for both gasoline and diesel in the European Union [3]. The main technology used to remove S from fuels is hydrodesulfurization (HDS), which is conducted under harsh conditions (260-425 °C, 5-170 bar) and requires expensive hydrogen. Furthermore, it suffers several drawbacks [2]; and thus, alternatives to substitute or complement HDS have been proposed. Among them, oxidative desulfurization (ODS) is seen as the most suitable due to milder operating conditions (25 – 150 °C, 1 – 2 bar) [4]. ODS is a process deals with the oxidation of sulfur compounds and further extraction using a solvent. It can be either conducted in a two-step process or under a biphasic system (in the presence of the organic extractant) [2], however, the biphasic system presents drawbacks due to the limited interfacial area. ODS can be conducted under an emulsified system should allow overcoming this drawback, using Pickering Interfacial Catalysts (PIC), which is when a material behaves simultaneously as catalyst and as emulsion stabilizer [5]. On the other hand, humankind is also facing a serious issue related to the accumulation of plastic solid waste (PSW), innovative technologies being required to

significantly reduce it. One alternative is to take advantage of the carbon content of these plastic materials to transform them into carbon-based materials, especially carbon nanotubes (CNTs) [6]. CNTs have been shown to act as catalysts for oxidative based treatments and also as emulsion stabilizers [7]. Thus, this work aims at studying the ODS using H_2O_2 as oxidant, and thiophene (Th), as model compound, dissolved in 2,2,4-trimethylpentane to simulate a S-containing fuel. CNTs synthesized from PSW were tested as catalysts and as PIC to overcome the issue of the low interfacial area.

Methodology

Carbon nanotubes (CNTs) derived from polyolefins (LDPE, HDPE, PP), considering a composition representative of plastic solid waste (35:25:40, mass percentage), were used as catalysts in the process. The CNTs were grown over a $NiFe_2O_4/Al_2O_3$ substrate at 850 °C for 30 min under N_2 flow (20 $NmL\ min^{-1}$), and further modified with HNO_3 (130 °C, 24 h), leading to CNT-OX. The ODS reactions were conducted at 80 °C, with a volume ratio of oil-to-water (O/W) of 80:20, and aqueous phase consisted in a H_2O_2 solution 11.1 $g\ L^{-1}$ at pH = 3.0. The initial concentration of Th in the oily phase was 500 $mg\ L^{-1}$. The concentration of catalyst was 2.5 $g\ L^{-1}$, considering the whole volume of the system. The fuel and water phases were mixed and heated. Upon reaching the desired temperature, the catalyst was added, and this instant was considered as $t_0 = 0$ min. For the emulsified reaction, upon adding the catalyst, the reaction medium was sonicated for 10 min. The reactions were conducted for 8 h. Emulsion was observed considering the same conditions as those for the ODS reactions.

Results

CNT-OX was tested as catalyst for the ODS of Th considering a biphasic medium and an emulsified system, and the results are given in Figure 1. Under a biphasic system, it is possible to observe that CNT-OX is not very active towards the removal of Th by oxidation, allowing 50% of removal after 8 h of reaction, which is not much superior to the non-catalytic run, that resulted in 37% of removal in the same timeframe. On the other hand, the reaction conducted under an emulsified system resulted in an improvement for Th removal, reaching a value of 77% after 8 h of reaction. A non-catalytic run subjected to ultrasound did not lead to significant difference respect to that without sonication. The results reported here are similar to those reported in the literature for biphasic or emulsified systems considering water as extractant phase and a waste-derived catalyst [7-9].

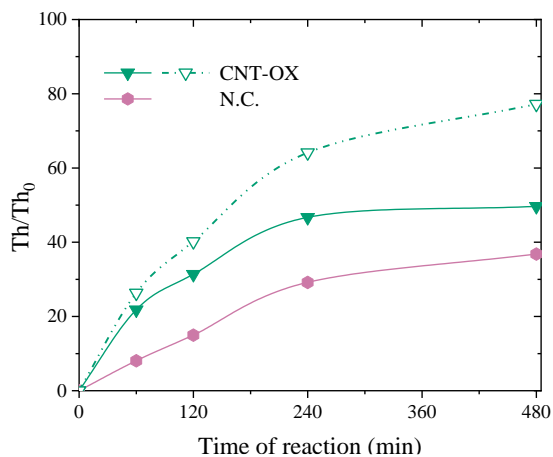


Figure 1. ODS of Th in the presence of CNT-OX under a biphasic system and an emulsified system. Conditions: $C_{\text{catalyst}} = 2.5 \text{ g L}^{-1}$, $O/W = 80:20$, $\text{pH} = 3.0$, $[\text{Th}] = 500 \text{ mg L}^{-1}$, $[\text{H}_2\text{O}_2] = 11.1 \text{ g L}^{-1}$, 10 min of sonication for emulsified reaction. **Solid** lines are for biphasic system and **dashed** line for emulsified system. N.C. = non-catalytic run.

The increased activity in the reaction conducted under an emulsified system has been ascribed to the ability of CNT-OX to stabilize a Pickering emulsion, having the dual role of catalyst and emulsion stabilizer. The formation of an emulsified layer increases the interfacial area between the organic and aqueous phases, which facilitates the contact between H_2O_2 and Th, and improve the mass transference between the phases. The emulsion formed in the presence of CNT-OX can be observed in Figure 2, with an average droplet size of $19.16 \pm 1.23 \mu\text{m}$. An

Acknowledgements

This work was financially supported by project "PLASTIC TO FUEL&MAT – Upcycling Waste Plastics into Fuel and Carbon Nanomaterials" (PTDC/EQU-EQU/31439/2017), by LA/P/0045/2020 (ALiCE), UIDB/50020/2020 and UIDP/50020/2020 (LSRE-LCM) funded by national funds through FCT/MCTES (PIDDAC), and CIMO (UIDB/00690/2020) through FEDER under Program PT2020. Fernanda F. Roman acknowledges FCT and FSE for the individual research grant with reference SFRH/BD/143224/2019. Jose L. Diaz De Tuesta acknowledges the financial support through the program of Atracción al Talento of Comunidad de Madrid (Spain) for the individual research grant 2022-T1/AMB-23946.

References

- [1] Complete Energy Balance. Eurostat. Accessed on Feb. 20th, 2023. Available online: https://ec.europa.eu/eurostat/databrowser/view/NRG_BAL_C__custom_5019982/default/table?lang=en.
- [2] F.F. Roman et al., *Catalysts*, 11 (2021) 1239.
- [3] Regulation (EC) N°. 715/2007 of the European Parliament and of the Council of 20 June 2007 on Type Approval of Motor Vehicles with Respect to Emissions from Light Passenger and Commercial Vehicles (Euro 5 and Euro 6) and on Access to Vehicle Repair and Maintenance Information. Available online: <https://eur-lex.europa.eu/eli/reg/2007/715> (accessed on Feb 20th, 2023).
- [4] A. Rajendran et al., *Journal of Materials Chemistry A*, 5 (2020) 2246.
- [5] M. Pera-Titus et al., *Angewandte Chemie*, 54 (2015) 2006.
- [6] C. Zhuo, Y. A. Levendis, *Journal of Applied Polymer Science*, 131 (2014) 39931.
- [7] A.A.S. Oliveira et al., *Applied Catalysis B*, 144 (2014) 144.
- [8] V. Tamborrino et al., *Fuel*, 296 (2021) 120693.
- [9] A.A.S. Oliveira et al., *Applied Catalysis B*, 162 (2015) 475.

emulsified layer was maintained for up to 8 h in the presence of CNT-OX under agitation.

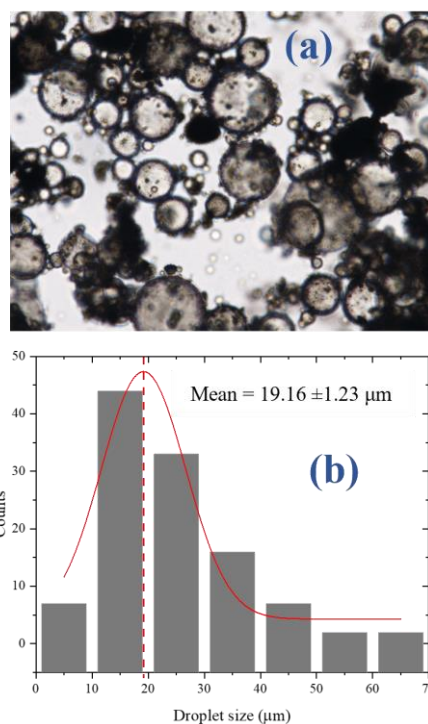


Figure 2. (a) Emulsion formation in the presence of CNT-OX with a 400x magnification and (b) distribution of droplet sizes. Conditions: $O/W = 80:20$, $\text{pH} = 3.0$; $C_{\text{catalyst}} = 2.5 \text{ g L}^{-1}$.

Conclusions

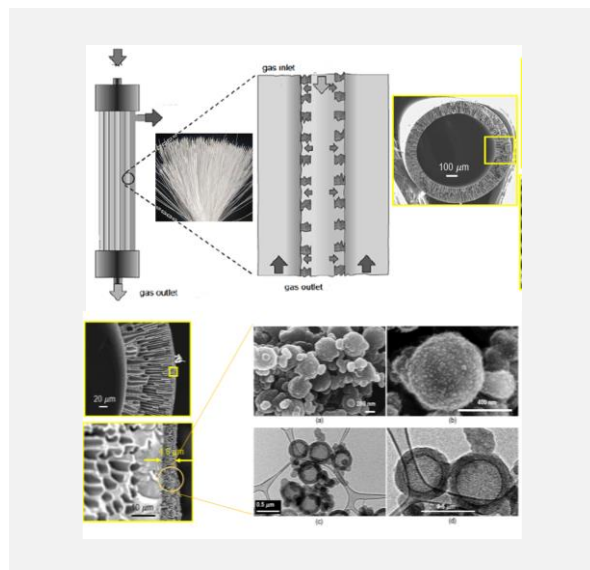
CNT-OX was tested as catalyst in a biphasic system without using sonication, leading to low removal of Th, due to the low interfacial area between water-oil phases. When the system was subject to ultrasounds, CNT-OX acted simultaneously as catalyst and as emulsion stabilizer, increasing the interfacial area and allowing an increased removal of Th from the oil phase. Thus, the results described here indicate that CNTs can act as PIC-like catalysts, and the conduction of reactions under PIC systems allows an improvement of the results. The results reported here should prompt further studies into the utilization of plastic solid waste for the production of active carbonaceous nanomaterials for catalytic applications and Pickering emulsifiers.

Hybrid hollow fiber membranes with encapsulated absorbents in sub-micron carbon capsules: A new technology for gas separation

P.J. Carvalho, R.T. Pais, I. Souza, L.P. Silva*

CICECO – Aveiro Institute of Materials, Department of Chemistry, University of Aveiro, 3810-193 Aveiro, Portugal.

**quijorge@ua.pt*



Dehydration technologies with low energy consumption using non-toxic materials are important in industrial, residential, and transport applications. In this work, nanocomposite polymeric hollow fibers with high dehydration capability were demonstrated with the incorporation of green amino acid-based ionic liquids. The ionic liquid was encapsulated in designed submicrometer carbon capsules and dispersed in thin polydimethylsiloxane coating layers. The effect of different coating compositions and operation conditions on the water vapor permeance and selectivity of water vapor over nitrogen was investigated using vacuum and sweep gas. Both sorption and permeation results suggested strong interactions between the water vapor and the encapsulated ionic liquid. The membrane systems had high water vapor permeances and selectivities, promising characteristics for application in membrane air dehumidification and other dehydration processes.

Over 90% of the world population is exposed to contaminated air. This is particularly relevant because air pollution, both outdoor and indoor, is associated with negative impacts on human health. In fact, nearly 1 in 10 deaths in the world can be attributed to air pollution, being the 4th highest risk factor for mortality, after high blood pressure, smoking, and high blood sugar. Indoor air pollution is caused by several types of contaminants, including gases (like CO, CO₂, O₃, NO_x, and SO_x), particulate matter (PM), volatile organic compounds (VOCs) with different types of volatility, and other compounds that, in the context of indoor air, are currently labelled as emerging. Each class of pollutants have specific characteristics in terms of size – as is the case with PM –, volatility and persistence in the indoor environment, which are responsible for their potential toxicity. These contaminants do not affect all the populations equally, with those living in high income countries being more exposed, as they also tend to spend most of their time indoors – up to 90% of their time – a reality that has become even more accentuated due to the COVID-19 pandemic. The relevance of this problem increases knowing that concentrations for several pollutants found indoors are usually higher than the ones found outdoors. Therefore, indoor air must be addressed in the most complete way to improve human health.

Several physical and chemical processes, based on absorption, adsorption, membranes and cryogenic separation, are

commercially available and widely used by the natural gas processing industry. However, when envisioning indoor air separation, the current technologies, requiring large separation units and high CO₂ partial pressures, stand unfeasible. Thus, innovative technological development, envisioned using greener solvents, is indispensable.

Innovative technology and emerging self-claimed green solvents for removing acid gases have been proposed but, none has reached a development level fit for deployment at an industrial level. Among those, physical and chemical absorption using ILs has attracted special interest due to the solvents' high capacity and selectivity. However, the use of ILs alone presents several drawbacks that hamper the development of new separation units capable of fulfilling industry demands.

Recently, we have shown that confining ILs in submicron porous inert matrices result in improved mechanical stability, higher mass transfer rates, virtually instant sorption kinetics and low energy regeneration demand at mild conditions, capable of overcoming the major drawbacks of the bulk solvents. Furthermore, the recent development of a matrix able to physically support the encapsulated solvent in the porous material, that minimizes the loss of surface contact area while presenting no resistance to the gas passage, has high potential to leverage the successful future of this novel technology [1].

Acknowledgements

This work was partly developed within the scope of the project CICECO-Aveiro Institute of Materials, UIDB/50011/2020, UIDP/50011/2020, and LA/P/0006/2020, financed by national funds through the FCT/MCTES (PIDDAC).

References

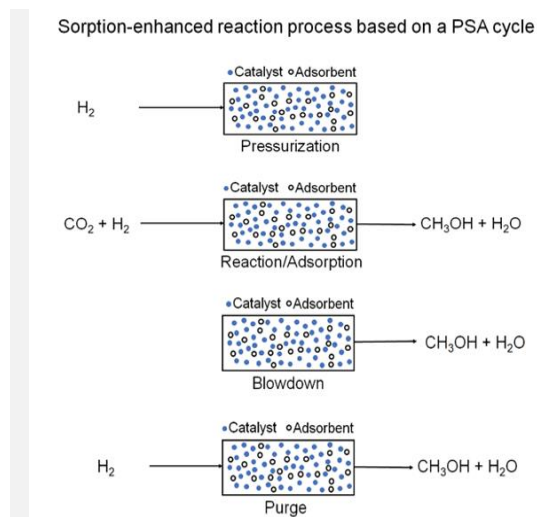
[1] A.Y. Gebreyohannes et al., ACS Sustainable Chemistry & Engineering, 8 (2020) 17763-17771.

Experimental PSA reactor for methanol-enhanced production via CO₂ hydrogenation

G. Pascual-Muñoz*, M. Larriba, V.I. Águeda, J.A. Delgado

Group of Catalysis and Separation Processes (CyPS), Department of Chemical Engineering and Materials, Universidad Complutense of Madrid, 28040, Madrid, Spain.

*gonzapas@ucm.es



Renewable methanol has emerged as a key component in the sustainable energy transaction. Methanol synthesis via CO₂ catalytic hydrogenation is one of the simplest ways to valorize captured CO₂. The main problem is the low CO₂ conversions of the process due to it being controlled by equilibrium.

Equilibrium conversion could be overcome by a sorption-enhanced reaction process (SERP), removing the products with a selective adsorbent.

The aim of the work is to study an experimental SERP process based on a PSA cycle. The PSA reactor has been filled with a commercial CuO/ZnO/Al₂O₃ catalyst and a commercial 3A zeolite. Total CO₂ conversion is achieved in the first cycle, and the conversion is established above 80% in the next cycles at 30 minutes of the reaction/adsorption stage.

Introduction

CO₂ utilization is crucial in the decarbonization process, and in the fight against climate change, avoiding greenhouse gas (GHG) emissions. [1]

CO₂ could be transformed into numerous commodities such as alcohols, olefins, dimethyl ether (DME) or methane. [1] One of the simplest and most feasible processes is methanol synthesis, but the catalytic hydrogenation reaction is exothermic and controlled by equilibrium. [1,2] Therefore, low conversion of CO₂ is achieved at high temperatures and pressures, around 25% at 250 °C and 50 bar. [3]

The equilibrium could be shifted to the products by a sorption-enhanced reaction process (SERP), removing the reaction products in situ. In SERP processes based on adsorption, the regeneration of the adsorbent is crucial to the process. In this context, PSA technologies are of great interest. [4]

The objective of the work is to design a SERP process based on a PSA reactor. The PSA cycle proposed consists of four steps: 1) Pressurization; 2) Reaction-Adsorption; 3) Blowdown; 4) Purge. [5,6]

Methods

The reagents, CO₂ and H₂, are fed with a 1:3 molar proportion. The reactor was filled with a homogeneous mixture of a commercial CuO/ZnO/Al₂O₃ and a commercial 3A zeolite as an adsorbent, with an 80:20 mass proportion. A scheme of the installation is presented in Figure 1.

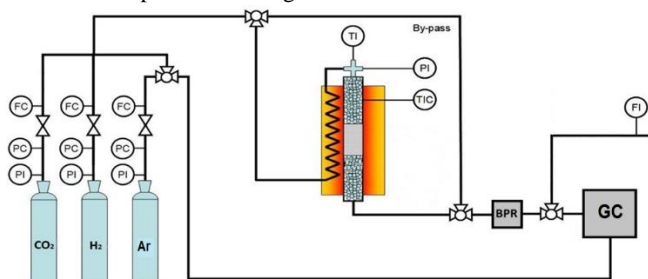


Figure 1. Experimental installation.

The installation was pressurized with a back pressure regulator (BPR) at the exit of the reactor. The effluent of the reactor was analyzed with a MicroGC Agilent 990

Results

CO₂ conversion and methanol selectivity results of six consecutive PSA cycles are shown below in Figure 2. The experiments were carried out at 250 °C, 45 bar and 1 g · mmol⁻¹ min⁻¹ contact time. The reaction-adsorption step was fixed in 30 minutes, and the blowdown and purge were in 20 minutes.

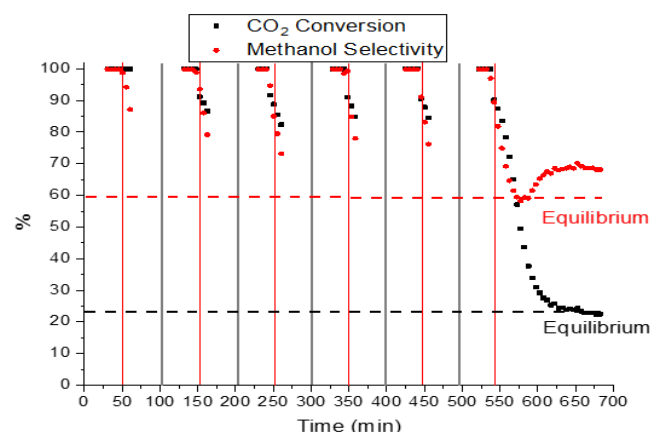


Figure 2. CO₂ conversion and methanol selectivity of six PSA cycles.

It is observed in Figure 2 that total CO₂ conversion could be achieved in the first cycle at 30 minutes of the reaction/adsorption step. In the following cycles, the conversion is stabilized at around 80-85%, still far away from equilibrium. Methanol selectivity is also higher than the equilibrium one in all cycles.

Conversion and selectivity decrease indicates that the adsorbent is not completely regenerated, so the blowdown and purge steps must be optimized.

Conclusions

Total conversion of CO₂ at 30 minutes of reaction is achieved in the first cycle of the PSA proposed. In the next cycles, conversions above 80% are achieved.

Methanol selectivity is also above equilibrium in all cycles. Blowdown and purge steps are crucial in the regeneration of the adsorbent, and, therefore, in the efficiency of the process.

Acknowledgements

Financial support from Ministerio de Economía y Competitividad of Spain through project CTM2017-84033-R is gratefully acknowledged. Gonzalo Pascual-Muñoz thanks Ministerio de Ciencia, Innovación y Universidades for awarding him a FPI grant (PRE2018-084805)

References

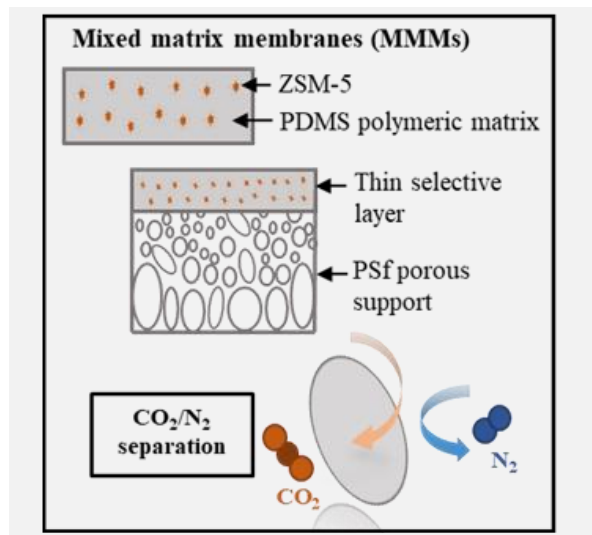
- [1] A. Goepfert et al., *Chemical Society Reviews*, 43 (2014) 7995-8048.
- [2] IRENA and Methanol Institute, *Innovation Outlook: Renewable Methanol*, International Renewable Energy Agency, Abu Dhabi, 2021
- [3] S. Dang et al., *Catalysis Today*, 330 (2019) 61-75.
- [4] B.T. Carvill et al., *AIChE J.*, 42, 1996, 2765-2772.
- [5] J.A. Delgado et al., *Separation and Purification Technology*, 262 (2021) 118292.
- [6] G. Pascual-Muñoz et al., *Chemical Engineering Transactions*, 86 (2021) 1081-1086.

Symmetric and asymmetric PDMS membranes for CO₂/N₂ separation using the inorganic filler ZSM-5

L. Rodrigues^{1,2*}, L. Martínez-Izquierdo^{3,4}, C. Téllez^{3,4}, J. Coronas^{3,4}, A.E. Rodrigues^{1,2}, V.J.P. Vilar^{1,2}, A.F.P. Ferreira^{1,2}

¹Laboratory of Separation and Reaction Engineering - Laboratory of Catalysis and Materials (LSRE-LCM), Department of Chemical Engineering, Faculty of Engineering, University of Porto, Rua Dr. Roberto Frias, 4200-465 Porto, Portugal; ²ALiCE – Associate Laboratory in Chemical Engineering, Faculty of Engineering, University of Porto, Rua Dr. Roberto Frias, 4200-465 Porto, Portugal; ³Institute of Nanoscience and Nanomaterials of Aragon (INMA), CSIC-University of Zaragoza, Zaragoza, Spain; ⁴Chemical and Environmental Engineering Department, University of Zaragoza, Zaragoza, Spain.

*inesmr@fe.up.pt



Bearing that CO₂ concentration in the atmosphere tend to increase, it is of utmost importance to consider solutions to mitigate CO₂ emissions, such as membrane-based CO₂ capture. PDMS/ZSM-5 symmetric membranes and PSf/PDMS/ ZSM-5 asymmetric membranes were prepared and tested for CO₂/N₂ separation. The embedment of ZSM-5 into the PDMS polymer matrix improved the performance of the membrane (with an increase of 26 % and 47 % in CO₂/N₂ selectivity and CO₂ permeance, respectively). PSf/PDMS/ ZSM-5 were superior to PDMS/ZSM-5, with an increase of 88 % in CO₂ permeance and no change in the CO₂/N₂ selectivity (12), considering optimal wt.% loading of ZSM-5. In summary, the developed membranes, particularly asymmetric membranes, have shown to be effective for CO₂ separation and are suitable for minimizing CO₂ emissions.

Introduction

One of the most significant environmental concerns nowadays corresponds to greenhouse gas (GHG) emissions, particularly CO₂ emissions. Although global CO₂ emissions decreased by 5.8% in 2020 as a consequence of the pandemic, the average annual concentration of CO₂ in the atmosphere, in 2020, from energy-related emissions reached its highest recorded value (412.5 ppm) [1,2]. For this reason, it is of utmost importance to consider strategies to decrease CO₂ emissions by using, for example, membrane-based CO₂ capture. Gas separation membranes have shown potential due to the reduction of electricity and fuel consumption, simplicity of operation and installation and to the fact that membranes can be adapted to fit separation requirements (for example incorporating fillers like zeolites, metal-organic frameworks (MOFs), etc.) [3,4]. Polymeric membranes have been widely studied and tested for CO₂ separation, particularly PDMS membranes, given their high permeability due to their flexible elastomeric structure. However, despite the excellent permeability results of PDMS and other polymeric membranes, the selectivity tends to be low due to the “trade-off” effect between permeability and selectivity discovered by Robeson in 1991 [5]. This can be reversed by surrounding fillers (such as zeolites, silica, activated carbons, metal-organic frameworks (MOFs), among others), which present higher separation characteristics into polymeric membranes, forming the so-called mixed matrix membranes (MMMs) [3-7]. Within MMMs, PDMS/MFI type zeolite (like silicalite-1 and ZSM-5) has shown promising results for gas separation [8,9].

Objectives

The main objective of this work consists of the development

of MMMs (PSf/PDMS/ ZSM-5 and PDMS/ ZSM-5) for CO₂/N₂ separation and the study of how the embedment of (ZSM-5 filler) improves the performance of the membranes.

Methods

The filler tested in this study was ZSM-5 (zeolite ammonium ZSM-5 powder with a 280 SiO₂/Al₂O₃ mole ratio supplied by Zeolyst and particle size of ca. 3-5 μm). The PSf porous support was prepared by immersion precipitation (phase inversion method), with casting the polymeric solution on a Teflon plate by an automatic film applicator (knife thickness of 250 μm) and immersion on a water coagulation bath, as shown in Figure 1. The selective layer of PDMS/ZSM-5 was formed by solvent evaporation after casting the polymeric solution embedded with filler on the porous support. Symmetric membranes of PDMS/ZSM-5 were prepared by solvent evaporation by placing the PDMS solution embedded with ZSM-5 in a metal petri dish [10].

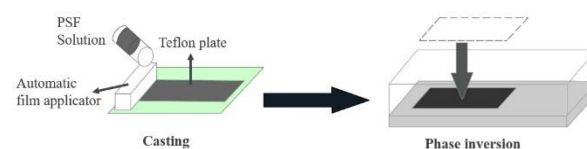


Figure 1. Schematic illustration of PSf support preparation, including casting and phase inversion technique.

The embedment of ZSM-5 in the PDMS selective layer and the thickness of the selective layer was studied by scanning electron microscopy (SEM), using an Inspect F50 model microscope (FEI), operating at 10 kV. The cross-sections of membranes obtained by SEM were prepared by freeze fracturing after immersion in liquid nitrogen [10].

The gas permeation tests were performed on a flat module, consisting of two stainless steel pieces and a 316LSS macro-porous disk support (Mott Co.) with a 20 μm nominal pore size, on which the membranes (2.12 cm^2 effective area) attached by a viton ring were placed. The tests were performed at 35 $^\circ\text{C}$ for a CO_2/N_2 mixture (15/85 cm^3 (STP) min^{-1}) at a pressure range of 1-3 bar and using helium as carrier gas (4.5 cm^3 (STP) min^{-1}). The permeances (in gas permeance unit (GPU) = $10^{-6} \text{cm}^3(\text{STP}) \text{cm}^{-2} \text{s}^{-1} \text{Pa}^{-1}$) were calculated based on N_2 and CO_2 concentrations in the permeate stream analyzed by an Agilent 3000 A micro-gas chromatograph at a permeate pressure of 1 bar [10].

Results

PDMS/ZSM-5 membranes showed a CO_2/N_2 selectivity increase of 26 % with the embedment of ZSM-5, reaching almost 15 for the highest ZSM-5 mass percentage (50 wt.%). The CO_2 permeance increased up to 10 wt.% ZSM-5 (47 %), which was considered the optimal value. The ZSM-5 was fully embedded in the PDMS matrix, as shown in Figure 2, and membranes thickness varied from 340 to 490 μm .

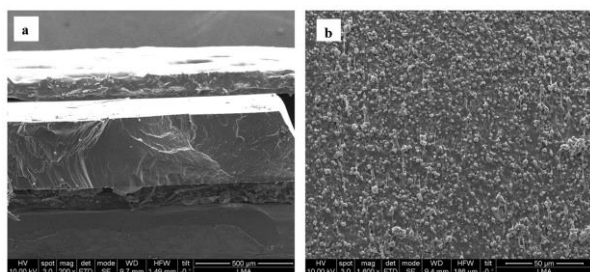


Figure 2. Cross-sectional SEM images of PDMS/ZSM-5 membranes with different ZSM-5 mass percentages: (a) 0 wt.% and (b) 50 wt.%.

PSf/PDMS/ZSM-5 membranes were firstly prepared at 10 and 20 wt.% PDMS, however the PDMS layer was not thick enough to fully embed the ZSM-5 (size range of 3-5 μm),

Acknowledgements

This work was financially supported by: LA/P/0045/2020 (ALiCE) and UIDP/50020/2020 (LSRE-LCM) funded by national funds through FCT/MCTES (PIDDAC); also financially supported by national funds through the FCT/MCTES (PIDDAC), under the project PTDC/EAM-AMB/4702/2020 (OZONE4WATER). Inês Rodrigues acknowledges FCT- Fundação para a Ciência e Tecnologia for funding the PhD Research Scholarship with the reference 2022.10784.BD. Grants PID2019-104009RB-I00 funded by MCIN/AEI/10.13039/501100011033 is gratefully acknowledged (Agencia Estatal de Investigación (AEI) and MCIN (Ministerio de Ciencia e Innovación), Spain). Grants T43-20R and T68_23R financed by the Aragón Government is gratefully acknowledged. L. Martínez-Izquierdo also thanks the Aragón Government (DGA) for her PhD grant.

References

- [1] IEA, 2019. Global Energy Review 2021. CO_2 emissions. <https://www.iea.org/reports/global-energy-review-2021/co2-emissions>. 7.2.23.
- [2] US EPA, 2022. Greenhouse Gas Emissions. <https://www.epa.gov/ghgemissions/global-greenhouse-gas-emissions-data>. 7.2.23.
- [3] C.C. Hu et al., Journal Taiwan Institute Chemical Engineers, 135 (2022) 104379.
- [4] S. Sridhar et al., Chemical Engineering Digest, 1 (2014) 1-25.
- [5] L.M. Robeson, Journal of Membrane Science, 320 (2008) 390-400.
- [6] T.S. Chung et al., Progress in Polymer Science, 32 (2007) 483-507.
- [7] Q. Zhao et al., Chemical Engineering Journal, 443 (2022) 136290.
- [8] H. Amiri et al., Chemical Papers, 71 (2017) 1587-1596.
- [9] M. Hussain, A.König, Chemical Engineering and Technology, 35 (2012) 561-569
- [10] L. Martínez-Izquierdo et al., Journal of Environmental Chemical Engineering, 9 (2021) 105624.

which remained on the surface, hindering the passage of gases. PSf/PDMS/ZSM-5 membranes were prepared using 80 wt.% PDMS, with fully embedment of ZSM-5. The thickness of the selective layer ranged from 60 to 80 μm . Compared with the PDMS/ZSM-5 results, for 10 wt.% of ZSM-5, the CO_2 permeance increased by 88 % (from 11 to 92 GPU) and the selectivity remained practically unchanged, in the order of 12 (Figure 3).

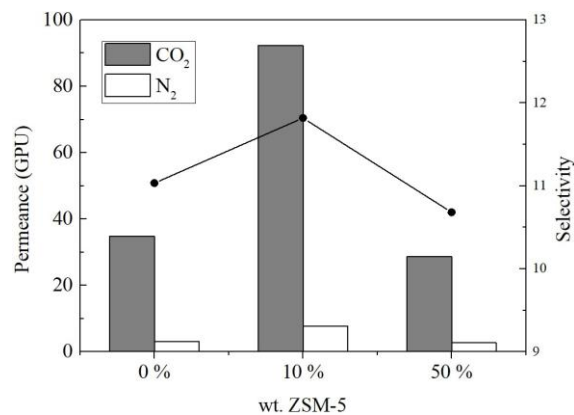


Figure 3. CO_2 and N_2 permeance (columns) and CO_2/N_2 selectivity (black dots) results for PSf/PDMS asymmetric membranes for different ZSM-5 mass percentages.

Conclusions

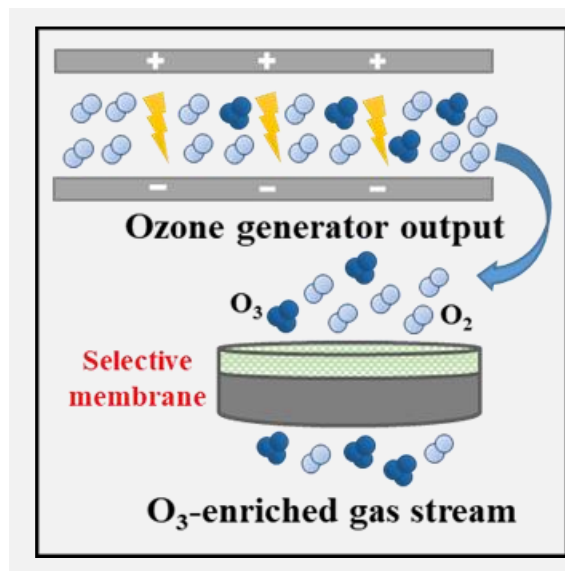
With this work it is possible to conclude that the embedment of fillers, particularly ZSM-5, in symmetric and asymmetric membranes is capable of improving the membranes performance. The PDMS polymeric matrix was able to completely embed ZSM-5 and due to the inherent smaller thickness (and therefore higher permeance), asymmetric membranes showed to be more effective for embedding fillers, improving the overall performance of membranes for CO_2 separation.

Development of functionalized membranes for O₂/O₃ gas separation

V.J.P. Vilar*, I. Rodrigues, A.E. Rodrigues, A.F.P. Ferreira

Laboratory of Separation and Reaction Engineering - Laboratory of Catalysis and Materials (LSRE-LCM), Department of Chemical Engineering, Faculty of Engineering, University of Porto, Rua Dr. Roberto Frias, 4200-465 Porto, Portugal; ALiCE – Associate Laboratory in Chemical Engineering, Faculty of Engineering, University of Porto, Rua Dr. Roberto Frias, 4200-465 Porto, Portugal

*vilar@fe.up.pt



Ozone (O₃) is an oxidant commonly used as a disinfectant in water and wastewater treatment technologies. However, ozone generation is an intense energy consumption process since the weight percentage of ozone that can be generated from oxygen-rich feed stream is very low (6-13 wt.%). It is possible to use ozone-selective membranes to purify the resulting ozone stream from the ozone generator by separating the oxygen and ozone, obtaining an O₃-enriched gas stream. The present work intends to evaluate the capacity of PVDF/PDMS asymmetric membranes to separate the O₂/O₃ mixture, enabling the ozone stream purification. The preliminary results showed that the PVDF/PDMS membranes can separate O₃ from O₂, achieving a selectivity of 2.1 for the highest PDMS weight percentage considered (20 wt.%) - an increase of 84 % in comparison with PVDF membranes. Further experiments will be carried out, such as increasing the PDMS wt.% loading of the asymmetric membranes and embedment of fillers in the polymeric matrix to increase the selectivity and improve the performance of the overall membranes.

Introduction

Ozone (O₃) is a major oxidant with a high oxidation potential (2.076 V), commonly employed as a disinfectant in water and wastewater treatment technologies. Ozone must be generated on-site since it is an unstable molecule, decomposing quickly into oxygen (few hours), and its generation on-site can be done by an electrical-discharge ozone generator (EDOG) [1,2]. However, ozone generation is a costly process mainly due to energy-intensive consumption, varying from 10 to 20 kWh/kg O₃ when ozone is generated from oxygen or air, respectively. The high generation costs are related to the low weight percentage of ozone generated from oxygen-rich feed streams (6-13 wt.%) [2,3].

A strategy to overcome this disadvantage is to purify the resulting ozone stream from the ozone generator by separating the oxygen and ozone, obtaining an O₃-enriched gas stream, using, for example, ozone-selective membranes [4]. In the past years, several studies have been carried out regarding polymers resistance to ozone. Polytetrafluoroethylene (PTFE), Polyvinylidene fluoride (PVDF) and Polydimethylsiloxane (PDMS) showed good ozone resistance without significant changes in the performance of polymeric membranes when continuously exposed to ozone [5,6]. Additionally, PDMS membranes are an exciting solution for O₂/O₃ separation since they exhibit an ozone permeability around four times higher than oxygen, enhancing the purification of the ozone feed stream [7].

Most studies currently available regarding O₂/O₃ separation through membranes are focused on membrane contactors, separating two phases (a gaseous ozone stream and an aqueous stream) and providing the contact between them to achieve wastewater treatment [8]. In this regard, no studies concerning O₂/O₃ gas separation processes using membranes exist. Despite some research works, such as the one by C.A. Jones et

al. [9], that analyze the permeation capacity of specific membranes resistant to ozone for certain gases to inquire about the potential of these membranes for O₂/O₃ separation, there are no guarantees that the O₂ and O₃ would behave the same way as these gases and that these membranes would be able to achieve good permeation results for O₂/O₃ mixture. Therefore, this work intends to overcome this research gap by evaluating the capacity of PVDF/PDMS asymmetric membranes to separate the O₂/O₃ mixture, enabling the ozone stream purification.

Objectives

The main objective of this research project is to develop functionalized membranes for O₂/O₃ separation to obtain an O₃-enriched gas stream. PVDF/PDMS asymmetric membranes will be synthesized and tested in a gas separation set-up, with the O₂/O₃ mixture being the feed stream and the permeate being the O₃-enriched gas stream to be achieved.

Methods

PVDF/PDMS membranes were synthesized by phase inversion (immersion precipitation and solvent evaporation). PVDF solution (14 % wt.) was first prepared by dissolving PVDF in NMP solvent under stirring conditions. PVDF porous support was synthesized by immersion precipitation by applying the degassed PVDF solution on a Teflon plate with the help of an Elcometer 4340 Automatic Film Applicator (thickness knife of 250 μm and a casting speed of 0.03 m s⁻¹) and immersion on a water coagulation bath. PVDF support is then placed in a deionized water bath for 24 h and dried at room temperature. PDMS coating solution was prepared by dissolving the silicone elastomer base and the respective curing agent at a 10:1 ratio (ratio suggested by the manufacturer) in hexane and stirring for 30 min. The selective

layer of PDMS was formed by solvent evaporation after casting the polymeric solution on the PVDF support using the Elcometer. The membrane was finished after 1 h at 75 °C until completely dry.

Before the gas permeation tests, the membranes were cut considering the size of the sintered disk (diameter around 19 mm), which gives support to the membranes. These were then placed inside the membrane module, consisting of two stainless steel pieces, on top of the disk and fixed with two Viton O-rings, one stainless steel O-ring, and an acme bronze.



Figure 1. Gas separation set-up.

The gas permeation tests were conducted at ambient temperature ($T=20-25\text{ }^{\circ}\text{C}$) and at a feed and permeate pressure of around 1-2 bar and 1 bar, respectively. The gas separation laboratory set-up, illustrated in Figure 1, consists of the following components: i) oxygen cylinder; ii) mass flow controller to regulate the flow of oxygen that is fed into the system; iii) corona discharge ozone generator; iv) diaphragm pump to compress the ozone stream up to 5 bar abs; v) membrane module made of stainless steel, incorporating the synthesized membranes (useful area of 2 cm^2 or 28 cm^2); vi) helium cylinder, where helium can be used as a carrier gas to decrease O_3 concentration and therefore increase the partial pressure difference (driving force in a gas separation system); vii) pressure gauge to measure the pressure in the retentate stream up to 10 bar; viii) mass flow meter to measure the permeate stream flow; ix) ozone analyzer capable of

Acknowledgements

This work was financially supported by: LA/P/0045/2020 (ALiCE) and UIDP/50020/2020 (LSRE-LCM) funded by national funds through FCT/MCTES (PIDDAC); also financially supported by national funds through the FCT/MCTES (PIDDAC), under the project PTDC/EAM-AMB/4702/2020 (OZONE4WATER). Inês Rodrigues acknowledges FCT- Fundação para a Ciência e Tecnologia for funding the PhD Research Scholarship with the reference 2022.10784.BD.

References

- [1] L.C. Cuong et al., Vietnam Journal of Chemistry, 57 (2019) 604-608.
- [2] C. Gottschalk et al., Ozonation of water and waste water: A practical guide to understanding ozone and its applications, 2nd Edition, Wiley-VCH Verlag GmbH & Co. kGaA, Germany, 2010.
- [3] M.J. Berry et al., Water, 9 (2017).
- [4] F. Fitch, A. Maheshwary, Methods for Separating Ozone, Google Patents, 2018.
- [5] F.R.A. dos Santos et al., Journal of Materials Research, 18 (2015) 1015-1022.
- [6] K. Li et al., Zhongguo Huanjing Kexue/China Environmental Science, 42 (2022) 1157-1163.
- [7] E. Bein et al., Chemical Engineering Journal, 413 (2021) 127393.
- [8] P. Janknecht et al., Separation and Purification Technology, 25 (2001) 341-346.
- [9] C.A. Jones et al., Polymer, 52 (2011) 901-903.
- [10] L.M. Robeson, Journal of Membrane Science, 320 (2008) 390-400

measuring ozone concentration in the feed, permeate, and retentate streams; x) catalytic O_3 destruction unit and O_3 destroyer bottle (containing a 2 wt.% KI solution) to ensure total ozone destruction.

Preliminary results

The PVDF/PDMS membranes were able to separate O_3 from O_2 , achieving a selectivity of 2.1 for the highest PDMS mass percentage (increase of 84 %), as can be seen in Figure 2. As expected, the permeance decreased with the PDMS coating due to the “trade-off” effect between permeance and selectivity considered in 1991 by Robeson [10].

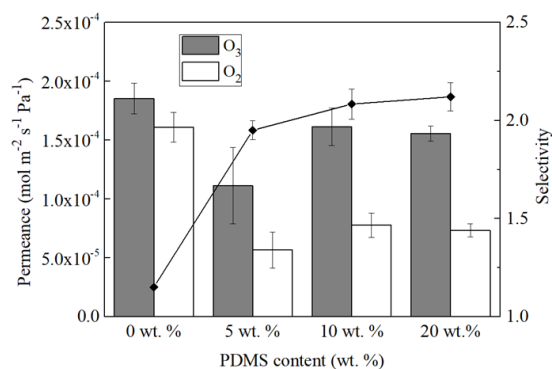


Figure 2. O_3 and O_2 permeance (columns) and O_2/O_3 selectivity (black dots) results for PVDF/PDMS membranes for different PDMS wt.%.

Conclusions and future work

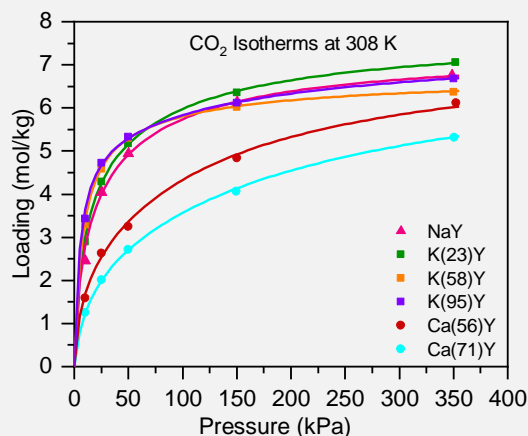
From the preliminary results obtained, it was possible to conclude that the PVDF/PDMS membranes are suitable for O_2/O_3 separation. Further experiments will be carried out to increase the selectivity of the membrane while maintaining or slightly decreasing the permeance values. For example, membranes with a higher weight percentage of PDMS coating will be tested to understand if it's possible to achieve a selectivity above 2.1, without significant changes in the permeance results (at higher PDMS wt. % the thickness of the PDMS selective layer increase, which leads to lower permeance values). The embedment of fillers in asymmetric (PVDF/PDMS) and symmetric membranes (PVDF) will also be tested.

Single- and multi-component fixed-bed adsorption of CO₂, CH₄, and N₂ on ion-exchanged binder-free NaY zeolites

E. Aly^{1,2*}, L.F.A.S. Zafanelli¹, A. Henrique¹, F.A. da Silva², A.E. Rodrigues³, J.A.C. Silva¹

¹Instituto Politécnico de Bragança, Campus Santa Apolónia, 5300-253, Bragança, Portugal; ²University of Aveiro, Portugal Campus Universitário de Santiago, 3810-168, Aveiro, Portugal; ³University of Porto, Rua Dr. Roberto Frias, S/N, 4099-002, Porto, Portugal.

*ezzeldin@ipb.pt



Ion-exchange was performed on bare commercial binder-free NaY zeolite with alkali (K⁺) and alkaline earth (Ca²⁺) metal cations in the range 23, 58, and 95% exchange for K⁺, and 56 and 71% for Ca²⁺, to be used as candidates regarding CO₂ post-combustion capture (PCC) and biogas upgrading by adsorption processes. Adsorption equilibrium isotherms of CO₂, CH₄ and N₂ were measured on all these cation-exchanged samples using a chromatographic technique between 308 and 348 K and pressures up to 350 kPa and modelled by the dual-site Langmuir isotherm. The CO₂ adsorption capacity increases as Na⁺ is exchanged further by K⁺ and the reverse for the Ca²⁺ exchange. The single- and binary-component breakthrough curves were numerically simulated and accurately predicted using the Aspen Adsorption package. This work discloses the importance of ion-exchange on binder-free beads of NaY zeolite to improve its performance in PCC and biogas upgrading applications.

Introduction

The generation of carbon dioxide is inherent in the combustion of fossil fuels, and the efficient capture of CO₂ from industrial operations is regarded as an important strategy to achieve a significant reduction in atmospheric CO₂ levels. Post-combustion capture (PCC) is referred to as the capture of CO₂ from sectors relying on fossil-fuel combustion such as power generation, steel making, and cement industries. It is a technically and economically viable solution to reduce carbon emissions as it can be implemented with ease into new and existing facilities without affecting the process upstream. Processes for removing CO₂ from methane (CH₄) are also important for upgrading both renewable and non-renewable energy sources such as landfill gas, biogas, and natural gas. These gases contain a large amount of CH₄ along with CO₂, nitrogen (N₂), and some traces of impurities, that need to be removed to meet pipeline grade specifications. Adsorption processes are promising capture technologies as they can use solid adsorbent to separate the CO₂ from other gas constituents, by using their cage-like structure to act in the limit as molecular sieves.

Zeolites Y and X belong to the family of aluminosilicate molecular sieves with a faujasite-type structure (FAU), being different only by the Si/Al atomic ratio (1.5 – 3.0 for NaY compared to 1.0 – 1.5 for NaX) [1]. The FAU structure demonstrates extreme versatility in gas separations through ion exchange and metal impregnation. The type of cation influences the electric field inside the pores, the available pore volume, and the adsorption of polar and non-polar molecules due to the induced electrostatic interactions of the ionic surface. Therefore, ion-exchange can be used as a tool for tailoring the structure to obtain specific performances. [2]

Objectives

This work aims to investigate by a series of fixed-bed breakthrough experiments the adsorption of single, binary and

ternary mixtures of CO₂/CH₄/N₂ in binder-free beads of K(23)Y, K(58)Y, K(95)Y, Ca(56)Y, and Ca(71)Y exchanged from the bare NaY zeolite, between 308 and 348 K and total pressures up to 350 kPa (under compositions typical of post-combustion and biogas upgrading processes).

Methods

The faujasite type-Y zeolites studied in this work were synthesized in the binder-free form in the labs of Chemiewerk Bas Köstritz GmbH (Germany). The beads particle diameter ranges between 1.6-2.5 mm. The exchange started from a commercial type of binder-free Y sodium zeolite form (Köstrolith NaYBfK) with a Si/Al ratio of 2.5 to achieve 23, 58, and 95% potassium- and 56 and 71% calcium-exchange degree value.

A single and multi-component breakthrough apparatus has been used to study the fixed bed adsorption of CO₂ and N₂ and their binary mixture. The apparatus is shown in previous works [3].

In chromatographic breakthrough experiments, the dynamic equilibrium loading is calculated by integrating the molar flow profiles of the breakthrough curves by using the following equation [4]:

$$q_{exp,i} = \frac{1}{m_{ads}} \left(F_{f,i} t_n - \int_0^{t_\infty} F_i dt - \varepsilon_b V_c C_{i0} \right) \quad (1)$$

where m_{ads} = adsorbent mass in the column; $F_{f,i}$ = feed molar flowrate of component i at the inlet of the fixed bed; F_i = molar flow rate of component i at the outlet of the fixed bed; t_∞ = saturation time; ε_b = bed porosity; V_c = column volume; and C_{i0} = feed concentration of component i at the inlet of the fixed bed.

Results

The Graphical Abstract shows a comparison of the CO₂ isotherms between NaY, K(23)Y, K(58)Y, K(95)Y, Ca(56)Y, and Ca(71)Y, collected at 308 K. The sorption hierarchy order

at low pressure (in the range until 50 kPa) observed is: Ca(71)Y < Ca(56)Y < NaY < K(23)Y < K(58) < K(95)Y. As the level of ion-exchange rate from Na⁺ to K⁺ increases, the CO₂ adsorption loading increases, where the opposite is observed when the ion-exchange changes from Na⁺ to Ca²⁺. At 25 kPa, the loading of binder-free NaY is equal to 4.05 mol/kg, compared to 4.29 for K(23)Y, 4.59 for K(58)Y, 4.72 for K(95)Y, 2.63 for Ca(56)Y and only 2.01 mol/kg for Ca(71)Y at 308 K. These results indicate a good response between the acidic CO₂ to the basic properties of the zeolites containing larger monovalent cations at low pressure. Larger cations such as K⁺ accept less charge transfer from the neighboring lattice oxygen atoms, these oxygen atoms therefore remain more negatively charged and hence more basic, increasing the binding energy to guest CO₂ molecule. Moreover, the CO₂ loading of Ca(71)Y is significantly lower than in all the rest (e.g. around a half of that on bare NaY), which is due to the decrease of the amount of exchangeable cations between the divalent Ca²⁺ cations and the adsorbate molecules.

The studied binary experiments consist of 15% CO₂ / 85% N₂ (vol.%) mixture, representing a typical post-combustion stream. Figure 1a shows the adsorption breakthrough curves in binder-free K(95)Y for the binary mixture at 313 K. Figure 1b displays the breakthrough curves for ternary mixtures feeds of CO₂/CH₄/N₂ (20/20/20 vol.% balanced with He) on binder-free zeolite KY. As can be seen in Figure 1c, the binary experiment shows a selectivity of CO₂ over N₂ around 105 at 10 kPa and 313 K; the ternary system resulted in a selectivity of CO₂ over CH₄ and over N₂ of around 19 and 45 at 313 K, respectively, under the same conditions. These results indicate that binder-free K(95)Y works well in the low-pressure region and therefore, is a promising adsorbent for the recovery of CO₂ from post-combustion streams. Numerical simulations were performed with a model implemented in Aspen Adsorption simulator, allowing to predict accurate breakthrough curves for dynamic experiments carried out in a fixed bed adsorption system, as shown in Figure 1.

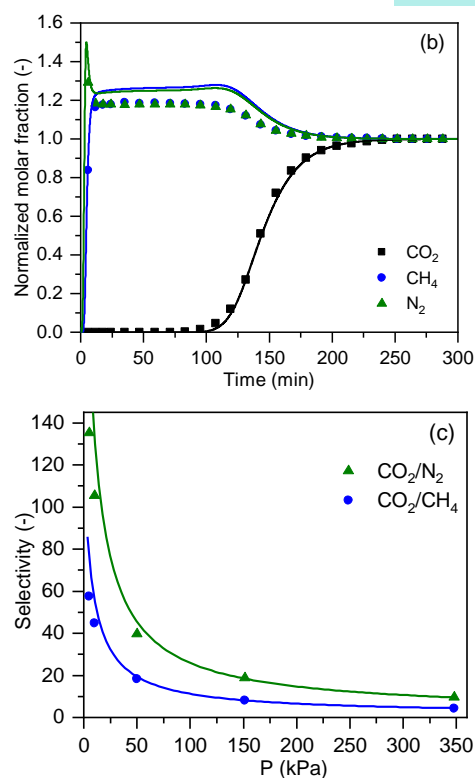
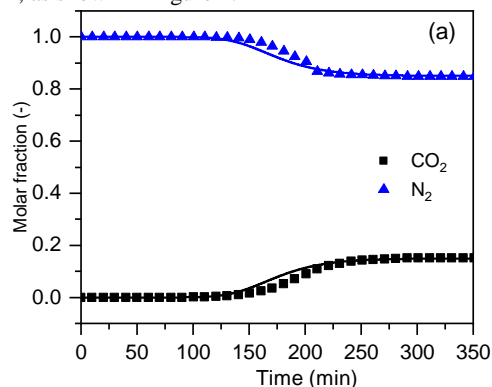


Figure 1. Breakthrough curves of (a) binary and (b) ternary fixed bed experiments, and (c) selectivity of CO₂/N₂ and CO₂/CH₄; at 313 K in binder-free K(95)Y zeolite.

Conclusions

Adsorption equilibrium measurements of CO₂, CH₄ and N₂ were performed on a series of ion-exchanged binder-free FAU type-Y zeolites using a chromatographic technique through a set of fixed bed breakthrough experiments. It was demonstrated that the CO₂ adsorption capacities at low pressure increases as follows: Ca(71)Y < Ca(56)Y < NaY < K(23)Y < K(58) < K(95)Y. The binary-component experiments of CO₂/N₂ mixture indicate that binder-free K(95)Y is a promising adsorbent for the recovery of CO₂ from post-combustion streams with a loading of 4.14 mol/kg, and a selectivity of around 105 over N₂ at 313 K. Aspen Adsorption v.10 was used to predict the single- and binary-component breakthrough curves. The mathematical model on the software was validated experimentally and the fitting of the numerical data through the transport and model parameters proves the capability of the model to describe the dynamics of adsorption in a fixed bed column.

Acknowledgements

The authors are grateful to the Foundation for Science and Technology (FCT, Portugal) for financial support through national funds FCT/MCTES (PIDDAC) to CIMO (UIDB/00690/2020 and UIDP/00690/2020) and SusTEC (LA/P/0007/2021). National funding by FCT, Foundation for Science and Technology, through the individual research grant under project PDTCEQU-EPQ/0467/2020. CICECO – Aveiro Institute of Materials, UIDB/50011/2020 & UIDP/50011/2020 & LA/P/0006/2020, financed by national funds through the FCT/MCTES (PIDDAC). Kristin Gleichmann and Chemiewerk Bad Koenstritz GmbH for kindly providing the binder-free beads of zeolites studied in this work.

References

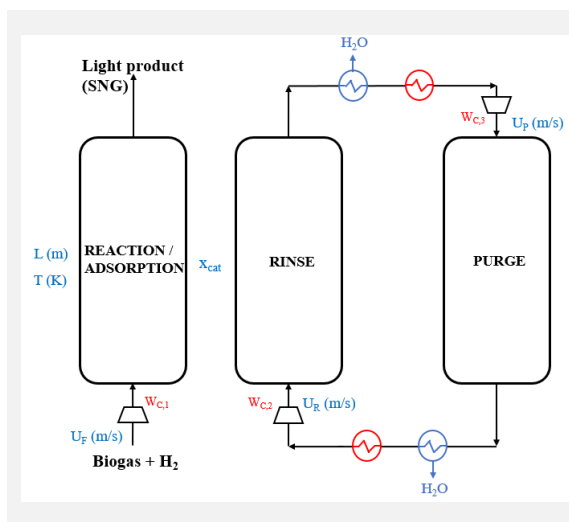
- [1] D.M. Ruthven, Principles of Adsorption and Adsorption Processes, 1st ed. New York, John Wiley & Sons, 1984.
- [2] O. Talu et al., Journal of Physical Chemistry, 97 (1993) 12894-12898.
- [3] E. Aly et al., Industrial & Engineering Chemistry Research, 60 (2021) 15236-15247.
- [4] D.D. Do, Adsorption Analysis: Equilibria and Kinetics, vol. 2. World Scientific, 1998.
- [5] D. Bonenfant et al., Science and Technology of Advanced Materials, 9 (2008) 013007.

Sorption enhanced reaction process designed for CO₂ methanation from biogas using different Ni-based catalysts

A. Cañada-Barcala*, M. Larriba, V.I.A. Maté, J.A.D. Dobladez

Catalysis and Separation Processes Group, Department of Chemical and Materials Engineering, Complutense University of Madrid. Spain. Avenida Complutense S/N 28040.

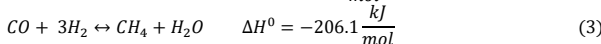
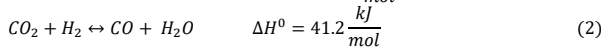
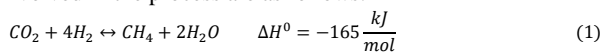
*acana01@ucm.es



Carbon dioxide is the gas with the greatest impact on climate change produced by humans since it is one of the main industrial by-products. Among the most attractive emerging solutions is the utilization of biogas as a biogenic source of CO₂ to produce synthetic natural gas. In this work, a cyclic SERP process to produce CH₄ from biogas hydrogenation has been designed by simulation, using different Ni-based catalyst such as NiAl₂O₃, Ni5A and the commercial Ni/SiAl. This last catalyst has been previously tested in the latest publication of this research group. For this purpose, catalytic tests were carried out in a reaction bed and the kinetics of the catalysts were studied. Once the catalyst kinetic model was obtained, these experimental data were used to develop the process, in which the influence of different operating variables (temperature, catalysis fraction, biogas composition or purge velocity) on productivity, energy consumption and process yields was studied.

Introduction

The capture and use of CO₂ to obtain methanol, formic acid or methane are one of the most viable technical-economic solutions to climate change. One solution to stop the use of fossil fuels can be their replacement by biogenic sources such as biogas. In addition, it is possible to contribute to a circular economy by using green hydrogen as an energy vector to transform carbon dioxide into synthetic natural gas (SNG) [1,2]. The reactions involved in the process are as follows:



As can be seen in the reaction scheme, CO production is favoured by temperature therefore decreasing selectivity towards CH₄. In addition, water is produced as a by-product and its accumulation shifts the equilibrium of the reaction towards the reactants. Therefore, it is essential to select a catalyst capable of maximizing reaction yields at relatively low temperatures (200-300°C). [2]

The most studied catalysts in CO₂ methanation are those based on nickel as active metal and supported on alumina, silica, or a mixture of both. However, the use of zeolites as a selective water adsorbent is well known throughout history, so it has been the subject of study for this reaction recently [1,3]. Thus, a cyclic SERP process to produce synthetic natural gas com CO₂ hydrogenation was recently designed in this research group, using Ni/SiAl commercial catalyst mixed with zeolite 3A as a water-selective adsorbent [4].

Experimental method and discussion

In this work, the mentioned SERP process has been used as the basis for the design of a biogas methanation process using three different catalysts. In this way, NiAl₂O₃ and Ni5A have been prepared by impregnation method for comparison with the commercial catalyst, as alumina is reported as one of the most

suitable catalyst for biogas methanation and 5A zeolite is reported as an excellent water-selective adsorbent [1,3]. The main target of this work is maximizing reaction yields at lower temperatures. For this purpose, a catalytic and kinetic study have been carried out first in a 19.12 mm long and 4.9 mm diameter reaction bed. The temperatures studied have been 200, 250, 300 and 350 °C. Furthermore, the partial pressure of CO₂ (PCO₂) has been modified in subsequent experiments to obtain the kinetic parameters. The experimental installation is shown in Figure 1.

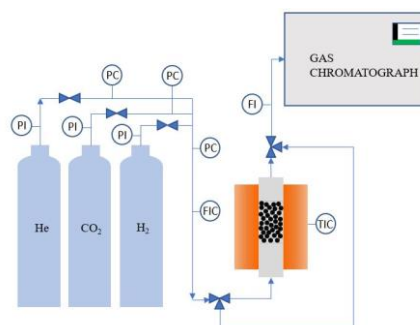


Figure 1. Catalytic and kinetic experimental installation.

Conclusions

Then, the kinetic data obtained have been used in the design and modelling of a methanation SERP process. The graphical abstract shows the designed process diagram, which has the typical elements of a Pressure Swing Adsorption (PSA) process [4,5]. Nevertheless, a pressure decrease is not necessary for the adsorbent regeneration since a minimum purge is enough to achieve it. In addition, the process has two condensers for the elimination of water. In this work, a 40% improvement in CO₂ conversion at 250° C is achieved using NiAl₂O₃ compared to the commercial catalyst.

Acknowledgements

Financial support from the Ministry of Economy and Competitiveness of Spain through project CTM2017-84033-R is gratefully acknowledged. Andrés Cañada-Barcala thanks Ministry of Universities of Spain for his FPU grant (FPU19/01451).

References

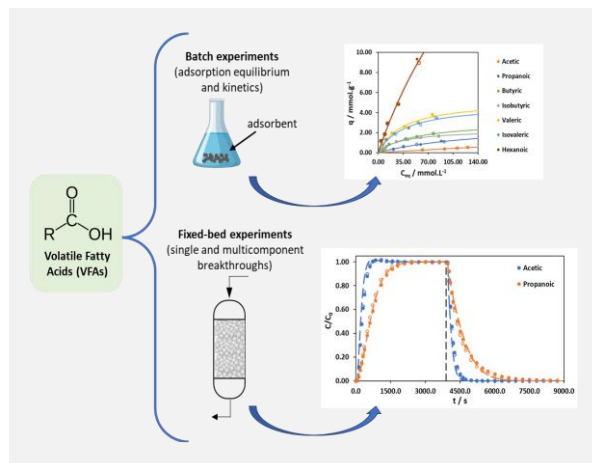
- [1] S. Nieß et al., *Catalysts*, 12 (2022) 374.
- [2] A. Ricca et al., *Chemical Engineering Journal*, 377 (2019) 120461.
- [3] M.C. Bacariza et al., *ChemCatChem*, 11 (2019) 2388-2400.
- [4] A. Cañada-Barcala et al., *Chemical Engineering Journal*, 461 (2023) 141897.
- [5] J.A. Delgado et al., *Industrial & Engineering Chemistry Research*, 53 (2014) 15414-15426.

Separation of volatile fatty acids with adsorption-based methods

C. Gomes*, A.M. Ribeiro, A. Rodrigues, A. Ferreira

LSRE-LCM – Laboratory of Separation and Reaction Engineering - Laboratory of Catalysis and Materials, Faculty of Engineering, University of Porto, Rua Dr. Roberto Frias, 4200-465 Porto, Portugal; ALiCE – Associate Laboratory in Chemical Engineering, Faculty of Engineering, University of Porto, Rua Dr. Roberto Frias, 4200-465 Porto, Portugal.

*up201403931@edu.fe.up.pt



The purpose of this work is to optimize the separation of the volatile fatty acids (VFAs), formed in the acidogenic fermentation of fish canning wastewater, using an adsorption-based process. To this end, the measurement of essential adsorption data (equilibrium and kinetics) on different adsorbents was analyzed, as well as the performance of a dynamic system (frontal analysis) and validation of the mathematical model. The equilibrium experimental data obtained allowed the selection of an adsorbent with higher potential for VFAs separation (a non-functionalized resin). The batch results were further used to design fixed-bed experiments and modelling. Fixed-bed adsorption experiments were run for single and multicomponent solutions and allowed the assessment of the dynamic adsorption behavior and the validation of the mathematical model.

Introduction

Fish canning is a significant sector worldwide and, to process the fish, this sector consumes large quantities of water in several operations, such as transport, cleaning, washing, cooking, cooling, defrosting, and sanitization. The resulting wastewater streams contain high organic matter content, which makes it challenging to treat. As a result, the development of valorization processes, such as wastewater acidogenic fermentation for volatile fatty acids (VFAs) production, is highly desirable [1-3]. However, not processed, and mixed VFAs are less valuable than the refined acids or even pure. Therefore, separating the acids into a worthier form is needed to be used for their intended purpose.

Several methods have already been researched for this end, such as precipitation, distillation, adsorption, and membrane-based technologies (e.g., nanofiltration, reverse osmosis, and vapor permeation membrane contactors). Adsorption is a highly studied method for VFAs separation, since it is relatively easy to operate, has high selectivity, and has a variety of materials [4, 5]. Different adsorbents have been tested to recover volatile fatty acids. Adsorbents with polystyrene-divinylbenzene or acrylic matrixes are most widely used for this end, especially those containing functional groups, such as primary, secondary, tertiary amines, or quaternary ammonium. The tertiary amino resins have the strongest interactions with VFAs at optimal pH 2.5-4.5, and non-functionalized ones present different affinities to each acid [3, 6-10].

This work intends to report a complete analysis of adsorption/desorption process on VFAs, to acquire the acids in a more refined and pure form (more worthy form). Therefore, batch experiments were carried out in different adsorbents to select the resin more suitable for VFAs separation and to determine the adsorption equilibrium and kinetics. Separation performance assessment by fixed-bed experiments was also accomplished for a better understanding of an adsorption dynamic system.

Materials and Methods

Different resins (one non-functionalized – Amberlite XAD-4, two functionalized with tertiary amines – Amberlite IRA-67 and Amberlyst A21, and one with quaternary ammonium – Dowex Marathon MSA) were selected and evaluated in terms of adsorption equilibrium and kinetics, in batch mode, with single-component aqueous solutions of the acids under study (acetic, propanoic, butyric, isobutyric, valeric, isovaleric and hexanoic acids). Different models (Single- and Dual-site Langmuir, Freundlich, Sips, and linear) were adjusted to the equilibrium experimental results to obtain the equilibrium parameters that best represent the results and best predicts the single adsorption isotherms. The experimental kinetic results were used to evaluate possible kinetic limitations and define the intraparticle diffusion by determining the mass transfer coefficient with Linear Driving Force (LDF) model regressed against the experimental results.

Single and multicomponent breakthrough experiments were also performed using a lab-scale fixed-bed set-up, packed with the adsorbent that achieved the best performance in the batch experiments, *i.e.*, that showed different affinities to each volatile fatty acid. Single and multicomponent breakthrough curves were used to assess the dynamic adsorption behavior and validate the fixed-bed mathematical model.

Results and Discussion

From the experimental data of the equilibrium adsorption, the predominant mechanism that stimulates the adsorption in each adsorbent in study was determined. Chemical adsorption was the principal adsorption mechanism in the Amberlite IRA-67 and Amberlyst A21 adsorbents since the acids exhibited similar adsorption capacities in concentration range tested. As for the Amberlite XAD-4 and Dowex Marathon MSA adsorbents, the results indicated an increase in adsorption capacity with the increase of the acid aliphatic chain length, which suggests that intermolecular interactions between the adsorbent and the adsorbates are the main adsorption mechanism. Single and Dual-site Langmuir models were selected to adjust the experimental results. From the equilibrium results obtained, it was concluded

that the non-functionalized resin (Amberlite XAD-4) would be the most suitable adsorbent to separate/fractionate the volatile fatty acids since it displays different selectivity to each acid, allowing a higher potential for the VFAs fractioning. The equilibrium data for Amberlite XAD-4 is represented in Figure 1.

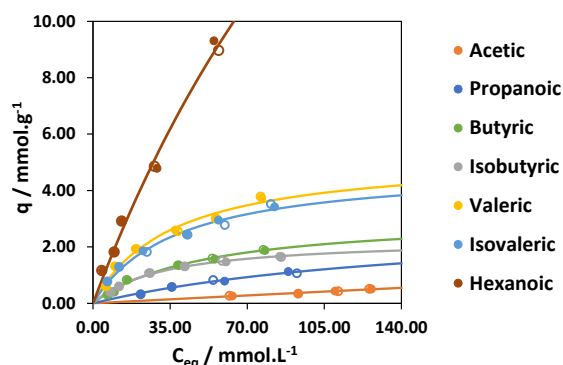


Figure 1. Adsorption equilibrium isotherms on the non-functionalized resin (Amberlite XAD-4).

The results obtained in the kinetic experiments showed an increase in the adsorption rate constant with decreasing in the acids' alkaline chain size.

Single-component breakthrough curves were determined in order to validate the fundamental properties determined in the batch essays. The results obtained were in agreement with each other, in terms of adsorption capacity. As for the mass transfer coefficient, it required tuning, having into account the fixed-bed experimental data, which means that the mass transfer in the batch and fixed-bed mode are slightly different. Both single and multicomponent breakthrough curves were used to evaluate the accuracy of the adsorption equilibrium model in predicting dynamic adsorption equilibrium. The mathematical model used had a good prediction of the fixed-bed experimental results, after

Acknowledgements

This work was financially supported by CONSERVAL Project, 0679_CONSERVAL_1_E, co-financed by the European Regional Development Fund (ERDF) through the Interreg V-A Spain-Portugal Program (POCTEP). This work was also financially supported by LA/P/0045/2020 (ALiCE), UIDB/50020/2020 and UIDP/50020/2020 (LSRE-LCM), funded by national funds through FCT/MCTES (PIDDAC). Cristiana Gomes acknowledges her PhD scholarship 2021.05666.BD funded by FEDER funds through NORTE 2020 and by national funds through FCT/MCTES.

References

- [1] R.O. Cristóvão et al., *Journal of Cleaner Production*, 87 (2015) 603-612.
- [2] N. Bermúdez-Penabad et al., *Waste Management*, 68 (2017) 96-102.
- [3] M. Atasoy et al., *Bioresource Technology*, 268 (2018) 773-786.
- [4] H. Yesil et al., *Water Science & Technology*, 69 (2014) 2132.
- [5] A. Silva et al., *Journal of Chemical & Engineering Data*, 58 (2013) 1454-1463.
- [6] E. Reyhanitash et al., *ACS Sustainable Chemistry & Engineering*, 5 (2017) 9176-9184.
- [7] S. Rebecchi et al., *Chemical Engineering Journal*, 306 (2016) 629-639.
- [8] C. Fargues et al., *Industrial & Engineering Chemistry Research*, 49 (2010) 9248-9257.
- [9] C.I. Cabrera-Rodríguez et al., *Bioresource Technology*, 237 (2017) 186-192.
- [10] T. Eregowda, *Separation Science and Technology*, (2019) 1-13.

the adsorption isotherms parameters were determined again since they did not represent accurately the multicomponent cases. An example case of a multicomponent breakthrough curve is represented in Figure 2 (experimental data and mathematical model prediction in dashed lines).

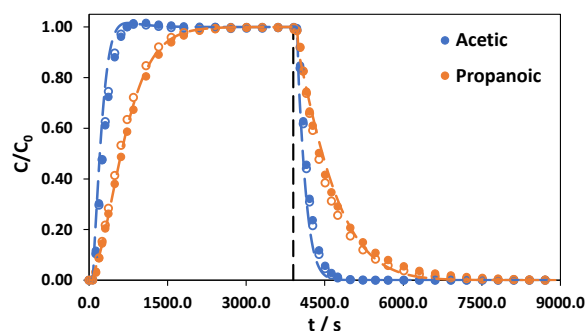


Figure 2. Acetic/Propanoic acids binary breakthrough curve.

Conclusions

This study explored the equilibrium adsorption of acetic, propanoic, butyric, isobutyric, valeric, isovaleric and hexanoic acids, in four different adsorbents. From the four adsorbents studied, the non-functionalized resin (Amberlite XAD-4) was selected, due to the different adsorption capacity achieved for each acid and higher potential to separate the volatile fatty acids. Single-site Langmuir model was used to fit the experimental data, in that adsorbent. The adsorption kinetics was also analyzed, and, with those results, the mass transfer coefficient was obtained by the regression of the experimental data against the LDF model.

In the fixed-bed experiments, the adsorption equilibrium was proved to be the same in batch and dynamic modes. However, the adsorption kinetics was a bit different from the batch essays. The mathematical model applied was capable of predicting the experimental data for the single and multicomponent breakthrough curves.

The logo for ChemPor 2023 features the word "ChemPor" in a white, sans-serif font, with "Chem" and "Por" separated by a thin vertical line. Below "ChemPor" is the year "2023" in a larger, bold, white, sans-serif font. The text is set against a white, rounded rectangular background that has a slight 3D effect, appearing to float above the dark blue background.

ChemPor 2023

**14th International Chemical and Biological
Engineering Conference**

Instituto Politécnico de Bragança | September 12-15



ORDEM
DOS
ENGENHEIROS

